NATIONAL AERONAUTICS AND

FACILITY FORM 602

(ACCESSION NUMBER) (THRU)

(PAGES) (CODE)

(NASA CR OR TMX OR AD NUMBER) (CATEGORY)

*Technical Report 32-1265*

# *Surveyor Project Final Report*

## *Part I. Project Description and Performance*

## *Volume II*

*Prepared by the Surveyor Project Staff*

CASE FILE
COPY

JET PROPULSION LABORATORY
CALIFORNIA INSTITUTE OF TECHNOLOGY
PASADENA, CALIFORNIA

July 1, 1969

NATIONAL AERONAUTICS AND SPACE ADMINISTRATION

*Technical Report 32-1265*

# *Surveyor Project Final Report*

## *Part I. Project Description and Performance*
## *Volume II*

*Prepared by the Surveyor Project Staff*

**JET PROPULSION LABORATORY**
**CALIFORNIA INSTITUTE OF TECHNOLOGY**
**PASADENA, CALIFORNIA**

July 1, 1969

***TECHNICAL REPORT 32-1265***

Copyright © 1969
Jet Propulsion Laboratory
California Institute of Technology

Prepared Under Contract No. NAS 7-100
National Aeronautics and Space Administration

# Contents


**XIII. Spacecraft System** . . . . . 1

A. Spacecraft System Design Objectives and Interface Constraints . . . . . 1

B. Flight Spacecraft Description . . . . . 3

C. Spacecraft System Design Development . . . . . 17

D. System Design Analysis and Verification Using Simulation Models and Programs . . . . . 41

E. Spacecraft System Performance . . . . . 49

References . . . . . 63

Bibliography. . . . . 64

**XIV. Spacecraft Structures and Mechanisms** . . . . . 67

A. Structural Design, Analysis, and Configuration . . . 68

B. Structural and Dynamic Testing . . . 84

C. Mission Structural Performance . . . . . 95

D. Mechanisms . . . . . 100

E. Electronic Packaging . . . 111

F. Cabling . . . . . 113

G. Spacecraft Alignment and Mass Properties Determination . . . 118

References . . . 121

Bibliography. . . 121

**XV. Thermal Control** . . . 123

A. Thermal Design . . . . . 123

B. Solar-Thermal-Vacuum Testing and Results . . . 137

C. Mission Performance. . . 147

D. Conclusions . . . 162

References . . . . . 163

Bibliography. . . . . 164

**XVI. Spacecraft Power** . . . . . 165

A. Early Design Evolution . . . . . 165

B. Design Used for *Surveyor I–IV* Missions. . . . . 171

C. Design Used for *Surveyor V–VII* Missions . . . . . 193

D. Construction Techniques and Manufacturing Experience . . 200

E. Testing . . . . . 207

## Contents (contd)


F. Mission Performance . . . . . 212

Bibliography. . . . . 216

**XVII. Spacecraft Propulsion** . . . . . 217

A. Vernier Propulsion System . . . . . 218

B. Main Retrorocket Motor . . . . . 282

C. Pyrotechnics . . . . . 300

References . . . . . 305

Bibliography. . . . . 307

**XVIII. Flight Control Subsystem** . . . . . 309

A. General . . . . . 309

B. Flight Control Subsystem Design. . . . . 309

C. Mission Sequence . . . . . 323

D. Construction Techniques and Manufacturing Experience . . . 326

E. Testing . . . . . 328

F. Flight Control Mission Performance Summary . . . . . 332

Appendix A. Flight Control Mechanization Diagram . . . . 335

Appendix B. Advanced Flight Control Programmer Mechanization Diagram . . . . . 339

Appendix C. Flight Control System Data . . . . . 343

Appendix D. Flight Control Power Distribution. . . . . 348

Appendix E. Design Requirements . . . . . 350

Appendix F. Detailed Canopus Sensor Mechanization Diagram . . . . . 354

**XIX. Spacecraft Radar** . . . . . 357

A. Altitude Marking Radar . . . . . 357

B. Radar Altimeter and Doppler Velocity Sensor . . . . . 363

Appendix A. Derivation of Radar Equations . . . . . 391

Appendix B. Research Triangle Institute Findings and Conclusions . . . . . 393

Appendix C. Lunar Reflectivity Model . . . . . 398

References . . . . . 399

Bibliography. . . . . 399

## Contents (contd)


**XX. Spacecraft Radio** . . . . . 401

A. Design Evolution. . . . . 401

B. Final Design Description. . . . . 403

C. Modification of Design, Specifications, and Procedures. . . . 411

D. Construction Techniques and Manufacturing Experience . . . 415

E. Testing . . . . . 418

F. Performance Summary . . . . . 419

Appendix A. Decibel Allocation Summary . . . . . 424

Appendix B. Radio System Active Elements . . . . . 443

Bibliography. . . . . 443

**XXI. Spacecraft Signal Processing and Command** . . . . . 445

A. Signal Processing Subsystem Design . . . . . 445

B. Command System Design . . . . . 452

C. Construction Techniques and Manufacturing Experience . . 459

D. Testing . . . . . 463

E. Mission Performance. . . . . 469

Bibliography. . . . . 473

**XXII. Spacecraft Scientific Instrument Payload** . . . . 475

A. Payload Evolution . . . . . 475

B. Television Cameras . . . . . 479

C. Soil Mechanics/Surface Sampler. . . . . 507

D. Alpha Scattering Instrument. . . . . 517

E. Instruments Not Used on *Surveyor* Missions . . . . 528

References . . . . . 548

**XXIII. Summary of Recommendations**. . . . . 549

A. Technology . . . . . 549

B. Qualification Testing and Quality Assurance . . . . 550

C. Contractual Aspects . . . . . 551

**Glossary** . . . . . 553

## Contents (contd)

### Tables


XIII-1. Spacecraft subsystem equipment and functions . . . . . 7

XIII-2. Flight spacecraft and payload configurations . . . . . 8

XIII-3. Summary of flight spacecraft weights . . . . . 8

XIII-4. Typical detailed spacecraft (*Surveyor V*) weight statement . . . . . 9

XIII-5. Flight spacecraft design changes and their effectivities . . . 10

XIII-6. Contractually defined spacecraft/payload configurations prior to *Surveyor* missions . . . . . 17

XIII-7. Mechanization sources of midcourse correction magnitude errors . . . . . 23

XIII-8. Mechanization sources of midcourse correction vector angle errors . . . . . 23

XIII-9. Summary of Spacecraft System performance during flight phase of *Surveyor* missions . . . . . 50

XIII-10. Lunar night survival performance summary . . . . . 55

XIII-11. Summary of SC-5 vernier weight of engine firings . . . . 59

XIII-12. Postlanding hop experiment parameters of SC-6 . . . . 61

XIII-13. *Surveyor* Spacecraft System and subsystem reliability estimates . . . . . 62

XIV-1. Boost-phase quasi-static load levels . . . . . 68

XIV-2. Boost-phase mechanical vibration input levels . . . . . 68

XIV-3. Boost-phase acoustic environment . . . . . 69

XIV.4. Relative vibration-level multiplying factors . . . . . 69

XIV-5. Descent-phase load levels . . . . . 69

XIV-6. Lunar-touchdown design conditions . . . . . 70

XIV-7. Minimum margins of safety . . . . . 70

XIV-8. Pressure vessel description . . . . . 78

XIV-9. Structural analysis summary . . . . . 79

XIV-10. Bulk yield pressure . . . . . 82

XIV-11. Test milestones of special test vehicles . . . . . 84

XIV-12. Result of S-2 modal survey . . . . . 85

XIV-13. S-2 vibration input level . . . . . 85

XIV-14. S-2 center-of-gravity and alignment shifts . . . . . 86

XIV-15. S-2A solar panel motion . . . . . 86

## Contents (contd)

### Tables (contd)


XIV-16. Results of S-2A modal survey landing configuration . . . . 87

XIV-17. Compartment modes, landing configuration . . . . . 87

XIV-18. S-9 torsional sinusoidal test inputs . . . . . 88

XIV-19. S-9 static test result summary . . . . . 88

XIV-20. Preliminary results of S-9 modal survey: launch configuration . . . . . 90

XIV-21. S-9 vibration test levels . . . . . 92

XIV-22. S-9 solar panel motion . . . . . 92

XIV-23. S-9 drop test conditions . . . . . 92

XIV-24. Burst test pressure data . . . . . 95

XIV-25. Summary of mechanical properties of propellant pressure vessel . . . . . 97

XIV-26. Landing conditions, *Surveyors I, III, V, VI,* and *VII* . 97

XIV-27. Leg touchdown sequence and relative timing . 97

XIV-28. Maximum shock-absorber axial loads during touchdown. . . . . 98

XIV-29. Performance parameters, *Surveyor VI* . . . . . 99

XIV-30. Maximum shock-absorber axial loads and times of initial ground contact (hop experiment of *Surveyor VI*) . . . . . 100

XIV-31. *Surveyor* assemblies, index . . . . . 101

XIV-32. Antenna/solar panel positioner configurations . 104

XIV-33. *Surveyor VII* wire harness description . . . . . 115

XIV-34. Component angular alignment tolerances relative to the spacecraft coordinate system . . . . . 120

XV-1. *Surveyor* payload configurations . . . . . 125

XV-2. Use of active and semiactive thermal control . 127

XV-3. Thermal radiative properties of *Surveyor* thermal finishes . . . . . 128

XV-4. Heater summary (typical) . . . . . 136

XV-5. Comparison of HAC and JPL STV data for sector 1 . . . 140

XV-6. Modifications to T-21 prototype spacecraft resulting from STV tests . . . . . 140

XV-7. S-10 tests . . . . . 141

XV-8. Lunar surface simulator calorimeter plate predicted and actual performance . . . . . 142

## Contents (contd)

### Tables (contd)


XV-9. Modifications to flight spacecraft during STV tests . . . . 143

XV-10. Effect of hardware changes on vernier propulsion system duty cycles . . . . . 145

XV-11. Spacecraft temperatures sensors . . . . . 148

XV-12. Operational and survival temperature limits and results . . . 148

XV-13. Flight and STV temperature comparisons . . . . . 151

XV-14. Spacecraft sensor temperatures at lunar noon, compared with solar-thermal-vacuum test results . 161

XVI-1. *Surveyors I–IV* power subsystem performance characteristics . . . . . 172

XVI-2. Launch-to-touchdown battery energy management, SC-1 through SC-4 . . . . . 183

XVI-3. User's load table . . . . . 184

XVI-4. Booster-regulator output characteristics . . . . . 186

XVI-5. Characteristics of the electrical conversion units . . . 188

XVI-6. Ground commands assigned to power subsystems . . . . 191

XVI-7. Launch-to-touchdown battery utilization, SC-5 through SC-7 . . . . . 194

XVI-8. *Surveyors V–VII* power subsystem performance characteristics of the new units . . . . . 197

XVI-9. Number of power subsystem units fabricated and their disposition . . . . . 204

XVI-10. Battery charge regulator type approval tests . . . . . 210

XVI-11. Hardline power subsystem measurements . . . . . 212

XVI-12. Power subsystem performance summary . . . . . 215

XVI-13. Solar panel preflight and mission performance data . . . 216

XVII-1. Vernier propulsion system requirements summary . . . . 221

XVII-2. *Surveyor* vernier engine major milestones . . . . . 224

XVII-3. Vernier engine requirements summary . . . . . 226

XVII-4. Flight vernier engine rework history . . . . . 230

XVII-5. Alternate vernier engine requirements summary . . . . 241

XVII-6. Vernier propulsion feed system major milestones . . . . 241

XVII-7. Vernier propulsion feed system component and control item flight acceptance tests . . . . . 253

XVII-8. Type approval tests performed on vernier propulsion feed system elements . . . . . 253

## Contents (contd)

### Tables (contd)


XVII-9. Sequence of vernier propulsion system tests conducted on flight spacecraft . . . . . 263

XVII-10. Vernier propulsion system test problems. . . . . 264

XVII-11. Vernier propulsion system transit phase performance summary . . . . . 271

XVII-12. Vernier propulsion system leaks and malfunctions after lunar landings . . . . . 278

XVII-13. Retro motor program milestones . . . . . 283

XVII-14. Retro motor development test history . . . . . 295

XVII-15. Flight retro motor data summary . . . . 299

XVII-16. *Surveyor* spacecraft pyrotechnic devices . . . . . 302

XVIII-1. Flight control modes . . . . . 310

XVIII-2. Flight control programmer technical characteristics . . 317

XVIII-3. Significant changes to Flight Control Sensor Group configurations . . . . . 319

XVIII-4. Flight control electronics unit construction changes . . . . 328

XVIII-5. Vibration test results . . . . . 329

XVIII-6. Comparison of earth measurement and inflight measurement of gyro drift . . . . . 334

XVIII-C-1. Flight control switch closure requirements . . . 347

XVIII-E-1. Inertial reference unit requirements . . . . 351

XVIII-E-2. Canopus sensor requirements . 351

XVIII-E-3. Electronics unit requirements . . . . . 351

XVIII-E-4. Acquisition sun sensor requirements . . . 351

XVIII-E-5. Inertia switch requirements . . . . . 351

XVIII-E-6. Telemetry accelerometer requirements . . . . . 352

XVIII-E-7. Primary sun sensor requirements . . . . . 352

XVIII-E-8. Secondary sun sensor requirements . . . . . 352

XVIII-E-9. Roll actuator requirements . . . . . 352

XVIII-E-10. Gas supply requirements . . . . . 352

XVIII-E-11. Gas jet requirements . . . . . 352

XVIII-E-12. Vernier engines requirements . . . . . 353

XVIII-E-13. Flight control system group weight summary . . . . . 353

XIX-1. Altitude marking radar performance requirements . . . . 357

## Contents (contd)

### Tables (contd)


XIX-2. Marking radar parameters . . . . . 359

XIX-3. Performance summary . . . . . 363

XIX-4. Radar altimeter and doppler velocity sensor parameters . . . . . 366

XIX-5. Klystron input power data . . . . . 368

XIX-6. Standard test conditions for vendor tests . . . . . 381

XIX-7. Outline of vendor tests on flight units . . . . . 383

XIX-8. Listing of buyer flight acceptance tests . . . . . 386

XIX-9. Outline of vendor system flight acceptance tests . . . . 387

XIX-10. Comparison of RADVS performance values: specification vs mission measurements . . . . . 388

XIX-11. RADVS mission events (time in seconds from RADVS on) . . . . . 389

XIX-12. Typical (*Surveyor I*) terminal-descent sequences . . . . . 390

XX-1. Receiver characteristics . . . . . 404

XX-2. Transmitter characteristics . . . . . 408

XX-3. Antenna and switching system characteristics . . . . . 412

XX-4. Subsystem hardware scheduled delivery vs actual delivery . . . . . 419

XX-5. Parameter comparison for radio system units . . . . . 421

XX-B-1. Receiver elements . . . . . 443

XX-B-2. Transmitter elements . . . . . 443

XXI-1A. Typical (SC-7) analog telemetry channel assignments . . . 449

XXI-1B. Typical (SC-7) digital telemetry channel assignments . . . 450

XXI-2. Commutation rates and frame lengths . . . . . 451

XXI-3. Command format and coding . . . . . 456

XXI-4. Typical (SC-7) command assignment list . . . . . 456

XXI-5. Unit module complement of signal processing and command subsystem . . . . . 461

XXI-6. Physical characteristics of the signal processing equipment . . . . . 461

XXI-7. Flight performance comparison of selected signal processing parameters . . . . . 470

XXI-8. Commutator word assignment changes for SC-3 and SC-4 . . . . . 471

## Contents (contd)

### Tables (contd)


XXII-1. Scientific instrument payloads . . . . . 476

XXII-2. Principal changes in the spacecraft scientific instrument payload definition . . . . . 477

XXII-3. Weight of scientific instruments . . . . . 478

XXII-4. Survey TV camera operating characteristics . . . . . 484

XXII-5. Composite video signal characteristics for *Surveyor III* . . . 502

XXII-6. Television camera configurations . . . . . 505

XXII-7. Major television operations performed on lunar surface . . . 506

XXII-8. Survey TV camera performance summary . . . . . 508

XXII-9. Summary of SM/SS operations on *Surveyor* missions . . . . 517

XXII-10. 1101 quartz peak characteristics of the X-ray diffractometer . . . . . 532

XXII-11. Touchdown dynamics experiment sequence of events . . . 544

XXII-12. Word-bit data . . . . . 545


### Figures


XIII-1. *Surveyor* spacecraft in postlanding configuration (*Surveyor VII* illustrated) . . . . . 3

XIII-2. *Surveyor* spacecraft configuration (*Surveyor VII* illustrated) . . . . . 5

XIII-3. Simplified spacecraft functional block diagram (*Surveyor VII*) . . . . . 6

XIII-4. Spacecraft coordinates relative to celestial references . . 13

XIII-5. Normal sequence of terminal-descent events . . . . . 13

XIII-6. Terminal-descent range-velocity diagram . . . . . 14

XIII-7. Radar altimeter and doppler velocity sensor beam orientation . . . . . 14

XIII-8. Thermal dissipating capability of main compartments on lunar surface . . . . . 16

XIII-9. Typical duty cycle capability of spacecraft on lunar surface . . 16

XIII-10. Battery charge and discharge profile for extended operation after sunset . . . . . 16

XIII-11. Retrorocket velocity vector diagram . . . . . 25

XIII-12. Velocity dispersions for vertical approach . . . . . 26

XIII-13. Retrorocket burnout velocity vs impact velocity . . . . . 26

## Contents (contd)

### Figures (contd)


XIII-14. Displacement vector diagram . . . . . 27

XIII-15. Altitude dispersions for vertical approach . . . . . 27

XIII-16. Vernier propellant margin vs impact velocity . . . . . 28

XIII-17. Nominal vernier descent propellant vs impact velocity . . . 28

XIII-18. Vernier propellant dispersion vs burnout velocity . . . . 29

XIII-19. Gravity turn descent geometry . . . . . 29

XIII-20. Thrust acceleration command . . . . . 30

XIII-21. Range-velocity trajectory relative to descent contour . . . 31

XIII-22. Acceleration vs velocity . . . . . 31

XIII-23. Final segment and corresponding trajectory . . . . . 32

XIII-24. Retroignition altitude vs unbraked impact velocity . . . 36

XIII-25. Altitude vs time during retromaneuver . . . . . 36

XIII-26. Velocity vs time during retromaneuver . . . . . 36

XIII-27. Nominal descent time from retroignition to touchdown vs retrorocket burnout velocity . . . . . 37

XIII-28. Time difference between unbraked impact and touchdown vs retrorocket burnout velocity . . . . . 37

XIII-29. Central angle difference between unbraked impact point and touchdown point as function of unbraked impact angle . . . . . 37

XIII-30. System plan for spacecraft sterilization (heat, liquid, and gas) . . . . . 39

XIII-31. Generalized block diagram of analog, six-degree-of-freedom model . . . . . 42

XIII-32. Bias closed loops of Surveyor five-degree-of-freedom simulation (nominal values) . . . . . 43

XIII-33. Thermal management program functional flow diagram . . . . . 44

XIII-34. General flow diagram of power management program . . . . . 45

XIII-35. Six-degree-of-freedom computation loop . . . . . 47

XIII-36. General diagram of landing dynamics space model and analysis procedure . . . . . 48

XIII-37. Idealized block diagram of attitude matrix assessment . . . 49

XIII-38. Terminal-descent and landing events of *Surveyor III* . . . 56

XIII-39. Landing sequence *Surveyor III* . . . . . 57

## Contents (contd)

### Figures (contd)


XIII-40. Comparison of nominal, predicted, and actual *Surveyor V* terminal-descent-event time intervals . . . . 60

XIII-41. Change in spacecraft position induced by hop experiment . . . . . 61

XIII-42. *Surveyor* Spacecraft System reliability estimates . . . . 62

XIV-1. Spacecraft coordinate conventions . . . . . 69

XIV-2. *Surveyor* spaceframe geometry . . . . . 72

XIV-3. Typical compartment substructure . . . . . 73

XIV-4. Landing gear assembly with crushable blocks . . . . . 74

XIV-5. Spaceframe with antenna/solar panel positioner support . . . . . 75

XIV-6. Solar panel bracket attachment . . . . . 76

XIV-7. Retrorocket mounting detail . . . . . 77

XIV-8. On-board arrangement of pressure vessels . . . . . 77

XIV-9. Landing stability boundaries for planar downhill landings on 15-deg slope . . . . . 83

XIV-10. Torsional test setup . . . . . 88

XIV-11. Strip chart timing record of torsional pulse inputs 89

XIV-12. Launch configuration modal survey setup . . . . . 89

XIV-13. Setup for evaluation of structural transfer function . . . . 91

XIV-14. S-9 unit on vibration test fixture . . . . . 91

XIV-15. S-9 unit shown suspended above landing platform . . . . 91

XIV-16. T-1 test vehicle. . . . . 93

XIV-17. Lunar gravity device . . . . . 93

XIV-18. Tensile test specimens in forged bar . . . . . 96

XIV-19. *Surveyor I* shock absorber strain-gage force histories . . . 98

XIV-20. *Surveyor* shock absorber column, design details . . . . 99

XIV-21. *Surveyor III* shock absorber strain-gage force histories . . . 100

XIV-22. *Surveyor VI* shock absorber strain-gage force histories . . . 100

XIV-23. Separation-sensing and -arming device . . . . . 103

XIV-24. A/SPP motors . . . . . 105

XIV-25. Deployment mechanisms for omnidirectional antennas A and B . . . . . 107

## Contents (contd)

### Figures (contd)


XIV-26. Extended-position locking mechanism, omnidirectional antenna A . . . . . 107

XIV-27. Omnidirectional antenna B locking mechanism . . . . . 107

XIV-28. Retrorocket release mechanism . . . . . 109

XIV-29. Basic straight-shaft pinpuller . . . . . 110

XIV-30. A/SPP tapered-shaft pinpuller . . . . . 110

XIV-31. Photo showing harness for bus 1 with insert showing cable-splicing technique . . . . . 115

XIV-32. Strain-relief methods for harnesses . . . . . 117

XIV-33. *Surveyor* spacecraft optical alignment dock . . . . . 119

XV-1. *Surveyor* mission sequence and thermal environment summary . . . . . 124

XV-2. Thermal design for *Surveyor VII* . . . . . 126

XV-3. Ultraviolet degradation of HAC inorganic white paint (from laboratory and *Surveyor I* data) . . . . . 127

XV-4. Vernier engine 2 solar reflector . . . . . 129

XV-5. *Surveyor* compartment A, showing T-top . . . . . 130

XV-6. *Surveyor* compartment A, showing T-leg . . . . . 131

XV-7. Typical conductivity curve for *Surveyor* thermal switches . . . . . 132

XV-8. *Surveyor* thermal switch . . . . . 133

XV-9. Thermal switch on *Surveyor* compartment . . . . . 134

XV-10. General test arrangement for *Surveyor* thermal switch . . . 135

XV-11. MT-1: sector I . . . . . 137

XV-12. MT-1: sector II . . . . . 138

XV-13. Hot cone simulator . . . . . 142

XV-14. Leg in sun test . . . . . 142

XV-15. Retro motor: flight temperature ranges for *Surveyors I* through *VII* (except *Surveyor II*) . . . . . 152

XV-16. Fuel tank 1: flight data envelope for *Surveyors I* through *VII* (*Surveyor II* through midcourse only) . . . . 152

XV-17. Fuel tank 2: flight data envelope for *Surveyors I* through *VII* (*Surveyor II* through midcourse only) . . . . 152

XV-18. Fuel tank 3: flight data envelope for *Surveyors I* through *VII* (*Surveyor II* through midcourse only) . . . . 153

## Contents (contd)

### Figures (contd)


XV-19. Oxidizer tank 1: flight data envelope for *Surveyors I* through *VII* (*Surveyor II* through midcourse only) . . . . 153

XV-20. Oxidizer tank 2: flight data envelope for *Surveyors I* through *VII* (*Surveyor II* through midcourse only) . . . . 153

XV-21. Oxidizer tank 3: flight data envelope for *Surveyors I* through *VII* (*Surveyor II* through midcourse only) . . . . 153

XV-22. Vernier line 2 temperature history on *Surveyor II* . . . . 154

XV-23. Transit thermal performance of vernier oxidizer tank 2 . . . 154

XV-24. Transit thermal performance of vernier fuel tank 2 . . . . 155

XV-25. Battery: lunar surface performance . . . . . 156

XV-26. Survey television camera electronics temperatures: lunar surface performance . . . . . 157

XV-27. Alpha scattering instrument sensor head: lunar surface performance . . . . . 158

XV-28. Alpha scattering instrument electronics: lunar surface performance . . . . . 159

XV-29. Soil mechanics/surface sampler auxiliary electronics: lunar surface performance . . . . . 160

XV-30. Typical output of shadow plot computer program . . . . 161

XVI-1. Simplified *Surveyor* power subsystem . . . . . 166

XVI-2. Block diagram of initial concept of radioisotope thermoelectric generator, solar panel, and battery power subsystem . . . . . 167

XVI-3. Initial concept of spacecraft requirements vs mission time . . . . . 168

XVI-4. Block diagram of initial concept of solar panel and battery . . . . . 169

XVI-5. Simplified electrical power subsystem functional block diagram, SC-1 through SC-4 . . . . . 170

XVI-6. Front view of SC-1 through SC-4 solar panel . . . . 173

XVI-7. Typical solar panel section wiring diagram . . . . . 173

XVI-8. Typical solar panel characteristics, SC-1 through SC-4 . . . 174

XVI-9. Simplified main battery schematic . . . . . 175

XVI-10. Typical flight battery . . . . . 176

XVI-11. Auxiliary battery . . . . . 178

XVI-12. Main power switch schematic diagram . . . . . 179

XVI-13. Auxiliary battery control . . . . . 180

## Contents (contd)

### Figures (contd)


XVI-14. Automatic battery transfer criteria . . . . . 181

XVI-15. Battery charge regulator, *Surveyors I–IV* . . . . . 182

XVI-16. Optimum charge regulator operating procedures . . . . 183

XVI-17. Booster-regulator block diagram . . . . . 185

XVI-18. Flight control three-phase power supply . . . . . 187

XVI-19. Simplified block diagram of engineering mechanism auxiliary . . . . . 190

XVI-20. Electrical power subsystem telemetry shunt locations . . . 192

XVI-21. Electrical power subsystem block diagram, *Surveyors V–VII* . . . . . 195

XVI-22. Cell side of solar panel . . . . . 198

XV-23. Block diagram of solar panel assembly, SC-5, SC-6, and SC-7 . . . . . 199

XVI-24. *Surveyor* solar panel SN-002, I-E characteristic curve . . . 200

XVI-25. Battery charge regulator block diagram, *Surveyors V–VII* . . . . . 201

XVI-26. Booster-regulator manufacturing flow chart . . . . . 203

XVI-27. Processing history of SC-1 booster-regulator (B/R 274200-96, SN-12) . . . . . 206

XVI-28. Processing history of SC-5 booster-regulator (B/R 3024240-1, SN-11) . . . . . 207

XVI-29. Processing history of SC-1 battery charge regulator (BCR 274100-3, SN-11) . . . . . 208

XVI-30. Processing history of SC-5 battery charge regulator (BCR 3024260, SN-11) . . . . . 209

XVI-31. Processing history of SC-1 auxiliary battery control (ABC 273000-2, SN-15) . . . . . 209

XVI-32. Typical power profile . . . . . 213

XVI-33. Spacecraft power requirements, SC-1 through SC-7 . . . . 213

XVII-1. Vernier propulsion system schematic . . . . . 219

XVII-2. *Surveyor* vernier propulsion system . . . . . 220

XVII-3. Flight configuration vernier engine . . . . . 225

XVII-4. Vernier engine flow schematic . . . . . 227

XVII-5. Vernier engine throttle valve . . . . . 228

XVII-6. Vernier engine combustion chamber assembly . . . . . 229

XVII-7. Vernier engine shutoff valve . . . . . 232

## Contents (contd)

### Figures (contd)


XVII-8. Vernier engine shutdown circuit . . . . . 233

XVII-9. Residue that caused propellant shutoff valve failure (engine SN 561) . . . . . 233

XVII-10. Typical uncommanded thrust excursion . . . . . 234

XVII-11. Effect of dissolved helium on vernier engine response to step thrust command . . . . . 234

XVII-12. Effect of dissolved helium on frequency response of vernier engines for small-amplitude signals . . . . . 234

XVII-13. Effect of dissolved gas on phase lag of vernier engines for small-amplitude signals . . . . . 235

XVII-14. Simulated closed-loop control system tests used for vernier engine development . . . . . 235

XVII-15. Alternate vernier engine configuration . . . . . 239

XVII-16. Alternate vernier engine external view . . . . . 240

XVII-17. Alternate vernier engine schematic . . . . . 242

XVII-18. Helium tank and valve assembly (spacecraft SC-1 through SC-4) . . . . . 243

XVII-19. Helium tank and valve assembly (spacecraft SC-5 through SC-7) . . . . . 244

XVII-20. Helium dump and release valve . . . . . 245

XVII-21. Helium pressure regulator . . . . . 246

XVII-22. Helium regulator (outlet port) . . . . . 246

XVII-23. Helium check valve . . . . . 247

XVII-24. Helium relief valve . . . . . 247

XVII-25. Vernier propellant tank assembly . . . . . 249

XVII-26. Propellant tank components without thermal wrap . . . . 250

XVII-27. Helium permeation of oxidizer tank bladder . . . . . 251

XVII-28. Helium solubility in propellants . . . . . 251

XVII-29. Helium pressure regulator seat that failed under possible *Surveyor V* conditions . . . . . 256

XVII-30. Vernier engine checkout equipment used at AFETR . . . . 267

XVII-31. Propulsion system temperature ranges during transit . . . 270

XVII-32. Typical propellant and helium tank pressure-vs-time curves . . . . . 272

XVII-33. *Surveyor II* strain gage and thrust command signals at midcourse . . . . . 273

## Contents (contd)

### Figures (contd)


XVII-34. Vernier propellant tank pressurization prior to *Surveyor V* midcourse correction . . . . . 274

XVII-35. *Surveyor V* helium tank pressure decay following midcourse correction . . . . . 274

XVII-36. *Surveyor V* vernier engine flow test results . . . . . 276

XVII-37. *Surveyor V* propellant supply pressure decay during terminal descent . . . . . 277

XVII-38. Postlanding vernier propulsion system temperature ranges . . . . . 277

XVII-39. *Surveyor V* engine thrust during vernier static firing experiment on lunar surface . . . . . 281

XVII-40. *Surveyor VI* vernier engine thrust during translation . . . 282

XVII-41. Retro motor section . . . . . 284

XVII-42. Main retro motor characteristics . . . . . 285

XVII-43. *Surveyor* main retro motor case assembly . . . . . 286

XVII-44. Retro motor case internal insulation . . . . . 286

XVII-45. Retro motor wrapped for installation . . . . . 287

XVII-46. Retro motor nozzle design evolution (early designs tested) . . . . . 288

XVII-47. Retro motor nozzle design evolution (redesigned structure and contour) . . . . . 289

XVII-48. Retro motor nozzle design evolution (final throat insert design tested) . . . . . 291

XVII-49. Main retro grain core configuration . . . . . 292

XVII-50. Typical retro motor thrust-vs-time curves (*Surveyor III*) . . . 300

XVII-51. Spacecraft roll moment torque during retro motor operation . . . . . 300

XVII-52. Spacecraft pitch and yaw resultant torque during retro motor operation . . . . . 301

XVII-53. Squib structure . . . . . 303

XVII-54. Pyrotechnic switches . . . . . 304

XVIII-1. Flight control block diagram . . . . . 311

XVIII-2. Spacecraft coordinates and location of FCS control elements . . . . . 312

XVIII-3. Primary sun sensor field of view . . . . . 313

XVIII-4. Acquisition sensor field of view . . . . . 313

## Contents (contd)

### Figures (contd)


XVIII-5. Spacecraft coordinates relative to celestial references . . . 314

XVIII-6. Canopus sensor field of view . . . . . 314

XVIII-7. Star Canopus location relative to sun–earth equatorial plane . . . . . 315

XVIII-8. Advanced flight control programmer block diagram . . . . 316

XVIII-9. Main retro-phase sequence of events before segment acquisition . . . . . 327

XVIII-A-1. Flight control mechanization diagram . . . . . 337

XVIII-B-1. Advanced flight control programmer mechanization diagram . . . . . 341

XVIII-C-1. Flight control system block diagram . . . . . 345

XVIII-D-1. Flight control power distribution . . . . . 349

XVIII-E-1. Output characteristics for Canopus sensor . . . 350

XVIII-E-2. Output characteristics for primary sun sensor pitch channel . . . . . 350

XVIII-E-3. Output characteristics for primary sun sensor yaw channel . . . . . 350

XVIII-E-4. Gas supply inlet-vs-discharge pressure . . . . 350

XVIII-F-1. Detailed Canopus sensor mechanism diagram . 355

XIX-1. Altitude marking radar, block diagram . . . . 359

XIX-2. Altitude marking radar, assembly photo . . . . . 360

XIX-3. Relation of RF energy to transit range . . . . . 361

XIX-4. Radar altimeter and doppler velocity sensor, block diagram . . . . . 365

XIX-5. Beam orientation . . . . . 367

XIX-6. Antenna and beam configuration . . . . . 367

XIX-7. Klystron power supply and modulator, block diagram . . . 368

XIX-8. Signal data converter, block diagram . . . . . 369

XIX-9. Antenna layout and signal flow . . . . . 371

XIX-10. Block diagram of preamplifiers . . . . . 373

XIX-11. Photo showing telemetry elements (less waveguide) . . . 378

XIX-12. Manufacture and test history of typical system . . . . . 380

XIX-13. Diagram of signal simulation subsystem . . . . . 382

XIX-A-1. Altimeter frequency diagram . . . . . 392

## Contents (contd)

### Figures (contd)


XX-1. Radio system block diagram . . . . . 403

XX-2. Receiver phase-lock-loop response . . . . . 404

XX-3. Receiver block diagram . . . . . 405

XX-4. Receiver crystal filter response . . . . . 406

XX-5. Receiver first discriminator automatic frequency control response . . . . . 407

XX-6. Transmitter block diagram . . . . . 409

XX-7. Transmitter TV wideband frequency modulator response . . . . . 409

XX-8. Transmitter scientific wideband frequency modulator response . . . . . 410

XX-9. Transmitter phase modulator response . . . . . 410

XX-10. Transmitter TV narrowband frequency modulator response . . . . . 410

XX-11. Local oscillator characteristics . . . . . 413

XX-12. Transmitter top view . . . . . 416

XX-13. Transmitter bottom view . . . . . 417

XX-14. Command receiver . . . . . 418

XX-15. T-bar module general arrangement . . . . . 419

XX-16. Typical receiver and transmitter processing history for a spacecraft . . . . . 420

XX-17. Typical transmitter wideband voltage-controlled crystal oscillator frequency output . . . . . 422

XX-18. Typical transmitter narrowband voltage-controlled crystal oscillator frequency output . . . . . 422

XXI-1. Simplified block diagram—signal processing subsystem . . . 447

XXI-2. Simplified commutation and analog-to-digital functions . . . 448

XXI-3. *Surveyor* simplified voltage-controlled oscillator and mixing functions . . . . . 453

XXI-4. Simplified *Surveyor* command block diagram . . . . . 454

XXI-5. Central command decoder block diagram . . . . . 455

XXI-6. Subsystem command decoder block diagram . . . . . 460

XXI-7. Rework/recycle graph for engineering signal processor SN 11 flown on SC-5 . . . . . 465

XXI-8. Rework/recycle graph for engineering signal processor SN 7 flown on SC-4 . . . . . 466

## Contents (contd)

### Figures (contd)


XXI-9. Rework/recycle operation failure report graph for engineering signal processor SN 9 flown on SC-3 . . . . 466

XXII-1. Exploded view of *Surveyor* TV camera . . . . . 481

XXII-2. Survey TV camera on the spacecraft (*Surveyor I*) . . . . 482

XXII-3. Cutaway view of the survey TV camera (model used on *Surveyor I*) . . . . . 483

XXII-4. One-inch vidicon tube assembly . . . . . 486

XXII-5. Vidicon tube assembly functional diagram . . . . . 486

XXII-6. Shutter assembly . . . . . 487

XXII-7. Variable focal length lens and iris assembly . . . . . 488

XXII-8. Survey TV camera . . . . . 489

XXII-9. Filter wheel assembly . . . . . 490

XXII-10. Relative tristimulus values of color filter elements . . . . 490

XXII-11. Mirror head assembly (as used on *Surveyor I*) . . . . . 490

XXII-12. Television photometric—colorimetric reference chart . . . . 491

XXII-13. Television calibration configuration at the Spacecraft Checkout Facility . . . . . 497

XXII-14. Television calibration at DSS 11 and the Space Flight Operations Facility . . . . . 498

XXII-15. Calibration test set . . . . . 499

XXII-16. Calibration light source . . . . . 500

XXII-17. Camera light transfer characteristics . . . . . 501

XXII-18. Television picture linearity correction . . . . . 503

XXII-19. Television picture intensity correction . . . . . 503

XXII-20. *Surveyor I* footpad pictures illustrating correction of modulation transfer function . . . . . 504

XXII-21. *Surveyor III* view of soil mechanics/surface sampler . . . . 504

XXII-22. Soil mechanics/surface sampler deployment envelope . . . 509

XXII-23. Soil mechanics/surface sampler . . . . . 510

XXII-24. Soil mechanics/surface sampler approaching footpad 2 . . . 512

XXII-25. Block diagram of soil mechanics/surface sampler auxiliary assembly . . . . . 515

XXII-26. Soil mechanics/surface sampler activity on *Surveyor III* mission . . . . . 518

XXII-27. Alpha scattering instrument simplified block diagram . . . .519

## Contents (contd)

### Figures (contd)


XXII-28. Sensor head interior . . . . . 521

XXII-29. Alpha scattering instrument deployment mechanism . . . . 522

XXII-30. Comparison of prelaunch and transit phase data . . . . 526

XXII-31. Comparison of standard sample spectrum and computer-generated curve . . . . . 527

XXII-32. X-ray diffractometer operation . . . . . 529

XXII-33. X-ray diffractometer 25-kV X-ray tube (lower unit) . . . . 529

XXII-34. P-3 X-ray diffractometer head without cover plates . . . . 530

XXII-35. P-3 X-ray diffractometer . . . . . 530

XXII-36. Comparison of *Surveyor* X-ray diffractometer and commercial X-ray diffractometer . . . . . 531

XXII-37. X-ray spectrometer operation . . . . . 532

XXII-38. Prototype model C X-ray spectrometer with dust cover removed . . . . . 533

XXII-39. Gas chromatograph schematic . . . . . 535

XXII-40. Typical gas chromatograph detector signal . . . . . 535

XXII-41. Subsurface sonde . . . . . 538

XXII-42. Acoustic velocity instrument, geophone sensor, and density instrument . . . . . 538

XXII-43. Thermal diffusivity instrument . . . . . 540

XXII-44. Seismometer major assemblies . . . . . 542

XXII-45. Seismometer sensor frequency response curve . . . . . 543

XXII-46. Prototype soil mechanics instrument . . . . . 547

# XIII. Spacecraft System

The *Surveyor* spacecraft was conceived and designed to effect a transit from earth to the moon, perform a soft landing, and transmit back to earth basic scientific and engineering data relative to the environment and characteristics of the moon.

Soft landing, as related to the *Surveyor* Program, is defined as a controlled landing method, employing required sensors, instrumentation, and throttlable engines for maintaining complete control of the spacecraft through the entire descent, that allows the spacecraft to settle gently onto the lunar surface. This method is in contrast with simpler landing methods such as the hard landing of probes by retroejection of smaller survivable packages. The *Apollo* soft-landing method was conceived similar to the *Surveyor* method, and it became a *Surveyor* objective to demonstrate the suitability of this technique for *Apollo*.

## A. Spacecraft System Design Objectives and Interface Constraints

In the *Surveyor* spacecraft design, an overall objective was to maximize the probability of successful spacecraft operation within the basic limitations imposed by launch vehicle capabilities, the extent of knowledge of transit and lunar environments, and the current technological state of the art. In keeping with this major objective, design policies were established that:

(1) Minimized spacecraft complexity by placing responsibility for mission control and decision-making on earth-based equipment wherever possible.

(2) Provided the capability of transmitting a large number of different data channels from the spacecraft.

(3) Included provisions for accommodating a large number of individual commands from the earth.

(4) Made all subsystems as reliable as practicable.

To establish more detailed spacecraft design objectives, the basic *Surveyor* Project objectives, which included development of soft-landing technology and the soft-landing of an instrumented payload for study of the lunar surface, were defined in more detail and related to hardware development. These design objectives were used to establish the system functional requirements and specifications for equipment and mission-related operations.

### 1. System Design Objectives

The following system design objectives evolved:

(1) Spacecraft size and weight would be compatible with the launch vehicle.

(2) Basic portion of all spacecraft would be uniform in design to the fullest possible extent.

(3) Each individual spacecraft would be capable of accommodating its selected payload.

(4) Materials used in spacecraft construction would not interfere with proper functioning of all spacecraft and payload elements.

(5) Spacecraft functional and structural capability for survival of both direct-ascent and parking-orbit boost trajectory environments.

(6) Capability for programmed search and acquisition of the required celestial bodies for attitude control.

(7) Spacecraft mechanization capable of executing two midcourse corrections of up to 50 m/sec between 4 and 40 hr after injection.

(8) Spacecraft instrumentation to permit adequate status and operating condition determination of the spacecraft during all phases of the mission.

(9) Normal planned transit time of 66 hr.

(10) The landing for each mission would occur in a preselected region of the visible lunar surface.

(11) Capability of landing at any approach angle between 0 and 45 deg.

(12) Landing accuracy for a 30-m/sec midcourse correction would be within 60 km for a vertical approach and 96 km for a 45-deg approach.

(13) Landing accuracy for a 50-m/sec midcourse correction within 100 km for a vertical approach and 160 km for a 45-deg approach.

(14) Spacecraft landing mechanization and sequence would be independent of local lunar lighting conditions.

(15) A 90-day period of flight and lunar surface operation.

(16) The design service life (defined as the total calendar time within which the spacecraft could be expected to operate without any wearout failures) of the spacecraft, including the mission payload would be 90 days.

(17) System reliability for the basic spacecraft and the payload for a 66-hr normal flight and landing of 0.75 and 0.85, respectively, at a confidence level of 80%.

### 2. Interface Constraints

In the evolution of spacecraft design objectives, other operational elements of the project with which the spacecraft would operate and which would constrain the spacecraft design were defined. Primary interfaces between the spacecraft and these elements, along with the associated set of constraints that each element imposed on the spacecraft design, are listed below.

*a. Air Force Eastern Test Range.*

(1) Spacecraft had to be delivered to Air Force Eastern Test Range (AFETR) in as near a flight-ready condition as possible, with testing being concentrated on system-level and calibration checks.

(2) Spacecraft design had to permit on-pad testing with communication limited to RF link.

(3) Spacecraft design had to accommodate built-in countdown holds.

(4) Spacecraft had to use 1-A, 1-W, no-fire (for 5 min) squib, and shielded wires so that squib circuits conformed to range safety requirements.

*b. Launch vehicle (Atlas/Centaur).*

(1) Size and weight of spacecraft had to be compatible with *Atlas/Centaur* launch vehicle configuration.

(2) In its stowed configuration, the spacecraft had to fit within a maximum payload dynamic envelope (under protective nose fairing).

(3) Spacecraft had to withstand predicted boost-phase acceleration and vibration conditions.

(4) Spacecraft had to null out rotational rates of up to 3.0 deg/sec imparted by the *Centaur*/spacecraft separation mechanism.

(5) Spacecraft had to have sufficient midcourse correction capability to correct for launch vehicle injection errors, which were not to exceed 16.7 m/sec (1 $\sigma$ rss).

*c. Deep Space Instrumentation Facility.* Spacecraft telecommunication design had to be compatible with the deep space instrumentation facility (DSIF) and provide

for transponders on the spacecraft to permit DSIF stations to make precise two-way (earth to spacecraft and spacecraft to earth) doppler measurements, as well as provide for adequate spacecraft transmitted power and spacecraft receiver sensitivity to ensure satisfactory telemetry and command link performance.

*d. Space Flight Operations Facility.* Spacecraft telemetry and command design had to provide:

(1) Sufficient data (number of channels and adequate sampling rates) to permit effective monitoring and assessment by Space Flight Operations Facility (SFOF) of spacecraft status and performance.

(2) Necessary command reception and processing capability to permit effective control of spacecraft operations.

Automatic on-board control of mission-critical sequences had to be provided when one or more of the following requirements existed:

(1) Rapid execution of commands.

(2) Absolute timing accuracy.

(3) Execution of a sequence when an earth-to-spacecraft command link could not be assured.

## B. Flight Spacecraft Description

### 1. Spacecraft Configuration

The *Surveyor* flight spacecraft was basically a three-cornered pyramidal, open-frame aluminum structure that carried a variety of reliable electronic and mechanical assemblies. Figure XIII-1 illustrates the fully deployed *Surveyor* spacecraft after soft-landing and identifies the spacecraft coordinate system and many major components that comprise the Spacecraft System. Components ejected from the spacecraft during final descent to the lunar surface, and not shown in Fig. XIII-1, included the spherical solid propellant retrorocket motor, which was located, prior to ejection, under and near the center of the spaceframe; and also the altitude marking radar (AMR) antenna, which, prior to ejection, was located (and held by friction clips) on the exit flange of the main retrorocket nozzle.

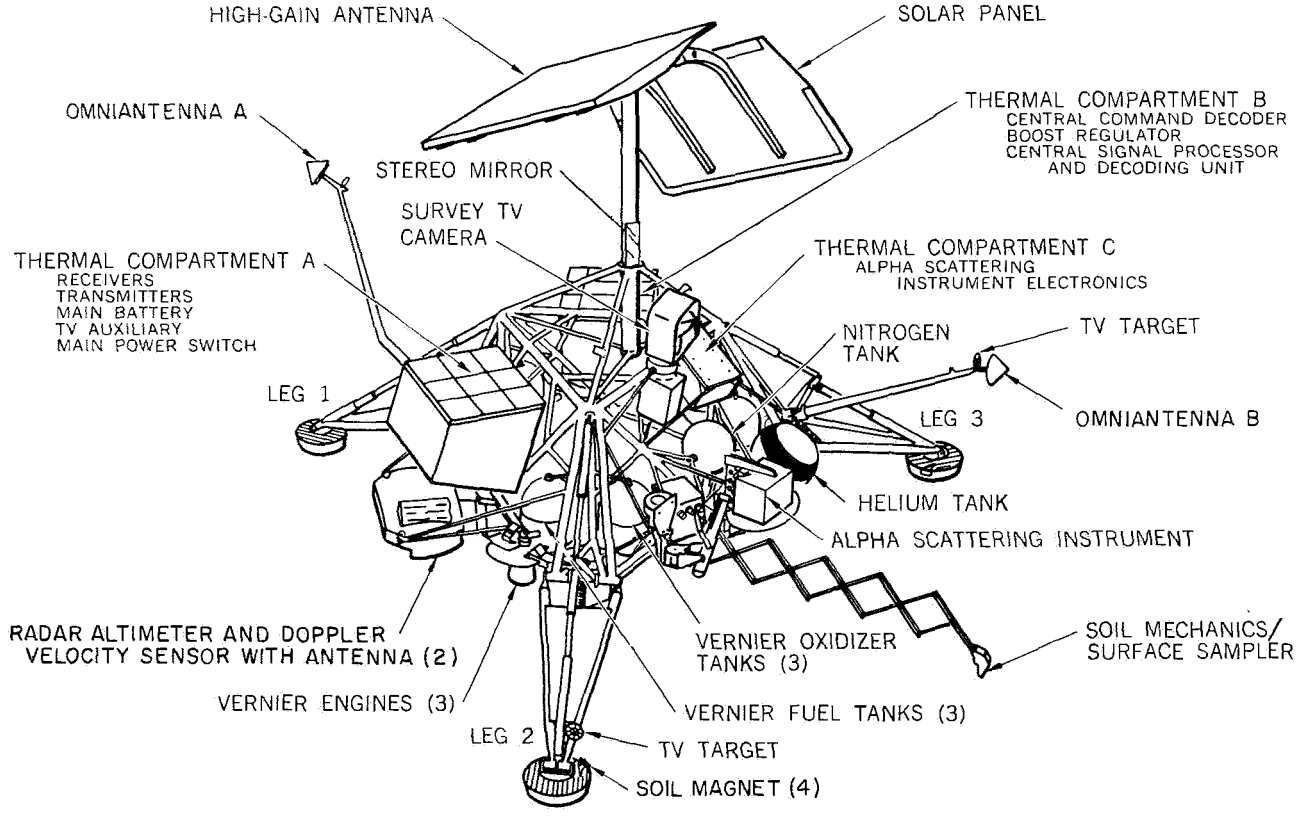



**Fig. XIII-1. Surveyor spacecraft in postlanding configuration (*Surveyor VII* illustrated)**

The spacecraft was designed with foldable antennas and landing legs to fit within the protective launch vehicle nose fairing during launch. During the boost phase, when the launch vehicle and spacecraft were about 60 mi above the surface of the earth, the nose fairing was jettisoned. At an altitude of about 100 mi and just before spacecraft separation from the launch vehicle, the legs and antennas were extended by preprogrammed commands from the launch vehicle. Figure XIII-2 shows the spacecraft in the stowed, midcourse, and postlanding configurations. Spacecraft CG was designed low to ensure stability over a range of landing conditions.

In terms of hardware, basic spacecraft subsystems were:

(1) Structures and mechanisms.

(2) Thermal control.

(3) Electrical power.

(4) Propulsion.

(5) Flight control and radar.

(6) Radio, signal processing, and command.

(7) Scientific instrument payload.

Subsystem functions and associated equipment are shown in Table XIII-1. More detailed subsystem discussions are presented in Sections XIV–XXII of this report.

The main scientific instrument carried by *Surveyor I* was the survey television camera. The success of *Surveyor I* resulted in additional instruments being added for later missions. The last five spacecraft, which carried the additional instruments, were designated the A-21E model. Actual spacecraft weight and scientific instrument configurations for each of the seven *Surveyor* missions are shown in Table XIII-2. A more detailed system weight summary for each flight spacecraft, to the subsystem level, is shown in Table XIII-3. Table XIII-4 shows a subsystem weight breakdown, to the control item level, for a typical spacecraft (SC-5).

Subsection C-1 cites the evolution of spacecraft configuration and weight during design development prior to the first *Surveyor* mission. After the first mission, design changes were incorporated in the spacecraft configuration as new information became available and as the flight program progressed.

Briefly, the major changes made between missions included:

(1) Approach television removed: effective on *Surveyors III–VII.*

(2) Soil mechanics/surface sampler incorporated: effective *Surveyors III, IV,* and *VII.*

(3) Alpha scattering instrument incorporated: effective *Surveyors V–VII.*

(4) Power system improved and auxiliary battery removed: effective *Surveyors V–VII.*

(5) Antenna/solar panel positioner (A/SPP) improved: effective *Surveyors V–VII.*

(6) High-impulse retrorocket incorporated: effective *Surveyors III, IV,* and *VII.*

(7) Redesigned TV camera incorporated: effective *Surveyors VI* and *VII.*

(8) Cross coupled side-lobe logic in radar altimeter and doppler velocity sensor (RADVS): effective *Surveyor IV* and up.

(9) Increased impulse retro motor: effective *Surveyors II, IV,* and *VII.*

More complete design change information is summarized in Table XIII-5. Further discussion of specific changes is presented in appropriate subsystem sections (Sections XIV–XXII) of this report.

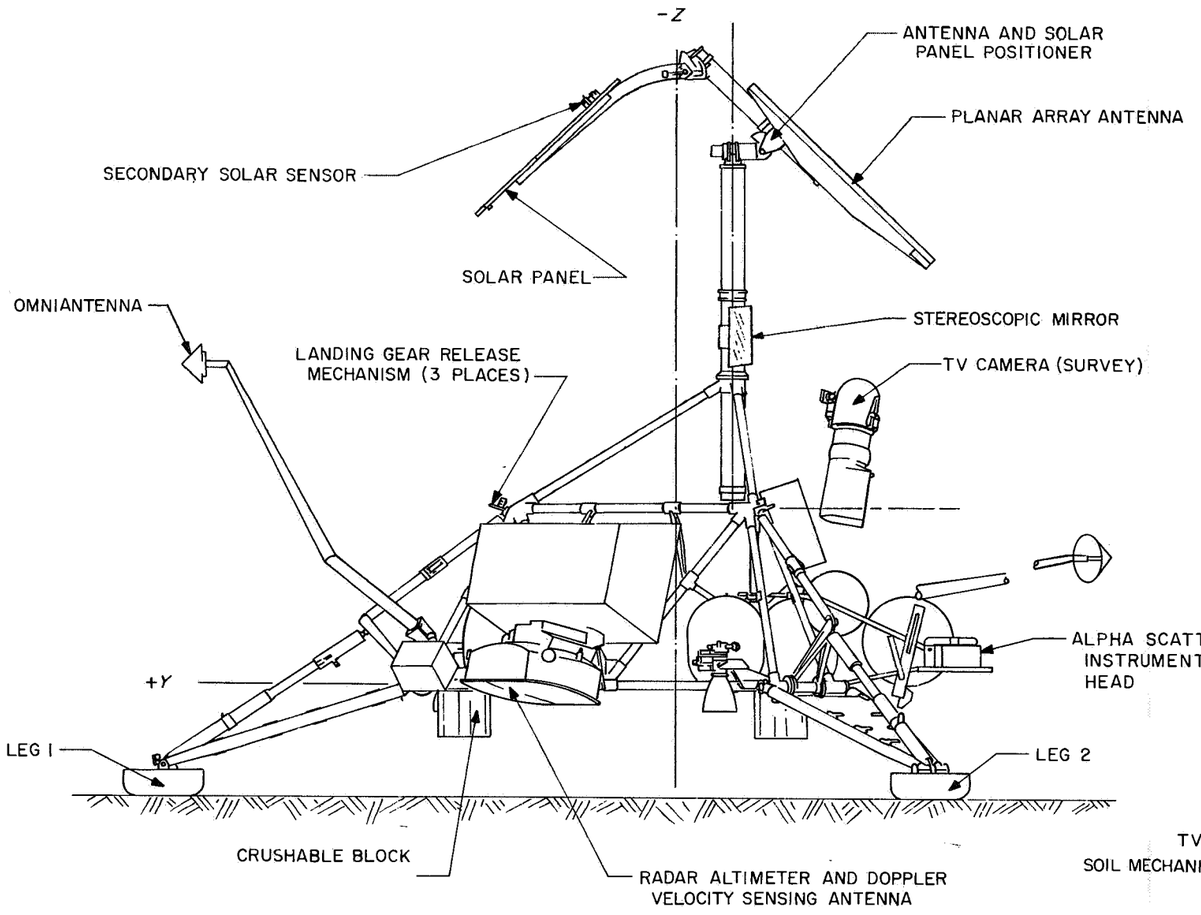
### 2. Spacecraft System Functional Description

The spacecraft achieved its system functional requirements through the integrated performance of several specialized, on-board subsystems. Figure XIII-3 is a simplified functional block diagram of the spacecraft system showing the subsystem interaction.

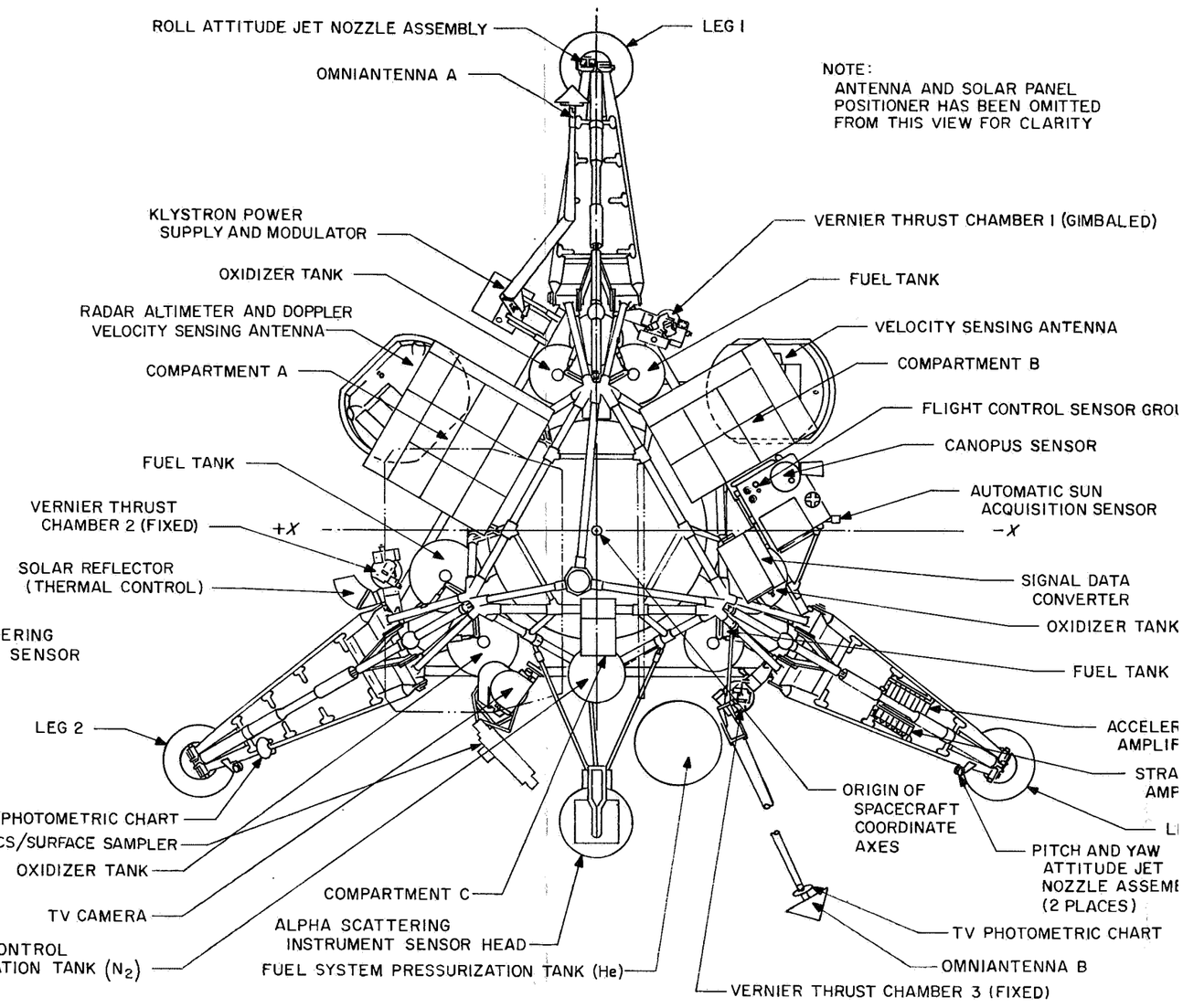
After separation from the launch vehicle, the spacecraft attitude was controlled by three cold-gas reaction jets located on the landing legs. Initially, control signals to the gas jets from the on-board flight control subsystem resulted in damping and nulling the small rotational rates that occurred at physical separation of the spacecraft from the launch vehicle. After rotational rates were nulled to negligible values, the spacecraft attitude was maintained by inertial control, with control signals being derived from gyro position signals.

#1

POSTLANDING CONFIGURATION




+Y MIDCOURSE CONFIGURATION



#2

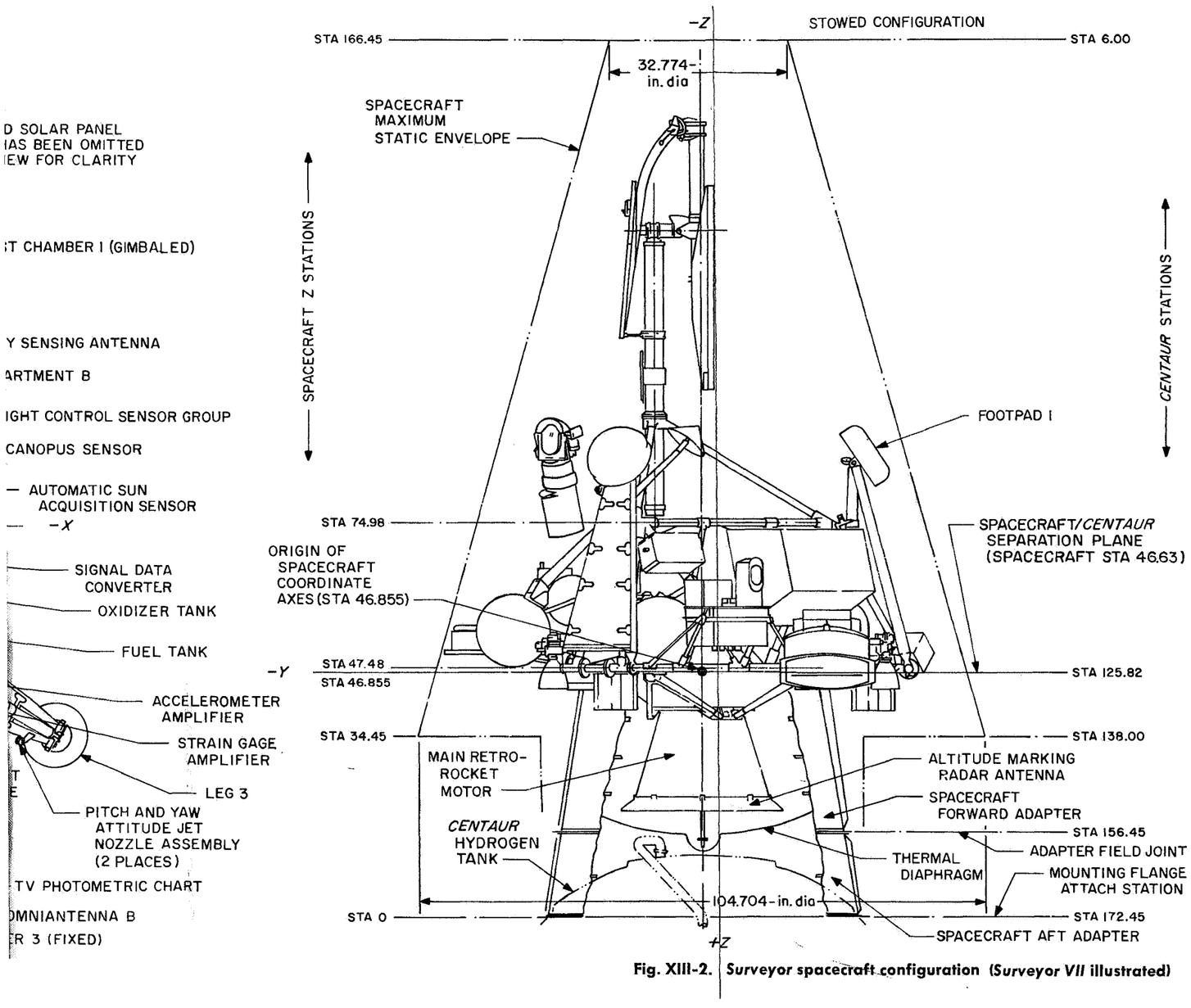



**Fig. XIII-2.** *Surveyor* **spacecraft configuration (*Surveyor VII* illustrated)**

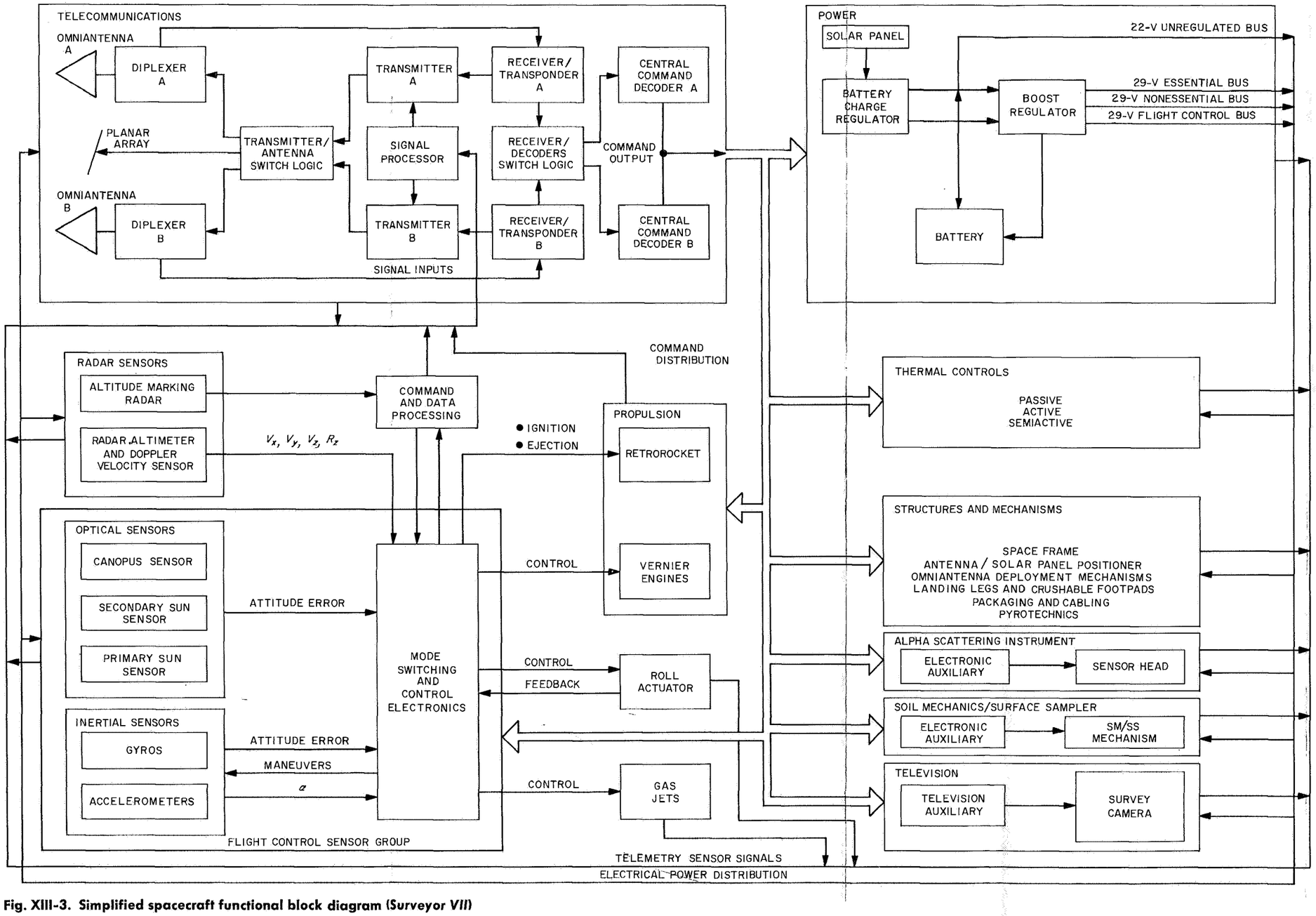



**Fig. XIII-3. Simplified spacecraft functional block diagram (*Surveyor VII*)**

## Table XIII-1. Spacecraft subsystem equipment and functions

| Subsystem | Equipment | Functions |
|---|---|---|
| Structures and mechanisms | Spaceframe and substructures; three landing legs with hydraulic shock absorbers, crushable block footpads | Mounting structure for all spacecraft equipment; absorption of landing loads |
| | Antenna/solar panel positioner, squib-actuated devices for deploying omniantennas and landing gears and for separating retrorocket | Positioning of solar panel and planar array, extension of omni-antennas and landing gears, separation of main retrorocket |
| Thermal control | Vernier fuel and oxidizer line heaters, super-insulated compartments with heaters and thermal switches, television electronic and vidicon heaters, alpha scattering and soil mechanics surface sampler heaters, aluminized Mylar wrapping and paint patterns | Active, semiactive and passive temperature control of spacecraft equipment to maintain temperature within specified operational and survival limits |
| Electrical power | Solar panel, main battery, auxiliary battery and contral (*Surveyors I–IV* only), power control units (including battery charge regulator), boost regulator, overload trip circuit, and optimum charge regulator (*Surveyors I–IV* only) | Power generation by conversion of solar energy to electrical energy required for spacecraft electrical loads and/or battery charging; energy storage to provide a source to help supply transit loads in excess of solar panel output and for supplying power during periods when solar panel was not illuminated; charge control of energy storage unit and conversion, regulation, control, and distribution of power to spacecraft loads |
| Propulsion | Solid propellant retrorocket | Retrorocket thrusting for removing bulk of incoming spacecraft velocity for lunar landing |
| | Three throttlable, bipropellant vernier engines, one of which was gimbaled for roll control, three sets of fuel and oxidizer tanks utilizing bladders, and helium pressurization system | Low-level thrusting and moment control during midcourse velocity correction and during the retrorocket firing vernier phases of the terminal descent |
| Flight control and radar | Flight control electronics, including control logic, programmer, and vernier engine control; gas jet system, vernier engine roll control actuator, and flight control sensor group, including inertial reference unit (gyros and axial accelerometer); optical sensors for celestial references (sun and star sensors); radar sensors for lunar reference (altitude marking radar, altimeter radar, doppler velocity radar) | Provided attitude stabilization and orientation during entire transit phase using inertial, celestial, and lunar reference systems, including dissipation of launch vehicle separation-induced rates, sun and star acquisition and lock-on; performed precise attitude maneuvers; precisely controlled propulsion system in performing midcourse velocity correction; caused ignition of vernier engines and retrorocket during terminal descent; controlled propulsion system to cause spacecraft to descend along desired range-versus-velocity profile |
| Radio, signal processing, and command | DSIF-compatible S-band system including omni-antennas, transponder/receiver, transmitter, demodulator, command decoder, modulator, high-gain antenna, diplexers, antenna switching, high-and-low RF power switching, and signal processor | Two-way DSIF-to-spacecraft transponder operation via omni-antenna to permit continuous angle and two-way doppler tracking to lunar distances; highly reliable, omnidirectional DSIF-to-spacecraft command link to monitor and control at lunar distances; spacecraft instrumentation signal processing and continuous omnidirectional spacecraft-to-DSIF telemetry link during transit from injection to lunar distances; low-power, directional spacecraft-to-DSIF telemetry link for lunar operations; high power, omnidirectional spacecraft-to-DSIF link for 200-line television transmission immediately after landing; high-power directional spacecraft-to-DSIF link for 600-line television transmission during postlanding operations |
| Scientific instrument payload | Survey television camera, auxiliary electronics, and auxiliary viewing and dust detection mirrors | Postlanding television surveys to permit observations of lunar topography, texture of lunar surface material, spacecraft structure, effect of landing gear and soil mechanics/surface sampler in disturbing lunar surface material, and other effects |
| | Soil mechanics/surface sampler instrument (Surveyors III, IV, and VII only) | Digging, scraping, trenching, impacting, and transporting lunar surface material |

## Table XIII-1 (contd)

| Subsystem | Equipment | Functions |
|---|---|---|
| Scientific instrument payload (contd) | Alpha scattering instrument (*Surveyors V* through *VII* only) | Elemental compositional analysis of lunar surface material |
| | Soil magnets | Determination of magnetic properties of lunar surface material |

## Table XIII-2. Flight spacecraft and payload configurations

| Surveyor mission | Spacecraft | | Injected weight, lb | Scientific instruments | Payload weight, lb[a] |
|---|---|---|---|---|---|
| | Serial No. | Model No. | | | |
| *I* | SC-1 | A-21 | 2193 | Survey TV[b] | 63[b] |
| *II* | SC-2 | A-21 | 2204 | Survey TV[b] | 63[b] |
| *III* | SC-3 | A-21E | 2281 | Survey TV and auxiliary mirrors, soil mechanics/surface sampler (SM/SS) | 88 |
| *IV* | SC-4 | A-21E | 2295 | Survey TV and auxiliary mirrors, SM/SS, soil magnet | 88 |
| *V* | SC-5 | A-21E | 2217 | Survey TV and auxiliary mirrors, alpha scattering instrument, soil magnet | 65 |
| *VI* | SC-6 | A-21E | 2220 | Survey TV and auxiliary mirrors, alpha scattering instrument, soil magnets | 66 |
| *VII* | SC-7 | A-21E | 2289 | Survey TV and auxiliary mirrors, SM/SS, alpha scattering instrument, soil magnets | 89 |

[a]Not including approach TV carried but not used on *Surveyors I* and *II*.
[b]Includes auxiliary battery (on *Surveyor I–IV* only) and added engineering instrument weight listed in Table XIII-3.

## Table XIII-3. Summary of flight spacecraft weights

| Item | Mission | | | | | | |
|---|---|---|---|---|---|---|---|
| | *Surveyor I*, lb | *Surveyor II*, lb | *Surveyor III*, lb | *Surveyor IV*, lb | *Surveyor V*, lb | *Surveyor VI*, lb | *Surveyor VII*, lb |
| Basic spacecraft | 703.30 | 708.94 | 709.02 | 724.58 | 718.95 | 719.86 | 717.92 |
| *Flight control* | 56.28 | 56.36 | 56.57 | 57.44 | 57.40 | 57.69 | 57.42 |
| Electronics | 120.72[a] | 120.81[a] | 115.76 | 114.65 | 116.49 | 117.40 | 117.09 |
| Electrical power | 54.32 | 54.74 | 54.64 | 54.70 | 54.59 | 54.67 | 54.61 |
| Mechanisms | 29.70 | 31.04 | 31.36 | 31.90 | 38.06 | 38.06 | 37.97 |
| Structure | 212.89 | 215.46 | 218.21 | 217.64 | 219.74 | 220.73 | 220.20 |
| Propulsion | 222.69 | 233.44 | 223.12 | 223.20 | 223.92 | 226.07 | 228.05 |
| Adjustment for actual weights | 2.06 | 0.62 | −0.03 | 3.45 | 1.82 | −0.16 | 0.81 |
| Ballast | 4.13 | 5.96 | 8.93 | 21.69 | 6.42 | 4.89 | 1.26 |
| Buoyancy | 0.51 | 0.51 | 0.51 | 0.51 | 0.51 | 0.51 | 0.51 |
| Uptrapped propellant | 1425.91 | 1431.16 | 148.94 | 1482.67 | 1432.68 | 1434.16 | 1482.22 |
| Retrorocket (including buoyancy) | 1244.07 | 1250.88 | 1302.25 | 1300.35 | 1251.37 | 1251.54 | 1300.51 |
| Vernier | 181.84 | 180.28 | 181.69 | 182.32 | 181.31 | 182.62 | 181.71 |
| Payload | 63.50 | 63.44 | 88.40 | 87.64 | 65.19 | 66.35 | 89.09 |
| Survey television | 22.46 | 22.13 | 26.20 | 25.62 | 26.86 | 28.15 | 29.44 |
| Auxiliary battery | 28.49 | 28.60 | 29.01 | 28.67 | 0 | 0 | 0 |
| Added engineering instrumentation | 12.52 | 12.88 | 12.89 | 12.83 | 10.74 | 10.65 | 10.77 |
| Soil mechanics/surface sampler | 0 | 0 | 20.05 | 20.32 | 0 | 0 | 21.20 |
| Magnets | 0 | 0 | 0 | 0.15 | 0.15 | 0.15 | 0.15 |
| Alpha scattering instrument | 0 | 0 | 0 | 0 | 27.35 | 27.35 | 27.46 |
| Buoyancy | 0.03 | 0.03 | 0.05 | 0.05 | 0.09 | 0.05 | 0.07 |
| Total separated weight | 2192.71 | 2203.74 | 2381.36 | 2294.89 | 2216.82 | 2220.37 | 2289.23 |

[a]Includes weight of approach television camera.

## Table XIII-4. Typical detailed spacecraft (*Surveyor V*) weight statement

| Item | Weight, lb |
|---|---|
| Total spacecraft injected weight | 2216.82 |
| Basic spacecraft | 718.95 |
| Flight control subsystem | 57.40 |
| Flight control sensor group | 38.49 |
| Inertial reference unit | 8.26 |
| Canopus sensor | 5.15 |
| Wiring harness | 1.05 |
| Electronics | 20.66 |
| Support | 3.37 |
| Secondary solar sensor | 0.29 |
| Attitude control system | 18.62 |
| Attitude jets (7) | 1.70 |
| Nitrogen tank and lines | 10.83 |
| Roll actuator | 1.52 |
| Nitrogen gas | 4.57 |
| Electronics | 116.49 |
| Radio subsystem | 35.07 |
| Planar array antenna | 9.64 |
| Omniantennas (2) | 0.64 |
| RF switches | 1.42 |
| Transmitters (2) | 15.60 |
| Command receivers and transponders (2) | 7.77 |
| Central command decoder | 5.73 |
| Central signal processor | 4.97 |
| Radar altimeter doppler velocity sensor | 34.07 |
| Signal data converter | 10.62 |
| Klystron power supply and modulator | 10.26 |
| Altitude/velocity sensor antenna | 6.12 |
| Velocity sensor antenna | 5.72 |
| Waveguide assembly | 1.35 |
| Boost-regulator | 8.22 |
| Engineering signal processor | 5.75 |
| Engineering mechanism auxiliary | 5.21 |
| Thermal control assembly | 0.24 |
| Altitude marking radar | 10.14 |
| Altitude marking radar insulation | 1.42 |
| Signal processing auxiliary | 0.31 |
| Battery charge regulator | 3.47 |
| Low dota rate auxiliary | 0.56 |
| Power switch | 1.00 |
| Buffer amplifiers | 0.18 |
| Diode assembly | 0.15 |
| Electrical power | 54.59 |
| Solar panel | 8.09 |
| Battery | 46.50 |
| Mechanisms | 38.06 |
| Antenna/solar panel positioner | 33.28 |
| Omniantenna booms (2) | 3.73 |
| Separotion sensor and arming devices (3) | 1.05 |
| Structure | 219.74 |
| Basic structure | 58.58 |
| Installation hardware | 20.27 |
| Thermal paint | 0.78 |
| Landing gear | 40.52 |
| Landing legs (3) | 37.32 |
| Leg release pinpullers (3) | 0.36 |
| Crushable blocks (3) | 2.66 |
| Kickout springs (3) | 0.18 |
| Thermal compartment A | 25.54 |
| Thermal compartment B | 17.66 |
| Basic spacecraft wire harness | 50.33 |
| Pneumatic lines | 1.00 |
| Main retro release mechanism | 2.43 |
| Engineering measurement sensor | 0.82 |
| Spacecraft to *Centaur* latch | 0.66 |
| Vernier engine thermal reflectors (2) | 0.88 |
| Heat shield | 0.27 |
| Propulsion subsystem | 223.92 |
| Vernier propulsion system | 76.34 |
| Helium check and relief valves (2) | 0.83 |
| Helium tank and valve | 29.68 |
| Fuel tanks (3) | 8.55 |
| Oxidizer tanks (3) | 8.55 |
| Thrust chamber assemblies (3) | 17.26 |
| Thermal control | 7.69 |
| Lines and miscellaneous fittings | 3.78 |
| Helium | 2.35 |
| Unusable propellant | 2.12 |
| Main retrorocket | 143.11 |
| Weight adjustment and ballast | 8.24 |
| Adjustment far actual weights | 1.82 |
| Ballast | 3.79 |
| Added to leg 2 pivot | 1.09 |
| Added to leg 3 pivot | 1.09 |
| Added to footpad 2 | 1.27 |
| Added to footpad 3 | 0.34 |
| Added to retrorocket struts | 2.63 |
| Buoyancy | 0.51 |
| Usable propellant | 1437.68 |
| Vernier propellant | 181.31 |
| Moin retrorocket propellant | 1251.37 |
| Payload | 65.19 |
| Survey television | 26.86 |
| Survey camera | 21.35 |
| Camera | 17.40 |
| Wire | 2.32 |
| Attaching hardware | 1.63 |
| TV auxiliary | 1.84 |
| TV targets (2) | 0.12 |
| Auxiliary TV mirror system | 3.55 |
| Added engineering instrumentation | 10.74 |
| Auxiliary engineering signal processor | 6.25 |
| Strain gages (6) and amplifier ossembly | 1.40 |
| Temperature sensors (10) | 0.22 |
| Current sensors (2) | 0.05 |
| Wire | 2.82 |
| Magnetic experiment—leg 2 | 0.15 |
| Alpha scattering experiment subsystem | 27.35 |
| Instrument | 8.98 |
| Sensor head assembly | 5.23 |
| Deployment mechanism | 3.55 |
| Standard sample | 0.20 |
| Compartment C | 12.08 |
| Compartment and structure | 5.79 |
| Electronics | 4.70 |

## Table XIII-4 (contd)

| Item | Weight, lb | Item | Weight, lb |
|---|---|---|---|
| Payload (contd) | | | |
| Auxiliary | 1.09 | Wire | 3.01 |
| Heater | 0.50 | Simulator | 0.40 |
| Installation hardware | 2.88 | Buoyancy | 0.09 |

## Table XIII-5. Flight spacecraft design changes and their effectivities

| Design change | Spacecraft effectivity | | | | | | |
|---|---|---|---|---|---|---|---|
| | SC-1 | -2 | -3 | -4 | -5 | -6 | -7 |
| Scientific instrument payload | | | | | | | |
| 1. Remove approach television camera | | | X | X | X | X | X |
| 2. Add soil mechanics/surface sampler | | | X | X | | | X |
| 3. Add two television viewing mirrors | | | X | X | X | X | X |
| 4. Add extension to television camera hood | | | X | X | X | | |
| 5. Add magnet control bar assembly to side of footpad 2 | | | | X | X | X | X |
| 6. Improve operation of television mirror's elevation and azimuth drive motors | | | | X | X | X | X |
| 7. Add alpha scattering instrument | | | | | X | X | X |
| 8. Add one television viewing mirror | | | | | | X | X |
| 9. Replace television color filters with polarization filters | | | | | | X | X |
| 10. Incorporate upgraded television camera with improved mirror hood assembly | | | | | | X | X |
| 11. Add photometric chart to the boom of omniantenna A | | | | | | | X |
| 12. Add magnet/control bar assembly to footpad 3 | | | | | | | X |
| 13. Add seven dust mirrors to spaceframe | | | | | | | X |
| 14. Add stereo viewing mirror to A/SPP[a] mast | | | | | | | X |
| 15. Add two horseshoe magnets to SM/SS scoop door | | | | | | | X |
| 16. Rotate SM/SS mounting to spaceframe by 30 deg | | | | | | | X |
| 17. Apply glare reducing black paint to TV mirror hood | | | | | | | X |
| 18. Add grasping knob to top of alpha scattering instrument sensor head | | | | | | | X |
| Structures and mechanisms | | | | | | | |
| 1. Incorporate improved pinpuller modules on A/SPP | | X | X | X | X | X | X |
| 2. Add kickout spring and otherwise modify omniantenna latch and release mechanisms | | X | X | X | X | X | X |
| 3. Replace A/SPP drive motor ball detents with roller detents | | X | X | X | X | X | X |
| 4. Add kickout springs to landing leg deployment mechanization | | | X | X | X | X | X |
| 5. Modify shock absorbers | | | X | X | X | X | X |
| 6. Incorporate improved landing gear locking squibs | | | X | X | X | X | X |
| 7. Add vent hole to A/SPP pinpuller modules | | | X | X | X | X | X |
| 8. Provide low-impedance ground path for landing leg locking squibs | | | X | X | X | X | X |
| 9. Strengthen A/SPP mechanism | | | | | X | X | X |
| 10. Incorporate new A/SPP drive motors | | | | | X | X | X |
| 11. Remove eight vibration accelerometers and amplifiers | | | | | X | X | X |
| 12. Modify main compartment shells for easy access | | | | | X | X | X |
| 13. Eliminate slippage in A/SPP potentiometer drives | | | | | | X | X |
| 14. Modify compartment B thermal blanket | | | | | | X | X |
| Telecammunicatians | | | | | | | |
| 1. Modify command assignments | | X | X | X | X | X | X |
| 2. Modify engineering signal process (including auxiliary) against solder splash | | X | X | X | X | X | X |
| 3. Add filter chokes to ESP,[b] AESP,[c] and CSP[d] | | X | X | X | X | X | X |
| 4. Add telemetry point: flight control return signal | | X | X | X | X | X | X |
| 5. Add two telemetry points; flight control unregulated current and SM/SS temperature | | | | X | X | X | X |

[a]Antenna solar panel positioner.
[b]Engineering signal processor.
[c]Auxiliary engineering signal processor.
[d]Control signal processor.

**Table XIII-5 (contd)**

| Design change | Spacecraft effectivity | | | | | | |
|---|---|---|---|---|---|---|---|
| | SC-1 | -2 | -3 | -4 | -5 | -6 | -7 |
| Telecommunicotions (contd) | | | | | | | |
| 6. Modify RF transfer switch ond associated microswitches | | | | X | X | X | X |
| 7. Modify data channel assignments | | | | X | X | X | X |
| 8. Increase low power output of transmitters | | | | | X | X | X |
| 9. Add telemetry transducers to fuel lines | | | | | X | X | X |
| 10. Reconfigure commutator modes | | | | | X | X | X |
| 11. Incorporate improved subcarrier oscillators | | | | | | X | X |
| Flight control | | | | | | | |
| 1. Modify Canopus window O-rings | | X | X | X | X | X | X |
| 2. Reduce the attitude loop gains of the $V_x$ and $V_y$ radar inputs | | X | X | X | X | X | X |
| 3. Reduce the filter factor of the Canopus sensor sun filter to 1.17 | | X | | | | | |
| 4. Reduce the filter factor of the Canapus sensor filter to 0.8 | | | X | X | X | X | X |
| 5. Remove Canopus window O-ring lubricant | | | X | X | X | X | X |
| 6. Increase capability for automatically timed midcourse burn time from 51 to 102 sec | | | | | X | X | X |
| Power | | | | | | | |
| 1. Disable overload trip circuit in boost regulator | X | | | | | | |
| 2. Reduce overload trip circuit susceptibility to transients | | X | X | X | X | X | X |
| 3. Add filter to flight control boost regulatar | | X | X | X | X | X | X |
| 4. Modify battery charge regulatar for lower A/SPP current pulse duration | | X | X | X | X | X | X |
| 5. Decrease voltage of optimum charge regulator trickle charge | | | | X | | | |
| 6. Increase efficiency of optimum charge regulator | | | | X | | | |
| 7. Replace optimum charge regulator with solar panel switch | | | | | X | X | X |
| 8. Redesign solar cell mounting and interconnectian scheme | | | | | X | X | X |
| 9. Remove auxiliary battery and battery control | | | | | X | X | X |
| Radar | | | | | | | |
| 1. Lower RADVS side-lobe rejection level | | X | X | X | X | X | X |
| 2. Limit $V_x$ and $V_y$ outputs with zener diodes | | | X | X | X | X | X |
| 3. Incorporate RADVS cross-coupled sidelobe logic for all radar beams | | | | X | X | X | X |
| 4. Modify RADVS to disable CCSLL at 1000 ft | | | | X | X | X | X |
| 5. Modify RADVS to delay the conditional reliable-operate logic disable signal until an an altitude of 1000 ft | | | | X | X | X | X |
| Thermal control | | | | | | | |
| 1. Alter thermal control paint pattern on auxiliary battery cover | | X | X | X | | | |
| 2. Set all thermal switches to open at 40 $\pm$5°F | | | X | X | X | X | X |
| 3. Incorporote specially processed thermal switch contacts | | | | X | X | X | X |
| 4. Set compartment A temperature control and heater assembly to 20°F | | | | | | | X |
| Propulsion | | | | | | | |
| 1. Incorporate higher specific-impulse retrorocket | | | X | X | | | X |
| 2. Relocate helium check and relief valve assembly | | | | | X | X | X |
| 3. Incorporate helium filters in vernier engine shutoff valves | | | | | | | X |
| Cabling | | | | | | | |
| 1. Modify squib firing harness and attoching hardware | | | X | X | X | X | X |
| 2. Pot connectors on RF cables | | | X | X | X | X | X |

The spacecraft functional configuration was altered as required during each mission for each of the following phases:

(1) Prelaunch phase. Prelaunch checkout and countdown.

(2) Launch phase. Power ascent through final *Centaur* burnout, preseparation events and injection (spacecraft separation) into lunar transfer trajectory.

(3) Postinjection attitude reference and DSIF acquisition phase. Included DSIF acquisition and celestial reference (sun and star) acquisition.

(4) Cruise phase one. The first coast period, ground tracking, orbit determination, and midcourse correction determination.

(5) Midcourse maneuver phase. Attitude maneuvers from celestial reference, firing of vernier engines

for midcourse velocity correction, and reacquisition of celestial references.

(6) Cruise phase two. The second coast period, ground tracking, and continued orbit determination.

(7) Preretromaneuver phase. Attitude maneuver from celestial reference to align retro thrust vector counter to the velocity vector.

(8) Retromaneuver phase. Deceleration along initial velocity vector until retrorocket burnout to remove most of spacecraft approach velocity.

(9) Terminal-descent phase. Radar-controlled descent under vernier thrust until preselected velocity and altitude (14 ft) were reached.

(10) Touchdown phase. Free fall from 14 ft to surface where touchdown loads were absorbed by the landing gear and crushable footpads.

(11) Postlanding phase. Spacecraft engineering assessment, orientation of the solar panel and the planar array antenna, and extended operations to perform engineering and scientific experiments on the lunar surface.

Because of the long duration of the transit phase and the small unavoidable drift error of gyros during cruise, celestial references were used to provide basic spatial references. Figure XIII-4 shows spacecraft coordinate axes relative to sun and star (Canopus) celestial references. The cone angle of the earth is the angle between the sun vector and the earth vector as seen from the spacecraft. The clock angle of the earth is measured in a plane perpendicular to the sun vector, from the projection of the Canopus vector to the projection of the earth vector in the plane. The spacecraft coordinate system was related to the cone and the clock-angle coordinate system after sun and Canopus lock-on had been achieved. The spacecraft minus Z-axis was directed toward the sun, and the minus $X$-axis was directed toward projection of the Canopus vector in a plane perpendicular to the Z-axis. The spacecraft $+Z$-axis was in the direction of the retrorocket exhaust, and leg 1 lay in the $Z$-$Y$ plane.

The sun was automatically acquired shortly after spacecraft separation from the launch vehicle. Sun acquisition was initiated with a spacecraft-commanded roll maneuver after a timed delay from separation. The roll maneuver was terminated and a yaw maneuver initiated automatically when the sun came into the 10-deg wide by 180-deg conical field of view of the automatic sun sensor. The yaw maneuver was terminated automatically when the narrow-view primary sun sensor acquired and locked-on the sun. Canopus acquisition was achieved a few hours after injection, following a roll command from earth.

Midcourse velocity-correction capability was required for the *Surveyor* spacecraft not only for correction of launch vehicle trajectory injection errors to improve spacecraft landing accuracy, but also to optimize several system terminal-descent and landing parameters to improve conditions needed for achieving a successful soft landing. The main parameters to be optimized were: (1) retrorocket burnout velocity, (2) vernier system propellant margin, and (3) landing time relative to the Goldstone tracking station view period.

To execute midcourse velocity correction, the spacecraft was accelerated constantly in the desired direction and for a precisely calculated time, by controlled thrusting of the vernier engines. Since the spacecraft (before midcourse correction) was locked on the sun and on Canopus in its cruise attitude, a series of spacecraft attitude rotations were commanded (using the gas jet system) before actual velocity could be corrected by vernier engine thrusting. In theory, the attitude rotations could have been performed in a number of ways; however, in practice only those spacecraft rotations that simultaneously satisfied several spacecraft subsystem (thermal, flight control, telecommunications, etc.) constraints, as well as the overall mission constraints of landing site and landing-site accuracy, were considered acceptable.

Upon initiation of earth command, the spacecraft executed the desired midcourse attitude maneuvers (roll, pitch, or yaw), which were accomplished serially by separate earth command sequences. The magnitude of the desired vernier thrust burning time for midcourse velocity correction was transmitted to the spacecraft, verified, and stored by the flight control. During the midcourse thrusting phase, the three vernier engines provided a constant spacecraft acceleration of about 0.1 earth $g$ until cutoff was commanded by flight control. The three vernier engines were differentially throttled, and one of the engines was gimballed by a roll actuator to achieve attitude stabilization under gyro control.

The typical sequence of terminal events is depicted in Fig. XIII-5. Approximately 30–40 min before touchdown, the terminal maneuvers were initiated by earth command to point the spacecraft thrust axis in a direction that was precalculated on earth to be nearly aligned with the velocity vector at the time of retrorocket ignition.

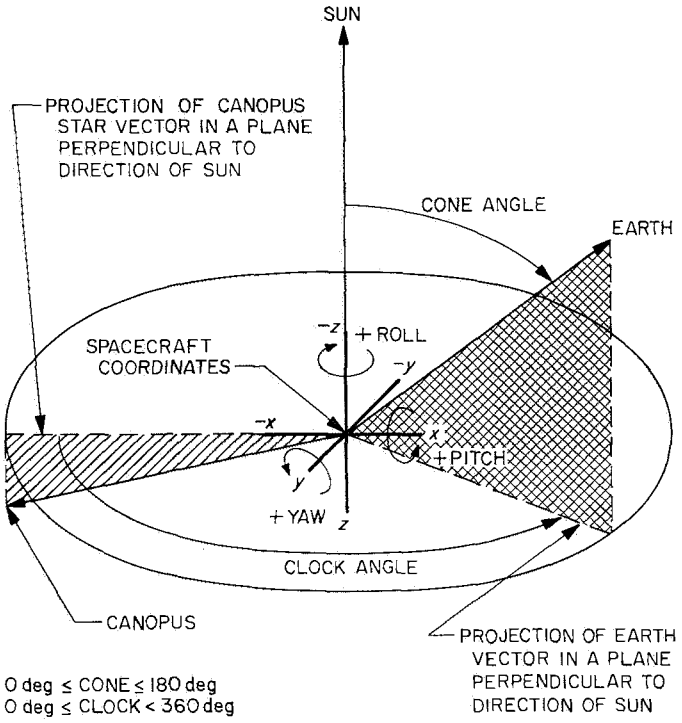



**Fig. XIII-4. Spacecraft coordinates relative to celestial references**

When the slant range to the lunar surface reached a preset value (about 60 statute mi), the pulse-type AMR generated a marking signal. After a suitable time delay, which was precomputed on earth and preset into the spacecraft flight control subsystem by command, the liquid-propellant vernier engines and the solid-propellant retro motor were ignited.

During retro-motor burning, the inertial attitude of the vehicle was maintained constant by differential throttling of vernier engines and control of the vernier engine roll actuator. The retrorocket burned at a thrust level of 8,000–10,000 lb for about 40 sec. Retrorocket burnout was detected by an acceleration switch which initiated a time delay of about 12 sec for thrust tailoff, after which the empty retrorocket case was jettisoned.

During the vernier descent phase, which began after retrorocket burnout and separation of retrorocket case, the vernier engines were controlled according to on-board sensors. Vernier descent phase information, which is helpful in understanding subsequent discussion, is depicted in Fig. XIII-6.

Shortly after separation of the retro-motor case, the vernier thrust was reduced so that the spacecraft would

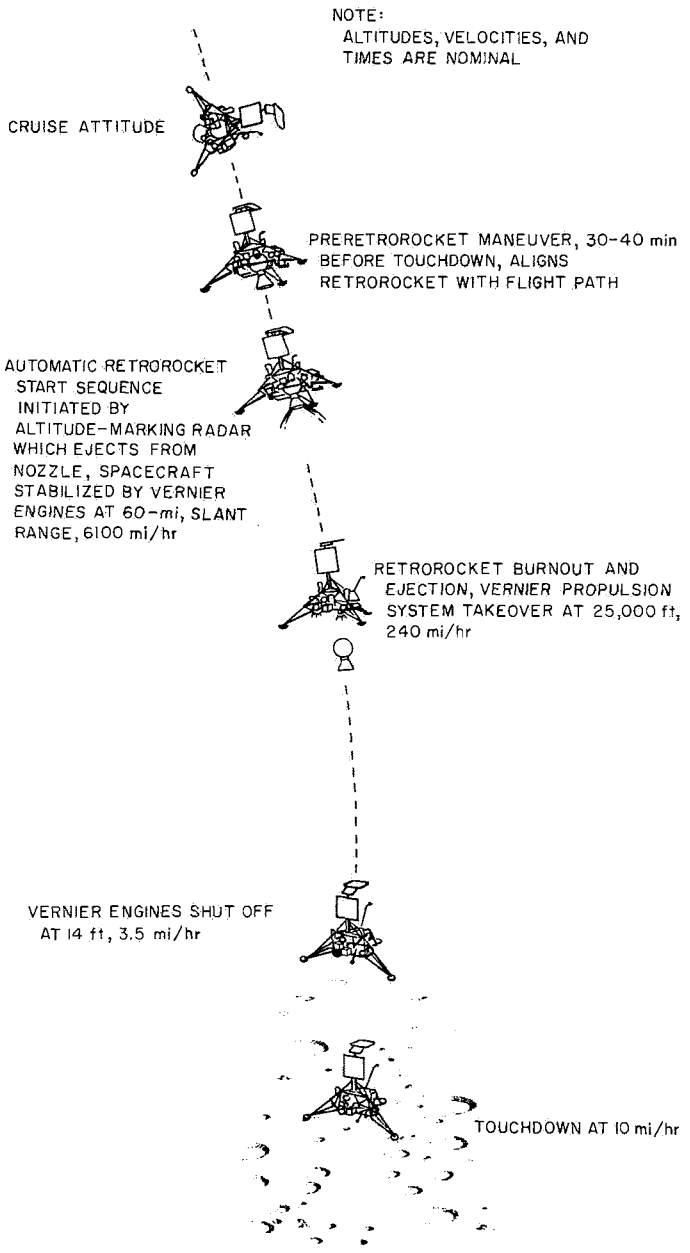



**Fig. XIII-5. Normal sequence of terminal-descent events**

descend with an acceleration of approximately 0.1 lunar *g*, as controlled by an axially oriented accelerometer, until the programmed descent contour (Fig. XIII-6) was reached. The spacecraft attitude was maintained in the retro-ignition position until the velocity radar locked on to the lunar surface. The thrust axis was then aligned automatically with the velocity vector and maintained throughout the remaining descent.

Continuous range and velocity information was provided by an on-board 4-beam RADVS as depicted in

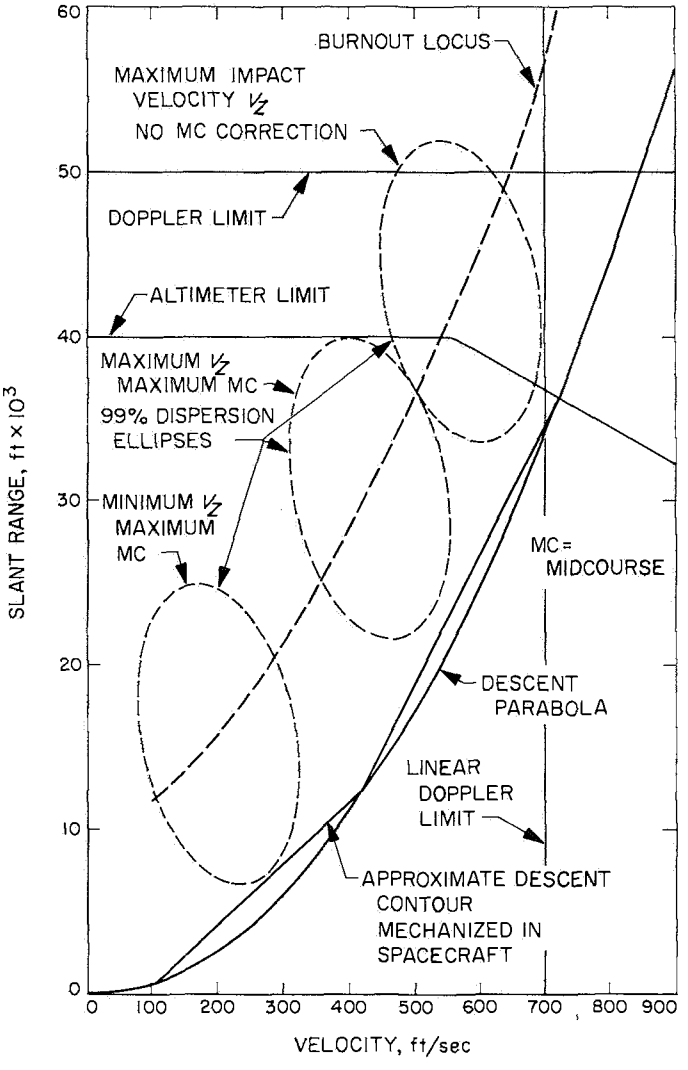



**Fig. XIII-6. Terminal-descent range-velocity diagram**

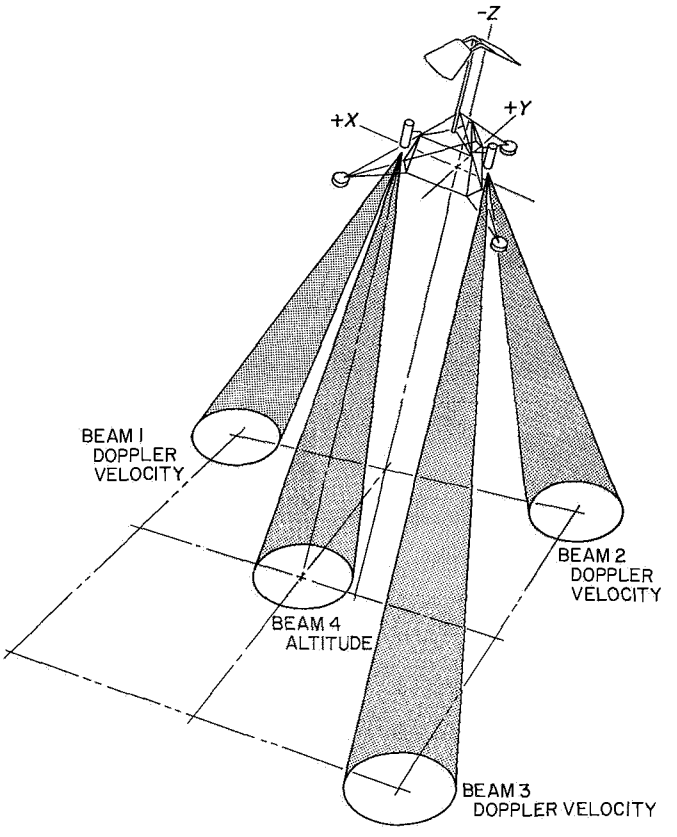



**Fig. XIII-7. Radar altimeter and doppler velocity sensor beam orientation**

Fig. XIII-7. The RADVS functioned in the flight control subsystem to provide three-axis velocity, range, and altitude signals for flight control during the vernier phase of the terminal descent. The RADVS consisted of a doppler velocity sensor, which employed three beams for computation of velocity along the spacecraft *X*, *Y*, and *Z* axes, and a radar altimeter using a single beam from which range data were obtained.

When the descent contour was reached, thrust level was commanded so that the spacecraft followed the descent contour until shortly before touchdown, when the final sequence was initiated. The descent contour was a straight line approximation to a parabola which corresponded, in the vertical case, to a descent at constant acceleration based on maximum thrust capability of the vernier engines.

The final phase of descent consisted of a constant-velocity descent from about 40 to 14 ft at 5 ft/sec, with the spacecraft attitude held inertially fixed. Vernier engines were cut off at the 14-ft mark, followed by a free fall to the lunar surface, and touchdown at approximately 13 ft/sec. The horizontal component of the landing velocity was essentially zero; however, the capability of withstanding small dispersions in lateral velocity without toppling was an essential requirement in the vehicle landing gear design.

The initial period after landing was utilized to turn off all terminal-descent-phase subsystems and functions not required during lunar operations. High electrical power dissipation within the thermally controlled compartments during a normal landing required immediate turnoff, particularly when the landing occurred under near-lunar-noon conditions. Engineering data transmission to verify the spacecraft response to turnoff commands was acquired by means of omniantennas, with the spacecraft transmitter in the high-power mode. Functions turned off included RADVS, flight control, temperature control, vernier line

fuel and oxidizer tank thermal control, and landing instrumentation electronics. Commands were then transmitted from earth to lock the landing gear and dump helium unless subsequent vernier engine firings were anticipated or under consideration. In a typical case, these operations were completed within 2 min.

Assessment of spacecraft survival of the landing shock was conducted to acquire reliability, design, and subsystem operating data for postlanding operational planning. Engineering assessment included verification of such functions as operation of the second transmitter, signal processing, planar array and solar panel positioning, solar panel output power, spacecraft temperatures, and the condition and response of the thermal control and electrical power systems.

The extent of the postlanding assessment of the spacecraft was dependent on solar lighting conditions, Goldstone visibility time remaining after touchdown, and payload operational requirements. For example, a night landing would have precluded the solar panel assessment as well as that of the survey television. Also, a noon landing might have reduced the extent of assessment possible by restricting the time available for continuous operation because of the high spacecraft temperatures that would be expected at that time. Finally, if touchdown occurred with a minimum of 3 hr of Goldstone visibility remaining, an evaluation of the relative importance of spacecraft assessment as opposed to the acquisition of initial scientific data by Goldstone, would have been desirable for optimum allocation of available time.

Postlanding positioning of the solar panel and planar array antenna was accomplished shortly after touchdown. Positioning was required to assure the necessary telecommunication bandwidth for television transmissions and for generation of solar energy for operations and battery charging. The procedures utilized and time required for initial positioning depended on lunar environmental conditions and on the thermally controlled compartment temperatures existing at touchdown. The solar panel was positioned by means of earth command in response to telemetered secondary sun-sensor output signals. Acquisition of the earth with the high-gain antenna was accomplished by conducting a search pattern with the planar array until the spacecraft signal received at the earth-monitoring point was maximized.

After initial positioning and at periodic intervals, the solar panel was repositioned to follow the changing solar incidence angle and the planar array and was positioned to correct for pointing errors resulting from lunar libration. To obtain optimum video signal-to-noise ratio, it was desirable to position the antenna approximately once per earth day at specific times, such as immediately before television operation.

Knowing the landing site lunar coordinates, the spacecraft attitude was determined from the position of two celestial bodies (sun and earth) given in spacecraft coordinates. The spacecraft provided sun and earth positions in spacecraft coordinates from the solar panel and planar array positions. Also, star positions from survey television frames, together with their corresponding mirror positions, were used to refine the spacecraft attitude determination.

The thermally controlled compartment heat-dissipating capability varied as a function of compartment environment. Electronics within the thermally controlled compartment were operated solely to maintain maximum thermal tray temperature below 125°F. The heat-dissipating capability of each compartment as a function of solar angle and percent of shading by other spacecraft elements is shown in Fig. XIII-8. The corresponding operational capability, in terms of duty-cycle or fraction of the time that typical operations were possible within the temperature constraints imposed by the thermally controlled compartments, is shown in Fig. XIII-9. (The conditions assumed in Fig. XIII-9 are compartments fully illuminated and total shutdown during "off" periods.)

Spacecraft thermally controlled compartment capability was a function of radiator view factor, lunar surface intrusion into the field of view due to spacecraft tilt or surface irregularities, solar loads, and solar panel and planar array reradiation of heat to the compartments. Compartment heat-dissipation capability and television camera temperature control were improved during the lunar noon interval by using the solar panel or planar array for shading these units. The main compartments were so designed that heat losses during the lunar night would not exceed 12 $\pm 3$°F for compartment A and 9 $\pm 3$°F for compartment B, with all switches open and the internal temperature maintained at 10°F.

Spacecraft postsunset operation was extended by using battery energy primarily to maintain thermally controlled compartments above the lower operating temperature limits. As shown in Fig. XIII-10, the time required to achieve a full battery charge before sunset, to permit postsunset operation of 150 hr was a function of battery charge at touchdown and charging rate. Spacecraft operational

and survival temperature limits are presented in Table XV-12. Lunar operational limits were defined as those temperature boundaries within which a unit had to be maintained in order for the unit to perform its normal function within specification. If the operational limit were exceeded, the unit would continue to function but not necessarily within its specified performance requirements. The unit, however, would not sustain permanent damage. Lunar operating survival temperature limits were defined as temperatures to which a unit could be exposed but at which operating performance or reliability might be degraded. The unit could sustain permanent damage if its survival temperature limits were exceeded.

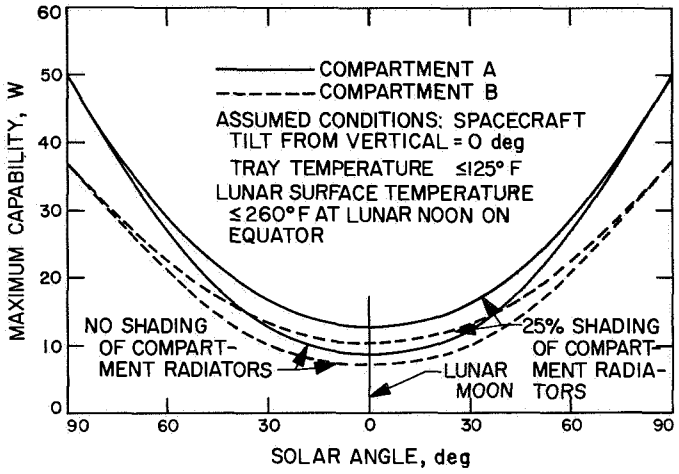



**Fig. XIII-8. Thermal dissipating capability of main compartments on lunar surface**

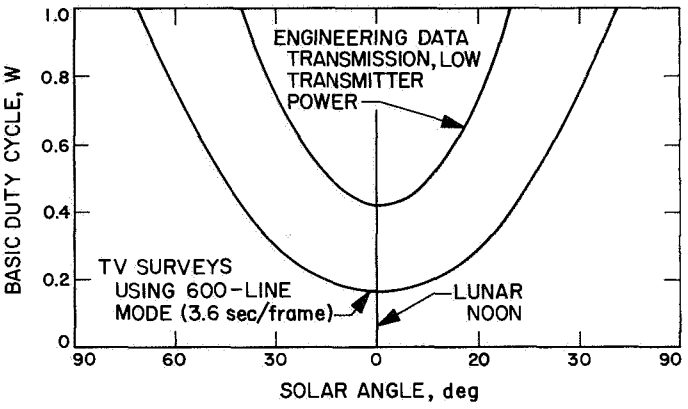



**Fig. XIII-9. Typical duty cycle capability of spacecraft on lunar surface**

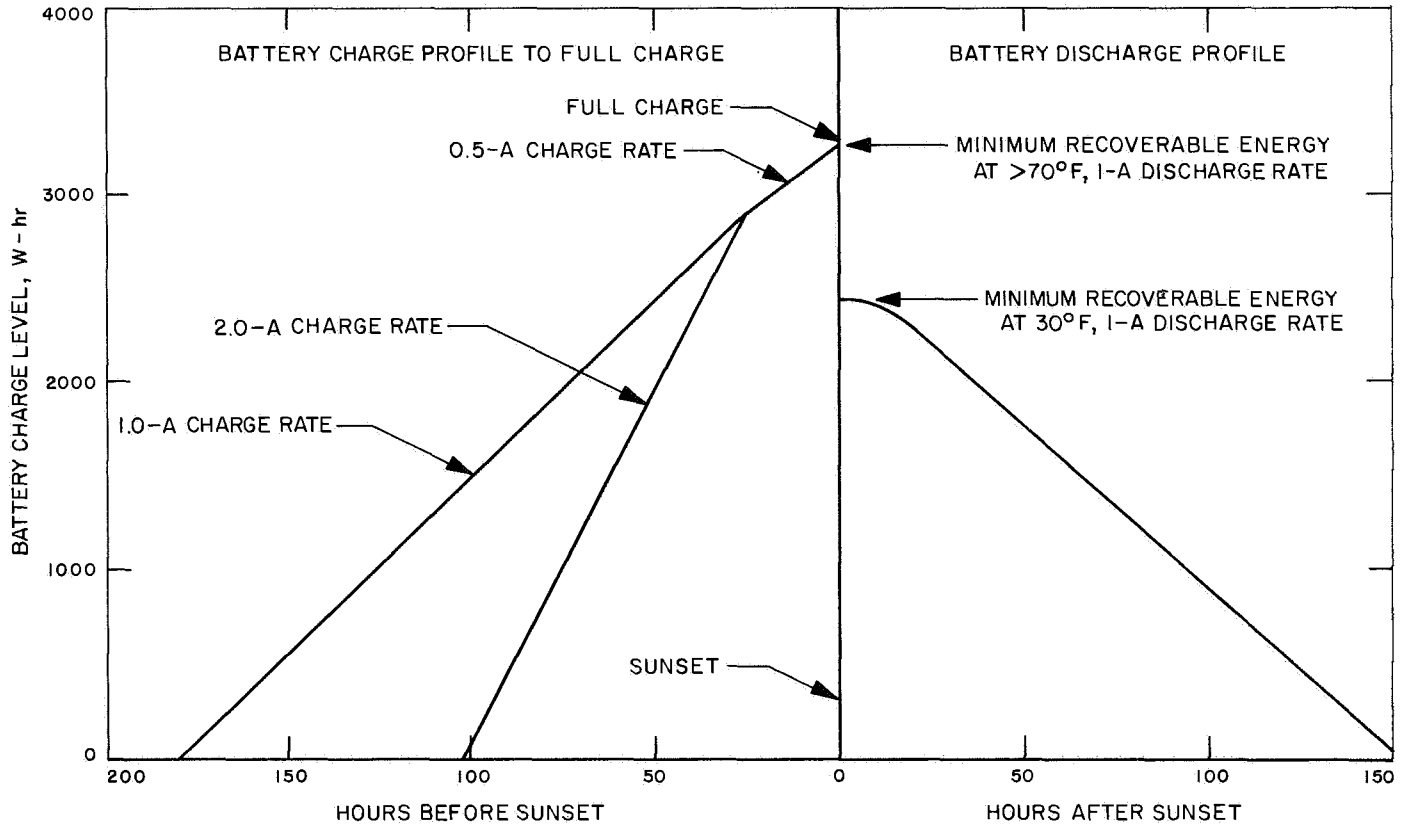



**Fig. XIII-10. Battery charge and discharge profile for extended operation after sunset**

## C. Spacecraft System Design Development

The following discussion includes main considerations and constraints pertinent to spacecraft system design and historical evolution of system design (Ref. XIII-1). Considerations related primarily to single subsystems are discussed in more detail within subsystem Sections XIV–XXII.

### 1. Spacecraft Configuration and Payload Weight Evolution Before the First *Surveyor* Mission

During spacecraft design and development, a number of different basic bus and payload configurations were considered as the result of changing constraints and differing specific mission objectives. Table XIII-6 indicates the evolution of several main spacecraft and payload configurations, together with associated hardware system weight limits (also refer to Fig. VIII-1). Scientific instrument payload evolution is shown in Section XXII-A.

The initially conceived spacecraft, which was designed to carry a minimum payload weight of 345 lb, was developed in accordance with a specified allowable 2500-lb injected weight established by assessed capability of the *Centaur* launch vehicle. This design was designated A-25. When later assessment of *Centaur* payload capability indicated that reduction in spacecraft weight to about 2100 lb was necessary, the spacecraft design was reevaluated for possible accommodation of a lighter payload.

Results of early analyses indicated that a 2100-lb spacecraft and payload design was feasible and could be achieved by making the following changes to the A-25 design:

(1) Removal of one of the two 45-lb batteries and the associated power management circuitry.

**Table XIII-6. Contractually defined spacecraft/payload configurations prior to *Surveyor* missions**

| Date | Configuration | JPL contract 950056 reference document | Allowable spacecraft injected weight, lb | Payload weight, lb |
|---|---|---|---|---|
| Sep 1961 | A-25 | Modification 6 | 2500 | 345 |
| Apr 1962 | A-21 | Modification 8 | 2100 | 115 |
| Apr 1962 | A-25 | Modification 8 | 2500 | 266 |
| Jan 1963 | A-21 | Modification 15 | 2100 | 114 |
| Apr 1963 | A-21 | Change order 18 | 2100 | 108 |
| Jun 1964 | A-21 | Modification 28 | 2150 | 62.5 |
| May 1965 | A-21A | Modification 43 | 2450 | 114 |
| Nov 1965 | A-21 | Change order 101 | 2250 | 62 |

(2) Removal of certain scientific instrument auxiliaries and an associated thermal compartment.

(3) Elimination of separate preseparation arming device by redesigning the engineering mechanics auxiliary unit.

(4) Reduction of retro motor solid propellant.

(5) Reduction of vernier engine propellant.

(6) Decrease of crushable footpad size.

(7) Reducing of scientific instrument weight.

(8) Modification of flight control subsystem and landing gear shock absorbers to account for the moment of inertia and landing weight changes, respectively.

Several lightweight spacecraft designs evolved for different estimated payload weights. The main effect of redesign was a more limited postlanding operational phase since less scientific data would be obtained due to payload reduction, and lunar night operating capability would be degraded due to removal of one of the two batteries.

Modification to the contract in 1962 established that the first five spacecraft be designed for 2100 lb (designated the A-21 design) and the last two for 2500 lb, in the hope that toward the end of the program the launch capability for the 2500-lb design could be realized. When it became apparent that a 2500-lb spacecraft could not be launched, effort was centered on the A-21 design with a reduced scientific payload.

Subsequently, two A-21 design configurations were established, each with the same basic bus but differing by the payloads they were to carry. The first four spacecraft were to carry engineering payloads, whereas the last three were to carry scientific payloads. The first four spacecraft (A-21) were to demonstrate the feasibility of a soft landing, whereas the last three (A-21A) were to carry specialized instruments for obtaining scientific data. The engineering payload included in the design of the first four spacecraft weighed 96 lb and included an auxiliary battery with associated controls, additional signal processing capability, four accelerometers, vernier engine and landing gear strain gages, and additional thermal, current, and position sensors. In 1965, the allowable spacecraft weight was increased. The first four spacecraft were to weigh 2250 lb and carry 62-lb payloads. The last three spacecraft were to weigh 2450 lb and carry

114-lb payloads (including a touchdown dynamics experiment). Significant changes to the A-21A spacecraft involved:

(1) Modification of spacecraft structural design to accommodate up to 2500 lb.

(2) Increased vernier propellant loading and flight control modifications to provide a 50-m/sec midcourse correction capability (instead of 30 m/sec) for a spacecraft weighing up to 2500 lb.

(3) Increased main retro propellant loading to accommodate a spacecraft weight of up to 2500 lb.

(4) Capability of transmitting engineering data and television pictures simultaneously.

(5) Current limiting capability in all scientific instrument auxiliaries.

In April 1966 the 2450-lb design effort (A-21A) was discontinued.

The final major changes resulted from the success of *Surveyor I* and were directed primarily toward providing scientific instruments on the remaining flight spacecraft as soon as possible.

The final major changes were made after the *Surveyor I* launch.

### 2. Command Link Considerations

A significant design philosophy established for the spacecraft and the mission operation sequence is the concept of placing major emphasis on the use of the earth-to-spacecraft command link for initiation and control of spacecraft operations. Inherent in this philosophy was the provision of a large number of earth commands and maximum utilization of sequences controlled from the SFOF, with a performance evaluation team assessing the spacecraft status and controlling the transmission of each command in real-time in accordance with the desired mission sequence and the assessed condition of the spacecraft.

Several automatically initiated and/or automatically controlled sequences incorporated in the spacecraft design were provided only when it was judged critical to mission success and when one of the following requirements existed:

(1) Rapid execution of a series of commands for which individual confirmation could not be achieved for each command prior to the required execution of a following command (the terminal descent sequence).

(2) Absolute timing accuracy was required for properly initiating a sequence (e.g., ignition of the vernier engines and retrorocket during terminal descent).

(3) Execution during a period of the mission when the existence of an earth-to-spacecraft command link could not be assured (spacecraft and *Centaur* preseparation sequences for extending the landing gear, deploying omnidirectional antennas, and turning on transmitter high power; or the postseparation sequences for achieving sun acquisition and deploying the A/SPP to the required transit position).

It is interesting to contrast the *Surveyor* philosophy with that used on *Ranger*, the predecessor of *Surveyor* in the lunar exploration program. The *Ranger* design emphasized the use of a relatively sophisticated on-board command computer and sequencer with minimum commands initiated from earth (fewer than 10, as compared with the more than 200 available for *Surveyor*) and with a spacecraft capability of storing many earth-commanded magnitudes (as opposed to the *Surveyor* design, which permitted only one earth-commanded magnitude to be stored at any time). Factors influencing the decision to implement the *Surveyor* concept included:

(1) Preliminary evaluation of mission sequence requirements, which indicated that the earth-controlled command concept was technically feasible for executing most spacecraft command sequences. This concept was based primarily on the fact that for most operations, high command rates were not required and the RF transit time would not provide significant communication delay in comparison with required execution times.

(2) Basic complexity of the *Surveyor* mission as originally conceived and the consequent large variety of scientific instruments which were expected to be controlled.

(3) A desire to provide maximum flexibility to accommodate changes in command and control requirements of the spacecraft subsystems and scientific instrumentation during hardware and program development, without requiring a complex and continually changing spacecraft command programmer and sequencer. Simplicity of spacecraft

design was retained in favor of increasing, if necessary, complexity of ground equipment.

(4) A recognized requirement that an effective earth-controlled command link would have to be developed under any spacecraft design and operational philosophy adopted. Even if extensive on-board sequencing and programming equipment were used, an effective earth-controlled command link would be necessary to provide for an emergency inflight backup capability.

In the interest of limiting the number of on-board automatically sequenced spacecraft operations to keep the spacecraft design as flexible, simple, and lightweight as possible, the initial design did not include circuitry for automatic initial sun acquisition and solar panel deployment. The original plan for achieving sun lock-on was by earth command, using information from the secondary sun sensor mounted on the active face of the solar panel, and the primary sun sensor located on the top of the flight control sensor group. This plan required that the sun acquisition sequence be initiated following completion of initial telemetry and command-links (two-way) acquisition by the DSIF ground station. The solar panel was positioned incrementally by successive earth commands.

Completion of the solar panel positioning sequence resulted in deployment of the solar panel to the transit position, which was required to place the secondary sun sensor in the proper position to achieve sun acquisition. Such a plan appeared reasonable for a standard mission in which initial DSIF station acquisition was assumed to be completed within 5 min after the spacecraft became visible to the station.

In 1962, the sequence for initial acquisition of spacecraft by the DSIF was investigated. Results indicated that 1 hr should be allowed for completion of the initial DSIF station acquisition, if 99% of all possible launch dispersions were considered. A delayed DSIF acquisition would

(1) Delay sun acquisition, which would delay battery charging by the solar panel and delay achievement of proper spacecraft attitude for thermal control.

(2) Delay reconfiguration of the spacecraft from the high-power transmitting mode to the low-power mode which, due to the thermal design, could cause excessive internal heating in compartment A.

The delay of spacecraft thermal control was the most severe effect of a delayed DSIF acquisition, since temperatures of one or more units could drop below their operational or survival limits. For a condition of 100% shading, it was estimated that the following units would fall below specified survival limits in the times indicated:

| Unit | Survival limit, min after liftoff |
|---|---|
| Vernier engines and propellant lines | 60 |
| Solar panel and secondary sun sensor | 72 |
| Shock absorbers | 87 |

Assuming that 60 min were required to complete the DSIF two-way acquisition, approximately 10 min were required for stepping the A/SPP axes to place the solar panel in the required transit position, and up to 18 min were required for performing the spacecraft attitude maneuvers to accomplish sun lock-on, sun acquisition could not be assured until approximately 88 min after liftoff. It was apparent that the success of the mission could be jeopardized by following the initial plan. Also, the large number of incremental movement commands (1160) that had to be transmitted to the spacecraft and executed properly to deploy the solar panel to the transit position was of concern. From the battery-charging consideration, it was desirable to have the sun acquisition sequence automatic and independent of DSIF acquisition.

It was established that the timely achievement of sun acquisition was crucial to mission success, and that the probability of mission success would be significantly increased by providing a method for sun acquisition that was independent of DSIF acquisition. On this basis, necessary spacecraft changes were incorporated to:

(1) Provide on-board automatically sequenced operations for sun acquisition following *Centaur* and spacecraft separation.

(2) Provide a new acquisition sun sensor, mounted on the flight control sensor group, to allow sun acquisition to be accomplished independent of solar panel deployment.

Although sun acquisition was made independent of the deployment of the solar panel, proper orientation of the panel was still required to ensure that proper solar energy would be converted to required electrical power as soon as possible and that the proper spacecraft shading pattern provided by the panel would be established

quickly. Therefore, circuitry was also added to provide automatic solar panel deployment capability. Incorporating an automatic deployment capability ensured that deployment would be accomplished as early as possible.

It should be noted that providing the automatic onboard sequencing circuitry for both sun acquisition and solar panel deployment enhanced the overall reliability of the spacecraft since there were two paths by which these operations could be achieved: either by means of the automatic sequencing circuitry or by the earth-to-spacecraft command link, once it was established.

Early command link calculations indicated that, even at lunar distances, a relatively strong signal strength would be available, and it also appeared that the maximum command transmission rate could be a modest two commands per second. Consequently, it was determined that there was no need for developing a relatively complex sophisticated coding scheme for increasing the command transmission rate for the available signal-to-noise ratio.

Selection of a command word structure with 4 bits for word synchronization, 10 information bits (5 for address and 5 for instruction), and 10 redundant bits for complement checking each of the information bits resulted from a desire to provide a conservative (from the standpoint of error detection), easy-to-implement design. Manchester coding was selected for the 10 information bits and the 10 redundant complementary bits. This enhanced the capability of spacecraft receivers to achieve bit synchronization by ensuring that one change of state would occur every bit time.

In addition to one central decoder and four subsystem decoders installed in a central command decoder unit, the spacecraft command link design provided for four more individual subsystem decoders for the scientific experiments and for the flight control subsystem, vehicle mechanisms, and television spacecraft subsystems.

In view of the complexity and large number of individual components required to operate simultaneously in a completely autonomous central command decoder capable of checking all commands arriving at the spacecraft and initiating the operation of all subsystems and experiments, a simpler spacecraft design could be developed by using a relatively simple central command decoder for checking and routing commands, and separate subsystem and experiment decoders for developing outputs required to execute commands. This design improved overall reliability by isolating experiment decoder failures to individual experiments (thereby providing minor degradation in the event of a single experiment decoder malfunction) and resulted in greater system flexibility and simplification of cabling problems within the spacecraft.

Although it was originally planned during the initial design to provide a separate decoder for each subsystem, the decision regarding which of the subsystems should have their own decoders was finally based on the number of commands used by the subsystem. Since 14 wires from the central command decoder to any subsystem decoder were required for routing the command address and instruction bits and associated enabling and timing synchronization bits, any subsystem had to have at least 14 associated commands to have its own decoder. Subsystems for which individual decoders were provided were flight control, mechanisms, and television, as well as each scientific experiment. All other commands, for subsystems not requiring at least 14 commands, were provided for in four subsystem decoders installed in the central command decoder unit.

### 3. Electromagnetic Interference Considerations

The spacecraft system was designed to ensure internal compatibility of the spacecraft with the electromagnetic interference (EMI) environment generated by the *Atlas* and *Centaur* and that which existed at the launch pad and other areas of AFETR.

Initial system design concepts included a complex 24-bit command code requiring a complement check of the command structure to minimize false triggering of commands by noise pulses, and use of a zener diode blocking technique to effectively block residual noise levels from activating the final command switching circuits.

Design concepts also included the requirement for an adequate margin (generally 6 db for low-frequency circuits and greater for high-frequency circuits) between noise-source output levels and circuit immunity levels. For this purpose, all internal and external noise sources were treated as transmitters and all susceptible circuits were treated as receptors, with appropriate coupling factors applied.

The EMI requirements were established as design guidelines for the A-21 program, to be followed as firm design requirements for the A-21A program. Hardware development had, in some cases, progressed beyond the

breadboard stage by the time EMI requirements were specifically defined. This posed a problem in achieving effective implementation without substantial impact on the program. The most significant areas of tradeoff were related to spacecraft weight limitations and the thermal control techniques utilized. As a result, for instance, overall application of EMI filtering techniques to each functional unit was not possible because of weight and volume requirements; however, studies were made to determine mission-critical functions on a system basis, and these functions were rendered immune to the anticipated EMI environment. Those functions not considered mission-critical were not corrected to the point of complete immunity if the weight penalty was excessive and the resulting functional characteristics were tolerable.

A typical condition considered critical, and therefore corrected by design modification, was the tendency of silicon controlled rectifier (SCR) switches to gate on relatively short-duration, low-level transients. This could result in the firing of critical squibs and loss of the mission. This intolerable situation was prevented by inclusion of adequate filtering.

On the other hand, an example of a noncritical function that was accepted rather than pay the necessary weight penalty for correction, was that of the compartment heater circuits. These circuits were susceptible to inadvertent turnon by negative noise transients. Since the thermostats were normally open during periods when it was desirable to leave the heaters off, it was decided that even if the circuits were triggered on during a period when the thermostats were closed, it would be simple to program a series of heater-off commonds for automatic transmission, ensuring that the heaters would not stay on during these periods.

Thermal control design techniques generally dictated that all compartments be thermally isolated from the spaceframe. This implied electrical isolation as well, which was undesirable from the EMI viewpoint, from considerations of electrostatic charge accumulation and range safety for electroexplosive devices. The large quantities of aluminized Teflon used on the spacecraft for thermal control were subject to high electrostatic charge accumulation.

It became necessary to minimize this charge accumulation, to provide electrical bonding of compartments and maintain low thermal conductivity in the process. Charge accumulation was minimized by sewing geometrical patterns on the Teflon insulation with fine stainless steel wire and bonding the wire to the spaceframe. Compartments and components were bonded to the spaceframe by paths of small cross section, minimizing thermal transfer.

As a result of rapid progress in hardware development, a philosophy was adopted early to provide for careful study and evaluation of possible problem areas to identify critical characteristics, determine tradeoffs, and correct the subsystems, where possible, before system assembly and test phases were reached. Several comprehensive studies were performed that pointed up potential problems, which were then attacked individually. Some of these studies were:

(1) Silicon controlled rectifier study. To determine whether there were any unusual sensitivities to transient spikes, thermal changes, or tolerance variations in components, all SCR circuits were investigated, identified, and tabulated, along with their circuit classification and function. The possible effects on the mission of inadvertent gating were identified, evaluated, and classified as to significance. This study also considered the effects of solar radiation on the stability of SCR characteristics and the associated SCR driving circuits. As a result of this study, several changes were made to desensitize and stabilize critical SCR circuits. The study showed that the effects of solar radiation on solid-state devices would not be a problem on *Surveyor* missions. The SCR types selected for *Surveyor* were found to be stable and reliable devices for their chosen applications.

(2) Noise transient study. An additional study of the susceptibility of circuits other than SCRs to noise transients was also conducted. For this study, a transient spike of 50-V peak amplitude and 10-$\mu$sec duration was postulated, based on earlier investigations of electrostatic phenomena. There were several cases of digital circuit sensitivity to the model noise transient, particularly in command circuits. These cases were reviewed and classified as to criticality; and after further investigation of the exact triggering levels of the suspect circuitry, design changes were recommended and incorporated to desensitize those circuits considered mission-critical.

(3) Harness shielding study. One of the problems posed to the spacecraft design resulted from restrictions imposed on cable harness shielding due to weight limitations. Proposed shielding for the spacecraft cabling would have added 9 lb, an unacceptable amount. Therefore, a study was made to determine

the possible shielding effectiveness of aluminized Teflon wrap used for thermal control on the harnesses. This study showed that, when properly applied and grounded, the aluminized wrap would provide greater than 40-db attenuation to high-frequency signals; the required shielding of individual wires was drastically reduced and the wrap was utilized for both shielding and thermal protection.

(4) Electrostatic investigation. Because of significant failure on the T-2 controlled-descent test program, probable electrostatic charge accumulation and discharge was postulated. It was theorized, and subsequently demonstrated possible, that an electrical charge had accumulated and subsequently discharged in a manner which caused accidental firing of one or more squibs, resulting in a hard drop of the early T-2 vehicle. Review of the T-21 design indicated that such a condition might occur on flight vehicles; therefore, an extensive study and test program was undertaken to determine the possible mechanisms of charge accumulation and release and the consequences.

#### 4. Midcourse Correction Considerations

The spacecraft's midcourse correction capability was designed to accomplish landing accuracy at selected landing sites and to satisfy specific system terminal descent parameters and conditions required for soft landing (Refs. XIII-2 through XIII-4). Inclusion of soft-landing constraints resulted in a relatively complex midcourse maneuver analysis as compared with the midcourse maneuver analyses required for previous *Ranger* and *Mariner* systems.

Proper selection of midcourse and terminal guidance maneuvers required consideration of various trajectory, spacecraft hardware, and operational constraints. Rough values and/or ranges could be assigned to particular system parameters, but the actual values and/or ranges (or limits) were subject to much speculation and would be influenced by particular flight circumstances. To serve as guidelines for spacecraft design and midcourse maneuver analysis (overall mission design and analysis of the midcourse maneuver is discussed in Section VI-F-3), the following constraints were identified and established:

(1) Normally, one midcourse correction would be performed at least 4.5 hr after the first Goldstone rise (approximately 15–20 hr after injection). The Goldstone tracking facility was desired for commanding at midcourse time, because of operational reliability and adequate accumulation of tracking data, to ensure orbit determination accuracy.

(2) Various thermal constraints would be satisfied at the time a midcourse maneuver was made. These constraints were concerned with various spacecraft subsystems being within the allowable operating temperature ranges for the duration of the nominal maneuver sequence. During the flight, this information would be provided by the spacecraft performance analysis and command (SPAC) group on the basis of real-time telemetry and thermal predictions.

(3) The preferred midcourse attitude maneuver would usually consist of two rotations: roll, then yaw. This combination would give the best control system accuracy. Also, thermal considerations indicated that an initial roll was highly desirable.

(4) Ideally, one of the spacecraft omniantenna should be used continuously during the maneuver to ensure minimum loss of telemetry and two-way doppler data. If antenna switching of the omniantenna would be required due to specific geometric and flight conditions, then switching between, rather than during, rotations would be preferred.

(5) The spacecraft could be at random attitudes with respect to the sun for up to ½ hr after separation from the *Centaur*, after which the vernier propulsion system temperatures could be outside the established engine operating and survival ranges.

(6) For radio communications capability lunar touchdown would take place 80 min after Goldstone rise and 3 hr before Goldstone set. Rise and set were defined as a 5-deg elevation angle at DSS 11.

(7) The spacecraft would remain in the lunar shadow no longer than ½ hr before touchdown.

(8) It would be desirable to perform the terminal attitude maneuver with two rotations, but three might be required to achieve the optimal tradeoff of mission-sequence capabilities, including those involving communications (omnidirectional antenna), operations, RADVS, TV, reliability, burnout conditions, and postlanding operation aspects.

(9) The off-vertical angle at which the spacecraft approached the lunar surface, before retrorocket ignition (called the *unbraked impact angle* in *Surveyor* trajectory analyses), would not be greater than the off-vertical landing capability (45 deg) of the spacecraft.

(10) The vernier propellant remaining in the tanks after midcourse correction would be sufficient to allow thrusting during terminal descent from vernier engine ignition to cutoff, a few feet above the lunar surface.

(11) Retrorocket burnout velocity would be within the maximum and minimum values of 550 and 280 ft/sec.

The upper limit was imposed by the altimeter limit in conjunction with the ability of the vernier engines to slow the vehicle velocity to a soft landing, the lower limit by doppler radar considerations. The lower limit varied as a function of unbraked impact angle and spacecraft roll attitude.

A perfect midcourse velocity correction would result in an accurate landing location and in terminal parameters as predicted by midcourse guidance evaluation. However, uncertainties resulting from two primary error sources were always associated with these parameters: orbit determination and mechanization (control and propulsion system uncertainties). Individual contributors and associated errors derived from hardware test data, and applicable to the midcourse velocity correction magnitude error, are shown in Table XIII-7. Table XIII-8 shows the 13 main contributors and errors to the spacecraft pointing error. An error analysis model, which assumed a spherical distribution of the execution errors, was used to map the effect of the errors onto the lunar surface.

### 5. Terminal Descent Considerations

Design of the terminal descent was strongly influenced by characteristics of the various sensors and propulsive units used. For various reasons, the two-stage descent was chosen, with the bulk of the approach velocity being removed by the solid propellant retrorocket, and the remainder by the vernier engine system. Because of variations in burn time and thrust of the retrorocket in the approach trajectory, and in the flight control and vernier propulsion subsystems, significant altitude-velocity dispersions could occur at retrorocket burnout. Enough vernier engine propellant had to be carried to provide for these dispersions. Sufficient propellant was provided to assure at least a 99% probability of not running out of propellant (Refs. XIII-5 through XIII-7).

For such a two-stage system, propellant consumption was minimized by optimum division between the characteristic velocities of the retrorocket and vernier systems. However, terminal sensor characteristics did not allow operation at this optimum; the retrorocket had to be sized so that burnout would occur within the operating ranges of the RADVS subsystem. The RADVS provided the information needed to control the vehicle attitude and thrust level during vernier engine phase. Because of the uncertain nature of the performance of the solid propellant retrorocket, these sensor constraints could be satisfied only in a statistical sense. Thus, it was required that with at least 99% of all possible conditions,

**Table XIII-7. Mechanization sources of midcourse correction magnitude errors**

| Random error source | 3 $\sigma$ acceleration error referred to 0.1 g, % | 3 $\sigma$ incremental velocity error, ft/sec |
|---|---|---|
| Accelerometer | $\pm$1.10 | |
| Reference signal | $\pm$0.50 | |
| Flight control electronics null | $\pm$0.15 | |
| Thrust bias variation | $\pm$0.09 | |
| Control channel gain variation | $\pm$0.07 | |
| Accelerometer misalignment | +0.6 | |
| Shutdown impulse dispersion | | $\pm$0.016 |
| Hysteresis limit cycle | | $\pm$0.035 |
| Ignition transient | | $\pm$0.30 |
| Timing granularity | | $\pm$0.11 |

**Table XIII-8. Mechanization sources of midcourse correction vector angle errors**

| Error source | 3 $\sigma$ error, deg |
|---|---|
| Optical mode | |
| Sensor null offset and alignment relative to sensor group coordinate system | 0.12 |
| Limit cycle | 0.18 |
| Electronic component drifts | 0.049 |
| Inertial mode | |
| Gyro alignment relative to sensor group coordinate system | 0.11 |
| Gyro drift (15 min of 1 deg/hr) | 0.25 |
| Gyro torquer scale factor (0.1 % for 90-deg rotation) | 0.9 |
| Timing accurocy (constant, independent of maneuver) | 0.10 |
| Control circuit accuracy ($\pm$0.1 %) | 0.09 |
| Spacecraft structure and alignment | |
| Sensor group alignment to spacecraft | 0.10 |
| Sensor group alignment change due to acceleration and heat loads | 0.20 |
| Engine alignment to spacecraft | 0.20 |
| Engine centerline variation | 0.06 |
| Engine centerline to thrust vector | 0.3 |
| Total | 0.697 |

retrorocket burnout would occur within the RADVS constraints and touchdown would occur before depletion of the vernier engine propellant supply.

*a. Sensor constraints.* Constraints on the allowable burnout region were imposed by the RADVS. In general, both the doppler velocity radar and range radar operating capability were defined by two equations.

Equation (1) described the reflected RF power returned to the radar receiving feedhorn, and Eq. (2) described radar tracker lock-on sensitivity.

$$P_r = \frac{P_t G \lambda^2}{2 (4\pi R)^2} [\eta F (\theta)] \tag{1}$$

where

$P_t$ = transmitter power

$G$ = peak antenna gain

$\lambda$ = operating wavelength

$R$ = slant range along beam axis

$\theta$ = incidence angle of beam

$\eta F(\theta)$ = Muhleman lunar reflectivity model

and

$$P_{\min} = f (f_i, \text{DGRD}) \tag{2}$$

where

$f_i$ = doppler frequency (velocity) along beam axis

DGRD = field degradation of sensitivity

For successful radar operation, $P_r \geq P_{\min}$

An additional constraint on radar operation was allowable reflected signal frequency variations as imposed by search frequency limits. The radar velocity sensors had a minimum frequency limit equivalent to a 30-ft/sec beam velocity and a maximum frequency limit equivalent to approximately 700–800 ft/sec, dependent on the radar model. Radar altimeter (RA) reflected frequency was a function of both range and velocity; therefore, the frequency limit resulted in a limit dependent on range-velocity as noted in Fig. XIII-6. The constant 40,000-ft limit, also noted in Fig. XIII-6, was the maximum range capability of RA due to power limitations.

Since a successful soft landing was contingent on the ability of the spacecraft to follow command descent segments, maximum spacecraft velocity at time of intercept of the internally programmed descent segments had to be less than the limiting velocity imposed by the RA operating limit. For the A-21 series spacecraft, this maximum burnout velocity was 650 ft/sec (Fig. XIII-6). The lower descent acceleration capability of the A-21A series spacecraft had the effect of decreasing this maximum allowable burnout velocity by approximately 100 ft/sec. This was effected by loading more propellant in the retrorocket and/or constraining launch vehicle weight. The minimum doppler velocity sensor (DVS) tracking velocity of 30 ft/sec, previously mentioned, had the effect of limiting minimum retrorocket burnout velocity because of flight-path angle dispersions.

*b. Propulsion constraint.* The allowable burnout velocity range was further restricted by maximum thrust capability of the vernier engine system, which had a throttling ratio of 3.5:1. To accurately control the final constant-velocity descent phase, minimum thrust capability had to be less than the least possible lunar landed weight of the vehicle so that 1-lunar-$g$ thrust acceleration could be maintained during the constant velocity phase. The result was a minimum thrust of 90 lb and a maximum of 312 lb. Terminal descent at maximum thrust to touchdown defined a curve in the range–velocity plane below which main retrorocket burnout could not be allowed to occur. Actually, since the vernier engines were also used for attitude control, it was necessary to allow some margin from the maximum thrust level. Since it was more convenient to sense acceleration than thrust, the terminal maneuver was designed for a constant acceleration rather than a constant thrust.

Acceleration level was determined from the maximum thrust capability of the engines and the maximum possible vehicle weight at retrorocket burnout, with suitable allowances for attitude control and control system mechanization errors.

Maximum command thrust acceleration $a$ defined a parabola in the altitude velocity plane given by Eq. (3):

$$V^2 = 2 (a_{\max} - g) h \tag{3}$$

where $g$ is equivalent unity gravity units and $h$ is spacecraft height above the lunar surface.

For vertical descents, the curve defined the minimum altitude at which retrorocket burnout was permitted to

occur for a given burnout velocity, and still achieve a soft landing. This parabola is indicated in Fig. XIII-6 along with the radar constraints. For ease of implementation, the parabola was approximated in the spacecraft control system by straight-line segments, also shown in Fig. XIII-6.

*1. Dispersion analysis.* Having defined the allowable burnout region, the retrorocket loading was determined so that burnout would occur within the region. It was necessary to provide for dispersions in engine characteristics, as well as for vehicle weight variations because of different amounts of propellant expended in performing the midcourse maneuver, and for the required range of approach velocities.

For vertical descent, burnout velocity can be expressed in terms of retrorocket ignition velocity $V_0$ and retrorocket characteristic velocity $\Delta V$ by the approximate relation of Eq. (4):

$$V_b = V_0 - \Delta V + gt \tag{4}$$

where $g$ is an equivalent average value of lunar gravity during the retroignition phase and $t$ is the retrorocket burning time. The characteristic velocity is given by Eq. (5):

$$\Delta V = c \ln \frac{w_0}{w_b} \tag{5}$$

where $w_0$ and $w_b$ are the vehicle weights at retroignition and burnout and $c$ is exhaust velocity (proportional to specific impulse). For off-vertical cases, the situation is shown in Fig. XIII-11.

The principal sources of burnout velocity dispersion were imperfect alignment of the vehicle prior to retroignition and variability of the total impulse. These variations, in the case of a nominally vertical descent, caused dispersions of the type shown in Fig. XIII-12, where the ellipse defined a region within which burnout would occur with a probability of 0.99. The scale of Fig. XIII-12 is exaggerated to illustrate the point. Actual retroignition velocities are approximately 8650 ft/sec, $gt$ is approximately 280 ft/sec, and nominal burnout velocities range from 200 to 525 ft/sec, depending on the magnitude of $\Delta V$. It is apparent that even relatively small percentage variations of $\Delta V$ can cause large percentage variations in burnout velocity and that $\Delta V$ alignment errors, although expected to be only 1 deg (3 $\sigma$), can cause substantial

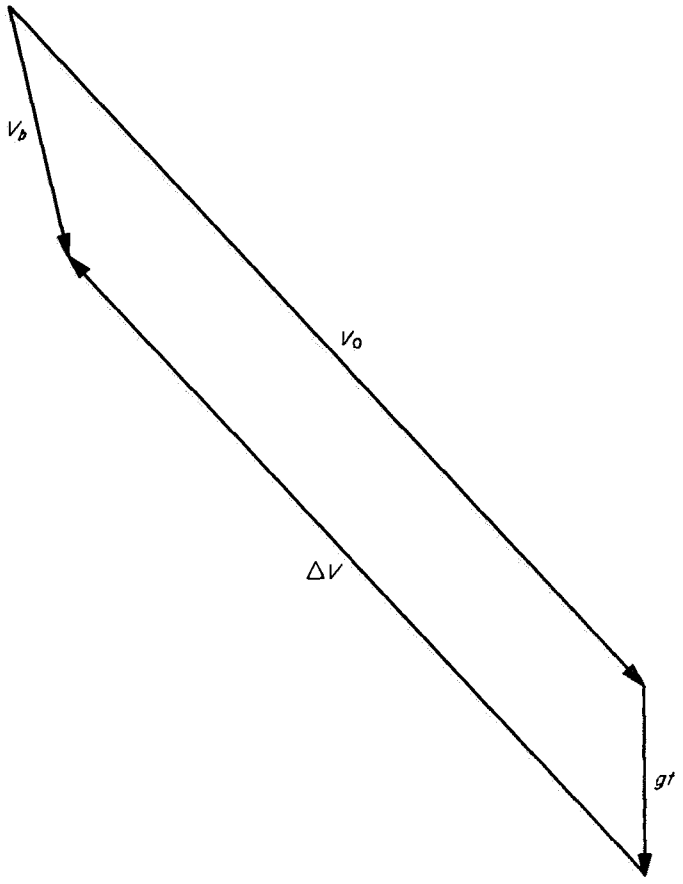



**Fig. XIII-11. Retrorocket velocity vector diagram**

variations in the burnout flight path angle, with the situation becoming more severe as nominal burnout velocity decreases. Thus, for low burnout velocities, there was danger of violating radar attitude constraints mentioned previously. In particular, for the planned design, these considerations restricted the minimum allowable nominal burnout velocity to about 200 ft/sec in the vertical case, 250 ft/sec for 25-deg approach angle, and 300 ft/sec for 45-deg approach angle.

The range of burnout velocity dispersions resulting from estimated subsystem error sources was $\pm$100 ft/sec (3 $\sigma$), as noted in Fig. XIII-13. However, design objective subsystem error sources resulted in $\pm$125-ft/sec dispersions.

While velocity dispersions were approximately the same for the A-21A spacecraft, the lower minimum acceleration capability required that maximum burnout velocity differ from the radar limit by the dispersions plus the increase in spacecraft velocity during the minimum acceleration phase from retrorocket burnout to command descent segment intercept.

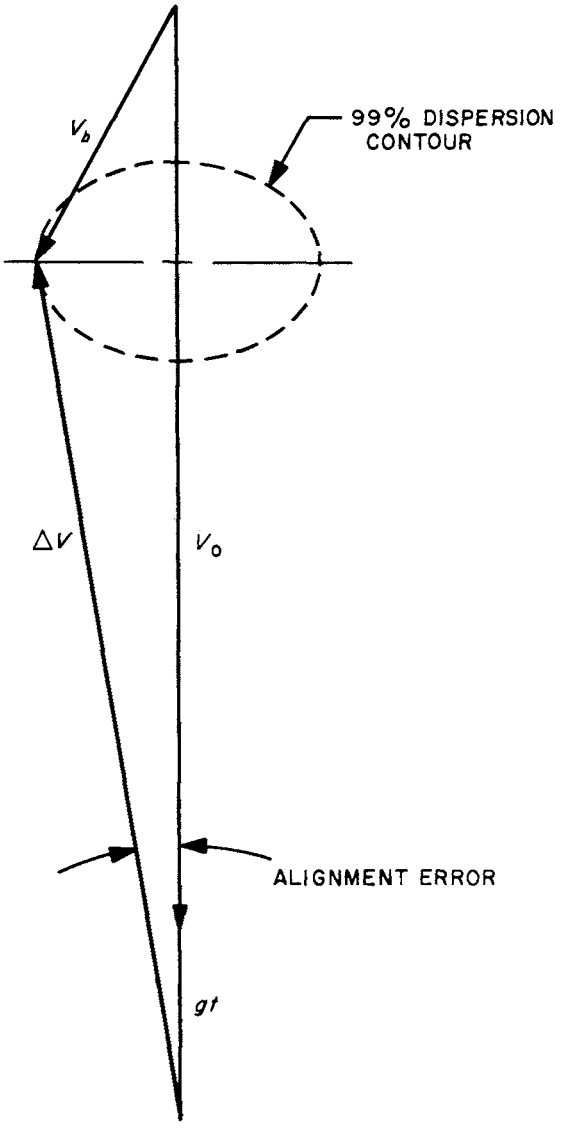



**Fig. XIII-12. Velocity dispersions for vertical approach**

Analysis of the burnout altitude dispersions followed similar lines. For a vertical descent, the burnout altitude is approximated by Eq. (6):

$$h_b = h_0 - V_0 t + \Delta D - \frac{1}{2} g t^2 \qquad (6)$$

where the characteristic distance $\Delta D$ is, according to Eq. (7), approximately

$$\Delta D = \frac{c^2}{g} \frac{w_0}{T} \left[ 1 - \left( 1 - \frac{\Delta V}{c} \right) e^{-\Delta V/c} \right] \qquad (7)$$

and $T$ is the retrorocket thrust, assumed constant here.

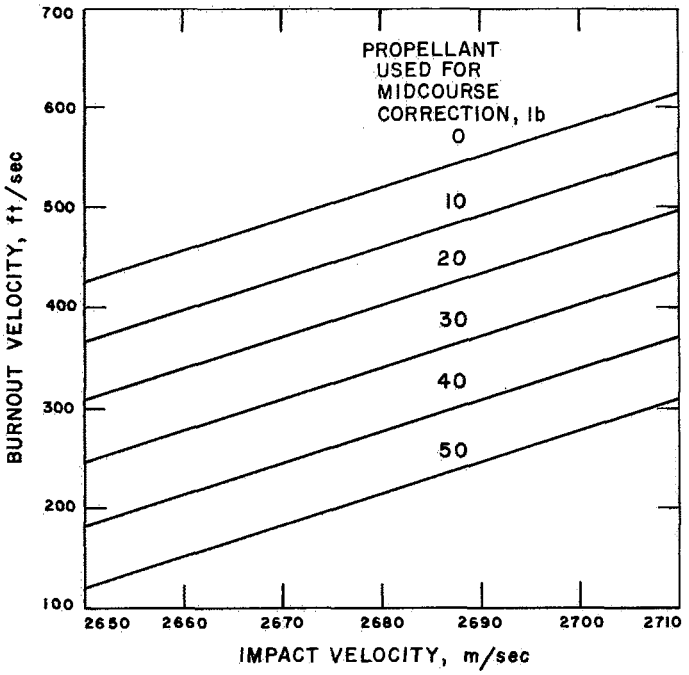



**Fig. XIII-13. Retrorocket burnout velocity vs impact velocity**

For off-vertical approaches, the vector diagram of Fig. XIII-14 applied, with the dispersion analysis for the vertical case indicated in Fig. XIII-15. Since the horizontal translation caused by thrust vector misalignment was of secondary interest for *Surveyor*, the principal point of interest was the altitude dispersion, caused principally by variation in retro engine burn time due to unpredictable temperature variations.

Once the disperson ellipse (Fig. XIII-6) was determined, the required burnout altitude, and hence ignition altitude, followed from the requirement that the probability of burning out within the constraints would be at least 0.99.

2. *Retrorocket sizing.* With the dispersions known, retrorocket propellant loading was determined for the A-21 spacecraft so that for the heaviest possible vehicle (no midcourse correction) approaching the higest possible velocity, burnout would occur at the highest permissible speed (that is, at the radar limit of 650 ft/sec less the 99% dispersion of 125 ft/sec). This policy allowed maximum reduction in burnout velocity due to variations in approach speed and in fuel consumed at midcourse. Since the sensitivity of burnout velocity to initial weight was about 6 ft/sec/lb, a 40-lb midcourse (50 m/sec) correction reduced nominal burnout velocity from 525 to

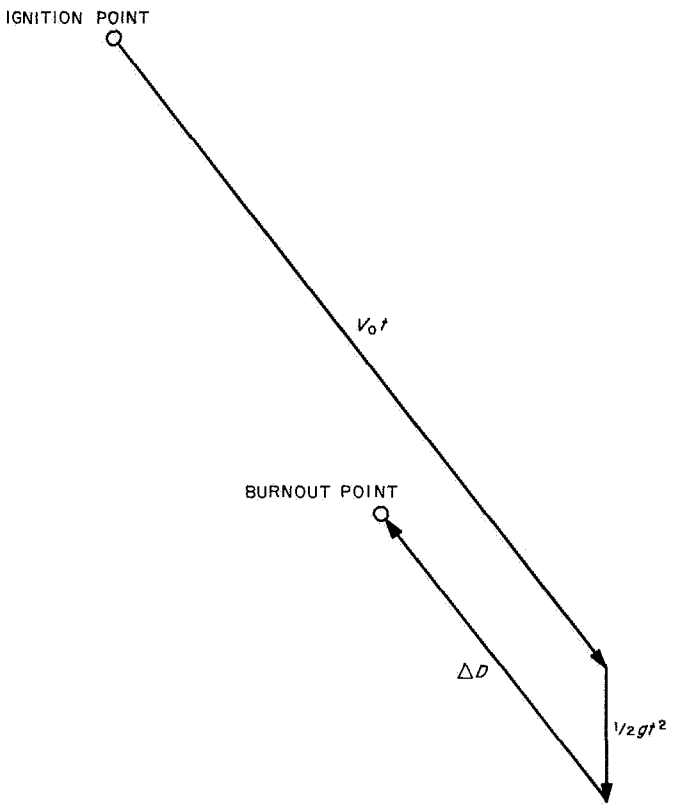



**Fig. XIII-14. Displacement vector diagram**

285 ft/sec. Remaining was 35 ft/sec for possible variations in approach velocity before the 250-ft/sec limit imposed by burnout attitude constraints was reached. As the required midcourse maneuver increased, the allowable variation in approach velocity reduced correspondingly. This is shown in Fig. XIII-13, which is a plot of burnout velocity vs unbraked impact velocity for various midcourse maneuvers with a maximum design unbraked impact velocity of 2682 m/sec.

Retrorocket sizing for the A-21A spacecraft was somewhat different because of a limited range in burnout velocities between 300 and 410 ft/sec. Because of the sensitivity of burnout velocity to midcourse maneuver, a maximum midcourse maneuver requirement of 50 m/sec could not be guaranteed, if a zero midcourse maneuver capability was also required. Therefore, the retrorocket was sized for the minimum expected unbraked-impact velocity, minimum allowable burnout velocity (300 ft/sec), and maximum midcourse maneuver. Thus, the burnout velocity range from 300 to 410 ft/sec was used to accommodate a combination of midcourse maneuvers less than 50 m/sec and unbraked impact velocities greater than the expected minimum.

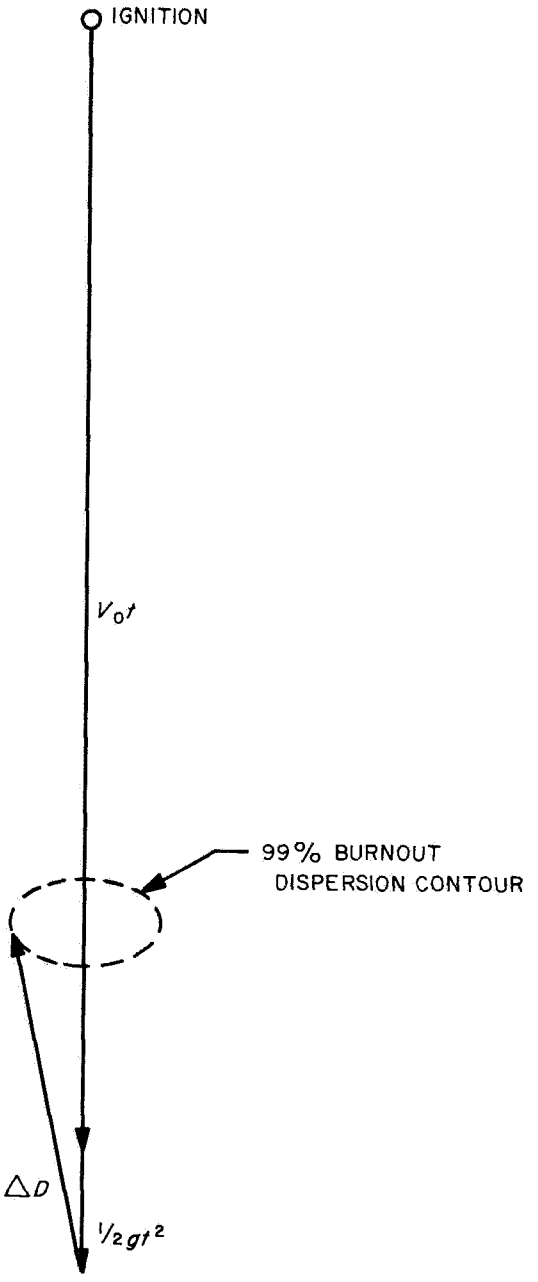



**Fig. XIII-15. Altitude dispersions for vertical approach**

The altitude at retroignition was established so that burnout would occur sufficiently above the descent contour (Fig. XIII-6) to allow time for spacecraft thrust axis alignment with the velocity vector before the trajectory intersected the descent contour. This established a burnout locus which allowed for altitude dispersions plus an alignment time that depended on the maximum angle between the flight path and roll axis at burnout. This locus is included in Fig. XIII-6.

3. *Vernier propellant analysis.* Maximum vernier propellant expenditure occurred when the executed midcourse velocity correction was maximum. The design was chosen to provide enough vernier propellant so that, given maximum midcourse velocity correction, the probability of sufficient propellant remaining for soft landing was at least 0.99. A Monte Carlo simulation program of the terminal descent had been developed which took into account dispersions in burnout velocity and altitude, specific impulse, mixture ratio, and other factors; this program was used to aid in determining the required propellant loading.

In addition, a more accurate simulation of terminal descent was used to determine nominal values of burnout velocity and propellant margin (expected usable vernier propellant remaining after touchdown) for varying values of unbraked impact velocity, unbraked impact angle, and midcourse correction. This program was a three-degree-of-freedom simulation using numerically integrated equations of motion.

Figures XIII-16 and XIII-17 are plots of propellant margin vs unbraked impact velocity, and approximations of-freedom simulation using numerically integrated equa- retrorocket burnout to touchdown vs unbraked impact velocity.

The essential output of the Monte Carlo simulation was a profile of vernier propellant dispersions vs burnout velocity. Figure XIII-18 is a typical plot of these parameters for midcourse corrections of 0 and 50 m/sec. For a given burnout velocity, the ordinate of the graph represents the required propellant margin to be expected at touchdown after a normal descent, in order to ensure 0.99 probability of sufficient propellant during descent when dispersions were present.

*c. Guidance considerations.* The basic closed-loop guidance method used during the vernier phase consisted of continual alignment of the thrusting direction antiparallel to instantaneous velocity vector, and thrust acceleration control in accordance with a nominal required velocity vs slant range descent contour (Fig. XIII-6). The attitude control law, known as the gravity turn, began after the doppler radar had acquired the velocity vector and the initial thrust axis pointing error had been corrected. Regardless of acceleration level, the gravity turn tended to force the flight path toward the vertical as time progressed. In fact, it had the very desirable property that as the velocity approached zero, the flight path angle, and therefore the vehicle thrust attitude, approached the vertical.

The thrust acceleration control law ensured that the cutoff velocity of 5 ft/sec was reached in a vertical attitude at some suitably low altitude above the lunar surface.

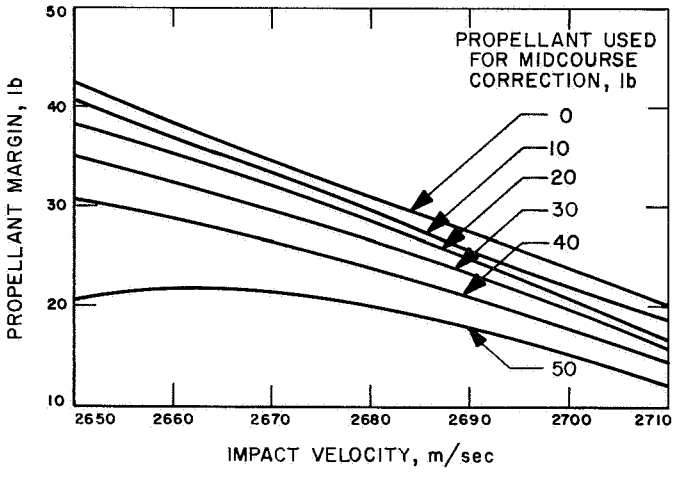



**Fig. XIII-16. Vernier propellant margin vs impact velocity**

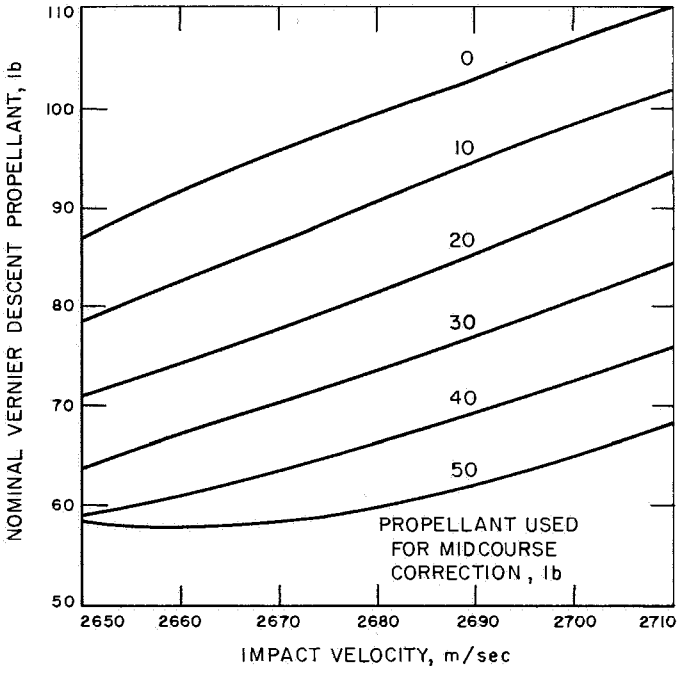



**Fig. XIII-17. Nominal vernier descent propellant vs impact velocity**

*1. Gravity turn.* Gravity turn geometry is shown in Fig. XIII-19. Differential Eqs. (8) and (9) describe motion:

$$\frac{dV}{dt} = -a + g\cos\psi \tag{8}$$

$$V\frac{d\psi}{dt} = -g\sin\psi \tag{9}$$

where

$\psi$ = flight path angle

The solution of constant thrust acceleration may be found by dividing Eq. (8) by Eq. (9), separating the variables, and integrating. The resultant expression of Eq. (10) relates velocity $V$ and flight path angle $\psi$ to the initial velocity $V_0$ and flight path angle $\psi_0$:

$$\frac{V}{V_0} = \left(\frac{\tan\frac{\psi}{2}}{\tan\frac{\psi_0}{2}}\right)^{\frac{a}{g}-1}\left(\frac{\sec^2\frac{\psi}{2}}{\sec^2\frac{\psi_0}{2}}\right) \tag{10}$$

*2. Constant low-acceleration phase.* The 0.9-lunar-$g$ gravity turn phase started from an initial velocity that depended on the main retro characteristic velocity and thrust attitude. This phase generally terminated at the descent contour with only a small change in velocity. Specifically, if the initial flight path is nearly vertical ($\psi_0 \approx 0$), the intersection velocity was slightly higher than the initial because the thrust acceleration was less than 1 lunar g. This fact affected the sizing of the main retro and the placement of the nominal main engine burnout point. If the initial flight path were off the vertical by some relatively large angle such as 45 deg, the velocity would first decrease, since the right hand side of Eq. (8) would be negative. As long as the spacecraft was still above the descent contour, this trend would continue until the flight path angle reached $\cos^{-1} a/g$ or 25.8 deg, after which the gradual reduction of flight path angle would be accompanied by a gradual increase in velocity.

*3. Turning rate.* Equation (10) may be substituted for Eq. (9), resulting in the expression of Eq. (11) for the spacecraft attitude rate:

$$\frac{d\psi}{dt} - = \frac{g\sin\psi}{V_0}\left(\frac{\tan\frac{\psi_0}{2}}{\tan\frac{\psi}{2}}\right)^{\frac{a}{g}-1}\left(\frac{\sec^2\frac{\psi_0}{2}}{\sec^2\frac{\psi}{2}}\right) \tag{11}$$

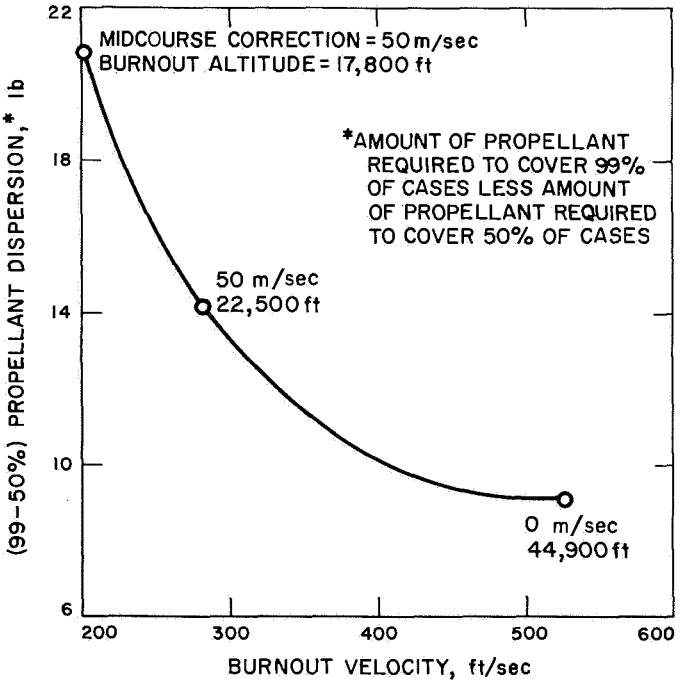



**Fig. XIII-18. Vernier propellant dispersion vs burnout velocity**

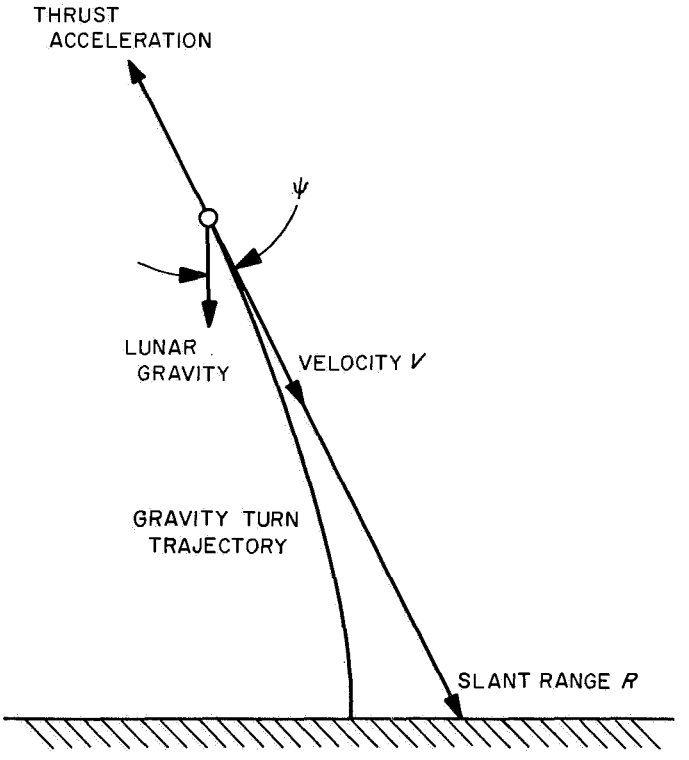
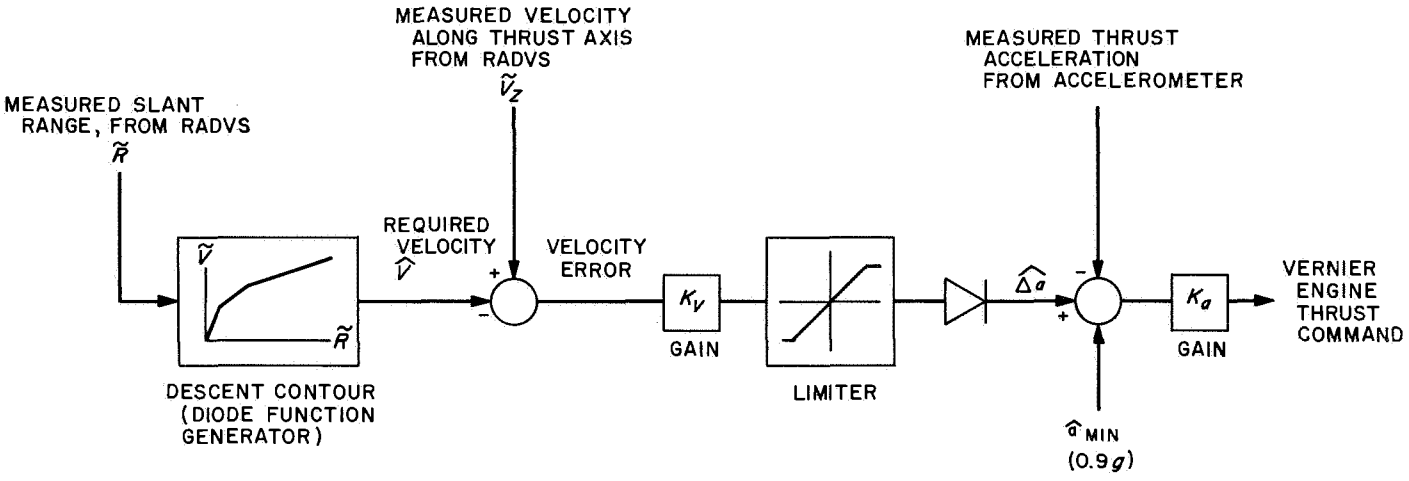



**Fig. XIII-19. Gravity turn descent geometry**

(a) MECHANIZATION




(b) CHARACTERISTICS

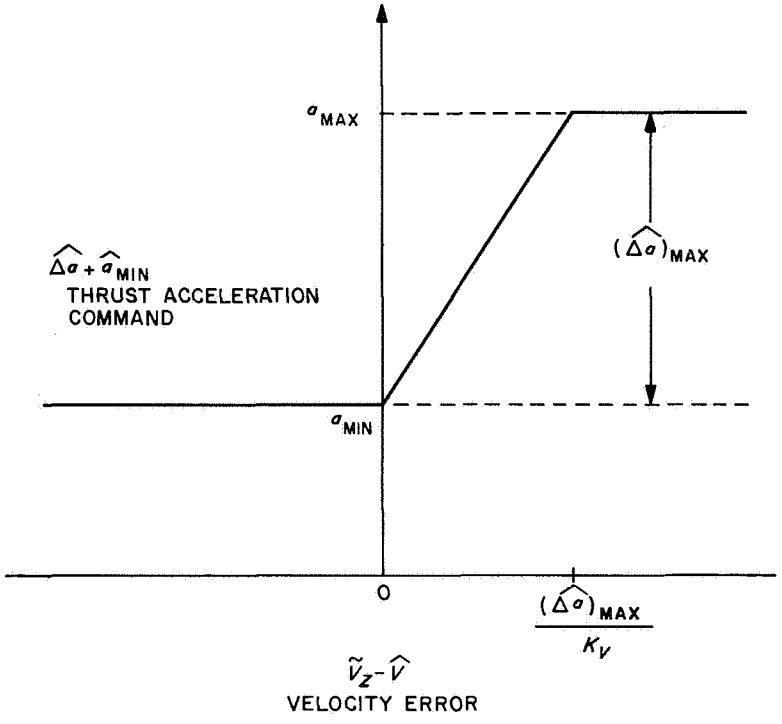



**Fig. XIII-20. Thrust acceleration command**

If the thrust acceleration $a/g$ were greater than 2, as would be the case during the major portion of descent following the 0.9-$g$ phase, Eq. (11) indicates that attitude rate $d\psi/dt$ diverges as the flight path angle $\psi$ approaches zero. Since the vehicle turning rate was limited because of finite gyro torquing capability, it was important to have a descent contour that did not require a large thrust acceleration (greater than 2 $g$) at the end of the closed-loop guidance phase. This was accomplished by employing a descent contour that used a final straight-line segment which passed through the origin of the range-velocity plane.

*4. Guidance during programmed descent contour.* In the vicinity of the descent contour, thrust acceleration command was proportional to velocity error, defined as the difference between measured velocity $\tilde{V}_s$ along the thrusting direction and required velocity $\tilde{V}$ programmed for the measured slant angle. The analog mechanization design used in the spacecraft is schematically shown in Fig. XIII-20(a). The actual characteristic relating thrust acceleration command and velocity error is shown in Fig. XIII-20(b). The linear region was necessary to prevent engine thrust from chattering between the upper and lower limits because of radar and system noise.

Figure XIII-21 shows a typical, actual range-velocity trajectory in relation to a particular straight-line segment of the mechanized descent contour. The velocity at which the 0.9-$g$ phase terminates ($V_s$) was a function of conditions at the start of the vernier phase, and was therefore variable. However, if $V_s$ were reasonably close to the upper velocity $V_2$ of the particular segment, the acceleration would be saturated almost immediately and would remain saturated until a lower velocity $V_a$ was reached, at which point the acceleration would be reduced to the value required to remain on the descent segment. This acceleration is given approximately by Eq. (12):

$$a \approx V\frac{dV}{dR} + g \approx V\frac{V_2 - V_1}{R_2 - R_1} + g \qquad (12)$$

where

$R$ = slant range along spacecraft thrusting axis

The actual trajectory, except for a small velocity error, then followed the straight-line segment to its lower velocity limit $V_1$. Typical acceleration versus velocity history is shown in Fig. XIII-22. The velocity $V_a$ depended primarily on $V_s$ and, to a lesser extent, on the flight path angle $\psi_s$. In general, the higher the value of $V_s$ and $\psi_s$, the lower $V_a$ tended to be. A finite tracking period between $V_1$ and $V_a$ was desirable so that the actual trajectory, in attempting to track the following segments, developed the same two-phase characteristic. This was the only method that could guarantee enough acceleration capability to soft-land at any subsequent time. Placement of

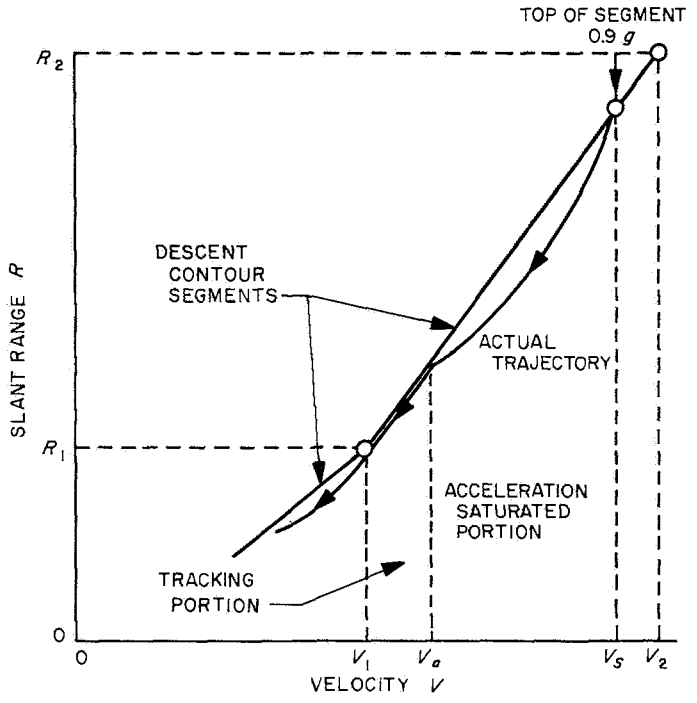



**Fig. XIII-21. Range-velocity trajectory relative to descent contour**

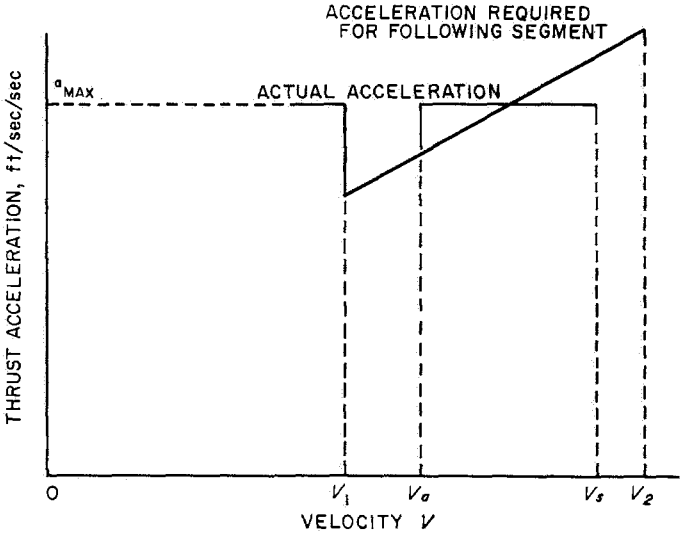



**Fig. XIII-22. Acceleration vs velocity**

the end points along the parabolic contour was based, therefore, partly on meeting certain minimum tracking period requirements for each and every segment. Other considerations that were not so obvious in the descent contour design were those relating to surface slope, system errors, and noise from radar outputs. These effects also influenced the margin required between the upper acceleration limit and the nominal acceleration level.

*5. Final segment and cutoff.* The final segment, crucial in design, is shown in Fig. XIII-23 along with a typical actual trajectory. Velocity $V_0$, corresponding to the top of the segment $P_0$, was so low that the probability of the 0.9-$g$ phase terminating at a lower velocity was negligible. Furthermore, for most retro-burnout conditions, the effect of gravity turn would have reduced the flight-path angle to a very small value when the starting point $P_0$ was reached. For practical purposes, descent from this point could be considered essentially vertical. The required acceleration for ideal tracking was, then:

$$a = V\frac{V_0}{R_0} + g \qquad (13)$$

Equation (13) shows that the required acceleration approached 1 lunar $g$ as $V$ approached zero. As was mentioned previously with regard to the spacecraft turning-rate [Eq. (11)] requirement, this reduction in acceleration to less than 2 lunar $g$ was beneficial in keeping the attitude rate expression $d\psi/dt$ from developing a divergent characteristic.

The trajectory possessed the usual acceleration-saturated and tracking portions until the velocity reached a preset value of 10 ft/sec. The required control velocity was then switched to a constant value $V_c$ of 5 ft/sec and the vehicle attitude was switched to inertial hold. A short transient appeared after $V_b$ during which acceleration was momentarily saturated again. Then the acceleration was automatically controlled to the required 1 lunar $g$ for a constant velocity descent at 5 ft/sec. This constant velocity descent removed any altitude error that might have existed at point B (Fig. XIII-23).

When the measured altitude reached 13 ft $R_c$, the vernier engines were shut off and the vehicle fell freely to the lunar surface. The vertical component of the landing velocity, nominally about 13 ft/sec, had an error largely dependent on the altimeter and doppler measurements at engine shutoff. Error analyses of the *Surveyor* system parameters indicated a 3 $\sigma$ dispersion of less than 2 ft/sec.

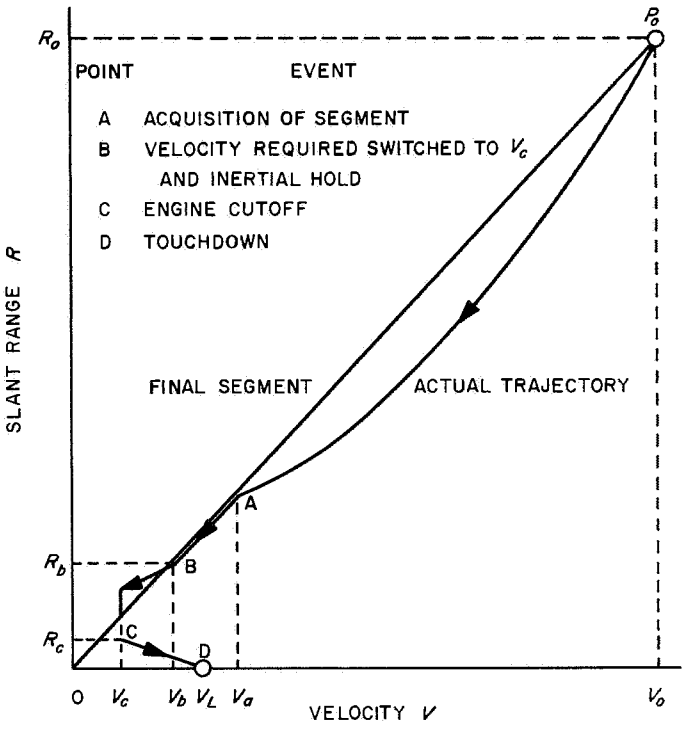



**Fig. XIII-23. Final segment and corresponding trajectory**

The horizontal component of the landing velocity was nominally zero. Dispersions arose, however, primarily because of the following two factors:

(1) Measurement error in the doppler system resulting in a velocity error normal to the thrust axis.

(2) Nonvertical attitude at point B in Fig. XIII-23, because of termination of the gravity turn at a finite velocity and attitude transients resulting from radar and other control-system noise sources.

Since the initial attitude was inertially held throughout the remainder of powered descent until cutoff, these errors gave rise to a small lateral velocity at touchdown. The capability of withstanding this lateral velocity without toppling was an essential requirement in the vehicle landing gear design.

### *d. Descent mechanization concepts.*

*1. Terminal descent initiation.* Accurate initiation of the terminal descent was mandatory. Uncertainties in retroignition altitude resulted in burnout attitude dispersions which required that the burnout altitude be biased above the vernier descent contour. This altitude bias is directly reflected in propellant requirements that restrict the payload under the fixed maximum launch

weight constraint. Use of an altitude marking radar reduces the retroignition altitude uncertainty from approximately 10 mi (based upon orbit determination from doppler tracking data) to 1 mi; this means of initiating the terminal descent sequence was selected. To obtain engineering data in the event of a failure of the radar, a backup marking capability was provided by earth command, delayed sufficiently so as not to affect the sequence, if the radar performed as expected.

2. *Descent sequence on-board control.* Mechanization of terminal descent control incorporated a fixed on-board analog control program, which was completely automatic, subsequent to terminal descent initiation (AMR mark). Major advantages of fixed analog control were small size, light weight, reliability, and simplicity; the major disadvantage was lack of flexibility.

3. *Inertial reference.* Major advantages of the strapdown gyro inertial reference over a stable platform were weight, size, cost, and reliability. Since celestial sensors could be used to accurately determine and control spatial attitude, except during the short periods of midcourse correction and retroignition, the strapdown gyro reference was selected for the *Surveyor*. Another compelling factor in design selection of strapdown gyros was the lack of a requirement for vertical reference.

4. *Velocity vector and range sensors.* The solid propellant retromaneuver phase of the descent could not be mechanized accurately enough to meet the desired soft-landing conditions. A subsequent vernier-descent phase was selected to achieve the soft landing. Determination of the velocity vector and range in spacecraft coordinates was required for the vernier phase.

Use of television as an assist to terminal descent was considered; however, the time needed to measure the velocity vector and command corrective action by the spacecraft precluded any serious consideration of this approach. Optical instruments were also investigated for use as active velocity vector sensors. Horizon scanner instruments were capable of measuring altitude and determining vertical and horizontal velocity from inertial rates of rotation. Major limitations of these instruments were the dependence on small deviations between landing site and horizon, the requirement for rotational isolation from the vehicle in order to maintain a fixed attitude to the vertical, and inadequate accuracy for altitudes less than 1000 ft.

Also considered was another optical instrument to measure the motion of the surface image across the optical field of view; however, its performance depended on the optical granularity of the surface, which imposed undesirable lighting constraints. Thus, optical systems had major limitations in addition to possible performance problems associated with the effect of engine exhaust on their field of view.

To accomplish the velocity and altitude sensing, frequency-scan continuous-wave radar was selected utilizing a combination of three side-looking doppler beams and one downward-looking altimeter beam. A significant advantage of the doppler radar was measurement of true velocity rather than rate of change in range, and its ability to sense lateral components of velocity.

5. *Constraints imposed by interaction between radar beams.* Antenna measurements indicated that under particular geometrical conditions it was possible for one velocity radar beam to lock on the sidelobe of another beam, resulting in erroneous steering and thrust control commands from the flight control system. One pair of radar beams which shared the same antenna structure was protected from this problem by logic designed into the radar to preclude possible interference resulting from this commonality. To prevent possible occurrence of a problem in the other beam pairs, the terminal maneuver roll angle of early *Surveyor* flights was restricted to particularly safe angular regions. Since these safe regions often resulted in undesirable lighting conditions for television pictures after landing, logic was subsequently added to the remaining beam pairs to remove this flight roll constraint.

Although relaxing (but not completely eliminating) the sidelobe acquisition problem, it was found that the added sidelobe logic could, through its normal logic action, cause beam unlock at low altitudes. This problem was resolved by a cross coupling scheme whereby the logic was inhibited with a signal generated by the radar when the range was reduced to 1000 ft (1000-ft mark).

6. *Liquid vs solid propulsion.* Propulsion requirements were of two categories. For the retromaneuver phase, a constant large thrust (approximately 10,000 lb) was required; for the vernier descent phases, a low-level variable-thrust propulsion system (approximately 300 lb) with a 3.5:1 throttle ratio was needed. Attitude control during these periods was also necessary. A single descent engine was rejected since it would require gimbaling or thrust vector control in order to stabilize the spacecraft; and a variable thrust engine, with acceptable dynamic response and variable thrust range to satisfy the low and

high acceleration requirements, would require extensive development. To satisfy the thrust range and attitude control requirements, the minimum practical requirement was three variable control engines; however, their throttle ratio would have to be an impractical 100:1 The next best choice was to have a large single rocket for the high thrust requirements and three small variable-thrust (limited-range) engines to satisfy the midcourse, vernier descent thrust, and attitude control requirements. Such a system was implemented. The remaining choice was between solid- and liquid-propellant retrorocket propulsion. A solid propellant was selected primarily for reliability considerations. Other advantages were in the areas of weight, development costs, complexity, personnel hazard, susceptibility to handling damage, spacecraft integration, and thrust-to-weight ratio.

*7. Attitude control during retromaneuver phase.* Because of possible misalignment between the retroignition thrust vector and spacecraft during the retromaneuver, under inertial control, large lateral velocities could exist at retrorocket burnout. Especially for low longitudinal velocity conditions, lateral velocity at burnout could yield large flight path angles between the velocity vector and the lunar vertical at retro burnout. Serious consequences of this condition would be lack of acquisition or loss of lock of radar beams and high residual lateral velocities at touchdown which could affect landing stability. Analysis revealed that during this phase, the spacecraft thrust vector could be pointed with sufficient accuracy under inertial and vernier engine control; therefore, radar attitude control was inhibited during this period because of uncertainty associated with performance of the radar under the influence of the retrorocket exhaust.

*8. Thrust control vernier descent.* Open-loop constant thrust control was initially considered for the vernier phase of the terminal descent; however, the best accuracy of thrust control with available electronics and engine hardware was found to be $\pm 10\%$, which exceeded trajectory requirements. Closed-loop acceleration control was then selected for *Surveyor* because the accelerometer yielded a simple, reliable, and accurate means of control.

*9. Vernier propellant feed system.* The initial vernier propulsion feed system design utilized fuel and oxidizer tanks for each of the three engines, with lines interconnecting the tanks. The major advantage of this approach was that if the propellant was depleted in one pair of the tanks because of unequal propellant consumption, the other two sets of tanks would supply propellant to the engines.

During the program, the design was changed to eliminate this tanking. This change was made because it was considered possible for the propellant to migrate to fill the ullage of a particular tank or tank pair and produce a significant shift in the spacecraft center of gravity, thus inducing catastrophic moment disturbance at retroignition. In addition, the large uncertainties associated with maintaining the retroignition disturbance within controllable limits during retromaneuver dictated the desirability of obtaining a corrective center of gravity shift to reduce the disturbance, as was achieved from the untanked system. (Under imbalance, propellant burned differentially, tending to correct the imbalance.)

*10. Vernier engine cutoff altitude.* Selection of the vernier engine cutoff altitude was a compromise among various tradeoffs involved. To minimize landing loads and landing instability, it would be desirable to effect cutoff at surface contact, since cutoff at some finite altitude allows (1) the velocity to increase during drop and (2) the attitude to degrade because of attitude rates induced by unequal shutdown of the vernier engines. The major reason for preimpact cutoff was to minimize disturbances of the lunar surface particles, which might be impelled by the engine exhaust plume and damage the television, science instruments, thermal surfaces, electronics, or liquid propellant tanks. A 14-ft cutoff altitude was selected because studies indicated that:

(1) Touchdown velocities with dispersions would satisfy landing stability and load requirements.

(2) Engine exhaust reaction with the surface would not be severe.

(3) The radar altimeter would operate to this altitude and could be used to provide the cutoff signal.

*11. Landing system configuration.* The leg configuration for the landing system was selected because it minimized problems associated with vehicle configuration and science equipment deployment, weight, and thermal control. The three-legged configuration was selected over designs with a greater number of legs for the following principal reasons:

(1) Stability for maintaining attitude on an uneven surface.

(2) Weight and reliability savings by minimizing the number of mechanisms.

(3) Superior truss strength of a triangular structure.

*e. Terminal descent parameters.* Figures XIII-24 through 29 present information of general interest on the A-21 terminal descent phase. The following paragraphs present a brief discussion of each figure.

Figure XIII-24 depicts the retroignition altitude as a function of unbraked impact velocity (velocity prior to retroignition) and midcourse maneuver magnitude. Although there was a difference in retroignition altitude of approximately 20,000 ft for the 0- and 25-deg approach-angle cases, it will be noted that variations in retroignition altitude as a function of midcourse maneuver and unbraked impact velocity are almost the same for both cases.

Figure XIII-25 depicts the spacecraft altitude as a function of time during the retromaneuver for an unbraked impact velocity of 2682 m/sec. Because of the relative difference in altitude scales, as compared to Fig. XIII-15, curves were plotted for only 0 and 40 lb of midcourse propellant expenditures.

Figure XIII-26 presents spacecraft velocity vs time during the retromaneuver, and for an unbraked impact velocity of 2682 m/sec. As noted in Fig. XIII-26, spacecraft velocity was not a strong function of midcourse maneuver. In addition, although not shown in Fig. XIII-26, there was even a smaller variation due to unbraked impact angle.

Figures XIII-27 and XIII-28 present normal powered-flight descent time (and the differential time between a soft landing and an unbraked impact) as a function of retrorocket burnout velocity. Primarily, because of retrorocket burnout dispersions, these times would vary approximately $\pm 45$ sec ($3\sigma$).

Figure XIII-29 presents the lunar central-angle difference in touchdown location for a powered soft-landing descent and an unbraked descent.

### 6. Lunar Night Survival Considerations

Spacecraft capability of surviving lunar night was studied in attempts to enhance the probability of achieving the desired objective of a 90-day period of flight and lunar surface operation of the spacecraft. Much of the electronic equipment needed to fulfill the experimental, control, and communication requirements of the spacecraft could not survive in the severe environments associated with outer space and the lunar surface. Therefore, it was necessary to create a thermally controlled environment for critical electronic equipment.

*a. Early design concepts.* Initially, in conjunction with the A-25 design studies two control concepts were studied to determine which would provide efficient thermal control of critical electronic equipment.

The first concept utilized by-product heat from a radioisotope thermoelectric generator (RTG) to keep equipment warm throughout the lunar night. The RTG would have been proposed as an integral part of the electrical power supply so that using its dissipated heat would constitute an increase in the efficiency of energy usage on the spacecraft. The by-product heat was to be so excessive with the RTG scaled to meet the electrical needs of the spacecraft, that little thermal insulation would be needed for the heated equipment. The plan required that as much equipment as possible be packaged in a container heated by conduction heat from the RTG. The remaining critical equipment would be heated electrically. The conduction process was to be controlled by bringing the RTG in contact with the container mechanically at night when heat was needed. Disadvantages of this system included the uncertain availability of a qualified RTG and radiation and lunar day thermal interfaces with the instruments and spacecraft.

The second concept considered involved packaging critical equipment in a thermally insulated compartment. Multiple radiation shields would have been required between the package and the thermal shell so that no more than approximately 8.0 W of power derived from the allocated 84-lb silver-zinc batteries would be needed to heat the package during lunar night. In addition, it would be necessary to use approximately 10 thermal control switches (mechanical device *switched* reversibly from conducting to nonconducting at a set temperature) to increase conductance during lunar day to such level that excess electrical dissipation in the compartment could be rejected. Design of the package, being isolation-critical, required miniaturization of all electrical and structural connections leading to the package. The life of this system depended on the operating lifetime of the battery. Since performance of this system was based on the use of simple thermal switches, its reliability was high. Components within the thermally controlled package were to have temperatures between 50 and 100°F at all times.

For more than a year after initiation of the design of the *Surveyor* spacecraft, development of a 2500-lb spacecraft was pursued. Development of the RTG system appeared technically feasible and desirable; however, potentially serious problems associated with prelaunch sterilization

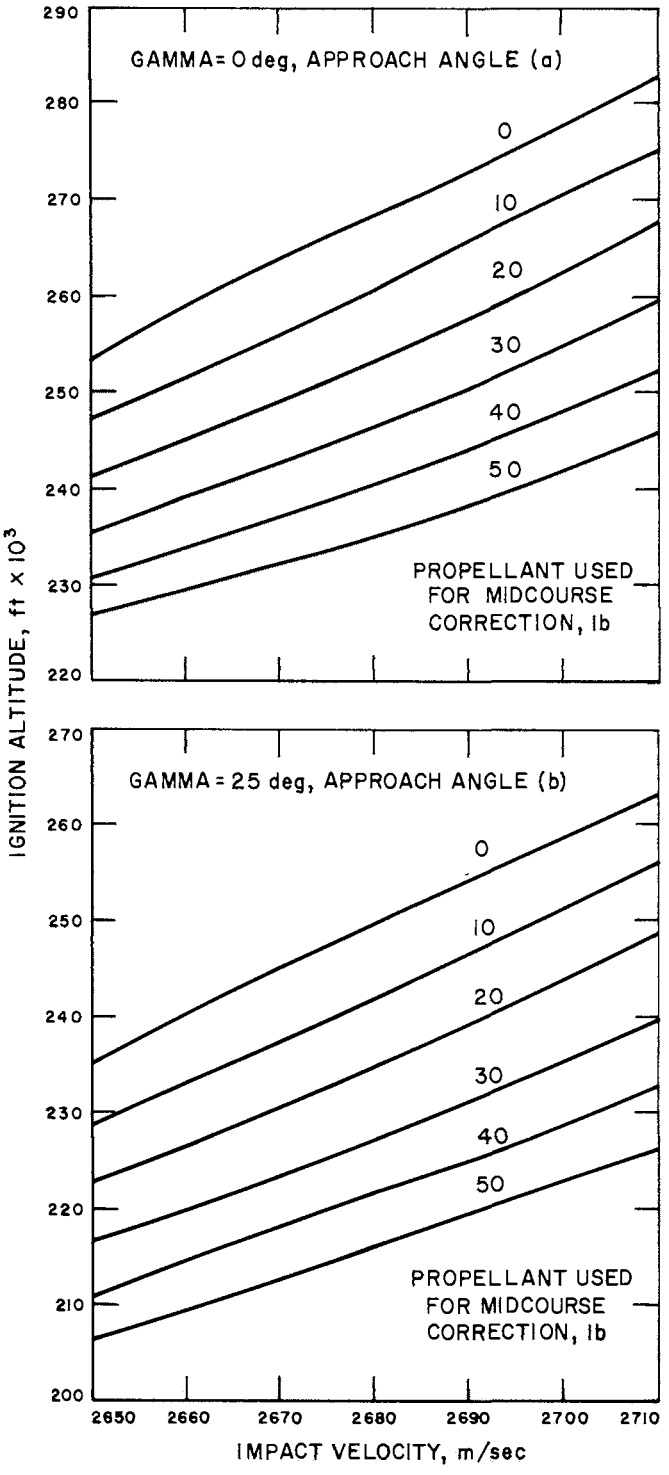



**Fig. XIII-24. Retroignition altitude vs unbraked impact velocity**

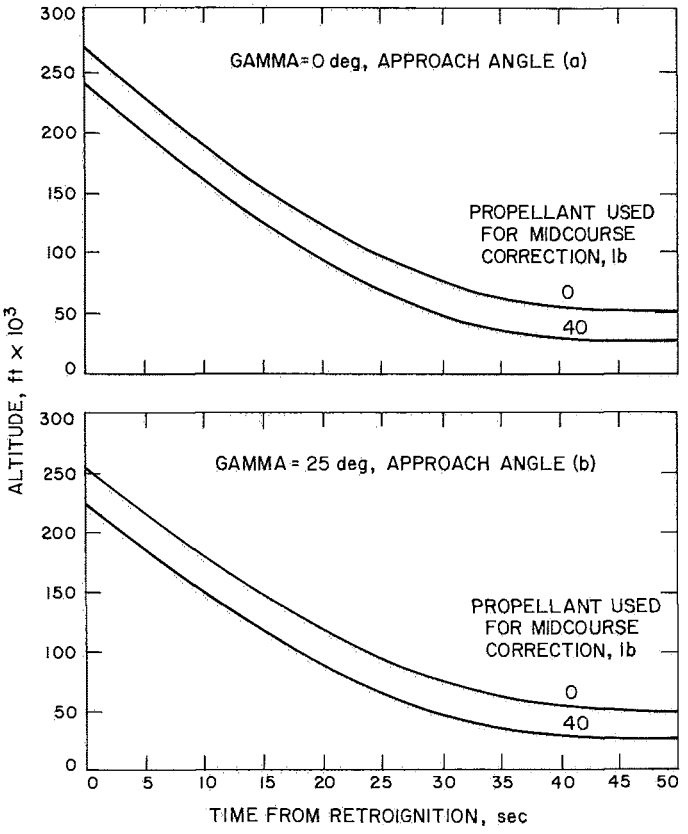



**Fig. XIII-25. Altitude vs time during retromaneuver**

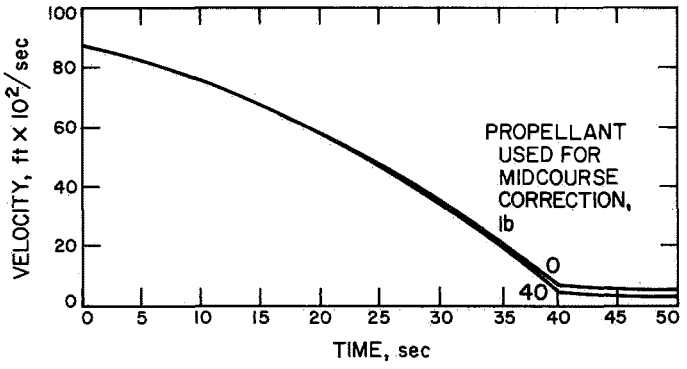



**Fig. XIII-26. Velocity vs time during retromaneuver**

and shielding requirements were apparent. Subsequently the plan was made to use the non-RTG system on the first four spacecraft and the RTG system on the last three.

The lunar-night survival plan for the A-25 spacecraft was merely to heat the thermal compartment so that each compartment maintained a temperature of 0°F throughout lunar night. First estimates placed total compartment heat losses during the lunar night at about 9.5 W, including a 3.3-W allowance for losses through wiring penetrations. Since storage batteries were designed to deliver 15 W for 350 hr when fully charged, sufficient energy would be available to satisfy the survival goal. Further analysis led to the recognition that heat losses through electric wiring

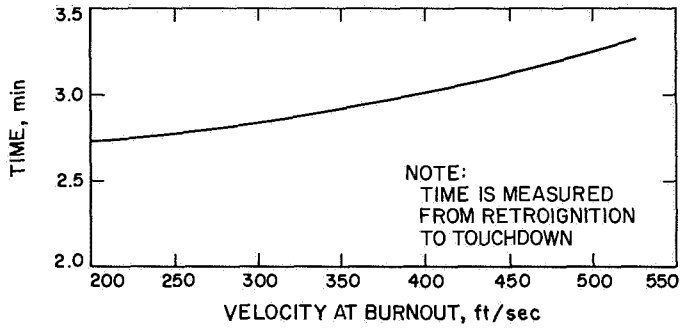



**Fig. XIII-27. Nominal descent time from retroignition to touchdown vs retrorocket burnout velocity**

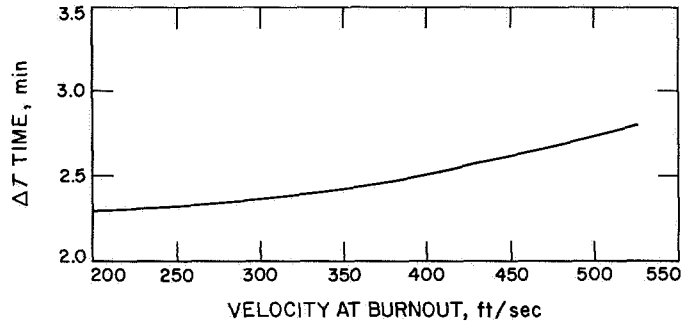



**Fig. XIII-28. Time difference between unbraked impact and touchdown vs retrorocket burnout velocity**

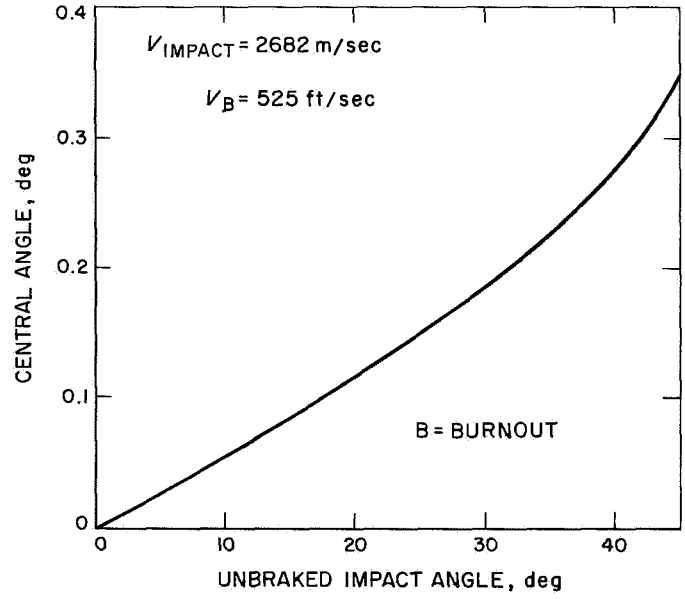



**Fig. XIII-29. Central angle difference between unbraked impact point and touchdown point as function of unbraked impact angle**

cables that penetrated the compartment walls would be closer to 7 W. Even with the additional loss, a small margin existed, ensuring the survival of A-25 through the lunar night.

When design of the A-25 was cancelled because of launch vehicle weight constraints, the RTG system was abandoned. Both the A-21 and A-21A designs included thermal compartments virtually identical in size and insulation to the compartments designed for A-25, thus lunar-night thermal losses were expected to be similar. The most severe effect of design change was removal of one of the batteries in the power system and hence half the energy available for lunar-night survival operations. Compartment thermal losses were estimated to be approximately 18 W during the lunar night, which far exceeded the electrical energy available for heating. Because of energy deficiency, compartment temperatures were expected to fall below −150°F.

*b. Final spacecraft design and survival plans.* Two approaches to lunar night survival of the A-21 spacecraft were examined. The first was to reduce compartment losses to a level which the battery was capable of supporting; the second was to try to develop an optimum procedure for bringing the spacecraft through the lunar night period while minimizing the probability of equipment failure during that period.

Significant results of the investigation of compartment losses and battery capability were:

(1) Redesign of the cable penetration interfaces in the thermal compartments could reduce thermal losses.

(2) Capacity of the battery was found to vary markedly between 0 and 40°F. The recoverable energy from a fully charged battery at 40°F could be as great as 40% more than from the same fully charged battery at 0°F.

Subsequently, cable penetration interfaces and thermal switch and heater assembly control adjustments were modified.

Utilizing all available characteristic data on compartment thermal losses and the spacecraft electrical power system, efforts were directed toward development of effective operational procedures for enhancement of spacecraft lunar night survival. Results of these efforts indicated that considerable additional system failure mode data was needed to establish an optimum procedure for survival at a reasonable confidence level.

After touchdown of *Surveyor I*, a lunar-night survival plan was prepared which included a requirement to retain as much charge as possible in the battery at the time of spacecraft shutdown. Lunar-night operations were designed primarily to acquire as much data as possible concerning compartment thermal losses and the lunar-night thermal environment and, secondarily, to maximize night-survival probability.

Success of the *Surveyor I* mission stimulated further interest in measures that would maximize night survival for future spacecraft. Special studies were conducted to determine survival improvements which could possibly be implemented on subsequent flight spacecraft. The scope of these studies included the effects on survivability of radioscope heaters in the compartments, further reduction of compartment thermal losses, and power system modifications. Low-temperature performance of the power, telecommunications, and television subsystems, related control items, and components, materials, and processes was considered; failure-mode effects of equipment not used after touchdown and their interface with the command decoding and signal processing subsystem were also considered. Recommending immediate procurement of radioisotope heaters for thermal compartments for SC-7, the study pointed out that the probability of survival without the addition of heaters in the compartment was difficult to determine. Although spacecraft survival was considered reasonable, not enough was known about the very-low-temperature performance of the spacecraft design and the effect of variations in components and production techniques from spacecraft to spacecraft for a specific statement of survival probability. However, it proved unfeasible to incorporate isotope heaters in SC-7, because they could not be procured in time to avoid jeopardizing the schedule and confidence in the spacecraft integrity.

Based on combined flight experience and survival studies, a lunar-night survival procedure was established for SC-5, which included the following five phases:

(1) Phase 1 was the first lunar day operating period, from approximately three days before lunar sunset. During this period efforts were expended to maximize battery energy at lunar terminator.

(2) Phase 2 was that period of approximately 24 hr after sunset, during which actual compartment losses were determined and the time to final spacecraft shutdown was computed. The duty cycle of compartment A heater for phase 3 was also determined during phase 2. Instead of using the compartment heater to provide desired electrical dissipation, power and thermal specialists elected to cycle spacecraft electronics.

(3) Phase 3 was the period from end of phase 2 until spacecraft shutdown. Compartment A temperature was maintained between 0 and 20°F, with the goal of operating toward 20°F. Compartment B temperature was maintained at 10 ±10°F. Periodic interrogation of spacecraft took place at least every 8 hr. This interrogation cycle was adjusted to coincide with computed duty cycle of compartment A heater or the spacecraft electronics as determined in phase 2.

(4) Phase 4 was the period of spacecraft cooldown and warmup starting at spacecraft shutdown and ending at first acquisition attempts on second lunar day. During this period spacecraft temperatures were uncontrolled.

(5) Phase 5 was the period beginning with attempts to acquire the spacecraft on second lunar day and ending when battery temperature had reached 40°F and compartment B temperature was 10°F or greater.

The choice of 20°F as the steady-state temperature for compartment A reflected a lowering of the thermal switch opening temperature for this spacecraft.

The plan of operation was to extend phase 3 until the battery was depleted by 115 A-hr from the fully charged state. Objectives of the plan were to maintain temperatures in the compartments within the prescribed operating range of the enclosed equipment during the lunar night and, at the same time, maintain sufficient battery charge to prevent mechanical damage by freezing.

Lunar night operations and survival performance for the landed *Surveyors* are summarized in Subsection E (Spacecraft System Performance).

### 7. Sterilization Considerations

Initially, the *Surveyor* design specification included the NASA requirement that the spacecraft be sterilized to reduce the probability of introducing viable organisms onto the surface of the moon.

The sterilization plan (Ref. XIII-8), as visualized early in the program, is illustrated in Fig. XIII-30. This plan incorporated three methods of sterilization: heat, liquid sterilants, and ethylene oxide/Freon 12 gas.

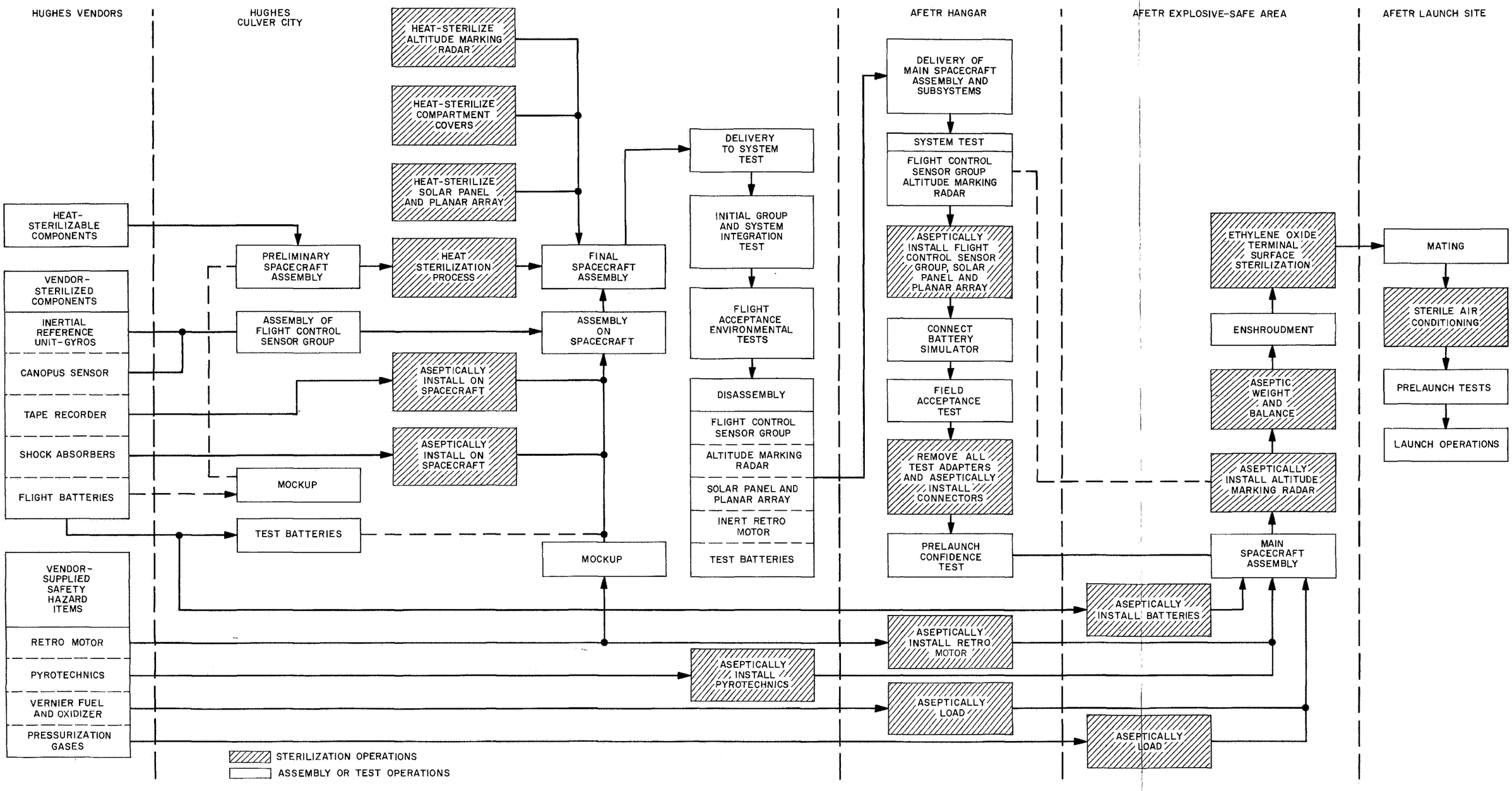



**Fig. XIII-30. System plan for spacecraft sterilization (heat, liquid, and gas)**

Heat sterilization by exposure to 125°C for 24 hr was established as the method to be used for internal sterilization. In the case of certain vital components which could not withstand heat sterilization, special techniques, including aseptic assembly with the aid of liquid sterilants, were to be used in an effort to retain the phisolosphy of internal sterilization. In addition, exposure to 12% ethylene oxide/88% Freon gas at 30–50% relative humidity and 100°F for 11 hr was defined for surface sterilization of the assembled spacecraft after final encapsulation in the nose fairing.

Each sterilization process had a success probability function with several independent variables. The best known process with a high success probability was that of thermal exposure. A high probability of sterilization success could be realized by subjecting the surfaces of an object bearing only a relatively few viable cells to special liquid sterilants or to the ethylene oxide gas sterilization process. However, the probability of these processes sterilizing large populations of spores deposited on the object was low.

The primary process of heat sterilization was to be accomplished on the spacecraft subassemblies of all items that could withstand the thermal process. However, studies had indicated that unless the complete *Surveyor* spacecraft was sterilized by thermal exposure while encapsulated in the nose fairing, the probability of launching a sterile vehicle would be low. Early component compatibility studies indicated that complete assembly of the spacecraft (with its 29,000 components) and total spacecraft heat sterilization did not appear to be feasible. Thus the sterilization plan included certain subsystem aseptic assembly steps before some of the subsystems could be integrated in the spacecraft. Subsystems requiring special sterilization processes included the flight control sensor group, tape recorder (originally planned), television cameras, batteries, shock absorber columns, and retrorocket.

Following internal sterilization, the spacecraft with all subsystems installed would undergo extensive system functional and environmental tests for complete system checkout. After system integrity was verified, those units sensitive to normal transportation environments were to be removed from the spacecraft and shipped to AFETR in protective containers. Assembly of these items into the spacecraft at AFETR would have then required aseptic techniques using liquid sterilants. To assure that transportation environments were not detrimental to the spacecraft, field-acceptance tests were to be performed on the spacecraft, using system test equipment. Once system integrity was verified, the system test adapters were to be removed and the equipment connectors aseptically installed. In the explosive-safe area at AFETR such safety hazard items as pyrotechnics, retrorocket, vernier engine fuel, oxidizer, and gases were to be aseptically installed and made ready for flight. The spacecraft would then be encapsulated within the nose fairing, and the final ethylene oxide gas terminal surface sterilization process would be performed using a mobile sterilization unit.

In December 1962, NASA relaxed the sterilization requirement for lunar missions. Thereafter, care was taken throughout the fabrication and testing of the *Surveyor* spacecraft to prevent physical contamination of the spacecraft. Wrapping of hardware with protective coverings, extensive use of dust covers and shields, and final cleaning operations were some methods used to assure a low particle count of contaminants before launch.

## D. System Design Analysis and Verification Using Simulation Models and Programs

The qualification and flight acceptance of the *Surveyor* spacecraft in system test is discussed in detail in Section XI. However, before the Spacecraft Systems test phase was reached, considerable effort was expended to verify Spacecraft System design by use of various simulations and analytical models discussed under the following paragraphs.

### 1. Mission Simulation Program

Digital computer simulation of a *Surveyor* flight, beginning at spacecraft separation from the *Centaur* and extending to lunar touchdown, had been designed, developed, and was used to study various aspects of the Spacecraft System design. This simulation, based on the Monte Carlo technique, used the best model of the system available, which characterized events from earth injection to lunar touchdown. In particular, the model included *Centaur* guidance system injection statistics, *Surveyor* midcourse guidance and maneuver logic, *Surveyor* terminal-descent guidance and maneuver system, the DSIF tracking statistics, and *Surveyor* spacecraft mechanization errors. This simulation, the most complete model of a *Surveyor* flight available, was developed mainly for use as a design and analysis tool.

The parameters describing a particular flight trajectory, spacecraft, etc., were correlated, and the statistics of key

system parameters were generated. These statistics described such items as probability of mission success, landing accuracy, midcourse propellant distribution, and probability of violating terminal descent sensor constraints.

Various system parameters were calculated for use as inputs to the program and the resultant statistics were studied as the inputs were varied. By use of this method each input parameter could be optimized. (Various parameters used by *Surveyor* operational programs had been optimized in a manner similar to that used for optimizing a single system parameter.)

The *Surveyor* vernier system propellant required to account for terminal phase uncertainties had been ascertained with the aid of this program. In addition, this program was used during *Surveyor* flights in real time as a decision-making tool and for performing error analyses during the flights.

The choice of the Monte Carlo technique in designing lunar mission simulation was predicated on various system characteristics. Chief among the reasons for selecting the Monte Carlo approach for the *Surveyor* system were:

(1) When dimensionality of the multivariable probability-density functions exceeded three or four, numerical integration techniques became difficult and impractical to use. Monte Carlo techniques circumvented this difficulty.

(2) The inherent system complexity and large number of parameters made it extremely difficult, if not impossible, to develop a complete analytical model of the system for predicting statistics.

The flight of a spacecraft was simulated and, at appropriate times, random errors were generated and inserted in the simulation, inducing changes in system parameters of interest. By repeating this procedure many times, the system parameter distributions obtained could then be used for analysis in the classical statistical fashion to generate such items as means and variances.

The simulation program utilized mapping matrix operations based on the linear perturbation theory to move from earth injection to midcourse and from midcourse (after correction) to the predetermined descent point. Computation of midcourse correction was based on actual *Surveyor* midcourse guidance logic. The terminal descent phase consisted of closed-form computations which resulted in computation times that were feasible for repeated calculation. Computations were based on the assumption of a flat moon and a piecewise uniform gravitational field, with suitable average values of lunar g used in various portions of the descent. Additional assumptions were that: (1) the alignment phase followed retrorocket burnout, (2) the vernier descent contour was a parabola in range and velocity, rather than a sequence of straight lines, and (3) the trajectory followed the descent contour exactly. At appropriate points, tests for mission failure were made, based on radar and propulsion system characteristics, fuel usage and touchdown dynamics.

### 2. Flight Control Simulation Programs

*a. Flight control analog computer simulation (Fig. XIII-31).* Equations of motion and all control loops involved in the vernier phase of the *Surveyor* terminal descent were mechanized. Simulation was limited in slant range from 1000 ft to touchdown and could run with or without radar noise, with different vernier engine characteristics, and with varying initial conditions of flight. Simulation differed from actual spacecraft operation in minor details of spacecraft dynamics and control-loop cross coupling. Since the flight control system was closed-loop (error-nulling), analog component accuracy did not affect the accuracy of the simulation. The most critical function was generation of the descent segments and here

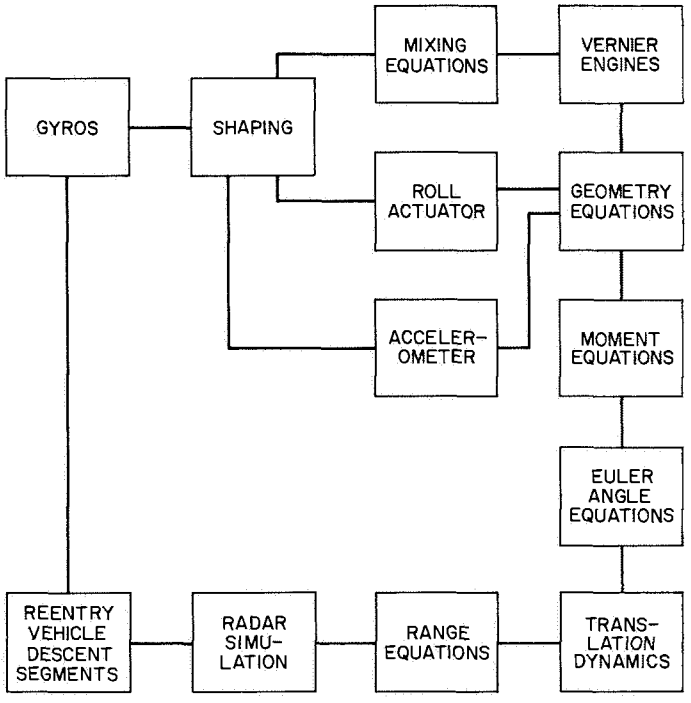



**Fig. XIII-31. Generalized block diagram of analog six-degree-of-freedom model**

0.1% accuracy was achieved (vs 2% accuracy in spacecraft hardware).

The following briefly describes the items mechanized:

(1) Equations used included moments, mixing, transformations, dynamics, and range.

(2) Component transfer functions used included radar filter, vernier engines (including hysteresis and maximum-thrust limit effects), roll actuator, accelerometer, shaping amplifier and command limits, velocity loop (range–velocity segments), doppler loop, and roll-shaping electronics.

(3) The simulation initial conditions were three vernier engine gains, initial angle off-vertical, slant range along Z axis; X, Y, and Z velocities; and radar noise level. The outputs included three vernier engine thrusts, acceleration command, pitch, yaw gyro outputs, Euler angle about final Z axis, pitch gyro command rate, Euler angles about X and Y axes, angular rates about spacecraft X and Y axes.

***b. Flight control digital simulation.*** A 5-deg-of-freedom simulation (Fig. XIII-32) had been developed for use on an IBM 7094 digital computer. The roll control loop did not materially affect the use of the model since many studies had been omitted. The main advantage of digital simulation was that various probability-density functions of certain error signals could be specified. The model has been programmed using MIMIC, a general purpose

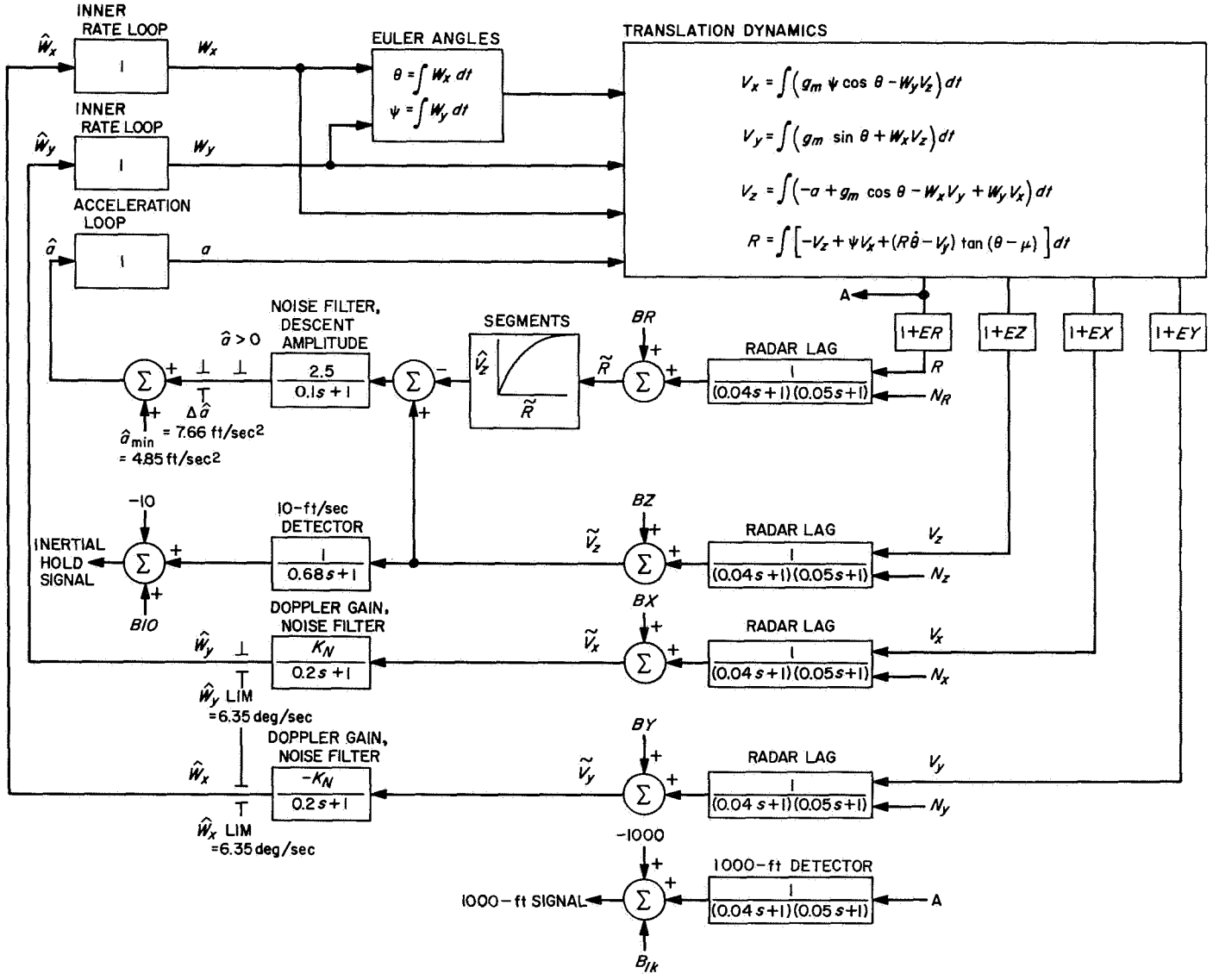



**Fig. XIII-32. Bias closed loops of Surveyor five-degree-of-freedom simulation (nominal values)**

simulator program. Inputs to this simulation included constant initial conditions, initial Euler angles, and initial range and initial velocity components. A total of 27 errors and biases could be varied on each run.

### 3. Thermal Models

Thermal problems could be approached from two levels: thermal subsystem and thermal subunits. Premission predictions resulted from the use of thermal models and tests at the subunit level. When compared to flight data in a few cases, a thermal model (Fig. XIII-33) was employed, but for the most part the effort was conducted by manual calculation.

For a particular thermal model, data input requirements included any changes to the model in geometry, heat capacitance, conductance, etc. Input parameters included initial temperatures, the solar constant, and all heat dissipations.

Accuracy was a function of input data to a particular thermal model. Where computer programs were not used, test data were used. Also, boundary conditions from one thermal model or calculation to the next affected accuracy and completeness of the analysis. Methods of comparing data varied as a function of the subunit and ranged from solar-thermal-vacuum (STV) test data to thermal model data for establishment of predictions. The predictions were compared to flight data which, in some cases, were used in a thermal model or used to update the validity of a thermal model.

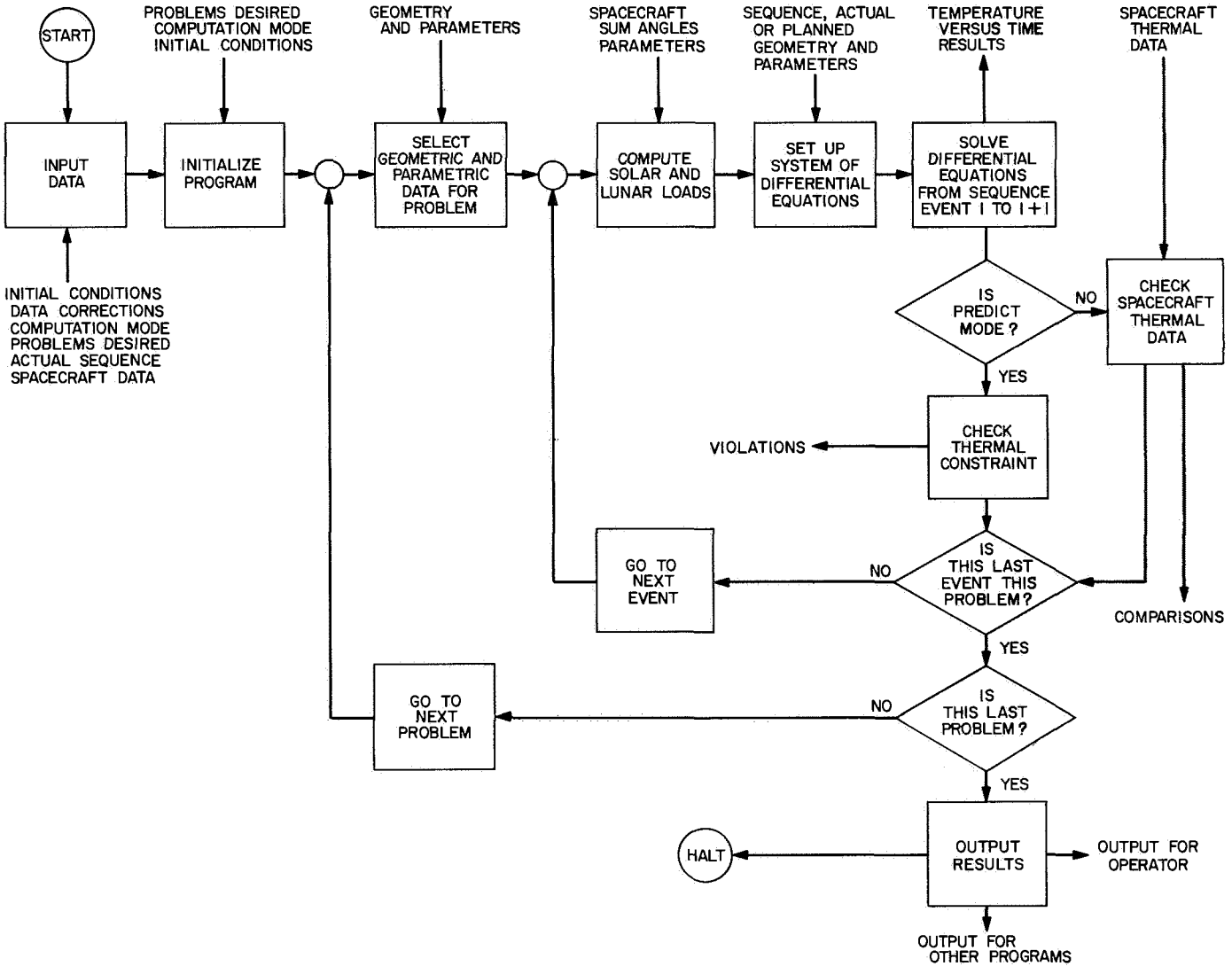



**Fig. XIII-33. Thermal management program functional flow diagram**

#### 4. Electrical Power Simulation Program

A power computer program, which simulated and solved the power subsystem transcendental equations, formed the basis of a power management program for the spacecraft. The power management program utilized energy profiles in conjunction with characteristics of such individual items as the predicted efficiencies of the boost-regulator and battery charge regulator to predict the profiles of the regulated and unregulated power demands (Fig. XIII-34).

Data input required command lists, processed spacecraft data from an engineering data reduction program, and the accuracies and standard deviations associated with the program data.

Calculated booster-regulator and battery charge regulator efficiencies and power profiles were compared

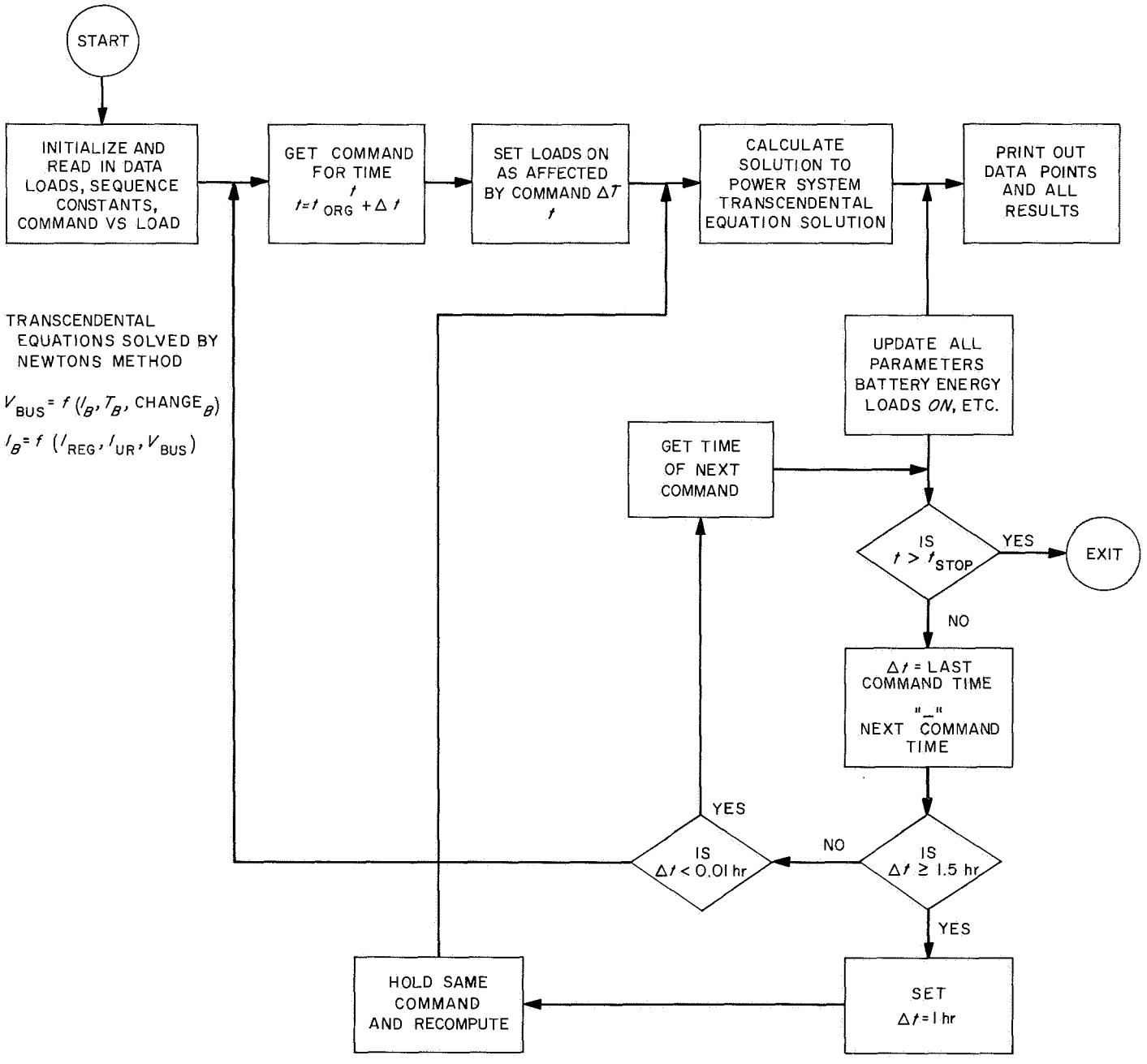



**Fig. XIII-34. General flow diagram of power management program**

to predicted values, test data, and specification data. Accuracy of calculations was dependent, primarily, on error growth associated with energy bookkeeping and load sharing assumptions between battery or batteries, solar panel outputs, etc. Instantaneous temperature effects of cyclic thermal loads were approximated in that only average temperatures were considered.

### 5. Terminal Descent Phase Simulation Programs

*a. Retrorocket.* Two procedures existed for constructing the retrorocket thrust curve. A descent-operations phase program consisted of a retromaneuver simulation which used a normal input thrust-time curve to compute simulated doppler data which would be received by an earth tracking station. This program computed the best-estimate curve from doppler data by perturbing the typical curve and using an iterative procedure until the simulated data agreed with the actual.

A thrust-time curve (TTC) program computed the retromaneuver profile from retrorocket accelerometer data by numerically integrating Eq. (14) for total thrust and then subtracting approximate vernier thrust.

$$T_{\text{total}} = \frac{a_{\text{total}}}{g}\left(W_0 - \int_0^t \frac{T_{\text{total}}\,dt}{I_{sp}}\right) \qquad (14)$$

If normal telemetry data existed in addition to doppler data, the descent operation program could compute a thrust curve which yielded a $\Delta V$ for the retrorocket plus verniers to within about 0.1% of the actual.

If only doppler data existed, this program could be operated only to within a thrust certainty of 290 lb. With telemetry and doppler data available, average computed thrust values between data points could be computed accurately to 20 lb. Accuracy in transient regions near ignition and tailoff was questionable because data were too widely spaced.

With normal telemetry data available, the **TTC** program could compute a thrust curve which also gave a $V$ to within 0.1% of the actual. Particular thrust values were accurate only to within 200–300 lb, because accelerometer hysteresis and stiction, along with telemetry bias and scale factor errors, made data difficult to correct.

Data inputs to the **TTC** program included retrorocket accelerometer (FC-32) flight data, spacecraft weight at retroignition, and other data from the midcourse and terminal guidance (MTG) operations programs.

Data inputs to the descent operations program included flight doppler data, in- and out-of-plane thrust misalignment angles, and telemetry data, as available. Other sources were MTG data, such as ignition position and velocity vectors.

The descent operations program computed the thrust–time curve by comparing simulated model data to actual flight data and perturbing the normal thrust curve until the model data agreed with the actual, whereas the accelerometer program used only a single comparison procedure.

*b. Six-degree-of-freedom terminal descent digital simulation.* The six-degree-of-freedom model was a digital simulation of terminal descent from vernier ignition to touchdown. It was used in conjunction with a Monte Carlo program, to calculate burnout dispersions. One of the prime uses of this program was for analysis of the overall terminal trajectory (Fig. XIII-35).

In general, the model was made as complete as possible to produce a truly faithful reproduction of a typical *Surveyor* descent. The following were typical of the corrections or calibrations that could be specified:

(1) Initial center-of-gravity offset

(2) RADVS antenna misalignments

(3) RADVS tracker bias errors

(4) RADVS signal-gain degradation

(5) Gyro torquer scale-factor errors

(6) Vernier thrust gain variations

The model was programmed on an IBM 7094 digital computer. The 7094 mechanization included the following general subroutines:

(1) Data block. Used to initially enter any spacecraft correction factors or other parameters.

(2) Initialization block. Accepted basic initial condition inputs to the model (body Euler angles, spherical position coordinates, velocity magnitude and direction) and converted as necessary.

(3) Main control block. Controlled sequence of computational blocks.

Computations were performed by the following subroutines, or blocks:

(1) Dynamics block. The spacecraft inertia tensor was computed within this block. In computing inertias of thrust and angular acceleration components, rigid body dynamics were assumed.

(2) Rotate block. The output was the coordinate transformation matrix between a moon-centered inertial coordinate system and the spacecraft axes.

(3) Acceleration, velocity, and range (AVR) block. The basic thrust acceleration in body coordinates was transformed within this block to acceleration expressed in inertial coordinates. Velocity and range were derived and expressed in both inertial and spacecraft coordinates. A nonrotating moon with constant gravitational acceleration (i.e., altitudes independent) was assumed. Various coordinate transformations relating the inertial coordinates, body coordinates, local vertical direction, and velocity direction were computed within this block.

(4) Radar block. True velocity in body coordinates was transformed to components along the radar beam axes. An option was provided in the block to compute power received for each beam as a function of velocity along the beam, beam incidence angle, lunar reflectivity, and RADVS performance parameters to test for tracker lock on. If one or two velocity trackers were not in lock, the system (and program) would operate in the conditional reliable-operate mode. Under these conditions, the apparent velocities (occurring as output from this block) could be significantly different from their corresponding true input values. Under fully reliable-operate conditions, the apparent and true velocities will differ only slightly (due to the effects of the RADVS lags).

(5) Control block. Flight control system time constants less than 1/30 sec were not included. In all other

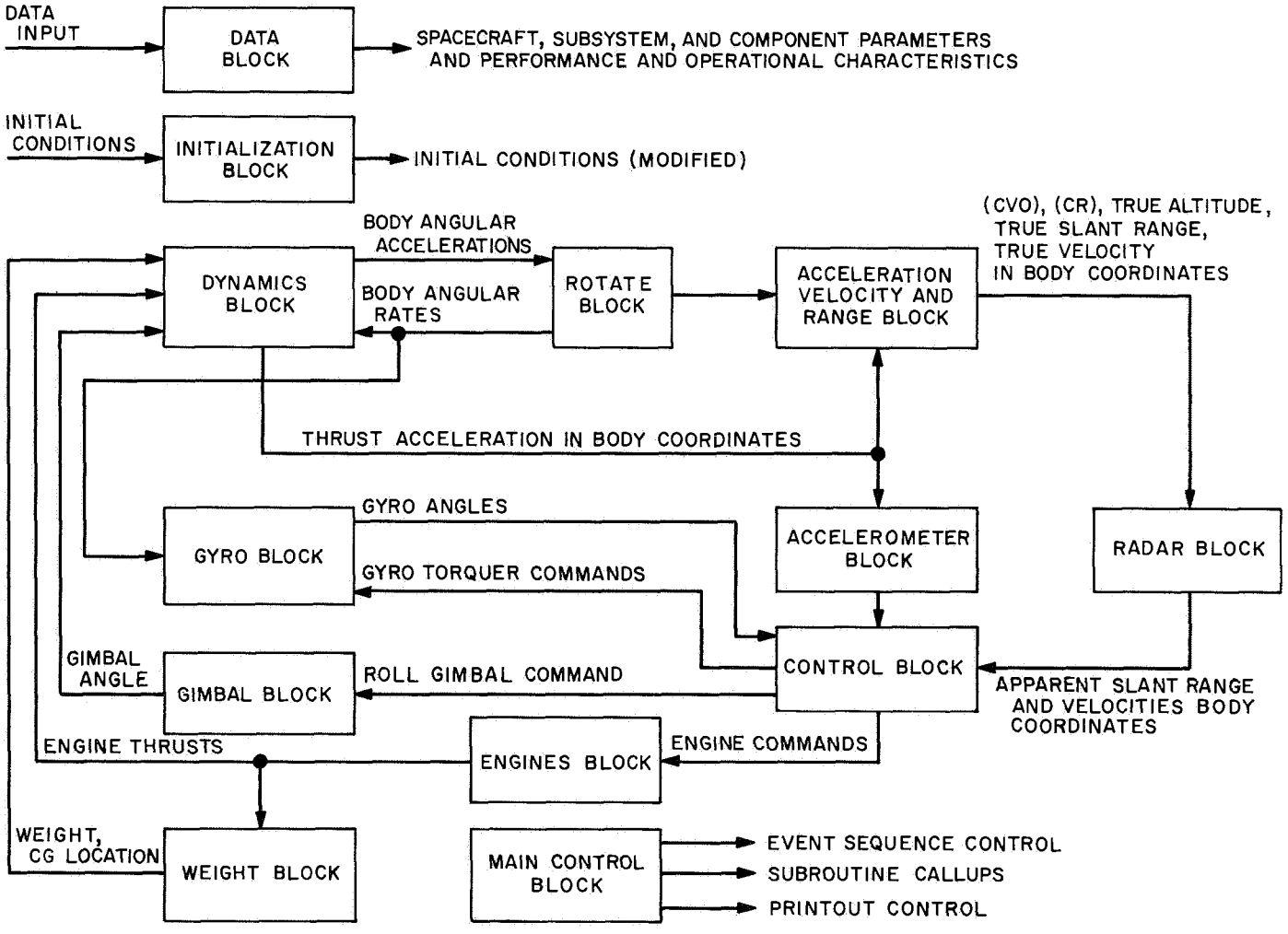



**Fig. XIII-35. Six-degree-of-freedom computation loop**

respects, the equations for this block have been written to preserve as much as possible the steady-state and transient stability characteristics of the present control system design.

(6) Weight block. Fuel weight losses of the tanks associated with each of the vernier engines were computed separately, and overall spacecraft center-of-gravity drift was determined. Inert losses were also accounted for in this block.

### 6. Landing Dynamics Model

A rigid body colliding with a surface of assumed properties and starting from given initial conditions was assumed for the landing dynamics surface analysis models (Fig. XIII-36). There were three basic types of models, corresponding to the following surface conditions:

(1) Bidimensional hard surface.

(2) Tridimensional hard surface.

(3) Bidimensional soft surface.

All models allowed for deflection of the legs, and the hard surface models included the crushing of footpads and crushable (body) blocks.

All models had digital computer mechanizations, so that numerous cases could be rapidly run. Time granularity for the approximate iterative solutions used was 2 msec.

The following initial conditions for the falling body (spacecraft) were input, in addition to the surface-type selection and specification:

(1) Longitudinal velocity.

(2) Lateral velocity.

(3) Incidence angle.

(4) Surface slope angle.

(5) Friction coefficient.

The main output of the model was a force–time history for each leg, which could be directly compared with the reduced strain gage oscillographs obtained from test or flight. Usually a series of model runs was made to determine which variation of initial parameters most nearly matched the strain gage data.

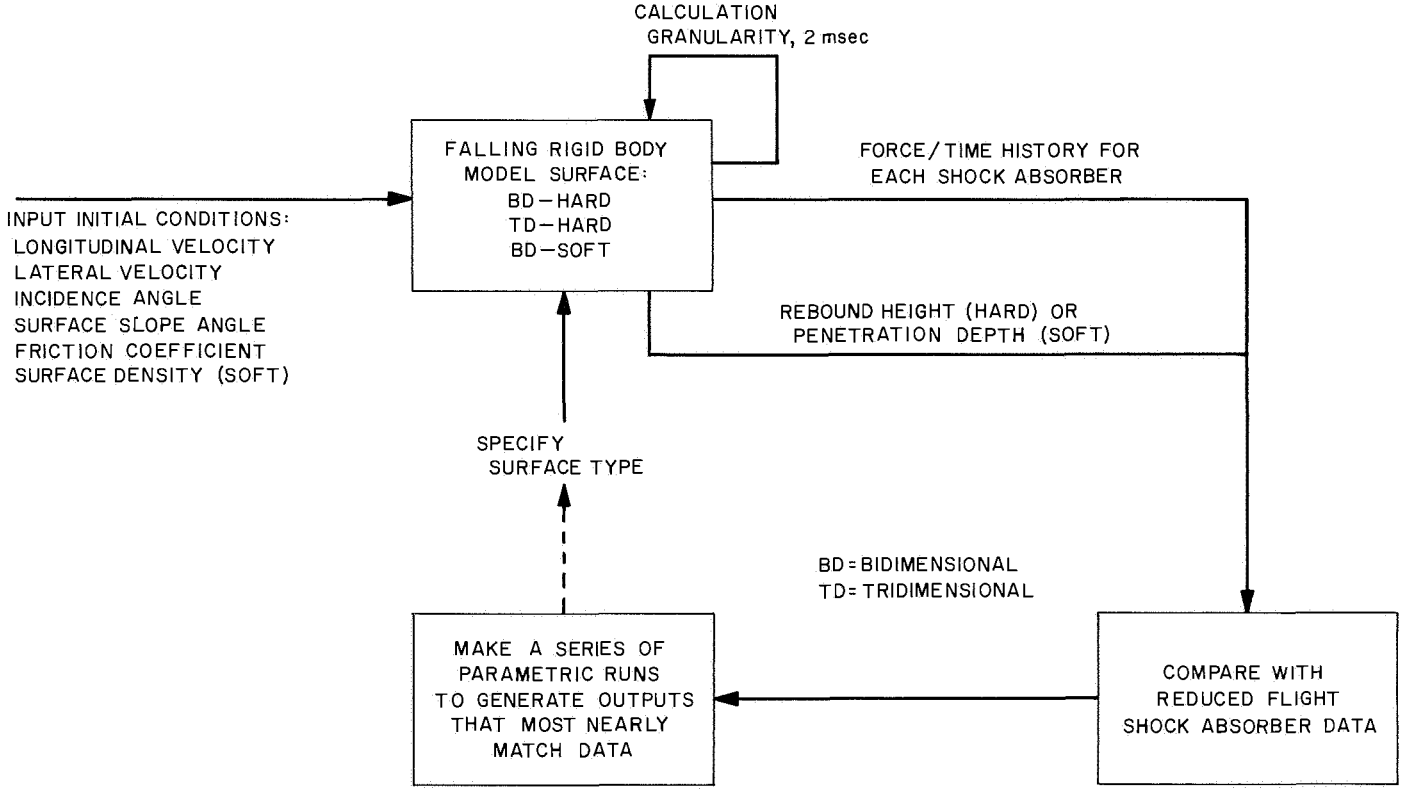



**Fig. XIII-36. General diagram of landing dynamics space model and analysis procedure**

### 7. Postlanding Attitude Assessment Program

No actual model was associated with attitude assessment; rather, there was a best-fit solution to a geometric problem. Typically the best transformation matrix between selenographic and spacecraft coordinates was found (Fig. XIII-37).

The initial estimate of the transformation matrix was calculated from a postlanded attitude assessment program. By knowing the landing coordinates of the spacecraft, the spacecraft attitude was then determined by establishing two vectors (sun and earth) to the selenographic and spacecraft coordinate systems. The two vectors were combined and resolved to yield the spacecraft attitude in selenographic coordinates.

The spacecraft–sun vector was established by positioning the solar panel until the output of the secondary sun sensor, which was located on the solar panel face, was maximum. The solar panel position, in spacecraft coordinates, was then determined from telemetered position potentiometer data. The spacecraft–earth vector was established by positioning the planar array until signal from the spacecraft was maximized. Telemetered data were then used to determine the position of the planar array in spacecraft coordinates.

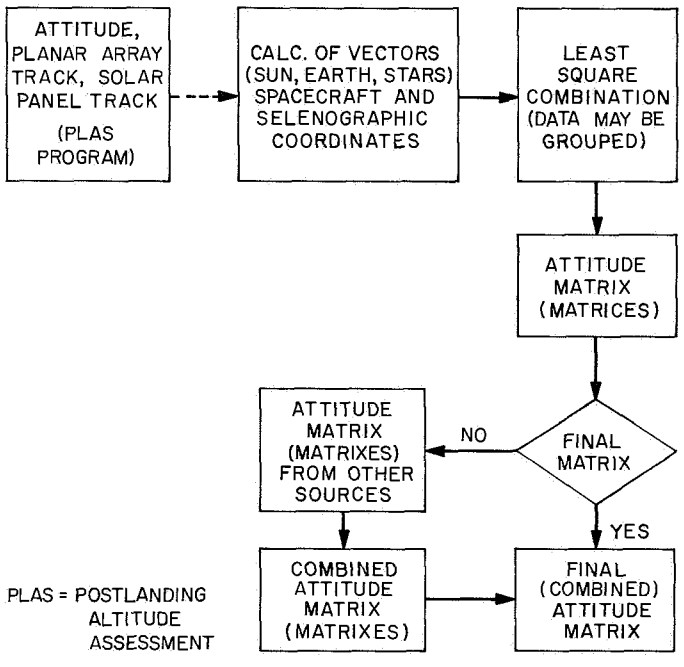



**Fig. XIII-37. Idealized block diagram of attitude matrix assessment**

The combination of more than two vectors during a calculation did not result in the averaging process that results when the attitude matrix is recovered by two vectors and then averaged with another attitude matrix recovered from a different pair of vectors.

In contrast, a least-squares fit was done upon the data set of vectors to obtain a best-fit transformation matrix.

Using as input a least-squares best estimate of the sun, earth, and star or stars, vectors in selenographic and spacecraft coordinates, an initial estimate of the spacecraft attitude was determined from the IBM 7094 postlanding attitude assessment program, and an improved least-squares attitude assessment was obtained using a GE 235 computer program.

## E. Spacecraft System Performance

The overall objectives of the *Surveyor* Project were met by five successful spacecraft flights (*Surveyors I, III, IV, VI,* and *VII*), which were successfully soft-landed on the lunar surface between May 1966 and January 1968. The successful soft landing of *Surveyor I* confirmed spacecraft design and soundness of the operational procedures. It also demonstrated that the *Atlas/Centaur* was a capable launch system, that transit maneuvers and soft landing were possible, and that the spacecraft communications interface with the Deep Space Network (DSN) was capable of providing continuous in-flight and postlanding engineering and science data. A summary of system performance is included in Table XIII-9.

Spacecraft postflight analyses (Refs. XIII-9 through XIII-22) were directed toward evaluation of system flight performance and timely recognition and analysis of spacecraft behavioral anomalies. In addition to postflight analyses, various studies were conducted throughout the program to fully understand and utilize *Surveyor* mission and spacecraft capabilities.

The unique performance on some of the missions is described in greater detail in Subsections E-2 through E-6, following a brief summary of the performance of each spacecraft, below.

### 1. Mission Performance Summary

Launched on May 30, 1966, *Surveyor I* achieved all its objectives. The only significant spacecraft anomaly in the mission was a failure that occurred in the extension mechanism of omniantenna A during the transit phase.

## Table XIII-9. Summary of Spacecraft System performance during flight phase of *Surveyor* missions

| Parameter | *Surveyor* mission | | | | | | |
|---|---|---|---|---|---|---|---|
| | *I* | *II* | *III* | *IV* | *V* | *VI* | *VII* |
| **Liftoff through sun acquisition phase** | | | | | | | |
| Liftoff time, GMT | 14:41:01 May 30, 1966 | 12:32:00 Sep 20, 1966 | 07:05:01 Apr 17, 1967 | 11:53:29 Jul 14, 1967 | 07:57:01 Sep 8, 1967 | 07:39:01 Nov 7, 1967 | 06:30:01 Jan 7, 1968 |
| Spacecraft separation, sec from liftoff | 757 | 753 | 2093 | 757 | 1166 | 1529 | 2115 |
| Time to null angular separation rates to 0.1 deg/sec, sec | ≤15 | <4 | <11 | <13 | <20 | <17 | <26 |
| A/SPP solar axis deployment time, sec | 617 | 360 | 358 | 348 | 298 | 337 | 323 |
| Spacecraft mass properties at separation | | | | | | | |
| Weight, lb | 2193 | 2204 | 2281 | 2295 | 2217 | 2220 | 2289 |
| CG location, in. | | | | | | | |
| X-axis | −0.12 | −0.10 | +0.06 | +0.04 | −0.07 | −0.06 | +0.34 |
| Y-axis | −0.09 | +0.01 | +0.18 | −0.19 | +0.78 | +0.73 | +0.11 |
| Z-axis | 59.18 | 59.16 | 58.95 | 58.88 | 59.69 | 59.7 | 59.7 |
| Moment of inertia, slug-ft$^2$ | | | | | | | |
| $I_{xx}$ | 195 | 200 | 202 | 204 | 210 | 210 | 215 |
| $I_{yy}$ | 192 | 196 | 198 | 200 | 211 | 211 | 213 |
| $I_{zz}$ | 213 | 215 | 223 | 225 | 211 | 211 | 216 |
| Sun acquisition maneuver | | | | | | | |
| Roll angle, deg | −87 | −71.5 | −181 | −59.4 | −342 | −264 | −224 |
| Yaw angle, deg | +99 | +15 | +38 | +42.1 | +18.0 | +22 | +37 |
| Total time, sec | 372 | 174.8 | 438.2 | 203 | 722 | 572 | 523 |
| **Canopus acquisition and coast phase** | | | | | | | |
| Mean roll rate during Canopus roll maneuver, deg/sec | 0.5004 | 0.4998 | 0.5011 | 0.5003 | 0.5007 | 0.5009 | 0.5018 |
| Total magnitude of Canopus roll maneuver, deg | +581 | +960 | +565 | +571 | +539 | +658 | +629 |
| Method of Canopus lockon | By earth command | By earth command | Automatic | Automatic | Automatic | Automatic | By earth command |
| Effective gain of Canopus sensar, relative to Canopus intensity | 1.5 | >1.5 | 1.03 to 1.22 | 1.16 | 1.32 | 1.10 | >1.5 |
| Attitude errors after Canopus acquisition | | | | | | | |
| Average error from sunline, deg | | | | | | | |
| Pitch | −0.058 | −0.07 | 0 | +0.009 | Very small | Very small | Very small |
| Yaw | −0.053 | −0.1 | +0.02 | +0.08 | | | |
| Roll | −0.055 | −0.08 | −0.06 | 0 | | | |
| Average error from Canopus line of sight, deg | | | | | | | |
| Pitch | −0.06 | −0.07 | 0 | 0 | Very small | Very small | Very small |
| Yaw | −0.05 | −0.1 | +0.02 | 0 | | | |
| Roll | −0.06 | −0.08 | −0.06 | +0.10 | | | |
| Limit cycle in optical mode | | | | | | | |
| Average roll amplitude, deg | 0.44 | 0.44 | 0.55 | 0.6 | 0.46 | 0.41 | 0.43 |
| Average pitch amplitude, deg | 0.47 | 0.45 | 0.51 | 0.44 | 0.37 | 0.52 | 0.44 |
| Average yaw amplitude, deg | 0.46 | 0.37 | 0.54 | 0.41 | 0.50 | 0.52 | 0.38 |
| Average period, sec | 65 | 64 | 68.5 | 64 | | | |

## Table XIII-9 (contd)

| Parameter | Surveyor mission | | | | | | |
|---|---|---|---|---|---|---|---|
| | I | II | III | IV | V | VI | VII |
| **Canopus acquisition and coast phase (contd)** | | | | | | | |
| Limit cycle inertial mode | | | | | | | |
| Average roll amplitude, deg | 0.415 | 0.47 | 0.46 | 0.48 | 0.30 | 0.48 | 0.49 |
| Average pitch amplitude, deg | 0.443 | 0.42 | 0.48 | 0.46 | 0.31 | 0.37 | 0.39 |
| Average yaw amplitude, deg | 0.417 | 0.43 | 0.50 | 0.53 | 0.36 | 0.20 | 0.59 |
| Average period, sec | 50 | 61 | 68.5 | 61 | | | |
| Gyro drift, deg/hr | | | | | | | |
| Roll | 0.2 | −0.8 | +1.1 | −0.5 | +0.8 | −0.6 | +0.6 |
| Pitch | 0 | 0.2 | +0.6 | −1.0 | +0.6 | 0 | +0.2 |
| Yaw | 0.7 | +1.1 | −0.8 | +0.1 | −0.6 | +1.4 | 0 |
| **Midcourse correction phase** | | | | | | | |
| Pre-midcourse maneuvers, deg | | | | | | | |
| First maneuver | 86.6 roll | +75.4 roll | +56.7 roll | +72.5 roll | +71.9 roll | +91.8 roll | −3.1 roll |
| Second maneuver | 58.0 yaw | +110.6 yaw | −39.1 pitch | −64.3 yaw | −35.5 yaw | +127.4 yaw | +117.1 yaw |
| Vernier ignition time from liftoff, hr:min:sec | 16:04:02 | 16:28:02[a] | 21:55:01 | 38:36:33 | 17:48:01[a] | 18:41:01 | 17:00:09 |
| Duration of midcourse firing, sec | 20.81 | 9.8[a] | 4.24 | 10.48 | 14.22[a] | 10.24 | 11.36 |
| Midcourse velocity correction, m/sec | | | | | | | |
| Magnitude | 20.26 | 9.587[a] | 4.2 | 10.13 | 14.2[a] | 10.1217 | 11.082 |
| Error | −0.081 | | 0.176 | −0.17 | | +0.058 | +0.001 |
| Peak attitude transients at ignition, deg | | | | | | | |
| Roll | −0.43 | | −1.0 | | −0.88[a] | | |
| Pitch | 0 | | −0.125 | −0.17 | −0.24[a] | 0.17 | −0.08 |
| Yaw | −0.08 | | +0.30 | +0.19 | +0.08[a] | 0.17 | −0.20 |
| Peak angular error at shutdown, deg | | | | | | | |
| Roll | | | +0.58 | +1.18 | +1.2[a] | +0.77 | +0.32 |
| Pitch | | | +0.96 | +1.09 | +0.13[a] | −0.33 | +1.24 |
| Yaw | | | +1.97 | +0.10 | +0.50[a] | −0.47 | +0.70 |
| Engine shutoff impulse, lb/sec | | | | | | | |
| Engine 1 | 0.27 | | −0.31 | −0.18 | −0.06[a] | +0.085 | −0.144 |
| Engine 2 | −0.37 | | +0.42 | +0.03 | +0.05[a] | −0.09 | +0.259 |
| Engine 3 | 0.10 | | −0.11 | +0.15 | +0.01[a] | +0.015 | −0.115 |
| Shutdown angular rate, deg/sec | | | | | | | |
| Pitch | | | | +0.24 | +0.06[a] | −0.08 | +0.08 |
| Yaw | | | | −0.01 | +0.06[a] | −0.1 | +0.32 |
| **Terminal descent phase** | | | | | | | |
| Approach flight path angle, deg | 6.13 | [b] | 23.6 | 31.5 | 46.4 | 24.5 | 35.9 |
| Terminal attitude maneuvers, deg | | | | | | | |
| First maneuver | +89.3 roll | | −158 yaw | +80.8 roll | +73.8 roll | +82.0 roll | +80.5 roll |
| Second maneuver | +60.0 yaw | | −76.8 pitch | +92.7 yaw | +119.6 yaw | +111.8 yaw | +96.1 yaw |
| Third maneuver | +94.4 roll | | −64 roll | −25.4 roll | None | +120.5 roll | −16.5 roll |
| Ignition delay time, sec | 7.85 | | 5.09 | 2.73 | 12.33 | 5.900 | 2.775 |
| Retroignition delay time, sec | 1.1 | | 1.1 | 1.12 | 1.07 | 1.100 | 1.100 |

[a] Initial midcourse firing.
[b] *Surveyor II* mission was terminated prior to lunar encounter.

## Table XIII-9 (contd)

| Parameter | Surveyor mission | | | | | | |
|---|---|---|---|---|---|---|---|
| | I | II | III | IV | V | VI | VII |
| **Terminal descent phase (contd)** | | | | | | | |
| Retrorocket thrust to CG offset at retroignition, in. | <0.02 | [b] | 0.02 | | 0.05 | 0.04 | 0.04 |
| Peak attitude transient at retroignition, deg | | | | | | | |
| Roll | — | | −0.22 | 0 | −0.16 | −0.77 | −0.23 |
| Pitch | −0.41 | | −0.10 | −0.09 | +0.5 | −0.17 | −0.08 |
| Yaw | −1.03 | | 0 | −0.35 | −0.5 | −0.08 | −0.44 |
| Main retrorocket burn time[c], sec | 38.9 | | 41.02 | [d] | 38.56 | 37.37 | 42.86 |
| Maximum retrorocket thrust, lb | 9,900 | | 9,550 | 9,250 | 9,950 | 9,700 | 9,200 |
| Average attitude error during retro-maneuver, deg | 0.26 | | 0.34 | 0.17 | 0.30 | 0.8 | 0.27 |
| Start of RADVS control | | | | | | | |
| Slant range, ft | 27,820 | | 36,158 | [d] | 6,300 | 40,574 | 51,259 |
| Altitude, ft | 27,800 | | 32,900 | | 4,139 | 36,625 | 41,510 |
| $V_z$, ft/sec | 425 | | 462 | | +46 | 463 | 428 |
| $V_x$, ft/sec | 71.3 | | 171 | | −41 | 225 | −56 |
| $V_y$, ft/sec | −4.1 | | | | +50 | 0 | −132 |
| Total velocity, ft/sec | 430 | | 483 | | 79 | 515 | 452 |
| Flight path angle from vertical, deg | — | | 26.8 | | −35.67 | 8.1 | 18.1 |
| RODVS[e] acquisition | | | | | | | |
| Slant range, ft | 55,000 | | 63,900 | 78,000 | | 68,022 | 80,639 |
| Velocity, ft/sec | 3,280 | | 3,230 | 3,414 | | 3,202 | 3,267 |
| RORA[f] acquisition | | | | | | | |
| Slant range, ft | 36,000 | | 43,700 | [d] | | 35,924 | 41,673 |
| Velocity, ft/sec | 690 | | 640 | | | 515 | 452 |
| Loss of lock of RADVS beams due to retrorocket case ejection | beam 3 once | | Beam 4 once | | Beams 4, 3 once | None | Beam 1 once |
| Due to other causes | None | | Beams 3, 4 once | | None | None | None |
| Programmed descent contour acquisition | | | | | | | |
| Slant range, ft | 18,000 | | 22,300 | | 806 | 24,730 | 20,246 |
| Velocity, ft/sec | 442 | | 495 | | 97 | 522 | 464 |
| 1000-ft mark | | | | | | | |
| Velocity, ft/sec | 103 | | 103 | | 96 | 106 | 102 |
| Attitude from vertical, deg | 1.1 | | 0.5 | | −7.5 | 1.0 | 1.6 |
| Time from 1000-ft mark to 10-ft/sec mark, sec | 18.2 | | 17.6 | | 17.4 | 17.1 | 16.9 |
| 10-ft/sec mark | | | | | | | |
| Slant range, ft | 43 | | 46 | | 46 | 50 | 46 |
| Attitude from vertical, deg | 0.7 | | 0.02 | | −0.53 | 0.03 | 0.03 |

[b] *Surveyor II* mission was terminated prior to lunar encounter.

[c] Until 3500-lb thrust level during burnout.

[d] SC-4 signal was lost 41.1 sec after main retroignition at an altitude of 49,400 ft and velocity of 1090 ft/sec.

[e] RODVS = reliable operate doppler velocity sensor.

[f] RORA = reliable operate radar altimeter.

**Table XIII-9 (contd)**

| Parameter | Surveyor mission | | | | | | |
|---|---|---|---|---|---|---|---|
| | I | II | III | IV | V | VI | VII |
| **Terminal descent phase (contd)** | | | | | | | |
| Time from 10-ft/sec mark to 14-ft mark, sec | 6.4 | [d] | [g] | [d] | 5.6 | 6.5 | 6.1 |
| 14-ft mark (vernier engine shutoff) | | | | | | | |
| Altitude (fram foot pads), ft | 13 | | | | 14.5 | 14 | 13 |
| Vertical velocity, ft/sec | 5 | | | | 5.2 | 5 | 5 |
| Lateral velocity, ft/sec | ≈0 | | | | ≈0 | ≈0 | ≈0 |
| Attitude from vertical, deg | 0.3 | | | | 0.1 | 0 | 0 |
| Time from 14-ft mark to touchdown, sec | 1.5 | | | | 1.7 | 1.3 | 1.3 |
| Touchdown conditions | | | | | | | |
| Based on trajectory data | | | | | | | |
| Vertical velocity, ft/sec | 12.2 | | 6 to 8 | | 13.5 | 12.5 | 12.5 |
| Lateral velocity, ft/sec | 0.6 | | 0 | | 0.5 | 0 | 0 |
| Attitude from vertical, deg | ≈0 | | ≈0 | | ≈0 | ≈0 | ≈0 |
| Based on strain gage data | | | | | | | |
| Vertical velocity, ft/sec | 10 | | 6 | | 12 to 13 | 11.5 | 12 |
| Lateral velocity, ft/sec | 2 | | 0.5 | | <1 | <1 | 1 |
| Attitude from vertical, deg | 1 | | ≈0 | | ≈0 | 2 | ≈0 |
| Spacecraft conditions after landing | | | | | | | |
| Roll orientation (+X-axis to north), deg clockwise | 179 | | 134.2 | | 114.5 | 149.0 | 290.2 |
| Tilt magnitude, deg | | | 12 | | 19.5 | 0.9 | 3.2 |
| Tilt direction, deg clockwise | | | 277 | | 7.6 | 335.04 | 279 |
| Weight, lb | 649 | | 659[h] | | 670 | 662 | 674 |
| Total vernier propellant used for mid-course and terminal descent, lb | 139.0 | | 140.1[i] | | 136.6 | 147.6 | 152.0 |

[b]*Surveyor II* mission was terminated prior to lunar encounter.
[d]SC-4 signal was lost 41.1 sec after main retroignition at an altitude of 49,400 ft and velocity of 1090 ft/sec.
[g]14-ft mark was not issued by RADVS on *Surveyor III* due to loss of beam lock at 37 ft.
[h]Weight at initial touchdown of *Surveyor III* was 674 lb.
[i]Until initial touchdown.

This failure gave very little trouble, since it was possible to perform the transit phase using omniantenna B, and omniantenna A was determined to be deployed after touchdown.

*Surveyor I* landed on a slope approximately 1 deg from the local horizontal. The television survey camera transmitted over 10,000 pictures during the first lunar day and approximately 900 additional pictures after lunar-night survival. *Surveyor I* demonstrated a remarkable capability of surviving the cold lunar nights, and its operation was extended to the eighth lunar day.

Launched on September 20, 1966, *Surveyor II* performed the early phases of the mission up to midcourse as planned. During execution of the midcourse maneuver, one of the three vernier engines failed to fire, resulting in spacecraft tumbling. Subsequent attempts (39 in all) to obtain normal firing of vernier engine 3 were unsuccessful and resulted in increasing spacecraft rotational rate to a maximum of 2.43 rev/sec. With available power decreasing steadily, it was decided to fire the main retro motor. Communication with the spacecraft was lost approximately 30 sec following ignition of the retro motor.

Launched on April 17, 1967, *Surveyor III* achieved a successful soft landing and met all objectives. As described later, the vernier engines did not shut off automatically before contact with the lunar surface, and the spacecraft lifted off after initial touchdown and again after second touchdown. The vernier engines were commanded *off* from earth just before third touchdown, and the spacecraft finally came to rest. Although telemetry failure during the landing impaired early lunar operations, corrective calibration permitted use of nearly all data received at low bit rates.

Landing inside a 200-meter-diameter crater on a sloping surface, *Surveyor III* tilted 12.5 deg. The SM/SS was used extensively, and more than 6000 television pictures were received after landing. The *Surveyor III* spacecraft did not survive the lunar night.

Launched on July 14, 1967, the mission of *Surveyor IV* was normal in all respects and the spacecraft performed flawlessly until the terminal-descent phase. About 2.5 min before predicted touchdown (2 sec before the expected time of retrorocket burnout), the spacecraft signal was lost. Exhaustive attempts to recover the signal proved futile.

After a successful launch on September 8, 1967, all *Surveyor V* mission objectives were achieved, even though high-pressure helium gas leakage occurred after the midcourse correction, which jeopardized the terminal descent. To enhance the chances for a successful landing, a series of additional vernier engine firings were performed which reduced the overall spacecraft weight and provided increased ullage in the vernier propellant tanks.

After successfully landing, *Surveyor V* transmitted over 18,000 television pictures and abundant alpha scattering experiment data from the surface during the first lunar day. Also, for the first time, the vernier engines were static-fired at low thrust for 0.55 sec to determine surface erosion effects of the rocket exhaust jets. On the second and fourth lunar days, the spacecraft was successfully revived and additional television pictures were obtained on both occasions.

Before the *Surveyor V* launch, a study was made to determine the spacecraft's capability of landing when approaching the moon at high incidence angles.

Launched on November 7, 1967, *Surveyor VI* achieved all mission objectives. In addition to acquiring about 30,000 television pictures, alpha scattering data, and other engineering and science data, *Surveyor VI* performed a hop experiment which resulted in the spacecraft landing about 8 ft from its original location. *Surveyor VI* spacecraft was revived only briefly during the second lunar day.

Launched on January 7, 1968, *Surveyor VII* achieved all mission objectives. The SM/SS operated successfully. In addition to performing its scheduled functions, it provided assistance for deployment of the alpha scattering sensor head to the lunar surface and, later, for relocation of the sensor head on the lunar surface for analyzing different samples. During the first lunar day, nearly 21,000 television pictures were acquired, and *Surveyor VII* survived the lunar night without battery damage. During the second lunar day, about 45 additional television pictures and engineering data were received.

Table XIII-10, a summary of lunar-night survival performance of the five soft-landed spacecraft, includes data on thermal switch operation, estimated low-temperature exposure of the main compartments, and second-lunar-day anomalies.

### 2. Failure of *Surveyor II* During Midcourse Correction

When the command to ignite the three vernier engines was sent to the spacecraft as part of standard midcourse velocity correction sequence, vernier engine 3 did not respond properly. The thrust provided by vernier engines 1 and 2 caused the spacecraft to spin at approximately 1.22 rev/sec. An initial attempt to halt the spinning, with the cold gas jets being controlled by the flight control subsystem operating in the rate mode, was terminated when approximately 60% of the available gas supply was required to reduce the spin rate to approximately 0.97 rev/sec, thereby indicating that the available gas supply would not be sufficient to stop spacecraft rotation.

The SC-2 failure was thoroughly investigated by a formally appointed Failure Review Board, which consisted of representatives from JPL, HAC, Reaction Motors Division of Thiokol, and NASA Offices of Space Science and Applications. After extensive review and analysis of the available flight data pertaining to vernier propulsion system performance during each thrusting period, it was concluded that:

(1) Engine 3 never ignited.

(2) Engines 1 and 2 operated inconsistently during some firings following midcourse, if not also during midcourse itself.

Although the precise failure mode could not be established, oxidizer injector clogging (Section XVII-A-2) was the most probable explanation. The board made many recommendations to provide, on later missions, greater assurance of spacecraft flight readiness and better preflight and inflight diagnostic data.

### 3. Final Descent and Landing of *Surveyor III*

The *Surveyor III* terminal-descent sequence was executed normally until shortly before touchdown. Approximately 2–3 sec after the 10-ft/sec mark, RADVS beam 3 tracker lost lock, thus preventing generation of the 14-ft

**Table XIII-10. Lunar night survival performance summary**

| Spacecraft | Thermal switch operation | | | | Estimated minimum compartmental temperatures reached during first lunar night, °F | | Anomalies observed during second lunar day operations |
|---|---|---|---|---|---|---|---|
| | Number opening within specified temperature limits | Number opening below specified temperature limits | Number opening at unknown temperature | Number failing to open[a] | Compartment A (battery) | Compartment B (upper tray) | |
| SC-1 | 2 | 4 | 5 | 4 | −205 | −280[b]<br>−300[c] | Main battery voltage dipped excessively when the unregulated bus was placed under a power load |
| SC-3 | 1 | 0 | 3 | 11 | −245[b]<br>−295[c] | −285[b]<br>−310[c] | Spacecraft could not be reacquired on the second lunar day |
| SC-5 | 5 | 1 | 8 | 1 | −187 | −268[b]<br>−280[c] | Signal-to-noise ratio for the television signal was extremely low<br>Spacecraft could not be commanded to bit rates lower than 550 |
| SC-6 | 1 | 6 | 1 | 7 | −225[b]<br>−290[c] | −280[b]<br>−290[c] | After a short period of erratic contact, the spacecraft signal was lost and could not be reacquired |
| SC-7 | 7 | 4 | 2[d] | 2 | −210[b]<br>−250[c] | −280 | Battery was severely degraded<br>Engineering and television data were satisfactory |

[a]Based on final interrogation before shutdown.
[b]All closed switches assumed to have opened at −50°F.
[c]All closed switches assumed to have remained closed.
[d]Based on observation of temperatures, it is believed that these two switches opened within specified temperature limits.

mark. Analysis indicates that the system behaved as though a false sidelobe rejection of the main beam had occurred. A momentary fade in signal of beam 3 or increase in signal of beam 2 (as might occur if the beams traverse a surface irregularity) induced the rejection logic to work. Once rejection occurred at low velocity, it was virtually impossible to reacquire lock. Upon loss of lock, flight control was mechanized to hold the spacecraft attitude fixed in the inertial mode and maintain a near-minimum vernier engine thrust level equivalent to 0.9 lunar *g*.

Loss of lock occurred at an altitude of about 37 ft and a velocity of approximately 5 ft/sec. The spacecraft then accelerated at about 0.1 lunar *g* for 6.5 sec, until contact was made with the lunar surface.

Normal and anomalous events which occurred during the *Surveyor III* terminal descent and landing are indicated in the chart of Fig. XIII-38.

Initial touchdown occurred on a slope of about 10 deg, with the verniers still operating at a thrust level almost equal to lunar weight. The spacecraft lifted off after initial touchdown and remained aloft for approximately 24 sec (Fig. XIII-39). Liftoff also occurred after second touchdown, and the spacecraft remained aloft for an additional 12 sec before third touchdown.

On each touchdown, leg 2 impacted the surface first in the uphill direction, followed by almost simultaneous impacts of legs 1 and 3. In attempting to correct the spacecraft attitude to the pretouchdown state, the flight control system momentarily increased engine thrust. This additional thrust and the spring forces in the landing legs caused the spacecraft to lift off in the downhill direction. The loads sensed by the touchdown strain gages indicated that forces in the shock absorbers were less than half those indicated on the landing of *Surveyor I*, as would be expected for landing with engines thrusting.

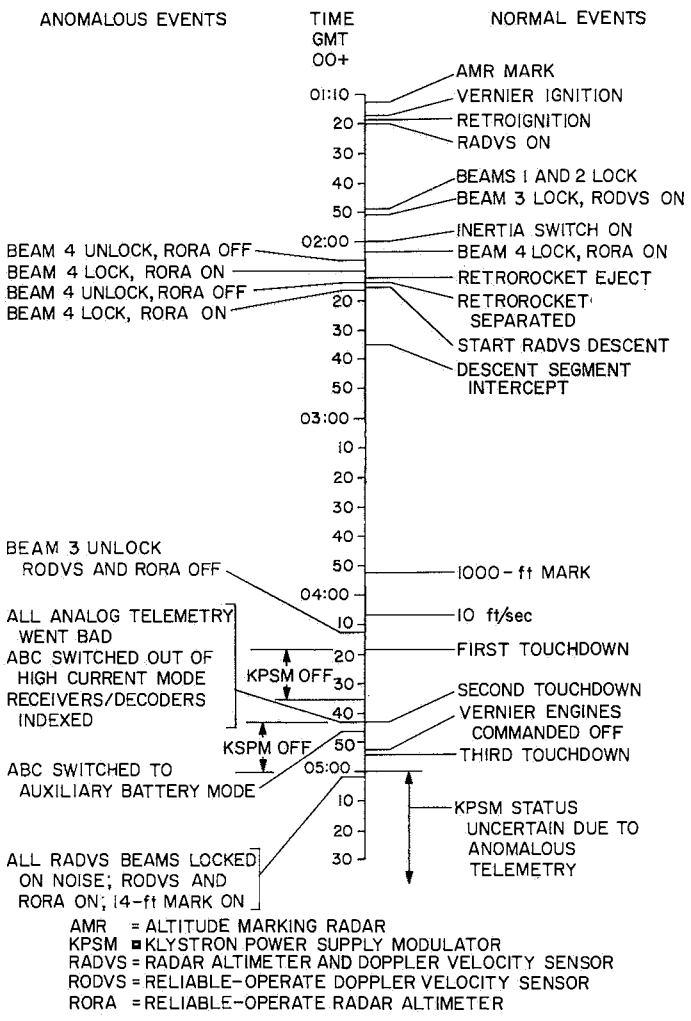



**Fig. XIII-38. Terminal-descent and landing events of *Surveyor III***

When spacecraft attitude was corrected following the first and second touchdowns, the attitude was held stable and a vernier thrust level of 0.9 lunar *g* was maintained while the spacecraft was aloft.

A ground command, sent 35 sec after initial touchdown, turned off the vernier engines approximately 1 sec before the third touchdown. After the spacecraft made contact the third time with the engines off, it moved only 1 ft laterally before coming to rest. As shown in Fig. XIII-39, the spacecraft traversed an estimated 50–70 ft between the first and second touchdowns and an additional 35–45 ft before the third touchdown. The spacecraft finally came to rest at an angle of about 12.5 deg, with the vertical about halfway between the eastern rim and the center of a crater approximately 200 mi in diameter.

Landing sequence adversely affected some spacecraft subsystems. Concurrently with both the first and second touchdowns, the RADVS klystron power supply and modulator (KPSM) switched off. The KPSM, which provided RADVS high voltage, came back on normally after 18 sec. Status of the KPSM after the second turnoff was uncertain owing to anomalous behavior of the RADVS current signal from which the KPSM voltage level was determined. Turnoff of the KPSM normally indicated a 6-V drop on the 22-V DC input for a duration of 3 msec.

At the time of second touchdown, all analog telemetry signals became erroneous, switching occurred from receiver/decoder B to A, and the battery control logic switched from the high-current mode to the main battery mode. Three seconds later, the control logic switched to the auxiliary battery mode, which was probably a normal occurrence considering the existing state of the battery charge.

Telemetry anomaly was found to be localized in the signal processing analog-to-digital converters, since the digital and television data remained normal. Analysis indicated that the direct cause of the data problem was serious degradation of transistor switches in the ESP and AESP. A suspected basic cause of signal processing failure is related to the anomaly in the KPSM. Analysis of the plasma dynamics, as the spacecraft touched down with engines operating, indicated that sufficient ionization may have entered the KPSM to cause high-voltage arcing. This would explain repeated KPSM turnoff coincident with the first two touchdowns and, if insulation had been burned away, could have resulted in high voltage being applied to the commutator transistor switches.

Initial indications after landing were that there was an acute power system problem. However, special sequences to investigate the problem and the general analog telemetry anomaly disclosed that the power system was normal, and that the problem was confined to the signal processing system. Further investigation led to the conclusion that most analog data obtained in the lowest-rate mode (17.2 bits/sec) was fairly reliable and could be corrected with simple calibration factors.

Considerable glare occurred on pictures taken by *Surveyor III* at some sun angles, due to contamination or pitting of the upper part of the camera mirror. This condition was believed to have been induced by landing with the engines thrusting. Moreover, the television camera developed stepping problems, which reduced the rate at which pictures were taken.

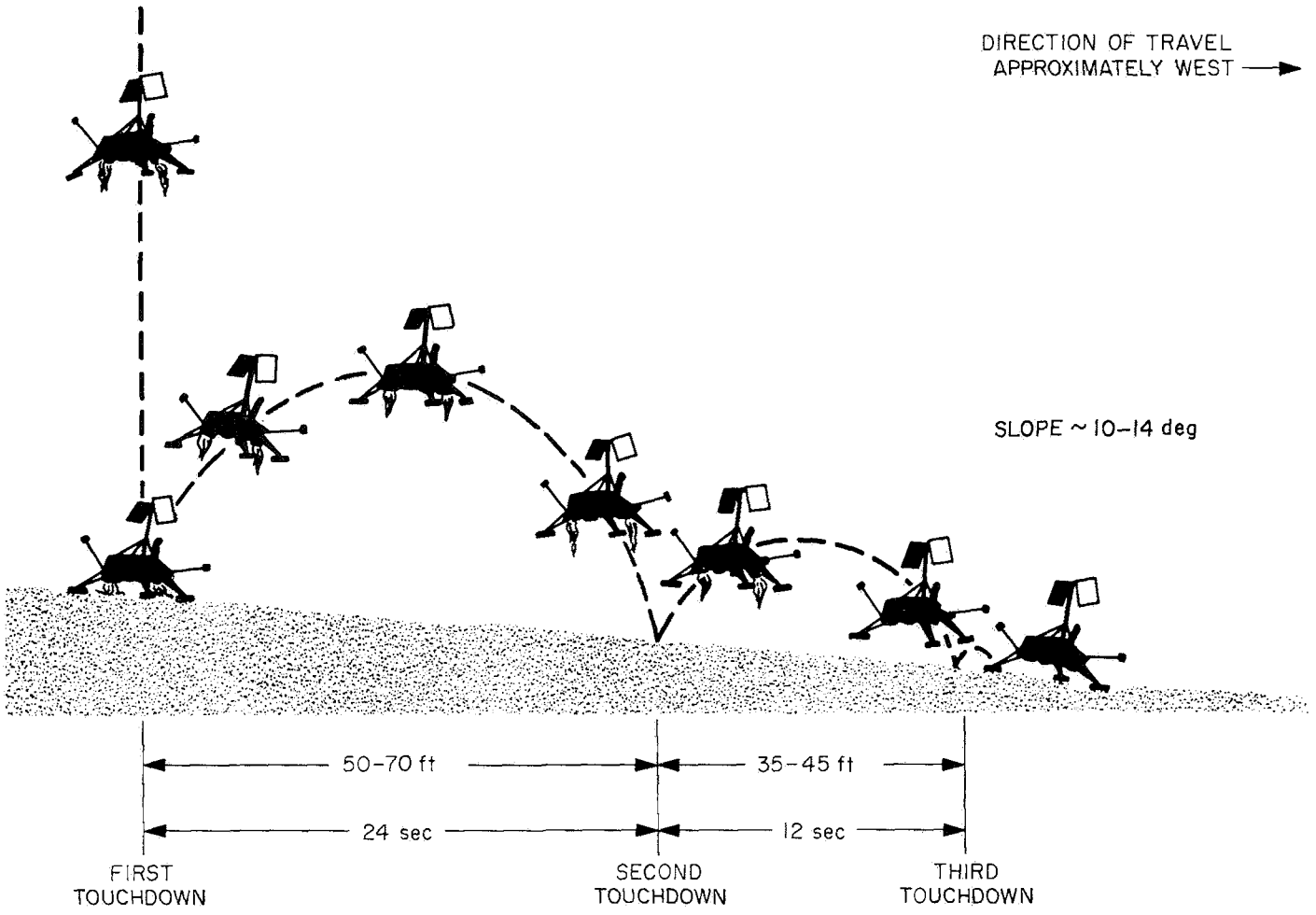



**Fig. XIII-39. Landing sequence of *Surveyor III***

#### 4. Failure of *Surveyor IV* During Terminal Descent

The *Surveyor IV* automatic descent sequence was satisfactorily initiated by the AMR mark signal. Ignition of the vernier engines and retrorocket was smooth, with only small changes in spacecraft attitude. The RADVS turn-on occurred at the expected time, and all three velocity beams acquired lock about 32 sec after retroignition. The spacecraft radio signal was abruptly lost about 41.1 sec after main retroignition, only 1.5 sec before predicted burnout, and about 2.5 min before expected touchdown. There was no evidence of subcarrier loss before carrier loss. Exhaustive efforts to regain radio contact with *Surveyor IV* were unsuccessful.

At the time of signal loss, the spacecraft was about 49,400 ft above the lunar surface, and its velocity was approximately 1090 ft/sec. Final data indicated that the spacecraft condition was completely satisfactory. The only significant anomaly that had appeared during the retromaneuver was greater-than-normal modulation of the thrust commands to vernier engines 1 and 2, which had not occurred during midcourse thrusting.

A formally appointed technical review board (TRB) conducted a thorough investigation of the *Surveyor IV* failure. Based on detailed examination of the telemetry records and other evidence, including the results of the working analysis group, the TRB was unable to identify any single or multiple cause for the failure of the *Surveyor IV* mission. The board did conclude, however, that the failure was in the spacecraft itself and could not be attributed to either the ground system (telemetry, tracking, or command links) or to human error. Many failure modes could be postulated, but from the direct evidence available it was not possible to pinpoint any single mode or combination of modes as a reason for the failure. Of the possible failure modes, the board considered the following to be the most likely:

*a. Breakage of critical power lead in wiring harness, or failure of connector or solder joint.* Abrupt and nearly simultaneous (within 0.25 msec) loss of carrier, subcarrier, and data was verified; and reacquisition after telemetry loss was unsuccessful. Problems had been encountered with manufacturing and reworking small-gage (22) wire to connectors and providing appropriate strain relief to multiwire harnesses.

*b. Main retromotor case rupture.* The motor still contained about 70 lb of propellant and was 1.4 sec from the end of burn. This time corresponded to reaching zero propellant web, and excessive case heating at this point would have been possible. X-rays of other motors indicate the possibility of liner separation, which could contribute to failure.

*c. Failure in transmitter that caused its power to drop to zero, or to a value below required carrier strength, and subsequent failure of spacecraft upon its landing in Sinus Medii area.* There had been instances of loss of transmitter high power on SC-1 and SC-6 during testing. Sinus Medii is considerably more hostile than the *Surveyor I* and *III* sites, and inability to reacquire telemetry could have been due to damage on landing.

*d. Failure of a helium pressure vessel, nitrogen tank, shock absorber, or propellant tank.* These units represented large sources of stored energy which could have caused substantial fragmentation. Imperfect welds, scratches, or local defects could have caused rupture of a pressure vessel a significant time after sustained stress had been applied.

The board had concluded that any of the above failure modes was a relatively low-probability occurrence, and could not single out any one as being more likely than another. Spacecraft telemetry indicated normal performance up to the time that carrier, subcarrier, and telemetry signals were abruptly lost. Detailed examination of telemetry dropout from the predetection tapes at DSSs 11 and 14 did not give further insight into the nature of the failure. The only two apparent anomalies which were considered significant prior to signal dropout were:

(1) A thrust modulation in vernier engines 1 and 2, indicating a relatively small moment disturbance of 300–500 in.-lb about leg 3, at a frequency of 5–25 Hz, not evidenced in previous missions.

(2) Several sharp accelerations (up to 8 *g*, measured peak-to-peak) at the spacecraft attach ring during *Atlas* and *Centaur* burns.

No reasonable correlation had been found between these and other less significant anomalies. Moreover, the board concluded that the two main anomalies, thrust modulation and shocks during launch, did not cause the signal dropout.

Because of the inability to identify a specific cause and the technical impracticability of conducting an extensive ground test program to duplicate the failure, the board recommended no significant spacecraft change, because such a change might of itself be the source of some unforeseen future problem. From available evidence and the two previous successes (*Surveyor I* and *III* missions), it appeared that the *Surveyor IV* failure was of sufficiently low probability that change in the current program was unwarranted.

The board did recommend, however, three general-type actions: (1) increasing the confidence of spacecraft preflight readiness, (2) providing some insight into the *Surveyor IV* failure, and (3) enhancing in-flight data retrieval for future missions.

### 5. Surveyor V Anomalies

When a helium squib valve was fired about 2.5 min before the *Surveyor V* midcourse correction to pressurize the vernier propulsion system, the helium regulator failed to lock up tight after propellant-tank pressure reached the regulated pressure setting of about 730 psia. This caused the tank pressure to rise slowly to the relief valve pressure setting of about 825 psia, where it was maintained by overboard venting of the helium. The midcourse firing of 14.25-sec duration was successfully executed. Afterward, however, the propellant tank pressure again rose slowly until venting occurred. The helium leak caused the helium tank pressure to drop at a rate of approximately 10 psi/min. In an attempt to actuate and reseat the helium regulator, three additional vernier engine firings (2–4) were performed; however, the leak persisted. Firing 4 consisted of a 12-sec burn, followed by two additional 0.5-sec burn periods with 1-sec interruptions. A summary of each of the vernier firings conducted on the *Surveyor V* mission is contained in Table XIII-11.

An intensive study of the situation, including special vernier engine tests at low supply-pressure conditions, indicated that a soft landing would still be feasible if (1) critical spacecraft propulsion system parameters were adjusted and (2) the spacecraft performed in a predictable manner during a terminal-descent sequence that would

**Table XIII-11. Summary of SC-5 vernier weight of engine firings**

| Burn sequence | Ignition time, GMT | Magnitude, m/sec | Duration, sec | Propellant used, lb | Purpose |
|---|---|---|---|---|---|
| 1 | 01:45:02 Sep 9, 1967 | 14.0 | 14.25 | 11.6 | Trajectory correction |
| 2 | 02:12:02 | 9.91 | 10.05 | 8.2 | Attempt to stop helium leak |
| 3 | 02:39:50 | 22.6 | 23.05 | 18.8 | Attempt to stop helium leak |
| 4 | 04:18:48 | 12.8 | 12.0<br>0.5<br>0.5 | 10.6 | Trajectory correction and attempt to stop helium leak |
| 5 | 08:24:02 | 32.4 | 33.0 | 26.8 | Adjust propulsion system parameters |
| 6 | 23:31:00 | 5.3 | 5.45 | 4.4 | Final trajectory correction |
| 7 | 00:44:51 Sep 11, 1967 | — | 111 | 58.4 | Terminal descent |
| 8 | 07:38:08 Sep 13, 1967 | — | 0.55 | — | Lunar surface erosion experiment |

be modified to minimize the required total vernier engine impulse. Two additional midcourse vernier firings (5 and 6) were performed to optimize vernier propulsion system parameters and to make final trajectory corrections. Vernier engine performance was smooth and spacecraft attitude was easily maintained during all the midcourse firings. The last two firings reduced the weight of the remaining vernier propellant to a desired minimum. Propellant weight reduction meant reduction in total spacecraft weight so that the retroignition impulse would decelerate the spacecraft to a much lower than normal velocity (≈100 ft/sec instead of 400–500 ft/sec) at retrorocket burnout and thus increase the helium ullage volume. The increased helium volume assured that maximum helium weight would be retained for blowdown during terminal descent, since the last vernier midcourse firing was made before helium tank pressure had dropped to the relief valve setting, which occurred about 1 hr before terminal descent. It had been determined that a minimum helium pressure of 500 psia was required to maintain vernier engine thrust.

The terminal-descent sequence was modified by sending the following earth commands in order to minimize vernier engine total impulse requirements:

(1) An unusually long delay time of 12.33 sec between automatic AMR 60-mi mark and vernier engine ignition was stored in the flight control programmer to delay the start of the retromaneuver so that retrorocket burnout (and the beginning of the RADVS-controlled vernier phase) would occur at a lower altitude.

(2) A 150-lb vernier engine thrust level (instead of the 200-lb level used on previous missions) was stored in flight control to increase the available burn time.

(3) At carefully selected times during the descent sequence, earth commands were sent overriding the flight control programmer to achieve retrorocket ejection about 4 sec early, to restrict the period of time that the vernier engines would be commanded to the high-thrust level following the burnout, and to begin the RADVS-controlled phase earlier relative to retrorocket burnout so that sufficient time would be available for the spacecraft to acquire the programmed descent curve.

The descent sequence was initiated automatically by the 60-mi mark signal from the AMR. All terminal descent events occurred very close to preretro predicted times. Comparison between the premission, preretro prediction, and actual event-time intervals is shown in Fig. XIII-40. Spacecraft performance was very nearly as planned in all respects. In particular, a very close agreement was achieved between predicted and actual retrorocket burnout conditions, which were severely constrained between narrow limits on this mission. As expected, vernier engine thrust command saturation was indicated near the end of the descent sequence due to low propellant supply pressure. Helium tank pressure was only 575 lb at touchdown.

Touchdown occurred inside the edge of a small, 30-ft-diameter by 5-ft-deep crater. Leg 1 contacted first, followed by almost simultaneous contact of legs 2 and 3. Having touched down on a slope of about 20 deg, the spacecraft slid along the surface approximately 30 in. while turning approximately 6 deg clockwise before coming to rest. No damage resulted from the landing, and it was possible to perform extensive postlanding operations, including television and alpha scattering experiments.

Approximately 53 hr after *Surveyor V* landed, a short (0.55-sec) vernier engine static-firing experiment was successfully performed for the first time on the lunar surface. It was estimated that thrust levels were about

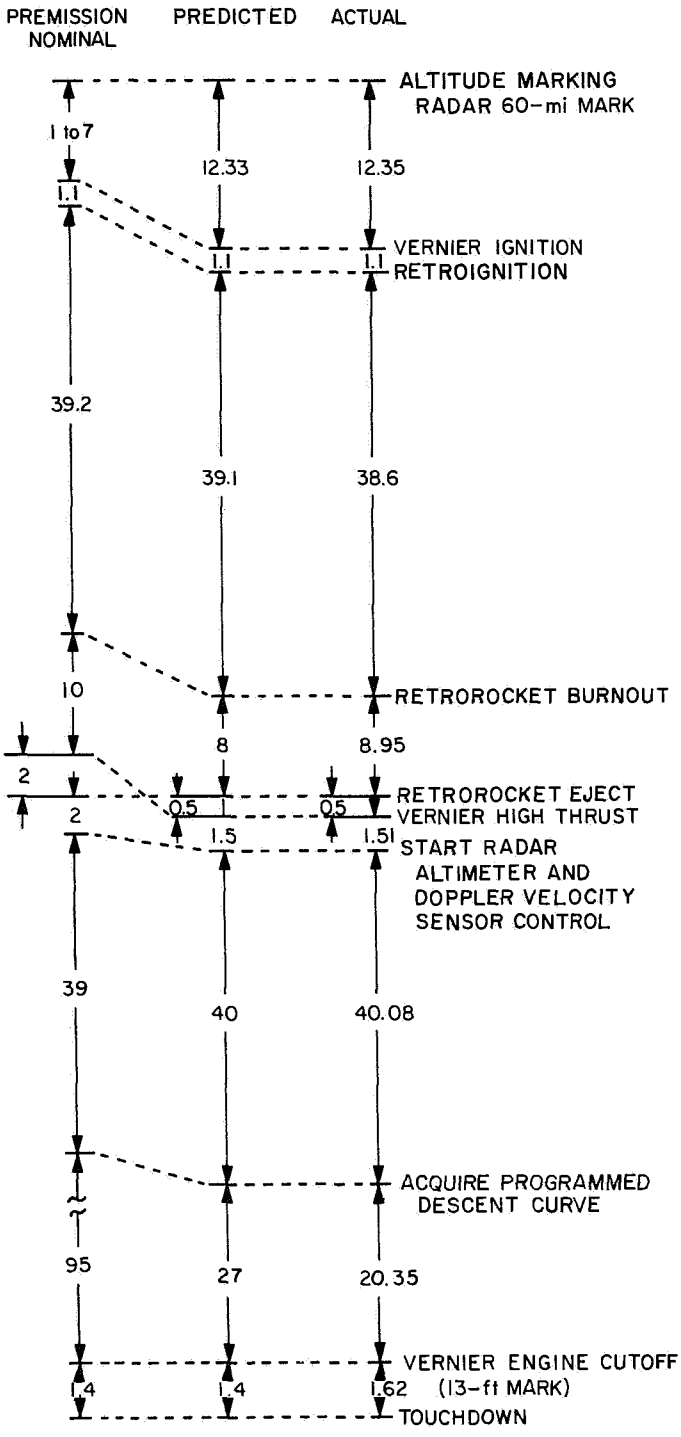



**Fig. XIII-40. Comparison of nominal, predicted, and actual *Surveyor V* terminal-descent-event time intervals**

24 lb for engine 1, 17 lb for engine 2, and 26 lb for engine 3. This variation from the commanded value of about 30 lb was expected because the temperature limits for normal operation of the vernier propulsion system had been exceeded. Lunar surface erosion by the vernier engines was clearly evident in television pictures taken after the firing. The firing also caused the alpha scattering sensor head (which had been deployed to the surface) to move a few inches down the slope. In addition, a very slight increase in the spacecraft tilt (about 0.3 deg) was indicated by gyro data and confirmed by postfiring A/SPP determinations. The firing also affected signal strength.

### 6. Postlanding Spacecraft Hop Experiment of *Surveyor VI*

About 7½ days after *Surveyor VI* landed on the moon, shortly after lunar noon, the spacecraft performed a successful hop experiment. To prepare for this experiment, the A/SPP was used to selectively shade the vernier engines to bring all the temperatures below the 222°F maximum operating limit. The A/SPP was then repositioned to a safe position. To achieve lateral translation 15 deg to the left of leg 1 (15 deg from the $+Y$ axis toward the $+X$ axis), the flight control system was commanded to achieve a +7-deg pitch attitude (leg 1 pitched down).

In performing the experiment, the vernier engines were fired for 2.5 sec at a total thrust level of about 150 lb. The resulting time of flight was 6.01 sec, with the spacecraft rising 10–15 ft and translating about 8 ft over the lunar surface. The planned thrusting time was 2.0 sec. However, the first shutdown command from earth was not effective at the spacecraft (possibly due to an antenna null) and the vernier engines were not shut down until the spacecraft received the backup command 0.5 sec later. A small pitch-up moment, induced by slightly delayed shutdown of engine 1, helped to level the spacecraft before landing.

Main hop experiment parameters are presented in Table XIII-12. Change in spacecraft position resulting from the hop is shown in Fig. XIII-41.

Although the translation was greater than expected because of the longer thrust time, the spacecraft made a completely successful landing, and no damage resulted from the experiment except for the alpha scattering instrument. Television pictures taken after the experiment revealed that the alpha scattering instrument sensor head was upside down. This was not unexpected, however, since the instrument design did not permit retraction to a safe position. Other pictures showed some lunar material was adhering to spacecraft surfaces, such as the photometric chart on the omniantenna B boom.

**Table XIII-12. Postlanding hop experiment parameters of SC-6**

| Item | Predicted | Actual | Item | Predicted | Actual |
|---|---|---|---|---|---|
| Total thrust level, lb | 150 | ≈165 | Maximum vertical height, ft | 7.9 | 10–15 |
| Thrust duration, sec | 2 | 2.5 | Vertical touchdown velocity, ft/sec | 8.6 | 13 |
| Flight time, sec | 4.56 | 6.01 | | | |
| Lateral displacement, ft | 4 | 7.9 | Lateral touchdown velocity, ft/sec | 1.22 | 1.4 |

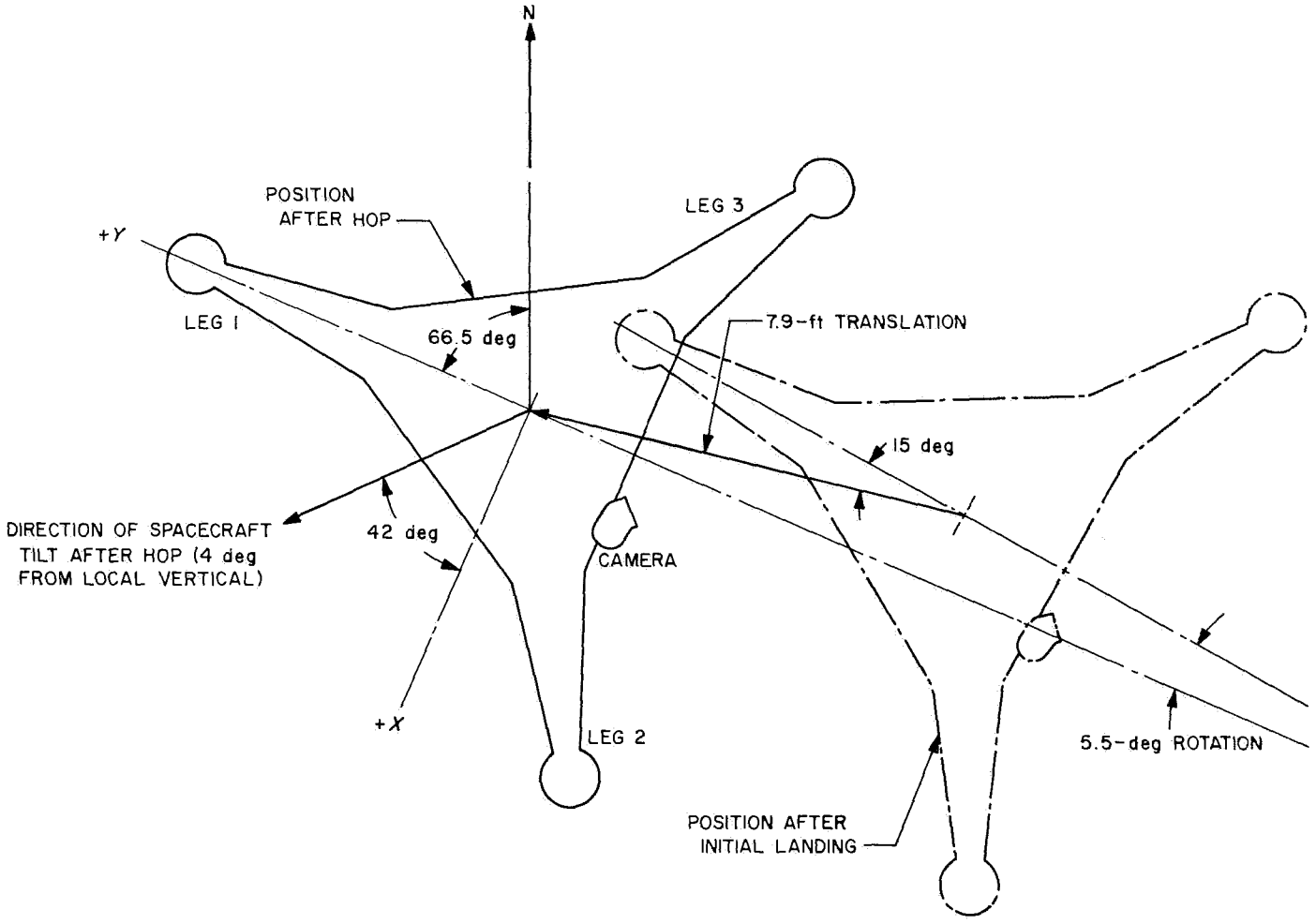



**Fig. XIII-41. Change in spacecraft position induced by hop experiment**

From the new spacecraft position, excellent pictures were taken of the footpad and crush block imprints made during the initial landing and the surface erosion caused by vernier firing during the hop.

### 7. Reliability

Estimated reliability of each of the *Surveyor* spacecraft for the transit phase between injection and touchdown, based upon systems test experience, is shown graphically in Fig. XIII-42. Table XIII-13 lists the detailed reliability estimates for each of the flight spacecraft. The primary source of data for these reliability estimates is the time and cycle information obtained by spacecraft control items during system tests. Tests and flight data from previous spacecraft were included in subsequent spacecraft reliability predictions, if there were no significant control-item design differences. More detailed reliability information is contained in Section XII (Quality Assurance and Reliability) of this report.

**Table XIII-13. *Surveyor* Spacecraft System and subsystem reliability estimates**

| Subsystem | Spacecraft | | | | | | |
|---|---|---|---|---|---|---|---|
| | SC-1 | SC-2 | SC-3 | SC-4 | SC-5 | SC-6 | SC-7 |
| Telecommunications | 0.926 | 0.941 | 0.965 | 0.920 | 0.987 | 0.989 | 0.991 |
| Structures and mechanisms | 0.816 | 0.865 | 0.905 | 0.910 | 0.850 | 0.820 | 0.884 |
| Propulsion | 0.991 | 0.991 | 0.967 | 0.945 | 0.945 | 0.934 | 0.928 |
| Electrical power | 0.870 | 0.938 | 0.932 | 0.952 | 0.985 | 0.986 | 0.975 |
| Flight control | 0.953 | 0.930 | 0.970 | 0.937 | 0.944 | 0.939 | 0.921 |
| Systems interaction factor | 0.737 | 0.930 | 0.959 | 0.964 | ~1.000 | ~1.000 | 0.895 |
| Overall spacecraft system | 0.457 | 0.655 | 0.732 | 0.681 | 0.738 | 0.702 | 0.655 |

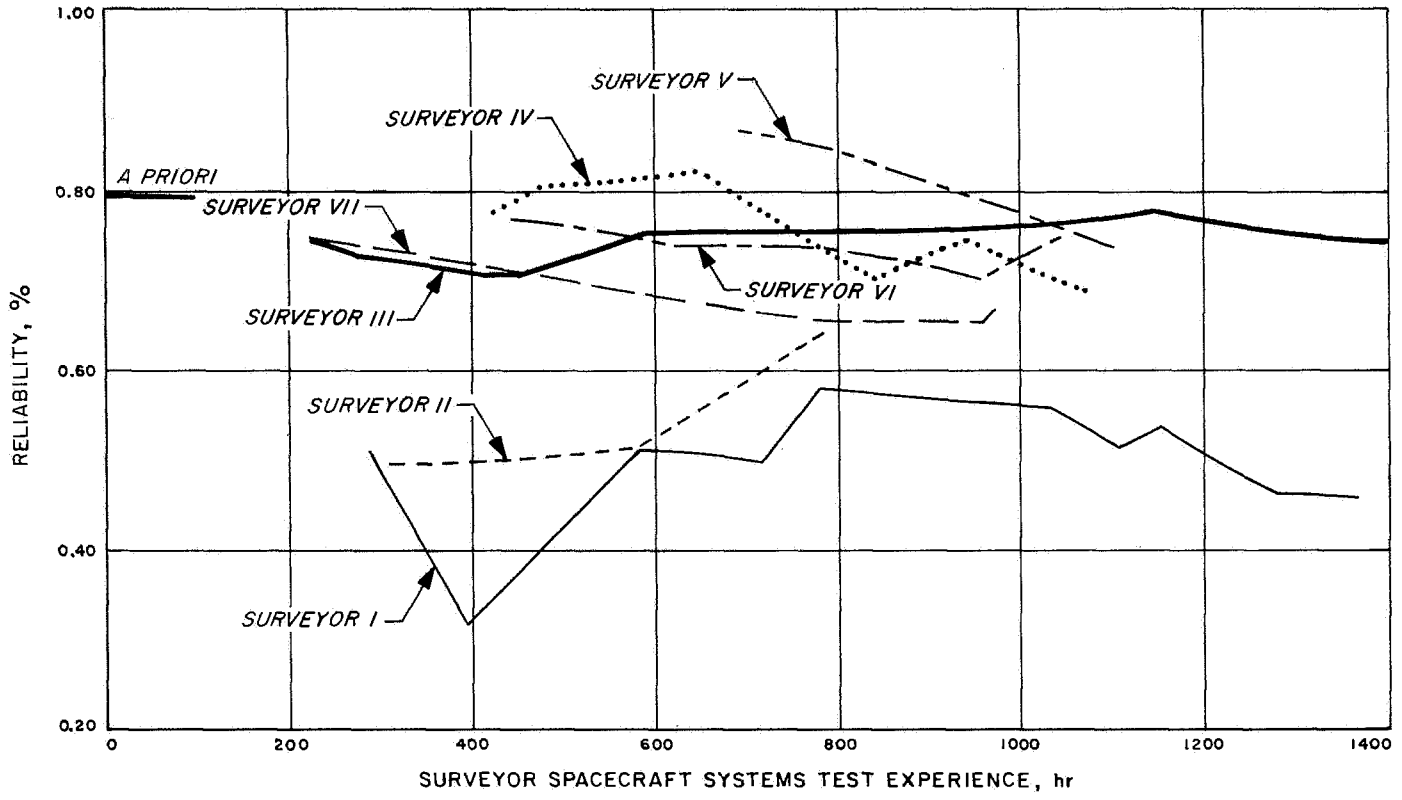



**Fig. XIII-42. *Surveyor* Spacecraft System reliability estimates**

## References


XIII-1. *Surveyor Final Engineering Report,* SSD 78175. Hughes Aircraft Co., El Segundo, Calif., May 1968.

XIII-2. Cheng, R. K., Meredith, C. M., and Conrad, D. A., "Design Considerations for *Surveyor* Guidance," *J. Spacecraft Rockets,* Vol. 3, No. 11, pp. 1569–1576. AIAA, Easton, Pa., Nov. 1966.

XIII-3. Ribarich, J. J., and Meredith, C. M., "Analysis of *Surveyor* Midcourse Guidance as a Problem in the Theory of Maxima and Minima," *J. Spacecraft Rockets,* Vol. 3, No. 7, pp. 997–1001. AIAA, Easton, Pa., July 1966.

XIII-4. Meredith, C. M., and Cheng, R. K., *Midcourse Guidance Equations for the Surveyor Spacecraft,* presented at AIAA/ION Astrodynamics Guidance and Control Conference, Los Angeles, Calif., Aug. 24–26, 1964.

XIII-5. Mason, M., and Brainin, S., "Descent Trajectory Optimization for Soft Lunar Landing," *Aerospace Engineering,* Vol. 21, No. 4, pp. 54–55 and 82–91. Institute of Aerospace Sciences, Easton, Pa., Apr. 1962.

XIII-6. Cheng, R. K., and Conrad, D. A., "Design Considerations for the Surveyor Terminal Descent System," *AIRA* paper No. 64-644, presented at AIAA/ION Astrodynamics Guidance and Control Conference, Los Angeles, Calif., Aug. 24–26, 1964.

XIII-7. Cheng, R. K., "*Surveyor* Terminal Guidance"; Chapter 7. *Lunar Missions and Explorations.* Edited by C. Leonides and R. Vance, John Wiley & Sons, Inc., New York, 1964.

XIII-8. *Final Sterilization Report,* Vols. I–III, SSD 3372R–3374R. Hughes Aircraft Co., El Segundo, Calif., June 1963.

XIII-9. *Surveyor I Mission Report: Part I. Mission Description and Performance,* Technical Report 32-1023. Jet Propulsion Laboratory, Pasadena, Calif., Aug. 31, 1966.

XIII-10. *Surveyor II Mission Report: Mission Description and Performance,* Technical Report 32-1086. Jet Propulsion Laboratory, Pasadena, Calif., Apr. 1, 1967.

XIII-11. *Surveyor III Mission Report: Part I. Mission Description and Performance,* Technical Report 32-1177. Jet Propulsion Laboratory, Pasadena, Calif., Sept. 1, 1967.

XIII-12. *Surveyor IV Mission Report: Mission Description and Performance,* Technical Report 32-1210. Jet Propulsion Laboratory, Pasadena, Calif., Jan. 1, 1968.

XIII-13. *Surveyor V Mission Report: Part I. Mission Description and Performance,* Technical Report 32-1246. Jet Propulsion Laboratory, Pasadena, Calif., Mar. 15, 1968.

XIII-14. *Surveyor VI Mission Report: Part I. Mission Description and Performance,* Technical Report 32-1262. Jet Propulsion Laboratory, Pasadena, Calif., Sept. 15, 1968.

## References (contd)


XIII-15, *Surveyor VII Mission Report: Part I. Mission Description and Performance,* Technical Report 32-1264. Jet Propulsion Laboratory, Pasadena, Calif. (to be published).

XIII-16. *Flight Performance, Surveyor I: Final Report,* Vol. I, SSD 68189R; Vol. II, SSD 68222R; Vol. III, SSD 68223R. Hughes Aircraft Co., El Segundo, Calif., Oct. 1966.

XIII-17. *Flight Performance, Surveyor II: Final Report,* SSD 68189-2. Hughes Aircraft Co., El Segundo, Calif., Jan. 1967.

XIII-18. *Flight Performance, Surveyor III: Final Report,* SSD 68189-3. Hughes Aircraft Co., El Segundo, Calif., July 1967.

XIII-19. *Flight Performance, Surveyor IV: Final Report,* SSD 68189-4. Hughes Aircraft Co., El Segundo, Calif., Sept. 1967.

XIII-20. *Flight Performance, Surveyor V: Final Report,* SSD 68189-5. Hughes Aircraft Co., El Segundo, Calif., Nov. 1967.

XIII-21. *Flight Performance, Surveyor VI: Final Report,* SSD 68189-6. Hughes Aircraft Co., El Segundo, Calif., Dec. 1967.

XIII-22. *Flight Performance, Surveyor VII: Final Report,* SSD 68189-7. Hughes Aircraft Co., El Segundo, Calif., Feb. 1968.


## Bibliography


*Design Change and Performance Summary A-21A,* SSD 5492B. Hughes Aircraft Co., El Segundo, Calif., Oct. 1965.

*Initial Acquisition Study for Surveyor on Direct Ascent Trajectories,* SSD 3466R. Hughes Aircraft Co., El Segundo, Calif., Aug. 1963.

*Isotope Heat Sources for the Surveyor Spacecraft,* SSD 84021. Hughes Aircraft Co., El Segundo, Calif., Sept. 20, 1967.

"Liftoff and Translation Analysis, *Surveyor* SC-2," *Surveyor Lunar Liftoff and Translation Study,* SSD 84029. Hughes Aircraft Co., El Segundo, Calif., Oct. 21, 1966.

"Liftoff and Translation Kit, *Surveyor* SC-3," *Surveyor Lunar Liftoff and Translation Study,* SSD 84030. Hughes Aircraft Co., El Segundo, Calif., Apr. 3, 1967.

*Lunar Night Survival Study Report,* SSD 78119R. Hughes Aircraft Co., El Segundo, Calif., May 1967.

"Lunar Static Firing Experiment, SC-5, Mission E," *Surveyor Lunar Liftoff and Translation Study,* SSD 84032. Hughes Aircraft Co., El Segundo, Calif., Sept. 6, 1967.

## Bibliography (contd)


*Midcourse and Terminal Guidance Operations Programs,* SSD 4051R. Hughes Aircraft Co., El Segundo, Calif., Apr. 1964.

"Postlanding Investigation of Lunar Translation, SC-5," *Surveyor Lunar Liftoff and Translation Study,* SSD 84033. Hughes Aircraft Co., El Segundo, Calif., Oct. 3, 1967.

*Potential Extended Capabilities, Surveyor Spacecraft,* SSD 84055. Hughes Aircraft Co., El Segundo, Calif., Feb. 1968.

*Preliminary Surveyor Midcourse and Terminal Guidance Equations,* SSD 3296R. Hughes Aircraft Co., El Segundo, Calif., Mar. 22, 1965.

"Proposal for *Surveyor* Liftoff and Translation," *Surveyor Lunar Liftoff and Translation Study,"* SSD 68161P. Hughes Aircraft Co., El Segundo, Calif., July 12, 1966.

*Space Flight Operations Detailed Operating Procedures for Missions A–G,* EPD-239. Jet Propulsion Laboratory, Pasadena, Calif., Oct. 1, 1964–Jan. 4, 1968.

*Space Flight Operations Plan, Surveyor Missions A–G,* EPD-180. Jet Propulsion Laboratory, Pasadena, Calif., Mar. 5, 1964–Dec. 19, 1967.

*Space Flight Operations System Design Specification,* EPD-233. Jet Propulsion Laboratory, Pasadena, Calif., Sept. 2, 1966.

*Space Flight Operations Report, Mission A:* Vols. I and II. SSD 64189R. Hughes Aircraft Co., El Segundo, Calif., Aug. 1966. (Also available as Addendum. Jet Propulsion Laboratory, Pasadena, Calif., Feb. 1967.)

*Space Flight Operations Report, Mission B,* SSD 64257R. Hughes Aircraft Co., El Segundo, Calif., Nov. 1966.

*Space Flight Operations Report, Mission C,* SSD 74071. Hughes Aircraft Co., El Segundo, Calif., May 1967. (Also available as Addendum SSD 7401-1. Jet Propulsion Laboratory, Pasadena, Calif., May 1967.)

*Space Flight Operations Report, Mission D,* SSD 74109. Hughes Aircraft Co., El Segundo, Calif., Aug. 1967.

*Space Flight Operations Report, Mission E,* SSD 78160. Hughes Aircraft Co., El Segundo, Calif., Oct. 1967.

*Space Flight Operations Report, Mission F,* SSD 78187. Hughes Aircraft Co., El Segundo, Calif., Dec. 1967.

*Space Flight Operations Report, Mission G,* SSD 88016. Hughes Aircraft Co., El Segundo, Calif., Feb. 1968.

"Static Fire Experiment Validation, SC-6 Mission F," *Surveyor Lunar Liftoff and Translation Study,* SSD 84034. Hughes Aircraft Co., El Segundo, Calif., Nov. 7, 1967.

"Static Fire and Lunar Translation Experiment, SC-7, Mission G," *Surveyor Lunar Liftoff and Translation Study,* SSD 84035. Hughes Aircraft Co., El Segundo, Calif., Jan. 25, 1968.

## Bibliography (contd)

"Static Firing and Liftoff and Translation Experiment Kit, *Surveyor* SC-4," *Surveyor Lunar Liftoff and Translation Study,* SSD 84031. Hughes Aircraft Co., El Segundo, Calif., July 12, 1967.

*Study of Lightweight Surveyor-A,* SSD 232P. Hughes Aircraft Co., El Segundo, Calif., Feb. 1, 1962.

*Surveyor Attitude Determination on the Lunar Surface,* SSD 88021. Hughes Aircraft Co., El Segundo, Calif., Jan. 1968.

*Surveyor Direct Ascent Trajectory Characteristics,* SSD 56028R. Hughes Aircraft Co., El Segundo, Calif., Dec. 1965.

*Surveyor High Incidence Angle Capability,* SSD 74160. Hughes Aircraft Co., El Segundo, Calif., Dec. 1967.

"*Surveyor* Hops Documentation (Lunar Liftoff and Translation Computer Program)," *Surveyor Lunar Liftoff and Translation Study,* SSD 84037, Hughes Aircraft Co., El Segundo, Calif., June 22, 1967.

*Surveyor Postlanding Attitude (PLAS) SPAC Program Description,* SSD 74008R. Hughes Aircraft Co., El Segundo, Calif., Jan. 13, 1967.

*Surveyor Spacecraft A-21 Model Description,* HAC 224847B. Hughes Aircraft Co., El Segundo, Calif., Mar. 1, 1965.

*Surveyor Spacecraft A-21A Model Description,* HAC 22848A. Hughes Aircraft Co., El Segundo, Calif., Jan. 1, 1965.

*Surveyor Spacecraft Development Plan,* SSD 68109. Hughes Aircraft Co., El Segundo, Calif., May 3, 1966.

*Surveyor Spacecraft/DSIF System Interface Requirements,* PD-6, Rev. 1. Jet Propulsion Laboratory, Pasadena, Calif., Jan. 1, 1964.

*Surveyor Spacecraft Functional Description,* HAC 239524E. Hughes Aircraft Co., El Segundo, Calif., Aug. 21, 1967.

*Surveyor Spacecraft/Launch Vehicle Interface Requirements,* PD-1, Rev. 3. Jet Propulsion Laboratory, Pasadena, Calif., Sept. 1, 1967.

*Surveyor Spacecraft Model A-21 Reliability Measurement,* SSD 78109. Hughes Aircraft Co., El Segundo, Calif., July 4, 1967.

*Terminal Guidance,* SSD 78069. Hughes Aircraft Co., El Segundo, Calif., June 1967.

# XIV. Spacecraft Structures and Mechanisms

The structural design concept used in the *Surveyor* Program evolved as the result of the high priority placed on the flexibility of the configuration. Whereas other programs emphasized integration of structure and other subsystems for consideration of weight efficiency, the capability to change subsystems and payload items individually dictated the opposite approach in the *Surveyor* Program. A truss frame with components mounted by an easily changed substructure was used. Changes were evaluated from static and dynamic tests on structural test model vehicles which were full-scale structural representations of flight spacecraft.

The most important requirement of the program was to soft-land a spacecraft on a surface whose parameters and scale were unknown. The landing loads were the critical design loads for much of the structure, and extensive analysis and test effort were devoted to landing dynamics and stability boundary determinations. The structural test models were drop-tested for loads and dynamics evaluation, and special drop-test vehicles were built to explore the limits of stability.

The *Surveyor* used many spring, explosive, and electrically powered mechanisms. Those mechanisms that were a part of major subsystems, such as the television and the soil mechanics/surface sampler (SM/SS), are described in other sections of this report as a part of the subsystems. Mechanisms that were individual, or which deployed structural elements of the spacecraft, are described in this section.

Electronic packaging and cabling are included in this section since the Mechanical Systems Section of the *Surveyor* Project Office was responsible for these areas along with those of the structures and mechanisms. Because HAC did not have a separate packaging group, packaging design was accomplished by electronic subsystem groups. The standards, philosophies, and problems discussed in this section usually involved more than one subsystem.

The spacecraft alignment and mass properties determination effort was also under the cognizance of the *Surveyor* Mechanical Systems Section of JPL, and is covered in this section of the report.

## A. Structural Design, Analysis, and Configuration

Determination of the loads or forces acting on the spacecraft was the first requirement for structural analysis. Shipping and ground-handling loads were considered early in the program, but were controlled by equipment and procedures that minimized such loads. Boost and lunar touchdown environments were considered to be the mission conditions of greatest structural importance.

In general, load levels expected during boost were derived from instrumentation on *Ranger* flights; however, the most critical condition for the majority of the spacecraft components was that of the lunar soft landing. Derivation of landing loads was necessarily preceded by a landing-dynamics study of spacecraft stability. A test and analysis procedure was used to generate a mathematical model of the spacecraft. This information was utilized in a computer program to determine the dynamic response of spacecraft components for various external inputs furnished by the landing dynamics study.

**Table XIV-1. Boost-phase quasi-static load levels**

| Flight condition[a] | Longitudinal force, g | Lateral force, g |
|---|---|---|
| Liftoff, maximum dynamic pressure, transonic | 2.2 | 0.4 |
| Remainder of powered flight | 0–5.9 | 0.4 |

[a]*Derived from history of Atlas flights.*

To assure structural adequacy, minimum margins of safety were established for comparison with analytically derived margins of safety. The determination of internal loads in the spaceframe and substructure members was accomplished by computer techniques. Detailed stress analyses were based on standard analytical methods.

### 1. Structural Design Criteria

*a. Loads and sources.* The external and internal loads experienced by the *Surveyor* spacecraft resulted from a variety of sources such as aerodynamic forces, engine thrust, pressurization, and other environmental conditions. Critical loads on a spacecraft could occur many times during production, ground-handling, prelaunch test phases, launch, transit, and lunar landing. However, because a *Surveyor* Program design goal was to minimize nonflight loading conditions, design loads were established based on the following conditions:

(1) Boost (combinations of quasi-static accelerations, sinusoidal and random vibration, acoustic excitation, and atmospheric pressure relief).

(2) Descent (quasi-static acceleration and random vibration).

(3) Lunar touchdown (a transient load which was treated in a quasi-static manner). This was the most critical loading condition for the spacecraft.

(4) Lunar operation (the loads resulting from operation of mechanisms such as the SM/SS and the alpha scattering instrument).

**Table XIV-2. Boost-phase mechanical vibration input levels**

| Frequency, Hz | Longitudinal force, g | Lateral force, g | Remarks |
|---|---|---|---|
| 5–50 | 1.5 (zero–peak) VFSW[a] | — | During powered flight |
| 50–1500 | 1.33 (zero–peak) VFSW | — | During powered flight |
| 100–1500 | 4.5 rms (white noise) | — | Liftoff, max dynamic pressure, transonic |
| 1–5 | — | 0.275 in. (zero–peak) VFSW | During powered flight |

| Frequency, Hz | Longitudinal force, g | Lateral force, g | Remarks |
|---|---|---|---|
| 5–15 | — | 0.7 (zero–peak) VFSW | During powered flight |
| 15–50 | — | 0.7 (zero–peak) VFSW | During powered flight |
| 50–1500 | — | 1.33 (zero–peak) VFSW | During powered flight |
| 100–1500 | — | 4.5 rms (white noise) | Liftoff, max dynamic pressure, transonic |

[a]VFSW is variable-frequency sinewave.

**Table XIV-3. Boost-phase acoustic environment**

| Octaves, Hz | Level, db (max)[a] | Level, db (min)[a] |
|---|---|---|
| 22–75 | 135 | 100 |
| 75–150 | 135 | 105 |
| 150–300 | 137 | 106 |
| 300–600 | 137 | 110 |
| 600–1200 | 134 | 109 |
| 1200–2400 | 131 | 100 |
| 2400–4800 | 130 | 95 |
| 4800–9600 | 130 | 90 |
| Overall | 145 | 115 |

[a]Derived from history of *Atlas* flights; results from *Atlas* engine noise at liftoff.

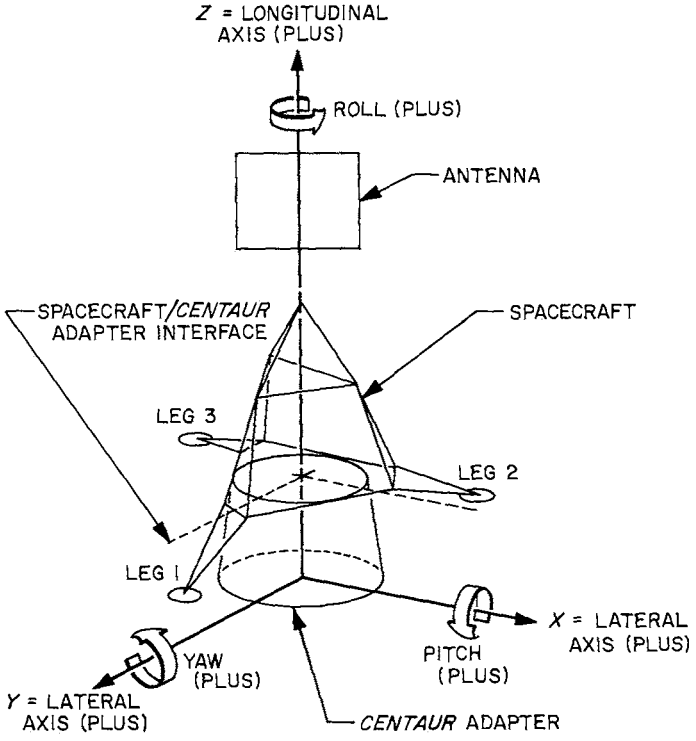



**Fig. XIV-1. Spacecraft coordinate conventions**

The loads from these sources were divided into two basic categories: general and specific. The general loads, presented in this section, were those applied to the overall spacecraft. The specific loads were the more definitive, internal forces arising within the spacecraft, dependent upon the structural response of the various components.

*b. General load criteria.*

*1. Boost.* The estimated load levels and factors for this design condition are summarized in Tables XIV-1, -2, and -3. With the exception of the acoustic environments, all loads were applied at the interface plane between the *Surveyor* spacecraft and the *Centaur* adapter (Fig. XIV-1). The vibration level multiplication factors are shown in Table XIV-4.

*2. Descent.* The descent loading condition shown in Table XIV-5 was quasi-static and vibratory. The quasi-static levels were derived from retrorocket tests; the vibratory loads were based on the vernier engine burning characteristics.

**Table XIV-4. Relative vibration-level multiplying factors**

| Frequency, Hz | Relative level | | |
|---|---|---|---|
| | FA[a] | PA[b] | STA[c] |
| | | Longitudinal (roll) axis | |
| 5–50 | 1.0 | 1.5 | 1.73 |
| 50–1500 | 1.0 | 1.5 | 1.5 |
| | | Lateral axes | |
| 1–15 | 1.0 | 1.25 | 1.44 |
| 15–50 | 1.0 | 1.50 | 1.73 |
| 50–1500 | 1.0 | 1.50 | 1.50 |

[a]Flight Acceptance. This level was associated with values listed in Table XIV-2.

[b]Prototype Approval. This level was used for type approval vibration tests of the prototype vehicle.

[c]Structural Test Acceptance. This level was defined as the boost-phase vibration design-load condition and was used for vibration tests of the structures tests vehicle.

**Table XIV-5. Descent-phase load levels**

| Level type | Longitudinal load[a] | Lateral load |
|---|---|---|
| Quasi-static levels: | | |
| Initial acceleration, g | −4.8 | ±0.1 |
| Final acceleration, g | −12.0 | ±0.1 |
| Vernier engine thrust, lbf | 104.0 | 1.0 |
| Vibration levels: | | |
| Vernier engine, lbf | +16.0 | — |
| Thrust (500 Hz), lbf | −5.0 | 0.0 |

[a]Minus sign indicates deceleration.

3. *Touchdown.* The critical transient loads at touchdown were a function of spacecraft approach velocities to the lunar surface and the physical characteristics of the surface. The design parameters are shown in Table XIV-6.

*c. Acceptance criteria.* Minimum acceptable margins of safety for the *Surveyor* spacecraft structures are presented in Table XIV-7. Margin of safety was defined as the figure obtained by dividing the allowable load by the design load and subtracting 1.0 from the quotient.

A structural member was considered inadequate if the computed margins of safety were less than those tabulated above, unless demonstrated adequate by test.

The limit load was defined as the maximum load that the structure was expected to sustain under specified conditions of operation. The design load was limit load multiplied by an appropriate hazard factor. For pressure vessels hazardous to personnel in the event of failure, the assigned hazard factor value was 1.76–2.40. The value was 1.35 for pressure vessels (and gearboxes) whose failure might jeopardize the mission itself. For components not hazardous to personnel and not mission-critical, the assigned hazard factor was 1.00.

**Table XIV-6. Lunar-touchdown design conditions**

| Description | Parameters |
|---|---|
| Approach velocity[a] | |
| Vertical | 20 ft/sec |
| Lateral | 7 ft/sec |
| Lunar surface characteristics | |
| Slope | ≤15 deg |
| Protuberances | ≤10 cm |
| Surface compressive strength | 50–25,000 psi |

[a]Vector sum ≤ 20.6 ft/sec.

**Table XIV-7. Minimum margins of safety**

| Mission phases | Boost and descent | | Touchdown and lunar operations | |
|---|---|---|---|---|
| | Yield | Ultimate | Yield | Ultimate |
| Simple unit stress | 0.00 | 0.25 | 0.00[c] | 0.10 |
| Combined stress[a] | 0.00 | 0.25 | 0.00[c] | 0.10 |
| Buckling; instability[b] | — | 0.25 | — | 0.10 |

[a]Computed using established interaction formulas.
[b]Includes all compressive elements such as columns and beam-columns.
[c]Applicable only to components with a posttouchdown function.

The allowable load for a structural component was that level at which either the yield or ultimate capability of the member was attained. Yield and ultimate material strength properties used in the analysis were the *B* values (90% probability) as published in MIL-HBK-5. The *A* values (99% probability) were used when the *B* values were not available. Fatigue strength of the material was taken from the lower edge of the scatterband of stress vs number-of-cycles data (stress–number curves). In the event that test data for the stress–number curves were insufficient to provide an adequate scatterband, the allowable life was reduced from the mean by a factor of 4. In addition, an appropriate stress concentration factor was used to determine the allowable fatigue strength value from published stress–number data. Where no notched fatigue data were available, the nominal stress levels were multiplied by the appropriate stress concentration factor. Temperature effects on strength, stiffness, and notch sensitivity were included.

The fatigue strength of the structure was such that, under the application of the design loads, associated load cycles, and Miner's rule for cumulative damage, the structure would not fail. Miner's rule was applied with a coefficient of unity and is written

$$\sum_{i=1\cdots j}\left(\frac{n_s}{n_f}\right)_i = 1$$

where

$n_s$ = number of cycles that a given stress level is applied

$n_f$ = number of cycles to failure by fatigue for the given stress level

$i = 1 \cdots j$ = stress levels

In general, the spacecraft structure was designed to conform to the rules stated, and the following structural acceptance criteria were used:

(1) The structure was not to rupture under any design load conditions.

(2) The structure was not to deform to the extent that spacecraft function was impaired. Where yield occurred, analysis or test verified the structural integrity and proper functioning of components.

## 2. Structural Configuration

The structure of the *Surveyor* spacecraft consisted of a tubular open-truss spaceframe. The framework concept proved to be very adaptable in accommodating changing payload requirements with minimum effects on tooling and spaceframe geometry. Truss assembly substructures of bipod and tripod configurations were used to attach equipment and payload to the spaceframe. Major components, such as landing gear assemblies, antenna/solar panel positioner, retrorocket, and propellant tanks were directly attached to the spaceframe with few secondary structures.

Excluding the retrorocket, the *Surveyor* pressure vessels consisted of six propellant tanks for the vernier propulsion engines, one helium tank for propellant tank pressurization, and a nitrogen tank for the gas-jet attitude control system and the shock absorber of the landing gear assemblies. These pressure vessels were fabricated from 6Al-4V titanium alloy and were man-rated.

*a. Spaceframe.* The open-truss spaceframe (Fig. XIV-2) which provided the basic structure for the spacecraft was constructed from 7075-T6 aluminum tubing joined with machined fittings. The tubular, open-truss concept was selected because of the ease of moving equipment and changing payload as the spacecraft evolved. The tubular elements were made of sufficient strength to allow configuration changes by simple substructure revisions. Round tubing was generally used because it permitted the use of precision boring and honing to obtain proper structural fits. The exception was the 1.5-in.-square tubing used for the periphery of the base where a flat surface interface was desirable.

An additional advantage of tubing was that the structural interface of the tube-socket joints could be fitted to the outside diameter of the tube, permitting wall thickness changes for more or less strength without upsetting the basic spacecraft geometry.

The spaceframe consisted of 95 members with 54 joints. Three column base fittings formed the lower corners of the spaceframe. Each fitting weighed 2.80 lb and was machined from a 125-lb 7075-T6 aluminum forging. Most of the joints in the spacecraft were made by this technique, resulting in a spaceframe which was less than 3% of the launch spacecraft weight.

*b. Substructure.* Aluminum truss assemblies were used to attach the spacecraft equipment and payload items to the spaceframe. Both bipod and tripod truss assemblies were used with fittings riveted to the spaceframe tubes and bolted to the equipment. Bosses were designed into the equipment to accept the truss fittings with alignment or antirotation capability. The following items used similar substructures:

(1) Helium tank.

(2) Nitrogen tank.

(3) Television camera.

(4) Soil mechanics/surface sampler.

(5) Alpha scattering instruments.

(6) Altitude/velocity sensor antenna.

(7) Doppler velocity sensor antenna.

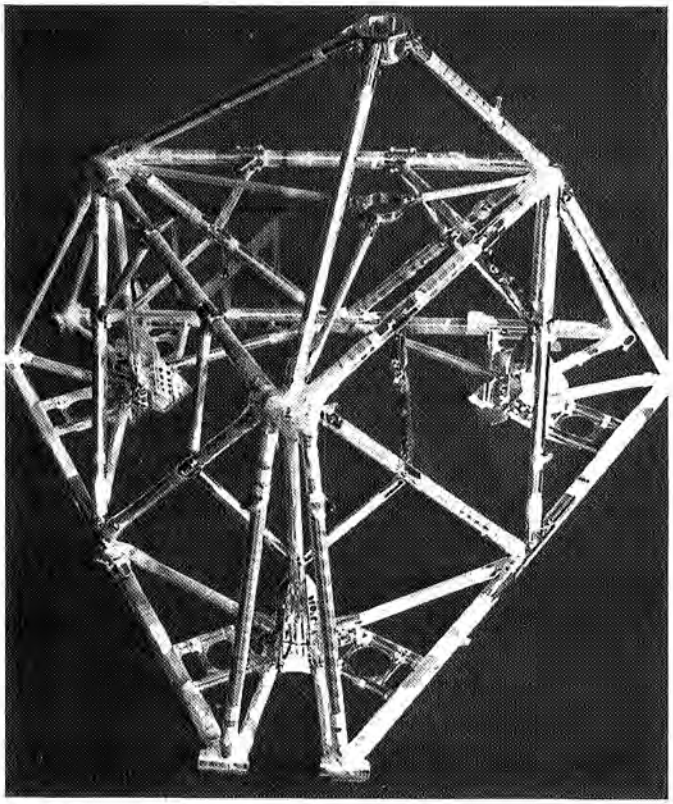
(8) Flight control sensor group.

(9) Auxiliary battery.

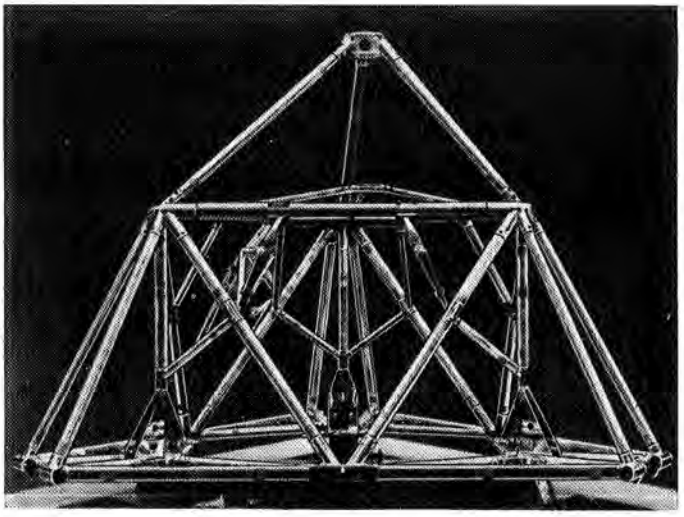
The substructures for the electronic compartments were unique in that they were required to carry structural loads and present a high resistance to heat flow. Fiber-glass inserts were placed in each aluminum tube of the compartment substructures to provide the insulation, as shown in Fig. XIV-3.

*c. Landing gear.* A photo of a typical *Surveyor* landing gear assembly is shown in Fig. XIV-4. Three such assemblies were used on each spacecraft, one hinged at each corner of the spaceframe. The landing legs were in the stowed position prior to nose fairing ejection; they were deployed, upon command, after ejection but before spacecraft separation from *Centaur*. Deployment was accomplished by a leaf spring and two torsion springs after a pyrotechnic pinpuller was fired. The leg rotated until two spring-loaded fingers in the telescoping lock-strut assembly locked the leg in the landing position. Each locking assembly had a switch which gave a telemetry indication that the leg was down and locked. A second switch sent the omnidirectional antenna (omni-antenna) deployment command at the same time. (The legs had to be deployed first due to physical interference.) Each leg had a potentiometer at the spaceframe hinge which provided a variable voltage to indicate the leg deployment angle.

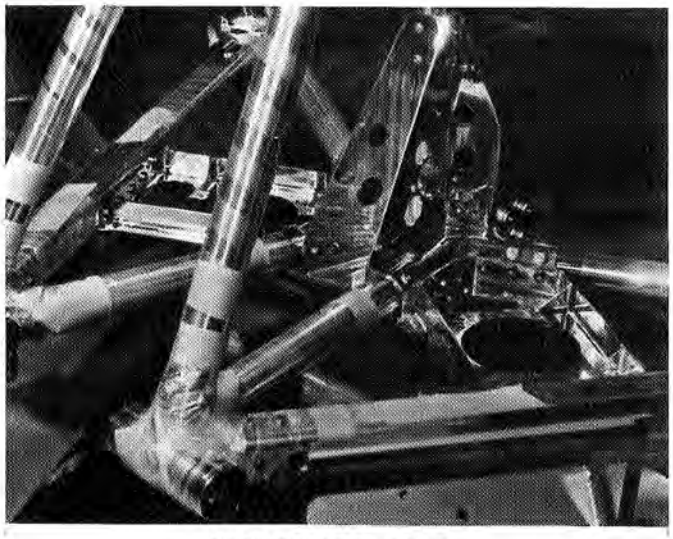
During landing, the legs rotated upward against the resistance of the shock absorber (described in Subsection C-2), which then reextended and was locked by a pyrotechnic device upon command. The crushable honeycomb footpads at the end of each leg were designed to act as mechanical overload filters for the shock absorbers



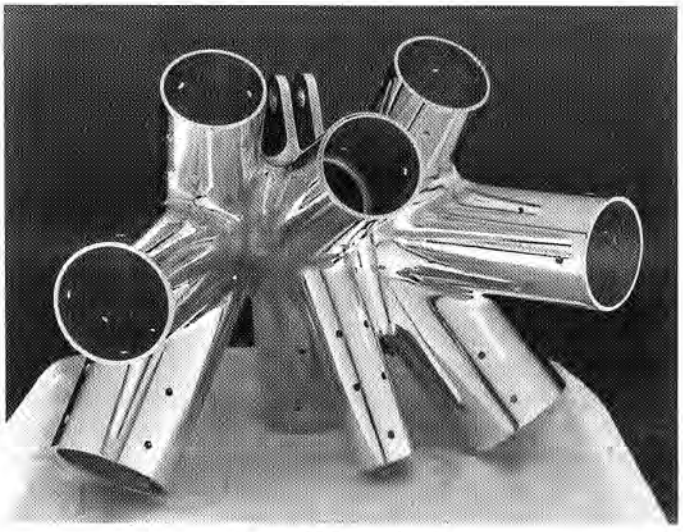
TOP VIEW



SIDE VIEW



CORNER STRUCTURE



CLUSTER FITTING

**Fig. XIV-2. *Surveyor* spaceframe geometry**

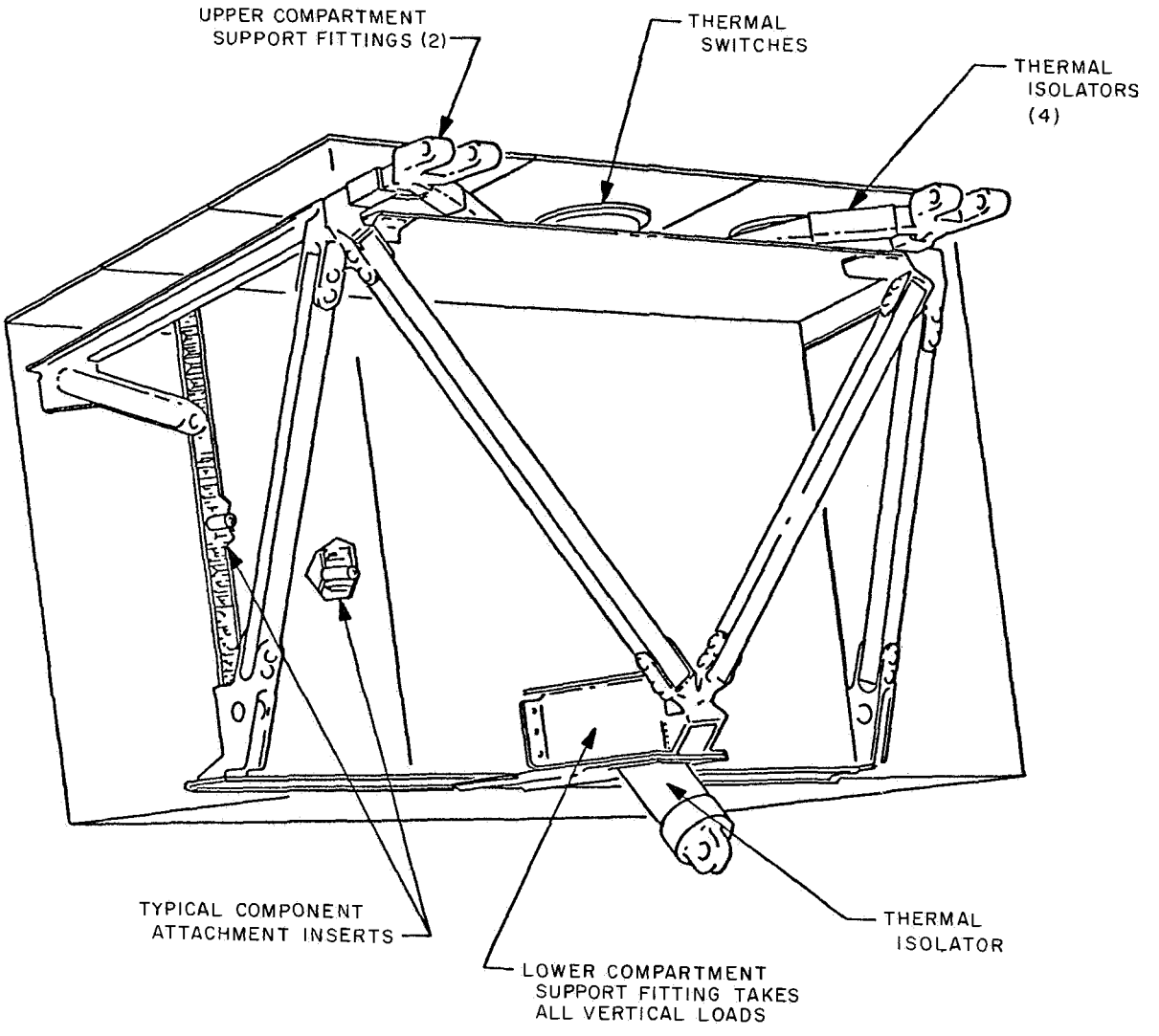



**Fig. XIV-3. Typical compartment substructure**

if landing speeds reached their upper limits. These footpads were made from aluminum and had a crush strength of 10 psi. The shock absorbers dissipated 80% of the landing energy, and the remainder was absorbed by the crushable blocks on the spaceframe as the landing gear deflected. These blocks had a crush strength of 40 psi and were also made from aluminum. The location of the crushable blocks with respect to the landing gear is shown in the insert of Fig. XIV-4.

*d. Antenna/solar panel positioner mast.* The mast provided elevated support for the antenna/solar panel positioner (A/SPP) and was machined from a 7075-T6 aluminum bar to give tapering thickness throughout the length for high structural efficiency. It was secured to the top of the spaceframe with an upper support, which consisted of a collar and tripod formed by members of the spaceframe, and a lower support consisting of a torque collar and hub, also supported by spaceframe trusses as shown in Fig. XIV-5.

*e. Solar panel substrate.* One of the major components on the A/SPP assembly was the solar panel. The panel structure was an adhesive-bonded aluminum honeycomb 0.47 in. thick with 4-mil aluminum facings to provide a flat substrate for the photovoltaic cells. The structural adhesive was FM-1000, an epoxy–nylon compound. After the panel was painted with epoxy dielectric material, the cells were bonded to one face with RTV-40, a silicone adhesive compound prepared by General Electric. The solar panel was attached to the A/SPP arms by brackets which were bonded to the uncelled side of the panel. The arrangement is shown in Fig. XIV-6.

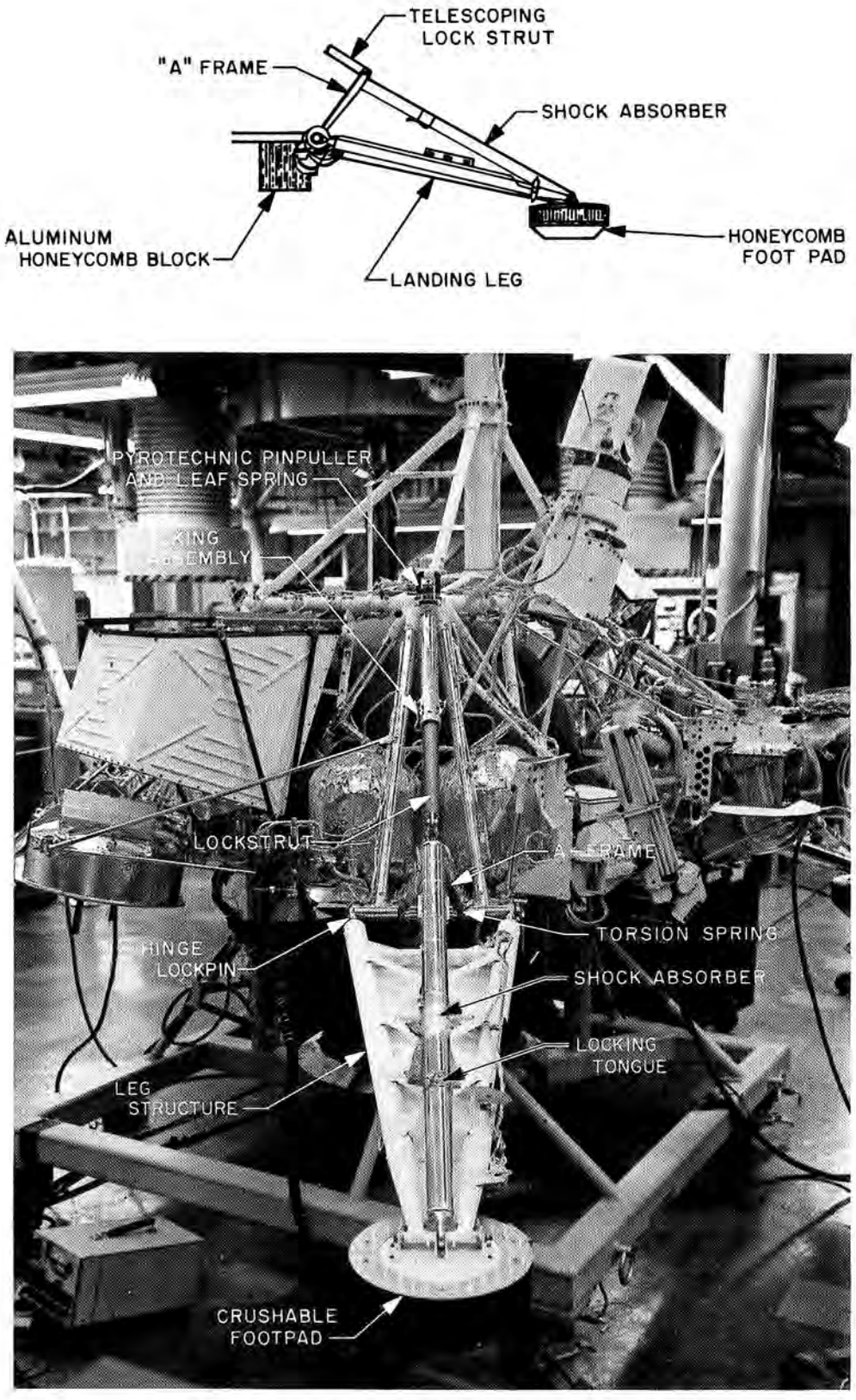



**Fig. XIV-4. Landing gear assembly with crushable blocks**

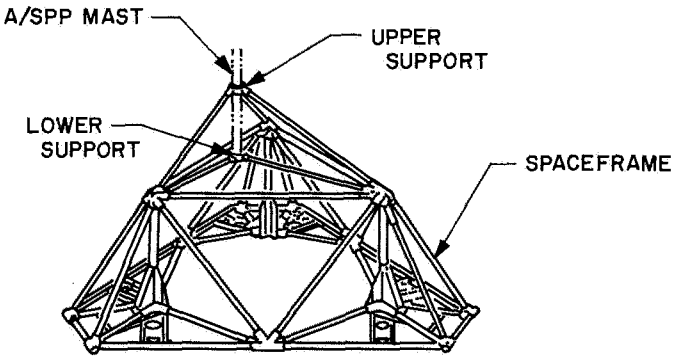



**Fig. XIV-5. Spaceframe with antenna/solar panel positioner support**

*f. Retrorocket case.* The retrorocket case was spherical with a diameter of 37 in. and a length of 55 in., including the nozzle. The total weight of the retrorocket was 1390 lb, of which approximately 1290 lb was propellant.

The retrorocket was attached to the spacecraft at three points inside the spaceframe near the landing leg hinges, as shown in Fig. XIV-7. Separation of the retrorocket after firing was accomplished by three release mechanisms which contained explosive nut disconnects. Friction clips around the nozzle flange provided attachment points for the altitude-marking radar. When the retrorocket ignited, the altitude-marking radar was blown clear of the nozzle by the exhaust gas. The retrorocket case was made of high-strength tool steel (Ladish D6AC), heat-treated to a minimum tensile-yield strength of 200,000 psi, with a minimum wall thickness of 0.037 in.

The support structure of the case consisted of a 4340 steel collar, three 7075-T6 aluminum wishbone struts, and three corrugated-steel thrust skirts. The skirts, welded to the spherical case at three locally thickened areas near the equator of the case at 120-deg intervals, extended aft to connect to the wishbone struts by means of roll pins. The steel collar was clamped on a bolt flange and connected to the wishbone struts by six bolts in spherical bearings. Figure XIV-7 shows how the struts interconnected the thrust skirts and collar to the spaceframe attach point.

Thrust was transferred from the case by the three skirts to the attach points. This loading was assumed to be equally distributed to the three attach points on the spaceframe. Transverse loading was taken out of the engine by differential bending forces through the skirts, while the major portion of the shear load was taken out of the aft closure flange–collar, up the struts to the attach points.

*g. Pressure vessels.* Excluding the retrorocket and shock-absorber vessels, the pressure vessels on the *Surveyor* consisted of an oxidizer and a fuel tank of the same design for each vernier engine (total of six propellant tanks), a helium tank which provided pressurization for the propellant tanks, and a nitrogen tank which contained high-pressure nitrogen for the gas jet attitude-control system. The physical position of the pressure vessels is shown in Fig. XIV-8.

The helium tank, 14.2 in. in diameter, was made from 6Al-4V titanium alloy, and had an operating pressure of 5175 psig at 100°F with a minimum burst pressure of 11,385 psig. The six propellant tanks also were made of 6Al-4V titanium alloy and were designed to: (1) have a prelaunch pressure of 346 psig, and (2) operate at a nominal pressure of 830 psig with a minimum burst pressure of 1038 psig. The propellant tanks were cylindrical with hemispherical ends; they had an overall length of 14 in. and a diameter of 10 in. The nitrogen tank was 9.6 in. in diameter and was also made from 6Al-4V titanium alloy. Its operating pressure was 5000 psi at 125°F with a minimum burst pressure of 11,000 psig. The description of all pressure vessels is summarized in Table XIV-8.

### 3. Evaluation of Design

*a. Structural analysis.* The structural analysis of the spaceframe and substructure was accomplished under the assumption that the external component loads would be transferred to the spaceframe at the substructure attach points. In general, the most critical spacecraft loads resulted from the inertia of the various components during touchdown on the lunar surface.

Internal loads in the spaceframe members were determined by the frame structure analysis program, a computer program designed by IBM to perform an elastic analysis of a tridimensional frame structure with arbitrary joint conditions, giving member forces and deflections under various loading conditions. The analyses were performed on a unit-load basis. Six loads (three unit loads and three unit moments) were applied separately at the center of gravity of each component of the assembly under analysis. Loading at any particular axis then was placed in static equilibrium by loads applied at the composite center of gravity of the assembly. The loads determined were multiplied by the computer unit-load solution, yielding the internal loads at the joints of the idealized structure. Once these forces and deflections were known, the stresses in all members were computed. Worst-case tolerance conditions were used since these could have affected the strength of the parts. The analyses

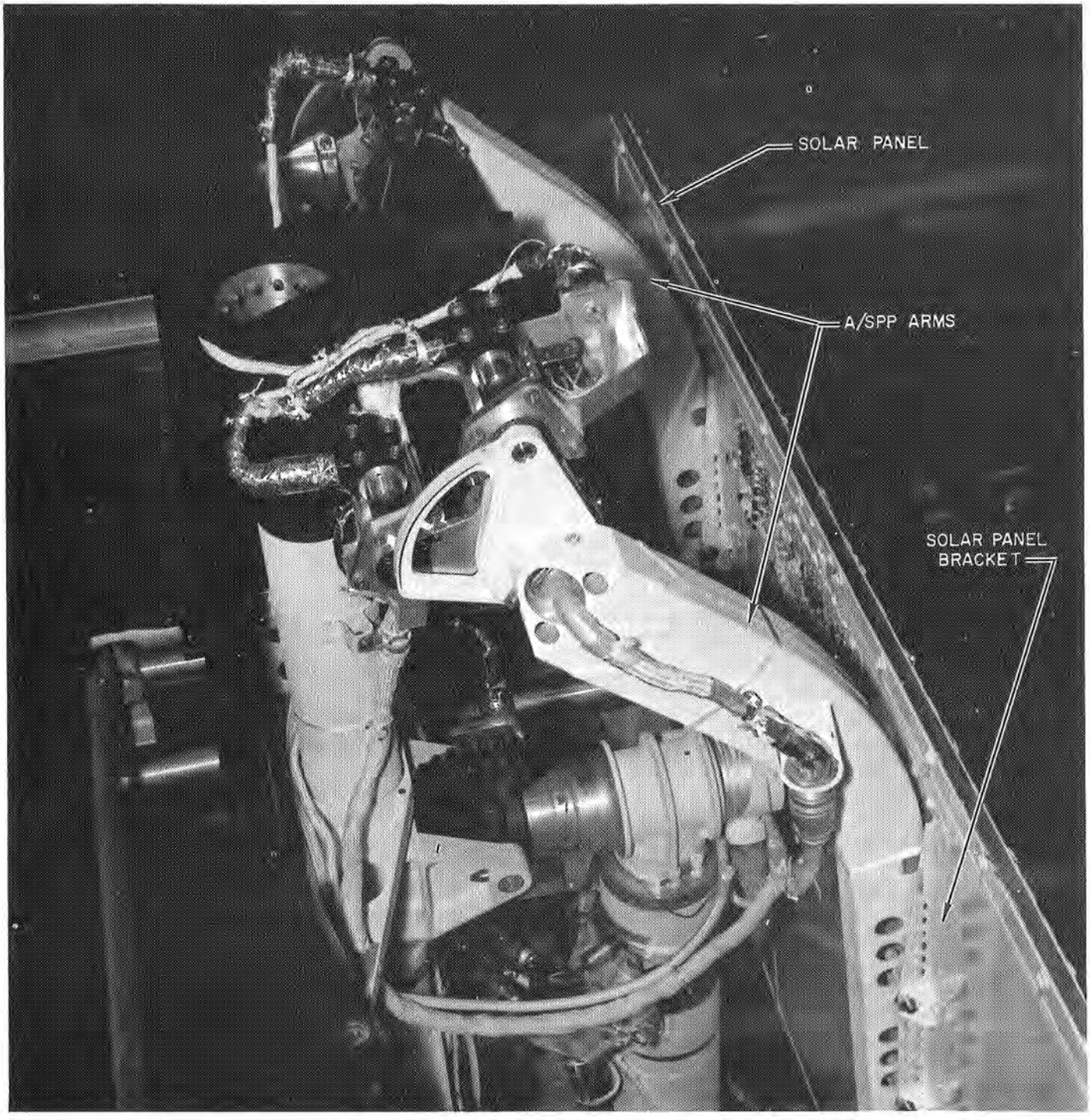



**Fig. XIV-6. Solar panel bracket attachment**

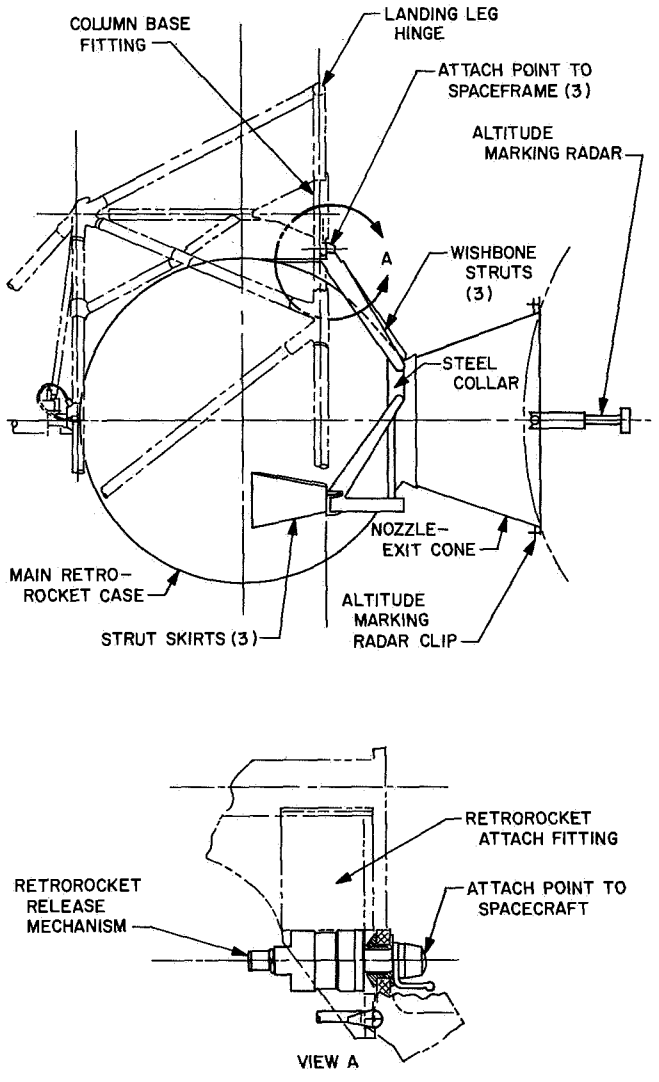



Fig. XIV-7. Retrorocket mounting detail

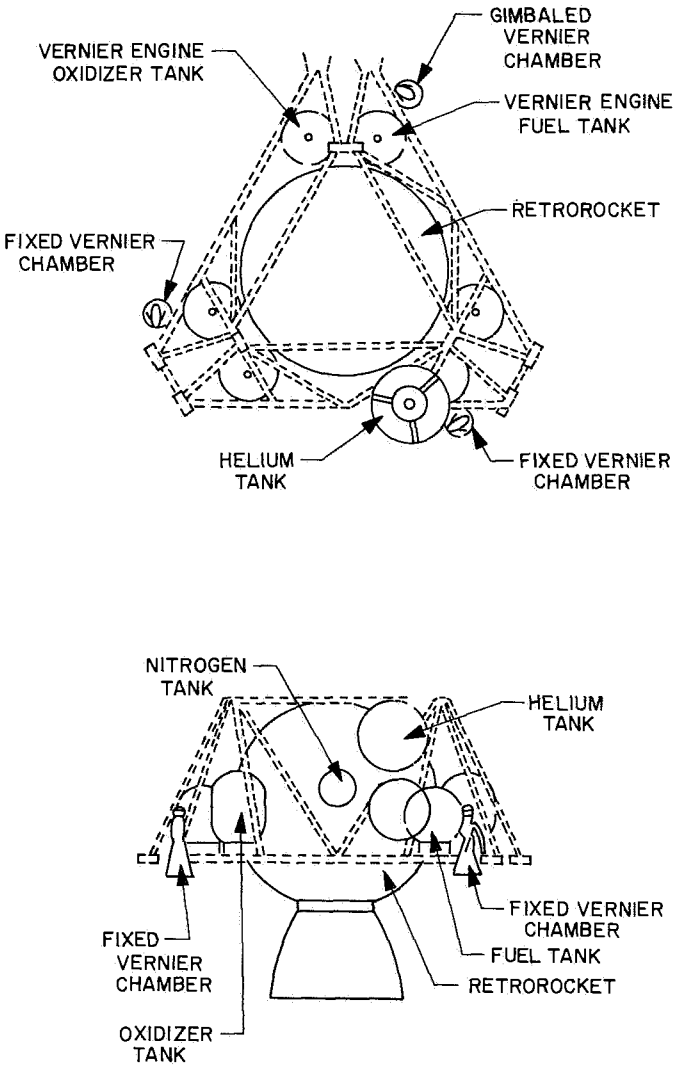



Fig. XIV-8. On-board arrangement of pressure vessels

**Table XIV-8. Pressure vessel description**

| Parameter | Propellant tank | Helium tank | Nitrogen tank |
|---|---|---|---|
| Shape | | Spherical | Spherical |
| Length of cylinder, in. | 3.23 | — | — |
| Ends | Hemispherical | — | — |
| Radius (internal), in. | 4.915 | 6.770 | 4.560 |
| Thickness, in. | 0.023 | 0.276 | 0.186 |
| Membrane | 0.018 | 0.270 | 0.181 |
| Weld | 0.048 | 0.316 | 0.225 |
| | 0.044 | 0.310 | 0.220 |
| Volume, in.$^3$ | | | |
| Min required | 736 | 1,291 | 395 |
| Actual | 742 | 1,298 | 398 |
| Weight, lb | | | |
| Max allowable | 2.28 | 27.80 | 9.98 |
| Actual | 2.11 | 27.04 | 9.10 |

| Parameter | Propellant tank | Helium tank | Nitrogen tank |
|---|---|---|---|
| Safety factor | 1.25 | 2.20 | 2.20 |
| Pressure, psig | | | |
| Operating | 830 | 5,175 | 5,000 |
| Proof | | | |
| Room temperature | 960 | 8,684 | 8,400 |
| −320°F | 1,325 | 12,158 | 11,725 |
| Burst | | | |
| Min required | 1,038 | 11,385 | 11,000 |
| Min actual | 1,370 | 12,215 | 13,500 |
| normalized | 1,235 | 11,670 | 12,250 |
| Number of units | 139 | 38 | 31 |
| Material | Ti 6A1-4V | Ti 6A1-4V | Ti 6A1-4V |

investigated a sufficient number of conditions to assure that all critical stresses were calculated.

Friction effects for load-carrying capability were used where the validity of such assumed load paths could be demonstrated by test. Thermal effects were not critical except in a few cases, such as bolt preloads and interference fits. The analytical methods used were from textbooks, structure manuals used by major aircraft companies, and government publications such as MIL-HBK-5 and NACA/NASA reports.

The criteria used for all analyses were those stated in Table XIV-6; that is, for the touchdown and lunar-operation phase of the mission, a minimum margin of safety of 0.00 was required when stresses due to limit loads were compared with the material allowable yield stress, and 0.10 when compared with allowable ultimate stresses. Moduli of rupture in bending and torsion were used where applicable to establish allowable stresses.

A summary of the structural analysis performed is presented in Table XIV-9. It describes the results of the analyses and contains a tabulation of minimum margin of safety for some of the components analyzed.

***b. Vessel design evaluation and qualification.*** All *Surveyor* pressure vessels were man-rated and designed for a 2.20 hazard factor over the maximum operating pressure for 6Al-4V titanium with an ultimate tensile strength of 145,000–160,000 psi. With an ultimate tensile-strength range of 155,000–170,000 psi, a safety factor of 3.0 was required. JPL specifications were used to establish design and qualification requirements of pressure vessels used in the vicinity of personnel.

For design evaluation and qualification of man-rated pressure vessels such as the propellant, helium, and nitrogen tanks, three vessels of each design were subjected to a bulk yield and burst test to obtain the pressure–volume data as well as burst-pressure data. From these data, the following parameters were determined:

(1) Bulk yield pressure.

(2) Normalized burst pressure.

(3) Normalized burst-pressure spread.

(4) Proof pressure for flight-hardware qualification.

Table XIV-10 shows tank hazard factors at two temperature ranges.

The burst pressures of the three vessels were not to exceed a spread of 5% when normalized. (Normalizing is that process which takes account of the ratios of *minimum required thickness* to *actual thickness* and *minimum required tensile strength* to *actual tensile strength* of the material to give a minimum normalized burst pressure.)

## Table XIV-9. Structural analysis summary

| Components | Part number and material | Critical loading condition | Critical loads | Maximum computed stress, psi | Margin of safety | Remarks |
|---|---|---|---|---|---|---|
| Spaceframe (1) Tube | 230301-5 (7075-T6) | Landing, leg 2 downhill | P = 1389 lb<br>M = 760 in.-lb<br>T = 250 in.-lb | 21.9 (compression) | 1.92 | Connects column base to main lower fitting |
| (2) Tube | 230301-4 (7075-T6) | Landing, leg 2 downhill | P = 1393 lb<br>M = 2510 in.-lb<br>T = 80 in.-lb | 54.6 (compression) | 0.21 | Connects column base to leg journal |
| (3) Tube | 230301-1 (7075-T6) | Landing, leg 2 downhill | P = 3320 lb<br>M = 4280 in.-lb<br>T = 320 in.-lb | 38.2 (tension) | 1.02 | Square tube; main lower member of spaceframe |
| (4) Socket | 230296 (7075-T6) | Landing, leg 2 downhill | P = 410 lb<br>M = 1870 in.-lb<br>T = 2160 in.-lb | 10.0 (tension) | High | One of three main sockets at top of spaceframe |
| (5) Column base | 230291 (7075-T6) | Boost<br>5.9-g vertical<br>0.4-g lateral | P = 2900 lb | 6.7 (tension) | High | One of three "keels" of the spaceframe–2.816; part machined from 125 lb billet |
| A/SPP support structure (1) Tube | 230301-9 (7075-T6) | Landing, leg 1 downhill, polar angle: 36.5 deg | P = 331 lb<br>M = 4120 in.-lb | 61.9 (compression) | 0.07 | Leg 2 of upper tripod support |
| (2) Tube | 230301-11 (7075-T6) | Landing, leg 2 downhill, polar angle: 70.5 deg | P = 2950 lb | 27.3 (compression) | 0.20 | Leg 3 of lower tripod; critical in elastic buckling |
| Landing gear (1) Lockstrut | 230257 (7075-T6) | Landing,<br>15 g vertical | P = 6480 lb | 35.2 (compression) | 0.32 | Strut critical in column bending |
| (2) Leg | 230262 (7075-T6) | Landing, side load of 1500 lb | 124 lb per spotweld | — | 0.19 | Spotwelds attaching skin to leg tubes are critical in shear |
| (3) Footpad bracket | 230477 (7075-T6) | Landing, side load of 1500 lb | P = 1875 lb<br>M = 5070 in.-lb | 57.4 (bending) | 0.12 | Margin based on interaction of shear and bending stress |
| (4) Pin | 230225 (6Al-4V Ti) | Landing | P = 6480 lb<br>M = 770 in.-lb | 203.0 (bending) | 0.11 | Pin connects lockstrut to A-frame. Margin based on interaction (shear and bending) |
| Compartment A substructure (1) Strut | 261520-3 | Landing,<br>18 g, vertical<br>9 g, lateral | P = 469 lb<br>M = 103 in.-lb | 21.9 (bending) | 0.15 | Upper right-hand strut (plastic tube used for thermal insulation) |
| (2) Clevis | 261268 (7075-T6) | Landing,<br>18 g vertical<br>4.5 g lateral | P = 4211 lb<br>M = 128 in.-lb | 51.3 (bending) | 0.385 | Upper left-hand bipod clevis |

## Table XIV-9 (contd)

| Components | Part number and material | Critical loading condition | Critical loads | Maximum computed stress, psi | Margin of safety | Remarks |
|---|---|---|---|---|---|---|
| Compartment B substructure (1) Strut | 261520-8 | Landing, 21 g vertical 5 g lateral | P = 1079 lb M = 30 in.-lb | 15.6 (bending) | 0.60 | Upper right-hand strut (plastic tube) |
| (2) Strut-to-clevis bond | | Landing, 21 g vertical 5 g lateral | P = 1079 lb | 1.2 (shear) | 0.70 | Margin established by testing |
| (3) Support-tube rivets | NAS-1398D (2017-T4) | Landing, 21 g vertical 9 g lateral | 499 lb shear per rivet | — | 0.26 | Rivets attach tube to compartment fitting |
| Helium tank substructure (1) Tube | 262850-12 (2029-T3) | Landing, 25 g vertical | P = 823 lb | 12.7 (compression) | 0.88 | Tube is left-hand member of upper support tripod; critical in column stability |
| (2) Yoke | 276945 (7075-T6) | Landing, 25 g lateral | P = 749 lb | — | 0.15 | Lug analysis indicated yoke critical in tension |
| TV camera substructure (1) Tube | 262850-26 (2024-T3) | Boost, 2.0 g vertical 16.4 g lateral | P = 732 lb M = 63.0 in-lb | 23.6 (compression) | 0.25 | Upper right-hand support tube; critical in bending plus column action |
| (2) Cluster | 230036 (7075-T6) | Boost, 2.0 g vertical 16.4 g lateral | Complex, multi-directional | 59.2 (bending) | 0.36 | Right-hand cluster fitting critical in shear and bending |
| Flight control sensor group substructure (1) Rivets | 261407 (2017-T4) | Landing, 25 g lateral | P = 327 lb to shear per rivet | — | 0.01 | Four rivets secure clevis to tube |
| (2) Fitting | 264228 (7075-T6) | Landing, 25 g lateral | P = 660 lb | 38.8 (bearing) | — | Upper right-hand fitting (forward) joins support tube to sensor group |
| RADVS substructure (1) B pod cluster | 264262 (7075-T6) | Landing, 25 g vertical | P = 179 lb | — | 0.16 | Cluster critical in buckling |
| (2) Yoke | 264222 (7075-T6) | Landing, 25 g vertical | M = 73.5 in.-lb | 102.5 (bending) | 0.10 | Attaches RADVS support tube to spaceframe square tube |
| A/SPP (1) Solar panel arms | 3028196 (6061-T6) | Landing, leg 1 downhill, polar angle: 36.5 deg | Multidirectional moments, (600–2200 in.-lb) | 12.1 (compression) | 0.17 | Arms critical in buckling; interaction of shear, bending, and compression |
| (2) Antenna support tube | 293458 (7075-T6) | Landing, leg 1 downhill, polar angle: 36.5 deg | M = 12,678 in.-lb | 66.8 (bending) | 0.04 | Maximum bending occurred at portion of tube between the square rings |

## Table XIV-9 (contd)

| Components | Part number and material | Critical loading condition | Critical loads | Maximum computed stress, psi | Margin of safety | Remarks |
|---|---|---|---|---|---|---|
| (3) Gear set, worm and sector | 3028029 (7075-T6) | Landing, leg 1 downhill, polar angle: 36.5 deg | P = 10,800 lb | 32.4 (shear) | 0.02 | Stress maximum in tunnel section of gear |
| (4) Tapered elevation lockpin | 302028 (7075-T6) | Landing, leg 1 downhill, polar angle: 36.5 deg | M = 12,588 in.-lb | 31.0 (tension) | 0.05 | Combined shear and tensile stress in elevation—axis lockpin ring |
| (5) Mast | 293451 (7075-T6) | Landing, leg 1 downhill, polar angle: 70.5 deg | M = 52,200 in.-lb | 71.0 (bending) | 0.03 | Critical section just above flanged portion of tube |
| SM/SS | | | | | | |
| (1) Elevation gear | 3024713 (2024-T4) | Lunar operation, digging | Elevation motor, stall torque = 68 in.-lb | 34.6 (bending) | 0.15 | Elevation internal gear teeth critical in bending |
| (2) Extension linkage tubing | 3024726 (7075-T6) | Lunar operation, digging | Elevation motor, stall torque = 68 in.-lb | 56.2 (bending) | 0.12 | Maximum stress occurs in area of central pin joints with linkage fully extended |
| (3) Extension linkage | 3024730 (7075-T6) | Lunar operation, picking | Impact transient, 274 lb | 52.2 (bending) | Predicted fatigue life: 1250 cycles | Transient based on shovel velocity of 10 ft/sec with a penetration of 0.072 in. |
| (4) Helical torsion spring | 3024787 (302 stainless) | Boost, stowed position | 185 deg twist<br>M = 0.23 in.-lb | 183.5 (bending) | 0.07 | Springs are wound when extension linkage is compressed to flight position |
| Alpha scattering instrument | | | | | | |
| (1) Nylon cord | 72NOB8 (#18) (nylon) | Deployment | P = 25.5 lb | — | 0.39 | Maximum tensile load of 25.5 lb occurred during earth deployment tests under 1 g |
| (2) Bracket, brace support | X3024822 (7075-T6) | Firing of pinpuller | P = 434 lb | 76.8 (bending) | 0.01 | Force can be generated if the pin and lugs lock up after firing pinpuller |
| (3) Pallet shaft | X3024808 (302 stainless) | Deployment | M = 7.23 in.-lb | 37.8 (bending) | 0.12 | Maximum load results from deployment tests under 1 g |

Three design reliability requirements were:

(1) A maximum spread of 5% normalized burst pressures on the initial three burst-test vessels.

(2) Use of ductile-type bursts.

(3) Satisfactory completion of type-approval test program with three production pressure vessels selected at random.

The design also required that every tenth production tank be subjected to a bulk yield and burst test for quality control. The reliability requirements for the one-in-ten burst test were:

(1) Normalized burst pressure equal to or greater than 95% of the average of the three initial burst vessels (burst must be of a ductile type).

(2) More than minimum volume.

(3) Less than maximum weight.

The 5% spread in burst pressure allowed in the three initial burst tests and the one-in-ten burst test emphasized the need for adequate control of the mechanical properties of the material and adequate dimensional control during fabrication of the vessels.

When stress corrosion problems were found in titanium tanks used in another NASA program in which the vehicle environment was similar to that of *Surveyor*, a special test program was initiated. Four propellant tanks were exposed to MON-10 at temperatures of 110–270°F, at pressures of 840–960 psig, and with exposure times of of 7–16 days.

Two pressure vessels were proof-tested after completion of the exposure tests. Sections taken from these vessels were metallurgically examined and found to be satisfactory; no stress-corrosion cracks were detected under a magnification of 1000×. Two other vessels were burst at 270 and 240°F, respectively, after completion of the exposure test. The burst pressures were 1375 and 1300 psig, respectively. The minimum required burst pressure was 1050 psig (see Section XVII-A-3).

**Table XIV-10. Bulk yield pressure**

| Conditions | Proof pressure safety factor | |
|---|---|---|
| | Helium and nitrogen tanks | Propellant tank |
| Room temperature | 0.85 | 0.90 |
| −300 to −320°F | 1.19 | 1.26 |

*c. Spacecraft landing dynamics analyses and testing.* Two important aspects of landing dynamics were considered: stability and structural survival. For an assessment of landing stability, a mathematical model was conceived to simulate the kinematic and dynamic characteristics of the landing gear mounted on a rigid body with estimated mass and inertia properties of the *Surveyor* spaceframe and components. This mathematical model was used to perform landing-dynamics analyses in the landing computer program, together with the various spacecraft initial conditions such as attitudes and velocities prior to touchdown on a constant landing-surface slope with a constant surface-friction coefficient.

Parametric studies, conducted with this landing simulation program, provided data for the detail design of the landing gear. As the spacecraft and landing gear design became firm, the program was used for investigation of combinations of landing parameters (spacecraft orientation and velocities at touchdown, lunar surface slope, and friction coefficient) for bidimensional or planar landings. In a planar landing, the spacecraft center of mass moves in a plane containing the lunar vertical and the maximum-slope direction of the assumed landing plane. This confines the landing conditions to velocities in this plane only and the spacecraft lands either uphill, downhill, or with zero horizontal velocity. Also, the spacecraft attitude is assumed to be symmetrical about this plane; i.e., one leg is either leading or trailing, and any initial spacecraft tilt is such that the spacecraft Z axis remains in this plane of symmetry.

While these studies provided a good assessment of the stability boundaries for planar landings, other environmental and spacecraft conditions had to be considered. A critical condition could have arisen if the bearing strength of the landing surface had not been sufficient to arrest the footpads vertically. However, a limited amount of analytical and experimental work showed that no significant degradation in landing stability occurs in soft-surface landings as long as the surface is strong enough to prevent excessive spacecraft sinkage. Footpad penetrations of several feet, however, might have seriously jeopardized the functioning of the spacecraft. This case was excluded from consideration by the design specification.

Tridimensional or nonplanar landings were also investigated. Under the original landing simulation program, it was impossible to handle other than planar landings. A new and more refined simulation (Ref. XIV-1) was conceived for the tridimensional landings and for checking the results obtained with the planar simulation. No significant degradation in landing stability due to cross-slope velocities or other tridimensional landing conditions was found. Only one combination of tridimensional conditions showed a stability below that of the comparable planar case. Therefore, the tridimensional effects were disregarded as long as the bidimensional stability boundaries were shown to be well outside the design conditions. This was shown by a comparison of analytical and test results for the worst planar case—a landing on a sloped surface with a downhill horizontal velocity and one leg trailing, minimizing the tipover radius.

The analytical points in Fig. XIV-9 are based on the second simulation program. The horizontal spacecraft velocity at initial touchdown, plotted along the abscissa, served as a stability indicator; the horizontal velocity was varied with all other parameters remaining fixed until an unstable landing was encountered.

The second simulation program indicated considerably more landing stability capability than the first, proving that the first program was excessively conservative.

Concurrent with the stability investigation, a structure and component landing-load analysis was performed which later was supplemented with a series of landing tests employing instrumented full-size structural test vehicles.

After the landing gear design parameters had been determined, it was apparent that the maximum landing-shock forces acting on the center of gravity of the spacecraft, assuming a nonelastic main structure, would never exceed 60% of the specification values of 12 and 30 g in the horizontal and vertical directions, respectively. While this indicated a satisfactory overall design of the landing system, individual component loads generally were higher than the center-of-gravity loads, depending upon their locations and support structures within the spacecraft.

Deriving the landing-induced component loadings was a complex task, and a semianalytical procedure was used in the *Surveyor* Program. After the bascic-frame and component support substructures had been designed based on estimated quasi-static loads, a structural test vehicle was built so a modal survey could be performed to experimentally determine natural frequencies and corresponding mode shapes. Using the modal information, the elastic spacecraft system was represented by 16 uncoupled differential equations (6 rigid-body modes plus 10 elastic modes) combined in one matrix equation by use of the generalized mass and stiffness matrices. This provided a forced-response solution for any excitation. Landing simulations then were performed, using as inputs the force-vs-time histories at the six ground-contact points obtained in the previously described stability program.

With accelerations of all important spacecraft components determined by this analysis, stresses in connecting structural members were computed. By this procedure, adequacy of the original design was verified and some redesign requirements were established, as in the case of the antenna/solar panel substructure, where peak loads of up to 90 g were shown to exist.

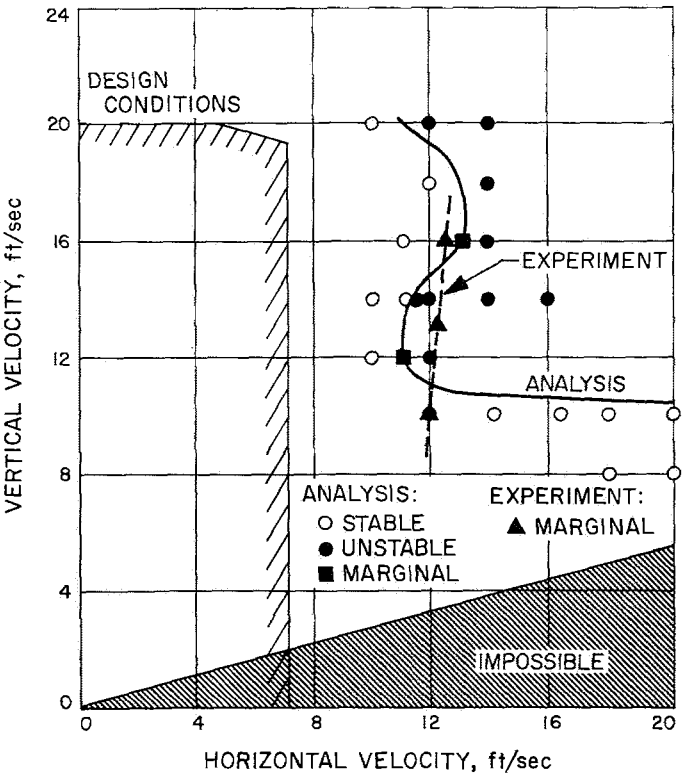



**Fig. XIV-9. Landing stability boundaries for planar downhill landings on 15-deg slope. Spacecraft orientation is with one leg trailing**

*d. Spacecraft boost-phase vibration testing.* Three distinct levels of vibration inputs were used for the evaluation of spacecraft component responses and system qualification.

The flight acceptance testing was based on an estimate of the 2 $\sigma$ or 95% flight environment (which includes all conditions that could occur with a 95% probability). Each flight spacecraft and its components were tested to this level (designated A) to assure flightworthiness.

Type approval testing was imposed on structures and assemblies which were identical to flight items to verify adequacy of the design and performance of the spacecraft system. Structures and assemblies exposed to type approval level tests (designated B) were not subsequently used as flight items.

Structural type approval testing (designated C) was used on structural test models of the spacecraft and its assemblies. The spacecraft or assemblies tested were normally identical to flight hardware, but some static and dynamic mockup assemblies were used. The amplitude or test level used with any particular component was defined in the appropriate unit specification.

## B. Structural and Dynamic Testing

The structural test effort on *Surveyor* was extensive since design of the spacecraft was initiated when there was only limited experience on space missions. Also, the dynamic characteristics of the launch vehicle were unknown since its development was concurrent with development of *Surveyor* itself. As a result, the *Surveyor* was developed by a process of evolution as design requirements and conditions became better defined. Early in the program, the need for special structural test vehicles was established, which resulted in development of the S-1, S-2, S-2A, T-1, S-9, and S-15 series of vehicles. These vehicles evolved along with the spacecraft in response to design changes and the need for structural test vehicles. The S-1, the earliest configuration, was used for the first vibration and static load tests. The S-2, S-2A, and S-9 were used for later structural and dynamic tests, with S-9 representing the final configuration. The touchdown stability of the spacecraft was evaluated with the T-1 and S-15 vehicles. Table XIV-11 is a summary of all tests (including their completion dates) performed on these test vehicles.

Because their performance was so critical to the success of *Surveyor*, the retrorocket and pressure vessels were subjected to a series of separate comprehensive tests. Among the retrorocket tests were separation tests and the static-firing tests to determine the nature of thrust transients. The pressure-vessel tests were composed chiefly of burst tests, and served to qualify the design as man-rated.

### 1. Structural Test Programs and Vehicles

*a. S-1 structural test vehicle.* The S-1 vehicle utilized a welded spaceframe structure with dummy units representing the mass properties of the various components. Vibration testing was performed on this vehicle to determine the following:

(1) Dynamic amplification of the *Centaur* adapter.

(2) Extent of spacecraft/*Centaur* nose fairing interference.

(3) Potential problems arising from unit response.

Vibration input to the vehicle was 0.25 $g$ rms from 5 to 200 Hz. Although this was only one-third the specified test level, failures occurred in welds on the mast support tube, in the mounting brackets for television cameras, and in an upper support tube for the helium tank. It was also found that due to excessive solar panel excursion during resonance of the A/SPP mast, the solar panel collided with the mast.

**Table XIV-11. Test milestones of special test vehicles**

| Vehicle | Type of test performed | Date of completion |
|---|---|---|
| S-1 | Vibration test (lateral axis) | November 1961 |
| | Static test | January 1962 |
| S-2 | Static test | June 1963 |
| | Modal survey | October 1963 |
| | Vibration test | |
| | Longitudinal axis | November 1963 |
| | Lateral axis | Incomplete |
| | Drop test (load investigation) | February 1964 |
| S-2A | Vibration test | |
| | Longitudinal and lateral axes | December 1964 |
| | Modal survey | January 1965 |
| | Drop test (load investigation) | August 1965 |
| S-9 | Torsional vibration test | October 1965 |
| | Static test | March 1966 |
| | Transfer function evaluation | November 1966 |
| | Modal survey | December 1966 |
| | Rough-ride road test | February 1967 |
| | Vibration test | |
| | Longitudinal and lateral axes | June 1967 |
| | Drop test | August 1967 |
| T-1 | Drop test (stability investigation) | April 1963 |
| S-15 | Drop test (stability investigation) | October 1966 |

Static testing was performed on the S-1 to verify analytically derived load and stress information. The S-1 was mounted on a model *Centaur* adapter, and loads were applied at the centers of gravity of the dummy units. Lateral loads were applied in the plane of the upper spaceframe and to the adapter at the spacecraft/adapter interface. Testing was completed in January 1962, and resulted in good load-vs-deflection data.

***b. S-2 structural test vehicle.*** The spaceframe and substructure of the S-2 test vehicle were similar to those of the A-21 spacecraft, but were made of the more brittle 7178-T6 aluminum alloy rather than the 7075-T6. The components installed on the S-2 vehicle were generally deadweight ballast units (proper weight simulation), although a few were dummy units (nonoperating components with proper mass-properties simulation). The retrorocket, where applicable, was fully loaded but inert. An empty retrorocket case was used during the static tests to simulate retrorocket burnout. The S-2 vehicle was subjected to:

(1) Modal survey.

(2) Type approval vibration testing.

(3) Drop tests.

(4) Static tests.

The modal survey was conducted to determine the elastic modes of the spacecraft for launch, flight, and landing configurations for the use of spacecraft dynamic loads or stability analyses. These surveys were by the use of controlled, low-level shakers located at strategic points of the spacecraft with sinusoidal inputs to excite its natural elastic modes. Due to the nonlinearity of the spacecraft and the test setup and accelerometer placement, many of the spacecraft modes could not be identified. In all cases, an acceptable relationship of mode orthogonalities was demonstrated before use of the set in analytical studies. The frequencies of the observed modes are shown in Table XIV-12.

**Table XIV-12. Result of S-2 modal survey**

| Spacecraft configuration | Frequencies of modes, Hz |
|---|---|
| Launch | 8.45, 16.8, 23.6, 35.9, 38.8, 48.1, 51.8, 57.4, 60.0, 71.2 |
| Flight | 11.1, 18.1, 19.7, 25.3, 36.3, 45.3, 47.9, 49.0, 62.1 |
| Landing | 12.2, 13.4, 19.5, 21.1, 23.8, 26.6, 28.5, 30.8, 35.2, 38.2, 47.4, 60.5, 75.5 |

The objective of the S-2 type approval vibration test was to qualify the *Surveyor* spaceframe and substructure for boost dynamic loads. The S-2 vehicle was upgraded to incorporate new compartments and a new flight control sensor group substructure. The vehicle was mounted to a test fixture by use of the spacecraft/adapter attach points. The test levels were as shown in Table XIV-13.

During the lateral test in the X-axis (input normal to leg 1), the upper supports for compartment B failed and the thermal switches on compartments A and B were damaged. Simultaneous response of compartment B about the X and Y axes resulted in an unforeseen increase in levels. Relative motion between the compartment canisters and thermal trays probably caused the damage to the thermal switches. The final test of the vehicle along the Y axis resulted in the failure of a welded joint on the A/SPP.

The objective of the S-2 drop test was to qualify the *Surveyor* spaceframe and substructure for dynamic loads resulting from lunar landing. The drop tests allowed free fall of the vehicle under earth gravity, but could be compared with lunar landing on the basis of total energy dissipated in the landing gear and crushable blocks. A standard vertical velocity of 20 ft/sec at touchdown was selected rather than a simulation of specific landing conditions. The first drop, onto a level surface, resulted in the fracture of a fiber-glass upper support member on compartment B. The third drop, onto an inclined surface of 15 deg, resulted in failure of a welded joint on the solar panel support structure. High-speed motion pictures disclosed that this failure probably was due to the snagging of the solar panel by one of the spacecraft support cables during the drop.

The primary purpose of the static test was to qualify the spaceframe and the unit support substructure design

**Table XIV-13. S-2 vibration input level**

| Axis | Frequency range, Hz | Level (zero–peak), g | Minimum sweep time, min |
|---|---|---|---|
| Longitudinal | 5–40[a] | 2.5[b] | 3 |
| | 40–200 | 2.0 | 5 |
| Lateral | 5–40 | 1.25 | 3 |
| | 40–200 | 2.0 | 5 |

[a]Input level at low frequency was not to exceed 0.7-in. double-amplitude and was controlled such that the response at the center of gravity of the retrorocket did not exceed 2.5 g (from zero to peak).
[b]Variable-frequency sinewave.

under quasi-static load conditions derived from launch, flight, and landing of the spacecraft. A secondary objective was to demonstrate that the functional requirements related to center-of-gravity shift and alignment during the retro phase of the trajectory were satisfied.

Static loads, simulating a 9.4-*g* inertia load due to retrorocket deceleration, were applied to various components of the spacecraft in increments of 10%. Dial gages were used to measure the movement of the components. The results of the test are shown in Table XIV-14.

*c. S-2A structural test vehicle.* The S-2A vehicle was an updated S-2 spaceframe with modified components as listed:

(1) Compartments A and B were changed from ballast units to dummy units.

(2) A battery pack was installed in compartment B.

(3) The A/SPP and mast were relocated to the present position near the *Y* axis of the spacecraft.

(4) The omnidirectional antenna booms were replaced with more representative dummy hardware.

(5) The helium tank was relocated to its present location.

(6) A vernier-engine roll actuator was installed on one dummy engine.

(7) The auxiliary battery and its support structure were installed.

(8) A dummy radar altimeter and doppler velocity sensor and waveguides were installed.

The S-2A vehicle was subjected to a type-approval vibration test, a drop test, and a modal survey.

Type-approval vibration testing was performed to verify the structural integrity of the spaceframe when subjected to C-level vibration inputs. Additional objectives were to verify compliance with the dynamic envelope and to satisfy the A/SPP functional requirements at B-level inputs. Numerous structural failures occurred during testing, including the elevation motor housing of the A/SPP and the thermal switches. Excessive excursions of the solar panel occurred as shown in Table XIV-15.

The objective of the S-2A drop tests was to verify the structural integrity of the upgraded structure under simulated lunar landing conditions. The drop tests were designed to subject the thermal compartments and the A/SPP to maximum levels, since these items were considered critical. Eight drop tests were accomplished. The first three drops of the S-2A (with a 287430 design A/SPP) caused the failure of the sector gear elevation-axis lock tab and the yoke plates which attach the planar array support tube to the sector gear.

The remaining five S-2A drop tests were accomplished with an upgraded 287550 design A/SPP. No further major failures occurred, although metal deformations at the elevation-axis tapered lockpin holes resulted in an inoperative elevation-axis drive. This condition occurred on two of the drop tests with a polar angle of zero degrees,

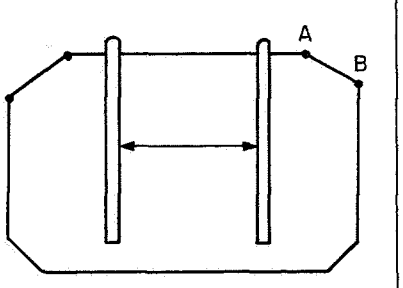
**Table XIV-14. S-2 center-of-gravity and alignment shifts**

| Measurement | Measured | Allowable error |
|---|---|---|
| Retrorocket lateral CG shift | 0.0325 in. | 0.100 in. |
| Flight control sensor rotation | 17 min of arc | 12[a] min of arc |
| Retrorocket nozzle centerline tilt | 8 min of arc | 9 min of arc |
| Doppler velocity sensor rotation | 10.4 min of arc | 30 min of arc |

[a]Subsequently changed so that 17 min is satisfactory.

**Table XIV-15. S-2A solar panel motion**

| Point | Direction of motion | Measured deflection, in. | Allowable deflection, in. |
|---|---|---|---|
| A | Parallel to plane of solar panel direction as shown | 0.63 | 0.88 |
| | Perpendicular to plane of solar panel | 2.15 | 1.33 |
| B | Parallel | 0.47 | 0.58 |
| | Perpendicular | 1.2 | 0.95 |



a solar angle of 270 deg (see Fig. XIV-9), leg 1 downhill, at equivalent lunar touchdown velocities of 17 and 20 ft/sec onto a surface slope of 15 deg.

A modal survey was performed on the S-2A to obtain data for generation of mathematical models for touchdown loads and stability studies. Before testing, the S-2A was made dynamically similar to a spacecraft at touchdown. It was then suspended by a very soft suspension system to simulate a free-flight condition. The criteria used to define the S-2A modes were:

(1) Presence of an in-phase relationship between exciting force and velocity at each driving point.

(2) Responses at all survey points with appreciable motion were either in or out of phase.

(3) Responses at all driving points decayed smoothly without evidence of a beat frequency.

The modal test results are presented in Tables XIV-16 and -17. The modes in Table XIV-16 were excited by inputs to the A/SPP in addition to shaker force applied at the crushable-block attachment points on the spaceframe. The modes presented in Table XIV-17 were obtained using shakers on the compartments in addition to inputs at the top of the A/SPP mast.

*d. S-9 structural test vehicle.* Six test programs were performed using the S-9 structural test vehicle as a test fixture to qualify newly developed components and evaluate special conditions. These programs were:

(1) Torsional test.

(2) Static test.

(3) Modal survey.

(4) Structural transfer-function evaluation.

(5) Rough-ride evaluation test.

(6) Boost vibration test.

(7) Drop test.

For the first four tests, S-9 had an A-21 spaceframe and substructure. The components were simulated with dummies which had the same mass properties as the flight hardware. Prior to the boost vibration and drop tests, the S-9 vehicle was upgraded to *Surveyor V* configuration.

The objective of the S-9 torsion test was to demonstrate that the vehicle could withstand the torsional environment experienced by some of the *Ranger* flights. A secondary objective was to measure dynamic response of the compartments and the 287550 design A/SPP for comparison with the original design loads. The tests were performed with the vehicle in the boost configuration and attached to the *Centaur* forward payload adapter. The torsional vibration inputs were applied to the base of the adapter (Fig. XIV-10). The initial test was a low-level (0.25 *g*, zero–peak) variable-frequency sine sweep (5–300 Hz) to verify the test setup. The second test was the qualification-level sine sweep with inputs as shown in Table XIV-18, followed by the torsional pulse test with inputs as depicted in Fig. XIV-11.

**Table XIV-16. Results of S-2A modal survey, landing configuration**

| Frequency, Hz | | | Principal motions |
|---|---|---|---|
| With planar array 45 deg to mast | With planar array 87 deg to mast | With planar array 17½ deg to mast | |
| 6.13 | 5.89 | 6.22 | Torsional about Z axis |
| 6.63 | 7.78 | 7.42 | Rocking about Y axis, node 2½ in. down on mast |
| 11.05 | 10.40 | 11.05 | Mast-bending normal to panels; node 17–20 in. down on mast |
| 12.88 | 12.80 | 13.63 | Mast-bending parallel to panels; node 15–19 in. down on mast |
| 13.95 | — | 14.80 | Solar panel rotating; planar array yawing |
| 19.56 | 24.30 | 20.20 | Solar panel rotating; planar array yawing |
| 33.75 | — | — | Complex panel motions |
| 37.60 | — | — | Complex panel motions |
| 45.80 | — | — | Complex panel motions |

**Table XIV-17. Compartment modes, landing configuration**

| Frequency with planar array 45 deg to mast, Hz | Frequency with planar array 17½ deg to mast, Hz |
|---|---|
| 22.2 | 21.1 |
| 23.6 | 22.55 |
| 28.0 | 23.55 |
| 30.9 | 28.55 |
| 34.8 | 30.4 |
| 60.2 | 36.0 |

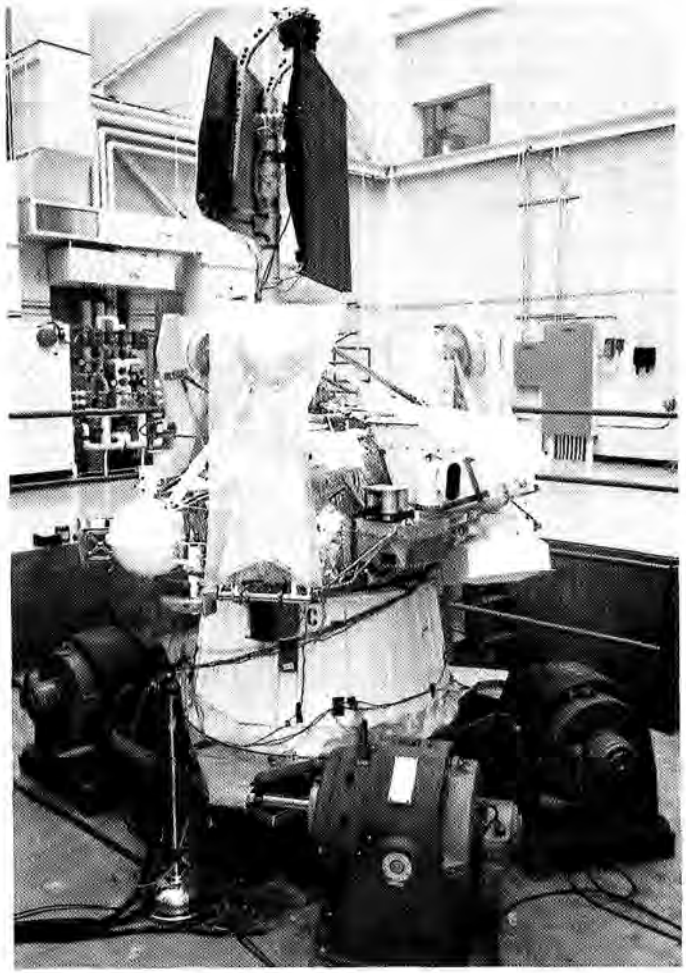


**Fig. XIV-10. Torsional test setup**

Following the sine sweeps, a visual examination of the spacecraft disclosed the following damage:

(1) Bond failure between helium line and spaceframe standoff.

(2) Loss of external nut on thermal standoff.

(3) Break in thermal standoff adjacent to tray in compartment B.

(4) Compartment B upper-support-tube failure.

Items (1) and (2) were found to be the result of manufacturing defects. Item (3) was attributed to increased loading resulting from failure stated in item (4). The torsional pulse test produced only low-level response throughout the vehicle structure with no failures.

A static test was performed on the S-9 to demonstrate the spaceframe's capability to meet functional requirement limitations on structural deformations. The spacecraft was mounted on three supports at the retrorocket attach fittings. Loads were incrementally applied through the center of gravity of all major components, up to 12 *g* to simulate retro deceleration. Deflection readings were recorded at each increment by dial gages and deflection beams. The center-of-gravity excursions or rotations are shown in Table XIV-19.

The primary objective in performing a modal survey on a flight-representative spacecraft such as the S-9 was to obtain modal information for mathematical models for use in the spacecraft dynamic loads and dynamic stability analyses. A secondary objective was to assess the ability to predict spacecraft modal characteristics from geometrical, inertial, and material descriptions by comparing analytical and experimental results.

The modal survey was performed with the spacecraft in two configurations:

(1) Launch mode with spacecraft mounted on the upper section of the *Centaur* adapter (Fig. XIV-12)

**Table XIV-18. S-9 torsional sinusoidal test inputs**

| Frequency, Hz | Angular acceleration, rad/sec[a] | Equivalent levels, g (zero–peak)[b] |
|---|---|---|
| 5–15 | 9.3 | 0.53 |
| 15–50 | 11.1 | 0.64 |
| 50–300 | 18.3 | 1.05 |

[a]Sweep rate = 0.5 octaves/min.
[b]Measured at point with arm radius = 22.4 in.

**Table XIV-19. S-9 static test result summary**

| Item | Requirement (max) | Test value |
|---|---|---|
| Vernier-engine bracket bending constant | 0.50 deg/ 100 lb | 0.46 deg/ 100 lb |
| Displacement between retrorocket nozzle centerline and combined spacecraft–retrorocket CG | 0.070 in. | 0.038 in. |
| Angle between retrorocket nozzle centerline and spacecraft roll axis | 0.15 deg | 0.05 deg |
| Angle between vernier-engine thrust vector and spacecraft roll axis | 0.55 deg | 0.51 deg |
| Angle between flight control sensor group and spacecraft roll axis | 0.20 deg | 0.56 deg |
| Angle between radar altimeter axis and spacecraft roll axis | 0.40 deg | 0.03 deg |
| Variation in doppler velocity sensor alignment | 2.00 deg | 0.19 deg |

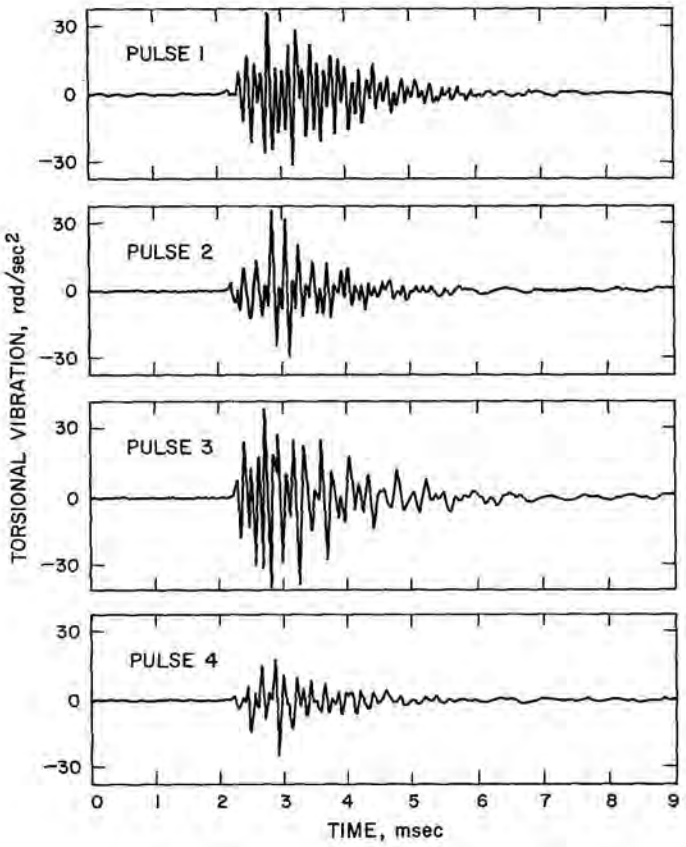



**Fig. XIV-11. Strip chart timing record of torsional pulse inputs**

with all four A/SPP drive axes clamped to produce a reasonably *linearized* spacecraft.

(2) Touchdown mode with landing legs detached for convenience. (The legs were considered to be rigid bodies and the test data obtained were modified analytically to include the effects of the mass of the legs.)

A second modal survey was performed with the spacecraft suspended to provide a very low natural frequency (less than 0.3 Hz) in each of the six rigid-body degrees of freedom.

The *Surveyor*, by virtue of its configuration, had a very high modal density in the low-frequency range. This was of potential importance to both loads and flight stability. Table XIV-20 shows the test results in launch configuration.

At the conclusion of the second modal survey, a structural dynamics test was performed with the S-9 vehicle in the touchdown configuration, the purpose of which was to determine the structural transfer functions relevant to flight stability during this phase of the mission.

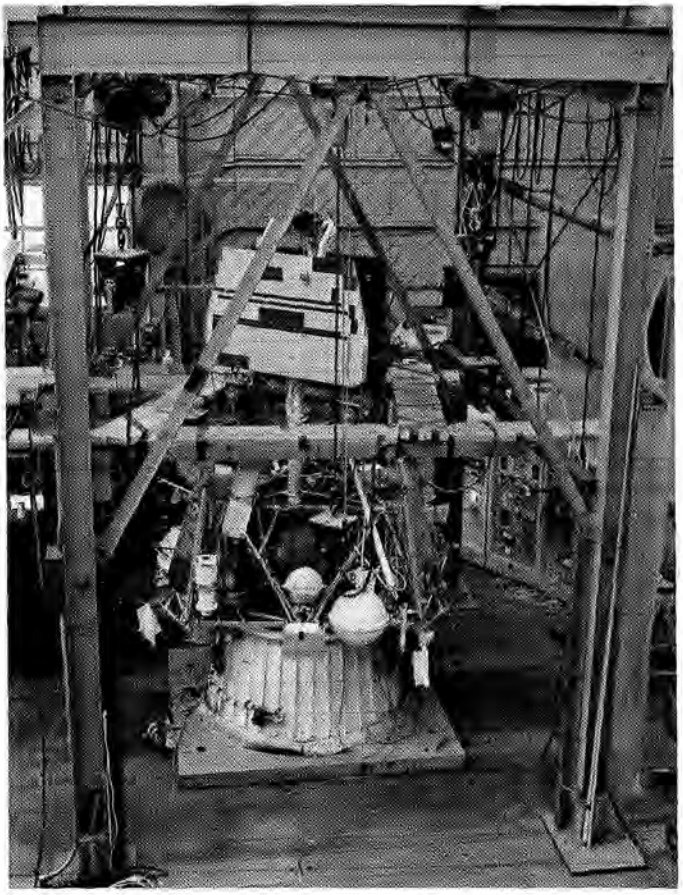


**Fig. XIV-12. Launch configuration modal survey setup**

Tests were performed with the vehicle suspended from a fixture to provide a very low natural frequency (less than 0.3 Hz) in all reference axes, as shown in Fig. XIV-13. The test results and subsequent analysis led to the conclusion that there were no adverse effects on spacecraft stability due to spacecraft structure and flight-control sensor interaction.

The S-9 spacecraft was used in a test program to evaluate suspected fatigue damage to *Surveyor III* spacecraft during its truck transport from Florida to California. A problem was first suspected when several damaged gear teeth were found in the television camera azimuth drive. A review of accelerometer data from the trip revealed unusually large input acceleration levels to the spacecraft. Concern about potential undetectable fatigue damage resulted in a test program in which the instrumented S-9 was transported over a test course in the same moving van used for *Surveyor III*. The response data obtained from the S-9 were used as inputs to a structural analysis program. Results of the analysis indicated that the *Surveyor III* fatigue level was 10% or less of its endurance capability.

**Table XIV-20. Preliminary results of S-9 modal survey: launch configuration**

| Mode | Mode freq, Hz | Qualitative description |
|---|---|---|
| 1 | 11.45 | Mast first torsion mode with some combined mast bending; virtuolly no spaceframe motion |
| 2 | 11.61 | Mast first bending mode with large in-phase flapping of planar array; virtually no spaceframe motion |
| 3 | 12.87 | Mast second bending mode (in-plane parallel to planar array), with some combined torsion, in-plane translation of solar panel and planar array in phase with mast bending. Significant rotation about the Z-axis ($\theta_z$). Rotation of A/SPP, planar array, and solar panel. In-plane rocking of planar array and solar panel opposed to tip slope of mast |
| 4 | 14.63 | General spacecraft mode with retro rocking in vertical plane 30 deg toward leg 2 from X–Z plane. Comparable amplitudes on other equipment items: mast bending; largest local amplitude on solar panel |
| 5 | 15.86 | General spacecraft mode with solar panel and planar array rocking in opposition about normal axes; rolling and twisting of solar panel. Significant motions of spaceframe and items maunted therean |
| 6 | 16.33 | Strong rocking of helium tank; motians above mast base similar to those described for mode 7, with less twisting and mare flapping in oppasite senses; some retro pitching |
| 7 | 17.41 | Mast bending and torsian, asymmetric twisting of solar panel and planar array abaut harizontal axis. Very little spaceframe motion |
| 8 | 17.9 | Survey camera rocking about centroidal X axis |
| 9 | 18.84 | General spacecraft mode with largest motions in solar panel and significant motions in compartments, flight control sensor group, helium tank, and survey camera |
| 10 | 19.71 | Strong spacecraft mode, principally first torsion. Largest motions on survey camera, bath compartments, and flight control sensor group. Relatively little motion above mast bose |
| 11 | 20.01 | Mast bending in plane normal to planar array; large flapping of planar array with rotation opposite to mast tip slope and salar panel. First symmetrical bending; motians on spaceframe relatively small |
| 12 | 22 | Auxiliary battery rocking about centroidal Y axis |
| 13 | 23.3 | Survey camera rocking about centroidal Y axis |
| 14 | 24.66 | Strong rolling of helium tank with significant motions of auxiliary battery, nitrogen tank, and survey camera. Motions above mast base are small |
| 15 | 25.51 | Mast bending in plane parallel to planar array; rigid-body roll plus twist af planar array, and smaller but opposed twist of solar panel; rocking motion of flight control sensor group |
| 16 | 26.07 | Mast torsion, coupled with bending. A/SPP motions similar ta those of mode 15 with some phase reversals; survey camera rocking about Y axis; significant matians of campartments A and B; retro vertical motion |
| 17 | 27.95 | Strang spacecraft made with largest amplitudes on auxiliary battery, nitrogen tank, both compartments, survey camera, and planar array |

The objectives of the S-9 vibration test were:

(1) Verify the structural integrity of *Surveyor V* hardware after exposure to simulated launch-vibration environment.

(2) Demonstrate adequate dynamic clearance between the A/SPP and the *Centaur* nose fairing during launch.

The spacecraft was mounted directly to a rigid test fixture as shown in Fig. XIV-14. Vibration input levels were as shown in Table XIV-21. The B-level tests were to verify the adequacy of the compartment B supports which had failed during the torsion test, and to measure the A/SPP dynamic envelope. Qualification of the 3035092 A/SPP and other *Surveyor V* hardware was accomplished by the three C-level tests. The only anomaly occurring during vibration was a tendency for the solar-axis launch lockpin to back out of its hole. The A/SPP motion did not violate the dynamic envelope, as shown in Table XIV-22.

The objective of the S-9 drop test was to verify the operation and structural integrity of *Surveyor V* hardware after simulated lunar landing. Figure XIV-15 shows the S-9 suspended above the sloped landing platform.

The conditions of the drop tests are shown in Table XIV-23. Following each drop, a functional check was performed on the A/SPP, including firing of the landing-lockpin pullers. No damage to the vehicle was observed until the completion of test 3. At that time, the solar-axis landing lockpins were found disengaged. The retraction of these pins was apparently due to lubricant contamination of the lockpin bearing surfaces; that is, the lockpins

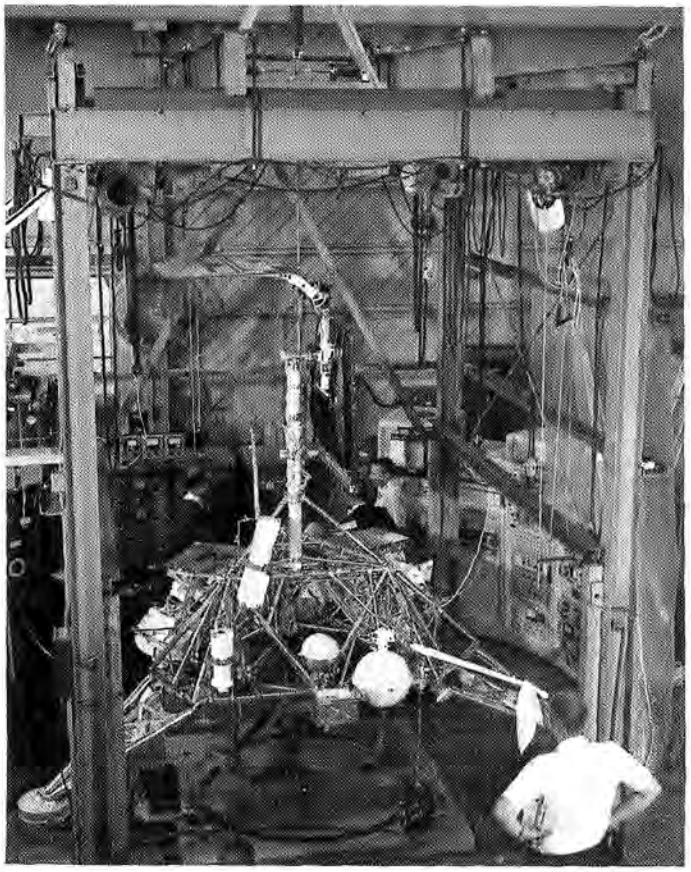


Fig. XIV-13. Setup for evaluation of structural transfer function

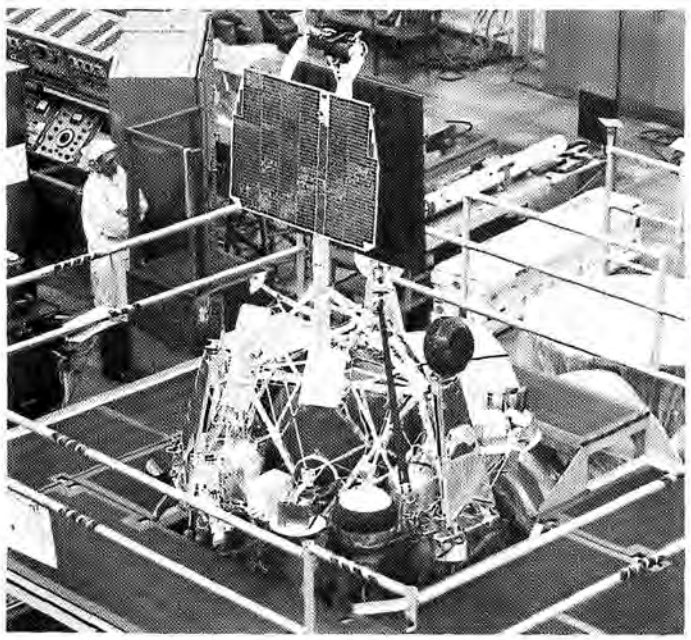


Fig. XIV-14. S-9 unit on vibration test fixture



Fig. XIV-15. S-9 unit shown suspended above landing platform

were literally squeezed out because of low friction. Disassembly of the A/SPP disclosed that the solar-axis driveshaft yielded in torsion enough to cause a solar-axis shift of 12 deg. Following corrective action, which included specified cleaning requirements for the lockpin assembly, two penalty drops (tests 4 and 5) with complete functional checks and alignment were conducted to assure no recurrence of this problem.

*e. T-1 and S-15 touchdown stability test vehicles.* Several test programs were conducted to check analytical predictions for landing stability (Ref. XIV-2) and to verify the adequacy of the landing gear design. After initial attempts with scale models, a full-size test vehicle was built, as scaling of the shock absorbers proved to be very difficult.

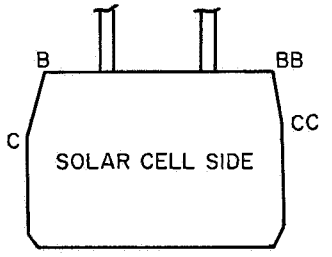
The full-size vehicle (designated T-1) had flight-like landing gear mounted on a frame that duplicated spaceframe landing gear attachment dimensions and inertial properties (Fig. XIV-16). Lunar gravity was simulated by an upward force of five-sixths of the spacecraft's weight

## Table XIV-21. S-9 vibration test levels

| Test level | Test run | Axis of vibration | Sweep frequency range, Hz | Sine level (peak), g | Random level, g (rms) | Test time, min | Sweep rate, octave/min |
|---|---|---|---|---|---|---|---|
| B | 1 | Lateral—normal to leg 2 | 5–15<br>15–50 | 0.88<br>1.02 | None | 3.25 | 1 |
| B | 2 | Lateral—normal to leg 3 | 5–15 | 0.88 | None | 1.5 | 1 |
| C | 3A | Lateral—normal to leg 3 | 5–15<br>15–50<br>50–100 | 1.0<br>1.2<br>2.0 | None | 4.5 | 1 |
| | 3B | Lateral—normal to leg 3 | 100–1500<br>1500–100 | 2.0<br>2.0 | 6.75<br>6.75 | 3.9<br>3.9 | 1<br>1 |
| C | 4A | Lateral—normal to leg 3 | 5–15<br>15–50<br>50–100 | 1.0<br>1.2<br>2.0 | None | 4.5 | 1 |
| | 4B | Lateral—normal to leg 3 | 100–1500<br>1500–100 | 2.0<br>2.0 | 6.75<br>6.75 | 3.9<br>3.9 | 1<br>1 |
| C | 5A | Longitudinal along roll axis | 5–50<br>50–100 | 2.5<br>2.0 | None | 3.9 | 1 |
| | 5B | Longitudinal along roll axis | 100–1500<br>1500–100 | 2.0<br>2.0 | 6.75<br>6.75 | 3.9<br>3.9 | 1<br>1 |

## Table XIV-22. S-9 solar panel motion

| Point | Measured deflection, normal to solar panel, (zero–peak), in. | | Allowable deflection, in. |
|---|---|---|---|
| | Film[a] | Accelerometer data | |
| C | 2.32 | 2.15 | 4.46 |
| B | 3.45 | — | 4.85 |
| BB | 3.32 | — | 3.44 |
| CC | 2.0 | 1.8 | 3.05 |




[a]Measured from movie taken during test.

## Table XIV-23. S-9 drop test conditions

| Test | Spacecraft orientation | Planar array position (deg polar angle)[a] | Slope of landing surface, deg | $\theta$, initial angle of spacecraft incidence, deg | Drop height,[b] ft | Equivalent lunar longitudinal touchdown velocity, ft/sec |
|---|---|---|---|---|---|---|
| 1 | Leg 1 downhill | 0 | 15 | −3 | 5.04 | 15 |
| 2 | Leg 1 downhill | 36.5 | 15 | 0 | 5.04 | 20 |
| 3 | Leg 2 downhill | 36.5 | 15 | 0 | 5.04 | 20 |
| 4 | Leg 2 downhill | 36.5 | 15 | 0 | 5.04 | 20 |
| 5 | Leg 2 downhill | 36.5 | 15 | 0 | 5.04 | 20 |

[a]Angle between planar array and A/SPP mast.
[b]Minimum vertical distance between footpad and surface.

applied at the center of gravity through a trailing cable system connected to constant-force pneumatic cylinders. Figure XIV-17 shows the schematic of this device.

Drops were made onto a 15-deg sloped platform with a variety of surfaces to simulate different frictional behaviors and surface hardness. Also, 2 × 4 × 4-in. and 4 × 4 × 4-in. wooden blocks were attached to the landing platform to simulate lunar surface roughness in accordance with the design specification.

The initial two-test series was performed to validate the planar-landing simulation program and to explore the influence of soft landing surfaces as well as tridimensional landing conditions.

In addition to proving the adequacy of landing gear design, these tests showed that the analytical predictions had been conservative. The soft-surface tests were inconclusive because the characteristics of a bearing strength of zero psi on the surface and 10 psi at 12 in. penetration (increasing linearly) were extremely difficult to simulate.

The tridimensional landing tests were also inconclusive because even a rough sampling of the three variables (horizontal spacecraft velocity, roll orientation, and incidence angle) resulted in such a large number of combinations that an investigation by test was not feasible.

After the second simulation analysis (including tridimensional capability) became available, a new series of tests with an upgraded test vehicle (designated S-15) was conducted to validate the analysis. The S-15 was first dropped onto a platform covered with rubber matting, and no instability occurred. To increase the effective coefficient of sliding friction, 2-in. cubes were attached to the landing platform. Total instability still did not occur at any landing condition of interest, but three drops were marginally stable. Figure XIV-9 shows the touchdown velocities for these cases.

The stability test program substantiated the conclusion that no danger of landing instability existed unless the specified landing conditions were considerably exceeded. However, close correlation could not be obtained between analytical and experimental stability boundaries. This was believed to be due to difficulties in the operation of the lunar-gravity simulation device and inability to control test conditions within close tolerances, particularly the friction between the footpads and the test surface. Undoubtedly, assumptions in the analysis (such as rigidity of the spaceframe and a constant coefficient of friction between footpads and ground) also contributed to the deviation between experimentally and analytically obtained

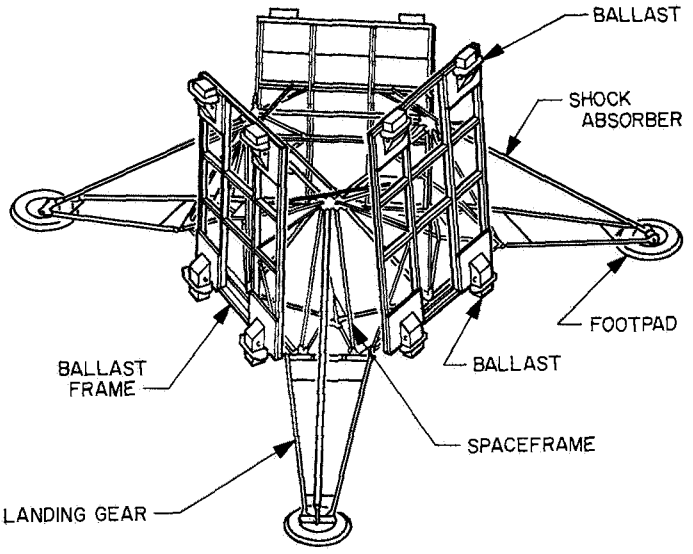



**Fig. XIV-16. T-1 test vehicle**

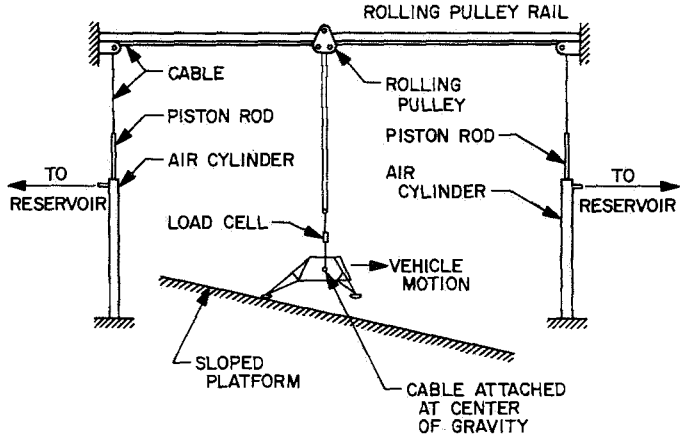



**Fig. XIV-17. Lunar gravity device**

stability boundaries. Therefore, the two stability boundaries shown in Fig. XIV-9 were not directly comparable. For the analytical boundary, the friction coefficient was assumed to be unity, but the friction in the tests (created by the 2 × 2 × 2-in. blocks) was not constant and was considerably higher. However, since the landing stability generally decreased with increasing footpad/ground friction, the experimental results indicated a higher landing capability than was found in the analytical investigation.

### 2. Test Programs of Major Components

#### *a. Retrorocket.*

*1. Static test.* An inert retrorocket was subjected to a lateral load test to determine the distribution of a lateral

load between the three sets of struts and skirts and between a single strut and skirt when the lateral load was applied to one attachment lug. The test objectives were accomplished by loading one strut pad from three different angles and measuring deflections with dial indicators. The spring constants for the attachment fittings were determined and the load distribution was computed. Another static test was performed to demonstrate the adequacy of a structurally improved version of the strut-and-skirt attachment of the retrorocket. In this test, a diagonal load was applied to the strut at the point where it was attached to the spaceframe. The condition simulated a 5 g lateral load combined with a 3 g axial load. The result of this test indicated that the attachment structure was adequate.

*2. Pressure test.* Pressure tests to qualify the design of the retrorocket case and flightworthiness of each production case were performed throughout the program.

*3. Static-firing test.* A series of static-firing tests were made on four *Surveyor* retrorockets to determine the magnitude and frequency contents of vibration generated during motor firing. Test results showed that the oscillatory forces appearing at ignition and thrust buildup were as expected (200–500 lb per attachment point). The occasional midburn transients were found to be due to spalling nozzle material, and their amplitude was in the range of 100–200 lb per attachment point. Aside from these specific phenomena, the *Surveyor* retrorocket operated smoothly. The vibration was small in amplitude (less than 6 lb rms total), random in character, and restricted to frequencies below 150 Hz.

***b. Retrorocket separation test.*** Two series of tests were conducted for verification of the spacecraft/retrorocket separation and for validation of the tridimensional analog computer investigation which was used to establish the reliability of this separation process.

The first test series (in 1963) consisted of eight separations simulating normal and extreme separation–acceleration conditions, delayed firing of one or two separation bolts, and thrust-axis tilting. Since actual *Surveyor* hardware was not available, the retrorocket was simulated by a cylinder with representative mass and inertia properties, and the spaceframe was simulated by a truss-type framework. To simulate lunar gravity, approximately five-sixths of the weight of the retrorocket was carried by a cable connecting its center of gravity to a pneumatic system designed to hold this compensation force constant during the separation. This device was also used for spacecraft drop tests for touchdown stability investigations. The retrorocket separated satisfactorily in all tests. However, the possibility of contact between motor and frame (bumping) during the separation, which was indicated by analytical separation investigations, could not be ruled out.

The second test series, conducted in 1965, was designed to determine whether this bumping, which had been shown to be tolerable to the flight control system, could possibly lead to a hangup condition. This test series employed a representative spaceframe and a geometrically and dynamically correct dummy retrorocket. The frame was mounted upside down on a platform that could be tilted, and the retrorocket was pulled out and up while the breakaway force was monitored. No case could be found in which a wedging condition exceeded the minimum available separation force. Also in this test series, the condition which occurs if one bolt fails to fire on first command was investigated. One edge of a 119-lb beam was connected to one of the spaceframe retrorocket attachment points, causing bending stresses in the bolt similar to the single-bolt retrorocket suspension condition. The separation device fired and separated without any indication of degradation.

***c. Pressure vessel test program.*** Since all pressure vessels in the *Surveyor* spacecraft were man-rated, test programs were conducted to qualify each design and each flight vessel in accordance with established requirements.

*1. Burst tests.* Table XIV-24 summarizes all burst tests, including determination of the actual burst pressure and the normalized burst pressure. The spread achieved for the initial burst tests was between 2.74 and 3.89%—well within the required maximum of 5%. The one-in-ten burst test results are also shown in Table XIV-24. The normalized burst pressure was divided by 95% of the average normalized pressure of the initial three burst tests or the minimum required burst pressure, whichever was the larger. If the ratio was less than 1:1, a lot of 10 vessels was subject to rejection. The data indicate that all tested vessels met the requirements.

*2. Type approval tests.* Samples of each type of pressure vessel passed the pressure hold, pressure cycle, vibration, and leak tests. Each test vessel was burst upon completion of type approval tests.

*3. Acceptance tests.* All flight pressure vessels passed the proof-pressure test (which constituted flight acceptance). The test was outlined as follows:

(1) The room-temperature proof pressures were established at 85% (for the helium and nitrogen tanks)

**Table XIV-24. Burst test pressure data**

| Pressure vessel | Propellant pressure, psi | | | Nitrogen pressure, psi | | | Helium pressure, psi | | |
|---|---|---|---|---|---|---|---|---|---|
| | Actual | Normalized | Normalized 1173 | Actual | Normalized | Normalized 11638 | Actual | Normalized | Normalized 11385 |
| Initial burst tests | | | | | | | | | |
| 1 | 1400 | 1237 | — | 14,475 | 12,360 | — | 12,790 | 11,761 | — |
| 2 | 1370 | 1258 | — | 13,500 | 12,000 | — | 12,215 | 11,465 | — |
| 3 | 1380 | 1210 | — | 13,800 | 12,390 | — | 13,000 | 11,785 | — |
| One-in-ten burst tests | | | | | | | | | |
| 1 | 1370 | 1180 | 1.006 | 11,850 | 12,050 | 1.035 | 12,475 | 11,711 | 1.029 |
| 2 | 1370 | 1285 | 1.095 | 13,050 | 12,570 | 1.080 | 12,000 | 11,544 | 1.014 |
| 3 | 1350 | 1202 | 1.025 | 12,850 | 12,360 | 1.062 | 12,900 | 12,054 | 1.059 |
| 4 | 1405 | 1205 | 1.027 | — | — | — | — | — | — |
| 5 | 1405 | 1268 | 1.081 | — | — | — | — | — | — |
| 6 | 1415 | 1246 | 1.062 | — | — | — | — | — | — |
| 7 | 1559 | 1243 | 1.060 | — | — | — | — | — | — |
| 8 | 1434 | 1193 | 1.017 | — | — | — | — | — | — |
| 9 | 1560 | 1270 | 1.083 | — | — | — | — | — | — |
| 10 | 1340 | 1193 | 1.017 | — | — | — | — | — | — |
| 11 | 1440 | 1197 | 1.020 | — | — | — | — | — | — |
| 12 | 1383 | 1195 | 1.019 | — | — | — | — | — | — |
| Average of initial three normalized burst tests | — | 1235 | — | — | 12,250 | — | — | 11,670 | — |
| 95% of normalized average burst pressure | — | 1173 | — | — | 11,638 | — | — | 11,087 | — |
| Minimum required burst pressure | — | 1050 | — | — | 11,000 | — | — | 11,385 | — |
| Percent spread, initial burst | — | 3.89 | — | — | 3.18 | — | — | 2.74 | — |

and 90% (for the propellant tank) of the pressure necessary for bulk yielding. (These bulk yielding pressures had been established during the design qualification tests.)

(2) Full proof pressure was applied three times and held for 5 min each time.

(3) A liquid-nitrogen proof test was performed at a pressure equal to 1.4 times the room-temperature proof pressure for 5 min. Temperature was maintained between −300 and −320°F throughout the test.

*4. Mechanical properties of 6Al-4V titanium.* Tensile coupons were cut from each end of a forged bar (typical locations are shown in Fig. XIV-18) from which the tank half was machined to final dimensions before the two halves were welded together to form a tank. This provided a minimum of 8 and a maximum of 12 tensile coupons to ascertain the material properties of that bar. A summary of some of the results for propellant pressure vessels for tensile ultimate, tensile yield, elongation, and reduction of area is shown in Table XIV-25. Weld-joint efficiency of 94% was determined from preproduction and post-production weld test data. In burst tests of pressure vessels, there were no instances of rupturing in the weld area.

## C. Mission Structural Performance

### 1. Flight Structural Performance

No structural failure was evident on any of the *Surveyor* missions. Communication with *Surveyor IV* was lost at maximum retrorocket deceleration loading (9 *g*) and also at the time when the retrorocket case was exposed to maximum internal pressure. Because of these circumstances, a complete review of the retrorocket was conducted.

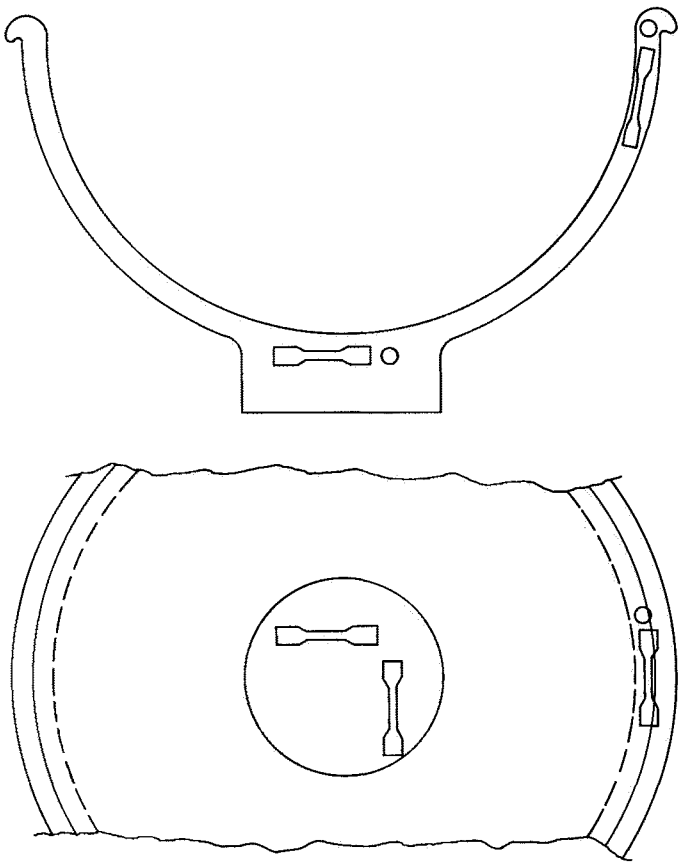


**Fig. XIV-18. Tensile test specimens in forged bar**

The fabrication records and X rays of the retrorocket cases revealed numerous welding defects, such as lack of penetration, lack of fusion, porosity (hook), and offsets (weld mismatch) as great as 50%. These defects were found mainly in the girth weld which joined the two hemispherical halves of the case. Structural and statistical analyses of the effects of these defects, particularly the weld mismatches, disclosed that the pressure capability of the retrorocket case was not impaired enough to affect mission performance. These findings were verified by the pressure-bursting of a retrorocket case with a combination of weld defects.

A review of the flight data from *Surveyor IV* revealed some anomalies which could have been related to structural problems:

(1) Transients observed during *Centaur* boost (8 *g* peak at approximately 1400 Hz).

(2) Canopus-sensor light obscuration approximately 8 sec after the 8 *g* transient.

(3) Seven false Canopus signals observed during transit.

(4) Gas jet on 41.3 sec after AMR mark.

(5) Pitch gyro noisy before and during retrorocket burn.

(6) RADVS oscillation (10 ft/sec, peak-to-peak) 36.5 to 40.5 sec after AMR mark.

(7) Thrust modulations in vernier engines 1 and 2, resulting in spacecraft attitude-control moments of 300–500 in.-lb.

The relevance of anomalies (1), (2), and (3) is questionable and may not have had direct bearing on loss of contact with *Surveyor IV*. For example, transients of a similar nature but of lower magnitude were observed on other *Centaur* flights. Also, a roll of the *Centaur* may have exposed the Canopus sensor to a low-level light source. A review of anomalies (4), (5), (6), and (7) first indicated that something in the flight control sensor group may have been loose. An examination disclosed that this was unlikely. The support of items immediately adjacent to the flight control sensor group was reviewed and found adequate. The two components that received the most attention were the signal data converter and compartment B. It was concluded that structural failure was probably not the cause of the loss of signal from *Surveyor IV*.

### 2. Landing Structural Performance

A summary of landing velocities, vernier engine cutoff altitudes, incidence angles, encountered ground slopes, leg touchdown sequence, and relative timing for all soft-landed *Surveyors* is given in Tables XIV-26 and 27. All soft-landed *Surveyors* (except *Surveyor III*, which is discussed in detail) succeeded in keeping the landing parameters within the design limits. Consequently, the landings of *Surveyors I, V, VI,* and *VII* were performed without any landing problems or anomalies. The landing loads, as indicated by the maximum axial shock-absorber forces in Table XIV-28, did not exceed the design maximum (8000 lb); also, no landing stability problem was encountered, although the ground slope at the landing site of *Surveyor V* was above the design limit of 15 deg.

The shock absorber force histories of *Surveyor I* spacecraft legs during touchdown are shown in Fig. XIV-19. One unpredicted condition can be seen in these traces (typical for the landings of *Surveyors I, V, VI,* and *VII*). After initial contact with the lunar surface, the force readings returned to zero for a duration of approximately 0.7 sec, indicating that the spacecraft rebounded from the lunar surface. *Surveyor I* rebounded approximately 3 in., but rebounding was more pronounced in the subsequent missions (where the spacecraft was equipped

## Table XIV-25. Summary of mechanical properties of propellant pressure vessel

| Parameter | Mechanical property | | | |
|---|---|---|---|---|
| | Ultimate strength ($F_{t_u}$), psi | Yield strength ($F_{t_y}$), psi | Elongation, % | Reduction of area, % |
| Specified requirement | Min 155,000 | Min 145,000 | 10 | 30 |
| | Max 170,000 | Max 160,000 | | |
| Boss area[a] | 165,250 | 153,870 | 13.50 | 45.36 |
| Rim area[a] | 164,210 | 153,040 | 13.92 | 46.03 |

[a]Average values obtained on the test results of approximately 80 specimens from both the boss and rim areas of differerent forgings.

## Table XIV-26. Landing conditions, *Surveyors I, III, V, VI, and VII*

| Parameter | Design requirement | Surveyor | | | | | Measurement tolerance |
|---|---|---|---|---|---|---|---|
| | | *I* | *III*[a] | *V* | *VI* | *VII* | |
| Vernier engine cutoff altitude, ft | 13±4.5 | 10.8 | — | 15.7 | 9.8 | 11.6 | ±0.8 |
| Vertical velocity at vernier engine cutoff, ft/sec | 5±1.5 | 4.3 | — | 5.4 | 4.6 | 5.3 | ±0.3 |
| Vertical velocity at touchdown, ft/sec | 12.6±2.5 | 11.6 | 6–4 | 13.9 | 11.2 | 12.4 | ±0.4 |
| Horizontal velocity at touchdown, ft/sec | <5.0 | 0.8 | 1–3 | <1.2 | 1.0 | <0.2 | ±0.2 |
| Spacecraft incidence angle at touchdown, deg | <7.0 | 1.8 | — | <3.2 | 2.3 | <0.5 | ±0.5 |
| Landing-surface slope angle, deg | <15 | 1.0 | — | 19.5 | 0.9 | 3.1 | ±0.5 |

[a]*Surveyor III* did not perform the final descent and landing sequence according to plan, as described in the text. The indicated values give the approximate range of touchdown velocities for the three touchdowns. Other landing conditions cannot be determined due to the nonstandard conditions during the first and second touchdowns and absence of meaningful digital telemetry during the third touchdown.

## Table XIV-27. Leg touchdown sequence and relative timing[a]

| *Surveyor* spacecraft | Leg contacting surface first | Next leg contacting surface | Time after first contact, sec | Third leg to contact surface | Time after first contact, sec | *Surveyor* spacecraft | Leg contacting surface first | Next leg contacting surface | Time after first contact, sec | Third leg to contact surface | Time after first contact, sec |
|---|---|---|---|---|---|---|---|---|---|---|---|
| *I* | 2 | 1 | 0.005 | 3 | 0.019 | (Third touchdown) | 2 | 1 | 0.240 | 3 | 0.275 |
| *III* (First touchdown) | 2 | 3 | 0.260 | 1 | 0.285 | *V* | 1 | 2 | 0.186 | 3 | 0.194 |
| | | | | | | *VI* | 1 | 2 | 0.023 | 3 | 0.039 |
| (Second touchdown) | 2 | 3 | 0.375 | 1 | 0.440 | *VII* | 1 | 3 | 0.022 | 2 | 0.048 |

[a]Time differences are considered accurate within ±2 msec.

**Table XIV-28. Maximum shock-absorber axial loads (lb) during touchdown[a]**

| Leg | *Surveyor I* | *Surveyor III* | | | *Surveyor V* | *Surveyor VI* | | *Surveyor VII* |
|---|---|---|---|---|---|---|---|---|
| | Touchdown | First touchdown | Second touchdown | Third touchdown | Touchdown | Original landing | Landing after translation | Touchdown |
| 1 | 1390 | 670 | 320 | 870 | 1240 | 1590 | 3350 | 1650 |
| 2 | 1600 | 690 | 630 | 550 | 1650 | 1810 | 1760 | 1760 |
| 3 | 1400 | 830 | 530 | 930 | 1660 | 1590 | 1940 | 1470 |

[a]All values are considered accurate within ±5% (except for the leg 3 force on *Surveyor I*, determined assuming nominal calibration factors due to an uncertainty in the preflight calibration).

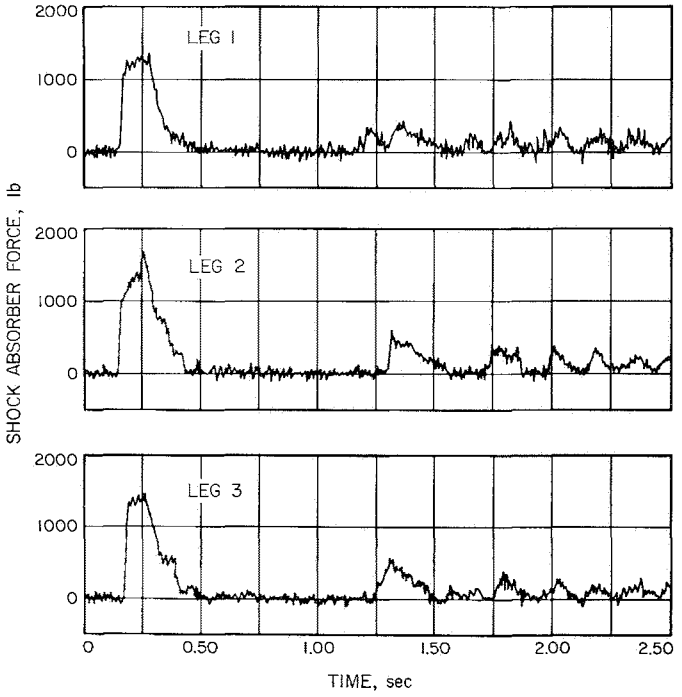



**Fig. XIV-19. *Surveyor I* shock absorber strain-gage force histories**

with redesigned shock absorbers). *Surveyor VII* bounced approximately 9 in., the highest rebound encountered; and a second slight rebound was indicated in the data of *Surveyors VI* and *VII*. A ringout oscillation with a frequency of between 4 and 7 Hz followed the last touchdown rebound in each case. The shock absorbers were designed to minimize rebounding, and no detrimental effects resulted from the impacts. Figure XIV-20 shows design details of the *Surveyor* shock-absorber column.

Calculations indicated that the body blocks would contact the surface for vertical touchdown velocities exceeding 8–9 ft/sec, and such contact was confirmed by photographic evidence for *Surveyors I, V, VI,* and *VII*. Block crushing did not occur, however, due to lack of resistance in the lunar surface, and it appears that no significant footpad crushing was ever experienced.

The final descent sequence was not followed properly in the case of *Surveyor III*. Engine cutoff, nominally occurring automatically at an altitude of approximately 13 ft above the lunar surface, was not executed at this time. Apparently the RADVS system temporarily lost lock before reaching engine cutoff altitude, in which case flight control was automatically switched back to the preacquisition mode (inertial hold with respect to angular motions, and constant vernier engine thrust equal to 90% of the lunar weight of the spacecraft).

In this condition, the lunar surface was encountered first by leg 2. In an attempt to resist the ensuing pitch–yaw motion—and also, possibly, as a consequence of the landing transient as sensed by the flight control sensor—all three vernier engines were commanded to increase thrust to various degrees. The result was a rebound and liftoff of the spacecraft after all three footpads contacted the ground. A second touchdown occurred 24 sec after the first, again followed by a rebound. A command from earth to terminate engine thrusting was sent and executed 35.8 sec after first ground contact. One-half second later, the third and final touchdown was registered, followed by a slight rebound and an elastic ringout similar to that of the other *Surveyor* landings.

Figure XIV-21 shows the shock absorber force histories throughout the *Surveyor III* landing. Rebounding was again observed, specifically on leg 2, resulting in two or more contacts for each of the three touchdowns.

Although the landing of *Surveyor III* was obviously nonstandard, landing velocities and forces were considerably below design values and caused no problems or failures in the dynamic landing performance.

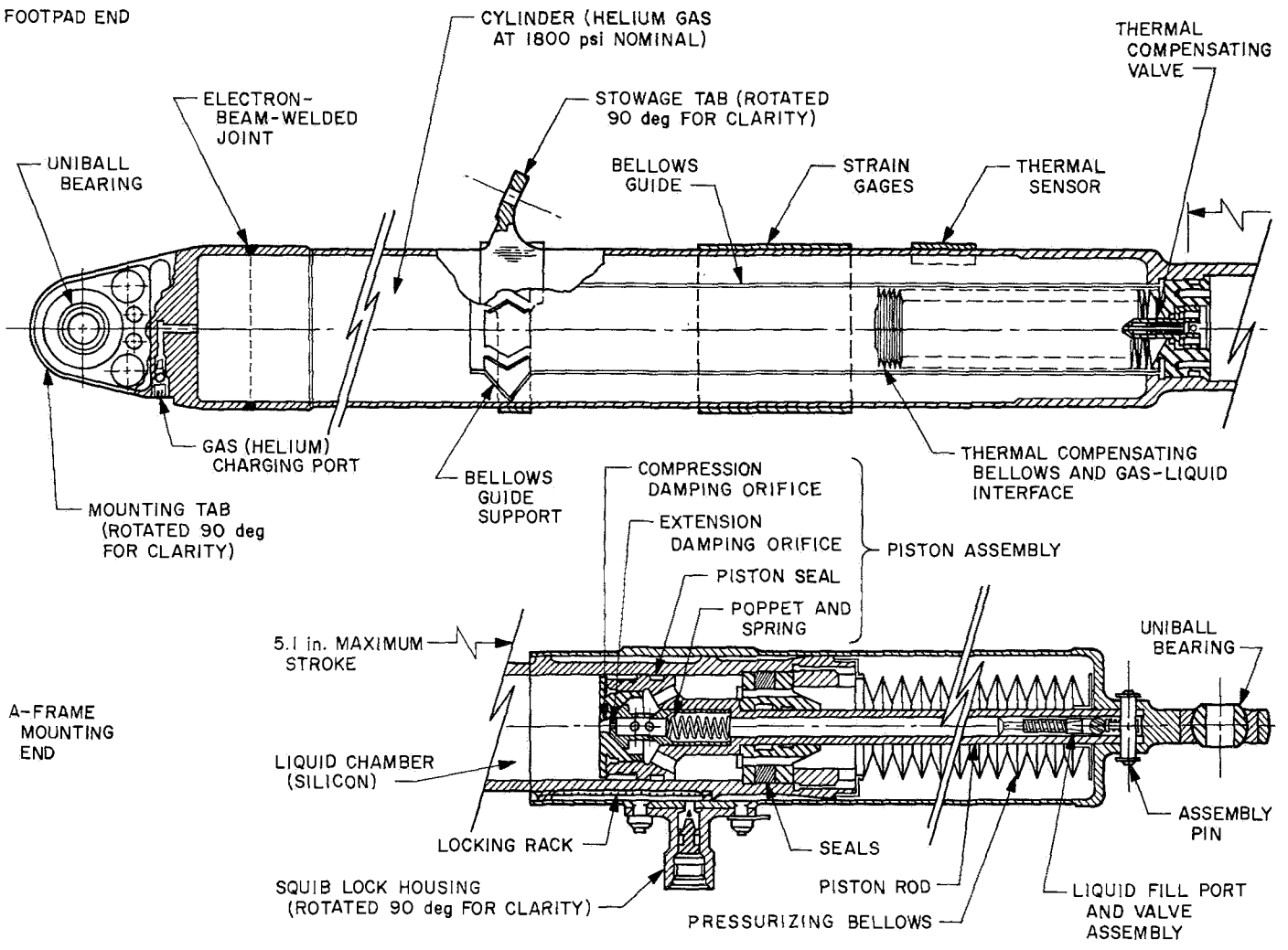



**Fig. XIV-20. Surveyor shock absorber column, design details**

### 3. Postlanding Spacecraft Hop Experiment

A postlanding *spacecraft hop* experiment was conducted with *Surveyor VI* with a desired translation in the leg 1 direction. Since no tilting of the vernier engines was possible, the flight control system was preset such that the closed-loop control system would acquire a +7-deg pitch attitude (angle at which leg 1 tilted downward) after liftoff. The vernier engines were ignited and commanded to sustain nominal midthrust, a combined thrust of 150 lb ±20% for 2.5 sec. The horizontal component of the tilted thrust vector provided the desired motion toward leg 1.

The three strain gages indicating the shock absorber axial loads were monitored in addition to commutated gyro and other telemetry signals. The strain-gage histories are shown in Fig. XIV-22. Liftoff and touchdown are clearly evident; engine ignition and shutoff were established from the commutated telemetry.

Using all available telemetry data, an estimated trajectory of the spacecraft translation was obtained. Since the thrust indications were not very accurate, event timing was used as a basis for the trajectory calculation. The following landing conditions were determined by this analysis and are shown in Table XIV-29.

**Table XIV-29. Performance parameters, *Surveyor VI***

| Parameter | Value |
|---|---|
| Maximum elevation reached | 14.3 (±1.8) ft |
| Vertical landing velocity | 12.3 (±0.8) ft/sec |
| Horizontal landing velocity | 1.8 (±0.2) ft/sec |
| Distance translated | 8.4 (±0.3) ft |

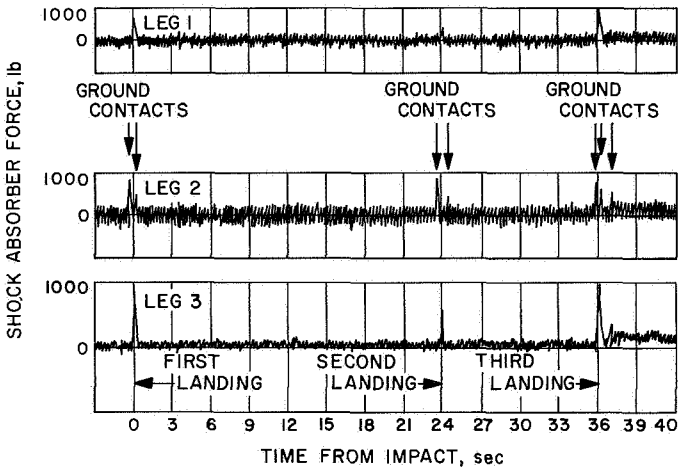



**Fig. XIV-21. *Surveyor III* shock absorber strain-gage force histories**

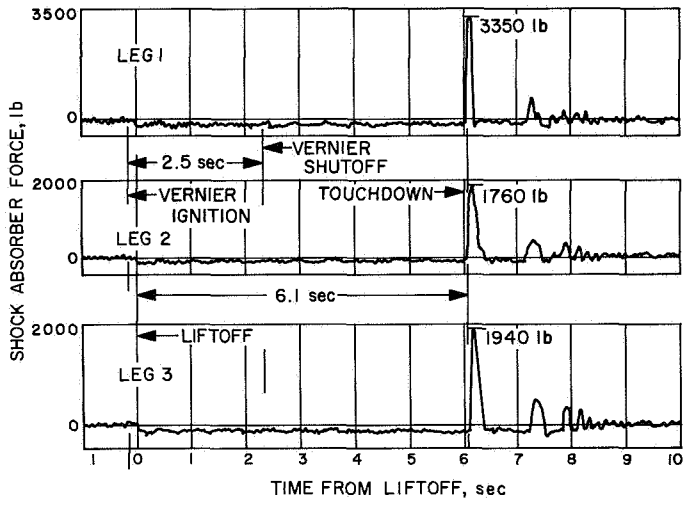



**Fig. XIV-22. *Surveyor VI* shock absorber strain-gage force histories**

The preprogrammed pitch angle of 7 deg was not maintained during the free-fall period. After engine shutoff, the pitch motion was reversed and a negative yaw motion introduced, probably due to uneven engine cutoff, resulting in a +2-deg pitch and −3.5-deg yaw position shortly before touchdown with respect to the prehop attitude of the spacecraft. Also, a negative roll motion was introduced at engine shutoff, resulting in a relative roll angle of −4.3 deg.

Leg contact timing and maximum shock absorber axial loads for the landing are given in Table XIV-30.

The high force encountered by leg 1, as compared with legs 2 and 3, can be explained in part by the horizontal velocity in this direction; however, a high-friction force is required to obtain the indicated level in a landing simulation. Therefore, it is assumed that leg 1 encountered some obstruction constraining its lateral motion during the hop landing.

**Table XIV-30. Maximum shock absorber axial loads and times of initial ground contact (hop experiment of *Surveyor VI*)**

| Leg | Max shock load, lb | Contact time, GMT |
|---|---|---|
| 1 | 3350 ±180 | 321:10:32:11.196 (±0.003) |
| 2 | 1760 ±90 | 321:10:32:11.178 (±0.003) |
| 3 | 1940 ±90 | 321:10:32:11.220 (±0.003) |

Following first contact, spacecraft rebounding and ringout were indicated in the strain-gage records as being quite similar to those of the initial landing of *Surveyor VI* and the landings of *Surveyors I, III, V,* and *VII.*

The hop experiment was designed to result in landing conditions within the spacecraft's capabilities. As the foregoing data show, this was achieved. No problems were encountered, although the force in the leg 1 shock absorber was unusually high—by far the highest shock absorber force ever experienced in a *Surveyor* landing.

## D. Mechanisms

The *Surveyor* mechanism concepts changed very little from those originally proposed by HAC in the early 1960s. The functions of the various mechanisms remained the same while the normal developmental changes were incorporated and qualified.

This section does not include descriptions of all spacecraft mechanisms. The mechanisms with functions integrally linked to operations of spacecraft subsystems are discussed within the respective subsystem sections of this report.

Table XIV-31 lists all of the *Surveyor* spacecraft mechanisms with references to the sections wherein their physical and functional descriptions are located.

Mechanisms were classified into two general categories: the event-actuated and the command-actuated devices.

**Table XIV-31. *Surveyor* assemblies, index**

| Mechanism | Reference section |
|---|---|
| Television mirror, focus and filter drives | XXII |
| Alpha scattering instrument deployment device | XXII |
| Soil mechanics surface sampler | XXII |
| Vernier engine roll actuator | XVII |
| Retrorocket safe–arm device | XVII |
| Helium release device | XVII |
| Helium dump device | XVII |
| Landing gear deployment device | XIV-A-2-c |
| Shock absorber device | XIV-D-1 |
| Separation sensing and arming device | XIV-D-2 |
| Antenna/solar panel positioner | XIV-D-3 |
| Omnidirectional antenna deployment mechanism | XIV-D-4 |
| Retrorocket release mechanism | XIV-D-5 |
| Pinpuller devices | XIV-D-6 |
| Thermal switch device | XV-A-3-b |

The units in the event-actuated category were the separation sensing and arming device, shock absorber, and thermal switch. The separation sensing and arming device and shock absorber were actuated by two physical occurrences: the separation of the *Surveyor* from the *Centaur* and touchdown of the *Surveyor* on the lunar surface. The thermal switch was actuated by a thermal occurrence: the temperature reaching a preset opening or closing position for the switch.

The units in the command-actuated category were all of the other units listed in Table XIV-31. The command-actuated units were triggered by discrete commands transmitted from an earth-based tracking station.

The command-actuated mechanisms were further divided into multiple- and two-position devices. During the conceptual study of the multiple-position actuation drive, it was concluded that the best solution was a stepper motor. Two sizes of stepper motors were chosen with corresponding planetary gear trains available in various ratios. The A/SPP drives were examples of the larger motor drives, and the televiewing camera mirror drives were examples of applications using the smaller motor drives.

The second type of command-actuated mechanism was the two-position unit which could be actuated only once. The original proposal described the single-actuation mechanism as being spring powered, which obtained release by a squib-actuated pinpuller. The omniantenna deployment mechanisms and the retrorocket release mechanisms were examples of the single-actuation type and are discussed in subsequent paragraphs.

### 1. Shock Absorber

The *Surveyor* shock absorber was a telescoping tubular column capable of dissipating the energy of landing and reextending to full length through damped spring action. It consisted of two pressure chambers made from one titanium billet. One chamber contained the damping–spring unit which used a silicone liquid for dissipating and absorbing the landing energy. A slow-bleed valve and a metal bellows extended into the second chamber. The second chamber contained helium gas which preloaded the liquid spring and, in combination with the bellows, enabled temperature compensation of the liquid pressure and volume. The preload was sufficient, at temperatures greater than 0°F, to keep the shock absorber fully extended when supporting the spacecraft lunar weight. After landing, in some cases, the shock absorber was mechanically locked in the extended position to prevent deflection in case of liquid or gas leakage. A strain gage mounted on the gas cylinder was calibrated to read the axial loads encountered. The shock absorber attached to the spacecraft at the landing gear A-frame/lockstrut juncture inboard and the footpad/landing-leg juncture outboard.

*a. Development of design for Surveyors I and II.* The HAC procurement specification established envelope, weight, and environmental constraints, outlined the variable damping feature and performance characteristics, and specified the quality controls and qualification programs required. National Water Lift Company (NWL) proposed two designs: a prime design to the HAC specification and an alternate fixed-orifice design, attractive from the viewpoint of simplicity. National Water Lift's prime proposal was accepted, and the procurement specification was revised to incorporate the details of that design.

The prime NWL design consisted of two basic parts: a liquid spring at one end and a tubular gas chamber at the other. The liquid spring chamber was completely filled and contained a rod and piston. As the piston moved, the liquid passed from one side of the piston to the other through two orifices. The first varied in size with piston position by a contoured, needle-like rod through the orifice and provided variable damping during compression. The second orifice was a check valve which opened when the shock absorber was compressed and closed during reextension to increase damping for rebound control. The liquid-spring action was accomplished by the change in volume of the liquid as the piston rod occupied more or less volume in the chamber. When the unit reextended to its initial length, it was held by cam detent lock fingers. Later, a squib-actuated positive lock

was added. A single prototype was fabricated, but significant vehicle weight decreases made a second one necessary.

The basic design, fabrication techniques, and functional performance were tested for verification. As changes were implemented, retests were performed. Redesigns were made to improve performance of the lock fingers and seals. Welding techniques and manufacturing facilities were improved but still required strict controls. Burst tests of the gas cylinder showed that, because of the high notch sensitivity and extreme brittleness of the 13V-11Cr-3Al titanium used, its man-rating as a pressure vessel was marginal. The fabrication of the metering rod was extremely difficult because its contour was determined by the performance of the unit. Nonrepeatable performance data complicated this problem.

Qualification tests (including pressure, temperature, shock, acceleration, vibration, and performance conformity) were initiated using units from the production run. Failure-mode tests demonstrated design margins, and drop tests were conducted with S-2, S-2A, and T-21 vehicles. The flight units were subjected to flight acceptance tests prior to HAC acceptance.

This original design was flown on *Surveyors I* and *II*. Development and fabrication attrition was high and, if continued at that high rate, would have expended the original "heat" of titanium material, leaving the program short of the required parts. At this point, an increased *Centaur* capability offered the possibility of an increased scientific payload. This increase of landed weight required that the shock absorbers be redesigned. JPL directed HAC to change the design and to change the material to 6Al-4V titanium. Later program decisions established the *Surveyor V–VII* landed weights at levels approximately the same as those of the earlier *Surveyors*, and it was determined that newly designed shock absorbers were suitable for application to *Surveyors V–VII*.

***b. Development of design for Surveyors III–VII.*** JPL's direction to change material afforded an opportunity to make other design improvements, and the NWL fixed-orifice design was reconsidered. Seal design was improved, as were welding techniques. The squib lock was maintained, but the troublesome cam–detent lock fingers were eliminated. The variable-compression damping feature, so difficult to fabricate, was replaced by a simple, fixed-orifice design. The spring-loaded, double-acting orifice feature was retained. The bellows assembly was changed so that it could be replaced without cutting welds. The housing was designed to a man-rated safety factor of 2.2. The result was a simplified, more reliable, and more easily fabricated unit with an increase in weight from 4 to 5 lb. Type approval tests were run on four units, and three were drop-tested aboard the S-9 and S-15 test vehicles. All flight units were subjected to flight acceptance tests prior to final acceptance. Shock absorbers of this design were flown on *Surveyors III–VII*.

***c. Posttouchdown performance.*** The *Surveyor V* shock-absorber squib locks were not fired until about 30 hr before lunar sunset because of the possibility of conducting a hop experiment. Near sunset and at different times, the leg position potentiometers on legs 2 and 3 were noted to change from less than 1 deg to 4.3 and 6.7 deg, respectively. This indicated that the shock absorbers on these legs were not fully extended. On the following lunar day at first interrogation, the legs were back to their original positions. The conclusion was that the locking squibs on shock absorbers 2 and 3 were not fired, and gas or liquid contraction allowed the two shock absorbers to retract as they cooled.

On the *Surveyor VII* mission, the shock absorbers were commanded to lock several earth days prior to the initial lunar sunset. The position potentiometer output on leg 2 showed 1.25 deg increased deflection at a shock absorber temperature about the same as that of the *Surveyor V* leg deflections, indicating a similar nonlocking anomaly. When *Surveyor VII* was first interrogated on the second lunar day, leg 2 had reextended but leg 1 had completely collapsed, indicating a total deflection of 23.5 deg. It has been concluded that leg 2 reextended upon warming up and that the shock absorber on leg 1 incurred a liquid or gas leak—probably the latter.

### 2. Separation Sensing and Arming Device

One separation sensing and arming device (SS&AD) was mounted on each of the three spaceframe column base fittings near each *Centaur* attach point. Three SS&ADs were used to provide redundant activation of the squib firing circuits and vernier engine solenoid circuit after the spacecraft separated from *Centaur*. Each of the SS&AD units performed the following functions:

(1) Prevented inadvertent firing of pyrotechnic devices prior to separation.

(2) Provided a delay between the closing of the two arming circuits and the closing of the third circuit which applied the power.

Initially, each SS&AD contained two microswitches actuated by a plunger bar-linkage mechanism. The bar-linkage slot was incorporated directly into the original plunger shaft. The two switches were mounted in the housing, one above and the other below the actuating-bar linkage. The switches were mounted to the case without tooling, which resulted in varying switch-actuation points with respect to plunger position. The assembly was attached to the column base fitting of the spaceframe, and the plunger protruded below the spaceframe, supported by an adjustable pedestal on the *Centaur* adapter.

During spacecraft/launch vehicle interface tests, it was found that the actuator shaft did not have sufficient travel to accommodate the interface displacement resulting from launch vibration without danger of premature switch operation. The actuator shaft was redesigned to incorporate a telescopic feature that would correct this discrepancy. To provide greater reliability, three switches were added to each housing, and all three SS&AD units on each spacecraft provided the same switching functions. Tolerances were tightened, and dry-film lubricant was added to the moving parts during the SS&AD redesign to provide more repeatable switch operation. Tests indicated that the dry-film lubricant had to be burnished to provide better mechanical operation. Special tooling was made to position the switches accurately in the housing. With these changes, the SS&AD became a very reliable unit. The redesign was accomplished in time to be effective for *Surveyor I*.

The SS&AD actuating mechanism consisted of a spring-loaded two-piece sliding plunger shaft and a pivoted bar linkage that operated three switches (Fig. XIV-23). The inner member of the plunger shaft was supported at both ends by two bushings in the top and bottom of the housing, and the attached collar restricted its downward axial movement. The outer sliding actuator member rode on the inner plunger member and was spring-loaded on both sides of a circumferential slot in which the free end of the bar linkage rode. The upper spring was supported by the upper housing, and the lower spring was supported by the inner telescopic plunger-shaft stop collar. When the inner plunger shaft was lowered to its full-travel position, the differential rate in the two springs allowed the outer switch-actuating sliding member to move down, lowering the bar linkage and actuating all three switches located between the plunger shaft and the bar-linkage pivot pin. Two switches were mounted above the pivot pin and one was mounted below, giving a delay between the closing of the arming circuits and the closing of the power circuit. The bar linkage was made in two parts: a solid piece that incorporated the pivot-pin hole and extended just beyond the switch-actuating arms, and a leaf spring that continued from that point to the actuating sliding member slot. The leaf spring allowed the bar linkage to have some overtravel without applying excessive force to the switches.

When the spacecraft was mounted on the launch vehicle, each plunger shaft rested on an adjustable pedestal on the *Centaur*, which compressed the two springs and held the outer sliding-actuator member against the top of the housing. In this position, the inner plunger shaft protruded from the top of the housing, and a groove was exposed into which a safety clip could be placed to prevent accidental switch actuation. In this position, the word *SAFE* appeared on the upper end of the plunger shaft, and a green band could be seen on the lower end. In any other position, the complete word *SAFE* would not be visible, and a red band became visible along with the green band on the lower plunger shaft. The *Centaur* adjustable pedestals were set so that all the plungers were supported in the safe position with the safety clip removed prior to launch.

All of the flight units went through a flight-acceptance test program with no apparent problems. The type-approval tests on two of the newly designed units indicated that the design was acceptable. No malfunction of the device occurred during any of the spacecraft missions.

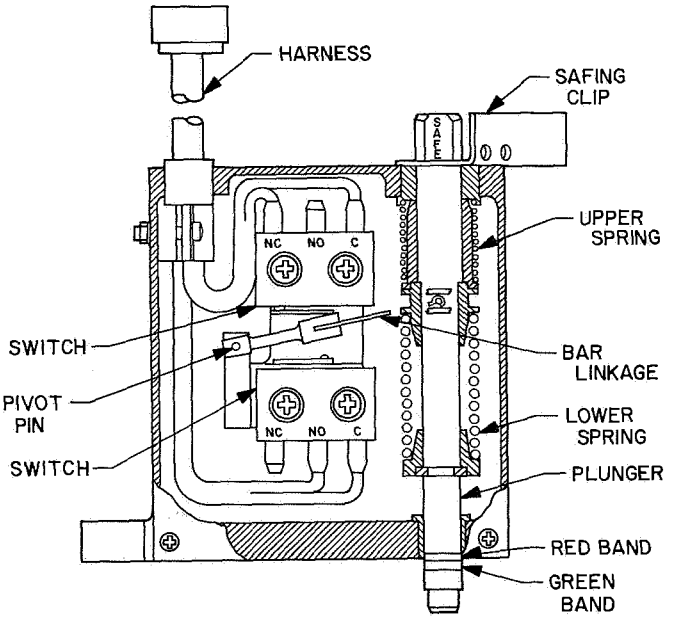



**Fig. XIV-23. Separation-sensing and -arming device**

### 3. Antenna/Solar Panel Positioner

The A/SPP was a four-axis (roll, elevation, solar, polar) gimbal mechanism that provided mounting, positioning, position indication, and launch and landing locks for the planar-array antenna and the solar panel. Positioning requirements included aligning the planar-array antenna toward earth, the solar panel toward the sun, and the antenna and solar-panel shadows over portions of the spacecraft or in special configurations such as for spacecraft attitude determination. These requirements had to be satisfied while the spacecraft was exposed to temperatures of −225 to 260°F, a vacuum of $10^{-12}$ torr, and lunar gravity.

The roll-, elevation-, and solar-axis drives utilized three-stage planetary gear reductions (288:1). The polar-axis drive used a two-stage (14.4:1) planetary and double-enveloping-cone worm drive (40:1). All axes used solenoid stepping motors for drive and wirewound potentiometers for position indication. Each motor step rotated the motor output shaft 36 deg. The solar-, elevation-, and roll-axis locking was achieved with tapered lockpins. Shear- and squib-actuated pinpullers were included for retraction. Spring-loaded, tapered lockpins were also utilized for relocking the roll- and solar-axis drives after stepping from launch configuration to transit/landing configuration. Polar-axis variable-position locking was accomplished with a worm-and-sector gear and detents in the drive motor.

*a. Design changes.* The basic A/SPP configuration remained unchanged after the initial configuration study. However, there were numerous engineering changes in components and parts to create approximately seven different versions: four that flew on various spacecraft, two that were built but never qualified for flight, and one design that was never converted into hardware. The principal areas of influence causing the changes were: dynamic loads and test results, low drive-motor output torque and life, and unsatisfactory position-potentiometer performance. The seven configurations are summarized in Table XIV-32.

The *Surveyor I* A/SPP configuration had the following design deficiencies which required operational restrictions:

(1) The A/SPP structural margins were negative, especially in the elevation-axis lock structure.

(2) The off-the-shelf solenoid-type stepper motors developed less than the required torque output and operating life.

**Table XIV-32. Antenna/solar panel positioner configurations**

| Surveyor | Serial number | Design deficiencies or changes | TA test completed |
|---|---|---|---|
| *I* | 287550 | Negative structural margins<br>Negative motor-torque margins | No |
| *II, III, IV* | 287580 | Improved stepper motor<br>Modularized pinpullers | No |
| | 293300 | Jackscrew polar axis<br>High-torque motor<br>New gearbox | No |
| | 293275 | Increased structural margins<br>Enlarged, tapered lockpins | No |
| | 3035049 | Dry-lube motor | No |
| *V* | 3035092 | Pin-and-bushing motor | Yes |
| *VI, VII* | 3035092-1 | Pinned position-potentiometer wiper | Yes |

The A/SPP used on *Surveyors II, III,* and *IV* (SN 287580) was an upgrade of the *Surveyor I* design in the following areas:

(1) The stepper motor was modified by replacing the ball detent mechanism with a roller detent mechanism to reduce friction and increase life. Dry lubrication was deleted to prevent slipping of the motor clutches. (See Fig. XIV-24 for comparison.) The stepper motor output shaft (without the planetary gearbox) still moved 36 deg per step.

(2) The tapered lockpin devices, squib-actuated pinpullers, and switches were modularized so that precision adjustments could be made on the assembly bench rather than on the spacecraft.

(3) Spring-loaded tapered lockpins were incorporated in the launch pinpuller assemblies of the roll and solar axes to provide greater assurance of proper seating during all environments.

The 293300 A/SPP configuration was basically the same as that for *Surveyors II, III,* and *IV*, but many detail design changes were incorporated to ease assembly and increase torque and structural margins. This design never was carried through to the point of fabricating flight hardware. Several design improvements resulted from the study and later were incorporated in the *Surveyor V, VI,* and *VII* units. These included:

(1) Development of a high-torque cam-type stepper motor to replace the detent stepper motor.

(2) A more efficient gearbox assembly.

(3) A new pinpuller assembly that incorporated a bulkhead mount, (allowing bench adjustment) and a retention device to prevent lockpin bounce after retraction.

(4) An improved structural stress margin due to increased tubular wall thicknesses.

The 293275 A/SPP configuration, which was never flown, incorporated significant engineering changes, but the basic configuration of 287580 was retained. Structural changes were made in the elevation- and roll-axis lock structures and the solar-panel support arms. Other structural changes accommodated the new solar-panel design which was considerably more rigid, and the tapered lockpins on the roll and elevation axes were enlarged. A new, interchangeable high-torque solenoid motor which rotated the motor output shaft 40 deg per motor step was incorporated along with a new potentiometer and two new planetary transmissions (289:1 for the roll, solar, and elevation axes, and 14.6:1 for the polar axis). Although the initial output torque of the new motors was high, dropoff was rapid after 50,000–60,000 cycles and was below the required torque. The degradation was caused by severe wear of the linear-to-rotary motion-conversion mechanism; therefore, the 293275 version was not flown.

Development work was continued to eliminate the premature wearout. The dry-film lubricant was changed to what was thought to be a superior lubricant, and the new version was designated 3035049. After considerable motor testing, it was found that 3035049 was not much of an improvement over the 293275, and a study was begun on different techniques of transferring linear motion to rotary motion without changing the motor envelope and other characteristics. The techniques studied were:

(1) A flexure connection to eliminate all of the friction-wearing surfaces. The design did not lead to successful results and was dropped.

(2) A pin-and-bushing design (Fig. XIV-24) which led to the next A/SPP version, designated 3035092.

The 3035092 A/SPP, used on *Surveyor V*, was the same as the 293275 design except that it incorporated the pin-and-bushing stepper motor with a 25% increase in initial output torque and a twofold increase in life at the minimum torque required. During flight-acceptance tests, the position-potentiometer output was irregular.

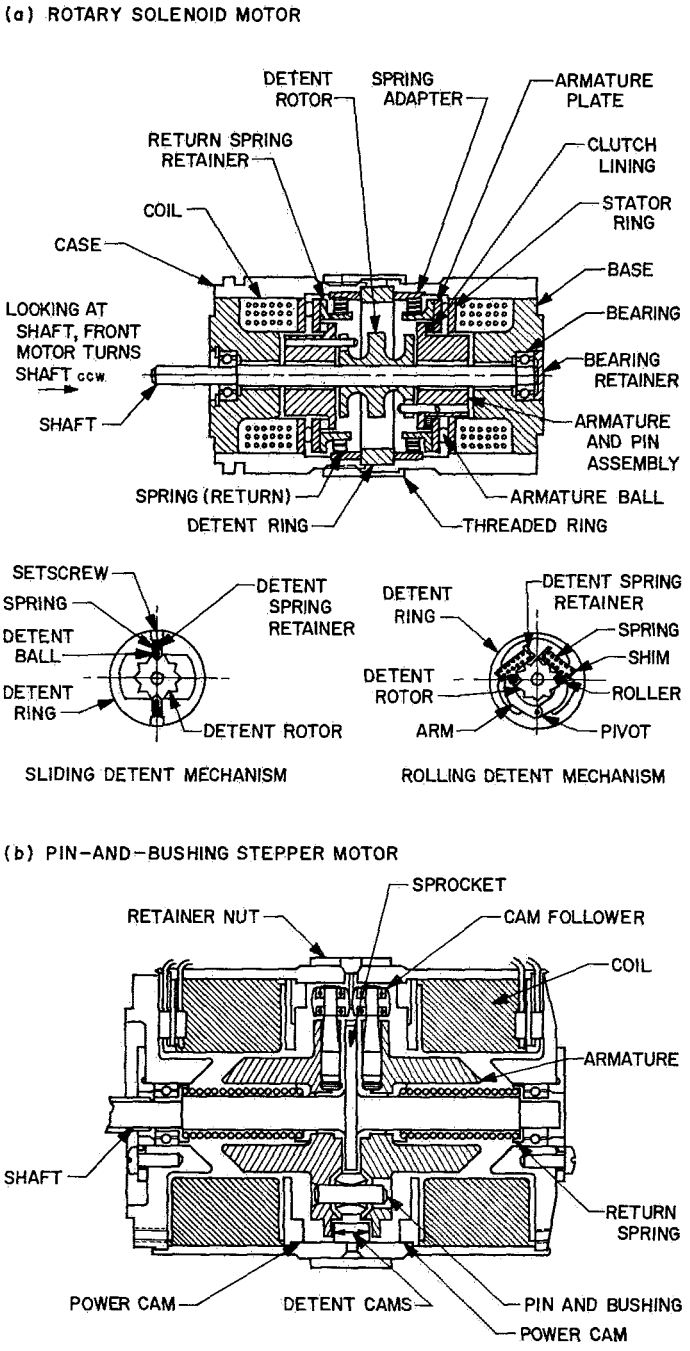



**Fig. XIV-24. A/SPP motors**

Upon investigation, the potentiometer pressfit wiper-to-shaft attachment, which involved two different materials, was found to be loose at −100°F due to dissimilar thermal expansion. The 3035092-1 model was used on *Surveyors VI* and *VII* and incorporated a different position potentiometer. The wiper-to-shaft attachment change incorporated a knurled pressfit combined with a riveted connection.

The 3035092 and 3035092-1 were the first units to have completed type-approval test programs. The most significant anomaly was the backing out of the solar-axis lockpins. These tapered pins were used to lock both solar arms in the transit position, not allowing the landing loads to be transmitted through the axis of rotation into the actuator. The taper was used to avoid close tolerances on the hold locations. The first failure occurred during an S-9 drop test when the two solar-panel *landing* lockpins popped out. Upon investigation, the lockpin hole was found to be coated with lubricant from the lockpin, which reduced the coefficient of friction to the point where the load cammed out the pin. The solution was to increase friction by removing the lubrication from the lockpin and to apply Alodine in the clean, bare, aluminum taper holes as a vacuum-welding deterrent. A second tapered lockpin failed on the solar-axis launch lock during S-9 spacecraft vibration testing. The spring-loaded lockpin slowly worked out of the hole due to vibration and the constant load imposed by the solar panel dampers. In order to overcome the effect of the damper force, a higher lockpin-spring preload was obtained by insertion of a plug behind the existing spring. This preload was effective, but the ability to check switch actuation by manual compression of the pin was lost because the spring was almost completely compressed.

*b. Mission performance.* The lunar landing loads encountered by the various *Surveyor* vehicles were far below the levels that could have been inflicted on the spacecraft by a maximum design condition. The early version of the A/SPP probably would have failed under the maximum design conditions. On *Surveyor I–IV* missions, operational restrictions were imposed on the A/SPP because of the design deficiencies. The polar axis was kept at zero degrees instead of at the minimum load position of 36 deg until after the landings. This restriction was imposed because the polar axis exhibited operational problems during low-temperature tests prior to installation on the spacecraft. These same temperatures were encountered during the *Surveyor* flights to the moon. Due to the uncertainty of operating the polar axis at these low flight temperatures, it was decided to leave it at the zero-degree position through the spacecraft lunar-landing sequence.

Since the polar-axis position would have affected the spacecraft center of gravity, the polar axis operational restriction had to be made prior to positioning the retrorocket centerline. The retrorocket was positioned for a polar-axis angle of zero degrees, and remained fixed until the *Surveyor* was on the lunar surface. This resulted in larger load inputs to the pinpuller for the elevation-axis transit lockpin and to the tapered hole. These load inputs would have caused local material yielding, for the maximum design landing loads, leaving the elevation axis inoperable. The planar-array antenna support tube was incapable of withstanding these maximum landing loads and would have suffered structural damage. The stepper motors were restricted in their operation time to avoid overheating and subsequent failure during the warmest part of the lunar day.

During the first lunar day of all *Surveyor* missions, the A/SPP functioned as required for spacecraft attitude determination, sun and earth tracking, and spacecraft shading. In addition, the *Surveyor VI* A/SPP survived the spacecraft hop experiment with the solar and roll axes unlocked.

The *Surveyor I* A/SPP survived the lunar night, but its performance was degraded during the second lunar day. *Surveyor V* A/SPP functioned normally through the second lunar day.

#### 4. Omnidirectional-Antenna Deployment Mechanism

The two omniantennas (A and B) used in the communication link with earth throughout flight and the initial lunar test sequences were not truly omnidirectional. A location remote from the spacecraft was required for minimum pattern distortion, but such placement was not compatible with the launch vehicle nose fairing. Foldable booms, stiff enough to keep the antennas from vibrating at a natural frequency that would interfere with the communication link, were developed.

The omniantenna cones were mounted on the ends of hinged, tapered, hollow fiber-glass booms which were 2 in. in diameter at the base and 1 in. diameter at the antenna attachment point (Fig. XIV-25). Each boom was formed at a different angle so that the antenna-head axis would be perpendicular to the Z axis of the spacecraft, in the deployed position, and so that the assembly would fit under the nose fairing for launch. Each boom had a unique hinge and telemetry position-switch mounting design (Figs. XIV-26 and 27). Both booms had tongue brackets near the omniantenna heads with holes in which the pinpuller shafts were placed to hold the booms in their stowed positions.

The omniantenna A hinge was a complete unit, both halves of which were attached to the boom which, in turn, was attached to the klystron power supply and modulator and had to be removed for access to the unit.

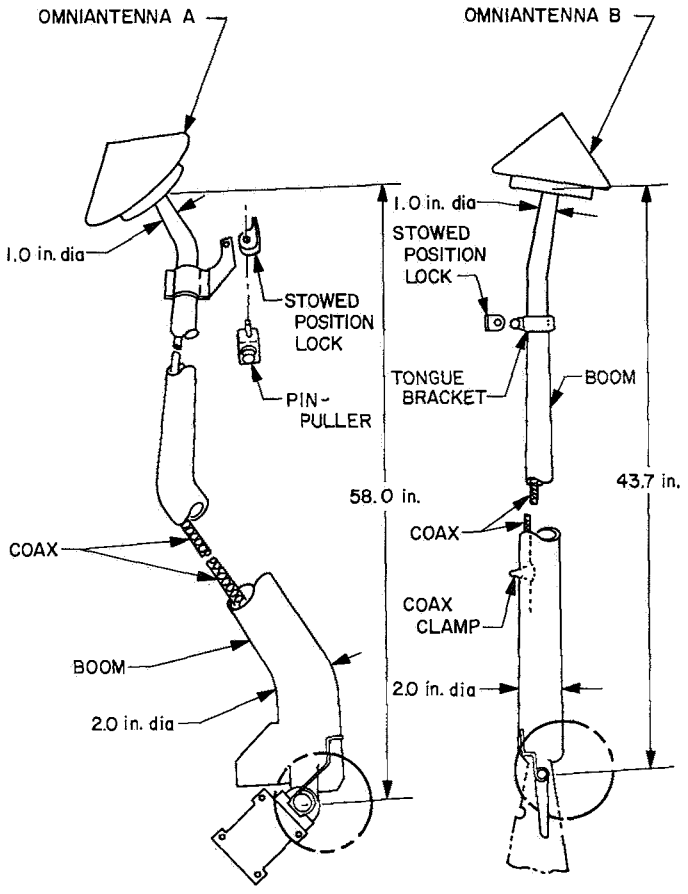



**Fig. XIV-25. Deployment mechanisms for omnidirectional antennas A and B**

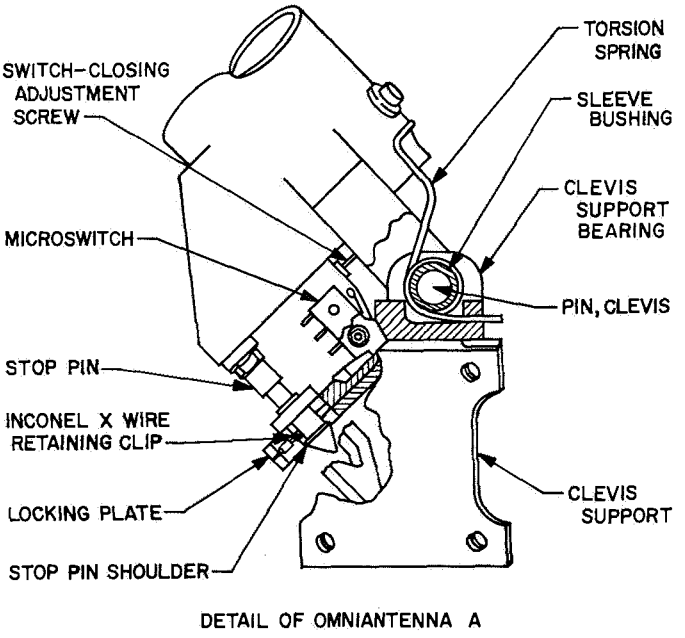



**Fig. XIV-26. Extended-position locking mechanism, omnidirectional antenna A (omni A)**

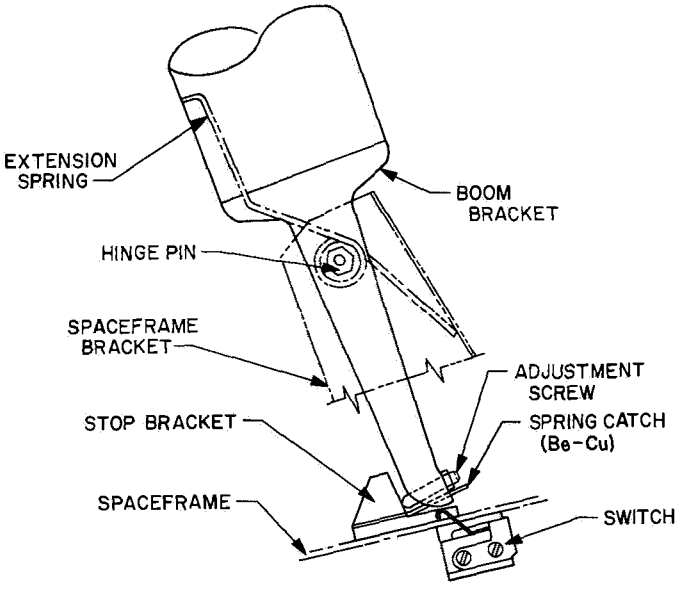



**Fig. XIV-27. Omnidirectional antenna B (omni B) locking mechanism**

The lower half of the hinge was made in two parts with a spherical interface to allow for antenna alignment and two index-pin holes so that alignment was retained when the boom was removed and replaced. A torsion spring on the hinge pin provided the deployment force, and all of the mating parts were coated with a dry-film lubricant. Omniantenna A was locked in the open position by a stop pin attached to the upper half of the hinge which passed through a hole in the lower half of the hinge and was trapped by a retaining clip made of spring wire lodged behind the stop-pin shoulder. Contact of the stop pin with the lower half of the hinge supported the boom in the deployed condition. Boom deployment was indicated when a microswitch on the hinge was actuated by an adjustable screw in the upper half of the hinge.

The omniantenna B boom design was much simpler since it was not constrained by the removal requirement. The hinge consisted of a boom bracket, a spaceframe bracket, and a pin-and-extension spring. The stop was an adjustable screw on the boom end which rested against the spaceframe stop bracket; the catch mechanism was a spring detent. A tongue on the end of the boom depressed a spring, fell into a slot in the spring, and was locked in place. The tongue also actuated an adjustable microswitch which indicated antenna deployment.

The *Surveyor I* omniantenna A boom did not indicate deployment until after the spacecraft had landed. This

problem resulted in the addition of a leaf-type kickout spring located at the pinpuller to initiate the boom movement. Even though omniantenna B deployed properly on *Surveyor I*, a kickout spring was also added as a safety precaution. The omniantenna B boom had no other significant changes from the initial design; but omniantenna A had several, including smaller allowable fit (tongue to stowed position lock) tolerances in the stowed position, better finishes and closer tolerances in the hinge mechanism, and the use of more dry-film lubricant on the hinge parts. The omniantenna A stop pin redesign was also necessary to obtain proper boom alignment with regard to the changing spaceframe alignment and boom manufacturing differences from unit to unit. A dogleg offset was used in the stop pin, but the omniantenna A booms were remade for proper bend angle control. The boom drawings were upgraded and new fabrication techniques used to form the new booms.

The antenna design was type-approval-tested as part of the S-9 vehicle. Most of the antenna mechanisms were flight-acceptance-tested as units before assembly on the spacecraft. This also included an antenna RF checkout. After the redesign following the *Surveyor I* mission, a few units were tested as part of the spacecraft during system test in order to meet the launch schedule. An additional flight acceptance test was added to each omniantenna boom after *Surveyor I* to determine the force necessary to lift the antenna from the pinpuller kickout spring and to verify that the kickout spring would kick the boom tongue clear of the stowed position lock. The force measurement was a check on the hinge friction. After incorporation of the design changes resulting from the malfunction of omniantenna A on *Surveyor I*, all booms functioned normally throughout subsequent *Surveyor* flights.

### 5. Retrorocket Release Mechanism

Three retrorocket release devices were used to secure the retrorocket to the spaceframe. Each was self-contained and operated independently. They were designed to support the load of the retrorocket until electrically activated, then to separate and release the retrorocket. Each device consisted of an explosive nut and associated support hardware, two dual-bridge wire squibs, a base backup plate, a ½-20 socket-head bolt, and two washers. When the devices were activated, the explosive nut freed the bolt and imparted sufficient force to expel it from the device and the retrorocket structure. The device retained all of the nut segments and fragments.

The main cylindrical body of each device radially supported the inner unlocking piston which, in turn, radially supported the three segments of the nut (Fig. XIV-28). The nut segments were supported axially by a conical, keyed seat at the lower end and by a conical separator piston at the upper end. The lower seat was cone-shaped so that the nut segments would slide down and out due to thread load when their radial support was removed by squib-firing. The keys were part of the seat and were used to prevent the nut from rotating and keep the segments equally spaced. When the separator piston was driven down by the squibs, its conical surface also forced the nut segments outward and would not allow them to go toward the center again. In the center of the separator piston was an ejector piston which applied a force to the end of the bolt, giving it the required parting impulse.

The following design change was made prior to the *Surveyor I* flight: The key seat was enlarged to preclude its being moved out of the lower part of the mechanism by the squib.

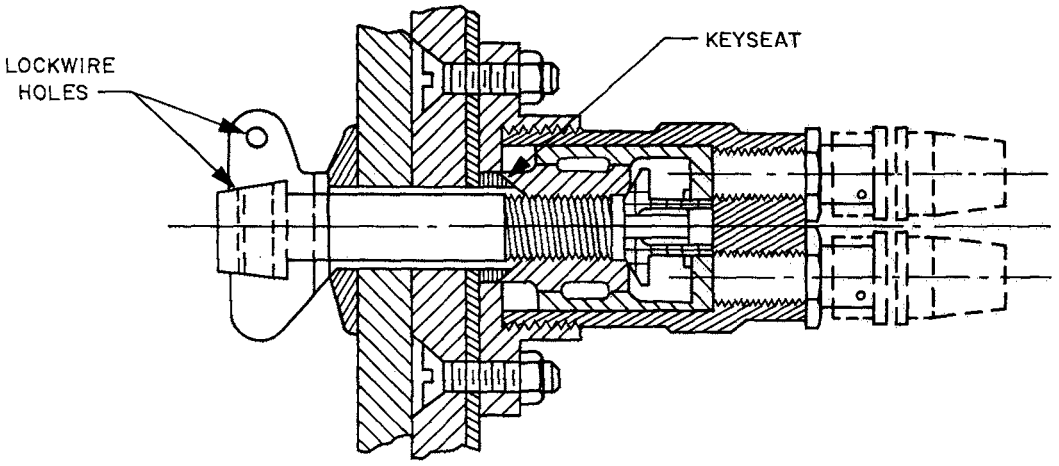
All of the retrorocket release mechanisms were procured early in the program from Hi-Shear Corporation. Hi-Shear also did qualification type-approval testing to prove the design. Flight acceptance testing of the flight units was done during the system vibration test series. All of the spares were flight-acceptance-tested separately in a simulated-retrorocket test fixture.

There were no malfunctions of the retrorocket release mechanisms during *Surveyor* missions.

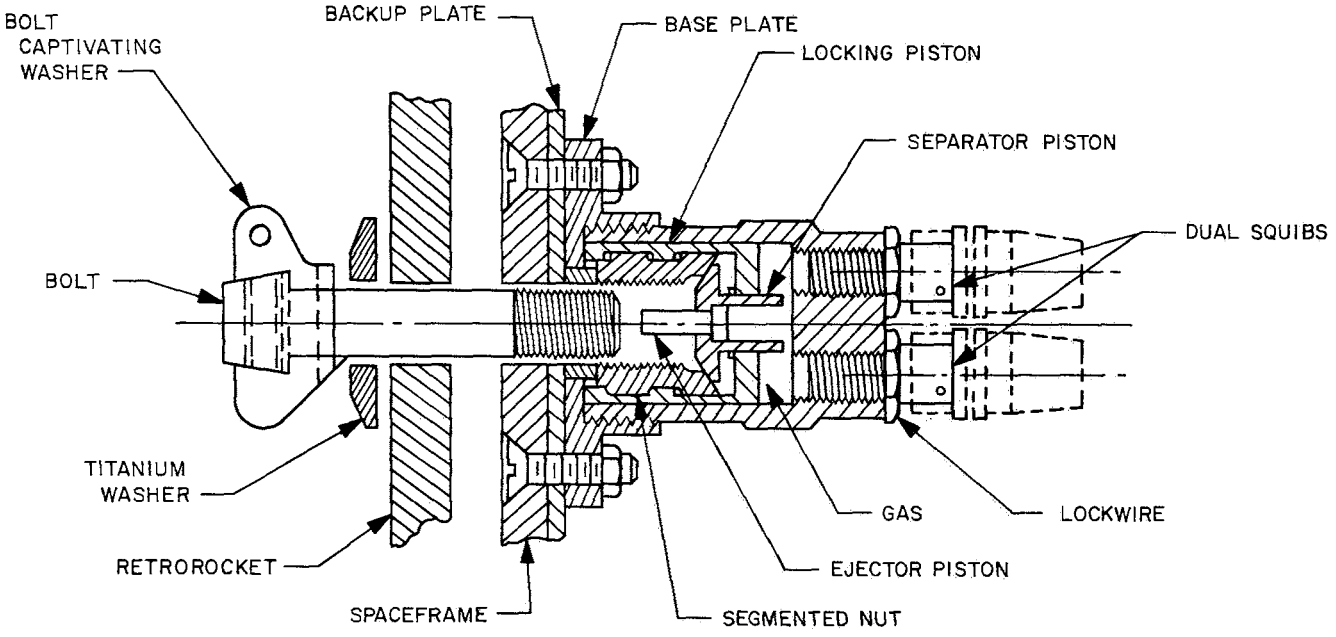
### 6. Pinpullers and Locking Devices

*a. Basic pinpuller.* The pinpullers represented an off-the-shelf Hi-Shear design, and were used to release the landing legs, omniantenna booms, vernier-engine roll actuator, and the science-instrument mechanisms. The basic pinpuller body was of aluminum with a stainless-steel pin protruding from one end. A capturing device on the opposite end held the retracted pin in place. A small shear wire was placed in the squib hole through the pin, and into the opposite body wall. The wire required about 60 lb to shear and kept the pin from inadvertently being retracted. The squib was installed toward the pin end of the body and perpendicular to the pin axis. O-rings were used to seal the body around the shaft hole and at the squib mounting hole (Fig. XIV-29).

The basic pinpuller design remained the same throughout the *Surveyor* Program. Some development work was done to determine the optimum explosive charge for safety and operational margins under various conditions of side loadings and temperature.




PRERELEASE




POSTRELEASE

**Fig. XIV-28. Retrorocket release mechanism**

A successful type approval test program was performed which included vibration, temperature shock, and acceleration to establish thermal reliability and confidence levels. All flight units were subjected to the flight acceptance test environment of vibration and thermal vacuum and X-rayed for proper assembly before acceptance.

*b. A/SPP pinpullers.* The pinpullers used on the A/SPP were of the same basic design as those previously described but were modified extensively for this application. The modifications included the addition of large, tapered stainless-steel pins which screwed onto the ends of the standard pinpuller shaft.

The A/SPP pinpuller design used for *Surveyor I* required that all of the pinpuller components be assembled individually on the spacecraft. The *Surveyor I* pinpuller bracket was installed on the A/SPP, and the pinpullers with solid taper pins were mounted to the brackets and carefully adjusted, after which the telemetry switches were installed and adjusted.

The first lot of the A/SPP squibs occasionally shorted out after firing. For this reason, the pinpullers which would be fired prior to landing were isolated from the spaceframe with a 500-ohm resistor. The resistor was connected between the pinpuller body and spacecraft ground so that a squib short would not drain the battery power.

A new module pinpuller assembly design was introduced prior to the flight of *Surveyor II*. (See Fig. XIV-30.) The tapered lockpins also were modified at the same time. These new lockpins were in several forms, both solid and spring-loaded. The elevation-axis lockpins were tapered and floating, which eliminated the need for precision alignment of these units. The tapered solar-axis lockpin was restricted so that its axial movement was very small compared to that of the roll-axis lockpin. The roll-transit and solar-transit lockpins were also spring-driven into the transit-position holes when the A/SPP was moved to the transit position after launch. The roll- and solar-transit lockpins and pinpullers were assembled on a bracket along with the lockpin-actuated switches used for automatic deployment sequencing and telemetry function indications. The complete roll- and solar-transit lockpin and pinpuller assemblies were set up and adjusted with a tooling fixture so that the units could be bolted onto the spacecraft without further adjustment, a considerable improvement over the original pinpuller design but one which required many hours for installation.

When the heavier tapered-lockpin assemblies for *Surveyors V, VI,* and *VII* were incorporated, the pinpuller piston seal was not capable of holding the increased pressure on the working side of the piston caused by the added inertia. Leakage resulted, and the lockpin either did not retract all the way or bounced back due to gas behind the piston. This condition was corrected by installing a new piston-cylinder endplug with a hole to vent blowby gas. The piston capturing device was also changed from a metal interruption design to an annular groove into which the piston O-ring seal would expand and hold the piston in the retracted position. The vented piston cylinder endplug, though designed for *Surveyor V,* was first used on *Surveyor III.*

A formal type approval unit test program was not completed on the A/SPP pinpuller assemblies, although specific tests were conducted to meet the most critical type approval unit test requirements.

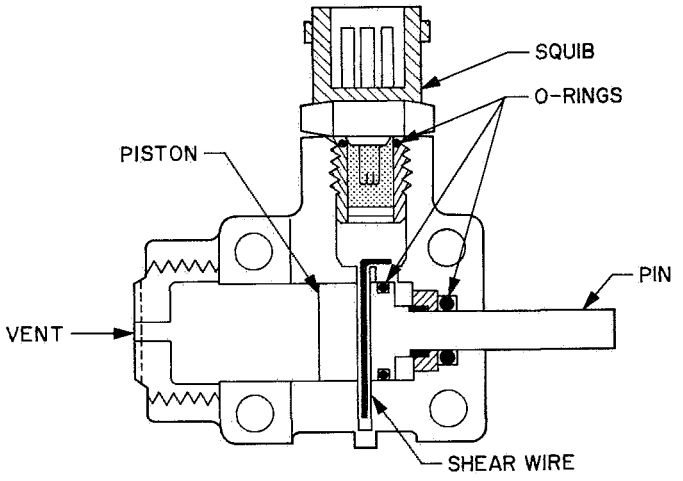



**Fig. XIV-29. Basic straight-shaft pinpuller**

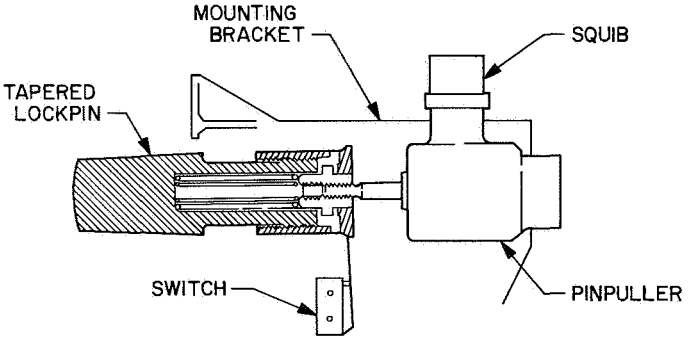



**Fig. XIV-30. A/SPP tapered-shaft pinpuller**

The pinpuller type approval (TA) tests were run as part of the total A/SPP assembly test which was performed prior to *Surveyor V*. The A/SPP system TA test did not meet the unit test requirements of the pinpuller specification, but the results were accepted as adequate qualification.

All flight and flight-spare A/SPP pinpullers and pinpuller assemblies passed the unit level flight acceptance tests. Once the A/SPP pinpuller modules were assembled and adjusted with the tooling fixtures, pinpuller problems vanished except for some which resulted from attempts to change the module adjustment on the vehicle.

There were no mission failures of A/SPP pinpullers.

***c. Shock-absorber locking device.*** The landing gear shock absorber locking device had a piston which rode in a bore perpendicular to the shock absorber axis. The piston had an O-ring seal around its circumference and a spike on its lower side, which was driven by a squib into the soft aluminum pad attached to the cylindrical part of the shock absorber. This locked the shock absorber in place axially.

The shock absorbers on legs 2 and 3 of *Surveyor V* and legs 1 and 2 of *Surveyor VII* collapsed, as was evidenced by the indicated changes in leg position. The shock absorber lockpins of *Surveyor V* were not commanded to fire at the normal time in order to maintain the capability of lunar hopping. The command to fire the locks was transmitted near the end of the lunar day after some of the component temperatures had dropped below the design operating levels. The low temperatures could have affected the squib firing capability; however, the reliability history of the squibs indicates that they would have fired.

The shock absorber lockpins of *Surveyor VII* were commanded to lock several days prior to lunar sunset. Temperature could not be considered a factor in the failure of the locking devices to function on this occasion. It is possible that the squibs did not receive the command.

Except for the shock absorber locks on *Surveyors V* and *VII*, all pyrotechnic devices on each of the vehicles functioned normally, as was indicated by telemetry signals and subsequent spacecraft operations.

## E. Electronic Packaging

### 1. Design Objectives and Standards

The primary electronic-packaging design objective was to achieve successful spacecraft operation in the environments encountered during prelaunch, launch, transit, and lunar-surface phases. In keeping with this objective, design policies were established to: minimize spacecraft electronic circuit complexity, save weight and conserve space by placing the spacecraft mission control and decision-making electronic circuitry on earth-based equipment wherever possible; package subsystems as autonomous and independent as possible for configuration flexibility; use components of proved reliability or establish test criteria for unknown components; use redundance in critical areas; and use technologically advanced designs and processes.

Some of the electronic components to be used could not survive the mission temperature extremes and required protection. Descriptions of the two temperature-controlled main compartments and other temperature-control measures are given in Section XV of this report.

The HAC electronic-packaging design standards often were inapplicable or incomplete because of the uniqueness of the *Surveyor* Program. Therefore, an effort was made during the initial design phase to establish a design standards manual for *Surveyor*. The resulting *Electronics Design Standards Book, Surveyor Spacecraft,* an informal working document, explains and depicts such items as:

(1) Method of mounting components to reduce the thermal gradients between them and the thermal control surface.

(2) Method of mounting components in terminals and on printed-circuit boards.

(3) Guidelines on selection of planar layout or modular construction.

(4) Design and materials information for the construction of the subchassis.

(5) Connector and component dimensions, lead lengths, and weight.

(6) Typical drawing callouts, notes, dimensioning for various methods, materials, and fabrication processes.

(7) Printed-circuit-board artwork layout and circuit spacing standards.

(8) Design and materials information for the construction of the T-bar module.

When new or revised information, processes, etc., were indicated as being necessary from test data or design requirements, the manual was updated as required; however, areas not given adequate coverage were standard

hardware (screws, nuts, terminals, washers, etc.), polymeric materials and their applications, and metallic and nonmetallic construction materials.

Each electronic subsystem was designed within the guidelines of the standards book, but there was no enforced uniformity in detail design or fabrication techniques.

### 2. Design Problems

The following paragraphs describe some of the more important design problems which arose and were solved during the program. Telemetry gave no indications of problems during any mission which were attributable to packaging techniques.

*a. Subchassis construction.* Originally, minimum weight was one of the prime considerations for *Surveyor* designs. The subchassis design consisted of a 16-mil aluminum sheet, a 125-mil plastic foam core, and a 31-mil-thick printed circuit board. During type approval environmental tests, several heavy components which were bonded to the subchassis had bonding failures attributed to the breakdown of the foam used in the subchassis "sandwich" construction. Substitution of a honeycomb material for the polyurethane foam and improved bonding techniques eliminated the problem.

*b. Circuit-board solder splash.* Short circuits occurred in sandwiched printed-circuit assemblies. X-ray examination revealed metallic bridges between adjacent terminals and etched-circuit lines on the concealed side of the boards. Prior to sandwiching of a circuit-board assembly, terminals were installed on the etched circuit board. The lower portion of the terminals protruded through the board and were rolled to come in contact with the etched circuitry on the back of the board, which was concealed after sandwiching. The rolled portion of the terminals was soldered to the circuitry to provide a positive electrical connection. The problem occurred when the components were soldered to the terminals of a sandwiched circuit board on which excessive solder had been used in installing the terminals. The temperature of the terminals was sufficient to cause the solder on the concealed end to melt. Since the terminals were solid and the sandwich was not vented, the pressure increased, causing the solder to be expelled into the spaces between the circuit board and the core and, in some cases, to contact an adjacent conductor.

The following actions were taken to prevent further failures:

(1) New boards were fabricated for the assemblies of *Surveyor II* and subsequent spacecraft. Minimum solder was used to secure terminals, and bond voids were provided to allow for thermal expansion of solder. Solder application time was limited to control terminal temperature. Inspection procedures were modified to include X-ray examination of all assemblies.

(2) X rays of analog electronic assemblies revealed the same problem but to a lesser degree because of the predominant use of hollow terminals. X-ray inspection was instituted for those assemblies containing solid terminals, and a repair procedure was developed and implemented. The material review board evaluated X rays and determined which solder splashes were to be removed and which were acceptable for flight.

*c. Printed-circuit tarnish.* In late 1964, it was determined that solder workmanship problems were occasionally caused by the poor surface condition of printed circuit conductors. The common process for preparing printed circuit boards was to apply a copper flash to conductors, followed by a silver underplate, and finally a layer of electrodeposited gold. Investigation revealed that the silver underplating migrated through the gold layer and oxidizer at a rate dependent on the sulfur and moisture content of the atmosphere. The oxide which formed prevented proper solder wetting action.

Use of this process was discontinued, and new circuit boards were produced by use of the solder plate process except for the digital-electronic units. The digital-electronic circuit boards were already fabricated when the problem was discovered. The problem had not yet been encountered, most probably because the boards were produced in the more favorable environment of the HAC facility at Tucson, Ariz.

*d. Flux corrosion.* Green discoloration on solder joints and under hookup wire insulation was first noted in February 1964. Investigation indicated that copper corrosion had taken place. The problem was similar to that encountered on the *Polaris* Mark I program in 1962. Activated liquid flux was a factor in both cases.

Tests were performed to determine the rate and time span of corrosion activity. Although the rate of corrosion was rapid, the duration was short and no deleterious

effects could be ascertained. Corrosion did not occur if the plating on the wire completely covered the copper.

Soldering methods were reviewed, since excessive use of activated liquid flux could have caused the problem. Moisture trapped under wire insulation also could have caused corrosion if the wire plating had been defective.

The following practices were recommended as a result of the review and tests:

(1) Avoid use of activated liquid flux and other liquid fluxes if possible.

(2) Use rosin-core solder having the smallest core consistent with adequate soldering.

(3) If liquid flux must be used, soak leads the minimum time necessary to prepare the lead for solder.

(4) Wire used in the assembly should be evenly and completely plated.

(5) Increase attention to flux removal and cleaning.

Application of these techniques on new assemblies minimized the corrosion. Existing corroded units were either reworked or sealed to inhibit further corrosion. A substitute activated-liquid rosin, placed in use in late 1965, did not cause a corrosion problem.

*e. Receiver crystal mounting.* The receive crystals were originally hard-mounted to the subchassis but lost phase lock at the resonant vibration frequency of the crystal (200 Hz) or the receiver (600 Hz). The crystals then were remounted in a flexible polyurethane foam in a metal case. Performance was greatly improved but it was still not up to specifications. The receiver performance met the specifications after the change to an advanced crystal design for low-jitter applications and improvement of the mounting design of the crystal to the crystal-case header.

*f. Transmitter high-voltage arcing.* Tests revealed that the pressure in the electronic compartment was at the critical range for ionization at the time when the transmitters were switched from low to high power. This caused the transmitters to arc and could have prevented normal acquisition by the Deep Space Instrumentation Facility during a mission.

Testing by JPL and HAC on encapsulation materials led to the selection of a foam with a density of 8 lb/ft$^3$ for encapsulating. Further testing indicated a possibility that outgassing of the foam could still cause the internal pressure to reach the critical range during mission life. Since additional testing verified the possibility as slight, flight units were then foam-encapsulated and data on subsequent missions indicated no arcing occurred.

## F. Cabling

The cables electrically interconnected the systems, subsystems, and assemblies of the *Surveyor* spacecraft by separable, branched cable assemblies of laced wire bundles terminating in electrical connectors, lugs, quick-disconnects, and splices. There were also RF cable assemblies which provided the RF transmission path between antennas, transmitters, receivers, and RF switches.

### 1. Design Requirements and Evolution

When the design was started, there was little experience with cable materials in a high-temperature, high-vacuum environment. Tests disclosed that materials which could withstand one environment or the other deteriorated or outgassed beyond acceptable limits under the combination of the two. Temperature capability of $\pm 300°F$ in vacuum was established for the harness so that they would not constrain spacecraft thermal design. Minimum conduction of heat from the thermal compartments was another requirement placed on the wire harnesses.

Materials were used that had proved to be successful on other spacecraft under similar conditions and in laboratory tests. In most cases, the requirements for low outgassing were met, but compromise was necessary. The encapsulation material used to cover the exposed solder pots on some connectors had to be flexible to allow the pins to float, but this material outgassed. However, no serious effects were noted on the optical devices, thermal paint, or arc-over characteristics of the spacecraft due, partly, to the fact that the connectors were wrapped to decrease heat loss and the fact that the outgas products were minimal and transparent.

During the early phase of harness design, an effort was made to minimize heat loss from the electronic compartments by use of a 3-in. length of high-resistance nickel-alloy wire inserted in conductors at the compartment exit. Two types of stranded, Teflon-insulated wire were developed: Nichrome V in 28 AWG (American Wire Gage) and Permanickel in 24 AWG. A crimp splice was developed to provide a reliable Nichrome-and-Permanickel/copper junction. The additional resistance in power leads required that the remaining

cable be increased in gage to prevent unacceptable voltage drop. An alternate proposal was made to disconnect transit loads after touchdown and before lunar night to avoid excessive wire weight of the resistance-wire insert design. The design consisted of a flat-cable tear strip which was to be torn out of the compartment after landing by an externally mounted linkage actuated by a pinpuller. The flat could pass through a narrow slit in the compartment thermal blanket so that heat loss would be negligible.

Prior to the fabricaton of flight harnesses, decisions were made to delete certain thermal control provisions, including most of the Nichrome wire inserts (except for the coaxial lines) and the lunar night tearaway cable. These changes were made to save weight, simplify the system, and alleviate voltage-drop problems, since the dual requirement of high electrical conductivity and low thermal conductivity proved to be incompatible.

Thermal control external to the compartments required that all harness bundles be wrapped with Teflon tape aluminized on one side only. It was suggested that this cover might serve also as an overall shield, both for electromagnetic interference (EMI) and for static-discharge protection. The proposed construction, which was applied to all flight spacecraft harnesses, was a double-wrap—an inner wrap of aluminized Mylar film with the metal surface out and an outer wrap of aluminized Teflon film with the metal surface in. Contact with the metal conductive surface was accomplished by a drain wire sandwiched between the wraps and grounded to the structure at appropriate points.

Low weight was a major factor in harness design, and small-gage wire (copper alloy for strength), thin-wall insulation, and miniature connectors were used to reduce weight. The selection of discrete junction-box or distribution-point areas contributed significantly to minimal weight. Multiple connections were made by permanent splices located in harness bundles, as required, to minimize wire length.

Routing paths and unit locations were selected to minimize cable length where alternatives were offered. Manufacturing break points were held to a minimum, consistent with installation and manufacturing requirements. Finally, every effort was made to avoid the use of shielding where it was not essential.

Apart from the *Centaur* interface, two mission in-flight disconnect requirements were: the altitude marking radar (AMR) must disconnect at retroignition and the retrorocket safe–arm device must disconnect at separation. The latter could be disconnected at any time after retroignition. The AMR dish was blown away at retroignition and supplied the pull force for lanyards used to separate both retrorocket and AMR leads. Separation was indicated when a small plastic plug, attached by a lanyard to the retrorocket case, pulled out of a phone jack mounted on the spaceframe, allowing a set of contacts to close.

Manufacturing schedules for harnesses required completion prior to spaceframe assembly; thus, all harnesses were bench-assembled rather than tailored on the spaceframe. The configuration for the T-21 vehicle was developed on the M-12 mockup and served as a guide for subsequent harnesses. Tridimensional jigs were built for the compartment harness assembly; other harnesses were formed on flat harness boards.

### 2. Description of Cabling and Harnesses

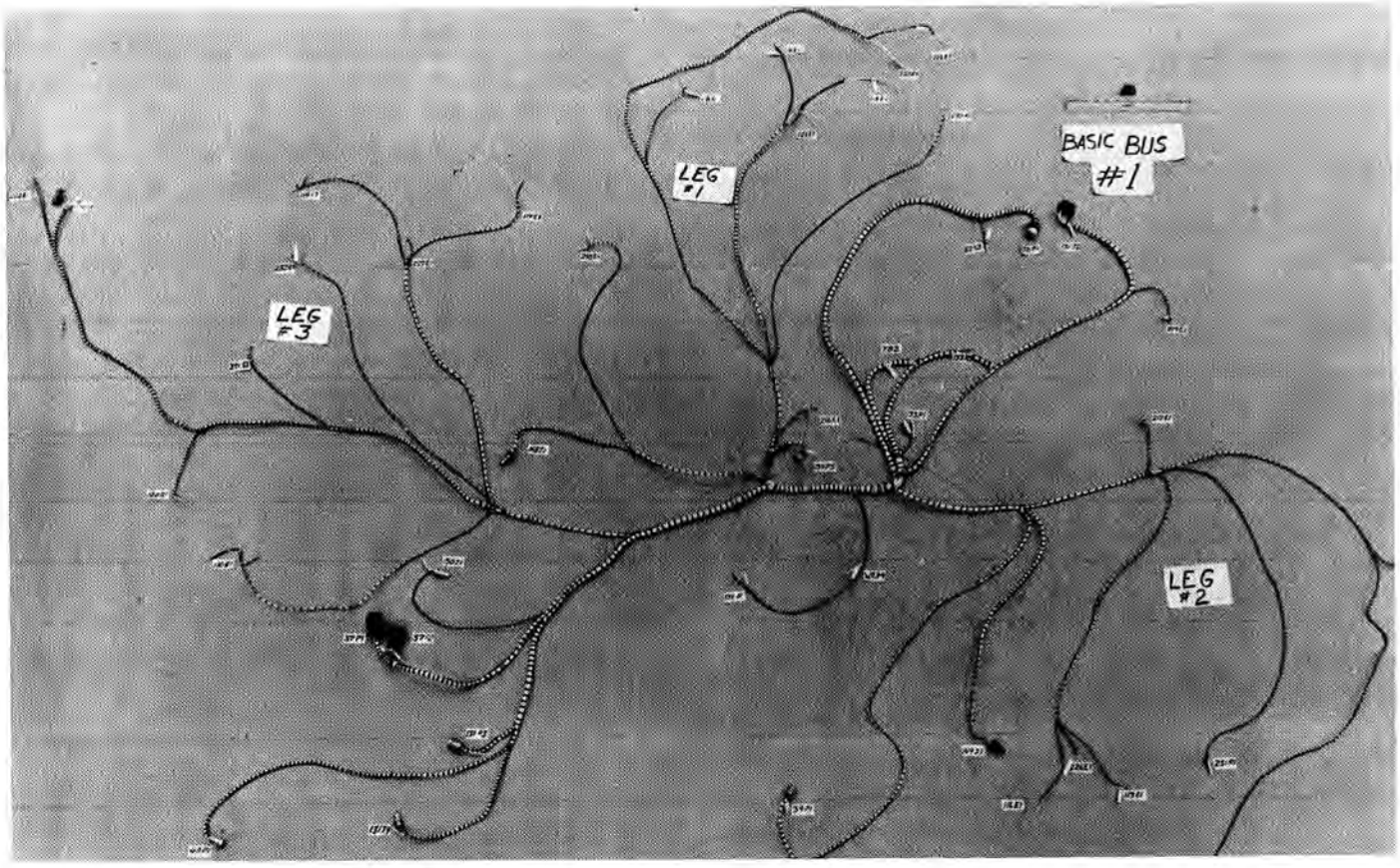
*a. Harnesses.* A description of the *Surveyor VII* harnesses is presented because this spacecraft carried both the alpha scattering instrument and the SM/SS. Intercabling on *Surveyor VII* consisted of 14 wire-harness assemblies and 17 RF cable assemblies, all designated as control items. These harnesses and RF cables were made up of the following elements: 206 electrical connectors with 3435 active pins, 8290 feet of electrical cable with 5930 wire ends or terminations, 596 cable-mounted distribution points (splices), four shunts, two amplifiers, two terminal boards, seven filters, two diode assemblies, and one temperature sensor. The total weight of all wire-harness assemblies and RF cables, excluding support provisions, was approximately 60 lb. The 14 harness assemblies and their major features are given in Table XIV-33.

In general, no special cable troughs or supports were provided in the spacecraft. The tubular spacecraft structure and the thermal tunnel running between compartments A and B acted as cable supports, as did a fiber-glass support on the retrorocket case.

Most of the harnesses were identified by the names of the items they connected to the electronics in one or both of the equipment compartments. The basic bus-1 harness (Fig. XIV-31), in general, carried high-level circuits such as vernier engine solenoids, attitude-control gas jets, helium valve actuation lines, propellant thermal control, etc. to the compartments. The basic bus-2 harness carried lower-level signals such as accelerometer

**Table XIV-33. *Surveyor VII* wire harness description**

| Harness | Number of connectors | Overall length, in. | Approximate weight, lb | Harness | Number of connectors | Overall length, in. | Approximate weight, lb |
|---|---|---|---|---|---|---|---|
| Alpha scattering instrument | 8 | 36 | 3.0 | Compartment B | 40 | 120 | 16.0 |
| SM/SS cable assembly | 2 | 27 | 0.2 | Basic bus 1 | 22 | 144 | 8.6 |
| SM/SS squib | 2 | 30 | 0.3 | Basic bus 2 | 35 | 54 | 6.5 |
| Battery cell voltage | 2 | 33 | 0.2 | A/SPP | 11 | 156 | 3.0 |
| Television auxiliary | 4 | 38 | 0.7 | Retrorocket | 3 | 60 | 0.5 |
| Retrorocket igniter | 2 | 18 | 0.2 | Separation squib | 7 | 96 | 1.5 |
| Television camera | 4 | 80 | 2.3 | | | | |
| Compartment A | 28 | 54 | 6.9 | Total | 170 | | 49.9 |



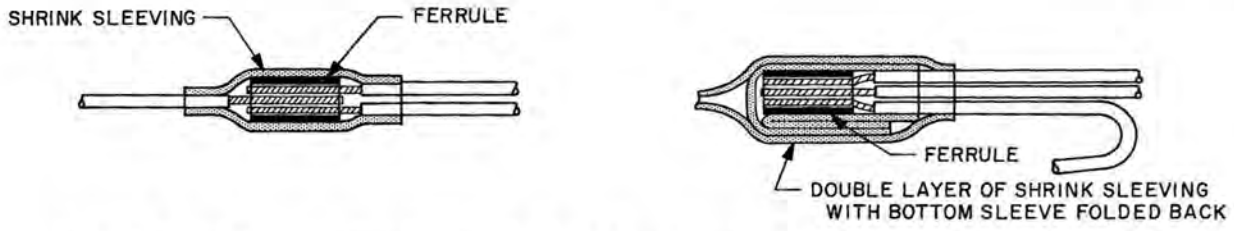




**Fig. XIV-31. Photo showing harness for bus 1 with insert showing cable-splicing technique**

amplifier, strain-gage amplifier, and various indicating circuits to the equipment compartments.

*b. Connectors.* Two basic types of connectors were used on the wire harness assemblies: miniature-rectangular and cylindrical. Selection was based on reliability, size, form, and qualification for space environmental conditions. The connectors used were:

| Manufacturer | Type |
|---|---|
| Cannon-Cinch | Rectangular (Golden D) |
| Atlas | Rectangular |
| Microdot | High-density, cylindrical |
| Bendix | High-temperature, cylindrical |
| Cannon | Cylindrical |

RF connectors used were:

| Manufacturer | Type |
|---|---|
| Microdot | 52-451 & 492 (subminiature) |
| General Radio Frequency | 83813-Al, 818-Al, 858-Al |
| General Radio Frequency | 3071-8004 |
| General Radio Frequency | 3046-8004 |
| General Radio Frequency | 3018-8003 |
| General Radio Frequency | 3049-8005 |

*c. Wire.* Of the candidate wiring materials, Surok was considered the best for meeting the requirements. Surok (tradename of the Suprenant Manufacturing Company) is a thin-wall FEP Teflon insulation with a modified polyimide lacquer coating, commonly referred to as ML. This wire became the basic *Surveyor* hookup wire, covered by HAC material specifications in gages 24–20 AWG and in multiple construction, including twisted quadruplets, both shielded and unshielded. For gages larger than 20 AWG, TFE Teflon wire per HAC-703 in 10-mil thick-wall construction was used.

### 3. Problems Encountered During Development and Test

*a. Connector pin retention.* A lower limit was placed on the force required to withdraw a test pin from a connector socket. It was intended that this test be applied at the receiving inspection level and that subsequent checks be made during spacecraft assembly and test. One of the difficulties of on-vehicle connector tests was that of manipulating the connector into position. Two methods were available: a deadweight tester which required that the connector be positioned so that the test pin would be vertical, and a test pin attached to a spring gage which also required connector manipulation to allow tool success.

A tool which had been used for Cannon DM connectors was modified late in 1965 for application to the Atlas connector for separation-force testing. This tool provided the withdrawal force by means of a calibrated spring. The tool was small and could be applied with the connector in any position. Its use on *Surveyor II* during an unscheduled troubleshooting sequence revealed numerous faulty connectors. The *Surveyor II* connectors were replaced, and an intensive investigation of socket contact performance followed. On-vehicle pin-separation-force testing was established for quality control (see Subsection XII-A-3-d-10). Recommendations on time and frequency of pin-separation-force tests were published in August 1966. When socket difficulties were discovered from the pin-retention tests, the defective sockets or the complete connector were replaced unless the launch schedule was jeopardized and the circuit was noncritical.

Some pin-retention failures were due to the connector design, and each of the two brands used presented problems. Atlas connectors have a split-sleeve design with two or four tines used interchangeably. The Microdot connector having a split-sleeve design was abandoned because, if the heat treatment allowed proper crimping, it did not give good spring action of the tines. The Microdot split-sleeve design also had a failure mode where the closed entry sleeve pressfit was sufficient to close the tines so that the mating pin could not enter. The other Microdot design utilized a pencil-clip spring which had no protection against being deflected into the socket where it would be bent over by entry of the mating pin.

Variations in socket material and heat treatment were the suspected causes of many sockets failing to have proper spring force. One connector was found to have three different materials with various heat treatments (bronze, beryllium–copper, and brass). Some sockets immediately lost spring force under use, while others were not damaged by repeated use.

The Cannon cylindrical connector design had an unplanted spring which forced the gold-plated pin against the opposite side of a gold-plated socket. In the event of a weak spring or misalignment, all contact was through the two surfaces of the spring. The stainless spring apparently developed a high-resistance surface coating which could not be cleaned off the side between

the socket and spring. This problem was somewhat alleviated by pin-retention testing which assured proper spring force.

Bent and oversized pins caused some socket difficulties. Pins on some Microdot connectors were bent when the flange was hit. The slipping of single sockets over single pins with a test wire attached and general rough handling resulted in other bent pins. Out-of-tolerance, oversized pins could have contributed to socket failure; but later indications were that, with properly designed and manufactured sockets, no failures resulted with slightly oversized pins.

***b. Connector cable entry.*** Cable entry into the connector was considered at the beginning of harness design work. Commercially available hoods and backshells for the miniature rectangular connectors were unacceptably bulky, and none of the resilient potting compounds could be qualified because of excessive outgassing. Epoxy potting agents were considered undesirable since work was difficult, and they tended to cut the wire insulation and prevent the pins from floating. In view of the weight penalty and difficulties stemming from the use of potting or backshell hardware, shrink-sleeving over solder pots was used as the basic cable entry treatment since testing had shown this method to be adequate.

During system testing of T-21, failures occurred at the solder pot of the miniature Atlas rectangular connectors. Usually the failure was induced when a wire which had been highly stressed in manufacture was flexed. Care was exercised to avoid wire stress during harness construction, but the effort was not always successful. Reworked harnesses, in particular, were subject to wire-stress problems. Several strain-relief designs were evaluated, and one was selected for test evaluation. The design proved effective, and the support was included on the Atlas connectors used on *Surveyors III–VII*. Beginning with *Surveyor V*, all other connectors were also supplied with strain-relief devices (Fig. XIV-32). The devices used on connectors other than Atlas rectangular types were extensions of the backshell with reduced-diameter openings to limit wire motion.

***c. Other connector problems.*** The jackscrews used in engaging and disengaging Atlas connectors presented problems. Screwing one side all the way out without the other caused trouble, but defective threads were discovered on many screws. The C-rings which held the jackscrew hardware in place were not always properly

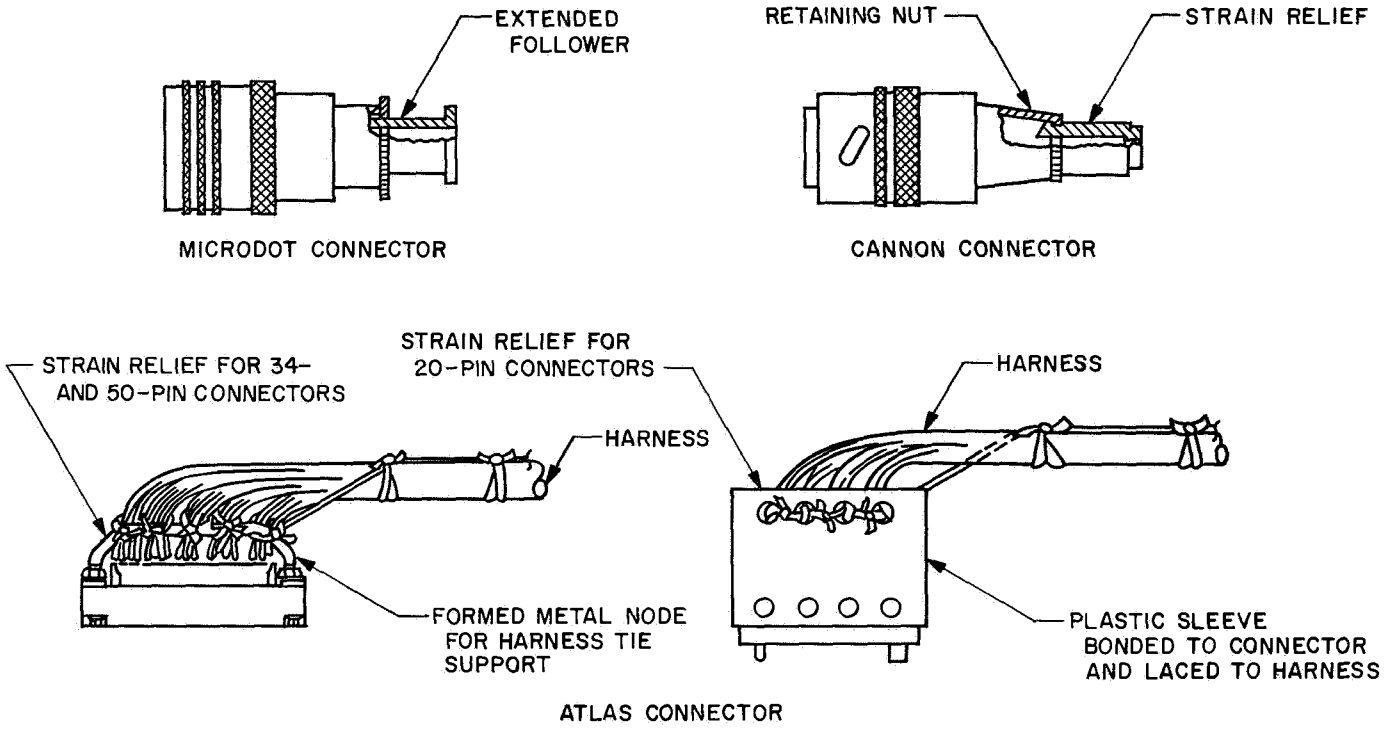



**Fig. XIV-32. Strain-relief methods for harnesses**

crimped when the jackscrews were replaced, resulting in lost hardware. Difficulties were experienced when O-rings on the Microdot connectors were changed to a nonoutgassing material, and dimensional changes on the mating connectors were not made on all hardware. On the Cannon connectors, it was difficult to get the washer spring and sealing O-rings to yield properly for mating the bayonet locks.

*d. Wire flaking.* Following successful test and qualification of the ML/FEP wire in early 1962, quantity orders were placed. The ML coating on some of the wire flaked during fabrication and handling. Wire was obtained from a second supplier for fabrication of the *Surveyor I* harnesses. Very little flaking was observed in the harnesses as delivered to system test; but, during the year of rework and upgrade, the wire flaked severely.

To avoid such flaking, new inspection criteria were established and all wire which failed to pass inspection, or which was delivered prior to manufacturing improvements, was removed from stores. On *Surveyor I*, that which could not be repaired by sleeving was replaced with reinspected wire. The new inspection criteria required a 100% visual inspection of the wire to detect flaking, bubbles, or cracking in the insulation and tight wrapping of the ends of every length of wire eight times around a mandrel which was one and one-half times the diameter of the wire. The wire then was inspected for flaking and cracks. Flaking was not observed on harnesses fabricated for *Surveyors IV–VII*. Splitting of the ML coating occurred, but there was no progression.

*e. Wire splices and terminals.* Two types of splices were considered: in-line and butt (insert of Fig. XIV-31). Since butt splices require that at least one wire be doubled back, the in-line splice was preferable for a minimum-weight design. During the extensive manipulation of the *Surveyor I* harness in rework and system test, a number of failed in-line splices were reported. The failure mode resulted from flexing the solder-wick wire area at the splice ferrule. Then, only butt-type splices were used since motion of the wire ends, with respect to the ferrule, was improbable. The splice change was introduced during the *Surveyor III* harness fabrication. *Surveyor III* had approximately 50% butt splices, and all later spacecraft had 100%.

Other breaks occurred when one or two wires were soldered to a switch or to another item of equipment and no strain relief had been provided. Loads applied to the terminal had to be carried by one or two wires, causing failure in the wick area of the solder joint. Failure-inducing loads were applied by dragging other cables or equipment over the wire, by moving the bundle from which the failed leads exited, or by manipulation of the equipment during spacecraft assembly and test operations.

Many high-voltage shorts occurred between the shield and lead at the termination on shielded wires during a special high-voltage test (1000 V rather than the normal 500-V test). The special test was conducted on all such cables when shorts occurred in several during the normal test. The shorts were attributed to heat-stripping, but this was not conclusive. A sleeve of insulating material was added to leads which failed the test.

#### 4. Mission Experience

No mission anomalies could be attributed definitely to harness failure. A change, resulting from the *Surveyor II* failure investigation, added a test access connector to the basic bus-2 harness. This allowed a low-current measurement of electrical continuity through all three vernier-engine solenoid-operated valve coils after the last mating of the electrical connectors. An intensive study was performed to isolate any electrical leads which could have resulted in the *Surveyor IV* loss of signal. These studies showed that failure of the 29-V low-ripple lead to the transmitters, or the coaxial cable interconnecting the RF transfer switch and RF single-pole, double-throw switch, could have resulted in the exact signature of the *Surveyor IV* failure. Proposed rework of the harness to add redundancy to the 29-V lines and RF cable was not shown to result in an increase in reliability and was not done.

### G. Spacecraft Alignment and Mass Properties Determination

The omniantennas, planar array, AMR, retrorocket, vernier engines, RADVS antennas, attitude-control gas jets, flight control sensor group, and secondary sun sensor required more stringent alignment with the spacecraft reference axes and planes than was possible in the manufacturing and assembly processes. The alignment was accomplished in an optical dock, as shown in Fig. XIV-33, and the alignment tolerances were achieved by shimming or by adjustable fasteners. The alignment was done in three steps for the early spacecraft and, later, in two steps. The first alignment of the three was performed at HAC, El Segundo, Calif., during the system test phase, preceding spacecraft vibration testing. Another was done

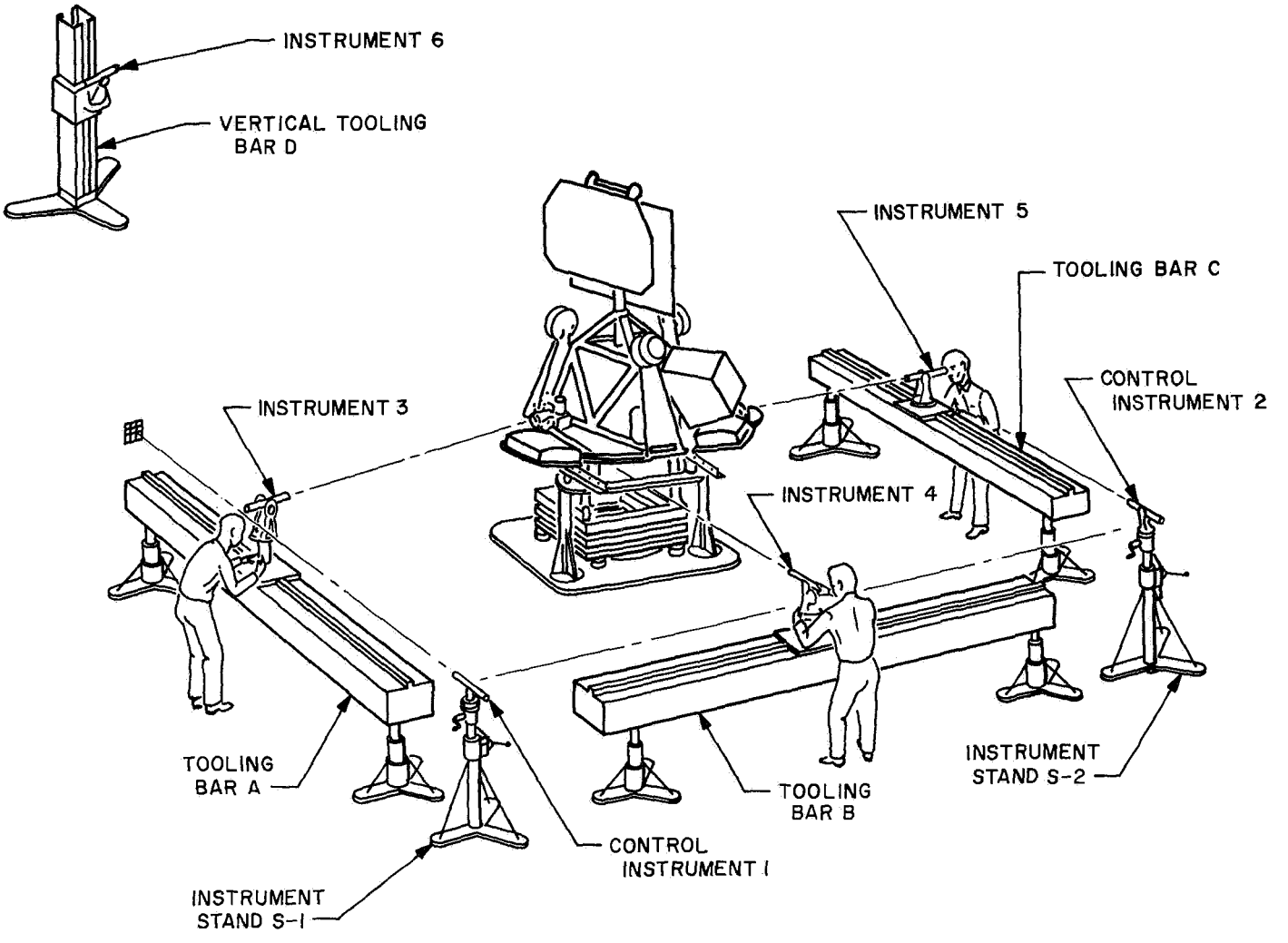



**Fig. XIV-33. *Surveyor* spacecraft optical alignment dock**

after vibration, as an engineering and quality check on the structural integrity of the spacecraft. The alignment to meet functional requirements was done at AFETR toward the end of the test cycle. As confidence in the spacecraft improved, previbration alignment was eliminated and factor alignment was restricted to only the RADVS antennas, omniantennas, secondary sun sensor, and vernier engines to assure that they were alignable. Table XIV-34 shows the alignment tolerances at the three stages.

Spacecraft weight and center of gravity were determined at the factory as a preliminary check of calculations to that point, with the final operation being done after propellant loading at AFETR. The comparison of calculations, factory measurements, and AFETR measurements served as a check on the accuracy of the operation. In flight, the mass properties of the spacecraft changed as a result of deployment of the landing gear and omniantennas, movement of the A/SPP, use of propellants and gas, and retrorocket ejection. An accurate determination of the center of gravity at retroignition was necessary for retrorocket alignment so that the thrust vector would pass close enough to the true spacecraft center of gravity to maintain stability during retromaneuver. Mass properties of the retrorocket and the spacecraft, separately and combined, were measured in the optical dock using optical instruments to level the spacecraft. A special fixture, employing Baldwin-Lima-Hamilton BLHC3P1 load cells, was used in conjunction with the dock for the weighing.

Retrorocket alignment was based on the assumption that the thrust vector was coincident with the nozzle centerline. The optical dock was used to determine the

relationship of this centerline with the retrorocket mounting holes and center of gravity. Ballast weights were added to the retrorocket struts for two reasons:

(1) To increase the spacecraft weight to the range necessary for maintaining the spacecraft terminal descent velocity profile within required limits.

(2) To adjust the center of gravity of the empty retrorocket to the nozzle centerline to minimize lateral movement of the spacecraft center of gravity during retro burning.

The retrorocket was placed in the spaceframe at the proper location by custom-drilling the attachment fittings for each spacecraft. Final adjustment of the center of gravity for retroignition was accomplished by ballast weights on the landing leg footpads and under the crushable body blocks.

No problems were encountered during any mission that were related to the mass properties or alignment of any components of the spacecraft. The source of telemetry data which would indicate errors in center-of-gravity determination was the vernier-engine strain gages; however, the uncertainty in these data was great in comparison with the assumed accuracy of the alignment and center-of-gravity determination. Thus, spacecraft stability was the criterion for assessment of the adequacy of the alignment.

**Table XIV-34. Component angular alignment tolerances relative to the spacecraft coordinate system[a]**

| Item | Final prelaunch requirement | Instrument error allowance | Remaining allowable indicated alignment tolerance | | |
|---|---|---|---|---|---|
| | | | Previbration | Postvibration change permissible from previbration measurement | Final prelaunch |
| Retrorocket | 0.050 | 0.005 | 0.054 | 0.15 | 0.045 |
| Vernier engines | 0.075 | 0.018 | 0.075 | 0.10 | 0.057 |
| RADVS antennas | 0.300 | 0.021 | 0.100 | 0.15 | 0.279 |
| Attitude-control jets—Leg 1 | 4.300 | 0.106 | 4.300 | 1.00 | 4.194 |
| Attitude-control jets—Legs 2 and 3 | 4.300 | 0.136 | — | — | 4.164 |
| Planar array | 1.000 | 0.022 | 1.000 | 1.50 | 0.978 |
| Secondary sun sensor | 1.000 | 0.038 | 1.000 | 1.50 | 0.962 |
| Flight control sensor group—roll axis | 0.100 | 0.009 | 0.100 | 0.20 | 0.091 |
| Flight control sensor group—pitch axis | 0.400 | 0.062 | 0.400 | 0.20 | 0.338 |
| Altitude marking radar | 0.200 | 0.003 | — | — | 0.197 |
| Omniantennas—angle of backface from vertical | 1.000 | 0.006 | — | — | 0.994 |
| Omniantennas—angle of backface from X–Z plane | 2.000 | 0.006 | — | — | 1.994 |
| Omniantennas—dipole orientation | 3.000 | 0.008 | — | — | 2.992 |
| Combined spacecraft and retrorocket CG-to-retrorocket centerline offset for retroignition | 0.180 in. | 0.175 in. (instrument and mission uncertainties) | — | — | 0.005 in. |

[a]Unless otherwise noted, all values are in degrees.

## References

XIV-1. Alderson, R. G., and Wells, D. A., *Final Report on Surveyor Lunar Touchdown Stability Study,* Report MM-66-19. Bendix Products Aerospace Division, South Bend, Ind., July 8, 1966.

XIV-2. Garba, J. A., *A Comparison of Some Predicated and Measured Variables for a Full-Scale Surveyor Drop Test,* Technical Report 32-1084. Jet Propulsion Laboratory, Pasadena, Calif., Mar. 1, 1967.

## Bibliography

Deitrick, R. E., and Jones, R. H., *Touchdown Dynamics Study, Surveyor Spacecraft System (Preliminary Report),* SSD 3030R. Space Systems Div., Hughes Aircraft Co., Culver City, Calif., Jan. 1963.

*Dynamic Analysis of Surveyor,* Report EC-6. MacNeal–Schwender Corp., Apr. 28, 1964.

Fisher, W. T., *Surveyor S-15 Lunar Landing Stability Drop Test Program,* SSD 68190R. Space Systems Div., Hughes Aircraft Co., Culver City, Calif.

Gammell, L. W., *Surveyor S-9 Torsion Type Approval Test Report,* SSD 74172. Space Systems Div., Hughes Aircraft Co., Culver City, Calif., Feb. 8, 1966.

Gammell, L. W., *Surveyor S-9 Structural Test Vehicle Vibration and Drop Test Program,* SSD 74170. Space Systems Div., Hughes Aircraft Co., Culver City, Calif., Aug. 1967.

Gayman, W. H., and Oliver, R. E., *An Experimental Test Program to Determine the Nature of Cause of the Vibrational Environment Encountered by SC-3 During Its Cross-Country Trip,* PD-602-12. Jet Propulsion Laboratory, Pasadena, Calif., July 10, 1967.

Gayman, W. H., Abbott, P. W., and Garba, J. A., *Modal Vibration Surveys of the Surveyor S-9 Spacecraft,* Technical Memorandum 33-388. Jet Propulsion Laboratory, Pasadena, Calif., Dec. 1968.

Gayman, W. H., Abott, P. W., and Trubert, M. R., *Measurement of Structural Transfer Functions of Significance to Flight Stability of the Surveyor Spacecraft,* Technical Memorandum 33-389. Jet Propulsion Laboratory, Pasadena, Calif.

Harter, R. J., and Switz, R. J., *Analytical and Experimental Techniques Used to Establish Structural Design Loads for the Surveyor Spacecraft During Lunar Landing,* Bulletin 35 (Shock and Vibration). Naval Research Laboratory, Washington, D.C., Jan. 1966.

Kornfeld, F., *Surveyor S-9 Static Load Test,* SSD 74171. Space Systems Div., Hughes Aircraft Co., Culver City, Calif., Jan. 1966.

## Bibliography (contd)

*Metallic Materials and Elements for Aerospace Vehicle Structure,* Specification MIL-HBK-5A. Department of Defense, Washington, D.C.

Schlue, J., and Wada, B., *Assessment of the Fatigue Damage to SC-3 Spacecraft During Its Transportation from Florida to California,* PD-602-32. Jet Propulsion Laboratory, Pasadena, Calif., Oct. 15, 1967.

*Stability Drop Tests, S-15/A21-E,* SSD 68250R. Space Systems Div., Hughes Aircraft Co., Culver City, Calif., Nov. 25, 1966.

Stafford, B. T., *Revised Surveyor Structural Landing Design Loads for Spaceframe Analysis,* SSD 74173. Space Systems Div., Hughes Aircraft Co., Culver City, Calif., Mar. 27, 1967.

*Stress Analysis Report, Antenna/Solar Panel Positioner (Model 293275), Surveyor Spacecraft,* Document SSD 64262R. Space Systems Div., Hughes Aircraft Co., Culver City, Calif., Oct. 1966.

*Stress Analysis Report, Anatenna/Solar Panel Positioner (Model 3035092), Surveyor Spacecraft SC-3,* SSD 64308R-1. Space Systems Div., Hughes Aircraft Co., Culver City, Calif., Aug. 1967 (and addendum dated Oct. 1967).

*Stress Analysis Report, Soil Mechanics/Surface Sampler, Surveyor Spacecraft SC-3,* SSD 64308R. Space Systems Div., Hughes Aircraft Co., Culver City, Calif., Dec. 1966.

*Stress Analysis Report, Soil Mechanics/Surface Sampler, Surveyor Spacecraft SC-3, -4 and -7,* SSD 64308R-1. Space Systems Div., Hughes Aircraft Co., Culver City, Calif., Dec. 1967.

*Stress Analysis Report, Alpha Scattering Instrument Deployment Mechanism, Surveyor Spacecraft SC-5,* SSD 64375R. Space Systems Div., Hughes Aircraft Co., Culver City, Calif., Dec. 1966.

*Stress Analysis Report, Compartment C and Substructure, Surveyor Spacecraft SC-5,* SSD 64381R. Space Systems Div., Hughes Aircraft Co., Culver City, Calif., Dec. 1966.

*Stress Analysis Report, Alpha Scattering Instrument Substructure Installation (Model 3025800), Surveyor Spacecraft SC-5,* SSD 74016R. Space Systems Div., Hughes Aircraft Co., Culver City, Calif., Feb. 1967.

*Stress Analysis Report, Basic Spaceframe and Substructure, Surveyor SC-5,* SSD 74151. Space Systems Div., Hughes Aircraft Co., Culver City, Calif., Dec. 1967.

*Stress Analysis Report, TV Auxiliary Mirrors for Surveyor Spacecraft SC-3 and -4,* SSD 74157. Space Systems Div., Hughes Aircraft Co., Culver City, Calif., Dec. 1967.

# XV. Thermal Control

## A. Thermal Design

The design and development of the *Surveyor* thermal control was started in March 1961, when experience in the space environment was limited and the thermal characteristics of the lunar surface were uncertain. *Surveyor* requirements were unique, not only from the standpoint of the lunar surface operations, but in the combination of random sun orientation and simultaneous firing of the solid propellant retrorocket and liquid propellant vernier engines during the retro sequence.

Described in this section are the design approach, passive and active thermal control techniques used, unit testing programs, and resulting configurations.

### 1. Design Requirements

*Surveyor* thermal design was considered from the standpoints of transit and lunar surface environments. *Surveyor* had unique mission characteristics. While other space programs had the problems of earth shadow and random sun orientation before acquisition and during midcourse, the *Surveyor* encountered:

(1) The retro sequence with the radiative and convective heating effects of firing the vernier engines for several minutes with exhaust cones reaching temperatures above 2000°F.

(2) The radiative heating environment when the 1200 lb of metal-doped propellant in the main retro rocket were burned in 43 sec.

(3) The possibility of up to 30 min of solar eclipse in the vicinity of the moon.

(4) The requirement to raise to the respective lower operational limits the temperatures of those items which had to function immediately after landing. Figure XV-1 shows the various mission operations that affected *Surveyor* during transit.

The lunar surface varies in temperature from +260°F, during the day, to −250°F during the night. The surface temperature profile has a parabolic shape, rising rapidly at

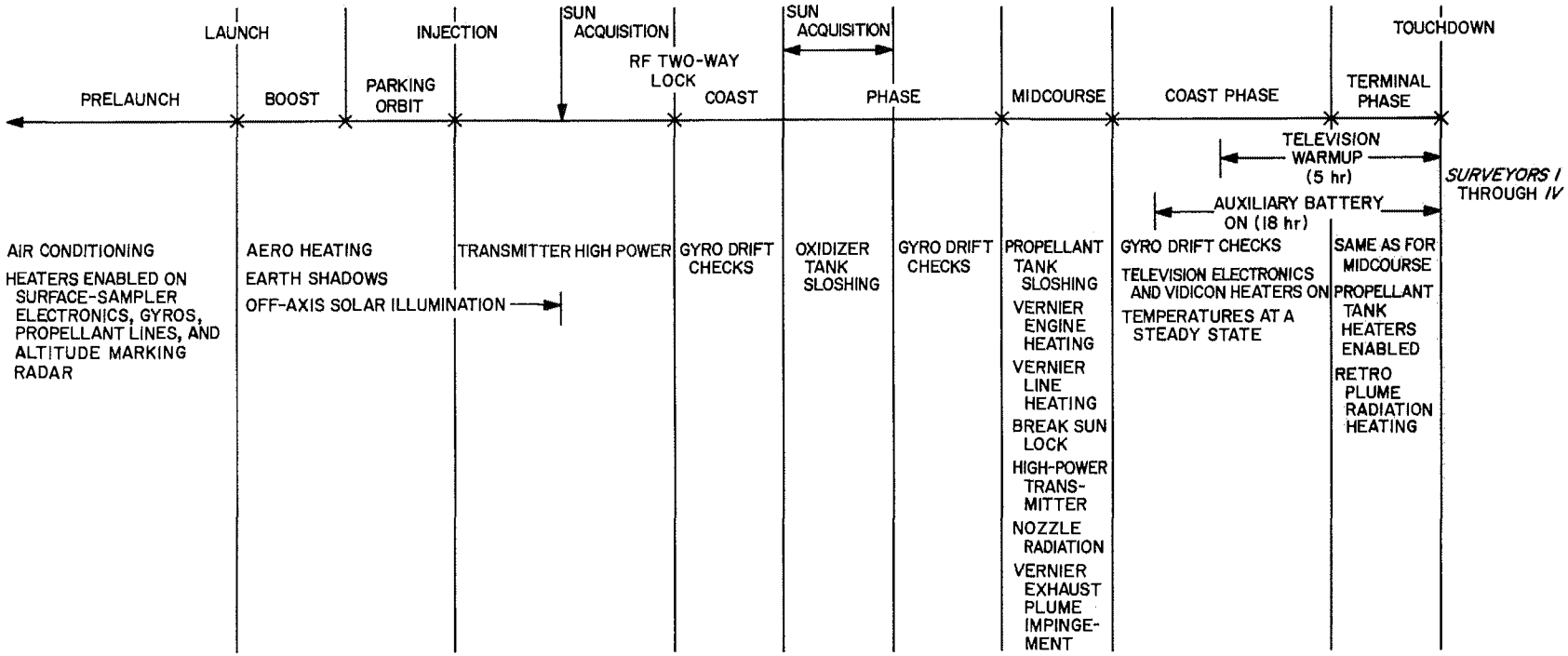



**Fig. XV-1. *Surveyor* mission sequence and thermal environment summary**

sunrise and falling rapidly at sunset to the minimum. The night temperature remains low until sunrise. Spacecraft components in general cannot operate at these temperature extremes, and some cannot survive. These environmental conditions resulted in a temperature control design keyed to the use and temperature limits of the various subsystems. The subsystems that operated only during the transit portion of the missions were not designed for postlanding survival, and those that functioned only on the lunar surface had to survive during transit.

It was also required that the thermal control design permit changing of the spacecraft payload. Table XV-1 shows the payload configurations of thermal significance.

While the design requirements called for the flight control system and the vernier propulsion system to survive only the transit portion of the mission, the desire developed during the later missions to fire the vernier engines of *Surveyor V* on the lunar surface and to carry out the hop experiment of *Surveyor VI*. These operations required the use of both the flight control and vernier propulsion systems and could be achieved only by judicious positioning of the antenna and solar panel positioner (A/SPP) to shadow critical items, as described in Subsection C-3.

### 2. Thermal Control Philosophy and Techniques

What is termed the "open system" of temperature control was used. Items with close temperature tolerances were grouped together in thermally controlled compartments, and items with wide tolerances were thermally decoupled from the compartments. Passive, active, and semiactive control techniques were applied, and subsystem steady-state temperatures were biased toward one end of the range to accommodate transient conditions. The approach used on the various subsystems is shown in Fig. XV-2; frequently, more than one control technique was used on a given subsystem.

The requirement for payload flexibility further complicated the thermal design. Payload variations and the complexity of *Surveyor* prevented use of a single thermal control computer program for the spacecraft. Programs were written for each subsystem and for some individual units, and each was studied both individually and for interaction with other portions of the spacecraft. The programs were updated as the design developed. A more detailed description of certain portions of the analysis is discussed in Ref. XV-1.

"Passive control" is defined as the use of the thermal radiative properties of external surfaces for temperature control. "Semiactive control" is defined as the use of a thermal–mechanical device to control a heat path. "Active control" is defined as the use of electrical heaters. The uses of active and semiactive control are shown in Table XV-2.

*a. Passive controls (finishes, insulation, reflectors, and shades).* Many types of thermal finishes were used on *Surveyor* including paints, polished aluminum and steel, vapor-deposited aluminum, platings, and aluminized plastic films, as shown in Table XV-3. The most critical requirement was for a white coating with a low solar absorptance and a high emittance within the design temperature range. Also, it had to have stable solar absorptance under solar exposure. In 1961, there was no white coating with the desired thermal radiative properties of solar absorptance less than 0.20, emittance greater than 0.90, and solar absorptance stability so that a change of less than +0.05 occurred with 1000 equivalent solar hours of ultraviolet exposure. A program to find such a coating resulted in the development of H-1, an inorganic white paint. The pigment chosen for the coating was a California

**Table XV-1. Surveyor payload configurations**

| Item | Surveyor I | Surveyor II | Surveyor III | Surveyor IV | Surveyor V | Surveyor VI | Surveyor VII |
|---|---|---|---|---|---|---|---|
| Auxiliary battery | X | X | X | X | | | |
| Approach television | X | X | | | | | |
| Survey television | X | X | X | X | X | X | X |
| Alpha scattering instrument and compartment C | | | | | X | X | X |
| Soil mechanics surface sampler | | | X | X | | | X |

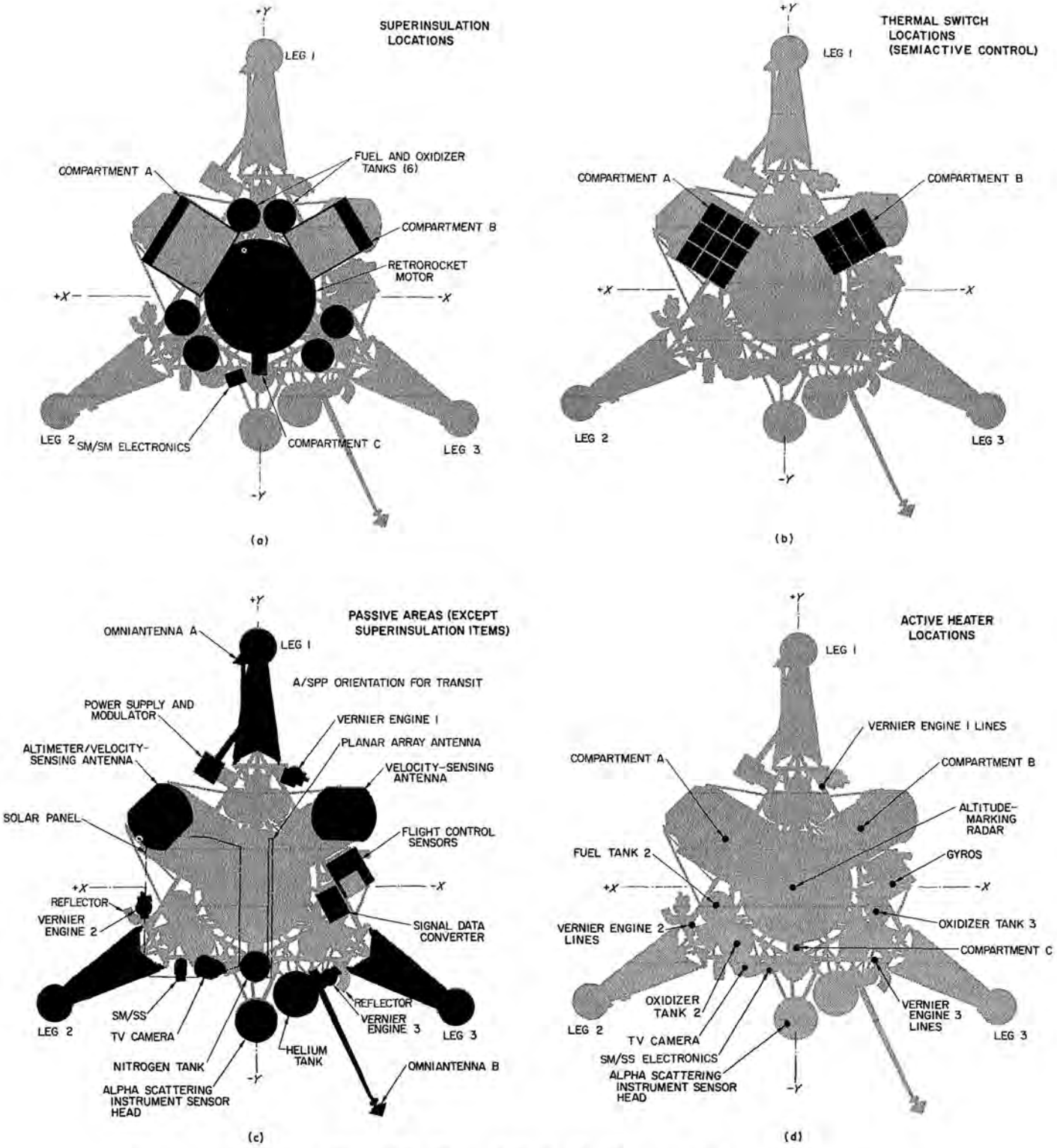



**Fig. XV-2. Thermal design for *Surveyor VII***

**Table XV-2. Use of active and semiactive thermal control**

| Unit | Type of control | Used during |
|---|---|---|
| Compartments A and B | Semiactive | Transit and lunar day |
| Compartments A and B | Semiactive and active | Lunar night |
| Flight control gyroscopes | Active | Transit |
| Altitude marking radar electronics | Active | Transit (unit jettisoned during terminal phase) |
| Vernier engine propellant lines | Active | Transit |
| Vernier engine 2 oxidizer and fuel tanks | Active | Transit (if required) |
| Vernier engine 3 oxidizer tank | Active | Transit (if required) |
| Approach television camera | Active | Transit (before terminal descent |
| Survey television camera | Active | Transit (before terminal descent and into lunar night) |
| Soil mechanics surface sampler | Active | Transit and lunar day |
| Alpha scattering instrument sensor head and compartment C | Active | Transit and lunar day |

china clay. Calcining this clay at 1275°C produced a brilliant, white pigment. The binder used was potassium silicate. Its laboratory properties were:

(1) Solar absorptance: 0.17.

(2) Emittance (normal, 70°F): 0.93.

(3) Change in solar absorptance in 500 equivalent solar hours of ultraviolet exposure: +0.05.

The stability of H-1 was satisfactory but not as good as was originally desired. The laboratory measurements of absorptance degradation of 0.05 in 500 hr of exposure to ultraviolet light have been confirmed by the progressive temperature increases from the first through the sixth lunar day of *Surveyor I* (Ref. XV-2). The *Surveyor I* surface evaluated was the front of the compartment A shell. A comparison of the laboratory and *Surveyor I* measurements of ultraviolet degradation is given in Fig. XV-3.

Use of the three white coatings shown in Table XV-3 was based on balance of physical and thermal radiative characteristics and ultraviolet stability. The inorganic white, H-1, was used only where the problems associated

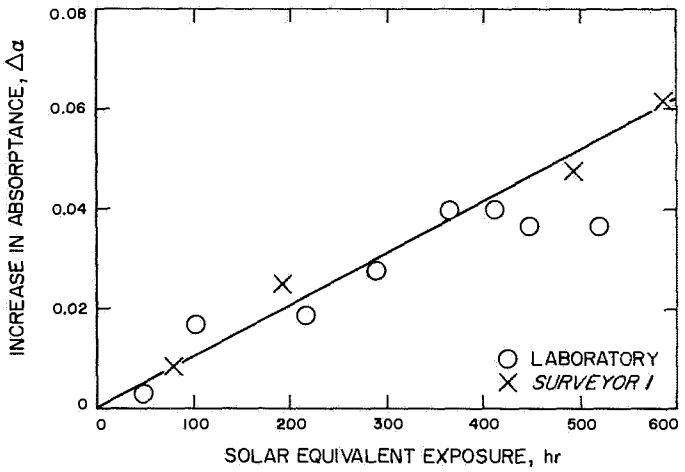



**Fig. XV-3. Ultraviolet degradation of HAC inorganic white paint (from laboratory and *Surveyor I* data)**

with its use were justified by initial property and ultraviolet stability requirements. The two organic whites were used in less critical applications. A discussion of the problems of applying and maintaining the inorganic white paint is included below.

A chrome-oxide-pigmented inorganic coating was applied to the vernier engine extension cones to provide oxidation protection before flight. Considerable difficulty was encountered late in the project in maintaining adhesion and coating integrity. Replacement would have been desirable but would have required disassembly and retest with resultant cost and schedule penalties. Extensive testing and repair techniques developed by JPL resulted in satisfactory mission performance.

Aluminized Teflon was bonded on some *Surveyor* subsystems to provide surfaces with a low solar absorptance-to-infrared emittance ratio ($\alpha/\epsilon$) surface and thermal radiative properties similar to white paint. This was done on simple shapes and where application of paint was not practical or where a high degree of ultraviolet stability was required. Aluminized Teflon was used on the shock absorbers, roll actuator, and early signal data converters. The bonding operation required both skill and patience to prevent bubble formation or stretching of the Teflon.

The initial optical properties of a coating, especially a low $\alpha/\epsilon$ coating, was only one of many of the aspects to be considered in its selection. Mechanical properties and the stability of physical and thermal radiative properties, from the time of application through the months of handling and testing, were also important factors.

**Table XV-3. Thermal radiative properties of *Surveyor* thermal finishes**

| Thermal finish | Process specification | Initial solar absorptance (nominal $\alpha$) | Increase in solar absorptance due to UV radiation for SEH,[a] $\Delta\alpha$ | Hemispherical emittance, $\epsilon_H$ |
|---|---|---|---|---|
| Inorganic white paint | HP 4-135[b] | 0.18 | 0.05 after 500 SEH | 0.87 |
| Organic white paint (3M) | HP 4-143 | 0.21 | 0.09 after 350 SEH | 0.86 |
| Organic white paint | HP 4-112 (PT-401) | 0.30 | — | 0.84 |
| Black paint (3M) | HP 4-143 | 0.97 | — | 0.85 |
| Aluminized kemacryl acrylic paint | HP 4-147 | 0.27 | 0.03 after 100 SEH | 0.31 |
| Aluminized Vycor mirrors | HP 4-138 | 0.11 | 0 | 0.79 |
| Aluminized Teflon (2 mil) Fep type A | HMS 16-1329 HP 16-121 | 0.14 | 0 after 100 SEH | 0.66 |
| Vapor deposited aluminum | HP 4-142 | 0.10 | 0 | 0.04 |
| Polished aluminum | HP 9-29 | 0.21 | 0 | 0.04 |
| Clear Teflon (2 mil) | Mil-P-22241 Etched per HP-30 | 0.80 | 0.04 after 100 SEH | 0.88 |
| Gold plate | Mil-G-45204 type II, CL 2 | 0.28 | 0 | 0.04 |
| Chrome oxide pigmented inorganic | RMD-7059 | 0.65 | — | 0.81 |

[a]SEH = solar equivalent hours.
[b]HP = Hughes Process Specification.

The sensitivity of the inorganic white coating to surface preparation, application, and protection was apparent in 1962, early in the *Surveyor* Project. The coating was applied for the first time in production quantities to a thermal test vehicle. The paint, sprayed too thickly to an inadequately cleaned structure, cracked and peeled during test. This led to thorough training of paint technicians, more thorough cleaning procedures, and rigid quality control of the entire paint preparation and application process. With these measures, adherence was excellent.

As is typical of all white inorganic coatings, the one used on *Surveyor* was easily contaminated. The paint was hard and porous, and dirt, oils, tool marks, fingerprints, and lint became entrapped. No simple washing or cleaning solvent could be used, as they would wash the contamination into the pores. Mechanical abrasion provided a practical, effective cleaning method and restored surfaces approximately to original thermal radiative property values and ultraviolet stability.

Maintenance of thermal finishes on *Surveyor* was performed by careful wrapping, inspection, and cleanups at certain points in the vehicle schedule. By inspecting the finishes before and after solar-thermal-vacuum (STV) flight-acceptance tests and prior to launch, comparative continuity was provided between the test data and surface condition. This record was used to evaluate changes to a surface after qualification testing and need for thermal finish rework.

Prelaunch rework was minimized by putting the thermal finishes in the best possible condition before shipment of the vehicle to Air Force Eastern Test Range (AFETR). The capability was maintained at AFETR *Surveyor* Spacecraft Checkout Facility to spray-paint entire units and bake out the coatings. During STV testing, the white paints yellowed despite the fact that the Xenon lamps used in the solar simulator were deficient in ultraviolet compared to the solar spectrum. Most of the yellowing occurred in the surface layers of the paint and was "skin" deep. It was possible to restore the surface to within 0.01 or 0.02 of the original solar absorptance by removing approximately 1.0 mil of the paint. To allow for necessary sanding and abrasion of the paint during cleaning, the original coating thickness was biased to the high side of the specification range.

The vernier engine thrust chamber thermal control design employed gold electroplate for a stable coating which would withstand thermal soak-back after engine firing. It was assumed that the gold plate would be resistant and compatible with the propellants, MON-10 and MMH monohydrate, since spillage, leaks, and vapor contacts with the gold-plated thrust chambers would be inevitable. This was not the case because of the inability to electroplate a pore-free gold coating on the stainless steel thrust chamber. The propellants entered the pores and attacked the silver and copper underplates, causing blisters and loose gold flakes. Of the propellants, the MON-10 was the worse offender. The loose plating was removed in each case, and the exposed stainless steel was polished to get as low an emittance as possible, with a limit of 1 in.$^2$ exposed substrate per engine. Engines with exposed stainless steel thrust chamber surfaces in excess of the limit were not flown. Just before the program was finished, a gold plate repair technique was developed which was compatible with the propellants and the high thrust chamber soak-back temperature from engine firing. The repair consisted of RTV 40 silicone adhesive bonded pure gold foil.

Other forms of equilibrium passive thermal control also were employed. A sun shade was used to cover vernier lines where they were exposed to direct solar radiation. The flight control sensor group (FCSG) utilized a passive radiator of the same type described later for the compartments; however, this was without the thermal–mechanical switch. Solar reflectors were used on two of the vernier engines (Fig. XV-4).

An early design called for an extensible antenna/solar panel positioner (A/SPP) mast to ensure clearance for the solar panel and planar array over science instruments placed high on the spaceframe. A secondary consideration was to reduce the radiation coupling between the backs of the panels and the tops of the compartments. Abandonment of this concept, while increasing the coupling, improved the shadowing capability by use of the panel and array, and contributed to successful lunar operations, including the hop experiment of *Surveyor VI*.

In most cases, passively controlled components reached equilibrium conditions rapidly; thus, their thermal radiative properties had to be designed so that the unit remained within operating limits only during the transients imposed by maneuvers. The retro motor, however, could not be held at the correct equilibrium temperature throughout transit, so it was covered by an insulating blanket and preconditioned before flight (see Section X-C-1). The preconditioning temperature was adjusted so that the solid propellant bulk temperature would fall to the correct temperature at the start of the terminal descent (see Subsection A-3).

A change in the vernier propellant tanks from aluminum to titanium necessitated an accompanying change from paint to superinsulation blankets to eliminate undesirable temperature gradients. Fuel tanks 1 and 3 and oxidizer tank 1, exposed to direct sunlight, were insulated with 25 layers of superinsulation. Fuel and oxidizer tanks near leg 2, shadowed by the solar panel, were insulated with 75 layers while oxidizer tank 3, partially shaded by the signal data converter (SDC), was insulated with 50 layers. The tanks performed satisfactorily during tests and flights (see Subsection C-1); the insulation retarded their cooling rates sufficiently that the propellant temperatures remained within the allowable 0 to 100°F range.

***b. Semiactive control (main electronic compartments utilizing thermal switches).*** The original thermal design specification called for daytime lunar operation on three successive lunar days. Semiactive and active techniques were required, in addition to the grouping of equipment in insulated compartments, if the battery, communications equipment, and signal processing units were to survive the nights. Thermal switches, low-conductance cable inserts, and a cutter to sever nonessential cables between the compartments were developed. The mission



**Fig. XV-4. Vernier engine 2 solar reflector**

requirement for night survival later was changed to 150 hr into the first night, and the cable insert and cutter development was abandoned. Thermal switch development continued, but reliability requirements were reduced since the lower requirement could be met with failure of one or two switches per compartment.

Two main compartments, A and B, and several additional small compartments, depending on the payload, were used for the electronic equipment. Compartment A construction is shown in Figs. XV-5 and XV-6. A "T" section was used as the principal structure of the main compartments. The top of the "T" (and of the compartment) was an aluminum plate which was also the mounting surface for the thermal switches. The leg of the "T" in compartment A and the leg of the "T" in compartment B were vertical honeycomb trays. Both compartment structures had insulated, tubular, triangular supports at their inside top corners and heavy, insulated, cylindrical supports at the bases of the vertical honeycomb structures. The supports first were made of magnesium. They broke during the initial type-approval

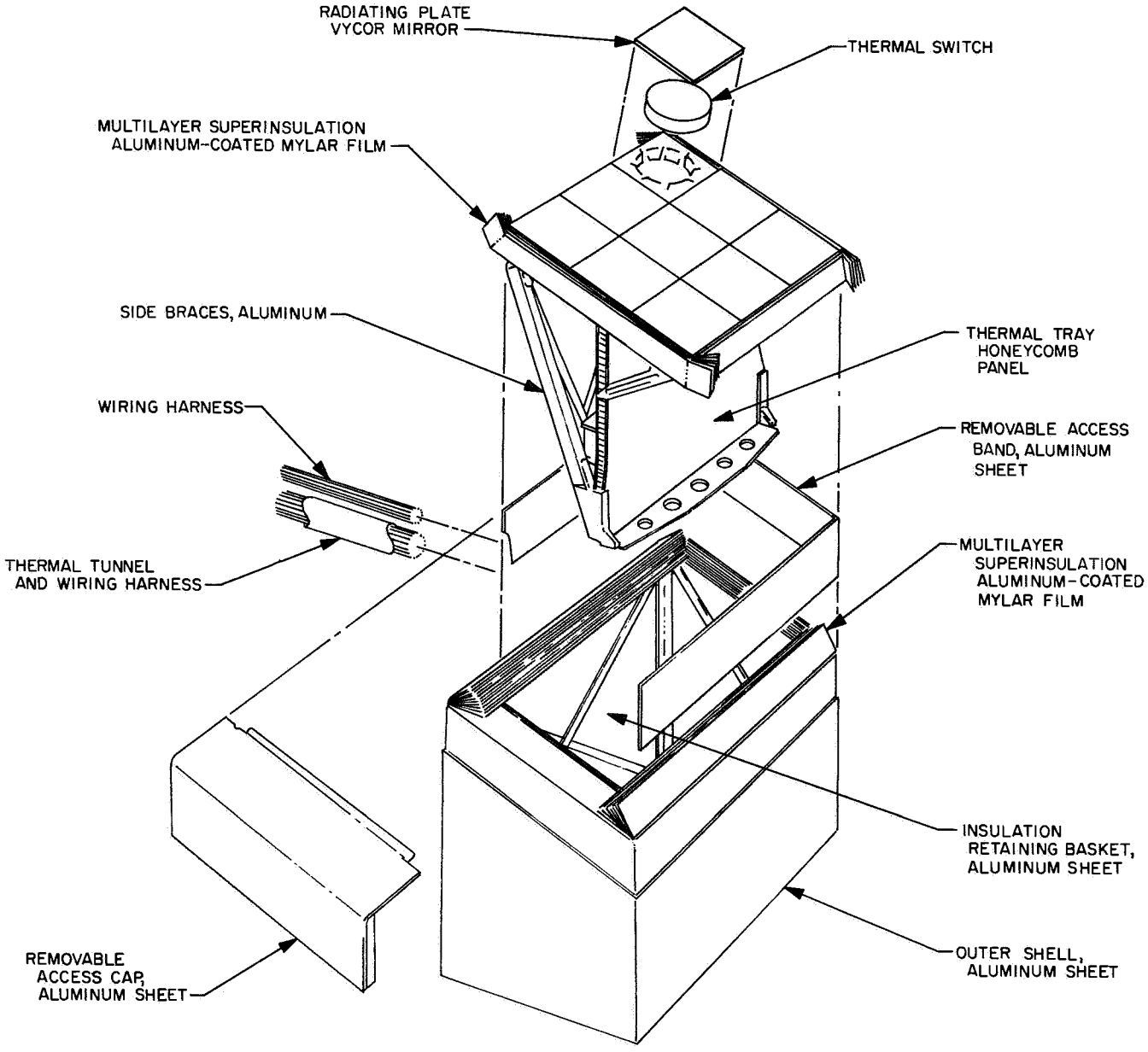



**Fig. XV-5. *Surveyor compartment A, showing T-top***

tests, and the material then was changed to aluminum. The insulated sections of the support structures provided thermal isolation from the spaceframe. The top and bottom supports were the primary structural members used to hold the compartments on the spaceframe. There were also several diagonal braces between the top plates and the vertical trays. The transmitters were fastened to the lower side of the top plate of compartment A for maximum heat conduction. The remaining electronic equipment was mounted on the honeycomb vertical trays by the use of many inserts installed from the side opposite the associated equipment. This was done so that only a small mounting bolt clearance hole was required in the tray honeycomb skin on the electronic mounting side, providing maximum area for heat transfer between the tray and the electronic equipment. Many fabrication problems resulted from this compartment design. The self-locking inserts were a swaged installation which made maintenance of flatness tolerances difficult. The flatness of this honeycomb structure was required to obtain intimate equipment-to-tray contact for optimum heat conduction.

The electronic units fastened to the thermal trays were removed and replaced often during the spacecraft buildup, resulting in many worn-out inserts. Since replacement of these inserts was difficult, several types of repairs were tried as a temporary remedy. The vertical tray assemblies were redesigned, beginning with *Surveyor V*, to eliminate galling problems resulting from the use of stainless steel bolts in stainless steel self-locking inserts. A nonlocking type was bonded into the trays. The

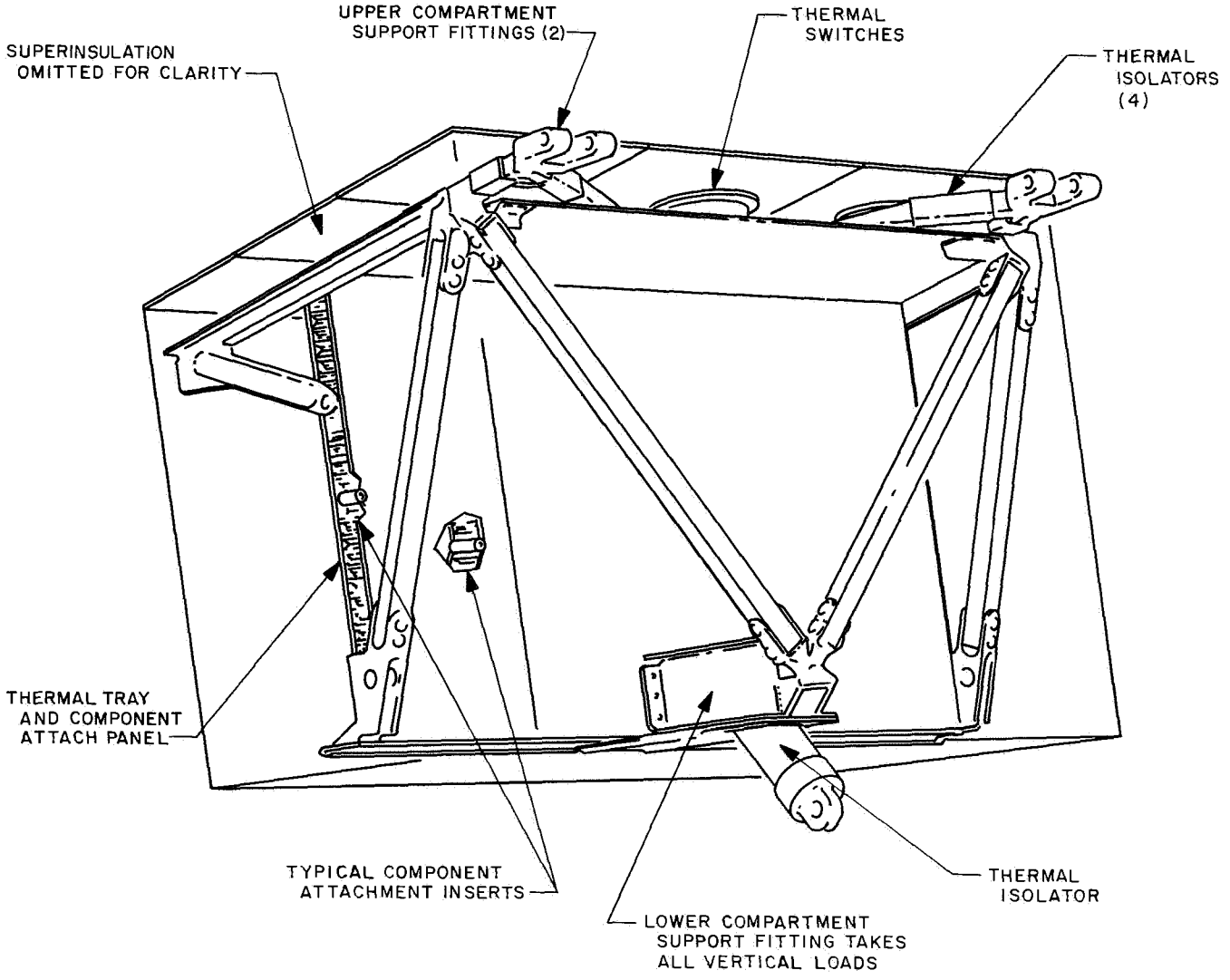



**Fig. XV-6. *Surveyor* compartment A, showing T-leg**

locking device was located on the bolt, which could be replaced if it showed evidence of galling or wear.

The sides and bottom of each compartment were insulated with a thermal blanket which, in turn, was covered with a thin, aluminum thermal shell to protect the thermal blanket and to provide a more uniform external thermal surface. The thermal shell and blanket were shaped like a box without a lid and were fastened together as a unit. A separate top thermal blanket for the top of the compartment tray had holes to accommodate thermal switches. The top and side corners of the blanket were interwoven, overlapped, and taped in place. Then a narrow thermal shell section was placed over this exposed blanket area. The lengthy installation and removal procedure for this blanket–shell design required that the whole compartment be rotated upward 45 deg with a special fixture. The entire process was repeated each time access was required to the electronic equipment and necessitated rerouting the cable service loop between the compartments.

The installation and removal problems encountered with the original shell and blanket were reduced by a new design used from *Surveyor V* on. This design permitted easier and faster access to the electronic equipment. The new blanket was designed to be installed as a separate item; however, it allowed loose aluminized Mylar fragments to enter the electronic area. Therefore, all of the electronic equipment was installed on the tray, and the entire unit except for the top plate was covered with a nylon net to keep the Mylar and foreign material out of the compartment. The thermal blanket, made of 75 layers of aluminized plastic sheets, then was installed over this assembly. The blanket was made in two pieces; one piece covered the back and bottom of the compartment and the other covered the top, sides, and front. The top piece of the blanket had cutouts for the thermal switches. The blankets were held in place with plastic, zipper-type fasteners, as were the overlap portions at the corners.

The new shell was made in two pieces, as was the blanket, to facilitate assembly. The front and side cover was easily removable for access to the electronics without rotating the compartment. The shell was supported by fiber-glass standoffs fastened to the top structural plate of the compartments and by two brackets which attached the back of the shell to the spacecraft frame. The thermal shell tolerances were also tightened, and the new thermal shell was made of fewer piece parts.

Beginning with the *Surveyor VI* spacecraft, an STV test cable access hole was added to the new compartment A blanket. On earlier spacecraft, a separate test blanket was used for STV; after testing, the test blanket was removed and the flight blanket installed.

Exchanging blankets required removal of the thermal switches after STV, violating system testing philosophy, since there were no further functional tests before flight. Concern about this resulted in redesign of the flight blanket with the test access hole. This test access hole was formed into the blanket by dividing it into three layers, each of which was cut so that, when folded flat, there was sufficient overlap to preclude any appreciable heat loss. Each layer was taped in place after the STV test harness was removed to keep the blanket functional.

Thermal switches were used on the top of each of the main electronic compartments (A and B) to control heat losses from the electronic equipment. Compartment A had nine switches and compartment B six, each of which was a self-contained unit capable of conducting heat at a rate of at least 0.5 Btu/hr °F, with the thermal contact closed (Fig. XV-7), and almost zero loss when open.

The thermal switch is shown in Figs. XV-8 and XV-9. Its basic components were

(1) Outer radiating face, exposed to space and containing an integral contact interface.

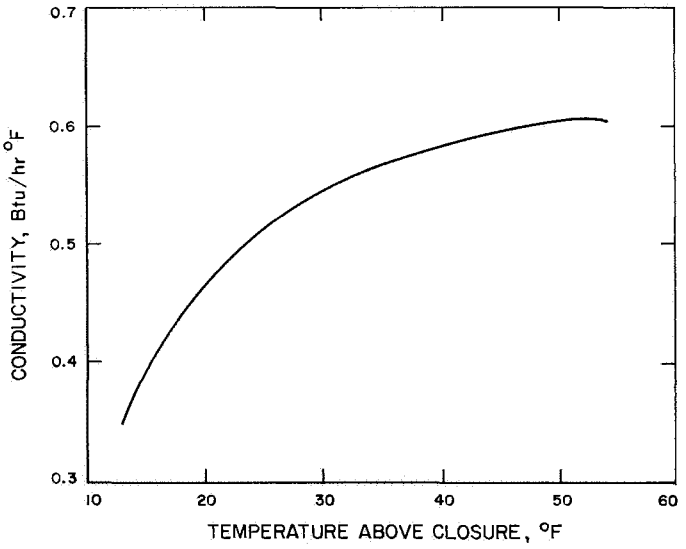



**Fig. XV-7. Typical conductivity curve for *Surveyor* thermal switches**

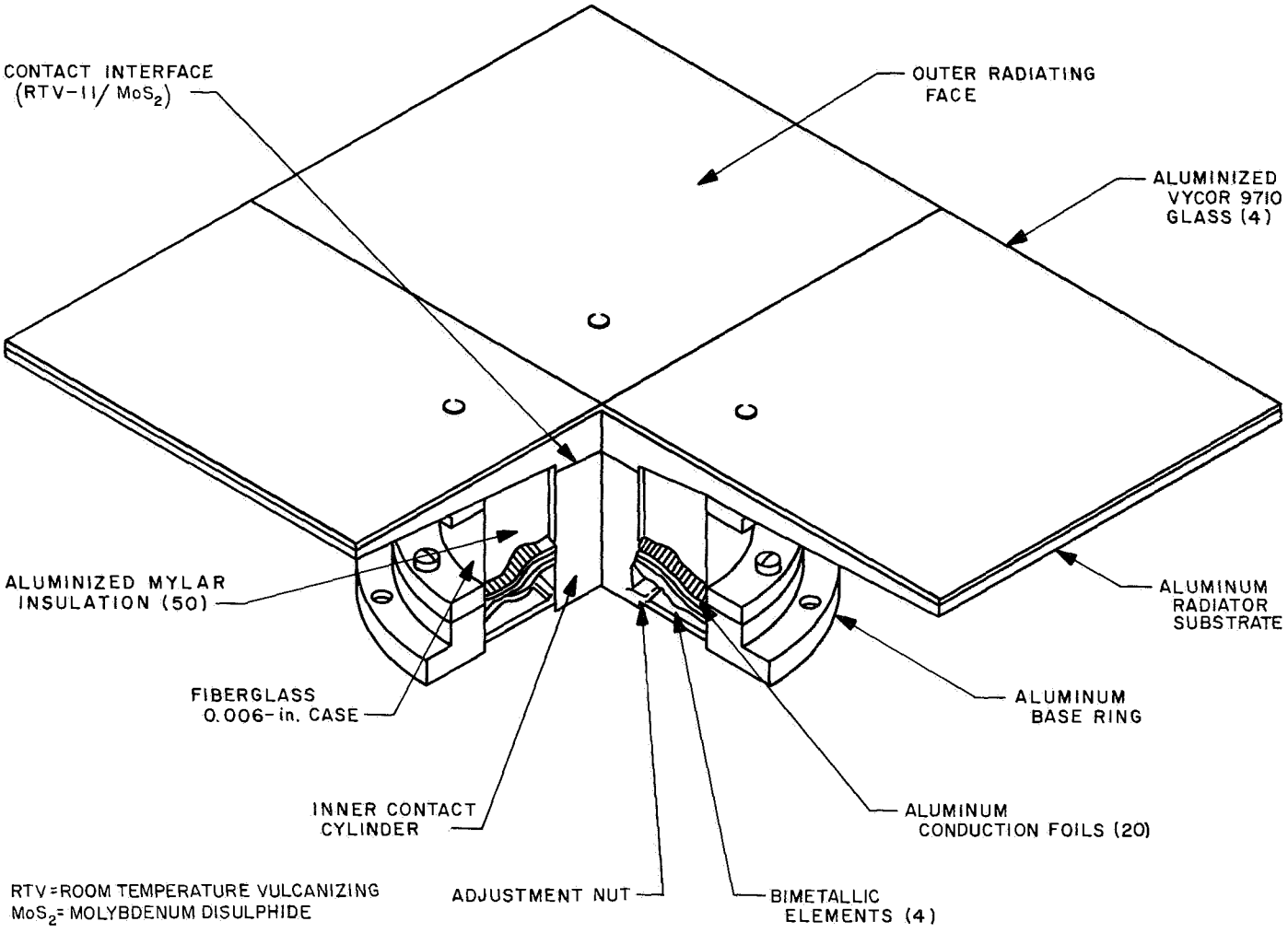



**Fig. XV-8. *Surveyor* thermal switch**

(2) An inner contact cylinder thermally connected to the base ring with multiple layers of aluminum conduction foil.

(3) Bimetallic elements cantilevered from the base ring and engaging the base of the inner contact cylinder.

(4) A low conductivity, fiber-glass case to support the outer radiator to the base ring.

The radiators on compartment A were 7.2 × 6.2 in. The radiator structure was a very shallow, inverted pyramid with a 0.7-in.-diameter contact protruding about 0.1 in. from its apex. The structure was made of 1100 aluminum for high heat conduction, and the contact was ground flat to 12 μin. The top of the radiator had four Vycor glass segments bonded to its surface. The back side of the Vycor glass had a vapor-deposited aluminum mirror finish. Vycor glass is transparent to the solar energy spectrum, so the absorption surface was the aluminized back sides, which absorbed only 11% of the incident solar energy. The heat loss was determined by the surface of the Vycor glass, which emitted 79% of the heat energy conducted to it. These characteristics enabled the switches to lose much more heat than they absorbed when the contacts were closed. Each radiator assembly had four screw holes so that it could be mechanically attached to the rest of the thermal switch structure. The compartment B radiator was identical to that of compartment A except that its dimensions were 7.2 × 6.6 in.

The heat path from each compartment to the radiators was from the base ring through the aluminum foil layers to the inner contact cylinder across the contact joint to the radiator. This inner contact cylinder had a diameter of 0.7 in. and a length of 0.92 in., and was made of 1100

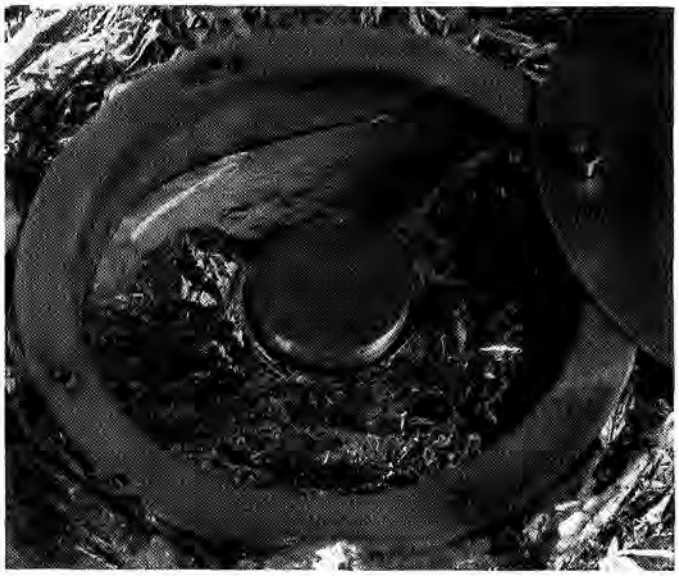


**Fig. XV-9. Thermal switch on *Surveyor* compartment**

aluminum. The contact (upper) end of the cylinder was ground flat to within 12 $\mu$in. To improve contact efficiency, a drop of RTV 11 was placed in the center of the flat contact surface, and an optical flat was pressed against it until most of the RTV 11 was forced out. The RTV 11 then was cured with the optical flat in place. When the optical flat was removed, a layer of RTV 11 about 0.0005-in. thick remained. The RTV 11 then was covered with a light coat of molybdenum disulfide, and all excess material was brushed off. The molybdenum disulfide was used as a parting agent to prevent the bonding material, RTV 11, from causing sticking.

The aluminum foil section, used as a flexible conductor, was in the form of a cross with a hole in the center in which the inner contact cylinder was bonded with silver-filled epoxy. There were 20 layers of foil material, and each arm of the cross was formed into a series of sine waves to allow flexibility for axial movement. The outer end of each foil arm was welded into the outer or base ring. The base ring was made of 1100 aluminum which was machined to accept the foil arms on the upper side and the four bimetal actuating springs on the lower side. The bimetal springs were trapezoidal with the small end toward the inner contact cylinder and the large end in the base ring. A flat strip of aluminum was placed over each spring. Two screws were used to hold each aluminum strip and the bimetal spring in place. The base ring assembly was then machined flat on the bottom to assure good thermal contact with the electronic compartment. The small end of each of the four bimetal springs rode in a slotted ring which was screwed to the bottom of the inner contact cylinder. The slotted ring could be screwed up and down on the lower contact to change the opening point of the contact with respect to the bimetal temperatures.

The switch case was the structure and thermal isolator between the base ring and the radiator. It was a fiber-glass cylinder with a wall thickness of 0.006 in. and a bolt flange on each end for attachment to the base and radiator. A small, 50-layer aluminized Mylar blanket was placed around the inner contact cylinder inside the switch case and just above the foil sections to reduce the radiation heat losses when the switch contacts were open.

Several fabrication techniques were developed to ensure proper switch function. A few examples are:

(1) Use of an optical flat for flattening the RTV 11 on the lower contact.

(2) Application of molybdenum disulfide as a parting agent.

(3) Fabrication of the bimetal actuators by rough-cutting them from the same piece of material, then finish-machining them in a stack so that all would have the same characteristics.

An unsolved design problem was that the thermal switch had to be disassembled prior to installation on the spacecraft after its flight acceptance test. The spacecraft STV test was used to verify final switch thermal conduction. Mission experience disclosed that the closer the switch installation (breaking the contact) was to flight time, the better the chances were for the switch to open properly at the end of the lunar day.

The thermal switch concept was not changed during the program, but several engineering changes were made to achieve the present performance. The mirror adhesive was changed to RTV 11 to prevent cracking caused by differential expansion rates of the glass and the aluminum at extreme temperatures. The case wall thickness was increased from 0.003 to 0.006 in. for structural stiffness. After the switches on *Surveyor I* stuck, a contact baking process was established to reduce contact sticking problems caused by the RTV 11 coating. The lower coated contact was baked in a vacuum chamber at 300°F to evaporate the remaining volatile material from the RTV 11. The contact opening temperatures were changed, along with the test tolerances, to reduce the tedious switch adjustment process required before *Surveyor IV*.

A type-approval test program was conducted on the flight-type thermal switches in late 1964 and early 1965. These tests included qualification level vibration, shock testing, high temperature soak, low temperature soak, and simulated aerodynamic heating. In September 1966, revised requirements were established for aerodynamic heating, and additional tests were run. A vacuum chamber was used in testing the *Surveyor* thermal switch to simulate the space environmental conditions. Figure XV-10 shows how the thermal switch was positioned in the environmental chamber and where thermocouples were located. Unit type-approval tests again were conducted.

The initial thermal switches were flight-acceptance-tested in a different sequence from that of later switches. Initially, the conduction test was the last operation performed, and many switches failed at this point and had to be reworked and completely retested. The procedure was changed and the conduction test was run first, allowing the bad switches to be removed and reworked before being put through the complete test program. A final conduction test was performed on these switches at 30 and 50°F above the contact-opening point, whereas the screening conduction test was only run at 50°F above the opening point. Contact-opening temperature tolerance was changed from +3 and −2 to ±10°F, the former being almost impossible to meet before and after vibration because of mechanical hysteresis.

*c. Active control (heaters).* Active thermal control consisted of electrical heaters operated by either external command or thermostats or both. Active control was used where survival could not be achieved by any of the previously described techniques alone; a close temperature control was required, as for the gyros; temporary heat was required to warm up electronics to their operating ranges, as for the television camera; and heat was required to provide lunar night survival. Wherever possible, active control was integrated with passive control to minimize energy requirements.

The major components utilizing active heaters are indicated in Fig. XV-2. The fuel and oxidizer tanks had continuous thermal transients. Two of the pairs of vernier propellant lines (the oxidizer and fuel lines ran close together with a common heater) and the altitude marking radar (AMR) fell rapidly to their heater actuation levels and cycled thereafter. The gyros cycled continuously from launch. Specific characteristics of the different heaters are given in Table XV-4.

### 3. Thermally Imposed Operating Restrictions

Restrictions were imposed upon the operation of the spacecraft so that the subsystems would remain within their thermal operating or survival limits.

*a. Air conditioning temperatures before launch.* Before the STV tests of *Surveyor I* were performed, the main retrorocket temperatures were predicted for various initial temperatures and solar intensities. The propellant bulk temperatures were calculated for STV phases II and IV

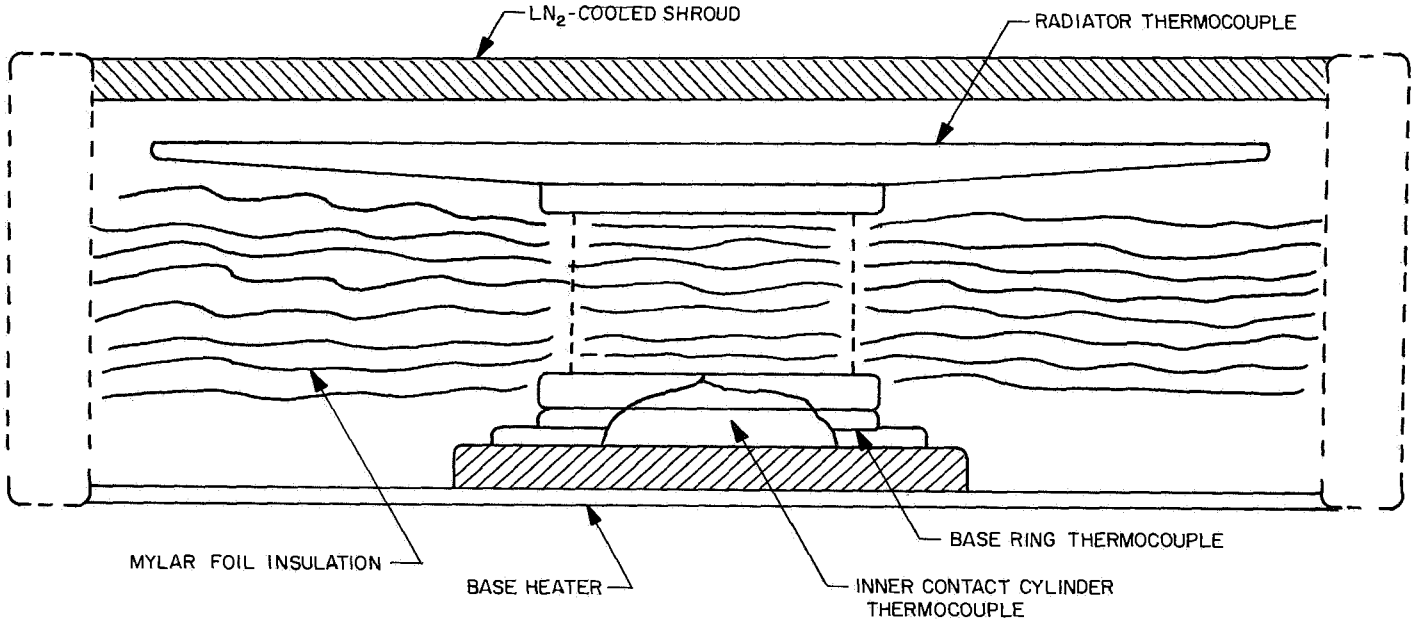



**Fig. XV-10. General test arrangement for *Surveyor* thermal switch**

**Table XV-4. Heater summary (typical)**

| Unit | Set point, °F | | Power capability, W | Time of first activation (time from liftoff), hr | Flight duty cycle, % |
|---|---|---|---|---|---|
| | On | Off | | | |
| Altitude marking radar | 20 | 26 | 5.0 | 7.5 | 52 |
| Soil mechanics surface sampler electronics | −5.8 to +5 | 10.4 to 21.2 | 7.75 | 3 | 100 |
| Vernier propellant lines | | | | | |
| 1 | 18 | 26 | 3.4 | — | — |
| 2 | 18 | 26 | 6.8 | 7 | 34 |
| 3 | 18 | 26 | 3.4 | 33 | 30 |
| Television mirror | 2 | 8 | 16.0 | 60 | 100 |
| Television electronics | 2 | 8 | 20.0 | 60 | 100 |
| Television vidicon | 75.2 | 78.8 | 2.24 | 63 | 100 |
| Compartment A | 50 ±5 | 50 ±5 | 19.4 | 51 | 100 |
| Compartment B | 10 ±5 | 10 ±5 | 19.3 | — | — |
| Compartment C | 14 to 27 | 32 to 43 | 9.5 | 61 | 100 |
| Alpha scattering instrument sensor head | 50 | 59 | 5.0 | 63 | 100 |
| Gyros (total for 3) | 180 ±0.2 | 180 ±0.2 | 30.0 | Pre-launch | 10 to 40 |

(nominal and high sun) conditions at the beginning of the mission and at launch plus 66 hr. The actual initial bulk temperatures for these phases were 82 and 85°F, whereas the final bulk temperatures were 66 and 70°F, respectively. Although the final bulk temperatures were within the specification limit of 70°F maximum at retro motor ignition, they were higher than predicted and higher than desirable.

The original specification for the air conditioning system used for the spacecraft from encapsulation until launch required the temperature to be maintained at 85 ±5°F (Ref. XV-3). If the bulk temperature of the retro motor had been at the upper limit of 90°F at launch, the temperature at retro motor ignition would have been undesirably high. For this reason, the air conditioning specification was changed and each spacecraft was conditioned first with 70°F air from the time of *Centaur* mating to 2 hr before launch, and then the conditioning temperature was raised to 85°F. The 70°F conditioning temperature was chosen so that the retro motor propellant, which was in a constant cooling transient throughout transit, would be close to the optimum bulk temperature of 55°F at the time of ignition. The final 2 hr of 85°F air provided a higher launch temperature for the low-heat capacity units (to offset the effects of potential earth shadowing and random sun orientation prior to sun acquisition); however, it had a negligible influence on the large mass of retrorocket propellant.

*b. Aerodynamic heating restriction on nose fairing ejection point and launch phase aerodynamic heating.* Potential aerodynamic heating of the spacecraft, caused by early nose fairing ejection during a single-burn *Centaur* launch or by a low parking orbit during a two-burn *Centaur* launch, was considered early in 1961. The final restrictions involved both the integrated and instantaneous heat loads due to aerodynamic heating, plus the solar and earth albedo heat loads, where appropriate. These were specified at nose fairing jettison and, from that point until the end of aerodynamic heating, for both direct-ascent and parking-orbit trajectories.

*c. Restriction on transmitter high-power time.* High-power operation periods for the transmitters were held to a minimum consistent with the accomplishment of the sequence requirements, but the maximum total unmonitored high-power-on time was 60 min to ensure that the transmitters would not be overheated. This imposed a launch constraint. It was required that the start of DSIF acquisition commence 40 min after spacecraft separation from the launch vehicle to allow at least 20 min to accomplish two-way lock so that the command to switch the transmitter back to the low-power mode could be sent.

*d. Restriction on time spent in shadow or not locked on the sun.* The sun acquisition sequence had to be completed within 60 min after liftoff to avoid overcooling of certain components. Sun acquisition required up to 18 min. Therefore, the spacecraft was required to be clear of the earth's shadow within 42 min after liftoff.

After sun acquisition, the spacecraft could be in the earth's shadow for not more than 30 min. The spacecraft could be in the shadow of the moon for not more than 30 min before touchdown (actually, all of the missions arrived during the lunar day, and this constraint was never involved).

Before the midcourse and terminal maneuvers, sun lock had to be broken and the following constraints applied:

The first maneuver before midcourse was to be executed less than 15 min before vernier ignition. This maneuver was to be roll, if possible, to minimize time off sun lock. The attitude maneuvers of the terminal sequence were to be initiated less than 33 min before the predicted time of retro motor ignition, but this time could be increased depending upon the results of the gyro drift checks.

*e. Restriction of time between last nonroll gyro drift check and vernier engine ignition.* The edge of the shadow of the solar panel lay across the head end of vernier engine 2, which was thus sensitive to slight movement of the spacecraft from direct sun lock. During gyro drift checks in pitch and yaw, the spacecraft Z-axis could move up to 2 deg away from the direct sun line, causing a change of $\pm 20°F$ in the temperature of vernier engine 2, depending upon the direction of the drift. For this reason, after the flight of *Surveyor I*, no gyro drift checks in pitch or yaw were done less than 4 hr before the vernier engines were required to ignite. This ensured that vernier engine 2 was within allowable limits at ignition.

## B. Solar-Thermal-Vacuum Testing and Results

The need for spacecraft STV tests as a development tool in conjunction with analysis was recognized early in the program, but there was no chamber with a simulated solar beam large enough to illuminate the complete *Surveyor* spacecraft, even with the legs removed. Sectors equal to about one-third of the spacecraft were built to allow testing in existing chambers.

Due to the fact that the open thermal control system was used, involving the discrete analysis of separate subsystems, thermal test behavior was analytically predicted test data were then used to modify the analyses where needed. The first complete vehicle to be STV-tested was the prototype spacecraft, T-21. Again, comparison of predicted and test behavior led to further analytical refinements. The prediction-test-comparison cycle was repeated on *Surveyor I*, the second complete vehicle tested, and again on the thermal control model, S-10, the third complete vehicle to be tested. The background gained in predictions and tests was applied to the prediction of the mission performance of the *Surveyors*, and mission data, in turn, were used to refine the predictions of future missions.

In order to illustrate the prediction-test-comparison cycle, particular attention has been paid to the vernier propulsion subsystem in the T-21 and flight spacecraft STV testing.

This subsection describes the STV tests on the sectors, T-21, S-10, and the flight spacecraft. Difficulties encountered and resulting design changes are discussed in conjunction with the tests.

The individual tests for a given flight spacecraft and for the prototype, T-21, were defined as test phases, starting with phase I for each vehicle. The thermal control model, S-10, went through two series of tests, one at JPL and the other at HAC, starting with phase I for each series.

### 1. Sector Testing (MT-1 Sectors I and II)

Tests on the first sector, MT-1, sector I, began in June 1962, under cold-wall, high-vacuum conditions in the Lockheed Aircraft Company facility in Saugus. This sector was the bay containing compartment A (Fig. XV-11), and was tested for up to 150 hr. The tests demonstrated the adequacy of the compartment A lunar night thermal isolation design, but, at the same time, indicated problems with the performance of the thermal switches.

MT-1, sector II (Fig. XV-12), was tested initially in October 1962, under cold-wall, high-vacuum conditions in the Hughes Aircraft Company facility. This sector was the bay containing compartment B. The 160-hr test demonstrated the adequacy of the compartment B lunar night thermal isolation design with improved thermal switches. The first transit test with solar simulation was

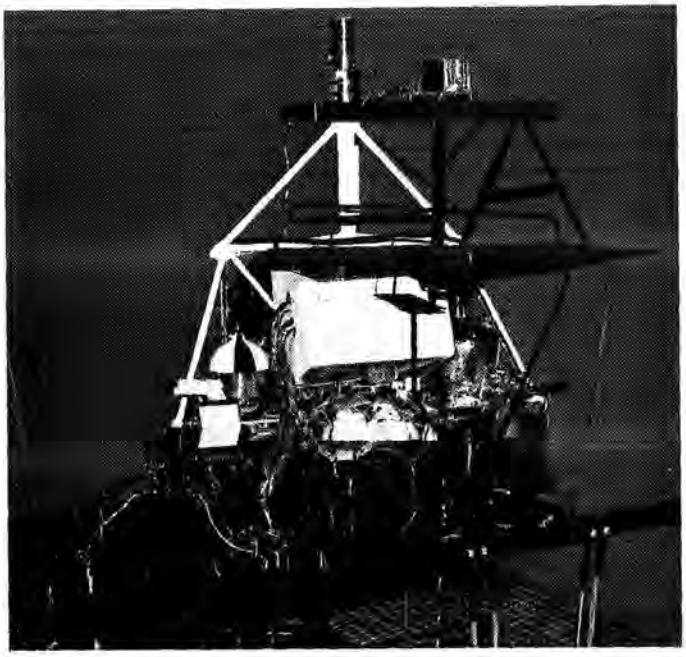


**Fig. XV-11. MT-1: sector I**

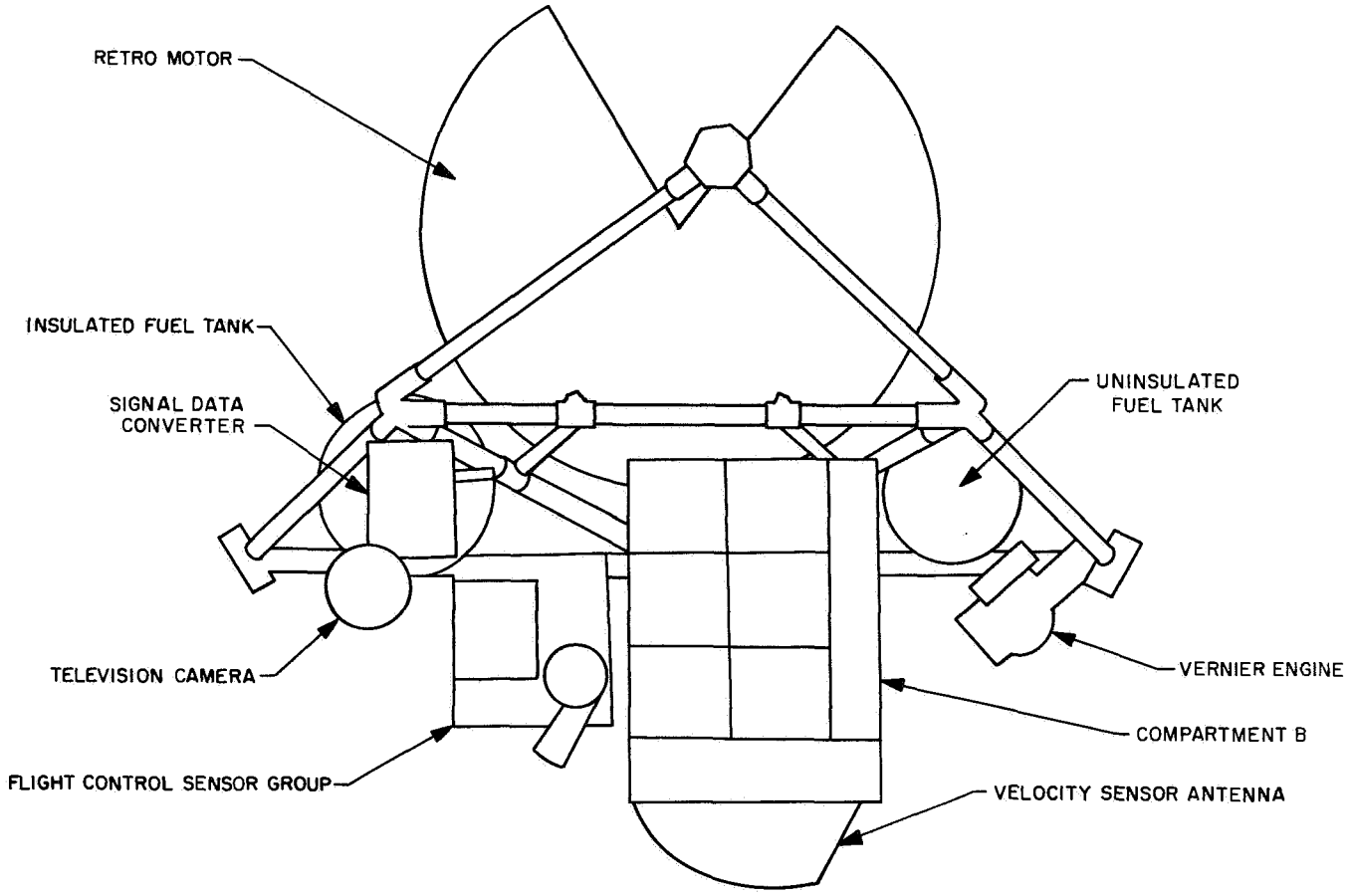



**Fig. XV-12. MT-1: sector II**

performed in the JPL 25-ft chamber in May 1963, using sector II. This 70-hr test showed some problems in the passively controlled units, but demonstrated the adequacy of the internal design of compartment B. Two more tests were run in the JPL chamber during July 1963: (1) a 37-hr transit test of modifications to the passively controlled elements of sector II and (2) a 50-hr test to evaluate lunar day performance and to provide an improved definition of the external environment of compartment B.

During September 1963, an MT-1 landing gear was tested in the JPL chamber and demonstrated the adequacy of the thermal control on the leg assembly and the attitude jet system; the shock absorbers were found to be sensitive to interreflections.

Sector I was tested in solar simulation for the first time in the JPL chamber in December 1963 and again in January 1964. The first test, lasting 70 hr, used liquid nitrogen-cooled shadow shrouds to simulate the shading of the solar panel. It was run first (40 hr) at 80% sun, and then retested (30 hr) at 100% sun. The second test, lasting 43 hr, had 100% sun and no shadow shrouds, fully illuminating the compartment, vernier fuel tank, and vernier engine. These tests showed that the shadow shrouds provided adequate simulation of the transit behavior of the spacecraft, that the thermal switches and radiators were adequate for control of the compartment, but that the solar collector used to thermally control the vernier engine was inadequate. The second test also was used to determine the reflective interaction between the retrorocket and other subsystems. The aluminized Teflon cover over the retrorocket was jettisoned by remote means, exposing a nonreflective undercoating to demonstrate in a gross manner the effect of this reflected solar energy on the temperature of the other subsystems.

During June 1964, the MT-1 landing gear test was rerun in the Hughes Aircraft Company C-4 simulator for a comparison between the JPL 25-ft chamber and the C-4 chamber. This was followed in July 1964 by a partial rerun of the sector I test conducted at JPL in December

1963. The comparison between the results obtained in the C-4 chamber and in the JPL chamber is shown in Table XV-5.

### 2. Prototype Spacecraft (T-21) Thermal Testing

The prototype spacecraft T-21 was tested in the HAC C-4 chamber during January and February 1965. The nominal (100%) solar intensity in the chamber was set at the level of the preamplifiers of the radar altimeter and doppler velocity sensor (RADVS); the intensity level at the top of the compartments was then 106% for the nominal setting, since intensity is a function of the distance from the source. At this setting, the solar intensity for most of the spacecraft in the chamber was higher than is encountered in space. Shadow shrouds were placed close to the shaded subsystems to simulate the effect of the antenna and solar panel positioner because the lack of collimation in the chamber resulted in a region of varying intensity 15 to 25 in. wide at lower levels on the spacecraft instead of a 1-in.-wide shadow line, as in flight. The landing gear and attitude control jet systems also required special hardware in test since both extended outside the 8-ft circle of solar illumination into a region where the intensity was between one-third and one-half of a solar constant. Blocking heaters were used to control the landing gear to $60 \pm 10°F$ and the attitude control jets to $120 \pm 20°F$ to prevent heat losses from the illuminated portion of the spacecraft.

The test was to have been run in two phases. Phase I, a 66-hr mission sequence at nominal solar constant, was aborted by nonthermal difficulties in the flight control sensor group (FCSG). The rerun, after repairs, was designated phase II. Phase III consisted of three abbreviated mission sequences at 80, 115, and 70% of nominal sun intensity, with a 1¼-hr eclipse between the high- and low-intensity tests. This phase was for demonstration of the subsystem thermal design margins (see Table XV-6 for problems and resulting modifications).

Vernier engine thermal control had been a continuing problem, and, by the beginning of phase I, a variety of engines, surface finishes, and solar collectors had been tested to meet the 0 to 125°F operating specification (later relaxed to 0 to 165°F). The thermal configuration of the vernier engine 1 barrel during phase I was gold-plated with black paint on the top. Since the engine ran too hot during the test, the black paint was removed from the head, black paint was added to the side of the barrel, and a 15-in.$^2$ solar reflector was added to warm the extension cone and to decrease the gradient from the top to the bottom of the barrel. The temperature was still too high during phase II.

The thermal configuration of the vernier engine 2 barrel during phase I was also gold-plated with black paint on top and an integral solar collector attached to the barrel. Since the temperatures during phase I were too low, the black paint and the solar collector were removed and a 15-in.$^2$ reflector was installed for phase II. Coast mode temperatures during phase II were satisfactory, and results indicated that engine 2 could be maintained above 0°F during the 30-min solar eclipse, but with very little margin.

The thermal configuration of the vernier engine 3 barrel during phase I was also gold-plated with black paint on top, and the temperature again was high. Before phase II, the black paint was removed and a 15.0-in.$^2$ reflector was installed. Test temperatures still were slightly higher than desired during phase II, and the black paint was changed to the side of the barrel as was done on vernier engine 1. The use of the reflector reduced the barrel gradient, but not below the 25°F design objective.

The predicted head end temperatures for the phase III test with reflectors on all vernier engines were 112, 70, and 99°F for 1, 2, and 3, respectively. The only significant discrepancy between test results and predictions occurred on vernier engine 1 where the bottom of the barrel cooled 40 to 45°F during a 30-min eclipse. Phase I results indicated that the barrel/cone interface conductance was low. After the T-21 STV phase III tests, the vernier engine thermal analytical models were upgraded to correlate with the test behavior. The barrel/cone conductance and cone emittance values were revised, based upon hardware characteristics.

During phase I, a special RADVS thermal development test also was run, including a 1-hr solar eclipse. After the mission sequence, other special thermal tests were run. The television cameras were warmed to equilibrium temperature by the electronics and vidicon heaters to demonstrate their maximum capabilities. The thermal performance of the FCSG also was demonstrated during a 7-hr period without power. The thermal switches did not perform as specified during phase II and were replaced before phase III. Later, it was found that the poor performance during phase II was due to faulty installation. In addition, transmitter A ran too hot as a result of improper tightening of the mounting screws. Paint patterns were modified before phase III on the Canopus sensor and the approach television camera. Areas where the white paint had degraded were repainted on the Canopus sensor and the FCSG.

During phase III, transmitter A performed better but still not as was desired. The general performance of

## Table XV-5. Comparison of HAC and JPL STV data for sector I

| Item | HAC C-4 chamber | | JPL 25-ft chamber | | Item | HAC C-4 chamber | | JPL 25-ft chamber | |
|---|---|---|---|---|---|---|---|---|---|
| | Temperature, °F | Intensity, W/ft² | Temperature, °F | Intensity, W/ft² | | Temperature, °F | Intensity, W/ft² | Temperature, °F | Intensity, W/ft² |
| Compartment A | | | | | Spaceframe | | | | |
| Switch radiators | 93 | 130 | 97 | 133 | Upper portion | −9 | 131 | −7 | 131 |
| Thermal tray (top) | 112 | — | 117 | — | Lower portion | 36 | — | 44 | — |
| Canister | | | | | Thermal tunnel | | | | |
| Sides | −88 | — | −80 | — | Inside | 62 | — | 68 | — |
| Back | 117 | — | 143 | — | Outside | −36 | — | −16 | — |
| Front | −23 | — | −1 | — | Radar altimeter and doppler velocity sensor | | | | |
| Bottom | −10 | — | −1 | — | Klystron power supply modulator | | | | |
| Vernier system | | | | | Top | 160 | 122 | 160 | 136 |
| Thrust chamber assembly | | | | | Bottom | 24 | — | 30 | — |
| 2 top | 104 | 125 | 130 | 134 | Waveguide | 45 | — | 55 | — |
| Solar collector | 211 | 119 | 220 | 110 | Altitude/velocity sensing antenna | | | | |
| Barrel | — | — | — | — | Septum (bottom) | 28 | — | 45 | — |
| Extension cone | 35 | — | 44 | — | Dish (in sun) | 85 | — | 108 | — |
| Oxidizer tank 2 | 67 | 124 | 80 | 135 | Dish (in shade) | 45 | — | 57 | — |
| Fuel tank 2 (inside) | 87 | — | 93 | — | Skirt (outboard) | −65 | — | −65 | — |
| Helium line (above tank) | 87 | — | 102 | — | Skirt (inboard) | −73 | — | −76 | — |
| Propellant lines | 37 | — | 47 | — | | | | | |

## Table XV-6. Modifications to T-21 prototype spacecraft resulting from STV tests

| Test phase | Sun level, % | Problem encountered | Modification |
|---|---|---|---|
| I | 100 | Vernier engines | |
| | | Barrel/cone interface conductance low | Interfaces reworked |
| | | Solar collector inadequate for engine 2 | 15-in. solar reflectors put on all three engines |
| | | Paint patterns incorrect on engines 1 and 3 | Black paint removed from top |
| II | 100 + eclipse | FCSG component problems | Early termination of phase I test |
| | | Thermal switches did not perform properly | Corrected installation |
| | | Transmitter A too hot during high power | Tightened mounting screws |
| | | Vernier engine 3 cool without black paint | Black added to side of barrel |
| | | Canopus sensor temperature 26°F higher than predict | Repainted because of white paint degradatian |
| | | FCSG base plate | Repainted because of white paint degradation |
| | | Approach television temperatures low with 50% white surface | Changed to fully polished surface |
| III | 70, 80, 100, and 115 + eclipse | Vernier engines | |
| | | 1 and 3 hotter than desired | Reflector removed from engine 1 |
| | | 2 cooler than desired | Larger reflector |
| | | Propellant lines lower than desired | |
| | | RADVS temperature variations bad for clase tolerances required | Minor surface finish changes |
| | | Helium tank temperature 15–20°F higher than predicts | Paint pattern changed |

compartments A and B was satisfactory. The vernier propellant line heaters were incapable of maintaining the lines above their desired minimum, and modifications were needed in the paint patterns on the RADVS and the helium tank.

### 3. Thermal Control Model (S-10) Testing

Flight-type thermal finishes were used throughout the thermal control model (S-10). Most of the vehicle had thermal heat capacity simulation since the electronic units used, with the exception of those within the compartments, were the actual units with nonfunctioning electronics. The basic construction of the compartments was of flight quality, as was the thermal control and heater assembly installed in each; the electronics, however, were simulated by heaters affixed to the flight-type mounting plates.

The S-10 tests were started in the JPL 10-ft chamber in January 1966, 3 mo after the beginning of *Surveyor I* tests in the HAC C-4 chamber. The timing resulted in the use of S-10 for the following purposes, rather than for the design of *Surveyor I:*

(1) To confirm the reproducibility of results obtained from different spacecraft.

(2) To confirm the reproducibility of results obtained from the same vehicle (S-10) in two different simulation chambers (JPL 10-ft and HAC C-4).

(3) To check the behavior of the spacecraft under lunar night conditions where temperatures were below the flight survival temperature limits.

(4) To check the thermal protection system devised for the vernier engine extension cone heating problem.

(5) To check the thermal protection of the legs with one leg directly in the solar simulation beam and certain other subsystems, which dropped below their flight survival limits, outside the beam.

(6) To check the behavior of the HAC lunar surface simulator with *Surveyor I* lunar surface behavior data.

The various phases of S-10 testing at JPL and at HAC are shown in Table XV-7. In JPL phase I shadow shrouds were employed instead of the A/SPP. JPL phase II included use of the A/SPP with the solar panel rotated down 6 deg from the horizontal to reduce the specular solar reflections caused by the chamber optical system. JPL phase III was a simulated lunar night test.

**Table XV-7. S-10 tests**

| Phase | JPL 10-ft chamber | HAC C-4 chamber |
|---|---|---|
| I | Transit coast mode; shadow shrouds; no legs; 80 and 100% sun; plus subsystem tests (January 1966) | Transit, hot cone; 1300 and 1600°F (4-min tests) plus 1900°F (6-min test); total 36 hr; 100% sun; (February 1966) |
| II | Transit coast mode; A/SPP, solar panel and planar array; power-on plus compartment and A/SPP tests; no legs; 100% sun (January 1966) | Transit coast mode; xenon and mercury–xenon mixtures for lamps; total 95 hr; 87% and 100% sun (March 1966) |
| III | Lunar night; determine heat losses; and television heaters plus thermal switch performance (January 1966) | Leg in the sun plus solar eclipse; total 40 hr; 87 and 100% sun (April 1966) |
| IV | — | Lunar noon; surface simulator only; no spacecraft; 100% sun; 260°F and $7.5 \times 10^{-7}$ mm Hg (March 1967) |
| V | — | Lunar noon; surface simulator plus spacecraft; *Surveyor I* and *III* lunar surface data used; 100% sun (April 1967) |

In HAC phase I, carried out in February 1966, midcourse propulsion thermal interactions were simulated by heating the vernier extension cones (Fig. XV-13). Electrical arcing problems experienced on the vernier engine 2 cone heater restricted the 1900°F run to 2.5 min. Thermal effects were extrapolated to the 2100°F expected in flight. The existing engine cone heating protection devices were found to be adequate.

The change in solar spectrum during the HAC phase II tests, conducted in March 1966, from pure xenon to 25% Hg-xenon, was made to observe the effect on the various subsystems because the latter spectrum is believed to be better for simulating the Johnson sun (Ref. XV-3) on the white painted surfaces. The spectral change caused temperature increases above the JPL test result.

The HAC phase III configuration (leg in sun), conducted in April 1966, is shown in Fig. XV-14. The leg temperatures were approximately 70°F, and shock absorber 80°F, during the 93% solar constant test. The shock absorber dropped to a minimum operating temperature of 20°F after 50 min of solar-eclipse condition, which agreed with predictions. Test data indicated that the shock absorber was relatively insensitive to leg temperature; however, the roll jet on leg 1 was coupled thermally to the leg.



**Fig. XV-13. Hot cone simulator**

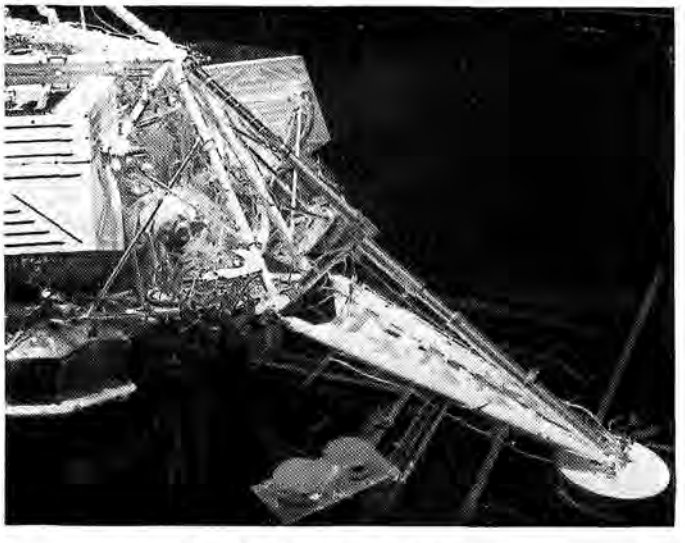


**Fig. XV-14. Leg in sun test**

The HAC phase IV test, conducted in March 1967, evaluated the thermal performance of the lunar surface simulator (LSS) as an infinite plane surface without the S-10. Table XV-8 indicates both the predicted and actual performance of six diffuse, black copper calorimeter plates mounted within the LSS during the test.

**Table XV-8. Lunar surface simulator calorimeter plate predicted and actual performance**

| Temperature, | Calorimeter plates | | | | | |
|---|---|---|---|---|---|---|
| °F | 1 | 2 | 3 | 4 | 5 | 6 |
| Actual | 121 | 145 | 184 | 130 | 162 | 175 |
| Predicted | 121 | 145 | 188 | 127 | 161 | 174 |

HAC phase V, carried out in April 1967, tested the S-10 on the LSS and compared results with those obtained from *Surveyors I* and *III* at lunar noon (see Subsection C-3).

#### 4. Flight Spacecraft Testing

The purpose of STV testing of flight spacecraft was to evaluate their performance at 87% of a solar contant (low sun) and at 112% of a solar constant (high sun). These tests were 66 hr each and were to be run without removal from the chamber or breaking vacuum. Each was followed by a period of television camera operation and operation of the surface sampler or alpha scattering instrument, when these were fitted. Since the total seasonal variation of solar intensity in the vicinity of the earth and the moon is less than $\pm 3.5\%$, the above tests provided adequate margin testing for thermal control design.

A third test followed which was run "plugs out," wherein the chamber was opened and much of the hard-line ground data system wiring was removed. The solar intensity for the last test varied from spacecraft to spacecraft, and it was varied during the test for sufficient time to obtain thermal stability on most of the subsystems.

The earlier spacecraft were tested long enough at one solar constant to determine their nominal performance, but this practice was abandoned later, and margin testing was used exclusively. Few of the spacecraft completed the sequential 66-hr tests without problems, but all were exposed to the full 66-hr simulated mission at low and high sun levels and to the "plugs out" test. The latter sometimes was shortened by reduction of the period simulating cruise between launch and midcourse and between midcourse and terminal maneuvers. Eclipse periods, varying from 30 to 60 min, were run to determine the system and subsystem performance during periods of earth shadow and off-sun maneuvers. Before testing, the solar energy, both incident and reflected, was mapped

with the spacecraft in the chamber to allow for variations of solar simulation intensity at various levels above the nominal test plane when analyzing the test results. The spacecraft modifications which resulted from the STV tests are shown in Table XV-9 and are discussed in the following paragraphs.

Preliminary calculations based on T-21 tests indicated that the existing *Surveyor I* vernier engine 1 would exceed the allowable 165°F temperature; therefore, the reflector was removed. Further analytical studies were made for *Surveyor I* based upon the 0 to 165°F range and 130°F steady-state operational level. Paint patterns were established and an increase was made in the vernier engine 2 reflector from 15 to 20 in.$^2$

*Surveyor I* STV flight acceptance (FA) test phase I indicated that vernier engines 1 and 3 performed as predicted. Solar intensity at the vernier engine level was determined to be 90% of a true solar constant (130 W/ft$^2$). The temperature of the head and the bottom of the barrel of vernier engine 1 dropped 24 and 8°F, respectively, during a 15-min solar eclipse test period. The head end and the bottom of the barrel of vernier engine 3 dropped 46 and 14°F, respectively, for the same time period. The *Surveyor I* STV phase I test also indicated that vernier engine 2 still was running too cool; therefore, the reflector size was increased again to 26.7 in.$^2$ Phase II tests were satisfactory with the enlarged reflector, which resulted in a temperature of 88°F at high sun (predicted at 99°F).

The flight sensor on vernier engine 1 indicated a steady-state temperature in high-sun STV testing about 20°F higher for *Surveyors III* and *VI* than for previous vehicles. A check revealed that the same engine (SN 551) had been on both spacecraft and that each had been exposed to similar test chamber pressure surges and vehicle contaminations. Both *Surveyors III* and *VI* compared favorably with other vehicles during the low-sun tests.

**Table XV-9. Modifications to flight spacecraft during STV tests**

| Spacecraft | Test phase | Sun level, % | Problem encountered | Modification |
|---|---|---|---|---|
| *Surveyor I* | I | 84 and 94 | Vernier engine 2 temperature ran cooler than expected | Vernier reflector increased in size |
| | | | Transmitter temperatures higher than desired | Indium foil between TWT and thermal tray |
| | II | 99 | Cracked glass and foreign material on thermal switches | Thermal switches replaced |
| | IV | 112 | Unreliable conductance between BCR and thermal tray | Indium foil between BCR and tray |
| | | | Localized hot spot on vernier lines 1 | Sunshade over vernier line 1 |
| | | | Regions of vernier lines 3 too cold | Vernier line 3 thermostat relocated |
| | | | Television mirror dropped below −50°F limit during operations | Thermostat control added to television mirror |
| *Surveyor II* | IA | 87 | Battery reached 152°F (limit: 125°F) | Four compartment A switches set from 65 to 40°F |
| | IB | 112 | Vernier line 1 temperature reached 130°F | Sunshade lengthened on vernier lines |
| | | | Two thermal switches stuck open | Corrected installation and cleanliness procedures |
| | IC and retest | 100 | Hot spot still existing on vernier line 1 | Tried aluminized Teflon wrap, approach abandoned |
| | | | Canopus sensor temperature high and window fogging | Canopus hood painted black |
| | IIIB | 112 | Compartments hot, main battery reached 124°F | Switches in both compartments set at 40°F |
| *Surveyor III* | IA | 87 | Auxiliary battery cold on Surveyor I flight; 30°F increase required | Auxiliary battery paint changed, also on *Surveyor II* at Cape Kennedy (discussed in Subsection XV-C-2) |
| | IC | 87 and 112 | Vernier tank 1 dropped rapidly; insulation tight | Control of insulation wrap for vernier tanks |
| | | | Vernier engine 1 20°F higher than normal (SN 551) | Replaced by another vernier engine |
| | IIC | 87 | *Surveyor II* vernier line 2 heater full-on in flight | Line 2 heater changed from 3.4 to 6.8 W |
| | IIIC | 100 | Surface sampler difficult to see with television camera | Surface sampler paint changed from black to pastel blue |
| *Surveyor IV* | IC | High and low sun | Sun too high; Eppley read 7°F lower than blackplate | Test procedures to control STV solar levels (discussed in Spacecraft Environmental Requirements) |
| *Surveyor V* | IA | 112, 100 and 87 | $N_2$ tank cold because of shading by new compartment C | New paint pattern and aluminum foil for $N_2$ tank |
| | | | Helium check and relief valves hotter in new location on spaceframe | White paint added and conductance to bracket increased by insertion of indium foil |
| | | | Aluminized Teflon bonding on SDC rough | Replaced by inorganic white paint |
| *Surveyor VI* | IA | 112 | Helium check and relief valves still hot; indium foil wrinkled | Changed to single layer of indium foil |
| | | | Vernier engine 1 20°F high (see *Surveyor III*, SN 551) | Nozzle/chamber conductance low and variable; replaced by SN 564 |

The thermal behavior of engine SN 551 did not appear to be reproducible during STV tests. For example, the temperature difference between the extension cone and the bottom of the barrel was 74°F during the initial *Surveyor III* high-intensity STV test, before the pressure surge. After the chamber pressure surge, SN 551 exhibited temperature differences of 103 and 107°F between the extension cone and the bottom of the barrel. Thermal conductance calculations showed that the extension cone/barrel bottom contact conductance changed from 0.782 to 0.200 Btu/hr °F. The conductance measurement was made on February 16, 1966, and the calculation on August 25, 1967. Thermal data seemed to indicate that the vernier engine conductance changed during *Surveyor III* STV testing. The vernier engine acceptance specification indicated that the extension cone/barrel bottom conductance should have been in the range of 0.70 to 3.50 Btu/hr °F.

Although the vernier engine did not exceed its upper temperature limit during *Surveyor VI* STV high-intensity tests, flight situations could have occurred whereby the extension cone/barrel bottom temperature differences would have become large, causing the thermal conductance to approach zero. An examination of the STV data from subsequent unit tests indicated that the interference fit between the extension cone and the bottom of the barrel and the thermal conductance were approaching zero. A zero conductance value between the extension cone and the bottom of the barrel could have resulted in vernier engine barrel temperatures in excess of 200°F during the coast phase. For this reason, it was recommended that vernier engine 1, SN 551, be replaced on *Surveyor VI* with a vernier engine that exhibited a larger interface conductance. This recommendation was implemented with SN 564 replacing SN 551.

Regions of fuel and oxidizer lines exposed to direct or reflected solar energy were a continuing problem throughout the project. Attempts to correct this problem with shades, wrapping, and finishes were not entirely successful. A primary concern about high line temperatures was in throttling control of the vernier engines.

The exposed leg 1 lines on *Surveyor I* ran hot in the STV tests at about 150°F for a high-intensity solar illumination. A maximum goal of 100°F was desired. A sunshade was fabricated, installed on *Surveyor I*, and proved to be satisfactory during the mission.

The leg 1 lines on *Surveyor II* ran hot in the STV tests, even with the sunshade installed. A hot spot developed on line 1 for each of the high solar intensity tests, ranging from 120 to 124°F, despite various thermal design modifications. The elevated temperature was attributed to a higher solar absorptance, or a higher solar reflection environment in the vicinity of the lines, or perhaps both. Subsequent overwrapping of the line with aluminized Teflon reduced the maximum temperature to 91°F for a nominal sun intensity but was not used in flight. A maximum line temperature during flight was predicted to be 85°F, based upon the *Surveyor I* flight, which ran below the STV nominal sun test levels.

On *Surveyor III*, the STV line temperatures also exceeded the 100°F goal for both the high-intensity sun and the nominal sun. After returning the spacecraft from the AFETR for retest, the line 1 temperature, even at low sun, was 91°F, which was 13°F higher than it had been previous to shipment. A waiver was obtained to allow the lines to reach 120°F during flight.

Vernier engine 1 propellant lines exceeded their maximum allowable temperature of 100°F in the high-sun intensity tests on subsequent spacecraft. The propellant lines for engines 2 and 3 also were warm, but to a lesser extent. A correlation of early flight temperature data revealed that the high-intensity test level provided an unrealistic environment for the lines. Flight intensities lay between the nominal and low-sun intensity levels experienced in the STV tests. The maximum temperature during high-intensity testing was redefined to be 120°F for lines 2 and 3, whereas it was more flexible for line 1, being a linear function of temperature change versus intensity change between low- and high-sun tests.

An analysis of *Surveyor II* data indicated that the heater on vernier line 2 had been "full on" before midcourse. An extensive study was undertaken to improve test procedures and test criteria to eliminate the possibility that this undesirable duty cycle might occur during subsequent missions. A correlation between STV test and flight intensities for *Surveyors I* and *II* indicated that the flight intensity for the lines closely approximated the low-sun (87% black plate) test intensity. Therefore, the maximum duty-cycle criteria for the vernier lines were specified by the low-sun test. A further review of STV test data indicated that the vernier line 2 heater also was "full on" in the *Surveyor II* low-sun test and was at an undesirably high duty cycle in the *Surveyor IV* low-sun test just being completed at that time. As a result of this investigation, the following engineering changes were made:

(1) Spacecraft wiring harnesses were rerouted to minimize their contact with vernier lines 2 and 3.

(2) Where these harnesses were in close proximity to vernier lines, they were wrapped with aluminum foil instead of the previously used aluminized Mylar.

(3) The heater capacity on vernier line 2 was increased from 3.4 to 6.8 W.

After these changes were made, the *Surveyor III* retest and *Surveyor IV* phase IC tests showed a heater duty cycle reduction greater than 50%, as shown in Table XV-10.

The superinsulation wrapping on the fuel and oxidizer tanks had to be tight enough to maintain reasonably uniform thickness but loose enough to be an effective insulator. On *Surveyor III* in STV phase IC testing, oxidizer tank 1 temperature decreased at a higher-than-normal rate because of a tightly wrapped insulation This tank was replaced; however, in flight, the *Surveyor III* oxidizer tank 3 temperature decreased more rapidly than on other missions. This has been attributed to a tight wrap. However, its temperature remained within the allowable range.

During the initial *Surveyor V* high-intensity solar thermal vacuum test, the helium relief and check valves (relocated from the positions they occupied on the first four spacecraft) experienced temperatures of 157 and 170°F, respectively, which were above the upper temperature limit of 125°F for the valves. Two thermal modifications were made, adding 1 in.$^2$ of white paint to the exterior surface of each valve and increasing the thermal conductance (reducing the insulator thickness) between valve and support bracket. The valves then experienced temperatures of 136 and 141°F during the second high-intensity test (phase IIA).

**Table XV-10. Effect of hardware changes on vernier propulsion system duty cycles**

| Vehicle/ STV phase | Solar intensity, % of nominal sun | Change description | Duty cycles, % | |
|---|---|---|---|---|
| | | | Line 2 | Line 3 |
| *Surveyor III*, phase IIC | 87 | None | 73[a] | 67[a] |
| *Surveyor IV*, phase IB | 87 | None | ≈100 | 54 |
| *Surveyor III*, retest | 87 | Rerouted/rewrapped vernier propulsion system harnesses on lines 2 and 3. Double heater power on line 2 only | 30 | 15 |
| *Surveyor IV*, phase IC | 87 | | 30 | 0[b] |

[a]Duty cycle still rising at conclusion of abbreviated 27-hr test.
[b]Temperature remained above thermostatic set point.

Thermal studies were made in an effort to understand the thermal behavior associated with the valves and to lower their temperatures to an acceptable level within the 0 to 125°F range. The findings could not be incorporated into *Surveyor V* in time, but did result in the addition of indium foil inserts in *Surveyor VI*. A study and a test program also were conducted which qualified the helium relief and check valves at an operational temperature of 145°F for *Surveyor V*.

During the initial *Surveyor VI* high-intensity STV test, the helium check and relief valve temperature was reduced (from 141°F during the *Surveyor V* test) to 126°F by increasing the conductive path (via indium foil inserts) between the valves and the spaceframe. However, this *Surveyor VI* high-intensity steady-state temperature still was considered marginal.

Between the STV test phases IB and IA, the valves were removed from the spacecraft, revealing that the indium foil had been wrinkled during the original installation, resulting in a decreased conductive path. Prior to reinstallation, the design was changed from multiple layers of indium foil to a single layer offering the same conductive path. This design change resulted in a steady-state temperature of 113°F during the next two high-intensity tests (phases IIA and IIIA).

The thermal control design for the *Surveyor V* nitrogen tank differed from that of *Surveyors I* through *IV* because of the incorporation of the alpha scattering instrument on the spacecraft. Compartment C (which housed the alpha scattering instrument electronics) shadowed approximately 45% of the tank projected (solar, insulation) area. On earlier spacecraft, the total projected area of the tank was sunlit during transit except for localized shadowing by struts. The tank temperature was predicted to be 77°F in high-sun conditions but was actually 27°F. The paint pattern was modified after this test, and aluminum foil was bonded to the inboard upper hemisphere which raised the temperature in high sun to 67°F and in low sun to 36°F. The behavior of the tank with the new design was well above the lower allowable limit and gave adequate eclipse capability. Results were good on this and on subsequent flights.

Three types of problems were encountered with thermal switches in solar thermal vacuum testing; these were associated with cracking of the Vycor glass radiators, foreign material between switch contacts, and improper assembly of matched pairs of contacts.

Following phase II testing of *Surveyor I*, two thermal switches on compartment A were replaced because of badly fractured glass. The glass fractures were the results of damage during pretest preparations. Also, during phases I and II, thermal switch 6 on compartment B exhibited anomalous thermal performance and was replaced before phase III. Investigation indicated a piece of foreign material embedded in the contact surface. It was noted that the defective thermal switches did not cause any large perturbations in the compartment performance.

Early in the *Surveyor II* phase IB test, abnormal temperature trends developed on compartment A. Thermal tray temperatures were 5–8°F higher than those observed in *Surveyor I* phases IV and VI high-level tests, at common points in the mission. Also, two thermal switch radiator temperatures were low, indicating an open switch condition. Switch 6 radiator was −174 instead of 30°F, and switch 5 radiator was −40 instead of 40°F. Extrapolation of the temperatures associated with operating in this mode revealed that battery temperatures in excess of 125°F would occur after midcourse and jeopardize the main battery; therefore, the test was aborted. Post-test examination indicated that both switches were operating improperly. Switch 6 malfunctioned because of an assembly error. During reinstallation of switches 2, 3, 6, and 9, the radiators of switches 3 and 6 were interchanged (the procedure called for the switch body and radiator to be assembled and installed as matched pairs), and switch 6 remained open throughout the test. Switch 5 radiator was removed as part of the installation operation of the other four, and, during reassembly, a hairline piece of foreign material inadvertently became lodged between the switch contacts, preventing normal contact at this critical thermal interface. Corrective action included cleaning and replacing radiator 5, and replacing the entire switch assemblies for 3 and 6, before STV phase IIB testing.

The thermal switch closure temperature settings also were changed several times as a consequence of the high compartment temperatures which resulted during STV tests. The thermal switch closure temperature for compartment A was 65°F and for compartment B was 50°F on *Surveyor I*. Compartment A tray temperatures ran slightly higher (5 to 10°F) in the *Surveyor II* low-sun sequence than in the *Surveyor I* sequence. All units except for the main battery remained within specification as predicted at high sun. The battery temperature limit of 125°F was exceeded at midcourse (130°F) and again late in the mission simulation where a 152°F peak temperature was reached. The latter temperature rise was attributed to increased energy dissipation within the battery. Corrective action was taken to reduce compartment tray temperatures by lowering the thermal switch closure temperature on four switches beneath the solar panel simulation shrouds. These switches (2, 3, 6, and 9) carried most of the internal dissipation load. Reducing switch closure from 65 to 40°F increased the conductance of the switch, causing increased disposal of heat.

In order to maintain lower peak temperatures for the main battery for *Surveyor III*, the compartment A thermal switches 1, 4, 5, 7, and 8 also were set to a closure temperature of 40°F. Resetting the thermal switches to 40°F and reducing the use of high power during transit sequence reduced the battery temperature after terminal descent from the 124°F, experienced in the *Surveyor II* high-intensity test (phase IIIB), to 108°F in the *Surveyor III* high-intensity test phase IB.

The closure temperature on all six compartment B thermal switches was reset from 50 to 40°F. This action and the decrease in power consumed by the flight control unit resulted in steady-state upper and lower tray temperatures of 105 and 110°F, respectively, in the high solar intensity test phase. These temperatures compared favorably with *Surveyor I* (phase VIB) and were 20°F cooler than *Surveyor II* at high intensity. All of the later spacecraft flew with the thermal switches in compartments A and B set to close at 40°F.

During phase I STV testing of *Surveyor I*, transmitter temperatures were too high during high-power operation. The temperature of transmitter A rose from 108 to 214°F after 22 min of high-power operation, and that of transmitter B rose from 108 to 150°F after 20 min of high power. The upper temperature limit was 210°F. Prior to phase II, a 0.005-in. sheet of indium foil was inserted between the thermal tray/transmitter mounting interfaces, and thermal performance was significantly improved. During phase II, transmitter B was operated in high power for 1 hr, 54 min, and the temperature rose to 137°F from a starting temperature of 71°F. In phase IV, transmitter A was operated for 68 min in high power during star acquisition. The temperature increased

from 75 to 155°F, and the rate of rise leveled off to 0.2°F/hr at high-power turnoff.

A series of tests was run on a mockup transmitter attached to a thermal tray to verify the conductance improvement. Phase II test data indicated a reduction in temperature difference across the transmitter B interface from 80°F (without foil) to approximately 35°F (with foil) at the end of approximately 1 hr of high power.

During *Surveyor II* phase IA testing (low sun), temperatures in compartment B were approximately 18°F higher than those experienced with *Surveyor I* under the same conditions, although they compared well with S-10. This trend existed throughout the ground testing of *Surveyor II* at high, nominal, and low intensities. No changes were made in the spacecraft since all temperatures were within specification limits. Flight temperatures, with the possible exception of the booster-regulator, did not show this effect since most of the temperatures in the compartment were within 5°F of the flight data from *Surveyor I*. While several explanations have been made for this behavior, none was provable, and the effect was not seen on any of the later spacecraft.

The *Surveyor I* STV tests also created some concern about the thermal conductance between the battery charge regulator and the thermal tray. Therefore, indium foil was added at that interface to increase the reliability of contact conductance.

The signal data converter (SDC) of the RADVS required modifications to the paint pattern and thermal finish. Changes were made between T-21 and *Surveyor I*, and the resulting design flew successfully on the first four spacecraft. On *Surveyor V*, the aluminized Teflon covering part of the SDC was replaced by inorganic white paint. This was not due to improper thermal performance but to difficulty in obtaining smooth aluminized Teflon with any bonding technique.

## C. Mission Performance

The results obtained from the flight phases of the seven *Surveyors* and the performance of the five spacecraft that landed successfully are discussed in this subsection. Analysis of the flight-phase performance of two spacecraft led to modification of the thermal control design of the auxiliary battery and the vernier engine propellant lines.

A shadow plotting technique was developed to determine attainable spacecraft shading—particularly that close to lunar noon.

Certain unusual and unexpected results obtained in the flight phase and on the lunar surface are discussed, together with the behavior of the thermal switches during the early part of the lunar night.

### 1. Thermal Control Flight-Phase Performance Summary

All thermal control specifications were met in the flight phase by all spacecraft. Based on trends during the premidcourse coast phase, it is estimated that *Surveyor II* might not have met the thermal specification for vernier oxidizer line 2 during the postmidcourse coast phase if a spacecraft failure had not occurred at midcourse. In the case of *Surveyor IV*, the thermal specifications were met until the last communication was received from the spacecraft.

Flight-phase performance was monitored by 74 or 75 temperature sensors distributed by subsystems, as shown in Table XV-11. The results of the seven flight phases and the operational and survival limits in transit are shown in Table XV-12 for the 85 different sensor locations which were read out in the engineering telemetry modes. It should be noted that no more than 75 of these were carried by any one spacecraft. Also listed are the preflight predictions for the first and last spacecraft; the major prediction improvement from feedback of flight-phase data is apparent.

Three additional sensors were telemetered only when operating in the television mode and do not appear in Tables XV-11 and XV-12. One was in the approach television camera which was carried on the first two missions but never used, and two were in the survey television camera used only on the lunar surface. The temperatures quoted fall into three categories:

(1) Steady-state temperatures in the cruise phase for those items which stabilized during the flight phase.

(2) Launch temperatures and final temperatures immediately before retro motor ignition for those items which were in a continuous cooling cycle during flight.

(3) Mean temperatures for those items controlled by thermostatic heaters.

It is impossible to show maxima and minima during such transients as occur during launch; before, during, and after midcourse; and in the maneuver before retrorocket ignition; however, none of the temperature limitations was violated. Plots of all thermal data for each

## Table XV-11. Spacecraft temperature sensors

| Subsystem | Spacecraft | | | | | | |
|---|---|---|---|---|---|---|---|
| | Surveyor I | Surveyor II | Surveyor III | Surveyor IV | Surveyor V | Surveyor VI | Surveyor VII |
| Flight control | 9 | 9 | 9 | 9 | 9 | 9 | 9 |
| Mechanisms | 3 | 3 | 3 | 3 | 3 | 3 | 3 |
| Radar | 7 | 7 | 7 | 7 | 6 | 6 | 6 |
| Electrical power | 5 | 5 | 5 | 5 | 4 | 4 | 4 |
| Transmitters | 2 | 2 | 2 | 2 | 2 | 2 | 2 |
| Approach television | 1 | 1 | 0 | 2 | 0 | 0 | 0 |
| Survey television | 2 | 2 | 2 | 2 | 2 | 2 | 2 |
| Structures | 30 | 30 | 30 | 29 | 27 | 27 | 26 |
| Propulsion | 16 | 16 | 16 | 16 | 19 | 19 | 18 |
| Alpha scattering instrument | 0 | 0 | 0 | 0 | 2 | 2 | 2 |
| Surface sampler | 0 | 0 | 1 | 2 | 0 | 0 | 3 |
| Total | 75 | 75 | 75 | 75 | 74 | 74 | 75 |

## Table XV-12. Operational and survival temperature limits and results

| Flight sensor location by subsystem | Transit temperature (steady state, except as noted), °F | | | | | | | | | Temperature limits, °F | |
|---|---|---|---|---|---|---|---|---|---|---|---|
| | Surveyor I | | Surveyor II | Surveyor III | Surveyor IV | Surveyor V | Surveyor VI | Surveyor VII | | | |
| | Predicted | Actual | Actual | Actual | Actual | Actual | Actual | Predicted | Actual | Operational | Survival |
| Compartment A | | | | | | | | | | | |
| Upper tray | 78 | 70 | 74 | 49 | 58 | 46 | 41 | 47 | 46 | 125/0 | 135/−10 |
| Lower tray | 98 | 93 | 94 | 70 | 76 | 56 | 51 | 57 | 56 | 125/0 | 135/−10 |
| Transmitter A | 76 | 68 | 71 | 49 | 55 | 42 | 38 | 42 | 43 | 185/5 | 210/0 |
| Transmitter B | 78 | 68 | 73 | 48 | 57 | 44 | 40 | 45 | 44 | 185/5 | 210/0 |
| Main battery | 98 | 97 | 99 | 69 | 75 | 58 | 52 | 58 | 58 | 125/40 | 125/0 |
| Battery charge regulator | 125 | 123 | 118 | 94 | 98 | 64 | 60 | 65 | 62 | 170/5 | 190/0 |
| Radiators | | | | | | | | | | | |
| No. 5 | 36 | 42 | 31 | 30 | 25 | −3 | 20 | 15 | 24 | 145/−300 | 150/−320 |
| No. 8 | 30 | 44 | 28 | 36 | 42 | 29 | 31 | 26 | 36 | 145/−300 | 150/−320 |
| No. 2 | 30 | 35 | 34 | 19 | 22 | −31 | 14 | 8 | −33 | 145/−300 | 150/−320 |
| No. 3 | [a] | [a] | [a] | [a] | [a] | 4 | 9 | 5 | −10 | 145/−300 | 150/−320 |
| Thermal shell inside | 102 | 92 | 92 | 68 | 74 | [a] | [a] | [a] | [a] | 125/0 | 130/−10 |
| Thermal shell outside | −110 | −85 | −82 | −84 | −87 | −93 | −82 | −90 | −86 | 160/−210 | – |
| Thermal switch No. 5 inside | 79 | 66 | 69 | 47 | 56 | 43 | 38 | 44 | 43 | 130/−5 | 150/−15 |
| Compartment B | | | | | | | | | | | |
| Upper tray | 97 | 93 | 99 | 76 | 77 | 74 | 77 | 77 | 81 | 140/0 | 150/−10 |
| Lower tray | 102 | 98 | 103 | 81 | 81 | 77 | 81 | 81 | 83 | 140/0 | 150/−10 |
| Boost regulator | 110 | 115 | 128 | 94 | 97 | 82 | 83 | 84 | 87 | 175/5 | 190/0 |
| Radiators | | | | | | | | | | | |
| No. 4 | 75 | 67 | 70 | 55 | 54 | 52 | 53 | 52 | 60 | 145/−300 | 150/−320 |
| No. 1 | 71 | 73 | 84 | 61 | 62 | 58 | 61 | 60 | 63 | 145/−300 | 150/−320 |
| No. 5 | 71 | 66 | 70 | 56 | 53 | 51 | 55 | 55 | 53 | 145/−300 | 150/−320 |
| Thermal shell outside | −78 | −70 | −72 | −64 | −72 | −78 | −77 | −82 | −72 | 160/−210 | – |

## Table XV-12 (contd)

| Flight sensor location by subsystem | Transit temperature (steady state, except as noted), °F | | | | | | | | | Temperature limits, °F | |
|---|---|---|---|---|---|---|---|---|---|---|---|
| | Surveyor I | | Surveyor II | Surveyor III | Surveyor IV | Surveyor V | Surveyor VI | Surveyor VII | | | |
| | Predicted | Actual | Actual | Actual | Actual | Actual | Actual | Predicted | Actual | Operational | Survival |
| Thermal switch No. 4 inside | 93 | 88 | 93 | 74 | 72 | 68 | 73 | 70 | 71 | 130/−5 | 150/−15 |
| Thermal tunnel | 75 | 89 | 91 | 72 | 74 | 67 | 68 | [a] | [a] | 125/0 | 135/−10 |
| Auxiliary battery | 60 | 35 | 64[b] | 54 | 60 | [a] | [a] | [a] | [a] | 130/40 | 145/15 |
| Outer compartment canister | — | 2 | 9[b] | 12 | [a] | [a] | [a] | [a] | [a] | 160/−140 | — |
| Landing gear assembly | | | | | | | | | | | |
| Leg 2 | 85 | 83 | 74 | 77 | 65 | [a] | [a] | [a] | [a] | 160/−140 | — |
| Crushable block | −50 | −62 | −48 | −63 | −55 | −68 | −76 | −61 | −57 | 160/−140 | — |
| Shock absorbers | | | | | | | | | | | |
| No. 1 | 90 | 84 | 76 | 74 | 77 | 80 | 79 | 80 | 79 | 125/20 | 125/−25 |
| No. 2 | 88 | 72 | 73 | 76 | 76 | 76 | 84 | 80 | 80 | 125/20 | 125/−25 |
| No. 3 | 90 | 82 | 82 | 79 | 74 | 70 | 76 | 80 | 76 | 125/20 | 125/−25 |
| A/SPP mechanism | | | | | | | | | | | |
| Solar panel drive | 40 | 60 | 45 | 51 | 46 | 45 | 62 | 64 | 60 | 260/−225 | 265/−235 |
| Elevation axis drive | −86 | 1 | −17 | −11 | −20 | −23 | −9 | −6 | −6 | 260/−225 | 265/−235 |
| Solar panel | 118 | 109 | 111 | 112 | 110 | 126 | 128 | 128 | 126 | 150/−150 | 235/−200 |
| Planar array | −60 | −50 | −50 | −50 | −52 | −50 | −44 | −45 | −40 | 275/−225 | 280/−255 |
| A/SPP mast | −114 | −84 | −88 | −88 | −90 | [a] | [a] | [a] | [a] | 264/−225 | — |
| Spaceframe and substructure | | | | | | | | | | | |
| Upper spaceframe | | | | | | | | | | | |
| Near leg 1 | 73 | 60 | 53 | 57 | 52 | 56 | 59 | 59 | 63 | 160/−140 | — |
| Near leg 2 | −70 | −79 | −81 | −82 | −84 | −82 | −82 | −80 | −78 | 160/−140 | — |
| Lower spaceframe | | | | | | | | | | | |
| Under compartment B | 46 | 48 | 42 | 43 | 38 | 39 | 40 | 40 | 46 | 160/−140 | — |
| Under compartment A | −21 | −27 | −24 | −32 | −34 | −31 | −25 | −25 | −26 | 160/−140 | — |
| Flight control | | | | | | | | | | | |
| Flight control electronics | | | | | | | | | | | |
| Chassis board 1 | 100 | 90 | 90 | 71 | 66 | 67 | 68 | 65 | 74 | 150/0 | 165/−20 |
| Chassis board 6 | 135 | 124 | 137 | 60 | 59 | 61 | 62 | 60 | 63 | 127/30 | 132/0 |
| Canopus sensor | 90 | 78 | 85 | 74 | 76 | 70 | 73 | 68 | 74 | 130/−20 | 145/−20 |
| Gyros | | | | | | | | | | | |
| Roll[c] | 178 | 170 | 175 | 173 | 175 | 175 | 173 | 175 | 175 | 185/165 | 190/120 |
| Pitch[c] | 175 | 175 | 175 | 172 | 175 | 174 | 173 | 174 | 173 | 185/165 | 190/120 |
| Yaw[c] | 177 | 180 | 174 | 172 | 174 | 174 | 173 | 174 | 173 | 185/165 | 190/120 |
| Roll actuator | 98 | 79 | 82 | 83 | 80 | 80 | 94 | 83 | 92 | 190/10 | 200/0 |
| Nitrogen tank | 71 | 45 | 40 | 50 | 41 | 45 | 52 | 53 | 60 | 130/0 | 135/−10 |
| Attitude control jet 2 | 87 | 88 | 86 | 105 | 91 | 94 | 103 | 95 | 97 | 150/−40 | 160/−50 |
| Radars | | | | | | | | | | | |
| RADVS | | | | | | | | | | | |
| KPSM | 22 | 12 | 11 | 17 | 18 | 20 | 23 | 22 | 22 | 100/−22 | 125/−49 |
| SDC | 53 | 56 | 63 | 55 | 53 | 60 | 66 | 63 | 64 | 105/15 | 125/5 |
| VS preamplifier | 32 | 22 | 14 | 16 | 15 | 16 | 27 | 16 | 22 | 122/−58 | 122/−58 |
| A/VS preamplifier | 45 | 33 | 20 | 27 | 36 | 25 | 34 | 34 | 35 | 122/−58 | 122/−58 |
| Altitude marking radar | | | | | | | | | | | |
| Electronics[a] | 21 | 15 | 18 | 17 | 15 | 22 | 19 | 20 | 11 | 125/10 | — |
| Electronics platform[c] | 0 | −12 | −14 | 3 | −7 | −6 | 2 | −5 | −4 | 100/−25 | 105/−30 |
| Edge of dish | −160 | −185 | −191 | −202 | −183 | [a] | [a] | [a] | [a] | 200/−300 | 300/−300 |

## Table XV-12 (contd)

| Flight sensor location by subsystem | Transit temperature (steady state, except as noted), °F | | | | | | | | | Temperature limits, °F | |
|---|---|---|---|---|---|---|---|---|---|---|---|
| | *Surveyor I* | | *Surveyor II* | *Surveyor III* | *Surveyor IV* | *Surveyor V* | *Surveyor VI* | *Surveyor VII* | | | |
| | Predicted | Actual | Actual | Actual | Actual | Actual | Actual | Predicted | Actual | Operational | Survival |
| Propulsion | | | | | | | | | | | |
| Vernier engine thrust chamber assemblies | | | | | | | | | | | |
| No. 1 | 76 | 59 | 54 | 58 | 50 | 60 | 65 | 60 | 72 | 145/5 | — |
| No. 2 | 81 | 72 | 84 | 81 | 80 | 72 | 80 | 80 | 74 | 145/5 | — |
| No. 3 | 62 | 59 | 63 | 69 | 66 | 68 | 73 | 65 | 78 | 145/5 | — |
| Propellant tanks[d] | | | | | | | | | | | |
| Oxidizer 1 | 74/45 | 75/41 | 76/50 | 76/41 | 75/42 | 75/39 | 76/44 | 76/41 | 77/42 | 100/0 | 120/−10 |
| Fuel 1 | 73/48 | 76/52 | 77/57 | 76/55 | 76/56 | 75/57 | 76/52 | 76/55 | 76/54 | 100/0 | 120/−10 |
| Oxidizer 2 | 74/35 | 77/24 | 75/35 | 75/18 | 76/19 | 74/14 | 74/21 | 74/21 | 77/14 | 100/0 | 120/−10 |
| Fuel 2 | 74/30 | 75/34 | 83/47 | 74/33 | 76/32 | 72/25 | 74/29 | 74/29 | 76/29 | 100/0 | 120/−10 |
| Oxidizer 3 | 73/45 | 79/40 | 75/46 | 77/30 | 76/42 | 74/34 | 76/38 | 76/39 | 77/41 | 100/0 | 120/−10 |
| Fuel 3 | 73/51 | 76/53 | 75/53 | 76/52 | 76/51 | 75/13 | 76/53 | 76/53 | 76/54 | 100/0 | 120/−10 |
| Propellant lines | | | | | | | | | | | |
| Engine 1 oxidizer | 35 | 26 | 23 | 30 | 39 | 30 | 51 | 32 | 37 | 110/0 | 145/−10 |
| Engine 2 oxidizer[c] | 24 | 24 | 14 | 21 | 20 | 20 | 23 | 23 | 23 | 110/0 | 145/−10 |
| Engine 3 oxidizer[d] | 30 | 24 | 24 | 22 | 20 | 23 | 20 | 23 | 23 | 110/0 | 145/−10 |
| Engine 1 fuel | [a] | [a] | [a] | [a] | [a] | 60 | 54 | 60 | 58 | 110/0 | 145/−10 |
| Engine 2 fuel[c] | [a] | [a] | [a] | [a] | [a] | 25 | 28 | 27 | 25 | 110/0 | 145/−10 |
| Engine 3 fuel[c] | [a] | [a] | [a] | [a] | [a] | 71 | 58 | 61 | 63 | 110/0 | 145/−10 |
| Helium tank | 75 | 60 | 72 | 73 | 76 | 79 | 84 | 80 | 84 | 110/0 | 110/−10 |
| Main retro motor[d] | | | | | | | | | | | |
| Upper case | 74/67 | 73/67 | 72/73 | 73/64 | 74/66 | 74/64 | 74/66 | 74/66 | 76/66 | 75/55 | 100/10 |
| Lower case | 74/36 | 74/46 | 76/59 | 78/41 | 76/44 | 76/43 | 76/41 | 76/42 | 78/42 | 75/35 | 100/10 |
| Nozzle | −222 | −124 | −118 | −130 | −127 | −123 | −122 | [a] | [a] | 300/−300 | — |
| Retro-motor attach points | | | | | | | | | | | |
| Leg 1 | 46 | 39 | 44 | 42 | 37 | 38 | 42 | 42 | 43 | 120/−95 | 140/−100 |
| Leg 2 | −21 | −36 | −32 | −52 | −53 | −41 | −37 | −52 | −47 | 120/−95 | 140/−100 |
| Leg 3 | 46 | 44 | 44 | 46 | 37 | 41 | 41 | 40 | 46 | 120/−95 | 140/−100 |
| Survey TV | | | | | | | | | | | |
| TV 3 mirror assembly | −162 | −120 | −120 | −120 | −126 | −126 | −125 | −120 | −115 | 180/−50 | 180/−200 |
| TV 3 ECU | −150 | −134 | −128[b] | −128 | −130 | −136 | −136 | −136 | −128 | 160/−20 | 250/−150 |
| Surface-sampler experiment | | | | | | | | | | | |
| Auxiliary electronics[c] | [a] | [a] | [a] | −35 | −35 | [a] | [a] | 6 | 6 | — | 200/−67 |
| Substructure | [a] | [a] | [a] | [a] | −104 | [a] | [a] | [a] | [a] | 0 | — |
| Retraction motor | [a] | [a] | [a] | [a] | [a] | [a] | [a] | −90 | −58 | — | 257/−180 |
| Elevation motor | [a] | [a] | [a] | [a] | [a] | [a] | [a] | −92 | −59 | — | 257/−180 |
| Alpha scattering experiment | | | | | | | | | | | |
| Instrument | [a] | [a] | [a] | [a] | [a] | 35 | 44 | 35 | 38 | 122/−40 | 167/−130 |
| Compartment C electronics | [a] | [a] | [a] | [a] | [a] | −20 | −10 | −10 | −3 | 131/−4 | 185/−67 |
| Approach television | −140 | −124 | −106 | [a] | [a] | [a] | [a] | [a] | [a] | 165/−20 | 250/−180 |

[a]Sensor not on spacecraft.
[b]Steady state not obtained.
[c]Mean cycling temperatures.
[d]Launch temperature/touchdown temperature for *Surveyors I, III, IV, V, VI,* and *VII*; launch temperature/midcourse temperature for *Surveyor II*.

flight are included in the documents listed under Refs. XV-4 through XV-10 and, for selected sensors, in Refs. XV-11 through XV-17. An important feedback from the flight results was that, in flight, the spacecraft behaved as if the solar simulation were slightly below the one-sun level in the test chamber. This is shown in Table XV-13, where flight-phase performance for *Surveyors I* and *III* is compared with STV data for *Surveyor I*, in the HAC chamber, and for S-10 in the JPL and the HAC chambers. The most important difference between the HAC and the JPL chamber tests is believed to be the difference in spectrum of the simulators. This information enabled more accurate prediction of flight-phase performance for the later spacecraft and a reduction in the prediction tolerances. This result has also been confirmed by the work of Drummond and associates (Ref. XV-18).

The retro motor and the vernier propellant tanks, in general, could not be passively temperature-controlled to a steady-state temperature within their operational limits during the flight phase.

The retro motor was covered with multilayer insulation and was instrumented at two points on the upper and lower case. Gradients through the propellant were important, but the most significant item was the bulk temperature of the propellant at the time of retro motor ignition with an optimum value of 55°F. Figure XV-15 shows the envelope of the results obtained from the six spacecraft, which operated successfully until retro motor ignition; the temperature limits for the upper and lower case; the bulk temperatures at retro motor ignition; and the optimum bulk temperature at retro motor ignition. It will be noted that the average spread of temperature for all of the spacecraft was 3°F, and that this spread also covered the bulk temperature at ignition although the flight durations varied by 4.5 hr, indicating very good reproducibility in the thermal wrap of the main retrorocket.

The vernier propellant fuel and oxidizer tanks were covered with varying numbers of insulation layers, depending upon the degree of shading they experienced in cruise configuration. In addition, the two tanks which were completely shaded by the solar panel, fuel 2 and oxidizer 2, and the tank largely shaded by the signal data converter, oxidizer 3, were fitted with thermostatically controlled electric heaters. The envelope of the results obtained from all of the spacecraft, omitting the data obtained from *Surveyor II* after midcourse, is shown in Figs. XV-16 through XV-21. On the plots for the fuel tanks (Figs. XV-16 through XV-18), the maxima (see Subsection C-2) occurring between launch plus 15 hr and launch plus 40 hr were caused by the midcourse maneuver firings, while the maximum occurring at launch plus 58 hr was due to the 360-deg yaw maneuver carried out with *Surveyor V* for the special landing sequence calibration for this spacecraft. The small peaks occurring before midcourse for the oxidizer tanks, shown in Figs. XV-19 through XV-21, were caused by the star search maneuver. The fuel, being more viscous, did not show this effect. Again, it will be noted that the total spread for the transients of the six propellant tanks was small, demonstrating good reproducibility of the thermal wrapping.

**Table XV-13. Flight and STV temperature comparisons**

| Component | Flight phase, °F | | Temperatures during solar thermal vacuum test, °F | | |
|---|---|---|---|---|---|
| | *Surveyor I* | *Surveyor III* | *Surveyor I* | JPL S-10 phase II (approximate change from Surveyor I) | HAC S-10 phase II (approximate change from JPL S-10, phase II) |
| Vernier engine 1 | 59 | 58 | 80 | +10 | +5 |
| Vernier engine 2 | 72 | 81 | 107 | −10 | +5 |
| Vernier engine 3 | 59 | 69 | 84 | 0 | +5 |
| Helium tank | 60 | 73 | 74 | +5 | +15[a] |
| Nitrogen tank | 45 | 50 | 86 | +5 | +10 |
| Compartment A | | | | | |
| Upper tray | 70 | 49 | 72 | +10 | +5 |
| Lower tray | 93 | 70 | 88 | +10 | +5 |
| Compartment B | | | | | |
| Upper tray | 93 | 76 | 89 | +10 | +5 |
| Lower tray | 98 | 81 | 91 | +10 | +5 |

[a]Paint pattern changed.

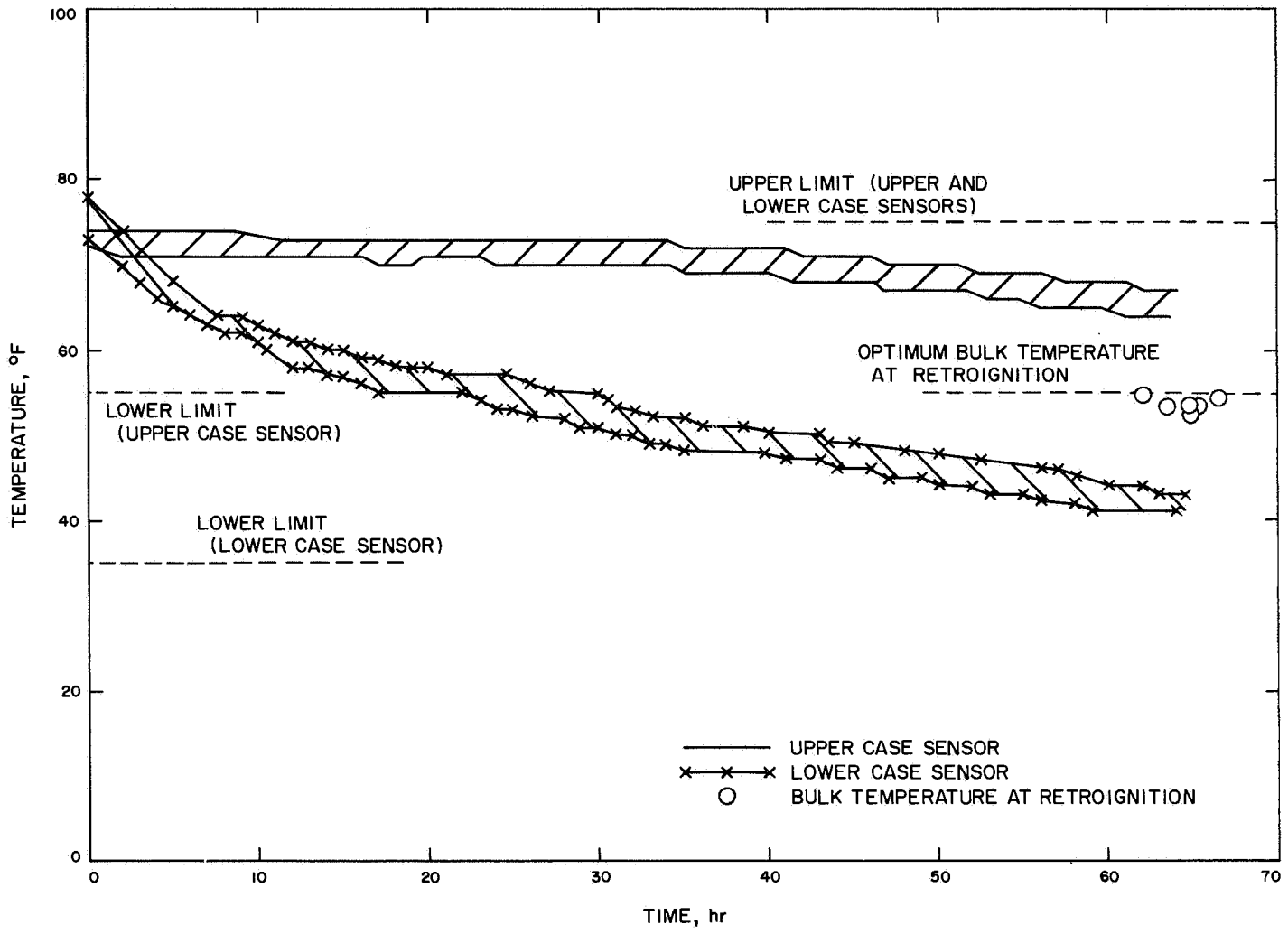



**Fig. XV-15. Retro motor: flight temperature ranges for *Surveyors I* through *VII* (except *Surveyor II*)**

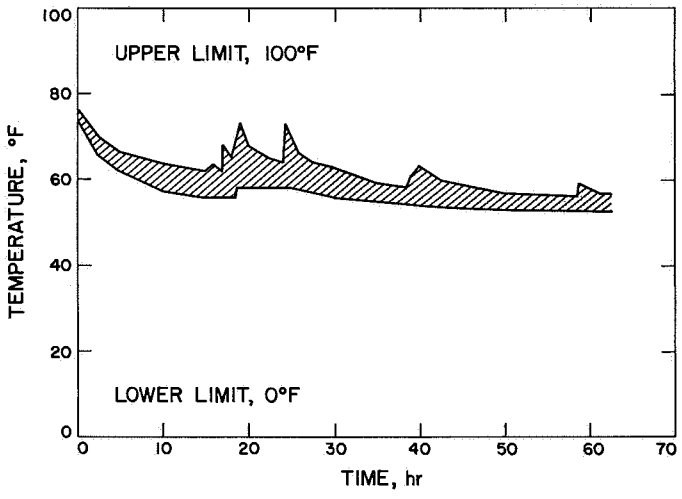



**Fig. XV-16. Fuel tank 1: flight data envelope for *Surveyors I* through *VII* (*Surveyor II* through midcourse only)**

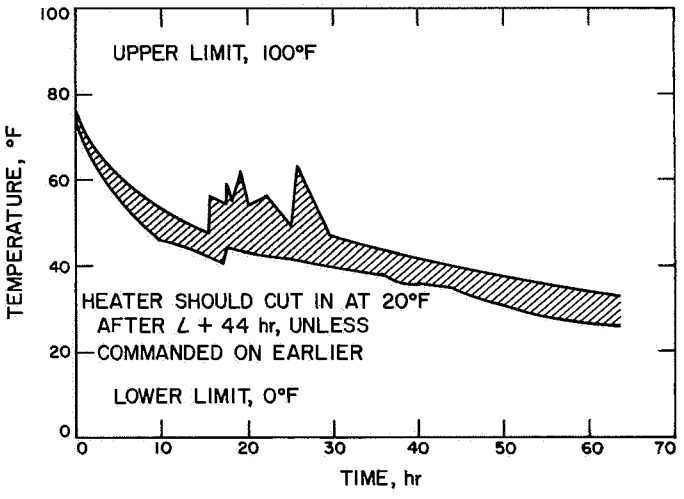



**Fig. XV-17. Fuel tank 2: flight data envelope for *Surveyors I* through *VII* (*Surveyor II* through midcourse only)**

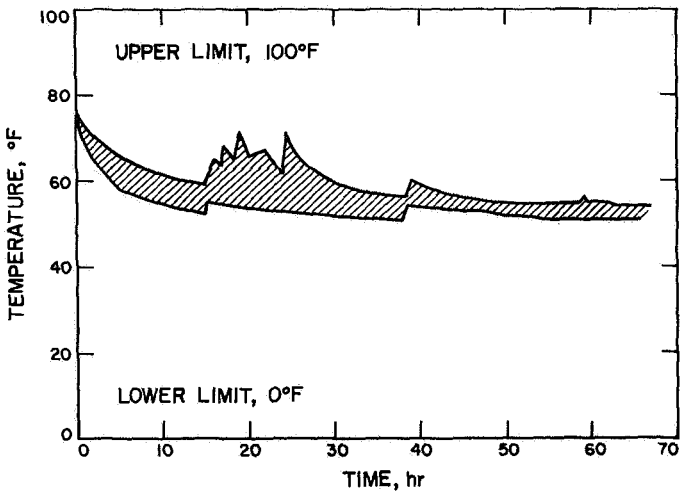



**Fig. XV-18. Fuel tank 3: flight data envelope for *Surveyors I* through *VII* (*Surveyor II* through midcourse only)**

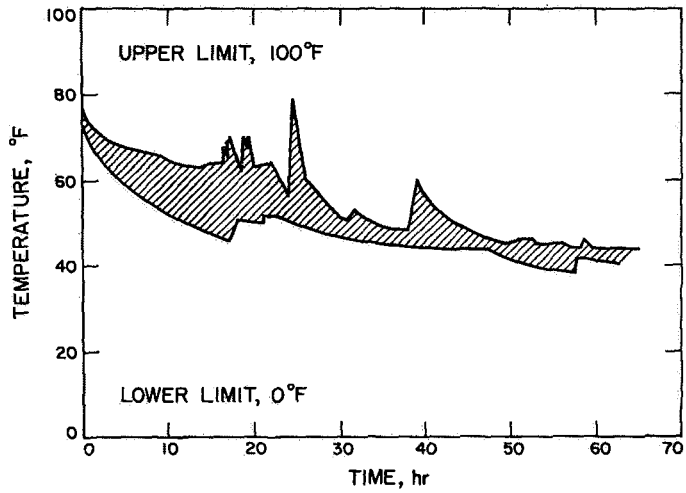



**Fig. XV-19. Oxidizer tank 1: flight data envelope for *Surveyors I* through *VII* (*Surveyor II* through midcourse only)**

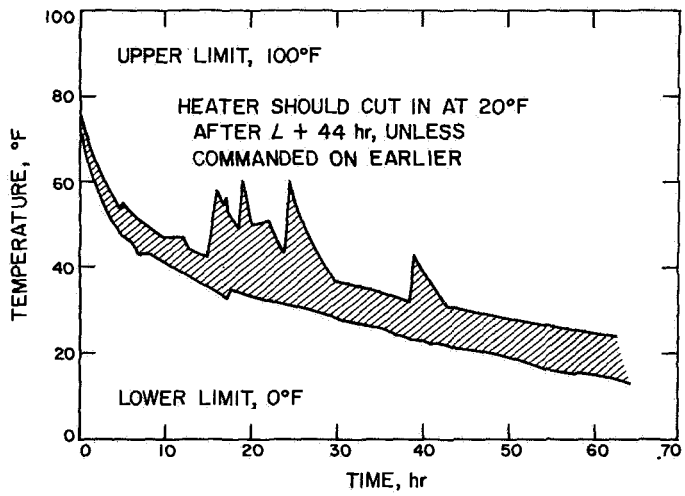



**Fig. XV-20. Oxidizer tank 2: flight data envelope for *Surveyors I* through *VII* (*Surveyor II* through midcourse only)**

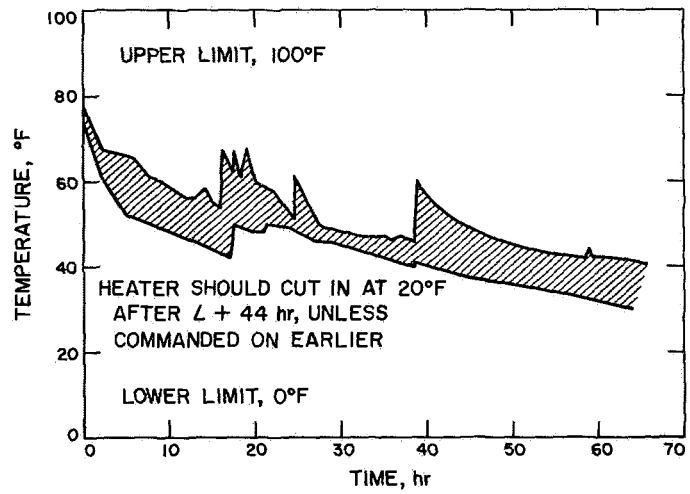



**Fig. XV-21. Oxidizer tank 3: flight data envelope for *Surveyors I* through *VII* (*Surveyor II* through midcourse only)**

### 2. Flight-Phase Results Leading to Spacecraft Modifications and Unexpected Flight-Phase Results

Two significant changes were made in the thermal control of *Surveyor* as a direct result of data obtained during the flight phase of the missions. These affected the auxiliary battery, flown only on the first four spacecraft, and the heaters for vernier line 2.

Before the launch of *Surveyor I*, the auxiliary battery had been predicted to cool to a steady-state unenergized temperature of 60°F. The flight-phase data indicated a steady-state temperature of 35°F. Review of the *Surveyor I* STV data indicated that the solar intensity simulated in test was higher than that encountered in the flight phase. The auxiliary battery thermal finish pattern of *Surveyor III* was changed to increase the predicted steady-state transit temperature by 30°F. The battery steady-state temperature was 28°F higher during phase IA of *Surveyor III* testing, compared to that obtained at the same solar intensity in *Surveyor II* testing. Because the design change goal was achieved, *Surveyor II* was modified before encapsulation. The failure of *Surveyor II* during the midcourse maneuver occurred before steady-state temperature was attained on the auxiliary battery; but *Surveyor III* and *IV* steady-state temperature of 54 and 60°F were very close to the design goal.

The flight data from *Surveyor II* indicated anomalous behavior of the vernier line 2 heater. It had cycled continuously during the flight phase of *Surveyor I*, but, as seen in Fig. XV-22, developed a steadily increasing cycle time for the first 7 hr of the flight phase of *Surveyor II*. The heater finally stayed on for the remainder of the time until the midcourse maneuver while the line temperature, after rising 3°F initially, fell continuously. This led to redesign of the temperature control of this line, which is described in Subsection B.

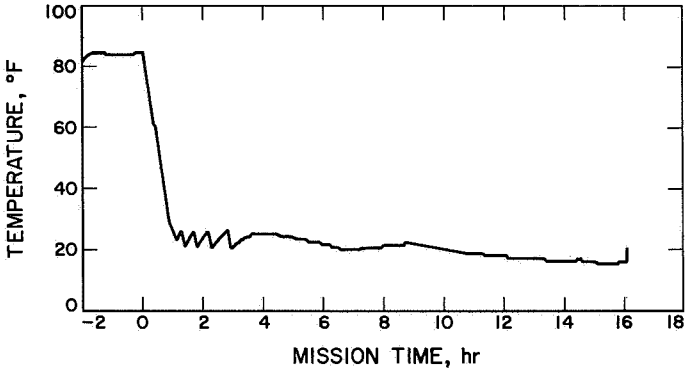



**Fig. XV-22. Vernier line 2 temperature history on *Surveyor II***

Another result from the flight-phase data that leads to some interesting conclusions is shown in Figs. XV-23 and XV-24. The most prominent feature is the sharp rise in temperature of both the fuel and the oxidizer tanks during the midcourse maneuver, while a more subtle feature was a slight rise in temperature of the oxidizer tank during the star mapping.

During the flight phase, both the fuel and oxidizer were cooled in an environment without the gravity effects that induce forces within a fluid which is cooling in a gravity field. The fluids cooled, as do solid bodies, with a thermal gradient from the part of the fluid in contact with the tank to the portion of the fluid remote from the metal. In addition, a standpipe runs from the center of the bottom of the tank almost to the top, causing a complex thermal field through the body of the fluid in the undisturbed state.

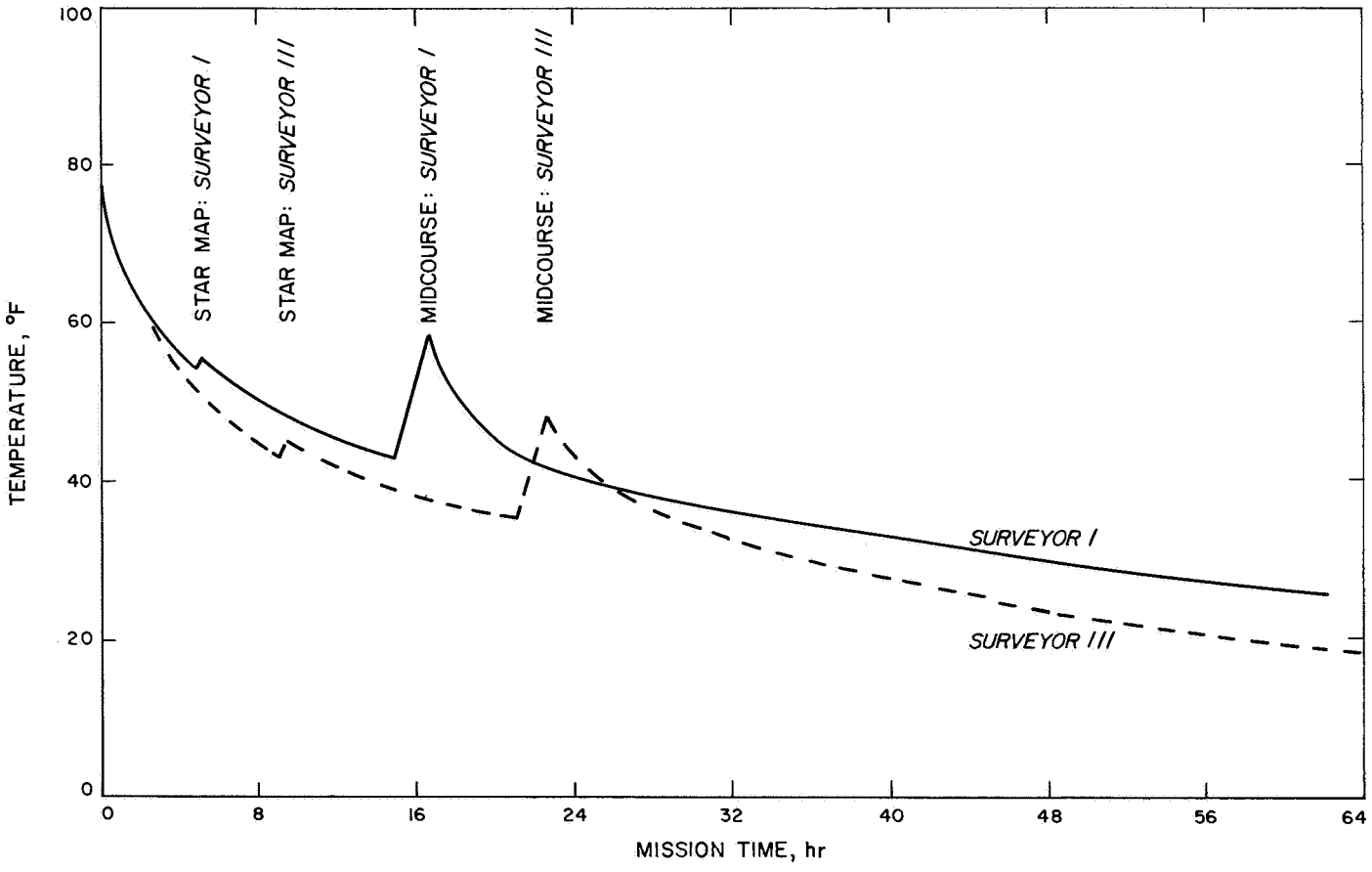



**Fig. XV-23. Transit thermal performance of vernier oxidizer tank 2**

During the midcourse maneuver, the spacecraft was rotated about at least two axes, producing accelerations within the fluids; and the engines caused an acceleration along the spacecraft Z axis. This mixed the parts of the fluid at different temperatures and densities. The sensor, mounted near the bottom of the standpipe, indicated a temperature immediately after the maneuver which was closer to the true bulk temperature of the fluid than at any other time during the flight phase.

The effect of these accelerations and body forces is also shown in the star mapping, a purely rolling maneuver, although in this case it affected only the oxidizer. The fuel, which is far more viscous, moved as a solid body and showed no change in temperature which could be detected by the telemetry. A similar effect showed up immediately after landing, when the more severe accelerations during retro firing and landing caused sufficient mixing of the fluids for the sensors to read the true bulk temperature of all propellant tanks.

### 3. Postlanding Performance During the Lunar Day

The behavior of certain units on the lunar surface is shown in Figs. XV-25 through XV-29. Note that the sun elevation angle is measured from 0 at dawn to 180 deg at sunset. For information on the behavior of additional units, see Refs. XV-1 and XV-10 through XV-17. For the detailed behavior of all units on the lunar surface, see Refs. XV-4 through XV-10. The battery (Fig. XV-25) was well within the temperature limits for most of the spacecraft during most of the first lunar day. The effect of one or more freezings during successive lunar nights is shown by the fact that *Surveyors I* and *VII* exceeded their upper operational and survival limits during the second lunar day.

The television camera electronics temperature is shown in Fig. XV-26. The upper and lower operational limits were not exceeded throughout the day. The lunar noon limitation on camera operation was based on the duty cycle temperatures on the vidicon, not on the electronics.

The alpha scattering instrument sensor head and electronics are shown in Figs. XV-27 and XV-28. Operations had to be stopped periodically because of excessive temperatures. The data for *Surveyor VI* are shown as a dotted line in Fig. XV-27 beyond 93-deg sun elevation, since the hop test occurred at this sun angle; and, on landing again, the sensor head was lying on its side. The *Surveyor VII* sensor head was moved twice after initial deployment; these points are shown at sun angles of 160 and 168 deg.

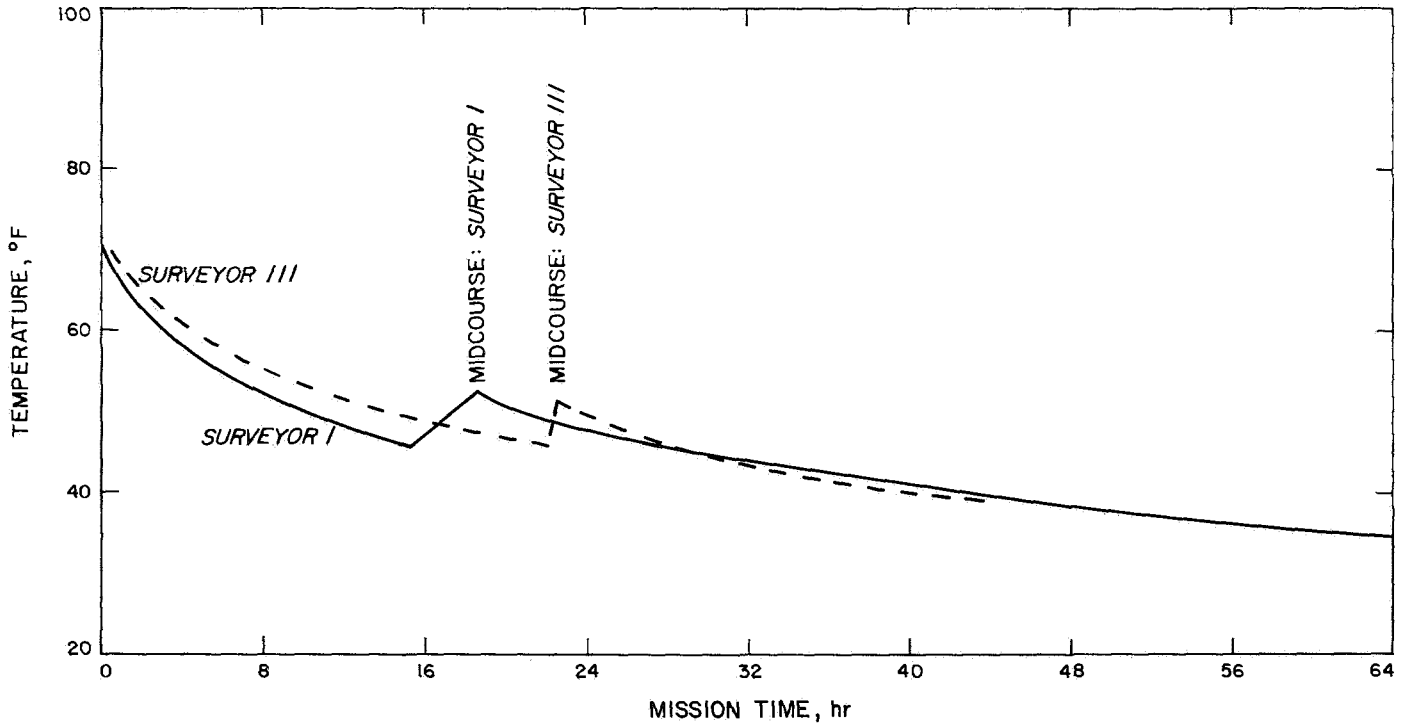



**Fig. XV-24. Transit thermal performance of vernier fuel tank 2**

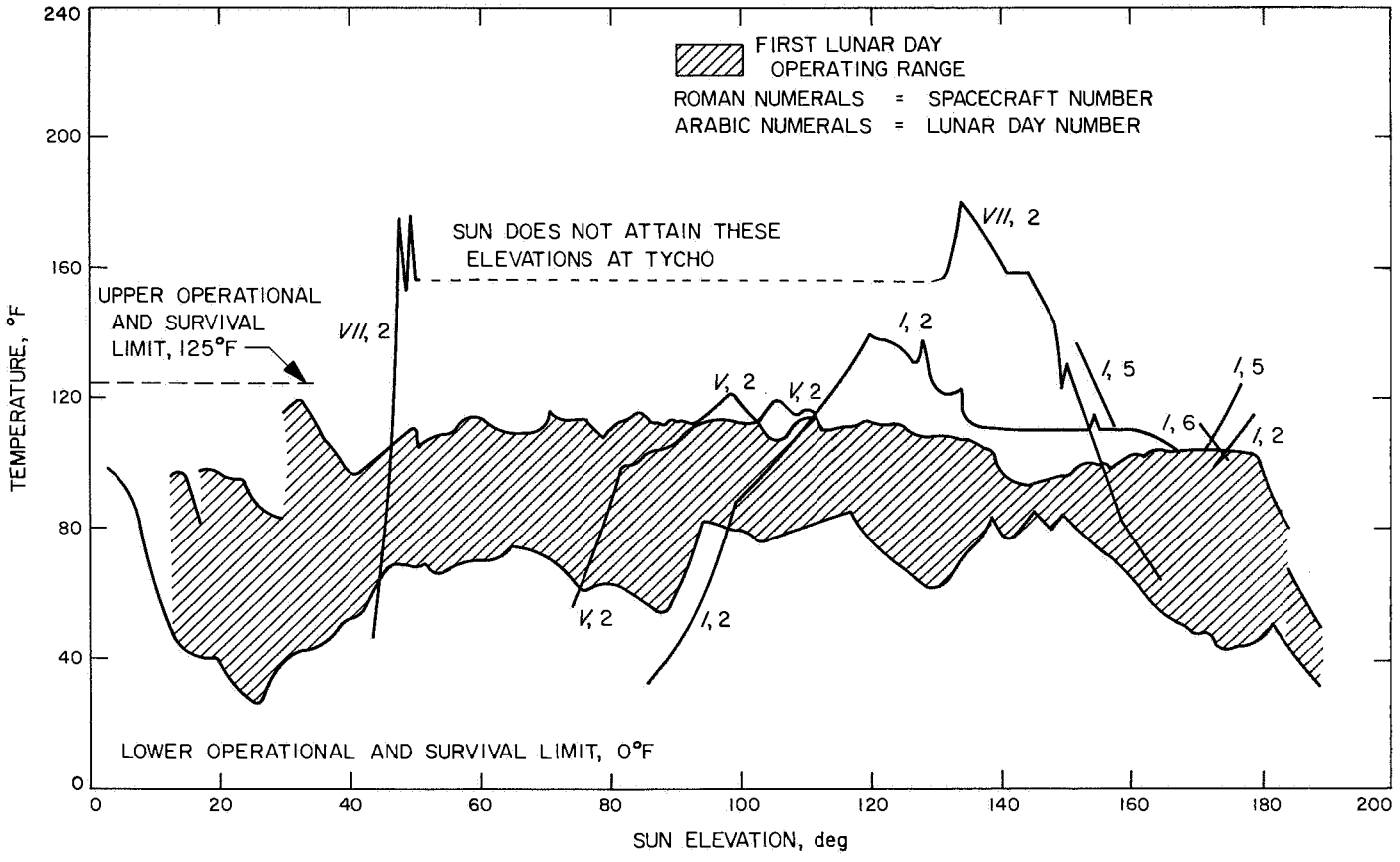



**Fig. XV-25. Battery: lunar surface performance**

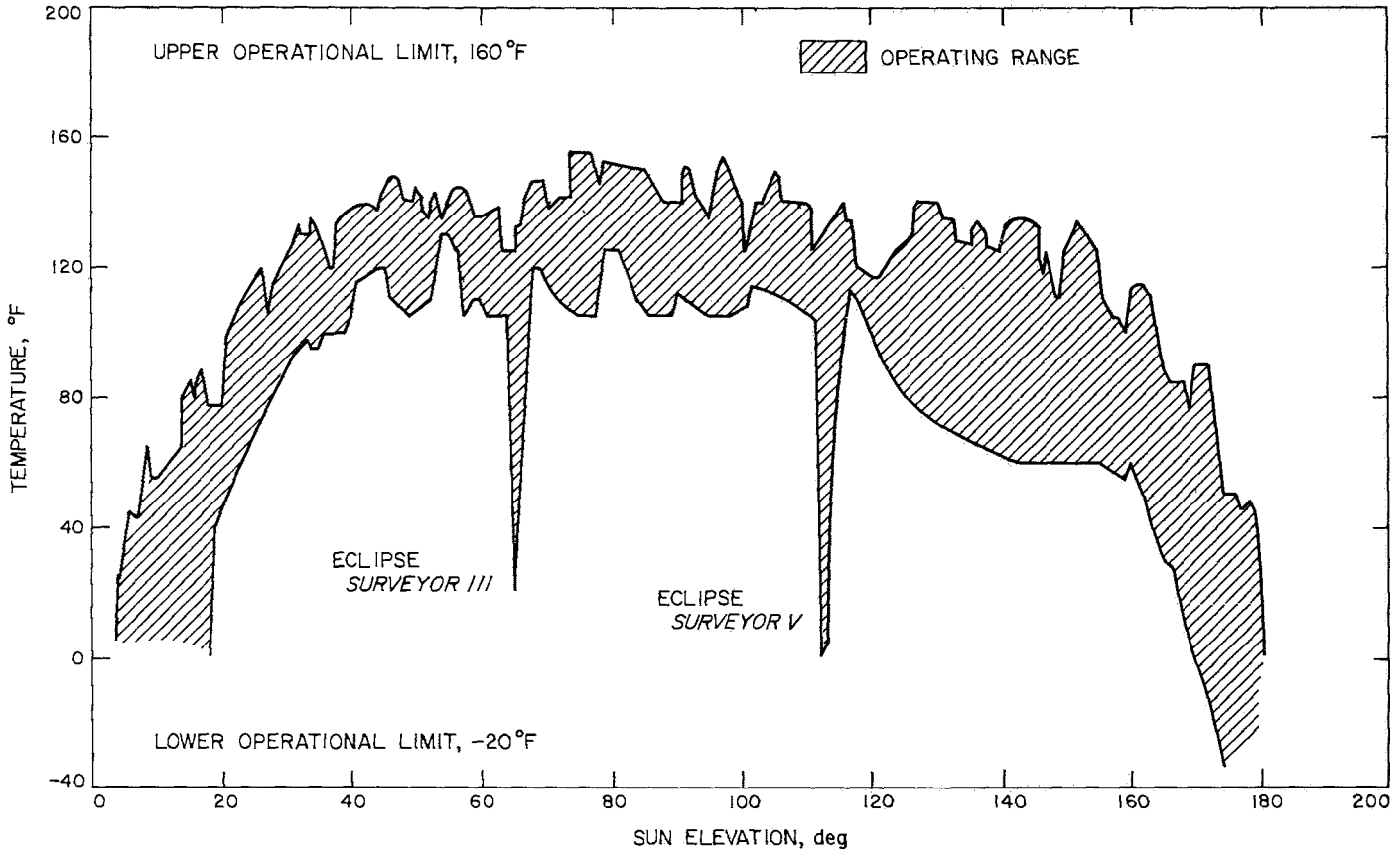



**Fig. XV-26. Survey television camera electronics temperatures: lunar surface performance**

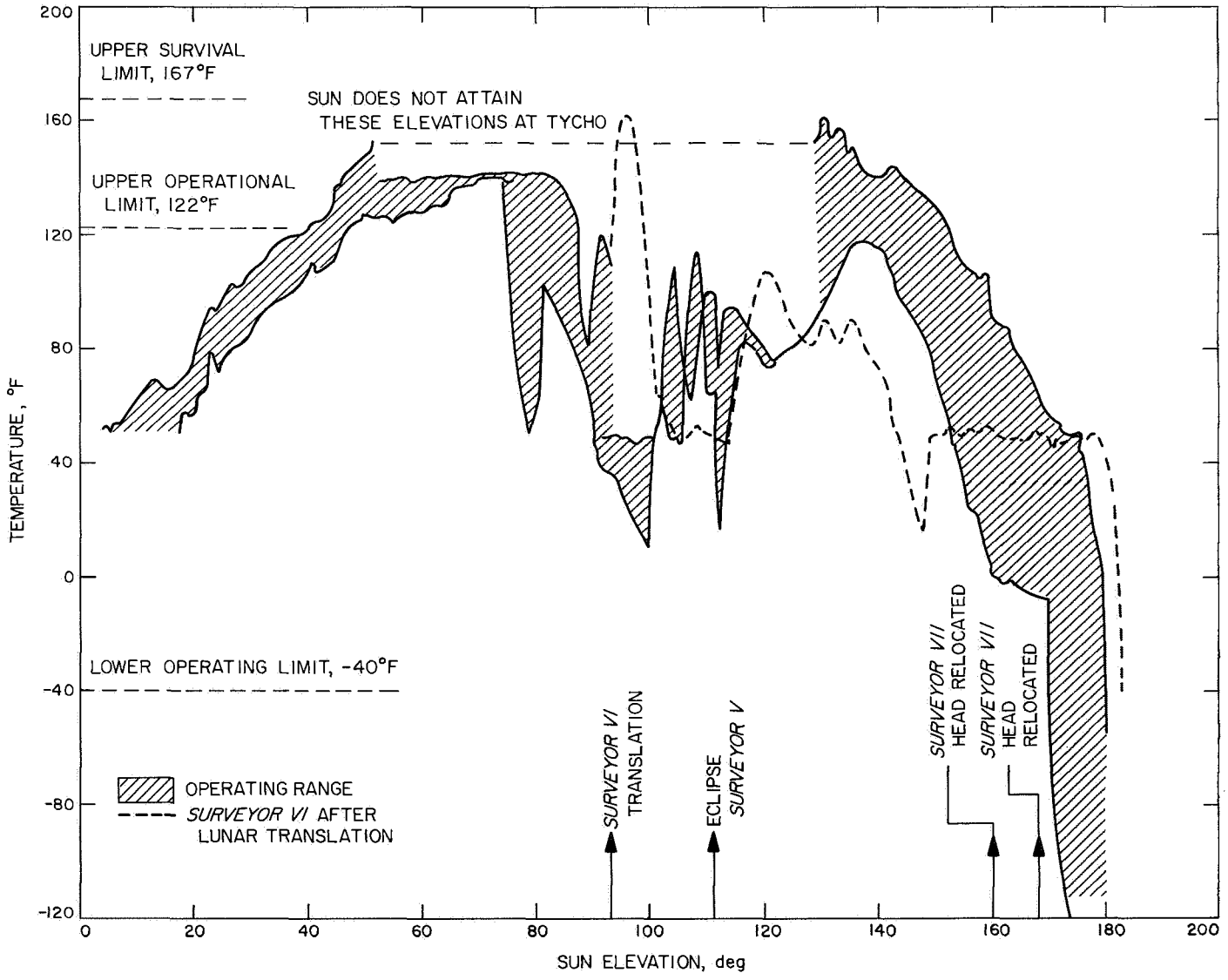



**Fig. XV-27. Alpha scattering instrument sensor head: lunar surface performance**

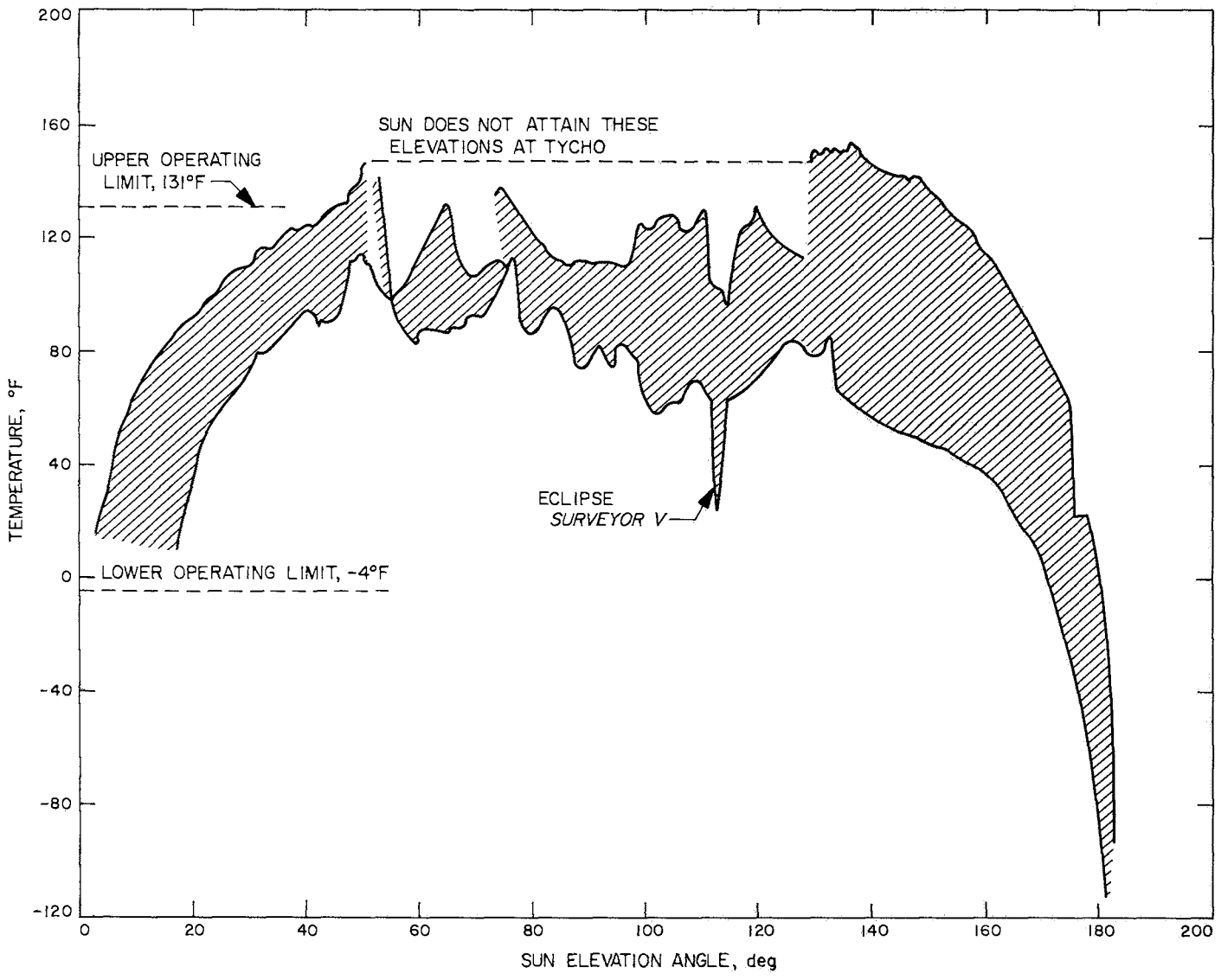



**Fig. XV-28. Alpha scattering instrument electronics: lunar surface performance**

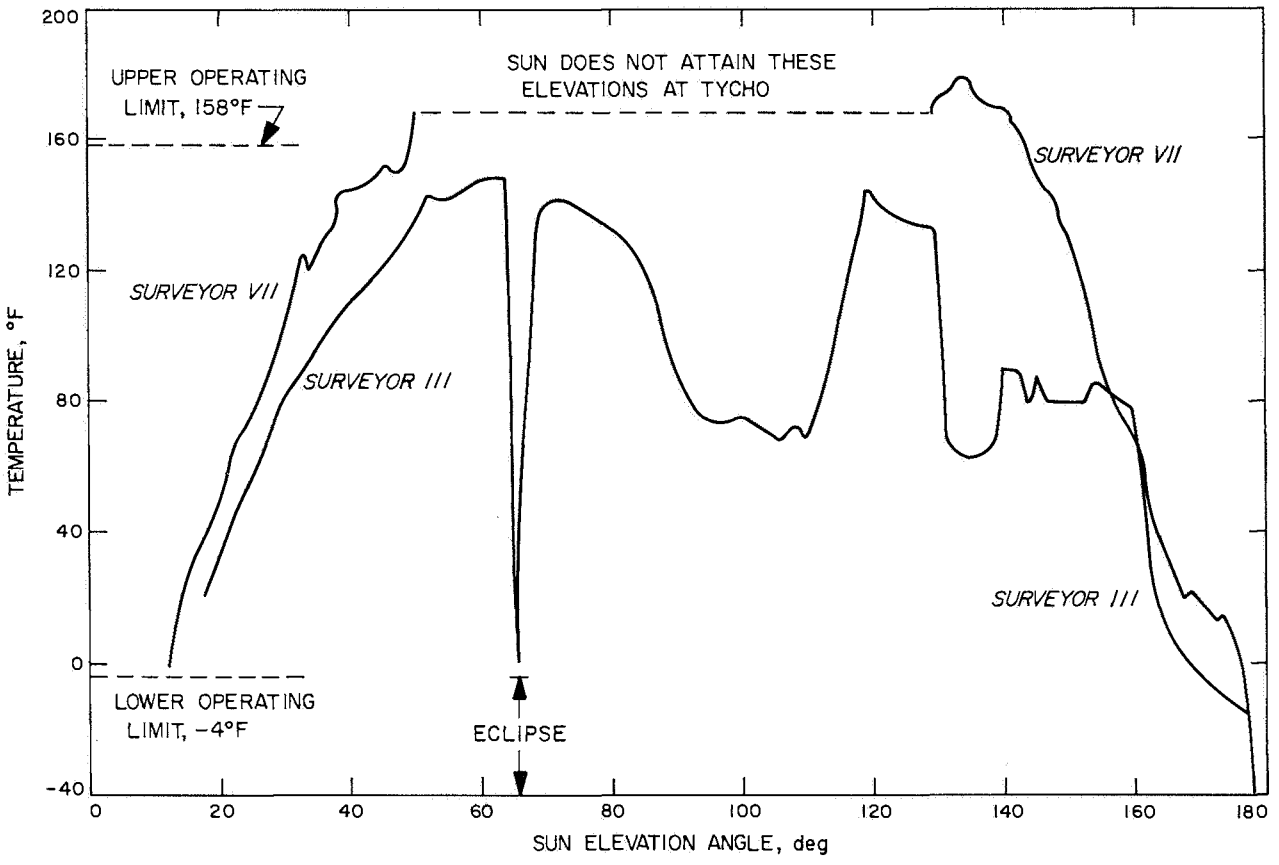



**Fig. XV-29. Soil mechanics/surface sampler auxiliary electronics: lunar surface performance**

The surface-sampler electronics are shown in Fig. XV-29. This instrument was flown successfully on *Surveyors III* and *VII*. On *Surveyor III*, the upper operating temperature never was exceeded; but for a period close to local noon on the *Surveyor VII* mission, operation had to be stopped because of temperatures above the upper operating limit.

Since, close to lunar noon, the television camera, the alpha scattering instrument, and the surface sampler were very near or above their upper operating temperature limits, the spacecraft were placed in standby operations. Shading from the solar panel and planar array considerably extended the period of time before and after noon that certain of these instruments and the compartments could be operated. This shading also was vital to the accomplishment of the static firing of the vernier engines for *Surveyor V* and the hop of *Surveyor VI* (by use of the vernier propulsion system), where shading was needed on the engines, the helium check and relief valve, and the FCSG.

A shadow plot computer program was used to generate shadow plots as a function of sun elevation angle for any orientation of the solar panel and planar array. A sample of these shadow plots is shown in Fig. XV-30. A second method, and a check on the shadow plots, was use of a one-fifth-scale model of the spacecraft and a collimated light source. The plots were usually generated after landing, using as inputs the real conditions of slopes, roll orientation, sun azimuth and elevation, and possible A/SPP positions. Utilizing the shadow plots and the JPL *Surveyor* Experiment Test Laboratory facilities, the possibility of shading certain areas could be determined. Whenever possible, spacecraft television pictures of shaded areas were used to verify the validity of recommended shading positions after the A/SPP was repositioned.

A comparison between the results obtained with S-10 in the HAC C-4 chamber with the lunar surface simulator and *Surveyors I* and *III* at lunar noon is shown in Table XV-14. This indicates good agreement between the sensors on most of the spacecraft and the S-10 data.

**Table XV-14. Spacecraft sensor temperatures (°F) at lunar noon, compared with solar-thermal-vacuum test results**

| Component | Surveyor I[a] | Surveyor III | Surveyor V | Surveyor VI | S-10 and lunar surface simulator | Component | Surveyor I[a] | Surveyor III | Surveyor V | Surveyor VI | S-10 and lunar surface simulator |
|---|---|---|---|---|---|---|---|---|---|---|---|
| Vernier engine 1 | 216 | 226 | 235 | 220 | 234 | Signal data converter | 145 | 155 | 160 | 130 | 123 |
| Vernier engine 2 | 226 | 224 | 180 | 210 | —[b] | | | | | | |
| Vernier engine 3 | 211 | 225 | 160 | 193 | 227 | Crushable block heat shield | 160 | 180 | 173 | 162 | 236 |
| Helium tank | 149 | 170[c] | 113 | 125 | 169 | | | | | | |
| Nitrogen tank | 165 | 170[d] | 125 | 110 | 194 | Auxiliary battery case | 190 | Shaded | Not fitted | Not fitted | 196 |
| Flight control sensor group | 187 | 200 | 166 | 180 | 205 | | | | | | |
| Klystron power supply and modulator | 201 | 218 | 223 | 195 | 235 | Television camera | 133 | Shaded | 135 to 150 | Shaded | 82 |

[a]*Surveyor I* data combine first and second lunar day information.
[b]Lost instrumentation during test.
[c]33⅓% increase in *Surveyor III* black paint over *Surveyor I*.
[d]Nitrogen tank shadowed.

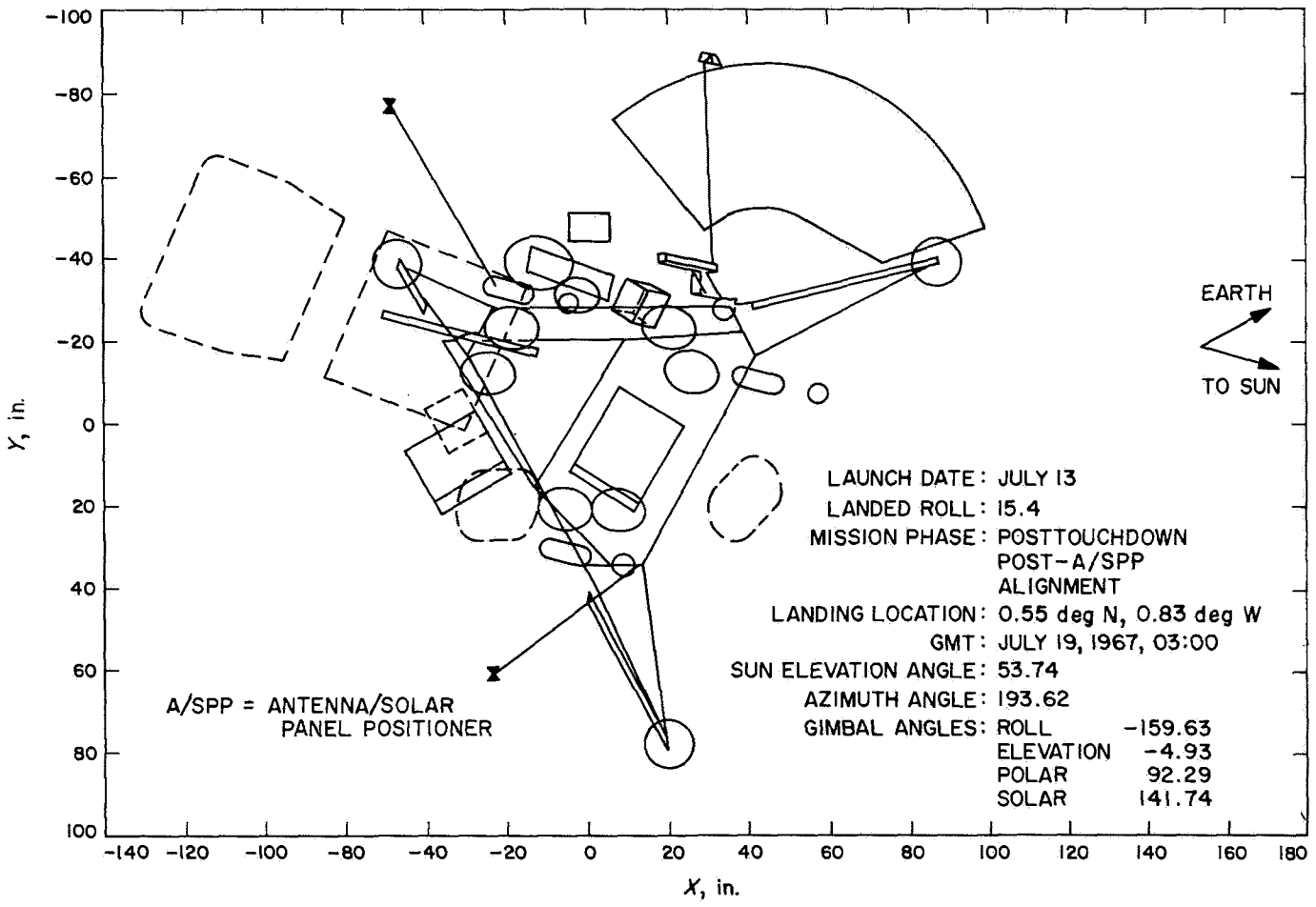



**Fig. XV-30. Typical output of shadow plot computer program**

Much of the discrepancy between ground test results and lunar surface data can be explained by variations in the solar intensity in the chamber, view factor to the lunar surface simulator, normal variations between spacecraft, or by the fact that many times the lunar surface data were in the middle of a transient due to shadowing. *Surveyor VII* data are not included since, at lunar noon, the solar elevation above the local (flat) horizon was only 50.5 deg; therefore, the results are not comparable to those obtained with a lunar noon sun elevation of 90 deg.

#### 4. Postlanding Performance During Lunar Night

*a. Supercooling of fuel.* *Surveyor V* telemetry data of fuel temperature "into the night" were surprising. In the vicinity of −110°F, each of the temperature curves rose rapidly to a plateau at about −80°F, then dropped at a different rate, showing that the fuel was supercooling. The fuel was a monohydrate of monomethylhydrazine (72% MMH and 28% $H_2O$ by weight) with an equilibrium freezing temperature of −78°F.

The temperature history of the fuel in tanks 1, 2, and 3 showed that the minimum points of the supercooling curves were −118, −110, and −115°F, respectively. At these temperatures, nucleation took place rapidly with evolution of fusion heat. The fuel tanks were insulated with multiple layers of aluminized Mylar, retaining the fusion heat and causing a rapid rise in fuel temperature and, in turn, a decrease in nuclei formation. This continued until thermodynamic equilibrium was reached at fuel temperatures between −80 and −94°F. Thermodynamic equilibrium continued (approximately 15 hr for tank 3) until the heat losses from the tanks allowed crystalline growth to proceed, followed by subsequent decreasing fuel temperatures after all of the fuel was frozen.

During the second lunar night, temperature data indicated that only the fuel in tank 3 experienced supercooling. It is important to note that at the time supercooling was first noticed in tank 3, temperature data were being taken once each 24 hr; therefore, supercooling may have occurred in the other fuel tanks undetected.

This same effect was noted in the data from *Surveyor VII* for fuel tanks 1 and 2; fuel tank 3 had not attained a sufficiently low temperature for this to occur at the time contact was lost with the spacecraft. Supercooling probably occurred on the other spacecraft, but none was interrogated long enough into the lunar night for determination of this effect.

*b. Thermal switch operation.* The performance of the *Surveyor* thermal control subsystem during the lunar night had a direct effect upon spacecraft revival the next lunar day. Equipment sensitive to the night temperature of −250°F was located in the insulated compartments. The battery was used to keep the compartments at or above 0°F for a part of the lunar night, and they cooled during the rest of the night.

Proper operation of the thermal switches was essential to the lunar night thermal performance, but each spacecraft had switches which remained closed well into the lunar night. *Surveyors I, III, V, VI,* and *VII* had the following number of sticking switches: 4, 11, 1, 7, and 2, respectively. The thermal switches were designed to open and reduce the outward heat flow when the compartment temperatures dropped below 65°F in A and 50°F in B on *Surveyor I.* Four switches were changed to 40°F settings in A on *Surveyor II*; all switches were set at 40°F on *Surveyors III* through *VII.* On *Surveyor I,* the compartment heater control was placed on manual mode, and temperatures were allowed to drop to increase the switch-opening bimetal forces. Not all switches responded. The baking process was used in the fabrication of the *Surveyor V* switches, and only one stuck.

Switches on *Surveyor VI* were the same as on *Surveyor V,* but seven were stuck at the last engineering interrogation. The only difference between the *Surveyor V* and *Surveyor VI* switches was the elapsed time after their installation. The *Surveyor V* switches had been closed for 4 mo, while the *Surveyor VI* switches had been closed for about 7 mo. Indications are that time, temperature, and contact pressure are governing factors associated with stuck thermal switches. On *Surveyor VII,* two switches stuck on compartment A at the final engineering interrogation at the conclusion of the first lunar day, and contact was lost before sunset of the second lunar day.

### D. Conclusions

The open system temperature control technique was used successfully to withstand the variable environment imposed by the flight phase of the mission and to make possible surface operation during the lunar day, operation into the lunar night, and, to a lesser extent, lunar night survival. This must be weighed against the added complexity of qualification and analysis.

Thermal switches are very effective temperature control devices when they open at the required set point.

Further work is needed to develop thermal switches of high reliability.

Most of the problems with the open system occurred in exposed items where temperature limits were stringent. One example of this is the propellant lines where it was difficult to maintain the required thermal radiative properties with the amount of handling involved, and reflections varied greatly among the spacecraft.

Indium foil was used successfully in a number of cases where a high-conductance, reproducible thermal path was required.

In any spacecraft program, it is vital to initiate the design and construction of test vehicles, such as the S-10, at a very early stage so that test data can make the maximum contribution to the thermal control development of the flight vehicle.

## References


XV-1. *Surveyor Final Engineering Report,* SSD 78175. Hughes Aircraft Co., El Segundo, Calif., May 1968.

XV-2. Hagemeyer, W. A., "Surveyor White Paint Degradation," *J. Spacecraft Rockets,* Vol. IV, No. 6, pp. 828–829, June 1967.

XV-3. Johnson, F. S., "The Solar Constant," *J. Meteorol.,* Vol. 11, p. 431, Dec. 1954.

XV-4. *Flight Performance, Surveyor I: Final Report,* SSD 68189R. Hughes Aircraft Co., El Segundo, Calif., Oct. 1966.

XV-5. *Flight Performance, Surveyor II: Final Report,* SSD 68189-2R. Hughes Aircraft Co., El Segundo, Calif., Jan. 1967.

XV-6. *Flight Performance, Surveyor III: Final Report,* SSD 68189-3. Hughes Aircraft Co., El Segundo, Calif., July 1967.

XV-7. *Flight Performance, Surveyor IV: Final Report,* SSD 68189-4. Hughes Aircraft Co., El Segundo, Calif., Sept. 1967.

XV-8. *Flight Performance, Surveyor V: Final Report,* SSD 68189-5. Hughes Aircraft Co., El Segundo, Calif., Nov. 1967.

XV-9. *Flight Performance, Surveyor VI: Final Report,* SSD 68189-6. Hughes Aircraft Co., El Segundo, Calif., Dec. 1967.

XV-10. *Flight Performance, Surveyor VII: Final Report,* SSD 68189-7. Hughes Aircraft Co., El Segundo, Calif., Feb. 1968.

XV-11. *Surveyor I Mission Report, Part I: Mission Description and Performance,* Technical Report 32-1023. Jet Propulsion Laboratory, Pasadena, Calif., Aug. 1966.

XV-12. *Surveyor Mission Report: Mission Description and Performance,* Technical Report 32-1086. Jet Propulsion Laboratory, Pasadena, Calif., Apr. 1967.

XV-13. *Surveyor III Mission Report, Part I: Mission Description and Performance,* Technical Report 32-1177. Jet Propulsion Laboratory, Pasadena, Calif., Sept. 1967.

## References (contd)

XV-14. *Surveyor IV Mission Report: Mission Description and Performance,* Technical Report 32-1210. Jet Propulsion Laboratory, Pasadena, Calif., Jan. 1968.

XV-15. *Surveyor V Mission Report, Part I: Mission Description and Performance,* Technical Report 32-1246. Jet Propulsion Laboratory, Pasadena, Calif., Mar. 1968.

XV-16. *Surveyor VI Mission Report, Part I: Mission Description and Performance,* Technical Report 32-1262. Jet Propulsion Laboratory, Pasadena, Calif., Sept. 1968.

XV-17. *Surveyor VII Mission Report, Part I: Mission Description and Performance,* Technical Report 32-1264. Jet Propulsion Laboratory, Pasadena, Calif., Feb. 1969.

XV-18. Drummond, A. J., et al., "Multichannel Radiometer Measurement of Solar Irradiance," *J. Spacecraft Rockets,* Vol. 4, No. 9, pp. 1200–1206, Apr. 1967.

## Bibliography

"*Surveyor* Spacecraft/*Atlas–Centaur* Launch Vehicle Interface Requirements," *Surveyor Project Control Document,* Project Document 1, Rev. 3. Jet Propulsion Laboratory, Pasadena, Calif., Oct. 1967.

# XVI. Spacecraft Power

The *Surveyor* spacecraft electrical power subsystem was designed to generate, store, convert, and distribute all electrical energy required by the other spacecraft subsystems (Refs. XVI-1 and XVI-2). The basic system used DC distribution of regulated 29 V. This power was converted by various subsystems to provide their particular power requirements. A simplified block diagram of the power subsystems is shown in Fig. XVI-1.

After the first four *Surveyor* missions, redesigns were incorporated in the power subsystem, which improved its performance characteristics and overall power efficiency.

## A. Early Design Evolution

The *Surveyor* spacecraft and mission requirements dictated a basic power subsystem configuration. During the transit period and most of the lunar day operations, spacecraft power demands were to be relatively constant. During lunar night, an energy storage source was required to supply the spacecraft thermal control demands. Considering this, and an overall minimum weight requirement, a combination of a sun-oriented solar panel, a radioisotope thermoelectric generator (RTG), and a storage battery to supply the high peak loads was proposed.

The RTG was expected to provide 15 W, the sun-oriented solar panel was expected to provide 68 W during transit and 44 W during lunar noon operations, and the silver–zinc rechargeable battery had a capacity of 1200 W-hr. Total weight of the power sources was estimated to be 60.5 lb. The block diagram of the subsystem is shown in Fig. XVI-2.

The solar panel and RTG were designed with sufficient capacity to supply spacecraft power requirements during transit. The rechargeable battery was required to supplement the power sources during peak-load demands, such as during launch, midcourse maneuvers, terminal descent, and lunar drilling operations. The expected power profile for transit and lunar operations is shown in Fig. XVI-3.

Power conditioning was to be accomplished by a booster-regulator (B/R) which maintained a regulated

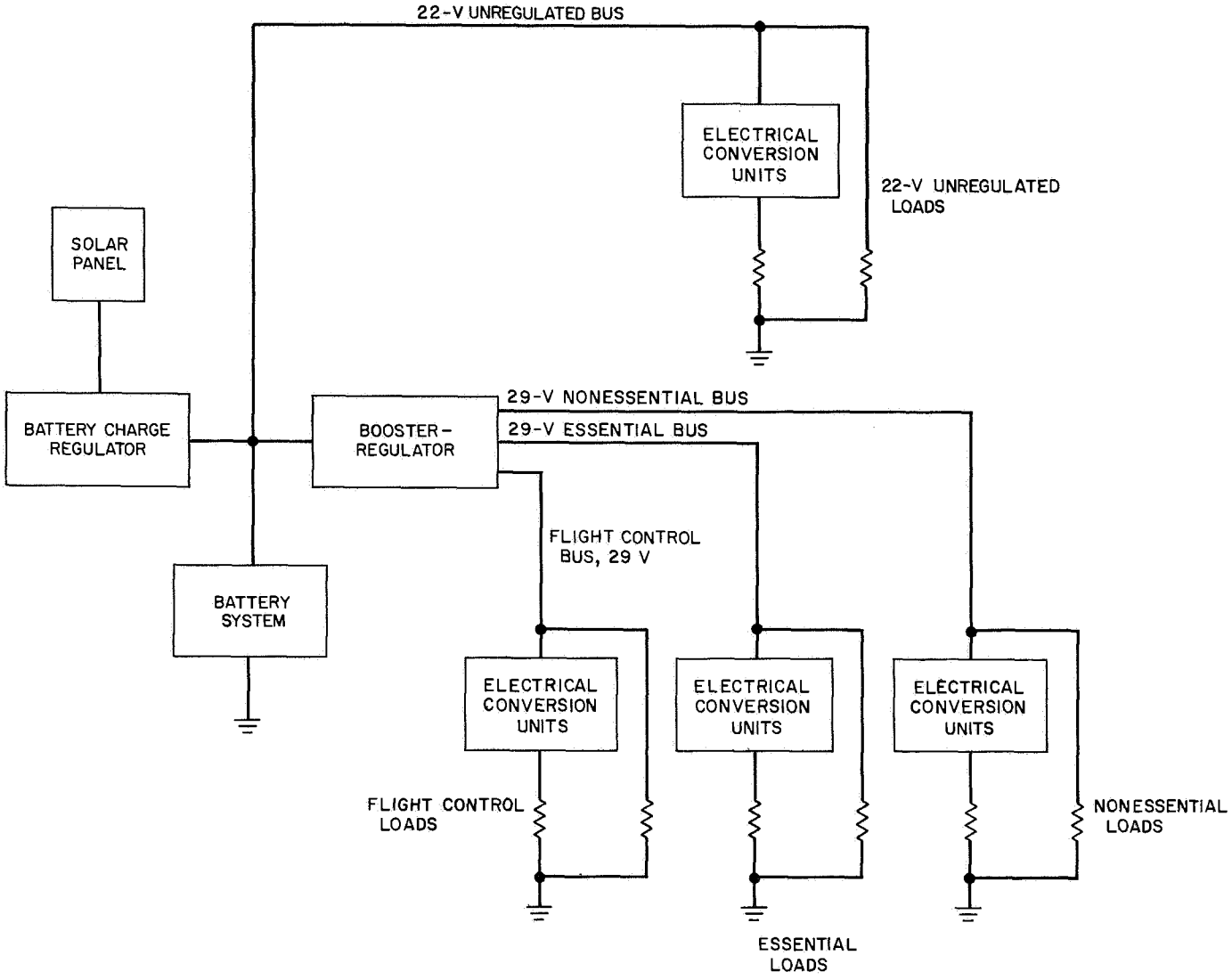



**Fig. XVI-1. Simplified *Surveyor* power subsystem**

bus at 29 V. The solar panel and the RTG fed directly to the regulated bus. Battery charging was accomplished through the regulated bus at the maximum rate available from the solar panel and RTG. When the battery voltage reached 28 V (2 V per cell), float charging was to be initiated until the charge current decreased to 0.1 A. A shunt regulator was available to keep the regulated bus voltage from rising after the battery was fully charged.

An overload trip circuit (OTC) was also included in the early design to turn off all regulated loads (with the exception of receivers and command decoders) when an excessive battery discharge was registered or a low regulated-bus voltage was present, indicating an overload condition.

In the event the RTG subsystem could not be available for *Surveyor* missions, an alternate power subsystem was considered. The block diagram of the alternate subsystem is shown in Fig. XVI-4. The alternate power subsystem consisted of a sun-oriented solar array and two 3650-W-hr rechargeable silver–zinc batteries for energy storage. This design was expected to weigh 103.5 lb. The solar panel had the same characteristics as in the RTG subsystem. The weight of the batteries was 47.5 lb. The solar panel design was expected to supply the spacecraft requirements during transit. The batteries were required for short durations during high-power demands, midcourse maneuvers, and terminal descent. After landing, power during the lunar day was expected to be supplied primarily by the solar panel. Battery charging to full capacity was

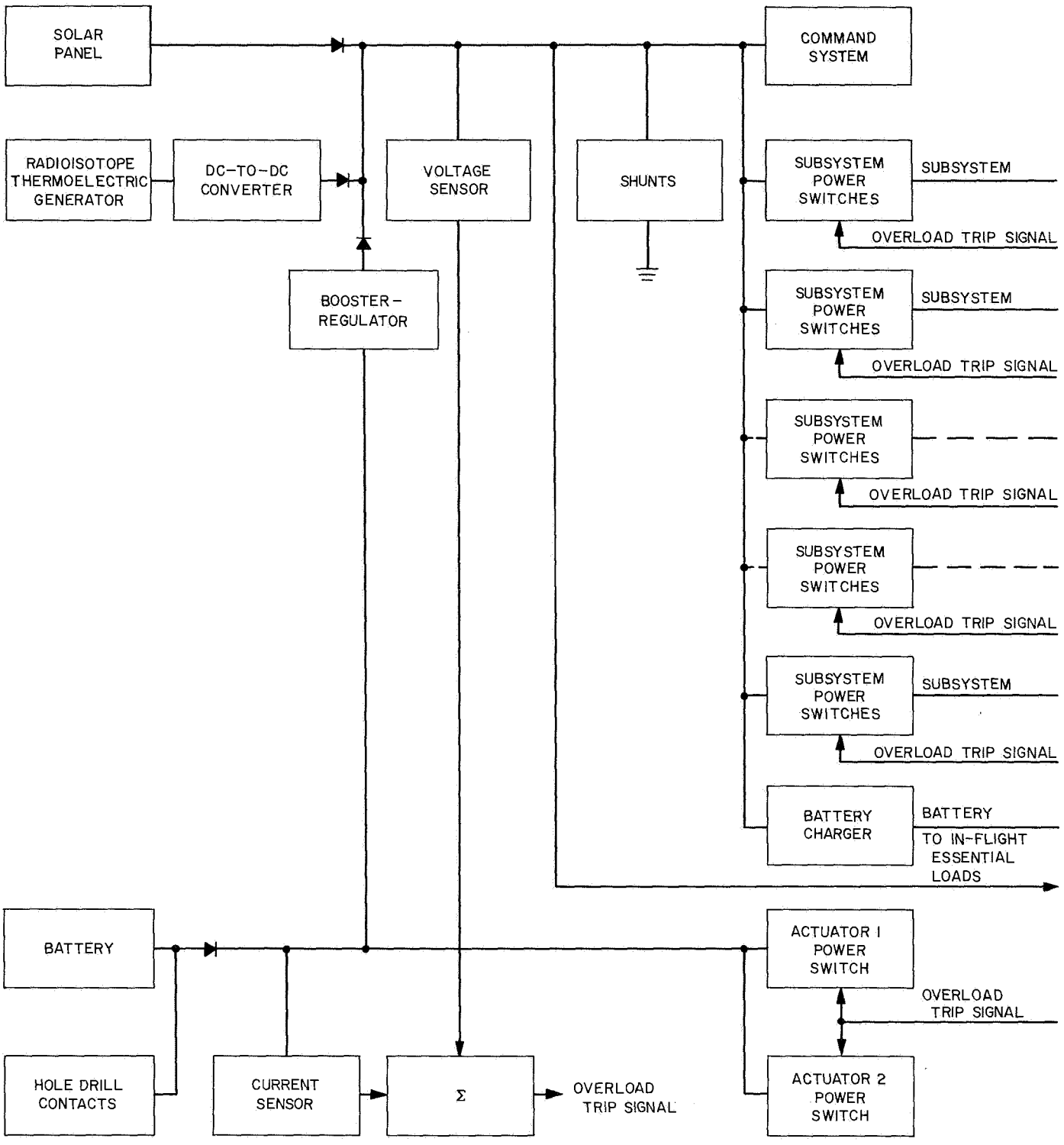



**Fig. XVI-2. Block diagram of initial concept of radioisotope thermoelectric generator, solar panel, and battery power subsystem**

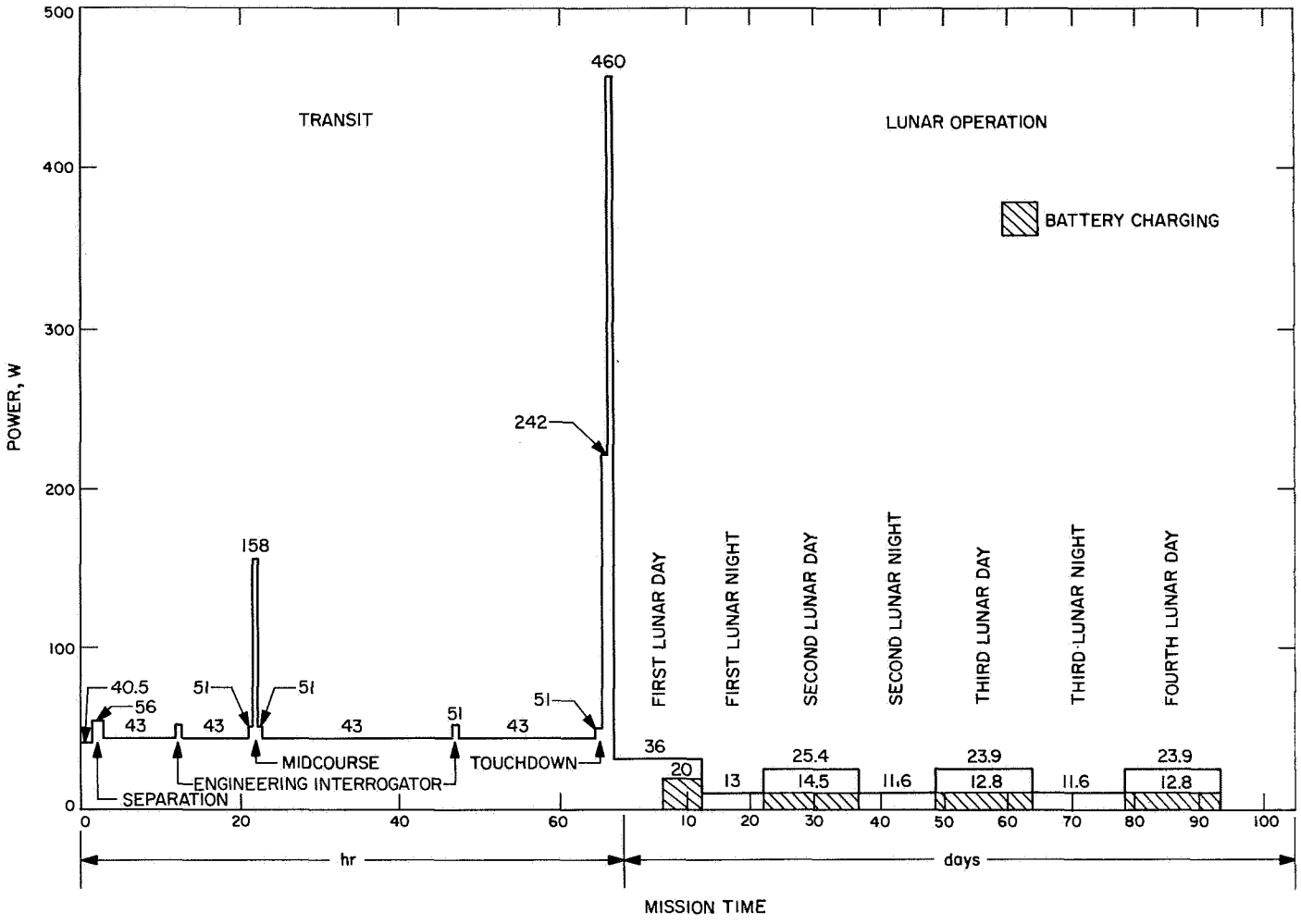



**Fig. XVI-3. Initial concept of spacecraft requirement vs mission time**

expected before lunar sundown. During lunar night, the batteries were to provide the spacecraft power requirements in order to survive the extreme environment.

New weight limitations, imposed by the redesigned boost vehicle, eliminated one of the rechargeable batteries in one of the temperature-control compartments. The night survival requirement was dropped. To solve the energy storage deficit, a nonrechargeable 1000-W-hr silver–zinc battery mounted to the spaceframe was proposed. An auxiliary battery control (ABC) unit was also developed to switch this auxiliary battery onto and off of the battery bus.

Computer power management evaluation of simulated missions showed that power sources could not supply spacecraft requirements under worst-case conditions. To obtain maximum power from the solar panel at all times, the optimum charge regulator (OCR) was designed and the output of the unit was connected to the unregulated bus. This modification provided additional energy; but the subsystem was still marginal, and the overall efficiency of the power subsystem remained a matter of primary concern. Power subsystem consumption measurements during the first spacecraft simulated mission revealed that the energy storage units would be heavily depleted during transit. The *Surveyor* mission requirements to land with sufficient energy to operate the spacecraft for 20 hr before sunrise had to be waived.

Modifications were introduced in the power distribution area that directly affected the B/R design. The essential, nonessential, and flight control loads were redefined and grouped. The essential loads were considered to be the command decoders and receivers. The signal processing and thermal control elements, transmitters, TV cameras, and strain-gage amplifiers were grouped in the nonessential category. A flight control postregulator with remote

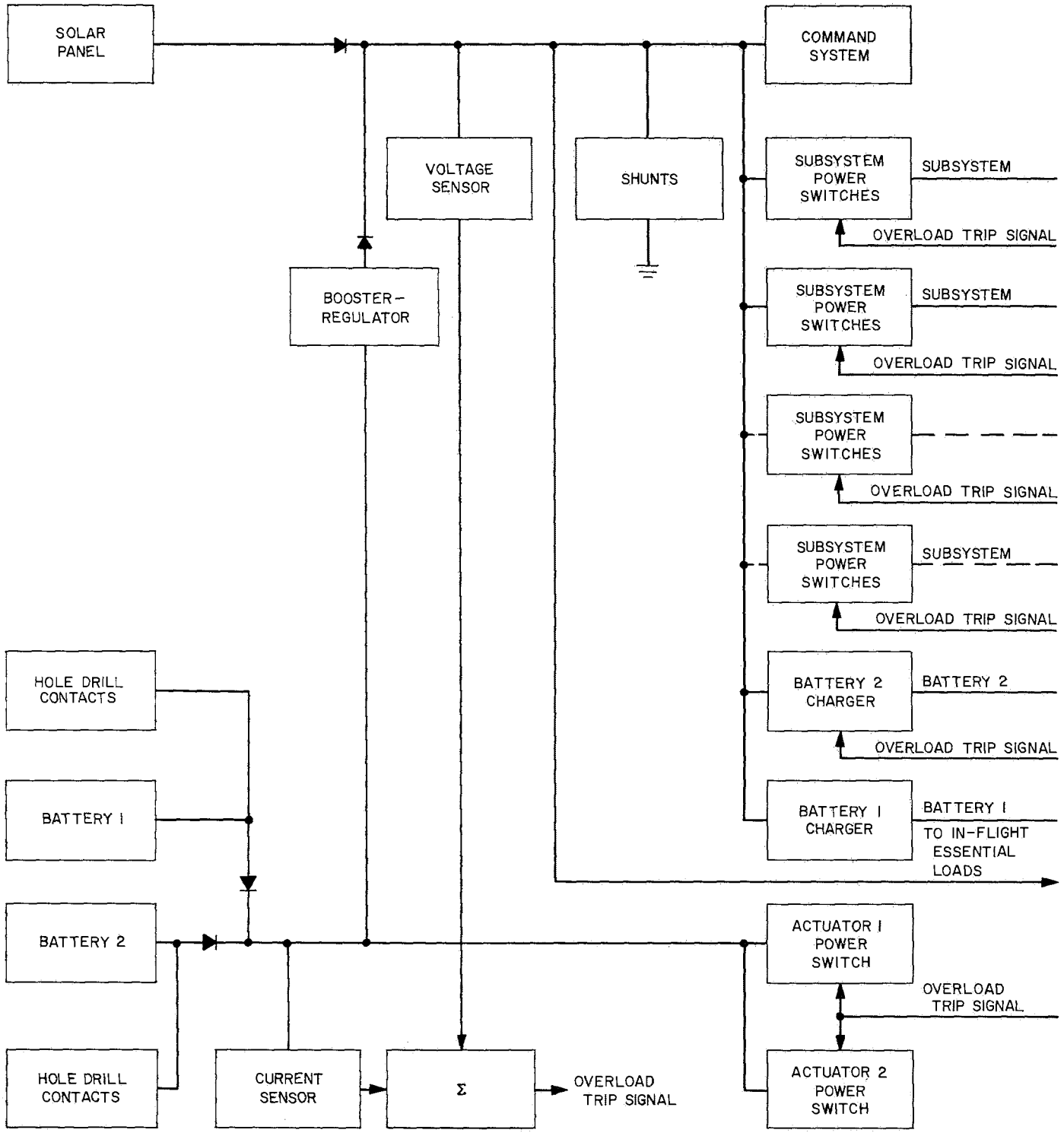



**Fig. XVI-4. Block diagram of initial concept of solar panel and battery**

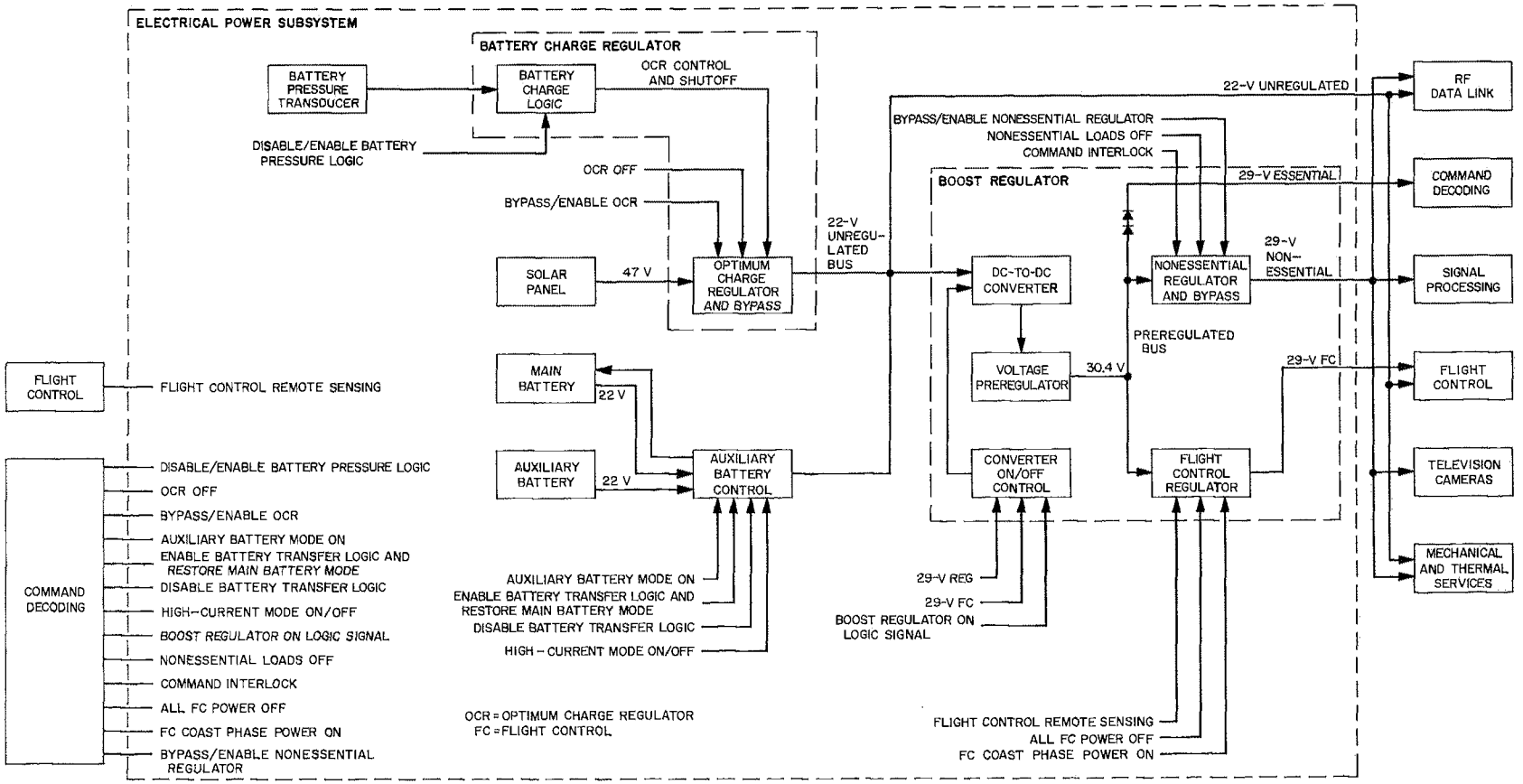



**Fig. XVI-5. Simplified electrical power subsystem functional block diagram, SC-1 through SC-4**

sensing was added to provide a low output impedance to the flight control electronic units. The receivers eventually were removed from the essential bus and transferred to the unregulated bus directly from the battery so the B/R could be turned off during the lunar night.

In addition, the OTC was combined with the nonessential postregulator to provide all features in one submodule.

Before the power subsystem design for the first flight was finally frozen, two other major modifications were made. The B/R and battery charge regulator (BCR) had previously been housed in one unit, the central power control unit, but temperature tests of the unit revealed that the power dissipation was excessive for the compartment. The unit was repackaged, separating the B/R and BCR and placing them in different compartments.

A motor-driven master power switch (MPS) was added to the subsystem to disconnect the power sources from the spacecraft. The switch also ensured the absence of voltage at the *Centaur* connectors during *Centaur–Surveyor* mating.

Additional modifications, which occurred after the basic power subsystem was established, are summarized in Subsection B-5.

## B. Design Used for *Surveyor I–IV* Missions

The *Surveyor I–IV* power subsystem, shown in Fig. XVI-5, derived its energy from the solar panel and the spacecraft battery system. The solar panel power capability, affected by temperature and the incidence of solar radiation, varied from 90 to 55 W.

The spacecraft battery system consisted of a 165-A-hr main battery and a 45-A-hr auxiliary battery. The main battery was a secondary (rechargeable) battery; the auxiliary battery was a primary (nonrechargeable) battery.

Power conditioning units controlled, regulated, and distributed the power received from the power sources to the various subsystems in the spacecraft.

The SC-1 through SC-4 power subsystems consisted of these units:

(1) Solar panel.

(2) Main battery.

(3) Auxiliary battery.

(4) Main power switch.

(5) Auxiliary battery control.

(6) Battery charge regulator.

(7) Booster-regulator.

(8) Engineering mechanisms auxiliary (EMA).

(9) Thermal control and heater assembly.

(10) Electrical conversion units (ECU) (distributed throughout the Spacecraft System).

Table XVI-1 summarizes the performance characteristics of each unit.

### 1. Power Sources

***a. Solar panel.*** The solar panel assembly was located at the top of the antenna/solar panel positioner (A/SPP) mast. It consisted of series–parallel-connected arrays of 792 solar cell modules (3960 cells) arranged on a planar honeycomb substrate approximately 9 $ft^2$ in area. During transit, the solar panel was erected and locked in a position normal to the sun (Z) axis of the spacecraft. After lunar landing, the panel was unlocked and could be adjusted to follow the sun in its transit. A front view of a solar panel is shown in Fig. XVI-6.

The solar panel substrate consisted of an expanded honeycomb aluminum core with a thin titanium facing sheet. Both sides of the substrate were coated with epoxy that isolated the cell modules and the wiring from the substrate. The substrate was grounded to the spacecraft frame.

The solar array had nine sections connected in parallel through diodes. The diodes provided isolation between sections in the event of a failure. Each section consisted of four parallel-connected strings of solar cell modules. The solar cell module consisted of five series-connected solar cells, each solar cell being a silicon P-on-N type semiconductor $1 \times 2$ cm. There were 22 series-connected modules per string. Each individual module within the string was also connected in parallel to its corresponding module on each of the three remaining strings in the section to ensure maximum reliability of operation. The wiring diagram of one diode isolation section is shown in Fig. XVI-7.

The modules were procured from Heliotek, Inc., Sylmar, Calif., and were of an overlapping shingle configuration construction. Each module was qualified and stored in bonded stores. The modules were mounted to

## Table XVI-1. *Surveyors I–IV* power subsystem performance characteristics

| Unit | Performance characteristics |
|---|---|
| Solar panel | Solar panel power at mean solar intensity: 89 ±5 W at 122 ±5.4°F<br>Open-circuit voltage: 107 V maximum at −320°F<br>Short-circuit current: 2.3 A maximum at 250°F |
| Main battery | Voltage: 22 $^{+4.0}_{-4.5}$ VDC Temperature: 40–125°F<br>Capacity (at 70°F): Load, A — Capacity, W-hr<br>1.0 — 3600<br>10.0 — 3250<br>20.0 — 3180 |
| Auxiliary battery | Voltage: 22 $^{+4.0}_{-3.5}$ VDC Temperature: 40–130°F<br>Capacity: 900 W-hr |
| Auxiliary battery control | Current handling: 50 A for 5 min, continuous 70 A for 20 msec, 5 times<br>Automatic transfer: to auxiliary battery from main battery |
| Battery charge regulator | Power transfer: operates close to maximum power point of solar panel current-voltage curve<br>Efficiency: 80%<br>Input current: 0–2.3 A<br>Input voltage: 30–90 VDC<br>Output current: 0–5 A<br>Output voltage: 17.5–27.5 VDC, unregulated |
| Battery charge regulator, battery charge logic | Unregulated bus sense:<br>Trickle charge: 27.16–27.30 VDC<br>Terminate charge: 27.5 VDC<br>Battery pressure sense:<br>Terminate charge: 65 ±3 psia<br>Restore charge: 60 ±5 psia |
| Battery charge regulator, antenna/solar panel positioner circuitry | Unregulated input:<br>Voltage: 18–27.5 VDC<br>Current: 4–30 A for 60 ±10 msec<br>Regulated input:<br>Voltage: 28.61–29.24 VDC<br>Current: 10 mA maximum, continuous |
| Booster-regulator | Unregulated input:<br>Voltage: 17.0–27.3 VDC<br>Current: 15.3 at 18 VDC maximum for 7-A output<br>Internal load on regulated bus:<br>Voltage: 29.0 ±0.58 VDC<br>Current: 25.0 mA maximum<br>Regulated output:<br>Voltage: 29 VDC<br>Continuous maximum current:<br>Essential bus: 0–0.06 A<br>Nonessential bus: 0–6.0 A<br>Flight contral bus: 0–3.0 A |
| Baoster-regulator overload trip circuit | Removes power from nonessential bus when:<br>Booster-regulator input voltage is less than 17 ±0.25 VDC<br>Output current is greater than 15 A with 18–22 VDC input<br>Series regulator output voltage:<br>29.00 ±0.29 VDC on nonessential bus<br>Overland trip circuit bypass:<br>Output current: 0.15–6.0 A |

**Table XVI-1 (contd)**

| Unit | Performance characteristics |
|---|---|
| | Output voltage:<br>29.00 (+0.87, −0.58) VDC with flight control off<br>29.00 (+1.015, −0.58) VDC with flight control on |
| Booster-regulator, flight control regulator | Output voltage: 29.0 ±0.29 VDC<br>Maximum output current: 3.0 A |
| Main power switch | Current ratios: make, carry, and break resistive loads of 74 A (2 A at 28 VDC)<br>Actuation voltage: 22–40 VDC at terminals<br>Actuation time: 85 msec maximum |
| Engineering mechanisms auxiliary, squib firing | Output: 20 ±5 msec squib firing of 9.5 ±0.5 A or 19.0 ±1.0 A<br>Interlocks:<br>Command interlock to selected circuitry separation sensing and arming switch interlock to selected circuits<br>Externally controlled turn-on of constant current generators |
| Thermal control and heaters | Ground-command controlled or automatically controlled; cycled to maintain: compartment A at 50°F, compartment B at 10°F |

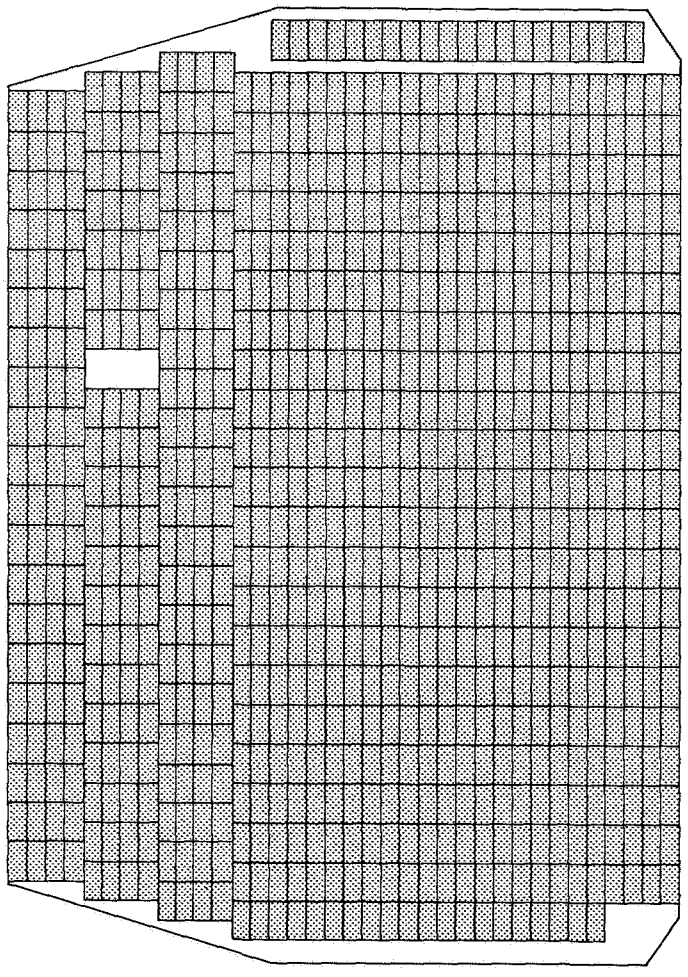


**Fig. XVI-6. Front view of SC-1 through SC-4 solar panel**

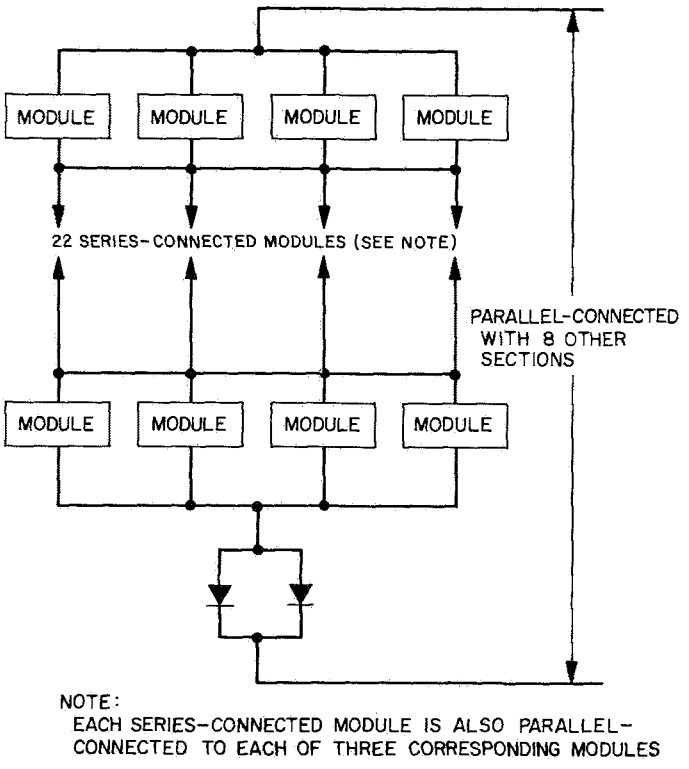



**Fig. XVI-7. Typical solar panel section wiring diagram**

the solar panel substrate with silicone rubber adhesive. The individual modules were hand-wired into strings. The series strings were connected through diodes encapsulated in the substrate to the contour table which was bonded on the rear substrate surface. The total weight

of the panel was 8.5 ±0.3 lb, and the panel was capable of producing 89 W at 50°C during the transit phase of the mission. A secondary sun sensor and a temperature transducer were also mounted on the cell side of the solar panel assembly. The sun sensor was used to optimize illumination level and served as a secondary aid to position the spacecraft during transit. Figure XVI-8 presents a typical current-voltage characteristic for the *Surveyor I–IV* solar panel.

***b. Main battery.*** The main battery was a sealed assembly consisting of 14 series-connected rechargeable silver–zinc cells housed in a magnesium canister. The nominal capacity of the battery was 3650 W-hr; dry weight was 18.28 ±0.28 lb; and the maximum wet weight was 46.8 lb. The battery design was greatly improved to achieve a 70-W-hr energy storage density. It was housed in compartment A for temperature environment control, and performed satisfactorily in the temperature range of 40–125°F. The output voltage was required to be from 17.5 to 27.3 V for all operating conditions of discharge, no load to full or peak load (50 A for 4 min, 70 A for 50 msec repeated 5 times), and for the entire life of 120 days, minimum. The battery was required to deliver the following energies when discharged at a constant rate from the fully charged condition at the battery temperature of 70°F:

| Constant discharge rate, A | Battery capacity, W-hr |
|---|---|
| 1 | 3600 |
| 10 | 3250 |
| 20 | 3180 |

The battery had a reliability factor of 0.998 for the 67-hr mission from launch to lunar landing, plus 80 hr during lunar operation on the first lunar day.

The battery was composed of two 3-cell and two 4-cell monoblocks cemented together on a 2- × 7-cell geometry configuration. The 14-cell cemented assembly was then sealed in the battery case. The individual cells were vented to a common manifold which was instrumented with a pressure transducer. Figure XVI-9 presents a simplified main battery schematic. Excessive pressure would have resulted in a signal to the battery charger which would determine charging. A temperature transducer was also available to measure the battery temperature.

There were two electrical connectors mounted on a magnesium bracket at one end of the case. One connector

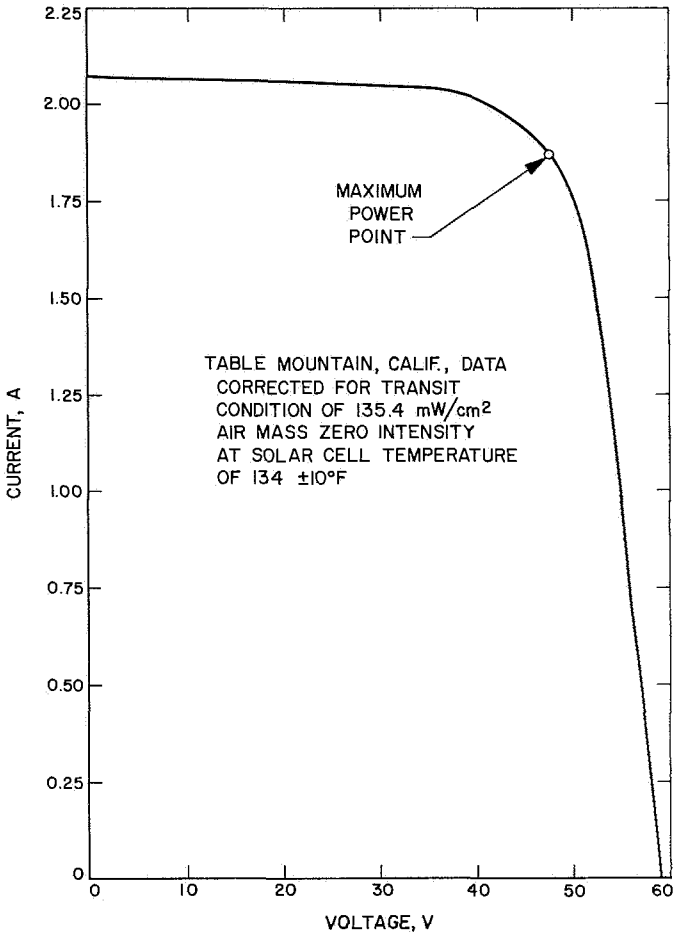



**Fig. XVI-8. Typical solar panel characteristics, SC-1 through SC-4**

provided connection for battery power and the pressure and temperature measurements. The second connector contained instrumentation leads for measuring the individual cell voltages during testing. A typical flight battery is shown in Fig. XVI-10. The battery was procured from Electric Storage Battery Co., Raleigh, N.C.

Initially, experimental cells supplied by Electric Storage Battery Co. were evaluated to determine their capability of meeting *Surveyor* design specifications. Eight experimental batteries were then constructed and tested. The test results concluded that the cells basically were satisfactory and only minor alterations were necessary. These alterations were incorporated in the 10 developmental batteries. A test plan for evaluating the developmental batteries was initiated and included (1) basic parameter tests, (2) system integration tests, and (3) environmental type-approval tests.

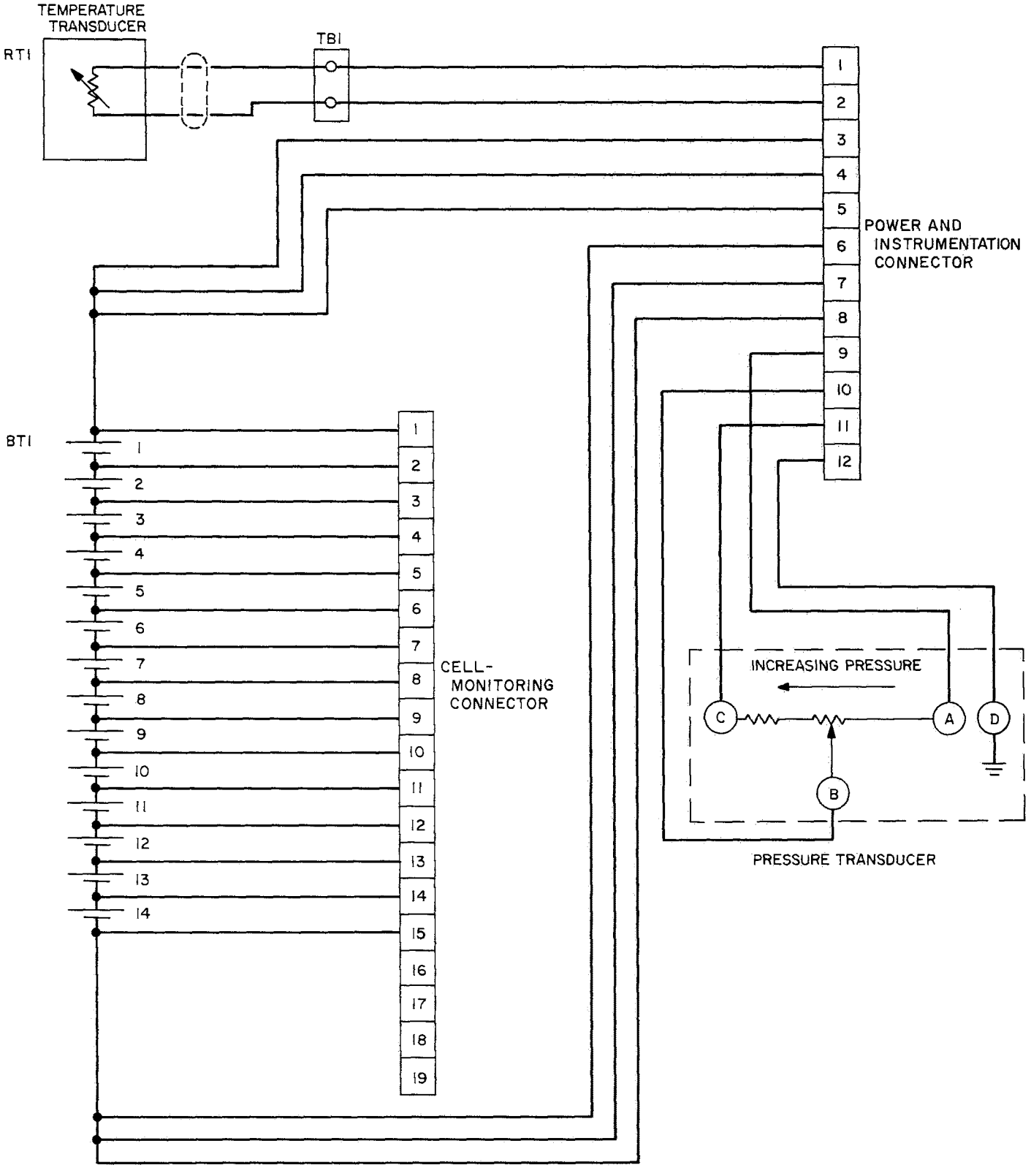



**Fig. XVI-9. Simplified main battery schematic**

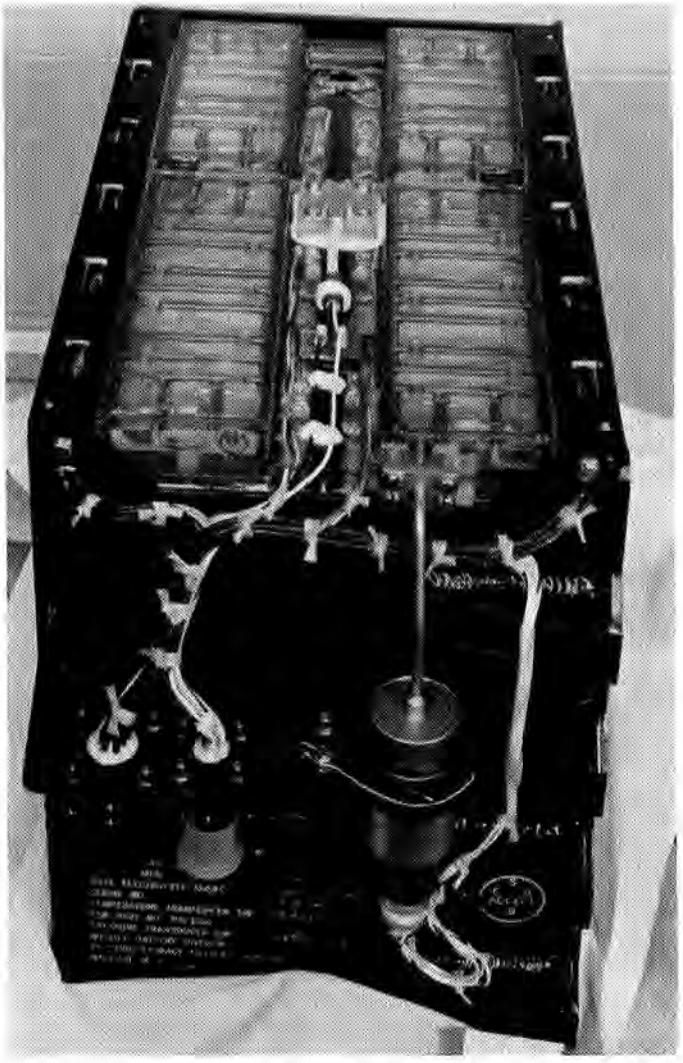


**Fig. XVI-10. Typical flight battery**

Developmental battery tests revealed that firm definitions of quality control procedures, manufacturing checkpoints, and test procedures were needed. This effort initiated testing of a number of reliability test cells, the development of a leak test method, development tests of cell cases, and a production lot-sampling of cells and cell cases.

Premature charge termination and cell unbalance at full charge were experienced in the testing of the developmental batteries, forcing an early termination of the test program. The problem was traced to the gassing of low-capacity cells in the battery at near full charge. Implementation of cell-forming charge techniques, to balance cell charge capacities at the full charge condition instead of at full discharge, corrected this problem.

The prototype battery test program followed. Twenty-six batteries were fabricated for this program. The prototype battery used manifolded cells instead of the individually sealed cells. Two other improvements were also introduced: a new separator folding technique and a modified manufacturing process for the negative plate to yield plates of more uniform density.

A pilot-run test of cells for the prototype battery disclosed that they did not accept the normal charge on the second charge cycle. To correct this problem, the separator combination was modified from one layer of nylon and seven layers of cellophane to only six layers of cellophane. The volume of the electrolyte was also increased.

During the flight acceptance vibration tests, a number of prototype batteries developed broken lug wires. This problem was corrected by strengthening the negative plates and tightening the cell pack. Two prototype batteries developed fractured positive plates in several cells during type approval vibration tests. The positive cell was redesigned with a more rigid canister design. The cell design consisted of a mesh screen for the positive grid and a rectangular frame with X-shaped reinforcing for the negative plate. Although the design change resulted in a 5% decrease of battery capacity, the redesign battery successfully completed the type approval program.

*c. Auxiliary battery.* The auxiliary battery provided limited backup for the main battery. It was chiefly used to augment the main battery during terminal descent to share the heavy load (as high as 70-A peak) caused by turn-on and operation of the landing radars. The battery capacity was 1000 W-hr. The output voltage level of the battery was required to be $22.0 + 4.0 - 3.5$ V for all operating conditions of discharge no load to full or peak load (50 A for 40 min, 70 A for 50 msec repeated 5 times). The operating temperature range was 70–110°F. The battery was procured from Eagle-Picher Co.

The additional battery was a manually activated, primary nonrechargeable unit. It was composed of 14 series-connected silver–zinc cells arranged in a 2- × 7-cell geometric configuration. The cells were assembled and potted in a sealed magnesium canister equipped with a pressure relief valve. The battery was supplied dry, and was activated at least 48 hr prior to spacecraft installation by manual injection of potassium hydroxide electrolyte. It was equipped with one connector that carried all the required power and instrumentation leads. The

battery maximum weight after electrolyte charge activation was 21.0 lb. The guaranteed activated stand life of the battery was only 15 days.

Studs mounted the battery on the auxiliary battery compartment, securing it to a platform cantilevered out from the spaceframe between legs 2 and 3. There was no active thermal control provided for the compartment, but its temperature was telemetered.

A complete auxiliary battery experimental test phase was not considered necessary since the selected battery had already been qualified to a Lockheed Missiles and Space Co. specification, indicating that the cells and method of packaging were compatible with space flight environments. The cells were similar to those used on the *Mercury* and *Agena* programs. Four developmental model batteries were subjected to a test program at HAC to determine electrical characteristics and structural integrity. Tests included discharge capacity, activated stand time, vibration, shock, and acceleration. Although activated stand time was less than desired, the electrical performance met all requirements. Figure XVI-11 presents a photograph of the auxiliary battery, the simplified schematic diagram, and the load and temperature profiles.

### 2. Power Sources Control

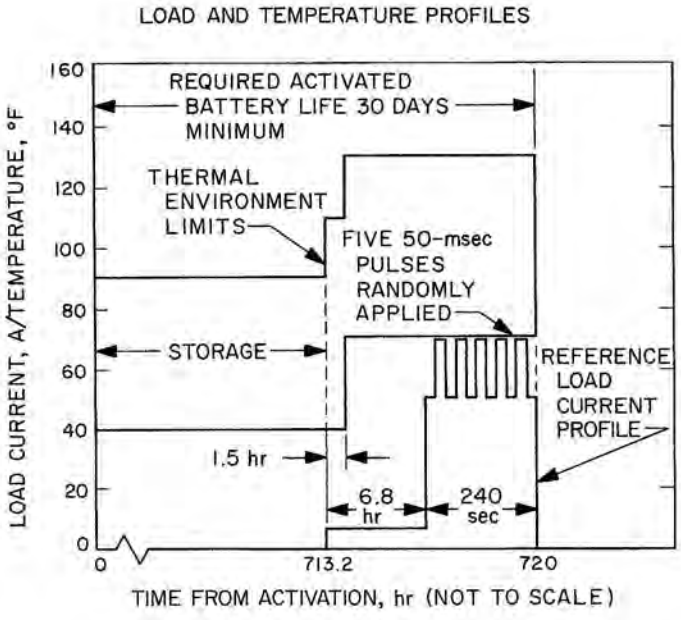
*a. Main power switch.* The power subsystem battery source could be disconnected from the spacecraft by means of the MPS. This arrangement assured a complete shutdown of the spacecraft. With the MPS open, the spacecraft could be powered from the ground power supply. This provided the flexibility of operating the spacecraft independently from either the ground power supplies or the internal batteries, and reduced the expensive use of flight batteries during testing. Prior to the incorporation of this switching, the only way the spacecraft could be shut down was by disconnecting the battery connector.

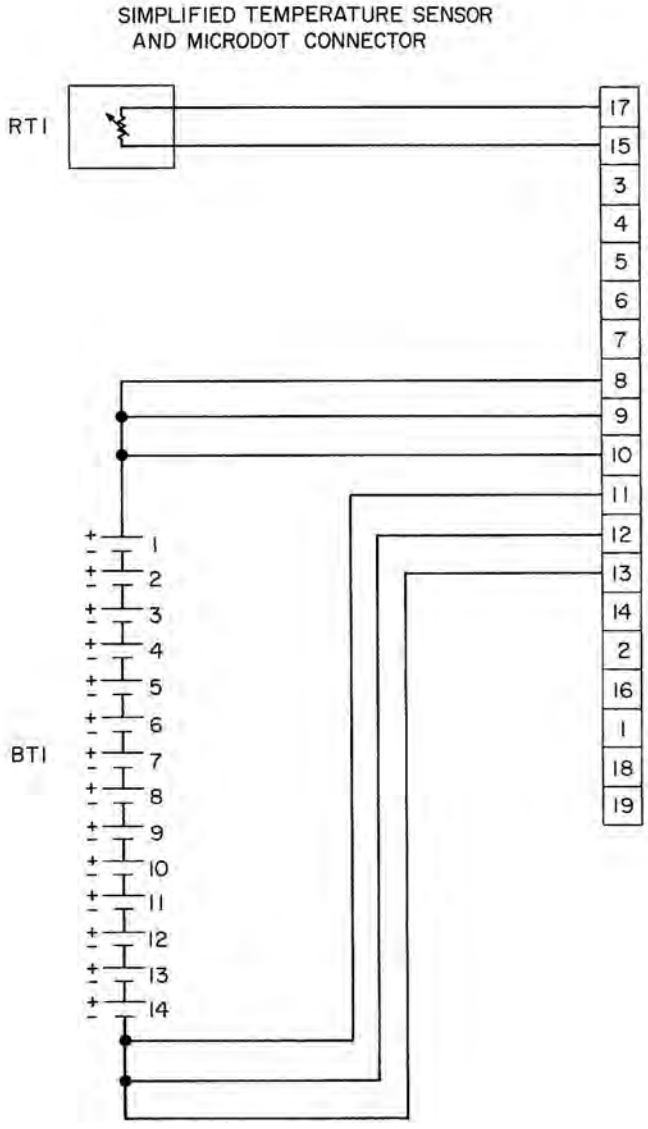
The MPS was a sealed, motor-driven, cam-operated, single-pole, single-throw (SPST) switch. The contacts of the switch were capable of carrying or breaking a maximum resistive load of 74 A at 28 VDC. In addition to the high-current contacts, there was an auxiliary 2-A contact used primarily for indication of the switch position. However, both sets of contacts were used functionally by the power subsystem. The high-current contacts allowed disconnection of the battery system from the spacecraft power as required before prelaunch operations. (Their contact resistance was less than 0.001 Ω at a current of 50 A-DC.) The low-current contact was used to disconnect the solar panel simulator power from the BCR during ground-testing operations. Figure XVI-12 presents the MPS schematic diagram.

The unit was actuated only on the ground and could not be operated after launch. It required an independent electrical drive source for "on" and "off" positions and it would self-interrupt its motor drive power at the completion of actuation. An integral, electrically released brake stopped the movement and held the position of the transfer mechanisms after the switch reached its selected position. The actuation voltage of the switch was 28 VDC; the motor current was less than 9.0 A. The actuation time for either operation was less than 85 msec. The switch was mounted in compartment A and its maximum weight was 1.15 lb. Procured from Kinetics, Inc., San Diego, Calif., the switch design had been previously qualified for both *Ranger* and *Mariner* spacecraft under similar environmental conditions.

*b. Auxiliary battery control.* The ABC provided automatic or command-controlled application of main and auxiliary battery power to the unregulated bus. There were three modes of battery operation: main battery mode, auxiliary battery mode, and high-current mode. In the main battery mode, only the main battery was connected to the unregulated bus. This was the mode in which the spacecraft operated during the major portion of the flight. In the auxiliary battery mode, the main battery was connected to the unregulated bus through a series diode while the auxiliary battery was directly connected. In the high-current mode, both the main and auxiliary batteries were connected to the unregulated bus without the series diode.

The ABC block diagram (Fig. XVI-13) shows both batteries connected directly to the unregulated bus. In the automatic controlled application, the voltage comparator circuit monitored the main battery voltage and, when the main battery voltage dropped below a transfer threshold dependent on the auxiliary battery voltage, the voltage comparator would initiate the automatic application of the auxiliary battery to the unregulated bus. Figure XVI-14 shows the automatic transfer criteria for the auxiliary battery. The automatic transfer logic could be disabled by ground commands. Switching was accomplished with two four-pole, double-throw magnetic latching relays. The unit also housed voltage dividers for sensing the voltage at the main and auxiliary batteries and circuits for indicating the position of the transfer relays.



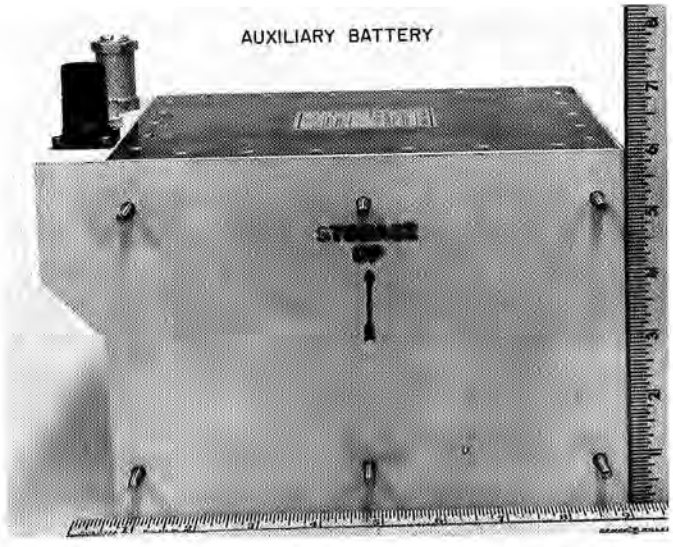




**Fig. XVI-11. Auxiliary battery**

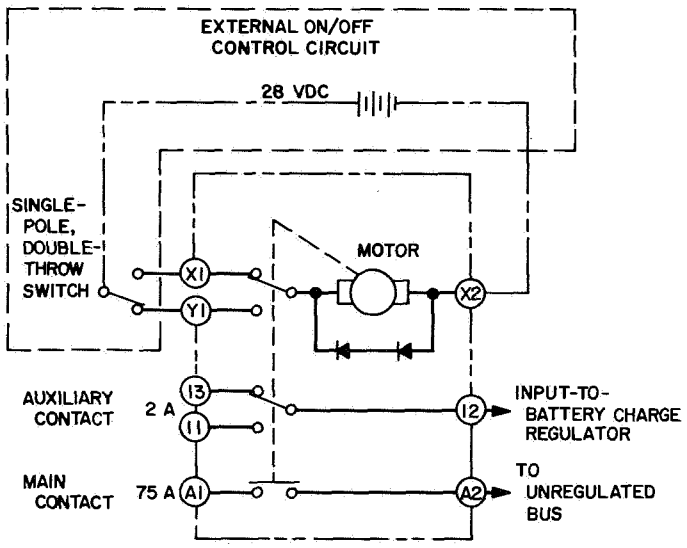



**Fig. XVI-12. Main power switch schematic diagram**

The ABC was located in compartment A. The maximum weight of the unit was 1.75 lb.

*c. Battery charge regulator.* The BCR was designed to regulate and control the power from the solar panel to the unregulated bus. The BCR contained the OCR, switches for controlling the A/SPP stepping motors, transducer devices to measure the solar panel voltage, current, and temperature of the unit, and the logic circuit for regulating the charge to the main battery. A block diagram of the BCR is shown in Fig. XVI-15.

The following four operational modes of the BCR controlled the solar panel output characteristics:

(1) On.

(2) Off.

(3) Bypass.

(4) Trickle charge.

In the "on" mode, the solar panel was switched to the OCR, which was designed to adjust the load on the solar panel to give maximum converted power into the storage battery and spacecraft loads.

The OCR operated over a solar panel voltage input range of 30–90 VDC and had an output of 17.5–27.5 V on the unregulated bus. Its input was exclusively from the solar panel and, when started from the "off" condition, it would operate automatically. The OCR consisted of a DC-to-DC converter, which acted as an impedance matching device between the solar panel and the unregulated bus, and extracted maximum power from the solar panel by shunting around the maximum power point of the solar panel voltage-current (E-I) characteristics.

The OCR used pulse-modulated regulation, the pulsewidth being determined by the solar panel current value around the maximum power point.

To describe how the output current was optimized, a complete cycle of operation will be explained. The solar panel E-I curve is shown in Fig. XVI-16.

Assuming the cycle started from a point A below the maximum power point, the pulsewidth of the modulator increased, supplying higher current, until maximum pulsewidth of the modulator was achieved. This point B corresponded to the maximum current from the solar panel. The pulsewidth of the modulator then decreased until zero pulsewidth was achieved. The cycle was repeated, swinging around the maximum power point of the solar panel. The operation range was approximately $\pm 5$ V around the maximum power point. The function of tracking the E-I characteristic curve was removed from SC-5, SC-6, and SC-7 by redesigning the subsystem to match characteristics between the battery and solar panel power sources. The efficiency of this circuit was a function of the unregulated voltage bus level and varied from 70 to 80% for 18–27 V output.

In the OCR "off" mode, the solar panel output was switched off. This mode was intended to prevent overcharging of the main battery by the solar panel. In the OCR bypass mode, the solar panel was connected directly to the unregulated bus. This mode was used in case of OCR failure.

In the trickle-charge mode, the main battery charging current was controlled by its terminal voltage. The battery-charge logic circuit, by sensing the battery voltage, terminated the operation of the charge circuit and reduced its output to a trickle charge at low current when the battery voltage reached 27.1 V. The trickle charge continued until the battery reached 27.3 V. The battery-case pressure-sensing circuit also terminated the battery charge if the pressure exceeded 65 $\pm 3$ psia. Charging was restored when pressure dropped below 60 psia. The trickle-charge mode was removed from SC-5, SC-6, and SC-7 because trickle-charging proved to be impractical.

All three BCR modes, excluding the trickle-charge mode, were controlled by earth commands. Also housed

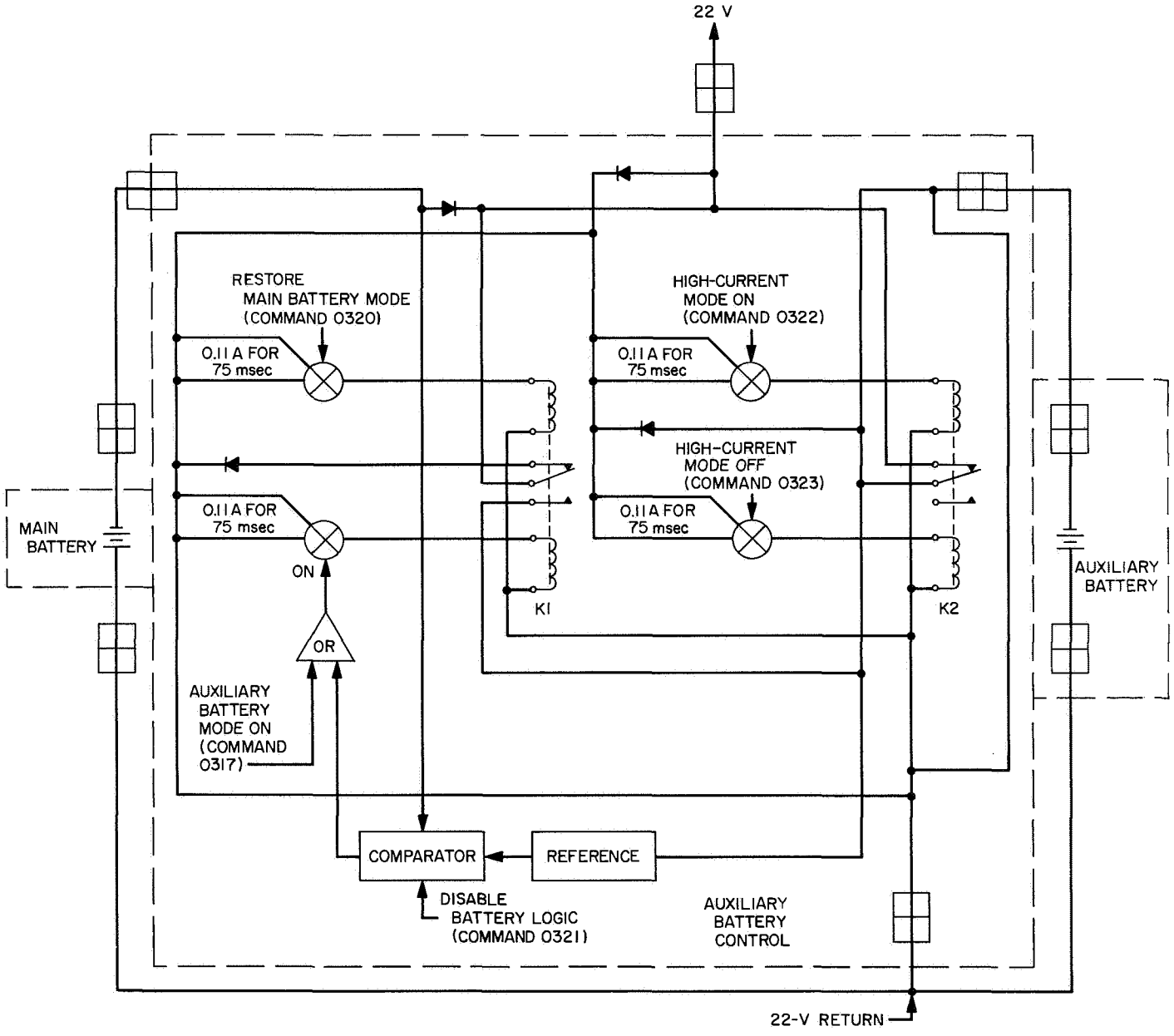



**Fig. XVI-13. Auxiliary battery control**

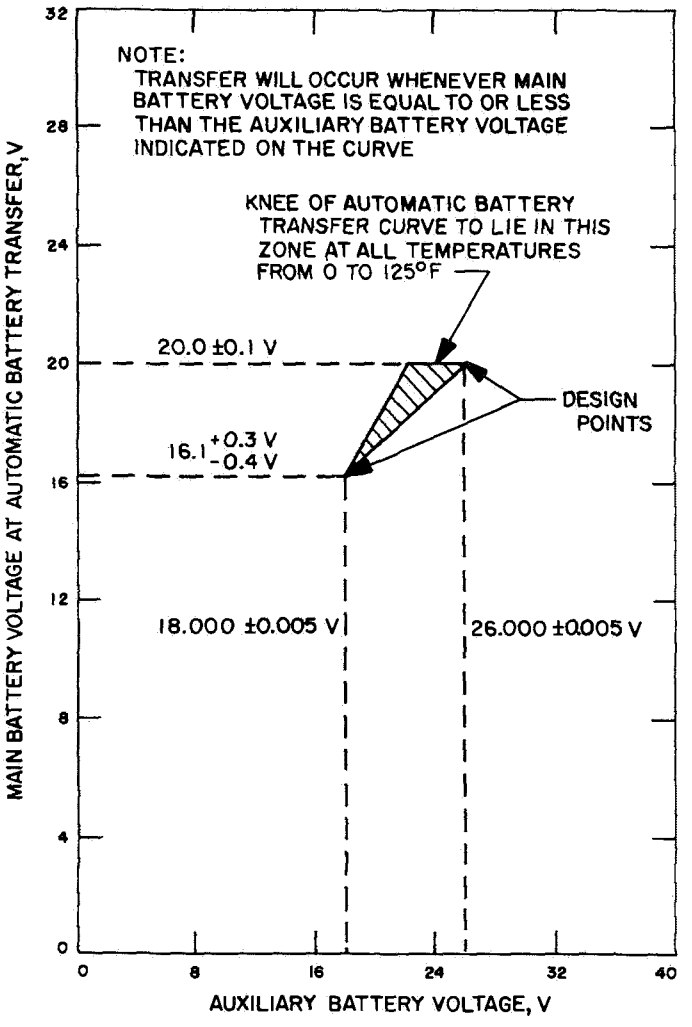



**Fig. XVI-14. Automatic battery transfer criteria**

in the BCR were the A/SPP switches that provided drive to the A/SPP motors and were controlled either by ground commands or command pulses generated by the automatic solar panel deployment logic.

These switches consisted of silicon controlled rectifiers (SCRs) to drive the stepping motors and a transistor switch in the motor's common return to reset the SCRs.

The BCR was housed in compartment A and had a maximum weight of 3.5 lb.

*d. Battery energy management plan.* The power subsystem derived energy from both the solar panel and the battery. The solar panel converted solar radiation into electrical energy, and the battery system supplied stored electrical energy. During the transit portion of the mission, both power sources were used to support the spacecraft power requirements. Even with the solar panel sun-oriented for maximum power, the battery system was required to supply power continuously to supplement the solar panel power. After lunar touchdown, spacecraft power requirements dropped, and battery charging was initiated and continued until the battery was fully charged. Table XVI-2 summarizes the battery energy management accounting that was used on *Surveyors I–IV*.

The power management computer program for SC-1 indicated that the battery energy remaining at touchdown would be dangerously low for a worst-case condition. Several high-power transmitter interrogations of the spacecraft had to be eliminated to reduce the demand on the power subsystem to that shown in Table XVI-2.

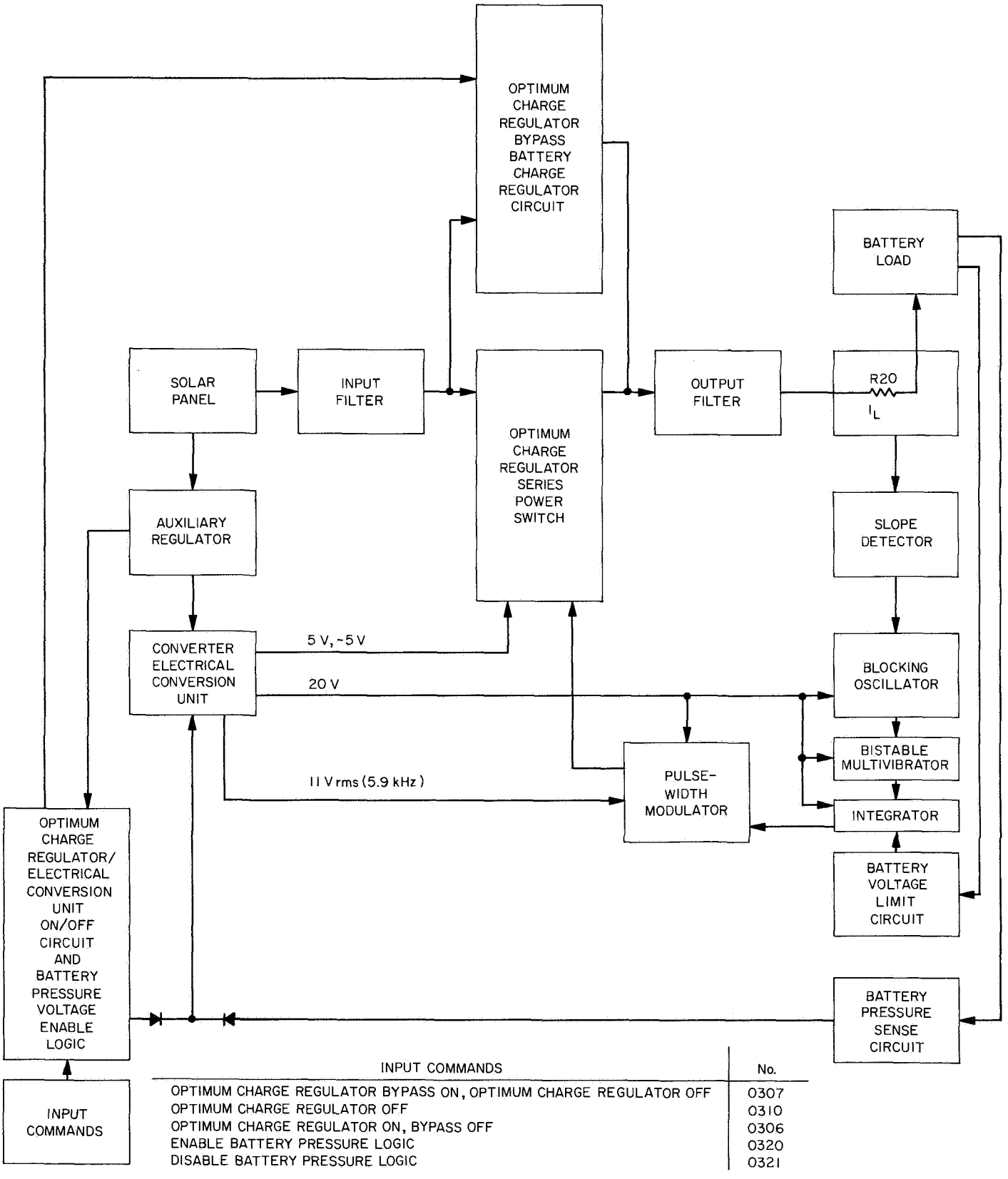
### 3. Power Distribution, Regulation, and Conversion

The power subsystem provided power to the spacecraft via one unregulated and three regulated voltage buses. They were the 22-V unregulated, 29-V essential, 29-V nonessential, and 29-V flight control buses. The 29-V essential bus supplied the spacecraft's command decoders. The 29-V nonessential bus supplied all regulated loads on the spacecraft with the exception of the flight control system. The 29-V flight control bus supplied the flight control loads exclusively.

Power from the BCR and spacecraft batteries was distributed to the B/R and also to the 22-V unregulated bus used for all spacecraft loads that did not require regulated voltage. Depending on the spacecraft battery's charge status, this bus varied in output between 17.5 and 27.3 V.

All regulated bus voltages were held on ±1% of their specified values. When voltages other than 29 V or 22 VDC were required by a spacecraft subsystem, they were made available by means of ECUs. The ECUs which were integral parts of the user's subsystem provided local power conditioning and isolation. Table XVI-3 lists the spacecraft power users and their load requirements from the various power subsystem distribution lines.

*a. Booster-regulator.* The B/R conditioned and controlled the power delivered to the spacecraft subsystems. It accepted unregulated power of 17.0–27.3 V from the unregulated bus and delivered regulated power to the three 29-V regulated buses: essential, nonessential, and flight control. The output ratings of the regulated buses are shown in Table XVI-4.




| INPUT COMMANDS | No. |
|---|---|
| OPTIMUM CHARGE REGULATOR BYPASS ON, OPTIMUM CHARGE REGULATOR OFF | 0307 |
| OPTIMUM CHARGE REGULATOR OFF | 0310 |
| OPTIMUM CHARGE REGULATOR ON, BYPASS OFF | 0306 |
| ENABLE BATTERY PRESSURE LOGIC | 0320 |
| DISABLE BATTERY PRESSURE LOGIC | 0321 |

**Fig. XVI-15. Battery charge regulator, *Surveyors I–IV***

**Table XVI-2. Launch-to-touchdown battery energy management, SC-1 through SC-4**

| Electrical system | Spacecraft 1 and 2, W-hr | Spacecraft 3 and 4, W-hr |
|---|---|---|
| Required system energy | 7230 | 6220[a] |
| Gross solar panel energy (90 W) | 5770 | 5770 |
| Net solar panel energy (75% efficiency) | 4330 | 4330 |
| Battery energy used through touchdown | 2900 | 1890 |
| Available battery energy at launch (two batteries) | 4400 | 4400 |
| Total battery energy remaining at touchdown | 1500 | 2510 |
| Main battery energy remaining at touchdown | 1050 | 2160 |
| Optimum charge regulator efficiency 75%<br>Booster-regulator efficiency 80%<br>Maximum power point of solar panel during transit<br>V = 47 V<br>I = 1.90 A<br>P = 80 W | | |

[a]For SC-3 and SC-4, the system energy required was reduced because of the improvements in the redesigned 3-phase power conditioning units.

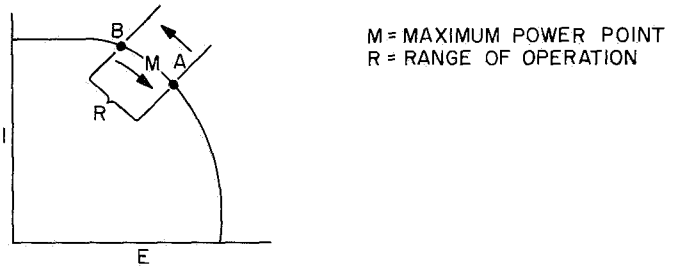



**Fig. XVI-16. Optimum charge regulator operating procedures**

The block diagram of the B/R is shown in Fig. XVI-17.

The B/R was composed of a DC-to-DC converter employing a square-loop oscillator–transformer to boost the voltage, full-wave rectifiers, and filters. The preregulator of the B/R converted the unregulated bus voltage to the regulated 30.5 V ±1% on what was known as the preregulated bus. Since the unregulated bus could vary above and below this voltage, a combination of boost, series, and shunt regulators was used to maintain 30.5 V ±1% on the preregulated bus. The series and shunt regulators functioned only when their input voltages exceeded predetermined limits.

The essential loads (loads considered essential to the operation of the spacecraft such as receivers and command decoders) were supplied from the preregulated bus through two series diodes. The diodes dropped the preregulated bus voltage of 30.5 V to the essential bus voltage of 29.0 V. The preregulated bus also supplied the flight control regulator and the nonessential regulator, which in turn supplied the flight control and nonessential buses, respectively. These regulators could be turned on and off by earth commands. As a subsystem protective measure, the B/R nonessential regulator also functioned as an OTC, removing power from the nonessential bus under abnormal load conditions. If an overload occurred on the nonessential bus, the OTC first limited the bus current to approximately 11 A for a maximum of 120 msec, and then, if the overload still persisted, the OTC would trip, shutting off the power to the loads on the nonessential line. The OTC could be enabled by ground command, returning power to the nonessential bus. Each load on the nonessential bus could then be turned on, and the problem load could be localized and removed from the system. The nonessential regulator OTC circuit could be bypassed, and turned on and off by ground command. The nonessential regulator also had a bypass mode of operation which connected the preregulated bus directly to the nonessential bus. This mode would have been used only if the nonessential regulator had failed.

The flight control regulator which was housed in the B/R used remote sensing to control the output voltage at the flight control load.

The B/R also housed logic circuits that provided the command output for automatic solar panel deployment initiated by the *Centaur/Surveyor* separation signal. A digital output registered whether the solar panel deployment logic was turned on, and various transducers gave temperature, voltage, and current measurements for telemetry.

## Table XVI-3. User's load table

| Status | Major users | 29-V essential bus load regulated current, mA | 29-V nonessential bus load regulated current, A | 29-V flight control bus load regulated current, A | 22-V unregulated bus load current, A |
|---|---|---|---|---|---|
| Continuous | Central command decoder | 28 (av)<br>150 (peak) | | | |
| Command | Analog-to-digital converter | | 0.053 (av) | | |
| Command | Engineering commutator | | 0.106–0.151 | | |
| Command | Signal processor | | 0.0083 (av) | | |
| | Altitude marking radar | | | | 3.3 |
| Command | Engineering mechanisms auxiliary | | 0.750 (max pulse) | | 19.0<br>9.5 (pulse) |
| Command | Transmitter | | 2.1 (max) 0.290 | | |
| Continuous | Receiver | | | | 0.072 |
| Command | Approach TV | (SC-1 only) | 0.350 | | 0.664 |
| | Approach TV temp control | (SC-1 only) | 0.097 | | |
| | Survey TV | | 0.350 | | 3.8 (motor) |
| | Surveyor camera temp control | | 0.097 | | 1.84 |
| Commond | Radar altimeter and doppler velocity sensor | | | | 29.0 |
| Command | Flight control coast phase | | | 1.350 | 0.010–2.0[b] |
| Command | Flight control thrust phase pawer | | | 1.6–21 | 2.6 |
| Command | Battery charge regulator | | | | 0.180 |
| Command | Booster-regulator antenna/solar panel positioner logic | | 0.016 | | 12.0 (pulse max) |
| Command | Narrow band voltage-controlled crystal oscillator | | 0.020 | | |
| Command | Transponder | | 0.029 | | 0.008 |
| Command | Compartment C temperature control[a] | | 0.004 | | 0.433 |
| Cammand | Compartment A heater with automatic control | | | | 0.907 |
| Command | Compartment B heater with automatic control | | | | 0.900 |
| Command | Strain gage power[c] | | 0.108 | | |
| Command | Vernier line thermal Centaur[c] | | 0.025 | | 0.117–0.275 |
| | Vernier oxidizer tank thermal Centaur | | 0.025 | | 0.320 |
| Command | Altitude Mark Voltor heater | | 0.057 | | 0.152 |
| Command | Alpha scattering | | 0.054 | | |
| Command | Alpha scattering heater | | 0.0097 | | 0.236 |
| Command | Soil mechanics/surface sampler | | | | 0.120 (max) |

[a]The heater was turned on 8 hr before touchdown and operated at a duty cycle of 100%. The transit switch drive was drawn from regulated power.

[b]Unregulated current varied due to gyro heater cycling. Average gyro heater duty cycle of 25%.

[c]There were three vernier lines heaters and three vernier oxidizer tank heaters. Under nominal conditions the heater may not be operative or may operate on a 50% duty cycle.

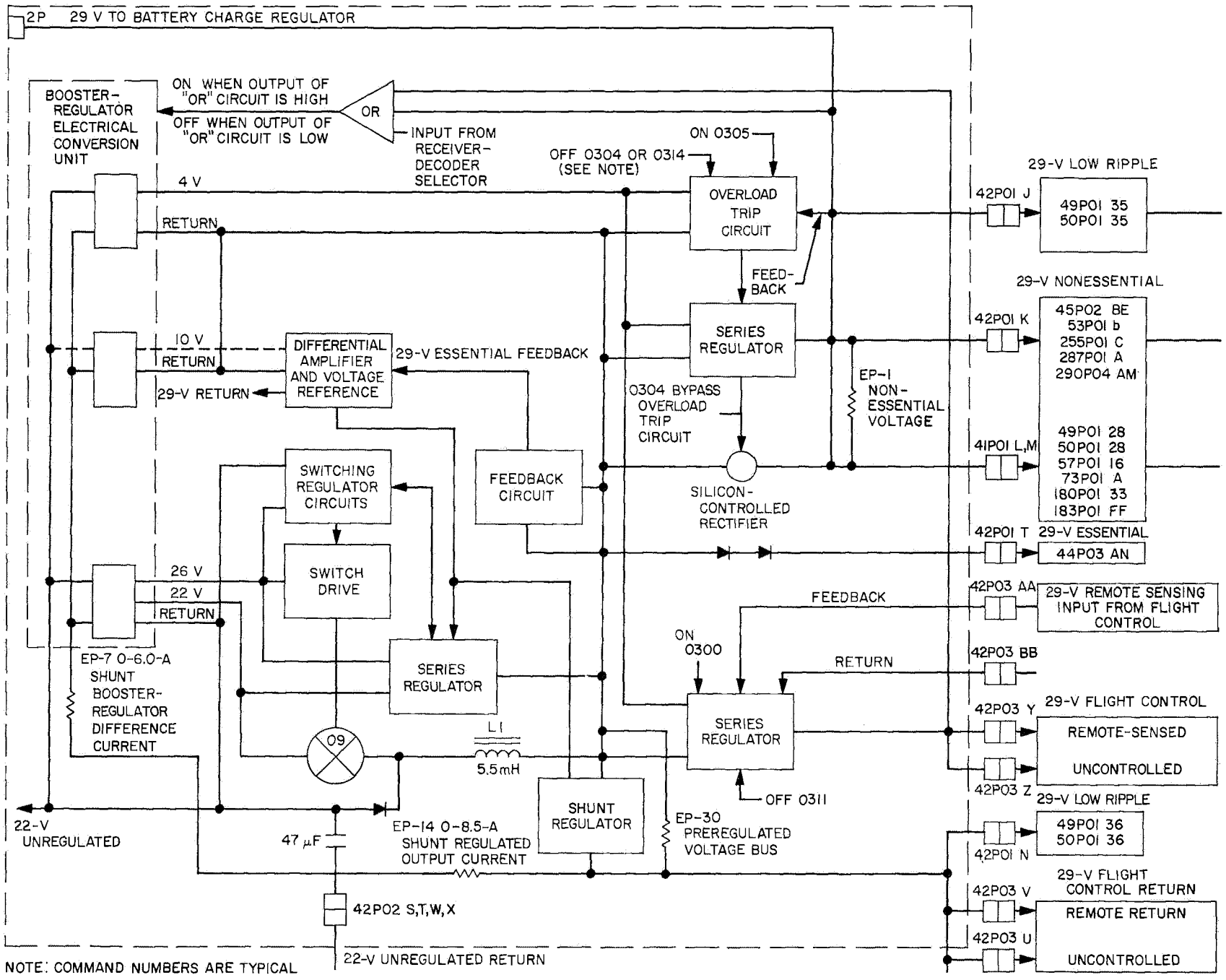



**Fig. XVI-17. Booster-regulator block diagram**

**Table XVI-4. Booster-regulator output characteristics**

| Output buses | Current, A | Voltage, VDC |
|---|---|---|
| Essential bus | 0–0.6 | 29.0 ±0.58 |
| Flight control bus | 0–3.0 | 29.0 ±0.29 |
| Nonessential bus (overload trip circuit enabled) | 0–6.0 | 29.0 ±0.29 |
| Nonessential bus (overload trip circuit bypass) | 0.15–6.0 | 29.0 (±1.01 −0.87) (worst condition) |
| The ripple and noise limits for all buses:<br>50 mV peak-to-peak below 100 kHz<br>2-V peak-to-peak periodic spikes whose lowest frequency component is greater than 100 kHz<br>0.1 V/rms above 100 kHz | | |

The B/R was located in compartment B. The maximum weight of the unit was 8.0 lb.

***b. Electrical conversion units.*** The ECUs operated from the 29 or 22 V supplied by the buses, and converted it to various other voltages required by each subsystem. The ECUs were physically integral modules of the subsystems. They were typically magnetic oscillators with transformer–rectifier outputs followed by capacitor filters. The voltages supplied by the ECUs ranged from 6 V to 3 kV. The flight control subsystem employed a 400-Hz three-phase supply which drove the gyro and Canopus sensor motors. This supply experienced an early redesign. The redesigned unit was installed and flown on *Surveyor III* and subsequent spacecraft.

Figure XVI-18 (top) shows the power supply used for *Surveyors I* and *II*, and Fig. XVI-18 (bottom) shows the supply used for all other *Surveyor* spacecraft. The *Surveyor I* unit utilized a Scott-T transformer to produce three-phase sinewave power from a two-phase drive signal. This method simplified the design of the supply, but was costly from an efficiency standpoint. The *Surveyor III* unit employed three separate amplifiers each driven by a separate phase signal generated in the flight control programmer. The output of each of the power amplifiers was a square wave. Previous experience with *Ranger* and *Mariner*, and tests performed on the *Surveyor* gyros, demonstrated that a square-wave source would be satisfactory. The redesigned unit eliminated sinewave filtering and improved the efficiency of the unit from 48 to 80%. A list of all ECUs, with their associated output capabilities, is given in Table XVI-5.

### 4. Auxiliary Functions

***a. Engineering mechanisms auxiliary.*** The EMA was part of the power distribution and control system and was located in compartment A.

The unit decoded signal commands and provided squib-firing power. A simplified block diagram of the unit is shown in Fig. XVI-19.

The switching capabilities of the EMA are:

(1) Switching of constant-current sources and SCRs, upon command or signal, to provide current pulses to the selected squib circuit.

(2) *On/off* transistor switching, upon command, to provide regulated nonessential voltage to the vehicle accelerometer amplifiers.

(3) *On/Off* transistor switching in return lines, upon command, to provide unregulated voltage to thermal control circuits for vernier lines, fuel and oxidizer tanks, altitude marking radar (AMR), and approach TV chassis electronics. After SC-1 and SC-2, the approach TV chassis electronics command was eliminated and these command circuits were assigned to the soil mechanics surface sampler (SM/SS) for SC-5 through SC-7.

(4) Irreversible "on/off" pyro switching, upon command or by signal from flight control subsystem (FCS), to provide unregulated voltage to the radar altimeter/doppler velocity sensor (RADVS). Unregulated voltage was removed by command to turn off all flight control power. The irreversible switch was replaced with an on/off relay circuit on SC-5 through SC-7.

(5) SCR turn-on upon receipt of the "flight-control-coast-phase-on" gate signal from an ECU in the FCS with unregulated voltage. The SCR was turned off by the "all-flight-control-power-off" signal which removed the SCR load current.

The EMA was composed of the following functional circuits and subunits:

(1) One subsystem command decoder.

(2) Two redundant constant-current generators that provided squib-firing current pulses. Either constant generator was capable of delivering the required output pulses of 9.5 ±0.5 or 19.0 ±1.0 A.

(3) Transistor switches to control the application of regulated and unregulated voltages.

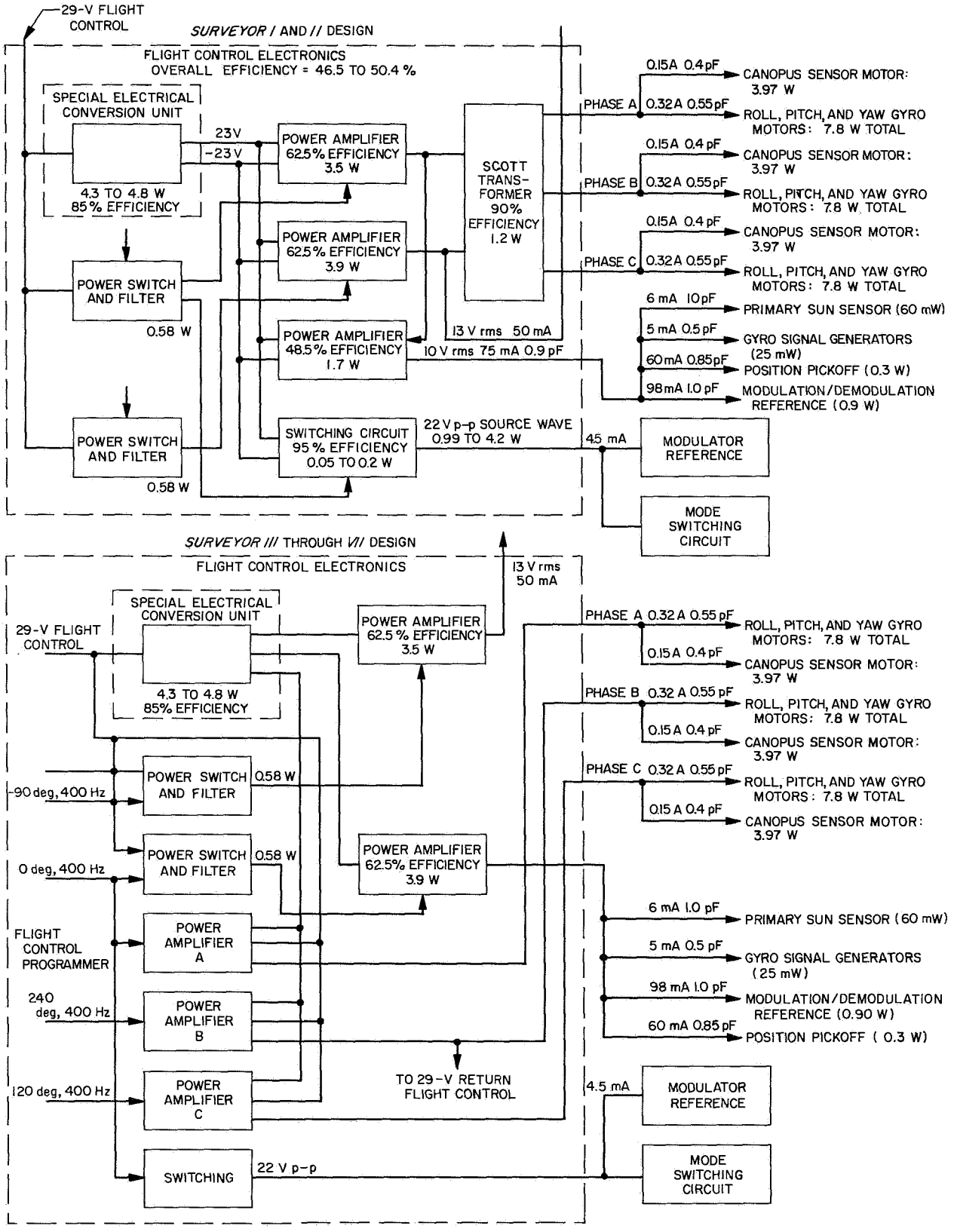



**Fig. XVI-18. Flight control three-phase power supply**

## Table XVI-5. Characteristics of the electrical conversion units

| Title | Input | | | Output | | | Efficiency, % | Status |
|---|---|---|---|---|---|---|---|---|
| | Voltage, V | Current, A | Power, W | Voltage, V | Current, A | Power, W | | |
| Flight control, thrust phase | 29 | 0.97 | 28.4 | 27<br>29<br>−29<br>4 | 0.590<br>0.447<br>0.347<br>0.600 | 25.4 | 89.5 | Commond |
| Flight control coast phase | 29 | 0.256 | 7.4 | 6<br>3<br>12<br>−12<br>−29 | 0.030<br>0.500<br>0.050<br>0.016<br>0.086 | 5.96 | 80.5 | Self-shorting |
| Flight control, AC three phase | 29 | 1.7 | 49.0 | 23<br>−23<br>28.5<br>13 rms<br>10 rms<br>22 P–P<br>25 phase A<br>25 phase B<br>25 phase C<br>25 phase A<br>25 phase B<br>25 phase C | 0.026<br>0.026<br>0.061<br>0.050<br>0.175<br>0.190<br>0.320<br>0.320<br>0.320<br>0.160<br>0.160<br>0.160 | 43.9 | 89.0 | |
| | | | | | Gyro motor | | | |
| | | | | | Canopus motor | | | |
| Transmitter A and B, each unit | 29 | 1.92 | 55.0 | 60<br>−425<br>−825<br>−1250 | 0.001<br>0.006<br>0.040<br>0.002 | 38.1 | 69.4 | Command |
| Traveling-wave tubes A and B, each unit | 29 | 0.79 | 2.3 | ±5.2 | 0.285 | 1.48 | 65 | Command |
| TV communication | 29 | 0.031 | 0.90 | 12<br>25<br>−25<br>−12 | 0.002<br>0.0095<br>0.0155<br>0.0025 | 0.68 | 75 | Command |
| Central command decoder, each unit | 29 | 0.0318 | 0.92 | 20<br>12<br>−8<br>−15 | | 0.76 | 70 | |
| Engineering signal processor | 29 | 0.005 | 0.145 | −25<br>12<br>−12 | 0.0002<br>0.0015<br>0.005 | 0.083 | 58 | Commond |
| Engineering signal processor and auxiliary engineering signal processor units, each unit | 29 | 0.103 | 2.94 | −25<br>25<br>12<br>−12<br>−30<br>29<br>4.85<br>−13<br>3<br>3<br>3 | 0.038<br>0.011<br>0.065<br>0.019<br>0.001<br>0.002<br>0.021<br>0.008<br>0.003<br>0.003<br>0.003 | 2.5 | 85 | Command |

Table XVI-5 (contd)

| Title | Input | | | Output | | | Efficiency, % | Status |
|---|---|---|---|---|---|---|---|---|
| | Voltage, V | Current, A | Power, W | Voltage, V | Current, A | Power, W | | |
| Central signal processor, two units, each unit | 29 | 0.053 | 1.54 | 25<br>−25<br>12<br>−12 | 0.006<br>0.003<br>0.053<br>0.029 | 1.35 | 88 | Command |
| Survey TV camera | 29 | 0.31 | 9.0 | 4.85<br>300<br>−100<br>25<br>−25<br>6.3<br>25<br>−25<br>25<br>−25 | 0.006<br>0.001<br>0.0006<br>0.0028<br>0.0010<br>0.175<br>0.050<br>0.024<br>0.052<br>0.029 | 5.45 | 60.5 | Command |
| | | Emergency modes | | | | | | |
| Altitude marking radar | 22 | 2.6 | 57.0 | −800<br>65<br>28.5<br>28.5<br>28.5<br>6.6 | 0.0001<br>0.330<br>0.310<br>0.054<br>0.054<br>0.720 | 38.16 | 67 | Command |
| Klystron power and supply/ modulator (radar altimeter and doppler velocity sensor) | 20 | 16.7 | 334 | 6.3<br>6.3<br>−400<br>−500<br>−800<br>−2150 | | | — | Command |
| Simulator data control (radar altimeter and doppler velocity sensor) | 20 | 8.35 | 167 | 100<br>−100<br>25<br>−25 | | | — | Command |
| Receiver 1, A and B, each unit, from 22 V regulated to 15 V | 15 | 0.004 | 0.060 | 29<br>−12 | 0.0014<br>0.0005 | 45.4 | 75 | Continuous |

(4) Transistor-controlled SCRs to channel constant-current pulses to those squib circuits selected by command and retroignition and separation.

(5) Pyrotechnic or relay switches to control RADVS power.

***b. Thermal control and heater assembly.*** In each thermal-controlled compartment there was an electrical heating element with sensing and control circuits which could be used to maintain the temperature of the compartment. The heaters operated from the unregulated bus and could be in any one of these modes by command:

(1) Heater power "on."

(2) Heater power "off."

(3) Temperature control "automatic."

Automatic control was achieved by a temperature-sensing diode that biased transistor control circuitry, which in turn controlled an SCR. Compartment A temperature control was set to 50°F and compartment B to 10°F.

***c. Ground command.*** The power subsystem had a number of ground commands assigned to perform functions scheduled during the mission and to overcome failure modes in key areas. Table XVI-6 lists all the

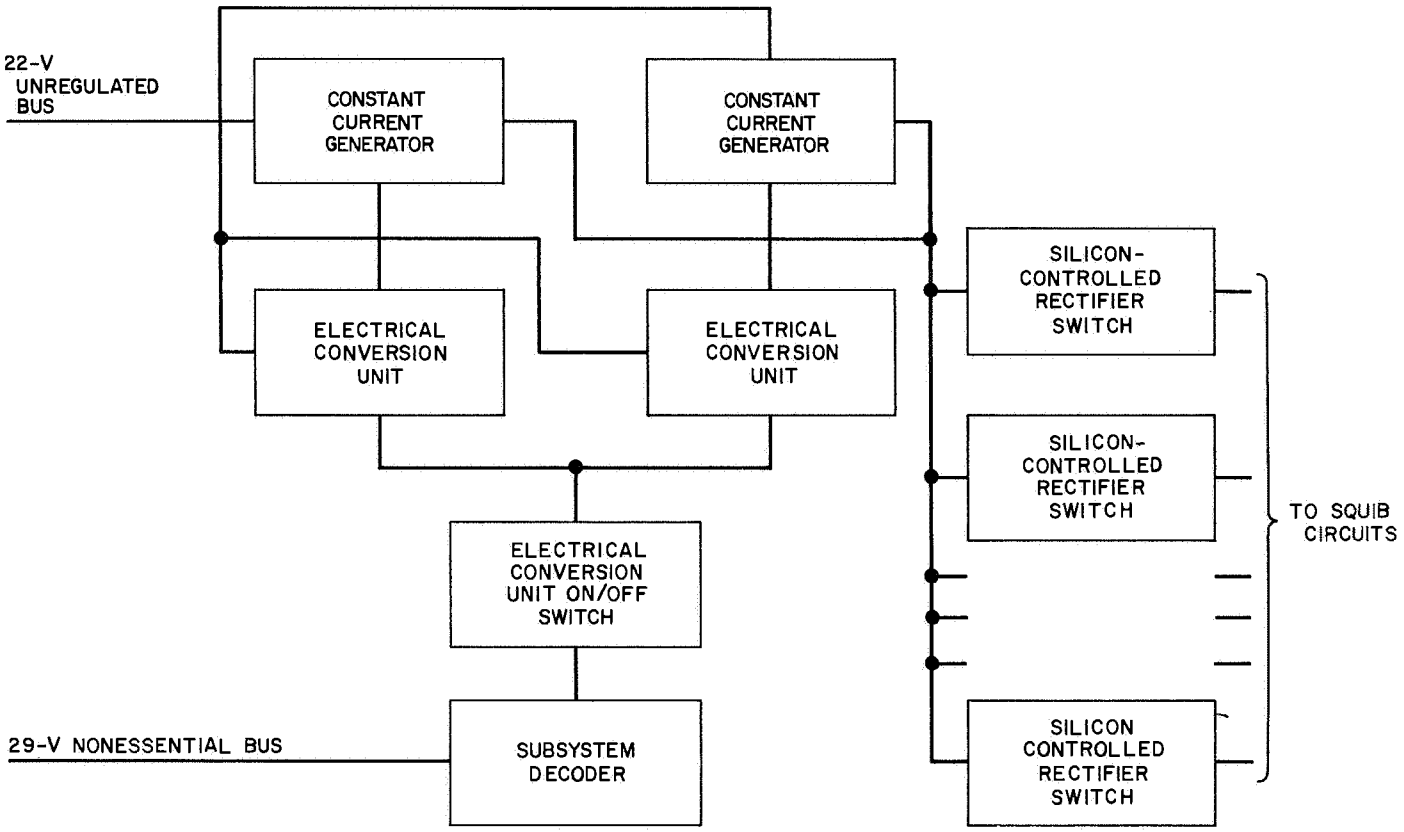



**Fig. XVI-19. Simplified block diagram of engineering mechanism auxiliary**

ground commands assigned to the power subsystem. The functions of the commands are self-explanatory. New commands were added and others deleted to support the revised requirements of the last three spacecraft.

*d. Telemetry transducers.* In-flight engineering evaluation of the power subsystem was accomplished by means of 30 telemetry voltage and current measurements. All voltage measurements were accomplished by means of voltage dividers. Current measurements were accomplished by means of shunts. Figure XVI-20 shows the location of the various telemetry shunts. Filtering was used across all shunts to reduce interference from spacecraft noise. The filtering, however, reduced the transient response of the current telemetry measurements.

A number of transducers for measurements were in the booster-regulator, and these measured the following:

(1) Nonessential bus voltage.

(2) Preregulated bus voltage.

(3) Nonessential bus current.

(4) Booster-regulator bus current.

(5) Booster-regulator temperatures.

A list of all measurements is contained in Section XXI.

### 5. Design Changes

Review of the circuit design of each power unit conducted at JPL and subsequent design reviews underlined a number of marginal areas.

Action directives were initiated and joint HAC/JPL meetings were held to resolve the problem areas. Functional testing of the units on the spacecraft also uncovered a number of problems. Additional circuit modifications were incorporated to reduce the power consumption and to increase the efficiency and reliability of the power distribution to the other subsystems.

To correct problems experienced in system testing and to modify circuits with marginal performance, engineering change requests (ECRs) were initiated.

**Table XVI-6. Ground commands assigned to power subsystems**

| Command No. | Spacecraft | |
|---|---|---|
| | SC-1 through SC-4 | SC-5 through SC-7 |
| 0300 | Flight control power on | Spare |
| 0301 | Enable battery pressure logic | Same |
| 0302 | Disable battery pressure logic | Same |
| 0304 | Bypass main overload trip circuit (29 V nonessential) | Same |
| 0305 | Enable main overload trip circuit (29 V nonessential) | Spare |
| 0306 | Optimum charge regulator on, bypass off | Solar panel switch off, bypass off |
| 0307 | Optimum charge regulator bypass on and optimum charge regulator off | Optimum charge regulator bypass on and solar panel switch off |
| 0310 | Optimum charge regulator off | Solar panel switch off |
| 0311 | Flight control power off | Same |
| 0312 | Spare | Battery charge regulator to preregulated bus |
| 0313 | Spare | Battery charge regulator to unregulated bus |
| 0314 | Nonessential loads off | Same |
| 0315 | Solar panel deployment logic on | Same |
| 0316 | Solar panel deployment logic off | Same |
| 0317 | Auxiliary battery mode on | Spare |
| 0320 | Restore main battery mode | Spare |
| 0321 | Disable battery transfer logic | Spare |
| 0322 | High-current mode on | Spare |
| 0323 | High-current mode off | Spare |
| 0331 | Spare | Flight control power on (SC-5 only) |
| 0332 | Spare | Enable main overload trip current (SC-5 only) |
| 0333 | Spare | Flight control power on (SC-6 only) |
| 0334 | Spare | Enable main overload trip circuit (SC-6 only) |
| 0335 | Spare | Flight control power on (SC-7 only) |
| 0336 | Spare | Enable main overload trip circuit (SC-7 only) |
| 0411 | Compartment A heater on | Same |
| 0412 | Compartment A automatic temperature control | Same |
| 0413 | Compartment A heater off | Same |
| 0414 | Compartment B heater on | Same |
| 0415 | Compartment B automatic temperature control | Same |
| 0416 | Compartment B heater off | Same |

The design changes described below were made to the SC-1 through SC-4 systems for the reasons indicated.

(1) During SC-1 system testing, several actuations of the overload trip circuitry were experienced. Modifications were recommended and were incorporated. For the SC-1 B/R, because of schedule constraints, it was decided to remove the overload tripping circuit.

(2) During SC-1 thermal-vacuum testing, the B/R and BCR units generated high levels of noise. A filter was designed to attenuate the noise.

(3) During SC-2 solar thermal-vacuum testing, the B/R experienced thermal runaway when the thrust phase power was commanded "on." The problem was traced to parasitic oscillation induced by the increased load to the flight control regulator and preregulator. The feedback loops of both units were subsequently stabilized and additional filtering was introduced at the output of the preregulator.

(4) During system testing of SC-1 and SC-2, a number of battery failures were experienced. The failures were attributed to the excessive charge–discharge cycles of the battery caused by high noise and spikes on the unregulated bus. Filtering was introduced in the output and input of the BCR and B/R.

(5) The OCR was turned off during thermal-vacuum tests at temperature near 155°F. The circuit was modified to permit reliable operation up to 160°F.

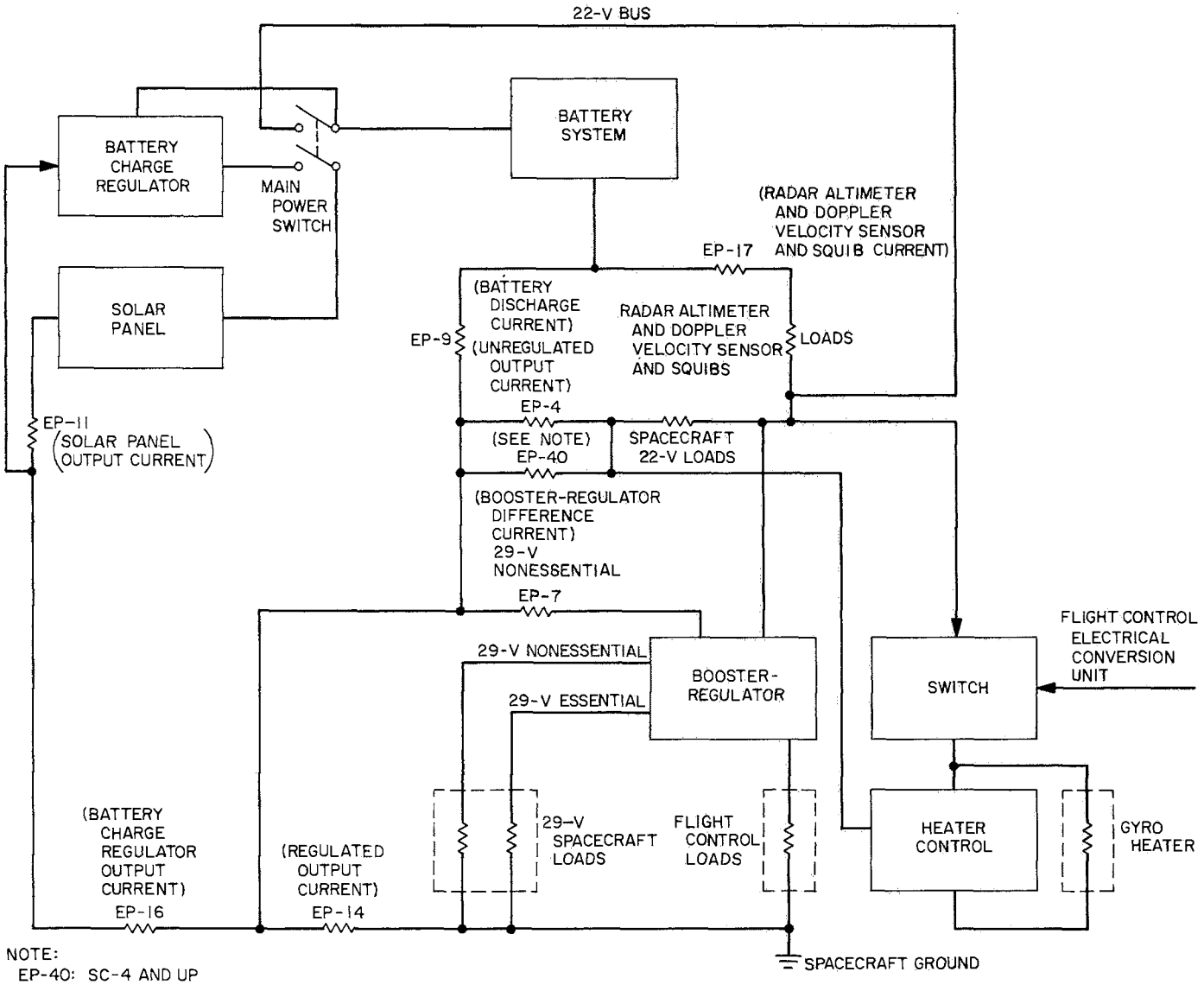



**Fig. XVI-20. Electrical power subsystem telemetry shunt locations**

(6) Motor stepping pulses were longer than required, causing excess heat dissipation. The motor pulse timing circuit was modified to change pulses from 60 ±10 to 48 ±8 msec.

(7) The OCR internal energy consumption was considered excessive, and it was redesigned. One unit was fabricated and used on SC-4.

(8) High-voltage spikes occurred on the 29-V essential bus when the OTC was recycled. The cycling function was removed from the B/R OTC.

(9) Sawtooth oscillation appeared on the nonessential bus when spacecraft loads were being supplied through the bypass circuit. Bypass circuit drive and stability were increased.

(10) The flight-control-regulator-on circuit was susceptible to negative transients. Circuitry was added to desensitize the flight control command circuit.

(11) Excessive voltage dip on the B/R essential bus caused command decoder turn-off. Circuitry was revised to improve transient response of the preregulated bus.

(12) During the SC-1 solar-thermal-vacuum test, squib-firing pulses were generated by the B/R during the stepping of the antenna/solar panel positioner. Noise-suppression circuitry was incorporated.

(13) Instability of an essential bus-to-preregulator feedback loop at high temperature was reported during

the thermal-vacuum test. Circuit modifications were introduced.

(14) The command lines of the EMA were noise-sensitive. The lines were desensitized by zener diodes.

(15) To provide actuation of solar panel and roll-axis squib firing for automatic solar panel deployment required an addition of OR gates to the EMA.

(16) Excessive vehicle accelerometer module heating was reported. The power transistor was mounted to the chassis to provide adequate heat sinking.

(17) Squib-firing SCRs could be dV/dt sensitive. The circuits were desensitized.

(18) The three-phase power supply, whose efficiency was about 48%, was redesigned.

The three-phase unit supplied sinewave power to the gyros and Canopus sensor motors. *Ranger* and *Mariner* gyros had successfully operated from a square-wave power supply. Tests performed with the *Surveyor* gyros verified that the square-wave source would be satisfactory. The redesigned unit eliminated sinewave filtering and improved the efficiency of the unit from 48 to 80%. The new unit became available for the *Surveyor III* spacecraft.

The modifications introduced in the SC-1 through SC-4 units improved the performance of the power subsystem, but performance was still marginal. Operational limitation and strict power management control had to be enforced to ensure satisfactory operation. The proposed modifications of the redesigned B/R and the BCR were found to be impractical. Therefore, a redesigned power subsystem was proposed which optimized the solar panel power utilization. The new subsystem required a new solar panel, a new B/R, and a new BCR. When developed, this new subsystem was used for the *Surveyor V–VII* missions.

## C. Design Used for *Surveyor V–VII* Missions

The *Surveyor V–VII* power subsystem was designed to provide better matching characteristics between sources and power conditioning units. Figure XVI-21 presents the block diagram. A number of improvements were introduced into the subsystem to increase the capability and the overall performance.

The power subsystem was required to provide power to satisfy the transit and touchdown requirements, and to land with enough capacity to operate the spacecraft in the event that solar panel power might not be available for about 20 hr.

In the *Surveyor I–IV* power subsystem, the solar panel maximum power point during transit was around 47 V. Through the use of the OCR, maximum power was obtained from the panel and converted to usable battery voltage. However, 16–20 W was lost during operation. The resultant power-source voltage, which was determined by the battery at a nominal 22 V, was boosted to 30.5 $\pm$1 V. The new solar panel eliminated the need for the OCR since power transfer could efficiently take place directly from the solar panel to the preregulated bus. This had a twofold advantage: it eliminated the losses in the OCR, and the losses internal to the B/R preregulator circuitry were considerably reduced because most of the preregulated output current was derived directly from the solar panel.

During lunar operation, the panel output was switched to the preregulator bus to directly charge the battery. The solar panel voltage during this time was still reasonably matched to the preregulated bus.

The redesigned BCR had the OCR circuits replaced by a transistor switch to perform the switching of the solar-panel output. The automatic trickle-charge circuitry was also removed to eliminate noise on the battery that had directly affected the charging characteristics of the battery. The power dissipation of the new BCR was decreased by 16–20 W.

The new B/R included circuitry to directly accept the solar panel output at the preregulated bus. A shunt regulator was also added to shunt any extra solar panel power to the battery.

Improvements accomplished by the redesigned power subsystem were:

(1) Increased efficiency of the power subsystem by eliminating losses in the OCR and B/R. Higher efficiency was especially pronounced during transit because the majority of the required regulator current did not have to pass through the preregulator.

(2) Improved thermal characteristics of the two thermal-controlled compartments for other subsystems by reducing the heat dissipated by the BCR and B/R.

(3) Spacecraft power requirements were reduced to the point that the auxiliary battery was not needed.

(4) The auxiliary battery and ABC unit were eliminated. Even without the auxiliary battery energy of 1000 W, the new power subsystem achieved an overall increase of landed storage energy of over twice the amount experienced on SC-1. The deletion of the auxiliary battery also made available space for the alpha scattering experiment.

(5) Use of a lower-power, more reliable solar panel was permitted. The new panel also reduced the hazardous high voltage expected at lunar sunrise.

(6) In-flight power requirement was reduced to the point that no battery discharge occurred during the cruise mode of the mission. (This was expected to improve the reliability of the mission and the battery performance during lunar operations.)

(7) Reliability of the power subsystem was improved by simplification and a reduction of the parts count.

The battery-power utilization plans for *Surveyors V–VII* are summarized in Table XVI-7.

The SC-5 through SC-7 power subsystem consisted of the following units:

(1) Solar panel (new).

(2) Main battery.

(3) Main power switch.

(4) Battery charge regulator (new).

**Table XVI-7. Launch-to-touchdown battery utilization, SC-5 through SC-7**

| Electrical system | Battery utilization, W-hr |
|---|---|
| Required system energy | 6520 |
| Gross solar-panel energy (81 W) | 5260 |
| Net solar-panel energy (battery charge regulatar efficiency 95%) | 4990 |
| Battery energy used through touchdown | 1530 |
| Battery energy available at launch (min) | 3500 |
| Battery energy remaining at touchdown | 1970 |
| Battery charger efficiency 95%<br>Booster-regulator efficiency 80%<br>Maximum power point of solar panel during transit<br>Potential: 30.5 V<br>Current: 2.66 A<br>Power: 81.0 W | |

(5) Booster-regulator (new).

(6) Engineering mechanism auxiliary (modified).

(7) Thermal control and heater assembly.

(8) Electrical conversion units.

The performance characteristics of the redesigned units are summarized in Table XVI-8. A brief description of the design parameters and major modifications incorporated in the SC-5 through SC-7 subsystem follows:

### 1. Solar Panel

The solar panel was redesigned to match the power subsystem requirement of maximum power point during transit and minimum open circuit during lunar day operations. The electrical performance acceptance criteria were as follows:

| Parameter | Criteria |
|---|---|
| Transit mode | |
| Power output at max power output | 81 W min at 143°F |
| Voltage output at max power output | 30.5 ±2 V at 56 ±5°C (133 ±10°F) |
| Lunar operations | |
| Power output at max power output | 60.5 W min at 121°C (250°F) |
| Voltage output at max power output | 22 V min at 121°C (250°F) |

*Mariner* spacecraft solar panel techniques of flat-cell construction were used to assemble 3626 solar cells on the 9-ft² substrate. A new substrate design was also required to satisfy the expected loads of the modified A/SPP. The new substrate used aluminum honeycomb and aluminum facing material. The cell layout on the solar panel consisted essentially of a folded voltage string. A view of the cell side of the panel is shown in Fig. XVI-22. The panel was divided into three isolated electrical sections: sections A, B, and C, as shown in Fig. XVI-23. The isolation diodes for each electrical section were included as subassemblies on the solar panel. Each section contained 74 submodules in series. Each submodule contained seven parallel connected 1- × 2-cm, P-on-N, silicon solar cells with Kovar bus bar interconnections. The voltage strings of each electrical section were parallel-connected (interconnected) at the midpoint of the voltage string, as well as at each end.

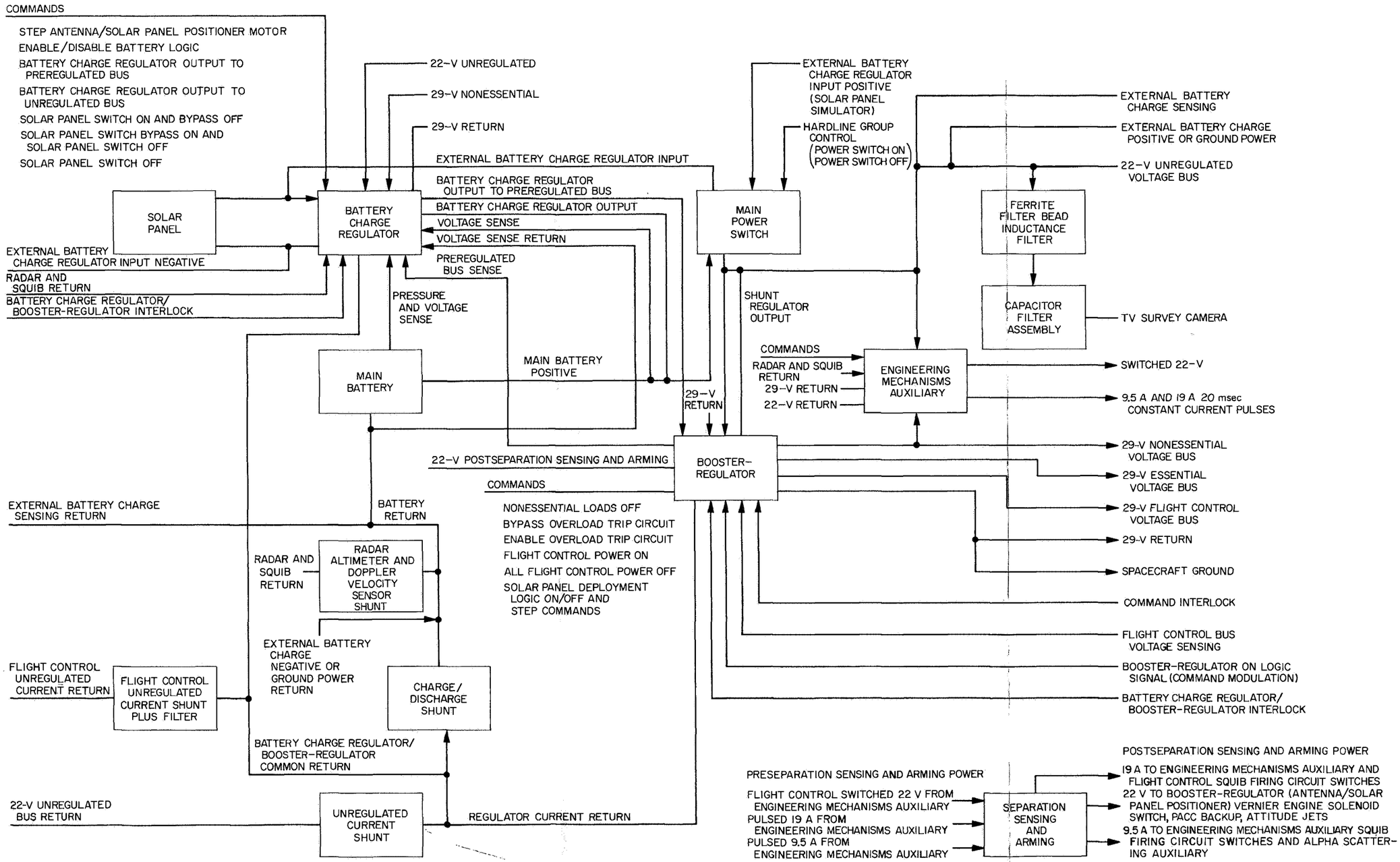



**Fig. XVI-21. Electrical power subsystem block diagram, *Surveyors V–VII***

**Table XVI-8. *Surveyors V–VII* power subsystem performance characteristics of the new units**

| Unit | Performance characteristics | | Unit | Performance characteristics | |
|---|---|---|---|---|---|
| Solar panel | Solar panel power at mean solar intensity: 81 W at 143°F, and 60.5 W (min) at 250°F | | Booster-regulator | Unregulated input: | |
| Battery charge regulator—output select switch | Positions: | | | Voltage: | 16.75–27.3 VDC |
| | Preregulated bus on command | | | Current: | 15.3 A at 18 VDC (max for 7-A output) |
| | Unregulated bus on command or when preregulated bus reaches 34 ±1 VDC | | | Regulated input: | |
| | Logic: | | | Voltage: | 29.0 ±0.29 VDC |
| | Off with battery voltage 21.16–27.30 VDC | | | Current: | 25 mA max (solar panel deployment logic on) |
| | Off with battery pressure at 65 ±5 psia | | | Efficiency: | 80% nominal |
| | Restored operation, with battery pressure between 55 and 65 psia | | | Regulated outputs: | |
| | Input voltage: | 17.5–70 VDC | | Flight control bus: | 0–3.0 A at 29.0 ±0.29 VDC |
| | Input current: | 0–3.5 A | | Nonessential bus: | |
| | Output voltage: | | | (overload trip circuit enabled): | 0–6.0 A at 29.0 ±0.29 VDC |
| | Unregulated bus: | 18–27.3 VDC | | (overload trip circuit bypassed): | 0–6.0 A at 29.0 ±0.87 VDC |
| | Preregulated bus: | 30 ±0.3 VDC | | Essential bus: | 0–0.6 A continuous at 29.3 ±0.586 VDC |
| Battery charge regulator—antenna/solar panel positioner circuitry | Output current: | 0–3.5 A<br>17.8 A (max) | | | 0–0.60 A (20-msec pulse) |
| | Pulsewidth: | 48 ±8 msec | Booster-regulator—overload trip circuit | Trip level: | 8.0 ±0.8 A for 40 ±20 msec |

Sections B and C each contained two voltage strings. Section A contained three voltage strings. Sections B and C and two of the voltage strings of section A were vertically arranged on the solar panel in a symmetrical form. The remaining string of section A was distributed over three areas of panel, along the right and the left edges of the panel, and along a small area in the midsection of the panel. This reduced the possibility of the loss of a complete section (two voltage strings) resulting from shroud damage during the shroud-separation event. If a shroud had damaged the edge of a panel, only section A would have been affected. Figure XVI-24 shows a typical current–voltage characteristic for the *Surveyor V–VII* solar panel design.

Transducers to measure temperature, short-circuit current, and open-circuit voltage were mounted on the panel to aid in the evaluation of the solar panel electrical performance during the spacecraft mission.

The flat series–parallel matrix configuration was selected in order to achieve the following:

(1) The cells could be directly interconnected in a series–parallel matrix so that the loss of a single cell would not cause the total loss of power in a circuit.

(2) The flat alignment of the cells permitted the use of less adhesive of lighter weight and better thermal conductivity to the panel substrate.

(3) The array had greater flexibility to survive thermal and vibration effects because the cells were interconnected with thin metallic or mesh connectors.

(4) The repair of a flat-mounted submodule was simpler as one individual cell could be renewed, if required.

The solar-panel weight remained at 8.5 ±0.3 lb. A computer reliability program was conducted to establish

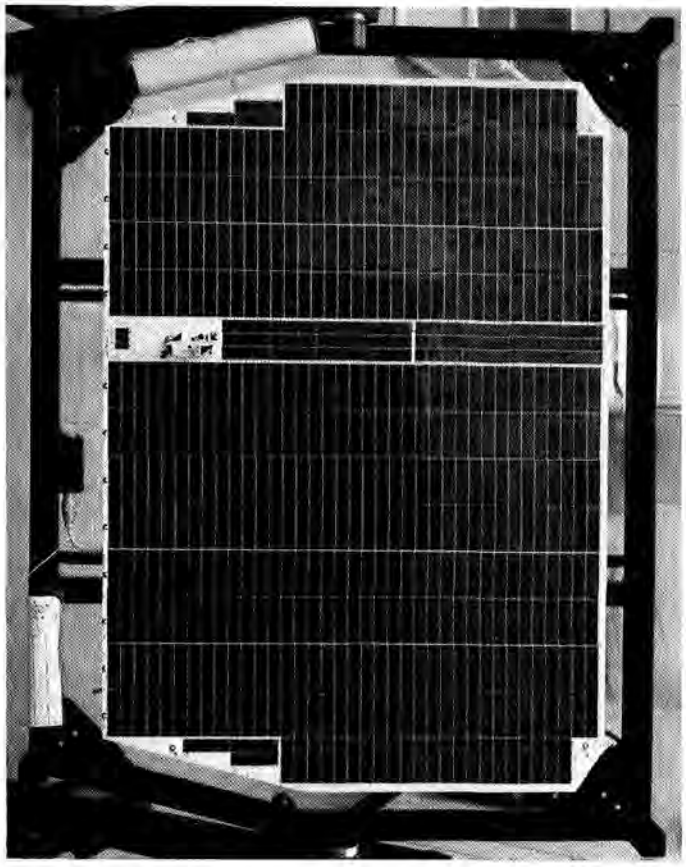


**Fig. XVI-22. Cell side of solar panel**

the confidence level of the new solar panel design. The program consisted of the evaluation of the following items:

(1) Mathematical mode.

(2) Failure mode audit of the design.

(3) Analysis of data.

(4) Confidence level of reliability.

(5) Control of parts, materials, and processes.

(6) Control of subtier contractor.

(7) Sustaining reliability.

See Section XII-B for a detailed discussion of this reliability program.

The new solar panel was fabricated by Electro-Optical Systems, Inc., Pasadena, Calif.

### 2. Main Battery

The same battery design used on *Surveyors I–IV* was used for *Surveyors V–VII*. To improve the quality of the battery, quality control check points were introduced. In addition, studies and qualification tests were initiated to verify the performance characteristics of the units and to improve the probability or survival of the battery through the low temperature of lunar night.

A review of the current manufacturing process of the vendor established that a number of processing control points and critical parameters must be monitored and statistically analyzed on control charts. The monitoring of the quality controls was expected to produce improved quality and uniformity of the product.

Improved control of cement composition and viscosity resulted in superior cement joints. The establishment of minimum lot sizes for all battery materials enabled the vendor to fabricate a minimum of six batteries per lot. This resulted in maximum uniformity of materials within the batteries. All battery cells, as well as the 12 Q cells (lot-qualifying test cells), were identical in plate material, separator, and electrolyte. The emphasis on uniformity was achieved through a detection of lot-to-lot differences in the electrical performance of positive electrodes. Small variations in capacity, efficiency, and discharge voltage were observed on the control charts. The clear reproducibility of battery performance was a direct reflection of the improved methods of fabrication. To maintain a timely flow of batteries, complete monoblocks, plus spares, were fabricated up to the point of activation and stored dry until needed. If problems had occurred in the manufacturing process, the spare monoblocks made from previously qualified materials would have maintained the production schedule until the problems were resolved. Most important, this procedure implemented battery age control by allowing tighter scheduling from activation to spacecraft delivery.

The studies and tests initiated were directed to produce the following information:

(1) Main battery lunar night survival study.

(2) Temperature condition in the batteries during simulated mission (thermocouple battery test).

(3) Low-temperature operation test.

(4) Battery performance under pulsed loads.

A 75-day activated life limit at spacecraft final encapsulation was stipulated for *Surveyor V–VII* flight batteries.

### 3. Battery Charge Regulator

The new solar panel allowed reduction of BCR complexity. The OCR circuit was replaced with a single

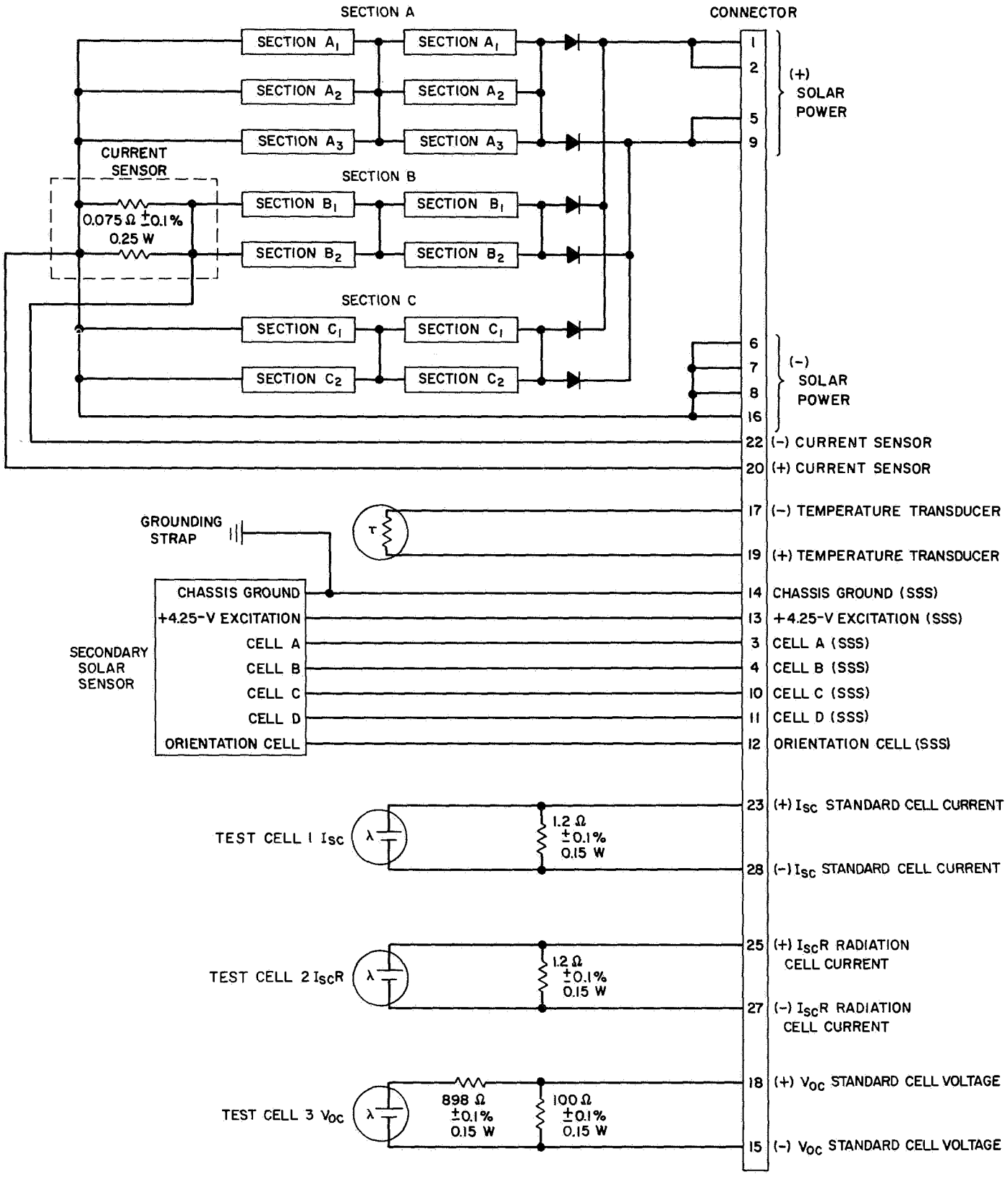



**Fig. XVI-23. Block diagram of solar panel assembly, SC-5, SC-6, and SC-7**

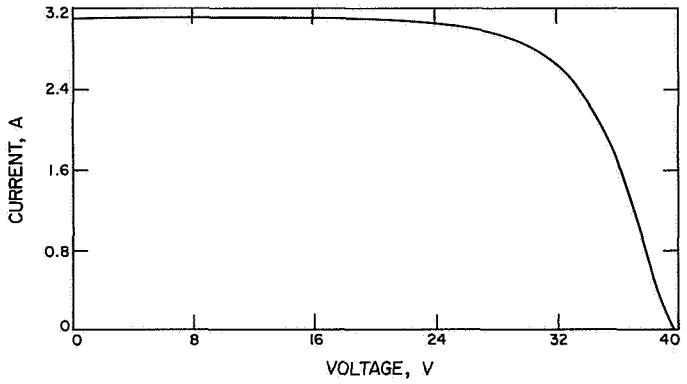



**Fig. XVI-24. *Surveyor* solar panel SN-002, I-E characteristic curve (transit temperature 62°C, solar intensity 140 mW/cm²)**

transistor switch that connected the solar panel to the power subsystem. There were only three modes of operation for the new BCR. In the "on" mode, the solar panel power was connected to the output of the BCR. In the "off" mode, the solar panel was left floating. The "off" mode could be commanded by an earth command or could be automatically switched by the battery voltage above 27.3 V or pressure logic above 65 psia. The automatic turn-off feature of the BCR could be enabled or disabled by earth command. In the bypass mode, an SCR could be energized, bypassing the switching circuit and its logic.

A block diagram of the simplified BCR is shown in Fig. XVI-25. The BCR output select switch logic housed in the unit determined the position of the BCR output to either the B/R preregulator or the unregulated bus. The preregulator logic automatically commanded the solar panel output from the preregulator bus to the unregulated bus when the preregulator voltage was above 34 V.

#### 4. Booster-Regulator

The redesigned B/R functions were essentially the same as in the previous unit. The B/R converter boosted the unregulated bus voltage to 30.0 V ±1%, and the preregulated bus essential loads were fed from the preregulated bus through a series diode which dropped the preregulated bus voltage to the essential bus voltage of 29.0 V. The preregulated bus also supplied the flight control regulator and the nonessential regulator, which in turn supplied the flight control and nonessential buses, respectively. The regulators could be turned on and off by earth commands. The nonessential regulator had a bypass mode which would have been used to connect the preregulated bus directly to the nonessential bus if the nonessential regulator had failed.

A shunt regulator was connected between the preregulated bus and the battery to supply excess solar panel current to the battery and to prevent the solar panel voltage from climbing. In the previous design, the shunt output was connected to ground so that no battery charging was possible. Other changes in the B/R included: (1) the use of higher gain transistors in the electronic conversion unit of the preregulator for increased efficiency, and (2) a closer control of the OTC trip time from the previous 20–120 msec range to a new range of 40 ±20 msec. The B/R also housed the latching relay that connected the output of the BCR regulator to either the preregulated bus during transit or to the unregulated bus during lunar operation.

The B/R operated at higher efficiency, approximately 85%. As a result of the BCR changes, even higher efficiency was achieved, especially during transit, since the majority of the regulator current did not have to pass through the preregulator.

#### 5. Engineering Mechanism Auxiliary

A design modification was introduced in the RADVS switching circuit of the EMA to enable the RADVS system to be turned off and on repeatedly. The old design employed squib switches capable of only one operation per mission. The new design used a latching relay. The standard 20-msec command pulse was not long enough to operate the relay in the new design, and a pulse stretcher circuit was added to the EMA gyro circuit board. Other minor changes included the addition of the SM/SS heater control circuit to the vernier thrust engine fuel line 1 heater-control circuit for *Surveyor VII* only, and the addition of a compartment C heater turn-on circuit.

### D. Construction Techniques and Manufacturing Experience

Power subsystem hardware was designed and packaged to satisfy the constraints of weight limitations and severe environmental requirements.

Structures used for power subassemblies were honeycomb sandwich chassis, which provided maximum strength with minimum weight. Aluminum alloy aircraft-style castings were used for the thermal structures. Manufacturer's cost and parts producibility were the

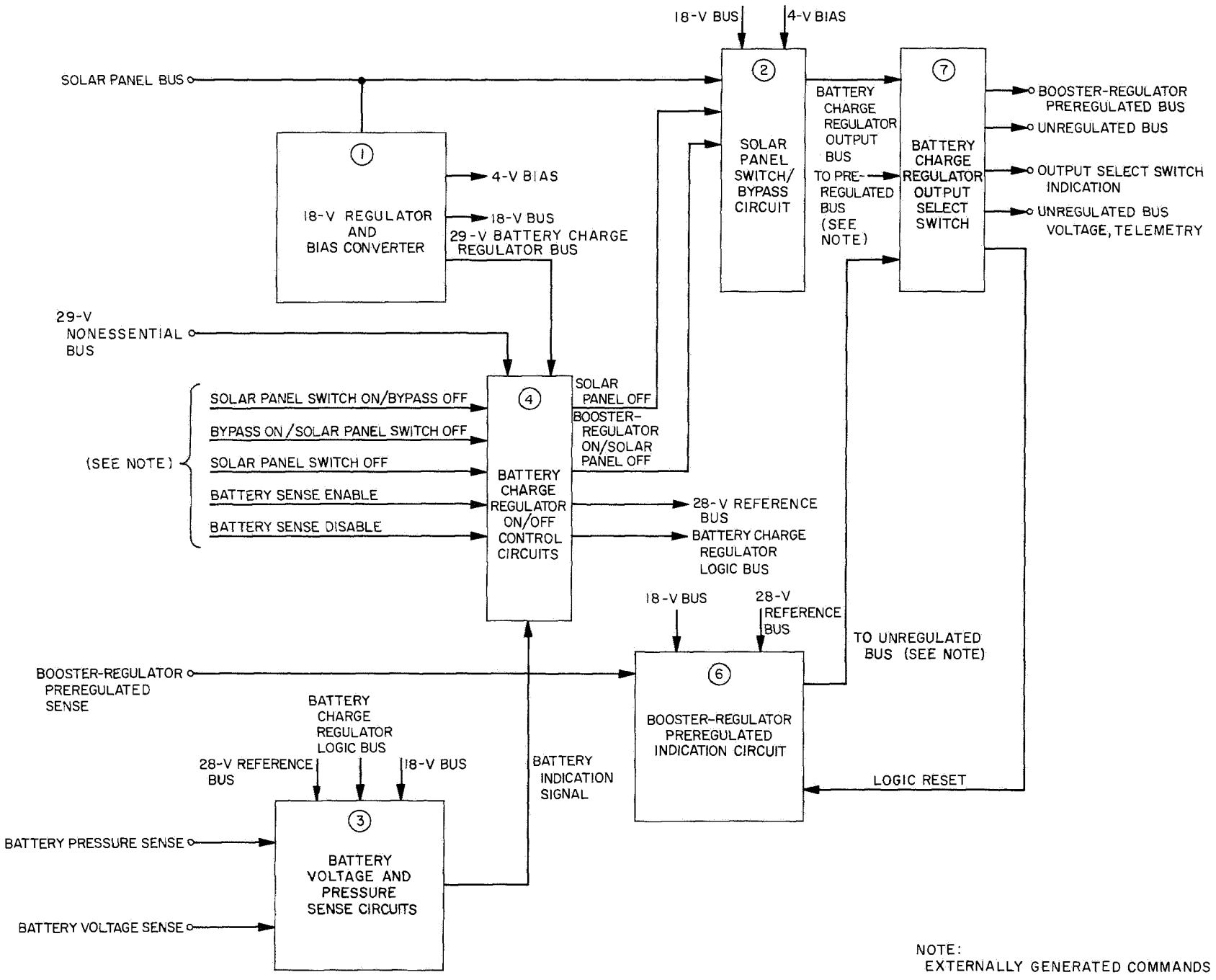



**Fig. XVI-25. Battery charge regulator block diagram, *Surveyors V–VII***

major considerations in the choice of this type of casting method. Other basic techniques were also employed in the fabrication of the power-unit structures. These were:

(1) Use of solid rivets for fastening sheet metal units or equivalent thin sections.

(2) Salt-bath brazing processes for joining aluminum alloys with minimum distortion.

(3) Use of nut plates to provide captive nuts, and to distribute stress.

Cordwood modules were used to achieve maximum packaging density of the electronic parts. The basic circuit boards were fabricated from laminated fiber-glass epoxy sheet. Prefabricated cables were used for interunit wiring to improve producibility. After fabrication, the chassis were coated with epoxy and the terminals and electronic parts were conformally coated to prevent possible contact with floating debris. All the power conditioning units were provided with covers to protect the unit from dust and facilitate handling and shipping. Permanent tool guides were used for locating and mounting screws on the thermal structure inside the cover.

All components used in the power unit had to be approved by the parts evaluation group and were assigned a special number for *Surveyor* use. The components were inspected and electrically tested at incoming inspection. Parts traceability was maintained through storage, assembly, and end item.

The processing of the hardware through manufacturing was as follows. Each control unit consisted of a subassembly (chassis) upon which a number of electrically independent submodules were assembled and wired. The construction of each submodule proceeded in parallel up to the final assembly. Any submodule problems that developed, such as late delivery of parts or circuit failure during submodule testing, did not affect the flow of production of the other submodules. Occasionally, when parts could not meet manufacturing schedules and delivery dates became critical to spacecraft testing schedules, HAC and JPL would meet and discuss the problem and find alternate solutions in order to continue the smooth flow of manufacturing the hardware. In this way, HAC manufacturing kept the production line operative and held wasted time to a minimum. Each submodule that completed fabrication was inspected by HAC quality control and checkers to verify the use of the proper parts, correctness of wire routing, placement of parts, and quality of workmanship. This was done before the submodule was authorized for an end item buildup. The final subsystem assembly was inspected by quality assurance and functionally tested by the unit cognizant personnel. After the electrical test, potting of components and conformal coating were performed. Final functional testing and flight acceptance testing were completed before the unit was stored in bonded stores for use on the spacecraft.

Inspection points were designated throughout the buildup cycle to assure the quality of the units. A typical flow sheet for the fabrication and qualification testing of the B/R is shown in Fig. XVI-26. JPL quality control personnel were additionally assigned to monitor HAC manufacturing and HAC testing functions. At specific manufacturing points, equipment was required to be approved by JPL before the units could proceed to the next point. Note that, on Fig. XVI-26, the *O*s are inspection points on the bar graph. Table XVI-9 lists the number of power units built and the number of submodules per unit. The physical description and special manufacturing techniques used in the fabrication of the solar panels and of each power conditioning unit are discussed in the next paragraphs.

### 1. Solar Panel

*a. SC-1 through SC-4.* The solar panel substrate consisted of an aluminum honeycomb core of 0.375-in.-thick, bonded-to-titanium facing sheets. Because 0.002-in. titanium sheets were not available in widths sufficient to span the substrate, two splice joints were made in each facing sheet using an adhesive bond. The available honeycomb material also required a center splice. Inserts were bonded to the honeycomb core for mounting the secondary solar sensor and brackets. The substrate was coated with a dielectric white epoxy paint. The solar cell modules were bonded to the substrate surface with silicone rubber adhesive. The individual modules were handwired into series strings. The same strings were connected through diodes encapsulated in the substrate to a contour electrical cable that was bonded onto the substrate surface.

*b. SC-5 through SC-7.* The solar panel substrate consisted of an aluminum honeycomb core of 0.5-in.-thick, bonded-to-0.004-in.-aluminum facing sheets.

The change in honeycomb core thickness and facing material was required to strengthen the substrate for anticipated increased landing loads caused by a concurrent stiffening of the A/SPP through redesign. Grommets inserted in the substrate were used to provide wire channels from one side of the substrate to the other. Grounding straps were bonded to the solar panel. Bus

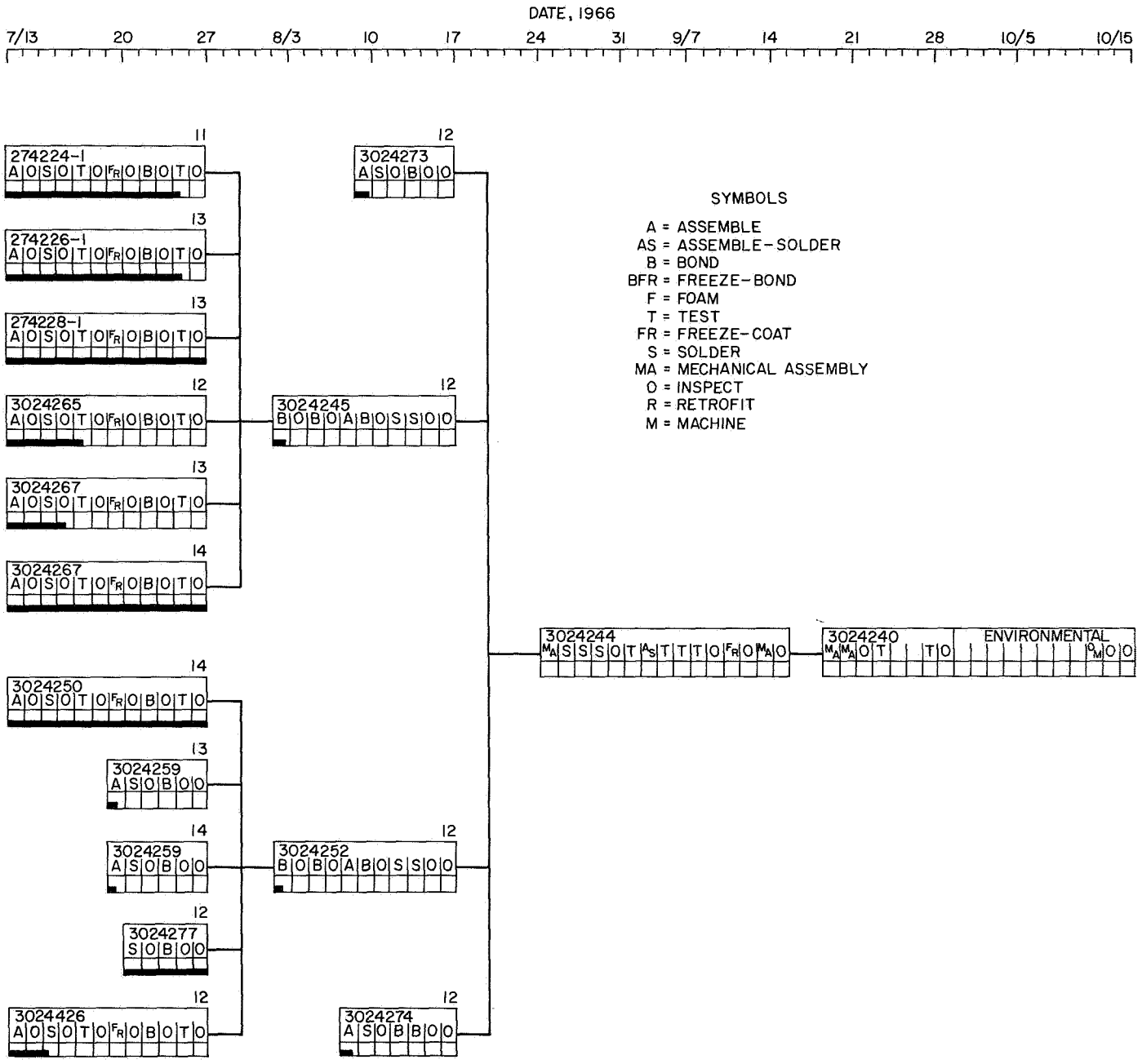



**Fig. XVI-26. Booster-regulator manufacturing flow chart**

bars were used for the interconnection of the solar cells. Alloy Kovar, an iron-nickel-cobalt alloy, was selected to match the thermal coefficient of expansion of the silicon solar cells.

### 2. Booster-Regulator

The B/R was mounted directly below the thermal radiating plane of compartment B. The shape of the unit was dictated by its location under the slant roof of the compartment. The unit's structure consisted of two wedge-shaped aluminum castings that supported two main structural member circuit boards. Each structural circuit board was bonded to a fiber-glass honeycomb-and-metal baseplate.

The total weight of the unit was 7.8 $\pm$0.2 lb and the volume of the envelope was 189 in$^3$.

Table XVI-9. Number of power subsystem units fabricated and their disposition

| Control Item | Total units fabricated | Flight units | Flight spares | Type approval | Prototype | Engineering test | Surveyor dynamic spacecraft | Modules per unit |
|---|---|---|---|---|---|---|---|---|
| Solar panel | 14 | 7 | 2 | 2 | 1 | 2 | — | 792/518 |
| Booster-regulator | 17 | 7 | 2 | 2 | 1 | 3 | 2 | 16 |
| Battery charge regulator | 13 | 7 | 2 | 2 | 1 | 1 | — | 15 |
| Engineering mechanism auxiliary | 12 | 7 | 2 | 2 | 1 | — | — | 19 |
| Auxiliary battery control | 9 | 4 | 3 | 1 | 1 | — | — | 2 |
| Temperature control and heater | 24 | 14 | 4 | 2 | 2 | — | — | 6 |

Cordwood modules were used for maximum packaging density. The top and bottom members of the cordwood modules were etched circuit boards. In the assembly process, these members were held in fixtures to obtain the correct alignment and the required spacing between boards. All components were threaded through the terminal pads of the etched circuit and were temporarily retained in position by bending the uncut leads. The holding fixture was then fitted with spacers that held the boards rigidly in correct proximity to one another. The component leads were trimmed and hand-soldered, first to one circuit board and then to the other. The module was then removed from the holding fixture, the circuit boards trimmed, and the entire module subjected to a microscopic visual inspection.

Some difficulty was experienced with the first cordwood modules produced. Glass base epoxy, 0.001-in.-thick stock, was used in the etched circuit boards. This material cracked along the edges and broke across the corners when subjected to handling in the assembly and inspection operations. The material also bowed during the component soldering operations, resulting in uneven top and bottom surfaces of the finished module. This condition was corrected on later productions by changing to plastic laminate stock for the circuit board.

Foam sandwich chassis provided mounting surfaces for the cordwood modules. The sandwich construction consisted of a sheet of polyurethane foam bonded between an etched circuit board and a formed sheet of 0.016-in.-thick aluminum. Photographic techniques were used to produce the etched circuit boards and to chemically etch the hole pattern and the perimeter of the aluminum chassis plate. The chassis plates were formed into shallow pans in a hydropress that used plastic forming dies and rubber pads.

A problem with metal cracking along the bond radii and fracturing to etched holes was experienced in the fabrication of the structure. The problem was corrected by increasing the bond radii and using a metal backing plate in the hydropress. Hole patterns on the chassis were fabricated by the use of drill jig fixtures. Problems in holding the dimensional tolerance were experienced in the metal-forming operation. The problem was eliminated when investment casting of this structure was used.

The B/R was composed of four subassemblies: structure assembly A1, structure assembly A2, chassis assembly A1, and chassis assembly A2.

All high-power dissipating elements of the unit were installed on structure assembly A2 to dissipate the heat to the thermal plate, radiating planes, and switches of the compartments. The heavy switching choke was tied directly to the compartment because of its weight.

On disassembly, the structural member would fold out and be held in place by the captive harness from the main chassis assembly. The disassembly feature provided maximum access to all unit components while the unit was still electrically operative.

### 3. Battery Charge Regulator

The BCR had a rectangular shape to fit in compartment A, being fastened to an inner vertical thermal tray. All the power dissipation stud-mounted components were distributed at each end of the thermal structure. One thermal wall was completely devoted to the A/SPP stud-mounted switching components, including the SCR motor switches, to ensure adequate heat transfer to the compartment tray. The other thermal wall was used for installation of the power-dissipating components of the solar panel output control and conditioning circuits. The magnetic devices and other bulky components were located at the bottom of the structure.

Etched circuit board chassis assembled on sandwich configurations were considered more practical here than the module method of packaging. Most components on the etched board were laid out in a straight-line pattern. Terminal tie points were provided for each component lead whenever practicable. The terminals used as ties to circuits external to each board were grouped at the edge of the board nearest to the other board ties. This permitted minimum cable lengths. The critical (or selected) components were mounted nearest the upper edge of the boards to facilitate insertion and removal without disassembly. Prefabricated harnesses were used for the internal wiring. Open-form wiring was used for short runs between boards, between closely spaced structure-mounted components, and to interconnect sandwiched chassis boards fed through holes. The unit weight was 3.5 lb.

#### 4. Auxiliary Battery Control Unit

The ABC unit was located on the inboard face of the mounting tray of compartment A, adjacent to the battery connection. The unit's dimensions were 6.3 × 3.5 × 3.2 in. Its weight was 1.75 lb. To minimize weight, no cover was provided. The unit consisted of two subassemblies: a printed-circuit board/foamed-aluminum sandwich and a bottom plate. Conventional printed circuit construction was used to facilitate assembly and component replacement. The bottom plate provided the heat sink for power diodes and structural support for the relays. There was access to all parts of the circuits without disassembly.

The standoffs and mounting tubes for the relays were machined aluminum parts. The bracketry and baseplates were formed aluminum sheet stock.

#### 5. Engineering Mechanisms Auxiliary

The EMA was installed in compartment A on the thermal tray. The unit's dimensions were 2.9 × 8.8 × 5.9 in. It consisted of four boards constructed of formed aluminum with foam spacer. Epoxy–glass printed-circuit boards bonded by epoxy adhesives provided the structure for the mounting of welded cordwood modules and electronic components. Provisions were made to remove chassis boards from the unit without affecting the rest of the unit in order to provide easy replacement of pyrotechnic switching boards.

The four special fabrication techniques used in this unit were:

(1) Plated-through connections on printed-circuit boards were redundant with wire interconnections.

(2) Fiber-glass module covers, coated with silver–epoxy, provided electrostatic shielding.

(3) Special sheet metal nuts to fasten stud-mounted SCRs and transistors were used for weight savings.

(4) Chassis were stiffened with tee brackets to increase their structural characteristics and were mechanically detuned to prevent resonances below 460 Hz.

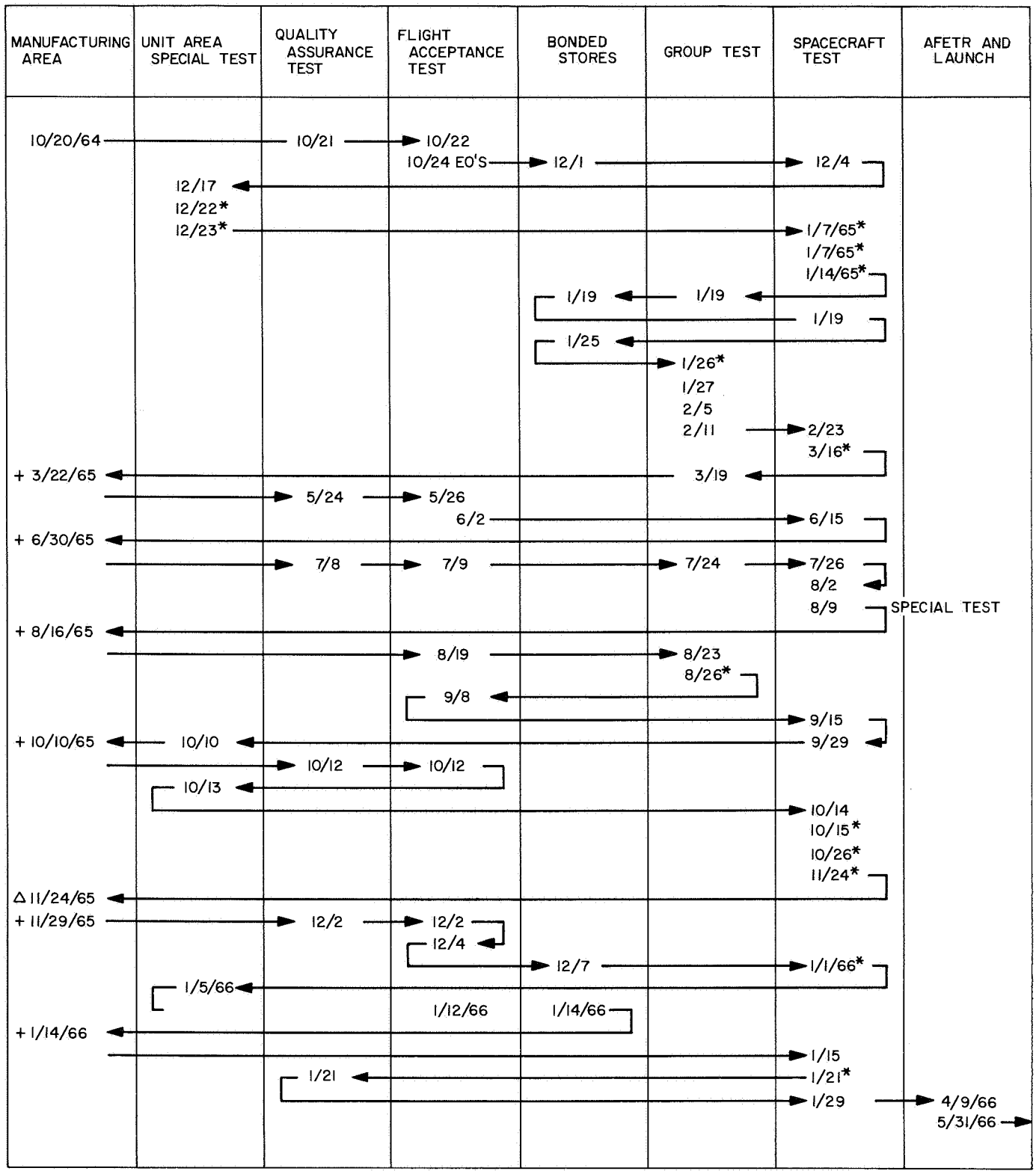
Stiffening of the chassis was necessary to eliminate chassis delaminations experienced, because of the poor geometry between the brackets and the chassis, so that the unit could survive shock and vibration levels.

#### 6. Summary of Manufacturing Problems

A number of problems were encountered during the manufacturing of the power conditioning and solar panel units, some of which have been mentioned. The majority of problems were with workmanship; i.e., personnel with little experience in the *Surveyor* fabrication procedure caused errors when the operator disregarded the layout instructions of the hardware or did improper cleaning and preparation of tooling. Other problems and failures can be directly attributed to poor manufacturing management, testing techniques, and engineering support. For example: some units did not use assembly fixtures, visual guides were seldom used, special fabrication instructions were not transmitted to the working level, test fixtures and jigs had ungrounded leads, testing instructions and test procedures were not available or were outdated, and marginal designs, problem areas, and failures were reported during spacecraft testing.

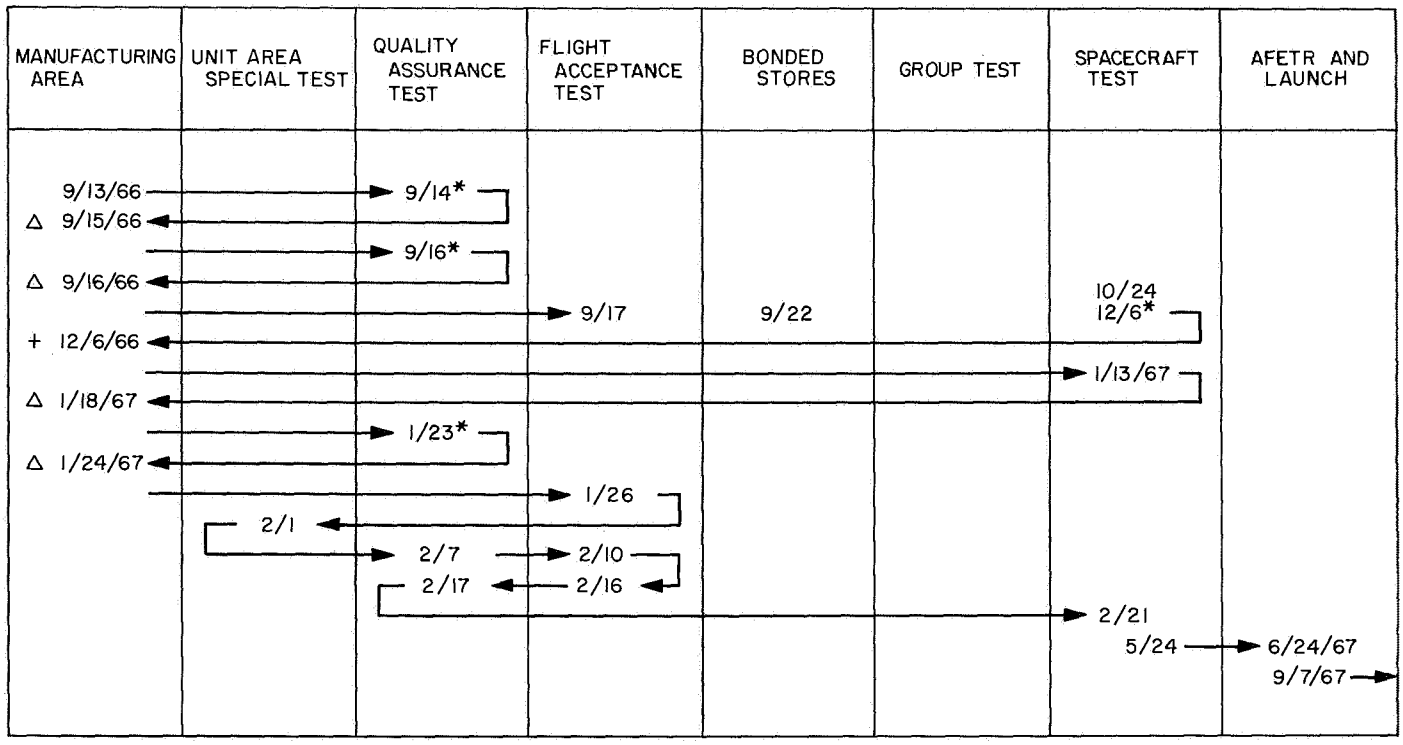
The cabling layout and cabling assembly techniques also generated failures, especially where cables between chassis were involved. Several problems were attributed to poor packaging techniques, such as wires pinched between chassis or modules. This problem was extremely difficult to detect because of the foldout construction. After the units were assembled, the only way to see if a wire was pinched was to X-ray the unit.

To show the amount of rework involved and the cycling experienced by the units—in and out of the fabrication, unit test, and spacecraft test areas—graphs have been prepared that chronologically show the sequence of events which took place from initial fabrication to launch for the B/R and BCR units flown on SC-1 and SC-5, and the ABC unit flown on SC-1. Figure XVI-27 presents this processing history of B/R unit 274200, SN-12, flown on SC-1. Figure XVI-28 presents the processing history




+ UPGRADE
Δ REWORK
* TROUBLE/FAILURE REPORT

**Fig. XVI-27. Processing history of SC-1 booster-regulator (B/R 274200-96, SN-12)**




+ UPGRADE
Δ REWORK
* TROUBLE/FAILURE REPORT

**Fig. XVI-28. Processing history of SC-5 booster-regulator (B/R 3024240-1, SN-11)**

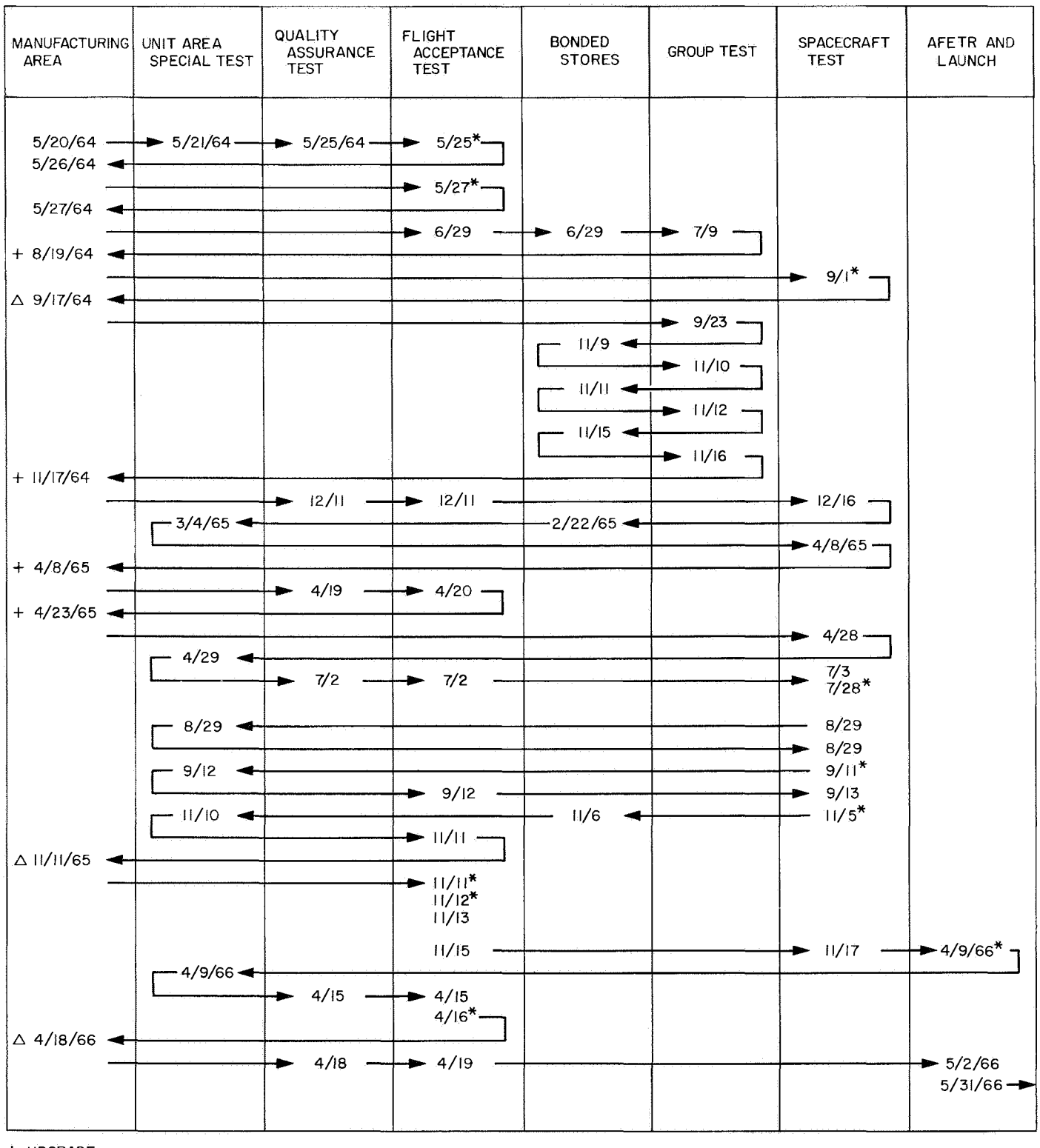
of B/R unit 3024240-1, SN-11, flown on SC-5. Figure XVI-29 presents the processing history of BCR unit 274100, SN-11, flown on SC-1. Figure XVI-30 presents the processing history of BCR unit 3024260, SN-11, flown on SC-5. Figure XVI-31 presents the processing history of ABC unit 273000-2, SN-15, flown on SC-1.

## E. Testing

### 1. Unit Level Tests

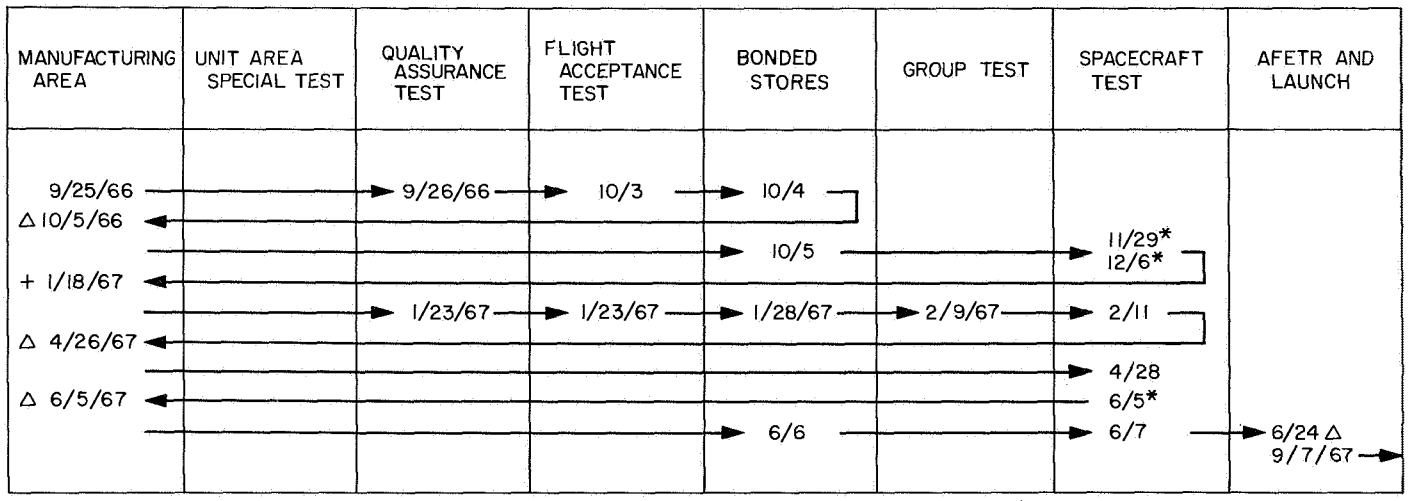
Preliminary evaluation of the design of each power subsystem unit was verified at the engineering laboratory by performing functional and marginal tests on prototype units. The formal qualification of the design was performed on the type approval unit. Type approval units were manufactured exactly the same as the flight units. As a typical example of the power unit qualification, Table XVI-10 summarizes and gives the results of type approval tests conducted on the BCR. Similar tests were conducted on the other power conditioning units to qualify their designs. In the power sources area, in addition to the type approval tests, a reliability program was conducted. Batteries were exposed to extreme environments, and qualification tests were performed at key intervals to verify the integrity of the units. Another set of batteries was life-tested on a group basis, each unit being discharged through a simulated mission (66 hr transit and 1 lunar day of simulated operation). Each group was exposed to a different temperature, within the anticipated use range, to explore the capability of the design. Similarly, in the solar panel area, a computer reliability program was conducted to examine design capability.

Qualification tests for the flight units were conducted to the flight acceptance specifications. JPL personnel verified all functional and flight acceptance testing. When all testing was completed and the requirements were met, the unit's history log, which included all flight acceptance test data, was submitted to HAC and JPL system engineering for unit buyoff. This qualified the item as a *Surveyor* flight accepted unit. At this time, any unexplained problems that occurred during flight acceptance testing constituted a lien on the unit. This lien then was worked independently so as not to delay the spacecraft testing schedules.



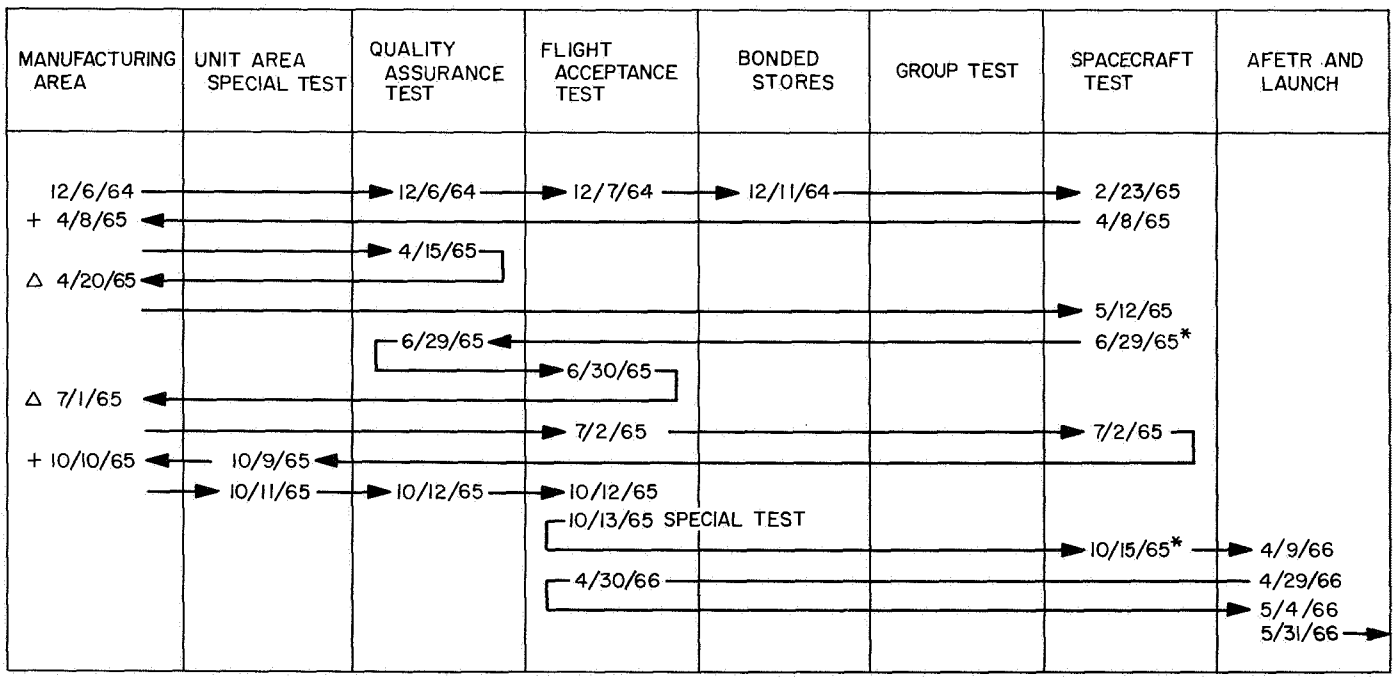

+ UPGRADE
△ REWORK
* TROUBLE/FAILURE REPORT

**Fig. XVI-29. Processing history of SC-1 battery charge regulator (BCR 274100-3, SN-11)**




+ UPGRADE
Δ REWORK
* TROUBLE/FAILURE REPORT

**Fig. XVI-30. Processing history of SC-5 battery charge regulator (BCR 3024260, SN-11)**




+ UPGRADE
Δ REWORK
* TROUBLE/FAILURE REPORT

**Fig. XVI-31. Processing history of SC-1 auxiliary battery control (ABC 273000-2, SN-15)**

### 2. Subsystem Level Tests

After completion of the flight acceptance tests on a unit level, each power system unit was qualified on a system basis before it could be installed on the flight spacecraft. For SC-1 through SC-4 hardware, each power conversion unit was initially qualified at group testing. The objectives of the system group testing were to confirm that each power conversion unit had successfully performed as part of the power subsystem and with other

## Table XVI-10. Battery charge regulator type approval tests

| Environmental condition | Test | Exposure time | Results |
|---|---|---|---|
| $10^{-6}$ torr at ambient temperature | All functions | 2 hr | All readings within limits of specification 231627 |
| $10^{-6}$ torr at 125°F | Five cycles on for 2 hr and off for 0.5 hr. Solar panel current monitored continously and all functions tested after 10 hr exposure | 12 hr | Same as above |
| $10^{-6}$ torr at 125°F | Four cycles on 2 hr and off for 0.5 hr. Solar panel current monitored continuously | 10 hr | Same as above |
| $10^{-6}$ torr at ambient temperature | Off during cooldown, then on for test of all functions | 4 hr | Same as above |
| $10^{-6}$ torr at 0°F | Off during cooldown, then on for test of all functions | 4 hr | Some as above |
| (Above sequence repeated three times with same results.) | | | |
| $10^{-6}$ torr at ambient temperature | On during warmup, then test of all functions | 4 hr | Same as above |
| Ambient temperature and pressure | Test of all functions and measure efficiency | 2 hr | Same as above |
| Vibration cycling: 100–1500 Hz at 2 *g* random vibration superimposed on five logarithmic sweeps of sinusoidal vibration; 40–125 Hz at 18 *g* and 125–1500 Hz at 4 *g* in *Z* axis and 40–125 Hz at 16 *g* in *X* and *Y* axes | Monitor solar panel current | 10 min | No major resonances detected |
| Vibration cycling: 100–1500 Hz at 4.5 *g* superimposed on one logarithmic frequency. Traverse of 40–125 Hz at 19 *g* and 125–1500 Hz at 4 *g* in *Z* axis | Monitor solar panel current | 2 min | No major resonance observed |
| Vibration survival test | All functions | 2 hr | All readings within limits of specification 231627 |
| Shock test: 4 shocks, half-sine pulse at 25 *g* peak acceleration and 5–7 msec duration. Applied in positive thrust direction of *Z* axis | Monitor solar panel current | 23 msec | No damage observed |
| Half-sine pulse at 15 *g* peak acceleration at 5–7 msec duration. Two shocks applied in each direction of *X*-axis and two shocks applied in each direction of *Y*-axis | Same as above | 28 msec | Same as above |
| Shock survival test | All functions | 2 hr | All readings within limits of specification 231627 |

subsystems. During the tests, the initial power profile data were obtained. For SC-5 through SC-7 hardware, the group test was replaced by the power subsystem test, which expanded the testing on the subsystem level to demonstrate the compatibility of the power subsystem, provided additional information on the margins, and characteristics over the critical mission sequence.

The test setup for the power subsystem included the following power subsystem items:

(1) Main battery.

(2) Battery charge regulator.

(3) Booster-regulator.

The test also included the following special equipment:

(1) Spacecraft type harnesses designed to simulate actual spacecraft hardware (i.e., wire gage, length, type, shield, etc.).

(2) Solar panel simulator — this unit simulated the spacecraft equipment with regard to voltage, current, and power parameters.

(3) Load simulation panel — this panel contained a flight control type ECU and a high-voltage transmitter ECU that were similar to the spacecraft hardware; all other loads were resistive and approximated the power requirements in the system.

(4) A command pulse generator was designed to provide spacecraft type pulses and was used to send the appropriate commands to control the B/R and BCR.

(5) Constant-current power supplies to excite spacecraft temperature transducers.

Data obtained verified interunit compatibility and provided additional confidence in the power subsystem design.

### 3. Spacecraft System Level Tests

After unit qualification, all power subsystem units, with the exception of the solar panel, were mated to the spacecraft in the integrated system checkout. During this and much of the subsequent testing, no batteries were used; instead, the spacecraft was operated from a ground power source which, through remote sensor leads, held the spacecraft unregulated bus at the simulated battery voltage. For all tests prior to shipment to AFETR, the solar panel power was provided by a specially designed solar panel simulator. This was also true of the solar-thermal-vacuum tests in which shadow shrouds were used that gave the same thermal shadowing as the solar panel. The reason for this was complex: the fragility of the solar panels, their high unit cost, and the impossibility of getting uniform radiation exposure in the vacuum test chamber.

Throughout the Spacecraft System tests, from integrated system checkout to solar thermal vacuum testing, the power subsystem had hardline measurements available. They were used to monitor the spacecraft power subsystem and to gain confidence in the calibration of the power telemetry channels. Table XVI-11 lists hardline measurements for SC-1 through SC-4 and SC-5 through SC-7. Additional monitoring of the main battery was performed on the spacecraft by using the battery scan rack, which sampled the terminal voltage and each cell voltage of the main battery. It was felt that a knowledge of the condition of each cell was necessary to assure a satisfactory long-term battery performance and to prevent any electrolyte overflow damage to the spacecraft. In addition, a log of the total remaining ampere-hours left in the main battery during system tests was kept to assure proper performance.

Battery charging on the spacecraft was reduced to a minimum, and a new battery was used during every major spacecraft qualification test. After the completion of the spacecraft qualification and mission verification tests, the spacecraft was shipped to AFETR with the power units in place. At AFETR, tests were performed to verify that the power system was not damaged in shipment to AFETR and to obtain final information data on the performance of the system. For the first time, the solar panel was installed on the spacecraft, and illuminated to verify the operations of the BCR and the spacecraft wiring harness with the actual solar panel as a source. The final power profile information was determined, and telemetry and hardline measurements were used to establish the accuracy of the current shunts and provide information about the actual loads and load changes that would be seen in flight.

The power sources of the subsystem, solar panel, and batteries were reevaluated before the installation of the spacecraft. Three main batteries were evaluated; one of these was selected for flight.

The solar panel was also sunlight tested at AFETR and the data obtained were compared to the latest data from tests at Table Mountain to determine whether any

**Table XVI-11. Hardline power subsystem measurements**

| Channel | SC-1 through SC-4 | SC-5 through SC-7 | Channel | SC-1 through SC-4 | SC-5 through SC-7 |
|---|---|---|---|---|---|
| EP-1 | 29-V nonessential voltage | 29-V nonessential voltage | EP-23 | Auxiliary battery voltage | — |
| EP-2 | Unregulated bus voltage | Unregulated bus voltage | EP-24 | Solar cell string 4 current | — |
| EP-3 | Main battery manifold pressure | Main battery manifold pressure | EP-25 | Solar cell string 6 current | — |
| EP-4 | Unregulated output current | Unregulated output current | EP-26 | Auxiliary battery temperature | — |
| EP-5 | Main battery voltage | — | EP-27 | Full scale current calibration (auxiliary engineering signal processor) | — |
| EP-6 | Battery charge current | Battery charge current | EP-28 | Mid-scale current calibration (auxiliary engineering signal processor) | — |
| EP-7 | Booster-regulator difference current | Booster-regulator difference current | EP-29 | Zero scale current calibration (auxiliary engineering signal processor) | — |
| EP-8 | Main battery temperature | Main battery temperature | EP-30 | Booster-regulator preregulatar voltage | Booster-regulator preregulator voltage |
| EP-9 | Battery discharge current | Battery discharge current | EP-31 | Auxiliary battery mode on | — |
| EP-10 | Solar cell array voltage | Solar cell array voltage | EP-32 | High-current mode off | — |
| EP-11 | Solar cell array current | Solar cell array current | EP-33 | Engineering mechanisms auxiliary radar altimeter and doppler velocity sensor pyro switches | Engineering mechanisms auxiliary radar altimeter and doppler velocity sensor power switch on |
| EP-12 | Solar cell array temperature | Solar cell array temperature | EP-34 | Battery charge regulator temperature | Battery charge regulator temperature |
| EP-13 | Booster-regulator temperature | Booster-regulator temperature | EP-35 | — | Solar cell short-circuit current |
| EP-14 | Regulated output current | Regulated output current | EP-36 | — | Irradiated solar cell short-circuit current |
| EP-16 | Optimum charge regulator output current | — | EP-37 | — | Solar cell section 2 current |
| EP-17 | Radar and squib current | Radar and squib current | EP-38 | — | Solar cell open-circuit voltage |
| EP-18 | Full-scale current calibration (engineering signal processor) | — | EP-39 | — | — |
| EP-19 | Mid-scale current calibration (engineering signal processor) | — | EP-40 | Flight control unregulated current | Flight control unregulated current |
| EP-20 | Zero scale current calibration (engineering signal processor) | — | | | |
| EP-21 | Compartment A heater current | Compartment A heater current | | | |
| EP-22 | Compartment B heater current | Compartment B heater current | | | |

damage had been sustained in shipment and handling. The solar panel was also cleaned before delivery to the spacecraft for installation. For SC-1 through SC-4, several auxiliary batteries were filled with electrolyte at AFETR and performance tested. The data obtained were reviewed; one battery was selected for flight.

## F. Mission Performance

Following mating to the launch vehicle, the spacecraft was operated from the ground power during the system readiness test. The voltage of the ground power supply was carefully adjusted to provide the spacecraft requirements and to maintain the charge on the main battery.

At launch −4 min, the main power switch was energized, transferring the spacecraft power requirements entirely to the spacecraft's main battery. At spacecraft separation, automatic deployment of the solar panel was initiated. This was followed by an automatic sun-acquisition sequence. With the sun acquired, both power sources provided power to the spacecraft as required for the remainder of the mission.

Figure XVI-32 shows the power-use profile for SC-1 through SC-7.

Table XVI-12 lists the actual values of various key power parameters telemetered during the mission. The values represent the average measured values and range of values recorded during the SC-1 through SC-7 transit portion of the mission.

During each spacecraft mission, the power consumption and the status of the power sources were continually evaluated. Plots of the parameters for SC-1, SC-3, and SC-6 are presented in Fig. XVI-33 for comparison to show the effect of the design modifications introduced during the design evaluation of the power subsystem.

The preflight and mission performance data of SC-1 through SC-7 solar panels are summarized in Table XVI-13, as an illustrative comparison of the solar panel preflight and mission data.

Experience with the power subsystem varied with each spacecraft only to the extent that was predicted by design changes, the varying power demands made during each flight as a consequence of other subsystem anomalies, and, of course, the battery degradation experienced in lunar night survival. Unless otherwise stated in the following discussion of the individual spacecraft, the power subsystem showed normal and predictable behavior during transit and lunar operations. Before each lunar night following the first lunar day's operations, the battery was charged to maximum capacity before going into the lunar night "keep-warm" survival attempts.

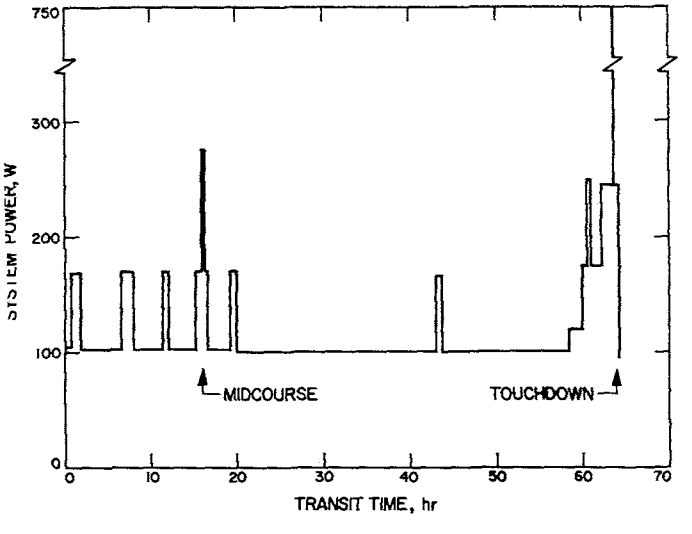



**Fig. XVI-32. Typical power profile**

The power subsystem performance during each of the *Surveyor* missions is covered in some detail in the following paragraphs:

(1) *Surveyor I:* The only anomaly reported during transit was that the auxiliary battery temperature dropped below the expected minimum value of 60°F during transit and 90°F at touchdown. The actual minimum values were 35°F during transit and 75°F at touchdown. To correct this anomaly, black paint was applied to the top coverplate of the auxiliary batteries on *Surveyors II–IV* to raise

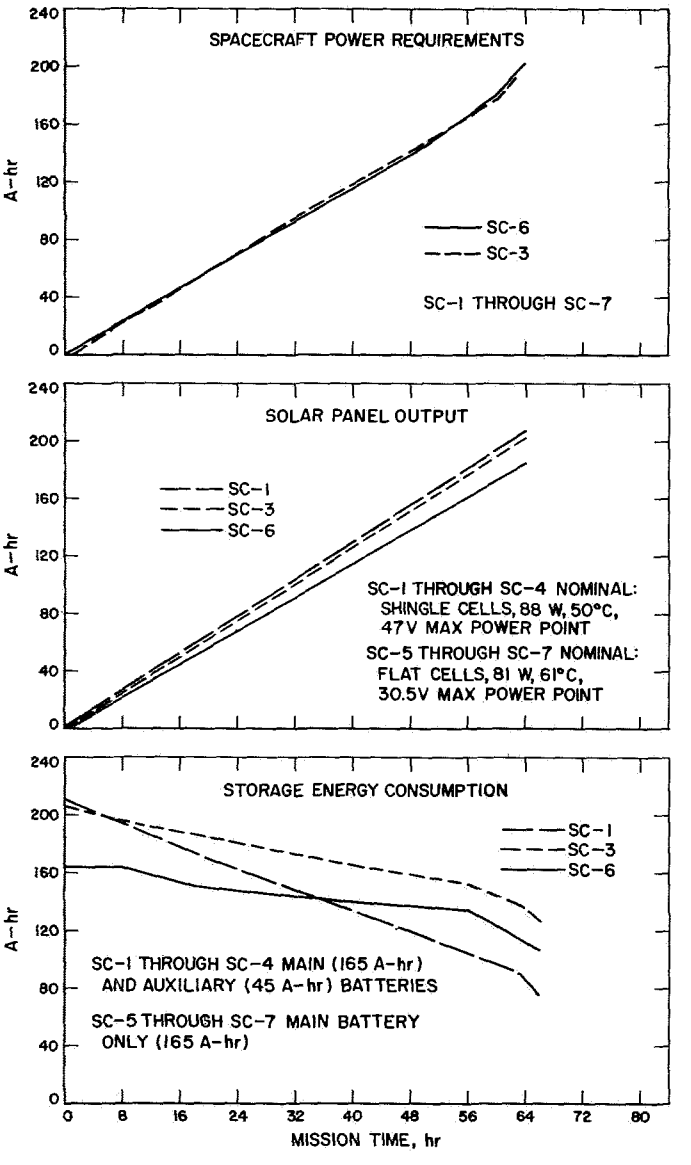



**Fig. XVI-33. Spacecraft power requirements, SC-1 through SC-7**

the operating temperatures. During lunar operations, using the bypass mode, the average power delivered by the solar panel was 48 W (24 V +2.0 W). At lunar noon, the solar panel recorded a high temperature of 213°F. After sundown, the spacecraft was operated for approximately 50 hr to obtain temperature measurements during the cooling of the spacecraft. The spacecraft was acquired on the second lunar day. All units of the power subsystem continued to function properly until a few hours before sundown. At that time, data from the main battery indicated that a number of cells were heavily discharged and damaged. No intelligible data were obtained during the next lunar day.

(2) *Surveyor II:* The performance parameters of the power subsystem followed closely the predicted values prior to the unsuccessful midcourse maneuver. Continuous solar panel illumination was lost after the midcourse maneuver because of the tumbling of the spacecraft, and the main battery was drained to 10 A-hr. The mission was terminated by firing the retrorocket.

(3) *Surveyor III:* The redesigned flight control system installed on this spacecraft lowered the operating temperature of both electronic compartments by approximately 20°F compared to the *Surveyor I* mission and improved the operating range of the electronic units. In addition, the battery energy residue at landing was relatively high compared to the *Surveyor I* mission.

An anomaly was reported during spacecraft landing. The spacecraft made three individual touchdowns before settling on the lunar surface. During the touchdowns, transients were generated which triggered a false "high-current mode off" command to the ABC circuit. The command removed the auxiliary battery from the bus. The main battery voltage dropped because of the heavy spacecraft loads. The automatic transfer circuitry in the ABC unit sensed the low spacecraft bus voltage and switched the auxiliary battery back to the battery bus in the auxiliary battery mode. After sundown, the spacecraft was operated for about 20 hr. Attempts to revive the spacecraft during the second lunar day were not successful.

(4) *Surveyor IV:* During the transit, midcourse, and terminal descent portions of the mission, and until radio communication was lost, all power subsystem performance parameters followed closely the predicted values.

(5) *Surveyor V:* Battery energy used during transit was above the predicted value because of additional midcourse maneuvers executed to correct the fuel regulator anomaly.

The temperature during coast was lower than for previous spacecraft. At 9.5 hr before touchdown, the compartment heater was turned on to bring the battery temperature to the optimum value of 90°F. After sundown, the spacecraft was operated for about 120 hr, keeping the battery warm at around 20°F and interrogating the spacecraft as little as possible. When the spacecraft was shut down, the battery was depleted to 30% of its capacity. The spacecraft was acquired during the second lunar day and all power subsystem units functioned properly. The battery again was fully charged before sundown.

During the second lunar night, the spacecraft was operated for about 210 hr. At the final interrogation, the data indicated that the main battery may have had 2 out of the 14 cells degraded. The battery was depleted to 39 A-hr or less than 25% of its capacity. The spacecraft did not respond to earth commands during the third lunar day. However, the spacecraft did respond on the fourth day. The transmitter signal was strong but the data obtained could not be analyzed.

(6) *Surveyor VI:* After sundown, the plans for operating the spacecraft for the night survival had to be modified because a number of the thermal switches of the compartment failed to function. The spacecraft was shut down after about 60 hr of post-sunset operation. The battery was depleted to about 60% of its capacity. The spacecraft responded to the earth commands during the second lunar day, but the data obtained had no intelligence value.

(7) *Surveyor VII:* After sundown, the spacecraft was operated for about 80 hr, keeping the battery warm at around 20°F and interrogating the spacecraft as little as possible. When the spacecraft was shut down, the battery was depleted to 30% of its capacity. The spacecraft was acquired during the second lunar day. Data obtained indicated that short circuits had developed in the battery, forcing limited operations of the spacecraft. During the last two days of operation, the battery appeared to be open, and the spacecraft was operated from the solar panel.

## Table XVI-12. Power subsystem performance summary

| Parameter | SC-1 | | SC-2 | | SC-3 | | SC-4 | | SC-5[a] | | SC-6 | | SC-7 | |
|---|---|---|---|---|---|---|---|---|---|---|---|---|---|---|
| | Spec | Actual | Spec | Actual | Spec | Actual | Spec | Actual | Spec | Actual | Spec | Actual | Spec | Actual |
| During transit phase | | | | | | | | | | | | | | |
| Solar panel temperature, °F | 122 | 129 | 122 | 133 | 122 | 135 | 122 | 136 | 146 | 135 | 146 | 136 | 146 | 136 |
| Solar panel power, W | 89 | 90 | 89 | 90 | 89 | 90 | 89 | 90 | 81 | 85.7 | 81 | 86.7 | 81 | 89 |
| Solar panel output energy, A-hr | 199 | 205 | 199 | — | 199 | 207 | 199 | — | 172 | 182 | 172 | 185 | 172 | 188 |
| Main battery temperature range, °F | <125 | 86–121 | <125 | — | <125 | 93–115 | <125 | 93–110 | <125 | 64–111 | <125 | 59–105 | <125 | 62–108 |
| Main battery maximum pressure, psia | <30 | 20.6 | <30 | — | <30 | 14.5 | <30 | — | <30 | 15.6 | <30 | 16.6 | <30 | 14.4 |
| Aux battery temperature range, °F | <110 | 35–78 | <110 | — | <110 | 54–80 | <110 | 59–79 | — | — | — | — | — | — |
| Battery discharge current during coast phases, A | — | 1.5 | — | 1.71 | — | 0.64 | — | 0.87 | — | 0.21 | — | 0.41 | — | 0.41 |
| Battery charge regulator temperature range, °F | — | 109–128 | — | — | — | 84–115 | — | 85–108 | — | 64–105 | — | 59–102 | — | 62–95 |
| Battery charge regulator efficiency, % | 75 | 80 | — | — | 75 | 80 | 75 | 80 | 95 | 94.5 | 95 | 94.5 | 95 | 94.5 |
| Booster-regulator temperature range, °F | — | 114–134 | — | — | — | 93–132 | — | 97–125 | — | 74–87 | — | 77–88 | — | 83–89 |
| Booster-regulator efficiency, % | 80 | 78.5 | — | — | 80 | 77 | 80 | 77 | 80 | 80 | 80 | 80 | 80 | 80 |
| Regulated output current during coast phase, A | — | 2.32 | — | — | — | 1.70 | — | 1.73 | — | 1.75 | — | 1.80 | — | 1.80 |
| Main battery energy remaining at touchdown, A-hr | 52 | 56 | 52 | — | 98 | 99.2 | 98 | — | 102 | 83 | 102 | 110 | 102 | 102 |
| During lunar operations | | | | | | | | | | | | | | |
| Solar panel temperature, °F | 200 | 237 | 200 | — | 200 | 241 | 200 | — | 230 | 254 | 230 | 240 | 230 | 240 |
| Main battery temperature max, °F | <125 | 142 | <125 | — | <125 | 115 | <125 | — | <125 | 118 | <125 | 114 | <125 | 114 |
| Main battery maximum pressure, psia | <60 | 44.4 | <60 | — | <60 | 35.5 | <60 | — | <60 | 23.5 | <60 | 17.0 | <60 | — |

[a]Additional midcourse maneuvers performed on this mission.

**Table XVI-13. Solar panel preflight and mission performance data**

| Parameter | SC-1 | SC-2 | SC-3 | SC-4 | SC-5 | SC-6 | SC-7 |
|---|---|---|---|---|---|---|---|
| Specification requirements | | | | | | | |
| SC-1 through SC-4 at 50°C | 89 W | 89 W | 89 W | 89 W | | | |
| SC-1 through SC-4 at 121°C | 2.3 A[a] | 2.3 A | 2.3 A | 2.3 A | | | |
| SC-5 through SC-7 at 62°C | | | | | 81.0 | 81.0 | 81.0 |
| SC-5 through SC-7 at 121°C | | | | | 60.5 | 60.5 | 60.5 |
| Preflight power meosurement | | | | | | | |
| SC-1 through SC-4 at 25°C | 103 | 102 | 102.5 | 102 | | | |
| SC-5 through SC-7 at 62°C | | | | | 85.6 | 84.9 | 86.6 |
| SC-5 through SC-7 at 121°C | | | | | 65.3 | 65.2 | 66.7 |
| Construction | Shingle cell | Shingle cell | Shingle cell | Shingle cell | Flat cell | Flat cell | Flat cell |
| Number of cells | 3960 | 3960 | 3960 | 3960 | 3660 | 3660 | 3660 |
| Effective area, $ft^2$ | 8.0 | 8.0 | 8.0 | 8.0 | 7.85 | 7.85 | 7.85 |
| Power during transient, W | 88[b] | 89 | 90 | 90 | 85.7 | 86.7 | 89 |
| Output during lunar noon corrected for sun angle, W | NA[c] | — | 70.5 | — | 64.0 | 65.4 | |
| Power during second lunar day, W | NA | NA | NA | NA | 84.0 | NA | |
| Percent of power less first lunar night | <10% | NA | NA | NA | 2% | NA | |

[a]Short-circuit current.
[b]SC-1 through SC-4, the optimum charge regulator was operating around the maximum power point.
[c]NA = not applicable.

## Bibliography


*Functional Description, Surveyor Spacecraft,* Vols. I, II, and III, HAC 339524E. Hughes Aircraft Co., Culver City, Calif., Dec. 1960.

*Surveyor Main Battery, A-21E Thermocouple Battery,* SSD 84023. Hughes Aircraft Co., Culver City, Calif., Nov. 30, 1967.

*Surveyor Main Battery—Lunar Night Survival,* SSD 84022. Hughes Aircraft Co., Culver City, Calif., Sept. 12, 1966.

# XVII. Spacecraft Propulsion

The primary objective of the *Surveyor* propulsion subsystem was to provide the thrust forces required by the spacecraft after separation from the *Atlas/Centaur* boost vehicle. Such thrusting was required for midcourse trajectory corrections and the main deceleration and vernier phases of terminal descent.

To accommodate these requirements, a fixed high-thrust system and a variable low-thrust system were provided. The high-thrust system consisted of a solid-propellant rocket motor that supplied the major portion of the impulse required to decelerate the spacecraft as it approached the moon. The low-thrust system consisted of three liquid bipropellant engines, coupled with an associated pressurization and propellant feed system that supplied the forces required for midcourse velocity correction, for attitude control during the retro deceleration phase of terminal descent and after retrorocket burnout, and for the final deceleration to the lunar surface. The vernier propulsion system (VPS) was also used for lunar operations. Although it was neither part of the design criteria nor an operational requirement, the VPS was successfully fired statically (*Surveyor V*) and successfully performed a spacecraft translation (*Surveyor VI*) as part of the science experiments after the moon landings.

Electrically initiated pyrotechnic devices provided helium valve actuation, landing leg and antenna deployment, retro motor separation, and other mechanical actuation functions. The squibs in these devices and the retroigniter were also part of the propulsion subsystem.

In a typical *Surveyor* flight, a midcourse maneuver was performed 15 hr after launch. At this time, the spacecraft was repositioned so that the vernier engines would thrust in the desired direction. A squib was then fired and helium was permitted to flow into and pressurize the propellant tanks at approximately 770 psi. Five minutes later, the vernier engines were ignited and fired for a predetermined time to produce the desired velocity vector correction. The engines thrusted at levels that resulted in a 0.1-$g$ spacecraft acceleration ($\approx$72 lbf per engine). Correction capability was limited by design to a maximum of 164 $\pm$1.3 and a minimum of 6.6 $\pm$1.3 ft/sec. Differential throttling of the three engines and hinging one of the engines stabilized the spacecraft during the correction.

At about launch plus 65 hr, the terminal sequence was initiated. With the spacecraft again reoriented at about 1000 mi above the lunar surface, the retroignition timer was set and enabled. At approximately 60 mi slant range

from the moon, the altitude marking radar marked and the timer began counting. The timer count reached zero after several seconds, and the vernier engines ignited and fired, producing total thrust of 200 lbf. After a 1.1-sec delay, the retro motor ignited. At this time, the spacecraft velocity was about 8700 ft/sec and the spacecraft was approximately 3 min from touchdown on the lunar surface. The retro motor burned for about 40 sec at a thrust level of 8000–10,000 lbf, reducing spacecraft velocity relative to the moon by 95%. Burnout, as indicated by a 3.5-g acceleration switch, nominally occurred at a 30,000-ft altitude and at a velocity of 400 ft/sec. The acceleration switch started a sequence that, after a 10-sec delay, increased the vernier engine thrust level to approximately 280 lbf. Two seconds later, three pyrotechnic release devices were actuated and the retro case fell from the spacecraft. Two seconds after case separation, the vernier engines were automatically downthrottled until the combined engine thrust was 0.9 of the lunar spacecraft weight ($\approx$105 lbf total thrust). At this time, the spacecraft altitude was approximately 25,000 ft and the velocity was about 350 ft/sec. The spacecraft remained at this thrust level until the radar altimeter and doppler velocity sensor (RADVS) signals indicated that the spacecraft had intercepted a series of preprogrammed line segments. These segments specified a profile of velocity vs slant range. At the time of intercept, the engines were upthrottled and the spacecraft decelerated until the velocity appropriate for that altitude was achieved. As the spacecraft descended the line segments, the flight control system, using RADVS range and velocity signals, controlled the total thrust in decelerating the spacecraft and differentially throttled the individual engines to provide attitude control. After the spacecraft had decelerated to 10 ft/sec, the on-board gyros maintained inertial attitude control and the engines upthrottled until a velocity of 5 ft/sec was attained. At 14-ft range, the engines were shut off in response to a signal generated in the RADVS, and the spacecraft fell under gravity to the lunar surface.

## A. Vernier Propulsion System

### 1. Introduction

*a. System description.* The VPS in its final design was composed of three independent, variable-thrust, bipropellant engines assembled to the thrust mounts on the spaceframe, one near each spacecraft leg. Each engine was connected to its own propellant feed or supply system via thermally controlled feed lines. The propellant tanks were pressurized by a common regulated source of high-pressure helium. Figure XVII-1 shows a schematic diagram of the VPS.

Each of the three vernier engines was continuously throttleable from 30 to 104 lbf thrust. Each engine had a dual-propellant throttle valve for thrust control and a dual-propellant shutoff valve actuated by helium from a solenoid pilot valve for on/off control. The combustion chambers had integral injectors and were regeneratively cooled by the fuel. Radiation-cooled, spun-molybdenum nozzle exit cone extensions provided an expansion ratio of 89:1. Passive thermal control using surface coatings was employed to maintain engine temperatures between 0 and 145°F during coast periods. Small valves mounted on each engine were used for propellant loading and servicing.

Propellants were fed to each engine through electrically heated propellant lines from an individual set of fuel and oxidizer tanks. These tanks, which were fabricated of titanium, were designed to operate at a nominal pressure of 730 psia. Housed within the tank shell was a bladder made of a tetrafluorethylene–fluorinated ethylene propylene (TFE–FEP) Teflon laminate for positive expulsion of propellant, and a central standpipe that contained concentric passages to permit: (1) propellant flow to the engine feed line, and (2) venting through a servicing valve during propellant filling operations. Three tank assemblies contained the monomethylhydrazine monohydrate fuel, and three assemblies contained the MON-10 (90% $N_2O_4$ + 10% NO) oxidizer. A pair of fuel and oxidizer tanks was located near each of the three landing legs as shown in Fig. XVII-2. Both active and passive thermal control methods were used to maintain the propellant tank temperatures within 0–100°F.

The propellant tanks were pressurized by a system that included a helium tank and high- and low-pressure valve asemblies. The helium tank was constructed of titanium and was loaded to an initial pressure of 5175 psia. The high-pressure valve assembly contained: (1) high pressure charging valves for helium fill and for preflight regulator checkout, (2) a helium pressure transducer, (3) a pyrotechnic helium release valve for in-flight propellant tank pressurization, (4) a pyrotechnic helium dump valve for postlanding or emergency prelaunch helium tank depressurization, (5) a filter unit, and (6) a pressure regulator to maintain the propellant tanks at a nominal 730 psig operating pressure.

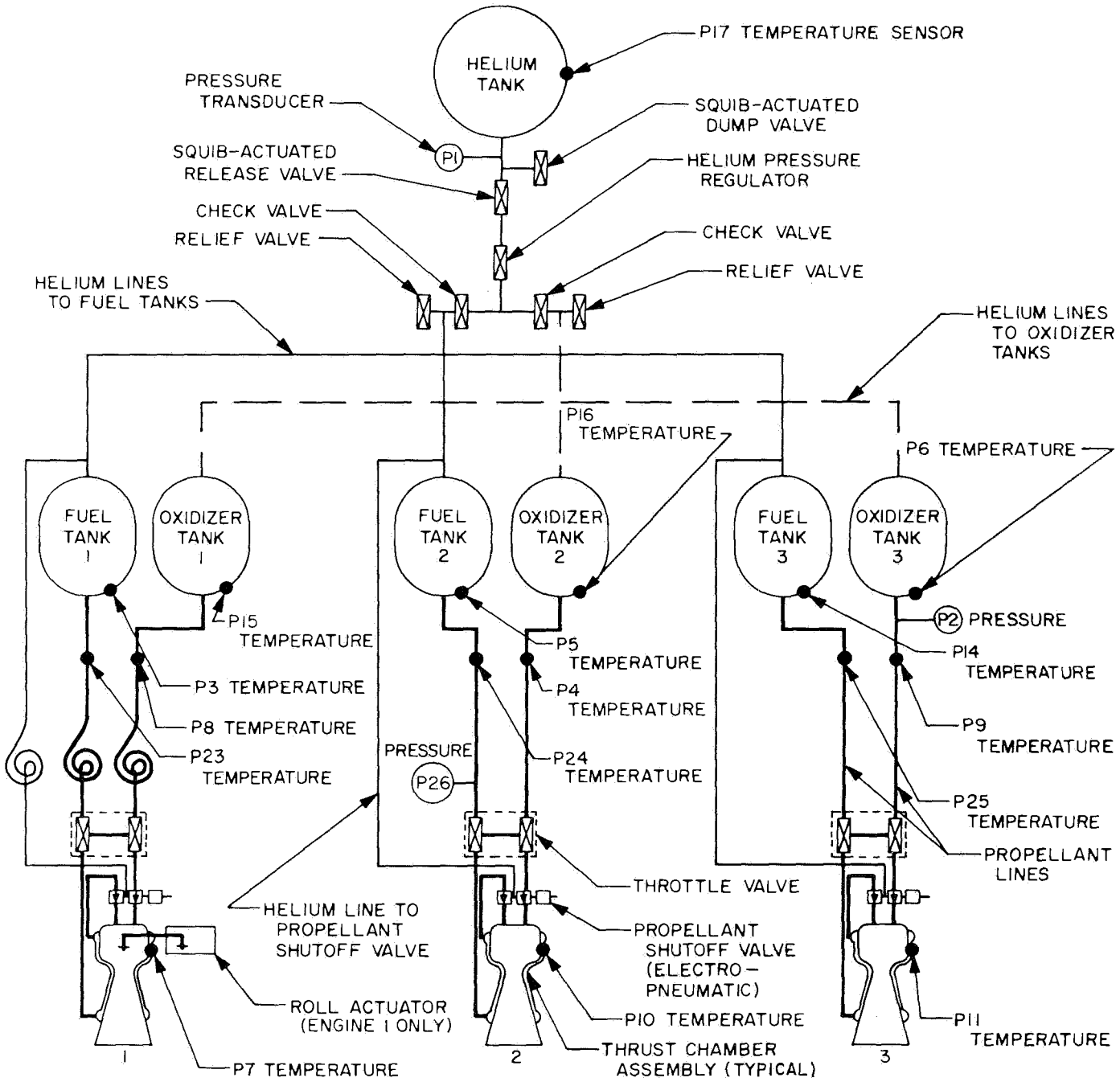



**Fig. XVII-1. Vernier propulsion system schematic**

**Fig. XVII-2. Surveyor vernier propulsion system**

The low-pressure valve assembly housed separate fuel and oxidizer pressurization branches, each containing: (1) a check valve to prevent intermixing of propellant vapors, (2) a low-pressure valve used for preflight checkout and prepressurization operations, and (3) a relief valve to prevent overpressurization of the propellant tanks. Passive thermal control, using surface coatings, maintained component temperatures between 0 and 125°F.

***b. System design requirements and evolution.*** The requirements established in the original design study are compared with the final system requirements in Table XVII-1. It should be noted that the engine throttling range and the number and sizes of engines and tanks were very similar in the original and final designs. Every portion of the VPS was substantially changed, however, and the control system interface was the area where requirements changed the most. Because the control system interface was inadequately defined initially, a number of problems remained undetected until quite late in the program. The specific impulse and sterilization requirements originally established could not be met and were later deleted after considerable effort had been expended. Many of the VPS design requirements and development problems were related to interface between the other spacecraft systems and the VPS.

**Table XVII-1. Vernier propulsion system requirements summary**

| Item | Requirement | |
|---|---|---|
| | Original design study (Dec 1960) | Final design (Jun 1965) |
| Engines | 3 | 3 |
| Throttling range (each) | 30–104 lbf | 30–104 lbf |
| Specific impulse (average) | 311 lbf-sec/lbm | 280 lbf-sec/lbm |
| Propellant capacity | 160 lbm | 180 lbm |
| Fuel tanks | 3 | 3 |
| Oxidizer tanks | 3 | 3 |
| Helium tanks | 3 | 1 |
| Roll actuator capability | ±3 deg | ±6 deg |
| Mixture ratio (oxidizer/fuel) | 2.1:1 | 1.5:1 |
| Total dry hardware weight | 77 lbm | 76 lbm |
| Propellant tank pressure | 610 psia | 730 psia |
| Sterilization | Required | Not required |
| Fuel | MMH | 72% MMH + 28% $H_2O$ |
| Oxidizer | 90% $N_2O_4$ + 10% NO | 90% $N_2O_4$ + 10% NO |
| Propellant temperature | 0–100°F | 0–100°F |
| Step-response time | <0.030 sec | <0.120 sec |
| Step-response overshoot | Not defined | <25% |
| Phase shift at 5 Hz | Not defined | <32 deg |
| Amplitude ratio at 5 Hz | Not defined | >85% |
| Hysteresis | Not defined | <1.4 lbf thrust |
| Start impulse variation | Not defined | <20 lbf-sec |
| Shutdown time | Not defined | <0.150 sec |
| Shutdown impulse variation | Not defined | <1.28 lbf-sec |

*1. Weight.* Initially, the constraint in the development of the VPS was the total weight of the system. The original design concept, therefore, emphasized minimum system weight consistent with functional requirements. This philosophy was followed wherever possible in any design changes that took place during the development phase of the VPS. Although every part of the system was redesigned from the original concept, the total system hardware weight was essentially unchanged from that of the original design (Table XVII-1).

*2. Moment and center-of-gravity control.* Mission requirements dictated that each of the three engines be continuously throttleable between 30 and 104 lbf thrust at vacuum conditions. With this range and the spacecraft geometry, the maximum moment correction capability about the pitch and yaw axes was 2065 in.-lb. This requirement was established in the original HAC design study and remained unchanged through the program.

The spacecraft CG was required to be within 0.2 in. of the retro motor thrust vector so that the moment control capability of the VPS would not be exceeded. This meant that the CG of the system could not vary significantly during the mission. In the original design, the propellant feed system had manifolds interconnecting propellant tanks. Investigations indicated that propellant migration from tank to tank could occur and could cause large CG excursions (Ref. XVII-1). After careful consideration of various means of reducing the magnitude of propellant imbalance, a decision was made to remove the propellant manifolds, and connect a pair of propellant tanks directly to each engine, thus eliminating the possibility of any propellant transfer between the propellant tanks during any portion of the mission. The elimination of the propellant manifolds had one additional advantage: It tended to correct misalignments between the main retro motor thrust vector and the spacecraft CG. The differential propellant usage between engines because of an initial misalignment actually caused the spacecraft CG to move toward the thrust vector. This, in effect, increased the moment control capability of the system

(Ref. XVII-2). This change had the disadvantage, however, of requiring additional propellant in each tank to ensure that depletion would not occur because of higher thrust on one engine. This required the addition of about 5 lb of propellant, which was balanced by a reduction of about 5 lb in manifold weight.

3. *Propellant tanks.* Configuration limitations precluded the use of a single fuel and oxidizer tank, which would have been advantageous from a reliability standpoint. Because of this restriction, a design evolved that used three oxidizer tanks and the three fuel tanks with each set interconnected by a manifold. As stated, after investigations indicated that propellant migration from tank to tank could occur and cause a CG shift large enough to exceed moment control capability during the retro motor firing, these propellant manifolds were removed and each pair of tanks was connected to the adjacent engine. Changes to the engine mixture ratio and the descent trajectory design required that the propellant tank volumes be changed; fuel and oxidizer tanks of equal volume were selected. Subsequent problems with propellant and helium tank burst-pressure reproducibility required that the materials also be changed.

4. *Helium supply system.* The helium package originally included three manifold, tubular high-pressure tanks that also provided structural support; however, the design concept was abandoned in the early stages of development in favor of a single spherical tank because of the weight penalty.

To preclude the possibility of back flow of helium from one side of the system to the other, the regulated helium supply was split into two systems, both of which incorporated one-way check valves. Since the bladders were permeable to a marked degree by the oxidizer and to a lesser degree by the fuel vapors, it appeared necessary to prevent possible mixing of the two vapors. To reduce the possibility of helium leakage, a squib-actuated valve was introduced between the high-pressure helium bottle and the helium regulator. A similar valve was used to dump high-pressure helium in the event of a mission emergency or to vent helium pressure after touchdown on the lunar surface.

5. *Engines.* An alternative vernier engine was developed at Space Technology Laboratories (STL). This engine used ablative cooling and an entirely different throttling technique than the Thiokol Chemical Corp. Reaction Motors Division (RMD) engine that was initially specified and finally used on the spacecraft. Very severe engine development problems nearly caused abandonment of the RMD engine and redesign of the spacecraft to accept the alternate engine. Subsequent redesign, however, resolved the major problems of the RMD engine.

6. *Flight control interface.* The VPS flight control interface created many of the major development problems. These problems are discussed in detail in Subsections A-2-d, -e, and -f. Many of these problems can be traced to an inadequate definition of requirements in the early phases of the program and the establishment of overconservative requirements late in the program. The T-2N descent tests and the S-6 closed loop test were invaluable in certifying adequacy of the interface (Subsection A-2-e).

7. *Impingement heating.* Impingement heating from vernier engine exhaust gases was another major concern during the development program. After an extensive analysis it was determined that the ablative heat protection on the crushable blocks and the retro motor nozzle were adequate (Ref. XVII-3). These conclusions were later verified during successful flight performance.

8. *Radar beam interference.* Interference of the radar beams by the vernier engine exhaust was of major concern during the program. A special study was performed to assess the problem (Ref. XVII-4). The conclusions indicated that, so long as the alkali metals content of the propellants was less than 500 parts/$10^6$ interference should not be a problem. The flight propellants had less than 5 parts/$10^6$ alkali metals, and no interference was noted during any of the missions.

9. *Surface contamination.* Surface contamination by propellants and exhaust products was an important interface with the scientific experiments. It was of particular concern to the alpha scattering experiment. Studies performed indicated that the possible level of surface contamination was on the same order as the sensitivity of the instrument (Ref. XVII-5). Mission results later showed no detectable evidence of surface contamination by the propellants.

10. *Lunar dust.* Dust during landing was a major concern for the spacecraft design. A detailed study was undertaken to determine the adequacy of the 14-ft cutoff altitude (Refs. XVII-6 and XVII-7). The results showed that the cutoff altitude could probably be reduced to 5 or 6 ft before dust transport by engine exhaust would be a problem. Mission experience demonstrated that the

14-ft cutoff altitude was adequate and that no detectable amount of dust was transported at that cutoff altitude. During the landing of *Surveyor III* when the spacecraft bounced across the surface before the engines were cut off, dust was noted on spacecraft equipment.

*11. Test and operations experience.* The test programs played an important role in the evolution of the final vernier propulsion design. Tests such as the T-2 tether test dramatically illustrated incompatibilities between the VPS and the spacecraft system that had not been covered by performance specifications. Other tests such as those performed on the S-6 vehicle showed incompatibilities between the vernier engine and the propellant feed system that also had not been covered in specifications. Later in the program the extensive prelaunch testing program for each spacecraft uncovered problems such as leakage, low thermal conductivity between engine barrel and nozzle extension, and foreign materials in the system. The problems encountered during testing led directly to redesign or procedural changes.

Significant VPS anomalies occurred on two of the seven missions. The failure of *Surveyor II* was traced to the VPS. A helium pressure regulator leak on *Surveyor V* was the only other anomaly, but this did not result in a mission failure. After each of these occurrences, special tests and changes to the test and launch preparation procedures were made to ensure against their recurrence. Test and operational problems and resulting corrective action are discussed in greater detail in Subsections A-2, -3, and -4.

### 2. Vernier Engine

This subsection summarizes the development of the vernier rocket engine that was used on the *Surveyor* spacecraft. As previously discussed, three vernier engines were required for each spacecraft to supply the thrust forces for midcourse velocity correction, attitude control during main retrorocket burning, and velocity and attitude control during terminal descent.

***a. Engine history.*** Hughes selected the Thiokol Chemical Corp. RMD as the vernier engine supplier during the original competitive design study in 1960. Shortly after HAC was selected as the system contractor in 1961, RMD was subcontracted to do the vernier engine and propellant feed system development. As originally proposed, the engine was to be a modification of a *Drone A* engine made by RMD. The modifications included changing propellants and valves and adding a throttle valve. In 1963, HAC terminated the propellant feed system portion of the RMD contract to allow the subcontractor to concentrate on serious engine development problems that had not been overcome. Also in 1963, a contract was let directly by JPL to STL for the development of an alternate vernier engine. Continued development problems at RMD forced the cancellation of the HAC subcontract in early 1964. A detailed evaluation of the STL vernier engine integration into the spacecraft and an evaluation of other engines that could be used with the throttle valve developed for the RMD engine were made in early 1964.

Evaluation of other engines, primarily the Rocketdyne *Gemini* engine and the Marquardt *Apollo* engine, revealed many then unknown and potential problem areas. Detailed studies indicated severe unanticipated problems associated with integration of the STL vernier engine into the spacecraft system. During this time, RMD, in a company-funded program, developed potential solutions to the major problems that had delayed the development program. Based on some encouraging results from RMD, and since using the STL engine would have required repeating much of the system tests that had been completed, a contract was let from JPL directly to RMD for a design demonstration program in mid-1964. After the successful completion of this program, RMD was contracted by JPL to continue the development of the vernier engine and later to do the qualification, production, and field service phases of the program. System test and flight engines were then supplied as customer-furnished equipment to HAC.

In addition to the formal qualification program conducted at RMD, other engine qualification tests were performed by JPL. The RMD engines were also used during VPS (S-6 and S-7) tests and descent simulation (T-2) tests conducted by HAC. A summary of the vernier engine program milestones is shown in Table XVII-2.

***b. Engine requirements.*** The engine requirements were basically the spacecraft control function, compatibility with the control system, compatibility with the propellant feed system, and operation or storage under various environmental conditions. A summary of the final requirements is presented in Table XVII-3. In the early phase of the engine development program, the control function requirements and control system compatibility were not well defined. This led to the late recognition of dynamic engine response problems. It was also found that a number of the requirements in the control function area were far too stringent and could be relaxed without degrading overall system performance. Definitions of

## Table XVII-2. *Surveyor* vernier engine major milestones

| Date | Milestone |
|---|---|
| Aug–Dec 1960 | RMD supported HAC in precontract design competition |
| Apr–Oct 1961 | RMD under limited contract to HAC for determining feasibility of *Drone A* (*Surveyor* precursor) to operate with MMH/MON-10 propellants in 30–104 lbf range; stable performance of vortex injector demonstrated |
| Aug 1961 | Initial HAC design review of RMD TD-280 vernier engine |
| Oct 1961 | RMD awarded full development contract by HAC |
| Nov 1961 | First successful demonstration by RMD of continuous throttling over full thrust range using spool-type throttle valve |
| Nov 1961 | Preliminary model specification for TD-280 engine submitted |
| Dec 1961 | HAC second design review of TD-280 engine |
| Feb 1962 | Finalized TA[a] test plan and start TA testing for TD-280 engine, scheduled for completion in Aug 1962 |
| Mar 1962 | First engine tests indicating overheating of fuel in coolant jacket |
| Jul 1962 | Third design review |
| Jul 1962 | Successful test, demonstrating engine survivability under constant g loading (centrifuge) and vibration loads |
| Aug–Sep 1962 | Recognition of continued severity of engine performance problems:<br>(1) Broad deviation in specific impulse<br>(2) Erratic engine start and restart<br>(3) Excessive nozzle throat erosion |
| Aug 1962 | Fuel pressure regulator incorporated to suppress fuel boiling in coolant jacket |
| Dec 1962 | Unstable T-2 tests traced to poor response characteristics of engine; HAC initiated backup design of throttle valve incorporating bellows in second stage |
| Apr 1963 | Alternate vernier engine development initiated at Space Technology Laboratories, Inc. (STL) |
| May 1963 | Initial integration of bellows throttle valve onto engine and incorporation of Teflon amniseals in throttle valve |
| Oct 1963 | RMD sole effort directed on engine as a result of HAC withdrawing responsibility of upstream system from RMD |
| Dec 1963–Feb 1964 | Intensive test and evaluation program at RMD to solve problems of:<br>(1) Excessive shifts in operating propellant mixture ratio<br>(2) Erratic start and restart<br>(3) Low specific impulse |
| Dec 1963–Jan 1964 | Alternate potential engine supplier reviewed by NASA/JPL/HAC |
| Mar 1964 | RMD activity terminated |
| Mar–Apr 1964 | In-house engine test activity at RMD to solve vernier engine problems |
| Jul 1964 | Letter contract (JPL Contract 950997) issued to RMD for 60-day design demonstration program |
| Sep 1964 | Program completed by demonstrating:<br>(1) Successful use of MON-10/MMH-$H_2O$ propellants<br>(2) Control and restart capability<br>(3) Long-duration firing without throat erosion |
| Dec 1964 | First JPL/RMD design review |
| Jan 1965 | Alternate vernier engine contract terminated at STL |
| Feb 1965 | Satisfactory demonstration of exposure to 96-hr hard vacuum, followed by engine test firing |
| Jan 1965 | Margin limit tests completed, successfully demonstrating:<br>(1) Engine and fuel have adequate heat transfer margins<br>(2) Sixty-two engine restarts<br>(3) Control after downthrottle |
| Jan–Apr 1965 | Prequalification testing completed, yielding necessity for additional evaluation of:<br>(1) Engine dynamic response problems<br>(2) Effects of helium gas solubility |
| Feb 1965 | Initial component fabrication for flight engines |
| Mar 1965 | Completed demonstration of 30- and 60-day storage tests with freon and isapropyl alcohol loaded in engine |
| Mar 1965 | Successful demonstration of engine survivability during revised vibration spectrum |
| Mar 1965 | Begin engine test program at JPL Edwards Test Station |
| Apr 1965 | Engine tests at JPL Test Station show major effects of helium dissolved in propellants on engine dynamic performance |
| Apr 1965 | Second JPL/RMD design review |
| May 1965 | First FA[b] test firing of flight engine |
| May 1965 | Initial delivery of flight engines to JPL |
| May–Jun 1965 | Roll actuator and mounting bracket tests with firing engine shows inadequate bracket design |
| Jun 1965 | TA test program initiated at RMD |
| Jul 1965 | Vernier engine successfully fired under high static acceleration at JPL Test Station |
| Aug 1965 | TA test program completed at RMD |
| Aug–Oct 1965 | Vernier engine successfully starts under cold hard vacuum conditions in test at JPL Test Station |
| Sep 1965 | Units S-6 and S-7 VPS TA tests successfully completed |
| Oct 1965 | Engine field service support established at AFETR |
| Nov 1965 | First successful T-2N descent test |
| Nov 1965 | Unit S-6 closed-loop test completed |
| Nov 1965 | Vernier engine fails part of lunar survival tests at JPL Test Station; failure caused by fuel poppet degradation at high temperature |
| Dec 1965 | Vernier engine operated successfully under nonfiring static acceleration at JPL Test Station |
| Dec 1965 | Vernier engine successfully completed storage and firing test at JPL Test Station |
| Feb–Apr 1965 | Vernier engine successfully completed thrust vector alignment tests at JPL Test Station |

[a]TA = type approval.

[b]FA = flight acceptance.

**Table XVII-2 (contd)**

| Date | Milestone |
|---|---|
| Mar 1966 | First rework required on flight engine previously delivered to JPL (TCA SN 536) |
| May 1966 | First successful T-2N landing test |
| Jun 1966 | *Surveyor I* successfully launched and landed |
| Jun 1966 | Successful simulated lunar firing experiment with vernier engine at JPL Test Station |
| June 1966 | Improved fuel poppet evaluation at JPL Test Station |
| Jul 1966 | Last flight engine delivered to JPL (SN 563) |
| Sep 1966 | Began *Surveyor II* failure review tests at JPL Test Station |
| Sep 1966 | Lunar dust tests at JPL Test Station |
| Oct 1966 | Changed lubricant (engine seals and threads) to Dupont PR 240AC |
| Dec 1966 | JPL initiated backup solenoid valves procurement at Valcor |
| Dec 1966 | Injector salting tests at JPL Test Station showed possible *Surveyor II* failure mode |
| Apr 1967 | Solenoid stroke problem: special tests at JPL Test Station |
| Apr 1967 | Completed *Surveyor II* failure review salting and oxidizer flow restriction tests at JPL Test Station |
| Apr 1967 | Successful completion of solenoid helium inlet filter qualification tests at JPL Test Station |
| Jun 1967 | Successful lunar hop simulation tests at JPL Test Station showed thrust increase at high temperature |
| Sep 1967 | Special engine flow tests at JPL Test Station for *Surveyor V* modified descent |
| Sep 1967 | First lunar static firing (*Surveyor V*) |
| Nov 1967 | First lunar translation (*Surveyor VI*) |
| Dec 1967 | Completed all engine rework at RMD |
| Jan 1968 | Lunar hop closed-loop test at JPL Test Station showed marginal shutdown capability for long hop |
| Jan 1968 | *Surveyor VII* successfully launched and landed |
| Jan 1968 | *Surveyor VII* engine 2 fuel poppet developed leak after 260 hr at high temperature on the lunar surface |
| Apr 1968 | Final report issued by RMD; program completed |

engine throttling duty cycle and environmental exposure requirements were formulated considerably after the beginning of engine development and resulted in the late recognition of some serious design deficiencies. Early requirements also included high specific impulse (312 lbf-sec/lbm) as compared with the actual delivered specific impulse of the flight engines (275 lbf-sec/lbm). The original high specific impulse could possibly have been met if the engine had been designed to operate at a fixed thrust. The many additional problems associated with throttling required the compromise of performance in their final solution.

*c. Flight configuration engine description.* The flight configuration vernier engine is shown in Fig. XVII-3, and the flow schematic is shown in Fig. XVII-4. It was basically a regeneratively cooled combustion chamber with a ceramic throat insert of silicon carbide and a radiation-cooled molybdenum nozzle extension. Propellant flow control was maintained by separate throttling and shutoff valves. Linked poppet-type fuel and oxidizer shutoff valves were actuated by a single helium piston. Actuation gas from the feed system was supplied through an electrical solenoid mounted on the shutoff valve casting.

Propellant flow rate was controlled by a separate valve as shown in Fig. XVII-5. A small thrust-command current was used to change the flow area in the first stage. A small-amplitude 400-Hz dither current was added to the command current to reduce hysteresis. A second stage was used to maintain a constant pressure drop across the first-stage flow-control area. A linear propellant flow rate (and thrust) variation with command current resulted from a constant pressure drop across an

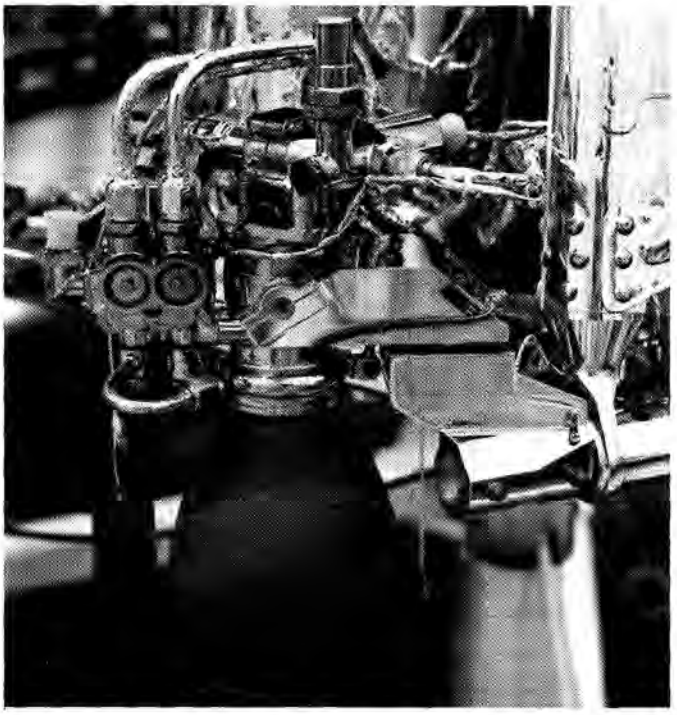


**Fig. XVII-3. Flight configuration vernier engine**

**Table XVII-3. Vernier engine requirements summary**

| Item | Requirement |
|---|---|
| A. Propellant feed system interface | |
| 1. Propellants | |
| Fuel | 72% MMH/28% $H_2O$ |
| Oxidizer | 90% $N_2O_4$/10% NO |
| 2. Propellant temperature | 0–100°F |
| 3. Propellant feed pressure | |
| Max | 830 psia |
| Min | |
| Fuel | 685 psia |
| Oxidizer | 687 psia |
| B. Mission and vehicle interface | |
| 1. Specific impulse | |
| Thrust level, lbf | Specific impulse, lbf-sec/lbm |
| 30 | 273 ±12 |
| 67 | 278 ±12 |
| 104 | 287 ±12 |
| 2. Mixture ratio (oxidizer/fuel) | 1.5 ±0.1 |
| C. Control system interface | |
| 1. Shutoff valve actuation voltage | 16–26 V |
| 2. Thrust range | |
| Min | ≤30 lbf |
| Max | ≥104 lbf |
| 3. Step response time | |
| Min–max | <0.120 sec |
| Max–min | <0.120 sec |
| 4. Overshoot on step command | <25% |
| 5. Thrust hysteresis | <1.5 lbf |
| 6. Frequency response | |
| Amplitude ratio (at 5 Hz) | >0.85 |
| Phase lag (at 5 Hz) | <32 deg |
| 7. Start characteristics | |
| Max thrust | <125 lbf |
| Impulse deviation from commanded | <20 lbf-sec |
| 8. Shutdown characteristics | |
| Shutdown time | <0.150 sec |
| Shutdown impulse variation | <0.63 lbf-sec |
| 9. Thrust command gain | ≥0.46 lbf/mA<br>≤0.69 lbf/mA |
| 10. Restart, min time between firings | 1 hr |
| D. Environmental | |
| 1. Operational temperature range | 0–145°F |
| 2. Life | |
| Shelf life | > 24 mo at 0–145°F |
| Service life–max thrust | 4 min |
| min thrust | 8 min |
| Starts | 4 |
| Lunar survival life | 1 lunar day |
| 3. Cycle life | |
| Solenoid valve | >250 |
| Shutoff valve | >250 |
| Throttle valve | >10,000 |
| 4. Vibration level (3 axes) | |
| Sinusoidal | |
| 5–35 Hz | 8.0 g |
| 35–150 Hz | 18.0 g |
| 100–1500 Hz | 6.0 g |
| White gaussian | |
| 100–1500 Hz bandwidth | 6.7 g |

orifice whose area changed linearly with current. The fuel and oxidizer sections of the throttle valve were independent except that a common torque motor was used to simultaneously control both first-stage flow areas.

After leaving the throttle valve, the fuel flowed through the cooling jacket and then through the propellant shutoff valve. A fuel pressure regulator was located in the fuel flow path just ahead of the injector. The regulator maintained the pressure above 450 psia in the cooling jacket. This suppressed fuel boiling in the jacket and limited the amount of dissolved gas which was released from solution in the fuel. The oxidizer flowed directly from the throttle valve through the shutoff valve to the injector.

The injector was a vortex type in which the fuel formed a sheet inside the injector cup as shown in Fig. XVII-6. Oxidizer was sprayed radially outward from a central spud into the fuel sheet. This injector was of the fixed-area type; i.e., the flow geometry remained constant but the injection velocities changed as the engine was throttled. The injector orifices were quite small so that the injection velocities were not too low for good propellant mixing at minimum thrust and there was sufficient hydraulic impedance between the combustion chamber and the injector to prevent instability. This meant that the engine operating at maximum thrust had a very large injector pressure drop. This engine required a propellant feed pressure of at least 700 psi, which was quite high considering that the maximum chamber pressure was 250 psia. A flame-sprayed Rokide Z coating on the interior surfaces of the combustion chamber, throat insert, and parts of the injector provided thermal protection from combustion gases.

The fuel was monomethylhydrazine monohydrate (72% MMH + 28% $H_2O$). The original fuel, which was

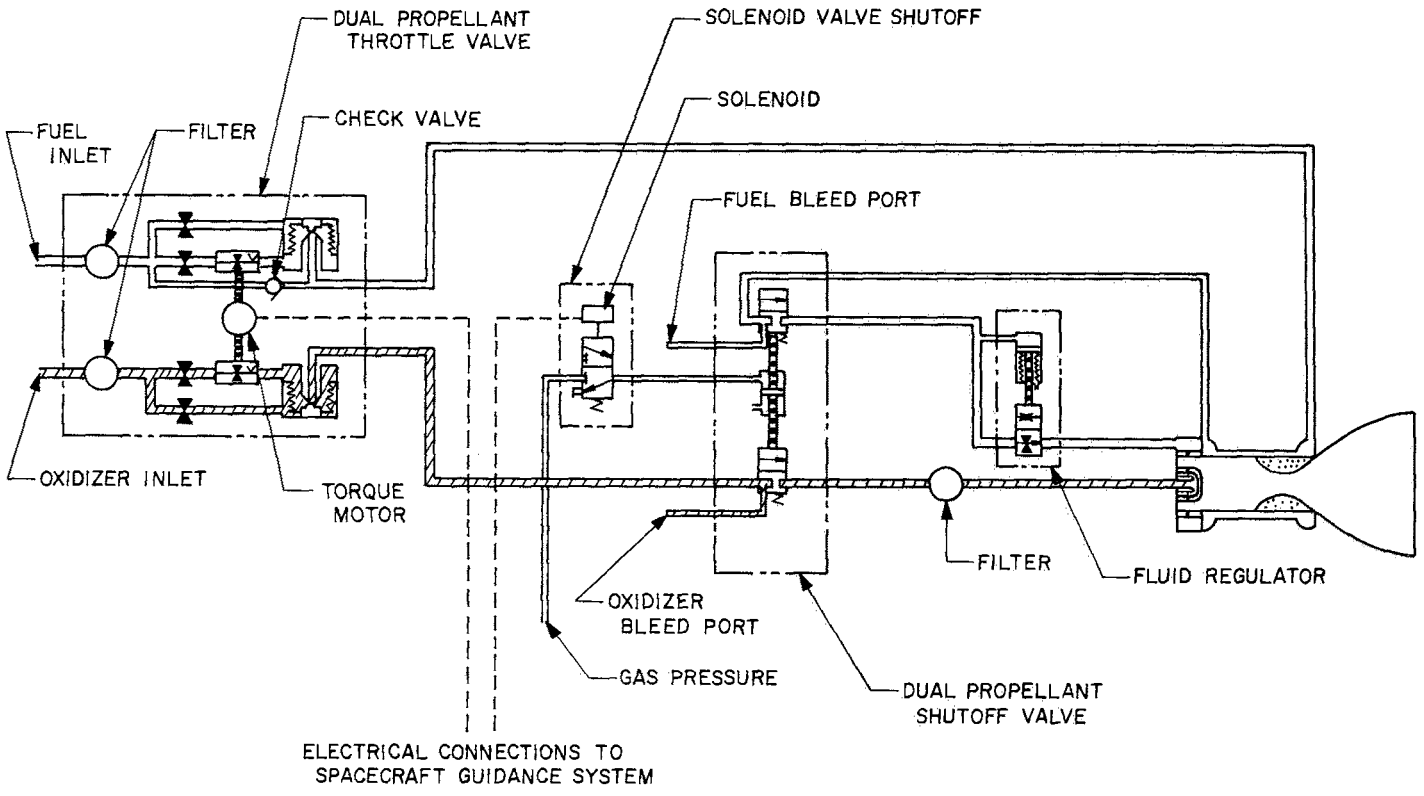



**Fig. XVII-4. Vernier engine flow schematic**

pure MMH, was found to undergo some thermal decomposition in the cooling jacket. The oxidizer was 90% nitrogen tetroxide with 10% nitric oxide (MON-10) added to depress the freezing point.

Black and white paints were applied to the top of the engine to control the solar heat input, and gold plating was applied to the remainder of the engine parts to prohibit excessive radiation during spacecraft cruise periods. The nozzle was coated with a pyrochrome paint of high emissivity to radiate heat during engine firing. Special reflectors on the spacecraft directed some solar energy onto the nozzle during cruise periods. This maintained the lower part of the engine at the required temperature without requiring an excessive thermal gradient along the engine barrel.

A temperature sensor was attached to the engine barrel for in-flight measurements. Strain gages attached to the engine mounting bracket were used to measure thrust. Thermal gradients in the brackets, which resulted from engine heating, degraded the accuracy of the strain gage circuit to about $\pm 20\%$. The engine thrust commands, spacecraft acceleration, and gyro angles were the main sources of dynamic performance data during flight.

*d. Early development problems and design modifications.* Demonstration tests performed before the beginning of the development program showed the feasibility of the throttling concept proposed by RMD. Early development efforts concentrated on improving the engine specific impulse to meet the 312-lbf-sec/lbm requirement. This performance level was never met. By the end of the program it was necessary to accept flight engines with a specific impulse of 275 lbf-sec/lbm. This large difference was attributed to an original specific impulse requirement that was far too optimistic and to changes that were required to solve controllability and chamber-life problems.

Engine controllability requirements were not well understood early in the program. One severe control problem was discovered during a T-2 tether test. The T-2 vehicle employed three vernier engines mounted on a spaceframe and fed by a single set of propellant tanks (see also Subsection A-4). An inertial attitude control system generated throttle commands to maintain attitude stability. Engine throttle valve hysteresis caused a large-amplitude limit cycle to develop during a tether test. This hysteresis was caused by friction in the second stage of the throttle valve, which required a large change in

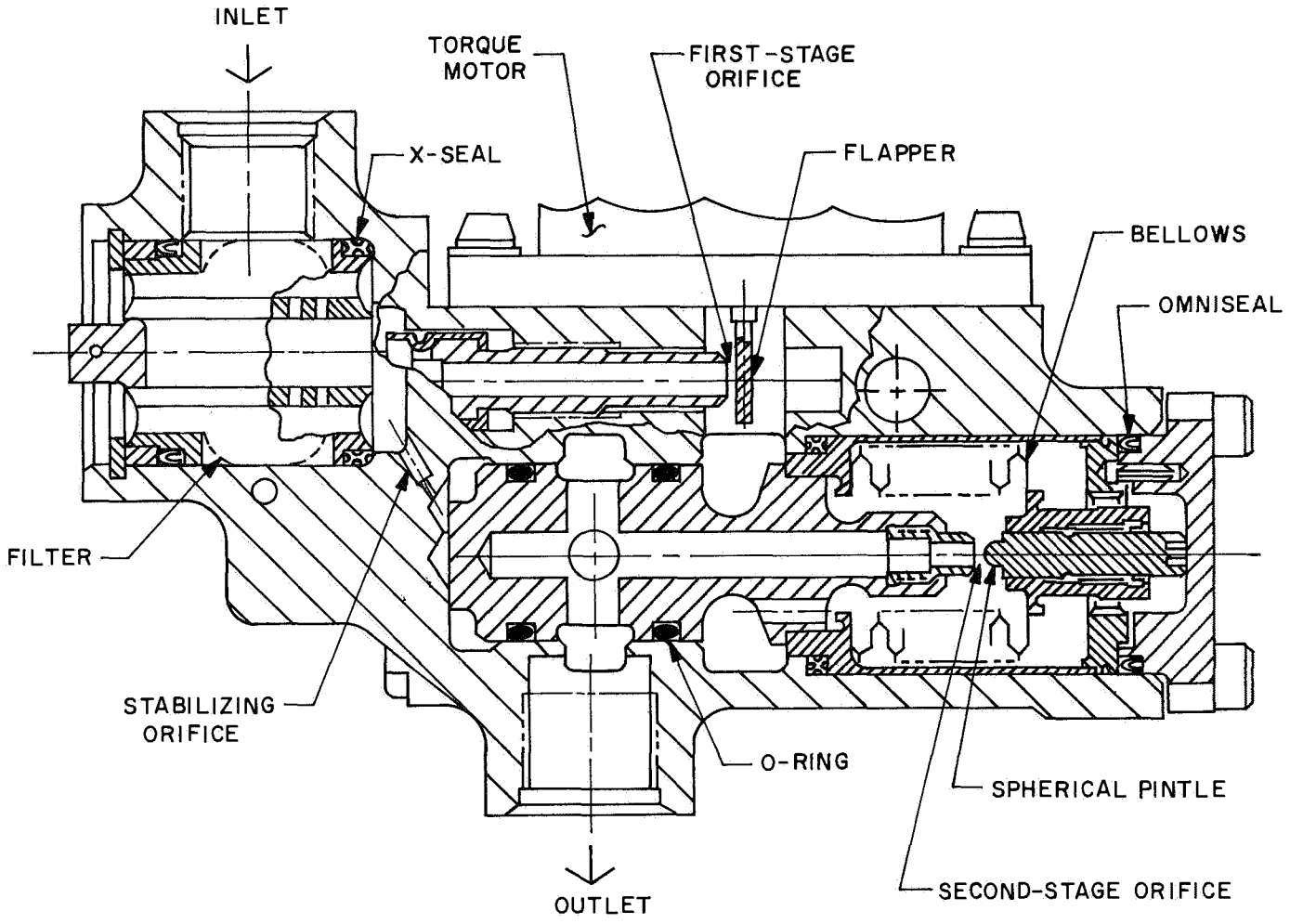



**Fig. XVII-5. Vernier engine throttle valve**

thrust command before a change in thrust would occur. This problem was solved, after considerable redesign, by using a bellows to replace the sliding spool in the second stage. This bellows was also used in the final throttle valve design (see Fig. XVII-5) and reduced the actual hysteresis to less than 0.5 lbf thrust.

Much of the early testing involved steady-state operation to determine performance parameters. The engine performed adequately at various steady-state thrust levels through the thrust range; however, it did not perform well on transients. These problems were not discovered until attempts were made to test the engine over parts of a simulated mission duty cycle. Severe throat erosion and injector-face erosion were noted on some engines. The engine could not be controlled after a downthrottle following a long high-thrust run. Upon restart, the engine showed large uncommanded thrust variations during the first 2 sec.

It was determined after an extensive investigation that all these problems were related to heat transfer in the cooling jacket. The basic engine construction, which used a large ceramic nozzle insert and a fixed-area injector with upstream throttling, contributed to the problem. During operation, heat from the combustion gases was transferred through the nozzle insert to the cooling jacket. Because the silicon carbide had a relatively low thermal conductivity, a large (2000°F) temperature gradient occurred during steady-state operation at high thrust. At low thrust the chamber pressure was approximately 70 psi, in contrast to the 250 psi at high thrust. This reduced chamber pressure decreased the heat flux by a factor of approximately three. Because the nozzle insert area and thermal conductivity were unchanged, the temperature gradient across the nozzle insert was only 700°F at low thrust, much lower than the 2000°F at high thrust. The nozzle insert, however, had a significant thermal capacity because of its size.

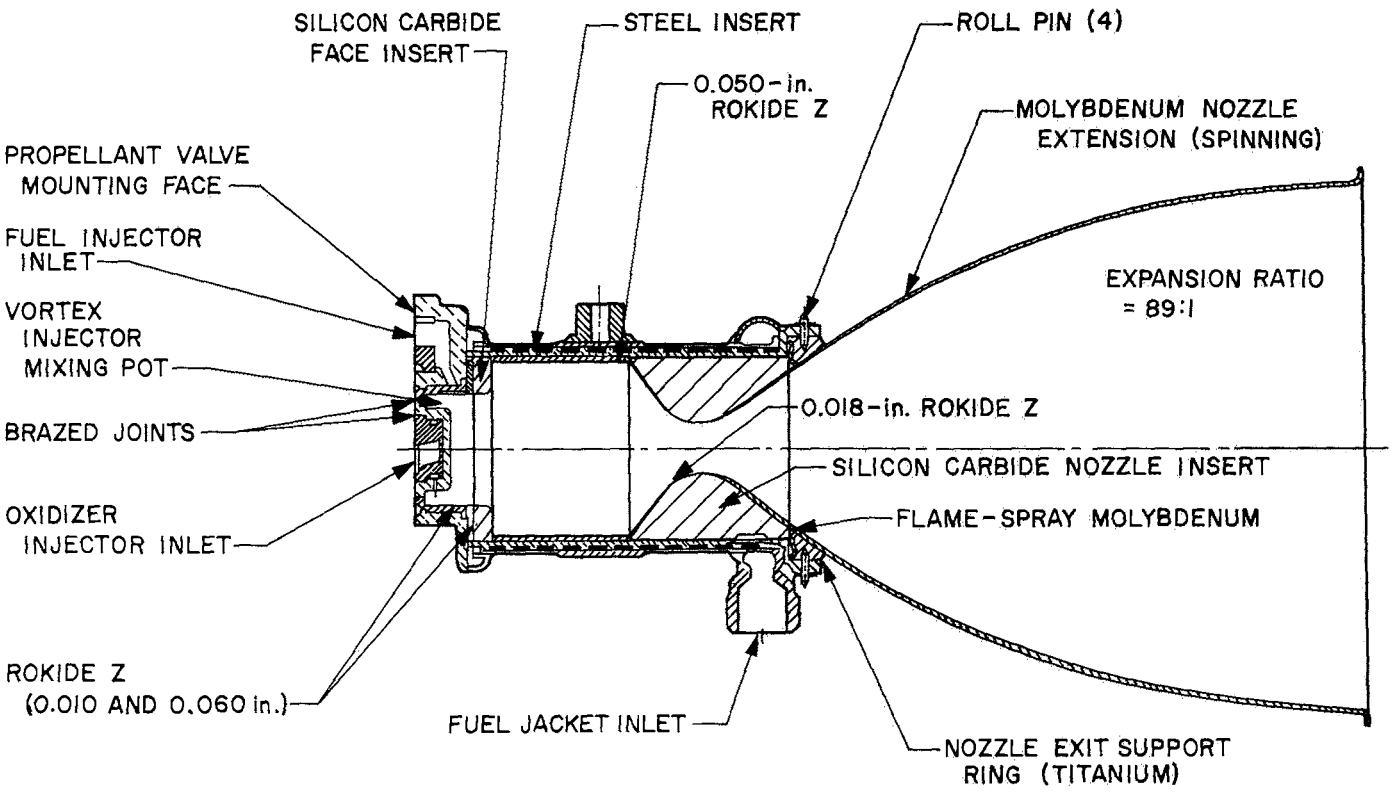



**Fig. XVII-6. Vernier engine combustion chamber assembly**

This caused the heat flux to the coolant, which was present at high thrust, to persist for an appreciable time after the engine was downthrottled to low thrust or shutoff. After downthrottle to low thrust, the coolant flow was greatly reduced, but the high heat flux present at high thrust persisted and caused the fuel to reach a very high peak temperature. This caused boiling and fuel decomposition after a downthrottle or shutdown. Fuel vapor and gaseous decomposition products were responsible for the loss of controllability after downthrottle and for erratic restarts.

Fuel decomposition was caused by localized overheating during boiling and a basic thermal instability of the fuel at temperatures above 350°F. This decomposition was exothermic, which tended to "boot strap" the decomposition reaction. Surface impurities in the cooling jacket also contributed to decomposition caused by catalytic effects.

The addition of a fuel pressure regulator just upstream of the injector and downstream of the cooling jacket helped prevent boiling in the cooling jacket after a downthrottle; this maintained the upstream pressure above 450 psia. Without this regulator the pressure would have dropped to 90 psia at low thrust. This significantly reduced, but did not completely resolve, the downthrottle problem; neither did it alleviate the rough restart problem.

A check valve was added to prevent throttle valve damage after shutdown by allowing vapor and decomposition products formed in the cooling jacket to bypass the throttle valve components. Also tried was a vent-reprime valve that vented the cooling jacket overboard and then refilled the engine after each firing. The valve was later abandoned because of its complexity and the potential damage to the spacecraft by the fuel dumped overboard; in addition, the valve did not solve the basic problem.

The thermal stability of the fuel was found to be greatly improved by the addition of water. A fuel of 28% water and 72% MMH, which actually forms monomethylhydrazine monohydrate, was finally adopted for use in the engine. This change increased the fuel decomposition temperature from 350 to 450°F and decreased the performance by about 3%. The use of this fuel in conjunction with the fuel pressure regulator, and a special passivation technique to remove impurities from

the cooling passages, eliminated the downthrottle problem and greatly reduced erratic restarts. It also completely eliminated throat erosion that was traced to excessive throat temperatures caused by high combustion temperatures and high cooling-jacket wall temperatures. The addition of a silicon carbide ring to protect the injector, the greatly reduced fuel temperatures because of the improved thermal stability, and Rokide coatings eliminated the injector-erosion problem. These changes moved the engine design close to the final configuration.

*e. Prequalification and flight engine problems.* During a design demonstration program in mid-1964, six engines were run through a complete mission profile, including downthrottles after sustained high-thrust periods, small- and large-amplitude cycling (2.5–1000 Hz) at various thrust levels, step changes in thrust, hysteresis loops, and restarts. These tests were conducted with engines using propellants at either 0 or 100°F. The program was quite successful and proved that the earlier heat-transfer problems had all been overcome. Several new problems appeared during the demonstration program and many more appeared later in the prequalification and flight phases of the program. Table XVII-4 contains a summary of engine problems encountered on flight engines during the preflight phase.

**Table XVII-4. Flight vernier engine rework history**

| Engine SN | Initial delivery date | Problem summary[a] | | | | | | | | | Re-work cycles | Final delivery date | Flight spacecraft allocation |
|---|---|---|---|---|---|---|---|---|---|---|---|---|---|
| | | Seal leakage | Torque tube rupture | Shutoff valve response | Contamination | Thrust command calibration or M.R.[b] shift | Manufacturing error | Foreign material | Low thermal conductance at nozzle/injector joint | Other[c] | | | |
| 536 | 5/28/65 | 1 | | *1* | *1* | | 2 | 1 | | | *5* | 8/28/67 | *7* |
| 537 | 5/28/65 | | | | *1* | 2 | | | | | 3 | 11/17/67 | Flight spare |
| 539 | 6/4/65 | | | | | | | | | | 0 | 6/4/65 | 1 |
| 540 | 6/17/65 | | 1 | | *1* | | 1 | | | | 2 | 8/23/67 | 6 |
| 541 | 6/17/65 | | | | | | | | | | 0 | 6/17/65 | 1 |
| 542 | 7/30/65 | | | | | | | | | | 0 | 7/30/65 | 2 |
| 544 | 7/30/65 | | | | | | | | | | 0 | 7/30/65 | 2 |
| 545 | 2/4/66 | | | | | | | | | | 0 | 2/4/66 | 1 |
| 546 | 7/30/65 | | | | | | | | | | 0 | 7/30/65 | 2 |
| 547 | 8/3/65 | | *1* | | | *1* | | | | | 1 | 5/13/67 | 4 |
| 548 | 8/3/65 | | | *1* | *1* | *1* | | | | | 1 | 11/3/67 | Flight spare |
| 549 | 8/3/65 | | | | *1* | *1* | | | | | 1 | 1/7/68 | Rework not complete |
| 551 | 2/9/66 | | | *1* | *1* | | | 1 | | | 2 | 1/7/68 | Rework not complete |
| 552 | 2/9/66 | | | | | 3 | | | 1 | | 4 | 1/7/68 | Rejected |
| 553 | 6/30/66 | *1* | | | | | | *1* | | | 1 | 6/30/67 | SC-5 |
| 554 | 5/21/66 | *1* | | | | | | *1* | | | 2 | 10/2/67 | SC-3 |
| 555 | 4/1/66 | | | | *1* | *4* | | | | | 3 | 11/22/67 | Flight spare |
| 556 | 2/4/66 | | | | | | | | | | 0 | 2/4/66 | SC-3 |
| 557 | 4/2/66 | 1 | | | | 1 | | | | 1 | 1 | 5/20/66 | SC-4 |
| 558 | 4/2/66 | 1 | | *1* | *1* | 1 | | | | | 1 | 7/22/67 | SC-7 |
| 559 | 4/2/66 | 1 | | *1* | *1* | | | | | 1 | 2 | 9/15/67 | SC-7 |
| 560 | 4/2/66 | | | | | | | | | | 0 | 4/2/66 | SC-5 |
| 561 | 5/20/66 | 1 | | | *1* | 2 | | 1 | | | 1 | 1/7/68 | Rework not complete |
| 562 | 3/26/66 | | | | 1 | | | | | | 1 | 2/28/67 | SC-6 |
| 563 | 7/12/66 | | | | | | | | | | 0 | 10/1/66 | SC-3 |
| 564 | 5/23/66 | *4* | | | *1* | | | | | 1 | 2 | 6/13/67 | SC-6 |
| 565 | 3/26/66 | | | | | | | | | 1 | 0 | 3/26/66 | SC-5 |
| 566 | 3/26/66 | | | | | | | | | 1 | 0 | 3/26/66 | SC-4 |

[a]Numbers in italics signify related problems, or problems occurring during same test/rework cycles.
[b]Mixture ratio.
[c]Individual problems of seized threads, chipped paint, electrical current overload, or questionable current traces.

*1. Thrust overshoot on ignition.* During the design demonstration program it was noted that the engine would always go to maximum thrust during startup before reaching its commanded level. This problem was solved by adding a mechanical stop to keep the second-stage pintle in the throttle valve from moving far away from its operating position when the engine was off. This reduced the time required for the throttle valve to begin control and completely eliminated the start-overshoot problem.

*2. Shutdown impulse dispersion.* This problem was first recognized during the design demonstration program, but continued in various forms throughout the program. Eventually the solution required a complete redesign of the solenoid valve, a change in lubricant, a redesign of the seals, an extensive preflight testing program, and greatly improved quality control procedures. During the design demonstration program, one engine shutdown was late by 0.15 sec. The maximum allowable shutdown time dispersion between engines on the spacecraft was 0.015 sec. This problem was first attributed to high friction in the shutoff valve seals.

Upon detailed investigation it was found that the magnetic gap in the solenoid valve was very small in the actuated position (Fig. XVII-7). This gap was also reduced by coining of the nylon seat. Since the magnetic force was approximately inversely proportional to the magnetic gap squared, a gap that was much smaller in the actuated position than in the unactuated position caused the solenoid dropout current to be much less than the pull-in current. The spacecraft side of the shutdown circuit used a resistor and diode to eliminate a voltage spike across the transistor switch at engine cutoff as shown in Fig. XVII-8. This circuit caused the solenoid current to decay exponentially after shutdown. With very small magnetic gaps the dropout current was very small and was not reached until late in the exponential decay. This problem was solved by increasing the magnetic gap from 0.004 to 0.012 in. so that the dropout current would be high and gap variations caused by coining would not greatly affect the dropout time and, therefore, not cause large variations in engine shutdown time. Upon detailed investigation it was also found that very little quality control was being exercised during solenoid fabrication. The procedure included such things as randomly winding the solenoid coil until the spool was full. No corrosion protection was applied to internal magnetic parts, which rusted quickly when exposed to air.

During the flight phase of the program, it was discovered that the solenoid valves were not being built to the dimensions shown on the drawings. Solenoids were built with a stroke of 0.007 in. rather than the 0.012–0.014 in. shown on the drawings. It was also discovered that the nylon seats in the solenoid valve armature increased the length of the armature on some units sufficiently to prevent movement when heated to only 190°F. This growth was caused by differential thermal expansion between the nylon seat and the magnetic steel armature. During flight, the initial temperature of the engine was always below 145°F. However, during engine firing, fuel heated in the cooling jacket passed through the solenoid end of the shutoff valve before entering the combustion chamber. Heating from the hot fuel, together with electrical heating, raised the solenoid temperature while the engine was operating.

The major concern with these solenoid valves was that one or more engines might not shut off when commanded at 14 ft above the lunar surface. Several flight solenoids were found that would fail when heated to 190°F; however, others would function at temperatures to 250°F (Ref. XVII-8). Solenoid plungers were cut to fit on each unit. The manufacturer discovered in the latter part of the program that valves with slightly oversized plungers would nevertheless pass acceptance testing without additional machining. Acceptance testing did not require the measurement of armature stroke or operating parameters at elevated temperatures. Valves were supplied if they passed the acceptance test even though they were not made according to the dimensions on the drawings. As a result, flight valves delivered late in the program often had plunger strokes shorter than valves delivered earlier for development and type approval (TA) test programs.

During the development and TA test programs, no shutdown problems were caused by this differential thermal expansion. Later during the flight phase, just before the launch of *Surveyor III*, it was discovered that the strokes of the flight valves were shorter than those of previous valves and maximum operating temperatures had been severely reduced. This problem very nearly caused the delay of the *Surveyor III* launch; the engines were already mounted on *Surveyor III* and propellants were loaded when the problem was discovered. Just before the launch, a series of special tests were conducted to determine the amount of solenoid heating which would occur (Ref. XVII-6). These tests showed that the maximum solenoid temperature would probably be less than 185°F at engine shutoff. Based on the distribution of strokes on the other flight solenoids, it was estimated that the probability of having a solenoid

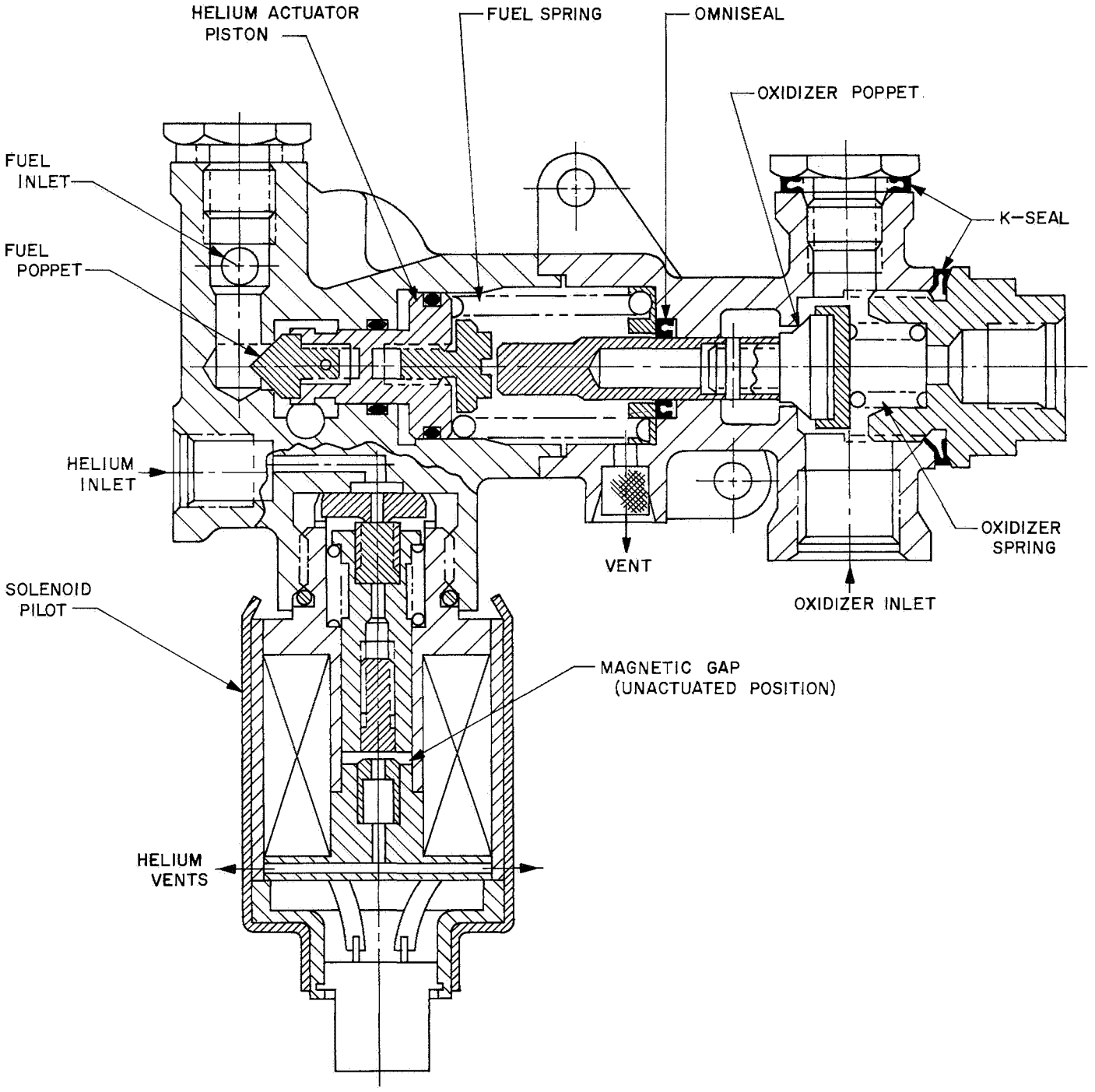



**Fig. XVII-7. Vernier engine shutoff valve**

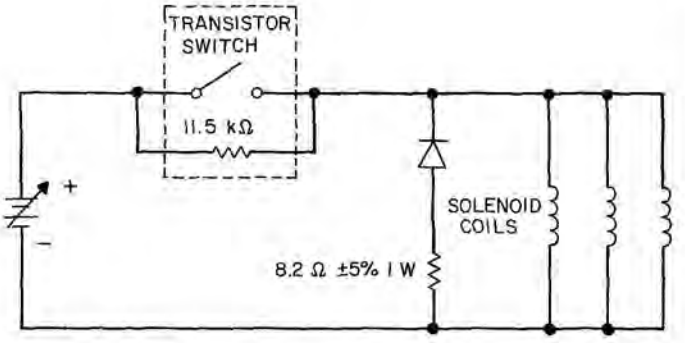



**Fig. XVII-8. Vernier engine shutdown circuit**

that would not shut off on SC-3 was about 14%. Based on this and many other considerations, SC-3 was launched without removing solenoids and measuring solenoid valve strokes. This removal and measurement would have imposed at least a 1-mo delay in launch schedule. The flight performance of *Surveyor III* engines was excellent even though the RADVS did not command the engines off, and the spacecraft lifted off from the surface after the first two touchdowns before the engines were turned off by ground command (Subsection A-5).

Viton A O-rings in the shutoff valve and the throttle valve were replaced by Teflon omniseals. This solved a serious compatibility problem between the Viton A material and the oxidizer. It also corrected leakage problems and the high friction problems caused by seal swelling. However, friction problems continued into the flight test phases because of a latent incompatibility between the fuel and the Kel-F-90 lubricant. This lubricant was used in the helium piston cavity. Fuel that seeped into this cavity reacted with the lubricant over a long period of time and formed a tacky black residue (Fig. XVII-9) that caused delayed shutdown of many engines during preflight checkout (Ref. XVII-9). The Kel-F-90 lubricant was also responsible for the galling of fittings on disassembly. Both of these problems were eliminated by using a Dupont PR-240AC perfluorinated grease. Engines using the Dupont grease were flown on SC-6 and SC-7. Earlier spacecraft had engines with the Kel-F-90 grease, which were carefully checked before flight. However, slow shutdowns of up to 1.5 sec on engine 1 of SC-2 during 3 of the 41 firings were probably caused by high friction which was attributed to the Kel-F-90 grease. On one of the 2-sec firings the shutdown delay was 1.5 sec. However, the engine 3 failure that resulted in the *Surveyor II* mission failure was not caused by high friction.

*3. Uncommanded thrust excursions.* During VPS development testing with the S-6 and S-7 propulsion test

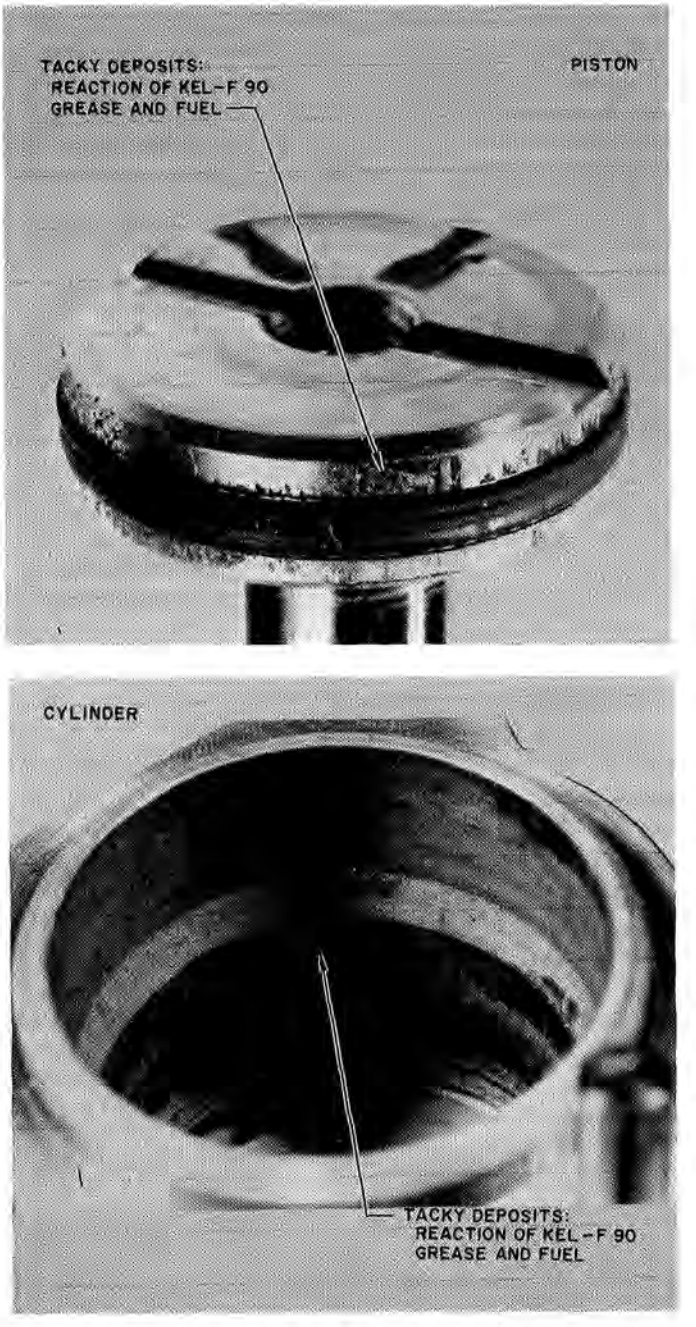



**Fig. XVII-9. Residue that caused propellant shutoff valve failure (engine SN 561)**

vehicles and the T-2 system test vehicle, uncommanded thrust excursions of up to 15 lbf were noted. One of these excursions is depicted in Fig. XVII-10. This excursion occurred while the thrust commanded level was nearly constant. After careful analysis it was determined that this anomaly was caused by gas bubbles in the propellant passing through the engine. When gas bubbles reached the throttle valve they caused the volumetric

flow rate to increase, since, at a constant thrust command, the throttle valve acted as a fixed-area orifice with a constant pressure drop. This increase in volumetric flow through the throttle valve pushed the gas-free propellants into the combustion chamber at an increased rate and raised the thrust. When the gas and propellant mixture finally reached the combustion chamber, it produced a lower than normal thrust. As shown in Fig. XVII-10, the times required for gas bubbles to reach and pass through the engine are all consistent with the actual data (see Ref. XVII-8). The gas bubbles were from inside the bladder and were caused by inadequate bleeding during loading or dissolved gas released from solution by tank depressurization, as discussed in Subsection A-3. This problem was solved by: (1) eliminating gas bubbles from the propellant feed system through improved propellant-loading procedures; and (2) redesigning, later in the program, the standpipe that removed the holes in the vertical tube to prevent ingestion if gas bubbles did get in the propellants.

*4. Pressurant gas dissolved in the propellants.* The effects of gas dissolved in the propellants were much more subtle than those of gas bubbles passing through the engine. With the engine operating at low thrust, the chamber pressure and the oxidizer injector pressure drop totaled approximately 100 psia. When propellants saturated with helium in the propellant tanks at 750 psia passed through the throttle valve with an outlet pressure of 100 psia, most of the dissolved helium was released from solution. This formed a compressible two-phase mixture in the lines and fittings between the throttle valve outlet and the injector. Although this had no effect on engine steady-state operation, it grossly affected dynamic controllability. The effect of dissolved gas on step response is shown in Fig. XVII-11. It should be noted that the engine step response with gas-free propellants required 0.030 sec, whereas with helium-saturated propellants 0.170 sec was required. Figures XVII-12 and XVII-13 show the effect of dissolved gas on engine frequency response for small-amplitude signals. Amplitude ratio is defined as the ratio of output thrust amplitude to commanded thrust amplitude. Phase lag is the time displacement between the fundamental of the output wave and the thrust command. With gas-free propellants the response was flat to about 20 Hz. Mechanical

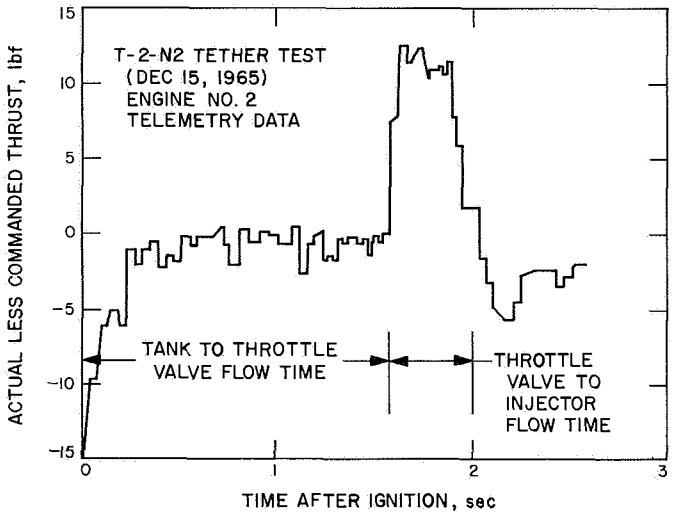



**Fig. XVII-10. Typical uncommanded thrust excursion**

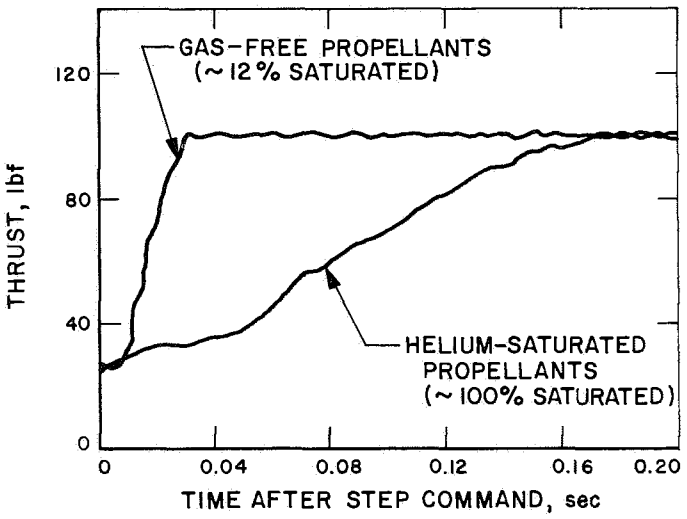



**Fig. XVII-11. Effect of dissolved helium on vernier engine response to step thrust command**

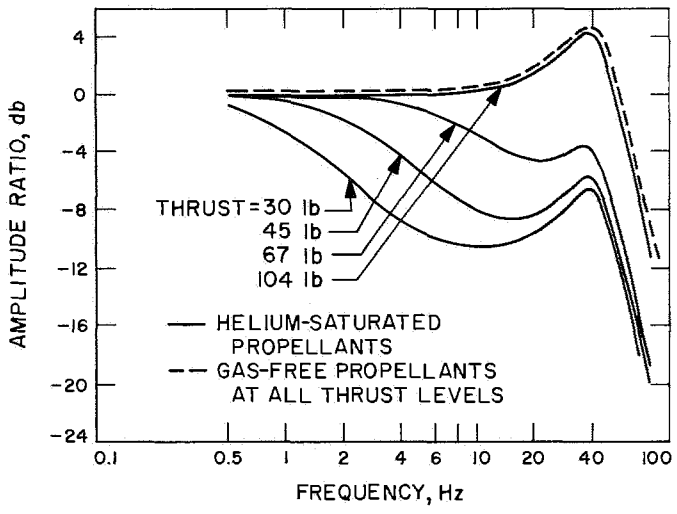



**Fig. XVII-12. Effect of dissolved helium on frequency response of vernier engines for small-amplitude signals**

resonance and damping in the throttle valve second stage caused rolloff at frequencies above 50–70 Hz. When dissolved gases were present, compressibility of the gas in the oxidizer line between the throttle valve and the injector caused major changes in the frequency response data.

An analytical model was developed which very accurately described the vernier engine response characteristics (Refs. XVII-10 and XVII-11). This mathematical model was used as part of a complete analog computer simulation of the control system. Using this simulation, vernier descents starting from a wide variety of initial conditions were conducted. Simulated RADVS noise was added to make the simulations more realistic. The results indicated that while the degraded dynamic response resulting from dissolved helium reduced damping in the control loop, the system still had adequate stability margins for the *Surveyor* mission. These results were confirmed by performing a closed-loop test using the analog computer to simulate the spacecraft and flight control system. The engines were fired at the HAC Placerita Canyon test site while being commanded via telephone lines from the analog computer in El Segundo. Engine chamber-pressure measurements were sent via telephone lines to the computer and scaled to represent thrust in the simulation as shown in Fig. XVII-14.

The results of these tests confirmed earlier results obtained using mathematical engine models that had shown adequate dynamic performance. Flight spacecraft performance also confirmed adequate dynamic performance with helium-saturated propellants.

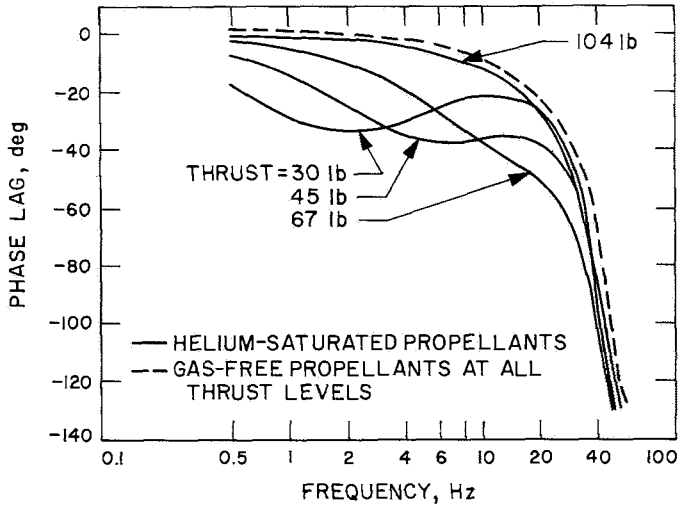



**Fig. XVII-13. Effect of dissolved gas on phase lag of vernier engines for small-amplitude signals**

*5. Salt formation in oxidizer injector.* During restarts or flow checks after atmospheric firings of the early SC-6 and T-2 test vehicles the oxidizer flow was found to be limited when high thrusts were commanded. The oxidizer flow restriction was found to be caused by salts formed in the injector orifices. These salts resulted from chemical action of the oxidizer remaining after shutdown and water from the atmosphere on the nickel injector face. Water from the atmosphere combined with the nitrogen tetroxide in the oxidizer to form nitric acid. The nitric acid attacked the nickel injector to form nickel nitrate salts. These salts did not form during vacuum testing because of the absence of atmospheric moisture. During tests in the atmosphere it was necessary to completely flush the engine with warm water, which readily removed the salts, after each firing. Another method was to provide a closure over the end of the engine and apply a vacuum on the engine; this method was used during system tests where restart was one of the test objectives.

During the *Surveyor II* mission engine 3 failed to fire for midcourse correction and the 40 subsequent firing attempts (Subsection A-5). Detailed examination of the data indicated normal fuel flow to the engine but only approximately 5% normal oxidizer flow. After an exhaustive examination of data from the prelaunch gas-phasing test before propellant loading, it was concluded that the engine was not restricted at that time.

A detailed analysis was conducted which showed that the point of restriction must have been near the injector orifice. After many of the possible failure modes were

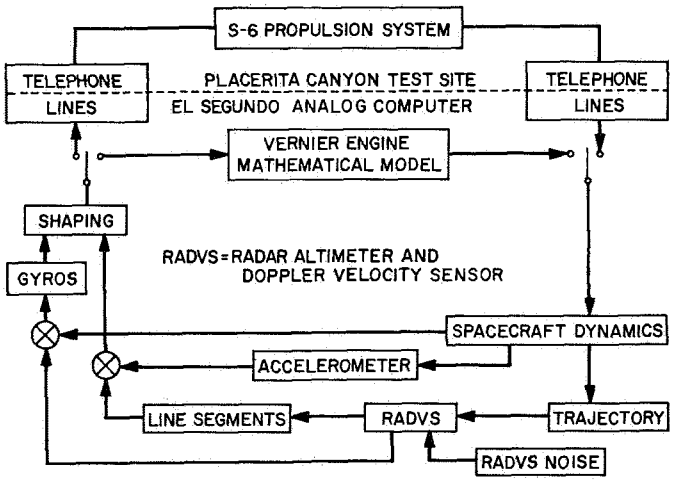



**Fig. XVII-14. Simulated closed-loop control system tests used for vernier engine development**

eliminated, another investigation of injector salting was undertaken. Salting had not occurred either during tests in a vacuum chamber or during the first atmospheric test firings. Salting had only caused flow restriction on restarts or flow tests after an atmospheric firing (see Ref. XVII-7). Among these occurrences the oxidizer flow was never restricted below about 50% of normal flow. The added investigation showed that the nickel nitrate salts were insoluble in the propellants. A series of 41 sequential flow tests, simulating all the trial firings on SC-2, were conducted on an engine with salts purposely formed in the injector (see Refs. XVII-8 and XVII-9). The results showed no change in the restriction.

Another series of tests were conducted to investigate the possibility of salt formation caused by a very small seepage of oxidizer past the shutoff valve and into the injector. The results confirmed that, over a period of five days when the spacecraft was encapsulated, leakage which was so small that it would not have been detected by the propellant vapor sensors (because of dilution with conditioned air flow) could cause injector salting sufficient to severely restrict the oxidizer flow. Prior to encapsulation this test leak rate would have been detected by periodic samplings from the engine injector area with a propellant vapor sensor.

This problem was solved on SC-3 and subsequent spacecraft by continually drawing a vacuum on the engines until only a few hours before flight. The gas drawn from the engines was also analyzed for the presence of oxidizer vapors, which would have been an indication of seepage. Plugs in the engine nozzles before launch contained hoses to the vacuum pump and gas analyzer. These plugs were forced out of the engine with nitrogen gas and removed from the vehicle while the spacecraft was atop the launch vehicle during the final stages of the countdown. Although this solved the salting problem, a much better solution would have been to eliminate all nickel parts from the injector. However, this would have required considerable time and development that was not compatible with the *Surveyor* schedule.

6. *Torque motor problems.* During overhaul checkout of two engines at RMD, leakage from the flexure tube in the torque motor was noted. Investigation disclosed that the torque tube had developed a crack that had probably resulted from improper heat treatment of the 17-7 PH stainless steel, together with surface discontinuities or stress risers from a previous machining operation.

On one torque motor, a silicon carbide disk-brazing operation was omitted; although this was not responsible for any failure, it was indicative of poor quality control procedures. One other torque motor had a chip of epoxy potting compound wedged into the magnetic gap so that the engine could not be commanded above 75% of maximum thrust. These problems were all caused by poor quality control by the subcontractor; tighter processing and inspection procedures were considered necessary to prevent recurrence.

7. *Leakage problems.* Severe leakage at a throttle valve bellows end cap seal was discovered during solar thermal vacuum (STV) testing. The engine had satisfactorily passed all previous leakage checks. After the STV test it was found that this seal would leak only under conditions where a large thermal gradient was present. After disassembly, it was found that the omniseal had been improperly installed. Leakage at K-seals was also a frequent occurrence requiring rework.

8. *Mixture ratio variation.* Mixture ratio variation during solvent flow tests was a frequent problem. This was generally caused by a slightly loose first-stage orifice in the throttle valve. The original staking provisions for this orifice at times allowed the orifice to rotate slightly and change the thrust or mixture ratio calibration. The staking technique was improved, resolving the problem in many instances. The continued recurrence of the problem of mixture ratio variability, even with improved staking techniques, required a further redesign of the first-stage orifice with closer tolerances and a thicker orifice wall in the staked area.

Mixture ratio variations with temperature also appeared to be a major problem. Differential thermal expansion in the throttle valve caused mixture ratio shifts which varied with propellant temperatures. This was not a problem in flight since the bulk of the fuel and oxidizer was at nearly the same temperature. The engine performed adequately on propellants at temperature extremes. Since these temperatures were only encountered during startup, the mixture ratio variation did not significantly affect overall propellant utilization. Based on these considerations, the specifications were revised to require a mixture ratio of 1.5 $\pm$0.1 only over a limited temperature range.

9. *Cleanness problems.* Foreign materials in the engine were responsible for a number of failures. The tacky black residue caused by Kel-F-90 grease and fuel

reaction is discussed above under shutoff impulse variation problems. Solenoid leakage, which occurred frequently during preflight checkout, was caused by foreign particles in the valve. This problem was solved by developing more definitive checkout test and procedures before flight, and finally by the addition of a filter on the solenoid helium supply port (see Ref. XVII-8). In one instance, the fuel pressure regulator was completely blocked by fuel residue that had not been flushed out and dried adequately after the acceptance test firing. During the disassembly of an oxidizer line to replace a leaky seal, some brown stringy fibers were found. Investigation disclosed that a large clump of steel wool had been left in the oxidizer line leading from the throttle valve to the injector (steel wool had been used to clean the line during engine fabrication). The engine had successfully completed many flow tests, an acceptance test firing, and vibration tests. Subsequent engines were radiographically inspected for foreign material and improperly assembled parts.

*f. Qualification program.* A limited engine qualification program was conducted at RMD in mid-1965 when two engines were subjected to a series of tests totaling more than two complete mission duty cycles for each engine. The test-commanded thrust profiles were designed to give a full set of dynamic and steady-state performance data on each engine under various temperature conditions. The performance of each engine was very good except for a delayed shutdown during one test.

The program did not, however, contain all the variations in hardware and a complete simulation of expected conditions. The testing of more engines was not possible at the time because of fiscal constraints. Time factors prevented a complete simulation of flight engine environmental conditions. A true simulation would have required one year or more of shelf life, many weeks of continuous exposure to solvents, repeated flow testing with solvents and drying, and, finally, exposure to loaded propellants held in the atmosphere for several weeks before undergoing launch vibration and vacuum firings.

Because some of these environmental conditions were not simulated, problems developed during the later phases of the program. A test program was undertaken in March 1965 at the JPL Edwards Test Station to supplement the formal qualification test program. These tests included: (1) performance under high static acceleration (see Refs. XVII-2 and XVII-9); (2) effects of RADVS-noise-induced, large-amplitude thrust commands; (3) effects of two-week engine storage with propellants loaded (see Refs. XVII-6 and XVII-7); (4) determination of thrust vector misalignment (see Refs. XVII-5 and XVII-10); and (5) survival of the lunar day and night environment. The engine passed all the tests with performance well within specification limits except for the lunar survival tests (Refs. XVII-2, XVII-12, and XVII-13). The engine successfully withstood −300°F temperature conditions for 14 days without leakage, but could not withstand 300°F for 14 days; the nylon fuel poppet was severely degraded by chemical action of the fuel at high temperature (see Ref. XVII-5). Later in the program Fluorosint-TFE (a glass-filled Teflon) was found to be a superior poppet material that would resist chemical action of the fuel while remaining free from creep and sealing well at low temperatures (see Refs. XVII-7 and XVII-12). This development came too late in the program to permit its incorporation into flight hardware without an extensive requalification program.

Another closely related series of tests was conducted to determine engine performance characteristics for firings at high temperatures as on the lunar surface (Refs. XVII-6 and XVII-12 through XVII-15). These tests showed that the engine behaved normally up to approximately 170°F. Above that temperature the minimum attainable thrust rose until about 250°F when it reached approximately 10 lbf above the normal minimum thrust capability. Above 250°F the attainable thrust began to decrease. These thrust elevations were caused by thermal expansion of parts in the throttle valve and increased oxidizer vapor pressure. Thrust elevation had serious implications for postlanding static firing or hop experiments. A special series of single-engine, closed-loop tests was conducted to evaluate the possibility of performing a lunar hop experiment. This series involved the firing of an engine at the JPL Edwards Test Station with a closed-loop control system utilizing, via telephone lines, an analog computer located at HAC in El Segundo.

Many other special tests were conducted to investigate potential problems, to simulate possible failure modes of *Surveyor II* (Refs. XVII-12 through XVII-14), and to check out possible solutions to existing problems. These tests included firing a vernier engine with a molybdenum nozzle at an initial temperature of −100°F to determine if the thermal shock would shatter the brittle material (Refs. XVII-2 and XVII-16). A special series of tests were also conducted to validate the suitability of pyrochrome paint repairing techniques or the effect of pyrochrome paint blisters on the nozzle. In the task conducted to simulate possible failure modes, a number of firings were conducted with oxidizer flow restricted at various points

in the engine (Refs. XVII-11 and XVII-14). The results showed that when the point of restriction was placed near the injector the thrust profile was similar to those observed on SC-2.

Vernier engines also played a major role in the VPS qualification tests conducted on the S-6 and S-7 vehicles. These tests successfully validated the interface between the propellant feed system and the vernier engine. The T-2 descent system tests helped validate the interface between the engine and the flight control system. These tests are described in more detail in the propulsion system performance section.

*g. Alternate engine development.* The development of an alternate vernier engine was initiated by contract from JPL to TRW/STL* in April 1963. The initial contract included a feasibility demonstration and the preparation of a flightweight design (Ref. XVII-17).

*1. Engine description.* The TRW engine was designed with a throttling range of 30–150 lbf (*Mira* 150 engine) which could be extended to a 20–180-lbf range (*Mira* 180 engine). The engine was made up of a throttling mechanism, propellant on/off valves, and and ablative thrust chamber with a hard throat insert (as shown in Figs. XVII-15 and XVII-16). Table XVII-5 contains a list of the required performance characteristics (Ref. XVII-18). The throttling mechanism consisted of two variable-area cavitating venturis to control the propellant flow rates as shown schematically in Fig. XVII-17. These venturis controlled flow by accelerating the flow until the pressure was equal to the vapor pressure. This established the limiting velocity. Flow-rate control was maintained by controlling the minimum venturi area where the flow reached its limiting velocity. The kinetic energy of the flow stream was then converted back into pressure as required by the other engine pressure drops. With this design, flow-rate control was unaffected by variations in pressure downstream of the throttle valve. This type of flow-rate control, however, was sensitive to variations in propellant feed pressure, propellant vapor pressure and dissolved gases; nevertheless, for the conditions tested, the thrust variations were within allowable tolerances. If the minimum pressure caused by propellant vapor pressure and dissolved gas released from solution was small compared with the propellant feed pressure, the effects on flow-rate control would have been small.

*STL, TRW/STL, and TRW are used as designations of the same subcontractor, reflecting the name at the time of the context.

The variable-area injector was used to maintain high injection velocities over the entire throttling range. High injection velocities were necessary to maintain good performance and stability over a wide throttling range. The single-injector pintle formed intersecting conical sheets of fuel and oxidizer. A single servoactuator was used to operate both the flow control valves and the variable-area injector. The servoactuator was controlled by a small electrical current from the flight control system. This control current was then used to position the actuator using hydraulic fluid power. The monomethylhydrazine fuel was to be used as the actuation fluid and then dumped overboard after flowing through the actuator. This required an additional valve for each actuator to prevent overboard leakage during nonthrusting periods. Approximately 8 lb of fuel would have been required by all three servoactuators during a mission. Propellant shutoff valves were located downstream of the flow-control valve. These valves were actuated by a helium pilot valve in a similar manner to the RMD design.

The combustion chamber was constructed with a JTA graphite throat insert which extended upstream and formed the convergent section. The insert was retained in an ablative chamber made of randomly oriented $0.5 \times 0.5$-in. chopped Refrasil phenolic with an overwrap of Refrasil phenolic. The ablative chamber was encased in a titanium shell which also formed the nozzle extension.

*2. Engine history.* The TRW engine was intended to be used as an alternative to the RMD engine. When this engine contract was let and for the following year there were major development problems with the RMD engine. The TRW contract was terminated in January 1965 after prequalification testing had been completed. By this time the RMD design demonstration program and the margin limit test programs had shown that the major development problems had been overcome. Meanwhile, integrating the TRW engine into the spacecraft was studied in detail. The major problem was the means for powering the servoactuator. A separate battery-driven hydraulic-power system was studied as one possibility. This system was very complex, had a high weight, required thermal control of a network of hydraulic lines, and appeared to have a long development time. Fuel used for hydraulic power and then dumped overboard was studied as another alternative. Because fuel tank sizes were already established, the fuel used for the servoactuator decreased the amount available to accomplish the mission. Spacecraft contamination by dumped

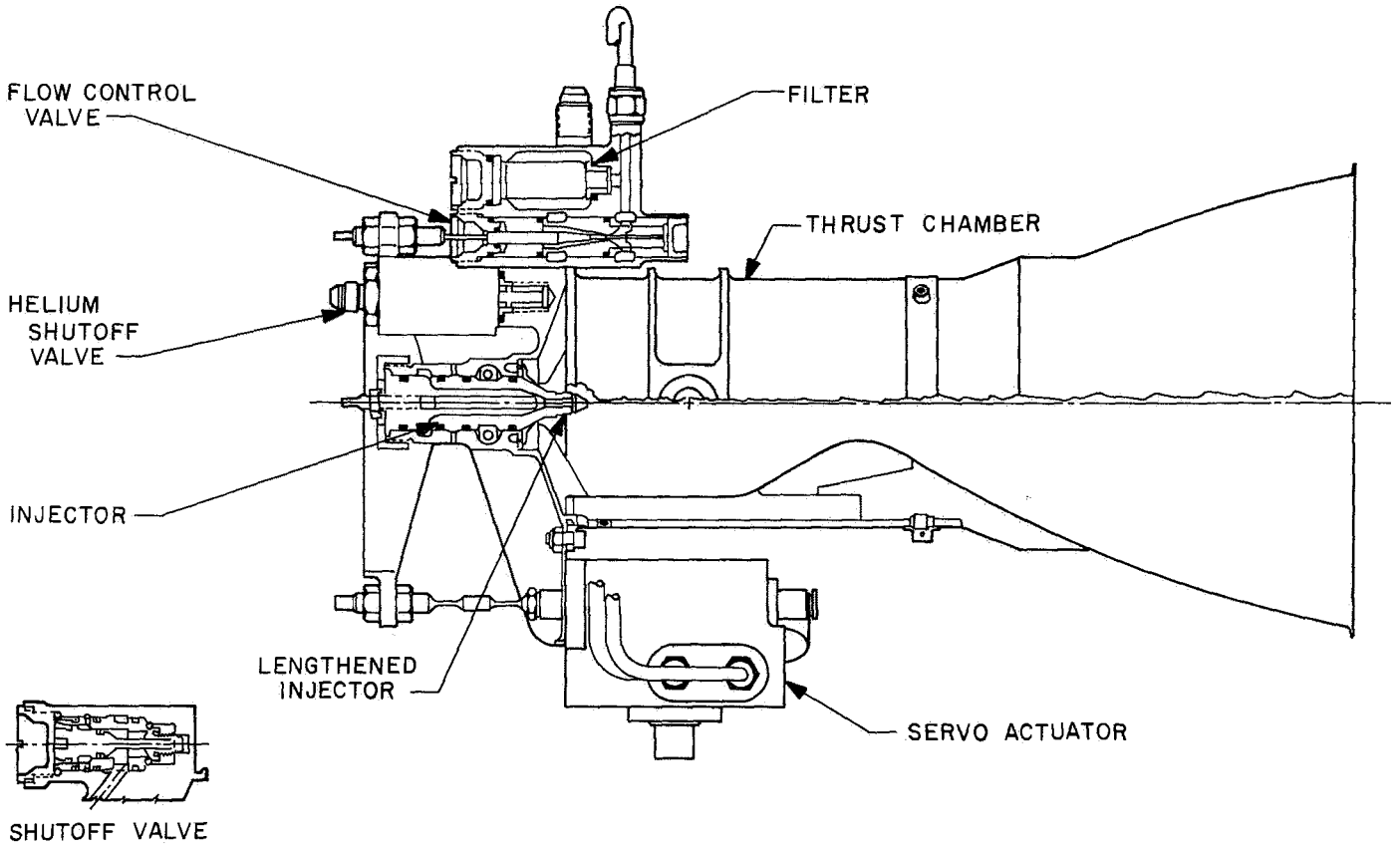



**Fig. XVII-15. Alternate vernier engine configuration**

fuel was another potential problem. The low chamber pressure (110 psia) of this engine made it impractical to use it in the T-2 atmospheric descent test program. This meant that RMD engines would still have been required for the T-2 program.

The greater throttling range and higher thrust of this engine would have substantially increased the moment control capability during the main retro phase of terminal descent. During this development period, moments created by the retro motor were unknown and suspected to be of the same order as the vernier system control capability. The major advantage of the alternate engine was the elimination of the heat-transfer problems associated with the RMD regeneratively cooled engine. The integration problems outlined above, however, seriously detracted from the otherwise attractive features of the alternate engine.

### 3. Vernier Propulsion Feed System

The Thiokol Chemical Corp., RMD, under subcontract to HAC, began the development of the vernier propulsion feed system in 1961. The RMD designed the feed system based on mission requirements and the spacecraft envelope as defined by HAC. All components of the upstream system were subcontracted except for the propellant tanks, which were built by RMD.

Development of the feed system was encumbered by problems with the helium regulator and propellant tanks. Although satisfactory redesigns to correct the problems were being made, in 1963 HAC terminated the feed system portion of the contract with RMD to allow RMD to concentrate on the engine problems which remained to be solved (see Subsection A-2). Upon contract termination, HAC assumed responsibility for the upstream feed system and completed the development and qualification.

Table XVII-6 lists significant milestones in the development of the feed system.

***a. Feed system description.*** The final feed system configuration consisted of a high-pressure regulated helium pressure source, a check and relief valve package, three oxidizer tank assemblies, three fuel tank assemblies, and line assemblies for both pressurant and propellants (see Fig. XVII-1).

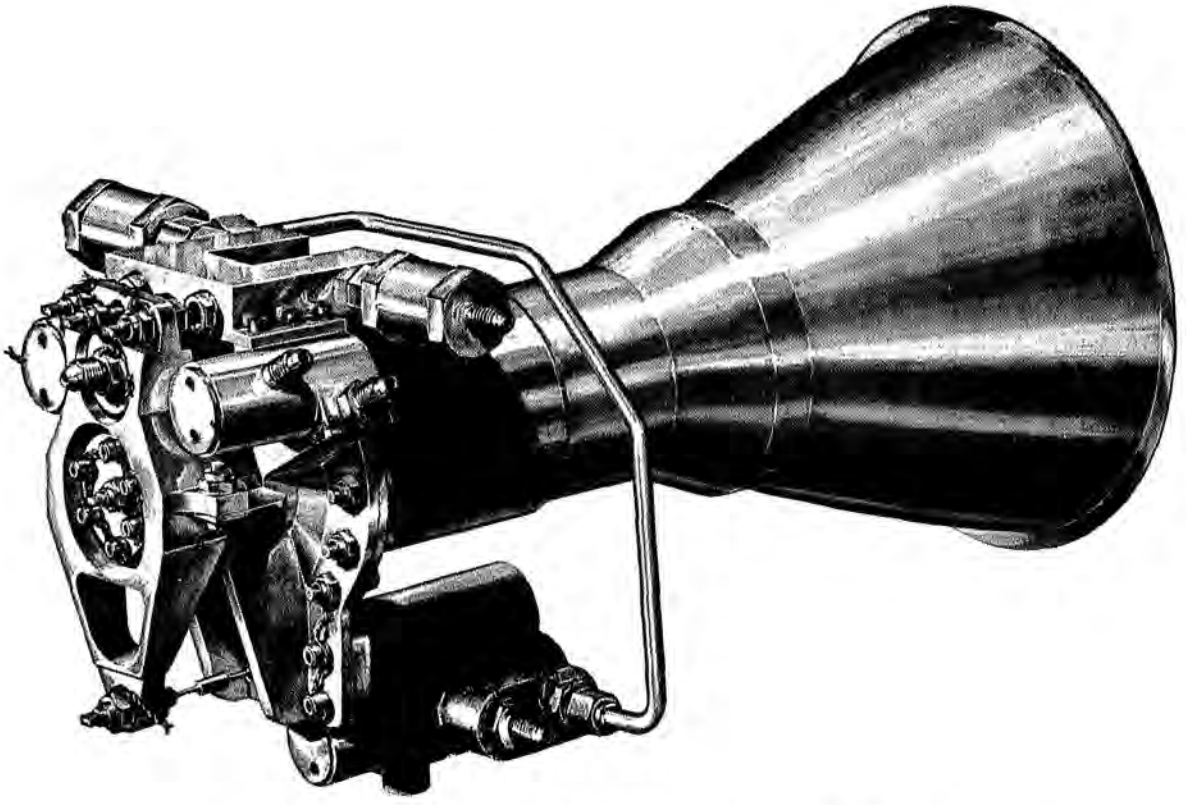


**Fig. XVII-16. Alternate vernier engine external view**

A single spherical tank was used to store 2.3 lb of helium at 5175 psig. A squib-operated helium release and dump valve was attached at the helium tank outlet. The squib-actuated valve performed two functions: (1) releasing helium to the regulator and/or (2) dumping helium overboard in the event of an emergency (see Subsection C). Additionally, the assembly provided porting for the high-pressure fill valve and the helium pressure transducer. A filter assembly was located upstream of the regulator valve to filter out squib valve debris. The pressure regulator supplied the helium for the expulsion of propellant from the tanks to the vernier engines, regulating at 730 (+25, −30) psi. During no-flow conditions, the regulator locked up at less than 795 psi to prevent flow of helium through the two helium relief valves, which were designed to vent overboard at a pressure of 840 psig to protect against overpressurization of the propellant tanks.

On spacecraft SC-1 through SC-4, two check valves and two relief valves were mounted to the regulator outlets on the helium tank and valve assembly, as shown in Fig. XVII-18. The check valves were designed to prevent mixing of the propellant vapors through the common pressurant supply system, and the two relief valves were used in the helium system to preclude excessive propellant tank pressures. On spacecraft SC-5 through SC-7 the check valves and the relief valves were incorporated into a housing and placed on the spaceframe as separate control items. A high-pressure valve and two low-pressure valves were in the system for checkout of the regulator, check, and relief valves.

The helium tank and valve assembly weighed 33.21 lb, including 2.3 lb of helium. The helium tank and valve package surfaces were polished and painted to maintain passive thermal control, as shown in Figs. XVII-18 and XVII-19.

The propellant tank assembly was a 4-in.-long, 10-in.-diameter cylinder with hemispherical ends and with an overall length of 14 in. The tank shell was made of 6Al-4V titanium alloy and was designed to operate at a nominal pressure of 730 psig. Housed within the tank shell was a bladder made of a TFE–FEP Teflon laminate for positive expulsion of propellant. A central standpipe bolted to the bottom tank flange contained concentric passages that permitted propellant flow to the engine feed line and provided venting during propellant filling operations. A ball seat valve was connected to an inner

## Table XVII-5. Alternate vernier engine requirements summary

| Item | Requirement |
|---|---|
| Propellant feed system interface | |
| Propellants | |
| Fuel | MMH |
| Oxidizer | 90% $N_2O_4$/10% NO |
| Propellant temperature range | 0–100°F |
| Propellant feed pressure | |
| Max | 830 psia |
| Min | |
| Fuel | 685 psia |
| Oxidizer | 686 psia |
| Mission and vehicle interface | |
| Specific impulse | |
| Thrust level, lbf | Specific impulse, lbf-sec/lbm |
| 30 | 260 ±7 |
| 90 | 292 ±5 |
| 150 | 290 ±5 |
| Mixture ratio (oxidizer/fuel) | 1.5 ±0.1 |
| Control system interface | |
| Shutoff valve actuation voltage | 16–26 V |
| dropout voltage | <13.5 V |
| Thrust | |
| Min | ≤30 lbf |
| Max | ≥150 lbf |
| Step response time | |
| Min–max | ≤0.060 sec |
| Max–min | ≤0.060 sec |
| Thrust control hysteresis | ≤4 mA |
| Frequency response | |
| Amplitude ratio (at 5 Hz) | ≥0.95 |
| Phase lag (at 5 Hz) | ≤28 deg |
| Start time | 0.125–0.300 sec |
| Shutdown characteristics | |
| Shutdown time | 0.070–0.135 sec |
| Shutdown impulse variation | <2.8 lbf-sec |
| Environmental | |
| Operationol temperature range | 0–145°F |
| Life | |
| Shelf life | >24 mo at 0–145°F |
| Service life | |
| Max thrust | >4 min |
| Min thrust | >8 min |
| Starts | 4 |
| Lunar survival life | 1 lunar day |
| Cycle life | |
| Solenoid valve | >250 cycles |
| Shutoff valve | >250 cycles |
| Throttle valve | >10,000 cycles |
| Vibration level (3 axes) | |
| Sinusoidal | |
| 5–35 Hz | 8.0 g |
| 35–150 Hz | 18.0 g |
| 100–1500 Hz | 6.0 g |
| White gaussian | |
| 100–1500 Hz bandwidth | 6.7 g |

## Table XVII-6. Vernier propulsion feed system major milestones

| Date | Milestone |
|---|---|
| Aug–Dec 1960 | Reaction Motors Division supported HAC in precontract design competition |
| Oct 1961 | Full vernier propulsion system development contract awarded to RMD by HAC |
| Dec 1961 | Hughes second design review of VPS |
| Jul 1962 | Third design review of VPS |
| Oct 1963 | Hughes assumed responsibility of *Surveyor* vernier feed system from RMD |
| Jul 1964 | Change propellant tank material from 7078 T-6Al to 6Al-4V titanium |
| Aug 1964 | Change helium tank material from 7Al-4Mo titanium to 6Al-4V titanium |
| Sep 1964 | Qualification of propellant tank shell completed |
| Jan 1965 | Qualification of helium tank shell completed |
| Mar 1965 | Qualification of helium release and dump valve completed; qualification of helium check valves completed |
| Apr 1965 | Qualification of helium regulator for A21 completed |
| May 1965 | Qualification of helium relief valves completed; delivery of FA tested propellant tanks to spacecraft SC-1; T-21 spacecraft shipped to Convair, San Diego for combined systems test; S-6 preliminary closed-loop test conducted; S-6 open-loop test with saturated propellants conducted |
| Jun 1965 | Qualification of helium filter completed |
| Jul 1965 | Delivery of FA-tested helium tank and valves to SC-1 |
| Aug 1965 | Loading tests (T-21) completed at AFETR |
| Sep 1965 | Unit S-6 firings at 0 and 100°F completed; S-7 pressurized hot shake program completed |
| Oct 1965 | Unit S-7 pressurized drop tests completed |
| Nov 1965 | Qualification of helium tank and valve assembly for A21 completed |
| Dec 1965 | Unit S-6 closed-loop test with gas-saturated propellants |
| Mar 1966 | Qualification of propellant tank assembly completed; qualification of A21E helium regulator completed |
| May 1966 | Successful *Surveyor I* mission; VPS performance verified |
| Nov 1966 | Qualification of A21E helium tank and regulator assembly completed; qualification of A21E helium check and relief valve assembly completed |
| Sep 1967 | *Surveyor V* mission problem with helium regulator malfunction; successful soft landing achieved |
| Jon 1968 | *Surveyor VII* successfully launched and soft-landed |

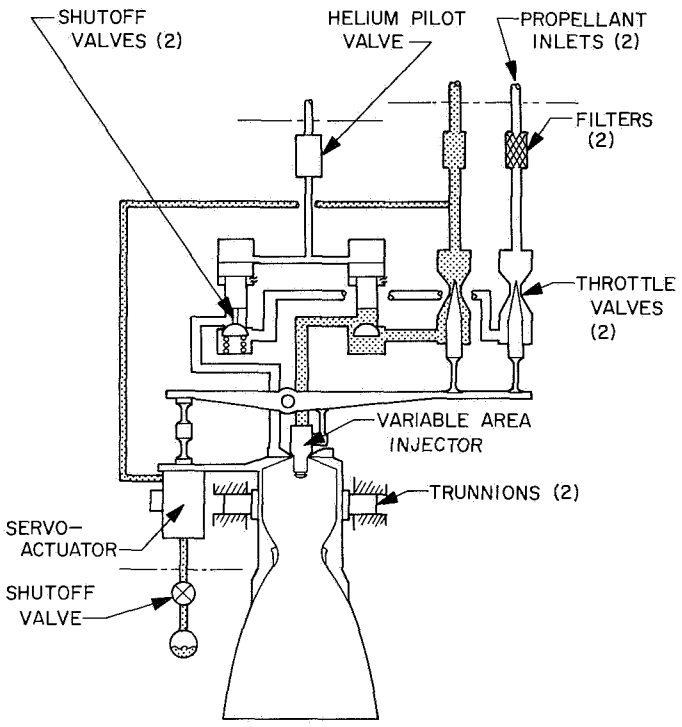



**Fig. XVII-17. Alternate vernier engine schematic**

standpipe tube that led to the top of the tank for venting and bleeding during propellant loading. Three tank assemblies contained the monomethylhydrazine monohydrate fuel, and three assemblies contained the MON-10 (90% $N_2O_4$ + 10% NO) oxidizer. A pair of fuel and oxidizer tanks was located near each of the three landing legs. Both active and passive thermal control methods were used to maintain the propellant tanks within the 0–100°F operational limits prescribed.

To satisfy the mission requirements the vernier propulsion feed system had to be capable of meeting certain design, performance, and environmental requirements. Among these requirements were pressure, thermal, vibration, acceleration, shock, and radiation environments.

***b. Component development.*** Vernier propulsion feed system component development is described in the paragraphs that follow.

*1. Helium tank.* In the original design, the helium package included three manifold, tubular high-pressure tanks that also served as a support structure; however, that design concept was abandoned in favor of a single spherical tank in the very early development stages because of the weight penalty. To optimize the weight of an unheated helium system (tank and helium), a study program was conducted to evaluate factors such as compressibility, storage pressure, tank diameter, and system leakage at an initial helium temperature of 0°F.

The initial tankage was fabricated from 7Al-4Mo titanium alloy using a pressure weld joint. Difficulties arose when the tank manufacturer failed to properly control the internal radius on the weld bead and the surface cleaning process, Ti-Brite, necessary for this titanium alloy. As a result, several tanks burst at proof pressure or less and the vendor could not guarantee a minimum burst pressure.

A number of 7Al-4Mo helium tanks with properly controlled manufacturing processes were subjected to a TA test program. Although this configuration satisfactorily met the TA test requirements, the brittle nature exhibited by the 7Al-4Mo alloy led to development of 6Al-4V titanium tanks.

After analysis of the results of the competitive bidding, the Airtek Division of Fansteel was selected to fabricate the helium tank.

Several serious problems, which also threatened the concurrent propellant tank program, arose during the development of the helium tank. The most critical of these involved the microstructure of the 6Al-4V titanium alloy. If the material temperature exceeded the beta-transus temperature, an undesirable grain structure was created. Although the measurable physical properties of the alloy were basically unaffected by exceeding the beta-transus temperature, subsequent problems involving tank life and strength were possible because of more readily induced interstitial corrosion.

To solve this problem, appropriate heat treating and handling procedures were developed for the 6Al-4V alloy to assure the absence of the beta-transus microstructure while losing none of the superior physical properties of the material. Moreover, HAC specified a sampling procedure for each forging produced. This extensive procedure established standard mechanical tests, a microstructure examination, chemical, ultrasonic and fluorescent penetrant tests, and grain size inspection. Furthermore, sufficient samples from each forged bar and from each metal heat were taken to assure representative results.

Intensive development tests were designed and conducted to determine the necessary metallurgical processes. These processes involved heat treating at 1750°F,

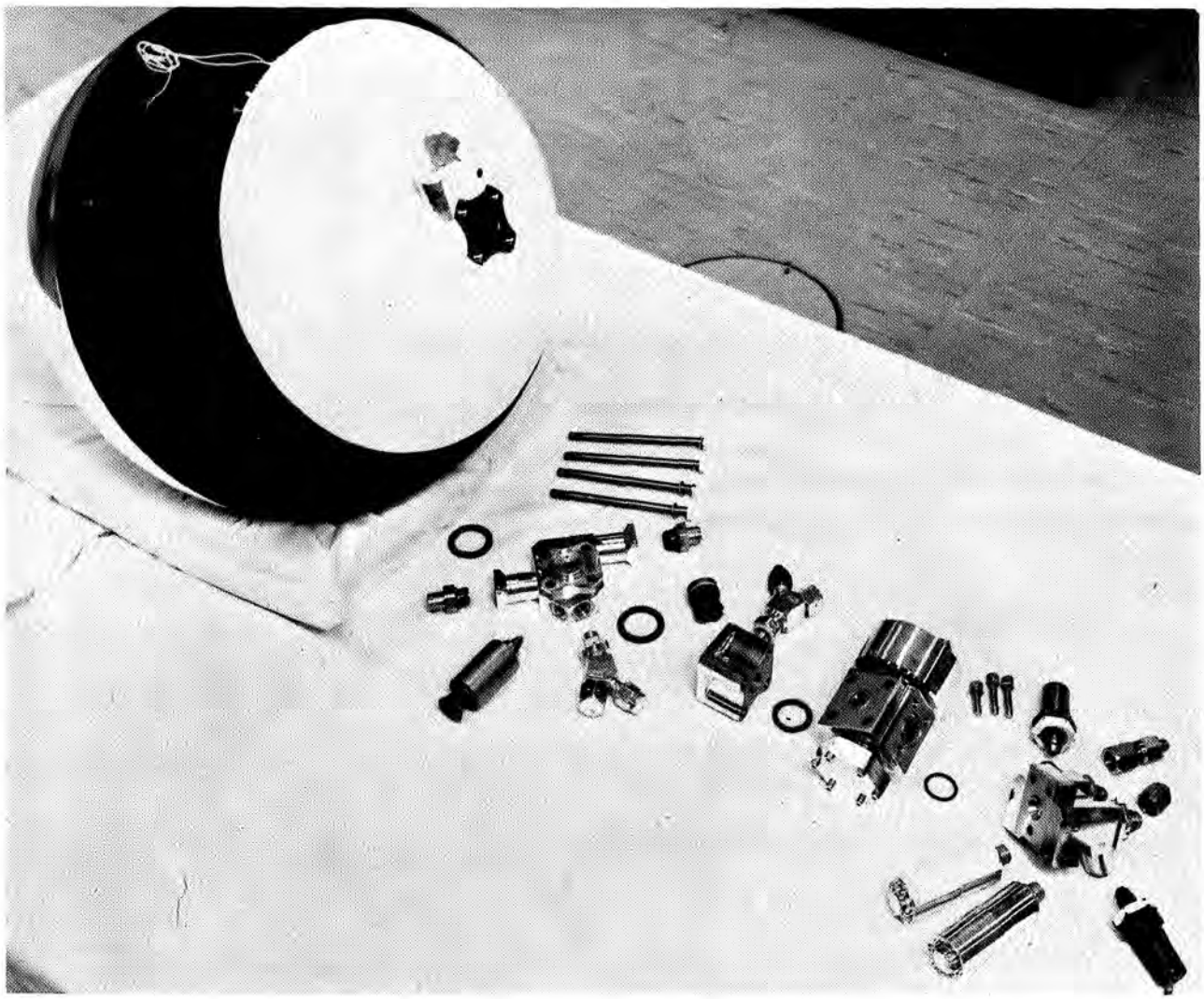


**Fig. XVII-18. Helium tank and valve assembly (spacecraft SC-1 through SC-4)**

quenching in less than 6 sec, and aging at various temperatures calculated for each specific batch of material.

Considerable effort was expended in developing techniques for producing nonporous welds. The final solution involved close controls over all steps in the process, including cleanness of the surfaces. These processes, in conjunction with the others required, resulted in a successful development program. As was the case with the propellant tanks, a normalized burst pressure range was maintained within 5% to demonstrate strict adherence to all dimensional and procedural requirements.

2. *Helium release and dump valve.* The squib-actuated helium release and dump valve assembly (Fig. XVII-20) had ports for a pressure transducer and for filling the helium tank. The 1-W, 1-A no-fire squibs, were manufactured by Holex, Inc., of Hollister, Calif. (Subsection C).

Results of initial valve tests revealed that the squibs provided insufficient force to the valve piston to completely shear the seal cup in all cases. A change was made to increase the amount of explosive charge.

Also during the initial qualification program, the shock generated by the release squib operation caused movement of the ceramic cup in the dump squib that housed the bridgewires. To overcome this deficiency an aluminum retainer sleeve was designed and incorporated.

During the development of the valve assembly, some sections of the valve body were thinned to save weight.

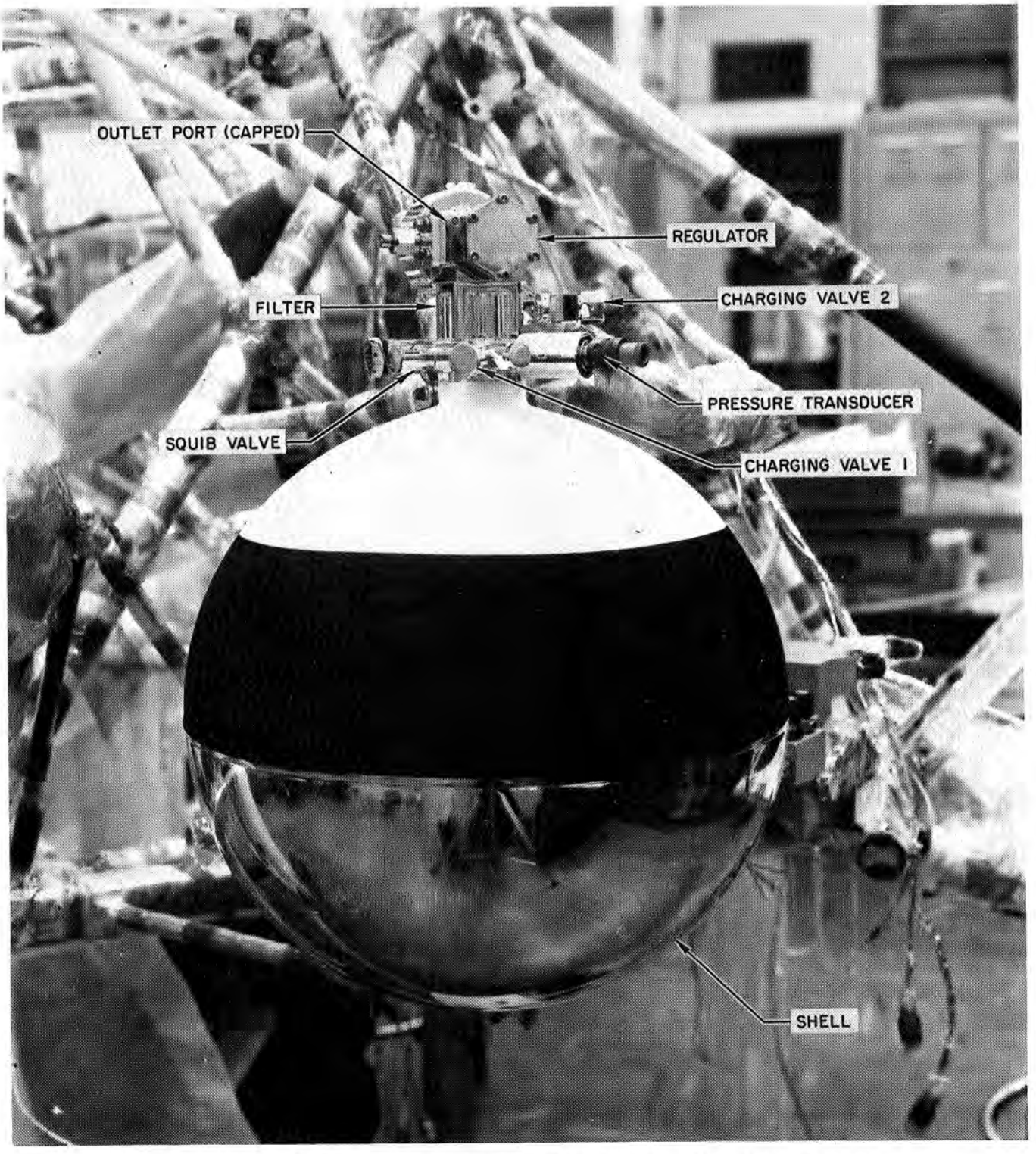



**Fig. XVII-19. Helium tank and valve assembly (spacecraft SC-5 through SC-7)**



**Fig. XVII-20. Helium dump and release valve**

Subsequent testing, with the squibs carrying the increased explosive charge, revealed some sections were too thin to withstand the loads imposed when the squibs were fired. The original thickness was restored in these sections.

*3. Helium filter.* The initial filter design used on the helium supply system upstream on the regulator was one of folded (pleated) 304 stainless steel wire mesh with 2-$\mu$m (nominal), 15-$\mu$m (absolute) filtration requirements. During squib firing and vibration testing, bowing of the pleated wire mesh and shredding were apparent because of the presence of wire mesh particles downstream of the filter.

A design developed by the Vacco Corp. of El Monte, Calif. incorporated multiple layers of 300-series stainless steel disks with flow paths etched into the surfaces. The disks were stacked and joined in a welded assembly using the same filter housing design. This filter design provided: (1) a labyrinth-like path capable of removing absolute size particles of 15-$\mu$m diameter or larger from the gas stream; (2) nominal filtration of two 2 $\mu$m; and (3) a structure that successfully withstood shock and vibration testing.

*4. Helium pressure regulator.* In the initial system, regulation of the propellant tank operating pressure at a nominal 725 psig was accomplished by means of a lightweight, two-stage regulator package containing relief valve and check valve provisions. Because of regulation problems and failure to maintain lockup, use of an alternate regulator was investigated. A single-stage regulator was under development by the Carleton Controls Corp. of Buffalo, N. Y. With this unit, limited redesign and a reappraisal of operating requirements were necessary.

Initial testing of the single-stage regulator revealed several design deficiencies requiring modifications as follows:

(1) Expansion of the Teflon seat material, which was corrected by replacing the Teflon with Kynar.

(2) Erosion of the Kynar seat because of pressure surge into the regulator as a result of firing the squib-actuated helium release valve. This design deficiency was corrected by incorporating an anti-surge valve into the regulator helium inlet.

(3) The original design incorporated elastomeric seals, which leaked at low temperature. Replacement of the seals with a special butyl compound effectively eliminated seal leakage.

(4) The spring package was redesigned to increase the regulator sensing area, and the springs were strengthened by substituting maraging steel for 17-7 PH steel.

When all of the above design changes were completed, production regulators were subjected to TA testing, and were used on the flight spacecraft (Fig. XVII-21).

Minor design changes were effected on the regulator design used on SC-5 through SC-7. These changes were limited to the mounting provisions at the outlet port with minor internal passage geometry changes dictated by the relocated mounting holes (Fig. XVII-22).

*5. Helium check valve.* The check valve assembly was designed and developed by the Pneu-Hydro Co. of Cedar Knolls, N.J. This valve, as originally designed, required little additional work.

The initial helium check valve assembly was designed as an integral part of the early helium regulator and incorporated a piston using a 45-deg-angle Teflon washer seat. The piston was preloaded with a small spring so that the nominal pressure required to open the valve was between 4 and 8 psi. This check valve did not change in basic concept, although the check valve housing was modified, once to provide mounting provisions for adapting to the new regulator, and again when the check valve was designed as an integral part of the check and relief valve assembly for SC-5 through SC-7 (Fig. XVII-23). The manufacturing procedure was also modified for the integral check and relief valves design so that the final machining of the sealing material seating surface was accomplished after assembly to the piston

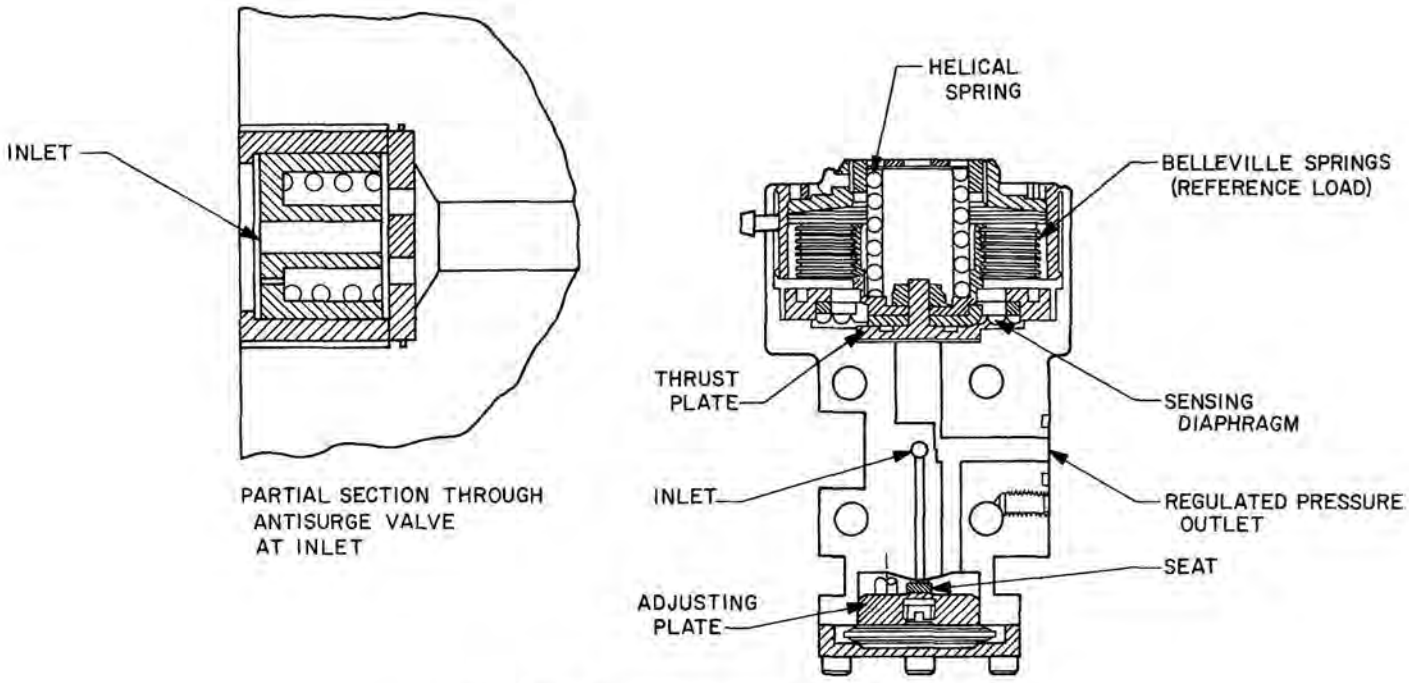



**Fig. XVII-21. Helium pressure regulator**

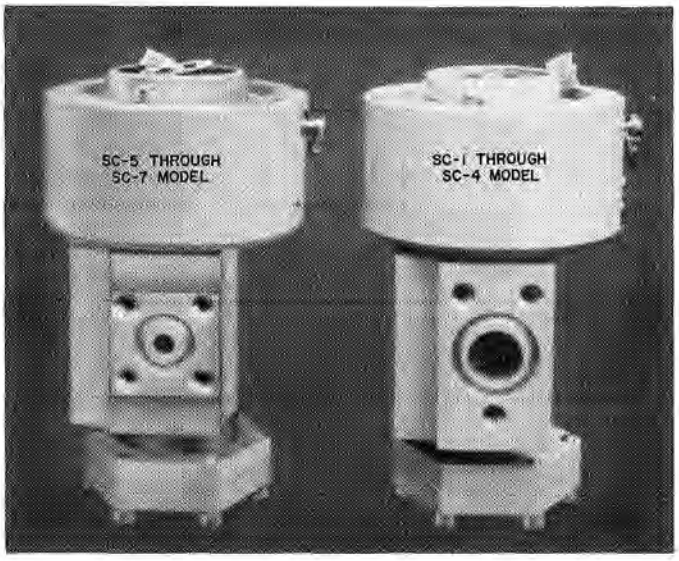



**Fig. XVII-22. Helium regulator (outlet port)**

and the final torquing of the retaining screw. This redesign, although very minor, greatly reduced the problems associated with leaking check valves.

*6. Helium relief valve.* Two helium relief valves, one each for the fuel and oxidizer tank pressurization manifolds, provided a means of eliminating the possibility of an overpressurization of any sort in the propellant tank system. Initially the valves were a part of the regulator package and utilized a spring-loaded piston, with the piston housing containing an O-ring seal. Valve operation was accomplished by movement of the vent port across the dynamic seal. Postpropellant exposure tests during development showed unduly large changes in the crack and reseat performance of the valve as well as a large increase in the spread between crack and reseat pressures.

The initial design was superseded by an inverted check valve type. The flight relief valves, designed by Carleton Controls, featured a metal bellows arrangement incorporating an integral stem poppet that functioned as a piston counterbalanced by a spring (Fig. XVII-24). The integral stem poppet sealed against a floating, travel-limited Kynar seat. As the inlet pressure increased, the bellows assembly and floating seat moved simultaneously until the seat assembly pin struck a stop. The pressure-actuated stem poppet continued to move away from the seat, venting pressure until the inlet pressure decreased to allow the poppet to reseal on the seat.

Design problems included spring and bellows sizing, bellows attachment, and bellows stress relieving procedures. After both electron-beam welding and soldering techniques to attach the nickel bellows to a stainless steel piston were investigated, a good soldered joint was produced and used.

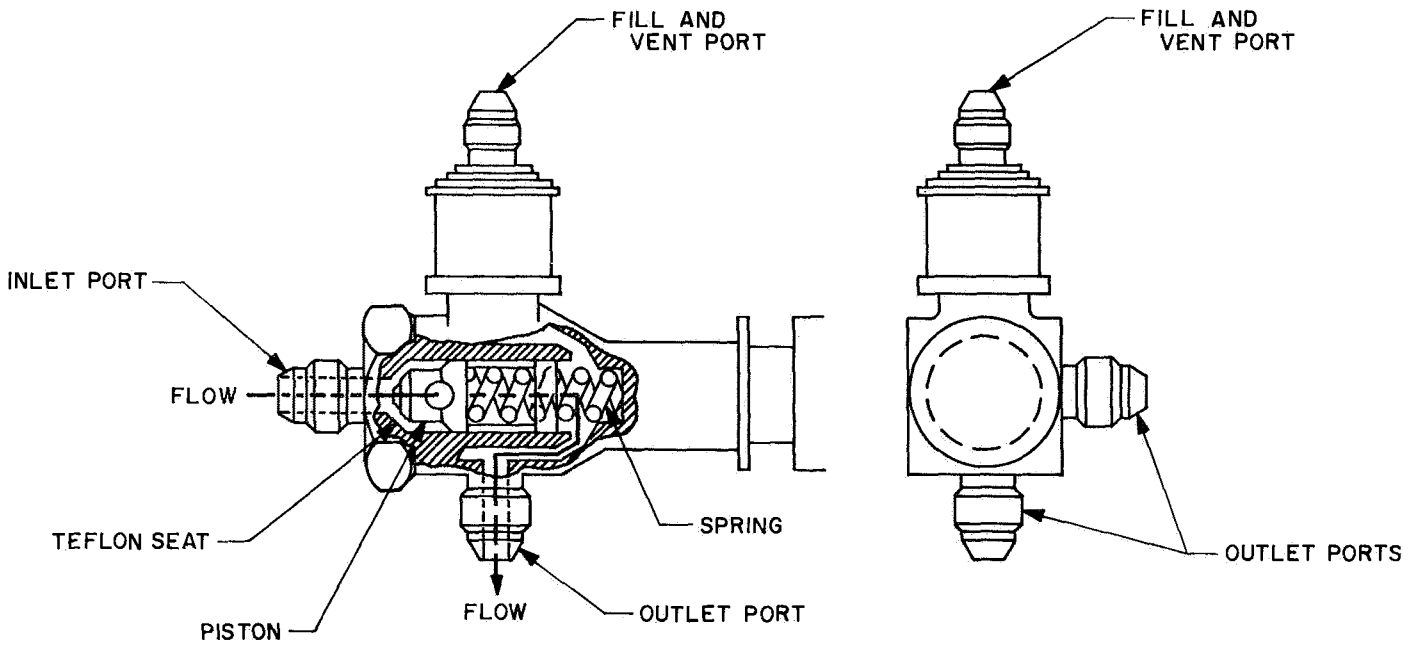



**Fig. XVII-23. Helium check valve**

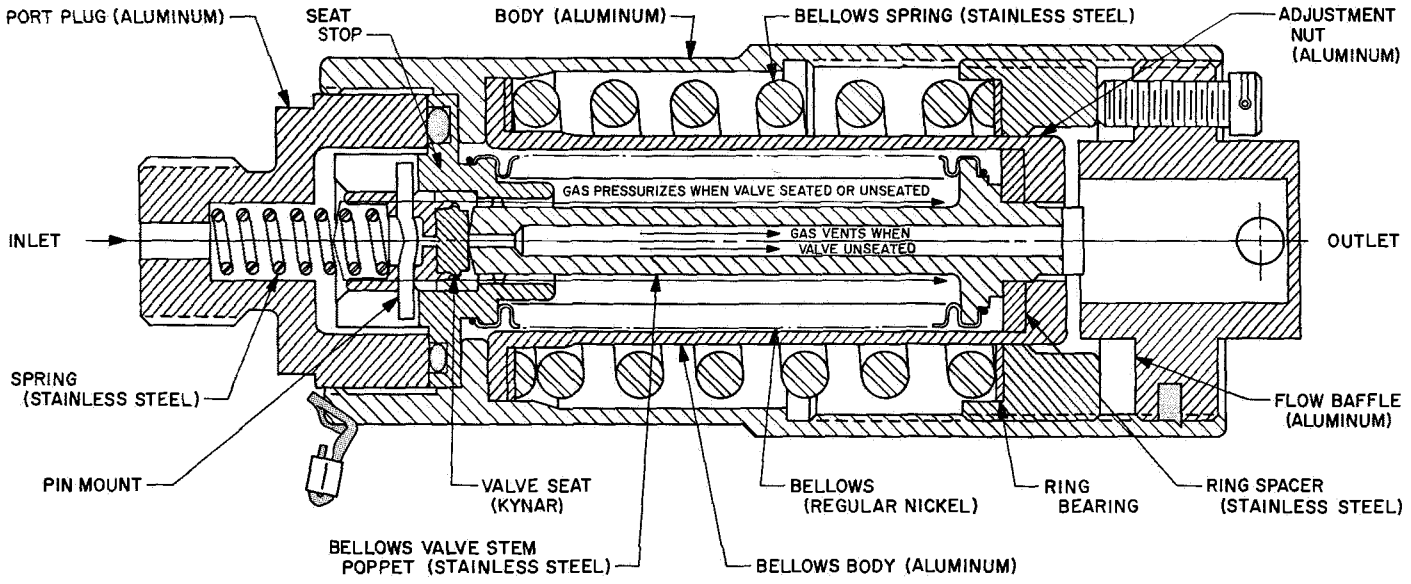



**Fig. XVII-24. Helium relief valve**

A method including thermal cycling was developed for relieving residual stresses in the bellows assembly. These residual stresses were responsible for drift of the relief pressure setting.

*7. Access ports and valves.* The initial design of the vernier propulsion feed system contained two high-pressure (5175 psi) helium quick-disconnects, two low-pressure (840 psi) helium disconnects, and 12 low-pressure (840 psi) propellant disconnects for various servicing and checkout operations. All quick-disconnects incorporated the same basic design; however, different materials and seals were used to meet the particular strength and compatibility requirements for a given application. Unique keying was employed to prevent misconnection. Among the problems incurred with the quick-disconnect were: (1) The high-pressure series often extruded an internal static O-ring seal, (2) high flow

rates would dislodge the elastomer from the nipple poppet, and (3) the low-pressure propellant units failed to close when disconnected, resulting in propellant leakage during field operations. The cycle life was not consistent and failure sometimes occurred after the first use.

Replacement of the quick-disconnects was initiated on the first flight spacecraft when the two high-pressure units in the helium system were replaced by Y-shaped needle valves which were modifications of an existing 3000-psi valve design from another program. The modification included the use of a Teflon backup ring added to inhibit O-ring extrusion at the higher operating pressure (5175 psi).

The low-pressure helium disconnects were replaced with fill valves incorporating an in-line ball valve design. A floating ball seat was used to reduce concentricity tolerance requirements. These valves were qualified and incorporated into the feed system.

As in the case of the low-pressure helium fill valves, the propellant disconnects originally used were replaced by ball valves.

8. *Propellant tank shells.* Space limitations precluded the use of a single fuel and oxidizer tank, which would have been more advantageous from a reliability standpoint. The use of multiple tanks located at each of the spacecraft legs resulted from this constraint.

The original propellant tank shell, which was fabricated from 7178-T6 aluminum alloy, caused many development problems. The machining of the hemispheres from forgings resulted in rejection rates of 30–50% because of the difficulty of working with this material. The low strength of girth welds was also a problem. This was attributed to the difficulty of arriving at optimum weld parameters and weld tooling that would eliminate excessive mismatch, weld defects, and many weld repairs. Because of the weld defects, stresses imposed on the weld joint at operating pressure equaled or exceeded the yield stress of the material. Several tanks that were subjected to operating pressure in a pressure hold test failed in a few hours which verified the high stress concentrations at the weld defects.

The weld design dictated that the tanks be heat-treated after welding to develop maximum strength in the weld joint; this presented problems in obtaining uniform strength properties in the weld joint.

While no evidence of stress corrosion was found in the 7178 series tanks, all the 7000 series aluminum alloys were known to be susceptible to stress corrosion, particularly as the operating stresses approach the yield stress. A local stress caused by an undetected discontinuity could approach or exceed the yield stress and thereby introduce a design uncertainty.

The rejection rate was drastically reduced by the introduction of a magnetic-tape-controlled metal cutting machine, and by the development of an automatic, direct-current, straight polarity welding process, which permitted elimination of heat treating after welding.

Tank shells of 7178-T6 alloy, fabricated by the improved procedures, were successfully subjected to qualification testing consisting of proof-test, pressure hold test for 14 days, pressure cycle test of 300 cycles, and burst tests of three separate tanks.

However, because of the uncertainty of the stress-corrosion problem, and the desirability of saving weight, the 7178-T6 aluminum alloy material was replaced by 6Al-4V titanium. (The final design of the propellant tank resulted in a weight reduction of 0.55 lb per tank shell and a 50-psig gain in burst pressure, which provided an extra margin of safety). Accordingly, detailed design specifications were prepared for an extremely lightweight (wall thickness varied from 0.018 to 0.031 in.) titanium pressure vessel. Bids were selected from six qualified pressure vessel manufacturers and, after careful analysis, the Airtek Division of Fansteel Corp. was chosen. The titanium forgings were produced by the Arcturus Corp. The problems encountered were similar to those experienced with fabrication of the 6Al-4V titanium helium tank.

Information was received that the *Apollo* program had experienced stress-corrosion failures of several 6Al-4V titanium alloy tanks that were used with nitrogen tetroxide at 105°F for 30 days. Since this was the same tank material and a similar propellant (the *Surveyor* oxidizer had 90% nitrogen tetroxide with 10% nitric oxide), there was concern that similar failures might occur on *Surveyor*. Several special test programs were conducted on the propellant tank shells. A *Surveyor* tank shell was sent to the Bell Aerosystems Co. for testing, and the tank ruptured after being exposed to nitrogen tetroxide for 24 hr at 112–115°F.

Another special test was made at HAC to determine the compatibility of 6Al-4V titanium tanks with the

*Surveyor* oxidizer MON-10 (90% $N_2O_4$–10% NO). The purpose of this test was to demonstrate the capability of a *Surveyor* propellant tank filled to 60–70% capacity, without a bladder, to withstand exposure to MON-10 oxidizer at a pressure of 850 psig for 14 days at 110°F. The tank shell successfully completed the exposure and proof tests without any sign of bulking, warping, or deleterious metallurgical effects. The metallurgical examination of the tank shell consisted of cutting the tank in half and taking metallographic sections from both hemispheres and across the girth weld. There was no evidence of any pitting or cracking, and the appearance of the tank surfaces was that of an as-machined surface. An earlier tank that had been subjected to extensive testing was placed in storage for seven days at 850 psig and 110°F. Then the tank was successfully proof-tested at 960 psig and examined metallurgically; the final examination indicated no evidence of degradation. It was the consensus that the nitric oxide in the nitrogen tetroxide acted as an inhibitor to prevent stress corrosion.

9. *Propellant tank bladder.* The initial development of the propellant tank bladder dictated the selection of Teflon as the bladder material because of the combined requirements for flexibility and compatibility with MON-10 oxidizer. Teflon possessed the additional advantages of high lubricity and reasonably high strength. The bladders were manufactured by Dilectrix Corp. of New York.

Teflon is available in two chemical forms: TFE and FEP. Whereas TFE is noted chiefly for its strength and flexure life, FEP is more flexible at low temperatures and less permeable. The first bladders were made of FEP of about 14-mil thickness. These bladders were too stiff and the wall thickness was subsequently diminished to 5 mils. However, expulsion tests showed that the all-FEP bladder had an unsatisfactory flexure life. As a result, the design was changed to a composite laminate of TFE and FEP film having a combined thickness of 5 mils to give a combination of film flexibility, heat resistance, strength, and maximum impermeability.

Initial attempts to qualify the complete propellant tank assembly, which included vibration levels up to 12 *g* axially and 4 *g* along each of two lateral orthogonal axes, revealed that the vibrational modes caused excessive relative motion between the bladder and tank and between the bladder and standpipe elements; this resulted in scuffing and eventual tearing of the bladder. This problem was corrected by thickening the bladder to about 15 mils at the nipple end and adding a mushroom-shaped Teflon tip to the standpipe. The modified design (Figs. XVII-25 and XVII-26) permitted tank assembly qualification without further bladder problems, and this type bladder was used on all *Surveyor* missions.

Although the flight bladder design was generally adequate from the standpoint of strength, flexibility, and leakage, it was found to have high permeability. This resulted in two-way permeation: (1) helium through the bladder to dissolve in the propellants, and (2) propellant vapor into the pressurizing system. Gas dissolved in the propellants was found to cause degradation of engine dynamic performance. Figure XVII-27 shows the helium saturation level as a function of time after pressurization (see Ref. XVII-16). It should be noted that the *Surveyor* flight bladder had a saturation time constant of about 4 hr. Figure XVII-28 shows the helium solubility in the propellants. In this case, solubility increased with increasing temperature. To significantly reduce the amount of helium dissolved in the propellants between midcourse correction and terminal descent (approximately 50 hr), permeation resistance had to be increased by a factor of 10–15.

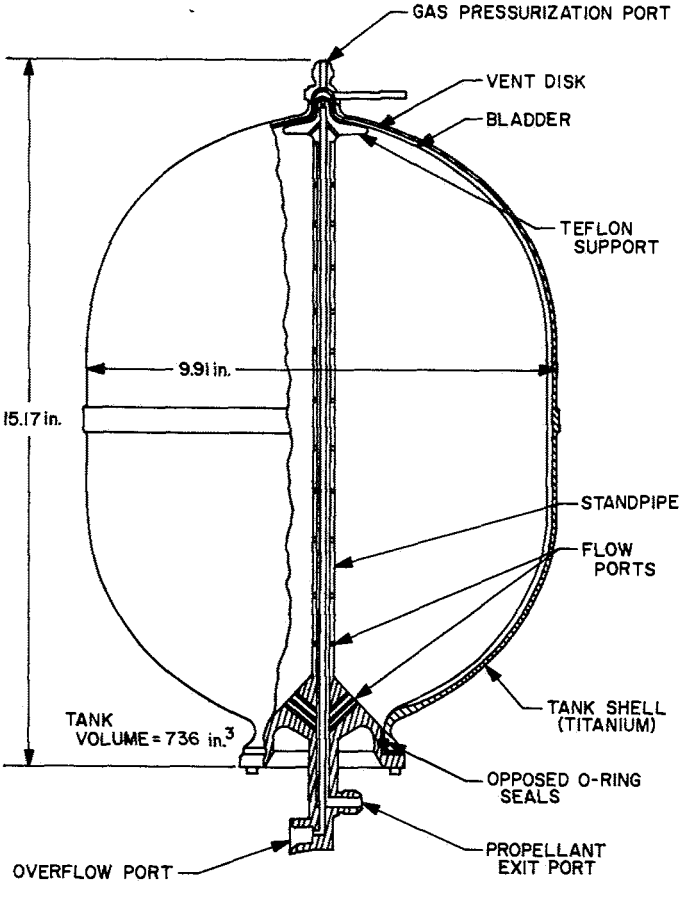



**Fig. XVII-25. Vernier propellant tank assembly**

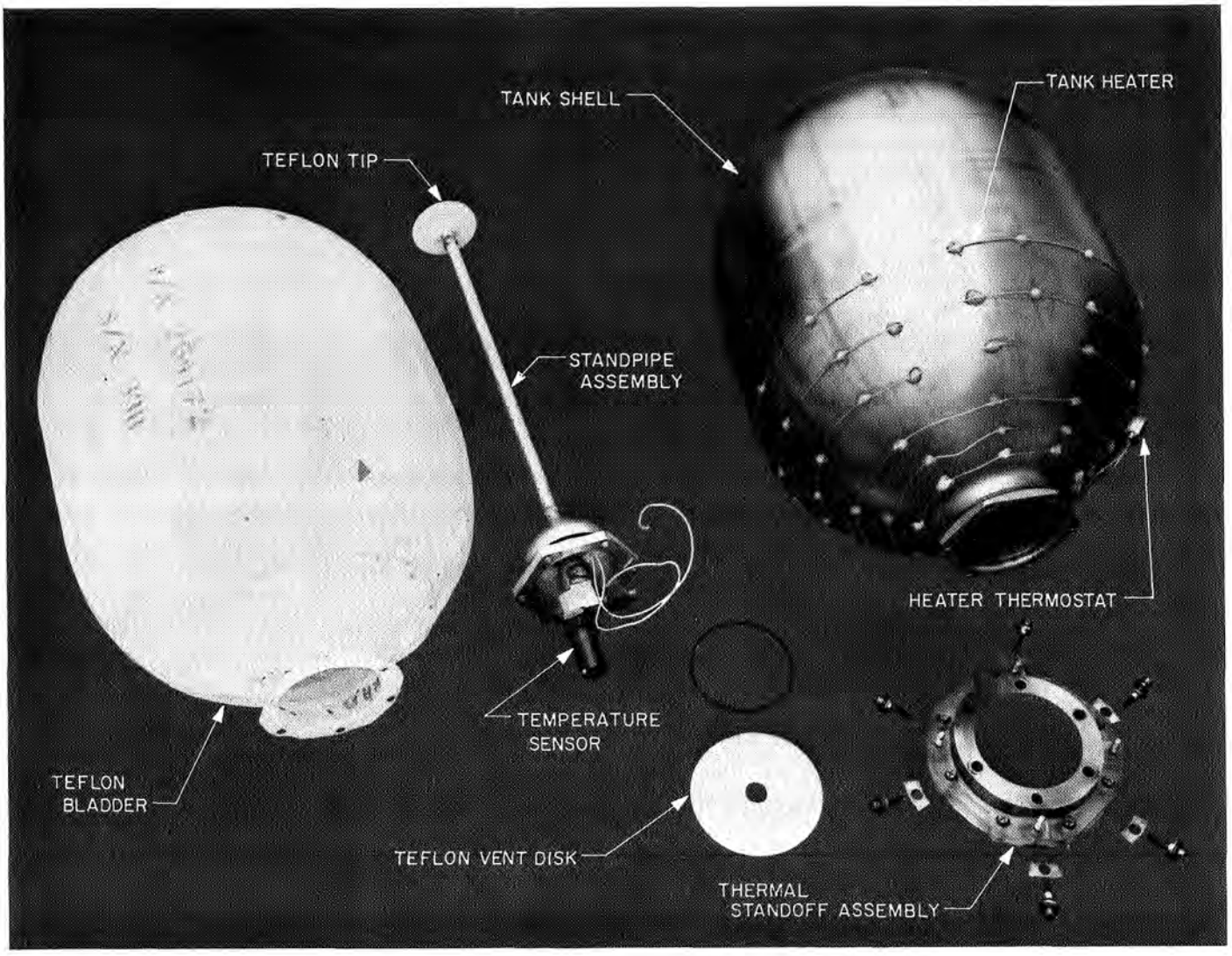



**Fig. XVII-26. Propellant tank components without thermal wrap**

On the basis of initial tests with bladder material samples, it appeared that a laminated Teflon–metal foil bladder would yield this improved resistance. Bladders of this material were manufactured using a process similar to that for the all-Teflon bladder, except that a ¼-mil-thick layer of Teflon-coated aluminum foil was sandwiched between the TFE and FEP layers. Sixteen of these bladders were procured and subjected to helium and nitrogen permeation, vibration, propellant exposure, and expulsion tests. It was found that, although propellant saturation level after exposure simulating the time from propellant loading to terminal descent was cut in half by use of a new Teflon–foil bladder, there was little, if any, reduction in saturation level when the bladder had been subjected to qualification (TA testing) vibration levels (see Fig. XVII-27). Damage to the foil during vibration was sufficient to nullify the permeation advantage of the metal foil. As a result, Teflon–foil bladders were not incorporated into *Surveyor* propellant tanks.

Because of the decreasing solubility with decreasing temperature and the short saturation time constant, concern developed over gas dissolved at a higher temperature being released as bubbles inside the bladder as the propellant tank temperature dropped during the mission. An additional concern was the condensation and freezing of propellant vapors in the sections of the pressurization lines that were exposed to very low temperatures. Special tests were conducted to evaluate these potential problems (see Ref. XVII-2). The results showed that a gradual temperature drop resulted in helium permeation

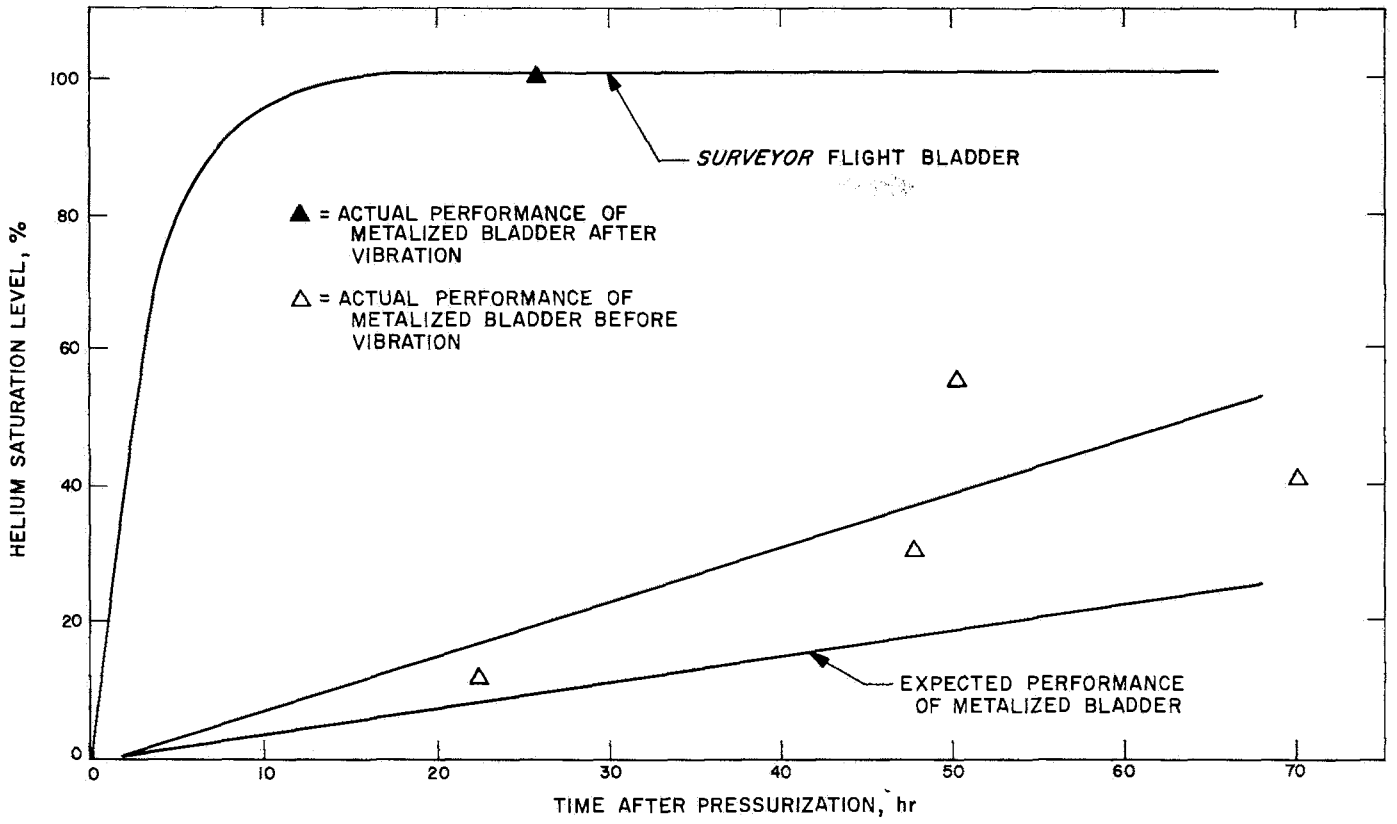



**Fig. XVII-27. Helium permeation of oxidizer tank bladder**

from the slightly supersaturated liquid back to the gas space, and bubbles were not formed. The results also showed that the fuel and oxidizer vapors would not freeze and block lines maintained at −100°F. The oxidizer vapor would contain a much higher concentration of NO than the liquid (about 40 rather than 10%). This means that vapor, which would condense in the pressurization lines, would have a freezing point well below the parent liquid.

*10. Propellant tank standpipe.* The functions of the propellant tank standpipe were to: (1) provide a flow port for propellant entry and exit, (2) provide a flow port for propellant overflow and for bleeding gases otherwise trapped as propellant was loaded, and (3) position and structurally support both ends of the positive expulsion bladder.

The standpipe design is shown in Fig. XVII-25. Positioning and support of the bladder at the nipple end was accomplished by a mushroom-shaped Teflon cap at the top of the standpipe, which was designed for a snug fit inside the bladder nipple. The mushroom shape, which provided uniform support for the top of the

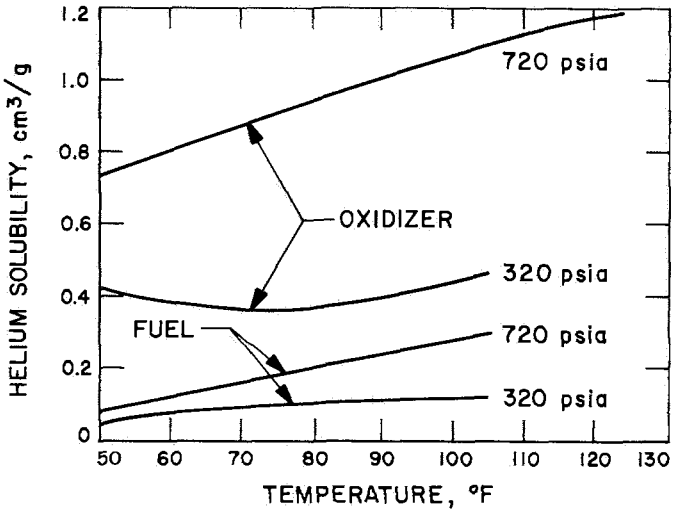



**Fig. XVII-28. Helium solubility in propellants**

bladder during vibration, was incorporated into the standpipe design after several bladder failures had occurred because of vibration. Holes were drilled through the cap connected to the inner flow tube to provide for gas bleeding and propellant overflow. At the flange end of

the propellant tank the standpipe fit snugly against the bladder and tank shell.

The original design, although functionally adequate and used for the first two missions, required eight welding operations, which resulted in a high rejection rate in manufacturing. In addition, cleaning was difficult because of the low velocity of flow in the standpipe base recesses. Consequently, for missions beginning with *Surveyor III*, an improved standpipe design was used in which the number of welds was reduced to two and all internal recessed cavities were eliminated. The inner overflow tube, which was located concentrically within the propellant flow passage, was positioned at both ends with a slip fit because a tight seal was not required at either location.

Early T-2N, S-6, and S-7 vehicle problems of uncommanded thrust excursions were traced to the presence of gas inside the propellant tank bladders, together with a standpipe hydraulic design that allowed gas from the top of the bladder to be ingested into the propellant flow. To help improve the hydraulic design while solving the fabrication problems outlined above, the number of holes in the standpipe base was increased from 8 to 48 and the diameter of the holes was doubled. This change, which was first incorporated on SC-3, lowered the standpipe pressure drop by a factor of 3 at maximum propellant flow rate and significantly reduced the probability that a helium bubble at the top of the tank would be ingested into the standpipe.

The standpipe design was further modified to eliminate entirely the holes in the vertical tube, leaving only the 48 base holes for propellant flow (Ref. XVII-19). This modification virtually eliminated the possibility of helium ingestion at some small sacrifice in expulsion efficiency. Expulsion tests of these standpipes did, however, prove them capable of 98% expulsion efficiency at 0.1 *g*. Several tanks having standpipes with no holes in the vertical tube were flown on spacecraft SC-5 and SC-7.

*c. Qualification test program.* Each flight component of the *Surveyor* vernier propellant feed system was acceptance tested before being assembled into a control item. The component level tests are listed in Table XVII-7. Upon assembly of the components into a control item, the assembly was flight acceptance (FA) tested. The FA tests, which were designed to demonstrate workmanship and the capability of the system to survive expected flight environments, are also shown in the table. Type approval tests were conducted on representative *Surveyor* vernier propellant feed system hardware at 1.5 times the FA test level to verify design concepts. These tests included all operating environments, as shown in Table XVII-8. All type approval hardware was subjected to component level and FA testing before being committed to TA testing.

*1. Helium tank and valve assembly.* Type approval tests were performed on the helium tank shell. All six helium filters subjected to TA testing passed the tests satisfactorily with no evidence of malfunction.

All the Carleton helium regulators, including the A21E configuration (spacecraft SC-5 through SC-7) passed TA tests satisfactorily without failure.

The helium relief valve also completed TA tests as part of the check and relief valve assembly for SC-5 through SC-7.

To verify the design of the helium tank and valve assembly, a complete assembly was subjected to TA testing. The qualification program was designed to exceed mission requirements by 150% with respect to acceleration, vibration, shock, and thermal vacuum. Leakage tests were conducted after each environmental test to reveal any system degradation. A series of functional tests was also performed to show the effect of the environment on the operational characteristics of the valve assembly. Functional tests, including regulator flow and lockup and relief valve crack and reseat, were performed during acceleration testing and after shock testing. The helium tank was pressurized to 6000 psig at 100°F to further demonstrate the capability of the pressure vessel to perform as designed.

As mentioned previously, the helium tank assembly was redesigned into two control items after the first four spacecraft were assembled. Both configurations (A21 and A21E) were subjected to TA testing.

During TA tests of the A21 helium tank and valve package, the shock of firing the helium release squib caused the helium pressure transducer reading to shift several hundred pounds per square inch. Many tests were made on similar transducers, but a zero shift was never observed. During the SC-2 flight, however, a zero shift of the transducer was noted (Subsection A-3-d). A similar shift was noted during the T-2 program. No shift has been observed in other missions.

In the A21E configuration the check and relief valves constituted a new control item. Check and relief valve TA testing was performed under dynamic and environmental conditions simulating a normal mission sequence of critical conditions, as outlined in Table XVII-8.

During FA testing of the A21-series helium tank assembly, considerable difficulty was experienced in achieving acceptable external leakage rates. The specification value of 100 $cm^3$/hr external leakage led to considerable rework of control items. The leakage was generally caused by the seals in the valve package buildup. To reduce the problem, several changes to the assembly were introduced. Torques of the mounting bolts were increased, the K seals were lubricated, and special attention was given to the sealing surfaces.

For spacecraft SC-5 through SC-7, the valve package was removed and the regulator mounting was moved to the CG of the tank assembly. The check valves, relief valves, and low-pressure fill valves were placed in a separate package to constitute another control item. With the separate helium tank and valve package, fewer problems were encountered during FA tests because of leakage.

*2. Propellant tank assembly.* The *Surveyor* Ti-6Al-4V propellant tank shells successfully completed the following tests: (1) twenty-two days of fuel storage in a standard

**Table XVII-7. Vernier propulsion feed system component and control item flight acceptance tests**

| Component/item | Test | | | | | | | | | |
|---|---|---|---|---|---|---|---|---|---|---|
| | Examination | Capacity | Leak | Proof | Cleanliness | Filtration | Functional | Vibration | Thermal | Vacuum profile |
| Component level | | | | | | | | | | |
| Helium tank shell | X | X | X | X | X | | | | | |
| Helium release and dump valve | X | | X | X | X | | | | | |
| Helium filter | X | | | X | X | X | X | | | |
| Helium regulator | X | | X | X | X | | X | X | | |
| Helium check valve | X | | X | X | X | | X | X | | |
| Helium relief valve | X | | X | X | X | | X | X | | |
| High- and low-pressure quick-disconnects | X | | X | X | X | | X | X | | |
| Propellant tank shell | X | X | X | X | X | | | | | |
| Expulsion bladder | X | | X | | X | | | | | |
| Control item level | | | | | | | | | | |
| Helium tank and valve assembly | X | | X | X | X | | X | X | X | |
| Propellant tank assembly | X | | X | | X | | X | X | X | X |
| Helium check and relief valve | X | | X | | X | | X | X | X | |

**Table XVII-8. Type approval tests performed on vernier propulsion feed system elements**

| Test | Helium tank and valve assembly | | Propellant tank assembly | | Helium check and relief valve | | |
|---|---|---|---|---|---|---|---|
| | Nonfunctional | Functional | Nonfunctional | Functional | Nonfunctional | Functional | Posttest Functional |
| Pretest examination | X | | X | | X | | |
| Propellant exposure | | | | | X | | X |
| Leak | | | X | | | | |
| Vibration | X | X | X | | | X | X |
| Leak | | X | X | | | X | |
| Shock | X | | | | X | | X |
| Leak | | X | | | | X | |
| Acceleration | | X | X | | | X | X |
| Leak | X | | X | | | X | |
| Thermal vacuum | | X | X | | | X | X |
| Leak | | X | X | | | X | |
| Squib firing | | X | | | | | |
| Expulsion | | | | X | | | |
| Leak | | X | X | | | | |
| Proof pressure | X | | | | | | |
| Endurance | | X | | | | X | |
| Posttest examination | X | | | | | | |

configuration tank at ambient temperatures and pad pressures; (2) one real-time mission sequence conducted under 0°F temperature conditions and operational pressures, followed by one real-time mission sequence conducted under 100°F temperature conditions and operational pressures; (3) shell TA tests involving 300 cycles, 150-hr pressure hold, vibration and burst tests, followed by a comprehensive metallurgical examination of the test specimens; (4) one standard tank configuration with oxidizer experienced several exposures at pad pressures totaling 64 hr and several to 750 psi totaling 62 hr at ambient temperature; (5) one standard tank configuration with fuel experienced several exposures at pad pressures totaling 96 hr and several at 750 psi totaling 62 hr at ambient temperature; (6) numerous exposures to oxidizer and fuel loadings at both pad and elevated pressures during S-6 development testing; and (7) seven-day direct exposure to tank shell followed by successful proofing and metallurgical examinations.

Early qualification tests of the TFE—FEP laminate bladders were performed on nine bladders at high pressure (650 psig) and three bladders at low pressure (25 psig). On the 9 bladders tested at high pressure, 10 runs were made at ambient temperature where 91–93% expulsion efficiency was achieved. Each of the three bladders tested at low pressure was subjected to one 99% expulsion at 0°F.

Qualification of the latter bladders was performed as part of the propellant tank assembly qualification.

The qualification of the propellant tank assembly was conducted to simulate actual mission requirements with respect to vibration, thermal vacuum, acceleration, and propellant expulsion. Bladder integrity was determined by leakage testing. A second leakage test was performed to determine the sealing capabilities of all other components, including all sealing surfaces.

Propellant tanks were pressurized before each vibration and acceleration test. The test assemblies were subjected to combined random and sinusoidal vibration. Propellant tanks were subjected to acceleration levels of 10 *g* for 4 min and 5 *g* for 8 min, applied through the propellant tank axes. The difference in levels simulated boost and retrodescent accelerations.

The thermal vacuum tests were designed to simulate mission transit, and coast vacuum and temperature conditions. Two tank assemblies were thermally wrapped with flight-type insulation and subjected to a hard vacuum.

The expulsion tests were made to demonstrate the capability of the bladder to expel 90–99% of the fluid.

As in the case of the helium tank and valve assembly, the propellant tank assembly performed as designed, demonstrating the capability of performing the requirements of the *Surveyor* mission. The tests for control item TA testing are shown in Table XVII-8.

Before the first spacecraft launch, a series of propellant tank lunar survival tests was made. The primary objective of these tests was to determine if the combined effect of high temperature and exposure to oxidizer vapor would materially reduce the burst pressure of the tanks to the point where a tank failure might occur. A secondary objective of the test was to gather lunar survival data relative to the oxidizer tanks.

Three flight-configuration oxidizer tanks were procured from the S-7 TA test vehicle for the series of lunar survival tests. The history of these tanks was essentially the same as expected for flight vehicle tanks after lunar landing. The first tank was loaded with 4 lb of MON-10 oxidizer, pressurized to a nominal 775 psig, and soaked at 240°F for 15 days. The second tank was loaded with 9 lb of MON-10 oxidizer, pressurized, and subjected to slow heating. The intended test temperature for the second tank was 270°F; however, at about 250°F the relief valve failed open and vented the gas pressure to ambient. Three tests were attempted with this tank; all resulted in relief valve failures, and the last included an O-ring failure, which permitted an oxidizer leak.

The third tank was also loaded with 9 lb of MON-10 oxidizer. It was pressurized to 775 psig and slowly heated to 270°F. After 30 hr at 249°F, the relief valve failed. The tank was held at 270°F for 16 days.

Both the first and third propellant tank assemblies survived the prolonged temperature soak test satisfactorily. Following posttest examination, each tank was filled with water, subjected to its respective test temperature, and gas pressure was increased until rupture occurred. Both tanks burst at pressures well above the design burst pressure of 1060 psig.

The results of these tests indicate there was no danger that the *Surveyor* propellant tanks would burst as a result of exposure to the worst-case condition of residual

propellant quantity and predicted tank temperature during the lunar day. Actual postlunar landing experience substantiated these results. However, on several missions there was a loss of tank pressure because of loss of liquid by O-ring and relief-valve failures.

*d. Spacecraft System test and flight problems.* Spacecraft System test and flight problems are discussed in the paragraphs that follow.

*1. Transducer shift.* As mentioned previously, upon helium pressurization during the *Surveyor II* mission, a 500-psi transducer zero shift was noted. This anomaly had no effect upon the mission; however, the failure of engine 3 to fire for midcourse correction and on subsequent attempts led to speculation that its fuel tank might have been empty. The transducer null shift was approximately the correct magnitude to permit pressurization of an empty propellant tank. Later, postflight analysis of point-by-point telemetry data revealed that the indicated helium tank pressure fell 530 psi in less than 0.25 sec after firing of the release valve squib. During the next 1.5 sec, an additional drop of 205 psi occurred; this rate of supply pressure reduction was characteristic for pressurizing the normal ullage volume and helium lines. It was concluded that the extreme shock load imposed by the release valve squib caused a shift of −500 to −530 psi in the null reading of the helium tank pressure transducer. On subsequent missions an analog recording of pressurization was made to allow immediate determination of a zero shift. Plots of the pressurization are given in another report (Ref. XVII-20).

*2. Surveyor V regulator failure.* The *Surveyor V* propulsion system successfully performed the midcourse correction and terminal descent sequences. However, the terminal descent sequence required major modifications during the flight because of a helium regulator malfunction.

Propulsion system performance during the launch and pre-midcourse coast phases was normal for all parameters and well within the allowable range. After completion of the pre-midcourse attitude maneuvers, vernier pressurization was commanded in accordance with the normal mission sequence. Vernier propellant tank pressurization was accomplished by firing the helium release squib and allowing high-pressure helium gas into the inlet port of the helium pressure regulator. The helium regulator allowed a high-rate flow of helium until the regulator outlet pressure reached the normal regulation pressure (approximately 730 psia). At this point, the pressure forces on the regulator diaphragm overcame the spring forces, and the regulator began to close and restrict the flow rate. (The regulator normally would have been completely closed at 770 psia and would have prohibited the further flow of gas until the downstream pressure decreased.) The downstream pressures rose rapidly to 750 psia and then continued to rise slowly until they reached 825 psia. Thus, it appears that the spacecraft SC-5 regulator functioned normally in attempting to completely stop the flow of gas to the propellant tanks when a pressure of 750 psia was reached. However, the regulator was unable to completely stop the flow of helium to the propellant tanks, and the pressures continued to rise until they reached the relief valve opening pressures. At this point, the relief valve opened just enough to allow overboard leakage such that the tank pressure remained constant. Therefore, the spacecraft data agree with what would be expected for a regulator that failed to lock up.

A review committee was established to investigate the *Surveyor V* regulator failure. A review was made of the manufacturing, assembly, test, preflight history, qualification tests, and flight data. The details of this review are contained in another report (Ref. XVII-21).

The conclusion of this review committee, based on the available data, was that the most probable cause of failure was contamination which damaged the helium regulator valve seat. This could have resulted in an internal leak through the regulator, causing the outlet pressure to increase to a level which would have caused the fuel or oxidizer relief valve to vent to space. A detail that would support the conclusion that contamination was the more probable failure mode was the fact that *Surveyor V* experienced four changeouts of check and relief valves. The last check valve changeout was caused by leakage attributed to contaminants.

A series of regulator tests to duplicate the *Surveyor V* regulator failure were made at JPL using flight-type hardware (Ref. XVII-22). Test results indicated abnormal coining of the regulator seat and contamination were necessary before a regulator failure such as that on *Surveyor V* could occur. A blocked antisurge valve was used to simulate an inoperative unit in each test in which a seat failed, but the contribution to the failure of the inoperative antisurge valve was not clearly indicated. Figure XVII-29 shows a regulator seat which was made to fail under conditions the *Surveyor V* regulator may have been exposed to. This failure apparently was triggered by contaminants cutting a small channel in the




**Fig. XVII-29. Helium pressure regulator seat that failed under possible *Surveyor V* conditions**

coined seat; subsequent high-pressure, high-velocity, gas erosion formed the large hole.

The regulator seat would have been abnormally coined because of as much as a 14% high back pressure that could have bled past the leakage check valve during the preflight pressure check of the relief valve.

On *Surveyor V* the helium regulator lockup test was performed prior to check and relief valve tests, which required flow through the regulator, and the regulator lockup test was not repeated after changeout of the check and relief valve assembly at AFETR.

Changes to the handling and checkout procedures for the helium pressurization system were made for spacecraft SC-6 and SC-7. These changes greatly reduced the probability of introducing contamination into the system, eliminated the possibility of abnormal coining of the regulator seat, and provided for a regulator lockup performance test in the final phase of preflight VPS testing.

*3. Check and relief valve thermal problems.* During spacecraft SC-5 STV testing, the fuel and oxidizer check and relief valves exceeded their design temperatures of 125°F. Since these control items were qualified to 125°F, a special series of penalty tests was conducted to determine their operating characteristics at higher temperatures. Test results verified that the check and relief valves could function to temperatures up to 165°F. Subsequent changes to the thermal control of the valve assembly for spacecraft SC-6 reduced the temperature environment during the mission.

*4. Check valve leakage.* During the system readiness test of spacecraft SC-5 at AFETR, it was noted that the oxidizer side helium check valve was leaking, and the valve was replaced. The cause of valve leakage was found to be contamination, presumably introduced because of the difficult earlier changeouts of check and relief valves as a result of the thermal problems.

*5. Relief valve leakage.* The oxidizer relief valve aboard *Surveyor I* failed about 100 hr after the lunar landing (Ref. XVII-23). Based on the results of lunar survival tests, it appears the most likely cause of this failure was erosion of the seat by oxidizer vapors during venting cycles. The fact that the *Surveyor VI* relief valve did not fail when exposed to about 200 hr of the lunar day while being shaded, and the fact that relief valves did not fail due to repeated venting cycles at ambient temperature suggests that the failure was probably induced by high valve temperatures during venting periods.

*6. Bladder leakage.* During the extensive system testing of each spacecraft, the propellant tanks were filled with referee fluids, and at specific intervals bladder leak checks were made. Many tanks failed the checks and required replacement. All failures were characterized by out-of-specification leakage rate of the bladder. The high leakage rates were attributed to excessive crazing of the bladder material, the formation of blisters, or tearing of the bladder. The crazing of the bladders manifested itself by thin lines or pinholes at the intersections of crazing lines. These failures were attributed to improper installation of the bladder into the tank.

The tearing of the bladder was investigated by subjecting production-type bladders to varying tank lengths. These tests showed that a short bladder would develop tears upon pressurization or loading sequences. The analysis of the production failures indicated that the bladders had become shortened since their delivery from the vendor. The installation of the bladder was reviewed and it was concluded that the insertion of the bladder into the tank shell by using a heat gun was causing the problem.

The blistering of bladders was discovered on a later procurement. The most probable cause of this failure was a contamination introduced during the spraying sequence.

To verify that a bladder with blisters could still function, a series of TA penalty tests were conducted. In all cases the bladder with blisters, and in one case with a blister torn through one layer, successfully demonstrated 99% expulsion at 0°F after an FA test vibration cycle.

*7. Thermal insulation problems.* Also during STV tests of spacecraft SC-3, it was discovered that one propellant tank had different cooldown characteristics than previous tanks. Upon investigation, it was determined that the thermal wrap had been installed tighter than on previous tanks. The tanks were removed and replaced, and procedures and drawings were changed to ensure proper wrapping on all other tanks.

*8. Propellant tank O-ring leakage.* Leakage at the oxidizer tank flange was discovered during performance verification tests at AFETR on spacecraft SC-3 and SC-5. Examination of the leaking tanks revealed defective O-rings. These O-rings were all traced to a common production lot, and all tanks with the O-rings were removed from the system.

To ensure against propellant tank leakage at flight pressures, a high-pressure leak check was made after the spacecraft completed environmental tests and again after spacecraft propellant loading. To verify the integrity of the bladders after propellant loading, a bladder leak check was made after propellant loading and again after the high-pressure leak check. These procedures are described in more detail in Subsection A-4.

The Viton A O-rings used in the oxidizer tanks proved to be adequate for normal spacecraft functions. The leg 1 oxidizer tanks on spacecraft SC-5 and SC-6 leaked at about 7 and 9 days, respectively, after landing. These leaks were shown to be a result of O-ring degradation caused by long exposures at temperatures above 160°F (Refs. XVII-23 and XVII-24). Some chemical degradation was also noted at ambient temperatures; however, it was not severe enough to be a major concern during a 30-day lifetime at ambient temperature.

*9. Propellant line heater problem.* The propellant lines that permit flow of propellant from the tanks to the engine were heated and thermostatically controlled to maintain the temperature from 18 to 21°F.

After analysis of *Surveyor II* data, it was noted that one line had a duty cycle that lengthened gradually until it was 90% at 15 hr after launch. (Details of this problem are given in Section XV of this report.) This was corrected on subsequent spacecraft by increasing the heater capacity on this line. This change reduced the duty cycle on this line to 30%. No further problems were encountered on the heaters or temperature sensors on the lines.

*10. Line fitting leakage.* Most of the helium and propellant lines were connected to the component by standard AN fittings. To enhance the sealing capabilities, soft aluminum conical seals were used. Early in the program leakage problems were encountered by using nickel seals or inadvertently using more than one seal. Careful inspection of seals and proper assembly procedures corrected this problem.

### 4. Vernier Propulsion System Testing

The system test program was conducted in two general phases: (1) VPS development tests, and (2) flight spacecraft system tests. The development tests can be classified into the following types: propellant servicing and deservicing, storage, flow, vibration, open-loop firings, closed-loop firings, and TA tests. Descriptions of VPS testing in these areas as well as the flight spacecraft system tests are described below. The system test program plans and operations are detailed in Section IX of this report.

***a. Development and type approval testing programs.*** The development and TA testing programs are described in the paragraphs that follow.

*1. T-2 test program.* The T-2 program was originally designed to demonstrate the capability of the RADVS/flight control/propulsion subsystems to control the vehicle while it performed a stable soft landing. The program was conducted at the Air Force Missile Development Center (AFMDC) at Holloman Air Force Base, Alamagordo, N. Mex.

The stated objectives were to:

(1) Perform an overall dynamic test of the final portion of the vernier descent phase (excluding actual touchdown) in as near normal conditions as possible.

(2) Determine the capability of the VPS (in conjunction with the attitude reference system) to hold vehicle attitude during dynamic descent under minimum and maximum vernier thrust conditions.

(3) Determine the capability of the VPS (in conjunction with the doppler velocity sensor) to correctly align the thrust velocity vector under dynamic conditions.

(4) Determine the capability of attaining predicted touchdown conditions using representative velocity and attitude control equipment under typical conditions.

The VPS was modified to meet the T-2 requirements, primarily by reducing the weight of the propulsion feed system. In addition, nozzle expansion ratios of the engines were reduced to prevent flow separation at sea-level test conditions.

The first test phase was a tethered hover test during December 1962. The vehicle was suspended 30 ft above the ground from an *Aerobee* tower, using ballast in place of the RADVS system. After two engine firings, the first test phase was terminated because of design problems; these were excessive hysteresis in the engine throttle valves and an uncommanded thrust transient that appeared about 1 sec after ignition of the engines. At this time the static engine response test was added. The engine was mounted rigidly to a static test stand to investigate engine operation. After the throttle valves were modified, an acoustic coupling problem was noted during tether tests with the RADVS system installed. Polyethylene foam was used to isolate the RADVS system from the vernier engine noise.

The second test phase was a drop test series that consisted of several free-fall drops from a balloon followed by parachute recovery at the required altitude. During the first drop test, the test vehicle was prematurely dropped from 1200 ft because of an inadvertent firing of the release squib. Another failure occurred during the second test because of problems including: (1) A short circuit disrupted the roll control loop and allowed the vehicle to continue in a slow roll, (2) a failure in the engine shutoff circuitry prevented shutdown of the vernier engines on initiation of recovery, and (3) a short circuit in the oxidizer manifold dump squib prevented the relieving of the oxidizer pressure at initiation of recovery.

The T-2 descent test program was then completely reoriented, and a program plan incorporating revised test objectives was prepared.

*2. T-2N test program.* The new program was formulated with the prime objective of providing extremely high confidence that the terminal descent phase would be performed successfully on operational lunar flights. This included provision for a minimum of 10 successful 500-ft drop test recoveries and 6 consecutive successful soft landings.

Typical propulsion activities for a given test included the following:

(1) Solvents were flowed through the vernier engines to simulate propellant flow. Checks were made of steady-state flow levels, hysteresis loop width, and dynamic response times.

(2) Solvent flow rates were monitored as the T-2N vehicle was tilted up and down to check for proper phasing between the engines and the flight controller. The solvents were removed by purge and vacuum cycles.

(3) A feed system functional test involved calibration of the helium, fuel, and oxidizer pressure transducers, measurement of the crack and reseat pressures of the relief valves, and leak-checking the helium tank and lines, check valves, bladders, and engines.

(4) Propellant tanks were loaded full, then off-loaded to the desired mission load. After the first tether test of vehicle T-2N2 in which a gas entrainment problem was indicated, a test was performed during propellant loading to measure system "softness." While the tanks were loaded full, a gas-entrainment device was used to provide a finite increase in the volume of the propellant system. The amount of volume increase required to cause a pressure decrease of 5 psi indicated the amount of system gas entrained.

(5) The helium tank was pressurized to desired mission level and a pad pressure was applied to the propellant tanks.

(6) During a mission, the propulsion console in the control room monitored the following parameters:

(a) Fuel manifold pressure.

(b) Oxidizer manifold pressure.

(c) Helium tank pressure.

(d) Total thrust.

(e) Three chamber pressures.

(f) Three delta chamber pressures that represented the difference between the actual chamber

pressure and the chamber pressure equivalent of the throttle valve command; these data provided the variation of engine performance from that commanded, which was used to indicate injector salting.

(7) Vacuum plugs were inserted in the engine chamber throats as soon as possible after landing to prevent injector salting.

(8) Propellants were removed and solvents were loaded for flushing, in conjunction with the engine solvent flow check for the succeeding mission. If the solvent flow check indicated injector salting, the engine oxidizer system was flushed with warm water, which dissolved the salts. The squib valves were rebuilt for the succeeding mission.

During the T-2N program, in 1965 and 1966, five tether tests, six descent/altitude recovery tests, and two touchdown tests were successfully accomplished. Indications of gas entrainment were noted on one of the tether tests. Several cases of posttest injector plugging were found during solvent flow tests of the engines. This was attributed to injector salting. The final report for the T-2N program is contained in another document (Ref. XVII-25).

3. *Spaceframe S-6 and S-7 system development and type approval test programs.* Two spaceframes, S-6 and S-7, were utilized for the VPS development tests, margin limit tests, and TA test programs. Development tests included propellant migration, propellant storage, and open-loop tests. The TA tests comprised mission-sequence vibration and firing, thermal environmental, and pressurized drop tests. The margin limit tests involved control margin with helium-saturated propellants.

The S-6 test vehicle was a rudimentary frame that provided spatial support for buildup and operation of the VPS; the S-7 test vehicle was a dynamic equivalent of the flight vehicle that included simulated masses for the nonpropulsion elements. Both vehicles used the sea-level version of the vernier engine.

Results of S-6 and S-7 tests performed in 1964 at AFMDC, Holloman AFB, revealed a major problem in the vernier propulsion system: anomalous performance was observed in vernier engine firings conducted during the S-7 propellant storage test. The anomalies included sudden uncommanded thrust excursions and also a degradation of dynamic performance with increased storage time. It was hypothesized that these anomalies were caused by the presence of free gas and dissolved gas in the liquid propellants. A program of open-loop tests was established to investigate further the effects of gas ingestion.

Open-loop dynamic performance tests were conducted on the S-6 vehicle at the HAC propulsion system field laboratory (PSFL), Placerita Canyon, Calif., in the second quarter of 1965. Objectives of the test program were to: (1) verify the cause of uncommanded thrust excursions that had occurred in the propellant storage test firings, (2) investigate the dynamic characteristics of the VPS, and (3) develop servicing procedures for the nonmanifolded propellant feed system. Objective (3) was accomplished in the course of pretest preparation.

Two runs with helium-saturated propellants were made to determine the open-loop dynamic characteristics of the VPS. The results of both runs were quite similar. It was proved that open-loop dynamic characteristics of the propulsion system are markedly changed by the presence of dissolved gas in the propellants (see Subsection A-2).

The S-7 TA test program was conducted in August and September 1965. The objective of the program was to demonstrate that the VPS would meet prescribed performance criteria after exposure to launch-phase vibration and during exposure to retrophase vibration. The test criteria were as follows:

(1) The VPS must be capable of providing propellants to the vernier engine such that a minimum thrust range of 30–104 lbf shall be attained.

(2) For a thrust range of 30–104 lbf the throttle valve inlet pressure as measured at oxidizer leg 3 must be greater than 687 psig. The no-flow system pressure must not exceed 830 psig.

(3) The vernier propulsion thrust chambers must be capable of providing a thrust differential between two engines such that a minimum moment control capability of 2065 in.-lb is attained as measured about an axis through the spacecraft center of gravity parallel to the $X$–$Y$ plane.

(4) The vernier propulsion feed system must be capable of providing propellants to the vernier engines for three commanded starts with no less than 1 hr between starts.

(5) There must be no evidence of mechanical failure of Class IV VPS parts at the conclusion of the vibration phase.

Before TA testing, the S-7 test vehicle was subjected to system-level, three-axis FA vibration, system functional checkout, and system leakage tests at HAC, El Segundo. To provide simulation of the vibration retest for which spacecraft SC-1 was scheduled, S-7 was subjected to twice the standard duration of FA vibration on each axis.

Following completion of FA tests, the S-7 vehicle underwent system-level TA vibration on the two lateral axes at HAC, El Segundo, and on the vertical axis at JPL, Edwards. For tests at El Segundo the system was loaded with referee fluids; for tests at Edwards the system was loaded with actual propellants.

After the vertical-axis simulated launch-phase vibration test, a complete real-time mission simulation was performed, with the test vehicle mounted on the shaker. The simulation included coast phase I, two midcourse firings, coast phase II, and terminal descent firing. During the main retro portion of terminal descent, with the vernier engines firing, the system was subjected to a vibration and shock environment approximately twice as severe as the expected flight environment due to retrothrust variations.

The performance of the VPS, as measured against all the test criteria, was found to be satisfactory.

Type approval tests to demonstrate satisfactory performance of the VPS at extremes of the predicted thermal environment were conducted at HAC PSFL in September and October 1965.

The conditions to be met by the VPS, when operated in a real-time mission sequence while exposed to thermal environments of 0 and 100°F, included thrust range, helium regulator, and moment control criteria as prescribed for the S-7 TA tests described above. Additional criteria prescribed were: (1) The VPS must be capable of four satisfactory starts, two starts during the high temperature TA testing and two during the low temperature TA testing; and (2) The vernier propulsion feed system must be capable of providing a minimum of 179 lb of usable propellant to the thrust chamber assemblies.

The test program consisted of two real-time simulated missions and a propellant capacity verification test. In the first two tests, the vernier propulsion feed system was operated through a selected real-time mission profile while subjected to thermal environments of 0 and 100°F, respectively. Data from the low temperature tests were also used to verify the capacity of the helium supply. The capability of the vernier propulsion feed system to supply the specified quantity of propellant was demonstrated in the propellant capacity verification test.

The S-7 VPS test vehicle was subjected to a lunar landing impact simulation at HAC PSFL on October 11, 1965. The purpose of this test was to demonstrate: (1) that the system could survive lunar landing without developing propellant leakage or catastrophic failure of the helium system, and (2) that the helium regulator and check and relief valves would perform their required functions after lunar landing.

A wooden platform set up in a horizontal position was used for the impacting surface; simulated lunar rocks were not included on this surface. The propellant tanks were filled with referee fluids to the maximum weight expected at vernier engine cutoff; similarly, the helium tank was pressurized to the maximum expected residual pressure. The vehicle was released from a height of 6.16 ft (as measured from the bottom of the footpads), to provide a spacecraft velocity at impact of approximately 20 ft/sec.

Inspection and functional checkout of the vernier system subsequent to the drop revealed that neither the structural nor functional integrity of the system was affected by this drop test.

In November and December 1965, a series of closed-loop firings was conducted to explore the limits of control margin available with helium-saturated propellants as compared to limits with unsaturated propellants. For these firings an analog computer at El Segundo was used to control the vernier engines of the S-6 propulsion system at PSFL. Inputs to the computer were in the form of simulated moment disturbances whereas feedback to the computer was by means of chamber pressure transducer signals.

Although control of the propulsion system was adequately maintained on all four runs, a comparison of three helium saturated runs with one unsaturated run indicated that the system dynamic characteristics changed with the addition of dissolved helium gas in the propellants. Qualitatively, the saturated runs evidenced longer settling times than did the unsaturated run.

The results of the tests showed that even though the dynamic response of the system was deteriorated by the presence of entrained gas in the liquid side of the

system, with an increase in the doppler loop gain, there was sufficient flexibility in the flight control propulsion system to provide spacecraft system stability.

*4. Type approval spacecraft test program.* The TA spacecraft, designated T-21, was developed to qualify the *Surveyor* functional and thermal design through a series of tests at environmental levels greater than those anticipated during the actual mission, and also to prove through usage the equipment, facilities, test techniques and test procedures to be utilized for FA tests performed on the flight spacecraft. Section IX of this report contains detailed descriptions of the test programs from an overall spacecraft standpoint.

The T-21 test program from the standpoint of the VPS accomplished the following:

(1) Demonstrated the compatibility of the propulsion ground support equipment with the spacecraft.

(2) Demonstrated the adequacy of propulsion off-site planning and procedures.

(3) Demonstrated the propulsion system test team capability in a field environment.

(4) Validated facilities and facility support activities.

(5) Established the adequacy of the system under simulated mission environments and operational constraints.

The VPS that was installed on the T-21 spacecraft comprised three nonflight but propellant serviceable vernier engines, six flight-type propellant tanks, a flight-type helium tank and valve assembly, and associated gas and propellant feed lines.

On December 27, 1963, the system functional test was started on the T-21 spacecraft. The tests that concerned propulsion were:

(1) Spacecraft harness verification to perform a quantitative test within each wiring group.

(2) Gross error check to verify the proper resistance to ground on all connections to the spacecraft units and the proper voltages on all connections.

(3) The group test, which included electrical and mechanical compatibility tests, mechanical alignment, overall group transfer functions, calibration of transducers, and signal conditioning circuitry.

On March 6, 1964, the spacecraft was placed in the high-bay area of the Space Systems Environmental Laboratory for modal vibration testing. These tests were performed to determine structural coupling to the RADVS subsystem on other T-21 subsystems. The test was accomplished by suspending the spacecraft a few feet above the floor with lifting sling attached to the overhead crane. Portable shakers were used to vibrate the vehicle during system testing. This test was the forerunner to vernier engine vibration tests that were to be performed on all flight spacecraft. The results of the test indicated that no detrimental effects were noted by the other subsystems (including propulsion) during RADVS operation.

At the completion of a major system test equipment assembly upgrade, a mission sequence test was performed on July 2, 1964 (Section VI).

The VPS was generally in a passive mode during this test; however, thermal and engine strain gage data were obtained as a verification of the correctness of the data link to the spacecraft.

The STV test phase utilized the test facilities available at the HAC space simulation laboratory.

The VPS tanks, lines, and engines were filled with referee fluids and charged to pad pressure level while the helium bottle was pressurized to a safe working level for STV testing.

In this condition the thermal mass of the propellant-loaded VPS was simulated and temperature data from the various elements of the system were representative of what would be expected under actual flight environments.

On March 11, 1965, the vibration test phase was started. The effects of boost and retro vibration on the loaded VPS were obtained during this test phase. Specific areas of the system were observed for their capabilities to withstand the vibration environment: propellant tank bladders, propellant and gas line connections, structural interfaces, and valves. The T-21 vibration tests were completed by April 10, 1965.

The referee fluid was removed from the propellant tanks and the tanks were replaced with Class IV hardware in preparation for combined systems tests at GD/C in San Diego.

The spacecraft VPS underwent a leak check before leaving El Segundo for combined systems tests with the

*Centaur* vehicle in San Diego. The following control items were pressurized with nitrogen for transport:

(1) Each propellant tank (10 psig on the liquid side through the tank bleed quick-disconnects).

(2) Each propellant tank (5 psig on the gas side through the vent or pressurize quick-disconnects).

(3) The helium bottle (approximately 50 psig through an AN fitting in lieu of the helium fill quick-disconnects).

The oxidizer relief valve leaked helium at a rate of 25 $cm^3$/min, three orders of magnitude more than the maximum specified. Furthermore, the white paint on the relief valve should have been on the top portion of the valve, whereas this valve was painted on its side. The valve was removed from the helium package and returned to El Segundo for rework.

The VPS was in a passive mode during conduct of the combined systems test. However, the test demonstrated the correctness of the RF link under combined systems operations.

The pressures in the system were checked in San Diego and were satisfactory with the following exceptions:

(1) The fuel tank gas side pressure had dropped from 5 to 3.7 psig.

(2) The fuel tank pressure on the liquid side of tank 3 was zero, indicating a fully collapsed bladder.

A leak test of the collapsed bladder showed that at 4 psi the leak rate was 40 $cm^3$/hr , which was within the specified limit (72.7 $cm^3$/hr). The bladder was considered satisfactory. It was apparent that the loss of bladder pressure during shipment of the spacecraft to GD/C occurred through the nonflight engine.

The telemetry power turnon test data for the VPS indicated that both pressure transducers, all temperature pickups, and one strain gage were functioning through the complete loop on RF. Only one of three strain gages was operating, because of faulty amplifiers in the system test equipment assemblies.

The spacecraft arrived at AFETR with many problems in the VPS. These were mostly leaks that were repaired in the course of the system tests. The primary propulsion effort at AFETR on the T-21 spacecraft was the establishment of the adequacy and compatibility of the ground support equipment/spacecraft interfaces, the propellant loading and vernier system test procedures, and the facilities. Details of the operations performed on the spacecraft are included in Section IX of this report.

The operations performed on the T-21 spacecraft provided valuable experience in propulsion for flight spacecraft servicing.

***b. Flight spacecraft system testing.*** Vernier propulsion system tests were performed on flight spacecraft at HAC, El Segundo, and at AFETR as part of preflight testing. Aside from data monitoring, no vernier propulsion tests were performed during the combined systems tests at San Diego. After the failure of SC-2, tests were added to gain added confidence in the areas of contamination, injector salting, bladder integrity, engine compatibility with the flight control system, and propellant feed system flow testing. Table XVII-9 lists the chronological sequence of VPS tests that were conducted on the flight spacecraft. Table XVII-10 lists, chronologically, the problems encountered with the VPS of each spacecraft during the course of spacecraft testing at El Segundo and AFETR.

*1. Helium system testing.* The helium tank was leak-checked at HAC, El Segundo by pressurizing the tank to 2500 psig and taking pressure decay readings. A highly accurate pressure transducer was connected to the helium tank charging valve for this purpose. At AFETR the helium tank was leak-checked by pressurizing the tank to 5200 psig and taking pressure decay readings. This was performed in parallel with joint flight acceptance composite testing (J-FACT). Although the helium tank was insulated for this test, inconsistent data were common because of temperature variations occurring through encapsulation, transportation, and mating to the *Centaur* vehicle. The gas bulk temperature could not be measured accurately enough to fully correct these pressure variations. Some of the observed data were only marginally acceptable.

The charging valves and check valves were leak-checked as part of the VPS functional test. This included measurement of the cracking pressure, reseat pressure, and leakage of the relief valves, and a performance test of the helium regulator. The regulator test measured output pressure at the propellant tank inlet fittings (each set of tanks) at minimum and maximum flow rates.

Before the assembly of SC-6, flex lines were used between the gas supply filters and the spacecraft fittings

## Table XVII-9. Sequence of vernier propulsion system tests conducted on flight spacecraft

| Test | Location | Spacecraft effectivity | Description | Procedure No. |
|---|---|---|---|---|
| Thrust chamber assembly preflight checkout | AFETR | SC-2 to SC-7 | Measurement of engine flow rates of solvents at commanded thrust levels, hysteresis, and dynamic response times; measurement of engine leakage | JPL 65-759 |
| Nozzle emissivity and joint conductance | JPL | SC-1 to SC-7 | Measurement at engine nozzle emissivity and nozzle joint conductance at near ambient temperatures in vacuum | JPL ETP-SUR-002 |
| Bladder leak | HAC, El Segundo | All | Measurement of individual bladder leakage | — |
| Engine 1 torque | HAC, El Segundo | All | Measurement of leg 1 engine resistance to roll actuator torque | — |
| VPS solvent leak | HAC, El Segundo | All | Measurement of pressure decay of VPS with solvents loaded and helium pad pressure applied | — |
| Solvent high pressure | HAC, El Segundo | SC-4 to SC-7 | Visual observation for solvent leakage from system pressurized to flight pressure | — |
| Helium pressure decay | HAC, El Segundo | All | Measurement of pressure decay of helium high pressure system at one-half flight pressure | — |
| Solar thermal vacuum | HAC, El Segundo | All | Measurement of temperatures and pressures during simulated flight environment | — |
| System flow | HAC, El Segundo | SC-3 to SC-7 | Measurement of solvent flow rate with engines removed | — |
| VPS functional | HAC, El Segundo | SC-7 | Measurement of individual bladder leakage | — |
| Thrust chamber assembly preflight checkout | AFETR | All | Same as mentioned above | JPL 65-759 |
| VPS functional | AFETR | SC-3 to SC-7 | Measurement of individual bladder leakage, charging valve, and check valve leakage, relief valve cracking pressure, reseat pressure, leakage, helium regulator performance (flow and lockup) | HAC 288107 |
| Engine/spacecraft functional | AFETR | SC-3 to SC-7 | Measurement of engine flow rates of solvents at commanded thrust levels, with commands from the spacecraft; measurement of dynamic response times and engine leakage | HAC 229155 |
| Thrust chamber assembly installation and phasing | AFETR | All | Measurement of leg 1 engine torque resistance, measurements of gas flow rates through engines at spacecraft commanded thrust levels, audible check of engine solenoid operation, and measurement of connected solenoid electrical resistance | HAC 288416 |
| VPS solvent final leak | AFETR | All | Measurement of pressure decay of VPS with solvents loaded and helium pad pressure applied | HAC 288109 |
| | | SC-3 to SC-7 | Visual observation for solvent leakage at flight pressures | — |
| Helium pressure decay | AFETR | All | Measurement of pressure decay of helium high pressure system at flight pressure | — |
| Composite bladder leak | AFETR | SC-3 to SC-7 | Measurement of composite bladder leakage | HAC 229151 |
| Spacecraft oxidizer and fuel servicing (propellant sample analysis) | AFETR | SC-3 to SC-7 | Chemical and particulate analysis of propellants loaded on the spacecraft | HAC 288117 and HAC 288118 |
| Bladder integrity | AFETR | SC-4 to SC-7 | Titration of propellant vapors from gas vented after propellant loading to establish integrity of bladders | HAC 229167 and HAC 229166 |
| Spacecraft fuel and oxidizer servicing (propellant high pressure) | AFETR | SC-5 to SC-7 | Visual observation for propellant leakage from system pressurized to flight pressures | HAC 288117 and HAC 288118 |
| Bladder integrity | AFETR | SC-5 to SC-7 | Titration of propellant vapors from gas, vented after high pressure propellant test to establish integrity of bladders | HAC 229167 and HAC 229166 |
| Toxic gas detector | AFETR | All | Periodic measurement of propellant vapor concentration near components | HAC 229153 |

## Table XVII-10. Vernier propulsion system test problems

| Spacecraft | Test location | Problem description |
|---|---|---|
| SC-1 | HAC, El Segundo | (1) Two propellant lines damaged; kinked line straightened; scratched leg 3 oxidizer replaced |
| | | (2) Leg 3 tank replaced when B-nut during above line replacement cross threaded |
| | | (3) Bladder collapse when pressure was not relieved during (1) above; no damage |
| | | (4) Helium leakage from gas line because of use of nickel and stainless steel conical seals instead of aluminum [a] |
| | | (5) Oxidizer tank O-ring material incorrect; tanks replaced after rebuild with proper O-rings |
| | | (6) Short circuit of heater wire pinched during tank installation in (5) above; wire repaired and rerouted |
| | | (7) Helium actuation line damaged and replaced |
| | | (8) One fuel and one oxidizer tank replaced because of leaky bladders [a] |
| | AFETR | (1) Test gage exploded during vernier engine phasing test because of improper use of gage; replaced by proper device |
| | | (2) Quick disconnect leaked during solvent decay test and reseated when cycled; gas charging quick disconnect leaked and was replaced [a] |
| | | (3) Inadvertent power application to engine solenoid valves after propellant loading (test is normally part of performance verification test 1). Engine did not fire because of lower than normal pad pressure; leaky gas filter in fuel servicing cart reduced pad pressure below level at which thrust chamber assembly (TCA) would operate |
| | | (4) Loss of gold plate and presence of greenish liquid at various external seal areas of engines. Material analyzed to be lubricant reacted with oxidizer vapors and copper oxide (gold plate substrate). Material neutralized with ammonia solution |
| SC-2 | HAC, El Segundo | (1) Bladder damage on leg 2 fuel and oxidizer tanks; solvents were observed at gas charging valves during loading; tanks replaced [a] |
| | | (2) Leg 3 propellant lines heater "hi-pot" failure; lines replaced |
| | | (3) Presence of solvent at fuel charging valve during leg 3 solvent download. Insufficient removal of solvents caused by (1) above [a] |
| | | (4) Leg 2 line heater thermostat unconnected and repaired |
| | | (5) Leg 2 oxidizer tank heater wires line-to-line short; repaired and rerouted |
| | AFETR | (1) Solvent observed in two engine helium actuation lines during engine installation attributed to earlier bladder problem at El Segundo; lines purged [a] |
| | | (2) Leg 3 line heater failed "hi-pot"; line assembly replaced |
| | | (3) Tank quick disconnect leak during solvent decay test; replaced [a] |
| | | (4) During propellant loading, leg 2 oxidizer engine quick disconnect leaked in coupled condition; leg 3 oxidizer tank quick disconnect leaked uncoupled; sealed when cycled [a] |
| | | (5) Oxidizer tank caps lost VDA finish and were covered with aluminum tape. Engines as on spacecraft SC-1, "weeped" a green, sticky liquid and lost some gold plate |
| SC-3 | HAC, El Segundo | (1) Prior to solar thermal vacuum (STV) testing, bladder leakage of legs 1 and 3 oxidizer tanks discovered. Tank replacement postponed until after STV [a] |
| | | (2) Leg 1 thrust strain gage indicated negative offset throughout STV until the three strain gage amplifiers were replaced |
| | | (3) A loss of chamber vacuum occurred during STV. A cloud of vapor was seen under the spacecraft, and "snow" was seen on the chamber end bell. Solvents were sampled, and the following samples appeared yellow: legs 2 and 3 fuel tanks, legs 1 and 2 engines. Later determined to be due to iron oxide from a Bourdon gage in the sampling line. Legs 1 and 3 oxidizer tanks replaced because of earlier bladder leaks. The leg 3 fuel tank was found to have been 67% empty. All fuel tanks, the engines and the fuel lines were replaced because of suspicion of contamination |
| | | (4) Actuator arm hole on the leg 1 engine undersized and required reaming to mate with roll actuator |
| | | (5) Thermal data disclosed that insulation on legs 1 and 3 oxidizer tanks was too tightly wrapped. The leg 1 oxidizer tank was replaced; the leg 3 tank was left installed, being heated [a] |
| | | (6) A tear in the leg 1 fuel tank insulation cover was repaired |
| | AFETR | (1) Leg 2 oxidizer tank removed to replace the thermal standoff, of a former design prone to cracking during vibration |
| | | (2) Pressurization lines not disconnected from the tanks (part of the bladder leak check), and the bladders were partially collapsed while pressurization to leak check the charging valves. A bladder leak check indicated that all bladders were acceptable; problem attributed to bypassing bladder leak check because of tank replacement [(1) above] |
| | | (3) The spacecraft was returned to El Segundo for additional STV testing |

[a]Problems discussed further in Subsection A-3.

## Table XVII-10 (contd)

| Spacecraft | Test location | Problem description |
|---|---|---|
| SC-3 | El Segundo (STV rerun) | (1) The leg 2 propellant lines were replaced with lines having greater heater capacity. These failed "hi-pot" test and were again replaced [a]<br>(2) Prior to vibration, the eyebolt nuts were found to be missing from legs 2 and 3 engines |
| | (AFETR final) | (1) The long extension cables connecting the spacecraft to the engines during the TCA/spacecraft functional test acted as capacitors and amplified the 400-Hz dither signal to the throttle valves. The 18-V signal at the spacecraft measured 29 V at the engines. Test performed on the engines using spacecraft for shutoff valve signal only; the engine flow bench provided the throttle valve commands. The engine preflight tests were repeated to confirm that the high dither current had not damaged them. One engine experienced degraded shutdown times believed caused by a loss of lubricant on the shutoff valve poppet seals and was replaced. One engine indicated a "double blip" on the solenoid actuation current trace and was set aside pending a better understanding of this characteristic<br>(2) The leg 1 oxidizer tank leaked Freon during the TV-monitored high pressure test and was replaced<br>(3) During propellant loading, leg 2 oxidizer tank fill and vent valve leaked vapor until retorqued. After propellant loading, a vapor leak was found at the bottom of the leg 1 oxidizer tank, using the toxic gas detector. Leak reduced when pad pressure was increased<br>(4) Slight "weeping" of green liquid noted from the engine seals, and some loss of gold plate |
| SC-4 | HAC, El Segundo | (1) All propellant tanks remaved from the spacecraft because of tight insulation wrapping [a]<br>(2) All vernier engines were replaced with engines that had been validated clean<br>(3) The temperature pickup on the leg 1 engine was replaced<br>(4) The leg 2 propellant line heater was cycling too fast in STV; lines were replaced with lines having more heater capacity [a]<br>(5) A loose strain gage connector was repaired<br>(6) The vernier engine vibration was initially performed without the leg 2 engine heat deflector installed, and was repeated |
| | AFETR | (1) Unacceptable leak found at oxidizer check valve. Cycling and purging the valve reduced the leakage to acceptable values<br>(2) During the engine/spacecraft functional test, a ground loop existed at the spacecraft and signal drift occurred. Command sequence was changed and the test performed successfully<br>(3) Leg 3 engine removed for special testing of the throttle valve bellows end cap seal. Legs 1 and 2 engines removed for special solenoid valve testing. Solvent flow test and leak check were repeated before reinstallation. While engines were removed, the leg 2 fuel line was damaged when caught by smock packet; the line was replaced<br>(4) During propellant loading, an electrical storm forced evacuation of the loading area, a standard safety procedure. Electrical power was off for 45 min, allowing the propellant loading building to heat to 78°F. Two oxidizer tanks were locked in the filled condition during this time |
| SC-5 | HAC, El Segundo | (1) Leg 2 oxidizer tank removed to check the tightness of the insulation wrapping. Remaining tanks removed to replace standoffs, which were of inadequate design. All three engines replaced with ones that had been validated clean<br>(2) Leg 2 engine removed for further testing and replaced<br>(3) After a pressure decay test was successfully completed, a leak was discovered at the oxidizer charging valve. Valve was replaced<br>(4) The oxidizer tank maunting bolts were loose<br>(5) A bad connector for the leg 3 fuel line temperature sensor was repaired<br>(6) During STV testing, a liquid leak was visually observed in the leg 3 area. Spacecraft removed from the chamber and leak tested, with negative results. The relief and check valve assemblies were too hot during STV, and were replaced with pained assemblies. After beginning another mission cycle in STV, the liquid leak at leg 3 was again nated. Mirrors placed under the spacecraft aided in locating the leak, which was from the throttle valve bellows end cap area of the engine. When pad pressure vented, liquid observed at the fuel gas charging valve. The normal bladder leak check indicated all fuel bladders to be good; probably the wet bladders were sealing test gas flow by clinging to the tank walls. The bladders were filled with solvent with pressurization lines removed, and the leg 2 fuel tank overflowed. This tank was replaced and the gas system vacuum purged of residual solvent. The leg 3 engine was replaced because of the above problem |
| | AFETR | (1) The leg 1 engine indicated slow shutdown response times during the engine/spacecraft functional test and was replaced<br>(2) Leg 1 fuel tank replaced because of unacceptable bladder leakage. Oxidizer check valve leaked and was replaced [a] |

[a]Problems discussed further in Subsection A-3.

**Table XVII-10 (contd)**

| Spacecraft | Test location | Problem description |
|---|---|---|
| SC-5 (contd) | | (3) During high-pressure solvent leak test, leg 2 oxidizer tank and the leg 1 oxidizer tank leaked at the O-ring seal; tanks reploced. The O-rings were not properly made. When venting pressure from the fuel system, alcohol was found in the gas manifold. Bladders in legs 2 and 3 fuel tanks were found to be damaged, and the tanks were replaced |
| | | (4) Slight gold loss from the engines after propellant loading |
| SC-6 | HAC, El Segundo | (1) The leg 2 strain gage failed calibration and was replaced. The leg 1 engine trunnion mount was too narrow, and restricted engine rotation, and was reworked |
| | AFETR | (1) During the engine/spacecraft functional test, the leg 2 TCA exhibited erratic response during start and shutdown and was replaced |
| SC-7 | HAC, El Segundo | (1) The propellant lines for legs 2 and 3 were installed interchanged and had to be corrected |
| | | (2) Because of a suspicion of faulty O-rings, legs 1 and 2 oxidizer tanks were replaced [a] |
| | | (3) The engines on legs 2 and 3 were replaced to provide confidence in the shutoff valve lubrication |
| | AFETR | (1) Two of the fuel bladders (legs 1 and 3) were replaced because of marginal or out-of-specification leak rates [a] |
| | | (2) Helium bottle pressure decay rate was greater than the allowable. One observed leak-pressure transducer seal was repaired by replacement of the O-ring. Another leak at the valve-bottle K-seal joint was observed; however, the decision was made to accept the leak rate as having no detrimental effect on the SC-7 mission [a] |

[a]Problems discussed further in Subsection A-3.

during the functional test. After the SC-5 helium pressure regulator failure, tubing was used to connect the supply filters to the spacecraft to minimize the possibility of introducing contaminants during the regulator tests. Typical problems included leaking check valves and leaking quick-disconnects.

2. *Propellant tank bladder leak tests.* After installation of the propellant tanks on each flight spacecraft, an individual leak check was made of each of the tank bladders to assure integrity before loading solvents in the tanks. Checking each bladder individually required disconnecting the pressurization line from each tank, evacuating the space between the bladder and the tank wall, supplying a low-pressure gas to the inside of the bladder, and measuring gas flow through the bladder by means of a bubble-O-meter attached to the tank pressurization port. It was sometimes difficult to fully evacuate the space between the bladder and the tank wall, and trapped gas would be released when pressurized, giving an apparent high leak-rate indication. Cycles of pressurization and venting were sometimes performed in an attempt to disturb the bladder–tank wall contact. Repeated readings would eventually stabilize near the actual leak rate. As a part of the VPS functional test another individual bladder leak test was performed at AFETR during prelaunch preparations. Faulty bladders were discovered and replaced on SC-1, -2, -3, -5, and -7.

Before propellant loading at AFETR, a composite leak check of the propellant tank bladders was made by measuring leakage out of the oxidizer and fuel access ports with bladders pressurized. Results were compared with the sum of the individual bladder leak rates measured previously to indicate any changes because of solvent exposure and pressure cycling during leak check operations. This check was a recommendation of the *Surveyor II* failure review board and was introduced because bladder leakage had occurred much more frequently during test operations than had been expected. Composite bladder leakage data were acceptable for all spacecraft tested.

A bladder integrity test was initiated on SC-4 as recommended by the *Surveyor II* failure review board. After propellant loading, the gas on the outside of the bladders was examined for gross propellant vapors to determine whether exercising of the bladders during the filling operation had caused any degradation. On the oxidizer side, a vacuum was required prior to taking samples to remove accumulated quantities of MON-10 caused by its high permeability. The samples were taken by pressurizing the gas manifolds and venting through a "cold-trap" sample tube in $LN_2$. Frozen propellant vapors were diluted with water and titrated to determine propellant quantity. A series of repeated readings was compared with test values obtained in control tests performed at the HAC PSFL facility to determine bladder integrity. After a tank leakage test at flight pressure, further cold-trap samples were taken while venting to 300 psig pad pressure. Bladder integrity data were acceptable for all spacecraft tested.

3. *Propellant system flow tests.* The solvents were downloaded after solar thermal vacuum testing and the vernier engines were removed for separate shipment to AFETR. A feed system flow test was then performed at HAC, El Segundo (beginning with SC-3), as recommended by the *Surveyor II* failure review board. Solvents were flowed from the tanks through the propellant lines at two pressure levels, pressurizing through the standpipe to prevent bladder collapse. Measured flow rates were compared with baseline test data obtained at PSFL on the S-6 propulsion system to check for gross blockage in the tank standpipe or propellant lines. The system flow test data were acceptable for all spacecraft tested.

4. *Vernier engine testing.* Following delivery of the vernier engines, the first test performed was the nozzle emissivity and nozzle joint conductance test conducted at JPL, Pasadena. The first group of engines was shipped to HAC, El Segundo after FA testing at RMD. Later the engines were shipped directly from RMD to AFETR for an additional preflight flow test in which solvents simulated propellants. Electrical resistances of the throttle and shutoff valves were measured, and solvent samples were drawn from the engine for a particular contamination check. Equivalent propellant flow rates were measured at nine static flow command levels. The throttle valve maximum and minimum flow settings were located, and a hysteresis check was made of the throttle valve. Start, downthrottle, and shutdown response times were measured by pressure transducers. After solvents were removed, a leak check was made of the thrust chamber assembly using a gas mixture of 99% $N_2$ − 1% He and a helium mass spectrometer. The vernier engine checkout equipment is shown in Fig. XVII-30.

After receipt of the engines at El Segundo, the leg 1 engine was tested for torque resistance during installation on the spacecraft. Measured was torque resistance of the trunnion, the trunnion and propellant line coils combined, and the trunnion, line coils, and thermal shield combined. The engines underwent a final preflight checkout after arriving at AFETR. This was essentially identical to the initial preflight checkout, including a posttest leak check.

An engine/spacecraft functional "long-line" test was instituted beginning with SC-3 to confirm system compatibility before installing the engines on the spacecraft. Throttle valve and shutoff valve commands were given by the spacecraft to the particular engine being tested on the solvent flow bench. The two engines not being flow-tested were also connected to the flight controller

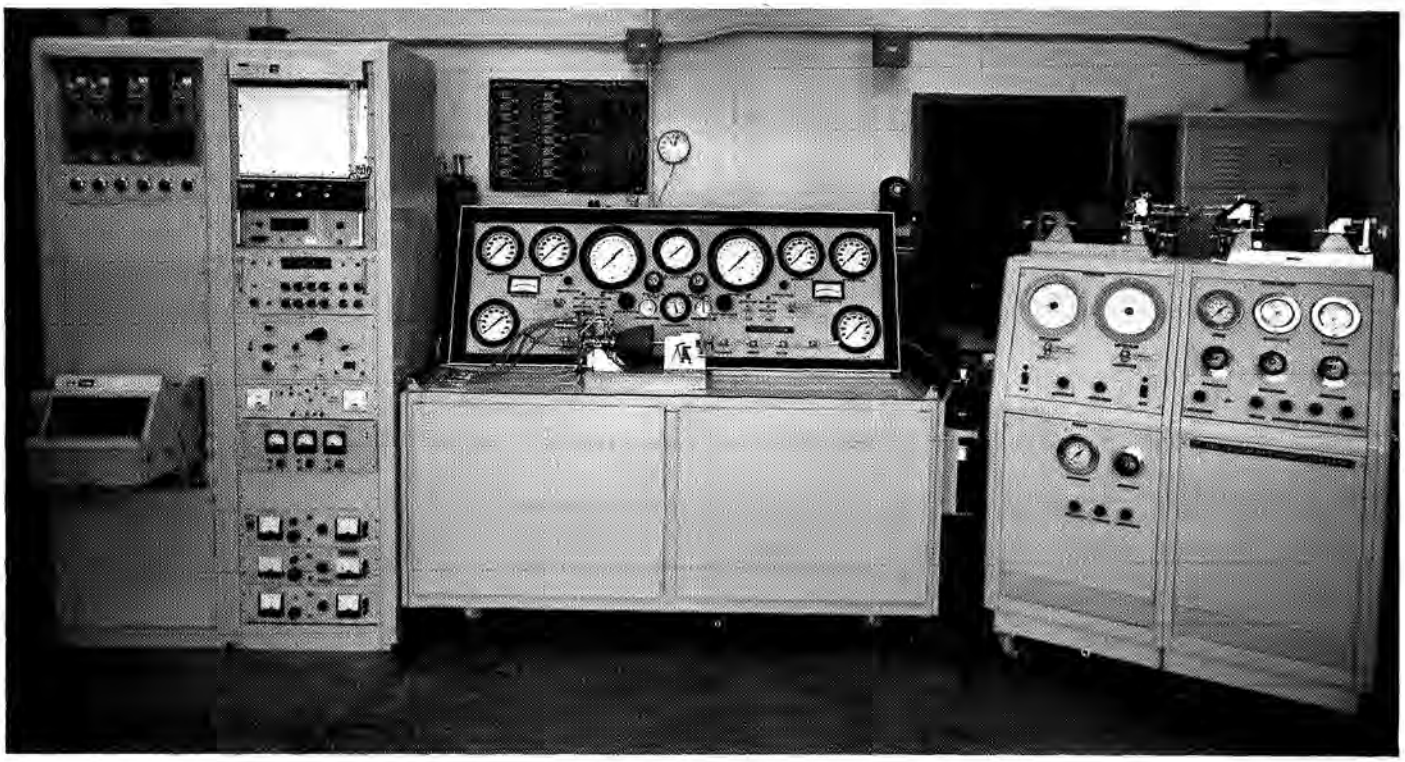


**Fig. XVII-30. Vernier engine checkout equipment used at AFETR**

to provide electrical load. Flow rates and dynamic response times were measured at five different flow command levels. A leak check was made of the engines after removing solvents.

The leg 1 engine was tested for torque resistance during installation on the spacecraft, as performed at HAC, El Segundo.

The engines were tested for proper phasing during installation on the spacecraft before propellant lines were connected. Only the oxidizer side could be gas-phased because the gas pressure used for this test was below that required to open the regulator in the fuel side. However, because there was a common actuator in the throttle valve, a check of the oxidizer side phasing was adequate. Helium gas was supplied to the throttle valve oxidizer inlet of the engine and exhausted out the shutoff valve bleed port to a gas flowmeter. Gas flow rates were measured while the spacecraft commanded the throttle valve to three thrust levels. An audible check was made of engine solenoid operation, and solenoid current was measured. Resistance of the connected shutoff valves was measured for reference data. Before final encapsulation, the valves were electrically connected, and a resistance check was made to confirm continuity.

A toxic gas detector was used preceding launch to examine the environment around the engines for propellant leakage. To minimize the possibility of injector salting in case of an oxidizer leak, a nozzle plug was developed to permit keeping a vacuum on the injector between propellant loading launch. (Section II-E of this report contains details of the injector salting problem.) This prevented salting by eliminating atmospheric moisture or oxidizer from accumulating in the injector in the event of leakage past the shutoff valve. The plug was made with two lines entering the chamber so that a nitrogen purge could be made of the thrust chamber, carrying any propellant leakage to the toxic gas detector. Subsequent to SC-2, periodic readings were taken to detect presence of vapors in the thrust chamber.

Many problems were discovered during the vernier engine preflight checkout, including flow restriction, calibration shifts, and seal leakage. Several engines exhibited loss of gold plating around seal areas after propellant loading. The toxic gas detector indicated slight vapor leakage only if placed adjacent to the seal area.

*5. System leak tests.* In preparation for STV testing and during the solvent final leak tests performed at AFETR, the spacecraft propellant tanks were loaded with solvents to simulate propellant density and thermal mass. A pressure decay leak test of the propellant and low pressure helium systems was performed at man-rated pressure (365 psig). Starting with SC-4, a short-duration visual check at 750 psig was performed to assure that under flight pressure the system was leak-free—this because earlier pressure cycling of the propellant tanks caused movement of the tank O-rings. This test was introduced in response to a *Surveyor II* failure review board recommendation. At El Segundo the flight pressure leak test was performed using barricades for personnel protection. At AFETR six TV cameras were focused on the tanks and vernier engines to check for leakage.

The 365-psig pressure decay test was conducted following an 8- to 12-hr soak period. This time was required to saturate the solvents with the pressurizing gas before a valid pressure decay measurement could be made. During the high-pressure test, if an appreciable amount of pressurant was allowed to be dissolved in the solvent (because of extended pressurization time), the gas was released during subsequent venting of spacecraft pressure and required immediate venting through the tank standpipes. This prevented a large pressure differential across the bladder wall. Solvent leakage occurred near the leg 1 propellant tanks during the high-pressure test of SC-3. Although it was difficult, because of the restricted view, to determine the exact location of the leak, it was concluded to have come from the oxidizer tank on leg 1. This tank was replaced and the monitoring system was improved by the addition of the six TV cameras.

Because the O-rings in the propellant tanks move during pressure cycling, a final high-pressure test was made at AFETR after loading propellants to determine that the tank O-ring was in its proper position. The test was performed at 750 psig and monitored by remotely operated TV cameras. This test was initiated with SC-5 because of tank leakage during testing at high pressure with solvents. A toxic gas detector was used before launch to examine the environment around the propellant tanks for propellant leakage.

The system leak tests revealed some liquid leakage at the tank bladder O-rings at flight pressure on SC-4 and SC-5, and gas leakage at the propellant tank helium inlet manifold on SC-1. A slight leak at a propellant tank on spacecraft SC-3 was located with the toxic gas detector.

*6. Contamination testing and propellant analysis.* Beginning with SC-3, solvent samples were taken from the supply lines, engines, and tanks each time solvents were loaded or downloaded, as recommended by the *Surveyor II* failure review board. The purpose of this procedure was to assure that no particulate contamination was introduced to the system and that the system itself was free of contamination. Propellant samples from the overflow lines were also analyzed for particulate content. Solvent samples were taken from the vernier engines, both in the forward and in the reverse flow directions, preceding the preflight checkout flows. Of all the particulate data, the samples that were unacceptable were believed to be caused by poor sampling techniques, a contaminated sampling gage, or improper sample filter assembly.

The propellants used on *Surveyor* spacecraft, including MON-10 oxidizer and MMH monohydrate fuel, were provided as customer-furnished propellant. Specifications were generated to establish controls on the chemical constituents of the propellants.

To establish that the propellants met the requirements of the specification, procedures for sampling and analysis of the chemical constituents had to be generated.

Initially, analyses of both fuel and oxidizer were accomplished at AFETR by the USAF laboratory at Patrick Air Force Base. Analysis of the fuel was performed in a relatively straightforward manner. However, because of the small tolerance on water content of the oxidizer, it was determined that the existing standard analysis techniques were subject to too much error. Consequently, personnel from the JPL Bioscience Section developed procedures for determining within a small error band the chemical constituent percentages of the sampled oxidizer and particularly the water content. A report defining these techniques has been prepared (Ref. XVII-26).

Two methods for determining water content were established: chemical and nuclear magnetic resonance (NMR). In the latter method, the sample is placed in a magnetic field. A signal based on the number of protons is generated, which in turn is proportional to the amount of water in the sample. Comparison of the chemical and NMR results showed close agreement in all analyses performed.

### 5. Vernier Propulsion System Mission Performance

Propulsion performance was monitored with telemetry sensors located on the propulsion system (vernier, Fig. XVII-1, and retromotor, Fig. XVII-41) and with thrust commands, gyro and acceleration errors, and spacecraft acceleration telemetered from the flight control system. Strain gages located on the engine mounting brackets gave an indicated engine thrust, although their output was greatly affected by engine heating and inertial forces.

***a. Nominal mission description.*** The final propulsion system prelaunch activity consisted of loading oxidizer and fuel and pressurizing the helium tank to flight pressure. During encapsulation, transportation to the launch pad, and while on the launch vehicle, the propulsion system status was monitored by means of system readiness tests and frequent engineering telemetry interrogations.

Continuous monitoring of the propulsion system was initiated at the Space Flight Operations Center at $L-90$ min. The propellant line heaters were enabled at $L-70$ min, and all temperatures and pressures were monitored for any significant changes during the final prelaunch period.

The propulsion system was in a passive condition during launch, injection, sun and star acquisition, and the remainder of the coast phase preceding midcourse. Operations during this period consisted of monitoring pressures and temperatures.

The first coast phase of the mission was terminated with the premidcourse attitude maneuvers. These maneuvers oriented the spacecraft such that the midcourse thrusting was done in the proper direction. At the termination of these maneuvers, vernier system pressurization was accomplished with a squib fired by ground command and was observed on helium, oxidizer, and fuel pressure telemetry. This same command also unlocked the engine 1 roll actuator and resulted in a change in the telemetered roll actuator position.

After pressurization, midcourse thrusting was initiated by ground-commanded vernier engine ignition. The engines fired for a predetermined time, which was set by a previous ground command, at a total thrust equivalent to a 0.1-g acceleration of the spacecraft. Differential throttling of the engines provided the required attitude stability during the midcourse velocity correction. The engine performance was monitored with engine thrust, thrust command, engine temperature, gyro error, and acceleration error telemetry.

Following midcourse, the postmidcourse attitude maneuvers repositioned the spacecraft by reacquiring the

sun and the star Canopus. The spacecraft then coasted towards the moon until the preterminal descent maneuvers began.

These maneuvers were initiated with a repositioning of the spacecraft in space so that the retro motor thrust would be in the correct direction to provide the proper deceleration. The altitude marking radar then generated an electrical signal at a predetermined altitude which started a timer to count down from a preset value. When the timer counted down to zero the vernier engines were ignited, which was followed 1.1 sec later by main retro motor ignition. Approximately 40 sec later, retro motor burnout occurred and, after an additional 12 sec, the retro case was separated from the spacecraft. The vernier engines were then throttled until the total thrust was equal to 90% of the lunar weight of the spacecraft. The spacecraft remained at this acceleration until the RADVS sensed that the spacecraft had intercepted a series of preprogrammed line segments. These segments specified a profile of velocity vs slant range. At the time of intercept the engines were upthrottled and the spacecraft decelerated until the velocity appropriate for that altitude was achieved. As the spacecraft descended the line segments, the RADVS controlled the total thrust in decelerating the spacecraft and differentially throttled the individual engines to provide attitude control. When the spacecraft had decelerated to 10 ft/sec, the engines were upthrottled and the spacecraft slowed to 5 ft/sec. The spacecraft then descended at this velocity until an altitude of 14 ft was reached, at which time the engines were commanded off and the spacecraft fell to the lunar surface. Vernier engine performance was monitored with vernier engine thrust, thrust command, gyro and acceleration errors, and temperature telemetry. Retro motor performance was obtained from vehicle acceleration telemetry.

***b. Transit performance.*** The above briefly describes the standard *Surveyor* mission sequence. This nominal sequence was followed closely by *Surveyors I, III, VI,* and *VII.* These four missions were characterized by as-predicted performance of the propulsion subsystem throughout the coast and thrusting phases (Refs. XVII-27 through XVII-30).

The *Surveyor III* spacecraft experienced a RADVS loss of lock condition during the final phase of terminal descent, which precluded the generation of a 14-ft mark and normal termination of vernier engine thrust. The spacecraft landed and bounced twice before engine cutoff was commanded from the Deep Space Instrumentation Facility. Upon this command the vernier engines cut off normally.

The overall temperature range to which the VPS components were exposed during the cruise portions of the mission is shown in Fig. XVII-31. These temperatures were well within the allowable range in all cases. Table XVII-11 shows values of the vernier engine performance parameters during the transit phases of the missions. It should also be noted that the startup and shutdown impulse dispersions, as indicated by postmission analysis, were quite small. The shutdown impulse variation, the more critical of the two, was less than 0.7 lbf-sec during each mission. Figure XVII-32 shows typical behavior of the helium and oxidizer pressures during system pressurization, midcourse, and touchdown.

In *Surveyor II* and *V*, in-flight component malfunctions occurred in the VPS. An altered flight plan resulted in a successful soft landing in the *Surveyor V* mission; the *Surveyor II* mission was lost. The *Surveyor IV* mission was, until terminal descent, normal in every respect except that at approximately 39 sec after retroignition the spacecraft RF signal was abruptly lost by the Deep Space Instrumentation Facility (Ref. XVII-31). The performance of the VPS on these three missions is discussed in greater detail below.

*1. Surveyor II.* During the period from launch to midcourse correction, all of the telemetered propulsion system data indicated normal operation, with two minor

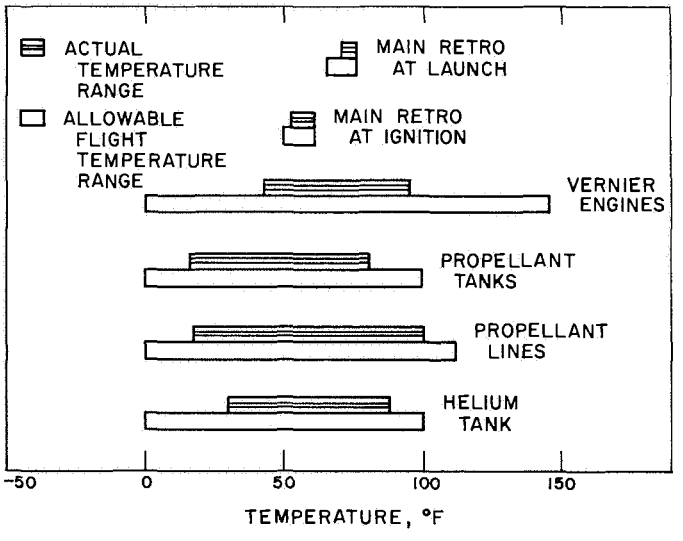



**Fig. XVII-31. Propulsion system temperature ranges during transit (all spacecraft except SC-2)**

**Table XVII-11. Vernier propulsion system transit phase performance summary**

| Parameter | SC-1 | SC-2 | SC-3 | SC-4 | SC-5 | SC-6 | SC-7 |
|---|---|---|---|---|---|---|---|
| Usable oxidizer loaded, lb | 107.9 | 108.1 | 107.9 | 108.1 | 107.8 | 108.6 | 109.3 |
| Usable fuel loaded, lb | 73.9 | 72.2 | 73.8 | 73.9 | 73.6 | 74.0 | 74.6 |
| Prelaunch helium pressure, psia | 5303 | 5168[a] | 5408 | 5269 | 5342 | 5219 | 5227 |
| Prelaunch helium temperature, °F | 88 | 71[a] | 84 | 84 | 83 | 81 | 83 |
| Squib release helium consumption, lb/in.$^2$ | 188 | 211[b] | 220 | 217 | 182 | 179 | 185 |
| Midcourse burn time $t_b$, sec | 20.8 | 9.8 | 4.2 | 10.5 | 98.1[c] | 10.2 | 11.3 |
| Midcourse helium consumption, lb/in.$^2$ | 383 | — | 102 | 208 | — | 208 | 248 |
| Midcourse propellant consumption, lb | 16.5 | — | 3.5 | 8.7 | 77.0[c] | 8.5 | 9.6 |
| Terminal-descent vernier burn time $t_b$, sec | 166.6 | — | 217[d] | — | 111.3 | 181.2 | 201.6 |
| Terminal-descent helium consumption, lb/in.$^2$ | 2122 | — | 2775[d] | — | — | 2539 | 2666 |
| Terminal-descent propellant consumption, lb | 122.5 | — | 154.7[d] | — | 59.6 | 139.1 | 142.4 |
| Main retro burn time (to 3500-lb-thrust tailoff level), sec | 38.9 | — | 41.0 | — | 38.6 | 39.4 | 42.9 |
| Helium pressure at touchdown, psia | 2457 | — | 2167[c] | — | 560 | 2314 | 2135 |
| Propellant remaining at touchdown (oxidizer and fuel), lb | 42.8 | — | 23.4 | — | 44.8 | 39.0 | 152.0 |

[a]Launch −2.5 hr.
[b]Corrected for zero shift.
[c]For six burns.
[d]For all three touchdowns.

exceptions: an acceptable but lower-than-expected temperature on the oxidizer line to engine 2; and an unexpectedly large drop in helium supply pressure when the release valve was actuated to pressurize the propellant feed system. Postflight analysis indicated that the oxidizer line heater did not have sufficient capacity to keep the line temperature in the thermostat cycling range, although it was adequate to keep it above the 0°F lower limit. The larger than expected pressure drop was found to be caused by a transducer null shift which occurred at firing of the pressurization squib (Ref. XVII-32).

During the 9.8-sec midcourse firing the vernier engine strain gages indicated that engines 1 and 2 fired normally and that engine 3 failed to fire, as shown in Fig. XVII-33. Note that engines 1 and 2 were initially throttled down in an attempt to maintain a stable vehicle attitude, but, during the thrusting, the acceleration loop partially overcame the attitude loop and raised their thrust commands. The difference between the thrust commands and the strain gage thrust telemetry was caused by engine heating effects on the strain gages.

These thrust levels resulted in a spacecraft spin rate of 1.22 rev/sec. Thirty-nine subsequent attempts to obtain ignition of vernier engine 3 were unsuccessful and resulted in the spacecraft rotational rate being increased to 2.43 rev/sec. The thrust pattern for each attempt was the same: engines 1 and 2 throttled to a minimum thrust, and engine 3 commanded to maximum thrust, but never produced more than approximately 2 lbf.

Strain gage data, supported by changes in other telemetry data, indicated that during burn 27, the shutoff valve on the leg 1 thrust chamber assembly failed to close until approximately 1.5 sec after engine shutoff was commanded. This anomaly may have been caused by high friction in the shutoff valve and did not appear to be related to the engine 3 failure (see Subsection A-2-e).

When the available battery power decreased steadily, it was decided to fire the main retro engine at $L+45$ hr, and communication with the spacecraft was lost approximately 30 sec after retro motor ignition.

An extensive review of the behavior of the *Surveyor II* spacecraft propulsion and associated systems during the mission was performed during and after the flight. Although it was not possible to pinpoint the precise failure mode, it was possible to establish that the fuel flow through engine 3 appeared normal for all attempted firings and that the oxidizer flow was approximately 5% of the commanded rate. The most probable explanation of the failure was oxidizer injector clogging caused by corrosion of the nickel injector with MON-10 in the presence of atmospheric moisture during prelaunch

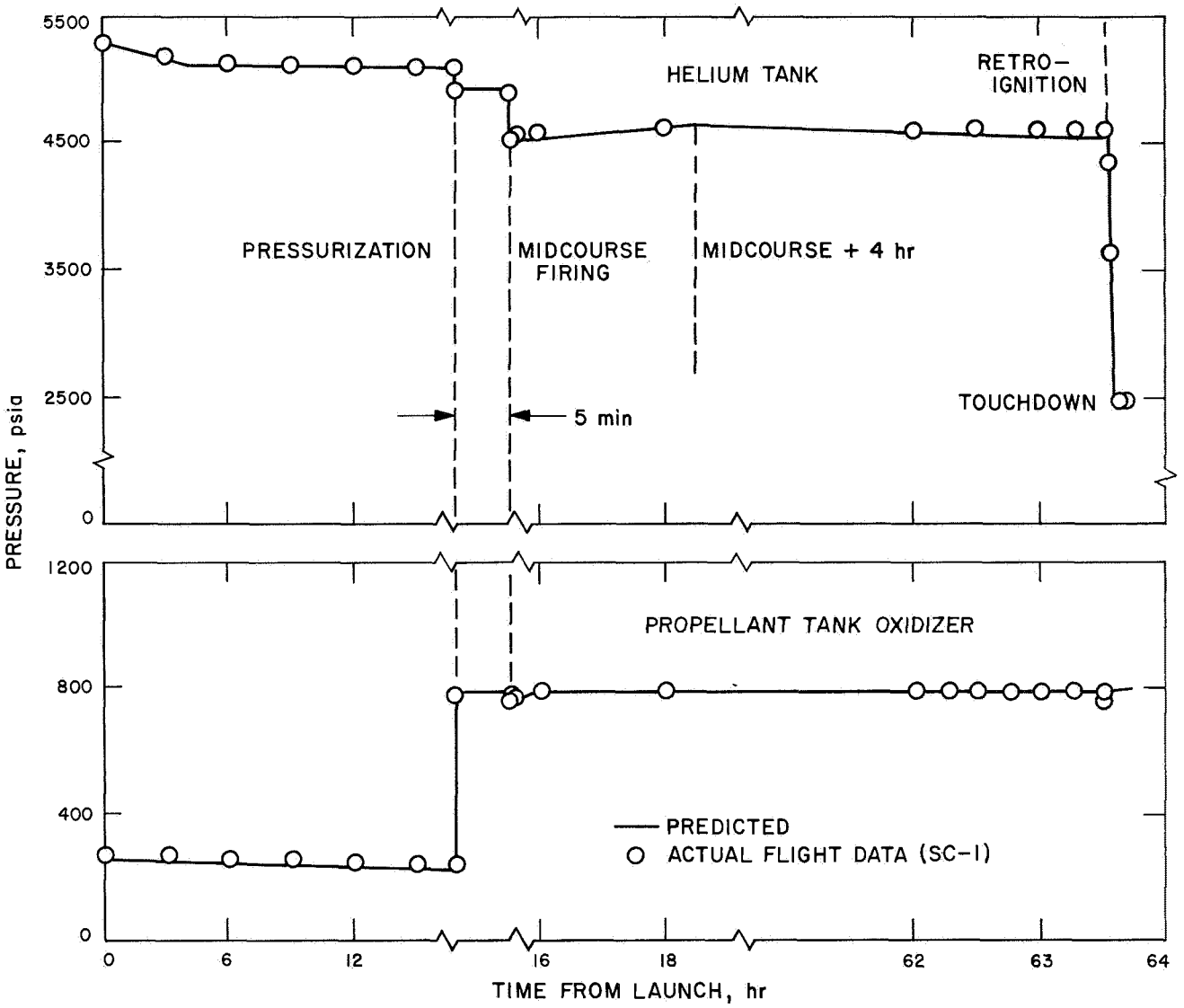



**Fig. XVII-32. Typical propellant and helium tank pressure-vs-time curves**

activities (see Subsection A-2-e). Consequently, on SC-2 and subsequent spacecraft the vernier engines were vacuum purged from the time of propellant loading to $L - 90$ min. In addition, preflight testing was extended to include a flow bench test of the engine using referee propellants, with commands to the engine supplied from the vehicle flight control unit. Increased emphasis was placed on system and fluid cleanness, and at each loading and offloading of the system, fluid samples were subjected to millipore filter analysis. Engine preflight testing was also extended to define the cleanness level of solvents flowing through the engine and to define the on/off valve electrical characteristics. A flight pressure solvent leak test before propellant loading was also incorporated. The tests are described in Subsection A-4.

2. *Surveyor IV*. In the period from *Surveyor IV* launch to main retro motor ignition, all the spacecraft telemetry indicated a normal mission. Before the abrupt loss of signal 39 sec after main retro ignition, all *Surveyor IV* VPS parameters were normal and at or near their predicted levels with only one difference from previous missions. This difference was the modulation of the thrust command to engines 1 and 2 during the retro period. Thrust command to engine 3 were only slightly modulated during this period; no modulation in any of the engine thrust commands occurred during the midcourse correction. The peak-to-peak modulation of engines 1 and 2 thrust commands was 3–6 lbf, compared to an engine throttling range of ±37 lbf. The average values of engines 1 and 2 thrust were close to the anticipated

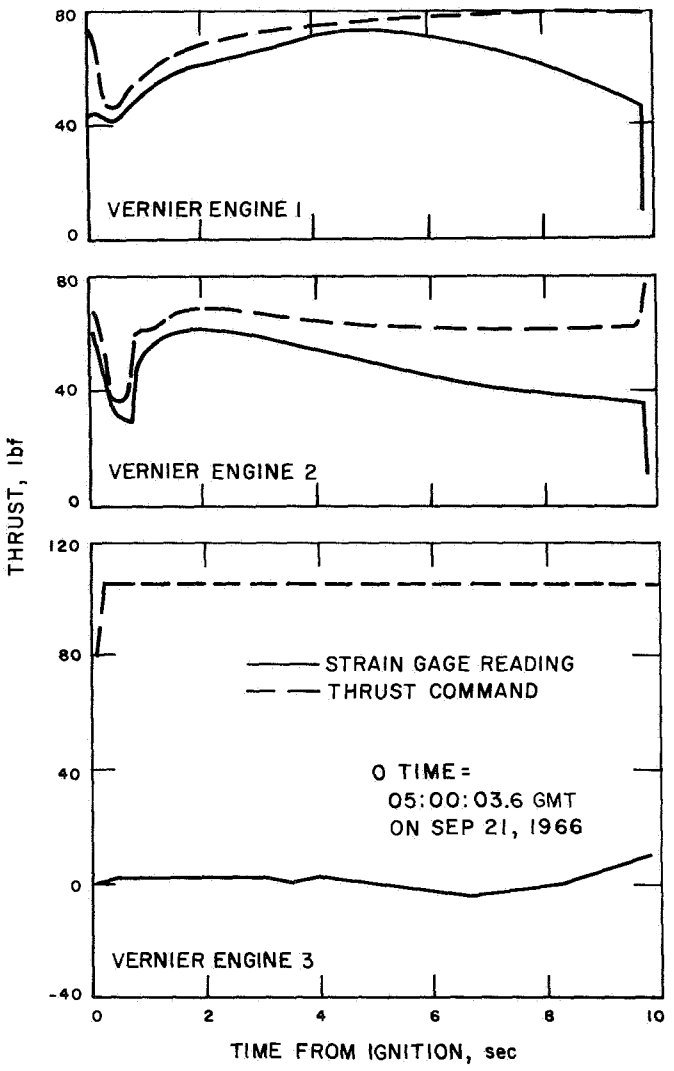



**Fig. XVII-33. *Surveyor II* strain gage and thrust command signals at midcourse**

midthrust level of 66.7 lbf. This small-amplitude modulation did not threaten the capability of the vernier engines to control the attitude of the spacecraft because the amplitude of the modulation was much less than the throttling range of the engines. It does not appear that this anomaly was symptomatic of a failure that could have caused the abrupt loss of signal from the spacecraft.

3. *Surveyor V.* The *Surveyor* V VPS successfully performed the necessary midcourse correction and terminal descent sequence. However, the terminal descent sequence required major modifications during the flight because the helium regulator failed to lock up after premidcourse pressurization. A postlanding vernier engine static firing experiment was also conducted successfully on this mission (Ref. XVII-33).

Vernier propulsion system parameters during launch and the premidcourse coast period were all normal and well within the allowable range. After completion of the premidcourse attitude change maneuvers, vernier pressurization was commanded in accordance with the normal mission sequence. Vernier propellant tank pressurization was accomplished by firing the helium release squib and allowing high-pressure helium gas to enter the inlet port of the helium pressure regulator. The helium regulator allowed a high flow rate of helium until the regulator outlet pressure reached the normal regulation pressure ($\approx$730 psia). At this point the pressure forces on the regulator diaphragm overcame the spring forces and the regulator began to close and restrict the flow rate. The regulator was normally completely closed at 770 psia and prohibited the flow of gas until the downstream pressure was decreased. Figure XVII-34 shows the fuel and oxidizer tank pressures at vernier pressurization. It should be noted that the pressures rose rapidly to 750 psia and then slowly rose to 825 psia, the relief valve opening pressures. At this point the relief valve opened just enough to allow overboard leakage such that the tank pressures remained constant. Thus, the spacecraft data agreed with what would be expected for a regulator that failed to lock up.

The first midcourse correction (vernier firing 1) was executed normally about 2 min after vernier pressurization. The regulator leakage in the lockup condition did not affect the midcourse correction. Vernier engine performance during the midcourse correction was normal, and start and shutdown transient performance were well within allowable limits.

After vernier engine cutoff, the propellant tank pressures returned to the relief valve settings. Overboard leakage was confirmed by a drop rate of 10 psi/min in the helium supply tank pressure. The helium supply tank pressure history is shown in Fig. XVII-35.

Three additional vernier engine firings were then performed in an attempt to clear and lock up the pressure regulator. During each firing the flow of propellants from the tanks caused the pressure to drop until it reached the regulation level. At this point the regulator opened and permitted helium to flow and prevent the pressure from dropping further. It was hoped that this repeated opening action would clear the seat area and allow the regulator to close completely. Vernier engine firings 2–4 were executed for this purpose, but did not significantly reduce the helium leakage rate, and attempts to stop the leakage were abandoned.

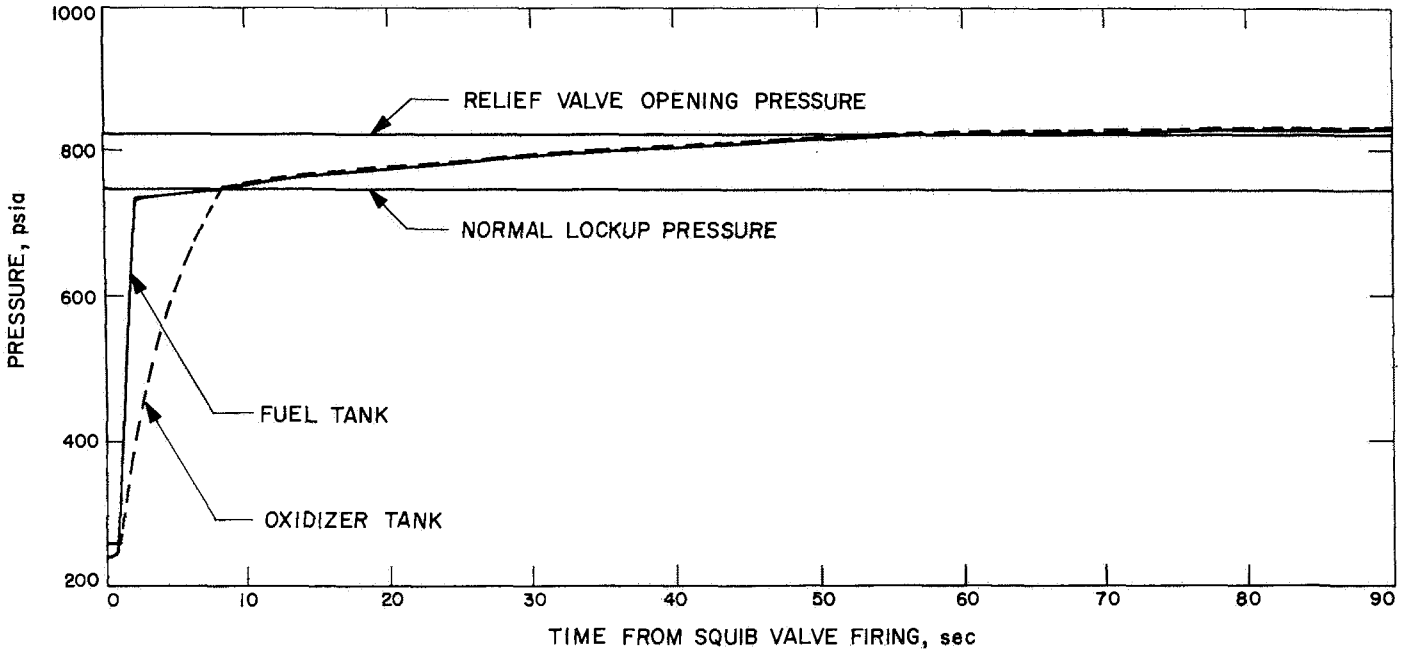



**Fig. XVII-34. Vernier propellant tank pressurization prior to *Surveyor V* midcourse correction**

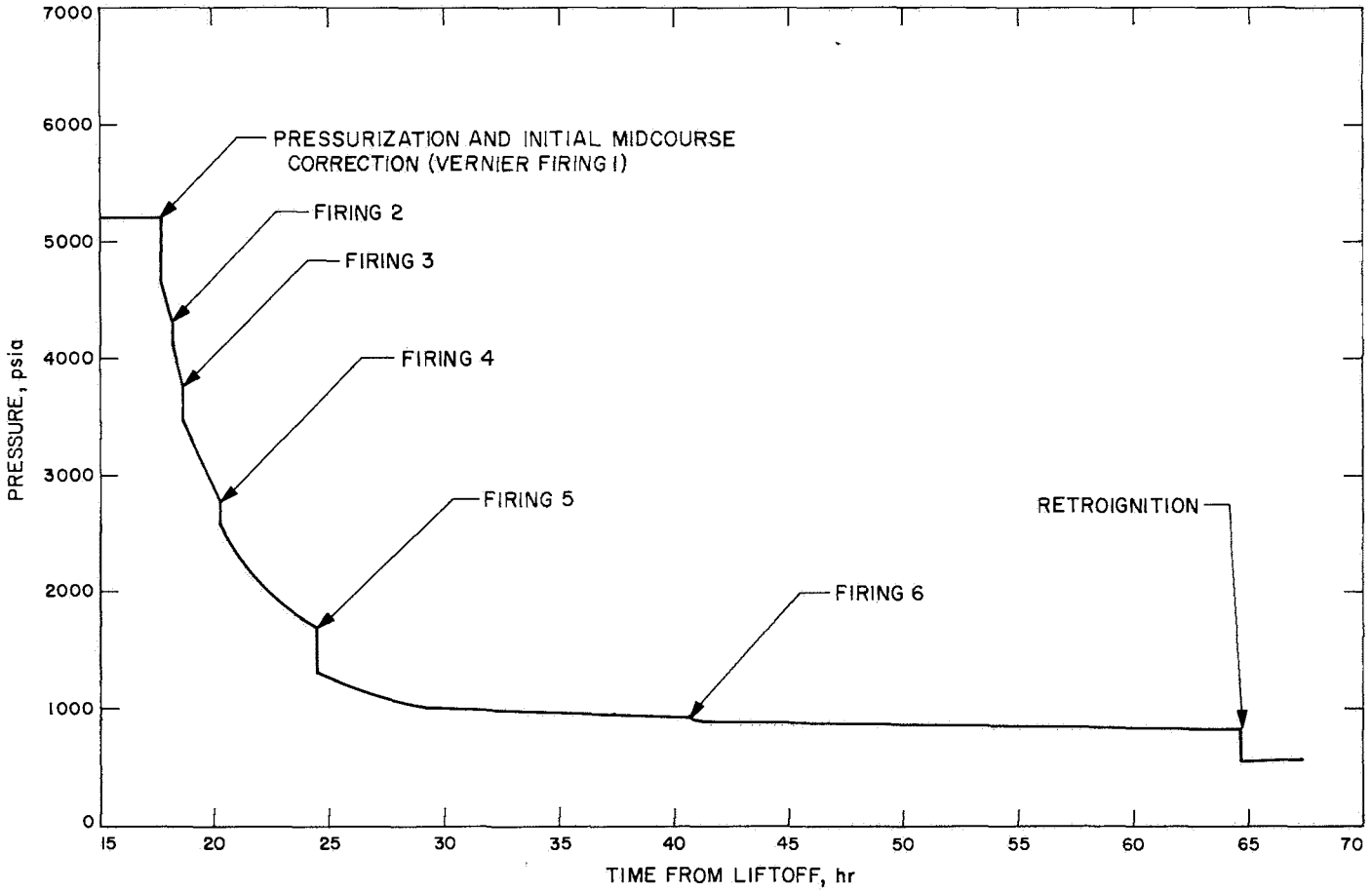



**Fig. XVII-35. *Surveyor V* helium tank pressure decay following midcourse correction**

The operation of the system, when the pressure regulator failed to lockup, was to slowly leak gas overboard through the relief valves. Eventually, when the helium tank pressure dropped to the relief valve setting, the overboard leakage would stop and the system would remain at just below the relief pressure. (The *Surveyor V* system reached this point about 10 hr before terminal descent.)

The capability of the vernier engines to operate at low propellant feed pressures was evaluated in detail during the mission. Special engine flow tests simulating low propellant pressures were conducted at the JPL Edwards Test Station to determine the thrust control capability as a function of propellant feed pressure. The results are shown in Fig. XVII-36. It should be noted that at propellant supply pressures between 550 and 500 psia, the oxidizer-to-fuel mixture ratio begins to vary significantly from the nominal 1.5, and, as a result, the thrust capability begins to drop substantially. This characteristic and the loss of all thrust capability at a pressure of 450 psia are caused by a fuel pressure regulator in the engine that closes when the pressure in the engine cooling jacket drops below 450 psia. The thrust characteristics calculated for each *Surveyor V* engine were very similar to those of the test engine shown in Fig. XVII-36. A minimum operating propellant supply pressure of 500 psia was established from these data.

Vernier engine firing 5 was performed to lighten the spacecraft and reduce the vernier propellant requirements during terminal descent. Burning this additional propellant also increased the volume of gas inside the propellant tanks for the terminal descent sequence. A final midcourse correction (firing 6) was made to correct the trajectory aiming point to the preplanned location; this also slightly increased the volume of gas inside the propellant tanks. Since all the vernier engine firings were conducted before the helium tank pressure had leaked down to the propellant tank pressure, the final state of the propulsion system for the terminal descent was at 825 psia (the relief valve settings) for the propellant tanks and the helium tank. Because of the many vernier engine firings, the total gas volume was 3240 $in.^3$, which included the 1290 $in.^3$ volume of the helium tank.

The results of calculations made to determine the predicted drop in propellant supply pressure as propellants were used from the tanks are shown in Fig. XVII-37. This prediction was verified before the *Surveyor V* lunar landing by a special test at the HAC propulsion test site. A complete VPS on the S-6 test vehicle was loaded with alcohol to simulate the fuel, and freon to simulate the oxidizer. The liquid volumes and pressures in each tank simulated the *Surveyor V* system. The S-6 engines were operated with a mid-thrust command until the propellant tank pressure dropped to 500 psia. The simulated propellants that flowed through each engine were caught and weighed. The total weight expelled was in good agreement with the analytical predictions (Fig. XVII-37). These data and the engine thrust capability for reduced supply pressures yielded a maximum allowable propellant usage during terminal descent of 70 lb. This limit was used to determine the optimum burnout altitude and velocity. The actual propellant usage during the *Surveyor V* terminal descent and the final supply pressure were in good agreement with predictions and special test data as shown on Fig. XVII-37.

The terminal-descent sequence was also modified to maximize the vernier propellant available for the RADVS-controlled phase of the terminal descent. One important part of the modification was reducing the delay time between retrorocket burnout and retro case ejection. A delay time of 5 sec was initially chosen, but after reexamination of retro thrust tailoff characteristics, an 8-sec delay was adopted. This should be compared with the 12-sec delay normally used.

The vernier engine thrust command signals indicated that thrust command saturations occurred just before the 10-ft/sec mark during terminal descent. This was caused by the low propellant supply pressure near the end of the terminal descent. These data indicate that the vernier engines were approaching the point where their thrust capability was severely degraded. This was as predicted based on the preterminal descent calculations.

Results of an extensive review of the helium pressure regulator failure (Subsection A-3-b) show the most probable cause was contamination that triggered major gas erosion damage to the helium regulator valve seat. This would result in an internal leak through the regulator, causing the outlet pressure to increase to a level which would cause the fuel or oxidizer relief valve to vent to space. Changes to the handling and checkout procedures for the helium pressurization system were made significantly to reduce the probability of introducing contamination into the system. These included a lockup performance test in the final phase of preflight testing.

***c. Postlanding performance.*** After the soft landing on the lunar surface the VPS components were exposed to the sun for the major portion of the lunar day. The

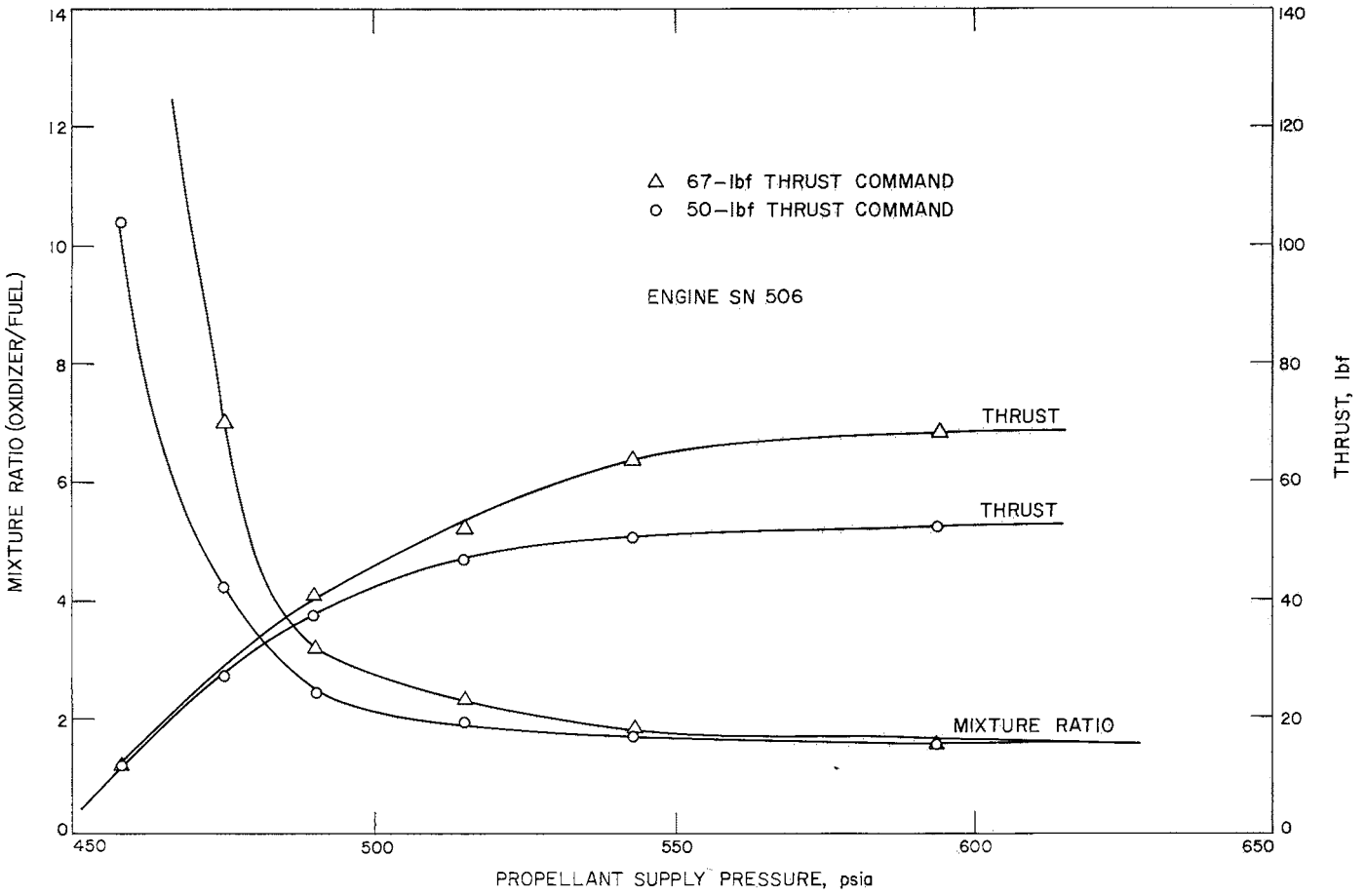



**Fig. XVII-36. *Surveyor V* vernier engine flow test results**

resulting temperatures were well above the operational limits set for the elements of the system. Shown in Fig. XVII-38 are the overall temperature ranges to which the VPS components were exposed during the lunar day following touchdown. The consequent helium expansion and elevation of propellant vapor pressures caused the oxidizer and fuel relief valves to cycle, venting excess gas from their respective systems. Table XVII-12 contains a summary of propulsion system leaks and malfunctions during the postlanding phases of each mission (see Refs. XVII-23 and XVII-24).

On *Surveyor I*, the oxidizer relief valve eventually failed open during this venting process because of high temperature exposure, and vented the oxidizer system. A similar loss of oxidizer and helium pressure occurred on spacecraft SC-3. The cause of this pressure loss has not been determined.

On *Surveyors V*, *VI*, and *VII*, the location of the check and relief valves was changed to the upper spaceframe member above the helium tank. On previous vehicles these valves were mounted on the helium tank. Also on *Surveyors V* and *VI* attempts were made to shade the check and relief valves with the antenna and solar panel. This helped prolong the life of the system. Positions of the antenna and solar panel to provide the desired propulsion system shading, while not sacrificing science and TV requirements, were determined using a ⅛ scale model of the *Surveyor* spacecraft and a collimated light source (see Section XV-C-3).

This shading was done to permit a vernier engine static firing experiment to be made with *Surveyor V* and a spacecraft hop experiment to be performed with *Surveyor VI*. (These postlanding firings are described in detail below.) The attempts to prolong the life of the propulsion subsystem were quite successful. *Surveyors V* and *VI* both survived until late in the lunar day when in each case the oxidizer tank 1 liquid side O-ring failed, causing the loss of liquid oxidizer and subsequent loss of pressurant.

The *Surveyor VII* spacecraft also survived essentially intact until late in the lunar day (Ref. XVII-34). The low

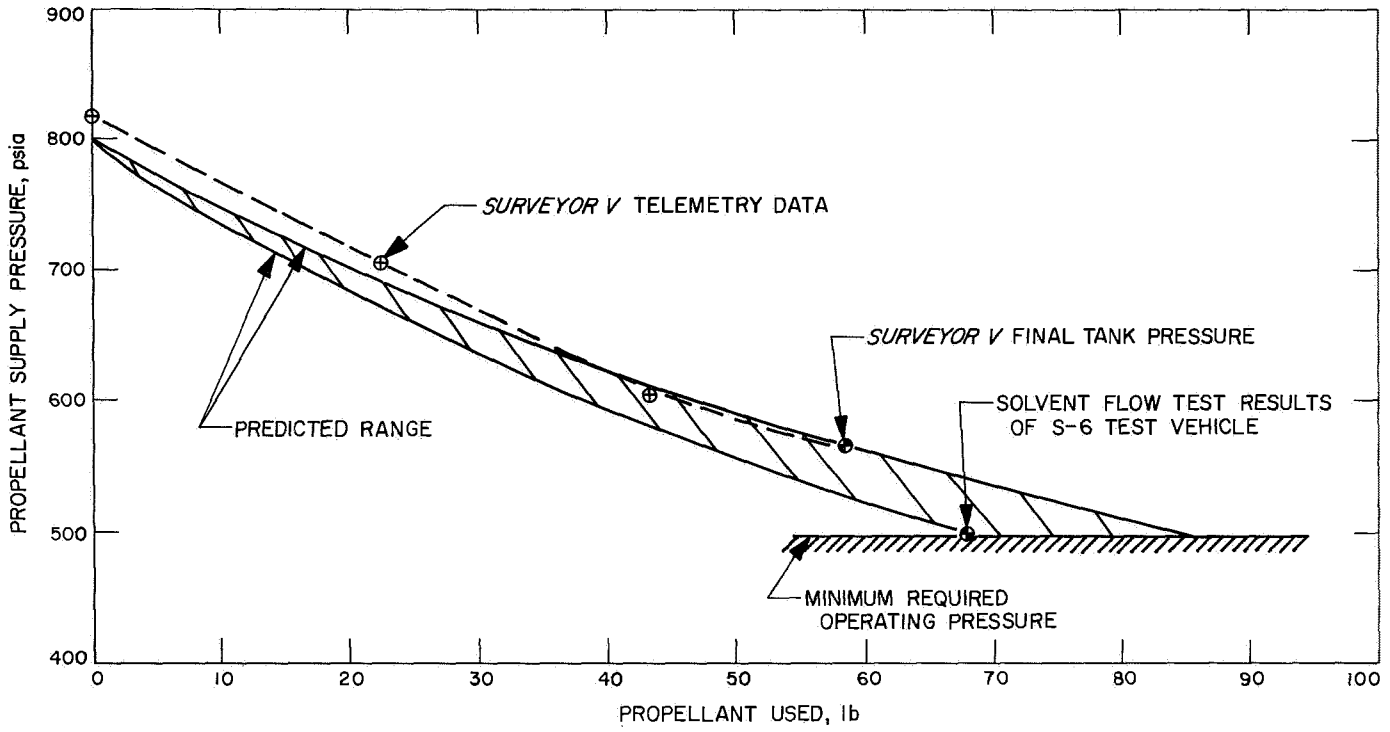



**Fig. XVII-37. Surveyor V propellant supply pressure decay during terminal descent**

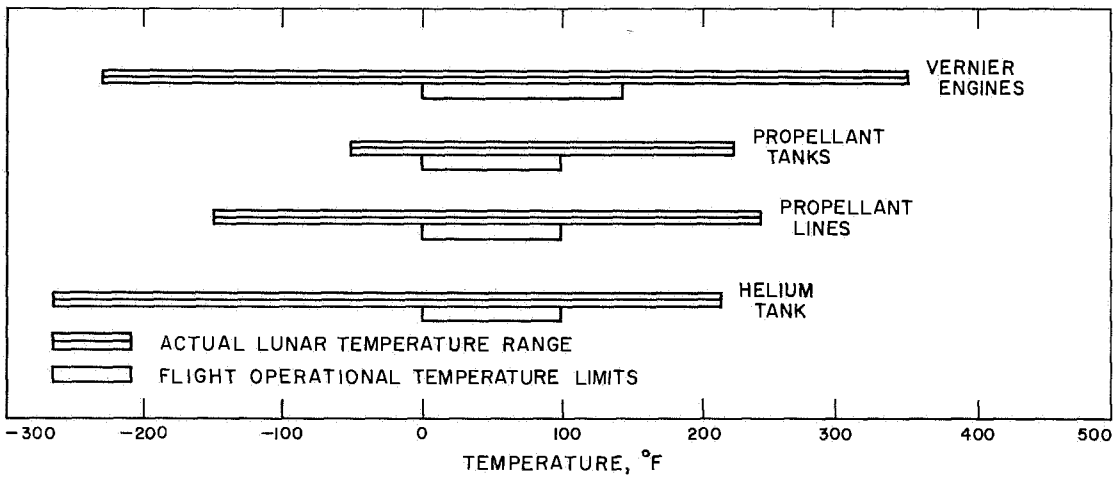



**Fig. XVII-38. Postlanding vernier propulsion system temperature ranges (except *Surveyors II and IV*)**

latitude of the landing site resulted in sun elevation angles always less than 50 deg. This made it impossible to shade the propellant tanks and engines by moving the solar panel and antenna. Shading the relief valve was difficult because of the low sun angle and because it conflicted with higher priority shading requirements for the science experiments. Since the sun remained between legs 2 and 3 during the entire lunar day, propulsion system components in this area reached temperatures higher than recorded on previous spacecraft.

Midway through the lunar day, when the check and relief valves were exposed to direct sunlight and were venting, some erratic behavior of the oxidizer check and

## Table XVII-12. Vernier propulsion system leaks and malfunctions after lunar landings

| Spacecraft | Time on moon before leak or malfunction occurred, hr | Type of leak or malfunction | Telemetry indications | Probable cause of leak or malfunction |
|---|---|---|---|---|
| *Surveyor I* | 104 | Gas leak on oxidizer side | Rapid loss of oxidizer and helium pressures<br>Smooth temperature drops of about 20°F on helium and oxidizer tanks<br>Oxidizer line temperatures increased approximately 25°F, indicating flow from hot engines to cooler tanks as tanks were depressurized; tank temperatures were initially cooler than line temperatures, whereas engines were hotter | Oxidizer relief valve failed |
| *Surveyor III* | 165 | Initially a gas or liquid leak on oxidizer side; if initially a liquid leak, it developed into a gas leak at time of pressure loss | Rapid loss of oxidizer and helium pressure | Undetermined |
| *Surveyor V* | 178 | Liquid oxidizer leak at tank 1 followed by gas leak after depletion of oxidizer in tank | Loss of oxidizer and helium pressure<br>100°F drop in oxidizer tank 1 temperature<br>20°F drop in retro attach bolt 1 temperature<br>Surveyor pictures showed that Mylar wrap on oxidizer tank 1 had been pressurized from within during time of pressure loss<br>Tank cooldown rate after sunset was greater for oxidizer tank 1 than for other two tanks. This indicated liquid loss of about 5 lb from tank 1 | O-ring on oxidizer tank 1 degraded by high temperature liquid oxidizer |
| | 273 | Gas leak on fuel side | Loss of fuel pressure<br>Second lunar day tank temperatures indicated that liquid fuel had not leaked from tanks but had frozen in the tanks during the lunar night | Undetermined whether failure occurred at fuel relief valve, solenoid valve, or gas-side O-ring on any of three fuel tanks |
| *Surveyor VI* | 228 | Liquid oxidizer leak at tank 1 followed by gas leak after depletion of oxidizer in tank | Temperature perturbations of about ±10°F on oxidizer tank 1<br>Loss of oxidizer and helium pressure<br>Tank cooldown rate after sunset was greater for oxidizer tank 1 than for other two tanks; as on *Surveyor V*, this indicated liquid loss from tank 1, loss was approximately 5 lb of liquid oxidizer | O-ring on oxidizer tank 1 degraded by high-temperature liquid oxidizer |
| *Surveyor VII* | 91–191 | Erratic cycling and leakage at oxidizer relief valve | When exposed to the sun on eleventh vent cycle, oxidizer relief valve crack and reseat pressures began deviating from those established during first 10 vent cycles; those established were an 850-psi crack and an 830-psi reseat. On eleventh cycle valve cracked at close to 850-psi, but did not reseat until 790-psi<br>During twelfth vent cycle valve did not crack until 870-psi<br>After twelfth vent cycle oxidizer pressure began to decay at 1.6 psi/hr; calculations proved that the oxidizer system had developed a slow gas leak<br>Leak stopped after relief valve was reshaded by repositioning planar array antenna | Coining and degradation of the valve seat, reduction in spring constants, and differential thermal expansion between parts of valve resulted in erratic behavior and leakage when valve was at high temperature |

## Table XVII-12 (contd)

| Spacecraft | Time on moon before leak or malfunction occurred, hr | Type of leak or malfunction | Telemetry indications | Probable cause of leak or malfunction |
|---|---|---|---|---|
| *Surveyor VII* (contd) | 260 | Liquid fuel leak at engine 2 | Rapid 90°F negative change in engine 2 temperature as fuel vaporized and cooled engine<br>Elevated fuel line temperature as line was heated by warm propellant<br>Analysis of pressure and temperature data indicated a loss of liquid fuel<br>Analysis of tank cooldown rates after sunset indicated liquid leakage of about 1 lb | Fuel poppet in engine 2 shutoff valve failed; cause was seat degradation after high-temperature (288°F) exposure to fuel |
| | 270 | Oxidizer check valve stuck almost shut | Oxidizer pressure fell below the helium regulator pressure<br>Correct regulator operation confirmed by fuel pressure data | Check valve malfunction probably resulted from seat degradation after high-temperature exposure |
| | 289 | Gas leak developed and resealed on oxidizer side | Rapid loss of 100-psi oxidizer pressure at a level less than the relief valve cracking pressure<br>Relief valve had shown erratic behavior on Jan 14<br>Calculations indicated a loss of approximately 0.08 lb of helium and that leakage stopped after several hours | Oxidizer relief valve cycled at pressures lower than normal; this resulted from seat coining, a decrease in spring constant at high temperatures, and differential thermal expansion within the parts of the valve |
| | 305 | Oxidizer check valve opened slightly but remained stuck | Rapid gain of 70 psi in oxidizer pressure as orifice area increased<br>Helium flow through stuck check valve resulted in oxidizer pressure remaining approximately constant even through vapor pressures within the tanks were dropping due to dropping temperatures<br>Helium flow and oxidizer pressure stablized after downstream pressure reached 650 psi<br>Helium pressure continued to drop but remained above 2000 psi; because fuel pressure was being maintained above 730 psi, indications were that oxidizer check valve was still stuck almost closed<br>Calculations based on temperatures and pressures indicated no gas leakage | Pressure drop of 150 psi across valve caused it to open slightly; degraded seat still prevented normal operation and caused valve to stick |
| | 316 | Oxidizer check valve opened further | Rapid goin of 110 psi on oxidizer pressure as orifice area was again increased; oxidizer pressure stabilized at 760 psi | Pressure drop of 80 psi across valve caused it to open |
| | 320 | Gas leak on oxidizer side | Loss of more than 600 psi in oxidizer pressure; leak continued through loss of data 24 hr later | Oxidizer relief valve finally failed; failure was probably the result of an eroded seat |

**Table XVII-12 (contd)**

| Spacecraft | Time on moon before leak or malfunction occurred, hr | Type of leak or malfunction | Telemetry indications | Probable cause of leak or malfunction |
|---|---|---|---|---|
| *Surveyor VII* (contd) | ≈320 | Oxidizer check valve was again stuck in an almost closed position | During and after the oxidizer relief valve failure, fuel pressure was still being regulated but oxidizer pressure dropped more than 400 psi below regulated pressures | After the check valve had opened as indicated above and after the oxidizer pressure had risen to 760 psi, the pressure drop across the valve was near zero; the pressure gradient then became negative and the valve closed; after closing the valve again became stuck |
| | ≈324 | Continuing gas side leak on fuel side | Analysis of fuel side pressure and temperature data indicated the continued loss of pressurant from the fuel side | Most probable cause is that gas leakage developed through engine 2 fuel poppet after liquid leak depleted fuel not yet frozen in tank; other sources would have been the fuel relief valve, the solenoid valve seat, and gas-side O-rings on fuel tanks |
| | ≈335 | Loss of liquid oxidizer from oxidizer tank 3 | The general behavior of the oxidizer tank 3 postsunset cooldown indicated the tank liquid content to be approximately normal at sunset and that later the tank was nearly empty<br>An increase in the temperature decay rate indicated a large reduction of tank thermal capacity<br>Tank temperature profile during propellant freezing indicated little oxidizer remaining<br>Analysis of above indicated that aproximately 3 lb had leaked from the tank | Leak at liquid side O-ring on oxidizer tank 3 after O-ring had been degraded by high-temperature oxidizer |

relief valves was noted. The relief valve ultimately failed and caused loss of pressure from the system. However, the failure of the oxidizer relief valve was not the failure that first caused the loss of system capability. This resulted from a liquid fuel leak at the vernier engine 2 shutoff valve fuel poppet.

*1. Vernier engine static firing experiment (Surveyor V).* A vernier static firing experiment was performed onboard *Surveyor V* at about 53 hr after landing (see Ref. XVII-33). Minimum vernier thrust (approximately 25 lbf for each engine) was commanded for 0.55 sec. Figure XVII-39 shows the vernier engine thrust profile during the static firing experiment. A very limited amount of telemetry data was available during the firing; this made it necessary to use engine data to construct the best estimate thrust profile through the limited *Surveyor V* data points. The 17 lbf of thrust measured for engine 2 was as expected based on the initial engine temperature of 274°F. At this temperature the oxidizer vapor pressure is 1100 psia. Because the oxidizer tank pressure was only 750 psia at this time, the oxidizer side of the engine must have been filled with oxidizer vapor rather than liquid. Because of this, the oxidizer flow rate was well below normal, resulting in the lower-than-normal minimum thrust level. The 274°F engine 2 temperature at ignition was well above the 220°F maximum limit for normal operation. For this very short (0.55-sec) firing it

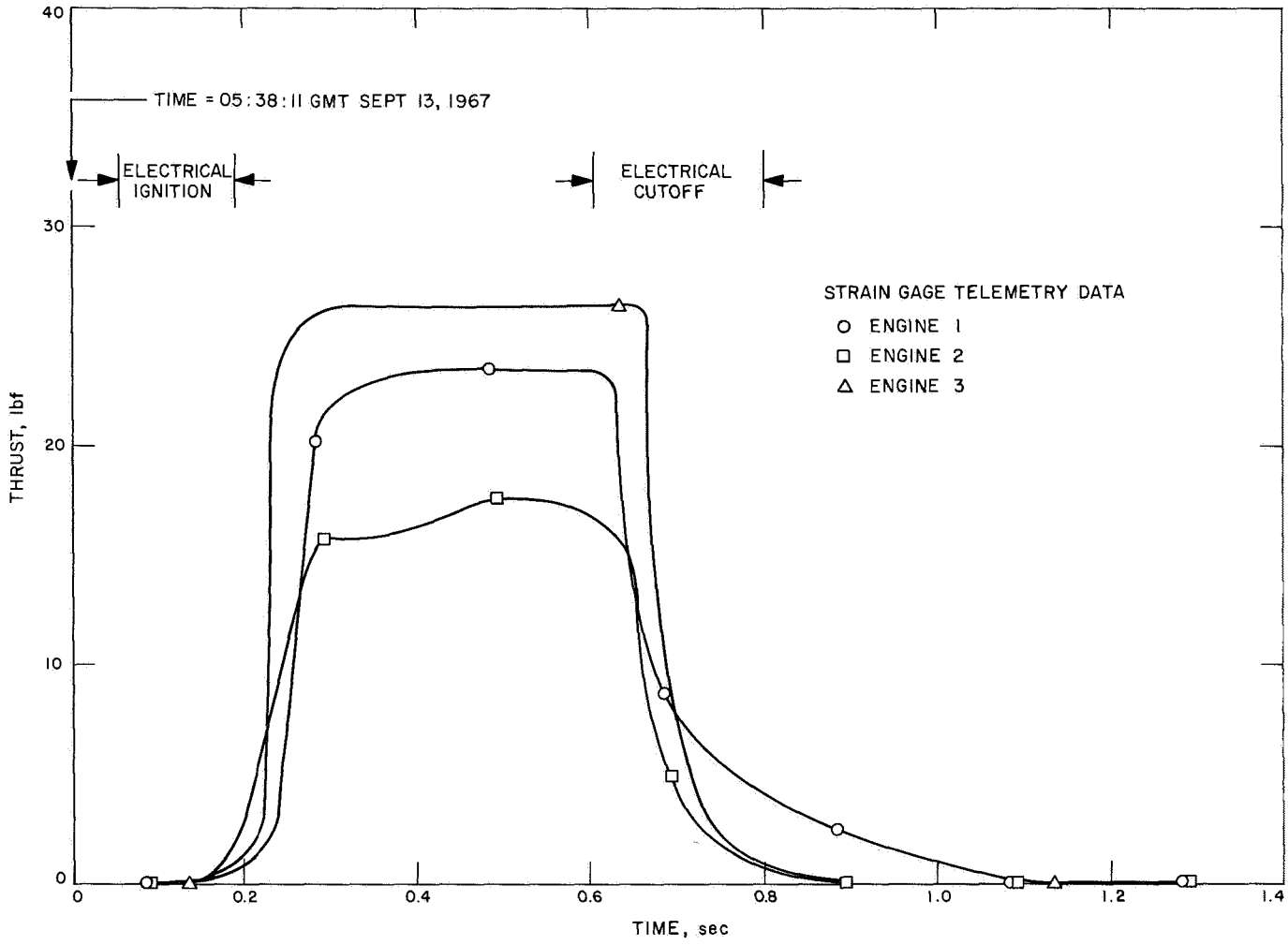



**Fig. XVII-39. *Surveyor V* engine thrust during vernier static firing experiment on lunar surface**

was not necessary that the engines perform normally. Even if the hot engine had failed to ignite, it would not have endangered the spacecraft.

*2. Vernier engine postlanding spacecraft hop experiment (Surveyor VI).* Shortly after landing, special precautions were taken to maximize the *Surveyor VI* VPS life (see Ref. XVII-32). On the *Surveyor V* spacecraft a liquid leak in oxidizer tank 1 had occurred about 7 days after landing. On *Surveyors II* and *III* oxidizer system leaks had occurred before lunar noon. The *Surveyor VI* antenna and solar panel assembly was used to shade the relief valves and hot oxidizer tanks in an attempt to extend the life of the VPS. The optimum positioning was determined using a ⅛ scale model and a collimated light source. In most instances a compromise between alpha scattering, TV, and propulsion system shading had to be made. The relief valves were kept continuously shaded using this method. This reduced their temperature by an estimated 100°F and prevented failure. Oxidizer tanks 2 and 3 were on the sunlit side before lunar noon. By shading these tanks whenever possible, oxidizer tanks 2 and 3 temperatures were prevented from exceeding 160 and 180°F, respectively. On *Surveyor V*, oxidizer tank 1 leaked when the temperature reached 193°F.

Near lunar noon, when the sun was almost directly overhead, all three engines could be shaded with the antenna and solar panel, although not all at the same time. After lunar noon, it was impossible to shade engine 1 because of the sun position. This meant that the lunar noon period was the last opportunity to perform a spacecraft translation until late in the lunar day. Since it was considered unlikely that the VPS would

remain leaktight until late in the lunar day and since the major science experiment commitments had already been satisfied, it was decided to perform a lunar hop experiment.

The vernier engines were brought below their 220°F limits by alternately shading each of the engines. At the time of firing, the engine temperatures were all below 210°F. The thrust-vs-time curve for each of the vernier engines is shown in Fig. XVII-40.

The planned profile utilized a 2-sec firing at 150 lbf total thrust with an initial pitch offset of 6 deg. The vernier firing was normal except that the firing time was 2.5 rather than 2 sec because the spacecraft did not respond to the first shutdown command but did respond to the second (a redundant command). All engines shut down normally. The propulsion system performed as predicted; however, engine 1 appears to have shut down slightly later than engines 2 and 3. This caused the spacecraft to pitch up about 3 deg before landing. Because the gyro null position during flight was with leg 1 pitched down 6 deg, this small cutoff dispersion helped level the spacecraft before landing. The landing was completely successful.

## B. Main Retrorocket Motor

The *Surveyor* main retro motor provided the major portion of spacecraft deceleration during the terminal descent. It was attached at three points on the spacecraft frame near the landing leg hinges with explosive nut disconnects for postfiring ejection of the spent rocket hardware. Friction clips around the nozzle exit plane provided attachment points for the altitude marking radar, which was ejected by exhaust gases at retro motor ignition.

The main retroignition and release device squibs were operated from a 19-A constant current source. Commands were initiated by the flight control system.

Table XVII-13 shows a summary of the retro motor program milestones.

### 1. Flight Configuration Design Description

The main retro motor (Fig. XVII-41) was a spherical, solid-propellant unit with a partially submerged nozzle to minimize overall length. The motor was nominally 37 in. in diameter and had an overall length of 55 in. Total weight was about two thirds of the injected spacecraft weight. The main retro motor had two configurations, designated A21 and A22, which contained nominally

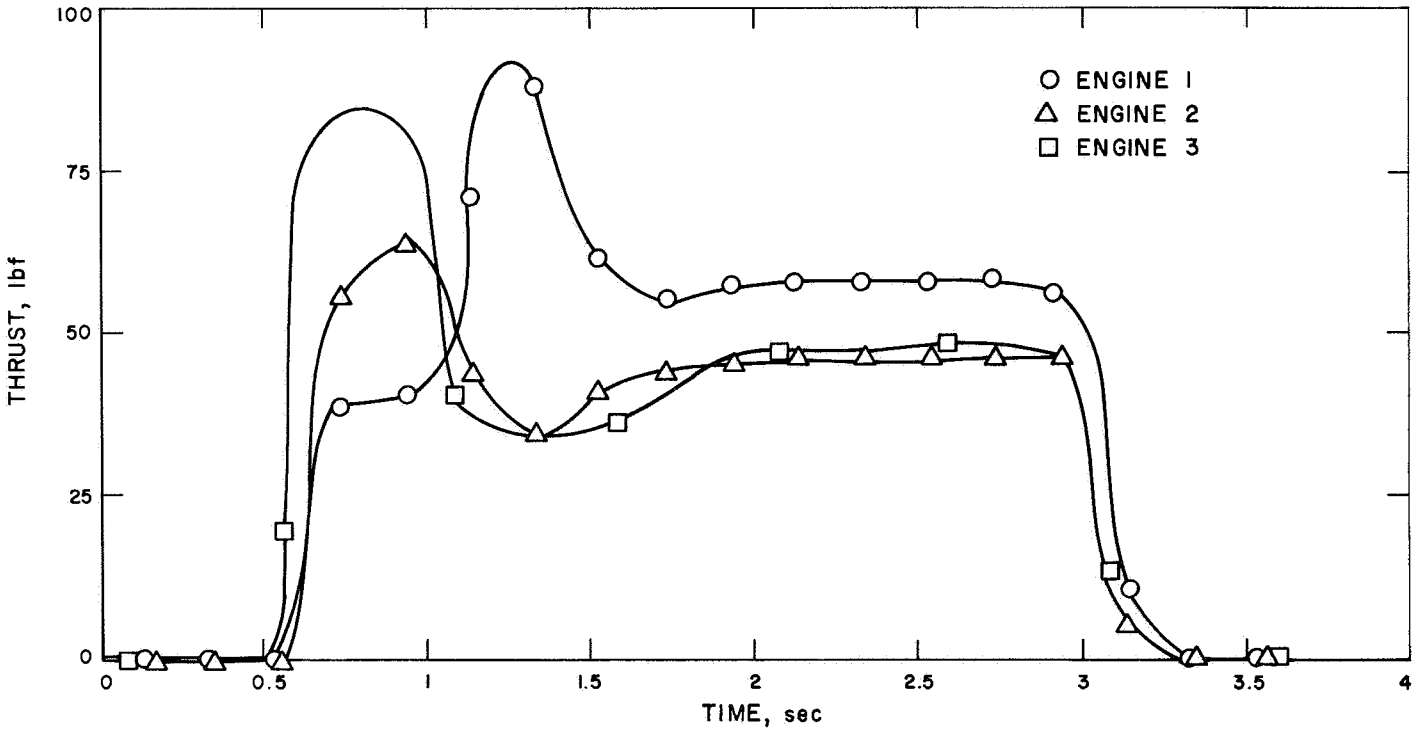



**Fig. XVII-40. *Surveyor VI* vernier engine thrust during translation**

**Table XVII-13. Retro motor program milestones**

| Date | Milestone |
|---|---|
| Apr 1961 | Contract awarded and design activities started |
| Aug 1961 | First heavywall full-scale motor manufactured and tested |
| Oct 1961 | First motor temperature-cycled |
| Feb 1962 | Propellant changed to TPH-3062, final flight formulation |
| Mar 1962 | Flightweight case evaluated in static firing; first test in altitude simulator |
| Apr 1962 | A21 motor introduced into the program to replace the A25 configuration |
| Jun 1962 | First altitude tests at AEDC revealed low delivered specific impulse; nozzle contour and structural redesign begun |
| Oct 1962 | New nozzle contour tested at AEDC; low performance problem resolved |
| Feb 1963 | First redesigned nozzle structure tested; nozzle throat failed |
| Apr 1963 | Flight design motors vibrated and drop tested |
| Oct 1963 | First successful test of final flight nozzle design |
| Dec 1963 | Final flight nozzle design confirmed and accepted for qualification testing |
| Feb 1964 | Development program concluded |
| Apr 1964 | Began fabrication of qualification motors |
| May 1964 | Began environmental testing of qualification engines |
| Sep 1964 | Six-component static firings conducted under altitude conditons at AEDC |
| Dec 1964 | Environmental testing of motors completed; grain design for A22 configuration begun |
| Feb 1965 | Manufactured A22 configuration motors for qualification testing |
| May 1965 | Motor qualification program completed |
| Jun 1965 | Three flight motors manufactured |
| Sept 1965 | First flight lot acceptance test motor successfully static fired |
| Mar 1966 | Two-year-old retro motor successfully static-fired |
| Jun 1966 | A21 retro motor operated successfully during *Surveyor I* mission |
| Dec 1966 | First rejection occurred of a flight motor |
| Apr 1967 | First A22 retro motor operated successfully during *Surveyor III* mission |
| Jan 1968 | Retro motor operated successfully during final mission, *Surveyor VII* |

1250 and 1300 lb of propellant, respectively. A data sheet showing motor weight breakdown and operating characteristics is shown in Fig. XVII-42. The major components of the retro motor were the case and attachment structure, nozzle assembly, internal insulation, ignition system consisting of igniter and safe-arm device, propellant grain, and external insulating blanket.

The case was a 36.7-in.-ID sphere made from Ladish D6AC steel, heat treated to a minimum yield strength of 200,000 psi (uniaxial). It was fabricated from two hemispherical forgings that were rough-machined to contour, then heat treated and final-machined to a minimum wall thickness of 0.037 in. The hemispheres were joined by tungsten insert-gas welding. The case wall was thickened adjacent to the weld area to provide additional strength in the heat-affected zone and to provide the strength required to accept and distribute the thrust loads from the thrust structure. Forward and aft ports were provided for installation of the igniter and nozzle, respectively.

The case was designed for a minimum yield pressure of 700 psi and a minimum burst pressure of 770 psi. Operating pressure of the retro motor was 585 psi maximum.

The structure that transmitted the rocket motor thrust to the spacecraft frame was made up of three skirts, three struts, and a collar. The three steel skirts were welded to the case at three locally thickened areas equally spaced around the equator. The collar was a split ring, fabricated from AISI 4340 steel and heat-treated to 150,000 psi ultimate strength, which was friction-fitted around the aft closure boss of the case. The strut was a wishbone structure machined from 7075 T-6 aluminum that connected the collar and the skirt and provided the point of attachment of the retro motor to the spacecraft. Figure XVII-43 shows the completed case and attachment assembly.

The nozzle assembly was approximately half submerged in the motor to minimize overall motor length. It was a composite structure consisting of a glass cloth–phenolic structural member running the length of the nozzle, an aluminum attachment ring, a monolithic throat insert of high-density graphite, a throat backup structure and exit cone liner of carbon cloth–phenolic material, and asbestos–phenolic insulating material on the outside of the submerged portion for protection from hot combustion-chamber gases. The nozzle exit cone was contoured for optimum multiphase flow expansion and had an expansion ratio of 53:1. The exit cone contained eight aluminum inserts for mounting of the altitude marking radar.

The case insulation provided thermal protection to the case during propellant burning to prevent weakening of

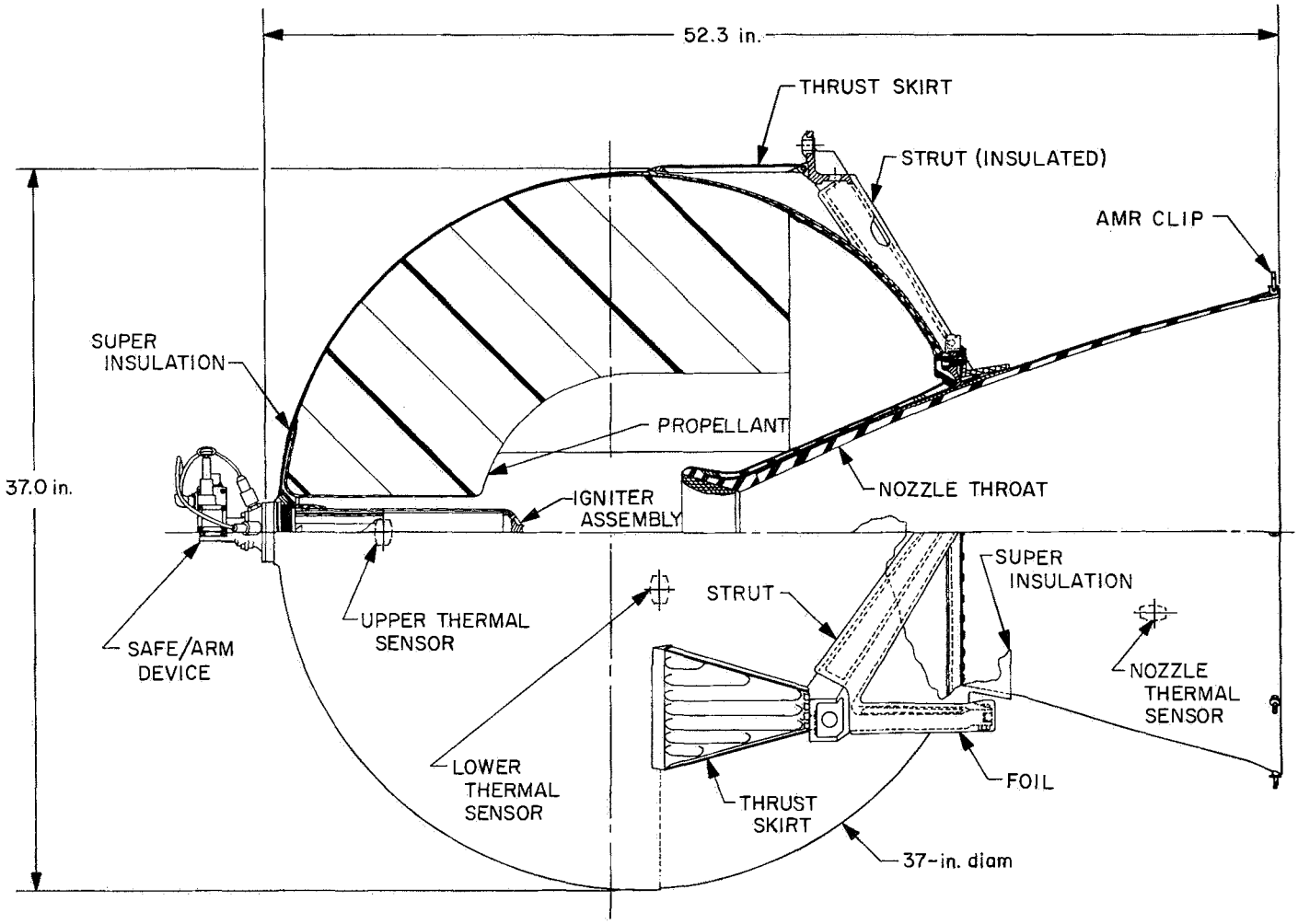



**Fig. XVII-41. Retro motor section**

the pressure vessel. The insulation, which was designed to keep the case temperature below 300°F during motor operation, consisted of a forward insulator and stress relief boot and an aft insulator and stress relief boot. These boots provided relief of thermally induced stresses in the propellant grain. The insulation material was an asbestos- and silicone-dioxide-filled Buna-N synthetic rubber designated Gen-Gard* V-44. The retro motor case insulation details are shown in Fig. XVII-44.

The propellant, designated TPH-3062, was a conventional composite-type solid propellant containing ammonium perchlorate oxidizer, powdered aluminum fuel additive, and a carboxyl-terminated polybutadiene binder system. The propellant solids loading was 86%.

The propellant grain was cast in an internal-burning, seven-point-star configuration and was bonded to the case. The grain configuration was designed to produce a nominally neutral thrust curve. Forward and aft insulation boots provided stress relief to prevent propellant cracking or separation from the case.

The ignition system consisted of an igniter threaded into the motor case and an externally mounted safe/arm device. The igniter was a cylindrical fiber glass case containing a cartridge-loaded, internal-burning, star-configuration propellant grain. The igniter grain was 0.6 lb of TPH 3062 propellant, the same propellant as the main motor grain. The igniter operated for approximately 1.2 sec at a maximum internal pressure of 1500 psi.

The safe/arm assembly, which was required by AFETR Range Safety, was an electromechanical assembly that performed the dual function of initiating rocket motor operation while in the armed condition and precluding

*Trademark of General Tire and Rubber Co.

| Weight, lb | Configuration | |
|---|---|---|
| | A21 | A22 |
| Total inert material | 139 | 139 |
| Case and attachments | 69 | 69 |
| Internal insulation | 12 | 12 |
| Nozzle | 49 | 49 |
| Ignition system, including safe/arm | 6 | 6 |
| External insulation | 4 | 4 |
| Miscellaneous | 3 | 3 |
| Propellant | 1250 | 1300 |
| Total assembly | 1389 | 1439 |
| Burnout weight | 125 | 125 |
| **Impulse** | | |
| Total impulse, lbf-sec | 362,000 | 376,000 |
| Specific impulse, lbf-sec/lbm | 289.5 | 289.5 |
| **Balance and alignment** | **Required** | **Actual** |
| CG shift, empty to loaded, in. | <0.030 | <0.011 |
| Nozzle CL offset from loaded CG, in. | <0.110 | <0.007 |
| Nozzle CL concentricity to mount hole circle, TIR, in. | <0.013 | <0.006 |
| Nozzle CL misalignment from attachment plane, in. | <0.970 | <0.640 |

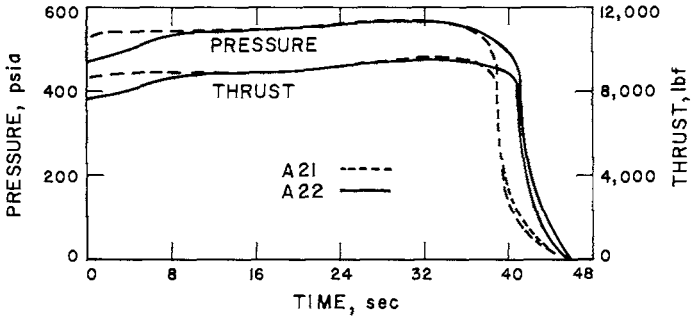



**Fig. XVII-42. Main retro motor characteristics**

the inadvertent ignition of the motor while in the safe condition. It was provided with a safety pin that mechanically prevented inadvertent electrical arming of the motor.

Both a visual and an electrical indication denoted whether the device was in the safe or arm position. The unit could be mechanically or electrically safed or electrically armed, and then, only when the safety pin had been physically removed. The safe/arm device upper housing performed the electromechanical drive function and contained a DC torque motor, gear train, friction clutch, and electrical switching components. The lower housing contained the ignition squibs, a blocking rotor, and a basket of pyrotechnic initiator pellets. Two electrically operated single-bridgewire squibs were provided for initiation of the firing train.

The thermal control design of the main retro motor was completely passive, depending on its own thermal capacity and external insulation during earth–lunar transit to minimize the decrease in temperature of the propellant grain and minimize the thermal gradient through the propellant grain, both of which tended to produce internal stresses in the grain.

The external insulation was a blanket consisting of 21 layers of aluminized Mylar plus an outer cover of aluminized Teflon. Very fine stainless steel wire was sewn into the Teflon cover to bleed off any static electrical charge that might have developed during handling. Figure XVII-45 shows the retro motor completely wrapped and ready for installation.

### 2. Design Evolution

The design philosophy of the retro motor development program was to use the most advanced technological concepts which had been demonstrated by testing. All components were designed and fabricated to close tolerances to ensure that the motor assembly met reproducibility requirements for specific impulse, thrust alignment, CG, and excursion, and burn time predictability requirements.

*a. Case and attachments.* The original retro motor design had a 36.7-in.-diameter spherical steel case of 0.035-in. minimum wall thickness. Before fabrication began, the wall thickness was increased to 0.037 in. minimum, and the diameter of the aft end port was increased. These changes were made to increase design flexibility for either increased propellant weight or a larger propellant core to accommodate the reduction in required propellant weight associated with a reduction in total spacecraft weight. The attachment fittings were originally designed as three foam-filled sheet metal structures bonded to the exterior of the case. Early testing of the proposed thrust fittings indicated that the design would not be sound without a marked improvement in the technology of bonding. The thrust fittings were redesigned to the final flight configuration, which consisted of three thrust skirts welded near the meridian of the case, three struts, and a collar. These fittings were redesigned after excessive deflection in the skirts was observed during structural testing; the redesign also was intended to reduce total weight.

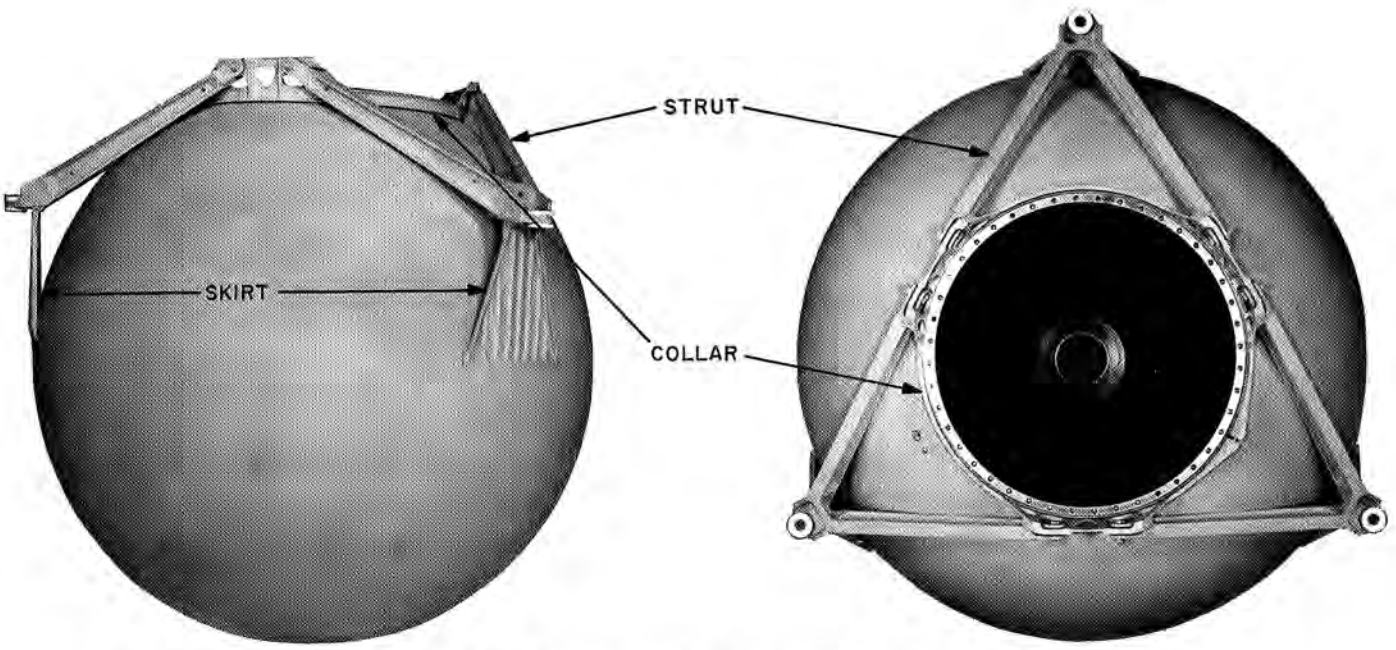



**Fig. XVII-43. *Surveyor* main retro motor case assembly**

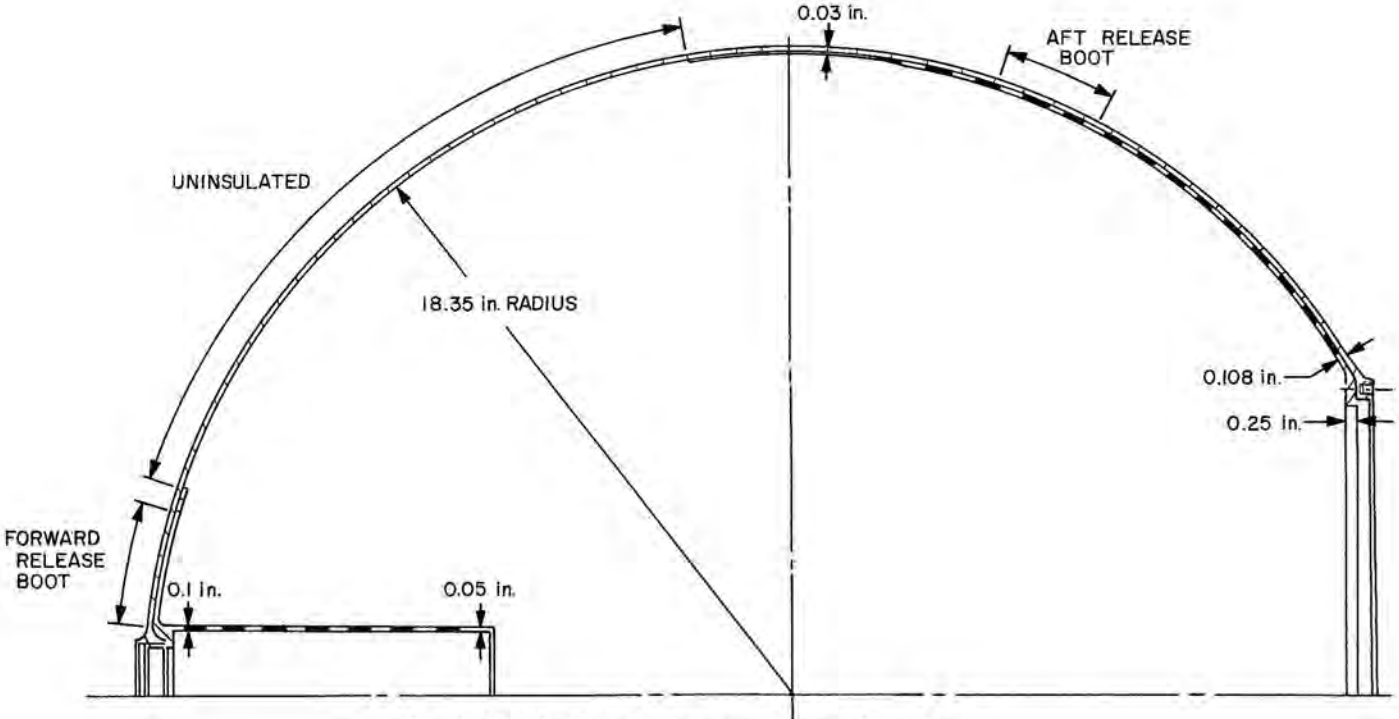



**Fig. XVII-44. Retro motor case internal insulation**



**Fig. XVII-45. Retro motor wrapped for installation**

To reduce the error in chordal dimensions, the motor attachment holes were drilled in the struts after hydrotest. Additionally, two strut ballast holes were located in each aluminum strut leg as a provision for spacecraft ballast, and a requirement was established to anodize the struts and passivate the steel collar.

***b. Nozzle.*** The original nozzle design (Fig. XVII-46) was a submerged configuration with a cantilevered, monolithic ATJ graphite insert used in the throat and leading section of the expansion cone. The remaining nozzle exit cone was vitreous-silica–phenolic molded directly to a completely machined aft case closure.

Early fittings yielded graphite erosion rates (25% area increase) that were excessive for adequate performance. To reduce throat erosion, tungsten, pyrolytic graphite, and high-density graphite were next considered as possible nozzle throat candidate materials. A U-shaped tungsten insert designed to fit over the leading edge of the graphite insert developed an axial crack during static firing and there was considerable exhaust flow between the tungsten and the parent graphite material. The pyrolytic-graphite throat design used 0.25-in. wafers installed perpendicular to the gas flow. During a static firing the pyrolytic graphite wafers were ejected from the nozzle. This effort was then dropped in favor of high-density graphite.

The first high-density graphite selected was HLM-85. It was used in seven nozzles and resulted in an average of 11% throat erosion. Nozzle firings at AEDC substantiated the structural integrity of the design, but the measured specific impulse was 280 lbf-sec/lbm, whereas the predicted value was 294 lbf-sec/lbm.

The nozzle contour was recalculated by using the "method of characteristics" and empirical data from the *Minuteman* Program. This redesigned contour resulted in a 9-in. increase in the expansion nozzle length to meet design performance requirements. To accommodate the longer nozzle within the motor envelope, it was necessary to submerge the assembly even farther into the motor. Thus, in turn, increased the loads on the nozzle, and a redesign was required using plastic materials to keep within the allocated weight limit. The redesign featured a fiber glass structural member, a good thermal insulating plastic (asbestos-filled phenolic) for insulating the structural member, and a good erosion-resistant plastic (bulk molded carbon cloth–phenolic) for use adjacent to the gas stream (Fig. XVII-47). This design effort was aided by a two-dimensional heat-transfer and thermal-stress analysis. Early retro motor tests with the redesigned nozzle contour resulted in a delivered vacuum specific impulse of 290 lbf-sec/lbm.

Because of continued difficulties with nozzle throat section design, a comprehensive nozzle development program was undertaken to produce a configuration that would be structurally adequate and have acceptable erosion characteristics.

A design with a two-piece ZTA graphite throat insert was tested in an attempt to reduce erosion. Excessive thermally induced structural loads caused the insert to break up and be ejected during a static firing.

A modified design using AHDG graphite, a material with low thermal shock sensitivity, was successfully tested two times before the material failed in a third firing, indicating a marginal condition.

A fine-grain molded graphite (TS-325) was next tested in a one-piece throat insert design. The throat sustained a full-duration static firing; however, the design was unacceptable because postfiring examination revealed a crack in the insert.

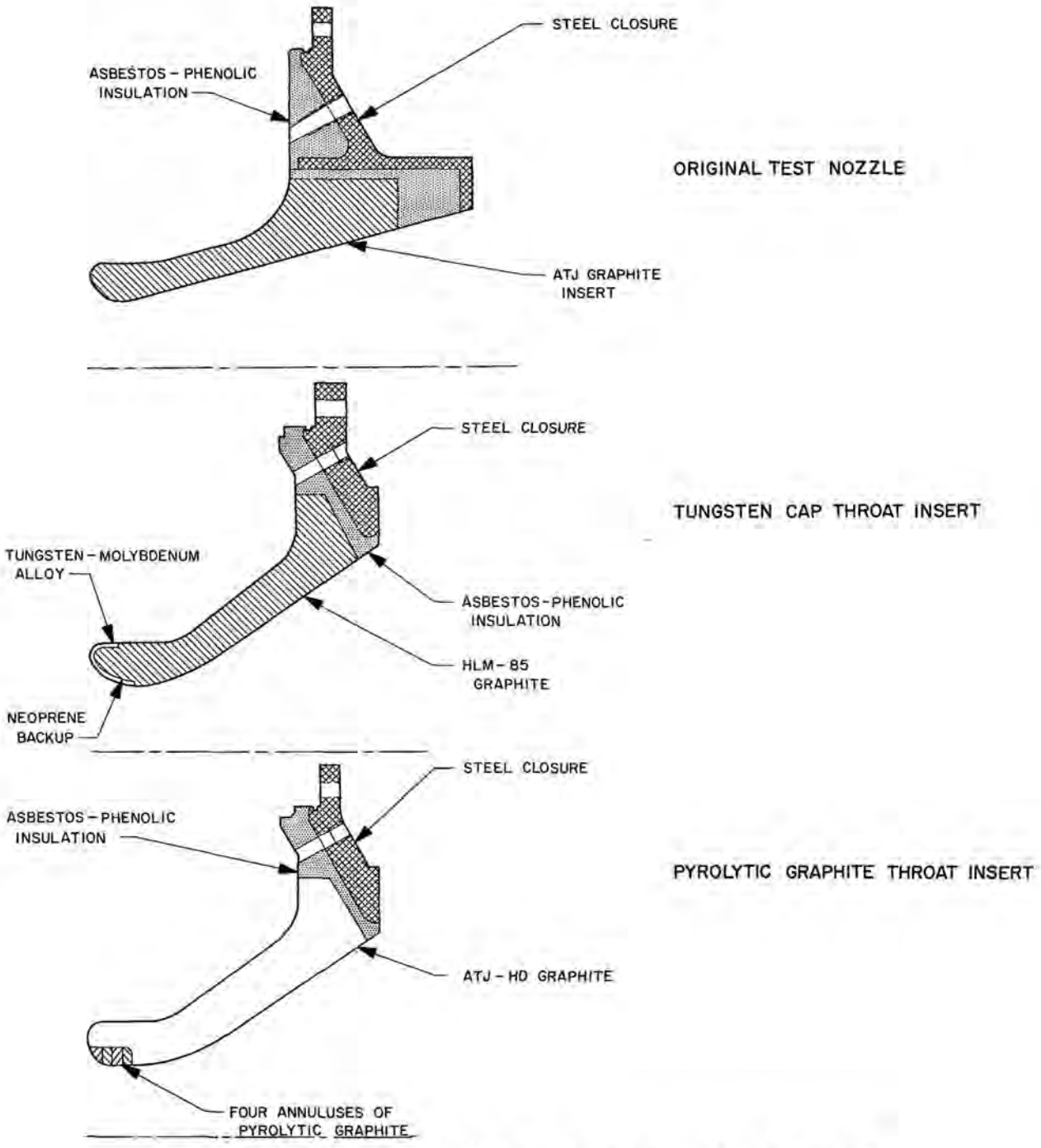



**Fig. XVII-46. Retro motor nozzle design evolution (early designs tested)**

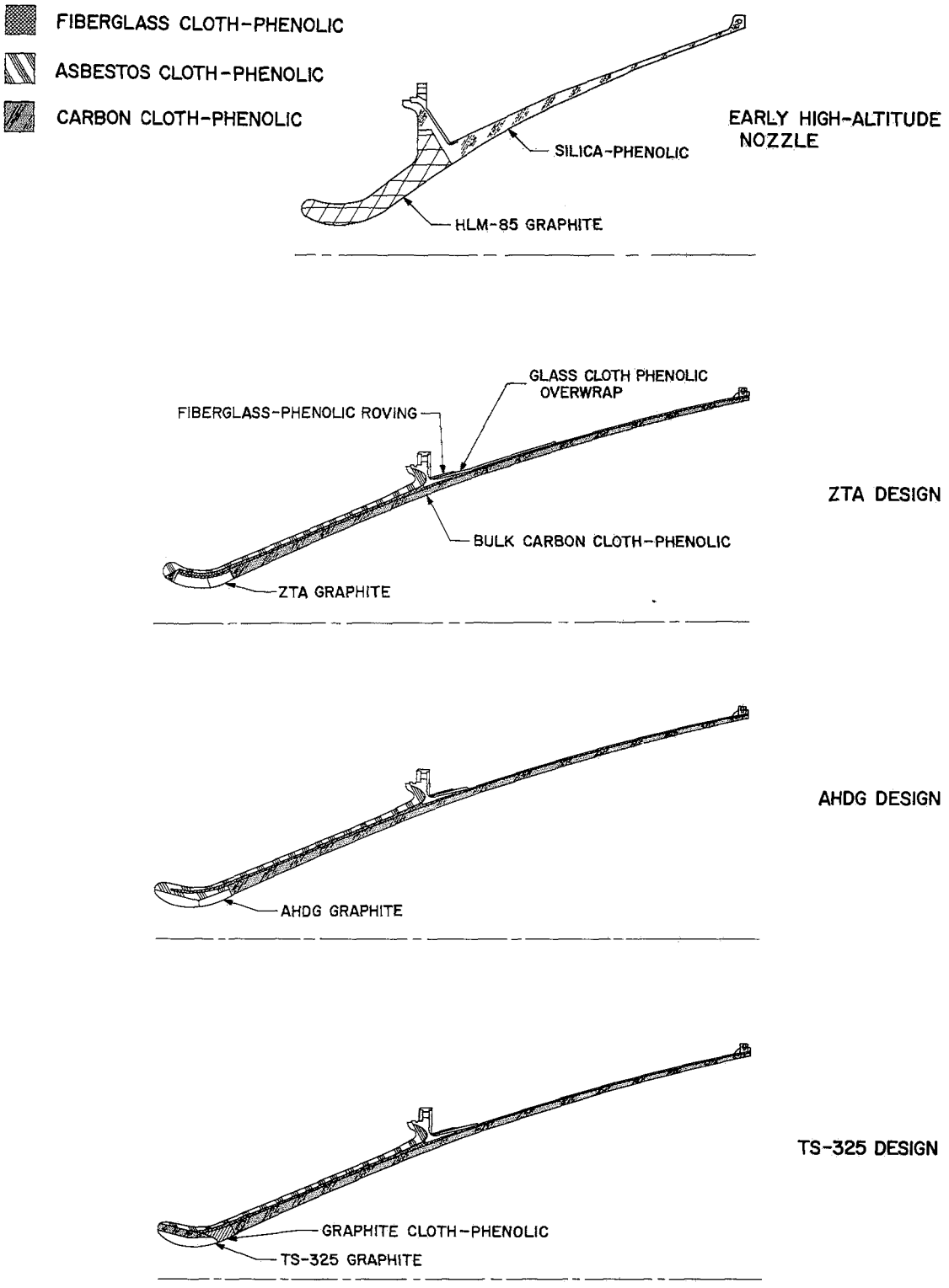



**Fig. XVII-47. Retro motor nozzle design evolution (redesigned structure and contour)**

The three final throat insert configurations are shown in Fig. XVII-48. Tests of the Mod I and Mod II designs resulted in circumferential cracks in the TS-325 graphite inserts.

The final configuration tested in the nozzle throat development test series was the Mod III configuration, which had a monolithic insert of graphite G-90 material uniformly supported by a carbon cloth–phenolic backup structure. The insert was unrestrained during firing to eliminate thermally induced compressive loads. The final configuration was successfully tested and was used in subsequent main retro motor tests, including all qualification and flight firings without a single failure.

*c. Internal insulation.* The initial internal insulation was an asbestos–phenolic material that was installed by hand layup and then cured. Early firing results indicated that the material was satisfactory as an insulator, but that propellant stress-relief boots were necessary to prevent propellant cracks or separations. Because the asbestos–phenolic material was relatively hard and stiff, it could not be used for stress-relief boots. The initial relief boots were manufactured from cured sections of Buna-N rubber bonded to the asbestos–phenolic insulation.

Although this insulator–relief boot combination of asbestos–phenolic and Buna-N rubber performed successfully in static firings, the amount of manual work required in the layup technique unnecessarily exposed the thin-wall case to damage. In addition, it was not possible to reproducibly control the thickness and contour of the insulation without an impractical machining operation.

The design was changed to use a flexible material: asbestos and silicon-dioxide-filled Buna-N synthetic rubber, designated Gen-Gard V-44, for both the insulator and relief boots. The parts were premolded outside the case, then bonded and cured in the case. After initial successful static firings indicated conservative thicknesses throughout, the insulation was thinned to the flight design of about 11 lb. This design maintained case temperatures below 250°F during retro motor operation. The flight configuration is shown in Fig. XVII-44.

*d. Propellant and grain.* One of the original requirements placed on the retro motor was sterilization. Heat sterilization, chemical sterilization, and gamma irradiation sterilization techniques were considered, studied, and evaluated with several propellants.

The original propellant formulation considered was TPH-3053 with a binder system of polybutadiene acrylic acid (PBAA) copolymer cured with an aziridine. This propellant system was considered to have the best high-temperature-resistant properties and, therefore, was considered a good candidate for heat sterilization, although the physical properties of the propellant were less than desired. An extensive propellant development effort was expended, optimizing the TPH-3053 formulation, which contained aluminum fuel additive and ammonium perchlorate oxidizer.

Early attempts to statically fire a heat sterilized retro motor resulted in motor failure, and the requirement for sterilization was eliminated from the program. In addition, a dual payload capability requirement was established for the retro motor that dictated a grain design change and a propellant burning-rate change. On the basis of these developments, the propellant formulation was changed to one with poorer heat sterilizable qualities but with superior physical properties and a modified burning rate. This propellant, TPH-3062, was similar to the original formulation except for the binder system. The TPH-3062 propellant utilized a carboxyl-terminated polybutadiene polymer cured with a mixed system of an imine and an epoxide. Considerable effort was spent adjusting the formulation to achieve the desired burning rate and physical properties. Propellant TPH-3062 was used for most of the development tests, all the qualification tests, and all the flight units.

The original grain design, designated A25, was for a propellant weight of 1388–1445 lb with an eight-point-star core configuration. Early in the program, when the spacecraft weight was reduced from 2500 to 2100 lb, the propellant weight requirement was reduced to 1200 lb. A new grain configuration, designated A21, had a seven-point-star core designed for propellant weights of 1200–1250 lb. As the spacecraft weight gradually increased back to 2300 lb, another seven-point-star grain (A22) was designed for propellant weights in the range of 1250–1300 lb. The qualification and flight units contained propellant grains of both the A21 and A22 configurations.

Figure XVII-49 shows a cross section for each grain core configuration.

*e. Ignition system.* The main components of the retro motor ignition system consisted of a pyrogen igniter, initiator basket, safe/arm assembly, and squibs.

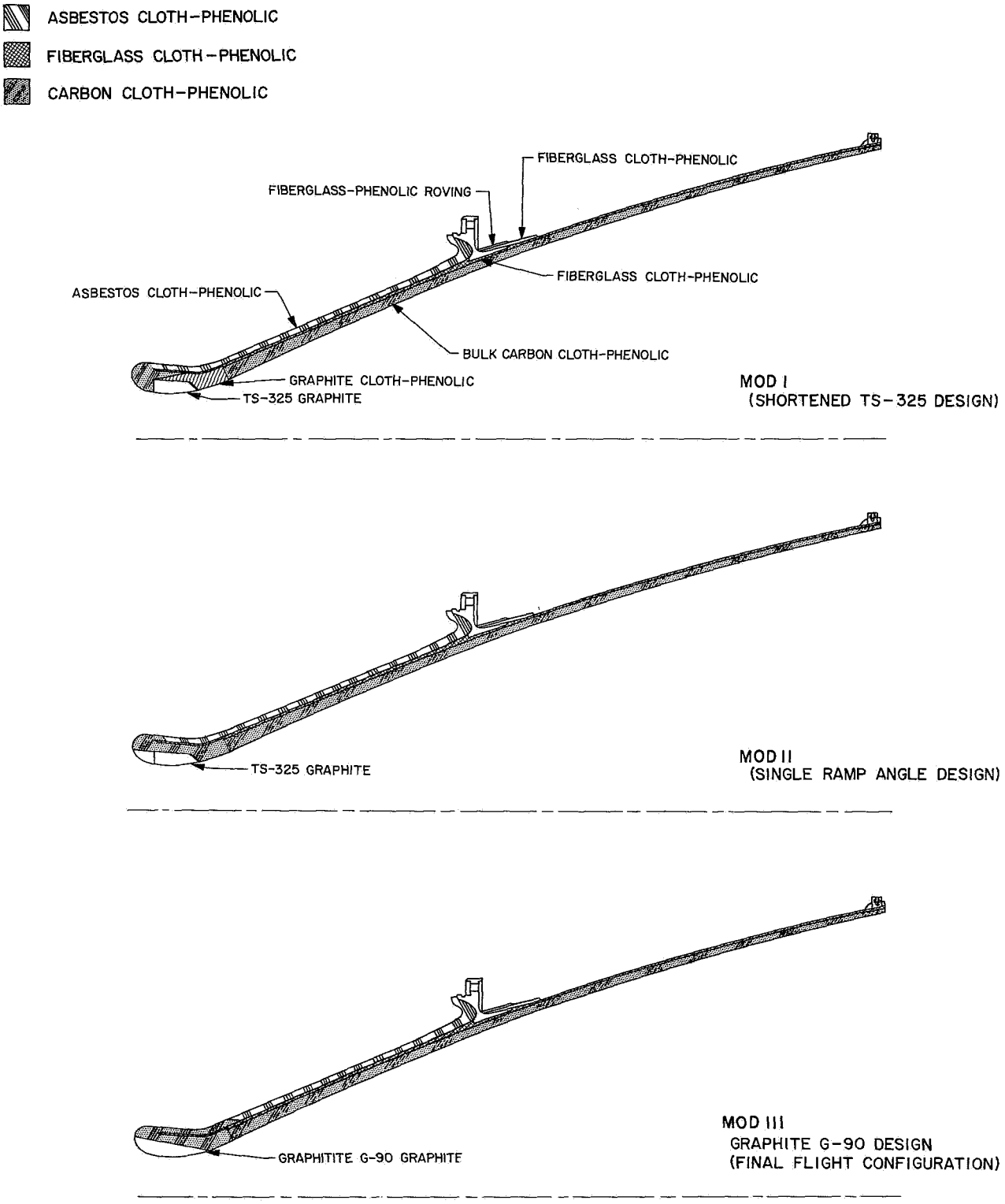



**Fig. XVII-48. Retro motor nozzle design evolution (final throat insert design tested)**

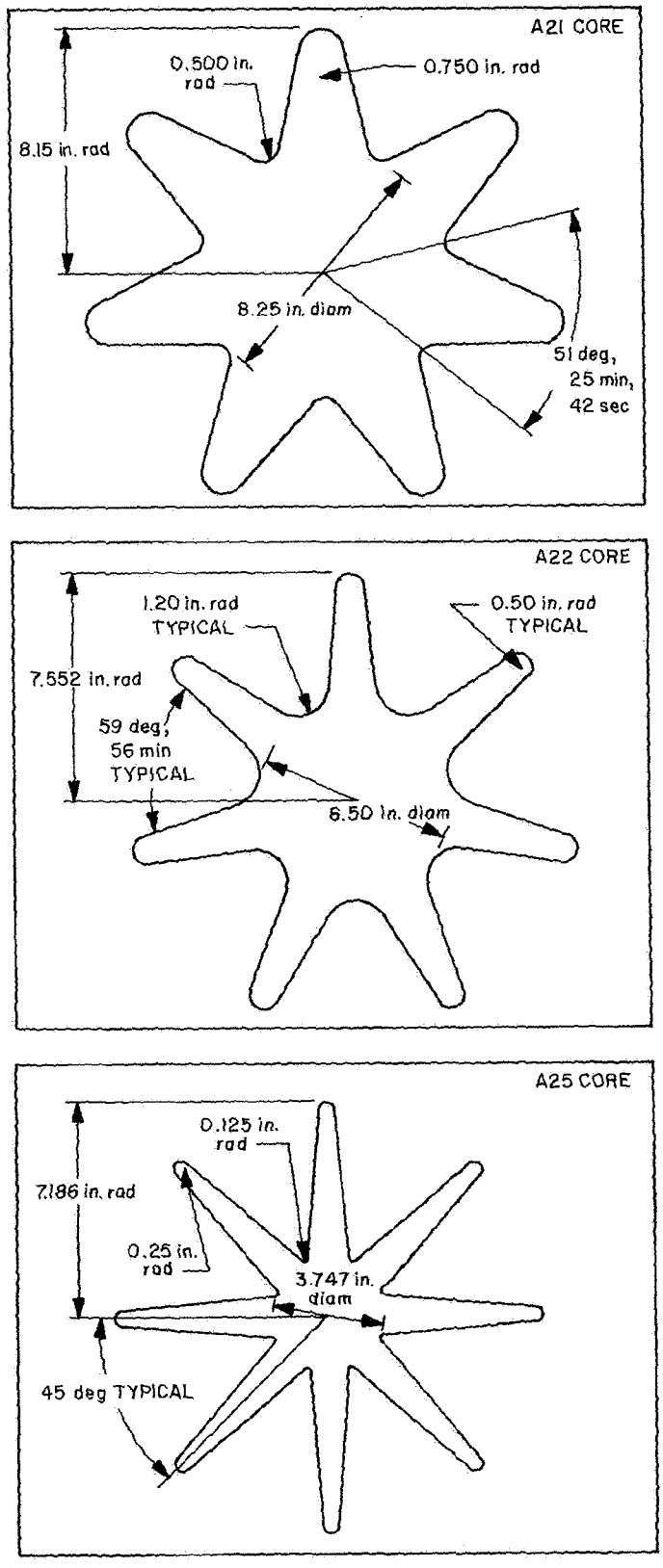



**Fig. XVII-49. Main retro grain core configuration**

The pyrogen igniter was selected because of its capability to produce reliable motor ignition under a wide range of environmental conditions. The cartridge grain concept provided the capability to change the pyrogen output to meet exacting requirements. The filament-wound fiber glass pyrogen case was selected because of its high strength-to-weight characteristics.

The first motor static test revealed ignition overpressurization of the motor, and this resulted in shortening the pyrogen propellant cartridge length and reducing the discharge port diameter. When the propellant was changed from TPH-3053 to TPH-3062, the cartridge propellant was also changed to eliminate the need for two different propellant systems within the main retro motor.

The original retro motor ignition system did not include a safe/arm device. In 1963, requirements were issued by AFETR Range Safety which dictated the use of a safe/arm device and the use of squibs that could pass a no-fire test with the application of 1 W and 1 A to the bridgewire. The safe/arm device development program extensively used designs and components already developed for other rocket motor programs.

The squib selected was the Hi-Shear PC-37, which was in qualification testing for the Air Force *Dynasoar* Program at that time.

### 3. Development, Qualification, and Flight Acceptance Program

The philosophy applied to main retro motor development (Ref. XVII-35), qualification (Ref. XVII-36), and FA was typical for high-performance, solid-rocket units. The retro motor was somewhat different from other components of the spacecraft in that the units to be flown could not be nondestructively tested for evaluation, adjusted or modified if necessary, and reoperated for FA in a manner similar to most spacecraft components. Confidence in the acceptability of the unit for flight use was based primarily on earlier successful static firings of units of the same design during the development and qualification program and on the ability to repeatably manufacture motors to rigid quality control and processing procedures. Only a minimal nondestructive testing effort could be applied to the retro motor assembly. This consisted principally of mechanical inspection for compliance to dimensional requirements and radiographic inspection of the propellant grain for voids, cracks, and separations.

*a. Retro motor component testing.* Adequacy of the flightweight case as a pressure vessel was demonstrated by the hydroburst testing of two cases, the hydroproof testing of 48 cases, and the static firing of 28 motors. The hydroproof tests were conducted at 683 psia, 15% over the maximum expected operating pressure of the motor. Two cases were subjected to hydroburst testing while simulated thrust loads were applied through the attachment-fitting structure. The cases burst at 960 and 976 psia, which is about 60% greater than the maximum expected operating pressure and about 40% greater than the design minimum yield pressure.

The thrust-attachment structure was subjected to vibration, acceleration, and various static load tests, and approximately 40 motor static tests. On the basis of some early structural tests, the skirt and strut were redesigned to improve their load-carrying capability, and the collar was redesigned to effect a weight savings. The redesigned attachment-fitting structure was retested and found to meet all design load requirements.

Fifty-nine production batches (115,000 lb) of the flight motor propellant, TPH-3062, were processed for the *Surveyor* Program. Chemical analysis and physical and ballistic testing were conducted on each batch. The chemical analysis included solids, heat, and aluminum content. The physical testing included density, tensile strength, elongation, and modulus of elasticity. The ballistic evaluation was performed by static firing ten 5-in.-diameter batch check motors each containing 6 lb of propellant, to determine burn rate and sensitivity of chamber pressure to temperature.

Problems with nozzle throat structural integrity resulted in the nozzle throat development program described in Subsection B-2. The TE-359 heavy-wall *Surveyor* retro motor was used extensively for nozzle evaluation. The 44-sec action time, 625 psia maximum operating pressure, and 1440-lb propellant load provided a significant overtest condition for the nozzle. In addition to the special static firings for nozzle evaluation, two flight design nozzles were hydrostatically tested to failure. As a result, the design was modified to redistribute the load-carrying mechanism in the nozzle.

Igniter tests were conducted to determine igniter propellant charge length and to optimize the igniter nozzle design. Tests were conducted with the safe/arm device to demonstrate the safety features and reproducibility of ignition.

*b. Retro motor environmental testing.* The environmental capabilities of the *Surveyor* retro motor were evaluated in acceleration, vibration, drop testing, and temperature cycling. Two motors, one inert and one live, were acceleration tested. The inert motor was subject to two tests to determine the adequacy and integrity of the thrust-attachment structure. Test results demonstrated that the motor attachment components were structurally adequate and capable of withstanding a 9-*g* acceleration longitudinally and a combination of 5 and 0.4 *g* axially and laterally. The live motor was accelerated to 6 *g* for 15 min. It was not damaged or deformed in any way by the test, nor were any propellant cracks or separations detected after the test.

Five complete vibration tests, three during development and two during qualification, were conducted on the retro motor. The motors typically were instrumented with accelerometers at points likely to exhibit maximum resonance (i.e., pyrogen boss, nozzle exit plane, case meridian weld, and aluminum strut). Rosette strain gages were applied above the skirt-to-case weld and strut-attachment holes. The motors were tested in both the transverse and longitudinal axes with sinusoidal, random, and combined vibration inputs. Test results in the most severe load regime of 5–40 Hz indicated a substantial margin of safety under vibration loading.

The retro motor shipping container with an inert motor installed was subjected to 38 environmental tests. The series included vertical and rotational drop tests, pendulum impact tests, tipover, drag, and handling tests. Both the motor and the container successfully passed the test series.

Two live development motors and two qualification motors were subjected to two 18-in. vertical drop tests in the shipping container. Both motors were visually and radiographically acceptable on reinspection and performed satisfactorily during static firing tests.

Three development motors, one inert and two live, and four qualification motors were cycled three times through the temperature limits of 20–110°F without adverse effect to the propellant grain. One of the qualification motors was cycled between 15 and 110°F. The live motors subsequently were successfully statically fired.

The environmental test program was satisfactory except for an attachment-structure failure during vibration testing, which necessitated the redesign and retesting of the strut–skirt interface. This redesign was completed and the redesigned parts performed satisfactorily during retest.

*c. Retro motor static firings.* Forty-nine retro motors were statically fired during the development, qualification, and FA programs (Table XVII-14).

The development program included 35 static firings, 14 of which were of the original A25 configuration, 7 were of the heavywall A25 case for the nozzle development test program, and 14 were of the A21 flight configuration. Twenty-eight of these firings were successful; five motors sustained failure of the nozzle throat insert, one A25 motor was destroyed at ignition because of complete propellant unbonding as a result of an unsuccessful sterilization attempt, and the last failure occurred when backside heating from the test setup resulted in a nozzle ejection. After incorporation of the final flight nozzle design, the last 11 development firings were completely successful.

Firing temperatures ranged from 20 to 70°F, with motors being tested under simulated flight temperature gradient condition, the flight gradient condition plus 15°F and the flight gradient minus 15°F.

The qualification program included a total of ten full scale static firings, six A21 motors and four A22 motors. Four A21 and three A22 configuration motors were statically fired at the AEDC, Tullahoma, Tenn. (Ref. XVII-37). The A21 motor was fired in a six-component-of-thrust test stand. The other qualification motors were fired by Thiokol Chemical Corp. at Elkton, Md. (see Ref. XVII-21). All 10 static firings were conducted under simulated high altitude conditions. Of particular interest during the qualification program was the reproducibility of specific impulse and burn time, tailoff characteristics and thrust alignment, and center of gravity data from the six-component-of-thrust test stands. Evaluation of test data indicated that the motors met or exceeded the requirements of the spacecraft system and the units were considered qualified for flight use.

Following the formal qualification test program four flight design retro motors were successfully statically fired. One (A21) motor was successfully fired under a propellant thermal gradient condition after having been aged for 23 mo at ambient temperature. One A21 and two A22 FA test motors were statically fired at the flight temperature gradient condition and simulated high altitude.

*d. Flight retro motor integrity.* During the flight program a total of 15 retro motors were manufactured, as shown in Table XVII-14. Of these, seven were used in flight, three were statically fired in lot acceptance tests, four were rejected, and one spare flight unit was unused.

Three reject motors exhibited propellant- or liner-to-insulation separations; in addition, one unit had an insulation-to-case separation. These defects were observed during routine radiographic inspection of the motor during flight preparation at AFETR. One motor was rejected because of a weak liner-to-insulation bond visually observed during manufacture.

The initial flight motors were delivered to AFETR without having had tangential radiographic inspection for propellant-to-case bond integrity. After motor A22-5 was rejected for flight use because of insulation-to-case separations, radiographic inspection of the insulated case was added to the manufacturing process.

Exhaustive investigations were conducted to determine the cause of the poor propellant, liner, and insulation bonding.

Radiographic inspection of insulated cases was added to ensure insulation bond integrity prior to propellant loading. Early flight motors were delivered to AFETR without having had tangential radiographic inspection of case bond integrity during the manufacturing cycle and tangential radiographic inspection after propellant loading was added to the manufacturing process. After the in-process radiographic inspection failed to reveal a separation and a fold in the aft boot in one motor delivered for flight use, the technique was changed to be identical to the AFETR radiographic procedure, which required twice as many exposures; i.e., tangential X rays every 13 instead of every 26 deg.

It was recognized that because the development and qualification motors had not received high-resolution tangential X rays prior to testing, these motors may have contained minor propellant separations and that the flight motors being rejected could in fact be of the same quality as the qualification motors. However, because of a lack of successful firings with known propellant separations, the philosophy applied to the flight units was that only retro motors without known propellant separations should be used for flight. Two reject flight retro motors and two spare retro motors left from the qualification program were subjected to radiographic inspection at reduced temperatures (40 and 20°F) in an attempt to better characterize the propellant separation phenomenon. In radiographic inspections two of the

## Table XVII-14. Retro motor development test history

| Test date | Motor SN | Motor type | Hardware type | Propellant TP-H | Nozzle | Test temperature | Environmental test | | | | Test location | Results |
|---|---|---|---|---|---|---|---|---|---|---|---|---|
| | | | | | | | Drop | Temperature cycle | Vibration | Acceleration | | |
| **Development** | | | | | | | | | | | | |
| 8/61 | A25-1 | TE-359 | HW[a] | 3053 | Trun[b] | 70 | | | | | Thiokol | Ballistic evaluation, A25 grain, successful |
| 10/61 | A25-2 | TE-359 | HW | 3053 | Trun | 20 | | | | | | Grain cracked, potted and fired, high initial press |
| 12/61 | A25-3 | TE-359 | HW | 3053 | Trun | 73 | | X | | | | First stress relief boot, pyrolytic graphite nozzle throat ejected |
| 1/62 | A25-R1 | TE-359 | HW | 3053 | Trun | | | X | | | | Grain altered to remove cracks, tested successfully |
| 1/62 | A25-4 | TE-359 | HW | 3053 | Trun | | | | | | | Sterilized, motor failed at 120 msec, propellant-liner separation |
| 2/62 | A25-1A | TE-359 | HW | 3062 | Trun | | | | | | | Ballistic evaluation, TP-H-3062 propellant, successful |
| 2/62 | A25-5 | TE-359 | HW | 3062 | Alt[c] | 56 | | | | | | C-21 diffuser malfunction, motor successful |
| | A25-6 | TE-360 | FW[d] | 3062 | | 20 | | X | | | Thiokol | Low temperature grain evaluation, motor successful |
| 6/62 | A25-9 | TE-359 | HW | 3062 | Alt | 50 | | | | | AEDC | Altitude ballistic evaluation, low specific impulse, nozzle contour |
| 6/62 | A25-10 | TE-359 | HW | 3062 | Alt | 50 | | | | | AEDC | Altitude ballistic evaluation, low specific impulse, nozzle contour |
| 6/62 | A25-12 | TE-359 | HW | 3062 | Alt | | | | | | Thiokol | C-21 altitude lost, 31 sec, motor performance satisfactory |
| 6/62 | A21-1 | TE-364 | FW | 3062 | Trun | 28 | | X | | | Thiokol | Ballistic evaluation, successful |
| 7/62 | A21-2 | TE-364 | FW | 3062 | Trun | | | | | | Thiokol | Ballistic evaluation, successful |
| 10/62 | A21-3 | TE-364 | FW | 3062 | Alt | 50 | | | | | AEDC | Altitude ballistic evaluation, nozzle contour evaluation, successful |
| 10/62 | A25-7 | TE-360 | FW | 3062 | Alt | 50 | | | | | AEDC | TS-325 throat ejected at 5.5 sec, delivered specific impulse 285.4 |
| 1/63 | A25-11 | TE-360 | FW | 3062 | Alt | | | | | | Thiokol | Obsolete nozzle failure, leak started at 2.3 sec, altitude simulator evaluation |
| 2/63 | A21-4 | TE-364-1 | FW | 3062 | Trun | | | | | | | Nozzle throat ejected at 4 sec, ZTA graphite evaluation |
| 3/63 | A25-8 | TE-360 | FW | 3062 | Trun | Grad[e] | | | | X | | AHDG graphite evaluation, successful static test |
| 3/63 | A21-5 | TE-364-1 | FW | 3062 | Alt | | | | | | Thiokol | AHDG graphite evaluation, successful static test |
| 4/63 | A21-9 | TE-364-1 | FW | 3062 | Alt | | | | | | AEDC | Nozzle throat failure at 20 sec, AHDG graphite |
| 5/63 | A21-6 | TE-364-1 | FW | 3062 | Alt | | X | | | | Thiokol | Nozzle throat cracked, TS-325 graphite, successful test |
| 7/63 | A25-14N | TE-359-1 | HW | 3062 | Trun | | | | | | | Nozzle throat cracked, TS-325 graphite, overtest, successful |

[a]HW = Heavyweight case.
[b]Trun = Truncated or sea level nozzle.
[c]Alt = Altitude or flight nozzle.
[d]FW = Flight weight case.
[e]Grad = Gradient.

## Table XVII-14 (contd)

| Test date | Motor SN | Motor type | Hardware type | Propellant TP-H | Nozzle | Test temperature | Environmental test | | | | Test location | Results |
|---|---|---|---|---|---|---|---|---|---|---|---|---|
| | | | | | | | Drop | Temperature cycle | Vibration | Acceleration | | |
| **Development (contd)** | | | | | | | | | | | | |
| 7/63 | A25-13N | TE-359-1 | HW | 3062 | Trun | | | | | | | Exit cone failure at 34 sec, TS-325 graphite, overtest |
| 9/63 | A25-15N | TE-359-1 | HW | 3062 | Trun | | | | | | | Nozzle throat cracked, G-90 overtest, successful |
| 10/63 | A25-16N | TE-359-1 | HW | 3062 | Trun | | | | | | | G-90, overtest, successful |
| 11/63 | A25-17N | TE-359-1 | HW | 3062 | Alt | | | | | | | G-90, overtest, successful |
| 12/63 | A25-19N | TE-359-1 | HW | 3062 | Alt | | | | | | | G-90, overtest, successful |
| 12/63 | A25-18N | TE-359-1 | HW | 3062 | Alt | | | | | | | G-90, overtest, successful |
| 1/64 | A21-7 | TE-364-1 | FW | 3062 | Alt | Grad | X | X | X | | | Environmental motor, successful |
| 2/64 | A21-14 | TE-364-1 | FW | 3062 | Alt | Grad | | | | | | Ballistic performance thermal gradient, successful |
| 2/64 | A21-8 | TE-364-1 | FW | 3062 | Alt | Grad | | | | | Thiokol | Ballistic performance thermal gradient, successful |
| 12/63 | A21-10 | TE-364-1 | FW | 3062 | Alt | 50 | | X | | | AEDC | Environmental motor, successful |
| 12/63 | A21-13 | TE-364-1 | FW | 3062 | Alt | 50 | | | | | | Altitude ballistic performance, successful |
| 6/64 | A21-11 | TE-364-1 | FW | 3062 | Alt | 50 | | | | | | Multicomponent test stand, successful |
| 6/64 | A21-12 | TE-364-1 | FW | 3062 | Alt | 50 | | | | | AEDC | Multicomponent test stand, successful |
| **Qualification** | | | | | | | | | | | | |
| 8/64 | A21-17 | TE-364-1 | FW | 3062 | Alt | 50 | | | | | AEDC | Successful altitude ballistic qualification, multicomponent tests |
| 8/64 | A21-18 | TE-364-1 | FW | 3062 | Alt | 50 | | | | | | Successful altitude ballistic qualification, multicomponent tests |
| 9/64 | A21-23 | TE-364-1 | FW | 3062 | Alt | 50 | | | | | | Successful altitude ballistic qualification, multicomponent tests |
| 9/64 | A21-24 | TE-364-1 | FW | 3062 | Alt | 50 | | | | | AEDC | Successful altitude ballistic qualification, multicomponent tests |
| 2/65 | A21-19 | TE-364-1 | FW | 3062 | Alt | Grad | X | X | X | | Thiokol | Environmental qualification, 1230-lb grain, successful |
| 2/65 | A21-22 | TE-364-1 | FW | 3062 | Alt | Grad | X | X | X | | Thiokol | Environmental qualification, 1230-lb grain, attach hinge failure in vibration, redesign incorporated, successful |
| 3/65 | A22-1 | TE-364-5 | FW | 3062 | Alt | Grad | | X | | | Thiokol | Reused case and attach fittings, ballistic qualification of 1300-lb grain, environmental, successful |
| 5/65 | A22-2 | TE-364-5 | FW | 3062 | Alt | Grad | | | | | AEDC | Reused case and attach fittings, ballistic qualification of 1300-lb grain, successful |
| 5/65 | A22-3 | TE-364-5 | FW | 3062 | Alt | Grad | | | | | AEDC | Reused case and attach fittings, ballistic qualification of 1250-lb grain, successful |
| 5/65 | A22-4 | TE-364-5 | FW | 3062 | Alt | Grad | | | | | AEDC | Reused case and attach fittings, ballistic qualification of 1250-lb grain, successful |

Table XVII-14 (contd)

| Test date | Motor SN | Motor type | Hardware type | Propellant TP-H | Nozzle | Test temperature | Environmental test | | | | Test location | Results |
|---|---|---|---|---|---|---|---|---|---|---|---|---|
| | | | | | | | Drop | Temperature cycle | Vibration | Acceleration | | |
| **Qualification (contd)** | | | | | | | | | | | | |
| — | A22 16 | TE-364-1 | FW | 3062 | Alt | — | | | | | — | In storage at Thiokol, Elkton (qualification program spare) |
| — | A21-20 | TE-364-1 | FW | 3062 | Alt | — | | | | | — | In storage at Thiokol, Elkton (qualification program spare) |
| — | A21-21 | TE-364-1 | FW | 3062 | Alt | — | | | | | — | In storage at Thiokol, Elkton (qualification program spare) |
| **Aging** | | | | | | | | | | | | |
| 3/66 | A21-15 | TE-364-1 | FW | 3062 | Alt | Grad | | | | | Thiokol | Aged motor—22 mo, no change in performance |
| **Flight program** | | | | | | | | | | | | |
| 9/65 | A21-25 | TE-364-1 | FW | 3062 | Flt | Grad | | | | | Thiokol | Lot acceptance test motor, successful |
| 5/66 | A21-26 | TE-364-1 | FW | 3062 | Flt | | | | | | Launch | *Surveyor I*, successful |
| 9/66 | A21-27 | TE-364-1 | FW | 3062 | Flt | | | | | | Launch | *Surveyor II*, tumbling, operation satisfactory until data lost |
| — | A22-5 | TE-364-5 | FW | 3062 | Flt | | | | | | — | Reject: weak liner to insulation bond |
| 12/66 | A22-6 | TE-364-5 | FW | 3062 | Flt | Grad | | | | | Thiokol | Lot acceptance test motor, successful |
| — | A22-7 | TE-364-5 | FW | 3062 | Flt | — | | | | | — | Reject: liner-insulation separation |
| 4/67 | A22-8 | TE-364-5 | FW | 3062 | Flt | | | | | | Launch | *Surveyor III*, successful |
| 7/67 | A22-9 | TE-364-5 | FW | 3062 | Flt | | | | | | Launch | *Surveyor IV*, performance normal, 41 sec |
| 4/67 | A22-10 | TE-364-5 | FW | 3062 | Flt | Grad | | | | | Thiokol | Reused fired hardware lot acceptance test motor, successful |
| 9/67 | A21-28 | TE-364-1 | FW | 3062 | Flt | | | | | | Launch | *Surveyor V*, successful |
| 11/67 | A21-29 | TE-364-1 | FW | 3062 | Flt | | | | | | Launch | *Surveyor VI*, successful |
| — | A22-11 | TE-364-5 | FW | 3062 | Flt | — | | | | | — | Reject: propellant separation |
| — | A22-12 | TE-364-5 | FW | 3062 | Flt | — | | | | | — | Flight spare |
| — | A22-13 | TE-364-5 | FW | 3062 | Flt | — | | | | | Thiokol | Reject: propellant separation |
| 1/68 | A22-14 | TE-364-5 | FW | 3062 | Flt | — | | | | | Launch | *Surveyor VII*, successful |

engines showed separations at 40°F and all four showed separations at 20°F. The separations were more pronounced at 20 than at 40°F. In addition, as the motor temperature was increased to ambient, some of the separations disappeared in the radiographs. A positive conclusion could not be made as to whether the low temperature was actually causing the separations or simply making them more visible by X-ray inspection.

To positively correlate propellant separations suspected on the basis of radiographic inspection, a reject retro motor was dissected and the suspect areas were examined in detail. The results indicated that the suspect areas were separated and that the propellant-to-insulation bond failures were cohesive (within the propellant and not an adhesive bond failure). In-process cleanness and quality control measures were improved to reduce possible process variations, particularly those associated with insulation preparation, cleaning, and lining prior to the propellant loading. A change in insulation vendors prompted a change to improve the method of installing the insulation into the case. Additional control features were added to minimize process variations.

When a change in design of the aft release boot resulted in rejection of another flight motor, investigation

revealed that the modified design had been installed incorrectly, which prompted a review of prior work. The review indicated the aft boot release distance was varying more than desirable and the manufacturing technique was changed to minimize the variation. The final conclusion was that the aft release boot design may have been marginal. This conclusion was made just before manufacturing the final flight unit. Because of flight experience and cost and schedule considerations, no design change was made, and final flight motor integrity was confirmed by radiographic inspection at AFETR.

#### 4. Flight Performance

Inflight performance data on the main retro motor was obtained from instrumentation on the retro motor and other portions of the spacecraft. Flight instrumentation directly on the retro motor consisted of three thermal sensors: two on the motor case underneath the thermal blanket, and one on the nozzle exit cone. These temperatures were monitored periodically during transit to the moon. About 4 hr before retroignition, the data were used to make a final prediction of retro propellant grain temperature and corresponding retro burn time for final adjustment or retroignition altitude.

Retro motor thrust and burn time data were calculated from doppler trajectory data and from an on-board accelerometer located in the flight control sensor group in conjunction with time-phase calculation of total spacecraft weight during the retro maneuver. Additional configuration of burn time was achieved by observing the timing sequence of retromaneuver events such as vernier engine ignition, RADVS power-on, VPS commands, a burnout switch, and retro motor ejection. Total and specific impulse were calculated from velocity increment data that were based on doppler, accelerometer, and RADVS velocity data. Retro motor roll torque, thrust alignment, and CG shift during burning were reflected in the total spacecraft moment control required during retro motor burning. These control requirements were determined from the demands on the VPS as evidenced by vernier engine thrust commands.

A summary of retro motor flight data is shown in Table XVII-15. On the *Surveyor IV* mission, the spacecraft signal was lost abruptly approximately 1.4 sec before expected retro motor burnout (3.5-g level). Spacecraft telemetry data received before loss of signal indicated normal operation. The propulsion analysis group of the Technical Review Board, which conducted a thorough investigation of the *Surveyor IV* failure, concluded it was unlikely that the retro motor or the VPS contributed to the loss of signal, but the group could not conclusively rule out the possibility.

***a. Thermal data.*** Prelaunch air conditioning of the spacecraft held the retro motor temperature to a uniform 70 ±5°F until launch. During transit to the moon, the retro motor cooled at a rate predicted by STV tests of the spacecraft before launch. The actual retro motor temperature decay followed very closely to the predicted. The maximum deviation occurred on *Surveyor III* where the final bulk temperature was 3°F lower than predicted. Thermal data are summarized in Section XV of this report.

***b. Burn time.*** The technique for predicting flight motor burn time was empirical based on test data developed during the qualification phase, and from the specific propellant batch burn-rate data for the flight motors as determined by testing 10 small batch check motors. Preflight burn time predictions were made assuming a final bulk propellant temperature of 55°F. This prediction was adjusted for real-time in-flight temperatures by using the burn rate temperature-dependent constant. The real-time bulk temperature was obtained by averaging the two case thermal sensor temperatures, a technique established during STV testing. The requirement for predicting burn time to 3500 lbf thrust level at tailoff (T-3500) was ±1% at a known bulk propellant temperature. Burn time prediction errors were all within the capability of the spacecraft. The maximum deviation from prediction for flight motors was 1.3%, which occurred on *Surveyor V*. Part of the inflight prediction error was associated with errors in knowing exactly the bulk temperature at retroignition.

***c. Impulse and thrust.*** The retro motor specific impulse was obtained from analysis of measured spacecraft velocity increment during retro motor burning using a calculated spacecraft weight and assumed VPS performance. The difference between actual and predicted change in velocity was assumed to be due entirely to the retro motor. This approach was conservative from the retro motor point of view since the velocity increment error was actually caused by a number of factors in addition to the retro motor, such as vernier engine performance, retro motor pointing errors, and predicting spacecraft weight-vs-time. The allowed deviation in specific impulse was ±1%; the maximum deviation was 0.4%, which occurred on *Surveyor I*.

Maximum thrust allowed for the retro motor was 10,000 lbf; the maximum thrust achieved during any flight was calculated to be 9950 lbf, which occurred on

**Table XVII-15. Flight retro motor data summary**

| Parameter | Requirement | Spacecraft | | | | | | |
|---|---|---|---|---|---|---|---|---|
| | | SC-1 | SC-2 | SC-3 | SC-4 | SC-5 | SC-6 | SC-7 |
| Retro motor SN | | A21-26 | A21-27 | A22-8 | A22-9 | A21-28 | A21-29 | A22-14 |
| Propellant weight, lb | | 1243 | 1250 | 1300 | 1300 | 1250 | 1250 | 1300 |
| Thermal data | | | | | | | | |
| Bulk temperature at launch, °F | 70 ±5 | | | | | | | |
| Bulk temperature at ignition, °F | 55 ±15 | 54.0 | — | 52.0 | 54.5 | 52.5 | 52.5 | 54.0 |
| Burnout time data (ignition to 3500-lbf thrust level at burnout) | | | | | | | | |
| Predicted at final temperature, sec | 38-44 | 38.5 | 39.22 | 41.09 | 42.55 | 39.06 | 39.60 | 42.78 |
| Actual, sec | — | 38.9 | — | 41.02 | — | 38.56 | 39.37 | 42.86 |
| Prediction error, % | <±1% | 1.0 | — | 0.2 | — | 1.3 | 0.6 | 0.2 |
| Specific impulse, lbf-sec/lbm | 289.5 | 288.4 | — | 288.9 | 288.0[a] | 288.4 | 289.3 | 289.8 |
| Error, % | <±1 | 0.4 | — | 0.2 | 0.5[a] | 0.4 | 0.1 | 0.1 |
| Maximum thrust, lb | <10,000 | 9850 | — | 9550 | 9250 | 9950 | 9700 | 9200 |
| Balance and alignment | | | | | | | | |
| Maximum distance, retro thrust axis to total spacecraft CG, in. | <0.200 | 0.008 | — | 0.017 | — | 0.013 | 0.027 | 0.010 |
| Spacecraft attitude control torque requirements | | | | | | | | |
| Spacecraft pitch/yaw torque maximum, in.-lb | <2000 | | | | | | | |
| At retroignition, in.-lb | | 80 | — | 390 | — | 100 | 350 | 340 |
| Steady state, in.-lb | | 75 | — | 175 | — | 125 | 275 | 200 |
| Spacecraft roll torque maximum, in.-lb | <90 | | | | | | | |
| At retroignition, in.-lb | | 47 | — | 20 | — | 25 | 28 | 20 |
| Steady state, in.-lb | | 62 | — | 35 | — | 60 | 60 | 40 |

[a]Data transmission stopped approximately at retro web burning point.

*Surveyor V*. The retro motor thrust curves followed the predicted very closely. However, in general, the flight motors burned at a slightly higher initial and slightly lower final thrust levels than predicted. This was probably caused by a thermal gradient through the propellant grain slightly different than predicted. Typical thrust-vs-time curves are shown in Fig. XVII-50.

*d. Moment control during retro motor burning.* Spacecraft attitude during retro motor burning was maintained by throttling three vernier engines and by swiveling one vernier engine. The moment control demands on the vernier engines during retro burning were caused by the retro motor thrust misalignment, thrust excursion, CG shift, etc., as well as by nonretro items such as VPS CG shift and thrust variations. During retro motor burning the spacecraft moment control minimum capability was approximately 90 in.-lb roll moment control and approximately 2000 in.-lb pitch and yaw moment control.

Mission moment control experience during retro motor burning is shown in Figs. XVII-51 and XVII-52. The roll moment control requirement characteristically had a small ignition transient and then increased with burning time, probably due to increased bending of the vernier engine mounting bracket as spacecraft acceleration increased. The maximum roll torque required for all missions was 62 in.-lb which occurred on *Surveyor I*. The maximum pitch and yaw torques occurred as spikes at retro ignition. The peak yaw and pitch resultant torque for all missions was 470 in.-lb. which occurred during ignition on *Surveyor III*. The maximum steady-state resultant torque was 290 in.-lb which occurred on *Surveyor VI*.

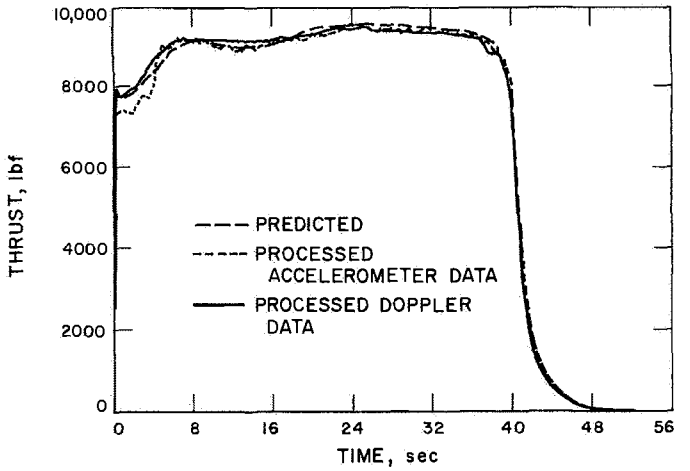



**Fig. XVII-50. Typical retro motor thrust-vs-time curves (*Surveyor III*)**

*e. Retro engine ejection.* During retro motor tailoff at approximately 3500 lbf thrust, a 3.5 $\pm$0.5-g accelerometer switch was activated. Twelve seconds later the retro motor release mechanisms were actuated and the retro motor was dropped from the spacecraft. To accomplish a successful retro motor ejection, the retro thrust had to be less than 30 lbf at that time. For all missions the retro motor was successfully separated from the spacecraft with little or no disturbances imparted to the spacecraft, as indicated by pitch and yaw gyros, the retro accelerometer data, and vernier engine thrust commands.

## C. Pyrotechnics

The *Surveyor* spacecraft used pyrotechnics and pyrotechnic-actuated devices for single-performance features such as locks, valves, switches, plungers, and main

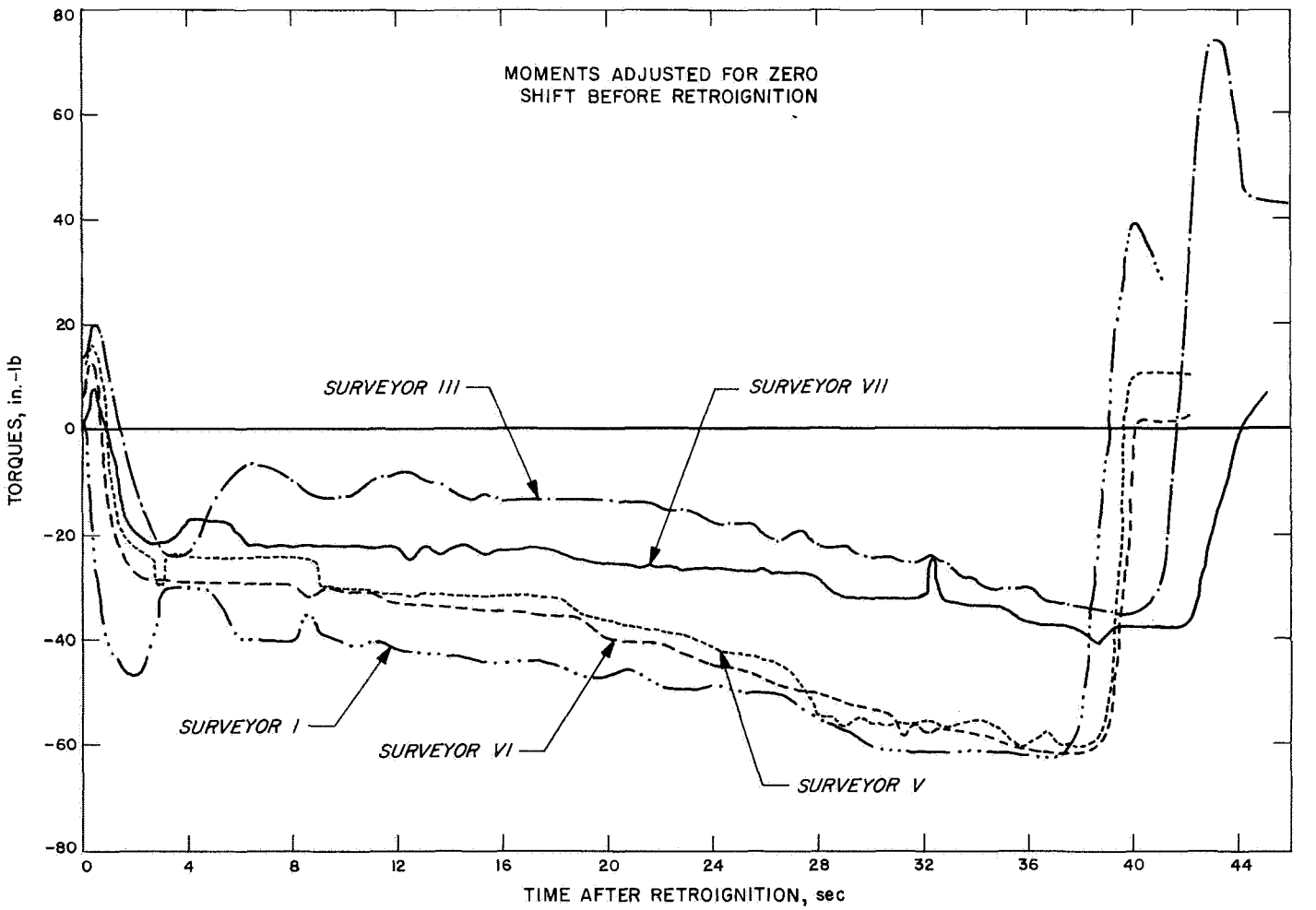



**Fig. XVII-51. Spacecraft roll moment torque during retro motor operation**

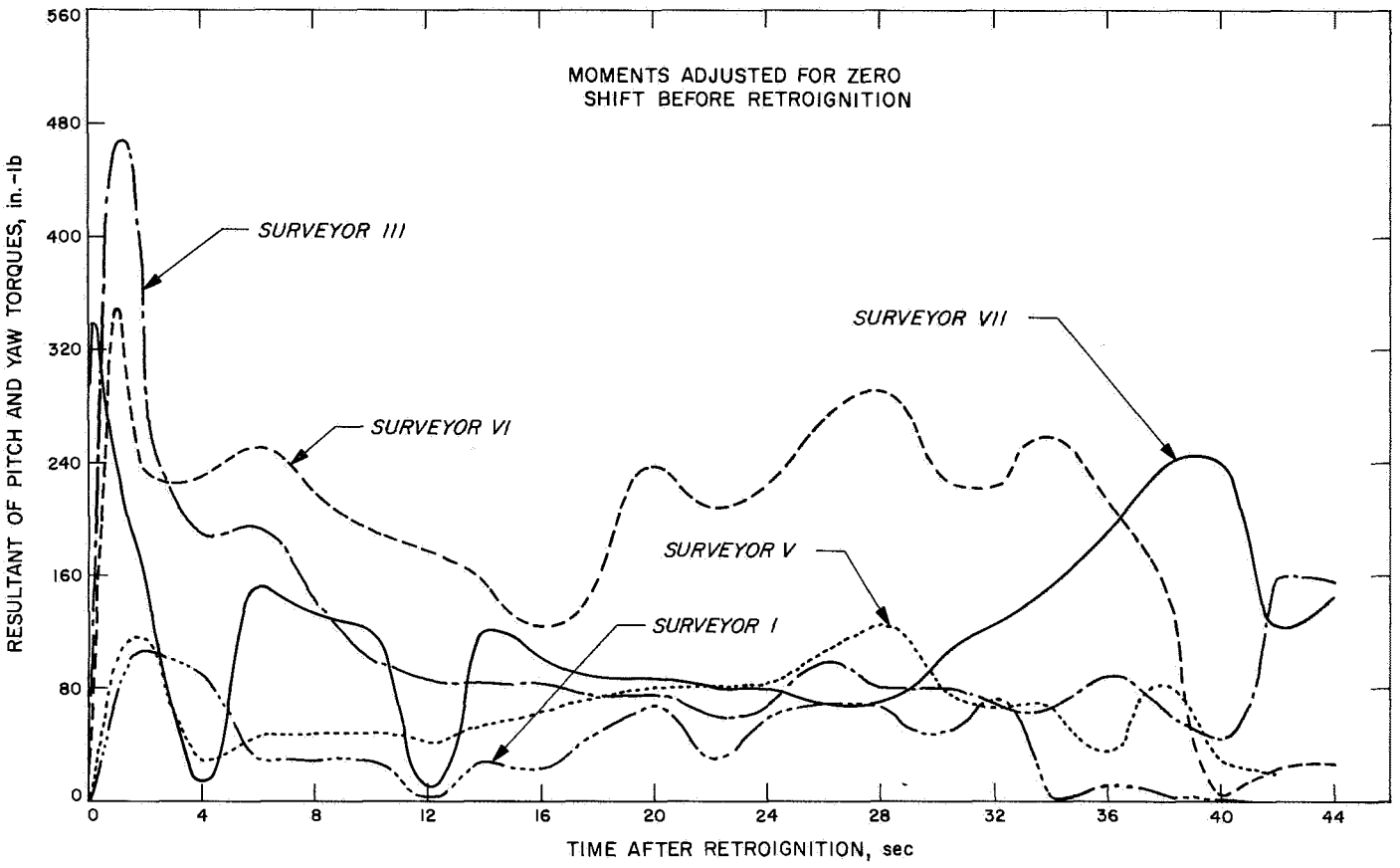



**Fig. XVII-52. Spacecraft pitch and yaw resultant torque during retro motor operation**

retrorocket initiation. The pyrotechnics (squibs and switches) were electrically initiated, hot-bridgewire, gas-generating devices. Electrical power required to initiate the pyrotechnic devices was provided by the spacecraft main battery. Power distribution was through 10.9 and 9.5 A constant-current generators in the engineering mechanisms auxiliary. Commands for operation came from various sources, including the *Centaur* vehicle programmer, separation sensing and arming device, flight control subsystem, and ground stations. The various pyrotechnic devices operated upon command during the entire mission, starting at vehicle injection and continuing until after touchdown on the lunar surface.

A summary of *Surveyor* spacecraft pyrotechnic devices is shown in Table XVII-16. Pinpuller separation devices and locking devices are discussed in Section XIV-D-6.

### 1. Squibs

A squib is a one-shot, electroexplosive device that is fired by an electrical stimulus. Squibs were used on *Surveyor* spacecraft to actuate pinpullers, release and eject bolts, operate valves, and ignite the retro motor. The high reliability of the squib, its low power consumption, high energy output, small size, and light weight made it a desirable component for these applications.

The design philosophy for pyrotechnic-actuated devices was to use a single squib per device with a dual bridgewire circuit for redundancy. This philosophy was adhered to for all the devices on the spacecraft except for the retro motor safe/arm device and the retro motor release device. The safe/arm device used two single-bridgewire squibs. Both the device and the squibs had been partially qualified in another program when they were procured for the *Surveyor* application, and the mechanical and electrical interfaces were already established. Therefore, the design was not changed. The retro motor release device was a modification of a device already in production that used two squibs. In this case, the two dual-bridgewire squibs were retained for the device. The basic philosophy of a single squib with a dual bridgewire was selected over the concept of two squibs

**Table XVII-16. *Surveyor* spacecraft pyrotechnic devices**

| Type | Application | Number of squibs | Command source |
|---|---|---|---|
| Pinpullers | Lock and release omni-antennas A and B | 2 | *Centaur* programmer |
| Pinpullers | Lock and release landing legs | 3 | *Centaur* programmer |
| Pinpuller | Lock and release planer antenna and solar panel | 7 | Separation sensing and arming device and ground station |
| Pinpuller | Lock and release vernier engine 1 roll actuator | 1 | Ground station |
| Valves | Helium release for VPS pressurization and helium dump | 2 | Ground station |
| Pyrotechnic switches | RADVS power "on" and "off" | 4 | Ground station and flight contral sub-system |
| Initiator squibs | Initiate retro motor ignition | 2 | Ground station and flight control sub-system |
| Separation device | Retro motor release | 6 | Flight control sub-system |
| Locking plungers | Landing leg shock absorber locks | 3 | Ground station |
| Pinpuller | Soil mechanics/surface sampler release | 1 | Ground station |
| Pinpullers | Alpha scattering release | 2 | Ground station |

with a single bridgewire each for the reasons described in the paragraphs that follow.

Less weight and space were required because one less squib, one less connector, and one less harness were needed per device. Greater spacecraft reliability was obtained because of the elimination of 50% of the required electrical connectors and solder connections. Less expense was incurred since a fewer number of squibs was required in the system test and flight use.

A wider operational margin was obtained between the nominal explosive charge and the minimum charge that would operate the device, and a wider safety margin was achieved between the nominal charge and the charge that would damage the device. The reasons for this were that in a device with two squibs the explosive charge must be of sufficient magnitude to provide assurance that one squib would operate the device reliably at the coldest-temperature (highest-friction) condition, and still not deform, shatter, or rupture the device when both squibs were fired simultaneously at the highest temperature (greatest-output) condition.

A dual-bridgewire circuit provided redundancy for the critical element of the squib circuits. The simplicity of desgn and reduction of components achieved with the single squib, dual-bridge system further enhanced reliability.

A typical squib (Fig. XVII-53) used a unitized contact pin and header cup assembly brazed to the housing to provide a high-pressure seal on the electrical end. The internal surface of the cup was ground flush after the contact pins were brazed in to provide a flat and smooth surface for maximum weld strength of the bridgewire to the pin. An insulator was included on the inside of the power cavity to provide a high electrical resistance after firing from the contact pins to the body. The insulator was bonded to the body to prevent it from being ejected during the operation. The closure was welded to the one-piece body construction.

Five different squibs were used on the spacecraft: pinpuller, retro motor igniter, helium release, helium dump, and shock absorber lock squib. In the pinpuller, the squib was used to retract a pin a finite distance. There were 16 such applications. The two retro motor igniter squibs were used to initiate an explosive train that resulted in the ignition of the main retro motor. One helium valve release and one helium dump squib were used to operate valve assemblies. The release squib pressurized the VPS, and the dump squib vented the pressurization gas to the atmosphere. The landing gear shock squib was used to provide a positive lock for the landing gear to maintain a constant spacecraft attitude with respect to the lunar terrain.

The squib designs were subjected to a design verification test program to provide a safety and operating margin for the device under various conditions of temperature extremes, maximum loads, and variations in hardware tolerance. A total of 982 squibs were fired in various development and assurance tests that demonstrated squib performance over the range of environmental conditions. Type approval tests were conducted to qualify the reliability and confidence levels of the squibs. These tests consisted of hot and cold environments, cold and hot storage, temperature shock, sealing, acceleration, mechanical shock, 5-ft drop, and thermal vacuum. All test units fired satisfactorily and met their requirements. A total of 1159 squibs were used in these tests. Flight-acceptance tests including vibration, mechanical shock, and thermal vacuum were conducted on all squibs designated for flight. Nondestructive electrical tests were made after the environmental exposure.

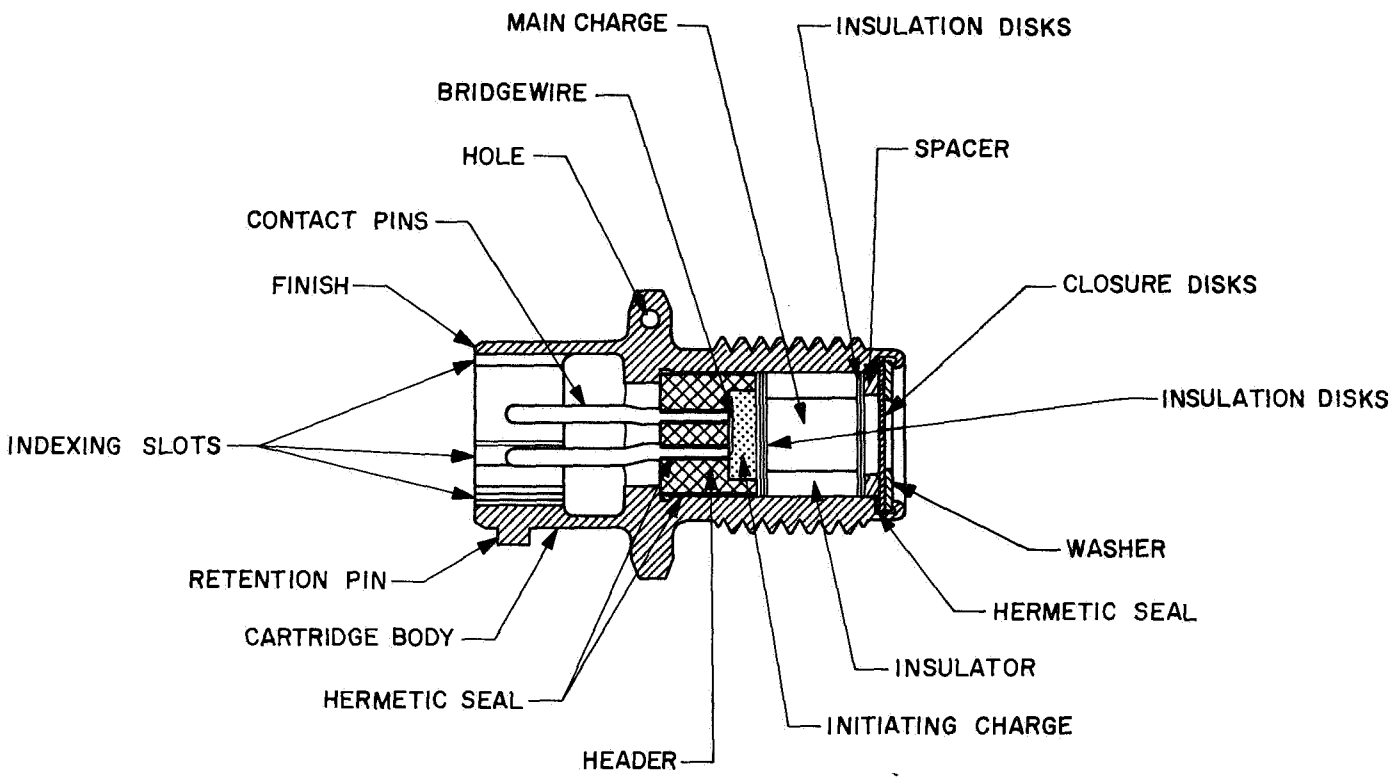



**Fig. XVII-53. Squib structure**

In all the reliability testing of pyrotechnic devices, the margins testing technique was employed. Essentially, this technique amounted to structuring the test and performance requirements so as to impose extremely severe operating conditions. The rationale behind such testing was that the reliability of the device could be established through margins testing of relatively few devices, as compared to a very large number of test samples under simple go/no-go attributes testing. Based on this concept of margins testing, the following reliability (at the 80% confidence level) was demonstrated:

| Squib type | Reliability |
|---|---|
| Pinpuller | 0.9999 |
| Helium dump and release | 0.9999 |
| Retro motor igniter | 0.988 |
| Shock absorber | 0.998 |

### 2. Pyrotechnic Switch

The hermetically sealed assembly consisted of an explosive squib and an eight-pole, single-throw switch. An electrical signal ignited an explosive charge that moved a slider, closing or opening a group of circuits. Two normally open and two normally closed units were used for each spacecraft (Fig. XVII-54). Squib circuits of the normally open units were wired in parallel and the circuits of the normally closed units were wired in series, thereby providing a redundant circuit. The switches were used to turn on and off the high current circuits used in operating the radar altimeter/doppler velocity sensor. On spacecraft SC-5 through SC-7 this switch was replaced with a solid-state relay switch.

Development tests were conducted to determine the design safety and operating margins using minimum crimp strength vs maximum squib output pressure for the safety margin, and the required maximum force to move the switch assembly vs the available minimum squib output force for operating margins. Type approval tests were conducted to qualify both the normally open and normally closed designs and to demonstrate the reliability and confidence levels of the unit. The TA tests included radio interference, vibration, high-temperature storage, cold-temperature storage, temperature shock, sealing, acceleration, mechanical shock, 5-ft drop, thermal vacuum, and postfiring vibration. All units performed satisfactorily. Based on the principle of margins testing, a demonstrated reliability of 0.999 at an 80% confidence level was achieved on each switch assembly.

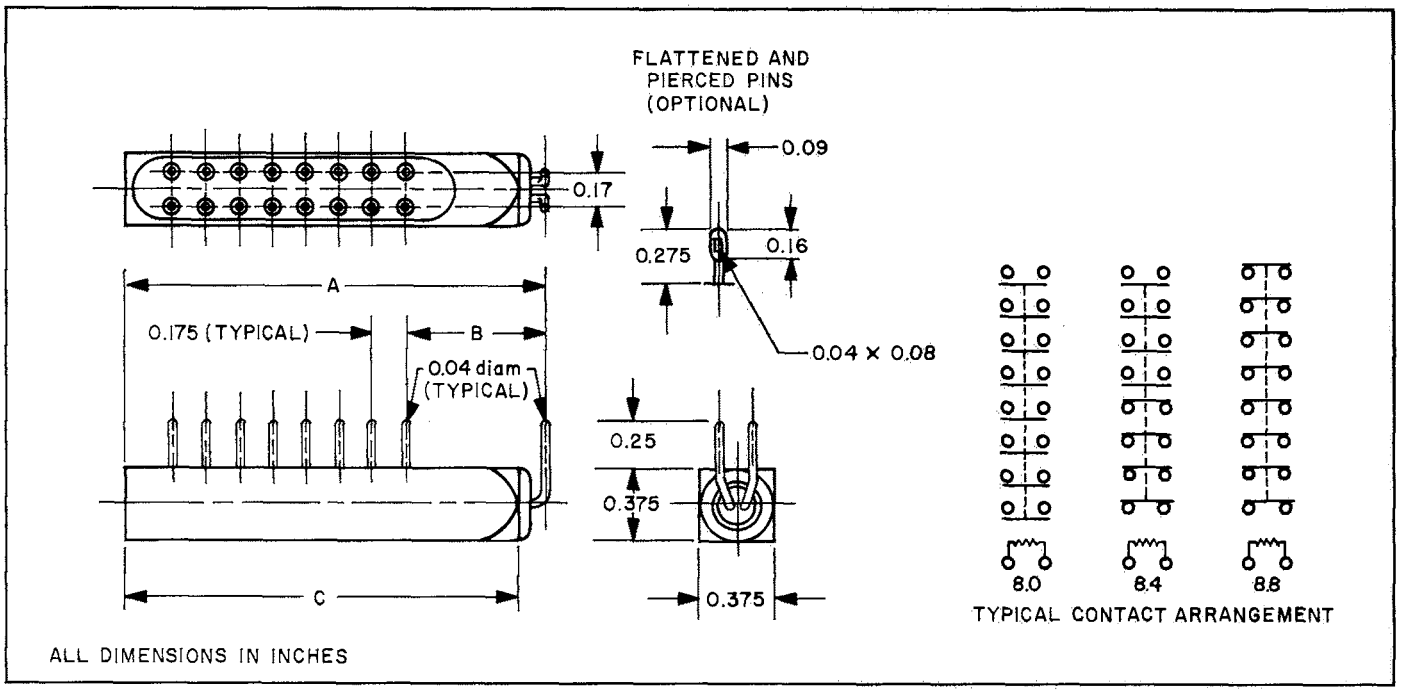



**Fig. XVII-54. Pyrotechnic switches**

### 3. *Safety*

To prevent any hazards to personnel during handling test, all squibs were installed in either a safety guard or a device to safely contain any inadvertent explosion. A shielding cap was installed on every squib connector to shield the pins from RF sources so that the input of stray energy to the squib bridgewire circuit, could be minimized.

The pyrotechnic devices were shipped in metallic containers that were lined with a soft, resilient material. The metal shielded the pyrotechnics from RF sources, minimizing the exposure of the units to such hazards, and the liner prevented physical damage from rough handling. All packing and shipping containers conformed to the Interstate Commerce Commission regulations pertaining to explosives.

All squibs were subjected to a 1-A/1-W, no-fire current for 5-min on both bridgewires simultaneously. The AFETR requires that squibs be capable of passing this test to minimize hazards to personnel or spacecraft when the pyrotechnics might have been subjected to an RF environment. The pyrotechnic devices were subjected to a safety margin test to provide assurance that the devices could safely contain the explosion under the most adverse conditions, such as an inoperative device or a possible overloaded charge.

### 4. Flight Performance

Use of pyrotechnic devices during *Surveyor* missions is summarized in Table XVII-16. There was no spacecraft instrumentation located directly on any pyrotechnic device. However, positive indication of satisfactory pyrotechnic operation was achieved by observing related and associated events and operations that were instrumented, such as retroignition, helium tank pressure, omniantenna and landing leg extension, and antenna/solar panel positioner position. On all missions there was positive indication that the pyrotechnic devices functioned normally upon command, excludng the shock absorber lock squibs. During *Surveyors V* and *VII* lunar surface operations there was evidence that one or more shock absorbers had not locked when commanded. However, there was no positive indication that this malfunction was caused by inoperation of the squibs. Details of this malfunction are contained in Section XIV-D-1.

## References*


XVII-1. "Vernier Engine Migrated Propellant Redistribution During the Main Retro Deceleration Phase," in *The Lunar Program*, Space Programs Summary 37-32, Vol. I. Jet Propulsion Laboratory, Pasadena, Calif., Mar. 31, 1965 (Confidential).

XVII-2. "Retro Phase Moment Control Compensation Due to Vernier Propellant Usage," in *The Lunar Program*, Space Programs Summary 37-37, Vol. I. Jet Propulsion Laboratory, Pasadena, Calif., Jan. 31, 1966 (Confidential).

XVII-3. "An Approximate Conservative Method to Determine Exhaust Plume Impingement Heating Rates of the RMD Vernier Engine on Other Spacecraft Components," in *The Lunar Program*, Space Programs Summary 37-33, Vol. I. Jet Propulsion Laboratory, Pasadena, Calif., May 31, 1965 (Confidential).

XVII-4. Kelly, A. J., *Analysis of the Interaction of the Surveyor Radar Altimeter Doppler Velocity Sensor System and Vernier Thrust Chamber Plumes*, Technical Report 32-927. Jet Propulsion Laboratory, Pasadena, Calif., Apr. 15, 1966.

XVII-5. "Lunar Surface Contamination Due to *Surveyor* Vernier Engine and Main Retro Exhaust Products," in *The Lunar Program*, Space Programs Summary 37-38, Vol. I. Jet Propulsion Laboratory, Pasadena, Calif., Mar. 31, 1966 (Confidential).

XVII-6. "*Surveyor* Vernier Engine/Surface Interaction Experiment," in *Flight Projects*, Space Programs Summary 37-47, Vol. I. Jet Propulsion Laboratory, Pasadena, Calif., Sept. 30, 1967.

XVII-7. *Surveyor* Vernier Engine Plume Interactions with the Lunar Surface," in *The Lunar Program*, Space Programs Summary 37-38, Vol. I. Jet Propulsion Laboratory, Pasadena, Calif., May 31, 1966 (Confidential).

XVII-8. *The Lunar Program*, Space Programs Summary 37-46, Vol. I. Jet Propulsion Laboratory, Pasadena, Calif., July 31, 1967 (Confidential).

XVII-9. *The Lunar Program*, Space Programs Summary 37-44, Vol. I. Jet Propulsion Laboratory, Pasadena, Calif., Mar. 31, 1957 (Confidential).

XVII-10. McDermott, C. E., Breshears, R. R., and McCafferty, J., "Dynamic Performance of *Surveyor* Throttleable Rocket Engine Operating on Propellants Containing Dissolved Gas," AIAA Paper 66-949, presented at AIAA Third Annual Meeting Nov. 29–Dec. 2, 1966, Boston, Mass.

XVII-11. *The Lunar Program*, Space Programs Summary 37-35, Vol. I. Jet Propulsion Laboratory, Pasadena, Calif., Sept. 30, 1965 (Confidential).

XVII-12. *The Lunar Program*, Space Programs Summary 37-43, Vol. I. Jet Propulsion Laboratory, Pasadena, Calif., Jan. 31, 1967 (Confidential).

XVII-13. *Flight Projects*, Space Programs Summary 37-48, Vol. I. Jet Propulsion Laboratory, Pasadena, Calif., Nov. 30, 1967.


*The material dealing with propulsion in Refs. XVII-1, -2, -3, -5, -7, -8, -9, -11, -12, -15, -16, -17, and -19 is unclassified and is available as JPL Re-order 68-207, dated May 15, 1968.

## References (contd)


XVII-14. *Flight Projects,* Space Programs Summary 37-47, Vol. I. Jet Propulsion Laboratory, Pasadena, Calif., Sept. 30, 1967.

XVII-15. *The Lunar Program,* Space Programs Summary 37-40, Vol. I. Jet Propulsion Laboratory, Pasadena, Calif., July 31, 1966 (Confidential).

XVII-16. "Predicted Dissolved Helium Gas Levels in Propellants with Use of a Teflon–Aluminum Laminate Bladder," in *The Lunar Program,* Space Programs Summary 37-36, Vol. I. Jet Propulsion Laboratory, Pasadena, Calif., Nov. 30, 1965 (Confidential).

XVII-17. *The Lunar Program,* Space Programs Summaries 37-22 through 37-32, Vol. I. Jet Propulsion Laboratory, Pasadena, Calif., July 31, 1963–Mar. 31, 1965 (Confidential).

XVII-18. *Surveyor Vernier–MITA 150A Thrust Chamber Assembly Final Report Phase III,* Report 8422-6013-TU-000, Vols. I and II. TRW Space Technology Laboratories, Redondo Beach, Calif., Feb. 26, 1965.

XVII-19. "*Surveyor* Bladder Expulsion Tests Using a Redesigned Standpipe," in *The Lunar Program,* Space Programs Summary 37-41, Vol. I. Jet Propulsion Laboratory, Pasadena, Calif., Sept. 30, 1966 (Confidential).

XVII-20. *Surveyor II Mission Report–Mission Description and Performance,* Technical Report 32-1086. Jet Propulsion Laboratory, Pasadena, Calif., Apr. 1967.

XVII-21. *Surveyor SC-V Review Committee Report,* Report 2227.1/2177. Hughes Aircraft Co., El Segundo, Calif., Sept. 1967.

XVII-22. "Experimental Investigation of *Surveyor* Helium Regulator," in *Flight Projects,* Space Programs Summary 37-49, Vol. I. Jet Propulsion Laboratory, Pasadena, Calif., Sept. 30, 1967.

XVII-23. "Loss of Oxidizer Pressure on SC-VI After Landing on the Moon," in *Flight Projects,* Space Programs Summary 37-50, Vol. I, pp. 127–138. Jet Propulsion Laboratory, Pasadena, Calif., Mar. 31, 1968.

XVII-24. "Loss of Oxidizer Pressure on SC-V After Landing on Lunar Surface," in *Flight Projects,* Space Programs Summary 37-49, Vol. I. Jet Propulsion Laboratory, Pasadena, Calif., Jan. 31, 1968.

XVII-25. *T2N Surveyor Test Vehicles–Tether and Descent Test Series Final Report,* Report SSD 68149, JPL Contract 950056. Hughes Aircraft Co., El Segundo, Calif., July 1966.

XVII-26. *Improved Sampling and Analytical Procedure for Nitrogen Tetroxide and Mixed Oxides of Nitrogen,* Technical Report 32-1282. Jet Propulsion Laboratory, Pasadena, Calif., Oct. 15, 1968.

XVII-27. *Surveyor I Mission Report, Part I: Mission Description and Performance,* Technical Report 32-1023. Jet Propulsion Laboratory, Pasadena, Calif., Aug. 31, 1966.

## References (contd)


XVII-28. *Surveyor III Mission Report, Part I: Mission Description and Performance,* Technical Report 32-1177. Jet Propulsion Laboratory, Pasadena, Calif., Sept. 1, 1967.

XVII-29. *Surveyor VI Mission Report, Part I: Mission Description and Performance,* Technical Report 32-1262. Jet Propulsion Laboratory, Pasadena, Calif., Sept. 15. 1968.

XVII-30. *Surveyor VII Mission Report, Part I: Mission Description and Performance,* Technical Report 32-1264. Jet Propulsion Laboratory, Pasadena, Calif., Feb. 15, 1969.

XVII-31. *Surveyor IV Mission Report, Part I: Mission Description and Performance,* Technical Report 32-1210. Jet Propulsion Laboratory, Pasadena, Calif., Jan. 1, 1968.

XVII-32. *Surveyor II Mission Report, Part I: Mission Description and Performance,* Technical Report 32-1086. Jet Propulsion Laboratory, Pasadena, Calif., Apr. 1, 1967.

XVII-33. *Surveyor V Mission Report, Part I: Mission Description and Performance,* Technical Report 32-1246. Jet Propulsion Laboratory, Pasadena, Calif., Mar. 15, 1968.

XVII-34. "*Surveyor VII* Propulsion System Performance During First Lunar Day," in *Flight Projects,* Space Programs Summary 37-50, Vol. I. Jet Propulsion Laboratory, Pasadena, Calif., Mar. 31, 1968.

XVII-35. *Surveyor Main Retrorocket Engine Development Program, Final Report,* Report E78-64. Thiokol Chemical Corp., Denville, N.J., June 30, 1964 (Confidential).

XVII-36. *Surveyor Main Retrorocket Engine Qualification Program, Final Report,* Report E70-65. Thiokol Chemical Corp., Denville, N.J., Aug. 13, 1965 (Confidential).

XVII-37. *Altitude Performance Evaluation of the Main Retrograde Thrust Rocket for the Surveyor Lunar Spacecraft (Summary of Nine TE-364 Firings),* Report AEDC-TR-65-244. Arnold Engineering Development Center, Tullahoma, Tenn., Dec. 1965 (Confidential).


## Bibliography


*AFETR Range Safety Manual,* AFETRM 127-1. Nov. 1, 1966.

*An Evaluation of Composite Teflon–Aluminum Foil Bladders for the Surveyor Vernier Propulsion System,* SSD 78020. Hughes Aircraft Co., Culver City, Calif., Mar. 1967.

## Bibliography (contd)

*A31E Helium Check and Relief Valve Assembly, Type Approval Test Report,* SSD 78017. Hughes Aircraft Co., Culver City, Calif., May 1965.

*Interface Document Surveyor Vernier Propulsion Thrust Chamber Assembly,* SSD 287015. Hughes Aircraft Co., Culver City, Calif., Feb. 18, 1965.

*Pad Safety Report for Surveyor Model A21–Project Surveyor,* HAC 227651, Rev. A. Hughes Aircraft Co., Culver City, Calif., July 18, 1966.

*Project Surveyor A21 Spacecraft, Pyrotechnic Handling, Testing, and Installation Procedure,* HAC 227431, Rev. G. Hughes Aircraft Co., Culver City, Calif., Oct. 18, 1967.

*Quality Assurance Testing of Surveyor Main Retro Engine at AEDC,* SSD 5118R. Hughes Aircraft Co., Culver City, Calif., Feb. 1965 (Confidential).

*Surveyor Helium Tank and Valve Assembly Type Approval Test Report,* SSD 68067R. Hughes Aircraft Co., Culver City, Calif., Jan. 1966.

*Surveyor Helium Tank and Valve Assembly Type Approval Test Report,* SSD 78014R. Hughes Aircraft Co., Culver City, Calif., Jan. 1967.

*Surveyor Propellant Tank Type Approval Test Report,* SSD 68103R. Hughes Aircraft Co., Culver City, Calif., May 1966.

*Surveyor S-6C Flight Control System Verification Test,* SSD 56037R. Hughes Aircraft Co., Culver City, Calif., Feb. 1966.

*Surveyor S-6 Type Approval Test Report,* SSD 5000R, Rev. A. Hughes Aircraft Co., Culver City, Calif.

*Surveyor S-7 Pressurized Drop Test Report,* SSD 50078R. Hughes Aircraft Co., Culver City, Calif.

*Surveyor* S-7 *Type Approval Test Report,* SSD 50001R. Hughes Aircraft Co., Culver City, Calif.

*Surveyor Spacecraft SC-2 Mission Failure Review Board Report,* Project Document 108. Jet Propulsion Laboratory, Pasadena, Calif., Jan. 10, 1967.

# XVIII. Flight Control Subsystem

## A. General

The flight control subsystem (FCS) was designed to control the velocity and attitude of the *Surveyor* spacecraft during the transit phase of the mission: from separation from the *Centaur* vehicle to touchdown on the lunar surface. The basic functions performed by the FCS included those to: (1) reduce *Centaur*/spacecraft separation rates to a minimum within the design requirements; (2) acquire and maintain a sun–Canopus orientation and attitude stabilization for spacecraft attitude reference during the entire transit phase; (3) perform pre-midcourse-correction, spacecraft attitude orientations and provide the necessary timing and control signals for stabilization and velocity correction to the flight path based on radio commands; (4) orient the spacecraft to the desired retro motor and vernier engine thrust attitudes for terminal descent; and (5) in conjunction with a FCS flight programmer and a radar system, generate a series of automatic commands during the descent sequence to reduce the vehicle velocity to a value required to soft-land in an upright position on the lunar surface.

## B. Flight Control Subsystem Design

The FCS, as conceived, embodied all the basic concepts of the final design described below. Although no basic changes were made during development, some detailed changes were required relatively late in the program; these are described in Subsection A-2.

### 1. Functional Description

The FCS consisted of the Flight Control Sensor Group (FCSG), the gas-jet attitude control system and the roll actuator. A pair of gas jets was located on each of the three landing legs to provide pitch, yaw, and roll attitude control during periods when the vernier engines were not used.

The gas jets used clean, dry, pressurized nitrogen gas to produce a low-level thrust for the attitude corrections.

To establish a spacecraft reference required for all phases of operation during the spacecraft transit phase, and to maintain adequate thermal control, the vehicle

had to be aligned with the sun and the selected reference star Canopus shortly after *Centaur*/spacecraft separation.

This was accomplished after a rate-dissipation phase by means of an automatic sun acquisition sensor. Upon acquisition of the sun, a primary sun sensor controlled pitch and yaw attitudes to maintain vehicle alignment.

Acquisition of Canopus was achieved by means of a star sensor for a roll attitude reference. All maneuvers for the midcourse correction and the terminal-descent phase were performed with respect to the sun–Canopus reference established.

The midcourse velocity correction, all maneuvers, and the radar range and velocity information were processed by the FCS after being initiated by either radio or radar command to the spacecraft.

Figure XVIII-1 indicates the functional elements of the FCS grouped into four principal categories: input stimuli, sensors, electronic controls, and vehicle controls. The main retro motor and vernier engines have been included in the diagram for functional completeness.

Vehicle responses in attitude, acceleration, and velocity were controlled as needed by various control loops during the coast and thrust phases of flight as shown in Table XVIII-1.

A complete presentation of control loop gains, transfer functions, and logic keys associated with the modes of operation described herein is contained in the flight control mechanization, flight control programmer mechanization, and the flight control system block diagrams (Appendixes XVIII-A, XVIII-B, and XVIII-C, respectively).

In addition, Appendixes XVIII-D, XVIII-E, and XVIII-F contain detailed descriptions of the sun sensors, inertial gyro reference unit, attitude gas system elements, Canopus sensor, FCSG electronics, and the roll actuator, which supplement the description of the FCS given in the body of this report.

*a. Gas-jet attitude control system.* The gas-jet attitude control system provided the torques required to stabilize the spacecraft during initial acquisition, and to maintain attitude control during the coast phases of flight.

This system (Fig. XVIII-2; also see Fig. XIII-24) was made up of three assemblies: the gas-jet supply assembly, the manifold, and the jet valves. The supply assembly consisted of a 9.6-in.-diameter tank that was assembled to an integral fill valve, pressure regulator, pressure transducer and temperature transducer. The required safety margin was a minimum burst pressure of 2 times, and proof pressure of 1.5 times the maximum operational charge pressure. (Maximum design pressure was 5000 psi; flight pressure was 4600 psi.) The uncharged weight of the supply assembly was 9.1 lb (charged to 46,000 psi, this weight was 13.67 lb). The pressure regulator regulated to 44.37 psi under lockup (no gas flowing), and to 37.7 psi during the flowing of two jets (average of data from spacecraft SC-2 through SC-5 PVT-3 tests). Included in the regulator assembly was a low-pressure relief valve designed to open at 75 psi if the low-pressure system should become pressurized above this value. The minimum reseating pressure for this valve was 62 psi.

A 0–5000-psi pressure transducer, with a total error of less than 5% of full-scale measurement and a scale

**Table XVIII-1. Flight control modes**

| Control loop | Flight phase | Mode | Remarks |
|---|---|---|---|
| **Attitude control loop** | | | |
| Pitch and yaw | Coast | Rate<br>Inertial<br>Celestial | Gas jet matrix signals |
| | Thrust | Inertial<br>Lunar radar | Vernier engine matrix signals |
| Roll | Coast | Rate<br>Inertial<br>Celestial | Leg 1 gas jet signals |
| | Thrust | Inertial | Vernier engine 1 gimbal command |
| **Acceleration control loop** | | | |
| Thrust axis | Thrust (midcourse)<br>Thrust (terminal descent) | Inertial (with accelerometer)<br>Inertial (with accelerometer) | Nominal 3.22 ft/sec$^2$<br>Minimum 4.77 ft/sec$^2$<br>Maximum 12.56 ft/sec$^2$ |
| **Velocity control loop** | | | |
| Thrust axis | Thrust | Lunar radar | Command segment signals to 43-ft altitude<br>Constant 5-ft/sec velocity signals to 14-ft altitude |
| Lateral axis | Thrust | Lunar radar | Lateral/angular conversion signals |

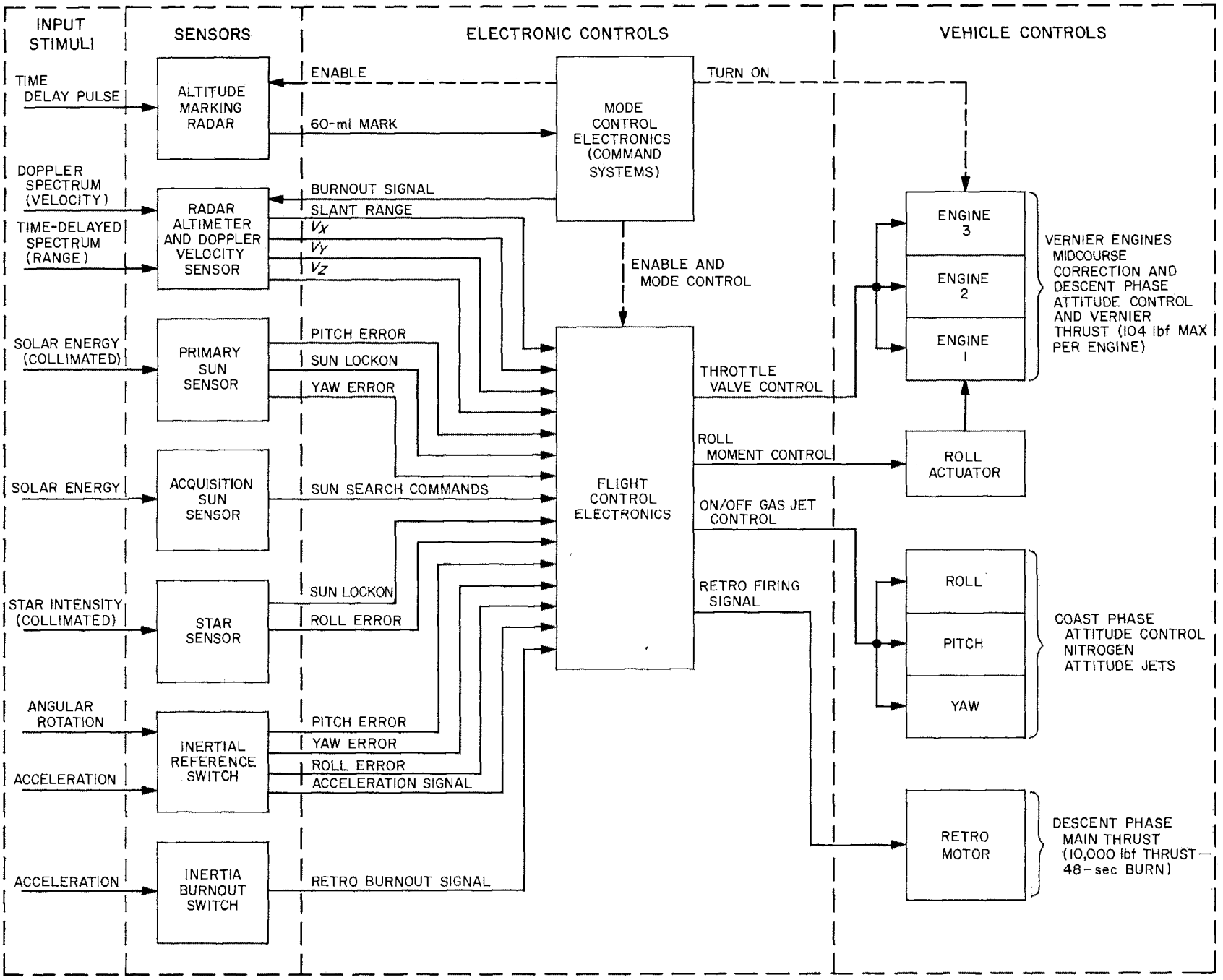



**Fig. XVIII-1. Flight control block diagram**

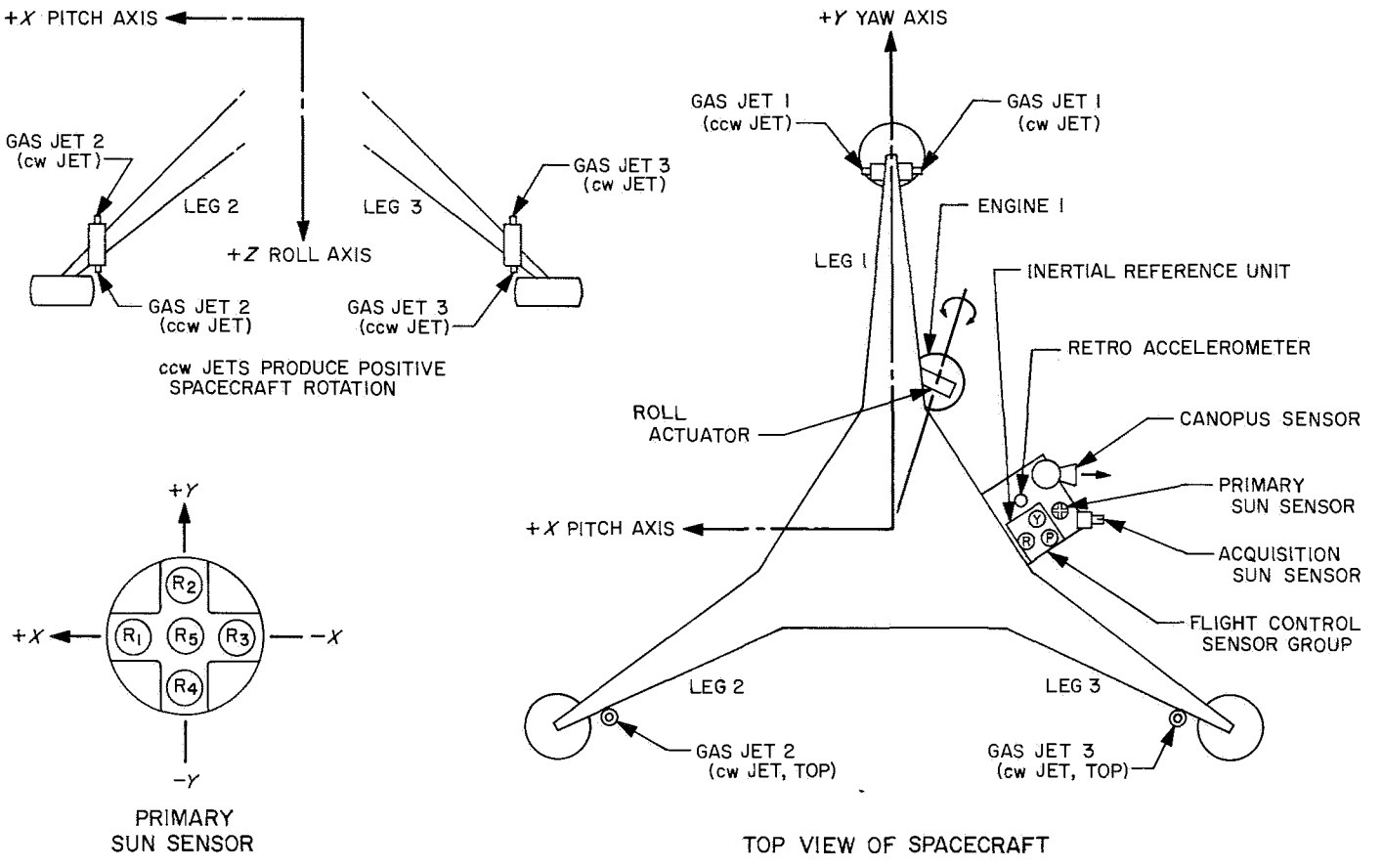



**Fig. XVIII-2. Spacecraft coordinates and location of FCS control elements**

factor of 1000 psi/V ±3% with 5 VDC excitation, was used. The power rating was 1.5 W continuous at 165°F, with a proof pressure of 7500 psi.

The temperature transducer was of the resistance type (500 ±100 Ω at 0°C) with a range of −135 to +170 ±0.5°C. The scale factor was 8 Ω/°C. The transducer was bonded to the tank in the upper rear quadrant (toward the spacecraft).

Lightweight tubing, B-nuts, and fittings constituted the manifold system that distributed the low-pressure nitrogen to the jet valves mounted on the legs of the spacecraft.

A thrust of 0.057 lb +30, −10% was provided by each of two jet valves mounted on the spacecraft legs just inboard of the footpads. The jet valves were electric solenoid type with a coil resistance of 180 Ω ±5% at at 70 ±5°F and a frequency response to 20 Hz. Operation of the valves was controlled by solid-state switches in the flight control unit. The operational temperature range of the jet valve was −50 to +160°F.

Overall leakage limits of the gas-jet attitude control system (174 $cm^3$/hr) was met on all spacecraft. One jet valve each on spacecraft SC-1 and SC-5 was leaking out of specification (20 $cm^3$/hr) at launch. However, because of the tightness of the rest of the system, these leaks in no way endangered the mission, and the systems were flown without repair.

Original design requirements were stringent enough to ensure reliability but not impossible of accomplishment.

*b. Primary sun sensor.* The primary sun sensor provided the required optical pitch- and yaw-error signals to the appropriate gas-jet activation circuits while in the celestial reference mode to maintain an accurate sunline coast reference. The sensor also supplied a switching signal, sun lockon, to logic circuits whenever the sun was in its field of view (FOV). The sensor FOV is shown in Fig. XVIII-3. The control system would not respond to the sensor-error signals unless this switching signal was present. A radio commandable manual lockon signal could also be initiated to back up the same function.

The sensor unit consisted of five light-sensitive cells; one was the lockon cell, and two each were for the pitch- and yaw-error signals. Each pair of cells was used in a bridge circuit and was excited by a 10 V rms 400-Hz reference.

Because cell resistance was proportional to light intensity, any off-sunline angle unbalanced the on-sun bridge null. The output of the bridge was phase-sensitive in response to the cell resistance changes so that the properly phased voltage was conducted to the appropriate gas-jet-firing circuits for accurate sunline-orientation correction of the spacecraft.

*c. Acquisition sun sensor.* Upon *Centaur*/spacecraft separation, the spacecraft was commanded by means of the acquisition sensor to seek the sun. Illumination of the acquisition sun sensor provided the necessary switching signal to the logic circuits during initial sun acquisition when the sunline did not fall within the FOV of the primary sun sensor; its FOV is depicted in Fig. XVIII-4. The sensor consisted of two light-sensitive cells that produced a FOV resembling a spherical sector. The FOV of the combined cells was slightly more than 180 deg in the $X$–$Z$ plane and about 6 deg in the $X$–$Y$ plane. The FOV pointed in the $-X$ axis direction. Each cell saw slightly more than 98 deg in the $X$–$Y$ plane and their FOVs overlapped at the $-X$ axis. The top cell saw slightly beyond the $-Z$ axis into the opposite hemisphere, and the bottom cell saw slightly beyond the $+Z$ axis into the opposite hemisphere. Because the sensor was used to seek the sun for initial sun lockon, the design provided that the sun would have come into view sometime during a 360-deg spacecraft roll.

*d. Secondary sun sensor.* The secondary sun sensor was disassociated from the flight controls as a logic input after the acquisition-sun-sensor development; it was used primarily to provide sun-position information after the lunar landing so that the solar panel could be stepped perpendicular to the sun and the planar array could be more quickly pointed towards the earth. Because the secondary sun sensor was mounted on and in the same plane as the solar panel, it could still be used as a backup indicator for an emergency sun lockon procedure in the event of an acquisition-sensor failure. The sensor was composed of four light-sensitive cells arranged to view hemispherically a 180- × 360-deg solid angle. Each cell viewed 90 deg of that hemispherical solid angle. The cells were connected into a voltage-divider circuit so that the resistance change per cell as a function of the amount of light seen by the cells produced four separate telemetered voltages proportional to the pitch–yaw plane alignment to the sunline.

*e. Roll actuator.* Vernier engine 1 mounted on the spacecraft leg, position 1, was free to swivel ±5.50 deg from null about an axis perpendicular to the Z axis. A roll actuator was used to control a small component of

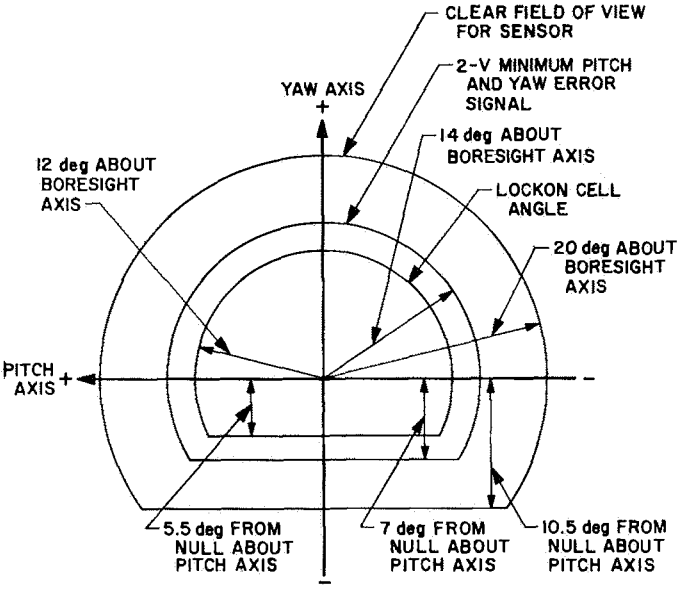



**Fig. XVIII-3. Primary sun sensor field of view**

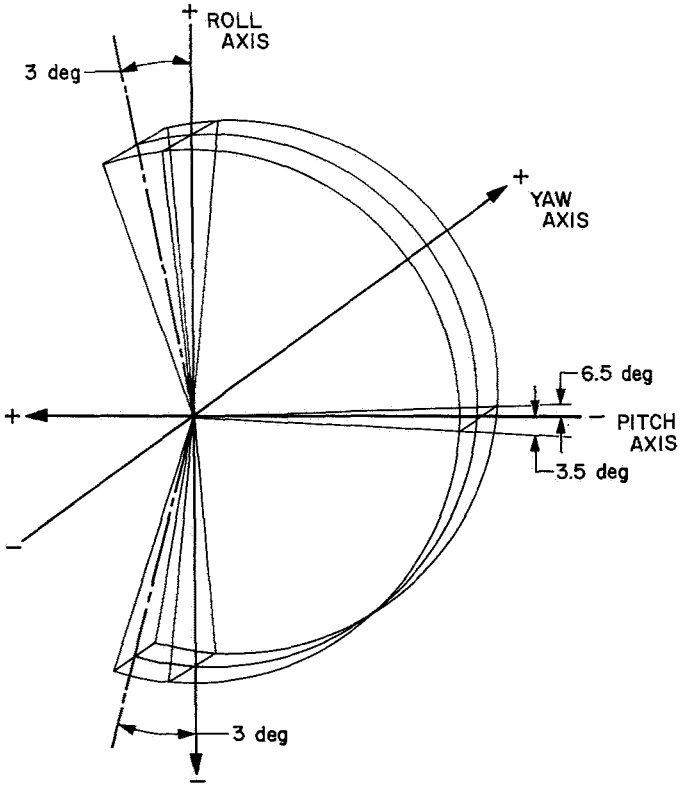



**Fig. XVIII-4. Acquisition sensor field of view**

thrust so that roll-moment disturbances during any vernier engine-thrusting periods could be corrected for. The roll actuator consisted of a servomotor, a reduction-gear train for torque magnification, and a linear potentiometer.

*f. Canopus sensor.* The Canopus sensor provided optical roll-error signals in the celestial-reference mode of operation when the spacecraft roll axis was pointed toward the sun (Fig. XVIII-5). The star window was covered by a shutter that did not open until a primary sun sensor lockon (or manual lockon) was present. This prevented possible damage to the photomultiplier tube by the sun when the spacecraft was in a random space orientation prior to sun alignment. The Canopus sensor FOV is shown in Fig. XVIII-6. Means were provided to adjust the colatitude angle of the center of the FOV to correct for Canopus line-of-sight variations of ±15 deg during the course of a year (Fig. XVIII-7). The sensor produced a logic switching signal (star lockon) whenever a star of the correct magnitude appeared in its FOV. The roll control system would not respond to a star-reference error signal unless the switching signal (or manual lockon) was present. The sensor also supplied a star-mapping output voltage that was proportional to the intensity of the star appearing in its FOV.

A detailed description of the mechanization of the sensor such as error-signal generation for a star of proper intensity (Canopus) is presented in Appendix E.

*g. Inertial reference unit.* The inertial reference unit included three strapped-down integrating-rate gyros with associated temperature-control modules and a linear force-balance accelerometer. The accurate-angle spacecraft maneuvers were accomplished by electrically torquing each of three body-fixed, rate-integrating gyros about its output axis, producing a rate about the input axis. Since torquing of the gyros results in an essentially constant and known angular-rate command, the desired maneuver magnitudes could be obtained by precessing the gyros for precise periods of time.

In addition, by electrically caging the gyros, and operating in servo-loop control, the gyro loop-error output signals provided a first-order lag measurement or angular velocity that was used as a control signal to reduce separation-induced angular velocities to acceptably low values. The gyros were also used in the rate configuration to provide some damping when the control system was operating in the optical-reference mode. The accelerometer sensed acceleration along the roll (thrust) axis and supplied a signal input to the flight control electronics unit for accurate control of the thrust magnitude during

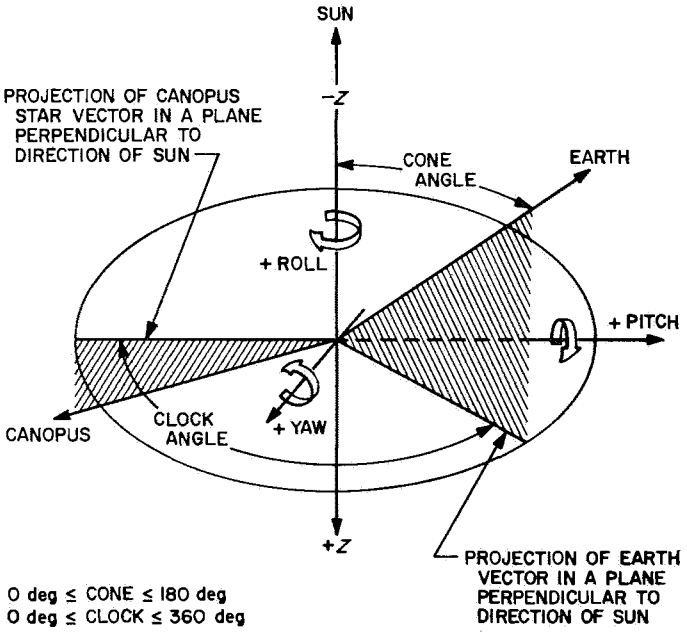



**Fig. XVIII-5. Spacecraft coordinates relative to celestial references**

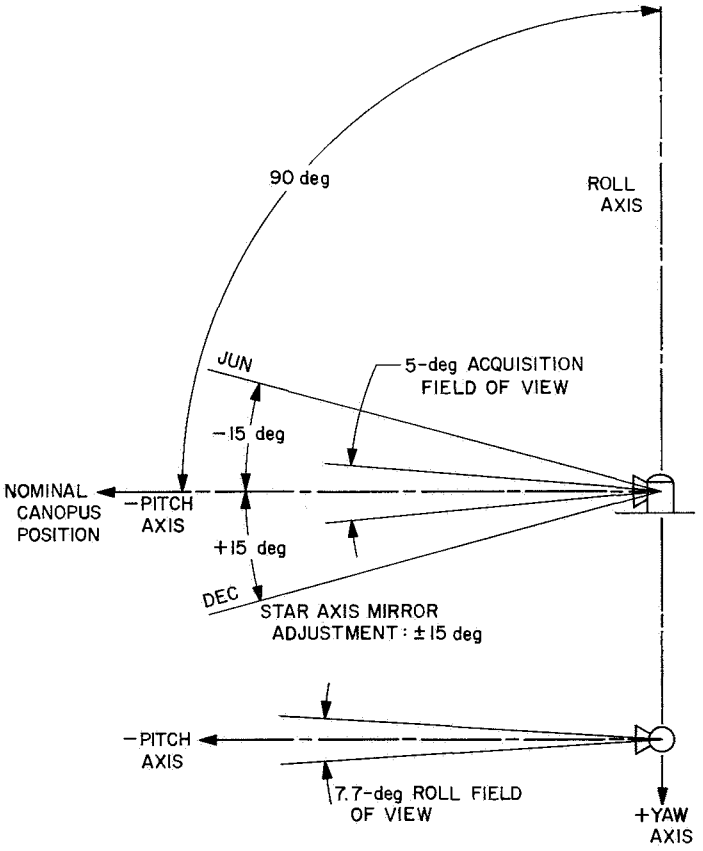



**Fig. XVIII-6. Canopus sensor field of view**

midcourse velocity correction and terminal descent. The range was ±0.75 g and was accurately calibrated for a constant acceleration command.

*h. Surveyor advanced flight control programmer.* The advanced flight control programmer (AFCP) was a digital unit that provided on/off output signals for initiating and controlling sequences within the flight control electronics and power management units of the spacecraft.

Basically, the programmer performed the following major functions:

(1) Generated the signals for attitude control, sun lockon and star lockon according to certain command sequences.

(2) Provided a timed sequence of output signals during the main retro staging sequence.

(3) Generated precision time delays whose durations were radio commandable for controlling attitude maneuvers, midcourse velocity correction, and retro delay.

A simplified block diagram of the AFCP is shown in Fig. XVIII-8; technical characteristics are shown in

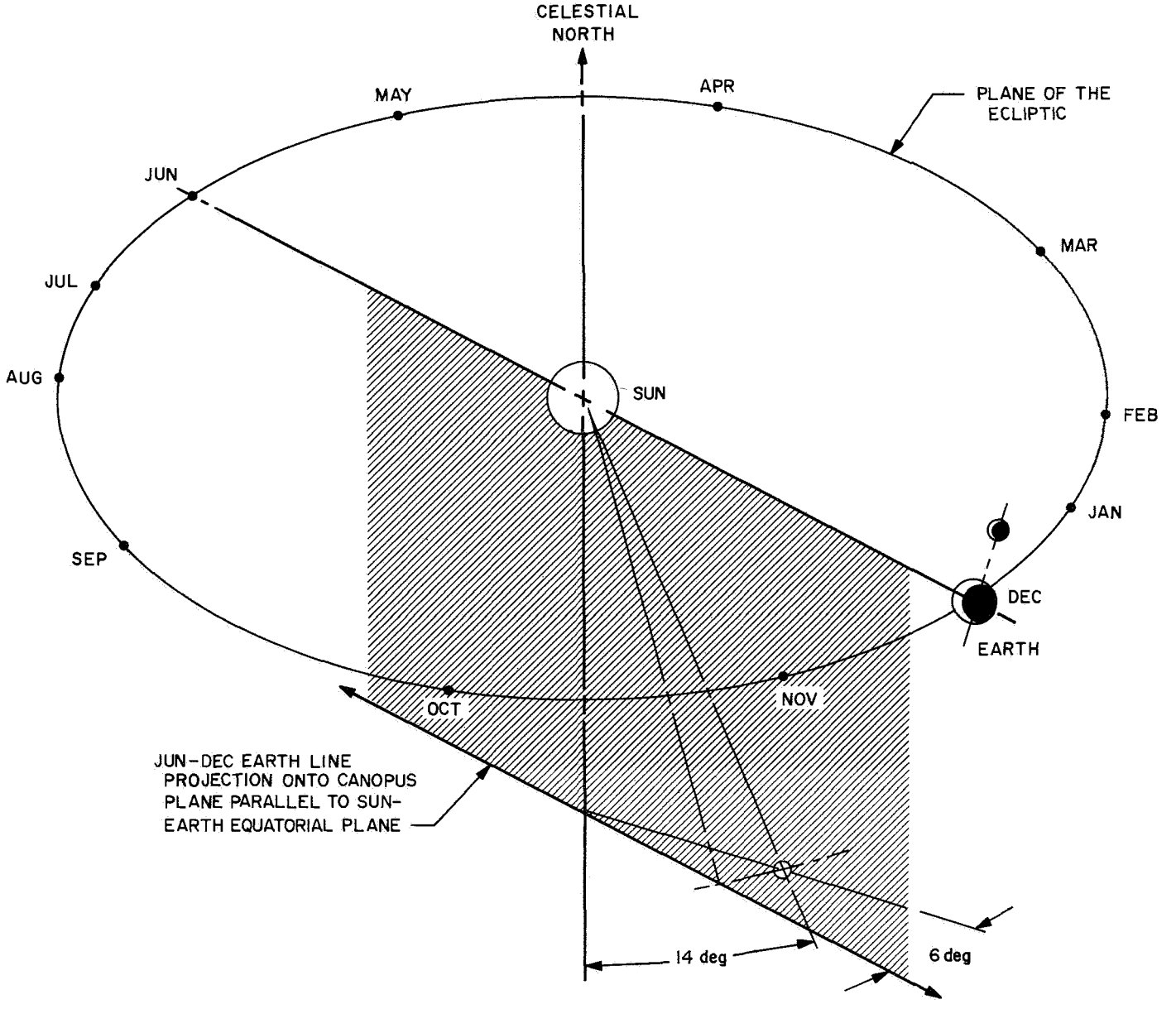



**Fig. XVIII-7. Star Canopus location relative to sun-earth equatorial plane**

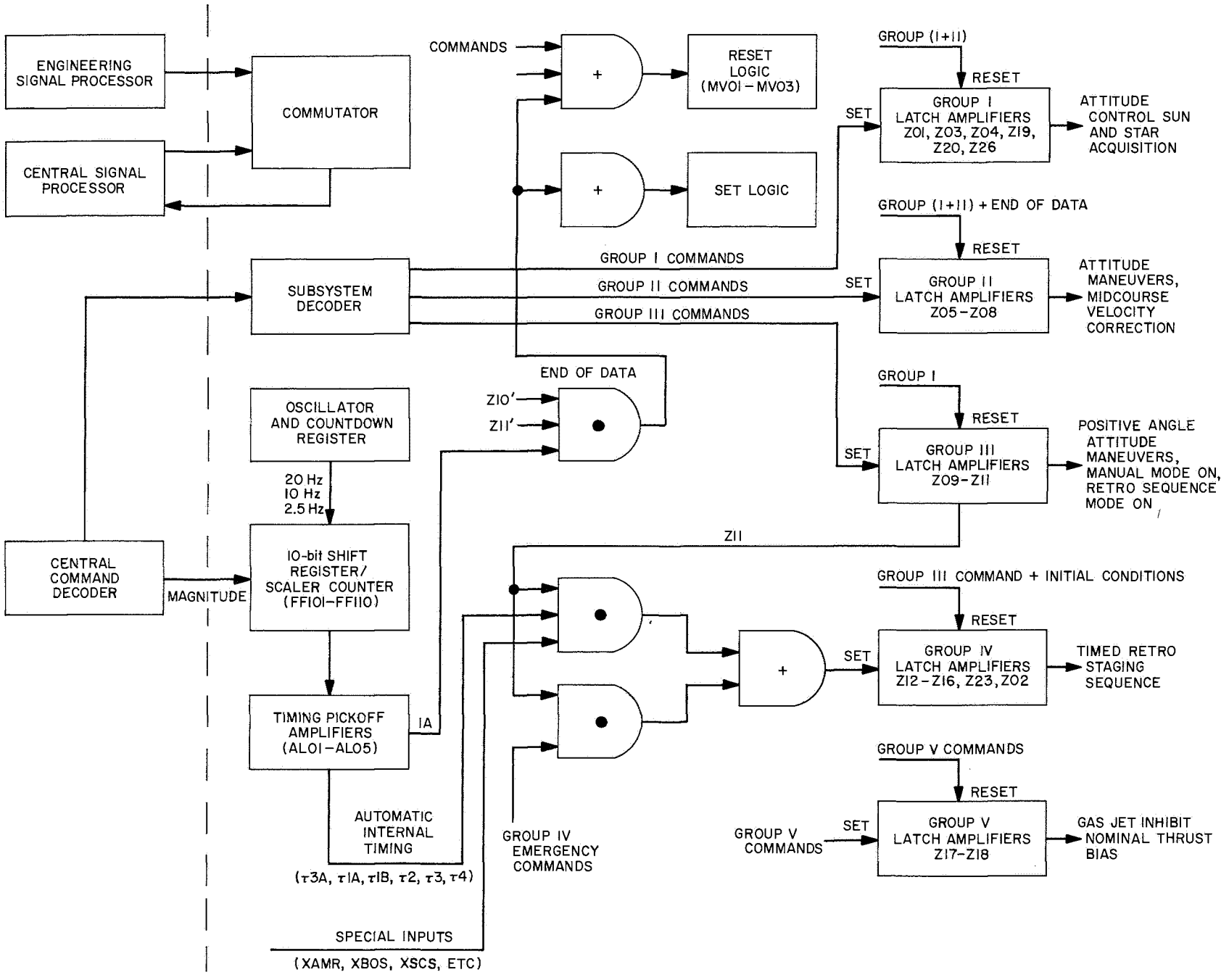



**Fig. XVIII-8. Advanced flight control programmer block diagram**

Table XVIII-2. Most of the inputs to the AFCP were transmitted commands or magnitude information from the AFCP subsystem decoder or the central decoder unit, respectively. Other inputs which were classified as special inputs, were from the altitude marking radar (AMR), the legs-down switches, the spacecraft separation sensors, and the inertia switch. These input signals, when they arrived in certain predetermined sequences, enabled the AFCP logic to generate the outputs for controlling the flight operation or retro staging sequence.

The output latch amplifiers served a dual purpose of providing mode memory capability and interface buffering between the programmer and the flight control electronics.

Operations involving time delays were performed by the 10-bit magnitude shift register/scalar counter. Basically, the shift register/counter provides two types of timing: auto-external time delays and auto-internal time delays.

Auto-external time delays consisted of counting a transmitted magnitude quantity down until the contents of a register equaled zero. The time delay was defined as the time interval between a start signal that initiated the countdown and the termination signal that occurred when the counter reached its zero state. This type of delay was used for initiating the retro staging sequence, automatically timing attitude maneuvers, and timing the midcourse velocity correction maneuver and automatic sun acquisition.

Auto-internal time delays provided the fixed timing associated with the retro staging sequence. Since the retro staging functions followed each other in a fixed-time sequence, each time interval was referenced with respect to the preceding time interval. The fixed internal time delays were provided by the timing-pickoff amplifiers associated with the 10-bit shift register/counter.

Reliability for the AFCP was calculated as the product of the reliability during orbit phase of the flight mission and the reliability during engine burn periods (launch, midcourse-correction, and retro phases). The estimated reliability of 0.9902 met the specified reliability of 0.99 required of the AFCP for a 66-hr mission.

### 2. Design Changes

No major FCS design changes were required during the project. Some details of the design were changed, however, to reduce the number of radio commands and incorporate additional automatic sequences to enhance mission reliability. Some of the more significant changes made relatively late in the program were: (1) The secondary sun sensor concept of sun acquisition was changed

**Table XVIII-2. Flight control programmer technical characteristics**

| Parameter | Value | Parameter | Value |
|---|---|---|---|
| Operating temperature range, °C | −20 to +55 | 12 V ±4% | 725 mW peak average |
| Maximum component temperature range, °C | −20 to +70 | −12 V ±4% | 230 mW peak average |
| | | Total peak average | 2.091 W |
| Storage temperature, °C | −65 to +125 | Calculated average | 2.014 W |
| Total number of electrical components (including interface circuits) | 1842 | Internal delay timing accuracies | |
| | | Roll, pitch, or yaw maneuvers | 2.5-pulses/sec clock, maximum delay, 409.4 sec; maximum deviation, ±0.2818 sec |
| Volume, in.$^3$ | 180 | | |
| Dimensions, in. | 10 × 5.4 × 3.35 | Midcourse velocity correction, | 10-pulses/sec clock, maximum delay, 102.35 sec; maximum deviation, ±0.07047 sec |
| Number of electrical components per in.$^3$ | 10.2 | | |
| Weight, lb | 3.9 ±0.2 | | |
| Electrical components, lb/1000 | 2.12 | Sun acquisition delay | 20-pulses/sec clock, maximum delay, 51.125 sec; maximum deviation, ±0.035225 sec |
| Special tolerance limits | | | |
| Tuning fork oscillator | from 0 to +40°C, 0.02%<br>from −30 to +80°C, 0.05% | Vernier ignition delay | 20-pulses/sec clock, maximum delay, 51.125 sec; maximum deviation, ±0.035225 sec |
| Power requirements | | | |
| 29 V ±1% | 1.048 W peak average<br>10.6 W peak (20.8 msec) | | |
| −29 V ±1% (ripple <20 mV) | 110 mW peak average | Auto-internal time delays deviation | <±0.2740 sec |

to a separate automatic concept. (2) The main retro motor ignition and case separation circuitry was redesigned. (3) Filtering was added to reduce susceptibility of interaction of the FCS control circuitry to radar noise and structural resonance. (4) The bandpass of some telemetered flight control signals was increased to enhance postflight dynamic and failure analysis. (5) The FCS flight control programmer was redesigned to incorporate additional logic circuits and reduced noise susceptibility. Other changes are listed in Table XVIII-3.

*a. Sun acquisition.* The initial concept of a sun-orientation acquisition was by means of a secondary sun sensor. The mechanization required that the sensor have a four-quadrant hemispherical viewing capability along the $-Z$ axis of the spacecraft. Each quadrant would contain a light-sensitive device whose voltage output as a function of light intensity would be telemetered.

It was conceived that upon *Centaur* separation from the spacecraft, the position of the sun relative to the spacecraft $X$, $Y$, and $Z$ coordinates could be ascertained via the telemetry link. An appropriate positive or negative pitch- or yaw-maneuver command would be radio commanded to position the $-Z$ axis within the restricted view of the primary sun sensor. The primary sensor would then initiate final alignment and subsequent pitch/yaw control.

To eliminate this awkward method of sun acquisition and to minimize the total number of spacecraft commands, the manual sequence was changed to make the secondary sensor acquisition an automatic function.

This required addition of logic circuits to the flight-control programmer to respond to the secondary quadrant sensor output so that the appropriate maneuver of the correct polarity for placing the sun within view of the primary sensor could be generated.

Early in 1965, a review of the sun-acquisition sequence revealed a number of weaknesses. The secondary sensor was located on the solar panel (an array of light-sensitive cells that change solar energy to electrical power to supplement inflight power requirements in parallel with the battery power system). Before separation, the solar panel was required to be in a stowed position to fit within the spacecraft protective shroud during the launch boost environment.

At separation, the solar panel was erected in a series of steps to a position such that the solar panel plane was perpendicular to the $Z$ axis. This sequence took about 6 min to complete.

Decisions were made that: (1) Sun acquisition should be made independent of the solar panel deployment from a reliability point of view. (2) The time from separation to sun acquisition should be minimized because temperature-sensitive components were off the sunline orientation. (3) An automatic sun-acquisition device insensitive to earthshine effects such as were inherent in the secondary sensor would be designed. The new automatic device would have a very narrow restricted view. As a consequence of these decisions, the automatic sun-acquisition sensor was designed, developed, and qualified for incorporation into the SC-1 spacecraft. This unit was mounted on the FCSG and proved to be highly successful for all seven *Surveyor* missions. The secondary sensor on the solar panel was retained to be used only as a backup nonstandard acquisition sequence, and to aid in positioning the solar panel during lunar operations.

*b. Main retro motor ignition and case separation circuits.* The flight control programmer contained the logic circuits necessary to generate the automatically timed retro-ignite and retro-separate commands during the retro phase of the terminal descent.

Included in the flight control electronics were the necessary circuits to perform retroignition and case separation in response to those commands.

These circuits had two capacitive-coupled pulsed inputs, retroignite and retro eject, using a driver amplifier circuit with a 20-msec turn-on feature and a positive feedback resistance–capacitance network to accomplish the activation period desired. The circuit powered by the flight control 29-VDC thrust phase power circuits enabled a 19-A current source in the engineering mechanisms auxiliary, and simultaneously provided a gating voltage to a silicon controlled rectifier (SCR) for a 19-A current path to ignite three sets of explosive squibs, which ignited the retro engine.

The retro casing eject circuitry used two sets of three squibs each in the three explosive bolts for separating the empty case from the spacecraft. This was accomplished by using two SCRs, one was used to gate the 19-A current source to the first set of three squibs and after a delay of 20 msec past the initial 20-msec activation, the second SCR fired the second redundant set of three squibs for a period of 70 msec to ensure retro case separation.

During the course of JPL design reviews and analyses conducted, it was determined that the retroignite–retro-eject circuitry was susceptible to inadvertent activation.

## Table XVIII-3. Significant changes to Flight Control Sensor Group configurations

| Engineering change authorization | Problem | Change |
|---|---|---|
| | **Spacecraft SC-1 and SC-3** | |
| 111367 | Based on gyro and inertial reference unit test experience, it was deemed advisable to be able to turn on gyro heaters prior to turn-on of flight control power | Added necessary wiring and an OR gate that permitted either external warmup or regular flight control voltage to be applied to gyro heaters |
| 111348 | Analysis of possible mission problems revealed no backup Canopus lock-on signal in the event the star sensor failed to provide same | Added necessary logic circuitry so that a manual Canopus lockon signal could be commanded on |
| 111374 | During vibration tests, it was noted that the 0- to +0.5-$g$ acceleration loop accelerometer rectified the vibration, resulting in erroneous accelerometer signals and excessive acceleration error | Procured $\pm 0.75$-$g$ accelerometer that did not yield erroneous signals because of vibration, and larger acceleration range provided greater control range |
| 111630 | Analysis of retro-separation sequence indicated that vernier engine maximum thrusting period should be extended from 8 to 12 sec to ensure retro case separation | Timing sequencing changed inflight control programmer to provide 12 sec of maximum thrust after inertia switch closed at 3.5 $g$ |
| 111762 | During spacecraft solar–thermal–vacuum testing the AC portion of the electronics power supply oscillated | Circuit was changed to provide sufficient filtering, and thermal control was improved to provide cooler, more stable operation |
| 111838 | During spacecraft solar–thermal–vacuum testing, some gyro heaters in the inertial reference unit reoched a very low cycling rate, indicating almost no margin against an over-temperature condition | Additional thermal radiation area was added to the side of the inertial reference unit, which increased the heater cycling rates to acceptable limits |
| | **Spacecraft SC-3 and SC-4** | |
| 111699 | To decrease total spacecraft power requirements, each subsystem was investigated for the purpose of reducing its power requirements | Previous 400-Hz, three-phase sinewave power, generated in the flight control electronics unit, was replaced by 400-pulses/sec, three-phase quasi-squarewave power. The star sensor nodding mirror drive motor and the three gyro spin motors operating on this power decreased power requirements by approximately 10 W |
| 111777 | AFETR safety regulations required that all squib-firing circuits be separately shielded and externally available | Additional shielded wiring was added to the flight control electronics unit harness, and two external connectors were added to provide enough pins for the separate shields |
| 111863 | Through much of flight control sensor group testing, both at the subsystem and spacecraft level, breakout baxes and test tees had to be mated to the flight control sensor group flight connectors for access to various signals. All this mating increased the possibility of damage, with a resultant decrease in reliability | An external test access connector was added in conjunction with ECA 111777, which added two other connectors. The flight control electronics harness was revised to provide more optimum wire routing, and the test access connector was supplied with a flight cap when not used for testing |
| 112514 | Analog simulation studies indicated that, at high-burnout altitudes and high-incidence angles, the attitude loop gain margins were smaller than desired | The gain in the $V_X$ and $V_Y$ loops was reduced to provide sufficient gain margins at all terminal descent conditions |
| 113040 | During spacecraft testing, only indirect or implied knowledge about yaw gyro heater cycling was available | Existing yaw gyro heater cycling circuits were connected to a spare flight control commutator channel |
| | **Spacecraft SC-5, SC-6, and SC-7** | |
| 111874 | Systems guidance and trajectory studies indicated that at some spacecraft weights and trajectories, a midcourse velocity correction of greater than 50 m/sec would be required | Maximum midcourse vernier engine firing time was increased from 51 to 102 sec by utilizing a 10- instead of a 20-pulses/sec, clock pulse in the flight control programmer. The resultant maximum midcourse velocity correction was approximately 100 m/sec |
| 112365 | Systems trajectory studies indicated that, under certain burnout conditions, a marginal vernier fuel condition could exist. By continuing to burn the vernier engines at their retro-burn level after inertia switch closure instead of up-thrusting, some fuel could be saved | Flight control programmer was changed to add a 10-sec delay after inertia switch closure before commanding vernier engine maximum thrust to effect retro case separation |

Table XVIII-3 (contd)

| Engineering change authorization | Problem | Change |
|---|---|---|
| 112663 | Many production delays and some damage caused by handling occurred during fabrication of the inertial reference unit whenever wired-in gyros had to be replaced | Added gyro connectors in the inertial reference unit, thereafter requiring only minimal harness handling and connector mating during gyro changeout |
| 112283 | Systems studies indicated the possibility of a worst-case requirement for ±12-deg travel instead of ±6 deg on vernier engine 1. A ±12-deg roll actuator, plus improved response driving electronics, was developed to meet this contingency | Early mission experience indicated that roll moment disturbances were handled very well by the ±6-deg roll actuator, and the margin was very high; therefore, development of a ±12-deg roll actuator was discontinued. However, it was decided that the ±12-deg roll electronics offered improved response and more stability for no increase in complexity or adverse effect on schedule |
| 113163 | The maximum mapping voltage available out of the star sensor was about 6 V. During the *Surveyor I* and *II* missions, star sensor effective gain was sufficiently high to yield greater than 5 V, thus saturating the telemetry channel | A voltage divider was added at the input to the star mapping voltage telemetry channel to reduce the maximum available voltage from 6 to 5 V. |

In particular, the circuits were sensitive to noise on the FCSG +29-VDC supply as the SCRs were not protected against rapid voltage change rates (noise generated $dV/dt$) and the squib returns and the activation circuit return were referenced to separate grounds.

During the solar-thermal-vacuum test of the SC-1 spacecraft an inadvertent retro eject occurred just before the midcourse test phase.

The failure occurred when the 19-A current source had been activated for use in unlocking the roll actuator. The flight control +29-VDC thrust power had been previously commanded "on" in preparation for the thrusting phase.

When the command, unlock roll actuator, was sent, the 19-A current source was activated to fire a pinpuller squib to release the actuator for positioning the vernier engine 1 for midcourse roll-moment control during simulated retro thrusting.

The retro-eject squibs also fired. Because the +29-VDC power was on and the 19-A current source was activated, the retro circuit was now armed and susceptible to one of the referenced failure modes.

Although an engineering investigation could not pinpoint the exact nature of the failure mechanism, it was concluded that the activation of the roll actuator squib generated a transient on the 19-A bus. The nature of this transient apparently caused a difference of potential between the retro-eject squib return and the 70-msec redundant circuit ground return of sufficient amplitude to trigger the redundant circuit.

The retro circuits on the SC-1 through SC-4 spacecraft were reworked to desensitize the circuits, and, starting with spacecraft SC-5 through SC-7, the circuits were redesigned for higher reliability.

In addition, starting with the *Surveyor I* mission, the command sequences were changed so that the FCSG thrust-phase power was activated after the roll-actuator unlock sequence to prevent the retro circuits from being armed during any period when the 19-A source was used by other subsystem squibs.

***c. Radar noise.*** Parallel with the design, development, and test programs to produce a FCS for incorporation in the *Surveyor* spacecraft vehicle test and flights, FCS personnel at HAC conducted a series of computer programs to verify the analytical design of the FCS.

During the course of the six-degree-of-freedom analog computer studies relating to the terminal descent phase of the *Surveyor* spacecraft, it was determined that the FCS output commands to the vernier engine differential throttle valves were being noise-modulated. The basic frequency of 3 Hz caused engine excursions of low to high thrust (stop-to-stop).

The radar noise model used in the simulations was based on earth tests of the radar system and analytical data regarding the lunar surface terrain.

Since there was low confidence that the engines could perform properly under these conditions, low-pass filtering was added to the $V_X$ and $V_Y$ (lateral velocity commands to the FCS gyros), $V_Z$ (spacecraft velocity along the $Z$ axis), and the $R$ (slant-range altitude of the spacecraft) inputs to the FCS from the radar system that commanded the vehicle along the descent path during terminal descent.

***d. Resonance (40 Hz).*** In addition to the computer programs conducted to verify the analytical design of the FCS, *Surveyor* spacecraft structural vibration modal surveys were conducted to verify the structural and mechanical design of the vehicle and subsystem components. The FCS engineering was particularly interested in these tests for any resonances or disturbing frequencies during vernier engine and retro motor thrusting that could interact with the FCS control loops to cause either poor performance or instability of control of the vehicle during midcourse and the terminal-descent phase.

These tests were conducted on the representative structural S-2 model of the *Surveyor* spacecraft.

The results of these tests indicated that a particular frequency of 40 Hz predominated all others in magnitude. In fact, comparison of the midcourse-accelerometer inverse-transfer function of frequency and amplitude to the structural inputs revealed interaction of this frequency with the accelerometer control loop.

Midcourse velocity correction was based on a precise fixed command of 0.100 $g$, wherein the accelerometer in a closed-loop configuration sensed the thrust-to-mass ratio (acceleration) and controlled the three vernier engine thrust levels to the required telemetry to match the input command.

The accelerometer had a range of $\pm 0.75$ $g$. Since there was asymmetry of the plus and minus output of the accelerometer channel, it was possible for the 40-Hz input to cause averaging offsets in the control loop, thereby introducing error in the total acceleration achieved during the timed vernier engine burn.

To eliminate this possibility, a filter was added to the input of the acceleration amplifier to reduce the bandpass of the output to about 10 Hz before the *Surveyor I* mission.

***e. Flight control subsystem telemetry.*** To effectively perform both inflight and postflight mission analyses, about 79 FCS measurements were telemetered from the spacecraft. Starting at launch, through separation, sun acquisition, Canopus acquisition, coast, midcourse maneuvers, midcourse thrusting-trajectory correction, terminal maneuver, retro sequence, terminal descent, and touchdown, the 79 measurements were presented as sampled data measurements at high or low rates depending on whether the signal had a low- or high-frequency response and on mode and bit-rate selection.

Of particular importance during closed-loop thrusting were the roll-, pitch-, and yaw-gyro error signals; roll actuator error signal; engine 1, 2, and 3 thrust commands; radar lateral velocities $V_X$ and $V_Y$; radar range; and velocity of the vehicle. These data were necessary not only to analyze the dynamic performance of the vehicle during thrusting, but to aid in any possible failure analysis. Evaluation of these telemetry circuits revealed that the bandpass characteristics were not sufficient to obtain data of a dynamic nature. In particular, the three gyro errors were analyzed to be down 3 db at a frequency of 0.5 Hz and were, therefore, essentially DC-error indicators only.

Consequently, these circuits were redesigned to increase the bandpass telemetry capabilities where needed. These changes were made for all flight vehicles before the first *Surveyor* vehicle was launched.

***f. Flight control programmer.*** The flight control programmer conceived at the beginning of the *Surveyor* Project developed problems, particularly during the vibration-test phase. The HAC proposed a completely redesigned programmer and was authorized by JPL in April 1963, to start fabrication of the new programmer. The new programmer, renamed the AFCP, had significant changes in mechanical layout, better thermal design, reduction in the number of components, and components of higher reliability, in addition to a considerable reduction in weight. The total redesign resulted in a lower probability of failure and improved ability to withstand the simulated flight environment. A joint HAC–JPL design review was held on October 11, 1963, for the redesigned programmer.

Very few additional changes were made in the AFCP until early in 1965 when a few minor logic changes were made and a three-phase, 400-Hz frequency reference was incorporated. The three-phase frequency reference replaced a two-phase system requiring a Scott transformer

in the flight-control electronics to power the three-phase gyro spin motors and the motor in the Canopus sensor. At this time, two AFCPs were on hand: one with a two-phase, 400-Hz reference scheduled for the SC-1 spacecraft, and one with a three-phase reference scheduled for the SC-2 spacecraft.

In August 1965, a third AFCP was tested that not only had the three-phase frequency reference, but also included a major functional change: automatic sun acquisition that was initiated by legs-down and separation switches.

The decision was made to use the new programmer with automatic sun acquisition, and the schedule permitted its incorporation in the SC-1 spacecraft flight-control electronics. The same basic AFCP was subsequently flown on all seven *Surveyor* spacecraft.

During the SC-1 spacecraft testing phase at El Segundo, many electrical-transient-induced anomalies were revealed:

(1) Changes of contents of the magnitude register because of noise on the magnitude transfer line.

(2) "Setting" of latches in the absence of a command.

(3) Starting of automatic sun acquisition when legs-down and separation logic had not been satisfied.

The magnitude-register problem was corrected by the addition of a filter circuit in the magnitude transfer line, but shortly afterwards a new problem developed. The command system design provided fill-in words during the time no commands were being received; if the spacecraft receiver were operating at or below the threshold level, however, the command logic generated erroneous magnitude-transfer commands that changed the information content of the AFCP register. The problem was resolved by inserting additional logic in the AFCP so that an interlock command was required in conjunction with the magnitude-transfer command. This change was implemented on the SC-1 through SC-7 spacecraft.

Noise-sensitive logic latches were desensitized by diodes that isolated any positive pulses reflected into the output circuits, which might trigger the positive feedback circuits, causing an undesired latch set. The addition of a small capacitor at the input shunted spurious signals to the return. All latches were modified on spacecraft beginning with SC-3; however, only two latches that showed evidence of particular susceptibility to noise during spacecraft SC-1 testing were modified before flight on the SC-1 and SC-2 spacecraft.

The legs-down, *Centaur*-separation, sun-acquisition problem was very seldom repeatable and occurred with different spacecraft configurations. The first effective attention was given to the problem during SC-1 spacecraft testing at Kennedy Space Center. Normally, sun acquisition should begin only when the logic is satisfied by having all three legs down and *Centaur*/spacecraft separation. During testing, indications of starting sun acquisition occurred when only one or two legs were down, or *Centaur* separation "only" was "on." After extensive testing and troubleshooting, it was determined that this problem did not occur when all test cables were removed from the spacecraft. Finally, the SC-1 spacecraft was launched without modifications designed to solve this problem.

During the separation events of the launch phase of the SC-1 spacecraft, the flight control suddenly switched from rate mode to inertial mode, indicating that part of the automatic sun-acquisition loop (rate latch reset) had been disturbed by a signal. Fortunately, with the extension of the three legs the rate-mode latch was automatically reset and normal sun acquisition was accomplished. As a result, all of the latches were desensitized against noise on spacecraft SC-3 and subsequent spacecraft. A sensitive "one shot" triggered by legs down and separation was replaced beginning with the SC-5 spacecraft by a relatively insensitive latch providing further protection. No other failures of this type were noted on later missions or during spacecraft testing.

A review of procedures and mechanization indicated that there was a possibility of inadvertently restarting the vernier engines immediately after touchdown on the lunar surface. The flight-control logic provides for the shutting down of the vernier engines upon receipt of the radar altimeter and doppler velocity sensor (RADVS) 14-ft mark. The 14-ft mark is a logic inhibit function and, if RADVS power is turned off prior to turning off flight control power, the engines will restart because the inhibit function has been removed. The problem was partially solved on the SC-1 and SC-2 spacecraft by changing the operational procedures to command flight control power off first. A logic change in the AFCP on spacecraft SC-3 through SC-7 reset the vernier ignition latches when the 14-ft mark was generated; this assured that the engines would not accidentally restart regardless of the order of shutdown commands.

Beginning with the *Surveyor V* Mission, two changes were made in the fixed-time events for the descent phase of the mission. The timing logic was changed to increase

the time delay between the retro-separation event and start of RADVS-controlled descent. The AFCP latches retro separate and RADVS-controlled descent formerly had a time delay of 2.5 sec between them and this time was increased to 3.15 sec to allow the burned out retro motor to fall a greater distance from the spacecraft before RADVS control was begun; this procedure was designed to ensure against a false lockup by RADVS on the falling retro motor case.

The second change in the delayed-time events required the addition of a new output latch and a telemetry monitor of the state of the latch; provision of optional control of the latch-by-ground command; and the addition of timing logic to set the new latch 10 sec after the retro-motor burnout event. The function of the new latch was to command vernier engine high thrust 10 sec after retro motor burnout. The reason for adding the delay was to reduce the total fuel consumption in the vernier propulsion system to permit a reduction in fuel loading of about 3 lb. (The fuel-loading capacity of the vernier propulsion system was marginal relative to the required loading for the weight of the A21 model spacecraft.)

Another AFCP change was implemented to enhance mission objectives by increasing the maximum midcourse capability from 51.2 to 102.4 sec. The 51.2-sec maximum vernier burn time allowed a midcourse correction of 50 m/sec. If, on a mission, the injection errors were such as to require a greater correction, the 102.4 sec would increase the correction capability to a maximum of 100 m/sec. The change involved gating in a 10-pulses/sec signal from the timing logic, instead of the 20-pulses/sec signal, thereby doubling the time of the register counting sequence. The logic still allowed the register to count down at a 20-pulses/sec rate for sun-acquisition delay and AMR mark to vernier ignition delay. The first spacecraft to use the increased time capability was SC-5.

Only the roll- and pitch-gyro heater controls were telemetered on spacecraft until SC-3; beginning with spacecraft SC-3, a spare digital word was used for telemetered information of the yaw-gyro heater. Before the SC-3 spacecraft, the only way to determine if the yaw-gyro heater was cycling was to very carefully examine power data for increases and decreases in current on the unregulated bus.

Some minor logic changes were also made in the programmer to ensure that the latches were all in their correct states before beginning a major sequence during the mission. One such change was to automatically reset the clock-enable latch whenever radio command 0720 (reset group 4 latches) was transmitted. This command was normally sent just prior to the descent phase, to put all the descent-phase latches in their initial-condition positions. The clock-enable latch was included to make certain the latch was reset and ready to be set by the AMR mark, at which event the clock counting started for the proper delay. This change was included on all *Surveyor* spacecraft. Another reset logic change was to add a radio command 0717, which reset all latches in the AFCP achieving initial conditions. This addition of reset capability facilitated latch reset in the event of an inadvertent set because of transients or noise. This change was made effective with the SC-5 spacecraft.

## C. Mission Sequence

### 1. Prelaunch Operations

The FCS was given a final test during the systems readiness test and countdown before liftoff. The following operations were part of the countdown:

(1) Gyro preheat 22-VDC power was applied by hardline through the *Centaur* vehicle umbilical connector to increase the three gyro temperatures to at least 150°F before application of gyro motor power (29-VDC coast phase).

(2) Flight control 29-VDC coast phase power was commanded "on" between 1 and 2 hr before liftoff.

(3) The attitude control system was temporarily placed in the "inertial hold mode" by command.

(4) Flight-control-programmer clock-magnitude register was loaded to its maximum time delay (51 sec using the 20-Hz clock). This provided the attitude control system with sufficient time to dissipate any spacecraft rotation rates induced at mechanical separation from the *Centaur* booster.

(5) The FCS was placed in the rate mode to cage the gyros and maintain essentially zero rates about all three axes.

(6) The inhibiting of the gas-jet amplifiers was verified. (They were designed to be inhibited automatically upon application of flight control coast-phase power.)

(7) Nitrogen supply pressure and temperature were checked to verify that sufficient gas was available (approximately 4.5 lb was loaded).

(8) The speed of each gyro motor was checked.

### 2. Separation Rate Dissipation

During the launch phase, the gas-jet attitude control system was inhibited until after *Centaur*/spacecraft separation. About 8 min after the spacecraft nose fairing was jettisoned (mark 4) and immediately after injection (mark 9), the three spacecraft legs were extended to the landing position which provided the gas-jet attitude control system with the necessary moment arms to control the spacecraft. The legs-extended sensors provided three of the four signals necessary to enable the gas jet amplifiers. The fourth signal was supplied upon electrical separation (umbilical plug disconnect) from the *Centaur* vehicle. This signal not only enabled the gas-jet amplifiers, but also started the countdown of the flight control programmer 51-sec clock. Approximately 5 sec after electrical separation, mechanical separation was commanded automatically. Because the attitude control system-commanded rates about the spacecraft axes were essentially zero at this time, the appropriate gas jet fired to reduce the spacecraft body angular rates to a low value as determined by the gas-jet amplifier deadband. The spacecraft was therefore rate-stabilized within the approximately 46 sec allowed for maximum expected separation rates (5 deg/sec about each axis).

### 3. Automatic Sun Acquisition

When the flight control programmer clock counted down to zero (51 sec after electrical separation), the gas-jet AC system was automatically placed in the sun mode of operation. Simultaneously, a −0.5-deg/sec roll maneuver was initiated until the acquisition sun sensor was illuminated, at which time the roll maneuver ceased and a positive yaw maneuver was initiated. The spacecraft dynamics at the completion of the roll maneuver were such that the sunline remained in the acquisition sun sensor FOV. The yaw maneuver continued until the primary sun sensor was illuminated and a lockon signal was generated; at this time the primary sun sensor pitch- and yaw-error signals were nulled to point the negative roll axis of the spacecraft toward the sun.

The pitch and yaw axes were in the optical mode at this time, whereas the roll axis remained in the inertial or roll gyro attitude control mode.

### 4. Canopus Verification and Acquisition

The location of the star Canopus was verified prior to acquisition by performing a positive roll maneuver and monitoring the star intensity signal to obtain a star map. The roll maneuver was initiated approximately 6 hr after launch and continued until Canopus was positively identified on the basis of a comparison of the real-time map with a previously prepared map. At least one, and possibly two or more, complete revolutions were made (depending also upon the mapping of omniantenna nulls) before the command was transmitted to permit automatic acquisition of Canopus. Following receipt of the "sun and star mode on" command, the spacecraft continued to roll until the star Canopus appeared in the FOV of the Canopus sensor and a Canopus lockon signal was generated. This lockon signal stopped the maneuver and permitted nulling of the Canopus sensor roll-error signal by the gas-jet attitude control system.

At this time, the spacecraft pitch and yaw attitude limit-cycled about a null point determined by the primary sun sensor whereas the roll atttude limit-cycled about the Canopus sensor null point.

### 5. Pre-Midcourse Orientation Maneuvers

Normally, two attitude maneuvers were required to orient the spacecraft roll axis in the direction desired for the midcourse velocity correction. Although any combination of pitch, yaw, and roll maneuvers was possible, the preferred two-maneuver sequence was a roll maneuver followed by a yaw maneuver, assuming that the telecommunications link or the pointing accuracy was not adversely affected by this combination.

The first maneuver was initiated approximately 15 min before the scheduled midcourse velocity correction. For a roll maneuver the command "sun and roll" caused precession of the roll gyro in an open-loop manner at 0.5 deg/sec for the desired maneuver duration. The sun-and-roll command placed the roll-control loop in the inertial attitude-hold mode, whereas the spacecraft pitch and yaw attitude remained controlled by the primary sun sensor. At completion of the roll maneuver (approximately 1 min is allowed for settling of transients), a pitch or yaw maneuver was executed by precessing the pitch or yaw gyro at 0.5 deg/sec for the desired time interval. The pitch-completed or yaw-completed command placed the pitch- and yaw-control loops in the inertial hold mode so that at the end of the attitude maneuvers all three axes were in the inertial-hold mode.

### 6. Midcourse Velocity Correction

When the spacecraft roll (thrust) axis had been pointed in the desired direction, the midcourse velocity correction was made by thrusting at an acceleration level of

0.1 $g$ for the duration previously entered into the flight-control programmer clock-magnitude register. The attitude of the spacecraft was controlled by the three gyros; pitch and yaw control was achieved by differential thrusting of the three vernier engines, whereas roll attitude was maintained by positioning engine 1 with the roll actuator. The primary disturbance moment at this time was the result of any variation in startup impulses between any two engines.

### 7. Reacquisition of Sun and Canopus

When the vernier engines were shut off at the end of the midcourse velocity correction, the spacecraft would normally experience a change in attitude because of the nonsimultaneous shutoff of the engines. The angular rates caused by this disturbance were designed to be sufficiently small so that the gyro gimbals would not be driven against their stops ($<10$ deg) and a satisfactory gyro reference could be maintained. Reacquisition of the sun and Canopus would be accomplished by executing the reciprocal of the pre-midcourse maneuvers in the inverse order (i.e., pitch or yaw followed by a roll, for the example cited).

If the gyro limits had been violated at termination of or during the midcourse velocity correction, then reacquisition of the sun would have been accomplished by commanding "sun mode on," which would produce the same negative roll–positive yaw maneuver sequence described in Subsection B-3. Following sun acquisition, the command "sun and star mode on" could have been transmitted to produce a positive roll maneuver and subsequent automatic lockon to the star Canopus as described in Subsection B-4.

### 8. Gyro Drift Measurements

At least four gyro drift checks were to be made during a normal mission: one before and three after the midcourse velocity correction. Depending upon the validity of the gyro drift data, the preretro-orientation-maneuver magnitudes could be compensated for gyro drift to reduce the pointing error.

Drift measurements were made by placing the gas-jet-attitude control system in the inertial mode after sun and Canopus lockon had been achieved. The spacecraft was then free to limit cycle about a reference determined by the pitch-, yaw-, and roll-gyro input axes. Any gyro drift was detected by monitoring the primary sun sensor pitch- and yaw-error signals, as well as the Canopus sensor roll-error signal. The duration of the drift checks was approximately 3 hr unless the sunline went beyond the linear portion of the primary sun sensor error-signal curve or the Canopus line of sight neared the end of the Canopus error-signal linear range. If the linear range of the primary sun sensor was in danger of being exceeded, the gas-jet attitude control system was commanded to the sun mode of operation, which caused nulling of the primary sun sensor error signal without disturbing the Canopus error signal. If the linear range of the Canopus sensor was exceeded, the control system was commanded to return to the cruise mode of operation, which caused nulling of both the primary sun sensor and the Canopus sensor error signals.

### 9. Preretro Orientation Maneuvers

Although only two maneuvers were generally required to orient the spacecraft roll (thrust) axis in the direction desired before ignition of the main retro motor, a third maneuver about the roll axis could be necessary to satisfy a RADVS side-lobe constraint. This constraint required that the location of the radar beams relative to the lunar surface be such as to ensure that the signal levels received via the main lobes of beams 1 and 2, and beams 1 and 3 were sufficiently unbalanced to prevent any cross coupling (see Section XIX). The maneuvers were normally made with the telecommunications commutator in mode 1 at a data rate of 1100 bits/sec. Although commutator mode 5 could be used, it was less desirable because of the lower flight control telemetry-signal sample rates.

Again, the preferred initial two-maneuver sequence was a roll maneuver followed by a yaw maneuver, as described in Subsection B-5. The first maneuver was initiated between 23 and 33 min before the computed retro motor ignition time. The 23-min constraint was based primarily on the undesirable effect of light reflected from the lunar surface, which would have degraded the performance of the Canopus sensor (increase in roll deadband), whereas the 33-min constraint was based on the desire to limit the effect of gyro drift. Both of these effects could influence the spacecraft pointing accuracy. The actual time of first maneuver execution was based in part on the validity of the gyro drift measurements and subsequent compensation of the maneuver magnitudes to correct for gyro drift.

### 10. Retroignition and Case Staging

Upon completion of the orientation maneuvers and during the burning of the retro motor, the spacecraft attitude was maintained using the gyros as an inertial

reference. While still in telemetry mode 5, before retro ignition, either of two vernier engine thrust levels was selected by radio command: "select nominal thrust bias," 152 lb or "reset nominal thrust bias," 201 lb. The vernier ignition delay quantity (0–51 sec) was also entered into the flight-control programmer magnitude register at this time.

About 6 min later (retroignition R − 8 min), the thrust mode commutator was selected.

At 5 min before computed retroignition (R − 5 min), the AMR power was commanded "on"; at R − 4 min, the flight-control thrust-phase power was commanded "on."

At R − 2 min (nominally 205 mi from the lunar surface), the AMR was enabled by command.

At a slant range of approximately 60 mi, the AMR provided a signal to start countdown of the flight control programmer clock.

Figure XVIII-9 shows the sequence of events during the main retro phase of terminal descent. At the end of the time delay, the programmer provided a signal to ignite the vernier engines at one of the two preselected thrust levels (152 or 201 lb). A signal was provided to ignite the main retro motor 1.1 sec later. The RADVS power was turned on automatically approximately 0.55 sec later.

The retro motor burned for approximately 40 sec. At burnout, the acceleration decay was sensed by the 3.5-$g$ inertia switch on the FCSG. Closing of this switch: (1) caused the vernier engines to increase thrust to a higher level (approximately 280 lb) to assist in separation of the burned-out retro motor casing; (2) reduced the bandwidth over which the doppler velocity sensor searched; and (3) initiated a 12-sec delay to allow time for a sufficient reduction in retro motor thrust level before the signal was provided to release the empty retro motor case.

Approximately 2 sec later, a signal (start RADVS controlled descent) was generated to remove the high-thrust command from the vernier engines and replace it with a minimum thrust command (equivalent to an accelerating force of 4.79 ft/sec$^2$).

#### 11. *Terminal Descent*

When the doppler velocity sensor signals became reliable following receipt of the start-RADVS-controlled-descent signal, the spacecraft attitude was controlled to continuously null the pitch and yaw lateral velocities to align the spacecraft thrust axis with its velocity vector. Roll attitude was maintained using the roll gyro as the inertial reference.

When both the radar altimeter and doppler velocity signals were reliable, the thrust-control loop was placed in a configuration that permitted the spacecraft to follow a programmed range vs vertical velocity descent profile. The spacecraft descended at a vernier engine thrust level of 0.9 lunar $g$ until the programmed descent profile was intercepted, when the thrust commands were varied as necessary to track the programmed descent segments (see Fig. XIII-2).

At a slant range of 1000 ft, the radar altimeter generated a signal to increase the gain of the pitch/yaw lateral velocity control loops by approximately a factor of 6 while increasing the gain of the radar altimeter by a factor of 20. These gain changes were required to compensate for the roll-off of the RADVS resistance–capacitance coupled doppler amplifier and increase the resolution of control along the last 1000 ft of descent.

Tracking of the descent segments continued until a velocity of approximately 10 ft/sec was reached, when pitch and yaw attitude control were switched from doppler lateral-velocity reference to gyro-inertial reference. At the same time, control of the vernier engine thrust was switched from the descent segment reference (slant range vs vertical velocity) to a constant vertical velocity command of 5 ft/sec. Both of these events normally occurred at about 40 ft above the lunar surface.

At approximately 14 ft, the radar altimeter generated signal to shut off the vernier engines, and the spacecraft then fell free the remaining distance to the lunar surface.

Flight-control thrust-phase power, RADVS power, and flight-control coast-phase power were turned off by radio command as soon as touchdown was confirmed.

## D. Construction Techniques and Manufacturing Experience

The flight control electronics unit consisted of 10 sandwiched circuit board chassis, a wiring harness, and an etched aluminum housing. Seven of the 10 chassis were constructed of an etched circuit epoxy fiber glass board and a thin aluminum plate with a sheet of epoxy fiber glass honeycomb sandwiched between. The remaining three were similar except that aluminum honeycomb was used as the core material. Discrete components and

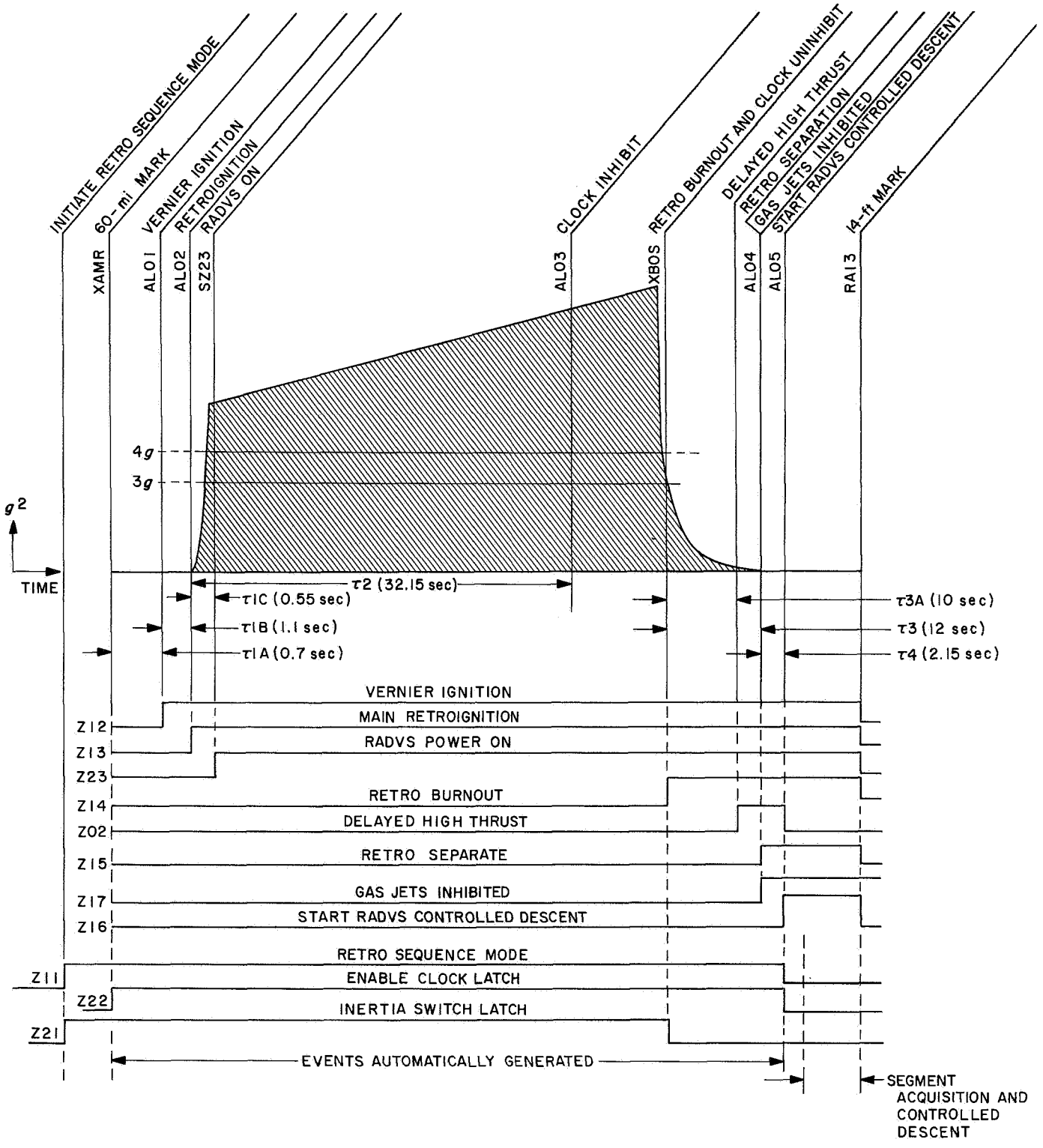



**Fig. XVIII-9. Main retro-phase sequence of events before segment acquisition**

conventional assembly techniques were used throughout. Several high-density modules were used: 5 were soldered-cordwood modules and about 30 were welded-foamed modules. Components were sealed and bonded with various polyamid resins and/or epoxies in a variety of structural to electrical applications.

Several minor circuit changes were successfully incorporated on completed circuit boards using standard techniques; i.e., cutting, hard-wiring, splicing, etc. Major circuit modifications generally required partial redesign and manufacture of new boards. The large number of selectable components (approximately 100), most of which were critical in establishing operational characteristics, caused some manufacturing difficulties, especially when reselection was required after conformal coating had been done.

Structural failures discovered during vibration testing necessitated considerable modification of the mechanical package, involving improvement of component mounting and chassis-sandwiching methods and materials. Wire breakage in the harness and on chassis connectors necessitated potting all connectors.

Some problems experienced with mechanical interference of components on adjacent chassis were eliminated by a slight increase in package size. Transistor heat-sink improvements were necessitated by occasional overheating and shorting of transistors to metal mounting surfaces. The major construction changes required to overcome problems are summarized in Table XVIII-4.

Most of the items comprising the FCSG were developed following the proven sequences of initial breadboarding. Prototype models for development engineering testing were followed by checkout testing of the first production units and flight acceptance (FA) testing of production hardware. Depending upon the extent of problems encountered in any of these phases, design changes were effected and remaining phases were repeated until the design was proven sufficient.

## E. Testing

### 1. Development Tests

*a. Closed-loop tests.* Single-axis, closed-loop gas-jet attitude control system tests were made using an air-bearing table and associated hardware. These tests were performed primarily to establish the system performance in the rate-dissipation, star-acquisition, and sun-acquisition modes. Other closed-loop tests were made using a single-axis, servo-rate table in conjunction with an analog computer to determine optical-mode, limit-cycle performance in terms of amplitude, frequency, and gas consumption.

Satisfactory performance of the FCS operating with a live vernier propulsion system was demonstrated during three test runs employing the S-6C development test vehicle. The vehicle, assembled with the engines, was located at the Placerita Canyon test facility and was linked via telephone lines to a six-degree-of-freedom analog simulation of the FCS, including spacecraft dynamics, in El Segundo. The tests consisted of:

(1) A firing to measure the open-loop vernier propulsion system frequency response with negligible amounts of dissolved helium in the system.

**Table XVIII-4. Flight control electronics unit construction changes**

| Construction change | Reason |
|---|---|
| Added riveted mounting bracket for each transformer. Used special epoxy for mounting | Heavier transformers broke loose from chassis plate during vibration |
| Used epoxy fiber glass honeycomb as core material instead of polyurethane foam. Increased height of flange on aluminum chassis plates | Chassis sandwich failed during vibration |
| Added mylar sleeving to stud of transistor. Used shoulder washer to center transistor in mounting hole. Used epoxy on mounting; added torque requirement for mounting | Power transistors shorted to chassis plate |
| Used beryllium oxide washers on mounting to decrease thermal resistance. Added torque requirement. Used epoxy on mounting hardware (reduced thermal resistance $<1°C/W$) | Power transistors overheated |
| Added insulating material to all exposed conductors. Increased spacing between chassis by increasing length of box | Components on adjacent chassis shorted (interference of components on adjacent chassis) |
| Added potting to harness and chassis connectors at point of attachment of wires | Wire breakage occurred in wiring harness and on chassis connectors |
| Strengthened internal connection by providing mechanical strength in addition to soldering | Scott T transformers developed internal open circuits because of subsegment soldering to etched circuit boards |
| Replaced the former toroidal-core transformers with flat laminated core transformers | During FA vibration tests on chassis 3, several transformers were discovered to be microphonic |

(2) A firing with helium-saturated propellant that included a closed-loop start; a small- and large-error signal, open-loop, frequency-response calibration; a closed-loop retro disturbance simulation; and a closed-loop terminal descent with and without radar noise.

Results of these tests were used to help establish a valid mathematical model of the vernier propulsion system. This model was then used in an analysis of the lateral-velocity-control loop that resulted in a doppler-loop gain reduction.

*b. Open-loop tests.* Three-axes, open-loop tests of both the gas-jet and vernier engine attitude control systems were performed with the system hardware. The tests were made primarily to assure electrical compatibility among the various pieces of hardware and to determine system null adjustment, circuit-balancing procedures, proper signal phasing, loop gains, and power requirements. Sensor linearity and alignment tolerances were also measured. The system was also exposed to a complete electromagnetic interference test per HAC Specification 226100 (see Section X). No significant degradation in performance was observed.

Roll-actuator frequency-response tests were also conducted. The two major problem areas uncovered during the open-loop tests were: (1) reduced saturation limits on the roll actuator position servo, and (2) poor self-starting characteristics of the attitude control in the electronics unit. Other minor problems were related to packaging deficiencies of the electronics unit.

*c. Elastic mode tests.* Vibration tests were made on the S-2A vehicle in a soft suspension to determine the effect of structural transmission from the vernier engines to the FCSG accelerometer. Unstable results were indicated for structural resonance at 40 Hz with marginal stability at 13 and 30 Hz. Stabilization was achieved by halving the DC gain of acceleration control loop and adding a low-pass filter, which combined to provide a gain margin of 6 db.

Vibration tests were also performed on the SC-6, SC-7, and SC-9 spacecraft vehicles with active electronics and inertial reference unit, following the *Surveyor IV* mission. The purpose of the tests was to measure the structural transmission into the attitude- or gyro-control loops. Results on the S-9 test vehicle indicated a potential low amplitude (less than 6 lb-peak) "buzz" limit cycle at frequencies of 18, 22, 28, and 40 Hz. The SC-6 spacecraft vehicle, however, had a sufficient gain margin (10 db). Each spacecraft structure and electronics unit was determined to be sufficiently different so that each combination had to be tested to measure buzz-gain margins. The results of these vibration tests are given in Table XVIII-5.

**Table XVIII-5. Vibration test results**

| Frequency, Hz | Spacecraft | | | | | | |
|---|---|---|---|---|---|---|---|
| | S-2 with retro (combined pitch and yaw inputs) | S-2 without retro (combined pitch and yaw inputs) | S-9 without retro (combined pitch and yaw inputs) | S-9 with retro | S-9 without retro (engines 1 and 2 out of phase) | *Surveyor VI* without retro (engines 1 and 2 out of phase) | *Surveyor VII* without retro (engines 1 and 2 out of phase) |
| | Attitude loop-gain margin, db | | | | | | |
| 5–10 | 19 | Not reduced | 4 | 6.0 | 8.2 | 9.6 | 5.0 |
| 10–20 | 25 | Not reduced | 20 | 1.5 | 10.5 | 9.8 | 13.5 |
| 20–30 | 39 | Not reduced | 16 | 3.5 | 0.9 | 12.6 | 7.5 |
| 30–40 | 32 | Not reduced | 28 | 12.4 | 12.4 | 27.3 | >10.0 |
| 40–50 | NA | Not reduced | 28 | 8.0 | 8.6 | 23.9 | 20.5 |
| Frequency, Hz | Spacecraft | | | | | | |
| | S-2 | S-2A | S-9 | *Surveyor I* | *Surveyor II* | *Surveyor VI* | *Surveyor VII* |
| | Acceleration loop-gain margin, db | | | | | | |
| 10–20 | 16 | 11 | 3 | 9 | 8 | 9 | 10 |
| 20–30 | 18 | 19 | 8 | 14 | 22 | 16 | >10 |
| 30–40 | 17 | 14 | 17 | 20 | 17 | 21 | >10 |
| 40–50 | 18 | 3 | 3 | 10 | 8 | 5 | 10 |

## 2. Type Approval Test Program

Type approval (TA) tests were performed on all control items according to the applicable TA test specification.

In general the TA test program consisted of:

(1) Pre-environmental functional performance tests, including measurements of nulls, gains, power consumption, and telemetry calibration.

(2) Environmental tests consisting of thermal vacuum, vibration, and shock.

(3) Postenvironmental functional performance tests per (1) for a quantitative comparison.

Results of the TA test program are summarized in the following paragraphs.

*a. Electronics unit.* Electronics unit performance was satisfactory during thermal vacuum tests, and all monitored chassis temperatures were in close agreement with predicted values. Several transformer-to-chassis bonding failures occurred during TA lateral vibration tests, primarily because a breakdown of the foam used in the sandwich-type chassis construction. Substitution of a honeycomb material for the polyurethane foam and improved bonding of the heavier transformers enabled the unit to complete vibration tests satisfactorily.

*b. Inertial reference unit.* The inertial reference unit (IRU) was incorporated in the thermal model of the spacecraft for thermal tests in the JPL solar-vacuum chamber. Because the unit was not mounted in its normal spacecraft orientation, it was necessary to simulate expected view factors. The solar intensity was estimated to be about 80%. Thermal control was satisfactory.

Analysis of several mechanical failures that had occurred during vibration testing indicated the primary cause of failure was poor workmanship rather than design deficiencies. Replacement of the air-filled, electrically damped accelerometer with a fluid-damped model corrected a scale-factor reduction problem caused by vibration. Earlier vibration tests of a mechanical model of the sensor group resulted in the addition of plastic stabilizing feet to reduce amplification factors by one-half at certain frequencies where a rocking mode occurred. This fix was successfully demonstrated during the TA vibration tests. Following TA testing, the IRU was also vibrated, with satisfactory results, as part of S-2 vehicle vibration testing.

*c. Gyros.* Type approval testing was successfully completed on two gyros. One of the gyros was vibrated at 30 $g$ without a failure (the required level was 18 $g$).

Of the 80 gyros procured for the *Surveyor* Project, 16 were expended and 28 were not flown because of allotments for prototypes, engineering evaluations, etc.; the remaining 36 gyros were flown on the flight *Surveyor* spacecraft and in the T-2N program.

The selected gyro was a fluid-floated, single-degree-of-freedom, Kearfoot 2514A series with a minimum of 10 deg input axis freedom. Detailed characteristics of the IRU are shown in Appendix A.

Hughes had experienced some difficulty in meeting performance requirements with these gyros. Most of the performance rejects occurred during receiving tests, others occurred at the IRU level, and a few at retest after spacecraft assembly. Until October 1965, a total of 110 trouble and failure reports were written covering the gyro problems. Of the 80 gyros ordered, only 62 had been received at this time, and multiple failures had occurred on a number of these.

To prevent serious schedule problems, HAC attempted to increase the yield of acceptable gyros. First, the test equipment and test techniques were modified so that the HAC and vendor test areas would conform. Second, the system requirements, as originally established, were reviewed and tolerances were broadened to be more compatible with the latest system re-evaluation. This approach sharply reduced the number of rejections and turnarounds.

It should be noted that the gyros, once selected and installed in an IRU, assembled to a FCSG, and delivered to a *Surveyor* spacecraft, rarely produced problems. In general, a gyro accumulated between 500 and 1000 hr of test history before launch. On the basis of their test history, a high level of confidence was warranted as to the flight worthiness of these gyros.

The gyro-transfer function change in value was of particular concern. The problem developed as follows: (1) A number of gyros exhibited a long-term decreasing change in transfer function of approximately 1 mV each 100 hr. (2) A few exhibited a short-term decrease of significant levels. (3) The short-term significant changes were confined to the roll gyro at the FCSG level. Despite extensive investigations by both HAC and Kearfott, the nature of this problem has not been determined. However, it is thought to be related to the pressure used to degas the damping fluid before a gyro fill.

The theoretical fluid damping number was 333,000 dyn-cm and was achieved by mixing a heavy and light fraction of fluorocarbon fluids. Because the precise value of damping coefficient was not critical, and because gyro gain, as a function of input angle vs gyro-gimbal-output displacement, was proportional to the microsyn transducer output for a given gimbal displacement, the gyro manufacturer controlled the gain by regulating the slope of the microsyn signal generator output as related to the input angle. The value of 44-mV output per degree of input angle was achieved by resistively padding the signal generator.

Results of fluid tests conducted by HAC indicated that the homogeneous fluid mix was being differentiated into its heavy and light components and some plating out of the heavy fluid was occurring, which affected internal gap clearances so that the fluid shear and damping was increased. The correlation of the roll gyro output axis position and the greater number of failures related to that position could not be explained.

Gyros exhibiting drastic changes in gain were screened out relatively early in the test cycle. Hughes system engineering determined as acceptable a total reduction of 30% in gain from FCSG testing through the terminal descent to touchdown. By examining the test history of each gyro, it could be predicted with confidence that long-term gain change of the gyros for each spacecraft would be within the 30% limit.

*d. Accelerometer.* Two accelerometers of the fluid-damped configuration passed TA testing successfully. Both were exposed to a maximum vibration level of 18 *g*.

*e. Canopus sensor.* During postenvironmental functional tests, the Canopus sensor failed to meet the noise and lockon signal specification requirements at the low-star signal level. Additional filtering of the roll-error signal minimized the noise problem, whereas the lockon signal performance was improved by choosing photo tubes whose characteristics were least temperature sensitive.

During TA cold soak tests at −40°F, the photomultiplier tube cracked because an improper potting procedure was used. Intermittent failure of a tantalum capacitor at 130°F also caused saturation of the roll-error signal. The capacitor was subsequently replaced with an acceptable type.

As part of the TA testing program, a sensor was exposed to radiation at Van Allen radiation belt levels. Test results indicated that the sensor would not perform reliably at radiation intensity levels of $10^5$ electrons/cm$^2$ sec or greater. No permanent damage was sustained up to a radiation intensity level of $10^{10}$ electrons/cm$^2$ sec.

*f. Primary sun sensor.* No significant problems were encountered during primary sun sensor TA testing. An investigation was made to determine the effect of electron radiation on the performance of the sensor. Photoconductive cells exposed to a radiation dosage equivalent to 20 trips through the Van Allen belt exhibited a maximum change in cell resistance of less than 0.75%.

*g. Inertia switch, telemeter accelerometer, and acquisition sun sensor.* Type approval tests of these units were completed with no significant discrepancies. A 0.2-*g* shift in inertia-switch contact-closing level after environmental testing was attributed to existing contamination in the mechanism. Subsequently, all switches were cleaned ultrasonically before final calibration to reduce the possibility of calibration shifts caused by contamination.

*h. Gas supply.* Excessive leakage of the pressure regulator during vibration testing resulted in the use of nonpermeable silicon seals. A "circle seal" pressure relief valve was also incorporated into the pressure regulator because of marginal low-temperature (−80°F) performance of the original valve. The regulator was successfully tested through 50,000 cycles of operation.

The gas tank was subjected to 500 pressure cycles at 110% of maximum operating pressure. The tank was finally burst at a pressure of 10,800 psig (the design minimum burst pressure was 10,000 psig).

*i. Gas jets.* Six gas-jet valves were operated satisfactorily after completing 100,000 on/off cycles. Some of the improvements made to the gas jet upon completion of TA testing included:

(1) More uniform gold plating in the valve seat.

(2) Improved ball-to-armature concentricity.

(3) Improved seat-sealing techniques.

*j. Roll actuator.* Initiation of TA tests was delayed after two taper pins coupling the last-stage gear to the output shaft sheared when the unit was exposed to launch-vibration levels. The failure was caused by a resonance of the actuator-engine spring/mass combination. A squib-actuated pinpuller was added to restrain the gimbaled engine during launch. The taper pin was also replaced with a more reliable square-shaft coupling. Following incorporation of these changes, the roll actuator successfully completed TA testing with no major discrepancies.

### 3. Flight Acceptance Tests

*a. Subsystem level tests.* All control items comprising the FCS underwent FA testing that consisted of temperature and vibration within the ranges expected during the flight. Although some failures of individual components occurred throughout the program, components replaced with subsequent retests revealed no continuing occurrences that were related to component or circuit design.

*b. Spacecraft system tests.* In general, the FCSG performed as expected during all spacecraft system level tests both at AFETR and at the HAC facility.

Some failures that occurred during the solar-thermal-vacuum tests and necessitated removal of the FCS for repair were attributed to nongeneric, random component failures, and were not related to the basic design. However, there was a continuing problem of adequately testing the Canopus sensor.

Four principal Canopus sensor testers (sun/star simulators) were used during the program. They were the HAC Santa Barbara Research Center (SBRC) primary standard simulator located in Tucson, Ariz., which was used to build the initial lot of sensors; the HAC secondary standard simulator located at Santa Barbara, Calif.; the Crowell secondary standard simulator located at HAC in El Segundo; and the De-Hass simulator located in the spacecraft test area at El Segundo. The SBRC, HAC, and Crowell simulators used a single light source, whereas the De-Hass simulators used separate light sources for the sun and star.

The Canopus tracker was designed to use intensity of the sun as a reference. Thus, the sun-channel input to the sensor so affected the gain of the photomultiplier tube that any deviations from the proper sun intensity affected the star-channel output. However, the De-Hass simulator test results could not be correlated with SBRC test results and the HAC–Crowell simulator test data.

Problems regarding Canopus sensor testers were as follows: (1) Sun bulbs supplied with the Canopus sensor were subject to aging and/or variations in light intensity and could not be reliably used as a substitute for "one sun." (2) There were problems in setting the proper current to the sun bulb. (3) The Canopus sensor output was sensitive to the characteristics of the sun/star simulators, including starlight intensity, diameter, collimation, and spectrum; and sunlight intensity, configuration on the sensor sun telescope diffuser, and spectrum. (4) The Canopus sensor was sensitive to various internal parameters, such as focusing of sun and star telescopes and spectral response of the photomultiplier tube. (5) The four Canopus sensor-type testers had variations in most of the parameters that caused changes in the Canopus sensor output.

After extensive investigation, it was concluded that it was unreasonable to expect a given Canopus sensor to test the same on two sun/star simulators of the same type because of the number of variables discussed.

In view of the problems, HAC and JPL agreed to rely extensively on the Crowell simulator used in HAC, El Segundo, based on the following test sequence:

(1) Calibrate the Crowell simulator at SBRC against the SBRC standard simulator and periodically recalibrate.

(2) Test at El Segundo at the unit level before delivery of the FCSG to the spacecraft.

(3) Test before the spacecraft solar-thermal-vacuum test.

(4) Test after solar-thermal-vacuum test.

(5) Test at unit level before delivery to AFETR.

(6) Test at AFETR at the unit level.

The Crowell simulator was selected because it: (1) had a single light source for both sun and star; (2) could be considered as a secondary standard, inasmuch as it could be transported to Tucson for comparison with the primary standard; (3) could be mounted on the spacecraft and could test the Canopus sensor in a flight configuration; and (4) was easily transportable (e.g., to Tucson and AFETR).

The successful Canopus acquisitions for spacecraft SC-1 through SC-7 demonstrated the soundness of the test plan adopted and confidence in the basic design of the Canopus sensor.

## F. Flight Control Mission Performance Summary

All FCS performance was nominal for all missions, including *Surveyor II* to the point of the failure of vernier engine 3 to ignite, and *Surveyor IV* to the point of complete loss of data near the end of the retromotor burn period.

The performance of the FCS was nominal for *Surveyor III*, even though the loss of the 14-ft mark

generated by RADVS allowed the vernier engines to continue to burn through the first and the subsequent touchdowns.

Although it was necessary to conduct a nonstandard terminal descent, *Surveyor V* spacecraft performance again demonstrated the design adequacy of the FCS. The *Surveyor I, VI,* and *VII* Missions were normal in all respects.

Just before loss of data on the *Surveyor IV* terminal descent, data indicated a buzz in the attitude control loops. This was the only *Surveyor* spacecraft on which this characteristic was detectable in flight (see Subsection D).

Because the Canopus sensor star window fogged during spacecraft SC-1 STV testing, which reduced the gain enough to lose Canopus lockon, it was decided to intentionally increase the spacecraft SC-1 sensor gain to compensate for any possible window fogging, although the material causing the fogging had been removed. Thus, the gain of the SC-1 spacecraft sensor was increased by filtering more of the sunlight entering the sun channel, which increased the gain electrically via the sun signal automatic gain control circuits. The sun filter value chosen for the SC-1 spacecraft was nominally 1.5 $\times$ Canopus, which would nominally yield an intermittent Canopus lockon signal. Spacecraft SC-1 flight results indicated a saturated star intensity signal when Canopus was centered in the FOV, and no Canopus lockon signal, thereby requiring use of the manual lockon mode to acquire Canopus. The saturated spacecraft SC-1 Canopus intensity signal rendered an exact calculation of the increased gain impossible, but the saturated signal indicated that the gain was probably well in excess of 1.5 $\times$ Canopus. On the basis of spacecraft SC-1 results, it was decided to launch spacecraft SC-2 with a sun filter that would have nominally yielded an equivalent gain of 1.17 $\times$ Canopus. Again, spacecraft SC-2 flight results indicated a saturated star intensity signal when Canopus centered in the FOV and no Canopus lockon, which again required use of the manual mode to acquire Canopus. Analysis of various star intensity signals, in addition to the saturated Canopus-intensity signal, indicated that the gain was still in excess of 1.5 $\times$ Canopus. On the basis of spacecraft SC-1 and SC-2 results, it was concluded that a substantial amount of uncertainty was involved in the earth-based testing of both sun- and star-channel characteristics and it was decided to fly spacecraft SC-3 with a 0.8 $\times$ Canopus sun filter. Canopus lockon was present during the flight of spacecraft SC-3, and the automatic Canopus-acquisition mode was utilized as it was during the flight of spacecraft SC-4, SC-5, and SC-6 which were all flown with 0.8 $\times$ Canopus-gain sun filters.

The calculated gains for spacecraft SC-3 through SC-6 were 1.17, 1.16, 1.32, and 1.10 $\times$ Canopus, respectively, which represented a fairly wide range of values; the 1.32 value approached the nominal lower edge, and the 1.35 value the upper lockon gate. Spacecraft SC-7 was launched with a 0.8-$\times$-Canopus-gain sun filter, but the Canopus intensity value was higher than expected and no Canopus lockon signal occurred; again, the manual mode was required to acquire Canopus. It was not possible, based on this telemetered information, to determine why the gain was higher; however, analysis of data from all seven flights lead to the conclusion that there was a substantial variation from sensor to sensor, probably caused by inconsistencies in sun filter transmissibility factors and/or sensitivity of the sun-channel optics-to-Canopus sensor alignment with the sunline, or possibly by the lodging of a small dust particle in the sun channel.

Several celestial bodies, other than stars, were recognized from the flight data and were used to verify the accuracy of the star maps and the identification of Canopus. The earth was consistently observed, and its wide-angle, high-intensity characteristic response proved to be a useful identifying signature, as was the moon to a much lesser extent. Furthermore, a number of noncelestial objects were observed and identified as particles or reflections by the different star angle and star intensity responses they presented.

The data for gyro drift in a 0-g environment vs earthbound non-g-sensitive testing are summarized in Table XVIII-6. From these data, it was not apparent that earthbound test data could be used for precise prediction of inflight values; however, from the inflght data, it appears that gyros that successfully completed earthbound testing were acceptable in flight (in the 0-g environment).

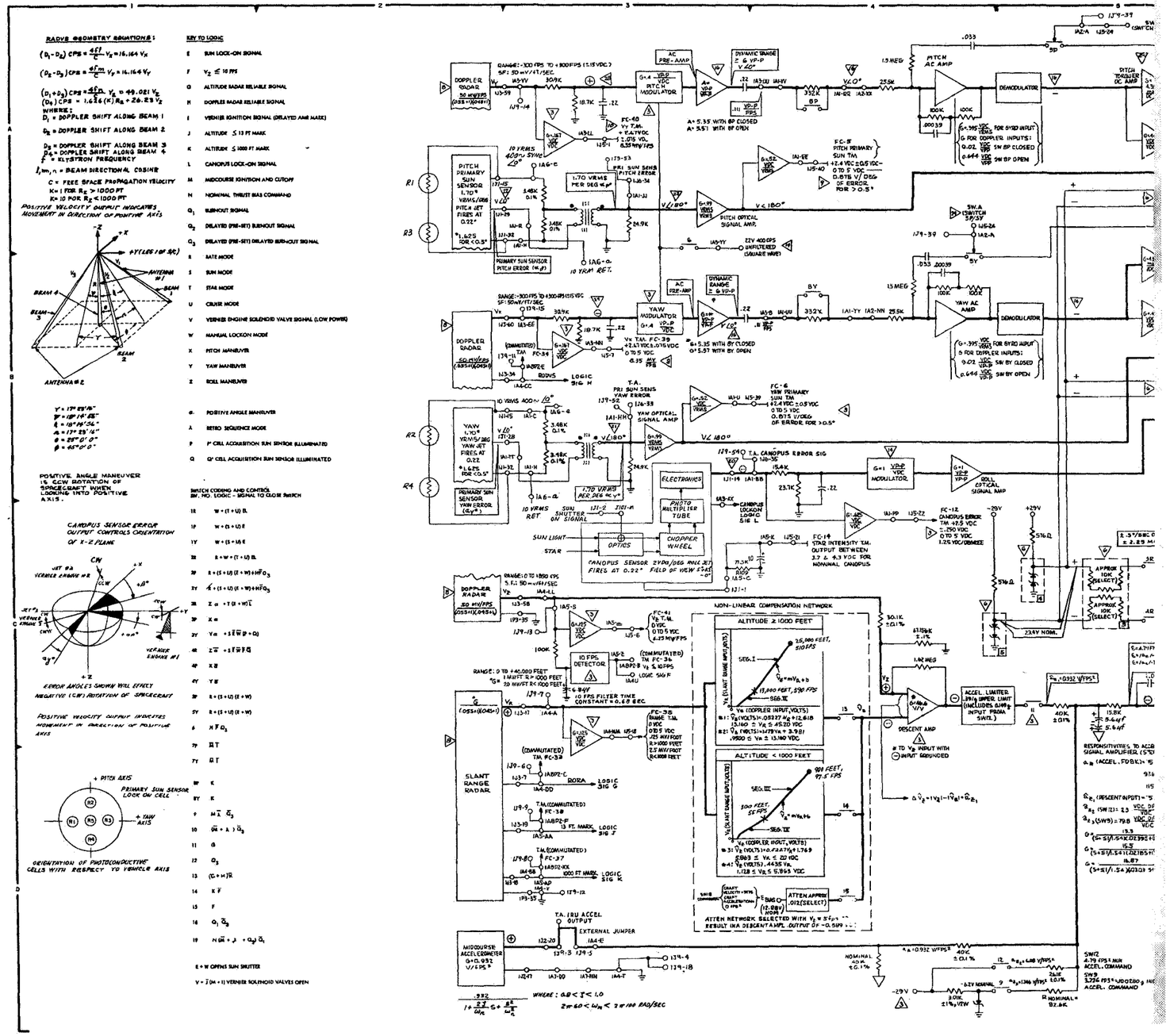
## Table XVIII-6. Comparison of earth measurement and inflight measurement of gyro drift

| Spacecraft/gyro SN | Gyro drift, deg/hr | | Spacecraft/gyro SN | Gyro drift, deg/hr | |
|---|---|---|---|---|---|
| | Earth[a] | Flight | | Earth[a] | Flight |
| *Surveyor I* | | | *Surveyor IV* | | |
| Roll, 57 | −0.2 to +0.95 | +0.2 | Yaw, 37 | −0.75 to +0.38 | +0.2 |
| Pitch, 61 | −0.9 to +0.4 | 0 | | | |
| Yaw, 25 | −1.1 to −0.05 | +0.7 | *Surveyor V* | | |
| | | | Roll, 74 | −0.95 to +0.3 | +0.9 |
| *Surveyor II* | | | Pitch, 71 | −0.7 to +0.2 | +0.6 |
| Roll, 72 | −0.95 to 0 | −0.8 | Yaw, 73 | −0.3 to +0.8 | −0.6 |
| Pitch, 70 | −0.3 to +0.2 | +0.2 | | | |
| Yaw, 51 | −0.2 to +0.9 | +1.0 | *Surveyor VI* | | |
| | | | Roll, 78 | −0.86 to +0.42 | −0.6 |
| *Surveyor III* | | | Pitch, 79 | −0.48 to +0.38 | 0 |
| Roll, 62 | −0.2 to +0.95 | +1.1 | Yaw, 75 | −0.9 to −0.06 | +1.4 |
| Pitch, 57 | −0.3 to +0.2 | +0.6 | | | |
| Yaw, 68 | −0.2 to +0.9 | −0.8 | *Surveyor VII* | | |
| | | | Roll, 53 | −0.85 to −0.2 | +0.65 |
| *Surveyor IV* | | | Pitch, 45 | −0.45 to +0.3 | +0.2 |
| Roll, 47 | −0.95 to +0.45 | −0.5 | Yaw, 39 | −0.6 to +0.3 | 0 |
| Pitch, 30 | −0.92 to +0.4 | −1.0 | | | |

[a]Range of test values.

# Appendix XVIII-A

## Flight Control Mechanization Diagram


RADVS GEOMETRY EQUATIONS:
KEY TO LOGIC
SUN LOCK-ON SIGNAL
ALTITUDE RADAR RELIABLE SIGNAL
DOPPLER RADAR RELIABLE SIGNAL
VERNIER IGNITION SIGNAL (DELAYED AMR MAKE)
ALTITUDE ≤ 13 FT MARK
ALTITUDE ≤ 1000 FT MARK
CANOPUS LOCK-ON SIGNAL
MIDCOURSE IGNITION AND CUTOFF
NOMINAL THRUST BIAS COMMAND
BURNOUT SIGNAL
DELAYED (PRE-SET) BURNOUT SIGNAL
DELAYED (PRE-SET) DELAYED BURNOUT SIGNAL
RATE MODE
SUN MODE
STAR MODE
CRUISE MODE
VERNIER ENGINE SOLENOID VALVE SIGNAL (LOW POWER)
MANUAL LOCKON MODE
PITCH MANEUVER
YAW MANEUVER
ROLL MANEUVER
POSITIVE ANGLE MANEUVER
RETRO SEQUENCE MODE
P CELL ACQUISITION SUN SENSOR ILLUMINATED
Q CELL ACQUISITION SUN SENSOR ILLUMINATED
POSITIVE VELOCITY OUTPUT INDICATES MOVEMENT IN DIRECTION OF POINTING AXIS
ANTENNA #2
Y = 179° 59' 8"
Y' = 179° 19' 58"
ϕ = 18° 54' 34"
A = 17° 29' 14"
θ = 29° 51' 0"
β = 45° 0' 0"
POSITIVE ANGLE MANEUVER IS CCW ROTATION OF SPACECRAFT, WHEN LOOKING INTO POSITIVE AXIS.
CANOPUS SENSOR ERROR OUTPUT CONTROLS ORIENTATION OF X-Z PLANE
ERROR ANGLES SHOWN WILL EFFECT NEGATIVE (CW) ROTATION OF SPACECRAFT
POSITIVE VELOCITY OUTPUT INDICATES MOVEMENT IN DIRECTION OF POSITIVE AXIS
ORIENTATION OF PHOTOCONDUCTIVE CELLS WITH RESPECT TO VEHICLE AXIS
SWITCH CODING AND CONTROL
E = W OPENS SUN SHUTTER
V = 1 (M = 1) VERNIER SOLENOID VALVES OPEN
DOPPLER RADAR
PITCH PRIMARY SUN SENSOR
YAW PRIMARY SUN SENSOR
SLANT RANGE RADAR
MIDCOURSE ACCELEROMETER
PITCH MODULATOR
YAW MODULATOR
PITCH AC AMP
YAW AC AMP
DEMODULATOR
PITCH OPTICAL SIGNAL AMP.
YAW OPTICAL SIGNAL AMP.
ROLL OPTICAL SIGNAL AMP
ELECTRONICS
PHOTO MULTIPLIER TUBE
OPTICS
CHOPPER WHEEL
SUN SHUTTER ON SIGNAL
SUN LIGHT
STAR
CANOPUS SENSOR 2YPD/DEG HALF JET FIRES AT 0.22° FIELD OF VIEW ±4°
NON-LINEAR COMPENSATION NETWORK
ALTITUDE ≥ 1000 FEET
ALTITUDE < 1000 FEET
DESCENT AMP
ACCEL. LIMITER
ATTEN NETWORK SELECTED WITH V_R = 37 FPS RESULT IN A DESCENT APPL. OUTPUT OF −0.599 V
ATTEN APPROX .012 (SELECT)
SLANT RANGE RADAR
MIDCOURSE ACCELEROMETER
T.A. IRU ACCEL OUTPUT
EXTERNAL JUMPER
WHERE: 0.8 < ζ < 1.0
2π 60 < ω_n < 2π 100 RAD/SEC
T.A. CANOPUS ERROR SIG
CANOPUS LOCKON LOGIC SIG L
STAR INTENSITY TM. OUTPUT BET WEEN 3.7 & 4.3 VDC FOR NOMINAL CANOPUS
SW. A (SWITCH SEQ)
SW. B (SWITCH SEQ)
SW. C (SWITCH SEQ)
SW. D (SWITCH SEQ)
SW. E (SWITCH SEQ)
SW. F (SWITCH SEQ)
SW. G (SWITCH SEQ)
SW. H (SWITCH SEQ)
SW. I (SWITCH SEQ)
SW. J (SWITCH SEQ)
SW. K (SWITCH SEQ)
SW. L (SWITCH SEQ)
SW. M (SWITCH SEQ)
SW. N (SWITCH SEQ)
SW. O (SWITCH SEQ)
SW. P (SWITCH SEQ)
SW. Q (SWITCH SEQ)
SW. R (SWITCH SEQ)
SW. S (SWITCH SEQ)
SW. T (SWITCH SEQ)
SW. U (SWITCH SEQ)
SW. V (SWITCH SEQ)
SW. W (SWITCH SEQ)
SW. X (SWITCH SEQ)
SW. Y (SWITCH SEQ)
SW. Z (SWITCH SEQ)

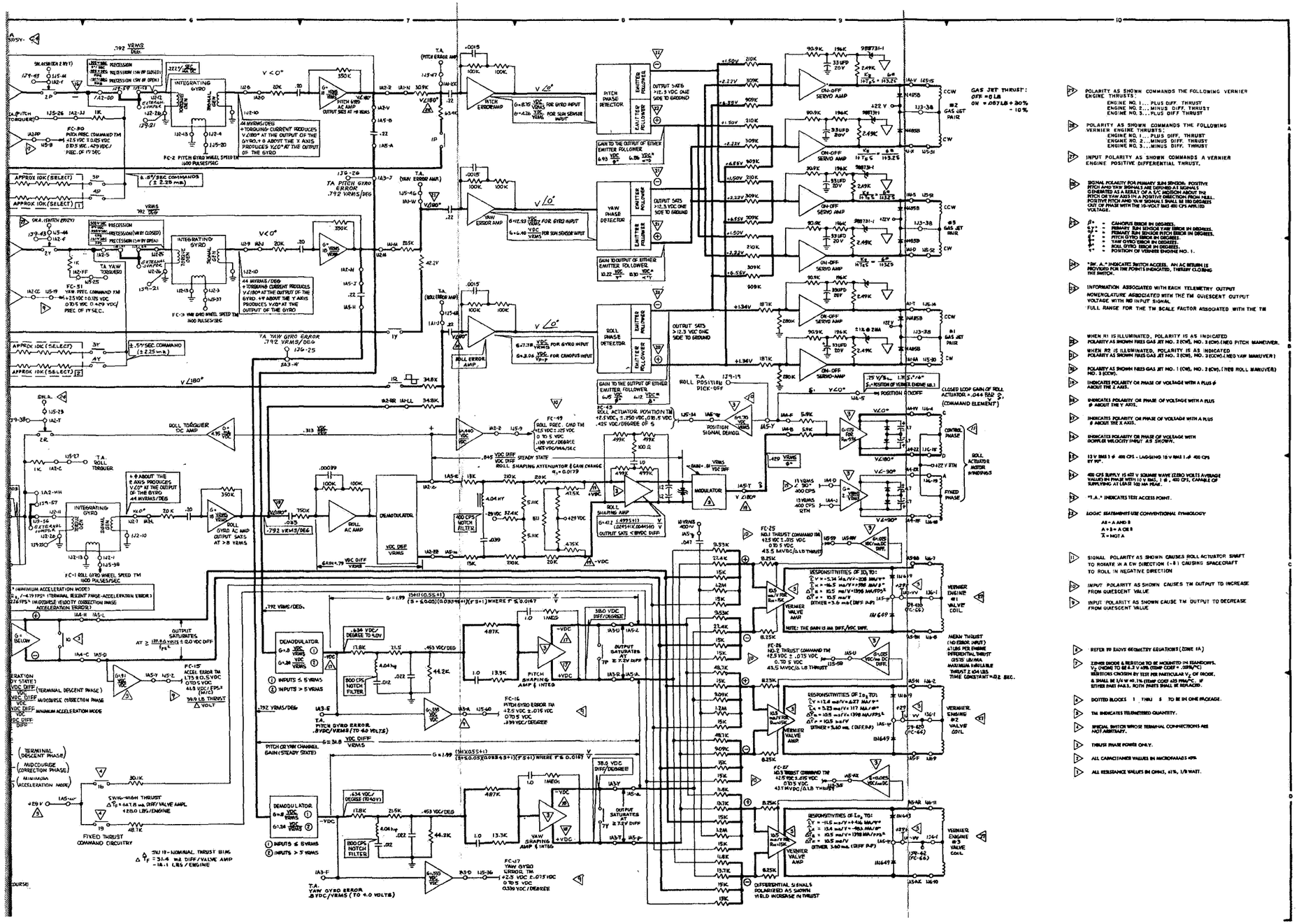


Fig. XVIII-A-1. Flight control mechanization diagram

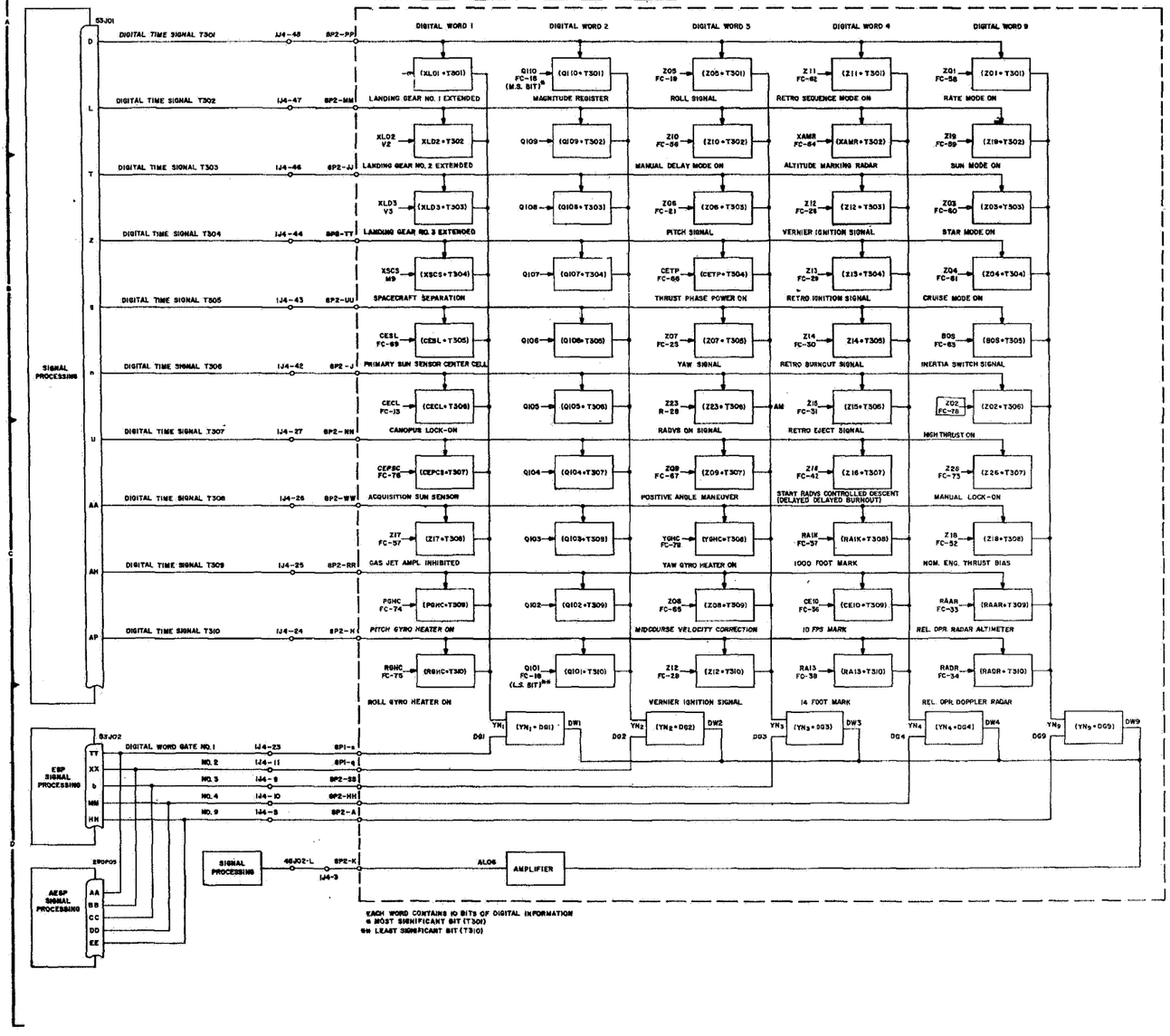
# Appendix XVIII-B

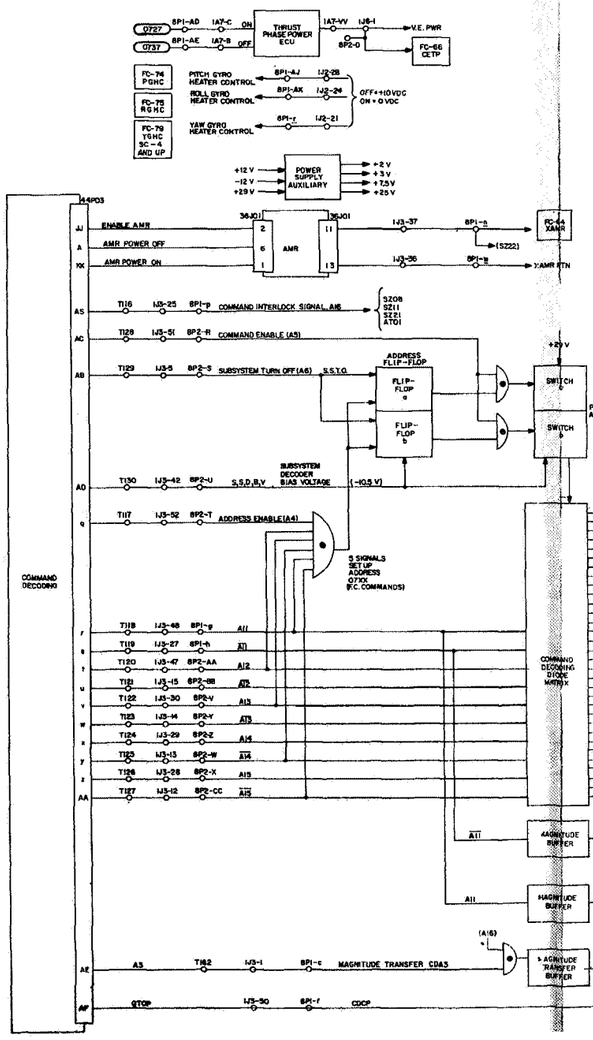
## Advanced Flight Control Programmer Mechanization Diagram

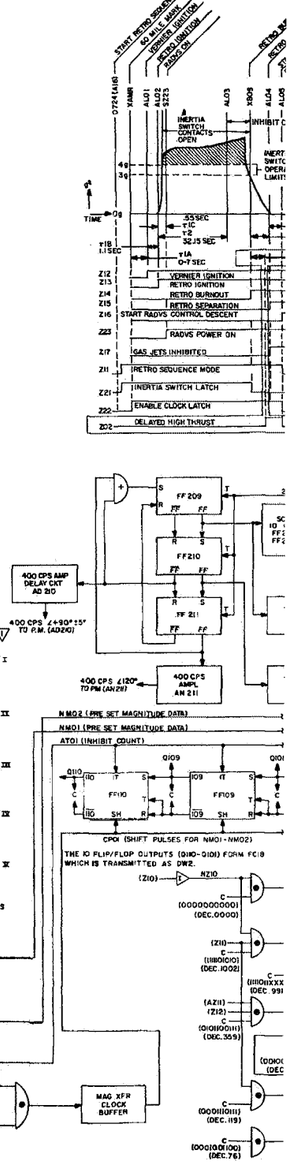
| WORD | SAMPLE TIMES PER MODE | | | | | |
|---|---|---|---|---|---|---|
| | 1 | 2 | 3 | 4 | C | T |
| 1 | 1 | 1 | 0 | 1 | 1 | 1 |
| 2 | 1 | 1 | 0 | 0 | 1 | 1 |
| 3 | 5 | 1 | 0 | 0 | 4 | 1 |
| 4 | 0 | 3 | 9 | 0 | 0 | 12 |
| 9 | 1 | 1 | 1 | 0 | 1 | 1 |

COMMUTATOR TABLES

| | | | | | | | | | |
|---|---|---|---|---|---|---|---|---|---|
| FC-13 | 186 | FC-33 | 989 | FC-59 | 981 | FC-87 | 387 | R-28 | 388 |
| FC-18 | 281 TO 2810 | FC-34 | 9810 | FC-60 | 982 | FC-88 | 185 | XLD1 | 181 |
| FC-19 | 381 | FC-36 | 489 | FC-61 | 983 | FC-73 | 987 | XLD2 | 182 |
| FC-21 | 383 | FC-37 | 488 | FC-62 | 984 | FC-74 | 189 | XLD3 | 183 |
| FC-23 | 385 | FC-39 | 4810 | FC-82 | 481 | FC-75 | 1810 | XSCS | 184 |
| FC-28 | 3810, 483 | FC-42 | 487 | FC-83 | 985 | FC-76 | 187 | | |
| FC-29 | 484 | FC-52 | 988 | FC-84 | 482 | FC-78 | 986 | | |
| FC-30 | 485 | FC-56 | 382 | FC-85 | 389 | FC-79 | 388 | | |
| FC-31 | 486 | FC-57 | 188 | FC-86 | 384 | | | | |



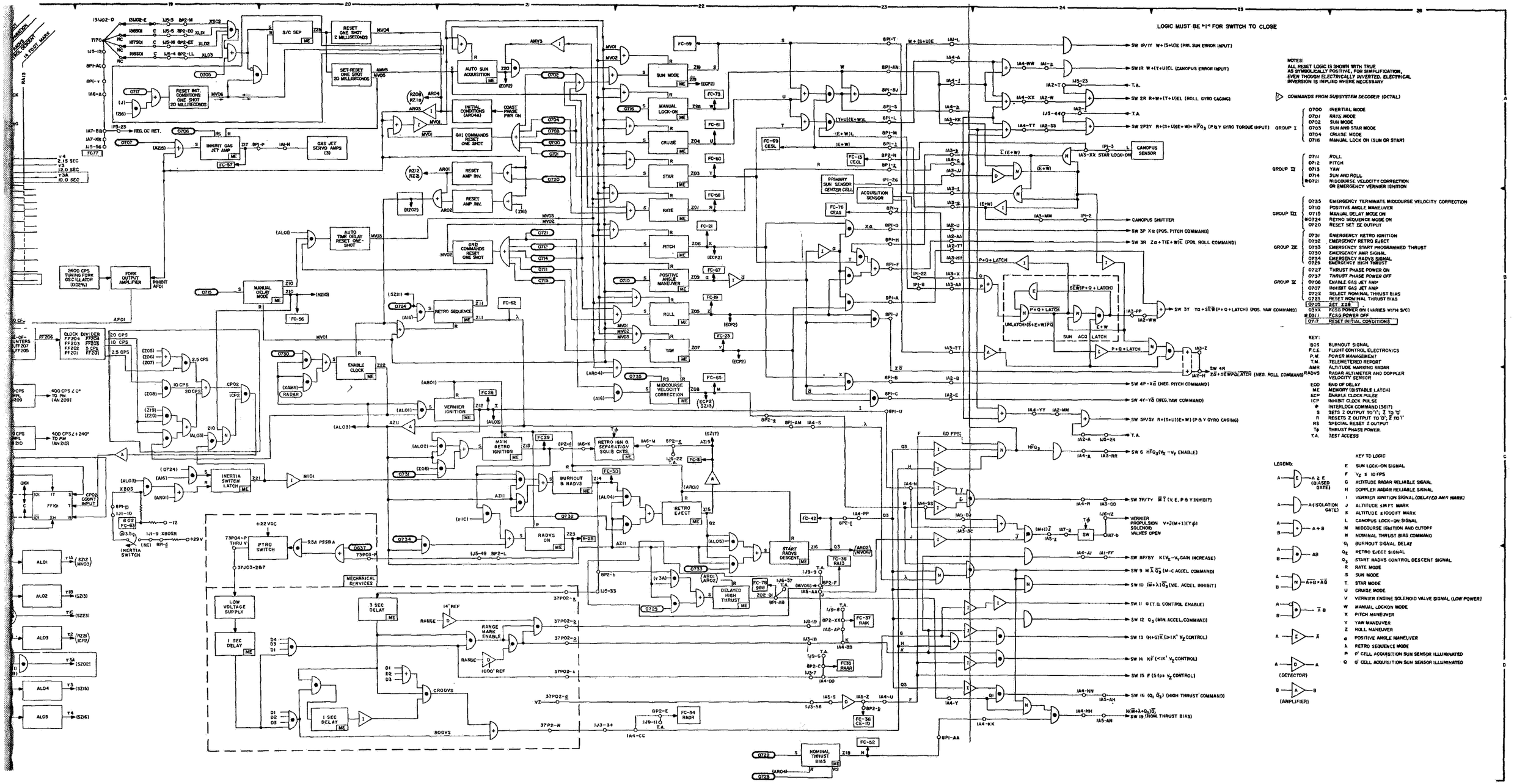
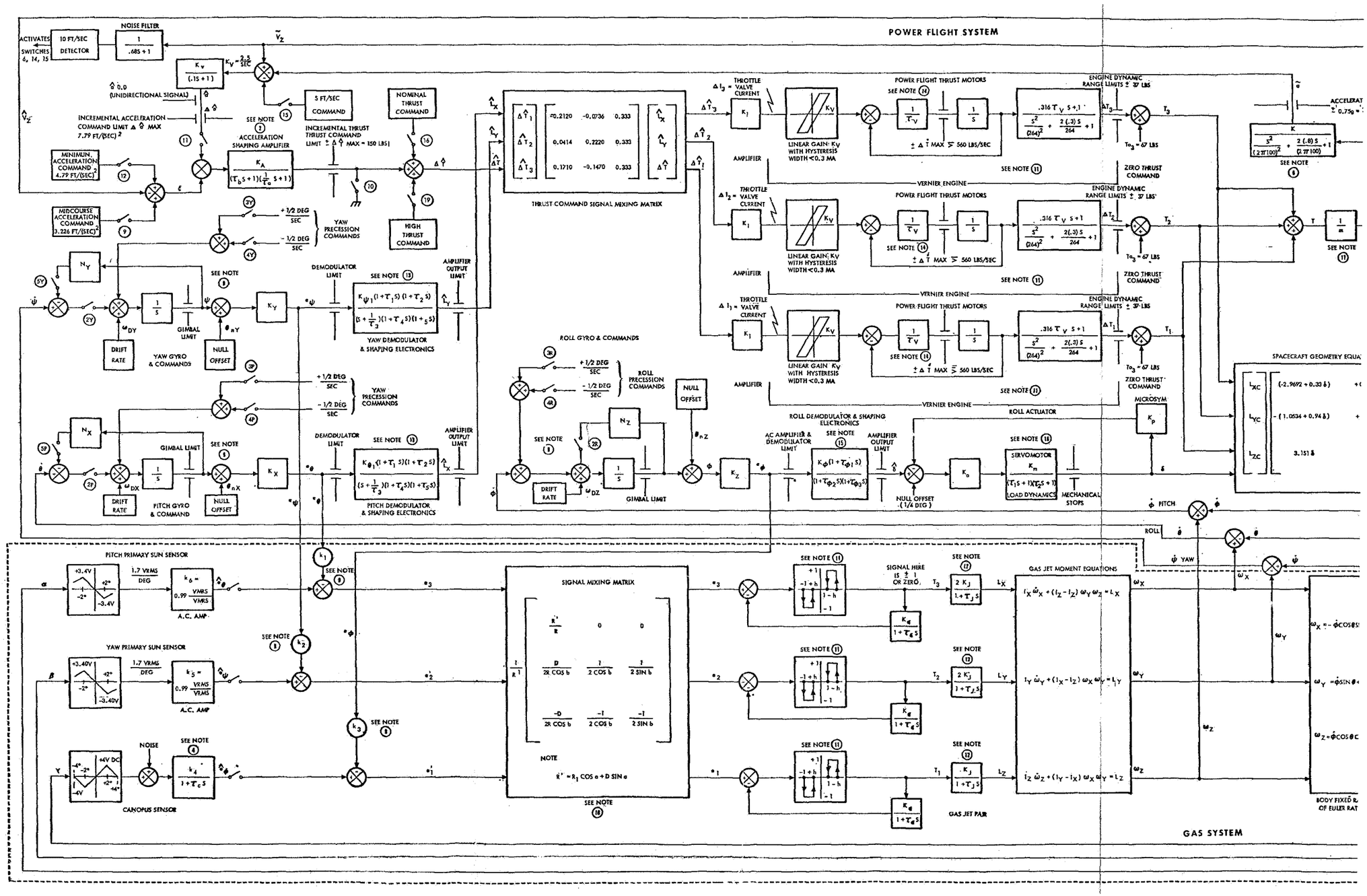
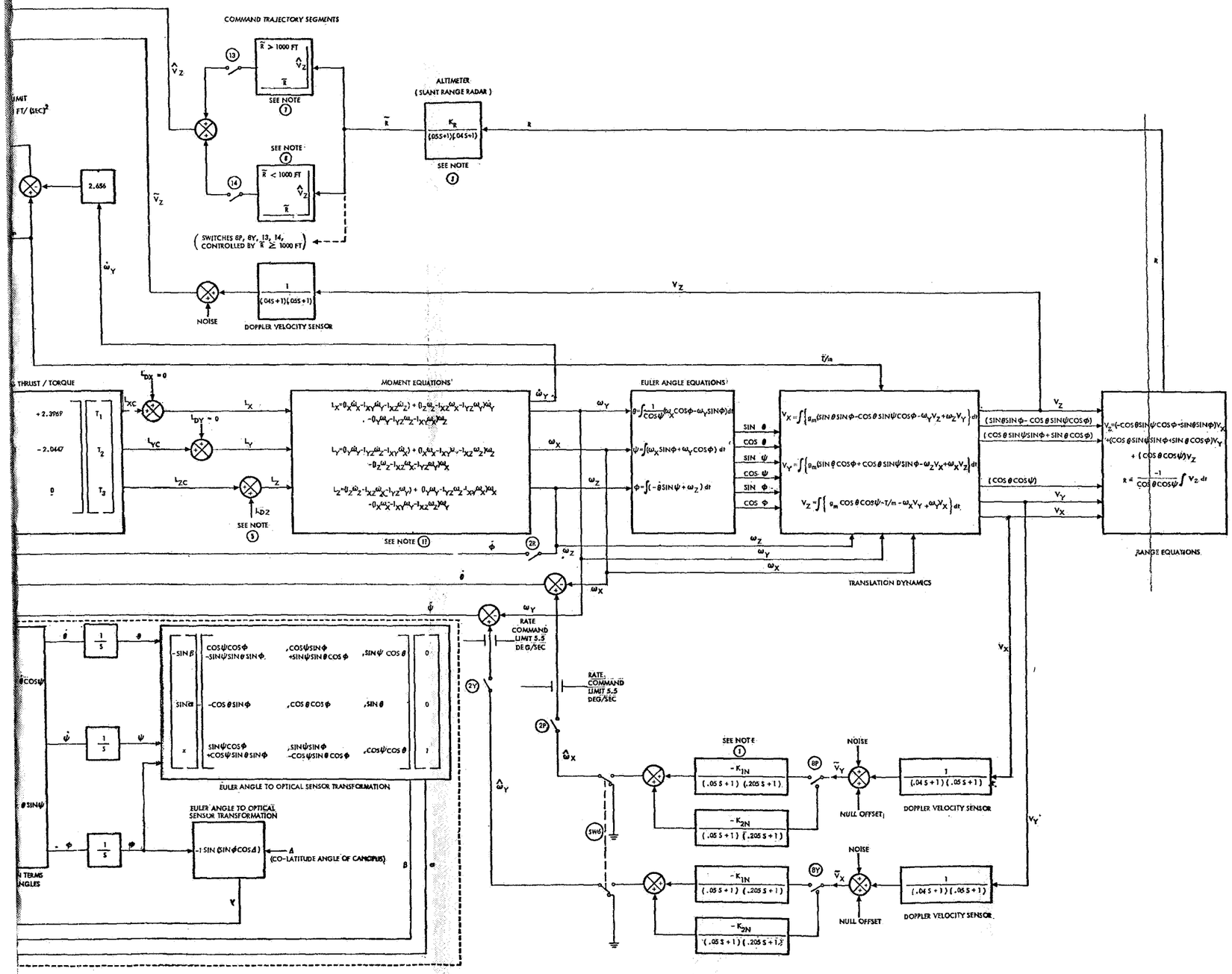



**Fig. XVIII-B-1. Advanced flight control programmer mechanization diagram**

# Appendix XVIII-C

# Flight Control System Data


POWER FLIGHT SYSTEM
NOISE FILTER
ACTIVATES SWITCHES 6, 14, 15
10 FT/SEC DETECTOR
INCREMENTAL ACCELERATION COMMAND LIMIT Δ MAX 7.79 FT/(SEC)²
MINIMUM ACCELERATION COMMAND 4.79 FT/(SEC)²
MIDCOURSE ACCELERATION COMMAND 3.226 FT/(SEC)²
ACCELERATION SHAPING AMPLIFIER
INCREMENTAL THRUST THRUST COMMAND LIMIT ± Δ MAX = 150 LBS
5 FT/SEC COMMAND
NOMINAL THRUST COMMAND
HIGH THRUST COMMAND
YAW PRECESSION COMMANDS
THRUST COMMAND SIGNAL MIXING MATRIX
THROTTLE VALVE CURRENT
LINEAR GAIN Kv WITH HYSTERESIS WIDTH <0.3 MA
AMPLIFIER
VERNIER ENGINE
POWER FLIGHT THRUST MOTORS
ENGINE DYNAMIC RANGE LIMITS ± 37 LBS
ZERO THRUST COMMAND
SEE NOTE 11
SEE NOTE 14
SEE NOTE 6
SEE NOTE 17
ACCELERATION ± 0.75g
YAW GYRO & COMMANDS
DRIFT RATE
NULL OFFSET
GIMBAL LIMIT
DEMODULATOR LIMIT
AMPLIFIER OUTPUT LIMIT
YAW DEMODULATOR & SHAPING ELECTRONICS
PITCH GYRO & COMMAND
PITCH DEMODULATOR & SHAPING ELECTRONICS
ROLL GYRO & COMMANDS
ROLL PRECESSION COMMANDS
ROLL DEMODULATOR & SHAPING ELECTRONICS
AC AMPLIFIER & DEMODULATOR LIMIT
ROLL ACTUATOR
MICROSYM
SERVOMOTOR
LOAD DYNAMICS
MECHANICAL STOPS
NULL OFFSET (1/4 DEG)
SPACECRAFT GEOMETRY EQUA
PITCH PRIMARY SUN SENSOR
YAW PRIMARY SUN SENSOR
CANOPUS SENSOR
A.C. AMP
NOISE
SIGNAL MIXING MATRIX
SIGNAL HERE IS ± 1 OR ZERO.
GAS JET MOMENT EQUATIONS
GAS JET PAIR
BODY FIXED R. OF EULER RAT
GAS SYSTEM




**NOTES:**

(1) LATERAL VELOCITY GAIN CHANGE

$K_{1N} = .0012 \frac{RAD - SEC}{FT}$ $R \leq 1000 FT$

$K_{2N} = .0170 \frac{RAD - SEC}{FT}$ $R \leq 1000 FT$

SW 6 = GROUNDED $V_Z < 10$ FT/SEC

(2) THRUST COMMANDS

| | $\frac{LB-SEC}{FT}$ $K_A$ | SEC $\tau_a$ | SEC $\tau_b$ |
|---|---|---|---|
| MID-COURSE | 262 | 5.4 | .028 |
| MINIMUM ACCLERATION | 284 | 5.4 | .030 |
| VERTICAL DESCENT | 225 | 5.4 | .024 |

(3) ALTIMETER

$K_R$ { 1m V/FT $\bar{R} \geq$ 1000 FT; 20m V/FT $\bar{R}$ (14 TO 1000) FT; $K_R$ (SWITCHED IN RADAR ELECTRONICS) }

(4) CANOPUS TRACKER

$\tau_c \geq 1.0$ SEC

$k_4 = 1.0 \frac{VP - P}{VP - P}$

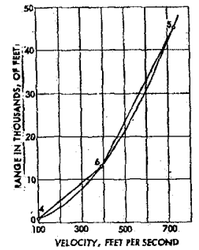
(5) DISTURBANCE TORQUE

$L_{DZ} = (T_1 \delta_1 + T_2 \delta_2 + T_3 \delta_3)\ 3.151$

(6) ACCELEROMETER

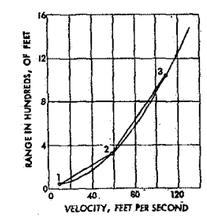
$K = \frac{30 \text{ VOLTS}}{g} = \frac{0.932 \text{ VOLTS}}{FT/(SEC)^2}$

(7) RANGE - VELOCITY DESCENT CURVE




RADAR ALTIMETER IN LOW GAIN MODE (RANGE > 1000 FEET)

(8) RANGE - VELOCITY DESCENT CURVE




RADAR ALTIMETER IN HIGH GAIN MODE (RANGE ≤ 1000 FEET)

(9) GYRO PARAMETERS

$K_X = K_Y = K_Z = 0.72 \frac{VRMS}{DEG}$

$N_X = N_Y = N_Z = 0.4167 \frac{DEG/SEC}{VRMS}$

STOPS $\geq \pm 10°$

$K_1 = 1.44$ VRMS/VRMS $\omega_{DX} = \omega_{DY} = \omega_{DZ} = 0.1$ DEG/HR

$K_2 = K_3 = 1.22$ VRMS/VRMS $\theta_{mX} = \theta_{mY} = \theta_{mZ} = 0.1$ DEG

(10) SIGNAL MIXING MATRIX

b = 24 IN a = 18 DEG

R = 77.64 IN h = 53.19 DEG

R' = 71.2 IN

(11) GAS JET AMPLIFIER

$K_a = 8$ V/V $\tau_a = 3.2$ SEC h = HYSTERESIS 7.5% (NOMINAL)

(12) GAS JETS

$K_J = 0.080$ LBS MAX, 0.05 LBS MIN } 2000 PSI SUPPLY

$\tau_J = .015$ SEC MAX

(13) PITCH OR YAW SHAPING

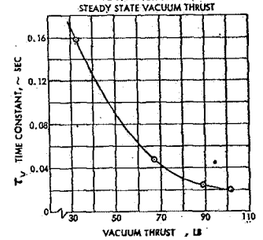
$\tau_1 = 1.0$ SEC $\tau_4 = 0.033$ SEC

$\tau_2 = 0.5$ SEC $\tau_5 = 0.0167$ SEC

$\tau_3 > 20$ SEC $K_{\psi 1} \approx \theta_1 \approx 3465 \frac{(FT - LBS)\ RAD}{SEC}$

(14) VERNIER ENGINE TRANSFER FUNCTION:

TIME CONSTANT, AS A FUNCTION OF STEADY STATE VACUUM THRUST




(15) ROLL DEMODULATOR & SHAPING ELECTRONICS

$\tau_1 = 0.50$ SEC $K_\phi = 0.428 \frac{DEG}{VRMS}$

$\tau_2 = 0.024$ SEC AMPLIFIER LIMIT

$\tau_3 = 0.055$ SEC $\theta \geq \pm 8.4°$

(16) ROLL ACTUATOR

$K_a = 185 \frac{VRMS}{VRMS}$ GIMBAL ANGLE STOPS 5.5 DEG ON ENGINE

$K_m = 1.66 \frac{DEG}{VRMS}$ ROLL SREVO AMPLIFIER SATURATION 26 VRMS

$\tau_1 = 4.8$ SEC NULL OFFSET ± 0.25 DEG

$\tau_2 = 0.024$ SEC

$K_p = 0.258 \frac{VRMS}{DEG}$

(17) SPACECRAFT STRUCTURAL DATA

MASS

$m = \begin{cases} 69 \text{ SLUGS MAX} \\ 18.6 \text{ SLUGS MIN} \end{cases}$

MOMENTS OF INERTIA

$I_{XY} = 3$ SLUG - $FT^2$ $I_X = 200$ SLUG - $FT^2$

$I_{XZ} = 6$ SLUG - $FT^2$ $I_Y = 215$ SLUG - $FT^2$

$I_{YZ} = 6$ SLUG - $FT^2$ $I_Z = 200$ SLUG - $FT^2$

**Fig. XVIII-C-1. Flight control system block diagram**

## Table XVIII-C-1. Flight control switch closure requirements

| Mode | Switch[a] | Coast phase | | | | | | | | | | | Thrust phase[b] | | | | | | | | | |
|---|---|---|---|---|---|---|---|---|---|---|---|---|---|---|---|---|---|---|---|---|---|---|
| | | 1R | 1P/1Y | 2R | 2P/2Y | 3P | 3Y | 3R | 4P | 4Y | 4R | 5P/5Y | 6 | 7P/7Y | 8P/8Y | 9 | 10 | 11 | 12 | 13 | 14 | 15 | 16 | 19 |
| Inertial | | | | | | | | | | | | | | X[c] | | | X | | | | | | | |
| Rate | | | | X | X | | | | | | | X | | X | | | X | | | | | | | |
| Sun[d] | | | X | | X | | | | | | | X | | X | | | X | | | | | | | |
| Sun–star[e] | | X | X | X | X | | | | | | | X | | X | | | X | | | | | | | |
| Sun–star–cruise | | X | X | X | X | | | | | | | X | | X | | | X | | | | | | | |
| Sun–roll, + | | | X | | X | | | X | | | | X | | X | | | X | | | | | | | |
| Sun–roll, − | | | X | | X | | | | | | X | X | | X | | | X | | | | | | | |
| Pitch, + | | | | | | X | | | | | | | | X | | | X | | | | | | | |
| Pitch, − | | | | | | | | | X | | | | | X | | | X | | | | | | | |
| Yaw, + | | | | | | | X | | | | | | | X | | | X | | | | | | | |
| Yaw, − | | | | | | | | | | X | | | | X | | | X | | | | | | | |
| Roll, + | | | | | | | | X | | | | | | X | | | X | | | | | | | |
| Roll, − | | | | | | | | | | | X | | | X | | | X | | | | | | | |
| **Thrust phase events** | | **Thrust phase power on command** | | | | | | | | | | | | | | | | | | | | | | |
| Midcourse velocity correction | | | | | | | | | | | | | | | | X | | | | | | | | |
| Vernier engine ignition | | | | | | | | | | | | | | | | | X | | | | | | | X[f] |
| Main retroignition | | | | | | | | | | | | | | | | | X | | | | | | | X |
| Doppler radar reliable | | | | | | | | | | | | | | | | | X | | | X | | | | X |
| Altitude and doppler radar reliable | | | | | | | | | | | | | | | | | X | X | | X | | | | X |
| Retro burnout | | | | | | | | | | | | | | | | | X | X | | X | | | | X[g] |
| Retro separation | | | | | | | | | | | | | | | | | X | X | | X | | | X[h] | |
| Begin vernier descent | | | | | X | | | | | | | | X | | | | | X | X | X | | | X | |
| 1000-ft elevation | | | | | X | | | | | | | | X | | X | | | X | X | | X | | | |
| $V_z$ = 10 ft/sec | | | | | | | | | | | | | | | X | | | X | X | | | X | | |
| 14-ft elevation | | | | | | | | | | | | | | | X | | | X | X | | | X | | |
| Touchdown | | | | | | | | | | | | | | | X | | | X | X | | | X | | |

[a]Switch numbers correspond to numbers on FCS block and mechanization diagrams.
[b]All thrust phase events require thrust phase power-on command as well as coast phase power-on.
[c]Indicates switch closed; no "X" indicates switch open.
[d]Switch states for modes 3 through 7, coast phase, are true only if sun lock-on exists.
[e]Switch states for modes 4 and 5, coast phase, assume both sun and star lock-on exist.
[f]Radio command closes switch 19 to low thrust prior to vernier engine and retro motor ignition.
[g]Retro burnout plus 12 sec open switch 19.
[h]Retro burnout plus 12 sec closes switch 16.

# Appendix XVIII-D

# Flight Control Power Distribution

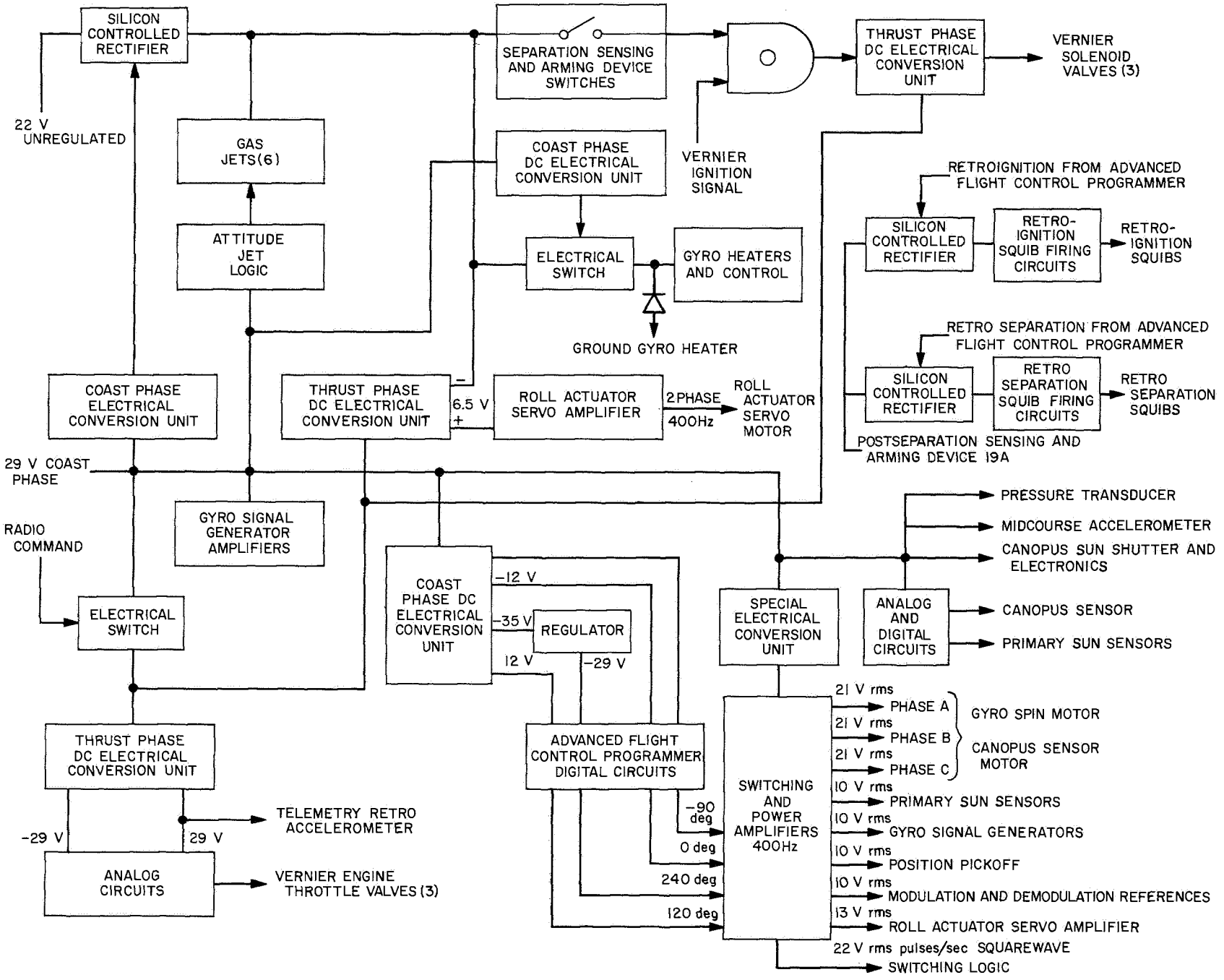



**Fig. XVIII-D-1. Flight control power distribution**

# Appendix XVIII-E

## Design Requirements

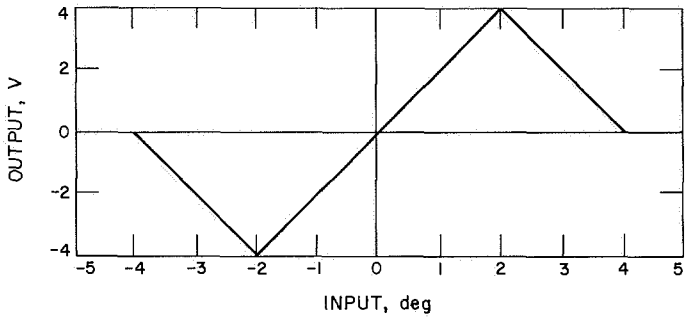



Fig. XVIII-E-1. Output characteristics for Canopus sensor

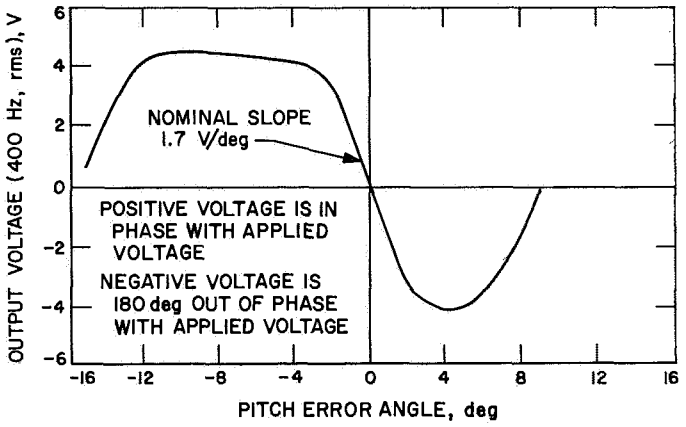



Fig. XVIII-E-2. Output characteristics for primary sun sensor pitch channel

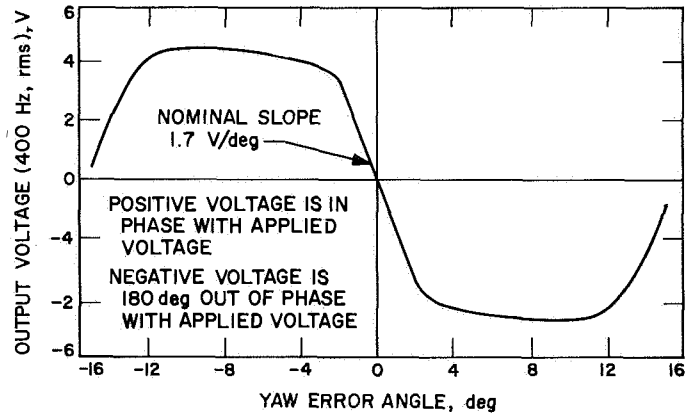



Fig. XVIII-E-3. Output characteristics for primary sun sensor yaw channel

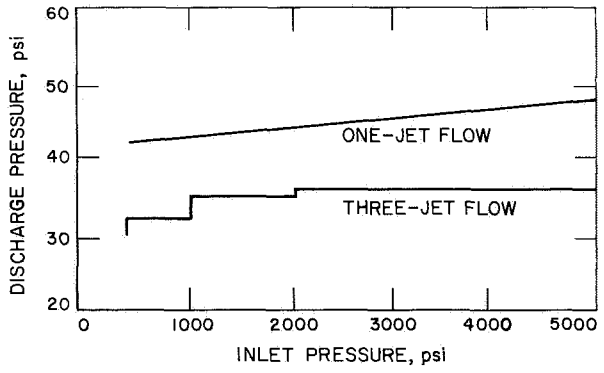



Fig. XVIII-E-4. Gas supply inlet-vs-discharge pressure

### Table XVIII-E-1. Inertial reference unit requirements

| Item | Requirement |
|---|---|
| Weight | 8.0 lb (max) |
| Thermal control | Three active temperature controllers; radiator with second surface mirrors |
| Gyro | Kearfott 2514A series, 10-deg input axis freedom, single degree of freedom, floated |
| Angular momentum | 100,000 gm-cm$^2$/sec |
| Motor | 3-phase, synchronous, 2.6 $\pm$0.3 W |
| Single generator | Electromagnetic, ac, $\pm$10% linearity over 10 deg |
| Signal generator scale factor at 180°F | 0.044 $\pm$5% V/deg |
| Torque generator | Permanent magnet, four pole, dc |
| Maximum torque rate at 100 mA | 80,000 deg/hr |
| Torque scale factor (calibrated at 1800 deg/hr = 0.5 deg/sec) | Input angle off null, deg / Max deviation, %<br>0–2 / 0.05<br>2–4 / 0.2<br>4–10 / 1.0 |
| Torquer linearity | Torque rate, deg/hr / % of 800 deg/hr/mA<br>0–$\pm$1800 / 0.5<br>1800–10,000 / 2.0<br>10,000–80,000 / 5.0 |
| Drift, non-acceleration sensitive | $\pm$1 deg/hr |
| Drift, acceleration sensitive | $\pm$2 deg/hr |
| Anisoelastic (from 500 to 700 Hz) | 0.02 deg/hr/g$^2$ (rms) |
| Elastic restraint | $\pm$0.6 deg/hr/deg off null |
| Heater power (warmup) | 50 $\pm$5 W (used in gyro test only) |
| Heater power (operate) | 10 $\pm$0.5 W |
| Accelerometer | Donner 431 linear force balance |
| Accelerometer weight | 8 oz |
| Accelerometer range | $-0.75$ to $+0.75$ g |
| Accelerometer scale factor | 30 V/g |
| Accelerometer accuracy (from $-0.2$ to $+0.2$) | $\pm$0.001g (1% full scale) |
| Natural frequency damping ratio | Between 60 and 100 Hz 0.9 $\pm$0.1 |
| Total electronic parts count | 175 |

### Table XVIII-E-2. Canopus sensor requirements

| Item | Requirement |
|---|---|
| Weight | 5.0 lb (max) |
| Thermal surfaces | Sun shade: black interior, white exterior; sensor: white top, polished aluminum sides and base |
| Field of view | 5 $\times$ 7.2 deg |
| Adjustment of 5-deg field | $\pm$0.15 deg |
| Null offset | 0.1 deg |
| Lockon threshold | $\pm$0.45 magnitude of Canopus |
| Scale factor | 2 V/deg (Figure XVIII-E-1) |
| Linear region | 2 deg (Figure XVIII-E-1) |
| Total electronic parts count | 166 |

### Table XVIII-E-3. Electronics unit requirements

| Item | Requirement |
|---|---|
| Weight | 18.9 lb |
| Thermal surfaces | White radiators on outboard side and bottom, all remaining external surfaces chem-milled aluminum |
| Total electronic parts boards | 2087 |

### Table XVIII-E-4. Acquisition sun sensor requirements

| Item | Requirement |
|---|---|
| Weight | 0.15 lb (max) |
| Thermal surfaces | Polished aluminum |
| Alignment | All axes within 0.5 deg of corresponding primary sun sensor axes |
| Field of view | 6 (narrow) $\times$ 196 deg |

### Table XVIII-E-5. Inertia switch requirements

| Item | Requirement |
|---|---|
| Weight | 0.17 lb (max) |
| Thermal surface | Polished aluminum |
| Switch setting | 3.5 $\pm$0.5 g (closed below set value) |

### Table XVIII-E-6. Telemetry accelerometer requirements

| Item | Requirement |
|---|---|
| Weight | 0.2 lb (max) |
| Thermal surface | Polished aluminum |
| Operating range | 0–15 ±1 g |
| Scale factor | 0.333 V/g |

### Table XVIII-E-7. Primary sun sensor requirements

| Item | Requirement |
|---|---|
| Weight | 0.4 lb (max) |
| Thermal surfaces | Polished aluminum with black aperture covers |
| Null offset | 0.1 deg |
| Scale factor for angles −2 to +2 deg. For angles greater than 2 deg | 1.7 V/deg (Figs. XVIII-E-2 and XVIII-E-3) |
| Alignment | 0.1 deg with respect to flight control sensor group axes |

### Table XVIII-E-8. Secondary sun sensor requirements

| Item | Requirement |
|---|---|
| Weight | 0.3 lb (max) |
| Power | 13 mW |
| Thermal control | White with black aperture |
| Field of view | Hemispherical, (180–360 deg solid angle) |
| Accuracy | 0.25 deg |
| Operating temperature | −100° to +160°F transit<br>−125° to +235°F lunar |

### Table XVIII-E-9. Roll actuator requirements

| Item | Requirement |
|---|---|
| Weight | 1.45 lb (max) |
| Power | 4.0 W per phase (max) |
| Motor size | 11 |
| Motor stall torque | 0.4 in.-oz (min) |

### Table XVIII-E-9 (contd)

| Item | Requirement |
|---|---|
| Travel | 11.5 ±0.5 deg |
| Thermal control | Polished aluminum or vacuum-deposited aluminum except top surface, which has an aluminized Teflon finish |
| Operating temperature range | 0–200°F |
| Loop gain | 1.65 deg of gimbaled engine angle/deg of roll gyro error |
| Mechanical null | ±0.5 deg |
| Electrical null | ±0.25 deg |

### Table XVIII-E-10. Gas supply requirements

| Item | Requirement |
|---|---|
| Weight (uncharged) | 9.1 ±0.1 lb |
| Gas | Dry nitrogen |
| Charge pressure and temperature | 5000 psi<br>125°F |
| Pressure regulation at 70 ±5°F | (Fig. XVIII-E-4) |
| Specific impulse | 63 lbf-sec/lbm |
| Pressure transducer accuracy<br>scale factor | 5%<br>1000 psi/V |
| Nitrogen bottle burst pressure | 10,000 psi (min) |

### Table XVIII-E-11. Gas jet requirements

| Item | Requirement |
|---|---|
| Weight | 0.52 ±0.02 lb (per gas-jet pair) |
| Alignment | 2 deg (thrust axis to nozzle CL) |
| Thrust | 0.057 lb +30% at −10% (inlet pressure, 40 ±2 psi) |
| Rise time | 0.015 sec (max) to two-thirds steady-state value |
| Moment control capability | Roll >4 in.-lb<br>Pitch >4.25 in.-lb<br>Yaw >7.00 in.-lb |
| Thermal surfaces | Gold plated |

## Table XVIII-E-12. Vernier engines requirements

| Item | Requirement |
|---|---|
| Alignment | Engines 2 and 3 nozzle CL to spacecraft roll axis shall be $+0.15 \pm 0.075$ deg. Engine 1 shall be $+0.15 \pm 0.1$ deg |
| Thrust misalignment | Angle between the thrust vector of any one engine and spacecraft roll axis shall not exceed 0.55 at mid-thrust (includes installation alignment errors, bracket bending, and thrust vector excursions) |
| Thrust vector excursions | 0.33 deg (max) prior to retro burnout<br>0.45 deg (max) after retro burnout |
| Thermal control | 0–165°F during inactive periods; Accomplished by selective treatment of external surfaces in conjunction with special solar reflector devices |
| Thrust misalignment with main retro off | 0.7 deg thrust vector of any one engine to spacecraft roll axis (includes alignment errors, bracket bending, and thrust vector excursions) |
| Engine mounting bracket bending constant | 0.5 deg/100 lb applied along engine CL |
| Moment arm | Distance from roll axis to nozzle CL shall be equal to within 0.1 in. |
| Ignition time delay | 0.075 sec (max) |
| Cutoff time | 0.075 sec (max) |
| Time constant | 0.015 sec |

## Table XVIII-E-12 (contd)

| Item | Requirement |
|---|---|
| Shutdown impulse | $\pm 0.66$ lb-sec (max) between any two engines when operating at same thrust within 4 lb |
| Electrical interface | Coil resistance: 400 Ω ±10% at 70°F (400 Ω +33%, operational)<br>Dither A-V: 18 V (peak to peak) $^{+30\%}_{-10\%}$<br>($\Delta I = 30$ mA)<br>Quiescent current $\leq$ 60 mA |

## Table XVIII-E-13. Flight control system group weight summary

| Item | Weight, lb |
|---|---|
| Flight control sensor group | 38.49 |
| IRU | 8.26 |
| Canopus sensor | 5.15 |
| Wiring harness | 1.05 |
| Electronics | 20.66 |
| Support | 3.37 |
| Secondary sun sensor | 0.29 |
| Attitude control system | 18.62 |
| Attitude jets (three pairs) | 1.70 |
| Gas supply | 10.83 |
| Roll actuator | 1.52 |
| Nitrogen | 4.57 |
| Total | 57.40 |

# Appendix XVIII-F

## Detailed Canopus Sensor Mechanization Diagram

## Explanatory Notes

*Description of Canopus mechanization and sequence of events for null star.* The star signal is being sinusoidally displaced by the nodding mirror such that an equal off-time (0.002 sec) or nonexcitation of the photomultiplier tube occurs at the $\pm$1-deg displacement angles of the nodding mirror and at 0.050-sec intervals (see star filter output).

In conjunction with the cam and nodding mirror displacement diagram, the magnetic pulses MP1 and MP2 are being generated 0.025 sec earlier than the peaks of the sinusoidal displacement diagram at an interval of 0.050 sec (see nodding mirror sinusoidal diagram).

Assumed states of multivibrator circuit are $Q_1$ on, $Q_2$ off, $Q_3$ on. At t = 0, MP1 switches $Q_1$ out of saturation, $Q_2$ into saturation, and $Q_3$ out of saturation.

Point B in the multivibrator circuit is effectively grounded. In the blanking pulse circuit, $Q_5$ and $Q_7$ are conducting and points D and E are effectively at ground potential.

$C_1$ and $C_2$ are charged to 28 VDC (29 VDC less drop through diodes $D_1$ and $D_2$ and $V_{5e}Q_5$ and $V_{6e}Q_7$).

When point B goes to ground, the action of $C_1$ discharging to ground potential back-biases $Q_5$ into cutoff.

Point D is raised above ground to bias on $Q_4$; $C_1$, being discharged to ground potential, charges through the adjustable 750-k$\Omega$ resistor at or approximately 1 VDC, whereby $Q_5$ is again biased on, pulling point D to ground and removing the drive for $Q_4$. $C_1$ now recharges to +28 VDC through the 57.6-k$\Omega$ resistor.

This action results in the wave shape tracking and command data (TCD) in the timing diagrams shown and, as can be seen, is of 0.024-sec duration.

Upon the negative TCD or $Q_5$ going into saturation at point D, the 0.002-sec blanking pulse is generated at point E, precisely as the symmetrical circuit of the 0.024-sec time constant is generated at point D. The blanking pulse generation is also shown time related to the TCD circuit.

As shown in the wave shape diagrams, the BP in time width (0.002 sec) and amplitude is generated symmetrically about the 0.050-sec point in time to fill in the no-star photomultiplier star output.

The star error blanking pulse pipper detector output are now inputs to the exclusive OR gate circuits time related as shown in the null star error diagrams.

The star voltage and blanking pulse inputs keep $Q_{10}$ and $Q_{11}$ in saturation alternately in time, and keep point F or the collectors of $Q_{10}$ and $Q_{11}$ at ground potential.

At t=0 the pipper detector output, being high, drives $Q_9$ into saturation for a period of 0.050 sec, $Q_9$ conducting through $Q_{10}$ and $Q_{11}$. Point G, therefore, including the diode drop through $D_4$, is at 1 VDC above ground.

For the 0.050-sec duration of the pipper output and with $Q_{10}$ and $Q_{11}$ conducting, the 1-VDC condition at point H is sufficient to drive $Q_{12}$ into saturation and cause $Q_{13}$ to nonconduct in the star error circuit. This is shown as the $Q_{12}$ and $Q_{13}$ conducting regions in the wave shape diagrams.

For the next 0.050 sec the pipper output is low or $Q_3$ is at ground, causing point D in the exclusive OR gate to be at ground potential. Since $Q_{10}$ and $Q_{11}$ are conducting, the 15-V supply through the 15-k$\Omega$ resistor input at $Q_8$ is effectively grounded. Thus, $Q_8$ is not biased on and point G rises to approximately 10.6 VDC. This condition is sufficient to bring $Q_{12}$ in the star error circuits out of saturation and drive $Q_{13}$ into saturation.

Thus, in 0.100 sec, +24 VDC and −24 VDC are symmetrically switched across the star error phi filter, resulting in an integrated output of 0 VDC null star error.

*Sequence of events off null star assumed −1 deg.* As seen in the wave shape diagrams for an assumed negative displacement of the vehicle, at t=0 the star voltage in time-off voltage decreases and 0.050 sec later in time increases.

#1

## Explanatory Notes (contd)

The sequence of events for $Q_{12}$ (+24 VDC) is the same as the null star condition described above.

However, in the next 0.050 sec, when the pipper output is low or ground for a portion of time, $Q_{10}$ is on and the +15 VDC is applied through the 15-kΩ resistor, making point G high and $Q_{13}$ (−24 VDC) is conducting. The off-time of the star now having been broadened in time, and since the blanking pulse is not yet in time being generated to fill in the off-time of the star voltage, $Q_{10}$ comes out of saturation and the +15 VDC is applied to $Q_8$, causing $Q_8$ to conduct into saturation. Point G is now reduced to +1 VDC through diode $D_3$ and $Q_3$ to ground. This permits $Q_{12}$ to conduct, $Q_{13}$ is cut off, and more +24 VDC is applied to the star error circuit. This action continues until at the proper time, and for 0.002 sec, the blanking pulse is generated, $Q_{11}$ conducts, and the +15 VDC through the 15-kΩ resistor is grounded, removing the drive for $Q_8$ and point A reset to −10.6 VDC. Again, $Q_{13}$ conducts, $Q_{12}$ is pulled out of saturation, and −24 VDC is applied to the star error circuit.

The net result is the average on-time of $Q_{12}$ increases, the average on-time of $Q_{13}$ decreases, and the star error ramps up to +2 VDC.

The same step-by-step analogy can be applied for a +1-deg spacecraft displacement with the result that the average on-time of $Q_{13}$ increases, the average on-time of $Q_{12}$ decreases, and the star error voltage ramps to −2 VDC.

Spacecraft displacement as a function of time generates the star error voltage as shown.

#2

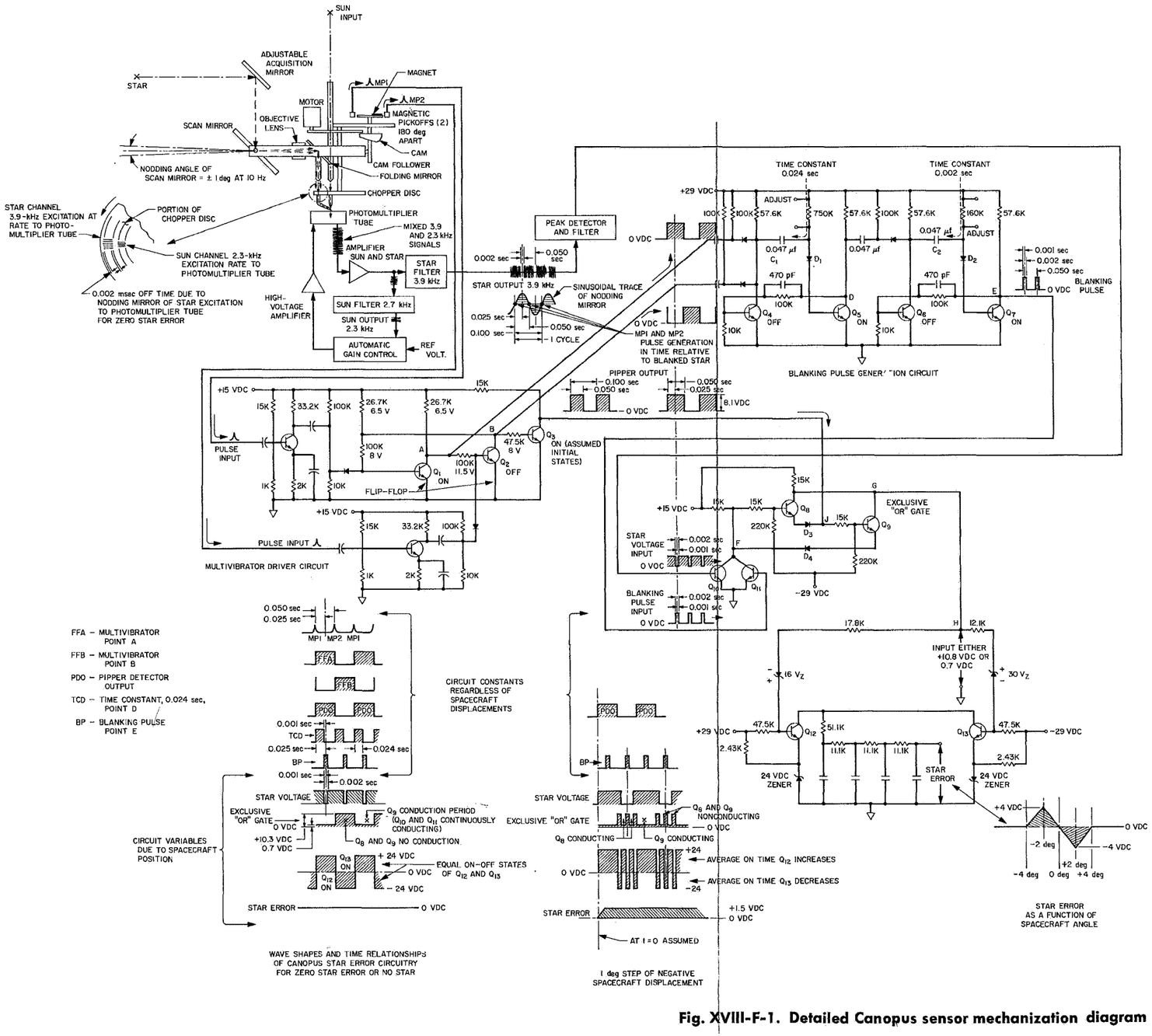



**Fig. XVIII-F-1. Detailed Canopus sensor mechanization diagram**

# XIX. Spacecraft Radar

The *Surveyor* spacecraft employed two radar systems, each with distinct responsibilities. The responsibility of the altitude marking radar (AMR) was to initiate the automatic terminal-descent sequence by providing a lunar altitude reference signal for precise timing of vernier-engine and main retro motor ignition.

The radar altimeter and doppler velocity sensor (RADVS) supplied the spacecraft flight control system with continuous velocity and slant-range measurements relative to the lunar surface to enable control of the spacecraft descent after retrorocket burnout in accordance with the desired velocity–range descent profile.

## A. Altitude Marking Radar

The *Surveyor* AMR was a small, conventional, fixed dual-range gate, marking radar. It provided, with high accuracy and reliability, a positive indication when the slant range from the *Surveyor* spacecraft to the lunar surface had reached a preset value (about 60 statute miles). Its performance requirements are summarized in Table XIX-1. The mark signal started an on-board timer (sequence time preset by ground command earlier in the flight) to initiate vernier-engine and main retro motor ignition. The AMR, installed in the exhaust cone of the main retro motor, served its purpose by providing retro-ignition timing; it was forcibly ejected from the spacecraft after ignition. The AMR was manufactured by Hughes Aircraft Company (HAC), the *Surveyor* prime contractor.

**Table XIX-1. Altitude marking radar performance requirements**

| Item | Value |
|---|---|
| Maximum approach angle | 45 deg |
| Velocity range | 8000–8850 ft/sec |
| Maximum acceleration | 6 ft/sec |
| Typical marking range | 60 mi |
| Calibrated marking range variation | ±1 mi |
| Random marking range variation | ±0.5 mi |
| Probability of false mark | 0.002 |
| Probability of reliable mark | 0.9975 |

### 1. Description, Flight Configuration

The *Surveyor* AMR was a pulsed, X-band, noncoherent radar system operating at a frequency of 9300 MHz (9.3 GHz). The transmitter was a magnetron with a peak output of 1500 W. The AMR block diagram is shown in Fig. XIX-1 and a list of its parameters is given in Table XIX-2. The receiver used a crystal-controlled local oscillator together with a low-noise crystal-mixer front end to provide a 30-MHz IF. The video detector was driven by the IF amplifiers to provide an output which was the envelope of the reflected RF pulse from the lunar surface. This reflected pulse was delayed from the moment of transmission by the transit time to and from the lunar surface. This delay was typically 643 $\mu$sec for a two-way range of 60 mi. The marking range could be preset by time-delay circuits in the AMR for any altitude within 52–70 mi of slant range above the lunar surface. The range for all missions was 60 $\pm$1 mi at mark. To assure a very low probability of false mark on noise, the output of two video gates (an *early* and a *late*) were summed and differenced.

The AMR marked when the sum of the video signal within the gates exceeded a fixed threshold and when the difference crossed zero with a positive slope. This excluded all normal noise pulses and image returns. Returns for multiples of the 60-mi distance were avoided by not enabling the AMR until it was less than 120 mi from the lunar surface. An excellent signal-to-noise ratio (20 db) at the design marking distance offered additional protection against false mark. A final precaution to guarantee retroignition was exercised during flight by ground transmittal of a backup mark which would start the retro sequence one second after the predicted time for a spacecraft range of 60 mi above the lunar surface.

The AMR antenna was a 30-in. parabolic dish which served for both transmit and receive through use of an RF circulator and a gaseous transmit–receive tube. The antenna had a gain of 34 db, with a 3.6 deg half-power beamwidth. The AMR electronics was mounted on the back of the antenna dish. The electronic package included the RF head, receiver, magnetron, local oscillator, and video processor. The AMR assembly is shown in Fig. XIX-2.

The entire AMR was mounted within the main retro motor exhaust nozzle and secured by friction clamps along the outer perimeter of the dish edge. Power was carried to the unit from the spacecraft by a quick-disconnect breakaway plug. After initiation of retroignition by the 60-mi mark signal of the AMR, the radar was forcibly jettisoned from the nozzle; it fell free, reducing the spacecraft weight for landing preparation (the spacecraft needed to be slowed for landing by some 11 lb).

### 2. Design Development

Type-approval (TA) tests of the original AMR prototype indicated serious mechanical, thermal, and electronic design deficiencies: The antenna dish exhibited dimensional instability, and the thermal control philosophy of maintaining only temperatures required for survival resulted in unacceptable instability in the receiver circuits during 1965. Special tests, based on newly developed scintillating lunar RF return predictions (Subsection A-3), proved the IF amplifier automatic gain control (AGC) to be incapable of functioning with noise-modulated return inputs. Continuing analytical studies and subsequent refinement to the functional-requirement definition proved that the parallel-channel gating system used in the video processor–mark detection functions could provide neither the required immunity from false marking nor the required accuracy for range marking. During 1965, a complete mechanical, thermal, and electronic redesign was initiated.

The redesigned AMR, in addition to meeting TA test requirements, could be defined by a more accurate mathematical model. (This model is described in Subsection A-4). Performance of the AMR was analyzed in a closely modeled computer program which used a modified Muhleman reflectivity model to evaluate the expected error in the predictable return RF power due to the random nature of the ground return signal, systematic range bias inherent in the design, and the probability of marking. This analysis confirmed the adequacy of the new design.

***a. Antenna reflector mechanical redesign.*** The antenna reflector, initially subcontracted, developed dimensional changes (warpage) with shelf life. The reflector was constructed of epoxy–Fiberglas with a corrugated core, and filled with polyurethane foam. When formed into the parabolic shape, the reflector exhibited dimensional instability in that the differential strength–stress parallel to (as opposed to *normal* to) corrugated planes caused the reflector shape to change. A new antenna design was initiated and an epoxy–Fiberglas honeycombed reflector was developed with adequate dimensional and structural integrity.

***b. Thermal redesign.*** The original thermal design, in which the AMR electronics was mounted directly to the back of the AMR antenna honeycomb platform, provided no thermal-radiation shielding. A total of 198 W-hr

## Table XIX-2. Marking radar parameters

| Parameters | Specified value | Parameters | Specified value |
|---|---|---|---|
| Operating frequency | 9.30 GHz | False alarm probability | $<10^{-3}$ |
| RF power output | | Transmitter | Magnetron self-excited oscillator |
| Average | 2 W | Video processor | Dual-channel, sum and difference gating with threshold detector |
| Peak | 1500 W | | |
| Pulse length | 3 $\mu$sec | Power requirements | |
| Pulse repetition rate | 350 pulses/sec | Voltage | 22 VDC unregulated |
| Antenna | Parabolic, 30-in., circular-polarized | Current before enable | 2 A |
| | | Current after enable | 3.5 A |
| Bandwidth | 3.6 deg at half-power point | Power before enable | $<$50 W |
| Gain | 34 db (over isotropic radiator) | Power after enable | $<$90 W |
| Intermediate frequency (IF) | 30 MHz | Spacecraft altitude-marking signal | |
| IF gain | 107 db | Level | 14 VDC |
| IF bandwidth | 5.5 MHz | Current | 0.3 mA |
| Receiver noise figure | 12 db | Weight | 11.8 lbs |
| Local oscillator | 9.330 GHz | Dimensions | 30 in. diameter; 17.125 in. deep |
| Receiver mixer | Passive, orthomode balanced 1N23 diodes | | |

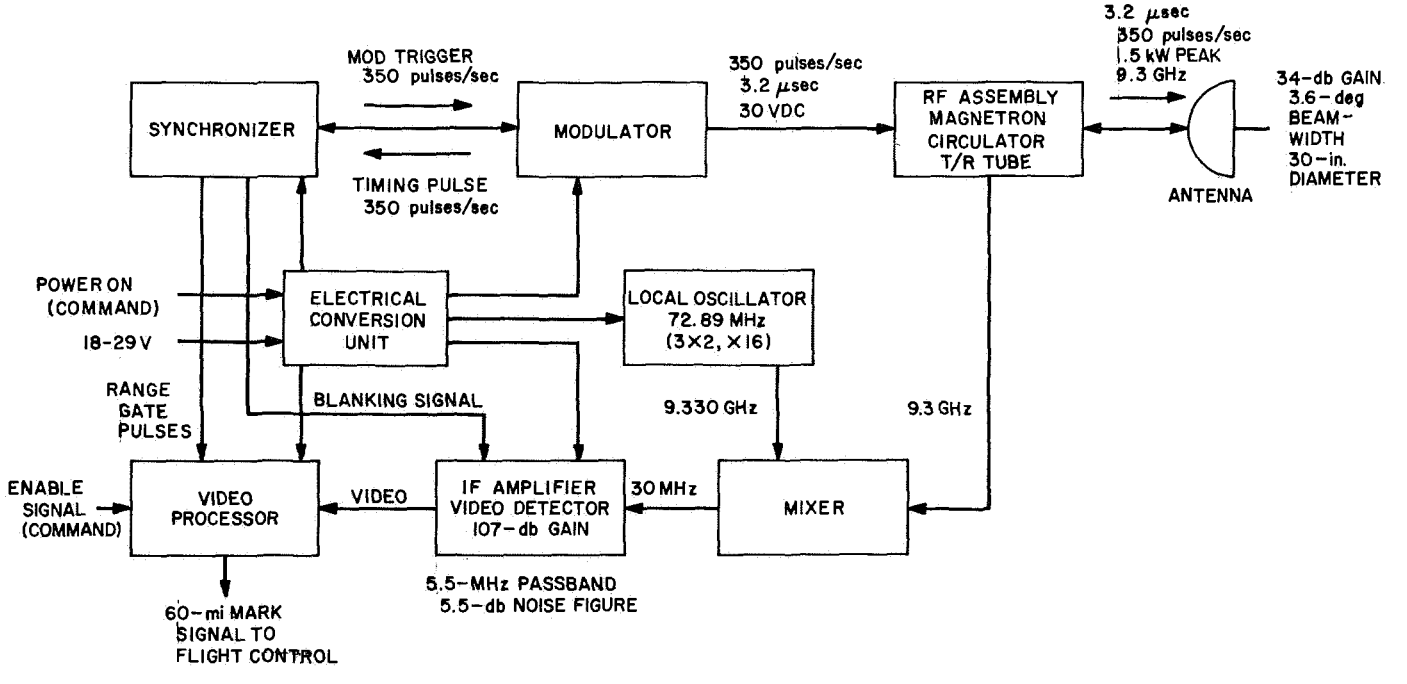



**Fig. XIX-1. Altitude marking radar, block diagram**

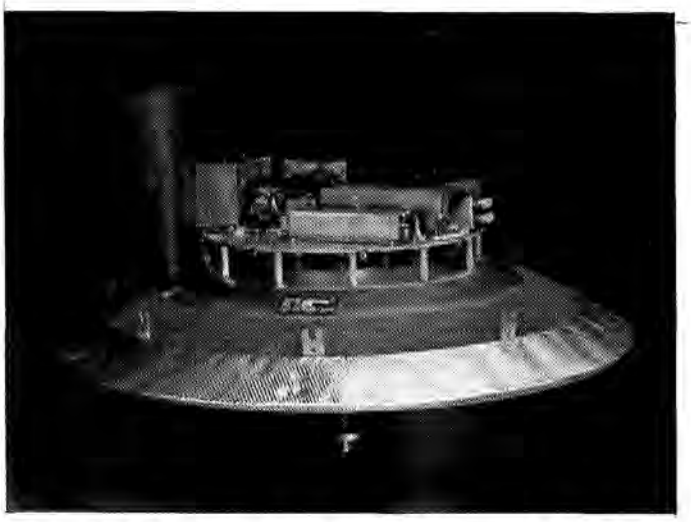


**Fig. XIX-2. Altitude marking radar, assembly photo**

of electrical energy was required during a 66-hr transit to maintain the magnetron at −42°F (−50°F specified lower limit for reliable operation). No heating was provided for other AMR electronics since its storage survival temperature capability of −130°F was then considered adequate.

To achieve maximum benefit from the electronic–thermal redesign, the requirement to maintain all AMR electronics between −10 and +50°F was established. This was accomplished in the following manner:

(1) The honeycomb electronics mounting platform was mounted to the AMR dish on low-conductivity epoxy–Fiberglas standoffs.

(2) Two aluminized Mylar film radiation barriers were placed between the AMR dish and the mounting platform.

(3) The AMR electronics (including magnetron) were enclosed in a removable thermal hat of multilayer aluminized Mylar superinsulation.

(4) Heater resistors were imbedded in aluminum blocks to improve energy transfer to the selected heated areas.

(5) The heater circuit thermostat control was mounted on the IF amplifier chassis (since this component exhibited the shortest thermal time constant).

(6) Due to the possibility that the edge of the AMR reflector dish might receive heat damage from the vernier-engine plumes during midcourse and terminal firings, a steel-and-Refrasil insulation ring was added to the back of the reflector dish.

These changes resulted in adequate thermal control, allowing the entire AMR electronics to be maintained at 17 ±5°F, utilizing approximately 198 W-hr of electrical energy during transmit.

*c. Electronic redesign.*

*1. Solid-state local oscillator.* Receiver instability because of temperature variations was eliminated by the addition of zener diodes in the varactor multiplier string which stabilized the bias level and drive current of these oscillator stages. Subunit flight-acceptance (FA) test procedures were modified to require 200 hr of operation for the complete local oscillator unit in order to eliminate aging shifts in the finely tuned varactor multipliers.

*2. Intermediate frequency amplifier.* The IF unit was incompatible with the video processor in the case of target scintillation. The averaging circuits could not average a randomly varying pulse. This caused range inaccuracies. To eliminate this IF amplifier saturation on scintillating input signals, the incoming signal was smoothed prior to noise separation, and the threshold detector was made to operate independently of the peak-averaging AGC circuitry. Unacceptable nonlinearity in the detector stage due to changing admittance of the following stages was eliminated by emitter-follower isolation. To improve the signal-to-noise ratio and sensitivity, a lower-noise transistor was added to the first IF amplifier following the mixer. This was contained within a four-stage 30-MHz IF strip having a bandwidth of about 5.5 MHz and a noise figure of 5.5 db.

*3. Video processor.* The original design approach of the video processor utilized parallel-channel sampling of the video in dual gates of 3 μsec width each and separated by 20 μsec. When staircase integration of the video pulses in each channel exceeded the high-impedance pulse-detector threshold, the circuit armed and marked. Marking accuracy was dependent upon constant video pulse amplitude, a condition not satisfied in the presence of scintillating signal returns. The redesigned processor utilized dual adjacent range gates (*early* and *late* gates) of 20 μsec width and zero separation. When both signals were approximately equal, and the sum of the signal in both range gates exceeded a threshold, the marking circuit armed. The possibility of false marking was additionally guarded against by providing that when the centroid of power of the video signal falls on the common boundary of the two gates, the difference of the signals in the two gates must pass through zero with a positive slope before the marking circuit would trigger. Analysis, test, and mission experience proved

this design to be reliable and accurate and to fulfill the functional requirements of the mission.

*4. Marking circuits.* Greater protection against externally generated false marks was achieved by replacing the original SCR mark trigger circuit with a transistor amplifier trigger, which clamped the mark signal line to zero potential until the internal AMR mark signal was generated.

The primary equation used for evaluation of AMR mission performance, which relates AMR transmitter–receiver characteristics to spacecraft trajectory parameters (Fig. XIX-3) and defines received RF power $P_r$ from the lunar surface, is

$$P_r = \left(\frac{1}{2}\right)\left(\frac{c}{4\pi}\right)^3 \left(\frac{P_{av}G^2}{f^2 f_p R^3}\right) \beta_1 \cot\theta\sigma(\theta)$$

$$G(\theta) = \eta\,(K/\alpha^3)\,f\,(\theta)$$

In this equation as well as those following, the elements are defined as:

$P_r$ = total received power at antenna

$P_{av}$ = average transmitted power

$\lambda$ = wavelength

$c$ = velocity of light ($f\lambda$)

$f$ = frequency

$G$ = one-way peak antenna gain

$R$ = slant range along beam axis

$\theta$ = incidence angle

$\sigma(\theta)$ = effective radar cross section per unit projected area

$f_p$ = pulse repetition rate $= \frac{P_{av}}{P_{peak}}\tau$ duty cycle

$\frac{P_{av}}{P_{peak}}$ = duty cycle (0.00133)

$A_p$ = projected area

$\beta$ = equivalent antenna beamwidth

$\frac{K}{\alpha^3}$ = 10.7 db = empirical AMR data

$$f(\theta) = \frac{\alpha^3}{(\sin\theta + \alpha\cos\theta)^3}$$

$\eta$ = power reflection coefficient = 0.065

A sample calculation using this equation and data from the *Surveyor V* mission are presented in Appendix A. Parameters of particular interest in the equation for $P_r$ are: the AMR slant range (60 mi), the incidence angle at the surface, and the received pulse stretching effect. The latter is seen to vary significantly because of slant range variation. It has been found that when $c\tau/2\cot\theta\beta_1 R$, the AMR antenna beamwidth would limit the peak value of the received power as the transmitted pulse $\tau$ is stretched in time as it traverses the illuminated patch of lunar terrain (Fig. XIX-3).

When $A_p \rightarrow (\beta_1 R)^2$ then $P_r \alpha R^{-2}$. Under condition $R$ (slant range) = 60 mi, $\beta_1 = 3.25$ deg; $\tau = 3.2$ $\mu$sec. There then occurred a crossover point for pulse-stretching at $\theta = 7.14$ deg incidence. Some pulse-stretching still occurs for $\theta = 7.14$, however. But when the incidence angle is greater than 7.14 deg, significant pulse-stretching occurs and $P_r \alpha R^{-3}$ is applied.

The pulse length of the reflected 3.2 $\mu$sec ($\tau'$) pulse is given by

$$\tau' = \tau + \Delta\tau \text{ (pulse-stretching)}$$

$$\tau' = 3.0\ \mu\text{sec} + 28.4\tan\theta$$

or

$$\Delta\tau = 28.4\tan G$$

$$\theta \geq 7.14 \text{ deg}$$

This derivation is presented with reference to Fig. XIX-3: At some point ($p_1$) two lines are drawn to $L$. The line associated with $\theta_1$ represents the first RF energy to reach the surface for transmitted pulse $\tau$. The line $L_2$ with $\theta_2$ represents the last energy from the transmitted

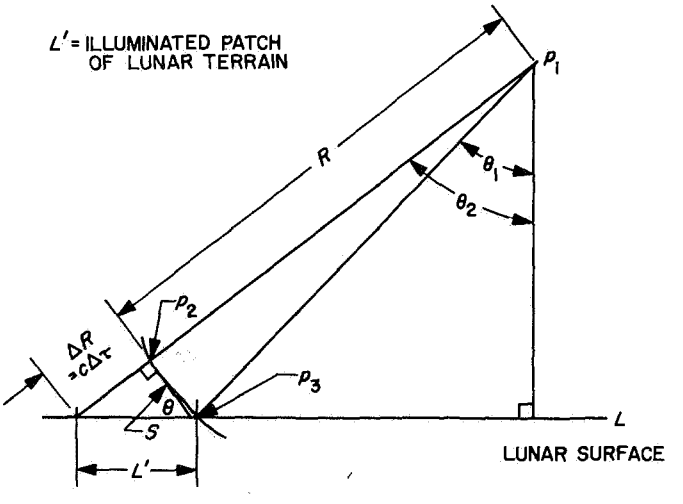



**Fig. XIX-3. Relation of RF energy to transit range**

pulse $\tau$ to reach the surface. $\Delta R$ is the extra range required for the RF energy to travel to reach the surface. The $\Delta R$ is associated with the $\Delta\tau$ (amount $\tau$ is stretched). With $R$ quite large it is assumed $\theta_1 = \theta_2$, and that the arc of $p_2p_3$ with center at $p_1$ is equal to S.

Then

$$\beta R = S$$

and

$$\tan\theta = \frac{\Delta R}{\beta R}$$

or

$$\Delta R = \beta R \tan\theta$$

But

$$\Delta\tau c = \Delta R$$

therefore:

$$\Delta\tau = \beta R/c \tan\theta$$

The expression $\beta R/c = 28.4$ was evaluated with

$R = 60$ mi

$c =$ velocity of light

$\beta =$ empirical AMR dish beamwidth (deg)

$$\beta = \frac{\text{AMR beamwidth}}{180}\pi(\text{rad})$$

The equation for $\tau'$ as derived above was used in determining and interpreting range marking performance. The calculated value of $\tau'$ established the proper operating point on the AMR automatic gain control calibration curve by knowing the AGC voltage (telemetry data) and the amount of pulse-stretching $\Delta\tau$. The actual RF return power was then determined from the AGC curves. This was compared to the theoretical return power as evaluated by the equation of $P_r$.

### 3. Test Program

*a. Type-approval tests.* The validity of the TA test as a proof of design procedure was demonstrated during AMR development. The results of the initial AMR TA and associated tests and studies indicated that the original design would not meet mission requirements (see Subsection A-2). The redesigned AMR successfully passed TA tests.

The two special tests described below figured prominently in the AMR development.

1. *Scintillating input signal test.* This test was performed in 1965 because of the result of continuous analysis upon most recent reflectivity data and studies which led to the prediction of significant noise-modulated amplitude scintillation of the returned AMR RF signal. The test proved that the IF AGC would block and saturate the IF amplifier gain with scintillating inputs, prompting the complete redesign of the IF subunit.

2. *Flight ascent pressure and profile test.* This test was performed to prove the design of the AMR as a unit, and particularly the honeycombed parabolic reflector structure, in a rapidly decreasing pressure environment as would occur in the boost phase of a *Surveyor* launch. Test results indicated the honeycombed structures were not subject to damage or boresight distortion during decompression by entrapped gases, and that the AMR met all operating requirements following such decompression.

*b. Flight-acceptance tests.* All flight AMRs received FA tests at both the unit and subsystem levels.

1. *Unit flight acceptance tests.* Before delivery to the spacecraft, all flight AMR units were required to demonstrate function, accuracy, and reliability in ambient and thermal-vacuum environments. Some of the major FA test parameters measured were: input power, transmitter frequency, RF power output, local-oscillator frequency, AGC and *late* gate curves, purge detection, marking sensitivity, and marking accuracy.

2. *System tests.* Following delivery to the spacecraft, all flight AMR units were required to demonstrate compatibility, function, accuracy, and reliability in the spacecraft mission environment. A most significant feature of system FA test was the use of computer-mechanized, real-time, closed-loop terminal descent. The computer simulated a range of 60 mi approximately 100 sec after the AMR was enabled. The order of test phases was as follows:

(1) Initial system checkout—AMR electrically mated to spacecraft. Compatibility tests and calibrations were performed in the ambient spacecraft environment.

(2) Mission sequence and electromagnetic interference —electrical and mechanical mating to spacecraft and plugs-out EMI compatibility testing.

(3) Solar thermal-vacuum (STV)—AMR mechanically and electrically mated to the spacecraft in both high- and low-intensity solar environment. This tested all active and passive thermal controls as well as compatibility, function, accuracy, and reliability in the STV environment.

(4) Boost vibration—AMR mechanically mated to spacecraft with functional closed-loop terminal descent following the vibration sweeps.

(5) Performance verification test at the Air Force Eastern Test Range (AFETR)—these included a unit test and a plugs-in test while electrically mated. After final mechanical mating, a power-on readiness test confirmed plugs-out mission readiness.

The results of the system FA tests demonstrated the reliability of the flight AMR. Although no AMR went through system FA testing without rework cycles, these rework cycles were usually minor. The AMR tested well and performed its flight requirements in all missions which required its operation.

#### 4. Altitude Marking Radar Performance

The AMR performed reliably on all spacecraft missions for which there was a terminal phase. The received-signal margins for all missions were over 26 db above the 0.999 probability threshold for marking.

A special two-body computer program having a high degree of accuracy was used to determine the predicted received-signal power for the AMR based on the Muhleman reflectivity model. This program predicted all significant AMR parameters throughout the 100-sec interval from enable to mark. The computer program was also used to apply calculated correction factors to observed telemetry AGC data before comparison with predicted received-signal power.

The telemetry data for all missions was in agreement with the predicted received-signal power based on the Muhleman reflectivity model. A summary of the performance for this mission is given in Table XIX-3. Additional details of mission performance are presented in the *Surveyor III* and *IV* final reports (Refs. XIX-1 and XIX-2).

### B. Radar Altimeter and Doppler Velocity Sensor

The radar altimeter and doppler velocity sensor (RADVS) was a four-beam, coherent, continuous-wave, doppler, microwave radar. Its primary function was to measure velocity and slant range relative to the lunar surface during the terminal-descent phase of the *Surveyor* flight (from 50,000 to 14 ft). These quantities were measured directly in spacecraft coordinates allowing direct utilization by the spacecraft flight-control system for both attitude control and deceleration thrust control. Additionally, the RADVS provided two range-marking signals. The first signal, which occurred at a range of 1000 ft, initiated an increase in RADVS output signal sensitivity and a flight control system gain change, which provided improved analog signal resolution and control for the last critical seconds of the flight. The second range signal, which occurred at a 14-ft altitude, was used

**Table XIX-3. Performance summary**

| Surveyor mission | Margin above 0.999 probability threshold for marking, db | Anomalies during operation | Correlation between processed AGC telemetry data and predicted signal strength |
|---|---|---|---|
| I | 37.0 | None | Very good[a] |
| II | No data | None — partial data from tumbling spacecraft | No AGC data — transit thermal control, AMR on, and AMR enable were normal |
| III | 27.7 | None | Within 2 — 3 db, good correlation, received signals somewhat weaker than expected. This might be due to lower than nominal terrain reflectivity |
| IV | 27.5 | High quiescent level (before enable) of AMR AGC[b] | Essentially the same as Surveyor III |
| V | 26.1 | None | Extremely good, generally within 1 db |
| VI | 31.5 | None | Within 1 — 2 db |
| VII | 29.3 | None | Within 5 db |

[a]The two-body program was not available at this time.
[b]This had no effect on the mission or the mark events.

to turn off the vernier engines. The spacecraft would then free-fall the last few feet to the lunar surface.

The RADVS consisted of a doppler velocity sensor for determining velocity and a radar altimeter (RA) for determining slant range and generating the altitude mark signals. The primary power of the RADVS was applied automatically 1 sec after retroignition. Approximately 20 sec after primary power application, circuits within the RADVS applied power to the radar transmitters. Beginning at that instant RF energy was transmitted in four beams via two antennas to the lunar surface. Since the reflected RF energy was shifted in frequency by doppler effect, and in time by the distance of travel, the signals contained the information as to spacecraft velocity and altitude. Determination of velocity components and slant range was accomplished within the signal data converter portion of the RADVS.

### 1. Radar Altimeter and Doppler Velocity Sensor Description, Flight Configuration

*a. Radar altimeter and doppler velocity sensor system.* As depicted in the simplified block diagram (Fig. XIX-4), the complete RADVS subsystem consisted of two radars, the doppler velocity sensors (which had three beams), and the radar altimeter (with one beam). The four beams were integrated into one subsystem. The five physical units that made up the RADVS system were the klystron power supply and modulator (KPSM); the altitude velocity sensor (AVS) antenna; the doppler velocity sensing (DVS) antenna, and the signal data converter (SDC) unit and interconnecting waveguide. A summary of RADVS system electrical and physical characteristics is given in Table XIX-4.

The DVS portion of the system was a three-beam continuous-wave doppler radar. A single klystron provided undeviated output at a nominal frequency of 13.3 GHz. Its output was divided equally among the transmitting antennas for beam 1 (contained on the AVS antenna) and beams 2 and 3 (contained on the DVS antenna). Each beam was constructed with separate receiving ports on its respective antenna. Adequate RF isolation against direct leakage was also implemented for each beam along with separate and independent receivers. These receivers utilized a small sample of the transmitted signal as a frequency reference which was compared with the returning signal to obtain the velocity-induced doppler shifts along each beam.

Associated with each of the three DVS beams was a separate and independent doppler signal processor and arithmetic unit. These units processed each beam's doppler frequencies and produced DC analog voltages proportional to the velocities associated with the spacecraft orientation of that particular beam (Fig. XIX-5).

The RA portion of the system was a single-beam frequency-modulated, continuous-wave (FM-CW) microwave unit. The RA beam was aligned with the spacecraft +Z-axis (Fig. XIX-6). The FM-CW RF energy was radiated via beam 4 from the AVS antenna, and received via the same antenna. The RA section had the same kind of transmitter-derived frequency reference used in the DVS system. The RA carrier was generated by use of a reflex klystron. The 12.9-GHz carrier was frequency-modulated by a ramp-voltage waveform using standard FM-altimeter techniques.

The returning RF energy contained an undesired doppler frequency shift and desired carrier-frequency time shift proportional to distance. The altimeter portion of the system also had an independent frequency processing and arithmetic section similar to the DVS system. It was within the arithmetic section that the undesired altimeter doppler shift was compensated for and the altitude information processed. The output of the altimeter portion of the arithmetic units was an analog voltage proportional to spacecraft slant range.

The antenna and beam configuration is shown in Fig. XIX-6. The operation of the RADVS subunits that made up the radar is described as follows:

*b. Klystron power supply and modulator.* The KPSM was installed on the spacecraft by six electrically isolated bolts attached to the velocity sensor and altimeter waveguide, and was connected to the spacecraft power and the SDC by one electrical connector. The functions of the various major components shown in the block diagram of Fig. XIX-7 are described in the following paragraphs; Table XIX-5 summarizes the parameters of the unit.

Basically, the power supply was a DC voltage converter, with the klystron tubes providing the conversion of high-voltage DC energy to RF energy. The preregulators compensated for variations in the spacecraft bus voltages and isolated the unit from spacecraft power interference, providing a stable input to the filament and high-voltage converters. These latter converters used voltage inverters for part of the circuitry, with a transformer primary as the inverter circuit load. The secondary windings of the transformer fed into full-wave rectifiers that provided the appropriate voltages for the postregulator and for

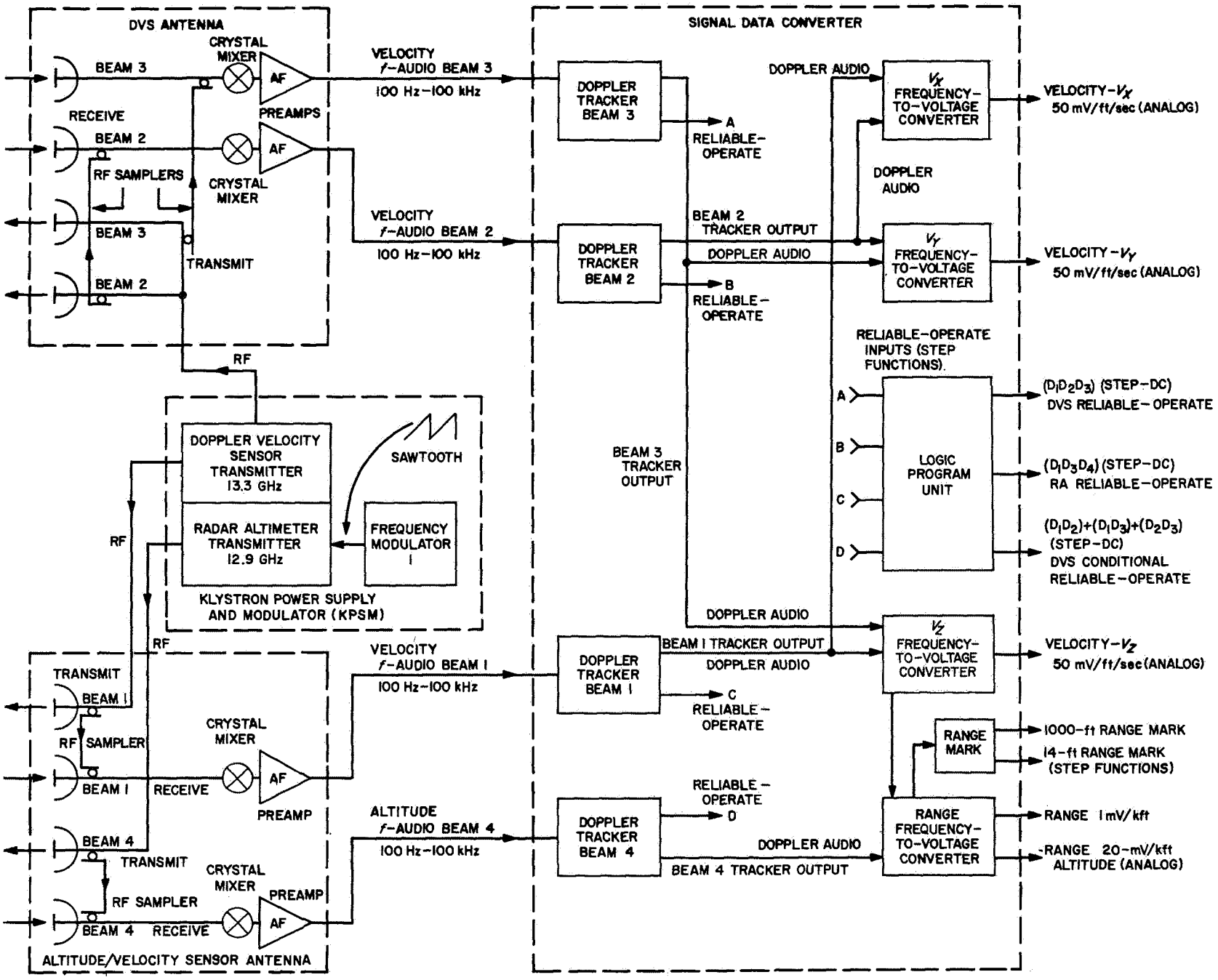



Fig. XIX-4. Radar altimeter and doppler velocity sensor, block diagram

**Table XIX-4. Radar altimeter and doppler velocity sensor parameters**

| Unit/parameter | Specifications |
|---|---|
| Physical characteristics | |
| Dual-beam DVS antenna | 17.27 × 21.57 × 11.65 in., 6.02 lb |
| Dual-beam AVS antenna | 17 × 21.6 × 10.8 in., 6.60 lb |
| Signal data converter | 5¼ × 6 × 12.4 in., 10.15 lb |
| Klystron power supply and modulator | 6.4 × 7.9 × 7.0 in., 10.75 lb |
| Electrical characteristics | |
| Power input (16.5–22.4 V) | 590 W (max) |
| Operating time (deep space) | 5 min (max) |
| Warmup time | 30 sec |
| Antenna beamwidth (2-way) | 5 deg (E-plane), 4 deg (H-plane) |
| Altimeter transmitter | |
| Power | 300 mW |
| Frequency | 12.9 GHz |
| Deviation (low) | 4 MHz (from 12.9 GHz) |
| Deviation (high) | 40 MHz (from 12.9 GHz) |
| Deviation frequency | 182 Hz |
| Deviation rate (low) | 800 MHz |
| Deviation rate (high) | 8 GHz |
| Velocity sensor transmitter | |
| Power (per beam) | 2.5 W |
| Frequency | 13.3 GHz |
| Performance | |
| Doppler velocity sensor | |
| Number of beams | 3 |
| Angle off vertical | 0–45 deg |
| Velocity (max) | 3,000 ft/sec |
| Linear range | |
| Beam 1 | 0 to ±300 ft/sec |
| Beam 2 | 0 to ±300 ft/sec |
| Beam 3 | +1 to +850 ft/sec |
| Accuracy | |
| ≤700 ft/sec | rss[a] of 1 ft/sec and 2% of total velocity vector |
| ≤ 850 ft/sec | rss[a] of 1 ft/sec and 3% of total velocity vector |
| Time constant | 0.1 sec |
| Radar altimeter | |
| Number of beams | 1 |
| Angle off vertical | ≤ 45 deg |
| Velocity (max) | 1 to 850 ft/sec |
| Slant range (total) | 14 to 40,000 ft |
| Low-deviation mode | 1,000 to 40,000 ft |
| High-deviation mode | 14 to 1,000 ft |
| Accuracy | |
| Low-deviation mode | rss[a] of 30 ft and 5% of slant range |
| High-deviation mode | rss[a] of 4 ft and 5% of slant range |
| Time constant | 0.1 sec |
| Electrical outputs | |
| Altitude (slant range) | 14–1000 ft, + 20 mV/ft<br>1000–40,000 ft, +1 mV/ft |
| Beam 1 | 0 to ±300 ft/sec, +50 mV/ft-sec$^{-1}$ |
| Beam 2 | 0 to ±300 ft/sec, +50 mV/ft-sec$^{-1}$ |
| Beam 3 | +1 to +850 ft/sec, +50 mV/ft-sec$^{-1}$ |
| Altimeter 1,000-ft mark | +5 V step voltage |
| Altimeter 14-ft mark | +5 V step voltage |
| Altimeter reliable-operate signal | +5 V step voltage |
| RADVS reliable-operate signal | +5 V step voltage |
| Number of discrete components | |
| Signal data converter | 4674 |
| Klystron power supply and modulator | 357 |
| Altitude velocity sensor antenna | 542 |
| Doppler velocity sensor antenna | 542 |
| Total components | 6166[b] |

[a]rss = root sum squared.

[b]Includes 51 minor components.

feedback control. A 20-sec time delay between applications of filament power and high voltage provided protection against erratic operation caused by klystron warmup. The filament regulators, in addition to providing regulation and very low ripple, provided current-limiting to the filaments of the klystrons. Because the resistance of the filaments may be low at turnon, the filament current had to be limited to less than 20 A to minimize filament distortion and subsequent klystron characteristic changes.

The high-voltage regulators utilized two 90-V outputs from the high-voltage converter, along with 2100-V and 455-VDC outputs, which provided the required −2150 V and −500 V for the klystrons.

The altimeter high-voltage regulator, which supplied −500 V beam voltage for the altimeter klystron, operated on the principle of regulating the 90-V input which was in series with the 455-VDC input, with the regulation loop closed on the total output of 500 V. The

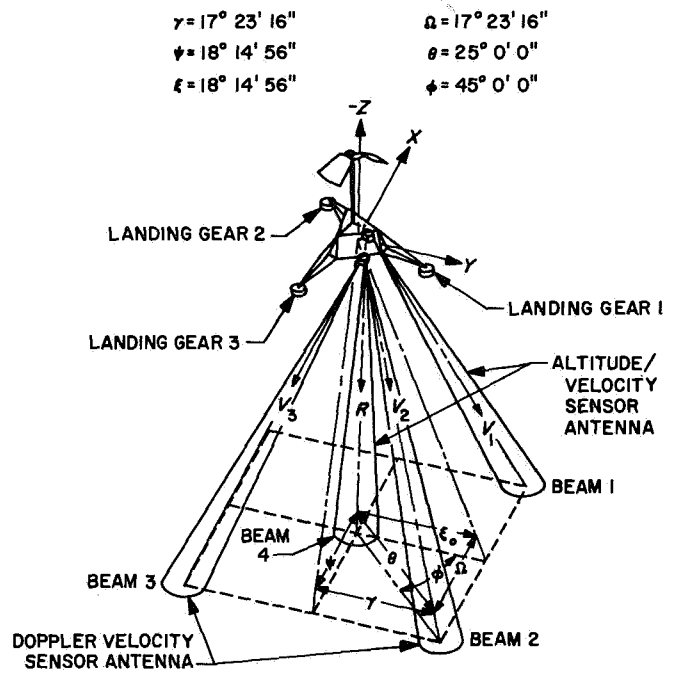



**Fig. XIX-5. Beam orientation**

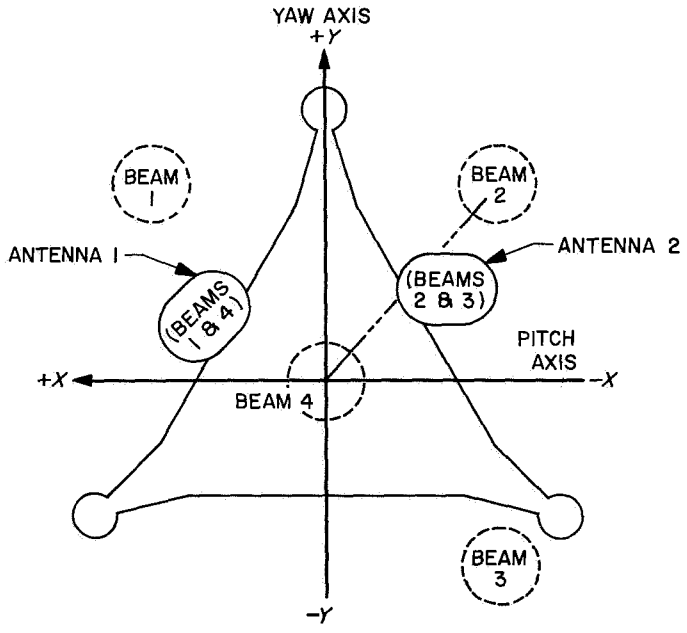



**Fig. XIX-6. Antenna and beam configuration**

velocity sensor high voltage regulator, which supplied −2150 V beams voltage to the velocity-sensor klystron, operated basically the same as the altimeter high voltage regulator.

A bridge was used to supply reflector voltage for the altimeter klystron by tapping to −800 V. The bridge was connected between the 500-V supply and the negative side of the 2150-V supply, with the tap adjusted to 300 V below the 500-V supply. The KPSM also possessed a short time constant to react on interruption of primary power: the KPSM would recycle to its 20-sec time-in period if primary power were interrupted for 30 msec. Successful system operation depended to a large extent on suppression of ripple and noise on the various klystron input lines. This made it necessary to precisely match a particular klystron over the ripple frequency spectrum.

The modulator provided a sawtooth voltage output which was transformer-coupled to the altimeter klystron reflector (high voltage) input. This output was temperature-compensated and matched to a particular klystron used. This matching was necessary to achieve a return signal spectrum which had as narrow a bandwidth as possible. The tradeoff between a narrow spectrum and the difficulties in matching the tube has given added ranging capabilities with the KPSM in the high-deviation mode. A change in klystrons would require a complete rematch to obtain this compensation. The linearity and accuracy of this sweep rate, coupled with the klystron characteristics, also determined the accuracy of the altimeter.

The KPSM weighed 10.5 lb and the package measured 7.66 in. wide, 5.46 in. high and 5.62 in. deep. Detailed test data are given in Ref. XIX-3.

*c. Signal data converter.* The DVS section of the SDC (Fig. XIX-8) consisted mainly of three frequency trackers and three frequency-converter functions. The frequency trackers acquired and tracked the doppler frequency shift from each of the DVS beams. These doppler frequencies were proportional to the relative velocities along each beam axis. The frequency-converter function of the SDC converted the velocity signals along each beam axis into the velocity components in spacecraft coordinates. The DC analog output signal scale factor for the three velocity converters was 50 mV/ft-sec. The $V_X$ converter output was proportional to the difference in doppler frequencies of beams 1 and 2. The $V_Y$ converter output was proportional to the differences in doppler frequencies of beams 2 and 3. Both $V_X$ and $V_Y$ converters have linear outputs in the range of ±300 ft/sec. The $V_Z$ converter output was proportional to the sum of the doppler frequencies of beams 1 and 3 and had a linear range of 1–850 ft/sec.

The RA sensor section of the SDC consisted of one frequency tracker and one frequency converter. The frequency tracker acquired and tracked the sum of the *doppler* and *range* frequency shifts from the altimeter

beam. The range frequency shift was proportional to the slant range of the spacecraft to the lunar surface. The altimeter converter used the vertical velocity component from the doppler velocity sensor to compensate for the doppler frequency shift in the altimeter radar beam return which provided true slant-range information to the flight control system. Linear range capability of the altimeter was 14–40,000 ft at a vertical velocity of 850 ft/sec.

The altimeter converter range signal also drove the range-mark programmer, which provided irreversible range mark signals at slant ranges of 1000 and 14 ft. At 1000 ft, the programmer provided a deviation control signal to the KPSM and altimeter converter, which increased the range scale factor from 1 to 20 mV/ft. The altimeter klystron deviation was increased from 4 to 40 MHz. To accommodate the change in altimeter tracker input signal frequency, the voltage-controlled oscillator of the altimeter tracker was stepped approximately 14.4 kHz by the deviation control to prevent loss of lock during the deviation change. A blanking signal from the KPSM was applied to the altimeter tracker IF amplifier, which blanked the altimeter beam-return flyback signal during the 500 $\mu$sec flyback period of the altimeter klystron. A portion of the signal present on all the IF amplifier AGC lines was filtered, and made available for telemetry as the reflectivity signal. Signals from these circuits were proportional to the RF power being received at the antenna feedhorn.

Because of antenna beam orientation, it was possible for the sidelobe of one beam to lie along the axis of another beam and be of sufficient amplitude to cause the tracker associated with that other beam to lock. This coupling placed serious threats on mission success. To correct for possible malfunction, circuitry was incorporated in the SDC to reject the cross-coupled sidelobe logic (CCSL), if it was essentially the same frequency (within 1.2 kHz) as a signal on a different beam and was simultaneously 25 db lower in amplitude than the other beam. Initially,

**Table XIX-5. Klystron input power data**

| Voltage[a] | Velocity klystron | Altimeter klystron |
|---|---|---|
| High voltage | −2150 ±75 V | −800 ±20 V |
| Regulation | ±0.25% | ±0.25% |
| Current | 40–55 mA | 0.5 mA (max) |
| Collector voltage | −500 ±10 V | −500 ±10 V |
| Regulation | ±1.0% | ±1.0% |
| Current | 10 $\mu$A (max) | 45–65 mA |
| Filament voltage | 7.2 ±0.3 V | +6.3 ±0.3 V |
| Regulation | ±0.15 V | ±0.15 V |
| Current | 0.8–1.1 A | 0.9–1.3 A |

[a]Typical ripple values over the frequency range of 0–10 kHz was 0.5 mV at discrete frequencies over most of the range.

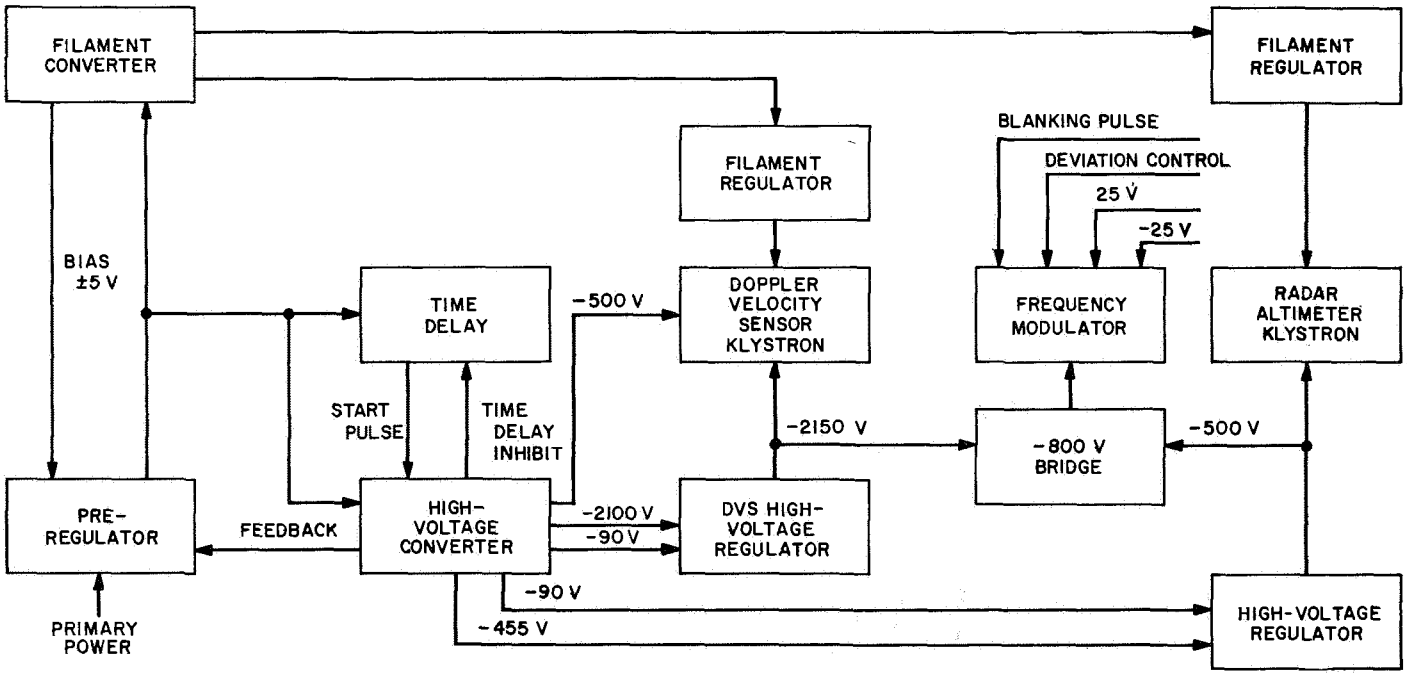



**Fig. XIX-7. Klystron power supply and modulator block diagram**

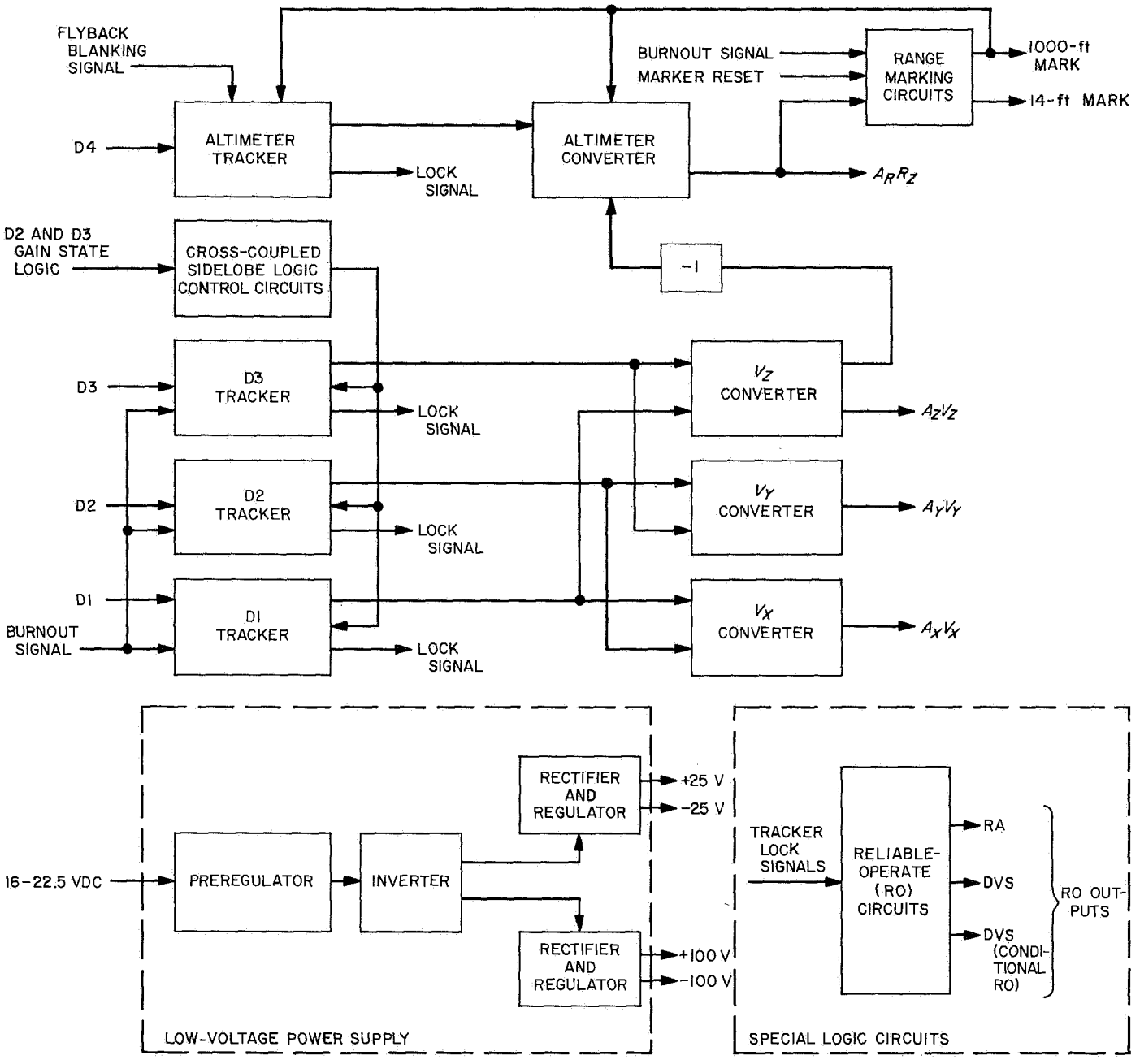



**Fig. XIX-8. Signal data converter, block diagram**

this logic circuitry was confined to beams 2 and 3; after *Surveyor III* it was added to include beam 1. This was not necessary on beam 4 because of the frequency difference. The burnout signal received by the SDC from the spacecraft was used to change the tracking bandwidth of the doppler velocity sensor trackers and to provide a timing delay function in the conditional reliable-operate mode. (Additional information about the CCSL can be found in Ref. XIX-4.)

The reliable-operate logic received a tracker lock signal from each tracker 0.1 sec after the tracker acquired a signal. The spacecraft then received a doppler velocity sensor reliable-operate signal when DVS trackers D1, D2, and D3 had acquired signals. This reliable-operate signal permitted attitude control of the spacecraft by the pitch and yaw flight control channel. Another reliable-operate signal was issued when DVS trackers D1 and D3 and RA tracker D4 acquired a signal. This concept permitted

control of altitude and rate of descent. When RADVS primary power was applied, a 1.0-sec time delay was provided to the signal-generation AND gates to prevent generation of false reliable-operate signals due to spurious tracker lock signals at turnon.

As a result of retrorocket burnout, the altitude of the spacecraft could possibly allow one or two of the velocity sensor beams to be at too low a frequency or signal-to-noise ratio for signal acquisition. If the *conditionally reliable* mode existed, velocity information would still be obtained from one or two velocity beams. To insure altitude recovery, the special logic circuitry provided the converters with a properly polarized signal to zero velocity along the beam for the tracker or trackers that had not acquired. These substitute signals would correct the altitude of the spacecraft and thereby orient the velocity sensor beams so that all three velocity trackers would acquire properly. Activation of the conditional reliable-operate (CRO) mode was delayed for 3.7 sec after receipt of the retro burnout signal to allow the tracker to search sweeps should the altitude of the spacecraft be such to allow normal DVS reliable-operate. If, after 3.7 sec, all velocity-sensor trackers had not acquired, a signal was sent to the CRO-enable AND gate, and an inhibit signal was applied to the DVS AND gate, thus providing any locked tracker signals to the spacecraft. The DVS reliable-operate signal was also present by virtue of the DVS reliable-operate OR gate. The CRO mode remained in operation until all three DVS trackers had been operating simultaneously for a period of 1 sec. For *Surveyor III* the CRO mode was automatically inhibited 1 sec after initiation, if spacecraft attitude initiated it. The CRO logic was modified after *Surveyor III* to increase CRO capability to the occurrence of the 1000-ft mark, where it was then inhibited. If a DVS beam broke lock, this increased CRO capability would allow spacecraft steering into the unlocked beam.

The special logic circuits shown in the block diagram (Fig. XIX-8) only involved the three DVS trackers. Their function was to select which of two tracker signals was to be supplied to the velocity converters, according to the *search* or *track* status of each tracker. When a DVS tracker was in the *track* mode, as evidenced by its tracker lock signal, the voltage-controlled oscillator (VCO) quadrature-generator frequency was supplied to the converters as a frequency associated with the signal being tracked.

When a DVS tracker lock signal was off, the special logic supplied instead the tracker single-sideband 800-kHz reference frequency to the converters. This action prevented the sweep voltage pattern of a DVS tracker (VCO) in the search mode from appearing in the converter analog output. This was unnecessary if the spacecraft used RADVS velocity information only when all three DVS beams were locked. This was not the case in the CRO mode, and application of the DVS tracker sweep voltages to flight control would cause erratic spacecraft steering.

The low-voltage power supply (LVPS) within the SDC supplied the unit with regulated outputs of $\pm 100$ V and $\pm 25$ V. The SDC LVPS was similar to the KPSM high voltage supply in that it was a DC converter. The LVPS primary was set up to drive a transformer load. The transformer outputs were fed through full-wave rectifiers, filters, feedback circuits, and regulators to supply the DC voltages. The 25-V output provided power to both antennas and the KPSM.

*d. Doppler velocity sensor antenna.* A portion of the block diagram in Fig. XIX-9 depicts the DVS antennas. Specifically, this antenna system radiated a carrier frequency of 13.3 GHz at an RF power of approximately 2.5 W per beam, transmitted in three narrow beams displaced 25 deg from the roll axis of the spacecraft and distributed at 90-deg intervals around the roll axis. Processing of the return RF energy began in the dual detectors. The dual microwave detector (Fig. XIX-9) heterodyned the return signal with a small portion of the transmitted carrier. The separation of three quarter-waves between channels was responsible for the zero-degree channel and the 90-deg channel. These quadrature channels were necessary to prevent trackers from locking on negative doppler returns (such as the negative return doppler signal at retrorocket ejection). For the positive doppler, the zero-degree channel led the 90-deg channel, and the trackers were able to lock to that signal. For the negative doppler, the 90-deg channel led the zero-degree channel signal (by 90 deg), and the trackers were unable to lock to a negative doppler signal.

Dual-channel amplifiers raised the level of the quadrature signals to values suitable for use as inputs to the DVS trackers. Low-frequency interference and high signal levels at low altitudes were attenuated by filter networks within the amplifiers. The preamplifier rolloff characteristics did present attenuation to low frequencies. The filter low-frequency rolloff began at a doppler frequency of approximately 20 kHz and was down 3 db at 3.2 kHz for the amplifier when return-signal power dictated operation in gain state 3. The approximate 3 db point for gain states 1 and 2 was at a frequency of approximately 2.7 kHz. The signal was reduced by 12 db/octave when the preamplifiers were in gain state 3, and 6 db/

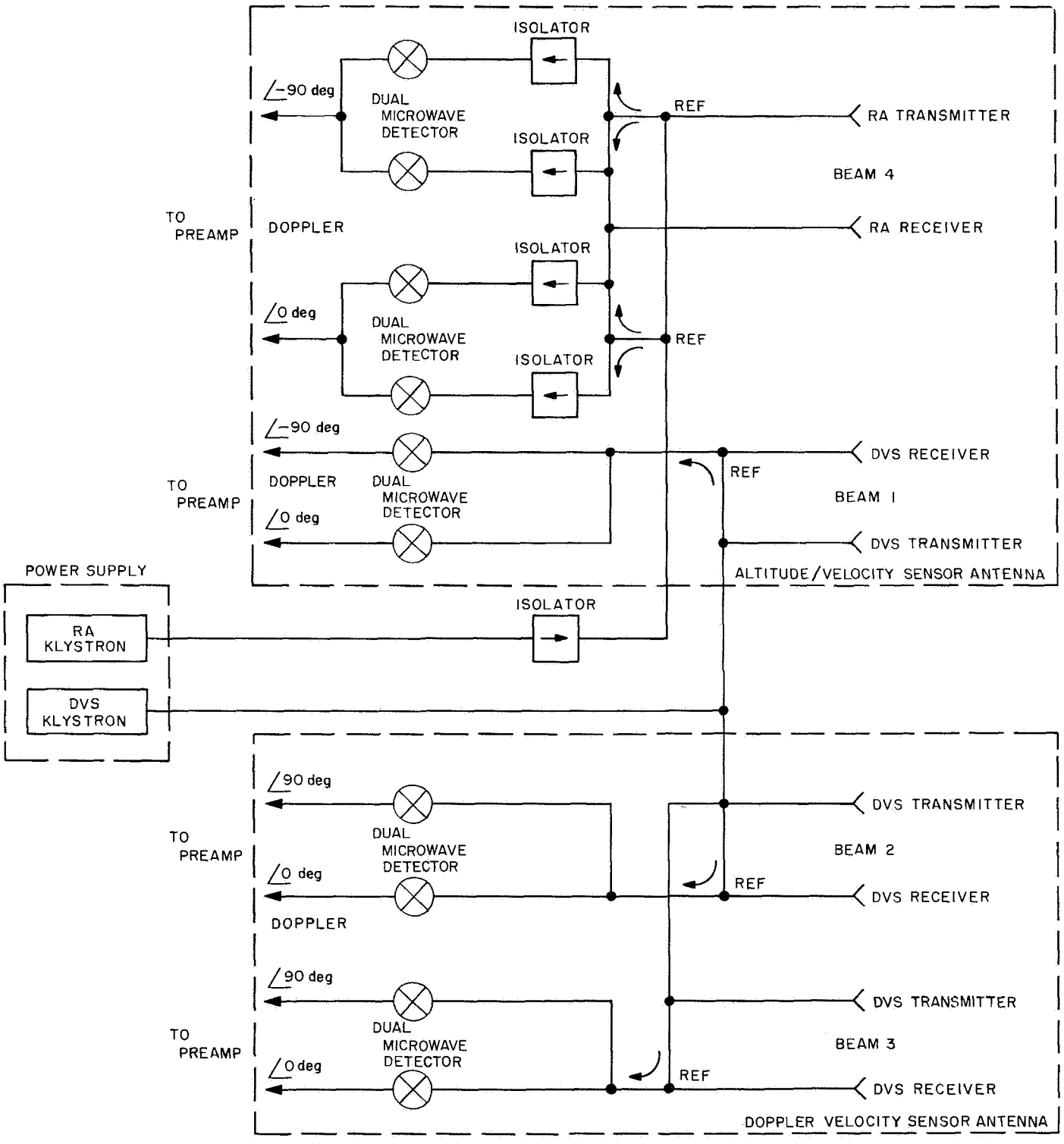



**Fig. XIX-9. Antenna layout and signal flow**

octave when in gain states 1 and 2. The corresponding gains of the zero- and 90-deg channel amplifiers were balanced to within 1 db, and the overall gain suitably held at 40, 65, or 90 db by a gate matrix working through two threshold detectors which kept the output signal levels of both channels within a range of 10–250 mV. Figure XIX-10 shows the block diagram of the preamplifiers.

*e. Altitude velocity sensor antenna.* Part of the block diagram in Fig. XIX-9 shows the AVS antenna. The signal from the altimeter beam was projected along the Z axis of the spacecraft; it operated at a carrier frequency of 12.9 kHz at a nominal CW output of 350 $\pm$100 mW. The transmitted output was frequency-modulated, with a linear ramp-voltage sweep of 5 msec duration; for altitudes above 1000 ft, it was swept through a 4-MHz range. For altitudes below 1000 ft, the radiated frequency was swept 40 MHz within the KPSM. The sweep voltage had a fixed repetition of 182 Hz at all altitudes and had a return sweep time of 500 $\mu$sec. To avoid false tracker locks during flyback, the tracker IF amplifier was blanked off during the flyback period. The altimeter signal reflected from the lunar surface provided slant-range information along the beam by a comparison of this signal frequency with that of the swept or reference frequency.

Microwave signal mixing took place in a pair of balanced mixers which produced two signal outputs to the two preamplifiers. The return signal to each balanced mixer was applied in phase quadrature with respect to the other signal so that the two beat-frequency signals to the preamplifiers were also in phase quadrature. The direction of rotation of the phase vector of these two quadrature signals determined the sign of the doppler signal as was done in the DVS portion. Any amplitude modulation of the transmitted beam accruing at the same time the signal was frequency-modulated was suppressed by use of balanced microwave mixers.

Beam 4 amplifiers had built-in filters. The 3-db point for all gain states was at approximately 30 kHz. The amplifiers did present a 6-db/octave attenuation to the mixer signal when the amplifiers were in gain state 1 or 2. The mixer signal was attenuated approximately 12 db/octave when the dual-channel amplifiers were in the high-gain (80 db) state.

As was the case of the DVS amplifiers, the gain of the dual-channel amplifier was balanced to within 1 db and the overall gain suitably held at 40, 60, or 80 db by a gate matrix, which worked through two threshold detectors to keep the output signal levels of both channels within a voltage range of 10–270 mV.

The discrete-step AGC system of all the receivers presented some difficulties with regard to transients earlier in the program, but sufficient smoothing was ultimately incorporated to negate the problem. The block diagram of the preamplifiers and gain switching matrix is shown in Fig. XIX-10.

*f. Waveguide.* The RADVS waveguide was used as a microwave transmission line for transferring the RF energy from the radar altimeter and velocity sensor klystrons in the KPSM to the subsystem antennas. As the velocity sensor used a single klystron for the three separate beams, it was necessary to use a power-dividing system to provide each radiating element with equal energy. The altimeter-beam waveguide was functionally entirely separate from the velocity half of the system. Load isolators were in series with antennas to provide attenuation to keep any reflected energy from reentering the transmitting system. Such reflections could affect the RF oscillator load impedance and cause energy from one beam to be retransmitted via another beam. Additional information on RADVS operation and maintenance will be found in Ref. XIX-5.

### 2. Design Development

The RADVS contract was awarded to the Ryan Aeronautical Corporation of San Diego by HAC in July of 1961. Breadboard operation of the radar was demonstrated in February 1962. From the outset, the RADVS was a difficult and complex system, both in test and operation. The necessity for the spacecraft flight control system to be provided continuous range–velocity measurements during terminal descent (due to the high approach velocity) dictated the choice of a CW doppler system.

Ryan Aeronautical Corporation was in a unique position for the *Surveyor* RADVS contract: As early as the late 1940s, Ryan had developed a frequency-modulated CW doppler radar for helicopter and aircraft use. These early doppler systems also found applications on the vertical takeoff and landing aircraft program of the 1950s as a supplement to pilot in-flight control of such aircraft. The spacecraft vertical approach was similar to a helicopter landing. It was decided that the low-altitude accuracy and RF power requirements at the time of the survey could be met by modifying the helicopter radar.

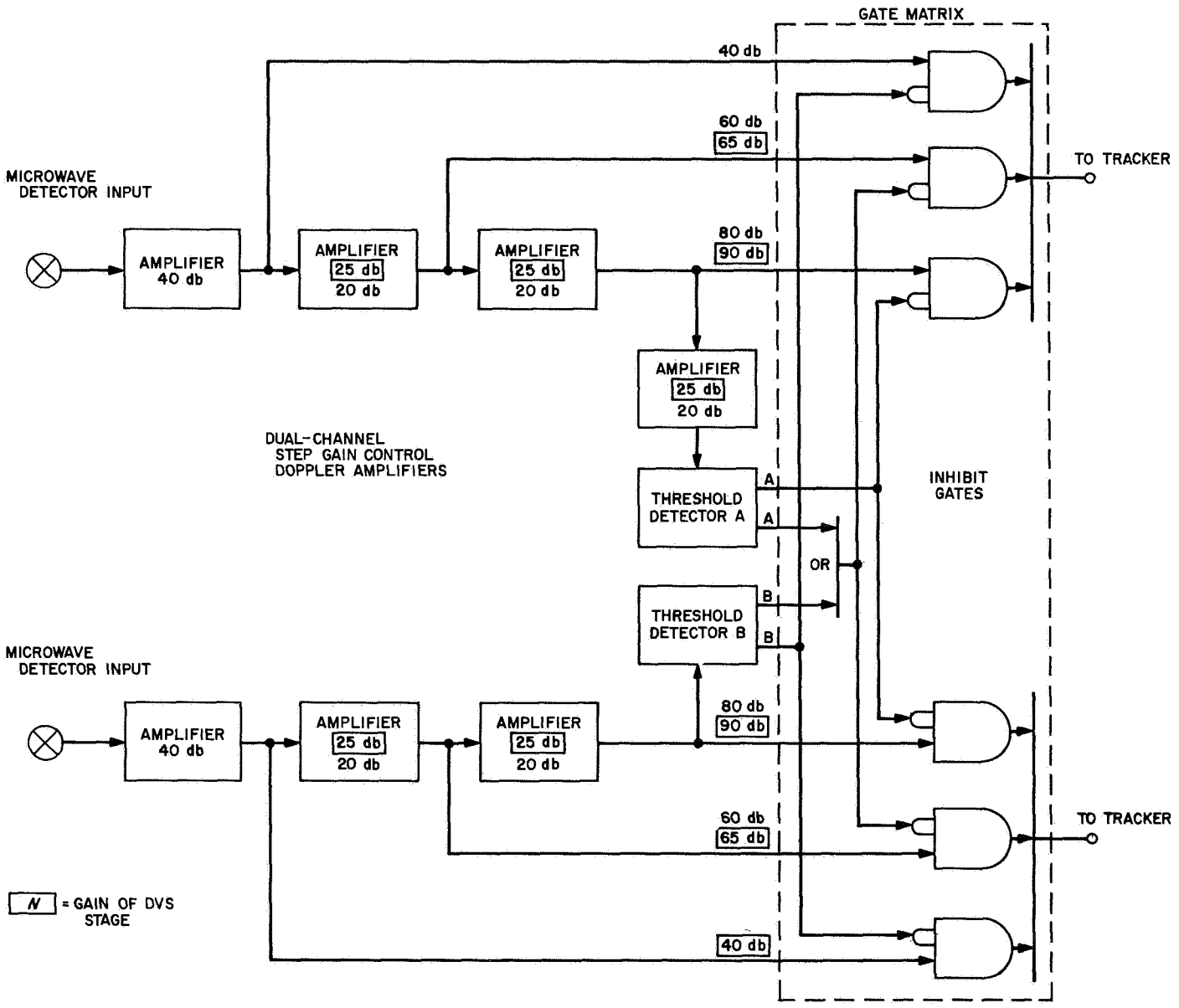



**Fig. XIX-10. Block diagram of preamplifiers**

The higher-altitude operation of *Surveyor* dictated greater RF power sources than previously used. This was directly related to the system receiver sensitivity because the return RF energy would be low at high altitudes (inversely proportional to the range squared). It was calculated that 2W of RF power per beam would be sufficient for the DVS beams. A lower value (250 mW) was established for the RA because its beam was aligned with the Z spacecraft axis.

The only RF source at the required frequency and power levels at this time were klystrons. The use of klystrons compounded design problems because of the necessity for development and modification of unconventional radar designs.

*a. Klystron power supply and modulator.* The use of klystron RF sources for both the DVS and RA required the generation of high repeller voltages, with concomitant insulation and arcing problems. Further, extremely well regulated supplies were required, for ripple on the klystron accelerating voltages would cause amplitude-modulated sideband frequencies with resultant false tracker locks. In addition, the klystron general structure

exhibited generic design difficulties with respect to klystron cavity resonance problems. When the RADVS subcontractor first solicited klystron procurement from Varian Associates, Palo Alto, California, the manufacturer took exception to most of the specifications contained within the procurement. At that time (September 1961), the specified klystron parameter tolerances (and the capability to measure them) were either at or beyond the state of the art. In addition, the manufacturer had never produced klystrons which were not externally cooled for the frequency and power required (8 W at 13.3 GHz). (The RADVS klystrons were to be heatsink-mounted and the heat was to be passively dissipated.) Varian agreed to design and produce the tubes based on an agreement that the requirements were to be design objectives rather than firm specifications.

Qualification testing for both klystrons was completed in September 1962. Klystron difficulties developed almost immediately after receipt of the Varian tubes. A high-frequency squeal problem persisted in the RF output of the velocity sensor klystrons and remained for several minutes after turnon. Varian attributed the problem to an ion cloud buildup in the electron-beam passageway (klystron drift channel) which was caused by the simultaneous application of filament and high voltages to the tube. It appeared that the ion cloud was caused by gas released from the heater as it changed from an inactive cold metal to an active hot one. A recommendation was made that klystron high voltage be applied 20 sec after the application of the filament potential. Additionally, Varian developed a depressed-collector ion pump that could be inserted into the tube to draw off the ions and prevent a cloud from forming. The new ion pump was incorporated into later tubes.

A severe resonance condition in the klystron grid circuit was next to appear. Manifestation was in the form of a 14-kHz signal in the output after about 2 min of klystron operation. It appeared that the grid structure was being mechanically excited by the high-voltage DC-converter transformer laminations and that the 14-kHz resonance was being driven by a harmonic of the converter input switching rate. The immediate Ryan solution, which was retained in the design, was to mechanically isolate the klystron corner section and mount the high-voltage DC converter transformer on silicone gaskets. Varian, however, came to the roots of the problem and succeeded in modifying the klystron grid structure so that self-resonance would occur at a higher frequency.

Other difficulties also appeared soon after the velocity sensor klystrons were put into service. Among them was a falling power output problem (caused by a displaced heater cup and focus ring), an RF wideband noise problem (caused by carbon monoxide molecules outgassing from the internal structure), and a mechanical resonance at 6.5 kHz. The first was solved by a change in the heater cup support structure to a material having higher thermal conductivity; the second by a special heat treatment of the nickel surfaces internal to the tube; and the third by a tightening of the klystron vibration specification.

The altimeter klystron faced different development problems due to the generic differences between the two tubes. The altimeter, being a wideband frequency-modulated CW device, was required to have a klystron having a wideband characteristic, good modulation linearity, and very little change in average modulation sensitivity across the required bandwidth range. These requirements were not easy to satisfy. Klystron spectrum difficulties caused by the nonlinear response of the tube to the modulator-forcing function were the basis for the bandwidth problem, and throughout the program it represented the most formidable problem inherent in the altimeter portion of the radar. Varian determined that the best way to approach the bandwidth problem was to add a double cavity with controllable coupling to the output of a reflex klystron. Other problems specifically dealing with modulation linearity were solved by employing tungsten for the klystron grids, and by an experimental selection of material for the double-cavity tuning screws. General klystron difficulties dealing with resonance excitation, vibration problems, power dropoff, wideband noise, and spurious signals were solved. However, an altimeter klystron difficulty dealing with wideband linearity persisted to the last, and only by individual attention to klystron tuning, modulator waveshaping and modulator–klystron matching was it brought within acceptable limits.

In addition to klystron difficulties, KPSM development was plagued with other problems—particularly those associated with preregulation noise immunity, DC converter switching, high-voltage stresses, temperature compensation, and modulator drive requirements.

The original power supply contained within the KPSM consisted of a DC converter utilizing the variable-pulsewidth-modulation principle to effect maximum efficiency and good regulation. The original specification anticipated an input primary voltage variation of up to 10 V, and the pulsewidth-modulated regulation principle was primarily necessary because of this constraint. The design, however, was found to suffer from a strong susceptibility to injected noise at the converter switching

frequency of 3 kHz. Additionally, the variable load impedance the klystrons would present to the high-voltage circuitry was not anticipated in the original design. As a result, very high potentials existed prior to tube cathode emission. Consequently, high-voltage arcing ensued upon turnon. The need for delayed high-voltage application was obvious, both because of the high-voltage constraint and the ion cloud problem.

Other problems with the KPSM DC converter did have considerable weight, due mainly to the iron-core switching transformer utilized. The open-frame, iron-core construction also presented some difficulty with regard to the elimination of eddy currents and high magnetic circulating currents.

Because of the difficulties with the KPSM design, a design team was established to look specifically at the problems of high-voltage breakdown, delayed klystron turnon, preregulator noise problems, ripple below the inverter switching frequency, and packaging. Concurrent with the above studies, HAC, as *Surveyor* prime contractor, submitted a schematic of a proposed new power supply design for the KPSM. Although slightly heavier in weight, the Hughes design was virtually immune to injected noise at the converter switching rate; utilization was made of squarewave oscillator circuitry (rather than the quasi squarewave Ryan design), resulting in lower peak voltages; the circuitry did not require any modulator decoupling from the 25 VDC line. The HAC design did, however, possess the same temperature-compensation problems as did the Ryan circuit. The basis for the design was the use of a shunt preregulator, rather than the variable-pulsewidth approach. Effort was immediately started on completing the electrical development and product design for a power supply which embodied the HAC preregulator concept, as the KPSM had become the limiting item for the RADVS development, and the shunt-regulation technique was obviously the superior approach.

The design and development program began with the construction of breadboard units for the preregulator, the high-voltage and filament converters, postregulators, and the altimeter modulator. Of prime concern was the thermal constraint, which necessitated a starting temperature of $-20 \pm 10°C$. In line with this, difficulty was encountered in getting both the preregulator and inverters to start at the lower temperature extreme ($-30°C$). The preregulator difficulty was solved by isolation of the input voltage from the regulator input line. Impedance changes with application of high-voltage load were deemed the cause of the starting problem, and isolation effectively removed changes with variable load currents. The filament inverter starting problem was solved by a stiffening of the inverter transistor specification to a lower beta under low temperatures.

Thermal problems in the high-voltage postregulators were resolved by temperature compensation of the postregulator feedback voltage and by stiff regulation of the regulator amplifier supply voltage.

As mentioned previously, ripple on the klystron accelerating voltages can produce amplitude modulation of the output, resulting in acquisition of spurious signals. It has been calculated that 10 mV of ripple on the klystron anode would keep the upper beam of a spacecraft (at 25 deg attitude) locked over slant ranges of 50,000–10,000 ft. Obviously, this cannot be tolerated, as it would be disastrous to mission success. Low ripple level on the high voltage output was attained primarily by good postregulation, very careful placement of power supply switching leads, magnetic shielding, and careful routing of interconnect wiring. Judicious attention was given to correct torquing of chassis screws to keep high magnetic circulating and eddy currents down to low levels. Careful consideration of these problems has alleviated the need for additional anode regulation, although the goals were extremely difficult to attain.

***b. Signal data converter.*** Design constraints and difficulties of this unit revolved around the thermal constraint of operation from $+5$ to $+25°C$, the packaging and interconnect problem, noise difficulties in the analog converter section, altimeter quantizing, and general output smoothing for spacecraft use. Basic design changes adopted during unit level manufacture are described below.

The SDC low-voltage power supply originally used the variable-pulsewidth modulation principle which was also utilized during initial design of the KPSM. It, too, was plagued by noise and whine at the prime converter switching rate, and was replaced by a design embodying the shunt-regulator technique with its associated noise immunity.

Temperature compensation of the constant pulse generators within the frequency-to-voltage converters was improved to effect a greater analog output accuracy. Additionally, DC amplifier drift within the converters was minimized by potting the amplifier and thereby improving its thermal environment. Analog output accuracy was

improved at the flight temperature extremes. An analog noise problem which caused the average analog noise level to be out of tolerance was found to be due to a poor discriminator (of the switching type) which was changed to a linear device, correcting the situation.

A spacecraft roll angle maximum contained within the procurement specification, coupled with an extreme attitude angle of the spacecraft as a result of retrorocket burnout, could have produced a difficult tracker acquisition problem. To insure the acquisition of velocity sensor beams which were low in frequency or power, an SDC special logic design was incorporated. Known as the conditional reliable-operate DVS mode, it provided a signal to the frequency-to-voltage converters when this extreme condition occurred, and in turn, provided the spacecraft flight control system with signals to enable attitude correction to bring the horizon-oriented radar beams within lunar view; that is, the spacecraft was tilted to enable all velocity sensor beams to be tracked during the terminal maneuver.

An altimeter quantizing or "bunching" effect was noted at low altitudes when testing with early RADVS experimental models. The effect was of such a magnitude to reduce the range output accuracy at low altitudes. A smoothing effect was provided through the use of a dither oscillator which provided a varying input to the integrator in the range tracker. This overcame the quantizing and produced a smooth, integrated tracker output with ample accuracy.

Early SDC units had transients on the tracker lock and retrorocket burnout signals. These would occasionally cause early triggering of the range-mark signals. A time-delay circuit was installed which inhibited range-mark triggering until the reliable-operate DVS signal was attained (indicating all velocity sensor beams had locked). This could only occur four seconds after the receipt of a retrorocket burnout signal, and served to prohibit false range-mark triggering. Because of antenna configuration and dish goemetry, it was possible for the radar to lock to and track a cross-coupled sidelobe from a beam other than the reflected main beam. This could have resulted in erroneous velocity and range information being fed to the flight control system, which would, in turn, result in faulty steering and thrust-control commands. An unstable condition and failure to soft-land would have been a probable consequence. For this reason, the radar was provided with a logic system between the six DVS beam combinations, which enabled it to reject a cross-coupled sidelobe, reset the tracker in question to the search (sweep) mode, and reacquire the main beam.

The SDC frequency trackers were originally designed for tracker acquisition with a 3-db signal-to-noise ratio. Because of experiences with the S-8 test program, frame transmittance difficulties, and spacecraft vibration problems, it was deemed advisable to change the velocity tracker sensitivity to the more realistic 9-db signal-to-noise ratio. This provided a 6-db margin to acquisition of false signals due to vibration-induced ripple components, and has been in effect on every flight spacecraft since.

During later unit-level testing and RADVS system tests on a production radar, it was discovered that a temperature gradient existed between the marker gate and the trigger submodules of the altimeter converter. This thermal differential created an inconsistency in the range-mark firing circuitry when flight covers (versus blower covers) were installed. (Blower covers are used whenever long operation of the radar is contemplated during test operations.) To provide for consistency of the range-mark firing point under all conditions, thermal shields were installed over the affected modules.

Initial SDC unit tests revealed a crosstalk problem between the signal trackers. This resulted in a higher noise level on the analog output signals and false locks of the trackers in question. Caused by signal coupling of the frequency of one tracker into an adjacent tracker, the problem was solved by placing shields on the tracker motherboards between the affected modules. Shielding also had to be added to several modules within the $V_z$ converter to cure a similar problem.

A change proposal was submitted by Ryan on November 30, 1965 to provide for the redesign of the SDC trackers to reject signals appearing within the tracker bandwidth that were double sideband in nature. This was primarily designed to discriminate against vibration- and ripple-induced signals, which manifest themselves as sideband signals because of their AM nature. The proposal was known as ECP-10. Although ECP-10 was never incorporated in a flight SDC, a breadboard model of the double sideband tracking system was demonstrated and all schematics and designs were completed.

Several mechanical changes were incorporated within the SDC during the initial stages of product development. These had no direct effect on electrical performance, but were deemed necessary for test access, operational adjustment during final system testing, and handling ease.

The SDC-module-to-motherboard interface was changed from a soldered-in configuration to a plug-in

connector configuration. This greatly eased the rework and servicing problem.

An outer-finish difficulty developed with handling. The finish was changed from vacuum-deposited aluminum to a polished surface. This was easily reworked and provided adequate thermal control. It was found that the SSB modulators on the tracker motherboard required readjustment after unit assembly. A convenient provision for adjusting the modulators when in the flight condition was made by locating holes in the motherboard to permit the installation of fine-adjust potentiometers without removing the submodule.

*c. Antennas.* The original antenna adapted for use in the *Surveyor* radar system was based upon a Ryan design already in existence. This antenna was circular in one plane while parabolic in another, and employed a side-looking feed system with a septum dividing both sides of the reflector (to accommodate two beams). Prototype antenna measurements revealed a serious sidelobe problem with the existing structure. Partial shrouds around the outer dish perimeter eliminated much of the difficulty, but there still existed sidelobes at an angle of 60–70 deg removed from the main beam. These were substantially reduced by the addition of a thin microwave-absorbing material over a small area of the inside of the shroud, but the relocation of a flight control compartment necessitated the use of a full shroud to prevent radar reflections from the box. Still the sidelobe problem persisted. Finally, to prevent lock to a cross-coupled sidelobe at high altitudes, it was deemed necessary to go to an electrical logic design in order that a cross-coupled sidelobe be rejected and the main beam acquired.

*d. Receiver/transmitter.* During and after radar design, it was found difficult to achieve acceptably low receiver noise figures with the mixer diodes then in use. At very low conversion frequencies, (typically to 80 kHz in RADVS) low-frequency diode noise presented a serious difficulty. Because of this, a large low-frequency rolloff characteristic was designed into both the velocity sensor and altimeter preamplifiers to limit the amount of mixer noise passing through the preamplifiers. Typical mixer noise figures range from a high of 24 db at 800 Hz to a low of 12 db at 80 kHz, the low-frequency characteristic being the predominant limiting factor.

Diode matching, balancing, and selection had proved to be a tedious process, with very low yields being the rule rather than the exception (typical yield is less than 2%). The RADVS microwave mixers were Type HDM-IE, manufactured by Hughes Semiconductor Division, Newport Beach, Calif. Diode manufacture technique improved with time, and acceptable diodes were found with careful selection procedures. The negative doppler rejection capability of the system added to the complexity of the situation, for it doubled the number of mixers in each beam (because of the necessity of a quadrature channel), and thus made the balancing and matching procedure more difficult, particularly with regard to AM rejection.

Along with the noise figure problem, there also existed a diode vibrational problem. Vibrational requirements were changed in a direction so as to increase the vibration level. It was found that the existing radar diode holder (of the friction-fit type) required a change to a more secure locking device which would lock both ends of the oscillator crystal. This was incorported with a set-screw type holder, but it necessitated more stringent requirements on the diode case mechanical characteristics due to increased stresses on the diode. Along with redesign of the diode holder, a variable shorted-stub device was added to further reduce the VSWR of the diode in the holder, thus reducing FM detection within the holder.

Two additional problems which were overcome by conventional corrective techniques were:

(1) The preamplifier AGC system acted as a *peak* rather than an *average* level detector.

(2) Ripple difficulty on the preamplifier input lines required increased filtering on these lines.

*e. Waveguide and isolator.* The waveguide system which interconnected both antennas and the KPSM exhibited some minor difficulties during initial design. A weight constraint at first dictated the use of cutaway waveguide flanges. These were later found to be impractical due to microwave leaks around the joints; they were then replaced with full flanges. Waveguide dampers were designed to secure the guide to the spaceframe and prevent lateral movement (lateral movement modulates the contained RF, producing a false return signal). It was also found necessary to *dent-tune* the guide to maintain as low a VSWR as possible.

Waveguide load isolators developed a loose magnet structure which required increased bonding material to be placed around the magnet. This was to prevent the isolator magnets from vibrating loose during the boost and vernier engine firing. Other waveguide difficulties were relatively minor in nature, having been confined mainly to areas involving the structural integrity of the

guide and power splitters. A minor power-splitter modification was made when it was decided to go to a one-piece casting rather than a separately welded construction technique. Crystal growth within the guide was a problem which occurred at the Air Force Eastern Test Range (AFETR), Kennedy Space Center, Fla. Because of high ambient-air moisture content, the interior of the waveguide was conducive to crystal growth. A specially prepared and etched waveguide alleviated the problem, although it was found that the particles were transparent to microwave energy and produced no detectable radar response.

### 3. Construction and Manufacturing

All elements of the RADVS system except the waveguide are illustrated in Fig. XIX-11.

*a. Klystron power supply and modulator.* The conventional electronic packaging design of the KPSM allowed normal electronic assembly techniques to be used in the fabrication and assembly of the various subchassis and printed circuit boards. The difficult part of the manufacturing cycle involved the adjustment of the various circuits by selection of components which would be compatible with the klystron characteristics over the intended range of performance. While the replacement components were available and easily installed, the circuit interaction severely complicated the KPSM rework process.

The dense packaging of the high-voltage power supply components and high thermal dissipation require care in spacing of leads and heatsinking of components. The relatively light sheetmetal structure of the unit did not aid in the precise location of components necessary; thus, extra care was required in assembly to assure adequate component spacing. Conformal coating was also used on all components and terminals for protection as well as to improve heat transfer under vacuum.

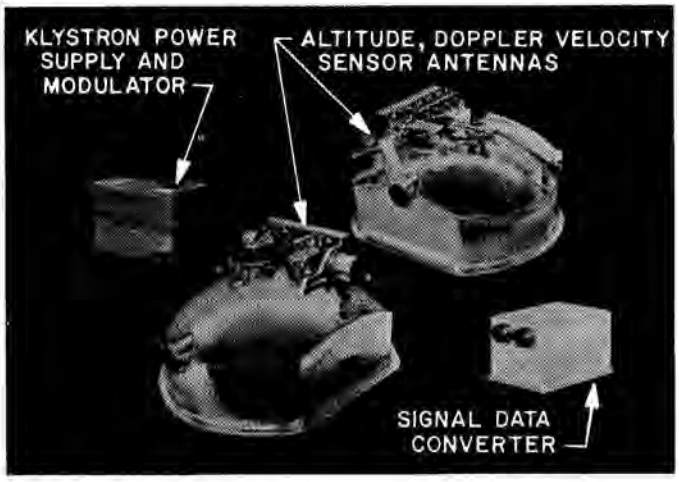



**Fig. XIX-11. Photo showing telemetry elements (less waveguide)**

*b. Signal data converter.* The SDC was housed in a polished aluminum structure measuring approximately $5.6 \times 6 \times 12.5$ in. and weighed 10.3 lb. The completed assembly was of cordwood construction; this, in turn, provided a major assembly, or motherboard, for each separate major function of the signal data converter. A multipin electrical connector was attached to the lower edge of each motherboard; this made the necessary mechanical assembly and electrical connection to the SDC interconnect board which was oriented parallel to the unit's bottom surface and extended the entire length of the SDC. The overall integrity of the SDC structure was further enhanced by a close-fitting sheetmetal cover secured not only to the assembly end plates but to each motherboard on all three upper surfaces. The unit assembly was held firmly on the longitudinal axis by five titanium skewer bolts—four that traversed the edge of every motherboard on the upper surface, and a fifth bolt that passed through the center of the assembly. Each motherboard had a series of submodules that were separately assembled and tested, thereby accelerating the process of product manufacture and simplifying the task of rework in the event of component failure during test.

*c. Antennas.* To meet the RADVS subsystem weight requirements, the receiver/transmitter antenna assembly was fabricated with a core made from aluminum alloy honeycomb, surfaced with fiber glass, all overlayed with vacuum-deposited aluminum. This surface deposition provided the necessary electrical conductivity for the radiation and receiving parabolas and also acted as a thermal finish.

Each half of the receiver/transmitter unit was fabricated separately of form-controlled fiber glass that extended from the inner surface of the central septum, across the parabolic surface, and down to the extreme outer edge of the antenna shrouds. After trim and finish, the two halves were assembled with the two separate inner walls of the septum, and were installed inside a separate pressure-formed aluminum honeycomb antenna shell. The peripheral stiffening ring around the shroud was added and all elements were structurally bonded.

After this assembly and bonding process, the inner surfaces of the composite antenna parabolas, shroud walls, and septum surfaces were given a coating of vacuum-deposited aluminum to provide the necessary conducting and reflective surfaces for beam-forming to support the boresight and preliminary installation of the septum and RF feed system. When measurements relating the boresight reference points to the space-radiated RF energy patterns were completed, each antenna feed assembly was bonded permanently to its structural assembly within the septum wall.

A new stiffening ring (attached to the leading edge of the antenna shroud) was designed after vibration tests verified that the first shroud caused sufficient modulation to the RF energy to effect tracker lockup. The ring material structure was similar in nature to that of the antenna (aluminum honeycomb and fiber-glass overlay); it was bonded into position with epoxy.

Upon completion, the entire assembly was again coated with the vacuum-deposited aluminum. The unit was then heat-cured at 275°F, and subsequently submitted for flight-acceptance (FA) testing.

*d. Waveguide.* The waveguide was fabricated from regular rectangular aluminum stock, and terminated appropriately at either end of each section with a carefully formed flange or RF choke joint. The system voltage standing-wave ratio was maintained within design tolerance by dent-tuning of both the waveguide and the power splitters.

*e. System rework cycle.* Virtually no radar flight system went through spacecraft system testing without additional rework and testing. The rework cycles were necessary to cover major or minor radar problems discovered in spacecraft testing and handling. A typical flow diagram showing the rework cycles for the SC-4 flight system is shown in Fig. XIX-12.

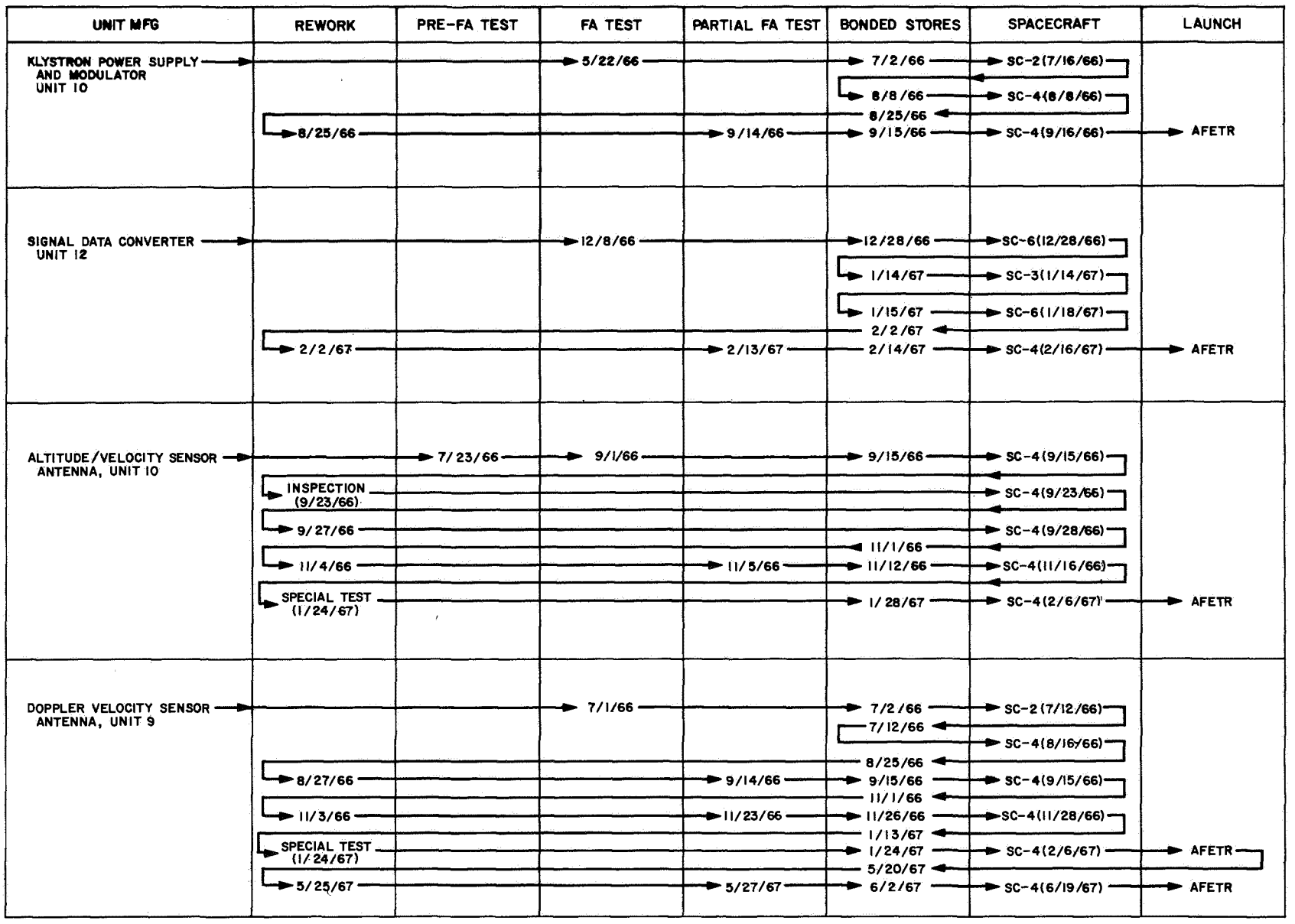
#### 4. Test Program

*a. Introduction.* The *Surveyor* RADVS test program was composed of three main facets: development tests such as the S-8 and T-2N programs, TA tests, and FA tests. The first two types of tests differed from the latter in that they did not generally involve flight hardware. Unit and subsystem development tests were necessary early in the program to prove that the modified radar design met its *Surveyor* design requirements. The validity of the TA tests as proof of radar design procedure was necessary to demonstrate that the radar did indeed meet its design goals. The results of the initial RADVS TA and associated tests and studies indicated that the existing design would not meet the mission requirements (refer to Subsection B-2).

Flight-acceptance tests were done to determine flight readiness of the systems which actually performed the flight missions. FA testing was performed at Ryan on the first flight system in 1965. This flight system was then delivered for further system testing.

All of the formal TA and FA testing was performed with the use of system test equipment assemblies (STEAs). The STEA consisted of three standard 8-ft racks containing assorted test equipment and simulation apparatus. Essentially, the STEA contained equipment to act on or modulate the radar system output to produce a single-sideband signal similar to that caused by a lunar return. This modulated signal was then fed back to the radar to be acted upon by it. The signals normally applied to the radar were generated from crystal-controlled oscillators whose outputs were mixed to produce a signal in the audio frequency range (corresponding to doppler information). The derived audio signal was then used to drive a set of single-sideband modulators (one for each beam) of the phasing type. These units modulated the incoming radar transmitter frequencies, suppressing the carrier and one sideband, and returned the single-sideband signal (equal to the carrier frequency plus doppler) to the radar receivers.

During testing it was found difficult to hold tolerances within the single-sideband modulators (contained in the STEA) with respect to sideband and RADVS carrier-frequency rejection. A large warmup period was necessary for all test equipment, because audio phase shift and single-sideband modulator imbalance was of constant concern. The only accurate generator with respect to amplitude and phase coherence was the RADVS itself, thereby necessitating continuous use of the radar with blower covers to remove the thermal constraint of 5 min. It was also difficult to test in the solar-thermal-vacuum test phase, because this was an actual test with flight covers (no thermal protection). This necessitated relatively short operation times with large cooldown periods —a time-consuming process and one of testing uncertainty. This was the case because of the difficulty in accurately simulating a spread single-sideband spectrum, rather than the line spectrum (sinewave) which normally comes from the STEA. With proper STEA single-sideband modulator tuning, various doppler frequencies could be




ALL DATES ARE DATES ACTION WAS COMPLETED
ALL WORK CYCLES AT RYAN WITH EXCEPTIONS NOTED

**Fig. XIX-12. Manufacture and test history of typical system**

selected for different desired standard test conditions. There were in fact some ten selectable test conditions which were employed. The simulated ranges and velocities for each of these test conditions will be found in Table XIX-6.

The STEA was also capable of simulating spacecraft dynamics in closed-loop control tests. The simulated signal received by the radar in these tests was essentially the same as that described earlier, except that the input audio frequencies (used to drive the sideband modulators) were determined by voltage-controlled oscillators (VCOs) instead of the crystal-controlled sources. The VCOs, in turn, were driven by signals which were derived from computed spacecraft motion. The radar then responded in a dynamic sense to continuously varying (rather than fixed) frequencies. A block diagram of the RADVS signal-simulation portion of the STEA is presented in Fig. XIX-13. (Additional information on operation and maintenance of the STEA will be found in Ref. XIX-6.)

***b. Unit level tests.*** Type-approval tests at the unit level were essentially completed in late 1964, and the unit tested was the first regular model radar produced, serial number 1. The first TA test covered application of the following environmental conditions (separately): vibration, constant acceleration, shock, thermal vacuum, low-temperature storage, and electromagnetic interference (EMI). The TA test revealed several equipment deficiencies (with particular respect to vibration) necessitating some equipment redesign. The following are the more significant results of the test:

(1) Structural resonances of the units were noted in the range of 100 to about 600 Hz.

(2) Preamplifier output noise rose to 40 mV in the 70-Hz range and to 70 mV at about 1.1 kHz during sinusoidal sweep on the vertical axis.

(3) Mechanical resonances appeared at 350 Hz, 1.2 kHz, and 1.6–2.0 kHz; preamplifier outputs did not exceed 6 mV.

(4) Arcing occurred in the altimeter klystron. The tube was redesigned and the KPSM was tested at a later date.

**Table XIX-6. Standard test conditions for vendor tests**

| Standard test condition | Altimeter sensor range $R_Z$, ft | Velocity $V_X$, ft/sec | Velocity $V_Y$, ft/sec | Velocity $V_Z$, ft/sec | Doppler shift $D_1$ Beam 1, kHz | Doppler shift $D_2$ Beam 2, kHz | Doppler shift $D_3$ Beam 3, kHz | Receiver frequency $f_r$ Beam 4, kHz | Velocity sensor signal power $P_{VS}$, dbmW | Altimeter sensor signal power $P_{RA}$, dbmW | Velocity sensor range $R_{VS}$, ft | Total velocity $V_T$, ft/sec |
|---|---|---|---|---|---|---|---|---|---|---|---|---|
| 1 | NR | 0 | 0 | 3310 | 81.13 | 81.13 | 81.13 | NR | −106 | | 50,000 | 3310 |
| 2 | 40,000 | −300 | −300 | 740 | 13.31 | 18.15 | 22.99 | 84.45 | −104 | −104 | 40,000 | 835 |
| 3 | search | 0 | 0 | 0 | −1.60 | −1.60 | −1.60 | −3.5 | −50 | −113 | | −65 |
| 4 | 36,530 | 300 | 300 | 325 | 12.80 | 7.97 | 3.10 | 67.925 | −100 | −104 | 36,530 | 530 |
| 5 | 14,000 | 0 | 0 | 850 | 20.83 | 20.83 | 20.83 | 45.06 | −95 | −93 | 14,000 | 850 |
| 6 | 2,000 | 0 | 0 | 67 | 1.64 | 1.64 | 1.64 | 4.995 | −106 | −77.4 | 50,000 | 67 |
| 7 | var 1,500–mark | −50 | 50 | 100 | 2.45 | 3.26 | 2.45 | var 5.06–17.26 | −74 | −74 | 6,800 | 122.5 |
| 8 | 300 | 0 | 0 | 38 | 0.93 | 0.93 | 0.93 | 5.88 | −104 −52 | −59 | 40,000 | 38 |
| 9 | 240 | −50 | −50 | 54.5 | 1.33 | 0.53 | 1.33 | 5.33 | −50 | −57 | 240 | 89.3 |
| 10 | Var 130–50 –mark | 0 0 | 0 0 | 5 10 | 0.123 0.245 | 0.123 0.245 | 0.123 0.245 | 2.24–1.075–mark | −42 | −47 | 100 | 5 |
| 11 | 29,757 | var | var | 67 | 1.64 | 0.100–1.64 var | 1.64 | 67.925 | −102 | −104 | 36,530 | var 60–120 |

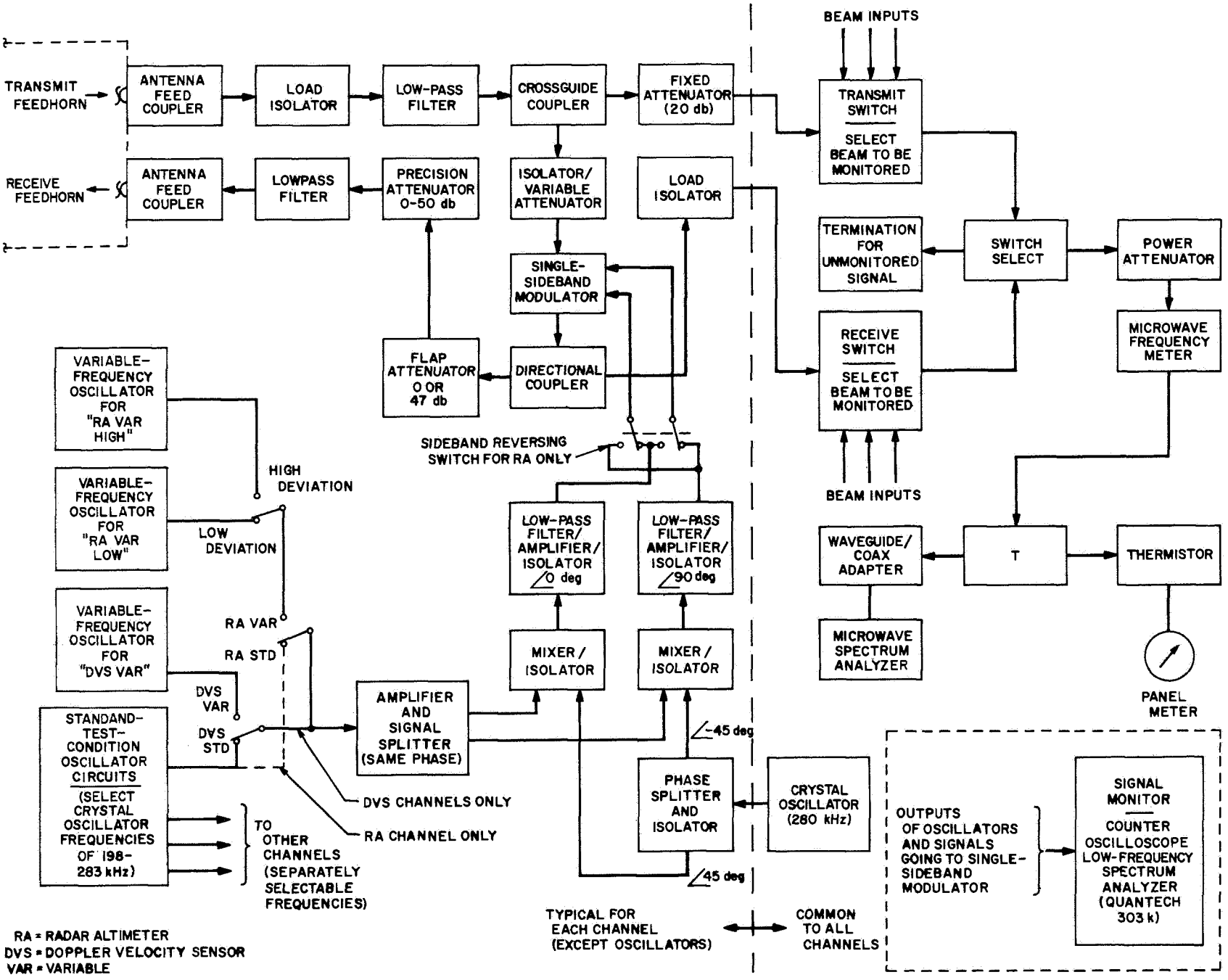



Fig. XIX-13. Diagram of signal simulation subsystem

(5) A bad diode was found in KPSM filament converter.

(6) A bad solder joint was found in the tracker low-pass filter during postreference run.

The solutions to these problems are described in Subsection B-2.

As part of construction verification of each of the RADVS flight units, the subassemblies were given a series of unit verification tests. In addition, the vendor (Ryan) performed a set of operational checks during a sequence of simulated operational conditions. These were performed at the subsystem level; that is, the completed RADVS subsystem was operating. A tabulation of vendor tests on flight units is shown in Table XIX-7.

*c. Special vehicle tests.* Development tests were conducted on several special vehicles. One of these tests, which had a direct bearing on RADVS development, was an upside-down vibration test (S-8).

A series of flight development tests was performed, known as the T-2 program. This program included a series of helicopter flight tests (T-2H) and several descent tests from a balloon-suspended gondola (T-2N) to investigate the terminal sequence. These tests are described below along with the salient results and conclusions.

The S-8 test vehicle consisted of a spaceframe fitted to simulate a standard spacecraft after the retrorocket had been ejected. The spaceframe was supported in an inverted position by a shock-cord system. Shakers attached at the three vernier-engine points were noise

**Table XIX-7. Outline of vendor tests on flight units**

| Unit | Characteristics tested | Unit verification | | Unit acceptance | | |
|---|---|---|---|---|---|---|
| | | Ambient | Temperature | Ambient | Vibration | EMI |
| Klystron power supply and modulator | Amplitude modulation | X | | | X | |
| | Other spurious outputs | X | | | X | |
| | Radar altimeter klystron rate | X | X | X | | X |
| | Output powers | | | X | X | |
| | Output frequencies | X | X | X | X | X |
| | Blanking signal amplitude, width, risetime | X | | | | |
| | Power consumption | X | | X | X | |
| | Warmup time | X | | X | | |
| | Time delay high voltage application | X | | | | |
| | Klystron supply voltages, regulation, ripple | X | | | | |
| | Modulation inhibit circuit (for test use) | X | | | | |
| Receiver/ transmitter | Antenna patterns | X | | X | | |
| | Noise figure | X | X | X | | |
| | Preamp gain, phase balance | X | X | X | | |
| | Preamp gain, selection accuracy | | | X | | |
| | Preamp possband, shape and gain | X | X | | | |
| | VSWR at transmit and receive | | | X | | |
| | Preamp microphonics | | | | X | |
| | Insertion loss of special test feedhorns | X | | | | |
| | Microwave isolation between feeds | X | | | | |
| Signal data converter | Reflectivity output calibration | X | | | | |
| | Signal-tracking thresholds (sine input) | X | | X | X | |
| | Signal-tracking thresholds (sine plus noise) | X | | | | |
| | Signal-tracking thresholds (doppler spectrum) | X | | | | |
| | Response time | X | | X | | |
| | Analog output accuracy, linearity (sine input) | X | | X | | |
| | Analog output ripple, noise (sine input) | X | | | X | |
| | Analog output accuracy, linearity (doppler spectrum) | X | | | | |
| | Range mark accuracies | X | | | | |
| | Cross-coupled sidelobe logic | X | | X | | |
| | Power consumption | X | | X | | |
| | Low-voltage power supply outputs and ripple | X | | | | |

driven and gave force outputs between 10 and 56 lb (rms) with flat spectra band-limited to the 80–2000 Hz range (expected mission level was 10 lb). Preamplifier outputs. The spectral content of the preamplifier output were radar analog outputs, the preamplifier medium-gain state, tracker lock signals, and other assorted digital outputs were recorded on magnetic tape. Also recorded signals was monitored, and significant results of the test were as follows:

(1) The early velocity-sensor tracker with a 3-db signal-to-noise acquisition threshold was very susceptible to false lock, but when the signal-to-noise ratio was raised to 9 db, there was no difficulty.

(2) Appreciable signal return from the spacecraft footpads and crushable blocks was noted before the radar antennas were shock-mounted. False tracker lock occurred when the shaker force level reached 28 and 56 lb rms.

(3) Evidence of leakage between antennas was noted.

(4) RF isolators within the waveguide were found to be required.

(5) The radar altimeter (beam 4) was found to be insensitive to vibration in this test.

The T-2H phase of the T-2 program included flight-testing of the RADVS with the use of a helicopter. The radar used in the tests was experimental but did contain all of the main features of an actual flight model. Altitude reached was about 6000 ft. The aircraft carried a magnetic tape recorder to monitor preamplifier outputs, analog outputs, range marks, and other assorted radar outputs. A strip-chart recorder was also utilized to display tracker lock signals and other radar outputs mentioned previously, and a downward-pointing camera was used to record the terrain being seen by the RADVS. An RF telemetry link also provided redundant coverage. Data analysis included spectral analysis of preamplifier outputs and a comparison of analog outputs with optical tracking data from ground installations. Some of the more significant results of the T-2H tests are described below:

(1) Analog output accuracy was found to be within tolerance when the trackers were locked and following a signal normally.

(2) When flown over water, it was found that the beam 2 and 3 trackers locked onto beam 1 through a sidelobe (hence the need for additional CCSL circuits). The CCSL between beams 2 and 3, tested over water, behaved properly, but the logic for these beams could not be tested over land.

(3) The 14-ft range mark was frequently triggered by noise at ranges greater than the 18-ft design maximum.

(4) Analog output noise was higher than expected.

(5) Although accuracy was not checked, the altimeter (beam 4) performance was satisfactory over mountainous terrain.

(6) Transients on the preamplifier (high-gain state) lines caused perturbation of the DVS analog outputs when switching occurred.

The primary purpose of the T-2N test program was to demonstrate the ability of the RADVS flight-control and propulsion subsystems to control a model spacecraft (equal in weight to the lunar weight of the flight spacecraft) while it performed a stable soft landing. The program was divided into three main categories of tests: tether tests, descent and recovery tests, and descent and touchdown tests.

The tether tests were designed to offer a pretest check of the vehicle's capability to undergo an actual descent test. Typically, the model spacecraft was raised to an altitude of 1500 ft by means of a large, helium-filled balloon. With the RADVS and flight control systems turned on, the vernier engines were ignited, and system operation was observed during both high and low thrust. An on-board telemetry transmitter provided a continuous RF link to the vital ground-telemetering functional parameters.

The descent and recovery tests were designed to prove the capability of the test vehicle using the radar flight-control loop by performing a programmed descent trajectory simulation within altitude limits which would enable safe recovery. The vehicle was not required to land, as such, but rather to *fly* a descent trajectory while maintaining a stable altitude. The vehicle was released from the 1500-ft altitude with vernier engines, RADVS, and flight control turned on. The vernier engines were commanded to low thrust, and the craft was released at a constant acceleration of 25 ft/sec$^2$. Vernier-engine thrust levels were modulated, and spacecraft altitude and velocity were controlled by the closed-loop RADVS/flight-control system. Recovery, in the form of a parachute deceleration system, was automatically commanded at an altitude of 600 ft and a velocity of 5 ft/sec.

The descent and touchdown tests were designed to verify that the craft could perform the *Surveyor* soft-landing sequence and a programmed-descent profile. The

test was similar to the descent and recovery test, except that the vehicle was released at a lower altitude (900 ft) and was not recovered. Descent was automatic to the surface, where a 2-ft fiber-glass probe shut down the vernier engines. The vehicle soft-landed to the ground on collapsible air bags (positioned where the *Surveyor* footpads would normally be).

The radar system used on these tests was essentially a flight system with the following exceptions:

(1) Waveguide runs were altered to fit the vehicle frame.

(2) The altimeter was locked in the high-deviation mode.

(3) Preamplifier high-gain states were bypassed (90 db).

(4) Cross-coupled sidelobe logic was bypassed.

(5) The RADVS trackers were locked in the narrow-band mode.

The above modifications were done primarily because the vehicle was at such a low altitude in the flight sequence. The high-gain state (90 db) lockout of the preamplifiers was done to disable the signal-to-noise acquisition mode of the radar to prevent vernier engine noise degradation due to acoustical coupling (because of the atmosphere environment).

Significant results of the T-2N series of tests were:

(1) The beam 1 tracker locked onto leakage from the radar altimeter feed.

(2) Transients appeared in the analog velocity outputs at preamplifier high-gain-state switching points.

(3) It was found necessary to mechanically isolate the klystrons.

(4) It was found necessary to develop a waveguide *scratch and thump* test to assess vibration sensitivity of the guide.

(5) It was found necessary to implement altimeter ranging techniques to insure spectrum compatibility with flight missions.

The first difficulty was solved by retuning the altimeter klystron for reduced AM emission, and by the addition of RF isolators to the velocity sensor waveguide runs. The second difficulty was caused by telemetry conditioning circuit leading of the high-gain-state lines and was solved by the addition of decoupling and isolation circuitry to the lines. In addition to these tests, HAC performed a series of regular FA tests, as follows. A more complete tabulation is shown in Tables XIX-8 and XIX-9.

***d. Prototype (T-21) and flight spacecraft system tests.*** A prototype *Surveyor* spacecraft (T-21), essentially identical to a flight model spacecraft, was used for the formal system TA test program. Its purpose was to verify design and check compatibility with ground equipment, including the DSIF, at all the test sites (El Segundo, San Diego, and the AFETR).

Spacecraft system FA tests were performed only on spacecraft which had been completely assembled and aligned. All units used were to have satisfactorily passed the appropriate lower-level FA test. The spacecraft system FA test was, therefore, mainly concerned with verifying the compatibility of units and checking that system functional requirements were met. This was accomplished through a sequence of eight phases, of which six concerned the RADVS.

The first phase, called initial system checkout (ISCO) test phase, gave initial verification of compatibility of subsystems and reference data for future phases. The next four phases in which the RADVS was exercised were environmental tests. These were the mission-sequence and electromagnetic interference test, the solar-thermal-vacuum test, the vibration test, and finally, the vernier engine vibration test phase. Additionally, a set of performance verification tests were performed prior to launch during final system testing at the AFETR.

***e. Test program review.*** Because of the highly complex nature of the RADVS, a degree of uncertainty existed in the methods of testing and simulation applied to the radar. Actual testing under realistic conditions at the limits of radar performance (50,000 ft range and 800 ft/sec velocity) was virtually impossible, and this made simulation a necessity. As a consequence, it was decided to solicit outside help to undertake a study and review of the radar system test program. The goal of this effort was embodied in the following points contained within a contract issued during mid-1966:

(1) An evaluation of system and unit tests for test adequacy, accuracy, redundancy, and proper tolerances relative to test level.

(2) A statistical evaluation of test data previously obtained from RADVS tests to determine the confidence levels and their relevance to radar system requirements.

**Table XIX-8. Listing of buyer flight acceptance tests**

| Characteristics tested | Operating conditions | | | | | |
|---|---|---|---|---|---|---|
| | Laboratory ambient | Vibration | Temperature | EMI | Vibration survival | Prelaunch |
| Ranging accuracy (waveguide simulator)[a] | X | | | | | X |
| Ranging accuracy (freespace simulator)[b] | | | | | | X |
| RA klyston deviation width (high and low) | X | | X | | | X |
| Transmitter output power | X | | X | | | X |
| Transmitter output frequency[c] | X | | X | | | X |
| Preamplifier output noise level and spurious outputs[d] | X | | | | | X |
| Preamplifier gain state logic and accuracy | X | | X | | | X |
| Preamplifier gain state signal false output[d] | | X | X | X | | X |
| Reflectivity-output calibration at one frequency[c] | X | | | | | |
| Reflectivity-output accuracy and repeatability[c] | | | X | | | X |
| Reflectivity-output in quiescent state [d] | | X | | X | | X |
| Signal-tracking thresholds (sensitivity)[c] | X | | | | | X |
| Acquisition time | | | | | | X |
| Analog output accuracy[c] | X | | X | | | X |
| False lock susceptibility and analog zero accuracy[d] | X | X | X | X | | X |
| Analog output noise and ripple | X | | | | | X |
| Range mark accuracies | X | | X | | | X |
| Range mark false-lock susceptibility[d] | | X | X | X | | X |
| Reliability circuit logic and delay | X | | X | | | X |
| Reliability circuit false outputs[d] | | X | X | X | | X |
| Cross-coupled sidelobe logic | | | | | | X |
| Waveguide leakage integrity[d] | X | | | | X | X |
| Waveguide grounding | X | X | | | | X |
| Warmup time from primary power to transmit | | | X | X | | X |
| Power consumption over input voltage range | X | X | X | X | | X |
| Tracker—lock indication by telemetry | X | | X | | | X |
| Unit temperatures indicated by telemetry | X | X | X | X | | X |
| Negative velocity and range rate rejection | | | | | | X |
| Range mark lockout until 3.7 after burnout | | | | | | X |

[a]About 600–900 ft.
[b]About 1700 ft equivalent free-space distance (both deviation modes).
[c]Test conducted with the KPSM undeviated.
[d]Measured with the simulated return signal level below acquisition.

(3) A study and determination of all RADVS operational parameters which were not being tested or were inadequately being tested by existing developmental, manufacturing, FA or other tests, and a written proposal giving specific practical recommendations for test improvements or additional tests which would close these test gaps and give greater confidence levels in those parameters.

This contract was issued to the Research Triangle Institute (RTI) of Durham, N.C. Three engineers, all eminently qualified in the microwave field, were assigned

**Table XIX-9. Outline of vendor system flight acceptance tests**

| Characteristics tested | Standard test conditions |
|---|---|
| Klystron sweep rate (radar altimeter) | Reference |
| Transmitter power levels | Reference |
| Transmitter frequencies | Reference |
| Preamplifier gain selection accuracy | — |
| Reflectivity–output | — |
| Signal tracking threshold (DVS) | 1, 4, 6, 8 |
| Signal tracking threshold (RA) | 2, 4, 6 |
| Acquisition time (DVS reliable-operate) | 1, 4, 6 |
| Acquisition time (RA reliable-operate) | 2, 4, 6 |
| Analog output accuracy, linearity (velocities) | 1, 2, 4, 5, 6, 7, 8, 9, 10 |
| Analog output accuracy, linearity (altitude) | 2, 4, 5, 6, 7, 8, 9, 10 |
| Analog output noise and ripple (at spacecraft filter output) | 10 |
| 1000-ft range mark accuracy | 7 |
| 14-ft range mark accuracy | 10 |
| Reliable-operation (indicating circuit operation) | Combination |
| Cross-coupled sidelobe logic operation (sine input) | 11 |
| Logic signal amplitudes | 7 |
| Analog transients due to preamplifier gain switching | 6 |
| Delay time from power-on to reliable-operate signals | 5 |
| Negative doppler rejection | 3 |
| Warmup time | 1, 5 |
| Mechanical test and inspection | — |

to the program. Two spent the total contract period (6 months) in residence at JPL; the third spent at least one-third of his time in residence.

Salient findings and recommendations of this effort are contained in Appendix B, but the most important was the conclusion that the doppler trackers were not being tested with realistic signal spectra. As sinewave-derived audio was serving as the STEA modulating waveshape, the trackers were not receiving a realistic input with regard to target scintillation; this tended to produce spread spectra rather than the line spectra used for the test purposes. In effect, it tested the system in a sort of *static* dynamic sense rather than a *dynamic* dynamic sense (corresponding to a fluctuating return). The findings of the RTI report were not incorporated into the test program because of schedule problems. Additional information about the RTI report is contained in Ref. XIX-7.

### 5. Mission Performance

*a. Mission performance summary.* The specification values and *Surveyor* mission values of RADVS terminal-descent parameters are presented in Table XIX-10. Event times for the missions are presented in Table XIX-11. Aside from one anomaly on the *Surveyor III* mission, the RADVS performed normally on all *Surveyor* missions where it was used. The RADVS was turned on during the *Surveyor II* mission even though that mission was terminated long before terminal descent would have been initiated. This was done to obtain thermal data after all hope of saving the mission was gone. The RADVS reflectivity data from the missions essentially confirms the Muhleman reflectivity model (see Appendix C) of the lunar surface within 4–6 db.

The terminal-descent event times and important RADVS parameters are given in Table XIX-12 for the

**Table XIX-10. Comparison of RADVS performance values: specification vs mission measurements**

| Parameter | Unit | Spec value | Surveyor mission values[a] | | | | | |
|---|---|---|---|---|---|---|---|---|
| | | | Surveyor I | Surveyor III | Surveyor IV | Surveyor V | Sureyor VI | Surveyor VII |
| RADVS power | A | — | 26.3 | 26.2 | 24.3 | 28.9 | 27.7 | — |
| Spacecraft attitude | deg | 0–45 | −4.09 | 23.8 | 31.5 | 45.7 | 25.4 | 34.86 |
| Reflectivity at lock on | | | | | | | | |
| Beam 1 | dbmW | −108 | −108 | −92.9 | −93.5 | −103.7 | −95 | −102.2 |
| Beam 2 | dbmW | −108 | −96.2 | −90.5 | −102 | −94.5 | −94 | −99.99 |
| Beam 3 | dbmW | −108 | −95.5 | −94.0 | −93 | −90.5 | −92 | −91.88 |
| Beam 4 | dbmW | −113 | −96.0 | −102.5 | —[b] | −96.5 | −92 | −96.18 |
| At DVS reliable-operate altitude | kft | <50 | 55 | 58.5 | 66 | 18.3 | 64.4 | 65.0 |
| Lateral velocity $V_X$ | ft/sec | — | 60 | −51.8 | —[b] | 30.7 | −3.3 | −37.9 |
| Lateral velocity $V_Y$ | ft/sec | — | −14 | 86.8 | —[b] | 27.0 | 135.8 | −568 |
| Lateral velocity $V_Z$ | ft/sec | — | 3280 | 3230 | ~3400 | 3332 | 3200 | 32, 50 |
| Beam 1 | kHz | <85 | 81 | 85.5 | 82.6–84.4 | 81.06 | 86.08 | 79.18 |
| Beam 2 | kHz | <85 | 81 | 86.3 | 82.6–84.4 | 88.14 | 86.12 | 79.79 |
| Beam 3 | kHz | <85 | 81 | 79.3 | 82.6–84.4 | 82.18 | 84.03 | 80.70 |
| At RA reliable-operate altitude | kft | <40 | 36 | 40 | —[b] | 11.3 | 35.5 | 39.5 |
| Total velocity | ft/sec | 1 + 850 | 690 | 632 | —[b] | 2349 | 501 | 452.5 |
| Range | kft | — | 36 | 43.7 | —[b] | 16.2 | 36.6 | 41.7 |
| Lateral velocity $V_Z$ | ft/sec | 1 | 690 | 632 | —[b] | 23.49 | 501 | 451.8 |
| Beam 4 | kHz | 91 | 76.6 | 91 | —[b] | 88.4 | 72.7 | 79 |
| Altitude at 1000-ft mark | ft | 1000 ±50 ft | 1028 | 998.9 | —[b] | 1048 | 1000 | 970 |
| Altitude at 14-ft mark | ft | 14 ±4 ft | 13 | —[c] | —[b] | 14.5 | 14 | 13.6 |

[a] Failed during midcourse maneuver.
[b] No data due to loss of telemetry signal.
[c] No 14-ft mark due to break-lock of beam 3 below 1000 ft.

*Surveyor I* mission, which was a typical mission. Various beams *locked on* during several missions, as noted in Table XIX-12. The majority of these locks occurred at the time of retrorocket ignition and it was concluded that the retrorocket case passed through and broke the tracker lock.

The range-vs-velocity descent profile of *Surveyor VI* is shown in Fig. XIX-13 as a typical example. It can be seen that SC-6 intercepted the programmed segment at about 25,000 ft. This segment acquisition occurred about 104 sec before touchdown.

On the *Surveyor III* mission, the terminal-descent sequence was normal until approximately 6 sec prior to touchdown, when beam 3 of the radar lost lock and did not reacquire for the remainder of the mission. Because the radar was required to generate the 14-ft range mark, which shuts down the vernier engines, the engines did not shut off but continued to burn through touchdown. Subsequent anomalies were probably a direct result of the beam 3 break-lock. Study has shown the break-lock was more than likely due to the rejection of the beam-3 tracker signal by the cross-coupled sidelobe logic. The basis for rejection by the logic is described in Subsection B-1. Essentially, the trackers for the specific beams being compared must be in a locked condition, the beam frequencies must be within 1.2 kHz of each other, and the amplitude difference between the beams must be at least 25 db after preamplifier rolloff. All data analyzed appeared to support the theory that cross-coupled sidelobe logic was responsible for this rejection. Performance just prior to the incident indicated that the preamplifier-gain states were switching quite rapidly; the spacecraft was nearly vertical, which means beam frequencies were certainly within 1.2 kHz; and there was a deep fade on

**Table XIX-11. RADVS mission events (time in seconds from RADVS on)**

| Event[a] | Telemetry signal | Surveyor | | | | | |
|---|---|---|---|---|---|---|---|
| | | I | III | IV | V | VI | VII |
| RADVS on | R-28, EP-17 | 0 | 0 | 0 | 0 | 0 | 0 |
| RADVS high voltage on | EP-17 | 24.5 | 19 | 21.3 | 22.9 | 20.7 | 21.6 |
| Beam 1 lock | R-15 | 27.5 | 29.6 | 30.9 | 27.0 | 26.8 | 31.0 |
| Beam 2 lock | R-16 | 27.5 | 29.6 | 30.9 | 26.1 | 26.8 | 32.2 |
| Beam 3 lock | R-17 | 27.7 | 30.5 | 30.4 | 27.0 | 26.8 | 30.8 |
| DVS reliable-operate | FC-34 | 27.7 | 30.5 | 30.9 | 27.0 | 28.3 | 32.2 |
| Beam 4 lock | R-18 | 33.7 | 41.1 | | 30.6 | 52.7 | 58.0 |
| RA reliable-operate | FC-33 | 36.7 | 41.1 | | 30.7 | 53.4 | 56.0 |
| RADVS control | FC-42 | 53.9 | 54.7 | | 48.9 | 51.9 | 56.4 |
| 1000-ft mark | FC-37 | 141.3 | 153.2 | | 86.2 | 114.7 | |
| 14-ft mark | FC-38 | 165.0 | —[b] | | 109.2 | 178.4 | 199.7 |
| Touchdown | | 166.5 | 178.1 | | 110.9 | 179.7 | 200.9 |
| Anomalies: | | | | | | | |
| | D3 unlock | 53.3 | | | 49.8 | | |
| | D3 RADVS | 53.3 | | —40.3: loss of data | 53.4 | | |
| | D3 RA reliable-operate | 55.3 | | | 53.4 | | |
| | D4 unlock | | 44.9 | | | | |
| | D4 RA reliable-operate | | 57.3 | | | | |

[a] Due to sampling rates for various signals, the sequence of two events at essentially the same time (<2.0 sec) is uncertain.

[b] D3 did not reacquire because spacecraft velocity was below the tracker design limit; therefore, 14-ft mark was inhibited from firing.

beam 3 just prior to the break-lock which could have been sufficient to have caused a 25-db amplitude difference.

Subsequent to the beam-3 break-lock and SC-3 first touchdown, the RADVS KPSM recycled for its normal 20-sec warmup period and then came on again at second touchdown. The KPSM again recycled for another 20-sec period (the 20 sec is the normal warmup time before application of klystron high voltage). The cycling repeated several times within the next several minutes, and the KPSM finally went off and remained off—probably because of a failure within the unit. The most likely cause for the KPSM recycles was a high-voltage arc in the plasma discharge caused by an exhaust plume from the vernier engines when the spacecraft was close to the lunar surface. It appeared possible for this plume to enter the side cover of the KPSM causing a glow discharge in the high-voltage circuitry.

As a result of the experience with the *Surveyor III* mission, it was decided to disable the sidelobe rejection logic by the 1000-ft mark. The effect was to remove sidelobe-logic discrimination below 1000 ft to prevent recurrence of the *Surveyor III* anomaly. As the sidelobe problem did not remain a problem at such low altitudes, the change did not affect the rejection logic effectiveness in any way.

A variation from the normal sequence was required for the SC-5 terminal descent due to the loss of vernier propulsion system helium pressure. The RADVS was required to perform its mission objectives in about half the typical operation time because retroignition was delayed the maximum of 13.35 sec (from standard 2–8 sec) after AMR mark. Main retro burnout occurred when the spacecraft was at 8000-ft range. The spacecraft acquired the descent profile curve at an altitude of about 850 ft. The RADVS performance was normal on this mission with all mission requirements fulfilled.

## Table XIX-12. Typical (*Surveyor I*) terminal-descent sequences

| Event | Time to touchdown, sec | Slant range, kft | $V_Z$ ft/sec | $V_X$ ft/sec | $V_Y$ ft/sec |
|---|---|---|---|---|---|
| AMR on | 455.0 | 2751.0 | 8700 | | |
| AMR enable | 275.0 | 1185.0 | 8900[a] | | |
| AMR mark | 175.0 | 315.0 | 8697.3 | | |
| Vernier ignition | 168.0 | 246.0[a] | 8565.5[a] | | |
| Retroignition | 166.0 | 236.6[a] | 8565.5[a] | | |
| RADVS on | 166.1 | 240.0[a] | 8540[a] | | |
| RADVS high voltage on | 142.1 | | | | |
| D1 and D2 lock | 137.9 | 62.00[a] | 3950[a] | | |
| D3 lock, DVS reliable-operate on | 137.0 | 55.0 | 3300 | | |
| D4 lock, RA reliable-operate on | 128.0 | 37.7 | >779 | 69.3 | −6.4 |
| Retrorocket burnout | 127.6 | 37.7 | >779 | 69.3 | −6.4 |
| Inertia switch closure | 127.0 | 37.3 | 670 | 69.3 | −6.4 |
| Retrorocket signal | 115.6 | 30.2 | 454 | 68.1 | −4.1 |
| Retrorocket ejected | 115.0 | 29.9 | 442[a] | 69.9 | −2.9 |
| Main retro sequence complete RADVS descent | 113.2 | 30.7[b] | 438 | 73.4 | −8.8 |
| Relible-operate lost | 111.5 | 30.2[b] | 434 | 73.4 | −8.8 |
| D3 unlock | 111.0 | 30.2[b] | 434 | 73.4 | −8.8 |
| DVS reliable-operate regained | 109.5 | 28.0[b] | 410 | 70.5 | No data |
| D3 lock | 109.5 | 30.2[b] | 410 | 72.2 | No data |
| RA reliable-operate regained | 109.5 | 28.0 | 410 | 72.2 | No data |
| Programmed-descent segment acquisition | 89.6 | — | 434 | +0.1 | 0.0 |
| 1000-ft mark | 25.0 | 1.070 | 125 | | |
| 10-ft/sec mark | 06.8 | 0.045 | 9 | | |
| 13-ft/sec mark | 01.4 | 0.015 | 4.3 | | |
| Touchdown | 00.0 | — | 11.7 | | |

[a]Typical value.
[b]Attributable to loss of D3 locking.

# Appendix XIX-A
# Derivation of Radar Equations

## A. Range Equation and Typical db Budget (*Surveyor V*)

$$P_r = \left(\frac{1}{2}\right)\left(\frac{c}{4\pi}\right)^3 \left(\frac{P_{av}\, G^2}{f^2\, f_p\, R^3}\right) \beta_1 \cot\theta\, \sigma(\theta)$$

for *Surveyor V*, $\theta = 46$ deg $\sigma(\theta) = \eta\,(K/\alpha^3)\, f(\theta)$.

The equation above for received power $P_r$ is the expression for the theoretical power level that would be reflected from the lunar surface and detected by the AMR for any operational range.

A sample calculation using *Surveyor V* data is given below.

For the AMR, using the Muhleman model, the calculation follows:

$$\alpha = 0.36$$

$$\frac{K}{\alpha^3} = +\ 10.7 \text{ db}$$

$$P_{av} = +\ 33.60 \text{ dbm}$$

$$G^2 = +\ 69.00 \text{ db}$$

$$c^3 = +122.12 \text{ db}$$

$$\eta\left(\frac{K}{\alpha^3}\right) = -\ 1.17 \text{ db}$$

$$f_3(\theta) = -\ 12.91 \text{ db}$$

$$R^3 = -\ 53.34 \text{ db}$$

$$f^2 = -199.37 \text{ db}$$

$$f_p = -\ 25.54 \text{ db}$$

$$\beta_1 = -\ 13.57 \text{ db}$$

$$\cot 46 \text{ deg} = -\ 0.19 \text{ db}$$

$-306.09$ db
$+224.72$ db

$-\ 81.37$ db prediction at 60-mi mark

The power value of $-81.37$ db calculated verified the measured data (via telemetry) from *Surveyor V*.

## B. RADVS Radar Altimeter/Doppler Velocity Sensor Equations

### 1. Doppler Velocity Sensor Equations

The spacecraft beam orientations were such that the typical velocity components $V_i$ ($i = 1,2,3$) along the axes of these three beams were determined by the spacecraft coordinate components of velocity according to the matrix multiplication:

$$\begin{bmatrix} V_1 \\ V_2 \\ V_3 \end{bmatrix} = \begin{bmatrix} +A & +A & +B \\ -A & +A & +B \\ -A & -A & +B \end{bmatrix} \begin{bmatrix} V_X \\ V_Y \\ V_Z \end{bmatrix}$$

where

$$A = (\sin 45 \text{ deg})(\sin 25 \text{ deg}) = 0.29884$$

$$B = \cos 25 \text{ deg} = 0.90631$$

and the spacecraft coordinates were a Cartesian right-handed triad with $+Z$ along the roll axis in the normally descending direction.

The solution of the matrix equation is:

$$V_X = \frac{V_1 - V_2}{2_A}\ ;\ V_Y = \frac{V_2 - V_3}{2_A}\ ;\ V_Z = \frac{V_1 + V_3}{2_B}$$

where $V_1$, $V_2$, and $V_3$ are proportional to the doppler frequencies detected for beams 1, 2, and 3, respectively.

The doppler shift along a particular beam is given by

$$D_i = \frac{2f}{c} V_T \cos\delta_i \qquad i = 1,2,3$$

where

$D_i$ = doppler shift in beam $i$

$f$ = transmission frequency (13.3 GHz)

$c$ = velocity of light

$V_T$ = total spacecraft velocity

$\delta_i$ = angle between $V_T$ and the axis of beam $i$

Substitution of the expression for the doppler shift into the expression for $V_X$, $V_Y$, and $V_Z$, and noting that $V_T \cos \delta_i$ is the velocity component along beam $i$, yields:

$$V_X = \frac{\frac{c}{2f}(D_1 - D_2)}{2A}$$

$$V_Y = \frac{\frac{c}{2f}(D_2 - D_3)}{2A}$$

$$V_Z = \frac{\frac{c}{2f}(D_1 + D_3)}{2A}$$

The above expression thus relates the spacecraft velocity components $V_X$, $V_Y$, and $V_Z$ to three doppler frequencies which were measured by the DVS channels.

### 2. Derivation of Radar Altimeter Equation

The radar altimeter was a single RF beam directed parallel to the spacecraft roll axis (+Z). The transmitted signal, at carrier frequency $f_0$, was frequency-modulated with a sawtooth waveform of fixed deviation $\Delta f$ and a repetition frequency $f_p$ (Fig. XIX-A1). Assuming that the transmitter frequency decreased linearly with time as shown, and that there was a reflecting surface or target at distance $R$, a reflecting signal or echo would return after a time $t = 2R/c$, where $R$ = range, $c$ = velocity of light.

If the transmitted frequency at some time $t$ was $f_1$ (Fig. XIX-A1), then the return frequency observed $t$ seconds later would be shifted by doppler $f_D$ and will thus be $f_1$ and $f_D$. If the echo was heterodyned with a portion of the transmitted signal a best frequency $f_b$ (i.e., the difference frequency between the transmitted and returned signals) will result. From the figure, the following ratio can be written:

$$\frac{f_b - 1 f_D}{t} = \frac{\Delta f}{1/f_p} = \Delta f f_p$$

Rearranging terms and noting that $t = 2R/c$, the above equation becomes:

$$R = \frac{c(f_b - 1 f_D)}{2 \Delta f f_p}$$

The doppler term $f_D$ is given by

$$f_D = \frac{2 V_Z}{c} f_1,$$

where

$V_Z$ = velocity along the +Z axis

$f_1$ = transmitted frequency

The inevitable but undesired velocity shift $f_D$ was compensated for within the SDC altimeter converter by subtraction of a scaled $V_Z$ component from within the $V_Z$ converter. This compensation produced the analog range signal used by flight control for vernier-engine control.

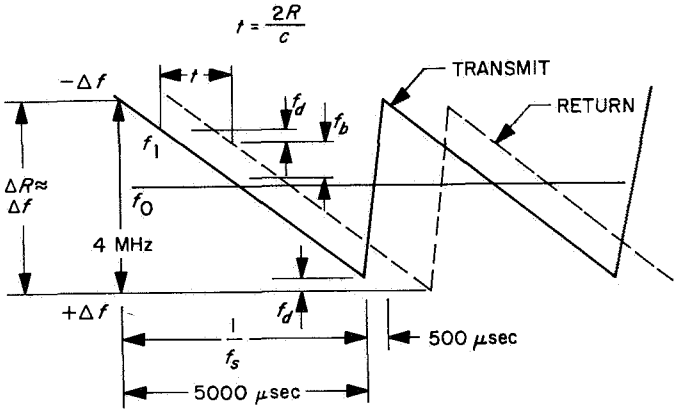



**Fig. XIX-A-1. Altimeter frequency diagram**

# Appendix XIX-B
# Research Triangle Institute Findings and Conclusions with Statements as to Applicability to Program

The following is a list of RTI suggested test modifications, additions, and deletions together with a discussion with regard to desirability and feasibility.

## A. Analysis and Experimentation of Problems

A suggested *cross-coupled sidelobe logic* (CCSL) study recommendation has already been implemented. Investigation has resulted in signal data converter (SDC) changes to include CCSL for all radar beam combinations. The RTI team suggested testing with spread spectrum input signals (fluctuating) to determine whether anomalous effects of the CCSL could occur, such as slow signal fades (causing errors in the CCSL decision outputs). This point was well taken and would have been a desirable modification to existing CCSL tests. It was conceivable that the Ryan-designed spread-spectrum simulator could be used at least in the unit test area. The RTI people further described a method of CCSL suppression by which the stronger of two or more signals was required for suppression to occur, and a widening of the tracker bandpass filter to accommodate all three main beams would have been required. As CCSL circuits between all pairs of antennas existed (SC-4 and up; ECP-23), it did not seem possible to consider the RTI-suggested method at that point in the *Surveyor* Program. It would be of interest for future CW doppler tracking radars, however.

## B. Transmitter/Receiver Leakage Tests

Transmitter/receiver leakage was a serious difficulty with all CW radar systems. The RTI representatives stated that to avoid degradation of tracker sensitivity, the product of the leakage factor and leakage power in the tracker-filter bandwidth must be of the order of $-160$ dbm. If this condition was not met, tracker acquisition sensitivity must be reduced to avoid locking to the leakage component. It was unfortunate that this leakage was difficult to assess quantitatively. The RTI-suggested approaches to the problem have merit but are difficult to incorporate. One approach involved incorporation of an on-board spectrum analyzer on the spacecraft to accurately measure the signal response in the preamplifier bandpass. This would be done by stepping a VCO doppler gate synchronously with the telemetry commutator through the preamplifier passband. It did not seem desirable at this late date, however, to incorporate so complex an addition to the system.

The wide bandpass necessary to monitor leakage spectrum in flight was not likely to be achieved practically. According to RTI, a ground-based free-space vibration and ranging test would accurately reveal all leakage paths with the exception of vernier plume reflection and modulation. The S-8 "upside-down" test, conducted early in the program, attempted to assess this vibration problem (vernier engines were not exercised, however). The RTI suggestion to compare vibration levels present in that test with flight vibration levels encountered in the SC-1 flight was worthy of consideration. Some study would be necessary to effect this, however, as the instrumentation differences between the tests were substantial. The importance of obtaining data on the spectral and time-behavior characteristics of the RADVS preamplifier signals is recognized. RTI stated that noise characteristics limiting tracker acquisition may be found in the doppler band below 10 kHz. It may well be that tracker search patterns might then be modified before burnout to lessen the chance of false lock. It was recommended that the vibration comparison be made.

## C. Klystron Coherence, Linearity, and Rate Measurements

Transmitter frequency coherence measurements should be made both at the unit level (ambient, vibration, and temperature) and at the system level (vibration, temperature, and EMI), that sweep linearity and width be measured at the unit level and system level; and that sweep-rate measurements be deleted from the ambient system test (at HAC and Ryan) and be added to a prelaunch test.

It was agreed that klystron frequency coherence measurements should be made. These would precisely define the maximum power supply ripple components and would pinpoint klystron AM and microphonic problems. The noncoherence problem was not evident in current STEA tests because of a lack of appreciable delay between the klystron reference and the return signal. (Normal propagation delay was of the order of $10^{-3}$ sec; the STEA delay more nearly approached $10^{-7}$ sec.)

It appeared that these measurements should be performed only during the unit level tests at Ryan. An FM microwave discriminator required for frequency coherence measurements was sufficiently complex to require a laboratory measurement; it was believed that field measurements of coherence would not be conclusive. Sweep nonlinearities should also be measured at the unit level. It was agreed that sweep linearity deficiencies could cause serious spectral spreading in the doppler preamplifier and result in poor frequency tracking together with suppressed acquisition sensitivity. For these reasons, it was recommended that sweep linearity be recorded. (It does not appear that sweep linearity would change noticeably from the unit level to the buyer acceptance-test stage.) Sweep rate should at least be recorded at the unit level; a measurement at the system level would be redundant. Analog output accuracy measurement would uncover faulty sweep-rate timing. Some indication of sweep linearity was obtained from current ranging tests.

## D. Test With Realistic Signal Spectra

The adequacy of the current flight-acceptance test program was of considerable concern because of a complete lack of realism with respect to signal simulation. The absence of any STEA time delay and the associated simulation with line spectra (sinusoidal input) resulted in serious deficiencies with regard to tests of acquisition sensitivity, tracker and converter operation, range mark accuracy, and CCSL circuit performance. A further effect is that closed-loop descent testing lacked the realism necessary to fully check subsystem interaction.

Lack of spread spectrum input testing raised a question concerning the validity of sensitivity measurements at various standard test conditions (STCs). If spectral spreading losses are computed and referenced to available return power during the descent, the current level (sensitivity) required for STC 1 is −108.3 dbm, the computed worst-case received power at 50,000 ft, 45-deg altitude, including spectral spreading loss is −109.6 dbm. This says STC 1 was testing about 1.3 db too high. Similarly, the worst-case computed condition for STC 8 (930 Hz) was −108.8 dbm, whereas the actual test was at +102.3 dbm, a discrepancy of 6.5 db. The former two levels are concerned with the DVS beams; the latter, low frequency sensitivity. As far as the altimeter was concerned, received power at 40,000 ft, 45-deg attitude was computed to be −106.6 dbm; STC 2 (84.45 kHz) actually tested at −104 dbm (vendor) and −113.3 dbm (buyer). It appeared that the HAC specification could be raised by about 6 db.

The fact that only the lab ambient unit verification test used spread spectra in the program should be of concern. All other tests applied either a sinusoidal input or no signal input. Filter bandwidths, threshold circuits; klystron AM effects; preamplifier gain, phase balance, and gain-selection operations; tracker search range; and blanking circuit operation were not adequately checked in system environmental tests.

## E. Further Analysis of Retrorocket Tankage Effects

There were questionable conditions for operation in the presence of retrorocket tankage separation. However, any analysis would have to make a free-fall assumption, or else be of the Monte Carlo type. The main reason for questioning a free-fall assumption was based upon the momentary unlock of beam 3 during the descent of *Surveyor I*, which could not be explained by assuming free-fall of the retrorocket casing.

The complete prediction and analysis for this type of situation was extremely difficult and would involve the computation of power density levels for various velocity–power profiles involving near field and minor lobe structures. The conclusions would be open to question at best.

## F. Renew Type-Approval Testing

Research Triangle Institute suggested renewal of the early TA tests. This was considered desirable if a test vehicle (T-21) could be used. Many spacecraft design problem areas have been uncovered. The use of a TA test vehicle would avoid flight spacecraft experimentation. To quote RTI: "Undertaking these tests in parallel to the current flight program ... might save time in analyzing possible flight failures. The fact that this testing would be important to other systems besides RADVS serves as additional justification."

In lieu of the several spacecraft design incompatibilities uncovered (particularly with regard to RADVS/flight control telemetry interface problems) it seemed highly advisable to have a spacecraft for experimentation. It was recommended that at least a vehicle be available for use. Justification for complete renewal of TA tests cannot be found, however.

## G. Constant-Acceleration Test

Research Triangle Institute recommended a constant-acceleration test to check component mechanical stress

on RADVS during retrorocket braking. Unfortunately, the problems faced to conduct such a test seemed almost insurmountable. Placing unit subassemblies or the complete system into a centrifuge with slipping pickoff of the RADVS SDC outputs would be difficult; RTI concluded that the constant-acceleration environment would induce the greatest mechanical stress on components and connections. (Wideband vibration: 0.2 *g* rms; sinusoidal vibration: 1.4 *g* rms; constant acceleration 10.8 *g* rms.) It did not seem likely that a realistic test of this environment could be feasibly engineered.

## H. Acquisition Sensitivity Levels Determination

Acquisition sensitivity specifications were constantly changing, and almost invariably the sensitivity requirement was decreasing. Based on spread-spectrum testing, and the coherence loss problem, sensitivity levels should be rigidly fixed; with all signal simulation done with spread-spectrum driving signals.

The suggested curve of *acquisition sensitivity* versus *doppler frequency* had already been incorporated into the system test specification (3023926-Revision B) as EO 34745. The curve was a step in the right direction; however, the input level should be changed to reflect a spread return signal.

It was recommended that the sensitivity specification be revised and rigidly adhered to.

It appeared that the system was not being operated on available return power (low-frequency signals) for all situations within specification. The sensitivity question related directly to the spread-spectrum tests, the coherence loss problem, and the unrealistic STEA propagation delay situation discussed elsewhere.

## I. Prelaunch Test Sequence

A brief prelaunch RADVS test sequence was suggested to check for damage during transit to the launch site. This was not done; however, the situation was investigated to determine whether RADVS could be turned on after spacecraft *Centaur* encapsulation. With a soon-to-be-installed EMA turnon/turnoff capability for the radar system (SC-5), a prelaunch test would seem more practical.

## J. Delay-Time-Constant Circuits

The delay circuits were necessary for proper radar operation with real signal inputs. No documented test existed in which they were checked. It was recommended that these be checked at least at the unit level with regard to proper timing. Time-delay circuits form the basis for any adaptive control errors which might appear later.

## K. Low-Pass Filter Bandwidth Change

There was a finite delay time between the receipt of the deviation signal and the bandwidth change of the low-pass filter in the RA. This was probably to insure against transients triggering the bandwidth change. This time delay was not checked. Research Triangle Institute suggested checking at both the ambient unit level and the thermal unit level. It was recommended that the delay time be checked at the unit ambient level; thermal checking seemed inordinately complicated and unwarranted.

## L. Analog Output Accuracy

Output accuracy was not measured under vibration or EMI. A lack of testing during vibration means that vibration-induced spurious signals or noise which would tend to disperse the spectrum being tracked would not be noticed. An RF access to RADVS during vernier-engine vibration would satisfy the vibration requirement. The EMI suggestion was not satisfied during spacecraft mission-sequence EMI testing when open-loop terminal descent was run, as EMI generators simulate only the AFETR preinjection EMI environment and not the spacecraft free-space situation. Further, open-loop terminal did no RADVS checking with signal input, as terminated dummy loads were used in place of feedhorn adapters. The test does give information relative to conductive (but not radiated) EMI. A RADVS spacecraft radiated-EMI test would have been desirable but did not prove practical.

## M. Range-Mark Testing and Ranging Test

Frequency coherence test difficulties have already been discussed as being a consequence of the practically nil propagation time delay of the STEA. The free-space ranging test possesses the same difficulty. Problems due to klystron AM spurious emissions would be no more apparent than STEA tests, as propagation delay was very small due to a maximum range length of about 1800 ft. The spectrum taken during the ranging test revealed nothing about blanking signal effectiveness as the flyback pulse was 10 times removed (in frequency) from the return spectrum. It was recommended that

spectrum measurements be made which include observation of the blanking pulse. It seemed impossible, however, to conduct a ranging test with a target located much further than the existing range. The ranging test did measure analog output accuracy, however.

Current tests of range-mark susceptibility to false mark are made with no signal input. The use of spread spectra was suggested to test the range-mark circuitry for false-mark susceptibility. If not spread spectra, then at least sinusoidal input should be used, and was recommended at the unit level.

## N. Vernier-Engine Vibration Test

Vernier-engine vibration tests, as conducted in the *Surveyor* Program, involved shaker vibration of the spacecraft at the three vernier-engine attach points. The RADVS was configured such that all four beams were operated into terminated dummy loads with no hardline access to the system. All four trackers were searching, and the radar reliable-operate signals and tracker-lock telemetry data were observed for indication of locks of any tracker. The RTI team suggested RF access to RADVS during the test through a flexible waveguide. This appeared feasible by equalization of the shaker drive to account for the waveguide addition. An RF access during the test would (1) satisfy the vibration test of analog output accuracy, (2) help to determine klystron vibration AM products, and (3) locate spurious transmitted outputs which otherwise would not be detected and might suppress acquisition sensitivity through spectrum dispersion. It was recommended that modification to the vernier-engine vibration test be given serious consideration.

## O. Determination of Required Levels of Analog Noise and Ripple

There was no pertinent test requirement specified for ripple on the DVS klystron anode supply lead. Vendor unit-level tests simply required that ripple be recorded. It was not required that it be measured anywhere nor were its FM effects to be observed. The RTI team calculated that 10 mV of ripple on the klystron anode would be sufficient to keep the upper beam of a spacecraft (at 25-deg attitude) locked over slant ranges of 50,000–10,000 ft. This would have been disastrous to the mission. RTI also stated that sideband levels relative to acquisition threshold are independent of range. Consequently, false locks will not be broken unless gain states are changed or attitude changes appreciably.

It was recommended that the RTI-computed minimum value of ripple voltage for which false lock could occur be considered a maximum test value. This computed to 1.33 mV. It was further recommended that unit test requirements be revised to require KPSM DVS klystron anode voltage ripple be less than 1.0 mV.

## P. Test Equipment Changes

Frequency coherence measurements, sweep linearity measurements, and spread-spectrum simulation have already been discussed. Test equipment changes to effect these measurements would consist of a microwave discriminator to measure instantaneous frequency and frequency-deviation linearity (including AM of the klystron), and the addition of a spread-spectrum simulator to accurately simulate the doppler spread spectrum.

A microwave discriminator consisted of a high-Q tunable cavity, a klystron local oscillator, a pair of mixers and associated IF amplifiers, a phase detector, and an audio amplifier. An audio spectrum analyzer or oscilloscope was required for display. It would be desirable to run the coherence measurement during vendor unit-level testing and it was felt that system testing at the buyer level was unnecessary.

Spread-spectrum testing was one of the more desirable test modifications. This necessitated STEA modification: the addition of a spread-spectrum simulator. The vendor used a simulator for SDC unit-level testing. It was recommended this be considered in whole or part for STEA use, at both the unit and system level. It was felt that all STEA tests should be done with spread-spectrum simulation.

## Q. Reliability Circuit Operation Under EMI

Circuit-operation reliability was not tested under EMI conditions. The test sequence did not include provisions for reliable-operate functions during open-loop terminal descent. All EMI generators were turned off upon spacecraft injection, as they were designed to simulate AFETR environment. Thus, there was no EMI test of any RADVS function. The only EMI source expected, however, was the high-power telemetry transmitter aboard the spacecraft. The RADVS was not tested under these conditions, as feedhorn adapters do not permit antenna utilization. It was conceivable that the reliable-operate logic circuitry could be susceptible to spacecraft EMI. Such a test did not seem feasible, however, because stray antenna radiation in a confined environment with no feedhorn adapters would cause numerous spurious returns to the trackers.

## R. Power Supply Transients

Some checks were run at the extremes of power supply voltage levels, but there were no tests made of transients on the spacecraft main power bus (unregulated output bus). It was recommended that the vendor run power supply transient checks at the unit level. It was doubtful that KPSM DC-converter problems would have appeared on the spacecraft had thorough power supply tests been run at the vendor.

# Appendix XIX-C
## Lunar Reflectivity Model

The lunar reflectivity model used for design and evaluation of both the RADVS and altitude marking radar was developed by Dr. Duane O. Muhleman. The surface backscatter function of the Muhleman model provided excellent fit to the complete-pulse return-time responses observed from earth, after convolution with pulse shape and determination of the mean slope at the radar wavelength. The angular dependence function as defined by Muhleman, therefore, was significantly strengthened as a concept and experimentally justified for earth-based observation.

Because of some uncertainties in the absolute calibration of the Muhleman experimental data, JPL, HAC, and Ryan agreed to use 0.075 (or −11.25 db) as the ratio of actual radar cross section to that of a lossless and isotropic sphere of lunar radius, where the latter is simply the area of the projected lunar disk. The impact of this decision was that the radar was required to operate against a moon which was 6 db below the normal moon. An additional 4 db was desired to maintain a reasonable margin against local terrain variations or scintillation.

The angular dependence derived by Muhleman is:

$$f(\theta) = \alpha^3/(\sin\theta + \alpha\cos\theta)^3$$

where $\theta$ was the angle of incidence (off local lunar vertical) and $\alpha$ was a wavelength-dependent mean-slope parameter. If this function were subjected to a hemispheric integral condition for normalizing, it must be multiplied by the factor $(K/\alpha^3)$. For RADVS, reasonable values are $\alpha = 0.39$ $K/\alpha^3/ = 10.15$ db. The total reflectivity factor was then $\eta\ (K/\alpha^3)\ f(\theta)$, where $\eta = 0.075$. This total factor was essentially a power reflection coefficient of the lunar surface, normalized to a lossless and isotropic sphere. It may also be viewed as the effective radar cross section per unit of surface area, a dimensionless ratio. It was not the surface backscatter function, which was $\cos\theta$ times this factor.

Using the Muhleman lunar reflectivity model and assuming the antenna gain pattern can be approximated by a gaussian pencil beam, the following expression can be derived for the received power on any beam $i$ $(i = 1,2,3,4)$

$$P_{r_i} = \frac{P_{t_i}\left(\frac{G_i}{2}\right)\lambda^2\,\sigma(\theta_i)}{(4\pi R_i)^2}$$

where

$P_{r_i}$ = received power on beam i
$P_{t_i}$ = transmitted power on beam i
$G_i$ = peak one-way antenna gain for beam i
$R_i$ = beam slant range
$\lambda$ = transmitted wavelength
$\theta_i$ = incidence angle (off local vertical) of beam $i$

$$\sigma(\theta_i) = \eta\left(\frac{K}{\alpha^3}\right)\left(\frac{\alpha}{\sin\theta_i + \alpha\cos\theta_i}\right)^3$$

The above expression for received power was an easily derived approximation which has been shown to be accurate to less than 1 db of error.

Using the radar equation just derived (expressed in db), the standard DVS db budget for minimum margin performance is shown below:

| | |
|---|---|
| $P_t$ | 31.76 dbm (1.5 watts/beam) |
| $G$ | 28.0 db |
| ½ | − 3.01 db |
| $\lambda^2$ | −22.64 db |
| $(4\pi)^{-2}$ | −21.98 db |
| $\eta(K/\alpha^3)$ | − 1.10 db |
| without $\frac{f(\theta)}{R^2}$ | 11.03 dbm |
| $f$ (25 deg) | − 8.94 db |
| $\cos^2$ 25 deg | − 0.86 db |
| without $R_z^{-2}$ | 1.23 dbm |

hence, the total DVS signal power per beam, with vertical spacecraft attitude, in dbmW, at receiving feedhorn is

$$P_r = [+\ 1.23 - 20\log_{10} R_z(\text{ft})\ \text{dbm}]$$

Similarly, the standard radar altimeter db budget for minimum margin hardware has consistently been as follows:

| | |
|---|---|
| $P_t$ | 23.22 dbm (210 mW min) |
| $G$ | 28.0 db |
| ½ | − 3.01 db |
| $\lambda^2$ | −22.36 db |

## References


XIX-1. *Surveyor III Flight Performance Final Report,* SSD 68189-3. Hughes Aircraft Co., Culver City, Calif., July 1967.

XIX-2. *Surveyor IV Flight Performance Final Report,* SSD 68189-4. Hughes Aircraft Co., Culver City, Calif., Sept. 1967.

XIX-3. *Klystron Power Supply Modulator Ranging Tests During Vibration, A Unit of Survey RADVS,* Report 51766-8. Ryan Aeronautical Co., San Diego, Calif., Aug. 1966.

XIX-4. *Cross-Coupled Sidelobe Discrimination by All-Doppler Velocity Sensor Trackers,* Document ECP-23. Ryan Aeronautical Co., San Diego, Calif., Oct. 1966.

XIX-5. *Operation and Maintenance Instructions for Radar Altimeter and Doppler Velocity Sensor, Ryan Model 517,* Report 51764-1A. Ryan Aeronautical Co., San Diego, Calif., Sept. 19, 1966.

XIX-6. *Operation and Maintenance Instructions for RADVS Test Equipment,* Report 51864-1B. Ryan Aeronautical Co., San Diego, Calif., Jan. 1967.

XIX-7. *Palmer, D. F., Smith, P. G., Borgiotti, G. V., Surveyor Landing Radar Test Program Review,* Report RTI-TRR-33 (NASA-CR-88883). Research Triangle Institute, Research Triangle Park, N.C., Jan. 24, 1967.


## Bibliography


*Decibel Allocation and Margin Summary,* SSD 4021 (Revs. 2 and 3). Space Systems Div., Hughes Aircraft Co., Culver City, Calif., Oct. 1966 (Rev. 2) and Jun. 1967 (Rev. 3).

*Functional Description of Surveyor Spacecraft: Volume III.* SSD 239524E. Space Systems Div., Hughes Aircraft Co., Culver City, Calif., Nov. 1964.

*Operation and Maintenance Instructions for RADVS Test Equipment,* Document 51864-1B. Ryan Aeronautical Co., San Diego, Calif., Jan. 1967.

*RADVS Mathematical Model,* Report 51769-8. Ryan Aeronautical Co., San Diego, Calif., Dec. 1965.

*Surveyor I Flight Performance: Volume III.* Report SSD 688223R. Space Systems Div., Hughes Aircraft Co., Culver City, Calif., Oct. 1966.

*T-2N Vehicle Design Requirements,* SSD 225410. Space Systems Div., Hughes Aircraft Co., Culver City, Calif., Aug. 1965.

# XX. Spacecraft Radio

A fundamental consideration for any remote-operated device is the method of maintaining control of the device and obtaining information about it. For the *Surveyor* spacecraft, a high-frequency radio system was the control link. The basic functions of the system were to provide: (1) earth-to-spacecraft command capability, (2) spacecraft-to-earth telemetry (both engineering and scientific), and (3) spacecraft tracking by means of doppler information.

To fulfill the stated requirements, the radio system contained a receiving subsystem (earth-to-spacecraft command link) and a transmitting subsystem (spacecraft-to-earth telemetry and tracking link). Additionally, provision was made to ensure command and telemetry capability for all spacecraft attitudes.

## A. Design Evolution

As in most complex designs, modifications were made to the spacecraft radio system throughout the project. Late modifications are covered in Subsection B. The early design evolution consisted of changes that occurred before a flight spacecraft was assembled.

### 1. Transmitter Evolution and Changes

Early design of the radio communication link incorporated redundant or stepped levels of performance from inception. In keeping with the precedent of previous spacecraft, several power levels were to be obtained by separate transmitters.

The transmitters, as originally proposed, were entirely solid-state, and could be considered as two subunits: (1) a power amplifier and (2) a varactor multiplier and exciter unit. A breadboard of the power amplifier, fabricated and tested during the study phase, consisted of transistors operated in parallel to drive a passive varactor multiplier chain to obtain an output of 1 W at 2.295 GHz. Both spacecraft transmitters were capable of operating in a high- or low-power mode by increasing the operating voltage of the power amplifiers and changing the bias voltage on the varactor diodes. Transmitter A, intended for lunar operation, operated at output of 1 W for TV transmission, 10 mW for low data-rate telemetry, and 50 mW for transponder operation during transmit. The difference in outputs was the result of optimizing the

multiplier chain of transmitter A for high-power operation and the multiplier chain of transmitter B for low-power operation. The transmitters could be switched between their associated omniantennas and one high-gain planar array antenna. This allowed the secondary transmitter to be used during transit or lunar operation if the primary transmitter failed.

The exciter design was based on the use of a demodulator with frequency-modulated feedback for TV transmission. As a result, the frequency modulator consisted of a voltage-controlled crystal oscillator (VCXO), with a modulation bandwidth of 0.5 Hz–440 kHz, slaved to a stable 99-MHz crystal oscillator in a crystal discriminator 3.4-MHz frequency-locked loop. In addition, the exciter could be operated in a transponder mode in which a signal from the receiver VCXO drove the transmitter. In this mode, the transmitter could be phase-modulated with engineering data. The frequency modulator was used to transmit either normal 600-line TV pictures through the planar array antenna, or 200-line TV pictures through the omniantenna.

During development of the transmitter, a detailed analysis of the minimum transmission margins for the TV and engineering modes revealed that some of these modes had negative margins. The amount of transmitted power necessary to ensure a positive margin with the worst combination of tolerances was 100 mW and 10 W for low- and high-power operation, respectively. Although the power amplifier and multipliers had been optimized since the first breadboard, they were capable of supplying only 2 W at 2.295 GHz. Because of this new power requirement, the solid-state power amplifier–multiplier chain development was terminated and a new design was investigated.

The new design retained transistor amplifiers and varactor multipliers to obtain the 100-mW output and a traveling-wave tube (TWT) was incorporated to obtain the 10-W output. This design required the addition of an electrical conversion unit (ECU) to provide the high accelerating voltages for the TWT. Since the low-power output had to be attenuated and matched to each TWT, a series of miniature attenuators from 4 to 10 db in half-decibel increments was developed and qualified. A latching RF transfer switch of the same type used for selecting the omnidirectional or planar array antenna was added to the transmitter to provide the switching between low- and high-power operation.

The exciter design was changed to improve the frequency stability of the wideband frequency modulator. This was achieved by eliminating the 99-MHz oscillator and applying the VCXO output directly to a crystal discriminator through an isolation amplifier. The modulation signals were AC-coupled to the modulator, and its frequency response was 0.5 Hz to 440 kHz. Design development was terminated when a new requirement, DC response of the wideband frequency modulator, was imposed on the transmitter for proper TV operation.

A new wideband frequency modulator design separated the TV and scientific inputs. The AC-coupling of the scientific data was retained and DC-to-220 kHz frequency response was added for TV modulation. In this design, a basic crystal oscillator was directly frequency-modulated from DC to 25 Hz for TV inputs and 250 Hz–50 kHz for scientific input. Higher frequency inputs were filtered and applied to a buffered phase modulator so that the deviation increased at +6 db per octave, supplying the equivalent high-frequency preemphasis. This composite design was necessary as a result of tests performed on the modulator. The tests showed that for input frequencies greater than 50 kHz that directly frequency-modulated the crystal, the output became distorted. There were spurious crystal responses for input frequencies above 100 kHz.

### 2. Receiver Evolution and Changes

The proposed receiver was a crystal-controlled, double-conversion receiver operating on the spacecraft 29-V nonessential bus. The receiver used two crystal oscillators: a fixed-frequency oscillator that supplied the second mixer local oscillator signal and a VCXO for supplying the first mixer local oscillator signal. The receiver operated in either of two modes: as an automatic phase-controlled (APC) receiver or as a fixed-frequency receiver. In the APC mode, the VCXO frequency was controlled by an error signal derived by comparing the receiver and received-signal phase relationship. In this mode, after establishing phase lock, the receiver was phase-coherent with the received signal and supplied a phase-coherent signal drive to the transmitter for transponding back to the ground station. When not operating in the APC mode, the VCXO was operated at a fixed frequency, converting the receiver to a fixed-frequency receiver with a 13-kHz bandwidth.

During the early development of the receiver, an automatic frequency loop that was active during nontransponder operation was added. It was clamped to a fixed value during transponder operation. This allowed the receiver to track the received signal greater than ±50 kHz in either the transponder or nontransponder modes. In

addition, the fixed-frequency crystal oscillator was eliminated and the second local oscillator signal was obtained by multiplying the VCXO frequency by two.

Three other significant changes were incorporated during the receiver development phase. First, the IF amplifier design was changed to use more advanced transistors. This change lowered the noise figure of the amplifier from 8.5 to 3 db, significantly lowering the signal power threshold of the receiver. Second, the crystal discriminator design was changed to improve its linearity and reduce its spurious responses. Third, the subcarrier discriminator was changed from a discriminator, amplifier, and gate combination to a discriminator, amplifier, Schmitt trigger, and wave-shaping circuit.

## B. Final Design Description

A simplified block diagram of the *Surveyor* flight radio system is shown in Fig. XX-1.

The two transmitters were identical crystal-controlled RF sources operated by ground command. Telemetry information could be supplied to either transmitter by the spacecraft signal-processing, TV, and science subsystems for broadcast to earth. Only one transmitter was operated at any given time. Either of the units could be commanded to transmit through any one of the three spacecraft antennas.

To obtain doppler information for spacecraft tracking, commandable interconnections were provided between each receiver and its respective transmitter (A to A or B to B) so that a coherent frequency relationship was maintained between the spacecraft received and transmitted signals (transponder mode).

The two omnidirectional antennas were positioned on the spacecraft so that their composite antenna patterns ensured reception of command information for any spacecraft attitude. Each omniantenna was permanently connected to a diplexer to permit simultaneous transmission and reception on the same antenna. The high-gain planar array antenna, which was used only for transmission from the lunar surface where wide information bandwidths were required, was a slotted waveguide array.

### 1. Receivers

The *Surveyor* spacecraft receivers were identical crystal-controlled, double-conversion, double-discriminator, frequency-modulation units. Table XX-1 lists the salient operating, physical, and functional parameters of the receivers. (All active elements used in the *Surveyor* receiver and typical decibel allocations are presented in Appendix B of this section.) Each receiver was entirely solid-state and had the capability of operating in either an automatic frequency control (AFC) mode or an APC mode. In the AFC mode, the received signal was acquired

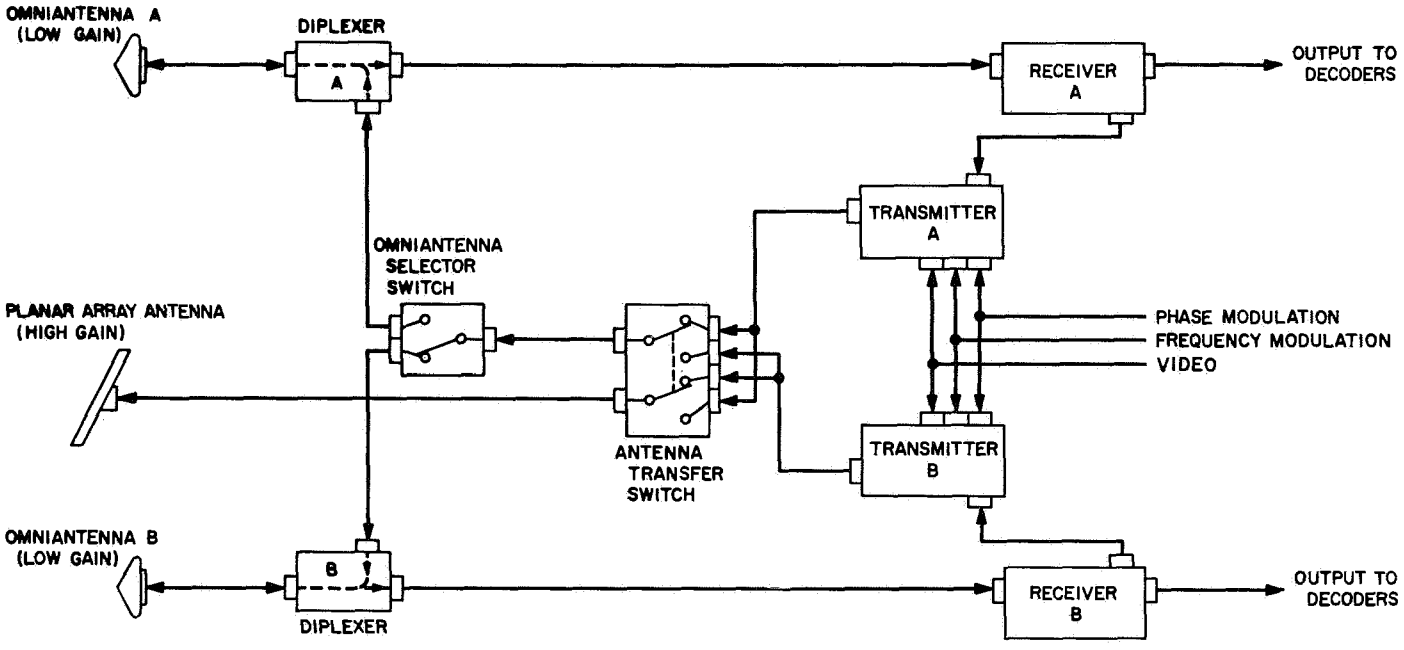



**Fig. XX-1. Radio system block diagram**

## Table XX-1. Receiver characteristics

| Parameter | Performance | Parameter | Performance |
|---|---|---|---|
| Operating frequency, GHz | 2.113312 | Receiver-to-transmitter isolation (nontransponder mode), db | ≥50 |
| Frequency drift (total), kHz | ±42.26625 (max) | Input power (DC) | |
| Noise figure, db | <13 | Voltage range, V | 17–27.5 |
| Threshold sensitivity (command)[a], dbm | <−114 | Current (transponder on), mA | 92 (max) |
| Input impedance (at frequency of operation), Ω | 50 | Current (transponder off), mA | 66 (max) |
| Dynamic range of automatic gain control, db | 40 (min) | Dimensions (overall, including power supply), in. | |
| IF bandwidth at 3 db down, kHz | 13 ±0.5 | Length | 8.0 |
| Tracking range of automatic frequency control, kHz | ≥50 (from zero) | Width | 3.0 |
| Phase stability (zero-to-peak)[b], deg | ≤36 | Height | 6.0 |
| Phase-lock-loop bandwidth (at receiver threshold)[c], Hz | 270 ±20 | Weight, lb | 4.0 |
| Phase-lock tracking range[c], kHz | ≥70 (from zero) | Active element quantity, units | 3 |
| Lockup slewing rate[a] (at −114 db sensitivity), kHz/sec² | ≥1 | Crystals | |
| Output power to transmitter (transponder mode), mW | 7.5 ±2.5 | Diodes | 43 |
| | | Transistors | 65 |
| | | Total number of discrete components | 1432 |

[a]Modulation index = 1.6.

[b]Translated to 2.113 GHz and measured in a noise-free phase-coherent receiver with a loop noise bandwidth of 30 Hz.

[c]Threshold = 0 db signal-to-noise ratio at receiver input.

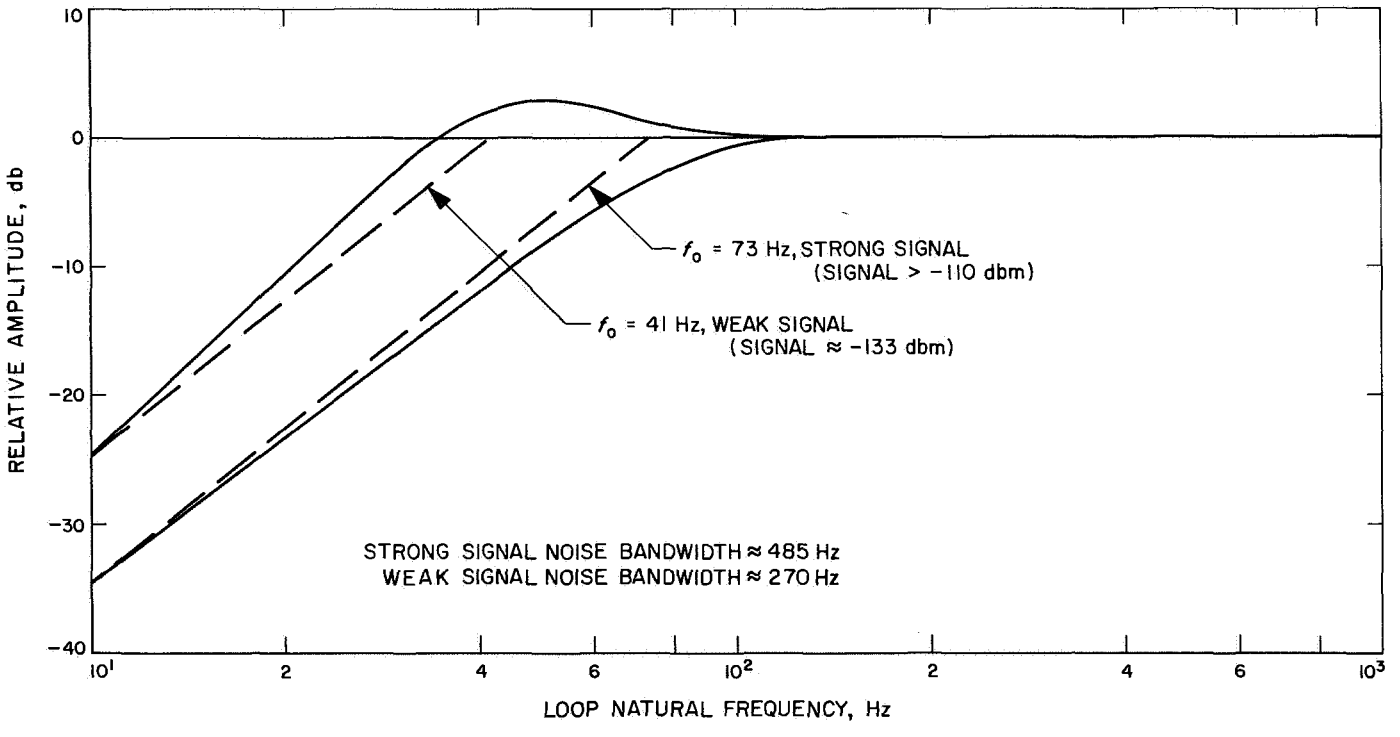



**Fig. XX-2. Receiver phase-lock-loop response**

and tracked in frequency by a VCXO, which in turn was voltage-controlled by the output of the IF discriminator.

In the APC mode, the control loop was similar, except that a phase detector provided the error voltage control of the VCXO, and thus the local oscillator tracked the input frequency in phase as well as frequency (Fig. XX-2). This coherent local frequency was switchable to control the associated transmitter for turnaround coherent phase-locked operation. The phase-lock mode enabled the ground stations to perform frequency-difference velocity determinations and cycle-count ranging.

Commands to the spacecraft were demodulated in the receivers. Commands from ground control were frequency-modulated on a subcarrier, which phase-modulated the main carrier of the earth-to-spacecraft transmissions. The first discriminator in the receiver detected the subcarrier signal. This signal was then applied to the subcarrier discriminator, which recovered the command information digits and supplied them to the command decoding subsystem.

Figure XX-3 is a simplified block diagram of the receivers. The first mixer stage was a tuned cavity device, which was used to produce a 47-MHz signal by combining the 2.113-GHz received signal with an internally generated 2.066-GHz reference.*

The 47-MHz signal output from the cavity mixer was applied to the first IF amplifier, where the signal was amplified and mixed* with a second locally generated reference signal to produce the 9.6-MHz second IF. An automatic gain control (AGC) signal, derived from the second IF amplifier, was used to maintain the first IF output at a fairly constant level.

At its input, the fixed-gain second IF amplifier contained a narrowband crystal filter that limited the noise output of the unit to a 13-kHz passband at 9.6 MHz. Figure XX-4 shows a typical frequency response curve

*In Fig. XX-3 the second mixer is shown (for clarity) separated from the first IF module. However, the mixer stage was actually a part of the IF module.

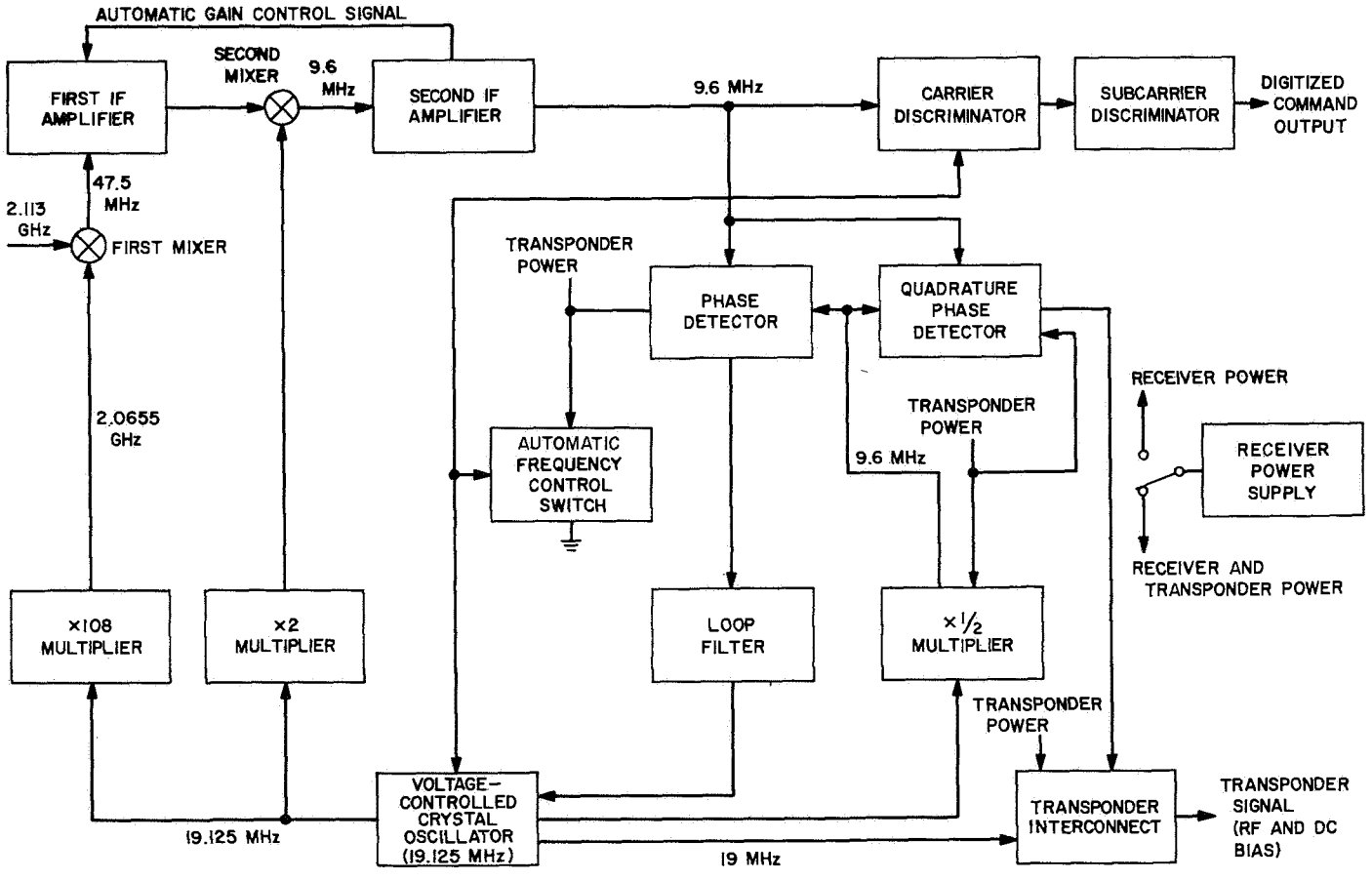



**Fig. XX-3. Receiver block diagram**

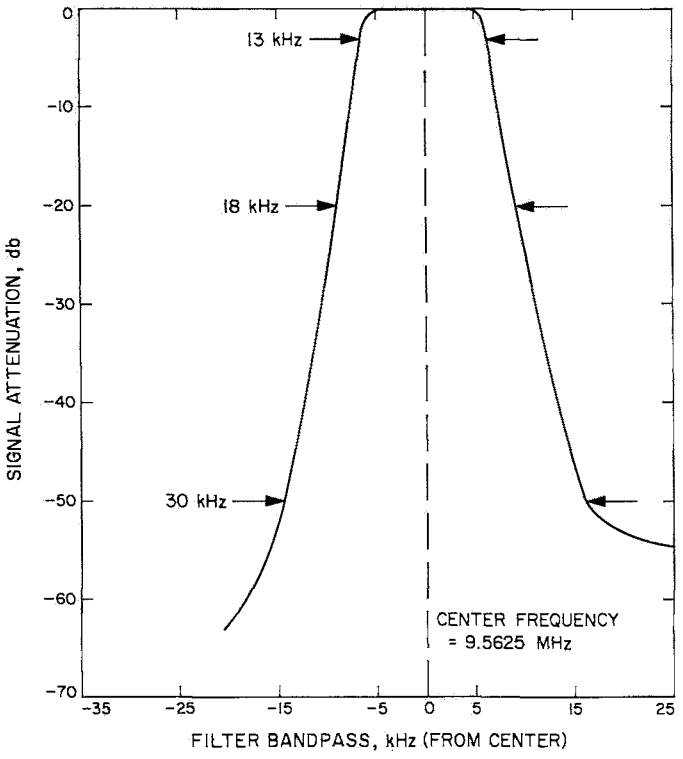



**Fig. XX-4. Receiver crystal filter response**

of the crystal filter, which determined the receiver bandpass. After additional amplifying, the 9.6-MHz signal was used to provide two outputs from the second IF. One output was the first IF AGC signal, which was a DC level proportional to the received RF power. The second output was limited to eliminate amplitude variations, and was fed to the first discriminator, the phase detector, and the quadrature phase detector. Signals to the phase detectors were significant only when the receiver was operated in the APC/transponder mode.

A double-tuned Travis type circuit was used in the first discriminator to separate the command sideband from the carrier and to provide a DC AFC signal, which had a magnitude and polarity directly related to the incoming frequency (Fig. XX-5) for control of the local VCXO. During receiver APC operation, the AFC signal was automatically switched out of the circuit. The command sidebands were applied to the second discriminator.

In the second discriminator, the command digital information was recovered from the subcarrier, and filtered and shaped. From this point, the command information was applied to the spacecraft command decoding subsystem for further processing.

Reference frequencies for the receiver and the transmitter control frequency during transponder operation were derived from the VCXO output. The highly stable VCXO frequency was governed at all times by either the AFC or APC signals, which were phased to maintain the incoming S-band signals in the center of the receiver passband. The 19-MHz outputs from the VCXO were supplied to the $\times 108$ multiplier, the $\times 2$ multiplier, the $\times \frac{1}{2}$ multiplier, and the transponder.*

A reference frequency for the cavity mixer was provided by the $\times 108$ multiplier by multiplying the 19-MHz signal from the VCXO in stages of three, three, two, and six. The first three stages of multiplication were accomplished by harmonic amplifiers tuned to a harmonic of the input frequency, while the final multiplication of six was performed by a varactor cavity multiplier.

The second cavity mixer reference frequency was obtained in the same manner except that the multiplication took place in a single $\times 2$ stage.

To obtain APC or transponder operation, a spacecraft command was required from the ground station.

Upon receipt of the proper command, the receiver ECU applied power to the receiver phase detectors, the $\times \frac{1}{2}$ multiplier, the transponder interconnect circuits, and the AFC grounding switch. All other receiver functions continued to perform as described here except that the VCXO was then controlled by the APC loop rather than the AFC loop. The VCXO 19-MHz output was processed by the $\times \frac{1}{2}$ multiplier to provide a 9.6-MHz reference for the two phase detectors.

The amplitude-limited output from the second IF module was phase-compared in the balanced phase detector to the input from the $\times \frac{1}{2}$ multiplier. An error signal from this comparison was applied to the loop filter, which provided the necessary time constants for the phase-tracking loop. The phase-tracking loop was closed by applying the loop filter output signal to the VCXO.

A 90-deg phase shift was applied to the reference signal of the quadrature phase detector so that, unlike the null-seeking tracking-loop detector, its output signal was at a maximum level when the receiver was operating at center frequency. This signal from the quadrature phase detector was used to gate the transponder interconnect circuitry, which allowed the 19-MHz VCXO

*Signals to the $\times \frac{1}{2}$ multiplier and the transponder were used only when operating in the APC/transponder mode.

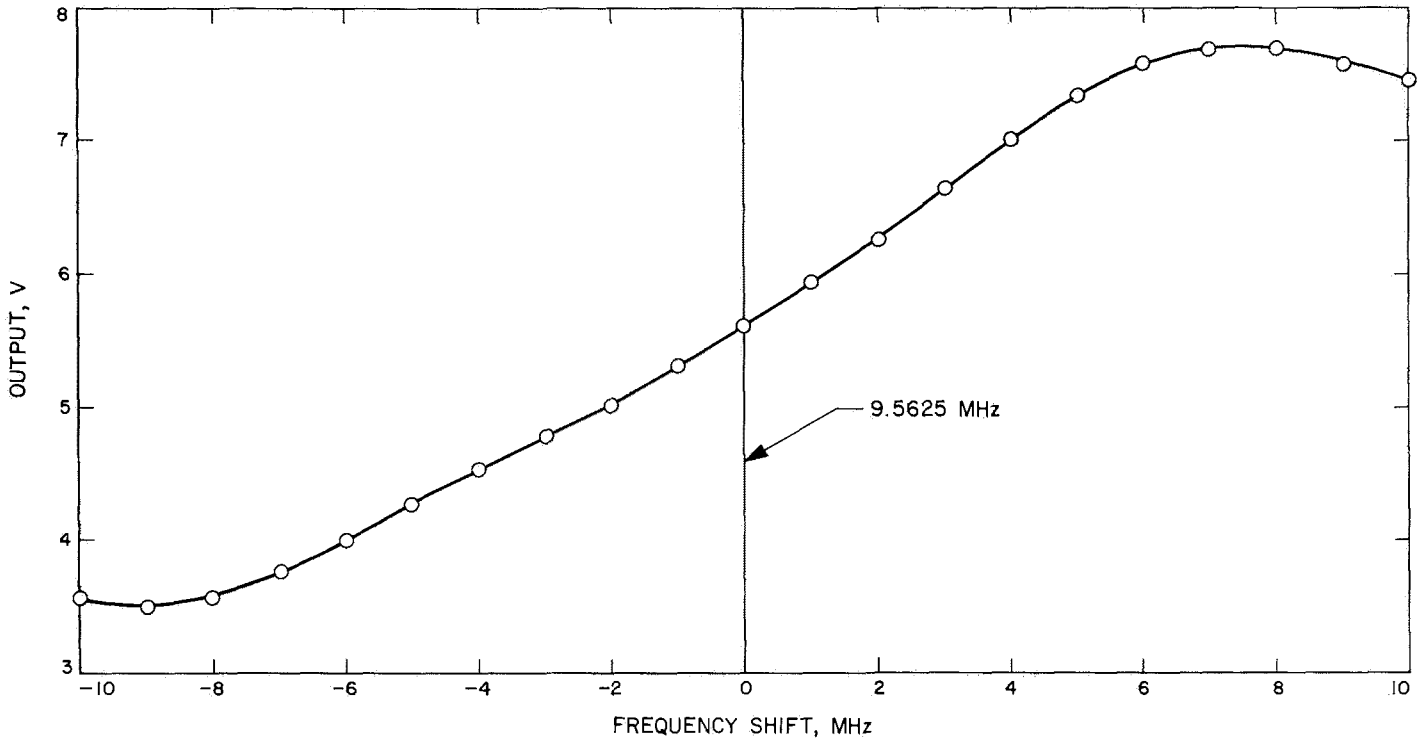



**Fig. XX-5. Receiver first discriminator automatic frequency control response**

signal to control the transmitter frequency for phase-coherent operations.

### 2. Transmitters

The two *Surveyor* transmitters were identical crystal-controlled units which, except for the power transfer switch and the TWT amplifier, were entirely solid-state. By command, each unit could be frequency-controlled from one of three separate sources: (1) the narrowband voltage-controlled crystal oscillator (NBVCXO), (2) the wideband voltage-controlled crystal oscillator (WBVCXO), or (3) the receiver VCXO (for operation in the transponder mode). Each transmitter also had the capability of operating in either high (10-W output) or low (100-mW output) power. The output power level was selectable by command. Each transmitter also had provisions for accepting a wide range of modulating signals. Table XX-2 lists the more pertinent transmitter parameters. Figure XX-6 is a block diagram of the transmitter.

The transmitters, unlike the receivers, were commanded on and off. Upon receipt of the "transmitter on" command from the spacecraft command subsystem, the ECU supplied power to the WBVCXO, the solid-state amplifiers, and multipliers (only the low-power wideband portion of the transmitters).

The WBVCXO was normally used only on the lunar surface where wideband TV and scientific data transmission were required. The oscillator, which was crystal-controlled for frequency stability, was provided with two modulation networks: one for wideband engineering/scientific data, and the other for TV data. Frequency response curves of the WBVCXO modulator are shown in Figs. XX-7 and XX-8. Both modulation networks used a combination of frequency and phase modulation.

The 19-MHz modulated carrier from the WBVCXO was applied to the input of the amplifier and $\times 5$ multiplier. Here the signal was amplified and multiplied to 95 MHz by the $\times 5$ varactor multiplier.

The output of the $\times 5$ multiplier was fed to a limiting amplifier to remove any existing amplitude modulation. The constant-amplitude 95-MHz modulated carrier received its final amplification in the three-stage power amplifier. Final frequency multiplication was accomplished by three varactor multiplier stages, which increased the frequency by factors of four, three, and two. The resultant output, nominally 100 mW of RF power at 2.295 GHz, was fed through a ferrite isolator which provided 40 db of attenuation against return energy to the antenna TWT switching circuitry.

## Table XX-2. Transmitter characteristics

| Parameter | Performance |
|---|---|
| Operating frequency, GHz | 2.295 |
| Wideband drift, kHz | |
| Long-term (lifetime of transmitter operating temperatures) | ±137.7 (max) |
| Short-term (1-sec period) | ±45.9 (max) |
| Narrowband drift, kHz | |
| Long term (lifetime, as defined above) | ±45.9 (max) |
| Short term (20-sec period) | 0.459 (max) |
| Phase stability[a] (zero-to-peak), deg | ≤ 36 |
| Power output, W | |
| Low-power model | |
| SC-1 through SC-4 | 0.1 (+2.5 db, −0.9 db) |
| SC-5 through SC-7 | 0.1 (min) |
| High-power mode | 10 (+2.5 db, −0.4 db) |
| Modulator characteristics | |
| Narrowband phase-modulated mode | |
| Bandwidth[b], kHz | 0.250 to 160 (min) |
| Sensitivity, rad/V | |
| At 2.295 GHz | 1 ±0.05 |
| At 250 Hz and 160-kHz band edge | 0.95 ±0.1 |
| Linearity, % of best straight-line characteristic | ±10 |
| Input level, V (p − p) | 5 (max) |
| Narrowband frequency-modulated mode | |
| Bandwidth[b] | DC to 1 kHz (min) |
| Sensitivity, Hz/V | |
| At 2.295 GHz | 1000 ±50 |
| At 1 kHz | 1000 + 50, −150 |
| Linearity, % of best straight-line characteristics | ±10 |
| Input level (zero-to-peak), V | ±5 |
| Wideband frequency-modulated mode | |
| Bandwidth, kHz | |
| Scientific data input[b] | 0.250 to 220 (min) |
| Television input | 0 to 220 (min) |
| Sensitivity, kHz/V | |
| Scientific data input | |
| At 2.295 GHz | 250 ±12.5 |
| At 25 kHz | 250 ±25 |
| At 250 Hz and 220 kHz | 250 + 12.5, −36.0 |
| Television input | |
| At 2.295 GHz | 250 ±25 |
| At 220 kHz | 250 + 25-50 |
| Linearity, % from best straight-line approximation | |
| Scientific data input | ±10 |
| Television data input | ±10 |
| Input level, V | |
| Scientific data (peak-to-peak) | 10 (max), AC-coupled |
| Television (referenced to ground) | ±5 (max) |
| Transmitter harmonic output (below carrier) | 35 (max) |
| Power requirements | |
| Low-power mode | |
| Input voltage, VDC | 29.0 +0.3, −0.4 |
| Input current, mA | |
| SC-1 through SC-4 | 235 |
| SC-5 through SC-7 | 365 |
| High-power mode | |
| Input voltage, VDC | 29.0 +0.3, −0.4 |
| Input current, A | |
| SC-1 through SC-4 | 2.4 |
| SC-5 through SC-7 | 2.54 |
| Traveling-wave tube amplifier | |
| Manufacturer | Hughes Aircraft Company |
| Type | 349-H-104 |
| Efficiency (including power supply), % | 15.9 |
| Voltage requirements, VDC | +60, −425, −1250 |
| Component quantity, units | |
| Crystals | 2 |
| Diodes | 88 |
| Transistors | 35 |
| Total discrete components | 1438 |
| Outline dimensions (including power supply) | |
| Length, in. | 15.225 (max) |
| Width, in. | 6.75 (max) |
| Height, in. | 4.5 (max) |
| Weight (including power supply), lb | 7.5 (typical) |

[a]Measured in a noise-free, phase-coherent receiver with a loop noise bandwidth of 30 Hz.
[b]This is 1-db point when excited from a source impedance of 1000 Ω.

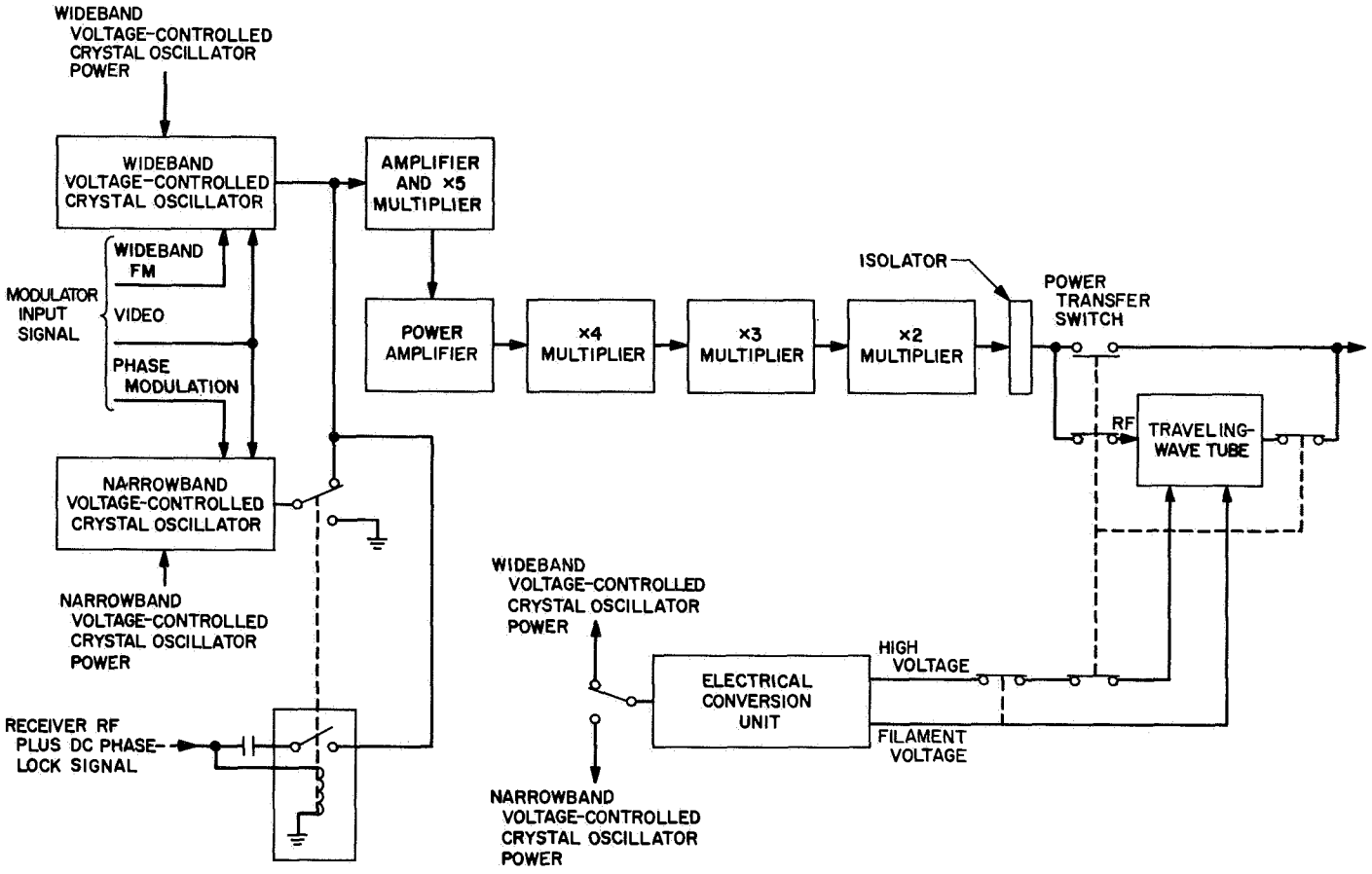



**Fig. XX-6. Transmitter block diagram**

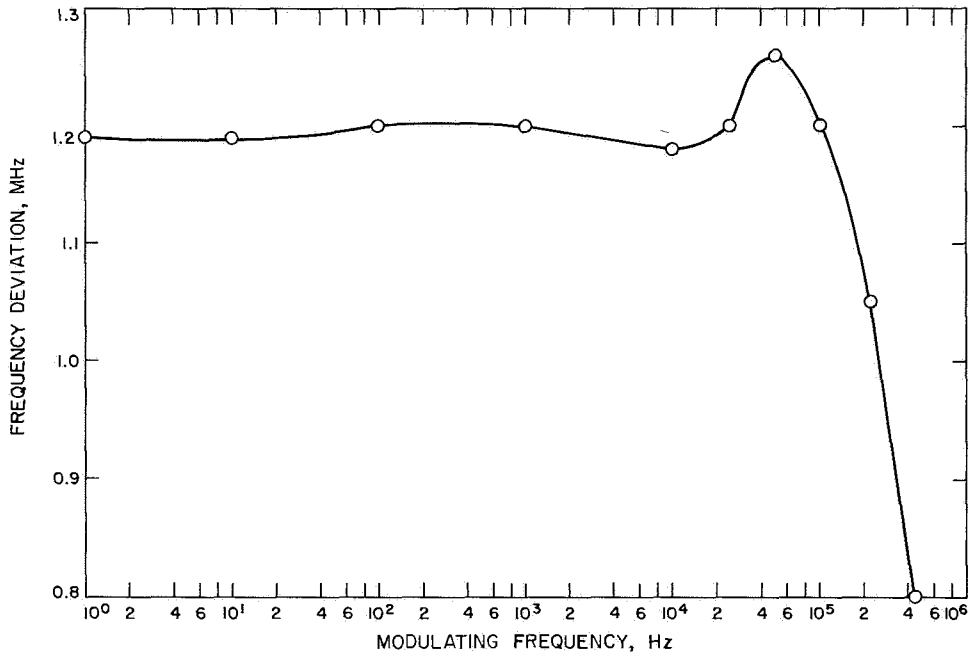



**Fig. XX-7. Transmitter TV wideband frequency modulator response**

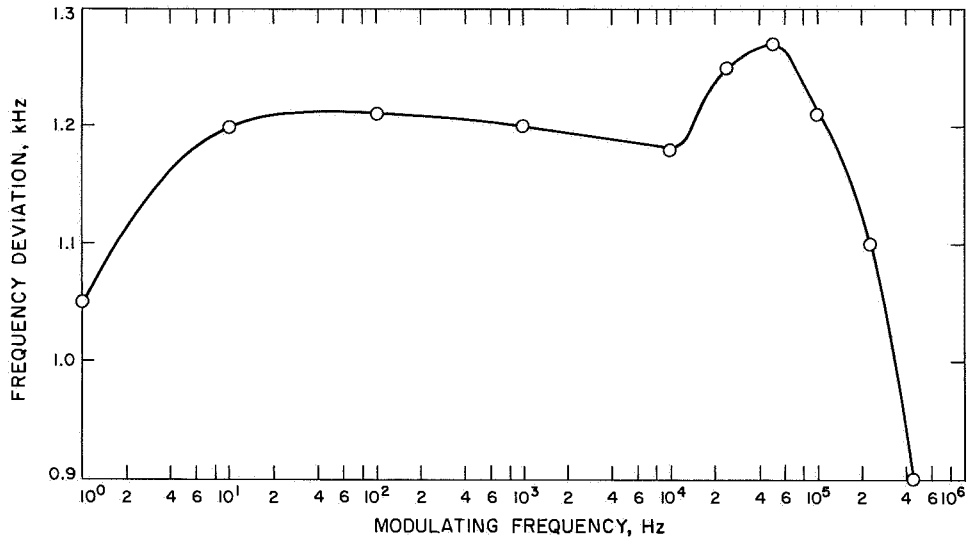



**Fig. XX-8. Transmitter scientific wideband frequency modulator response**

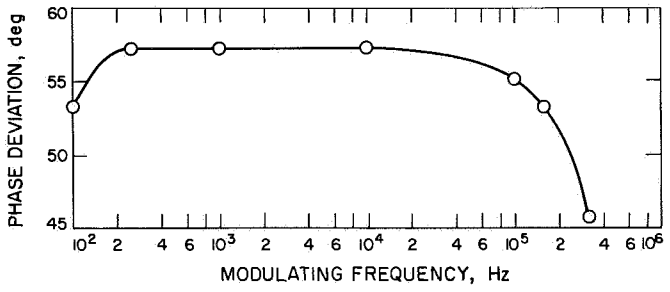



**Fig. XX-9. Transmitter phase modulator response**

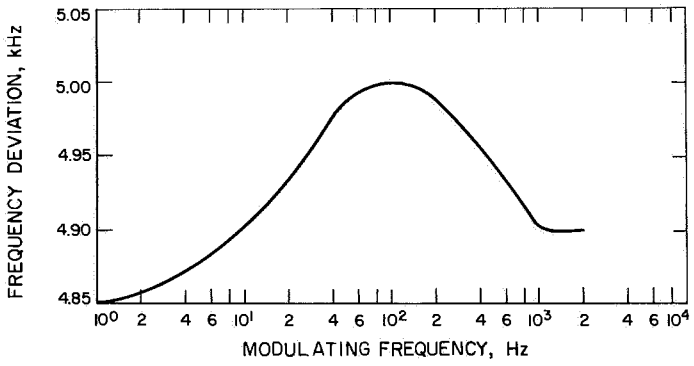



**Fig. XX-10. Transmitter TV narrowband frequency modulator response**

The NBVCXO was a high-$Q$ crystal oscillator with provisions for phase modulation (spacecraft engineering information) and narrowband frequency modulation (emergency TV data). Figures XX-9 and XX-10 show typical response curves. This oscillator, in conjunction with the receiver VCXO (transponder operation), was used during all spacecraft operations except those indicated for the WBVCXO. To achieve NBVCXO operation, the NBVCXO *on* command was transmitted to the spacecraft. Upon receipt of this command, the transmitter ECU turned off the WBVCXO and applied power to the NBVCXO. Under normal conditions, the 19-MHz carrier was applied to the phase modulator, where it was modulated by the telemetry information supplied by the spacecraft processing subsystem. After being amplified, the 19-MHz signal was fed to the amplifier and $\times 5$ multiplier, from which point the processing was as previously described.

During the major portion of the *Surveyor* flight, highly accurate doppler information was required for tracking purposes. To obtain the doppler data, phase-coherent receiver–transmitter (transponder) frequencies were required. Transponder operation was achieved by commanding either of the spacecraft receivers into the APC mode of operation (Section XV-B-1) and its associated transmitter (receiver A/transmitter A; receiver B/transmitter B) into the NBVCXO mode. Under these conditions, phase-locking the receiver to the earth-to-spacecraft signal applied a DC bias and the 19-MHz signal from the receiver VCXO to the transmitter NBVCXO module. The DC bias gated the transmitter NBVCXO signal to earth, while the 19-MHz carrier from the receiver was applied to the phase modulator as its replacement. This allowed the earth-to-spacecraft RF signal phase to coherently control the spacecraft-to-earth frequency by means of the APC loop.

When operating from the lunar surface, where wideband telemetry information was required, or during periods of spacecraft maneuvering and initial acquisition,

RF downlink signal levels, in the low-power mode, could become marginal because of spacecraft antenna attitudes and/or telemetry bandwidth requirements. To eliminate this possibility, each spacecraft transmitter had a commandable 10-W high-power capability. A series of three earth-generated commands was required to realize the high-power operation. First, the transmitter filament *on* command, which allowed the ECU to apply power to the TWT filaments, was transmitted. After a 90-sec warmup period, the power transfer switch was commanded to the high-power position, thus connecting the TWT amplifier in series with the transmitter. Finally, the TWT high voltage was commanded on. The filament and power transfer commands interlocked the high-voltage command to preclude any possibility of damaging the TWT.

Normal operational procedures required that only one transmitter be operated at any given time. However, the units were not interlocked and could be operated simultaneously. With both transmitters operating, no telemetry information could be transmitted, as operation of either unit automatically locked out the telemetry modulation signals to the other unit.

#### 3. Switching and Antenna System

The *Surveyor* radio switching and antenna system contained:

(1) Two omniantennas (A and B).

(2) Planar array directional antenna.

(3) Two diplexers (A and B).

(4) Two RF power monitors.

(5) Antenna transfer switch.

(6) Omniantenna selector switch.

Table XX-3 is a tabulation of the more pertinent equipment parameters. The purpose of this system was to connect the output of the operating transmitter to the appropriate antenna and to radiate and receive RF energy.

The two low-gain, omnidirectional turnstile antennas, which were circularly polarized, were used for simultaneous reception of command information and transmission of TV and engineering data. They were positioned on the spacecraft so that their composite antenna pattern ensured reception of command information for all spacecraft attitudes. The gain for the composite pattern of the two omniantennas for right-hand circular polarization was a minimum of 10 db in any given direction. Each omniantenna was permanently connected to a receiver through a diplexer. Located at the ends of fiber-glass booms, the antennas were extended away from the main body of the spacecraft during flight and lunar operations.

The high-gain planar array antenna, which was used only for transmission, was a slotted waveguide array. Radio-frequency energy was radiated through slots cut in the top surface of the antenna and fed in such a manner that the radiated energy was right-hand circularly polarized. In normal mission operations, the planar array antenna was used only on the lunar surface, and to take full advantage of the directional gain properties of the antenna, the unit was positionable by command from the controlling ground station.

Each diplexer was permanently connected to one of the omniantennas, and provided for simultaneous reception and transmission via that single antenna. Each unit was a double-tuned cavity device that had one arm tuned to pass 2.113 GHz and the other to pass 2.295 GHz. A minimum of 60 db of isolation was provided between the two arms.

The transmitter RF output from the diplexer was applied to the stripline power monitor. A small portion of the transmitter RF, during both high- and low-power transmission, was rectified and filtered by the power monitor and fed to the spacecraft signal processing system for transmission to ground control as an indication of transmitter output power.

Both the antenna transfer switch and the omniantenna selector switch were relay-operated coaxial switches commandable from ground control. The antenna transfer switch was a double-pole, double-throw unit connected to provide, as desired, the output of either of the transmitters to the input of the omniantenna selector switch or the planar array antenna. The omniantenna selector switch was a single-pole, double-throw device that directed the power to either of the two omniantennas.

## C. Modification of Design, Specifications, and Procedures

#### 1. Receivers

*a. Crystal mounting.* Extremely phase-stable signals were necessary to maintain phase-lock conditions in both the spacecraft and ground equipment. During the early test phases of the *Surveyor* receivers, phase jitter, particularly under vibration conditions, was excessive. Investigation of the problem, conducted primarily by HAC

## Table XX-3. Antenna and switching system characteristics

| Parameter | Performance |
|---|---|
| Omniantenna | |
| Type | Conical groundplane slot radiator |
| Feed | Turnstile |
| Polarization | Right-hand circular |
| Axial gain ratio, db | |
| At 2.113 GHz | 6 |
| At 2.295 GHz | 4 |
| Operating frequency, GHz | |
| Transmission | 2.295 |
| Reception | 2.113 |
| Operating bandwidth | |
| Lower edge, GHz | 2.110 |
| Upper edge, GHz | 2.30 |
| Impedance, Ω | 50 |
| Voltage standing wave ratio | |
| At 2.113 GHz | 2:1 (max) |
| At 2.295 GHz | 1.5:1 (max) |
| Overall dimensions, in. | |
| Diameter at base | 5.8 |
| Base to apex | 4.5 |
| Weight, lb | 0.33 (typical) |
| Planar array antenna | |
| Type | Nine-section, half-wave, crossed-slot, thin-wall waveguide, (parallel fed) |
| Feed | Slot-caupled feedbox (insertion screw tunable) |
| Polarization | Right-hand circular |
| Axial gain ratio, db | 2 (max) |
| Center frequency, GHz | 2.295 (factory tunable, ±5 (MHz) |
| Operating bandwidth, MHz | ±10 |
| Impedance, Ω | 50 |
| Voltage standing wave ratio | 1.5:1 (max) |
| Gain (over reference dipole), db | 27 ±0.5 |
| Beamwidth (3 db), deg | 7.0 |
| Overall dimensions, in. | |
| Length | 39.0 (max) |
| Width | 4.12 (max) |
| Height | 38.8 (max) |
| Weight, lb | 9.5 (max) |

| Parameter | Performance |
|---|---|
| Diplexer | |
| Resonant frequency, GHz | |
| Receiver arm | 2.113 ±5 |
| Transmitter arm | 2.295 ±5 |
| Image rejection (receiver arm), db | ≥ 20 (at 2017 ±5 MHz) |
| Insertion loss (resonant frequency each arm), db | ≤ 0.5 |
| Impedance (all arms), Ω | 50 |
| Voltage standing wave ratio (at resonant frequency) | 1.2:1 (max) |
| Isolation (at resonant frequency, each arm), db | 60 (min) |
| Weight, oz | 7.5 (max) |
| Overall dimensions, in. | |
| Length | 7 (max) |
| Width | 3.25 (max) |
| Height | 1.875 (max) |
| Manufacturer | Rantec Corp. |
| Part number | FSS 104 |
| Antenna transfer switch | |
| Switching action (RF) | Double-pole, double-throw; break before make |
| Voltage standing wave ratio (2.29–2.30 GHz) | 1.2:1 (max) |
| Crosstalk level, db | −40 (max) |
| Switching time, msec | 40 (max) |
| Insertion loss, db | 0.2 (max) |
| Pickup voltage (at 65°C), V | 16 (max) |
| Coil resistance (at 25°C), Ω | 5.0 (min) |
| Overall dimensions, in. | |
| Length | 4.64 (max) |
| Width | 2.0 (max) |
| Height | 2.0 (max) |
| Weight, oz | 14.6 (max) |
| Omniantenna selector switch | |
| Switching action | Single-pole, double-throw; break before make |
| Overall dimensions, in. | |
| Length | 3.03 (max) |
| Width | 2.45 (max) |
| Height | 1.09 (max) |
| Weight, oz | 9.0 (max) |
| All other parameters are identical to those of the antenna transfer switch | |

personnel, indicated that the major source of the excessive phase jitter was in the crystals used for frequency control of the receiver reference oscillator.

In the original receiver design, the crystal assembly was hard-mounted to the unit chassis. In an attempt to alleviate the phase instability problems, the hard-mounting of the crystals to the chassis was eliminated and the crystals were cushion-mounted. This was achieved by mounting the crystal in a flexible polyurethane foam block enclosed in a metal box to which the crystal case was grounded. This improved the performance by an order of magnitude, but still all receivers could not meet the phase-jitter requirements.

The next step in eliminating the instability was to modify the crystal. An advanced crystal design, using ribbon strips for mounting the crystal to the header of the crystal case, was substituted for the foam-mounted units. This crystal had been especially designed for low phase jitter, and tests showed that with it all flight receivers could satisfy the vibration and shock requirements.

*b. Local oscillator.* Early spacecraft testing of the *Surveyor* receivers revealed that some units would intermittently exhibit a degraded threshold operation. Symptoms of the problem were loss of receiver sensitivity, loss of tracking range, and a shift in the AGC curves.

Initial investigation of the problem at the unit level indicated the problem was temperature sensitive. Further investigation revealed the local oscillator bandpass was distorted (Fig. XX-11). The distortion was suspected to be a result of alignment procedures used in the original setup of the receivers. The practice at that time was to maximize the local oscillator power output while monitoring with a power meter. While providing slightly more power output at ambient temperature, this procedure did not take into account the tuning effects on the bandpass as a whole. As a result, the variation of the local oscillator frequency with temperature would cause the power output to fall unexpectedly.

To correct this problem, all receivers were recycled to a new procedure wherein some power output was sacrificed for bandwidth, and all local oscillators were frequency-swept at the conclusion of the tuning process to ensure proper bandwidth. Local-oscillator power output was far greater than that required for proper receiver operation, so that no reduction in performance was experienced in the bandwidth-vs-power tradeoff.

It was believed all local oscillator problems were resolved by these process changes. However, this was not true. During the SC-3 vibration testing, the symptoms reappeared. Upon examining the anomalous behavior of

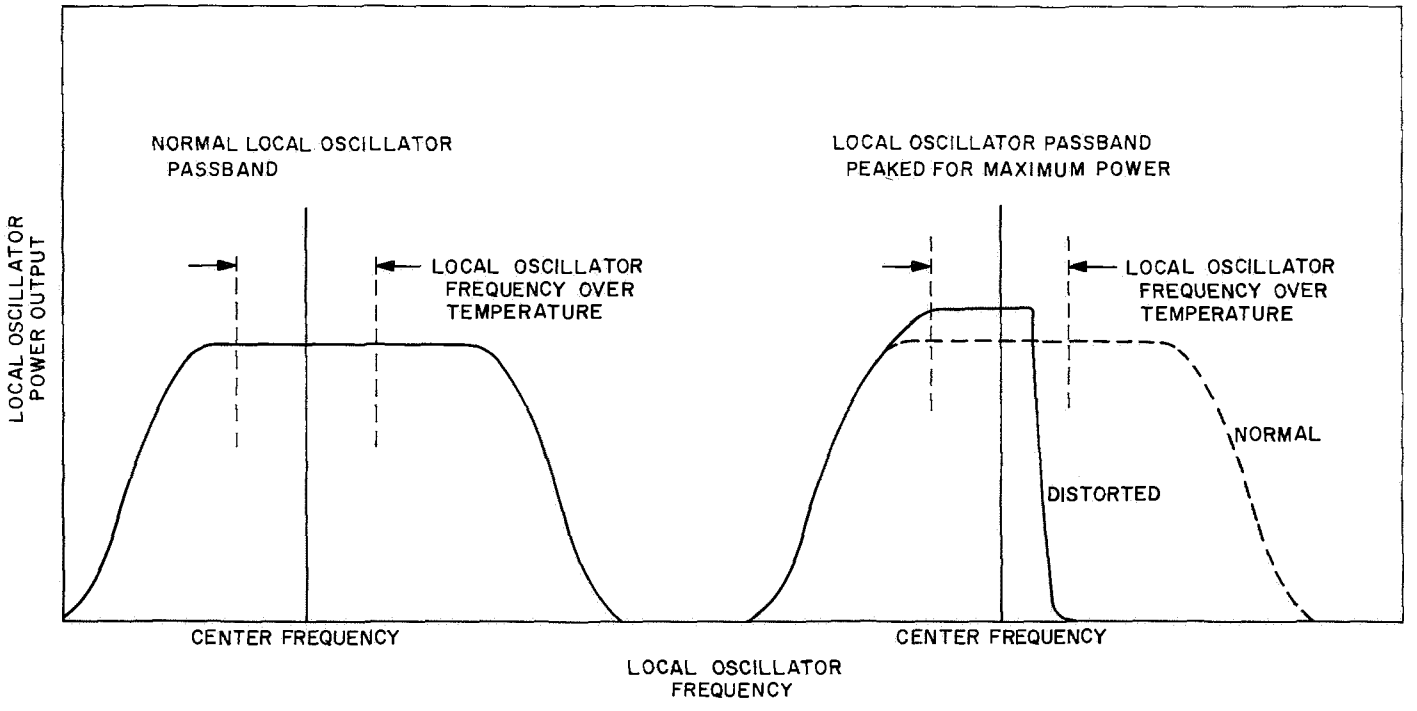



**Fig. XX-11. Local oscillator characteristics**

the receiver, discovery was made that the variable piston-type capacitors, used for trimming the local oscillator ×6 multiplier, could undergo a change in the tuning slug set position under vibration conditions. The variation in capacitance resulted in the same bandwidth distortion.

To eliminate the problem, the capacitor tuning slugs were staked in place with epoxy at the conclusion of final tuning. No further trouble of this type occurred.

*c. Interstage coupling.* Early in the receiver test phases, several instances of spurious internal oscillation and interference were encountered. The interference problems were caused by interstage coupling of high-frequency signals. The coupling problems were resolved by incorporating metallic shields between various stages of the first and second IF modules and in the phase detectors.

**2. Transmitters**

*a. Electrical conversion unit redesign.* A test of the *Surveyor* transmitters under thermal-vacuum conditions was not a flight acceptance requirement in early 1965. However, JPL experience indicated this should be an area of serious concern. To validate this concern, special tests were performed on the spacecraft electronics compartments. These tests indicated the compartment would have an internal pressure of approximately $10^{-2}$ torr at the time the transmitters would be commanded to high power for initial spacecraft acquisition. Additional tests, conducted on the transmitter, showed that the unit's high-voltage ECU would arc over at approximately $2 \times 10^{-2}$ torr. This indicated that the transmitter would arc when commanded to high power at injection, thus preventing a normal acquisition—possibly causing loss of the spacecraft mission.

To eliminate the possibility of critical pressure arcing, the high-voltage ECU was encapsulated with 8 lb of polyurethane foam. It was calculated that, although the foam would slowly outgas and eventually allow the ECU to reach its critical pressure, this would not occur during the normal lifetime of the spacecraft.

Tests conducted on the transmitters to verify the effectiveness of the foam insulation disclosed arcing at approximately $10^{-3}$ torr. Investigation of the ECU showed that the arcing occurred between the high-voltage printed circuit and the nut plates fastened to the metal backing plate, an area not penetrated by the foaming process.

To remedy this breakdown problem, all high-voltage printed circuits and high-voltage leads were replaced with point-to-point wiring methods so that the foaming process would be effective. Arcing of the transmitters did not occur after this change was incorporated.

*b. Transmitter thermal interface.* With approximately 74 W of power dissipated internally in the transmitter during high-power operation, a good thermal interface with the spacecraft mounting surface was required to maintain equipment temperatures within reasonable limits. During the T-21 spacecraft test phase, it was discovered the spacecraft/transmitter interface was not optimum. In fact, transmitter high-power operation was limited to 1 hr maximum to preclude overheating.

To overcome this characteristic, a sheet of 5-mil indium foil was installed between the unit and its mating surface, and an installation torquing sequence procedure was defined to minimize the thermal resistance between the transmitter and its mounting surface. These steps effectively overcame the thermal constraints on the transmitter operation.

*c. Transmitter multiplier redesign.* During thermal-vacuum testing, at a tray temperature of 125°F, the flight transmitters were unable to satisfy the minimum low-power-output specification. This was the combined result of the operating temperatures of the final power amplifier module and the ×6 varactor multiplier and the changes in the matching of these two modules over the temperature range. Although the mission signal level margins were adequate, even at the lower output levels, the internal component temperatures were of great concern.

The first attempt to alleviate the temperature conditions was to decrease the thermal resistance between the multiplier varactor diodes and their housing by coating the stripline in the vicinity of the diodes and the interior walls of the module with a heat-radiating and -absorbing material. While providing some improvement, this solution was unsatisfactory because it could not affect the power amplifier temperatures and did not completely eliminate the concern over the varactors.

The next approach was to redesign the power amplifier (A4 module) for higher efficiency, using newer types of transistors and improved thermal characteristics. The ×4 varactor multiplier, which had previously been contained in the A4 module, was redesigned as a separate assembly. Redesign of the ×6 multiplier entailed splitting the module into separate ×3 and ×2 units. In all of the new multipliers, the diodes were operated in a shunt rather than series configuration as they had been

previously. In the shunt configuration, the diodes were electrically and physically attached to the chassis, thus obtaining direct thermal dissipation.

### 3. Antenna Switching System

The RF coaxial relays were the only areas of concern in the antenna switching network. Inductive transients, generated by actuating the relay coils, could be coupled into other areas of the spacecraft and cause inadvertent commanding and/or possible damage to other electronic units. Additionally, if a switch chattered or did not completely transfer, its coil could not be removed from the power source because microswitches, activated by the transfer movement, were used to break the coil current. This condition could cause excessive battery drain that might have been catastrophic to a spacecraft mission.

Elimination of the inductively coupled transients was accomplished by installing flyback diodes across each relay coil. The possibility of a sticking switch causing excessive power drain was removed by adding a transistor switch in series with the return lead of each coil. This transistor was biased on and off by a monostable flip-flop keyed by the command pulse actuating the transfer switch. The time constant of the flip-flop was greater than the 40 msec maximum transfer time of the switch, and ensured that the coil current would be interrupted. With the addition of the transistor switches, the requirement for the microswitches ceased to exist. However, because the microswitches were inside the coaxial switch housing, it was decided to leave them in the circuit. This proved to be unwise. After numerous operations of the relay switches, it was found that the microswitch contacts had carbonized and were arcing when opening. Resultant transients were again causing inadvertent switching of other equipment.

The final solution was to open each coaxial switch and remove the microswitches. No further switching problems were encountered.

## D. Construction Techniques and Manufacturing Experience

The *Surveyor* radio subsystem was largely modular in construction (Figs. XX-12, XX-13, and XX-14). Except for the first mixer stage (a purchased tuned-cavity device), the modules of the high-frequency multipliers, the second discriminator, and the ECU, were of T construction (Fig. XX-15).

This basic chassis was adopted to provide necessary internal and external shielding, and permit close mounting of components for reduced parasitic inductance and capacitance effects. The DC and high-frequency portions of the circuits were separated by the vertical member of a T-bar. The T-bar was fabricated from two pieces of 0.010-in.-thick aluminum sheet that was gold-plated and then solder-brazed at the flange between the vertical member and the base. A typical T-bar measured 1 in. wide, 1 in. high, 6 in. long, and weighed only a few ounces.

Because of the high frequencies involved, only low-loss and low-dielectric-constant organic insulating materials were used. Most of the components were mounted to small sections of a sandwich composed of a fiber-filled Teflon terminal board bonded with epoxy resin to a sheet of polyurethane foam bonded to the T-bar. The components were installed on terminals mounted in the terminal board. Capacitance to ground was controlled by maintaining a close tolerance on the thickness of the foamed polyurethane sheet. As far as the circuits were concerned, the filled Teflon and polyurethane foam were electrically equivalent. Terminal locations were closely controlled in all three dimensions. This dimensional control was required to ensure the exact location of components within the three-dimensional array created by the T-bar.

To minimize inductive effects and power losses in component leads, solder joints were made within 0.011–0.050 in. from the component bodies. This spacing was much closer than was normally recommended by the component manufacturers, but experience showed that adequate reliability could be maintained with these lead lengths. This was possible through the use of low-wattage irons and clean surfaces. The latter permitted quick wetting by the solder and therefore a minimum application of heat. Two or three components were interconnected at each terminal through short, soldered-in leads. Very little discrete wiring was used.

Components that required grounding or heat sinks were mounted to the T-bar through any of the three surfaces. When good heat transfer and ground contact were required, the part was bonded with a silver-filled epoxy. To maintain good heat transfer, but with insulation from ground, a solid boron nitride cup or disk was included between the transistor and silver–epoxy interface. In most cases, electrical isolation and adequate heat transfer were achieved by bonding the part with a polyester, double-backed adhesive tape. This type of

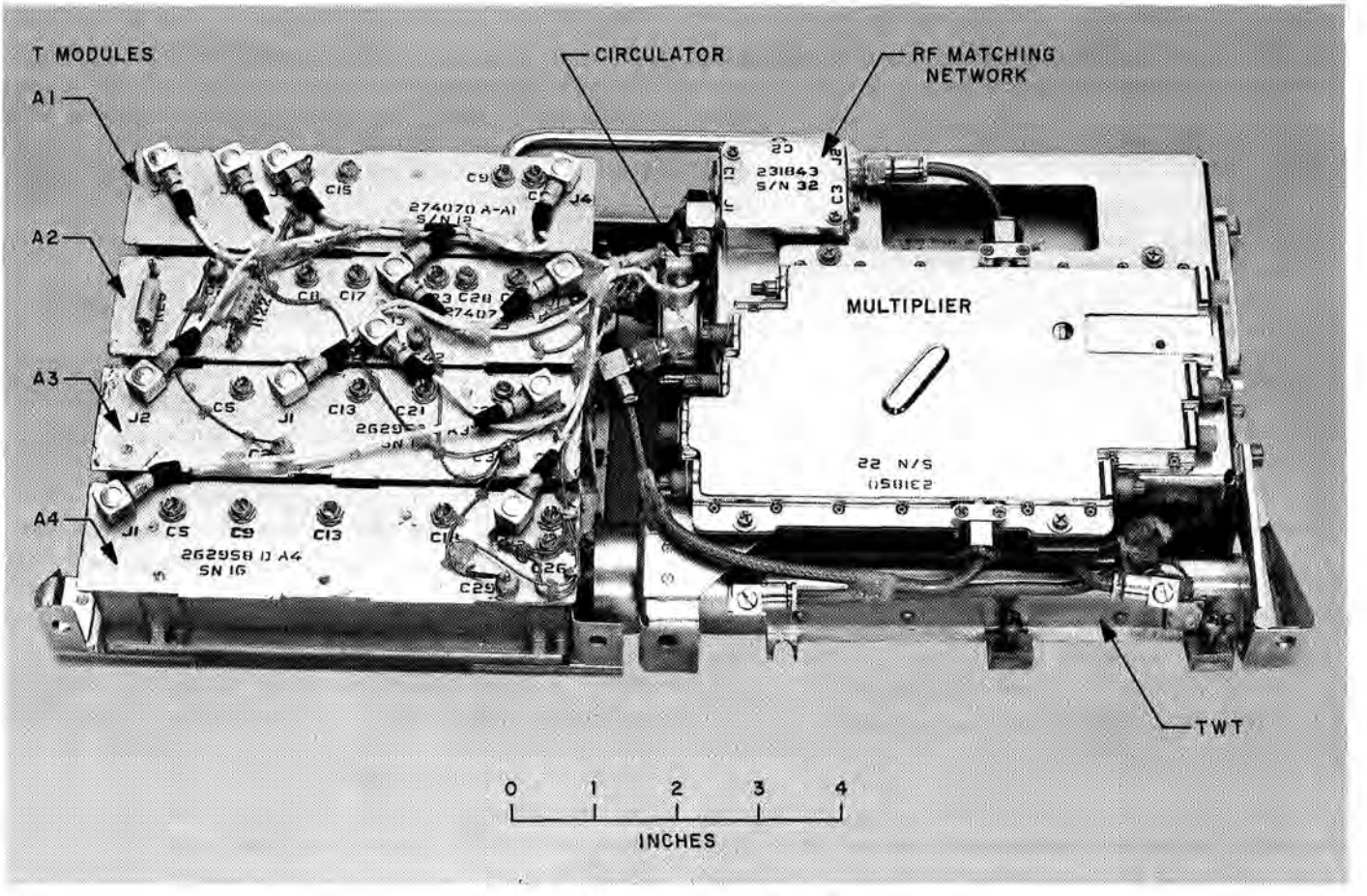



**Fig. XX-12. Transmitter top view**

mounting was preferred because it facilitated part replacement. Holes in the horizontal member of the T provided access to the adjustable piston capacitors for final tuning. Silver-filled epoxy resin or solder was used to ground one side of the piston capacitor.

The two sides of the T-bar were interconnected by feedthrough filters or capacitors mounted within the plane of the vertical member of the T. Input/output connections were made to coaxial fittings extending through the horizontal element of the T.

Where required, the IF stages were shielded from each other as well as from the DC portions by including an additional aluminum member normal to the elements of the T.

The assembled T-bar was contained within a can which was formed from 0.016-in.-thick aluminum sheet. The can was solder-sealed to the edge of the horizontal portion of the T after a foam-in-place polyurethane resin was deposited within the unit. To check the unit electrically before foaming, the effect of the resin was simulated by filling the unit with hollow glass spheres which had essentially the same dielectric constant as the foam. If the unit was still within tuning range, the spheres were replaced with foam to complete the assembly. The foam provided support for the components and, with the skin formed by the can, made a very rigid module. The thin aluminum sheet stock was used throughout to reduce weight.

Both the transmitter and receiver ECUs, as well as the second discriminator in the receiver, were of different construction and used point-to-point wiring.

The point-to-point assembly technique required an aluminum chassis (usually a rectangular box 1–2 in. deep) formed to the space and volume requirements. The chassis was plated for corrosion and solderability. The ground terminals and standoff terminals were installed as required. The transistors in the IF circuits were

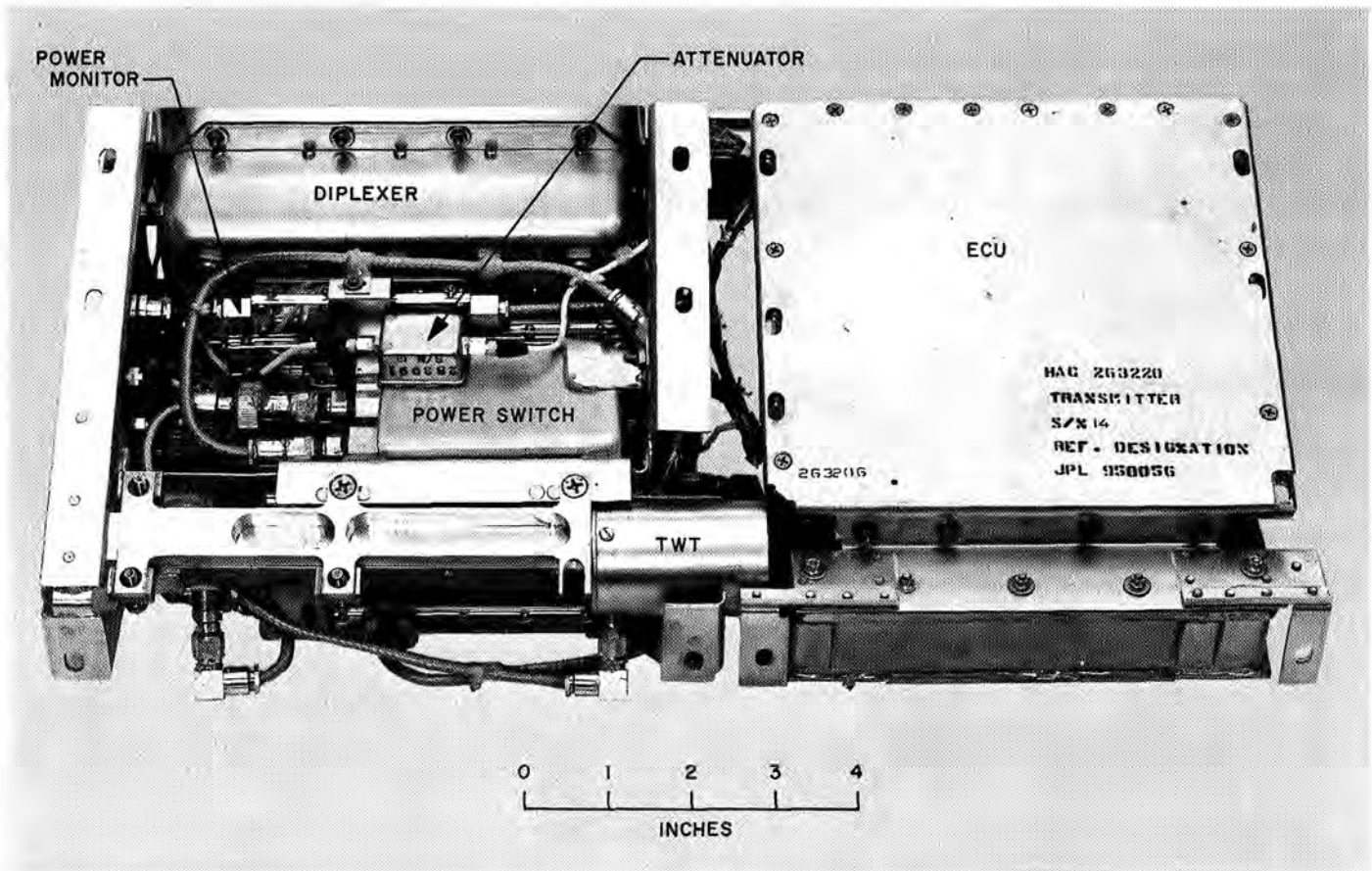



**Fig. XX-13. Transmitter bottom view**

bonded to the chassis with silver–epoxy. Other transistors were insulated with Mylar tape and epimided to the chassis. Large power-dissipating resistors were also epimided to the chassis. These components were soldered together, wire lead to wire lead. The wired parts were bonded or coated as required. The cover was installed and the unit was foamed (polyurethane) to give the unit and the components added mechanical strength.

This method was flexible to changes in development and allowed high-density packaging. However, the assembly method was usable for limited volume operation only because the foam encapsulant made rework operations extremely difficult.

Though most of the subsystem modules were not difficult to produce, the phase detector and the multiplier modules did introduce some problems.

The balanced phase detector was the most difficult unit to assemble. The primary reason for the problem was the variation in components, which made proper balance hard to attain. Balance was achieved by making component values selectable.

Problems in building the $\times\frac{1}{2}$ multiplier module early in the project stemmed from difficulty in obtaining varactor diodes that were matched to the degree necessary. Through experience, it was found that the requirements of the unit could be met by making other components selectable. From this point on, the units were producible in a reasonable amount of time.

Maintaining some semblance of hardware delivery schedules was a continuous problem throughout the program. Table XX-4 indicates the time differences between scheduled delivery and actual delivery of some selected control items. Optimistic scheduling consistently failed to allow for the problems which led to the design changes previously outlined. Human error during the manufacturing stage, component failures in the test cycles,

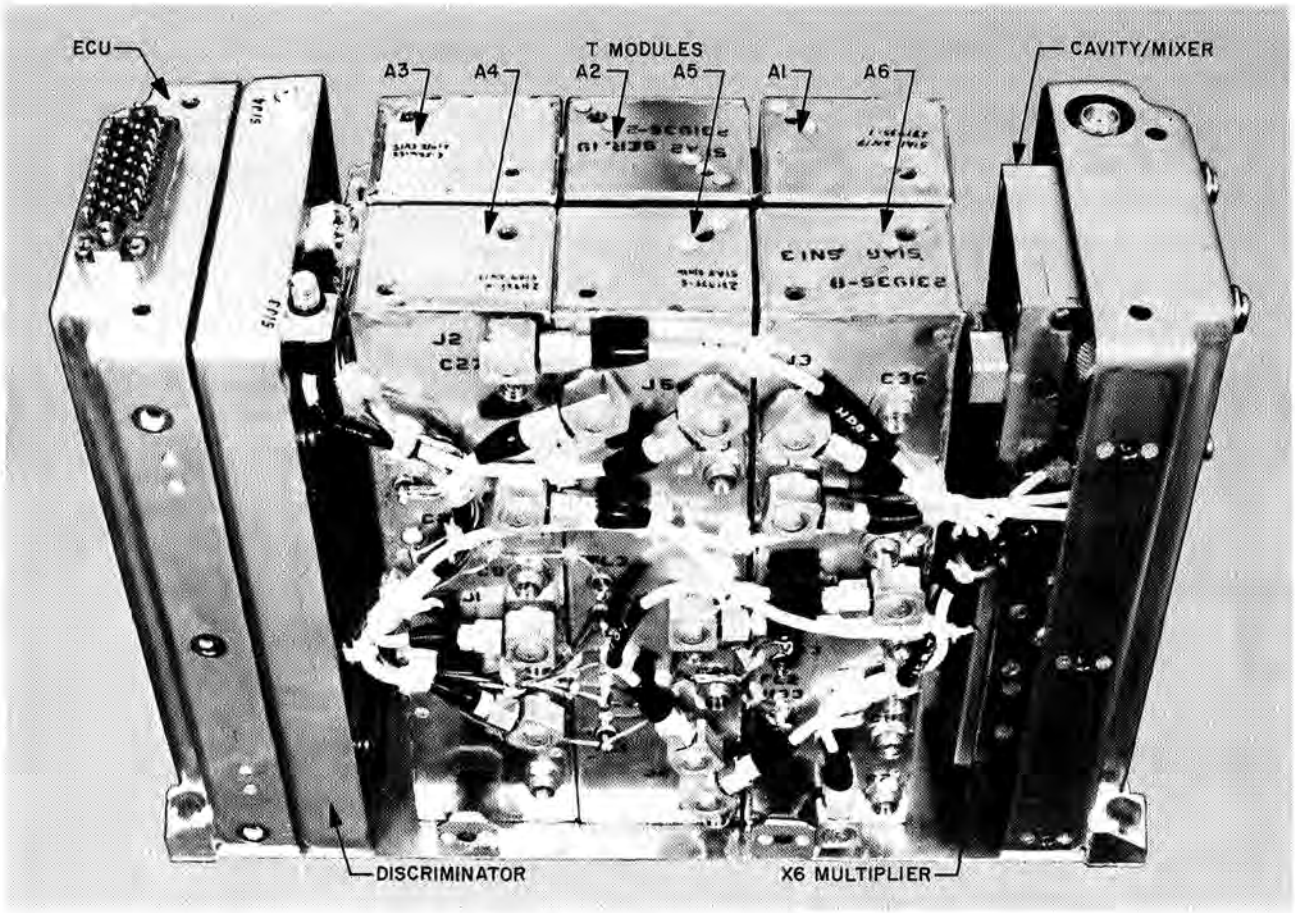



**Fig. XX-14. Command receiver**

and the difficulties involved in reworking foamed modules contributed heavily to schedule slippage.

To obtain an idea of the contribution to scheduling difficulties made by the almost continuous rework cycling, a bar chart of the history of the RF equipment required for a typical spacecraft (SC-5) is shown in Fig. XX-16. The continuous recycling of failed equipment from the test and spacecraft areas forced backlogging of work on new hardware for later flights.

## E. Testing

Specifications of the radio subsystem parameters were so broad at the beginning of the program that undesirable characteristics in the equipment could pass through the testing phase without detection. This was not a great problem during the design, prototype, and first-build phases because the testing was performed by engineering personnel. As the program matured and the acceptance testing was turned over to quality assurance personnel—who, by reason of unfamiliarity, were not as capable of detecting equipment faults—the looseness of specifications became intolerable. To overcome the shortcomings in the testing processes, a successive review of the test program was begun. Test procedures were reviewed and tightened, test methods improved where necessary, and various recording devices introduced. Cognizant engineering personnel were required to review all test records and information as a condition of acceptance.

At least one unit from each control item group (receivers, transmitters, etc.) was designated as a type approval unit. This unit was subjected to type approval testing to qualify the basic group for space application. Type approval testing was completed successfully for the basic design of all control items. Additionally, the major redesign of the transmitters was qualified by additional type approval testing.

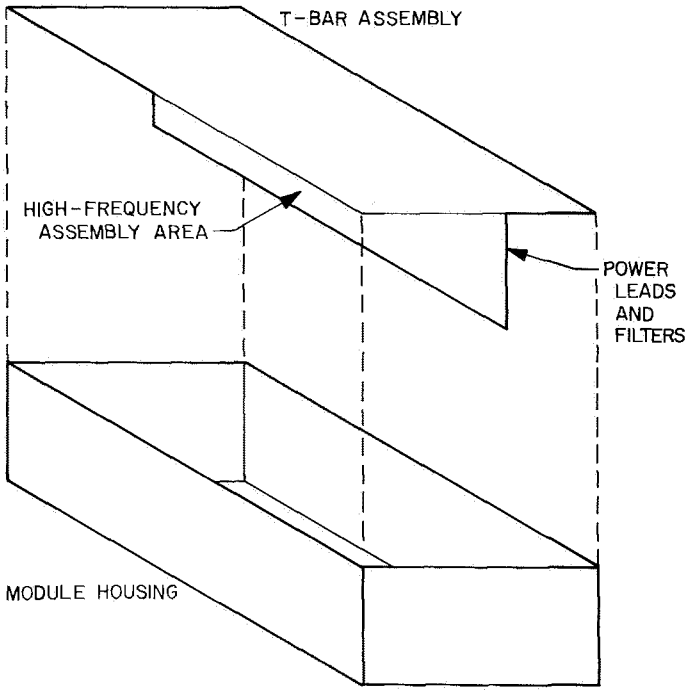



**Fig. XX-15. T-bar module general arrangement**

All flight units were exposed to a series of flight acceptance tests at least once before delivery to the spacecraft. Most equipment was processed through the test cycle several times (Fig. XX-16).

Normal flight acceptance testing of all units consisted of these tests:

(1) Preflight acceptance functional.

(2) Thermal cycle (atmospheric conditions).

(3) Thermal vacuum.

(4) Vibration (flight acceptance levels).

(5) Postvibration functional.

In both flight acceptance and type approval testing, all units were required to operate, both during and after exposure, with no significant degradation.

Phase jitter was the greatest single troubleshooting and evaluation problem encountered in testing the *Surveyor* radio equipment. Extreme sensitivity of the phase-lock loop to perturbations in phase, frequency, or signal interruptions resulted in problems originating from many sources being classified as phase jitter. The major sources of phase jitter were:

(1) Crystal instability.

(2) Intermittent solder joints.

(3) Intermittent cables.

(4) Variable piston-type capacitors.

(5) External interference signals.

Jitter problems caused by items 2, 3, and 5 were particularly difficult to isolate simply because of their intermittent nature. Temperature cycling at the unit area was the most useful tool for isolating solder joint and cable problems. Uncontrolled RF radiation at the HAC testing facility presented many interference problems that were classified as phase jitter. These problems were seldom pinpointed exactly because of the difficulty in maintaining and/or reestablishing exact conditions.

## F. Performance Summary

The performance of the communications equipment in flight was extremely good. All known major problems —and there were many—occurred during the manufacturing and test phases. Although some components (RF switches, variable capacitors, and crystals) and some areas (parameter stability and operating temperatures) could have been improved to ease the qualification process, the equipment was adequate for the required mission.

**Table XX-4. Subsystem hardware scheduled delivery vs actual delivery**

| Control item | Serial No. | Part No. | Scheduled delivery | Actual delivery | Difference, wk | Control item | Serial No. | Part No. | Scheduled delivery | Actual delivery | Difference, wk |
|---|---|---|---|---|---|---|---|---|---|---|---|
| Receiver | 11 | 231900 | 3/1/65 | 3/9/65 | 1 | Transmitter | 14 | 263220 | 6/20/65 | 5/17/65 | −4 |
| Receiver | 13 | 231900 | 4/30/65 | 4/22/65 | 0 | Transmitter | 18 | 263220 | 7/16/65 | 6/15/65 | −4 |
| Receiver | 20 | 231900 | 1/15/66 | 6/2/66 | 20 | Transmitter | 11 | 302440 | 5/9/66 | 7/26/66 | 10 |
| Receiver | 28 | 231900 | 5/11/66 | 12/8/66 | 30 | Transmitter | 14 | 302440 | 7/8/66 | 2/20/67 | 32 |
| Receiver | 29 | 231900 | 6/8/66 | 3/2/67 | 38 | Transmitter | 17 | 302440 | 9/10/66 | 3/21/67 | 28 |
| Transmitter | 12 | 263220 | 5/21/65 | 6/4/65 | 2 | Transmitter | 18 | 302440 | 10/1/66 | 5/8/67 | 31 |

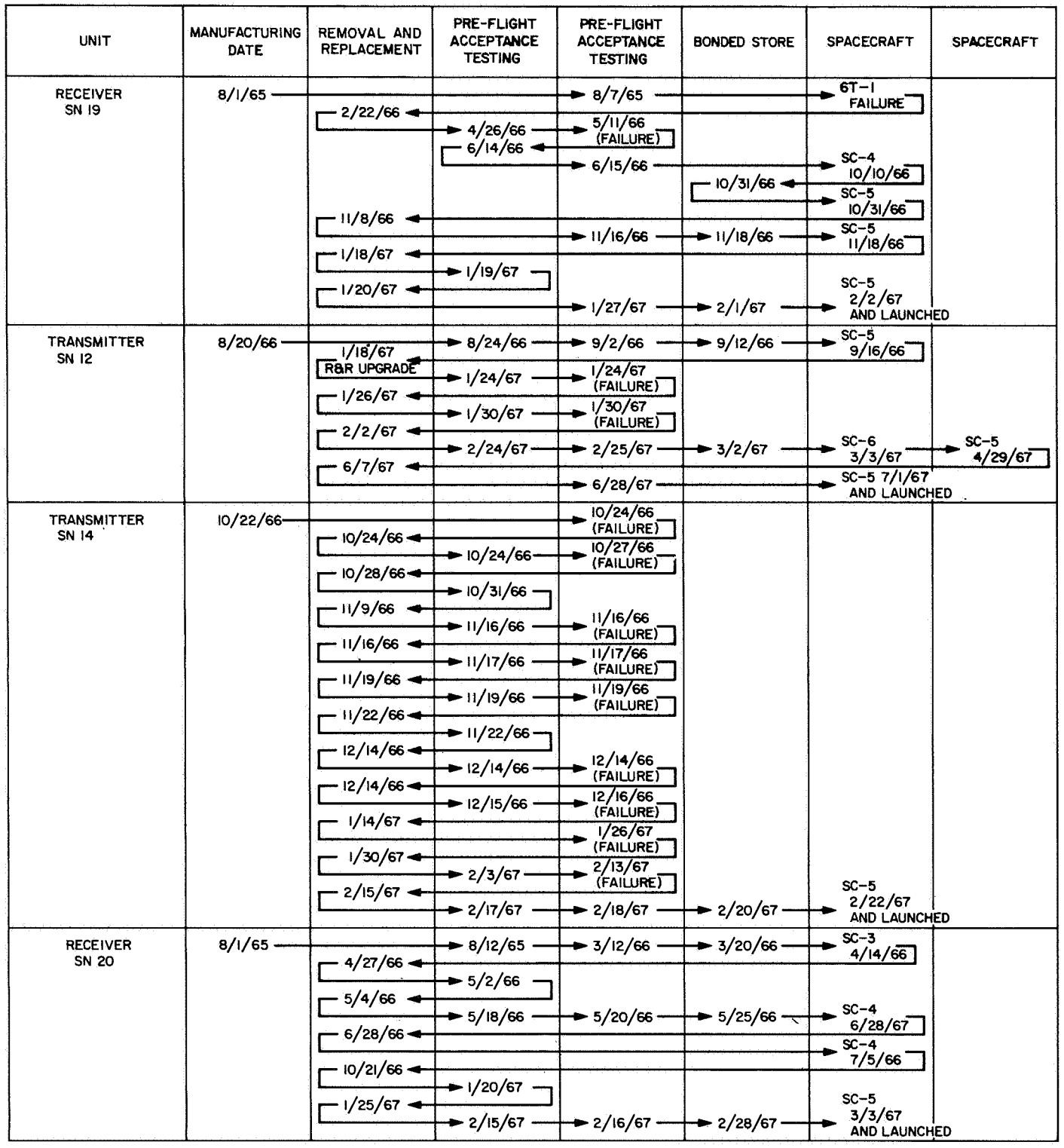



**Fig. XX-16. Typical receiver and transmitter processing history for a spacecraft**

The process of evaluation of the RF equipment for determination of flight acceptability was extremely difficult throughout the *Surveyor* Project because of parameter instability, measurement errors, and lack of documentation of parameter history. Looseness of parameter specifications was the greatest hindrance. Data values could, and usually did, vary considerably. Automatic gain control levels, receiver threshold levels, and the WBVCXO frequency were the worst offenders. Table XX-5 gives a comparison of like parameters for several units. The main concern in attempting evaluation of data with a wide range of nominal values is the possibility of overlooking significant anomalies.

The actual mission flight operation of the RF spacecraft equipment was marked by several events as exceptions to the otherwise excellent performance.

### 1. *Surveyor I* Omniantenna A Problem

During the *Surveyor I* mission, immediately after the spacecraft separation and legs-down events, it was noticed that the omniantenna A *antenna deployed* switch was not actuated.

Subsequent surveys of the RF levels while transmitting through omniantenna A confirmed that the antenna had not unfolded. Since the omniantenna is folded over center, the thrust from the midcourse maneuver and retrorockets only served to hold the antenna more tightly in its folded position. Not until actual touchdown did the *antenna deployed* switch show that the antenna had bounced out of its extended position. This was confirmed by signal strength measurements.

Because of the totally redundant omniantenna and receiver subsystem on board the *Surveyor*, this failure presented no hazard to the mission, but did put minor constraints on the landing roll attitude to keep omniantenna B effective.

### 2. *Surveyor II* Receiver B Threshold Sensitivity Degradation

In the early phases of the *Surveyor II* transit, a loss of 12 db was observed in the threshold sensitivity of receiver B. This did not interrupt full use of this receiver for spacecraft commands up until loss of the spacecraft when the retro motor was ignited. Subsequent analysis indicated that, if no further degradation had occurred, a normal mission could have been completed successfully without the use of the redundant system.

Testing and evaluation on the receivers led to the belief that the sensitivity loss was a result of local-oscillator detuning as discussed in Subsection C-1-b.

### 3. *Surveyor IV* Loss of Signal

*Surveyor IV* was in final retro motor descent when the RF signal suddenly disappeared.

A complete failure review and analysis of data to that time showed absolutely no signs of degraded or degrading performance in any of the spacecraft functions.

**Table XX-5. Parameter comparison for radio system units**

| Receiver parameter | Receiver | | | |
|---|---|---|---|---|
| | 18 | 19 | 20 | 22 |
| Threshold, dbm | | | | |
| AGC, V | −136 | −132 | −135 | −133 |
| At −80 dbm | 0.30 | 0.53 | 0.275 | 0.49 |
| At −120 dbm | 1.14 | 1.50 | 1.10 | 1.54 |
| Tracking range, kHz | | | | |
| High | 101.3 | 90 | 103 | 87.3 |
| Low | 105.7 | 100 | 125 | 102.2 |
| **Transmitter parameter** | **Transmitter** | | | |
| | 12 | 14 | 17 | 19 |
| Wideband voltage-controlled crystal oscillator frequency, MHz | | | | |
| At flight acceptance testing | 2295.008380 | 2295.025580 | 2294.978100 | 2295.030900 |
| At launch | 2294.992061 | 2294.972397 | 2294.918672 | 2295.007888 |

Further, it was established that loss of spacecraft power would have caused a signal tailoff which was not seen.

The only possible failure modes that satisfied the observed indications included a loss of the RF signal by RF subsystem failure. This could have been caused by catastrophic explosion of the retro motor, but also could have been a result of as simple a cause as an RF cable vibrating loose.

Unfortunately, the redundant transmitter was not immediately helpful because the time required to command it to warmup and then onto high power was a critical tradeoff against the possibility that the operating unit could be made to work in the very short time to touchdown.

Since the spacecraft was entirely under its own control to land on the lunar surface at this time, and since many subsequent efforts to raise the other transmitter were unsuccessful, indication is that the spacecraft met with disaster either at the time of the signal loss or on descent to the lunar surface.

For this reason, and this one only, there is slightly greater suspicion attached to the propulsion system than to the RF subsystems. However, this will not be known until the spacecraft or its pieces are found.

#### 4. *Surveyor VII* Multipath Reception

Immediately after touchdown of *Surveyor VII*, periodic fluctuations of about ±1.0 db were noted on the spacecraft receiver AGC at a 30-sec interval. These fluctuations were noted only on the omniantennas, but persisted through lunar operations, varying in both magnitude and period. The period varied from several seconds to several minutes; magnitude was as great as ±3.0 db.

A cursory effort was made to examine the terrain around the spacecraft, and also compare the observed geometry and angular rates against the observed frequencies. A study was also made of the change in amplitude and frequency during tracking station changeover when geometry was changed. The conclusion was that an RF multipath reception was being experienced by the spacecraft omniantennas with a probable differential path length of about 14 km with other distances being occasionally indicated.

These fluctuations did occasionally cause the signal level to dip below command threshold, causing a missed command, but these fluctuations were too infrequent to affect operations in any way. No corrective action was attempted on this problem.

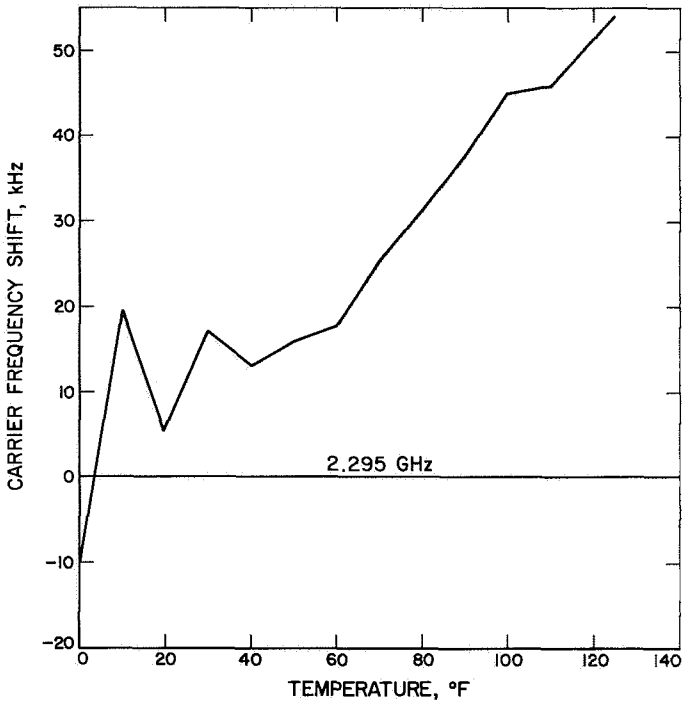



**Fig. XX-17. Typical transmitter wideband voltage-controlled crystal oscillator frequency output**

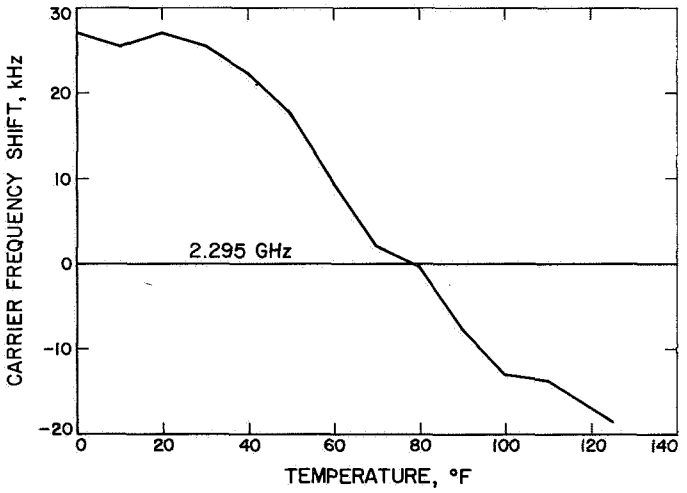



**Fig. XX-18. Typical transmitter narrowband voltage-controlled crystal oscillator frequency output**

#### 5. Transmitter Frequency Drift

One of the more troublesome signature list items of the *Surveyor* spacecraft was the frequency drift characteristics of the transmitters when operating with the WBVCXO. The WBVCXO was so heavily damped to widen its frequency deviation capability that it was not

a crystal-controlled oscillator at all, despite the presence of the crystal in the circuit.

Figures XX-17 and XX-18 show variations of typical frequency outputs of the WBNCXO and NBVCXO, respectively, as a function of temperature.

The NBVCXO frequency was predictable in flight according to the transmitter temperature, but the WBVCXO was not. Under vacuum conditions, an additional drift in frequency of as much as an additional 50–75 kHz occurred in the WBVCXO. This necessitated observance of the transmitters during lunar operations to enable prediction of the frequencies for reacquisition. This drift also imposed on the tracking net the nonstandard use of their frequency synthesizers to enable reception of *Surveyor* signals. This was a problem only on the lunar surface during transmission of TV or other wideband information, for at all other times the NBVCXO was used.

# Appendix XX-A
# Decibel Allocation Summary

DECIBEL ALLOCATION SUMMARY

MODE DESCRIPTION--SURVEYOR MISSION G
DSIF ACQUISITION OF S/C AT GREATEST RANGE
S/C HAS ACQUIRED SUN

| | | NOMINAL | + TOL | - TOL |
|---|---|---|---|---|
| TRANSMITTING SYSTEM | | | | |
| 1) RF POWER, DBM | | 40.60 | 0. | -0.30 |
| 2) CIRCUIT LOSS, DB | | -3.25 | 0.50 | -0.50 |
| 3) ANTENNA GAIN, DB | | -18.32 | 0. | 0. |
| PERCENT GAIN COVERAGE | | | | |
| 4) POINTING LOSS, DB | | 0. | 0. | 0. |
| PATH PARAMETERS | | | | |
| 5) SLANT RANGE (MAX), KM | 10423.0 | | | |
| 6) CARRIER FREQUENCY, MHZ | 2295.00 | | | |
| 7) ATMOSPHERIC ABSORPTION, DB | | 0. | 0. | -0.20 |
| 8) SPACE LOSS (MAX), DB | | -180.024 | | |
| RECEIVING SYSTEM | | | | |
| ANTENNA TYPE-- | | | | |
| 9) ANTENNA GAIN, DB | | 21.00 | 1.00 | -1.00 |
| 10) POLARIZATION LOSS, DB | | 0. | 0. | 0. |
| PREAMPLIFIER-- | | | | |
| 11) CIRCUIT LOSS, DB | | -0.50 | 0. | 0. |
| 12) SYSTEM NOISE TEMP, DEG. K | | 270.00 | 50.00 | -50.00 |
| 13) NOISE SPECTRAL DENSITY, DBM/HZ | | -174.29 | 0.74 | -0.89 |
| TOTAL RECEIVED POWER, DBM | | -140.49 | 1.50 | -2.00 |

| | CARRIER | CH 1 | CH 2 | CH 3 | CH 4 | IF |
|---|---|---|---|---|---|---|
| SCO CENTER FREQUENCY, KHZ | | 3.90 | | | | |
| DATA/SUBCARRIER MOD. INDICES | | 1.07 | | | | |
| SCO/CARRIER MOD. INDICES | | 0.300 | | | | |
| +-10 PERCENT | | | | | | |
| MODULATION LOSS, DB | -0.20 | -13.57 | | | | |
| + TOLERANCE | 0.04 | 0.81 | | | | |
| - TOLERANCE | -0.04 | -0.90 | | | | |
| SIGNAL POWER, DBM | -140.7 | -154.1 | | | | |
| + TOLERANCE | 1.54 | 2.31 | | | | |
| - TOLERANCE | -2.04 | -2.90 | | | | |
| PREDETECTION NOISE BW, HZ | 152.0 | 685. | | | | |
| +- HZ | 0. | 68.5 | | | | |
| NOISE POWER, DBM | -152.5 | -145.9 | | | | |
| + TOLERANCE | 0.74 | 1.15 | | | | |
| - TOLERANCE | -0.89 | -1.35 | | | | |
| THRESHOLD SNR, DB | 9.00 | 9.00 | | | | |
| +- DB | 0. | 1.0 | | | | |
| MAXIMUM MARGIN, DB | 5.21 | -12.47 | | | | |
| NOMINAL MARGIN, DB | 2.78 | -17.13 | | | | |
| MINIMUM MARGIN, DB | 0.00 | -22.18 | | | | |

DECIBEL ALLOCATION SUMMARY

MODE DESCRIPTION--SURVEYOR MISSION G
UP LINK ACQUISITION AT GREATEST RANGE - DSIF ON SAA
S/C HAS ACQUIRED SUN

| | NOMINAL | + TOL | - TOL |
|---|---|---|---|
| TRANSMITTING SYSTEM | | | |
| 1) RF POWER, DBM | 70.00 | 0.50 | -0. |
| 2) CIRCUIT LOSS, DB | -0.40 | 0.10 | -0.10 |
| 3) ANTENNA GAIN, DB | 20.00 | 2.00 | -2.00 |
| PERCENT GAIN COVERAGE | | | |
| 4) POINTING LOSS, DB | 0. | 0. | 0. |
| PATH PARAMETERS | | | |
| 5) SLANT RANGE (MAX), KM | 10423.0 | | |
| 6) CARRIER FREQUENCY, MHZ | 2113.00 | | |
| 7) ATMOSPHERIC ABSORPTION, DB | 0. | 0. | -0.20 |
| 8) SPACE LOSS (MAX), DB | -179.306 | | |
| RECEIVING SYSTEM | | | |
| ANTENNA TYPE-- | | | |
| 9) ANTENNA GAIN, DB | -10.00 | 0. | 0. |
| 10) POLARIZATION LOSS, DB | 0. | 0. | 0. |
| PREAMPLIFIER-- | | | |
| 11) CIRCUIT LOSS, DB | -4.00 | 0.50 | -0.50 |
| 12) SYSTEM NOISE TEMP, DEG. K | 2700.00 | 0. | 0. |
| 13) NOISE SPECTRAL DENSITY, DBM/HZ | -164.29 | -0. | -0. |
| TOTAL RECEIVED POWER, DBM | -103.71 | 3.10 | -2.80 |

| | CARRIER | CH 1 | CH 2 | CH 3 | CH 4 | IF |
|---|---|---|---|---|---|---|
| SCO CENTER FREQUENCY, KHZ | | 0. | | | | |
| DATA/SUBCARRIER MOD. INDICES | | 7.20 | | | | |
| SCO/CARRIER MOD. INDICES +-10 PERCENT | | 1.600 | | | | |
| MODULATION LOSS, DB | -6.83 | 0. | | | | |
| + TOLERANCE | 1.56 | 0. | | | | |
| - TOLERANCE | -1.96 | 0. | | | | |
| SIGNAL POWER, DBM | -110.5 | -103.7 | | | | |
| + TOLERANCE | 4.66 | 3.10 | | | | |
| - TOLERANCE | -4.76 | -2.80 | | | | |
| PREDETECTION NOISE BW, HZ | 240.0 | 13430. | | | | |
| +- HZ | 24.0 | 0. | | | | |
| NOISE POWER, DBM | -140.5 | -123.0 | | | | |
| + TOLERANCE | 0.41 | -0. | | | | |
| - TOLERANCE | -0.46 | -0. | | | | |
| THRESHOLD SNR, DB | 12.00 | 9.00 | | | | |
| +- DB | 0. | 0. | | | | |
| MAXIMUM MARGIN, DB | 23.06 | 13.40 | | | | |
| NOMINAL MARGIN, DB | 17.95 | 10.30 | | | | |
| MINIMUM MARGIN, DB | 12.77 | 7.50 | | | | |

DECIBEL ALLOCATION SUMMARY

MODE DESCRIPTION--SURVEYOR MISSION G
MIDCOURSE MANEUVER (FIRST PASS)
DOWN LINK -- 4400 BPS PCM

| | NOMINAL | + TOL | - TOL |
|---|---|---|---|
| TRANSMITTING SYSTEM | | | |
| 1) RF POWER, DBM | 40.60 | 0. | -0.30 |
| 2) CIRCUIT LOSS, DB | -3.25 | 0.50 | -0.50 |
| 3) ANTENNA GAIN, DB | -14.20 | 0. | 0. |
| PERCENT GAIN COVERAGE | | | |
| 4) POINTING LOSS, DB | 0. | 0. | 0. |
| PATH PARAMETERS | | | |
| 5) SLANT RANGE (MAX), KM | 188000.0 | | |
| 6) CARRIER FREQUENCY, MHZ | 2295.00 | | |
| 7) ATMOSPHERIC ABSORPTION, DB | 0. | 0. | -0.20 |
| 8) SPACE LOSS (MAX), DB | -205.147 | | |
| RECEIVING SYSTEM | | | |
| ANTENNA TYPE-- 85 FT. PARABOLIC | | | |
| 9) ANTENNA GAIN, DB | 53.00 | 1.00 | -0.50 |
| 10) POLARIZATION LOSS, DB | 0. | 0. | 0. |
| PREAMPLIFIER-- MASER | | | |
| 11) CIRCUIT LOSS, DB | -0.18 | 0.05 | -0.05 |
| 12) SYSTEM NOISE TEMP, DEG. K | 55.00 | 10.00 | -10.00 |
| 13) NOISE SPECTRAL DENSITY, DBM/HZ | -181.20 | 0.73 | -0.87 |
| TOTAL RECEIVED POWER, DBM | -129.18 | 1.55 | -1.55 |

| | CARRIER | CH 1 | CH 2 | CH 3 | CH 4 | IF |
|---|---|---|---|---|---|---|
| SCO CENTER FREQUENCY, KHZ | | 33.00 | | | | |
| DATA/SUBCARRIER MOD. INDICES | | 0.90 | | | | |
| SCO/CARRIER MOD. INDICES +-10 PERCENT | | 1.600 | | | | |
| MODULATION LOSS, DB | -6.83 | -1.87 | | | | |
| + TOLERANCE | 1.56 | 0.16 | | | | |
| - TOLERANCE | -1.96 | -0.33 | | | | |
| SIGNAL POWER, DBM | -136.0 | -131.1 | | | | |
| + TOLERANCE | 3.11 | 1.71 | | | | |
| - TOLERANCE | -3.51 | -1.88 | | | | |
| PREDETECTION NOISE BW, HZ | 152.0 | 5160. | | | | |
| +- HZ | 0. | 516.0 | | | | |
| NOISE POWER, DBM | -159.4 | -144.1 | | | | |
| + TOLERANCE | 0.73 | 1.14 | | | | |
| - TOLERANCE | -0.87 | -1.33 | | | | |
| THRESHOLD SNR, DB | 14.00 | 9.00 | | | | |
| +- DB | 1.0 | 1.0 | | | | |
| MAXIMUM MARGIN, DB | 14.35 | 8.06 | | | | |
| NOMINAL MARGIN, DB | 9.37 | 4.02 | | | | |
| MINIMUM MARGIN, DB | 4.13 | 0.00 | | | | |

***USE OF 210 FT. PARABOLIC ANTENNA (GAIN=61+-) DB) RESULTS IN THE FOLLOWING***

| | | | | | | |
|---|---|---|---|---|---|---|
| MINIMUM MARGIN, DB | 11.63 | 7.50 | | | | |

DECIBEL ALLOCATION SUMMARY

MODE DESCRIPTION--SURVEYOR MISSION G
MIDCOURSE MANEUVER (FIRST PASS)
LP LINK

| | | NOMINAL | + TOL | - TOL |
|---|---|---|---|---|
| TRANSMITTING SYSTEM | | | | |
| 1) RF POWER, DBM | | 70.00 | 0.50 | -0. |
| 2) CIRCUIT LOSS, DB | | -0.40 | 0.10 | -0.10 |
| 3) ANTENNA GAIN, DB | | 51.00 | 1.00 | -0.50 |
| PERCENT GAIN COVERAGE | | | | |
| 4) POINTING LOSS, DB | | 0. | 0. | 0. |
| PATH PARAMETERS | | | | |
| 5) SLANT RANGE (MAX), KM | 188000.0 | | | |
| 6) CARRIER FREQUENCY, MHZ | 2113.00 | | | |
| 7) ATMOSPHERIC ABSORPTION, DB | | 0. | 0. | -0.20 |
| 8) SPACE LOSS (MAX), DB | | -204.429 | | |
| RECEIVING SYSTEM | | | | |
| ANTENNA TYPE-- | | | | |
| 9) ANTENNA GAIN, DB | | -10.00 | 0. | 0. |
| 10) POLARIZATION LOSS, DB | | 0. | 0. | 0. |
| PREAMPLIFIER-- | | | | |
| 11) CIRCUIT LOSS, DB | | -4.00 | 0.50 | -0.50 |
| 12) SYSTEM NOISE TEMP, DEG. K | | 2700.00 | 0. | 0. |
| 13) NOISE SPECTRAL DENSITY, DBM/HZ | | -164.29 | -0. | -0. |
| TOTAL RECEIVED POWER, DBM | | -97.83 | 2.10 | -1.30 |

| | CARRIER | CH 1 | CH 2 | CH 3 | CH 4 | IF |
|---|---|---|---|---|---|---|
| SCO CENTER FREQUENCY, KHZ | | 0. | | | | |
| DATA/SUBCARRIER MOD. INDICES | | 7.20 | | | | |
| SCO/CARRIER MOD. INDICES +-10 PERCENT | | 1.600 | | | | |
| MODULATION LOSS, DB | -6.83 | 0. | | | | |
| + TOLERANCE | 1.56 | 0. | | | | |
| - TOLERANCE | -1.96 | 0. | | | | |
| SIGNAL POWER, DBM | -104.7 | -97.8 | | | | |
| + TOLERANCE | 3.66 | 2.10 | | | | |
| - TOLERANCE | -3.26 | -1.30 | | | | |
| PREDETECTION NOISE BW, HZ | 240.0 | 13430. | | | | |
| +- HZ | 24.0 | 0. | | | | |
| NOISE POWER, DBM | -140.5 | -123.0 | | | | |
| + TOLERANCE | 0.41 | -0. | | | | |
| - TOLERANCE | -0.46 | -0. | | | | |
| THRESHOLD SNR, DB | 12.00 | 9.00 | | | | |
| +- DB | 0. | 0. | | | | |
| MAXIMUM MARGIN, DB | 27.94 | 18.28 | | | | |
| NOMINAL MARGIN, DB | 23.82 | 16.18 | | | | |
| MINIMUM MARGIN, DB | 20.14 | 14.88 | | | | |

DECIBEL ALLOCATION SUMMARY

MODE DESCRIPTION--SURVEYOR MISSION G
MIDCOURSE MANEUVER (SECOND PASS)
DOWN LINK -- 4400 BPS PCM

| | NOMINAL | + TOL | - TOL |
|---|---|---|---|
| TRANSMITTING SYSTEM | | | |
| 1) RF POWER, DBM | 40.60 | 0. | -0.30 |
| 2) CIRCUIT LOSS, DB | -3.25 | 0.50 | -0.50 |
| 3) ANTENNA GAIN, DB | -9.94 | 0. | 0. |
| PERCENT GAIN COVERAGE | | | |
| 4) POINTING LOSS, DB | 0. | 0. | 0. |
| PATH PARAMETERS | | | |
| 5) SLANT RANGE (MAX), KM | 307000.0 | | |
| 6) CARRIER FREQUENCY, MHZ | 2295.00 | | |
| 7) ATMOSPHERIC ABSORPTION, DB | 0. | 0. | -0.20 |
| 8) SPACE LOSS (MAX), DB | -209.407 | | |
| RECEIVING SYSTEM | | | |
| ANTENNA TYPE-- 85 FT. PARABOLIC | | | |
| 9) ANTENNA GAIN, DB | 53.00 | 1.00 | -0.50 |
| 10) POLARIZATION LOSS, DB | 0. | 0. | 0. |
| PREAMPLIFIER-- MASER | | | |
| 11) CIRCUIT LOSS, DB | -0.18 | 0.05 | -0.05 |
| 12) SYSTEM NOISE TEMP, DEG. K | 55.00 | 10.00 | -10.00 |
| 13) NOISE SPECTRAL DENSITY, DBM/HZ | -181.20 | 0.73 | -0.87 |
| TOTAL RECEIVED POWER, DBM | -129.18 | 1.55 | -1.55 |

| | CARRIER | CH 1 | CH 2 | CH 3 | CH 4 | IF |
|---|---|---|---|---|---|---|
| SCO CENTER FREQUENCY, KHZ | | 33.00 | | | | |
| DATA/SUBCARRIER MOD. INDICES | | 0.90 | | | | |
| SCO/CARRIER MOD. INDICES +-10 PERCENT | | 1.600 | | | | |
| MODULATION LOSS, DB | -6.83 | -1.87 | | | | |
| + TOLERANCE | 1.56 | 0.16 | | | | |
| - TOLERANCE | -1.96 | -0.33 | | | | |
| SIGNAL POWER, DBM | -136.0 | -131.1 | | | | |
| + TOLERANCE | 3.11 | 1.71 | | | | |
| - TOLERANCE | -3.51 | -1.88 | | | | |
| PREDETECTION NOISE BW, HZ | 152.0 | 5160. | | | | |
| +- HZ | 0. | 516.0 | | | | |
| NOISE POWER, DBM | -159.4 | -144.1 | | | | |
| + TOLERANCE | 0.73 | 1.14 | | | | |
| - TOLERANCE | -0.87 | -1.33 | | | | |
| THRESHOLD SNR, DB | 14.00 | 9.00 | | | | |
| +- DB | 1.0 | 1.0 | | | | |
| MAXIMUM MARGIN, DB | 14.35 | 8.06 | | | | |
| NOMINAL MARGIN, DB | 9.37 | 4.02 | | | | |
| MINIMUM MARGIN, DB | 4.13 | -0. | | | | |

***USE OF 210 FT. PARABOLIC ANTENNA (GAIN=61+-1 DB) RESULTS IN THE FOLLOWING***

| | | |
|---|---|---|
| MINIMUM MARGIN, DB | 11.63 | 7.50 |

DECIBEL ALLOCATION SUMMARY

MODE DESCRIPTION--SURVEYOR MISSION G
MIDCOURSE MANEUVER (SECOND PASS)
LP LINK

| | NOMINAL | + TOL | - TOL |
|---|---|---|---|
| TRANSMITTING SYSTEM | | | |
| 1) RF POWER, DBM | 70.00 | 0.50 | -0. |
| 2) CIRCUIT LOSS, DB | -0.40 | 0.10 | -0.10 |
| 3) ANTENNA GAIN, DB | 51.00 | 1.00 | -0.50 |
| PERCENT GAIN COVERAGE | | | |
| 4) POINTING LOSS, DB | 0. | 0. | 0. |
| PATH PARAMETERS | | | |
| 5) SLANT RANGE (MAX), KM | 307000.0 | | |
| 6) CARRIER FREQUENCY, MHZ | 2113.00 | | |
| 7) ATMOSPHERIC ABSORPTION, DB | 0. | 0. | -0.20 |
| 8) SPACE LOSS (MAX), DB | -208.689 | | |
| RECEIVING SYSTEM | | | |
| ANTENNA TYPE-- | | | |
| 9) ANTENNA GAIN, DB | -10.00 | 0. | 0. |
| 10) POLARIZATION LOSS, DB | 0. | 0. | 0. |
| PREAMPLIFIER-- | | | |
| 11) CIRCUIT LOSS, DB | -4.00 | 0.50 | -0.50 |
| 12) SYSTEM NOISE TEMP, DEG. K | 2700.00 | 0. | 0. |
| 13) NOISE SPECTRAL DENSITY, DBM/HZ | -164.29 | -0. | -0. |
| TOTAL RECEIVED POWER, DBM | -102.09 | 2.10 | -1.30 |

| | CARRIER | CH 1 | CH 2 | CH 3 | CH 4 | IF |
|---|---|---|---|---|---|---|
| SCO CENTER FREQUENCY, KHZ | | 0. | | | | |
| DATA/SUBCARRIER MOD. INDICES | | 7.20 | | | | |
| SCO/CARRIER MOD. INDICES | | 1.600 | | | | |
| +-10 PERCENT | | | | | | |
| MODULATION LOSS, DB | -6.83 | 0. | | | | |
| + TOLERANCE | 1.56 | 0. | | | | |
| - TOLERANCE | -1.96 | 0. | | | | |
| SIGNAL POWER, DBM | -108.9 | -102.1 | | | | |
| + TOLERANCE | 3.66 | 2.10 | | | | |
| - TOLERANCE | -3.26 | -1.30 | | | | |
| PREDETECTION NOISE BW, HZ | 240.0 | 13430. | | | | |
| +- HZ | 24.0 | 0. | | | | |
| NOISE POWER, DBM | -140.5 | -123.0 | | | | |
| + TOLERANCE | 0.41 | -0. | | | | |
| - TOLERANCE | -0.46 | -0. | | | | |
| THRESHOLD SNR, DB | 12.00 | 9.00 | | | | |
| +- DB | 0. | 0. | | | | |
| MAXIMUM MARGIN, DB | 23.68 | 14.02 | | | | |
| NOMINAL MARGIN, DB | 19.56 | 11.92 | | | | |
| MINIMUM MARGIN, DB | 15.89 | 10.62 | | | | |

DECIBEL ALLOCATION SUMMARY

MODE DESCRIPTION--SURVEYOR MISSION G
TERMINAL MANEUVER
DOWN LINK -- 1100 BPS PCM

| | | NOMINAL | + TOL | - TOL |
|---|---|---|---|---|
| TRANSMITTING SYSTEM | | | | |
| 1) RF POWER, DBM | | 40.60 | 0. | -0.30 |
| 2) CIRCUIT LOSS, DB | | -3.25 | 0.50 | -0.50 |
| 3) ANTENNA GAIN, DB | | -5.57 | 0. | 0. |
| PERCENT GAIN COVERAGE | | | | |
| 4) POINTING LOSS, DB | | 0. | 0. | 0. |
| PATH PARAMETERS | | | | |
| 5) SLANT RANGE (MAX), KM | 406000.0 | | | |
| 6) CARRIER FREQUENCY, MHZ | 2295.00 | | | |
| 7) ATMOSPHERIC ABSORPTION, DB | | 0. | 0. | -0.20 |
| 8) SPACE LOSS (MAX), DB | | -211.834 | | |
| RECEIVING SYSTEM | | | | |
| ANTENNA TYPE-- 85 FT. PARABOLIC | | | | |
| 9) ANTENNA GAIN, DB | | 53.00 | 1.00 | -0.50 |
| 10) POLARIZATION LOSS, DB | | 0. | 0. | 0. |
| PREAMPLIFIER-- MASER | | | | |
| 11) CIRCUIT LOSS, DB | | -0.18 | 0.05 | -0.05 |
| 12) SYSTEM NOISE TEMP, DEG. K | | 165.00 | 35.00 | -35.00 |
| 13) NOISE SPECTRAL DENSITY, DBM/HZ | | -176.43 | 0.84 | -1.04 |
| TOTAL RECEIVED POWER, DBM | | -127.23 | 1.55 | -1.55 |

| | CARRIER | CH 1 | CH 2 | CH 3 | CH 4 | IF |
|---|---|---|---|---|---|---|
| SCO CENTER FREQUENCY, KHZ | | 7.35 | | | | |
| DATA/SUBCARRIER MOD. INDICES | | 1.00 | | | | |
| SCO/CARRIER MOD. INDICES | | 0.935 | | | | |
| +-10 PERCENT | | | | | | |
| MODULATION LOSS, DB | -2.01 | -4.56 | | | | |
| + TOLERANCE | 0.40 | 0.62 | | | | |
| - TOLERANCE | -0.46 | -0.73 | | | | |
| SIGNAL POWER, DBM | -129.2 | -131.8 | | | | |
| + TOLERANCE | 1.95 | 2.17 | | | | |
| - TOLERANCE | -2.01 | -2.28 | | | | |
| PREDETECTION NOISE BW, HZ | 152.0 | 1290. | | | | |
| +- HZ | 0. | 129.0 | | | | |
| NOISE POWER, DBM | -154.6 | -145.3 | | | | |
| + TOLERANCE | 0.84 | 1.25 | | | | |
| - TOLERANCE | -1.04 | -1.49 | | | | |
| THRESHOLD SNR, DB | 14.00 | 9.00 | | | | |
| +- DB | 1.0 | 1.0 | | | | |
| MAXIMUM MARGIN, DB | 15.35 | 9.19 | | | | |
| NOMINAL MARGIN, DB | 11.36 | 4.53 | | | | |
| MINIMUM MARGIN, DB | 7.52 | 0.00 | | | | |

***USE OF 210 FT. PARABOLIC ANTENNA (GAIN=61+-1 DB) RESULTS IN THE FOLLOWING***

| | | | | | | |
|---|---|---|---|---|---|---|
| MINIMUM MARGIN, DB | 15.02 | 7.50 | | | | |

DECIBEL ALLOCATION SUMMARY

MODE DESCRIPTION--SURVEYOR MISSION G
TERMINAL MANEUVER
DOWN LINK -- 550 BPS PCM

| | | NOMINAL | + TOL | - TOL |
|---|---|---|---|---|
| TRANSMITTING SYSTEM | | | | |
| 1) RF POWER, DBM | | 40.60 | 0. | -0.30 |
| 2) CIRCUIT LOSS, DB | | -3.25 | 0.50 | -0.50 |
| 3) ANTENNA GAIN, DB | | -9.70 | 0. | 0. |
| PERCENT GAIN COVERAGE | | | | |
| 4) POINTING LOSS, DB | | 0. | 0. | 0. |
| PATH PARAMETERS | | | | |
| 5) SLANT RANGE (MAX), KM | 406000.0 | | | |
| 6) CARRIER FREQUENCY, MHZ | 2295.00 | | | |
| 7) ATMOSPHERIC ABSORPTION, DB | | 0. | 0. | -0.20 |
| 8) SPACE LOSS (MAX), DB | | -211.834 | | |
| RECEIVING SYSTEM | | | | |
| ANTENNA TYPE-- 85 FT. PARABOLIC | | | | |
| 9) ANTENNA GAIN, DB | | 53.00 | 1.00 | -0.50 |
| 10) POLARIZATION LOSS, DB | | 0. | 0. | 0. |
| PREAMPLIFIER-- MASER | | | | |
| 11) CIRCUIT LOSS, DB | | -0.18 | 0.05 | -0.05 |
| 12) SYSTEM NOISE TEMP, DEG. K | | 165.00 | 35.00 | -35.00 |
| 13) NOISE SPECTRAL DENSITY, DBM/HZ | | -176.43 | 0.84 | -1.04 |
| TOTAL RECEIVED POWER, DBM | | -131.37 | 1.55 | -1.55 |

| | CARRIER | CH 1 | CH 2 | CH 3 | CH 4 | IF |
|---|---|---|---|---|---|---|
| SCO CENTER FREQUENCY, KHZ | | 3.90 | | | | |
| DATA/SUBCARRIER MOD. INDICES | | 1.07 | | | | |
| SCO/CARRIER MOD. INDICES +-10 PERCENT | | 1.150 | | | | |
| MODULATION LOSS, DB | -3.15 | -3.27 | | | | |
| + TOLERANCE | 0.65 | 0.51 | | | | |
| - TOLERANCE | -0.75 | -0.63 | | | | |
| SIGNAL POWER, DBM | -134.5 | -134.6 | | | | |
| + TOLERANCE | 2.20 | 2.06 | | | | |
| - TOLERANCE | -2.30 | -2.18 | | | | |
| PREDETECTION NOISE BW, HZ | 152.0 | 685. | | | | |
| +- HZ | 0. | 68.5 | | | | |
| NOISE POWER, DBM | -154.6 | -148.1 | | | | |
| + TOLERANCE | 0.84 | 1.25 | | | | |
| - TOLERANCE | -1.04 | -1.49 | | | | |
| THRESHOLD SNR, DB | 14.00 | 9.00 | | | | |
| +- DB | 1.0 | 1.0 | | | | |
| MAXIMUM MARGIN, DB | 10.32 | 8.98 | | | | |
| NOMINAL MARGIN, DB | 6.09 | 4.43 | | | | |
| MINIMUM MARGIN, DB | 1.95 | 0.00 | | | | |

***USE OF 210 FT. PARABOLIC ANTENNA (GAIN=61+-1 DB) RESULTS IN THE FOLLOWING***

| | | | | | | |
|---|---|---|---|---|---|---|
| MINIMUM MARGIN, DB | 9.45 | 7.50 | | | | |

DECIBEL ALLOCATION SUMMARY

MODE DESCRIPTION--SURVEYOR MISSION G
TERMINAL MANEUVER
UP LINK

| | NOMINAL | + TOL | - TOL |
|---|---|---|---|
| TRANSMITTING SYSTEM | | | |
| 1) RF POWER, DBM | 70.00 | 0.50 | -0. |
| 2) CIRCUIT LOSS, DB | -0.40 | 0.10 | -0.10 |
| 3) ANTENNA GAIN, DB | 51.00 | 1.00 | -0.50 |
| PERCENT GAIN COVERAGE | | | |
| 4) POINTING LOSS, DB | 0. | 0. | 0. |
| PATH PARAMETERS | | | |
| 5) SLANT RANGE (MAX), KM | 406000.0 | | |
| 6) CARRIER FREQUENCY, MHZ | 2113.00 | | |
| 7) ATMOSPHERIC ABSORPTION, DB | 0. | 0. | -0.20 |
| 8) SPACE LOSS (MAX), DB | -211.117 | | |
| RECEIVING SYSTEM | | | |
| ANTENNA TYPE-- | | | |
| 9) ANTENNA GAIN, DB | -10.00 | 0. | 0. |
| 10) POLARIZATION LOSS, DB | 0. | 0. | 0. |
| PREAMPLIFIER-- | | | |
| 11) CIRCUIT LOSS, DB | -4.00 | 0.50 | -0.50 |
| 12) SYSTEM NOISE TEMP, DEG. K | 2700.00 | 0. | 0. |
| 13) NOISE SPECTRAL DENSITY, DBM/HZ | -164.29 | -0. | -0. |
| TOTAL RECEIVED POWER, DBM | -104.52 | 2.10 | -1.30 |

| | CARRIER | CH 1 | CH 2 | CH 3 | CH 4 | IF |
|---|---|---|---|---|---|---|
| SCO CENTER FREQUENCY, KHZ | | 0. | | | | |
| DATA/SUBCARRIER MOD. INDICES | | 7.20 | | | | |
| SCO/CARRIER MOD. INDICES +-10 PERCENT | | 1.600 | | | | |
| MODULATION LOSS, DB | -6.83 | 0. | | | | |
| + TOLERANCE | 1.56 | 0. | | | | |
| - TOLERANCE | -1.96 | 0. | | | | |
| SIGNAL POWER, DBM | -111.3 | -104.5 | | | | |
| + TOLERANCE | 3.66 | 2.10 | | | | |
| - TOLERANCE | -3.26 | -1.30 | | | | |
| PREDETECTION NOISE BW, HZ | 240.0 | 13430. | | | | |
| +- HZ | 24.0 | 0. | | | | |
| NOISE POWER, DBM | -140.5 | -123.0 | | | | |
| + TOLERANCE | 0.41 | -0. | | | | |
| - TOLERANCE | -0.46 | -0. | | | | |
| THRESHOLD SNR, DB | 12.00 | 9.00 | | | | |
| +- DB | 0. | 0. | | | | |
| MAXIMUM MARGIN, DB | 21.25 | 11.59 | | | | |
| NOMINAL MARGIN, DB | 17.14 | 9.49 | | | | |
| MINIMUM MARGIN, DB | 13.46 | 8.19 | | | | |

DECIBEL ALLOCATION SUMMARY

MODE DESCRIPTION--SURVEYOR MISSION G
VERNIER DESCENT
DOWN LINK -- 1100 BPS PCM AND STRAIN GAGES MULTIPLEX

| | NOMINAL | + TOL | - TOL |
|---|---|---|---|
| TRANSMITTING SYSTEM | | | |
| 1) RF POWER, DBM | 40.60 | 0. | -0.30 |
| 2) CIRCUIT LOSS, DB | -3.25 | 0.50 | -0.50 |
| 3) ANTENNA GAIN, DB | -0.62 | 0. | 0. |
| PERCENT GAIN COVERAGE | | | |
| 4) POINTING LOSS, DB | 0. | 0. | 0. |
| PATH PARAMETERS | | | |
| 5) SLANT RANGE (MAX), KM | 406000.0 | | |
| 6) CARRIER FREQUENCY, MHZ | 2295.00 | | |
| 7) ATMOSPHERIC ABSORPTION, DB | 0. | 0. | -0.20 |
| 8) SPACE LOSS (MAX), DB | -211.834 | | |
| RECEIVING SYSTEM | | | |
| ANTENNA TYPE-- 85 FT. PARABOLIC | | | |
| 9) ANTENNA GAIN, DB | 53.00 | 1.00 | -0.50 |
| 10) POLARIZATION LOSS, DB | 0. | 0. | 0. |
| PREAMPLIFIER-- MASER | | | |
| 11) CIRCUIT LOSS, DB | -0.18 | 0.05 | -0.05 |
| 12) SYSTEM NOISE TEMP, DEG. K | 165.00 | 35.00 | -35.00 |
| 13) NOISE SPECTRAL DENSITY, DBM/HZ | -176.43 | 0.84 | -1.04 |
| TOTAL RECEIVED POWER, DBM | -122.29 | 1.55 | -1.55 |

| | CARRIER | CH 1 | CH 2 | CH 3 | CH 4 | IF |
|---|---|---|---|---|---|---|
| SCO CENTER FREQUENCY, KHZ | | 7.35 | 0.96 | 1.30 | 1.70 | |
| DATA/SUBCARRIER MOD. INDICES | | 1.20 | 2.00 | 2.00 | 2.00 | |
| SCO/CARRIER MOD. INDICES +-10 PERCENT | | 0.935 | 0.650 | 0.650 | 0.650 | |
| MODULATION LOSS, DB | -4.84 | -7.39 | -11.11 | -11.11 | -11.11 | |
| + TOLERANCE | 0.95 | 1.17 | 1.50 | 1.50 | 1.50 | |
| - TOLERANCE | -1.07 | -1.34 | -1.69 | -1.69 | -1.69 | |
| SIGNAL POWER, DBM | -127.1 | -129.7 | -133.4 | -133.4 | -133.4 | |
| + TOLERANCE | 2.50 | 2.72 | 3.05 | 3.05 | 3.05 | |
| - TOLERANCE | -2.62 | -2.89 | -3.24 | -3.24 | -3.24 | |
| PREDETECTION NOISE BW, HZ | 152.0 | 1290. | 169.0 | 169.0 | 169.0 | |
| +- HZ | 0. | 129.0 | 16.9 | 16.9 | 16.9 | |
| NOISE POWER, DBM | -154.6 | -145.3 | -154.1 | -154.1 | -154.1 | |
| + TOLERANCE | 0.84 | 1.25 | 1.25 | 1.25 | 1.25 | |
| - TOLERANCE | -1.04 | -1.49 | -1.49 | -1.49 | -1.49 | |
| THRESHOLD SNR, DB | 14.00 | 10.50 | 7.00 | 7.00 | 7.00 | |
| +- DB | 1.0 | 1.0 | 1.0 | 1.0 | 1.0 | |
| MAXIMUM MARGIN, DB | 18.01 | 10.36 | 19.29 | 19.29 | 19.29 | |
| NOMINAL MARGIN, DB | 13.48 | 5.14 | 13.75 | 13.75 | 13.75 | |
| MINIMUM MARGIN, DB | 9.02 | -0. | 8.25 | 8.25 | 8.25 | |

***USE OF 210 FT. PARABOLIC ANTENNA (GAIN=61+-1 DB) RESULTS IN THE FOLLOWING***

| | | | | | | |
|---|---|---|---|---|---|---|
| MINIMUM MARGIN, DB | 16.52 | 7.50 | 15.75 | 15.75 | 15.75 | |

DECIBEL ALLOCATION SUMMARY

MODE DESCRIPTION--SURVEYOR MISSION G
VERNIER DESCENT
DOWN LINK -- 550 BPS PCM AND STRAIN GAGES MULTIPLEX

| | | NOMINAL | + TOL | - TOL |
|---|---|---|---|---|
| TRANSMITTING SYSTEM | | | | |
| 1) RF POWER, DBM | | 40.60 | 0. | -0.30 |
| 2) CIRCUIT LOSS, DB | | -3.25 | 0.50 | -0.50 |
| 3) ANTENNA GAIN, DB | | -4.76 | 0. | 0. |
| PERCENT GAIN COVERAGE | | | | |
| 4) POINTING LOSS, DB | | 0. | 0. | 0. |
| PATH PARAMETERS | | | | |
| 5) SLANT RANGE (MAX), KM | 406000.0 | | | |
| 6) CARRIER FREQUENCY, MHZ | 2295.00 | | | |
| 7) ATMOSPHERIC ABSORPTION, DB | | 0. | 0. | -0.20 |
| 8) SPACE LOSS (MAX), DB | | -211.834 | | |
| RECEIVING SYSTEM | | | | |
| ANTENNA TYPE-- 85 FT. PARABOLIC | | | | |
| 9) ANTENNA GAIN, DB | | 53.00 | 1.00 | -0.50 |
| 10) POLARIZATION LOSS, DB | | 0. | 0. | 0. |
| PREAMPLIFIER-- MASER | | | | |
| 11) CIRCUIT LOSS, DB | | -0.18 | 0.05 | -0.05 |
| 12) SYSTEM NOISE TEMP, DEG. K | | 165.00 | 35.00 | -35.00 |
| 13) NOISE SPECTRAL DENSITY, DBM/HZ | | -176.43 | 0.84 | -1.04 |
| TOTAL RECEIVED POWER, DBM | | -126.42 | 1.55 | -1.55 |

| | CARRIER | CH 1 | CH 2 | CH 3 | CH 4 | IF |
|---|---|---|---|---|---|---|
| SCO CENTER FREQUENCY, KHZ | | 3.90 | 0.96 | 1.30 | 1.70 | |
| DATA/SUBCARRIER MOD. INDICES | | 1.07 | 2.00 | 2.00 | 2.00 | |
| SCO/CARRIER MOD. INDICES +-10 PERCENT | | 1.150 | 0.650 | 0.650 | 0.650 | |
| MODULATION LOSS, DB | -5.98 | -6.10 | -12.25 | -12.25 | -12.25 | |
| + TOLERANCE | 1.20 | 1.06 | 1.74 | 1.74 | 1.74 | |
| - TOLERANCE | -1.36 | -1.24 | -1.99 | -1.99 | -1.99 | |
| SIGNAL POWER, DBM | -132.4 | -132.5 | -138.7 | -138.7 | -138.7 | |
| + TOLERANCE | 2.75 | 2.61 | 3.29 | 3.29 | 3.29 | |
| - TOLERANCE | -2.91 | -2.79 | -3.54 | -3.54 | -3.54 | |
| PREDETECTION NOISE BW, HZ | 152.0 | 685. | 169.0 | 169.0 | 169.0 | |
| +- HZ | 0. | 68.5 | 16.9 | 16.9 | 16.9 | |
| NOISE POWER, DBM | -154.6 | -148.1 | -154.1 | -154.1 | -154.1 | |
| + TOLERANCE | 0.84 | 1.25 | 1.25 | 1.25 | 1.25 | |
| - TOLERANCE | -1.04 | -1.49 | -1.49 | -1.49 | -1.49 | |
| THRESHOLD SNR, DB | 14.00 | 10.50 | 7.00 | 7.00 | 7.00 | |
| +- DB | 1.0 | 1.0 | 1.0 | 1.0 | 1.0 | |
| MAXIMUM MARGIN, DB | 12.99 | 10.14 | 14.26 | 14.26 | 14.26 | |
| NOMINAL MARGIN, DB | 8.20 | 5.04 | 8.47 | 8.47 | 8.47 | |
| MINIMUM MARGIN, DB | 3.45 | -0. | 2.69 | 2.69 | 2.69 | |
| ***USE OF 210 FT. PARABOLIC ANTENNA (GAIN=61+-1 DB) RESULTS IN THE FOLLOWING*** | | | | | | |
| MINIMUM MARGIN, DB | 10.95 | 7.50 | 10.19 | 10.19 | 10.19 | |

DECIBEL ALLOCATION SUMMARY

MODE DESCRIPTION--SURVEYOR MISSION G
LUNAR OPERATION - OMNI A - XMTR A
DOWN LINK - LOW POWER - 17.2 BPS PCM DATA

| | | NOMINAL | + TOL | - TOL |
|---|---|---|---|---|
| TRANSMITTING SYSTEM | | | | |
| 1) RF POWER, DBM | | 23.70 | 1.60 | -0.60 |
| 2) CIRCUIT LOSS, DB | | -2.77 | 0.50 | -0.50 |
| 3) ANTENNA GAIN, DB | | -6.69 | 0. | 0. |
| PERCENT GAIN COVERAGE | | | | |
| 4) POINTING LOSS, DB | | 0. | 0. | 0. |
| PATH PARAMETERS | | | | |
| 5) SLANT RANGE (MAX), KM | 406000.0 | | | |
| 6) CARRIER FREQUENCY, MHZ | 2295.00 | | | |
| 7) ATMOSPHERIC ABSORPTION, DB | | 0. | 0. | -0.20 |
| 8) SPACE LOSS (MAX), DB | | -211.834 | | |
| RECEIVING SYSTEM | | | | |
| ANTENNA TYPE-- 85 FT. PARABOLIC | | | | |
| 9) ANTENNA GAIN, DB | | 53.00 | 1.00 | -0.50 |
| 10) POLARIZATION LOSS, DB | | 0. | 0. | 0. |
| PREAMPLIFIER-- MASER | | | | |
| 11) CIRCUIT LOSS, DB | | -0.18 | 0.05 | -0.05 |
| 12) SYSTEM NOISE TEMP, DEG. K | | 165.00 | 35.00 | -35.00 |
| 13) NOISE SPECTRAL DENSITY, DBM/HZ | | -176.43 | 0.84 | -1.04 |
| TOTAL RECEIVED POWER, DBM | | -144.77 | 3.15 | -1.85 |

| | CARRIER | CH 1 | CH 2 | CH 3 | CH 4 | IF |
|---|---|---|---|---|---|---|
| SCC CENTER FREQUENCY, KHZ | | 0.56 | | | | |
| DATA/SUBCARRIER MOD. INDICES | | 1.00 | | | | |
| SCC/CARRIER MOD. INDICES +-10 PERCENT | | 1.450 | | | | |
| MODULATION LOSS, DB | -5.36 | -2.18 | | | | |
| + TOLERANCE | 1.17 | 0.29 | | | | |
| - TOLERANCE | -1.42 | -0.44 | | | | |
| SIGNAL POWER, DBM | -150.1 | -146.9 | | | | |
| + TOLERANCE | 4.32 | 3.44 | | | | |
| - TOLERANCE | -3.27 | -2.29 | | | | |
| PREDETECTION NOISE BW, HZ | 12.0 | 27. | | | | |
| +- HZ | 0. | 2.7 | | | | |
| NOISE POWER, DBM | -165.6 | -162.2 | | | | |
| + TOLERANCE | 0.84 | 1.25 | | | | |
| - TOLERANCE | -1.04 | -1.49 | | | | |
| THRESHOLD SNR, DB | 11.40 | 9.00 | | | | |
| +- DB | 0. | 1.0 | | | | |
| MAXIMUM MARGIN, DB | 9.46 | 12.15 | | | | |
| NOMINAL MARGIN, DB | 4.10 | 6.21 | | | | |
| MINIMUM MARGIN, DB | -0. | 1.67 | | | | |

***USE OF 210 FT. PARABOLIC ANTENNA (GAIN=61+-1 DB) RESULTS IN THE FOLLOWING***

| | | |
|---|---|---|
| MINIMUM MARGIN, DB | 7.50 | 9.17 |

DECIBEL ALLOCATION SUMMARY

MODE DESCRIPTION--SURVEYOR MISSION G
LUNAR OPERATION - OMNI A - XMTR A
DOWN LINK - HIGH POWER - 1100 BPS PCM DATA

| | NOMINAL | + TOL | - TOL |
|---|---|---|---|
| TRANSMITTING SYSTEM | | | |
| 1) RF POWER, DBM | 40.60 | 0.20 | -0. |
| 2) CIRCUIT LOSS, DB | -2.77 | 0.50 | -0.50 |
| 3) ANTENNA GAIN, DB | -6.35 | 0. | 0. |
| PERCENT GAIN COVERAGE | | | |
| 4) POINTING LOSS, DB | 0. | 0. | 0. |
| PATH PARAMETERS | | | |
| 5) SLANT RANGE (MAX), KM | 406000.0 | | |
| 6) CARRIER FREQUENCY, MHZ | 2295.00 | | |
| 7) ATMOSPHERIC ABSORPTION, DB | 0. | 0. | -0.20 |
| 8) SPACE LOSS (MAX), DB | -211.834 | | |
| RECEIVING SYSTEM | | | |
| ANTENNA TYPE-- 85 FT. PARABOLIC | | | |
| 9) ANTENNA GAIN, DB | 53.00 | 1.00 | -0.50 |
| 10) POLARIZATION LOSS, DB | 0. | 0. | 0. |
| PREAMPLIFIER-- MASER | | | |
| 11) CIRCUIT LOSS, DB | -0.18 | 0.05 | -0.05 |
| 12) SYSTEM NOISE TEMP, DEG. K | 165.00 | 35.00 | -35.00 |
| 13) NOISE SPECTRAL DENSITY, DBM/HZ | -176.43 | 0.84 | -1.04 |
| TOTAL RECEIVED POWER, DBM | -127.53 | 1.75 | -1.25 |

| | CARRIER | CH 1 | CH 2 | CH 3 | CH 4 | IF |
|---|---|---|---|---|---|---|
| SCO CENTER FREQUENCY, KHZ | | 7.35 | | | | |
| DATA/SUBCARRIER MOD. INDICES | | 1.00 | | | | |
| SCO/CARRIER MOD. INDICES +-10 PERCENT | | 0.935 | | | | |
| MODULATION LOSS, DB | -2.01 | -4.56 | | | | |
| + TOLERANCE | 0.40 | 0.62 | | | | |
| - TOLERANCE | -0.46 | -0.73 | | | | |
| SIGNAL POWER, DBM | -129.5 | -132.1 | | | | |
| + TOLERANCE | 2.15 | 2.37 | | | | |
| - TOLERANCE | -1.71 | -1.98 | | | | |
| PREDETECTION NOISE BW, HZ | 12.0 | 1290. | | | | |
| +- HZ | 0. | 129.0 | | | | |
| NOISE POWER, DBM | -165.6 | -145.3 | | | | |
| + TOLERANCE | 0.84 | 1.25 | | | | |
| - TOLERANCE | -1.04 | -1.49 | | | | |
| THRESHOLD SNR, DB | 11.40 | 9.00 | | | | |
| +- DB | 0. | 1.0 | | | | |
| MAXIMUM MARGIN, DB | 27.88 | 9.09 | | | | |
| NOMINAL MARGIN, DB | 24.69 | 4.23 | | | | |
| MINIMUM MARGIN, DB | 22.15 | -0. | | | | |

***USE OF 210 FT. PARABOLIC ANTENNA (GAIN=61+-1 DB) RESULTS IN THE FOLLOWING***

| | | |
|---|---|---|
| MINIMUM MARGIN, DB | 29.65 | 7.50 |

DECIBEL ALLOCATION SUMMARY

MODE DESCRIPTION--SURVEYOR MISSION G
LUNAR OPERATION - OMNI A - XMTR A
200 LINE TV (ASSUMES 4 VOLT VIDEO SIGNAL) - HIGH POWER

| | | NOMINAL | + TOL | - TOL |
|---|---|---|---|---|
| TRANSMITTING SYSTEM | | | | |
| 1) RF POWER, DBM | | 40.60 | 0.20 | -0. |
| 2) CIRCUIT LOSS, DB | | -2.77 | 0.50 | -0.50 |
| 3) ANTENNA GAIN, DB | | -7.09 | 0. | 0. |
| PERCENT GAIN COVERAGE | | | | |
| 4) POINTING LOSS, DB | | 0. | 0. | 0. |
| PATH PARAMETERS | | | | |
| 5) SLANT RANGE (MAX), KM | 406000.0 | | | |
| 6) CARRIER FREQUENCY, MHZ | 2295.00 | | | |
| 7) ATMOSPHERIC ABSORPTION, DB | | 0. | 0. | -0.20 |
| 8) SPACE LOSS (MAX), DB | | -211.834 | | |
| RECEIVING SYSTEM | | | | |
| ANTENNA TYPE-- 85 FT. PARABOLIC | | | | |
| 9) ANTENNA GAIN, DB | | 53.00 | 1.00 | -0.50 |
| 10) POLARIZATION LOSS, DB | | 0. | 0. | 0. |
| PREAMPLIFIER-- MASER | | | | |
| 11) CIRCUIT LOSS, DB | | -0.18 | 0.05 | -0.05 |
| 12) SYSTEM NOISE TEMP, DEG. K | | 165.00 | 35.00 | -35.00 |
| 13) NOISE SPECTRAL DENSITY, DBM/HZ | | -176.43 | 0.84 | -1.04 |
| TOTAL RECEIVED POWER, DBM | | -128.27 | 1.75 | -1.25 |

| | CARRIER | CH 1 | CH 2 | CH 3 | CH 4 | IF |
|---|---|---|---|---|---|---|
| MODULATING FREQ. (MAX), KHZ | 1.20 | | | | | |
| PEAK CARRIER DEVIATION, KHZ | 5.00 | | | | | |
| SCO/CARRIER MOD. INDICES | 3.330 | | | | | |
| +-10 PERCENT | | | | | | |
| MODULATION LOSS, DB | 0. | | | | | |
| + TOLERANCE | 0. | | | | | |
| - TOLERANCE | 0. | | | | | |
| SIGNAL POWER, DBM | -128.3 | | | | | |
| + TOLERANCE | 1.75 | | | | | |
| - TOLERANCE | -1.25 | | | | | |
| PREDETECTION NOISE BW, KHZ | 11.4 | | | | | |
| +- KHZ | 0. | | | | | |
| NOISE POWER, DBM | -135.9 | | | | | |
| + TOLERANCE | 0.84 | | | | | |
| - TOLERANCE | -1.04 | | | | | |
| THRESHOLD SNR, DB | 4.50 | | | | | |
| +- DB | 0. | | | | | |
| MAXIMUM MARGIN, DB | 6.87 | | | | | |
| NOMINAL MARGIN, DB | 3.09 | | | | | |
| MINIMUM MARGIN, DB | -0. | | | | | |

***USE OF 210 FT. PARABOLIC ANTENNA (GAIN=61+-1 DB) RESULTS IN THE FOLLOWING***

| | |
|---|---|
| MINIMUM MARGIN, DB | 7.50 |

## DECIBEL ALLOCATION SUMMARY

MODE DESCRIPTION--SURVEYOR MISSION G
LUNAR OPERATION - PLANAR ARRAY
DOWN LINK - 4400 BPS PCM DATA - LOW POWER - XMTR A

| | NOMINAL | + TOL | - TOL |
|---|---|---|---|
| TRANSMITTING SYSTEM | | | |
| 1) RF POWER, DBM | 23.70 | 1.60 | -0.60 |
| 2) CIRCUIT LOSS, DB | -2.30 | 0. | -0.22 |
| 3) ANTENNA GAIN, DB | 27.00 | 0.50 | -0.50 |
| PERCENT GAIN COVERAGE | | | |
| 4) POINTING LOSS, DB | 0. | 0. | 0. |
| PATH PARAMETERS | | | |
| 5) SLANT RANGE (MAX), KM 406000.0 | | | |
| 6) CARRIER FREQUENCY, MHZ 2295.00 | | | |
| 7) ATMOSPHERIC ABSORPTION, DB | 0. | 0. | -0.20 |
| 8) SPACE LOSS (MAX), DB | -211.834 | | |
| RECEIVING SYSTEM | | | |
| ANTENNA TYPE-- 85 FT. PARABOLIC | | | |
| 9) ANTENNA GAIN, DB | 53.00 | 1.00 | -0.50 |
| 10) POLARIZATION LOSS, DB | 0. | 0. | 0. |
| PREAMPLIFIER-- MASER | | | |
| 11) CIRCUIT LOSS, DB | -0.18 | 0.05 | -0.05 |
| 12) SYSTEM NOISE TEMP, DEG. K | 165.00 | 35.00 | -35.00 |
| 13) NOISE SPECTRAL DENSITY, DBM/HZ | -176.43 | 0.84 | -1.04 |
| TOTAL RECEIVED POWER, DBM | -110.61 | 3.15 | -2.07 |

| | CARRIER | CH 1 | CH 2 | CH 3 | CH 4 | IF |
|---|---|---|---|---|---|---|
| SCO CENTER FREQUENCY, KHZ | | 33.00 | | | | |
| DATA/SUBCARRIER MOD. INDICES | | 0.90 | | | | |
| SCO/CARRIER MOD. INDICES +-10 PERCENT | | 1.600 | | | | |
| MODULATION LOSS, DB | -6.83 | -1.87 | | | | |
| + TOLERANCE | 1.56 | 0.16 | | | | |
| - TOLERANCE | -1.96 | -0.33 | | | | |
| SIGNAL POWER, DBM | -117.4 | -112.5 | | | | |
| + TOLERANCE | 4.71 | 3.31 | | | | |
| - TOLERANCE | -4.03 | -2.40 | | | | |
| PREDETECTION NOISE BW, HZ | 12.0 | 5160. | | | | |
| +- HZ | 0. | 516.0 | | | | |
| NOISE POWER, DBM | -165.6 | -139.3 | | | | |
| + TOLERANCE | 0.84 | 1.25 | | | | |
| - TOLERANCE | -1.04 | -1.49 | | | | |
| THRESHOLD SNR, DB | 11.40 | 9.00 | | | | |
| +- DB | 0. | 1.0 | | | | |
| MAXIMUM MARGIN, DB | 42.53 | 23.61 | | | | |
| NOMINAL MARGIN, DB | 36.79 | 17.81 | | | | |
| MINIMUM MARGIN, DB | 31.92 | 13.16 | | | | |

***USE OF 210 FT. PARABOLIC ANTENNA (GAIN=61+-1 DB) RESULTS IN THE FOLLOWING***

| | | | | | | |
|---|---|---|---|---|---|---|
| MINIMUM MARGIN, DB | 39.42 | 20.66 | | | | |

DECIBEL ALLOCATION SUMMARY

MODE DESCRIPTION--SURVEYOR MISSION G
LUNAR OPERATION - PLANAR ARRAY
6CC LINE TV(ASSUMES 4 VOLT VIDEO SIGNAL) - HIGH POWER

| | | NOMINAL | + TOL | - TOL |
|---|---|---|---|---|
| TRANSMITTING SYSTEM | | | | |
| 1) RF POWER, DBM | | 40.60 | 0.20 | -0. |
| 2) CIRCUIT LOSS, DB | | -2.30 | 0. | -0.22 |
| 3) ANTENNA GAIN, DB | | 27.00 | 0.50 | -0.50 |
| PERCENT GAIN COVERAGE | | | | |
| 4) POINTING LOSS, DB | | 0. | 0. | 0. |
| PATH PARAMETERS | | | | |
| 5) SLANT RANGE (MAX), KM | 406000.0 | | | |
| 6) CARRIER FREQUENCY, MHZ | 2295.00 | | | |
| 7) ATMOSPHERIC ABSORPTION, DB | | 0. | 0. | -0.20 |
| 8) SPACE LOSS (MAX), DB | | -211.834 | | |
| RECEIVING SYSTEM | | | | |
| ANTENNA TYPE-- 85 FT. PARABOLIC | | | | |
| 9) ANTENNA GAIN, DB | | 53.00 | 1.00 | -0.50 |
| 10) POLARIZATION LOSS, DB | | 0. | 0. | 0. |
| PREAMPLIFIER-- MASER | | | | |
| 11) CIRCUIT LOSS, DB | | -0.18 | 0.05 | -0.05 |
| 12) SYSTEM NOISE TEMP, DEG. K | | 165.00 | 35.00 | -35.00 |
| 13) NOISE SPECTRAL DENSITY, DBM/HZ | | -176.43 | 0.84 | -1.04 |
| TOTAL RECEIVED POWER, DBM | | -93.71 | 1.75 | -1.47 |

| | CARRIER | CH 1 | CH 2 | CH 3 | CH 4 | IF |
|---|---|---|---|---|---|---|
| MODULATING FREQ. (MAX), KHZ | 220.00 | | | | | |
| PEAK CARRIER DEVIATION, KHZ | 1250.00 | | | | | |
| SCO/CARRIER MOD. INDICES | 4.550 | | | | | |
| +-10 PERCENT | | | | | | |
| MODULATION LOSS, DB | 0. | | | | | |
| + TOLERANCE | 0. | | | | | |
| - TOLERANCE | 0. | | | | | |
| SIGNAL POWER, DBM | -93.7 | | | | | |
| + TOLERANCE | 1.75 | | | | | |
| - TOLERANCE | -1.47 | | | | | |
| PREDETECTION NOISE BW, KHZ | 3400.0 | | | | | |
| +- KHZ | 0. | | | | | |
| NOISE POWER, DBM | -111.1 | | | | | |
| + TOLERANCE | 0.84 | | | | | |
| - TOLERANCE | -1.04 | | | | | |
| THRESHOLD SNR, DB | 10.50 | | | | | |
| +- DB | 0. | | | | | |
| MAXIMUM MARGIN, DB | 10.68 | | | | | |
| NOMINAL MARGIN, DB | 6.90 | | | | | |
| MINIMUM MARGIN, DB | 3.59 | | | | | |

***USE OF 210 FT. PARABOLIC ANTENNA (GAIN=61+-1 DB) RESULTS IN THE FOLLOWING***

MINIMUM MARGIN, DB 11.09

DECIBEL ALLOCATION SUMMARY

MODE DESCRIPTION--SURVEYOR MISSION G
LUNAR OPERATION - PLANAR ARRAY
200 LINE TV(ASSUMES 4 VOLT VIDEO SIGNAL) - LOW POWER

| | | NOMINAL | + TOL | - TOL |
|---|---|---|---|---|
| TRANSMITTING SYSTEM | | | | |
| 1) RF POWER, DBM | | 23.70 | 1.60 | -0.60 |
| 2) CIRCUIT LOSS, DB | | -2.30 | 0. | -0.22 |
| 3) ANTENNA GAIN, DB | | 27.00 | 0.50 | -0.50 |
| PERCENT GAIN COVERAGE | | | | |
| 4) POINTING LOSS, DB | | 0. | 0. | 0. |
| PATH PARAMETERS | | | | |
| 5) SLANT RANGE (MAX), KM | 406000.0 | | | |
| 6) CARRIER FREQUENCY, MHZ | 2295.00 | | | |
| 7) ATMOSPHERIC ABSORPTION, DB | | 0. | 0. | -0.20 |
| 8) SPACE LOSS (MAX), DB | | -211.834 | | |
| RECEIVING SYSTEM | | | | |
| ANTENNA TYPE-- 85 FT. PARABOLIC | | | | |
| 9) ANTENNA GAIN, DB | | 53.00 | 1.00 | -0.50 |
| 10) POLARIZATION LOSS, DB | | 0. | 0. | 0. |
| PREAMPLIFIER-- MASER | | | | |
| 11) CIRCUIT LOSS, DB | | -0.18 | 0.05 | -0.05 |
| 12) SYSTEM NOISE TEMP, DEG. K | | 165.00 | 35.00 | -35.00 |
| 13) NOISE SPECTRAL DENSITY, DBM/HZ | | -176.43 | 0.84 | -1.04 |
| TOTAL RECEIVED POWER, DBM | | -110.61 | 3.15 | -2.07 |

| | CARRIER | CH 1 | CH 2 | CH 3 | CH 4 | IF |
|---|---|---|---|---|---|---|
| MODULATING FREQ. (MAX), KHZ | 1.20 | | | | | |
| PEAK CARRIER DEVIATION, KHZ | 5.00 | | | | | |
| SCO/CARRIER MOD. INDICES | 3.330 | | | | | |
| +-10 PERCENT | | | | | | |
| MODULATION LOSS, DB | 0. | | | | | |
| + TOLERANCE | 0. | | | | | |
| - TOLERANCE | 0. | | | | | |
| SIGNAL POWER, DBM | -110.6 | | | | | |
| + TOLERANCE | 3.15 | | | | | |
| - TOLERANCE | -2.07 | | | | | |
| PREDETECTION NOISE BW, KHZ | 11.4 | | | | | |
| +- KHZ | 0. | | | | | |
| NOISE POWER, DBM | -135.9 | | | | | |
| + TOLERANCE | 0.84 | | | | | |
| - TOLERANCE | -1.04 | | | | | |
| THRESHOLD SNR, DB | 4.50 | | | | | |
| +- DB | 0. | | | | | |
| MAXIMUM MARGIN, DB | 25.93 | | | | | |
| NOMINAL MARGIN, DB | 20.74 | | | | | |
| MINIMUM MARGIN, DB | 16.84 | | | | | |

***USE OF 210 FT. PARABOLIC ANTENNA (GAIN=61+-1 DB) RESULTS IN THE FOLLOWING***

MINIMUM MARGIN, DB 24.34

DECIBEL ALLOCATION SUMMARY

MODE DESCRIPTION--SURVEYOR MISSION G
ALPHA SCATTERING/550 BPS PCM DATA (LOW MI)
LOW POWER/PLANAR ARRAY

| | NOMINAL | + TOL | - TOL |
|---|---|---|---|
| TRANSMITTING SYSTEM | | | |
| 1) RF POWER, DBM | 23.70 | 1.60 | -0.60 |
| 2) CIRCUIT LOSS, DB | -2.30 | 0. | -0.22 |
| 3) ANTENNA GAIN, DB | 27.00 | 0.50 | -0.50 |
| PERCENT GAIN COVERAGE | | | |
| 4) POINTING LOSS, DB | 0. | 0. | 0. |
| PATH PARAMETERS | | | |
| 5) SLANT RANGE (MAX), KM | 406000.0 | | |
| 6) CARRIER FREQUENCY, MHZ | 2295.00 | | |
| 7) ATMOSPHERIC ABSORPTION, DB | 0. | 0. | -0.20 |
| 8) SPACE LOSS (MAX), DB | -211.834 | | |
| RECEIVING SYSTEM | | | |
| ANTENNA TYPE-- 85 FT. PARABOLIC | | | |
| 9) ANTENNA GAIN, DB | 53.00 | 1.00 | -0.50 |
| 10) POLARIZATION LOSS, DB | 0. | 0. | 0. |
| PREAMPLIFIER-- MASER | | | |
| 11) CIRCUIT LOSS, DB | -0.18 | 0.05 | -0.05 |
| 12) SYSTEM NOISE TEMP, DEG. K | 165.00 | 35.00 | -35.00 |
| 13) NOISE SPECTRAL DENSITY, DBM/HZ | -176.43 | 0.84 | -1.04 |
| TOTAL RECEIVED POWER, DBM | -110.61 | 3.15 | -2.07 |

| | CARRIER | CH 1 | CH 2 | CH 3 | CH 4 | IF |
|---|---|---|---|---|---|---|
| SCO CENTER FREQUENCY, KHZ | | 5.40 | 70.00 | 3.90 | | |
| DATA/SUBCARRIER MOD. INDICES | | 1.47 | 4.77 | 1.07 | | |
| SCO/CARRIER MOD. INDICES +-10 PERCENT | | 0.600 | 1.400 | 0.300 | | |
| MODULATION LOSS, DB | -5.93 | -12.97 | -3.31 | -19.30 | | |
| + TOLERANCE | 1.26 | 1.85 | 0.53 | 2.03 | | |
| - TOLERANCE | -1.49 | -2.16 | -0.69 | -2.35 | | |
| SIGNAL POWER, DBM | -116.5 | -123.6 | -113.9 | -129.9 | | |
| + TOLERANCE | 4.41 | 5.00 | 3.68 | 5.18 | | |
| - TOLERANCE | -3.56 | -4.23 | -2.76 | -4.42 | | |
| PREDETECTION NOISE BW, HZ | 12.0 | 948.1 | 1400.0 | 685.0 | | |
| +- HZ | 0. | 94.8 | 1140.0 | 68.5 | | |
| NOISE POWER, DBM | -165.6 | -146.7 | -135.9 | -148.1 | | |
| + TOLERANCE | 0.84 | 1.25 | 1.25 | 1.25 | | |
| - TOLERANCE | -1.04 | -1.49 | -1.49 | -1.49 | | |
| THRESHOLD SNR, DB | 11.40 | 10.00 | 11.00 | 9.00 | | |
| +- DB | 0. | 1.0 | 1.0 | 1.0 | | |
| MAXIMUM MARGIN, DB | 43.13 | 20.56 | 17.10 | 16.83 | | |
| NOMINAL MARGIN, DB | 37.69 | 13.08 | 10.94 | 9.16 | | |
| MINIMUM MARGIN, DB | 33.30 | 6.60 | 5.92 | 2.49 | | |

***USE OF 210 FT. PARABOLIC ANTENNA (GAIN=61+-1 DB) RESULTS IN THE FOLLOWING***

| | | | | | | |
|---|---|---|---|---|---|---|
| MINIMUM MARGIN, DB | 40.80 | 14.10 | 13.42 | 9.99 | | |

DECIBEL ALLOCATION SUMMARY

MODE DESCRIPTION--SURVEYOR MISSION G
ALPHA SCATTERING/1100 BPS PCM DATA
LOW POWER/PLANAR ARRAY

| | NOMINAL | + TOL | - TOL |
|---|---|---|---|
| TRANSMITTING SYSTEM | | | |
| 1) RF POWER, DBM | 23.70 | 1.60 | -0.60 |
| 2) CIRCUIT LOSS, DB | -2.30 | 0. | -0.22 |
| 3) ANTENNA GAIN, DB | 27.00 | 0.50 | -0.50 |
| PERCENT GAIN COVERAGE | | | |
| 4) POINTING LOSS, DB | 0. | 0. | 0. |
| PATH PARAMETERS | | | |
| 5) SLANT RANGE (MAX), KM | 406000.0 | | |
| 6) CARRIER FREQUENCY, MHZ | 2295.00 | | |
| 7) ATMOSPHERIC ABSORPTION, DB | 0. | 0. | -0.20 |
| 8) SPACE LOSS (MAX), DB | -211.834 | | |
| RECEIVING SYSTEM | | | |
| ANTENNA TYPE-- 85 FT. PARABOLIC | | | |
| 9) ANTENNA GAIN, DB | 53.00 | 1.00 | -0.50 |
| 10) POLARIZATION LOSS, DB | 0. | 0. | 0. |
| PREAMPLIFIER-- MASER | | | |
| 11) CIRCUIT LOSS, DB | -0.18 | 0.05 | -0.05 |
| 12) SYSTEM NOISE TEMP, DEG. K | 165.00 | 35.00 | -35.00 |
| 13) NOISE SPECTRAL DENSITY, DBM/HZ | -176.43 | 0.84 | -1.04 |
| TOTAL RECEIVED POWER, DBM | -110.61 | 3.15 | -2.07 |

| | CARRIER | CH 1 | CH 2 | CH 3 | CH 4 | IF |
|---|---|---|---|---|---|---|
| SCO CENTER FREQUENCY, KHZ | | 5.40 | 70.00 | 7.35 | | |
| DATA/SUBCARRIER MOD. INDICES | | 1.47 | 4.77 | 1.00 | | |
| SCO/CARRIER MOD. INDICES +-10 PERCENT | | 0.600 | 1.400 | 0.935 | | |
| MODULATION LOSS, DB | -7.74 | -14.78 | -5.12 | -10.29 | | |
| + TOLERANCE | 1.62 | 2.21 | 0.89 | 1.84 | | |
| - TOLERANCE | -1.91 | -2.57 | -1.11 | -2.18 | | |
| SIGNAL POWER, DBM | -118.4 | -125.4 | -115.7 | -120.9 | | |
| + TOLERANCE | 4.77 | 5.36 | 4.04 | 4.99 | | |
| - TOLERANCE | -3.98 | -4.64 | -3.18 | -4.25 | | |
| PREDETECTION NOISE BW, HZ | 12.0 | 948.1 | 1400.0 | 1290.0 | | |
| +- HZ | 0. | 94.8 | 1140.0 | 129.0 | | |
| NOISE POWER, DBM | -165.6 | -146.7 | -135.9 | -145.3 | | |
| + TOLERANCE | 0.84 | 1.25 | 1.25 | 1.25 | | |
| - TOLERANCE | -1.04 | -1.49 | -1.49 | -1.49 | | |
| THRESHOLD SNR, DB | 11.40 | 11.00 | 13.00 | 9.00 | | |
| +- DB | 0. | 1.0 | 1.0 | 1.0 | | |
| MAXIMUM MARGIN, DB | 41.68 | 18.11 | 13.65 | 22.90 | | |
| NOMINAL MARGIN, DB | 35.88 | 10.26 | 7.12 | 15.41 | | |
| MINIMUM MARGIN, DB | 31.06 | 3.37 | 1.69 | 8.92 | | |
| ***USE OF 210 FT. PARABOLIC ANTENNA (GAIN=61+-1 DB) RESULTS IN THE FOLLOWING*** | | | | | | |
| MINIMUM MARGIN, DB | 38.56 | 10.87 | 9.19 | 16.42 | | |

# Appendix XX-B
## Radio System Active Elements

**Table XX-B-1. Receiver elements**

| Element type | HAC Part No. | Standard component No. | Special No. | Component manufacturer | Quantity used |
|---|---|---|---|---|---|
| Crystal | 988666 | — | B613-1 | Bliley | 2 |
| Crystal | 988668 | — | B05-1 | Bliley | 1 |
| Diode | 988700 | IN485B | — | — | 8 |
| Diode | 988702 | IN3064 | — | — | 12 |
| Diode | 988703 | IN3070 | — | — | 4 |
| Diode | 988704 | IN757A | — | — | 2 |
| Diode | 988705 | IN1318 | — | — | 1 |
| Diode | 988710 | — | HU 103A | Hoffman | 1 |
| Diode | 988712 | IN2934 | — | — | 1 |
| Diode | 988723 | IN3730 | — | — | 1 |
| Diode | 988732 | — | CD34354 | Continental Devices | 2 |
| Diode | 988903 | — | PC4088 | TRW | 6 |
| Diode | 988909 | IN831 | — | — | 4 |
| Diode | 988929 | — | D5242 | Sylvania | 1 |
| Transistor | 988800 | 2N718A | — | — | 15 |
| Transistor | 988801 | 2N722 | — | — | 1 |
| Transistor | 988802 | 2N871 | S4966 | Fairchild | 3 |
| Transistor | 988805 | 2N869 | — | — | 1 |
| Transistor | 988808 | 2N930 | — | — | 2 |
| Transistor | 988810 | 2N871 | SP8285 | Fairchild | 2 |
| Transistor | 988811 | 2N917 | — | — | 22 |
| Transistor | 988824 | 2N2193A | — | — | 2 |
| Transistor | 988847 | — | S5872 | Fairchild | 2 |
| Transistor | 988852 | 2N918 | — | — | 11 |
| Transistor | 988879 | — | S18172 | Fairchild | 1 |
| Transistor | 988902 | — | FSP358 | Fairchild | 3 |

**Table XX-B-2. Transmitter elements**

| Element type | HAC part No. | Standard component No. | Special No. | Component manufacturer | Quantity used |
|---|---|---|---|---|---|
| Crystal | 988665 | — | B04-1 | Bliley | 1 |
| Crystal | 988687 | — | 00136 | McCoy | 1 |
| Diode | 988700 | IN485B | — | — | 1 |
| Diode | 988701 | IN645 | — | — | 6 |
| Diode | 988702 | IN3064 | — | — | 8 |
| Diode | 988703 | IN3070 | — | — | 3 |
| Diode | 988704 | IN757A | — | — | 7 |
| Diode | 988705 | IN1318 | — | — | 1 |
| Diode | 988719 | — | FA 3077 | Fairchild | 8 |
| Diode | 988723 | IN3730 | — | — | 25 |
| Diode | 988732 | | CD34354 | Continental Devices | 12 |
| Diode | 988903 | — | PC4088 | TRW | 12 |
| Diode | 988917 | IN1930 | — | Microwave Associates | 4 |
| Diode | 988924 | — | MA4078 | — | 1 |
| Transistor | 988801 | 2N722 | — | — | 2 |
| Transistor | 988802 | 2N871 | S4966 | Fairchild | 8 |
| Transistor | 988810 | 2N871 | SP8285 | Fairchild | 5 |
| Transistor | 988811 | 2N917 | — | — | 2 |
| Transistor | 988814 | 2N2891 | — | — | 1 |
| Transistor | 988816 | 2N1724 | — | — | 2 |
| Transistor | 988819 | 2N707A | — | — | 4 |
| Transistor | 988824 | 2N2193A | — | — | 2 |
| Transistor | 988846 | — | MHT8001 | Honeywell | 1 |
| Transistor | 988852 | 2N918 | — | — | 5 |
| Transistor | 988864 | — | S15644 | Fairchild | 3 |

## Bibliography


Herskind, R., *Surveyor Spacecraft Antenna Measurement Program,* Technical Manual 33-367. Jet Propulsion Laboratory, Pasadena, Calif., Mar. 1968.

Moore, W. G., and Weiner, M. R., *Telecommunications Subsystem Production and Performance Summary Document,* SSD 704097. Hughes Aircraft Co., Culver City, Calif., July 21, 1967.

*Surveyor Spacecraft Model A21 Equipment Specification,* HAC 224832, Rev. B. Hughes Aircraft Co., Culver City, Calif.

# XXI. Spacecraft Signal Processing and Command

The *Surveyor* signal processing subsystem accepted, encoded, and prepared the voltages, currents, and resistance changes for transmission that corresponded to various spacecraft parameters, such as events, voltages, temperatures, accelerations, etc. The signal processor employed both pulse code modulation (PCM) and direct frequency modulation (FM) telemetry techniques to encode spacecraft signals for frequency, or for phase modulating spacecraft transmitters.

## A. Signal Processing Subsystem Design

### 1. Design Evolution

In the initial design of the *Surveyor* spacecraft, the signal processor consisted of three major categories:

(1) Engineering signal processor (ESP).

(2) Central signal processor (CSP).

(3) Scientific signal processor (SSP).

Detailed decriptions of the ESP and the CSP are presented in Subsection A-2. Briefly, the ESP was used to process engineering data by using commutators for time-shared data channels and subcarrier oscillators, (SCOs) for continuous data channels. It also provided four modes for the commutated data to accommodate the needs of the different operational phases of the spacecraft. The CSP provided the basic clock for the entire signal processing function, performed the analog-to-digital (A/D) conversion, generated the data synchronization signal, and summed and conditioned the SCO outputs for transmission by the spacecraft transmitter. The SSP contained amplifiers, commutators, SCOs, and gating circuitry which converted the output of the scientific experiments to standard form for transmission.

In April 1963, the SSP was converted into the auxiliary engineering signal processor (AESP) when it was decided to turn the first four *Surveyor* missions into engineering missions. Subsequently, the number of engineering missions was increased to seven, and some scientific instrumentation additions were planned, such as a soil sampler, a lunar ejecta detector, or an alpha scattering device.

The AESP provided two additional engineering commutator modes and was intended to be completely

independent of the existing commutators. A coast phase mode was used to transmit information during the transit phase when the spacecraft was locked on to the sun and Canopus. A thrust phase mode was to be used in case of failure of the existing midcourse and terminal phase modes.

Another unit, the low data rate auxiliary (LDRA) was added in mid-1963 to ensure data reception throughout the transit phase when the transmitter was operating at low power and transmitting through the low gain antenna. With the above operating mode and at 550 bits/sec (550 bits/sec was the lowest bit rate available), continuous reception of data at the specified bit error rate of less than one in $10^5$ could be guaranteed to only approximately 68,000 km. The value of 68,000 km was equivalent to only 5 hr of transit time after injection. The LDRA provided two additional bit rates, 137.5 and 17.2 bits/sec. Two more SCOs were added in the LDRA to accommodate the additional low bit rates. This low data rate capability ensured reception of engineering data throughout the mission.

A third unit, the signal processing auxiliary (SPA), was added in 1963 to enhance the probability of carrier acquisition by the Deep Space Instrumentation Facility (DSIF). The SPA used a 3.9-kHz SCO which phase modulated the transmitter with a modulation index of 0.3 rad peak. This low modulation index increased the ratio of carrier power to sideband power. The normal modulation index at 550 bits/sec using the 3.9-kHz SCO in the CSP was 1.15 rad peak. This shift to a low modulation index provided an additional 3.5 db in carrier power.

Additional continuous-data channels were added during mid-1963. Four additional accelerometers were added to provide more information during the main retro motor burning period. Two SCOs were employed on a time-shared basis to transmit the accelerometer data. Because of the wide bandwidth required to transmit the accelerometer information, the transmitter would have been required to operate at high power and transmit through the planar array antenna. Operational constraints prevented this mode of operation, and the accelerometer channels were later removed for SC-5 through SC-7.

A decision was made at this time to add three strain-gage data channels to permit the reconstruction of touchdown dynamics. The three SCOs required for the strain gages plus the two accelerometer SCOs were located in the AESP.

### 2. Final Design Description

A simplified block diagram of the signal processing subsystem is shown in Fig. XXI-1.

In its first form, the signal processing equipment on *Surveyor* was made up of three commutators, two redundant analog-to-digital converters (A/DCs), two clocking oscillators, seventeen voltage controlled oscillators (VCOs), and associated mode control, rate switching, and signal conditioning amplifiers and networks.* This equipment was contained in several major units:

(1) The CSP contained the two A/DCs, the two sync clock oscillators, three SCOs, four summing amplifiers, and various switching and mode selection circuitry.

(2) The ESP contained a 100-signal commutator, digital word assembly circuits, signal selectors for four modes of operation, and six SCOs for gyro, command reject/enable, and accelerometer inputs.

(3) The AESP contained a 120-signal commutator, digital word assembly circuits, signal switching for the coast and thrust modes, and VCOs for accelerometer and strain-gage inputs.

(4) The SPA contained the low modulation index 3.9-kHz SCO.

(5) The LDRA contained a countdown clock to enable low-speed operation of the signal processing equipment, and two SCOs to provide PCM/FM output.

There were also elements of signal processing incorporated in other subsystems of the spacecraft, as follows:

(1) Part of the television auxiliary (TVA) contained two television subcarrier summing amplifiers, a 16-count commutator, and other signal processing related to television engineering information.

(2) Part of the flight control sensor group contained the quantitative command register/scaler, signal processing related to flight control, and digital word assembly circuitry.

The input signals to the signal processor were derived from various voltage or current pickoff points within the other subsystems as well as from standard telemetry transducing devices such as strain gages, accelerometers,

*Kirsten, C. C., *Surveyor Spacecraft Telecommunications*, Technical Report 32-1105. Jet Propulsion Laboratory, Pasadena, Calif., Mar. 15, 1967.

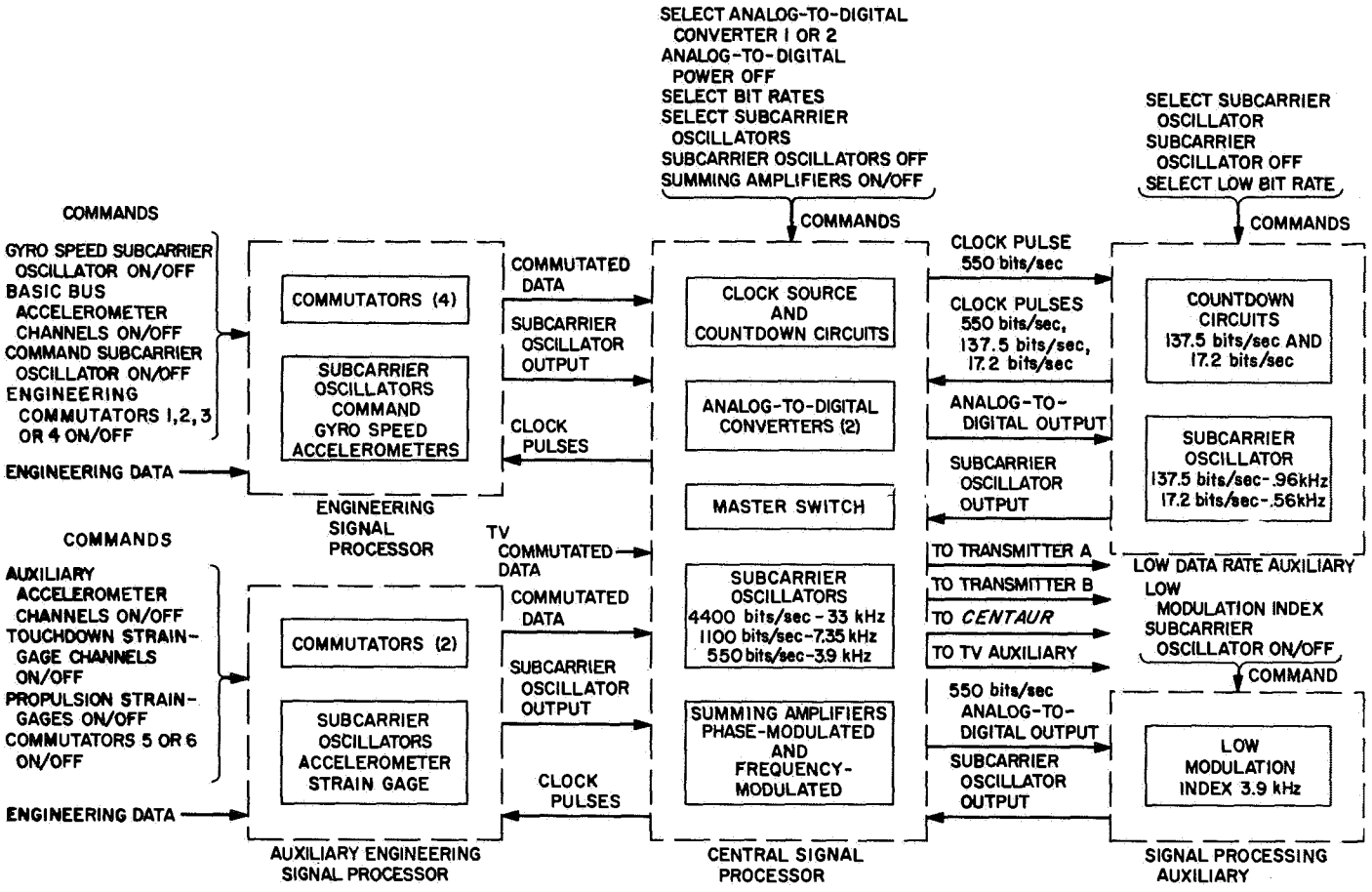



**Fig. XXI-1. Simplified block diagram—signal processing subsystem**

temperature transducers, and pressure transducers. Table XXI-1 depicts typical analog and digital telemetry channel assignments. These signals generally were conditioned to standard ranges by the originating subsystem so that a minimum amount of signal conditioning was required by the signal processor.

As illustrated in Fig. XXI-1, some of the signal inputs were commutated to the input of the A/DC while others were applied directly to SCOs. The directly applied signals were accelerometer and strain gage measurements which required continuous monitoring over the short intervals in which they were active.

The signal processing output was primarily PCM/FM, which phase modulated (PM) or FM the transmitters as commanded from the ground. The PCM comprised commutated signals encoded into 11-bit binary coded words, 10 bits of data for each signal sample plus a parity bit.

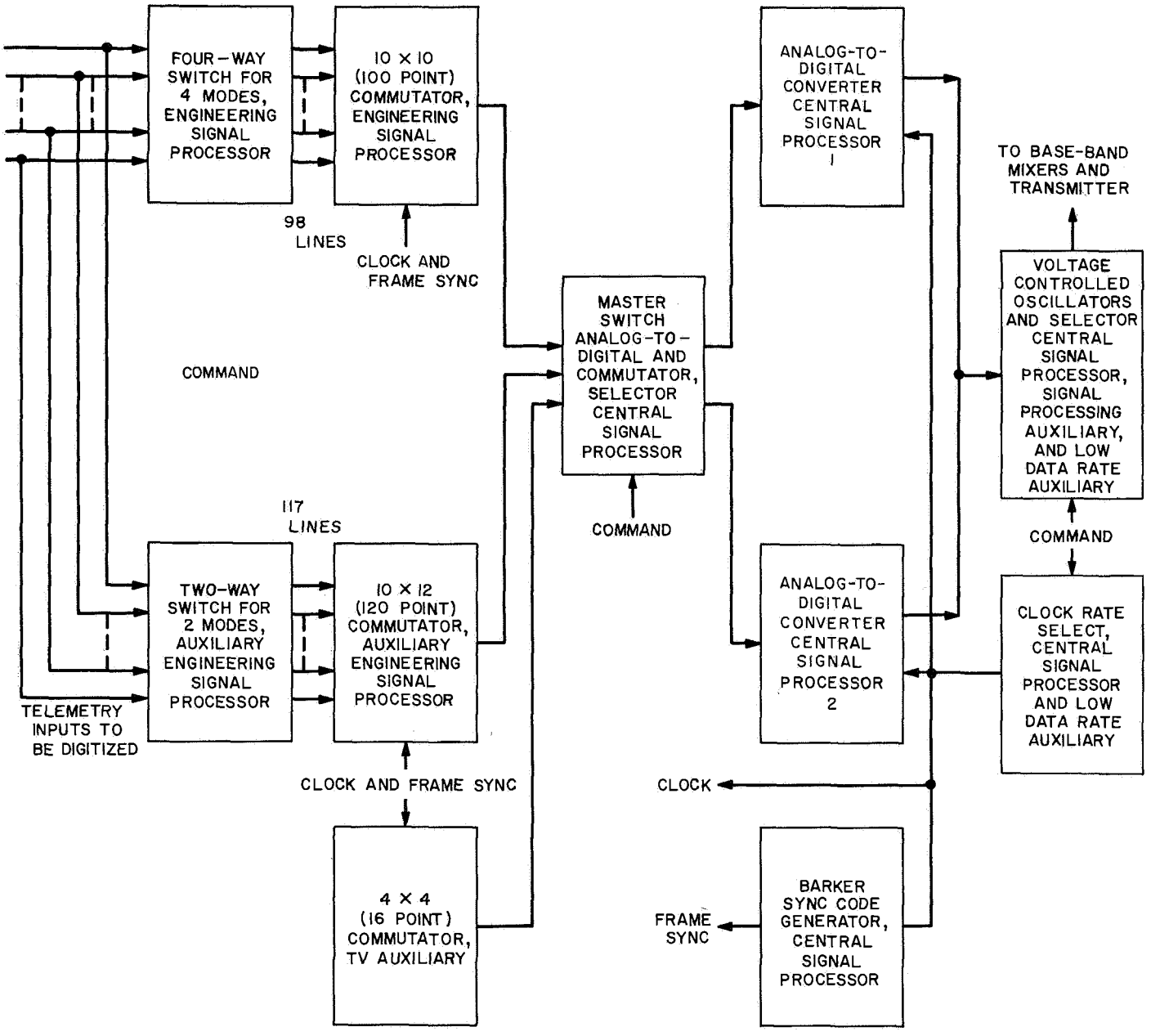
The accuracy requirements of the telemetered data were specified as follows:

(1) Continuous analog channels: The demodulated data channel output should be equal to the channel input to within $\pm 10\%$.

(2) Commutated analog channels:
   (a) Accuracy: The analog data should be converted to binary form to within $\pm 10$ mV.
   (b) Bit error rate: The bit error rate should be less than $3 \times 10^{-3}$ bits/sec.

*a. Commutation.* The six modes of the commutators and the commutation frame rates are shown in Table XXI-2.

The commutators routed the majority of telemetry input signals to the A/DC where they were converted to digital words. The commutators consisted of transistor switches and logic circuits which selected the sequence and number of switch closures. Figure XXI-2 depicts simplified commutation and A/D functions.




FORMATS

WORD = PARITY BIT + 10 BITS INFORMATION
SYNC = 11 BIT BARKER CODE

SYNC ADDRESSES

| | SYNC COMPLEMENT | SYNC | SYNC COMPLEMENT |
|---|---|---|---|
| 100 POINT | – | 00 | 0 |
| 120 POINT | 118 | 119 | 120 |
| 16 POINT | 0 | – | – |

| BIT RATE, bits/sec | VCO OUTPUT | |
|---|---|---|
| 4400 | 33 | kHz |
| 1100 | 7.35 | kHz |
| 550 | 3.9 | kHz |
| 550 | 3.9 | kHz (LOW MODULATION INDEX) |
| 137.5 | 960 | Hz |
| 17.2 | 560 | Hz |

**Fig. XXI-2. Simplified commutation and analog-to-digital functions**

| CHAN | NAME | MODE 1 WORDS | MODE 2 WORDS | MODE 3 WORDS | MODE 4 WORDS | MODE C (5) WORDS | MODE T (6) WORDS |
|---|---|---|---|---|---|---|---|
| **ALPHA SCATTERING INSTRUMENT** | | | | | | | |
| AS-3 | SENSOR HEAD TEMP. | | | | 60 | | |
| AS-4 | ELECTRONICS TEMP. | | | | 70 | | |
| AS-5 | GUARD EVENT MONITOR | | | | 91 | | |
| AS-8 | +7 VDC MONITOR | | | | 37 | | |
| AS-9 | +24 VDC MONITOR | | | | 41 | | |
| **RADIO AND COMMAND DECODING (DATA LINK)** | | | | | | | |
| D-1 | OMNI A TRANSMITTER POWER | | | | 1 | 87 | |
| D-3 | OMNI B TRANSMITTER POWER | | | | 11 | 117 | |
| D-7 | STATIC PHASE ERROR A | 66 | | | 3,23,43,63,83 | 17 | |
| D-8 | STATIC PHASE ERROR B | 98 | | | 13,33,53,73,93 | 27 | |
| D-9 | RECEIVER A AGC | 28,78 | 81 | | 81 | 31 | 81 |
| D-10 | RECEIVER B AGC | 38,88 | 55 | | 17 | 33 | 79 |
| D-13 | TRANSMITTER A TEMPERATURE | | 34 | | 2 | 6 | |
| D-14 | TRANSMITTER B TEMPERATURE | | 44 | | 12 | 30 | 30 |
| D-16 | RECEIVER A AFC | | 61 | | 61 | 37 | |
| D-17 | RECEIVER B AFC | | 15 | | 15,35,55,75,95 | 41 | |
| **ELECTRICAL POWER** | | | | | | | |
| EP-1 | 29V NON-ESSENTIAL VOLTAGE | 90 | 90 | | 27 | 59 | |
| EP-2 | UNREGULATED BUS VOLTAGE | 48 | 48 | 48 | 7,57 | 69 | 69 |
| EP-3 | MAIN BATT MANIFOLD PRESS. | | | | 51 | 63 | |
| EP-4 | UNREGULATED OUTPUT CURRENT | 22 | 22 | | 22 | 9 | 9 |
| EP-6 | BATTERY CHARGE CURRENT | | | | 49 | 45 | |
| EP-7 | BOOST REG DIFFERENCE CURRENT | | 69 | | 69 | 15 | |
| EP-8 | MAIN BATTERY TEMPERATURE | 44 | | | 4 | 40 | 40 |
| EP-9 | BATTERY DISCHARGE CURRENT | 72 | 72 | | 72 | 29 | 29 |
| EP-10 | SOLAR CELL ARRAY VOLTAGE | | | | 47 | 67 | |
| EP-11 | SOLAR CELL ARRAY CURRENT | 59 | 59 | | 59 | 25 | |
| EP-12 | SOLAR CELL ARRAY TEMPERATURE | | | | 8 | 36 | |
| EP-13 | BOOST REGULATOR TEMPERATURE | 24 | | | 10 | 20 | 20 |
| EP-14 | REGULATED OUTPUT CURRENT | 42 | 42 | | 42 | 39 | 39 |
| EP-17 | RADAR AND SQUIB CURRENT | | 89 | | 89 | 49 | 49 |
| EP-21 | COMPARTMENT A HEATER CURRENT | | | | 9 | | |
| EP-22 | COMPARTMENT B HEATER CURRENT | | | | 29 | | |
| EP-30 | BOOST REG. PREREG. VOLTAGE | 64 | 21 | | 21 | 93 | |
| EP-34 | BATTERY CHARGE REG. TEMP. | | | | 78 | 46 | |
| EP-35 | SOLAR CELL SHORT CKT. CURRENT | | | | | 35 | |
| EP-36 | IRRADIATED SOLAR CELL S.C. CURRENT | | | | | 65 | |
| EP-37 | SOLAR CELL SECTION 2 CURRENT | 79 | 79 | | 79 | | |
| EP-38 | SOLAR CELL OPEN CKT. VOLTAGE | | | | | 55 | |
| EP-40 | FLIGHT CONTROL UNREGULATED CURRENT | 32 | 32 | | 32 | 19 | 19 |
| **FLIGHT CONTROL** | | | | | | | |
| FC-4 | NITROGEN GAS PRESSURE | | | | | 89 | |
| FC-5 | PRIM. SUN SENSOR PITCH ERROR | 10,60 | | | | 71 | |
| FC-6 | PRIM. SUN SENSOR YAW ERROR | 20,70 | | | | 77 | |
| FC-7 | SECONDARY SUN SENSOR CELL A | | 27 | | | 99 | |
| FC-8 | SECONDARY SUN SENSOR CELL B | | 35 | | | 101 | |
| FC-9 | SECONDARY SUN SENSOR CELL C | | 47 | | | 105 | |
| FC-10 | SECONDARY SUN SENSOR CELL D | | 37 | | | 107 | |
| FC-12 | CANOPUS ERROR | 7,27,47,67,87 | | | | 109 | |
| FC-14 | STAR INTENSITY SIGNAL | 9,29,49,69,89 | | | | 115 | |
| FC-15 | ACCELERATION ERROR | 11,31,51,71,91 | 11 | 11 | | | 6,36,66,96 |
| FC-16 | PITCH GYRO ERROR | 12,62 | 12,73 | 12 | | 1 | 1,31,61,91 |
| FC-17 | YAW GYRO ERROR | 18,68 | 18,77 | 18 | | 3 | 3,33,63,93 |
| FC-25 | THRUST CMD TO VERNIER ENG 1 | 15,35,55,75,95 | 9,63 | 9,19,29,39 | | | 17,47,77,107 |
| FC-26 | THRUST CMD TO VERNIER ENG 2 | 16,36,56,76,96 | 1,49 | 1,21,31,41 | | | 15,45,75,105 |
| FC-27 | THRUST CMD TO VERNIER ENG 3 | 3,23,43,63,83 | 2,52 | 2,22,32,42 | | | 16,46,76,106 |
| FC-32 | RETRO ACCELEROMETER | | 7,57 | 24 | | | 8,38,68,98 |
| FC-35 | RADAR ALTIMETER RANGE SIGNAL | | 74 | 44 | | | 18,48,78,108 |
| FC-39 | DOPPLER VELOCITY Vx | | 51 | 38 | | | 24,54,84,114 |
| FC-40 | DOPPLER VELOCITY Vy | | 43,93 | 34 | | | 25,55,85,115 |
| FC-41 | DOPPLER VELOCITY Vz | | 3,53 | 3,23,33,43 | | | 26,56,86,116 |
| FC-43 | ROLL ACTIVATOR SIGNAL | 1,21,41,61,81 | 41,91 | 7,27,37,47 | | | 27,57,87,117 |
| FC-44 | FLIGHT CONTROL E/U TEMP 1 | | 70 | | | | |
| FC-45 | FLIGHT CONTROL E/U TEMP 2 | | 24 | | | 18 | |
| FC-46 | ROLL GYRO TEMPERATURE | | 60 | | | 68 | |
| FC-47 | CANOPUS SENSOR TEMPERATURE | | | | | 48 | |
| FC-48 | NITROGEN GAS TANK TEMP. | | | | 18 | 82 | |
| FC-49 | ROLL PRECESSION COMMAND | 17,37,57,77,97 | 17 | 17 | | 5 | 5,35,65,95 |
| FC-50 | PITCH PRECESSION COMMAND | | 10 | | | 7 | 58 |
| FC-51 | YAW PRECESSION COMMAND | | 87 | | | 11 | 109 |
| FC-53 | SEC. SUN SENSOR CENTER CELL | | 29 | | | 97 | |
| FC-54 | PITCH GYRO TEMPERATURE | | 20 | | | 110 | 110 |
| FC-55 | YAW GYRO TEMPERATURE | | 80 | | | 98 | |
| FC-70 | ATTITUDE GAS JET 2 TEMP | | | | | 102 | |
| FC-71 | ROLL ACTUATOR TEMPERATURE | | | | | 104 | |
| FC-77 | FLT. CONT'L REFERENCE RETURN | | 23 | | | | 99 |
| **MECHANISMS** | | | | | | | |
| M-3 | SOLAR PANEL POSITION | | | | 71 | 57 | |
| M-4 | POLAR AXIS POSITION | | 98 | | 98 | 61 | |
| M-6 | ELEVATION AXIS POSITION | | | | 77 | 79 | |
| M-7 | ROLL AXIS POSITION | | | | 87 | 91 | |
| M-8 | PLANAR ARRAY TEMPERATURE | | | | 14 | 38 | |
| M-10 | SOLAR PANEL STEP. MOTOR TEMP. | | | | 58 | 44 | |
| M-12 | ELEV. AXIS STEP. MOTOR TEMP | | | | 64 | 106 | |
| SPARE | (HIGH-ACC. TEMP) | | | | 80,90 | | |
| CHAN | NAME | MODE 1 WORDS | MODE 2 WORDS | MODE 3 WORDS | MODE 4 WORDS | MODE C (5) WORDS | MODE T (6) WORDS |

| CHAN | NAME | MODE 1 WORDS | MODE 2 WORDS | MODE 3 WORDS | MODE 4 WORDS | MODE C (5) WORDS | MODE T (6) WORDS |
|---|---|---|---|---|---|---|---|
| **PROPULSION** | | | | | | | |
| P-1 | HELIUM PRESSURE | 84 | 25 | | | 21 | 21 |
| P-2 | OXIDIZER PRESSURE 3 | 30 | 30 | | | 51 | 51 |
| P-3 | UPPER RETRO CASE TEMPERATURE | | 68 | | | 52 | |
| P-4 | VERNIER LINES 2 TEMPERATURE | 2 | | | | 80 | 80 |
| P-5 | VERNIER FUEL TANK 2 TEMP. | | 66 | | | 12 | |
| P-6 | VERNIER OXIDIZER TANK 3 TEMP. | | 86 | | | 56 | |
| P-7 | VERNIER ENGINE 1 TEMPERATURE | 26 | | | | 70 | 70 |
| P-8 | VERNIER LINES 1 TEMPERATURE | 52 | | | | 90 | 90 |
| P-9 | VERNIER LINES 3 TEMPERATURE | 82 | | | | 100 | 100 |
| P-10 | VERNIER ENGINE 2 TEMPERATURE | 80 | | | | 50 | 50 |
| P-11 | VERNIER ENGINE 3 TEMPERATURE | 46 | | | | 60 | 60 |
| P-12 | LOWER RETRO CASE TEMPERATURE | | 88 | | | 28 | |
| P-13 | VERNIER FUEL TANK 1 TEMP. | | 56 | | | 4 | |
| P-14 | VERNIER FUEL TANK 3 TEMP. | | 76 | | | 54 | |
| P-15 | VERNIER OXIDIZER TANK 1 TEMP. | | 82 | | | 92 | |
| P-16 | VERNIER OXIDIZER TANK 2 TEMP. | | 84 | | | 2 | |
| P-17 | HELIUM TANK TEMP. | | | | 20 | 86 | |
| P-18 | VERNIER ENGINE 1 STRAIN GAGE | 13,33,53,73,93 | 13 | 13 | | | 7,37,67,97 |
| P-19 | VERNIER ENGINE 2 STRAIN GAGE | 14,34,54,74,94 | 14 | 14 | | | 11,41,71,101 |
| P-20 | VERNIER ENGINE 3 STRAIN GAGE | 8,58 | 8 | 8 | | | 28,88 |
| P-23 | VERNIER FUEL LINE #1 TEMP | | 78 | | | | |
| P-24 | VERNIER FUEL LINE #2 TEMP | | | | | 84 | |
| P-25 | VERNIER FUEL LINE #3 TEMP | | 58 | | | | |
| P-26 | VERNIER FUEL LINE PRESSURE | 86 | | | | | |
| **RADAR** | | | | | | | |
| R-2 | RADVS-R AMPLITUDE | | 26 | 26 | | | 4,64 |
| R-3 | RADVS-D1 AMPLITUDE | | 28 | 28 | | | 44,104 |
| R-4 | RADVS-D2 AMPLITUDE | | 36 | 36 | | | 14,74 |
| R-5 | RADVS-D3 AMPLITUDE | | 46 | 46 | | | 34,94 |
| R-6 | AMR ANTENNA TEMPERATURE | | 54 | | | | |
| R-7 | AMR ELECTRONICS TEMPERATURE | | 64 | | | 26 | |
| R-8 | RADVS KLY. UNIT TEMP. | | 38 | | | 10 | 10 |
| R-9 | RADVS SIG. DATA CONVERT. TEMP. | | 62 | | | 22 | |
| R-10 | DOPPLER RADAR SENSOR TEMP. | | 94 | | | 76 | |
| R-12 | AMR PWR OUTPUT (MAG CURRENT) | | | | | | 59 |
| R-13 | ALTMETER RADAR SENSOR TEMP. | | 96 | | | 24 | |
| R-14 | ALTITUDE MARKING RADAR AGC | | 33 | | | | 43 |
| R-29 | AMR LATE GATE SIGNAL | | 71 | | | | 89 |
| **SURFACE SAMPLER EXPERIMENT** | | | | | | | |
| SS-10 | MOTOR CURRENT | | | | 5,25,45,65,85 | | |
| SS-12 | AUX. ELECTRONICS TEMPERATURE | | | | 62 | 42 | |
| SS-14 | MECHANISM TEMPERATURE | | | | 66 | | |
| SS-15 | ELEVATION MOTOR TEMPERATURE | | | | 76 | | |
| **SIGNAL PROCESSING** | | | | | | | |
| S-1 | REFERENCE VOLTAGE | | 67 | | 67 | | |
| S-2 | REFERENCE RETURN | | 97 | | 97 | | |
| S-5 | COMMUTATOR UNBAL. CURR. (ESP) | | 31 | | 31 | | |
| S-7 | COMMUTATOR UNBAL. CURR. (AESP) | | | | | 47 | |
| S-8 | AESP REFERENCE VOLTAGE | | | | | 81 | |
| EP-18 | FULL SCALE CURR. CALIB. (ESP) | 92 | 92 | | 92 | | |
| EP-19 | MID-SCALE CURR. CALIB. (ESP) | 39 | 39 | | 39 | | |
| EP-20 | ZERO SCALE CURR. CALIB. (ESP) | 19 | 19 | | 19 | | |
| EP-27 | FULL SCALE CURR. CALIB. (AESP) | | | | | 75 | |
| EP-28 | MID-SCALE CURR. CALIB. (AESP) | | | | | 85 | |
| EP-29 | ZERO SCALE CURR. CALIB. (AESP) | | | | | 95 | |
| **TELEVISION** | | | | | | | |
| TV-16 | SURV. CAM. ELECTRONICS TEMP. | | | | 16 | 62 | |
| TV-17 | SURV. CAM. MIRROR ASSY. TEMP. | | | | 82 | 116 | |
| **STRUCTURES (VEHICLE)** | | | | | | | |
| V-5 | LANDING GEAR 1 DEFLECTION | | 75 | | | | |
| V-6 | LANDING GEAR 2 DEFLECTION | | 95 | | | | |
| V-7 | LANDING GEAR 3 DEFLECTION | | 83 | | | | |
| V-15 | COMP. A TEMP. THERMAL TRAY TOP | | | | 24 | 66 | |
| V-16 | COMP. A TEMP. LOWER SUPPORT | | | | 26 | 78 | |
| V-18 | COMP. A TEMP. CANISTER | | | | 30 | 64 | |
| V-19 | COMP. A TEMP. SW. 5 IN CONT. RING | | | | 34 | | |
| V-20 | COMP. A TEMP. SW. 5 IN FACE RAD. | | | | 36 | 32 | |
| V-21 | COMP. B TEMP. TRAY TOP CENTER | | | | 44 | 58 | |
| V-22 | COMP. B TEMP. LOWER SUPPORT | | | | 46 | 74 | |
| V-23 | COMP. B TEMP. CANISTER | | | | 48 | | |
| V-24 | COMP. B TEMP. SW 4 IN FACE RAD. | | | | 52 | 34 | |
| V-25 | COMP. A TEMP. SW 8 IN FACE RAD. | | | | 38 | 94 | |
| V-26 | COMP. B TEMP. SW 4 IN CONT. RING | | | | 54 | | |
| V-27 | UPPER SPACEFRAME TEMP. NO. 1 | | | | 56 | | |
| V-28 | SPACEFRAME TEMP. UNDER COMP. A | | | | | 14 | |
| V-30 | SHOCK ABSORB 1 TEMPERATURE | | | | 68 | 16 | |
| V-32 | SHOCK ABSORB 2 TEMPERATURE | | | | | 8 | |
| V-33 | SHOCK ABSORB 3 TEMPERATURE | | | | | 96 | |
| V-35 | UPPER SPACEFRAME TEMP. NO. 2 | | | | 74 | | |
| V-36 | SPACEFRAME TEMP. UNDER COMP. 3 | | | | 96 | | |
| V-37 | RETRO ATTACH POINT 1 TEMP. | | | | 84 | | |
| V-38 | RETRO ATTACH POINT 2 TEMP. | | | | | 72 | |
| V-39 | RETRO ATTACH POINT 3 TEMP. | | | | 88 | | |
| V-44 | CRUSHABLE BLOCK TEMP. | | | | | 88 | |
| V-45 | COMP. B TEMP. SW 1 IN FACE RAD. | | | | | 108 | |
| V-46 | COMP. B TEMP. SW 5 IN FACE RAD. | | | | 94 | 112 | |
| V-47 | COMP. A TEMP. SW 2 IN FACE RAD. | | | | 86 | 114 | |
| V-49 | COMP. A TEMP. SW 3 IN FACE RAD. | | | | 28 | | |
| CHAN | NAME | MODE 1 WORDS | MODE 2 WORDS | MODE 3 WORDS | MODE 4 WORDS | MODE C (5) WORDS | MODE T (6) WORDS |

**Table XXI-1B. Typical (SC-7) digital telemetry channel assignments**

## COMMUTATED BINARY SIGNALS

### RADIO AND COMMAND DECODING (DATA LINK)

| CHAN | NAME | DIGITAL WORD (BIT) |
|---|---|---|
| D-2 | TRANSMITTER A FILAMENT ON | 6, 10(5) |
| D-4 | TRANSMITTER B FILAMENT ON | 6, 10(6) |
| D-5 | TRANSPONDER A PHASE LOCKED | 6, 10(3) |
| D-6 | TRANSPONDER B PHASE LOCKED | 6, 10(4) |
| D-11 | MESSAGE REJECT | 5, 6, 10, 12(2) |
| D-12 | CENTRAL DECODER A ON | 6, 10(8) |
| D-15 | MESSAGE ENABLE | 5, 6, 10, 12(1) |
| D-18 | CENTRAL DECODER B ON | 6, 10(7) |
| **ELECTRICAL POWER** | | |
| EP-33 | EMA RADVS POWER SWITCH ON | 11(8), 5(4) |
| EP-39 | BCR TO UNREG. BUS | 10(9) |
| **FLIGHT CONTROL** | | |
| FC-13 | CANOPUS LOCK-ON | 1(6) |
| FC-18 | MAGNITUDE REGISTER READOUT | 2 |
| FC-19 | PROGRAMMER ROLL SIGNAL | 3(1) |
| FC-21 | PROGRAMMER PITCH SIGNAL | 3(3) |
| FC-23 | PROGRAMMER YAW SIGNAL | 3(5) |
| FC-28 | VERNIER IGNITION SIGNAL | 3(10), 4(3) |
| FC-29 | RETRO IGNITION SIGNAL | 4(4) |
| FC-30 | RETRO BURNOUT SIGNAL | 4(5) |
| FC-31 | RETRO EJECT SIGNAL | 4(6) |
| FC-33 | RELIABLE OPERATION-RADAR ALT | 9(9) |
| FC-34 | RELIABLE OPERATION-DOPP. RADAR | 9(10) |
| FC-36 | TEN FOOT PER SECOND MARK | 4(9) |
| FC-37 | ONE THOUSAND FOOT MARK | 4(8) |
| FC-38 | THIRTEEN FOOT MARK | 4(10) |
| FC-42 | START RADVS CONTR'LD DESCENT | 4(7) |
| FC-52 | NOMINAL ENGINE THRUST BIAS | 9(8) |
| FC-56 | MANUAL DELAY MODE ON | 3(2) |
| FC-57 | GAS JET AMPL. INHIBITED | 1(8) |
| FC-58 | RATE MODE ON | 9(1) |
| FC-59 | SUN MODE ON | 9(2) |
| FC-60 | STAR MODE ON | 9(3) |
| FC-61 | CRUISE MODE ON | 9(4) |
| FC-62 | RETRO SEQ. MODE ON | 4(1) |
| FC-63 | INERTIA SWITCH SIGNAL | 9(5) |
| R-28 | RADVS ON SIGNAL | 3(6) |
| FC-65 | M/C VELOCITY CORRECTION SIG. | 3(9) |
| FC-66 | THRUST PHASE POWER ON | 3(4) |
| FC-67 | PROG. POS. ANGLE MANEUVER SIG. | 3(7) |
| FC-69 | PRIM SUN SENSOR CNTR. CELL L-O | 1(5) |
| FC-73 | MAN. L-O (SUN OR STAR) | 9(7) |
| FC-74 | PITCH GYRO HTR. CONTROL OFF | 1(9) |
| FC-75 | ROLL GYRO HTR. CONTROL OFF | 1(10) |
| FC-76 | ACQUISITION SUN SENSOR ILLUM. | 1(7) |
| FC-78 | VERNIER ENGINE HIGH THRUST | 9(6) |
| FC-79 | YAW GYRO HEATER CONTROLLER OFF | 3(8) |
| **MECHANISMS** | | |
| M-1 | OMNI ANTENNA A EXTENDED | 7, 11(9) |
| M-2 | OMNI ANTENNA B EXTENDED | 7, 11(10) |
| M-9 | VEHICLE ELECTRICAL DISCONNECT | 1(4) |
| M-11 | SOLAR PANEL LOCK IN TRANS. POS. | 7, 11(3) |
| M-13 | ROLL AXIS LOCK IN TRANS. POS. | 7, 11(4) |
| M-14 | SOLAR PANEL LAUNCH LOCK UNLOCKED | 11(2) |
| M-15 | SOLAR PANEL DEPLOY. LOGIC ON | 7, 11(7) |
| **RADAR** | | |
| R-1 | ALTITUDE MARKING RADAR ON | 5, 12(7) |
| R-11 | AMR ENABLED | 5, 12(8) |
| R-15 | RADVS-$D_1$ TRACKER LOCK | 8, 13(1) |
| R-16 | RADVS-$D_2$ TRACKER LOCK | 8, 13(10) |
| R-17 | RADVS-$D_3$ TRACKER LOCK | 5, 12(3) |
| R-18 | RADVS-R TRACKER LOCK | 5, 12(6) |
| R-19 | RADVS-$D_1$ GAIN 1 (65 TO 40 db) | 8, 13(2) |
| R-20 | RADVS-$D_1$ GAIN 2 (90 TO 65 db) | 8, 13, (3) |
| R-21 | RADVS-$D_2$ GAIN 1 (65 TO 40 db) | 8, 13(4) |
| R-22 | RADVS-$D_2$ GAIN 2 (90 TO 65 db) | 8, 13(5) |
| R-23 | RADVS-$D_3$ GAIN 1 (65 TO 40 db) | 8, 13(6) |
| R-24 | RADVS-$D_3$ GAIN 2 (90 TO 65 db) | 8, 13(7) |
| R-25 | RADVS-R GAIN 1 (60 TO 40 db) | 8, 13(8) |
| R-26 | RADVS-R GAIN 2 (80 TO 60 db) | 8, 13(9) |
| FC-64 | ALTITUDE MARKING RADAR SIG. | 4(2) |
| **SIGNAL PROCESSING** | | |
| S-3 | COMUT. SEL. F/F R500 (ESP MODE 2-3) | 5, 6(10) |
| S-4 | COMUT. SEL. F/F R501 (ESP MODE 3-4) | 5, 6(9) |
| S-6 | COMUT. SEL. F/F R500 (AESP MODE C) | 10(10) |
| **TELEVISION** | | |
| TV-18 | VID. SURV. HEATER OFF | 11(5), 7(8) |

| CHAN | NAME | DIGITAL WORD (BIT) |
|---|---|---|

### ALPHA SCATTERING INSTRUMENT

| CHAN | NAME | DIGITAL WORD (BIT) |
|---|---|---|
| AS-6 | BOTH ALPHA DETECTORS OFF | 7(6) |
| AS-7 | ALL PROTON DETECTORS OFF | 7(5) |
| **STRUCTURES (VEHICLE)** | | |
| V-1 | LANDING GEAR 1 EXTENDED | 1(1) |
| V-2 | LANDING GEAR 2 EXTENDED | 1(2) |
| V-3 | LANDING GEAR 3 EXTENDED | 1(3) |
| V-4 | RETRO NOT EJECTED | 5, 12(5) |
| **SURFACE SAMPLER** | | |
| SS-1 | DECODER POWER ON | 7, 11 (1) |
| SS-2 | COMMAND ENTERED | 7 (2), 11 (6) |
| SPARE | (AESP) | 12 (4, 9, 10) |

| CHAN | NAME | DIGITAL WORD (BIT) |
|---|---|---|

### DIGITAL WORD (DW) SUMMARY

| BIT | DW-1 | DW-3 | DW-4 | DW-5 | DW-6 | DW-7 |
|---|---|---|---|---|---|---|
| 1 | V-1 | FC-19 | FC-62 | D-15 | D-15 | SS-1 |
| 2 | V-2 | FC-56 | FC-64 | D-11 | D-11 | SS-2 |
| 3 | V-3 | FC-21 | FC-28 | R-17 | D-5 | M-11 |
| 4 | M-9 | FC-66 | FC-29 | EP 33 | D-6 | M-13 |
| 5 | FC-69 | FC-23 | FC-30 | V-4 | D-2 | AS-7 |
| 6 | FC-13 | R-28 | FC-31 | R-18 | D-4 | AS-6 |
| 7 | FC-76 | FC-67 | FC-42 | R-1 | D-18 | M-15 |
| 8 | FC-57 | FC-79 | FC-37 | R-11 | D-12 | TV-18 |
| 9 | FC-74 | FC-65 | FC-36 | S-4 | S-4 | M-1 |
| 10 | FC-75 | FC-28 | FC-38 | S-3 | S-3 | M-2 |

| BIT | DW-8 | DW-9 | DW-10 | DW-11 | DW-12 | DW-13 |
|---|---|---|---|---|---|---|
| 1 | R-15 | FC-58 | D-15 | SS-1 | D-15 | R-15 |
| 2 | R-19 | FC-59 | D-11 | M-14 | D-11 | R-19 |
| 3 | R-20 | FC-60 | D-5 | M-11 | R-17 | R-20 |
| 4 | R-21 | FC-61 | D-6 | M-13 | | R-21 |
| 5 | R-22 | FC-63 | D-2 | TV-18 | V-4 | R-22 |
| 6 | R-23 | FC-78 | D-4 | SS-2 | R-18 | R-23 |
| 7 | R-24 | FC-73 | D-18 | M-15 | R-1 | R-24 |
| 8 | R-25 | FC-52 | D-12 | EP-33 | R-11 | R-25 |
| 9 | R-26 | FC-33 | EP-39 | M-1 | | R-26 |
| 10 | R-16 | FC-34 | S-6 | M-2 | | R-16 |

✻ BRACKETED SCO'S TURNED ON BY A SINGLE COMMAND

## COMMUTATED DIGITAL WORDS

| DIGITAL WORD | COMMUTATOR WORDS | | | | | | |
|---|---|---|---|---|---|---|---|
| | MODE 1 | MODE 2 | MODE 3 | MODE 4 | MODE C (5) | MODE T (6) | |
| 1 | 40 | 40 | --- | 40 | 23 | 23 | |
| 2 | 50 | 50 | --- | --- | 53 | 53 | |
| 3 | 5, 25, 45, 65, 85 | 65 | --- | --- | 13, 43, 73, 103 | 13 | |
| 4 | --- | 5, 45, 85 | 5, 10, 15, 20, 25, 30, 35, 40, 45 | --- | --- | 2, 12, 22, 32, 42, 52, 62 72, 82, 92, 102, 112 | |
| 5 | --- | 6 | 6 | --- | --- | --- | |
| 6 | 6 | --- | --- | 6 | --- | --- | |
| 7 | --- | --- | --- | 50 | --- | --- | |
| 8 | --- | 16 | 16 | --- | --- | --- | |
| 9 | 4 | 4 | 4 | --- | 83 | 83 | |
| 10 | --- | --- | --- | --- | 111 | 111 | |
| 11 | --- | --- | --- | --- | 113 | 113 | |
| 12 | --- | --- | --- | --- | --- | 73 | |
| 13 | --- | --- | --- | --- | --- | 103 | |
| SYNC | (100) | (100) | (50) | (100) | 118, 120 | 118, 120 | |
| SYNC COMP | (99) | (99) | (49) | (99) | 119 | 119 | |

### TV COMMUTATOR

| CHAN | NAME | MODE 7 WORDS | |
|---|---|---|---|
| TV-1 | CAMERA NUMBER | 2 | |
| TV-2 | MIRROR AZIMUTH | 3, 11 | |
| TV-3 | MIRROR ELEVATION | 7 | |
| TV-4 | LENS FOCAL LENGTH SETTING | 12 | |
| TV-5 | LENS FOCAL SETTING | 5 | |
| TV-6 | LENS IRIS SETTING | 13 | |
| TV-7 | LENS IRIS SERVO ON | 15 | |
| TV-8 | FILTER WHEEL POSITION | 10 | |
| TV-9 | VIDICON FACEPLATE TEMP. | 8 | |
| TV-10 | CAMERA ELECTRONICS TEMP. | 4 | |
| TV-11 | SHUTTER MODE (OPEN OR NORMAL) | 9 | |
| TV-12 | CALIBRATE VOLTAGE | 6, 14 | |
| TV-13 | MULTIPLE STEP FOCUS ON | 16 | |
| SYNC | (BARKER WORD) | 1 | |

### SUBCARRIER SUMMARY

| CHAN | NAME | SCO FREQ. (KC) | CARRIER MOD. MODE ✻ |
|---|---|---|---|
| D-11, 15 | COMMAND REJECT/ENABLE | 2.3 | PM |
| FC-1 | ROLL GYRO SPEED | 5.4 | PM |
| FC-2 | PITCH GYRO SPEED | | |
| FC-3 | YAW GYRO SPEED | | |
| AS-1 | ALPHA PARTICLE COUNT (2200 BPS) | 70 | PM |
| AS-2 | PROTON COUNT (550 BPS) | 5.4 | |
| V-12 | LEG 1 SHOCK ABSORBER STRAIN GAGE | 1.7 | PM |
| V-13 | LEG 2 SHOCK ABSORBER STRAIN GAGE | 1.3 | |
| V-14 | LEG 3 SHOCK ABSORBER STRAIN GAGE | .96 | |
| TV-14 | COMPOSITE VIDEO | CARRIER | FM |

### COMMUTATED PCM DATA

| BIT RATE (BPS) | SCO CENTER FREQ. (KC) | CARRIER MODULATION |
|---|---|---|
| 4400 | 33 | FM OR PM |
| 1100 | 7.35 | FM OR PM |
| 550 | 3.9 | FM OR PM |
| 550 (LOW MOD INDEX) | 3.9 | PM |
| 137.5 | .96 | PM |
| 17.2 | .56 | PM |
| 4400 (NORMAL MODE TVID) | CARRIER | FM |

**Table XXI-2. Commutation rates and frame lengths**

| Mode designation | Frame length (word positions) | Primary use | Data rate | | | | |
|---|---|---|---|---|---|---|---|
| | | | 17.2 bits/sec 1.5625 words/ sec | 137.5 bits/sec 12.5 words/ sec | 550 bits/sec 50 words/ sec | 1100 bits/sec 100 words/ sec | 4400 bits/sec 400 words/ sec |
| | | | Frame length, sec | | | | |
| 1 | 100 | Attitude maneuver and midcourse velocity correction | 64 | 8 | 2 | 1.0 | 0.25 |
| 2 | 100 | Terminal descent (SC-1 and -2); backup for mode T and miscellaneous telemetry requirements (SC-3 and subsequent) | 64 | 8 | 2 | 1.0 | 0.25 |
| 3 | 50 | Vernier descent (SC-1 and -2); backup for mode T and miscellaneous telemetry requirements (SC-3 and subsequent) | 32 | 4 | 1.0 | 0.5 | 0.125 |
| 4 | 100 | Lunar operation and miscellaneous telemetry requirements | 64 | 8 | 2 | 1.0 | 0.25 |
| C (Coast) | 120 | Launch and coast periods | 76.8 | 9.6 | 2.4 | 1.2 | 0.3 |
| T (Thrust) | 120 | Backup for modes 1, 2, and 3 (SC-1 and -2); terminal and vernier descent (SC-3 and subsequent) | 76.8 | 9.6 | 2.4 | 1.2 | 0.3 |

The commutation in each commutator was accomplished by applying a "commutator advance signal" to the input of a 4-flip-flop, 10-count circuit which addressed one side of a $10 \times 10$ matrix. The output of this 10-count circuit was applied to another counter of a similar circuit, which addressed the other coordinate of the matrix cited above. The first counter may be said to have been the vertical, and the second counter the horizontal count of the commutator matrix. Thus, the commutator would count down in the vertical $Y$ circuit 10 counts before stepping to the next horizontal $X$ position. There were 10 $Y$ positions in both the ESP and the AESP and 10 $X$ positions in the ESP, but there were 12 $X$ positions in the AESP. This provided a 100-word count capacity in the ESP and a 120-word count for the AESP.

These count positions typically represented two possible information inputs for each count position in the AESP, and either three or four information inputs for each count position in the ESP. The inputs were divided into groups of similar nature, and these groups were separately selectable by the mode select commands from ground. Each mode selected many different groups, and a given group could be included in several different mode selections.

The complete sequence of all count positions in a commutator and in the transmission of the associated data words was called a frame of data, for the sequence was transmitted over and over in the same sequence just like elements of a picture frame.

Synchronization of the information frames was accomplished by sending a sync and sync-complement signal at specific word times at the beginning of the frame. These occurred at words 00 and 0 in the ESP, and at words 118, 119, and 120 in the AESP. The synchronization signal was a Barker code (11100010010), that was a calculated series of 11 digits that would be the least likely to occur at random in a binary digital sequence. In the ground decommutator, the Barker code and the Barker code complement were used as the commutator sync indication and sync-complement signal.

***b. Analog-to-digital conversion.*** The commutated measurement was applied to the A/DC. For each measurement, an 11-bit digital word was generated. Ten bits of this word described the voltage level of the input signal and the eleventh bit was used for odd-parity checking. The A/DC employed a 4-flip-flop, 11-count circuit, which provided the timing signals for the 10 binary voltage weighting switches. The incoming signal which had been commutated to the A/DC was compared to a precision reference voltage made of the algebraic sum of all previously selected voltage weightings, plus one-half of the last trial value.

Starting with one-half of the full-scale reference voltage, the incoming voltage was compared to this reference

voltage. If the input voltage was greater than the reference value, the one-half/full-scale weighting value was retained. If the input value was lower than the one-half value, then the reference was abandoned. Next, one-half of the previous trial value was added, making a three-quarter or one-quarter/full-scale reference, depending upon whether the input was above or below the half value. Again, a comparison was made and again the voltage weighting was added or abandoned, depending upon the input voltage.

This process was repeated 10 times, and a binary code of 10 bits was assembled by the binary weighting switches. At the end of assembly, the 10-bit code was provided with a one-bit parity, and transmitted serially by signals derived from the clocking of the active commutator.

The digital words modulated any of six subcarrier oscillators, as shown in Fig. XXI-3. Note that the selected SCO was a function of the selected bit rate. In the case of the normal 550-bit/sec rate, a special low modulation index mode was selectable wherein the RF transmitter deviation was held to approximately 0.3 rad. (This special low modulation index mode left most of the power in the RF carrier which facilitated ground acquisition of the spacecraft signal for launch tracking and doppler determinations.)

Binary measurements such as switch closures or contents of a digital register already existed in digital form and were therefore routed around the A/DC. In these cases, the commutator supplied an inhibit signal to the A/DC, and, by sampling, assembled the digital input information into 10-bit digital words. This binary input information was also passed through the parity checker.

The A/DC also provided the central timing and digital clock signals for the entire system. The selection of one or the other of these A/DCs was by ground command, and provided a backup if one of the A/DCs or its internal clock had failed. The oscillators which controlled the clock frequency in the A/DCs operated at 35.2 kHz and were under crystal control. This frequency was divided down to 8800 Hz. The 8800 Hz was counted down by a series of flip-flops in the bit rate selectors where 4400-, 1100-, or 550-bit/sec operation could be selected. To accommodate unexpected or degraded RF link performance, an additional LDRA had been provided wherein additional countdowns to 137.5 or 17.2 bits/sec could be selected by ground command.

***c. Multiplexing and summing.*** The SCOs were VCOs used to provide frequency multiplexing of the telemetry information. This technique was used to greatly increase the amount of information which was transmitted on the spacecraft carrier frequency as shown in Fig. XXI-3.

The summing amplifiers summed the outputs of the subcarrier oscillators and applied the composite signal to the modulator portion of the spacecraft transmitters. Two types of summing amplifiers were employed to take advantage of the transmitter's ability to transmit either a PM or an FM signal. Selection of the appropriate summing amplifier was by ground command.

***d. Power requirements.*** The entire signal processor system operated from the power bus on the spacecraft that was designated 29-V nonessential. This meant that, had a malfunction developed in the spacecraft which reduced its power delivering capability, the signal processing subsystem would be cut off along with other nonessential functions, to protect such functions as receiver, command decoding, and flight control that operated from the 29-V essential bus.

The signal processing maximum power requirement was 555.5 mA at 29 V. This maximum occurred during the terminal phase when the AESP and the propulsion and touchdown strain gages were all on.

## B. Command System Design

### 1. Design Evolution

The original design of *Surveyor* spacecraft was based on the concept of a completely ground-controlled operation. Since there were expected to be many commands to each subsystem, and a heavy reliance placed upon the reliability of the commands, a central command decoder/subsystem command decoder (CCD/SSD) concept was adopted very early. Reliability was assured by the transmission of complete complementation of both the address and the command word, and then requiring address recognition in both the CCD as well as in the SSD.

Later, the spacecraft experienced a reduction in the command requirements of the scientific experiments, as many of these were removed to meet new weight constraints. There was also a growing recognition that many of the fly-by-wire potentials of the spacecraft would not be realizable due to a very busy schedule of activities during actual flight. These factors generally caused the command system originally conceived to be more than

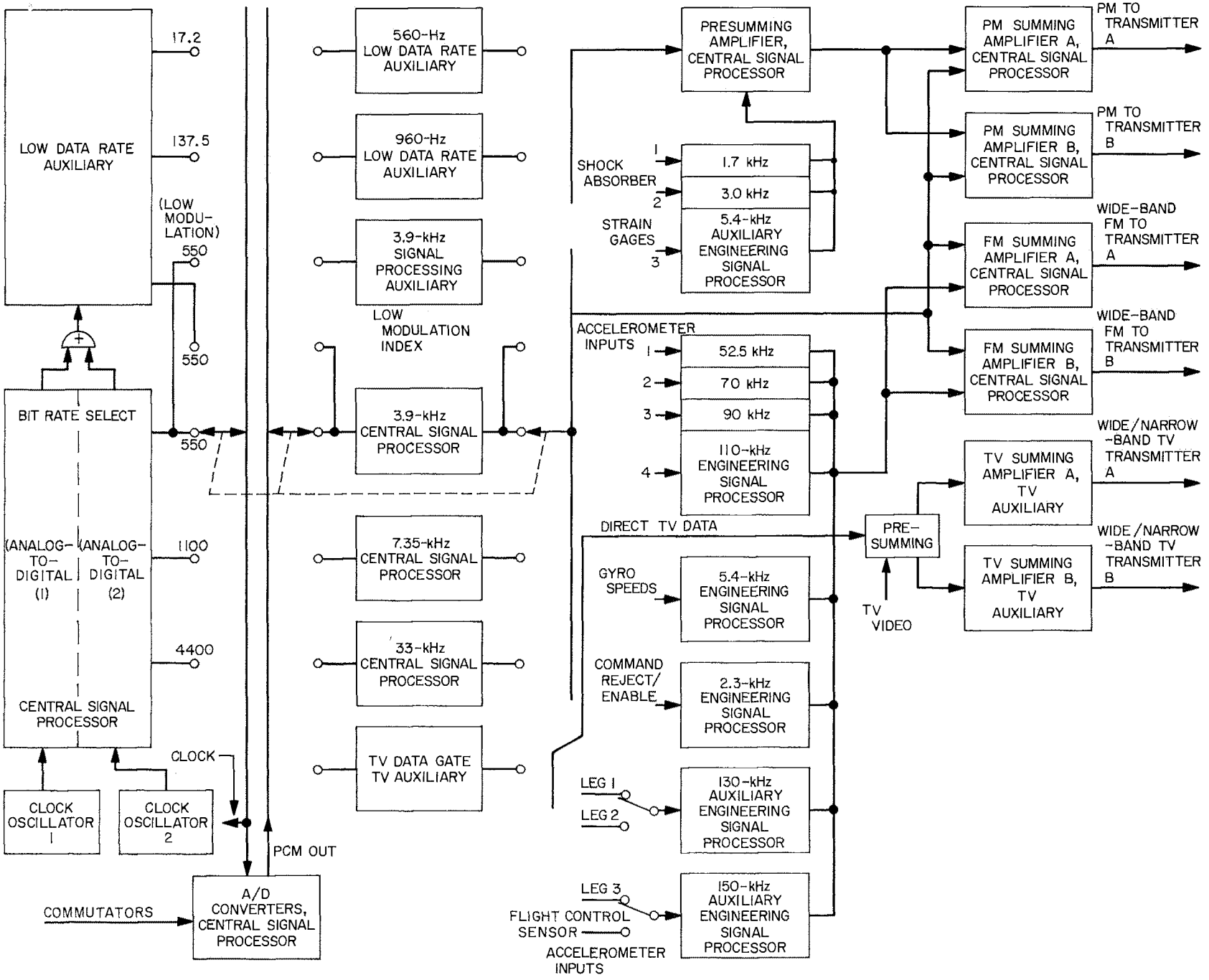



**Fig. XXI-3. *Surveyor* simplified voltage-controlled oscillator and mixing functions**

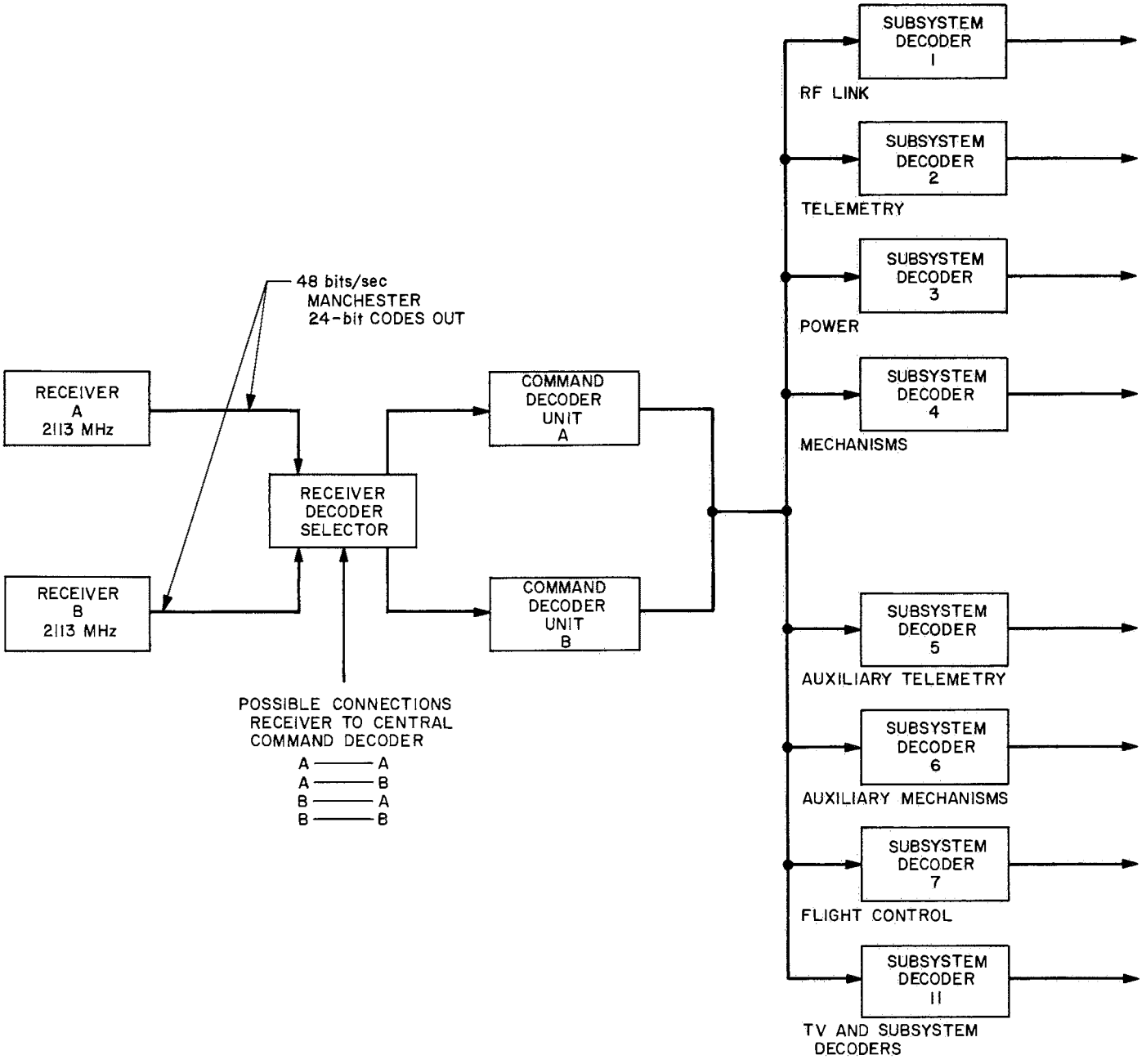



**Fig. XXI-4. Simplified *Surveyor* command block diagram**

adequate during subsequent changes in the spacecraft configuration. Later consideration of the internal digital logic reliability, in the face of power supply noise and other noise sources, led to the incorporation of the additional protection of an interlock command for critical squib firing, and for the magnitude commands after the testing of SC-1. This feature caused these command addresses to be inaccessible even to properly addressed commands unless they were preceded by the special interlock command.

### 2. Final Design Description

The command subsystem consisted of three serial functional elements: receiver decoder selector (RDS), CCD, and SSD.

These elements are readily identifiable in the simplified command block diagram on Fig. XXI-4.

The purpose of the CCD was to generate synchronization, timing, and control signals from each command

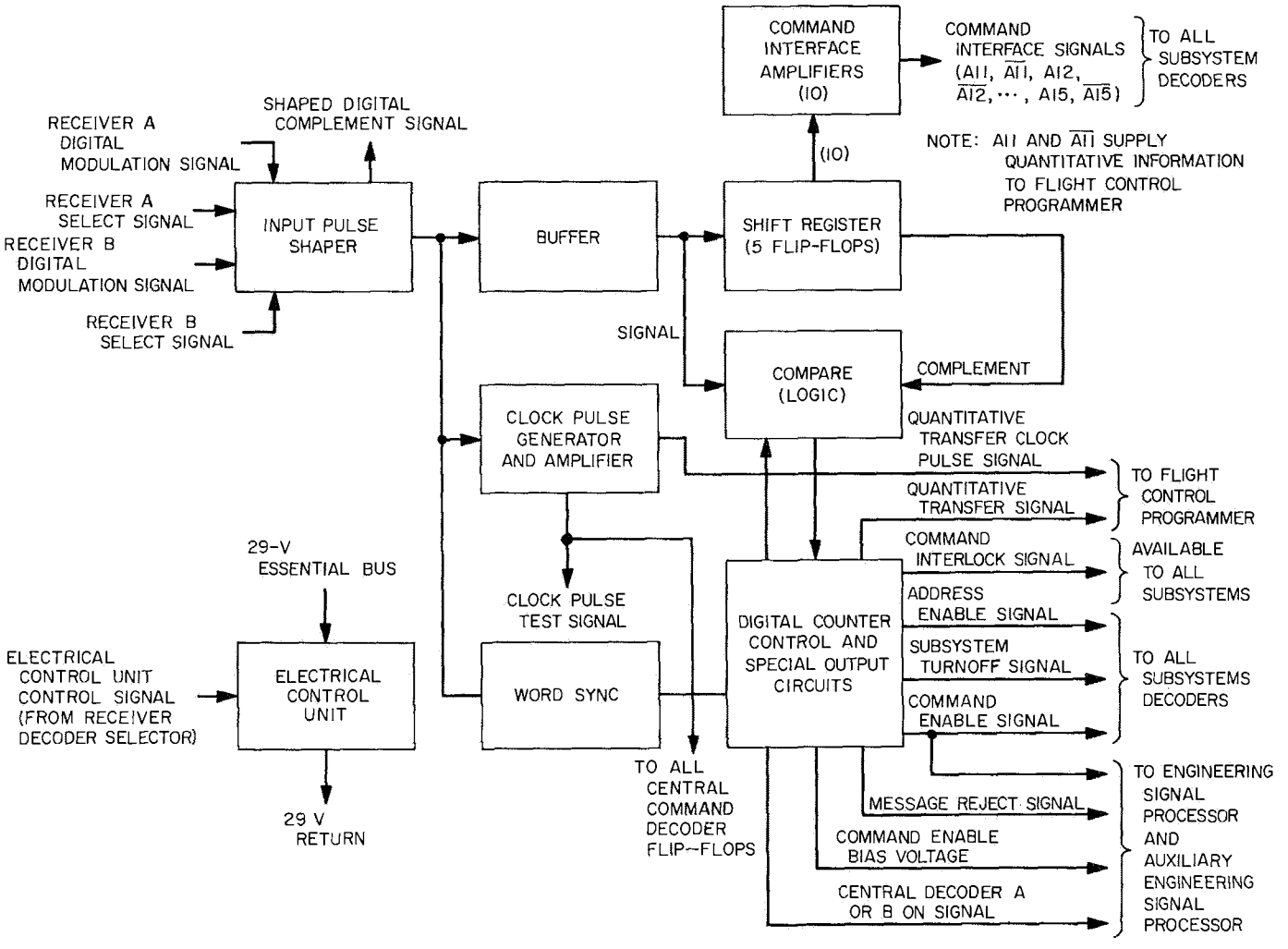



**Fig. XXI-5. Central command decoder block diagram**

word, check each command for the correct address and command, and provide the digital signals to the subsystem decoders. Figure XXI-5 is a simplified block diagram of the CCD. Table XXI-3 illustrates the format and coding of a typical direct command. The table also gives an example of the octal designation of commands that were used in identifying the commands in ground operations as may be seen later in the typical command listing in Table XXI-4 which uses octal numbers.

The command format was a 24-digit word using Manchester coding. The first four bits were used for synchronization and to identify the beginning of a command word. The next 10 bits comprised the address and address complement of the desired subsystem decoder. The last 10 bits, command complement and command proper, comprised the instruction to the SSD for the desired command to be implemented.

There were two types of commands used: the direct command and the magnitude or quantitative command.

The former was normally used for on/off switching and control and the latter was used to control the time duration of operations in the flight control and propulsion subsystems.

Upon receipt of the serial command bits from the receivers, the CCD decoded this digital output from the receiver for word sync, bit sync, the 5-bit address and its complement, and the 5-bit command and its complement. The address and its complement and the command and its complement were compared. If the comparison was successful, a signal was generated to energize the address matrix of the subsystem decoders. The address and command decoding was performed by the 5-bit shift register (Fig. XXI-5) and a bit-by-bit comparison was performed by the comparison logic.

## Table XXI-3. Command format and coding

| Function | | Synchronization | Address complement | Address | | Command complement | Command | |
|---|---|---|---|---|---|---|---|---|
| Fixed values | | 0 — — 1 | | | | | | |
| Octal digits | | Special | Address complement | 1st digit | 2nd digit | Command complement | 3rd digit | 4th digit |
| Sample: 0601- "extend omnis" | Octal | Special | 3 1 | 0 | 6 | 3 6 | 0 | 1 |
| | Binary | 0 — — 1 | 1 1 0 0 1 | 0 0 1 1 0 | | 1 1 1 1 0 | 0 0 0 0 1 | |
| | Code | | | | | | | |
| | Central command decoder | Synchronization | Check complement | Select subsystem command decoder No. 6 | | Complement check only | | |
| | | — | | | | | | |
| Bit position | | 1 2 3 4 | 5 6 7 8 9 | 10 11 12 13 14 | | 15 16 17 18 19 | 20 21 22 23 24 | |

Summary of subsystem decoder functions by address:

| | |
|---|---|
| 01XX = RF system and approach TV | 06XX = Mechanism and radar |
| 02XX = Telemetry control | 07XX = Spacecraft flight functions |
| 03XX = Power subsystem control | 11XX = Lunar television |
| 04XX = Mechanisms operation | 35XX = Alpha scattering instrument |
| 05XX = Telemetry control | 3617 = Special interlock |
| | 0000 = Fill-in command |

Quantitative commands are address 00XX after the interlock

## Table XXI-4. Typical (SC-7) command assignment list

| Command | Function | Command | Function |
|---|---|---|---|
| 0100 | Spare | 0126 | Transfer switch A low power |
| 0101 | Transmitter A lower power on (wide band) | 0127 | Transfer switch B high power |
| 0102 | Transmitter A filament power on | 0130 | Transfer switch B low power |
| 0103 | Transmitter high voltage on | 0131 | SM/SS decoder power on/execute |
| 0104 | Transmitter B low power on (wide band) | 0132 | SM/SS decoder buffer one input |
| 0105 | Transmitter B filament power on | 0133 | SM/SS decoder buffer zero input |
| 0106 | Transmitter high voltage on | 0134 | SM/SS power off |
| 0107 | Transmitter high voltage off | 0135 | Compartment C heater off |
| 0110 | Transmitter filament power off | 0136 | Compartment C heater on |
| 0111 | Transmitter low power off | 0137 | Spare |
| 0112 | Narrow band VCXO on | 0200 | Low modulation index SCO on (3.9 kHz-SPA) |
| 0113 | Narrow band VCXO off | 0201 | A/D converter 1 power on |
| 0114 | Spare | 0202 | A/D converter 2 power on |
| 0115 | Spare | 0203 | A/D converter power off |
| 0116 | Transmitter B to planar array (A to omni) | 0204 | A/D phase clock rates (17.2, 137.5, or 550 bits/sec) |
| 0117 | Transmitter A to planar array (B to omni) | 0205 | A/D clock rate 1100 bits/sec |
| 0120 | Select omni antenna A | 0206 | A/D clock rate 4400 bits/sec |
| 0121 | Select omni antenna B | 0207 | PM presumming amplifier on |
| 0122 | Transponder A power on | 0210 | PM summing amplifier A on |
| 0123 | Transponder B power on | 0211 | PM summing amplifier B on |
| 0124 | Transponder power off | | |
| 0125 | Transfer switch A high power | | |

## Table XXI-4 (contd)

| Command | Function |
|---|---|
| 0212 | FM summing amplifier A on |
| 0213 | FM summing amplifier B on |
| 0214 | Summing amplifiers off |
| 0215 | 3.9 kHz A/D SCO on (for 550 bits/sec) |
| 0216 | 7.35 kHz A/D SCO on (for 1100 bits/sec) |
| 0217 | 33 kHz A/D SCO on (for 4400 bits/sec) |
| 0220 | 33 kHz, 7.35 kHz, 3.9 kHz SCOs off |
| 0221 | Gyro speed signal processing on (5.4 kHz) |
| 0222 | Select next gyro speed channel (null, R, P, Y) |
| 0223 | Gyro speed signal processing off |
| 0224 | Spare |
| 0225 | Spare |
| 0226 | Engineering commutator 1 on |
| 0227 | Engineering commutator 2 on |
| 0230 | Engineering commutator 3 on |
| 0231 | Engineering commutator 4 on |
| 0232 | ESP commutators off |
| 0233 | Command reject/enable 2.3 kHz SCO on |
| 0234 | Command reject/enable 2.3 kHz SCO off |
| 0235 | A/D isolation amplifier on (Centaur, LDRA, SPA) |
| 0236 | A/D isolation amplifier off (Centaur, LDRA, SPA) |
| 0237 | Low modulation index SCO off (3.9 kHz SPA) |
| 0300 | Spare |
| 0301 | Enable battery pressure logic |
| 0302 | Disable battery pressure logic |
| 0303 | Spare |
| 0304 | Bypass main overload trip circuit (29 V nonessential) |
| 0305 | Spare |
| 0306 | Solar panel switch on and bypass off |
| 0307 | OCR bypass on and solar panel switch off |
| 0310 | Solar panel switch off (solar panel not used) |
| 0311 | All flight control power off (interlocked) |
| 0312 | BCR to preregulated bus |
| 0313 | BCR to unregulated bus |
| 0314 | Nonessential loads off (interlocked) |
| 0315 | Solar panel deployment logic on |
| 0316 | Solar panel deployment logic off |
| 0317 | Spare |
| 0320 | Spare |
| 0321 | Spare |
| 0322 | Spare |
| 0323 | Spare |
| 0324 | Spare |
| 0325 | Spare |
| 0326 | Spare |
| 0327 | Spare |
| 0330 | Spare |
| 0331 | Spare |
| 0332 | Spare |
| 0333 | Spare |
| 0334 | Spare |
| 0335 | Flight control C phase power on |
| 0336 | Enable main overload trip circuit |
| 0337 | Command pulse test |
| 0400 | Spare |
| 0401 | Step solar panel plus (0.125 deg) (down) |
| 0402 | Step solar panel minus (0.125 deg) (up) |
| 0403 | Step polar axis plus (0.0625 deg) (up) |
| 0404 | Step polar axis minus (0.0625 deg) (down) |
| 0405 | Step roll axis plus (0.125 deg) |
| 0406 | Step roll axis minus (0.125 deg) |
| 0407 | Step elevation axis plus (0.125 deg) |
| 0410 | Step elevation axis minus (0.125 deg) |
| 0411 | Compartment A heater on |
| 0412 | Compartment A temperature control automatic |
| 0413 | Compartment A heater off |
| 0414 | Compartment B heater on |
| 0415 | Compartment B temperature control automatic |
| 0416 | Compartment B heater off |
| 0417–0437 | Spare |
| 0500 | (for 137.5 bits/sec) Coast phase 1 960 Hz A/D SCO on |
| 0501 | Coast phase 2 560 Hz A/D SCO on (for 17.2 bits/sec) |
| 0502 | Coast phase 560 and 960 Hz A/D SCOs off |
| 0503 | A/D clock rate 550 bits/sec |
| 0504 | A/D clock rate 137.5 bits/sec |
| 0505 | A/D clock rate 17.2 bits/sec |
| 0506 | Coast phase commutator on (AESP) |
| 0507 | Thrust phase backup commutator on (AESP) |
| 0510 | AESP commutators off |
| 0511 | Spare |
| 0512 | Spare |
| 0513 | Spare |
| 0514 | Spare |
| 0515 | Touchdown strain gage power on |
| 0516 | Touchdown strain gage power off |
| 0517 | Touchdown strain gage data channel on (0.96, 1.3, 1.7 kHz) |
| 0520 | Touchdown strain gage data channel off (0.96, 1.3, 1.7 kHz) |
| 0521 | Propulsian strain gage power on |
| 0522 | Propulsion strain gage power off |
| 0523–0537 | Spare |
| 0600 | Extend landing gear |
| 0601 | Extend omniantennas |
| 0602 | Spare (9.5 A pre-SS&A) |
| 0603 | Spare (9.5 A pre-SS&A) (interlocked) |
| 0604 | AMR temperature control off |
| 0605 | Unlock engine 1 roll actuator and pressurize vernier system (helium) (interlocked) |
| 0606 | Spare |
| 0607 | Unlock roll axis (lunar) (interlocked) |
| 0610 | Dump helium (interlocked) |
| 0611 | Vernier lines 2 temperature control power on |

## Table XXI-4 (contd)

| Command | Function |
|---|---|
| 0612 | Vernier fuel tank 2 temperature control on |
| 0613 | Vernier lines 2 and fuel tank 2 temperature control off |
| 0614 | Vernier lines 1 and SM/SS electrical temperature control an |
| 0615 | Vernier oxidizer tank 2 temperature control on |
| 0616 | Vernier lines 1, oxidizer tank 2, SM/SS electrical temperature control off |
| 0617 | Vernier lines 3 temperature control on |
| 0620 | Vernier oxidizer tank 3 temperature control on |
| 0621 | Vernier lines 3 and oxidizer tank 3 temperature control off |
| 0622 | Spare |
| 0623 | Spare |
| 0624 | AMR temperature contral on |
| 0625 | AMR power on |
| 0626 | AMR enable |
| 0627 | AMR power off (interlocked) |
| 0630 | RADVS power off (interlocked) |
| 0631 | Unlock solar panel (launch lock) |
| 0632 | Unlock roll axis (launch lock) |
| 0633 | Spare (9.5 A post-SS&A) |
| 0634 | Unlock elevation axis (lunar) (interlocked) |
| 0635 | Unlock solar panel (lunar) |
| 0636 | Lock landing gear |
| 0637 | RADVS power on (interlocked) |
| 0700 | Inertial mode on |
| 0701 | Rate mode on (reduce angular motion $\leq$ 0.067 deg/sec) |
| 0702 | Sun mode on (acquire sun) |
| 0703 | Sun and star mode on (Canopus roll search) |
| 0704 | Cruise mode on (sun and star lockon) |
| 0705 | Set automatic sun acquisition |
| 0706 | Enable gas jet amplifiers |
| 0707 | Inhibit gas jet amplifiers |
| 0710 | Positive angle maneuver |
| 0711 | Initiate roll |
| 0712 | Initiate pitch |
| 0713 | Initiate yaw |
| 0714 | Sun and roll (initiate roll with sun lockon) |
| 0715 | Manual maneuver delay mode on |
| 0716 | Manual lockon (sun or star) |
| 0717 | Set programmer initial conditions |
| 0720 | Reset group IV outputs (retro sequence mode latches) |
| 0721 | Initial midcourse velocity correction (interlocked) |
| 0722 | Select nominal thrust bias (150 lb total) |
| 0723 | Reset nominal thrust bias (200 lb total) |
| 0724 | Retro sequence mode on (interlocked) |
| 0725 | Vernier engine high thrust |
| 0726 | Spare |
| 0727 | Flight control thrust phase power on |
| 0730 | Emergency AMR signal |
| 0731 | Emergency retroignition |
| 0732 | Emergency retro eject |
| 0733 | Emergency start programmed thrust |
| 0734 | Emergency RADVS on signal |
| 0735 | Emergency terminate midcourse velocity correction |
| 0736 | Spare |
| 0737 | Flight control thrust phase power off |
| 1100 | Survey camera start frame |
| 1101 | Vidicon survival heater on |
| 1102 | (TV null-spacer) |
| 1103 | Survey camera power on |
| 1104 | Survey camera power off |
| 1105 | Time exposure mode off |
| 1106 | Time exposure mode on |
| 1107 | 200 line scan mode on |
| 1110 | Set 25 mm focal length |
| 1111 | Set 100 mm focal length |
| 1112 | Iris servo on |
| 1113 | Step iris open (one step) |
| 1114 | Step iris closed (one step) |
| 1115 | Step mirror right (3 deg) |
| 1116 | Step mirror left (3 deg) |
| 1117 | 2 steps mirror right (6 deg) |
| 1120 | 2 steps mirror left (6 deg) |
| 1121 | Step mirror down (2.5) (5 deg line-of-sight) |
| 1122 | Step mirror up (2.5 deg) (5 deg line-of-sight) |
| 1123 | Step focus in (4 ft to $\infty$ in 50 steps) |
| 1124 | Step focus out (4 ft to $\infty$ in 50 steps) |
| 1125 | Multiple steps focus in (command repeat stops stepping) |
| 1126 | Multiple steps focus out (command repeat stops stepping) |
| 1127 | Step filter position right (CL, GR, BL, R, CL) |
| 1130 | Step filter position left (CL, R, BL, GR, CL) |
| 1131 | Shutter inhibit override (start frame) |
| 1132 | Spare |
| 1133 | Survey camera vidicon temperature control on |
| 1134 | Survey camera all vidicon temperature control off |
| 1135 | Spare |
| 1136 | Survey camera electronics temperature control on |
| 1137 | Survey camera electronics temperature control off |
| 3500 | Spare |
| 3501 | Alpha scattering power on |
| 3502 | Alpha scattering power off |
| 3503 | Alpha scattering heater power on |
| 3504 | Alpha scattering heater power off |
| 3505 | Deploy to background position (interlocked) |
| 3506 | Deploy to lunar surface (interlocked) |
| 3507 | Alpha detector 1 on |
| 3510 | Calibration on |
| 3511 | Proton detector 4 on |

Table XXI-4 (contd)

| Command | Function | Command | Function |
|---|---|---|---|
| 3512 | Proton detectors 3 and 4 off | 3520 | Calibration off |
| 3513 | Proton detector 2 on | 3521 | Spare |
| 3514 | Spare | 3522 | Proton detector 3 on |
| 3515 | Alpha detectors 1 and 2 off | 3523 | Alpha detector 2 on |
| 3516 | Proton detectors 1 and 2 off | 3617 | Interlock |
| 3517 | Proton detector 1 on | 00XX | Magnitude command (interlocked) |

The serial bits of the shift register were read into 10 command interface amplifiers. The contents of the command interface amplifiers were read out by the subsystem decoders in parallel.

The quantitative commands were treated somewhat differently by the CCD. Besides having a unique address, the last 10 bits of the command word contained quantitative information. The CCD recognized the unique address and shifted the 10 bits to the flight control sensor group magnitude register.

The receipt of a correct command by the CCD was verified via telemetry. A successful complement check generated a command enable signal whereas an unsuccessful complement check generated a message reject signal. The last 10 bits of the magnitude command were also verified by telemetry. After the magnitude command was stored in the flight control programmer, the bits were read out for verification during digital word No. 2 of the telemetry transmission.

The purpose of the SSD was to supply the decoded digital information from the CCD to the specific circuits being addressed. A block diagram of a typical subsystem decoder is shown in Fig. XXI-6. For SC-1 through SC-4 eight SSDs were used. An additional SSD was added to accommodate the alpha scattering instrument, and soil mechanics/surface sampler on SC-5 through SC-7.

The outputs of the command interface amplifiers were applied to all of the SSDs. A particular SSD was chosen by the address decoder matrix. The selected SSD then energized its associated command decoder matrix which then generated an output pulse. Since 5 bits were used for the command messages, 32 different commands were available from each SSD.

Some of the critical commands, associated with squib firings and other irreversible actions, were interlocked so that they would not be recognized or acted upon unless the command subsystem had first received the special interlock command (octal 3617). This interlock was also used as a protection on the magnitude command register. The reason for this provision was the feeling that the magnitude command register needed additional protection, since it might often be required to hold magnitudes for long periods of time without change. There were 14 interlocked commands as indicated in Table XXI-4 which shows a typical command assignment list.

The command assignments were changed from time to time to accommodate the needs of the different flights. The most notable change was the command "enable main overload trip circuit." As an example, this command was designated as 0332 on SC-6 and 0336 on SC-7. The reassignments were made in order to operate the two spacecraft simultaneously on the lunar surface.

## C. Construction Techniques and Manufacturing Experience

The six control items which comprised the signal processing and command subsystems, were basically made up of welded modules mounted on circuit boards. The welded modules used discrete components held and interconnected by welded nickel strip, and then potted and canned.

Table XXI-5 shows the number of units built, their disposition, the number of modules per control item, the number of parts per control item, the number of parts per module, and the number of etched boards used.

The size, weight, and physical characteristics of each unit of the digital units are summarized in Table XXI-6.

Once the material and individual components, i.e., transistors, capacitors, etc., were received, they were identified by lot number, and subjected to receiving inspection. Following acceptance, the parts were shipped to bonded stores where they were assembled into kits,

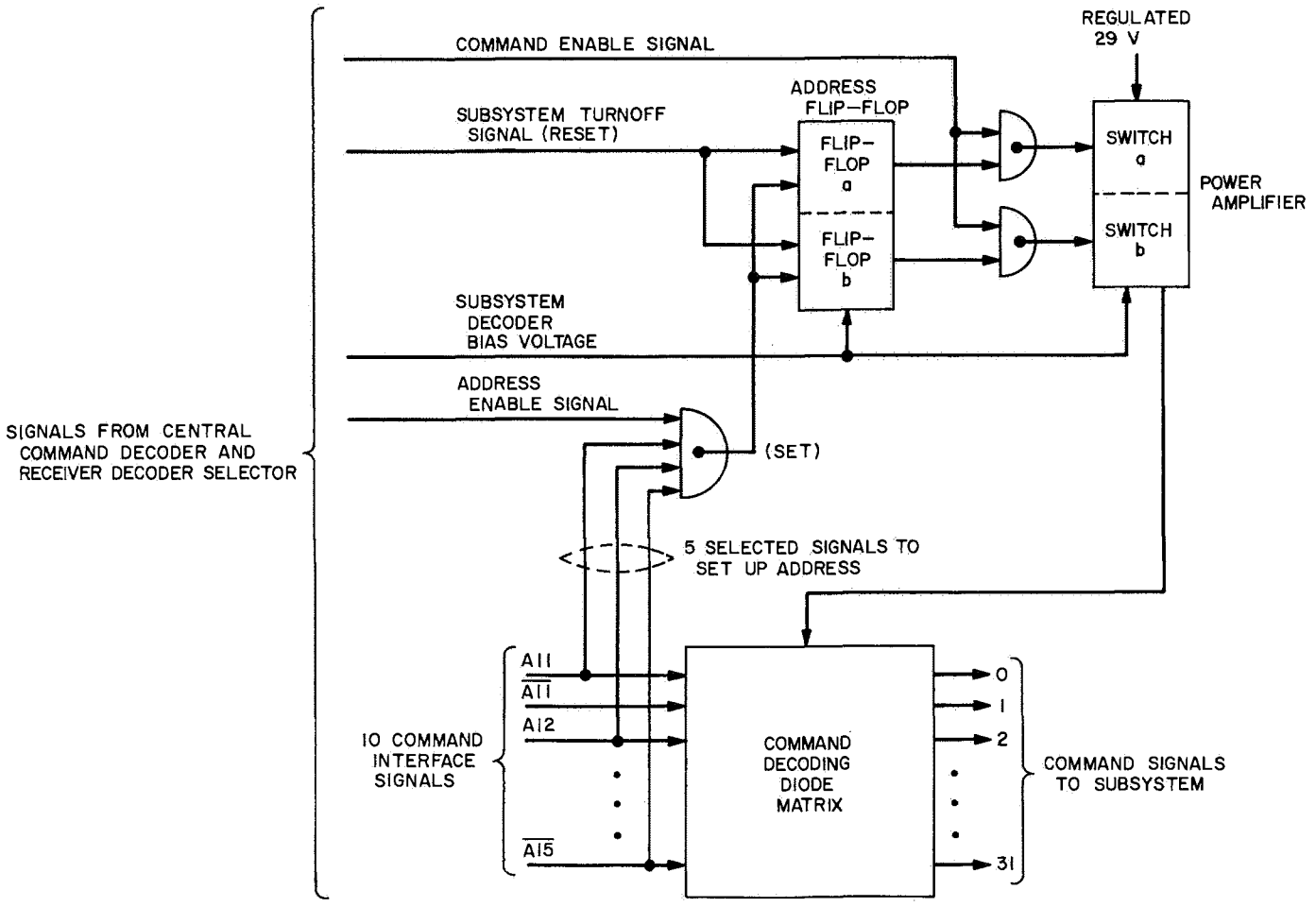



**Fig. XXI-6. Subsystem command decoder block diagram**

ready for fabrication. Each kit contained enough parts to build a module, the functional building block of the unit. The average module consisted of 40 parts in a volume of 1½ × 1½ × 1 in. The module parts were placed in a component holder made of polyethylene wax, with the proper hole pattern required for the module design. The components were then resistance welded to nickel interconnection ribbon. When the welding was complete a perforated header plate was placed over the module to protect the external pins. The module was then subjected to its first electrical test. Following successful electrical checkout, with the module still in the polyethylene holder, a polyurethane conformal coat was applied to the top and bottom weld levels to provide both electrical insulation and structural support. When the conformal coat had cured, the component holder was dissolved and the components were left free standing on the header plate. A final conformal coat was applied by dipping the module, thus completing the insulation. The module was then installed in a 10-mil aluminum can and placed in a potting tool for another electrical test. After successfully completing this electrical test the module was encapsulated using a polyurethane foam which provided both mechanical support and heat conduction paths for the components. After passing final electrical tests, the module was sent to bonded stores where it was held ready for assembly on the chassis.

Basically the chassis were formed from two 5-mil stainless steel plates with a ⅛-in.-thick aluminum honeycomb core bonded to the printed circuit board, and an insulator between the core and plates. The steel plates were chemically etched to provide clearance for the external module pins. The exposed edges of the cutouts and the chassis are filled with epoxy to prevent electrical shorts. The modules were mounted directly on the steel plates to maximize heat transfer. Unit wiring was completed using special lightweight abrasion resistant wire.

**Table XXI-5. Unit module complement of signal processing and command subsystem**

| Control item | Total units | Flight spares | Flight units | Proto-type T-21 | Type approval tests | Down-grade class three | Scrapped | Number modules per unit | Average No. parts per module | Total parts per unit | Etched boards per unit |
|---|---|---|---|---|---|---|---|---|---|---|---|
| AESP | 12 | 2 | 7 | 1 | 1 | — | 1 | 62 | 35 | 2185 | 6 |
| ESP | 15 | 2 | 7 | 1 | 1 | 2 | 2 | 86 | 35 | 3030 | 7 |
| CSP | 11 | 2 | 7 | 1 | 1 | — | — | 58 | 44 | 2570 | 5 |
| LDRA | 12 | 2 | 7 | 1 | 1 | 1 | — | 7 | 38 | 263 | 1 |
| SPA | 11 | 2 | 7 | 1 | 1 | 1 | — | — | — | 54 | — |
| CCD | 14 | 3 | 7 | 1 | 1 | 1 | 1 | 58 | 40 | 2350 | 6 |

**Table XXI-6. Physical characteristics of the signal processing equipment**

| Equipment | Weight, lb | Dimensions, in. | Volume (enclosed), $in.^3$ | Density, $lb/in.^3$ | Total parts count | Weight per 1000 elec-tronic parts, lb | Elec-tronic parts per $in.^3$ | Number of etched boards | Total module parts count | Number of modules | Parts per module (av) | Power dissipa-tion, W |
|---|---|---|---|---|---|---|---|---|---|---|---|---|
| Central command decoder | 5.7 | 5.3 × 6.0 × 13.3 | 240 | 0.024 | 3128 | 1.8 | 13.0 | 6 | 3050 | 58 | 53 | 1.9 |
| Central signal processor | 4.8 | 5.3 × 5.7 × 8.8 | 173 | 0.028 | 2607 | 1.8 | 15.1 | 5 | 2554 | 62 | 41 | 2.2 |
| Signal processor auxiliary | 0.34 | 1.8 × 2.4 × 4.4 | 10 | 0.034 | 57 | 6.0 | 5.2 | 1 | 39 | 1 | 39 | 0.15 |
| Engineering signal processor | 6.0 | 5.2 × 5.7 × 9.9 | 198 | 0.030 | 2832 | 2.1 | 14.3 | 7 | 2764 | 87 | 32 | 6.0 |
| Low data rate auxiliary | 0.55 | 2.4 × 3.0 × 5.0 | 21 | 0.026 | 257 | 2.1 | 12.2 | 2 | 256 | 7 | 37 | 0.10 |
| Auxiliary engineering signal processor | 6.1 | 5.3 × 8.0 × 8.0 | 260 | 0.023 | 2311 | 2.6 | 9.0 | 6 | 2246 | 72 | 31 | 3.9 |
| Total | 23.49 | NA[a] | 902 | NA | 11,192 | NA | NA | 27 | NA | 287 | NA | 14.25 |

[a]NA = not applicable.

### 1. Manufacturing Problems

A number of problems were encountered during the manufacture of the signal processing and command systems. The principal problems related to:

(1) Purchased items.

(2) Choice of components.

(3) Workmanship practices.

(4) Quality control.

(5) High density design.

Of the procured items for the signal processing, the most difficult items were the voltage controlled SCOs.

Originally the SCOs used were manufactured by Vector Manufacturing, Inc. These SCOs performed normally during all missions (from launch through lunar operations), but many problems arose during all phases

of the test program. The successful operation of the SCOs during the missions can be attributed to some extent to the natural selection process that took place during tests. However, this selection process was expensive in terms of test hours and spacecraft reliability.

Most of the problems with the SCOs had to do with center frequency and frequency deviation instabilities, output voltage tolerance, and too low a frequency response of the low pass input filter. These problems were principally due to occasions of poor workmanship, the use of commercial components, inadequate component screening, and a very crowded product design. Over a period of about 2 yr, the vendor instituted corrective steps to improve the product. Nevertheless, the early improvement factor was not considered adequate and in view of the difficulties experienced with the SCOs, it was decided to develop an alternate vendor. Motorola Inc., Scottsdale, Ariz., was chosen as the alternate.

The Motorola SCOs were used in SC-6 and SC-7 and proved to be highly reliable. Out of 111 SCOs tested, only two failures were experienced and these occurred early in the unit test phases.

The Motorola SCO utilized a partial hybrid component configuration. This approach was necessary in order to house the complex circuitry (which included an active rather than a passive filter) in a tight package configuration.

The high reliability of the SCOs was achieved by advanced design and engineering techniques and quality control practices. Using their experience in building units for space application, Motorola used space approved and screened parts and inspection requirements were set up at crucial points in the manufacturing cycle.

Fortunately, the effect of a failure of a single SCO would have been minimal to the overall mission because of the redundancy built into the system. As far as the A/D channels were concerned, the failure of an SCO would have caused some inconvenience if the particular data rate could not have been received at the maximum allowable rate. Complete touchdown dynamics data would not have been available if one of the continuous strain gage data channels failed, but the failure would not have been catastrophic.

Another purchased unit which was a source of problems was the strain gage amplifier. These problems involved oscillation of the units under certain environmental and dynamic loading conditions as discussed in Subsection D-3. Since the amplifier was purchased as a sealed, potted unit it was not possible to effect internal circuit changes, so stabilization was accomplished by an external filter.

Perhaps the single most serious cause of manufacturing recycle was the unfortunate selection of a low puncture voltage transistor for the telemetry commutator switches. This, coupled with a design which offered no protection to these transistors from voltages applied on the telemetry lines, led to many failures. Although the three types of alloy junction transistors used as switches were affected by identical problems, the bulk of the failures were with HAC transistors, part 988809. The commercial equivalent for this type of transistor is identified by part 2N2185.

Most of the failures of this part were collector-to-emitter shorts induced in test and are discussed in Subsection D-3-b. However, besides collector-to-emitter shorts, component tests demonstrated that the alloy junction transistors became degraded while on the shelf and during normal operations. Because of this fatigue, or shelf life problem, effective screening of the component was difficult. This was verified by the number of trouble failure reports written against these transistors in the unit area for excessive current leakage.

The alloy transistors were replaced with epitaxial devices for SC-5 and up. The latter transistors were superior from the point of stability, lower emitter-to-collector saturation voltage, higher power rating, and higher breakdown voltages. The superiority of the epitaxial transistor was illustrated by experiences with SC-5, SC-6, and SC-7. Because of procurement and installation problems only the switches that interfaced the outside world were changed. Nevertheless, switch failures on the later spacecraft were limited specifically to externally induced (operator error or environmental) causes.

A commutator switch failure during flight would have caused severe problems in evaluating the performance of the spacecraft. An open circuit failure would have caused the loss of one measurement, but a collector-to-emitter short could affect all of the A/D channels. Just such a failure did occur on SC-5 and is discussed in Subsection E-1-a.

The failure of Ultronix precision wire wound resistors was another component problem. These resistors were used in two places. In one application, they were used as

base resistors for the transistor switches. In the second application, they were used in a resistive ladder configuration as the binary voltage weighting circuit in the A/DC. The basic design of the resistors was the primary cause of failure. The base resistors had a tendency to develop a turn-to-turn short while the resistors in the ladder network tended to develop an open. The corrective action was to perform additional screening of the components. In the base resistor application, the additional screening consisted of a power burnin for 100 hr at 125°C. In the ladder network application the networks were vibrated to cull out those units that tended to open.

The impact on the mission could have been serious because of the failure of these components, especially in the ladder network case. Since the ladder network was used in the binary voltage weighting device an open circuit in the resistor would have resulted in improper digitalization of the measurement with possible loss of most of the data, and a horrendous task of deciphering the data.

Connector jack screws, that pulled the connector into full mate as they were screwed tight, caused much rework on the various units. This problem was jointly attributable to a poor choice in selecting the part, and a lack of adequate installation procedures and control.

Specific manufacturing problems which resulted in extensive rework, and, in some cases, scrapping complete control items, are delineated below:

(1) Digital modules and module to circuit boards built early in the program used an activated flux solder, and the soldering practices then used applied excessive solder that migrated between and to the rear of the laminated boards. The activated flux caused corrosion, leakage, and degradation of joints. The excessive solder caused subsequent shorts (solder splash) and intermittents. The solder splash problems ultimately resulted in the scrapping of CCD 6 and AESP 4. The rework and retest necessary to correct other units caused serious slippages in the schedule for all units in the digital area.

(2) Ungrounded soldering irons and bench fixtures were occasionally identified as the cause for transistor punctures and shorts. The final correction to this practice was motivated when in one two-week period, a shorted soldering iron and a shorted work lamp put 117 VAC directly on two completed digital control items. Engineering signal processor 8 was completely immolated when contacted by a shorted soldering iron. Engineering signal processor 10 was likewise electrocuted when a shorted bench lamp touched a holding fixture for the unit during rework. Both units were scrapped due to the extensive damage, and manufacturing controls were introduced to electrically isolate and ground manufacturing tools and fixtures.

(3) Contour cables, which were flat laminated flexible polyurethane printed circuit cables, were a source of great assembly and rework difficulties. These cables were subject to tearing, distortion, and end-connection breakage due to handling or improper soldering techniques. Rework of any sort involved considerable flexing and stressing of these cables, so they often became victims and subsequent objects of rework.

(4) Various other problems with varying degrees of severity included:

   (a) Noncompliance with the outline and mounting drawings.

   (b) Board discoloration, delamination, measling and lifted circuitry

   (c) Uncontrolled length of cover screws causing component damage and wiring shorts.

   (d) Loss of the traceability of bad part lots and modules.

A Material Review Board (MRB) was organized to disposition those discrepancies that manufacturing would, or could not rework. The MRB consisted of HAC and JPL quality control and engineering personnel. From July 13, 1966 to September 18, 1966, there were 186 MRB disposition requirements on signal processing equipment. In most cases corrective action was not taken. As an example, on November 18, 1966, an MRB meeting was held on a contour cable. The corrective action was to caution the operator to exercise more care during rework. Three days later the same cable was the subject of another MRB action as a result of additional mishandling by an operator. The corrective action this time was to replace the cable and again caution the operator. The additional manufacturing rework on this single discrepancy was 18 man-days.

## D. Testing

### 1. Module and Unit-Level Testing

Module testing was carried out during the manufacturing process prior to encapsulation and assembly into

units. After experiencing manufacturing delays due to the high rate of failures under test and the required rework, it beeame apparent that the module test program as a whole was suspect. Early in 1965, it was decided to review the module test procedures for evaluation, and to insure that the testing was adequate to properly screen the equipment for use as flight hardware. A 15% sample of all the test procedures was reviewed in detail. The test procedures proved to be inadequate and as a result many tests were not fully effective, causing defective modules to be installed in units. This later necessitated module removal and rework of finished control items, with attendant damage and delays.

Recommendations were made to improve the testing and to insure that modules would be flight worthy.

After completing all manufacturing assembly the units were subjected to a functional test to assure correct assembly. Then environmental and performance tests, called flight acceptance tests, were performed.

In addition, during the developmental phases of the equipment, type approval tests were run to verify that the subsystem design could perform under extreme conditions. Only one unit of each type was subjected to these tests. The type approval test environment was much more stringent than the flight acceptance tests environment, and any unit exposed to this environment was not flown.

The flight acceptance tests provided confidence in the ability of the unit to perform satisfactorily in the expected environment. The flight acceptance tests environment included vibration, temperature, and thermal-vacuum. The sequence of testing was as enumerated here, and the levels and duration used for each were:

(1) Each flight unit was subjected to three planes of vibration testing. One plane was parallel to the axis of thrust of the vehicle and the other two planes were orthogonal to this plane. Each plane consisted of 6 min of vibration which was swept over a frequency range from 25 to 1500 Hz at 9 g peak acceleration.

(2) The unit was subjected to thermal testing over temperature extremes of 0 to 125°F. After temperature stabilization at 125°F during which the unit was allowed to soak for 4 hr with no power applied, a complete functional test was performed. The procedure was repeated at 0°F.

(3) The thermal-vacuum test phase was not performed on the signal processing equipment of the command system units until the testing of equipment scheduled for SC-5. This test was then made a requirement to overcome the possibility that through spares interchange on the spacecraft, a subsystem which had not been tested in a vacuum environment might be flown. Up through SC-4, the subsystem units were exposed to the vacuum environment for the first time during the spacecraft solar-thermal-vacuum test phase at the system test level. An item replaced after this test would not then have been a fully qualified unit.

In the thermal–vacuum test, the chamber pressure was reduced to less than $10^{-5}$ mm of mercury and the unit was soaked for 2 hr at 130°F with power applied before a complete functional test was performed. This temperature was then reduced to −5°F and the functional test was performed again after the unit had soaked for 2 hr with power on.

Flight acceptance testing was required for all flight units and was performed after the manufacturing cycle and after each major rework. The original intent was to not subject equipment to more than one or two such tests. However, because of the number of subcarrier oscillator and transistor switch failures, some flight units were exposed to multiple cycles of flight acceptance testing. As an example, the AESP on SC-3 was exposed to four complete cycles and four partial cycles. (See Fig. XXI-7 and XXI-8.)

### 2. Spacecraft System Level Testing

Upon completion of the flight acceptance tests in the unit area, the signal processing and command units were delivered to bonded stores. From this point, the units were delivered to a particular spacecraft and were then ready for integration into a Spacecraft System. The integration procedures and all subsequent system level tests were controlled by requirements defined in the *Surveyor* spacecraft system test specification. This specification defined the test requirements for each test phase as well as for each subsystem. These requirements served as a basis for test procedures for each spacecraft test phase.

On SC-1, SC-2, and SC-3 a series of tests, called group tests, were performed on the control items before their installation on the flight spacecraft bus. A test jig, wired so that a large number of intrasystem signals were easily accessed, was used to test the various control items as a

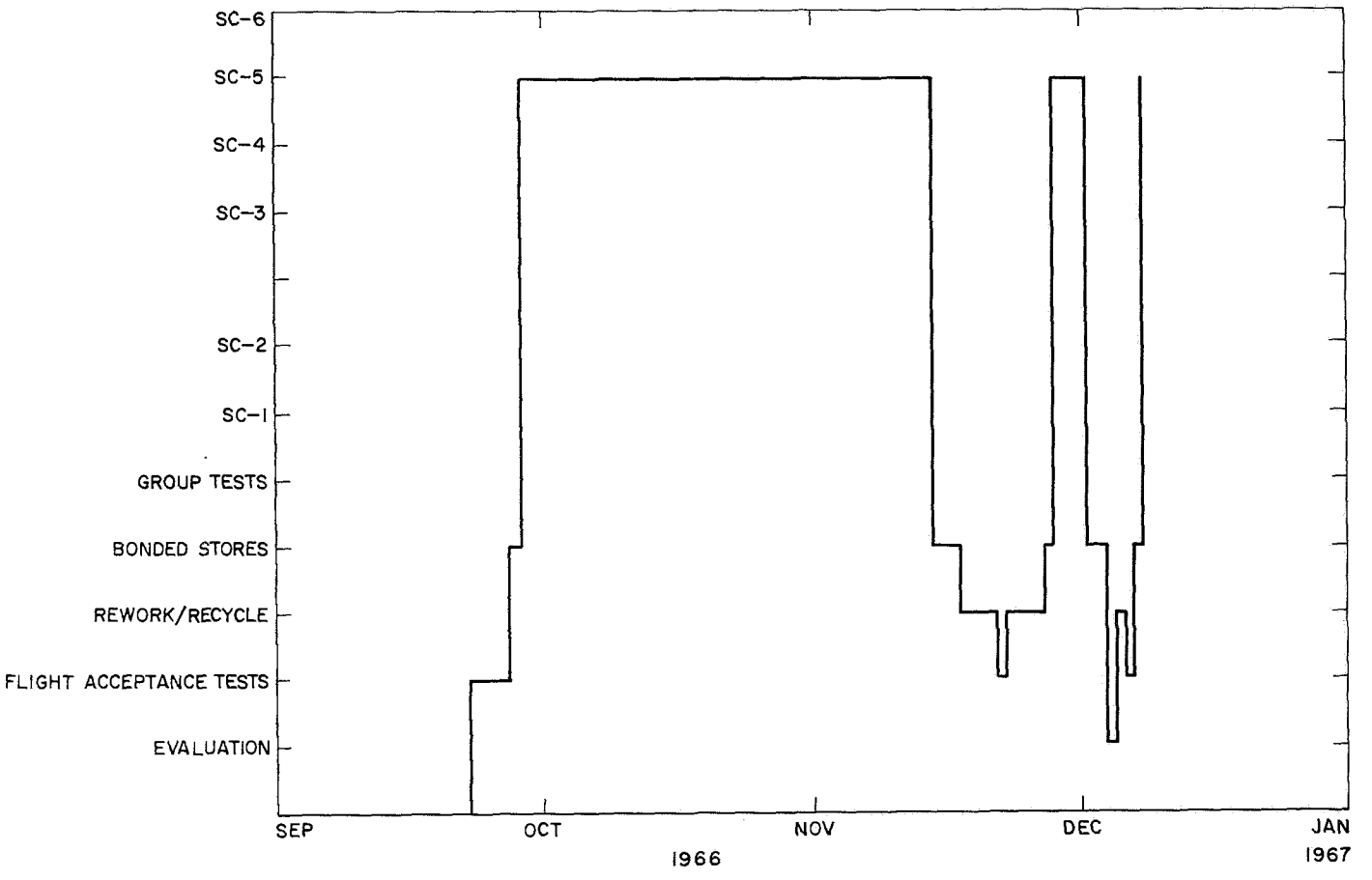



**Fig. XXI-7. Rework/recycle graph for engineering signal processor SN 11 flown on SC-5**

system. The group tests were deleted on the later spacecraft because it was found that many of the tests performed were either unnecessary, or that they could be performed as part of the initial system checkout tests on the flight spacecraft.

Throughout all of these test phases, spacecraft telemetry data were continually processed in real-time by the programmed automatic test equipment and the spacecraft computer data system (CDS) for real-time evaluation of the spacecraft performance. In addition to the real-time evaluation, telemetry records were reviewed after each major test and the results of this review and of the tests were included in quick-look reports.

The command subsystem was also a serial element in the testing of the spacecraft; in that, the command subsystem was the means used for activating the various spacecraft subsystems, inserting turn and burn durations in the flight control subsystem, and initiating changes in the position of the various spacecraft appendages such as antennas, solar panel, and legs. Because of this constant exercise of these communication subsystems, a very thorough test of their functional capabilities was obtained under all test conditions.

The test and operations personnel performed all work on the spacecraft and were responsible for the operation of the checkout consoles for the system test equipment assemblies (STEA). The data analysis personnel originally supported only the formal tests such as solar-thermal-vacuum or vibration, but beginning with SC-3, they were assigned to monitor all electrical testing of the spacecraft. The HAC signal processing subsystem engineers originally were on an on-call basis. This later evolved to be support at every test level and came about as a result of the nominal assignment of a HAC signal processing engineer to every spacecraft.

The JPL signal processing and command group also supported the Spacecraft System test operations through the assignment of an engineer to each spacecraft. The principal functions of this engineer were:

(1) Monitor tests.

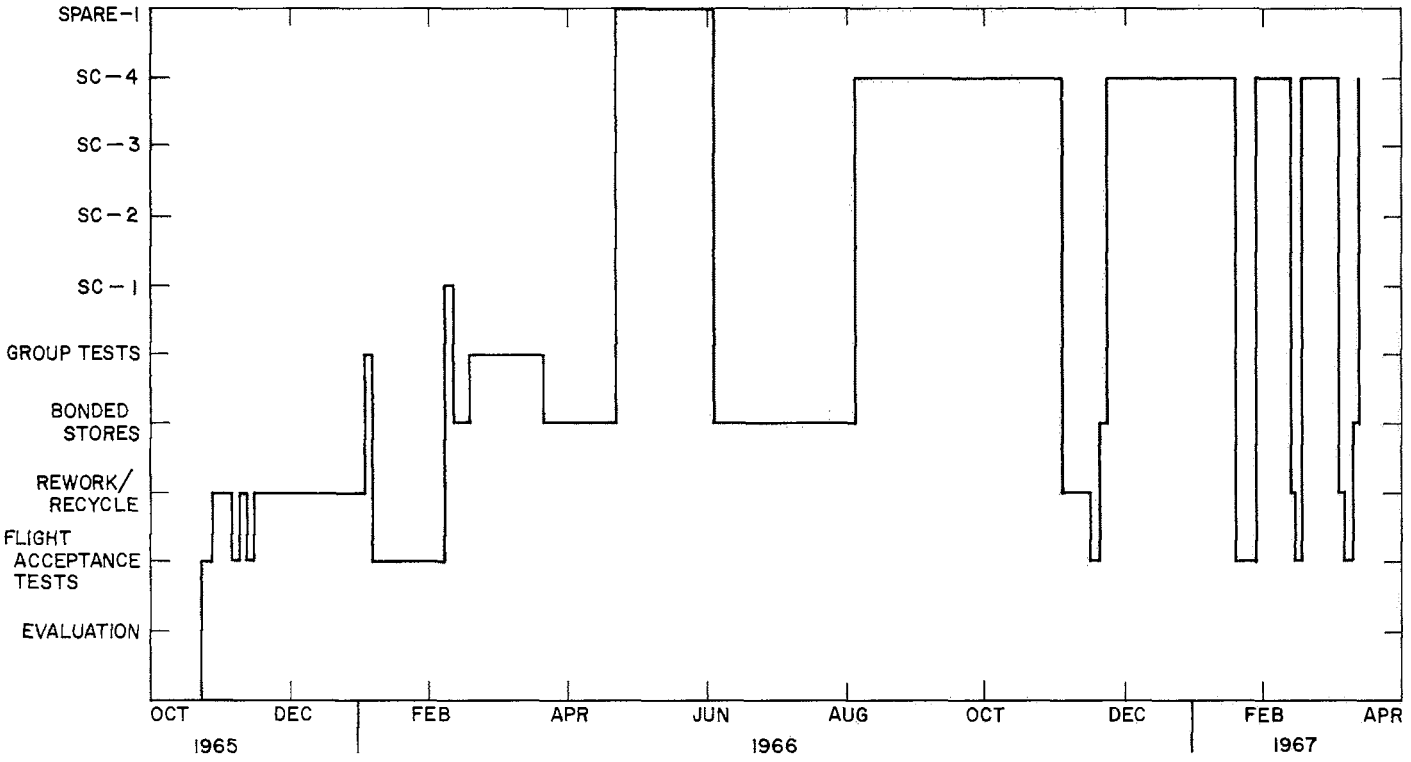



**Fig. XXI-8. Rework/recycle graph for engineering signal processor SN 7 flown on SC-4**

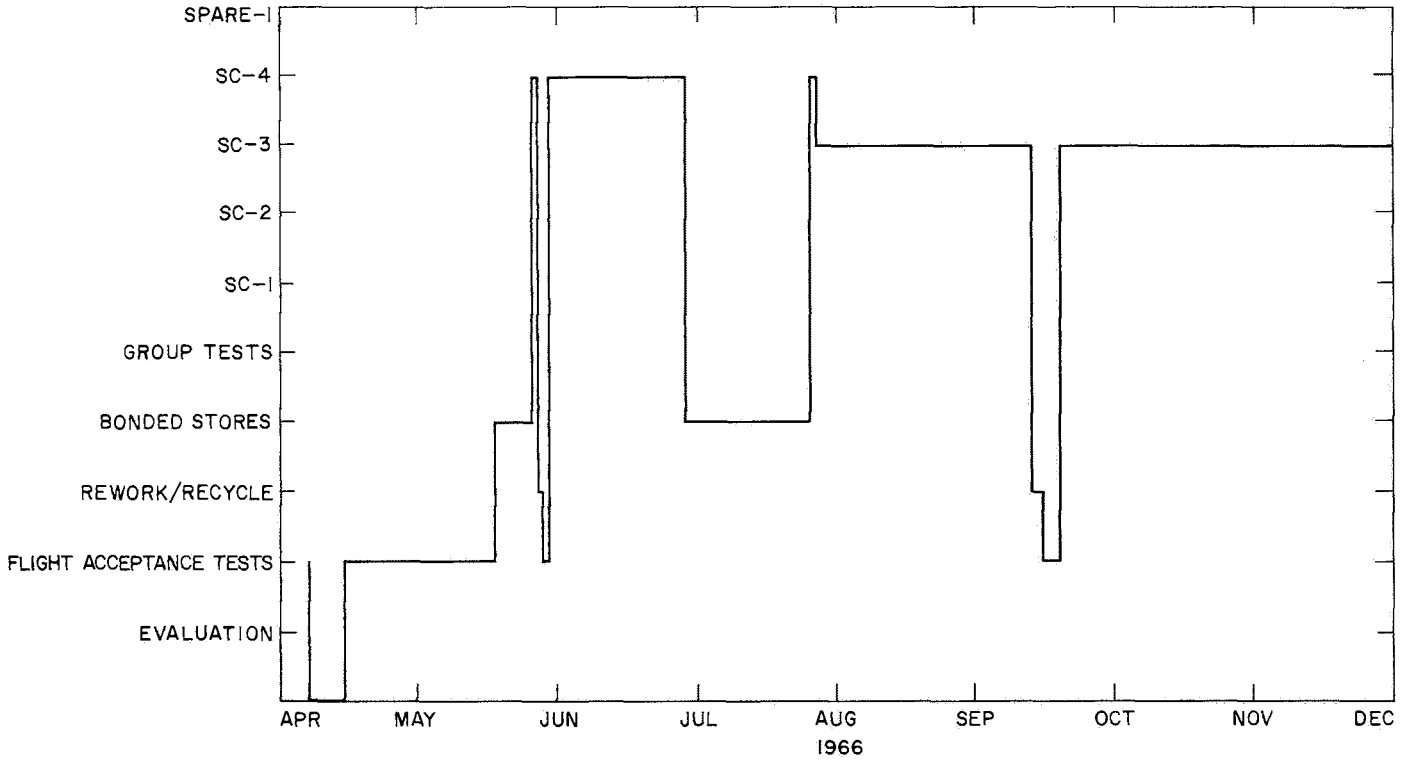



**Fig. XXI-9. Rework/recycle operation failure report graph for engineering signal processor SN 9 flown on SC-3**

(2) Review procedures.

(3) Review and analyze telemetry data.

(4) Serve in a liaison capacity between the JPL systems test and operations group and the JPL signal processing and command group.

### 3. Test and Operations Problems and Corrective Action

A brief description of the principal problems encountered during test and operations in the telemetry and command areas is given in the subsequent paragraphs along with the corrective action taken. Typical unit history diagrams are shown in Figs. XXI-7, XXI-8, and XXI-9.

*a. System noise/ground loops.* One of the more persistent problems encountered during system test was noise in the Spacecraft System which produced fluctuations of telemetry data read-outs. The principal causes of this system noise were; ground loops both in and between the various spacecraft subsystems, ground loops and pickup on STEA control and monitoring lines, and cabling design which was such that telemetry returns were often carrying excitation current for one or more subsystems. As a result, the amount and character of the noise on the telemetry channels was dependent upon the telemetry bit rate, the spacecraft power consumption, and the particular STEA used for a test.

To overcome some of these noise problems passive filters were added in the 29 V (nonessential) excitation lines to the ESP and AESP; in each current channel input to the signal processor; and in the gyro speed measurement inputs. In addition, several ground loops were eliminated by reworking the spacecraft harness on SC-5, SC-6, and SC-7 and by adding isolation amplifiers to several of the STEA lines.

*b. Commutator switch failures.* During the test program of SC-1 and the T-21 test model spacecraft, a large number of transistor commutator switch failures (typically collector-to-emitter shorts), occurred. The primary failure mode apparently resulted from a voltage transient. This was especially true in the T-21 spacecraft where at least 30 failures occurred during static discharge tests.

Seventeen transistor failures in the signal processor occurred during testing of spacecraft SC-1 through SC-7, and sixteen of these were commutator switches. The one exception was a transistor failure in the AESP master switch circuits on SC-2.

In many instances, the cause of failure was determined to be overvoltage through the use of ungrounded instruments, or soldering irons. This was not the case with the SC-4 spacecraft which had six transistor switch failures, five of which were associated with the auxiliary battery case temperature measurement.

A thorough investigation was conducted by both HAC and JPL and a joint failure review board was organized. While the board was not able to pinpoint the exact cause of the switch failures on SC-4, it was believed that the switches were damaged by an electrostatic discharge through the transistors. Tests performed at HAC showed that this component could be damaged by as little energy as 0.30 $\mu$J. This is approximately equivalent to a discharge of 620 pF at 30 V. It was demonstrated that sufficient charge could have been stored in the spacecraft harness during times when the ESP or AESP were disconnected, and this could have been caused by a static charge created or transferred by people or materials in contact with the spacecraft.

Primarily as a result of the SC-4 switch problems several actions were taken. An action directive was generated directing the test personnel to terminate all open telemetry input lines. The auxiliary battery compartment and soil mechanics/surface sampler chassis were electrically grounded, and it became a requirement before installation of the ESP or AESP to momentarily ground the harnesses to remove any built-up charges. A more detailed description of the failures and corrective action is contained in the final report issued by the failure review board.

*c. Excessive input voltages.* In early spacecraft, whenever the landing radar altimeter and doppler velocity sensor (RADVS) was operated, a degradation of data accuracy was experienced. This was due to a 10 VDC signal being applied to the FC-39 (doppler velocity $V_x$) and FC-40 (doppler velocity $V_y$) commutator switches. This voltage was sufficient to overcome the 9.6 VDC holdoff bias on the transistors in the switch. Beginning with SC-5, a modification was incorporated at the interface between telemetry and flight control that consisted of zener diodes to limit the applied input signal to 7 VDC.

A similar problem was experienced with the altitude marking radar (AMR), automatic gain control (AGC) measurement. This signal went to a very high voltage level (15 VDC) immediately after the AMR was turned on and then decayed to normal values within two or

three seconds. On SC-1, SC-2, and SC-3, the spacecraft signature list contained instructions to ignore bad telemetry during the AMR turnon transient. On SC-5, SC-6, and SC-7, a zener diode clamp was installed in the AMR circuitry to correct this problem.

*d. Deadband errors.* The design of the A/D conversion was a successive approximation process which repeatedly sampled the instantaneous applied input voltage. If the input voltage varied rapidly during the digitizing process, it was quite possible to have serious errors in the digital representation of the analog signal. This effect was quite predominant on temperature and current measurements at the higher bit rates and was called the deadband error.

Deadband errors on some of the temperature measurements were caused by slow response of the constant current sources. During periods when the commutator was not sampling a temperature measurement, the output of the constant current sources would rise to +7 V. When the +7 V were applied to the transducer, by the commutator current switch, the output would decay exponentially to a voltage determined by the resistance of the transducer. At a bit rate of 4400, this decay time was of sufficient length to cause errors of up to 60 binary-coded decimal (BCD) (out of a total of 1023 BCD) in the basic accuracy temperature channels and up to 20 BCD on the high accuracy temperature channels.

Beginning with SC-3 the basic accuracy constant current sources were modified by reducing the output capacitor from 2 $\mu$F to 0.2 $\mu$F. This eliminated the deadband problem in the basic accuracy channels.

The high accuracy temperature channels were not modified and deadband errors were present on all spacecraft. Data was generally accurate at 550 bits/sec, but positive shifts of 4–6 and 16–20 BCD were observed at 1100 and 4400 bits/sec, respectively. This behavior was included in the spacecraft signature lists.

There also existed a deadband error characteristic of the current (low-level) channels. In its most serious manifestation, this behavior caused all low-level channels which should have indicated greater than midscale to read 511 BCD, i.e., half-scale.

The characteristic was due to the relatively long (150 $\mu$sec) recovery time of a times-fifty differential amplifier in coming from its open input negative saturation state when the low level inputs were applied by the commutator. At 4400 bits/sec, this would cause the first bit to be a zero in the digitizing process, instead of the proper "one."

A fix was incorporated to force the amplifier into positive saturation when not being used, which gave a recovery time of 50 $\mu$sec. The fix was accomplished by inserting zener diodes at the input with the zener voltages unbalanced in the desired direction. This reduced the maximum deadband errors to less than 60 BCD at 4400 bits/sec. Tests were conducted on each spacecraft to calibrate the magnitude of the deadband for each low-level channel at 4400 and 1100 bits/sec.

*e. Erratic strain gage measurements.* The zero instability of the propulsion strain gage channels was troublesome throughout spacecraft testing. The normal zero force level readout by telemetry which should have been 200 BCD (full scale 1023) was often observed to be as low as 50 or as high as 300. These shifts were ascribed to a number of causes. These included: temperature effects on the strain gage amplifiers, tightening or loosening the vernier engine mounting mechanisms, moving the spacecraft, and even people bumping the mounted engines.

All observed changes in the strain gage channels were offsets (zero shifts), and not sensitivity shifts. Because no operational, or data interpretation problems, were caused by these offsets, no corrective action was taken and the offsets were included on the spacecraft signature lists.

*f. Oscillation of amplifiers.* Another problem involving the propulsion strain gage measurements was the tendency for the strain gage amplifiers to oscillate when sampled by their respective commutator switches. This was determined to be caused by a step voltage from the commutator on the output of the amplifier being fed via the samplifier feedback path to the amplifier input, shocking the amplifier into oscillation. A passive filter added on the output of the amplifiers, on SC-4 and subsequent spacecraft, eliminated this problem.

A tendency to oscillate was also encountered with the null error amplifier of the A/DC in the CSP used on SC-1 and SC-2. This problem was corrected by hand selecting some of the component values used in the amplifiers so that the amplifier was more stable over a wider temperature range.

*g. Loading of the signal processor timing signals.* During SC-1 testing, the signal processor timing signals

(T-301 through T-309) were loaded by the flight control subsystem. The symptom of the problem was that telemetry data would become badly degraded when flight control power was on. Installing series diodes in the timing lines to the flight control subsystem corrected this difficulty. This was distinctly different from the problem of over voltage from the flight radar system discussed previously.

***h. Command interface problems.*** The problems in the command area consisted primarily of missed commands, inadvertent command action, and erroneous message reject indications. Nearly all commands that were sent to the spacecraft during test and not executed were traced to a marginal RF uplink. This was never a problem during actual flight and operations, because the RF link was more closely controlled than during the various test phases.

Several cases of undesired command interaction were observed throughout system testing. The following list describes the most chronic occurrences of this type:

(1) Interaction between commands 0511 "accelerometer amplifiers on," 0510 "touchdown strain gage power on," and 0521 "propulsion strain gage power on." When one of these "power on" commands was transmitted, one or both of the other commands would also respond. This was attributed to poor noise immunity at the "on" input to the AESP power latches. No redesign was instigated, but procedures were altered to command all three amplifier units "off" after any one of them had been commanded on.

(2) Interaction between commands 1101 "vidicon survival heater on" and 1133 "survey camera vidicon temperature control on." This anomaly was noted on SC-5 only and was repeatable. Command 1133 would cause both heater circuits to latch. Investigation revealed that a switching transient on the TV 29-V line was causing the inadvertent turnon of the survival heater. A capacitor added in the TV heater control circuit corrected the problem.

(3) The susceptibility of the AMR heater control circuitry to inadvertent turnon was observed on all spacecraft, during test and during flight. The normal command for this action was 0624. Troubleshooting sequences indicated that this circuit was sensitive to any spacecraft transient involving the engineering mechanics auxiliary EMA, i.e., squib-firing, RADVS on and off, etc. No corrective action was taken and this problem was added to the spacecraft signature lists.

(4) Several other single-instance occurrences of noncommanded command activity were observed. Among these were:
   (a) Change from mode C to mode T without command (SC-1).
   (b) Dropout of transmitter high power (SC-6).
   (c) Failure of ESP to turn off (SC-5).

   These were, in general, attributed to noise or transients in spacecraft power and although considerable test time was spent on these problems, no appropriate corrective action was determined.

(5) Many cases were also observed of "message reject on" indications when no commands were being sent to the spacecraft. These indications were caused by the input noise of one of the receivers which was operating open mouthed, with no input signal; being interpreted by the command decoder as the word sync portion of a command word. This immediately caused the generation of the "message reject" signal because the complement check of the 10 bits preceding the erroneous word sync would not match. This was a known characteristic of the system and no circuit changes were made.

## E. Mission Performance

### 1. Signal Processing Subsystem

In general, the typical flight values of the signal processing parameters, taken as a percentage change from preflight test values as charted in Tables XXI-7 disclose the relative flight-to-flight stability of the subsystem, if actual flight data variations are discounted. In this and all other respects, signal processing performance was close to the expected nominals for the transit phase of all missions.

As discussed in the final design description under Subsection A-2, the vernier engine failure on *Surveyor II* precipitated a decision to allocate more telemetry information bandwidth to some of the propulsion and guidance functions. These changes are depicted in Table XXI-8.

This modified system was flown on *Surveyor III* and did provide improved visibility into spacecraft operation during the critical powered maneuvers in transit.

The transit telemetry performance on the *Surveyor IV* mission was excellent up to the time the RF carrier disappeared. The telemetry signal terminated suddenly as

**Table XXI-7. Flight performance comparison of selected signal processing parameters**

| Parameters | Tolerance | Spacecraft | | | | | | |
|---|---|---|---|---|---|---|---|---|
| | | SC-1 | SC-2 | SC-3 | SC-4 | SC-5 | SC-6 | SC-7 |
| Engineering signal processor | | | | | | | | |
| Reference (mode 2)—% | ±3 | +0.418 | +0.102 | −0.184 | +0.808 | 0.0 | 0.0 | 0.0 |
| Reference (mode 4)—% | ±3 | +0.418 | +0.102 | −0.204 | +0.810 | 0.0 | 0.0 | 0.0 |
| Reference return—% | — | 0.0 | 0.0 | 0.0 | 0.0 | 0.0 | 0.0 | 0.0 |
| Unbalance current (mode 2)—μA | ±12 | −0.10 | +0.20 | 0.0 | +0.29 | 0.0 | 0.0 | 0.0 |
| Unbalance current (mode 4)—μA | ±12 | −0.10 | +0.20 | +0.19 | 0.0 | 0.0 | 0.0 | 0.0 |
| Full-scale current calibration—% | ±2 | −0.33 | −0.1 | +0.09 | +0.195 | 0.0 | 0.0 | +0.097 |
| Mid-scale current calibration—% | ±2 | −0.40 | 0.0 | +0.10 | 0.0 | +0.39 | 0.0 | 0.0 |
| Zero-scale current calibration—% | ±2 | −0.20 | −0.3 | +0.10 | 0.0 | 0.0 | 0.0 | 0.0 |
| Auxiliary engineering signal processor | | | | | | | | |
| Full-scale current calibration—% | ±2 | −0.11 | +0.1 | +0.20 | +0.195 | 0.0 | 0.0 | 0.0 |
| Mid-scale current calibration—% | ±2 | +0.20 | +0.1 | −0.03 | +0.194 | 0.0 | 0.0 | 0.0 |
| Zero-scale current calibration—% | ±2 | 0.0 | +0.1 | +0.29 | +0.098 | −0.10 | 0.0 | 0.0 |
| Unbalance current —μA | ±2 | −0.82 | 0.0 | 0.0 | 0.0 | 0.0 | 0.0 | 0.0 |
| Reference—% | ±3 | — | — | — | — | −0.283 | 0.0 | +0.65 |

the *Surveyor IV* was in powered descent some 49,000 ft above the lunar surface. A detailed examination of the data just prior to the termination of signal showed no signal processing or spacecraft anomalies up to the RF signal disappearance.

During the transit of *Surveyor VI*, the data rate was experimentally increased for a time until the bit error rate caused approximately 15% of the received data to be unusable, thus confirming the design thresholds of the communication system, but no anomalies were exhibited by the data subsystem.

All other spacecraft transits showed normal, and uneventful data transmissions.

Lunar surface performance of the signal processing system was normal except for the anomalies discussed in the subsequent paragraphs.

***a. Surveyor III telemetry data failure during landing.*** Due to the loss of lock by one of the landing radar beams, during the final descent of *Surveyor III*, internal logic allowed the vernier engines to continue burning down to the lunar surface. Under these conditions, the spacecraft lifted off from the lunar surface twice before an earth command was transmitted to shut off the vernier engines, allowing the spacecraft to come to rest following the third touchdown.

Coincident with the second touchdown, the signal processing subsystem began transmitting garbled data. Several attempts were immediately made to discover the problem source. The alternate A/DC was turned on; another bit rate was selected; the RADVS was commanded off several times; flight control power was commanded off; the touchdown and propulsion strain gage data channels were commanded off; and the AESP was turned off. The ESP was turned on and several bit rates were attempted, including low bit rates and various modes. These attempts failed to clear the problem or to reveal the source of the trouble.

It was discovered, however, that all the digital words were reading correctly at all bit rates, and at the 17.2 bits/sec rate some of the analog channels were reading near their expected values. This was sufficient to enable the mission to proceed.

The investigation of the signal processing subsystem damage was limited to attempting to identify the trouble source by theoretical and computer simulations of the characteristics of the degraded telemetry.

The failure mode that best fit the characteristics of the data appears to have been shorted commutator switches. This failure mode could have been a single channel failure of a measurement which was sampled in both the AESP and the ESP and in which both the ESP switch and the AESP switch were partially shorted.

**Table XXI-8. Commutator word assignment changes for SC-3 and SC-4**

| Signal | | Changed from | | | Changed to | | |
|---|---|---|---|---|---|---|---|
| | | Mode 1 | Mode coast | Mode thrust | Mode 1 | Mode coast | Mode thrust |
| D-13 | Transmitter A temperature | — | 10 | 10 | — | 6 | — |
| EP-1 | 29 V regulated bus | — | 59 | 59 | — | 11 | — |
| EP-8 | Main battery temperature | — | 42 | — | — | 40 | 40 |
| FC-4 | $N_2$ gas pressure | 30 | 89 | 89 | 30 | 7 | — |
| FC-43 | Roll actuator | 48, 49 | — | 27...117, 34 | 48, 98 | — | 27, 57, 87, 117 |
| FC-45 | Flight control electronic control unit temperature 2 | 24 | 40 | 40 | 24 | 18 | — |
| FC-50 | Pitch precession | — | 7 | 7...97 | — | 59 | 59 |
| FC-51 | Yaw precession | — | 11 | 11...101 | — | 89 | 89 |
| P-4 | Vernier line 2 temperature | 2 | 6 | — | 2 | 80 | 80 |
| P-7 | Vernier engine 1 temperature | — | 70 | 70 | 26 | 70 | 70 |
| P-8 | Vernier line 1 temperature | 52 | 88 | — | 52 | 90 | 90 |
| P-9 | Vernier line 3 temperature | 82 | 84 | — | 82 | 100 | 100 |
| P-10 | Vernier engine 2 temperature | — | 50 | 50 | 80 | 50 | 50 |
| P-11 | Vernier engine 3 temperature | — | 60 | 60 | 46 | 60 | 60 |
| P-18 | Vernier engine 1 strain gage | 15...95 | — | 4, 64 | 15, 35, 55, 75, 95 | — | 7, 37, 67, 97 |
| P-19 | Vernier engine 2 strain gage | 16...96 | — | 14, 74 | 16, 36, 56, 76, 96 | — | 11, 41, 71, 101 |
| P-22 | Retro nozzle temperature | 80 | 100 | 100 | — | 42 | — |
| | Radar altimeter and doppler velocity sensor | | | | | | |
| R-2 | R amplitude | — | — | 43 | — | — | 4, 64 |
| R-3 | $D_1$ amplitude | — | — | 44 | — | — | 44, 104 |
| R-4 | $D_2$ amplitude | — | — | 58 | — | — | 14, 74 |
| R-5 | $D_3$ amplitude | — | — | 94 | — | — | 34, 94 |
| R-8 | Klystron temperature | — | 18 | — | — | 10 | 10 |
| | Altitude marking radar | | | | | | |
| R-12 | Magnetron current | — | — | — | — | — | 43 |
| R-14 | Automatic gain control | — | — | 104 | — | — | 109 |
| R-27 | Antenna temperature 2 | 26 | 80 | 80 | — | 84 | — |
| R-29 | Late gate | — | — | — | — | — | 58 |
| V-44 | Crushable block temperature spare | 46 | 90 | 90 | — | 88 | — |

The resistive load on the A/DC input was computed, from telemetry data, to have been approximately 10 kΩ when the AESP was being used, and approximately 20 kΩ when the ESP was used. The constraints on the inputs to both the ESP and AESP required a normal range of 0.0–5.0 V, never to exceed 10 V. An input of 12 V would produce a nondestructive malfunction by causing the sampling switch to turn "on" without signal processor control. Tests indicated that an input of 30 V or higher would produce a nonreversible, component-level, destructive malfunction. The result was to cause that particular sampling switch, and possibly others, to short with an impedance of 0 Ω–10 kΩ, and with either linear or nonlinear characteristics.

It was speculated that the principal cause of the signal processing failure on the *Surveyor III* mission was a high voltage arc or corona discharge somewhere on the spacecraft that induced a large transient (greater than 30 V) in some of the input lines to the ESP and AESP. This high voltage arc was believed to have been due to a plasma cloud around the spacecraft that was generated when the three vernier engines burned all the way through the initial touchdown and the two subsequent bounces when the RADVS failed to generate a 14-ft mark. The principal suspect was the radar subsystem, as this subsystem utilized very high voltages and was located in the bottom portion of the spacecraft, close to the vernier engines. It must be pointed out, however, that

this was only speculation and a definite failure cause was never confirmed.

This particular signal processor failure was well known before the *Surveyor III* mission and has been discussed previously in this Section. The effect of this type of failure was to constantly parallel the source impedance of the shorted channels with any channel the processor was attempting to sample. On *Surveyor III*, the shorted channels exhibited a source which contained a capacitor, the charging and discharging of which affected all samples based on the voltage of several previous samples and on the source impedance of the channel being commutated. At very low bit rates, this capacitor was able to discharge or charge to the current sample value, thereby allowing some of the channels to reach nearly the correct steady state value before being digitized for transmission. The resulting data could then be corrected for the resistive loading off-set which also existed.

After a thorough review of the data, and the construction of a mathematical model of a portion of the commutator, correction curves were provided for all affected temperature channels.

The data channels which could not be corrected were those in which the immediately preceding word on the commutator caused the sample to be of such value that the first decision (the most significant bit) was made incorrectly. The remaining bits in that word, then were incorrect and the data was irrecoverable.

The experience of *Surveyor III* caused no telemetry hardware changes in the subsequent missions because of cost and schedule considerations, but a change was made in the radar conditional reliable operate logic to prevent a reoccurrence of the loss of the 14-ft mark. For further discussion on this topic, see Section XIX B-1-c.

Signal processing changes which had been considered were: the complete redesign of the signal processing subsystem using higher voltage devices, the addition of fuses, or the addition of buffer transistors which would act as fuses. In addition an alternate means of insuring vernier engine cut off at the 14-ft mark was considered. For various reasons, none of these were implemented.

### 2. Command Decoding Subsystem Performance

The *Surveyors* responded to hundreds of thousands of commands in flight, and on the lunar surface. A rigorous evaluation of the mission performance of this subsystem was impossible for several reasons. The only command information sent back to earth was the position of a command reject/enable flip-flop. This flip-flop was set to the enable state only if the command met certain complement checks to determine if any noise had distorted the transmitted command. This noise could have been introduced at any point in the telecommunications loop from the command generator on earth, up to the complement checking circuitry on the spacecraft. If this noise indeed distorted the command, and the command subsystem rejected the erroneous command, but processed a subsequent proper command to the proper output, then the subsystem was functioning properly.

Alternately, the command subsystem was in error if a command with noise was enabled, or a command output was generated with no received command. In either case a spacecraft commanded function would occur without the proper input.

Since the state of the reject/enable flip-flop, and the effect on data of commanded functions were the only real information returned via telemetry about the command subsystem, these two were required to supply the total evidence for evaluation.

The state of the flip-flop could be sent to earth in two ways. The first way was as part of digital word in the signal processing subsystem. This digital word was not in all modes, and the indicated state of the flip-flop was a function of the sampling time of the commutator. This could, and did, result in a valid command being transmitted, received, decoded, and acted upon without the flip-flop having been sampled in that time span.

Additionally, a command could be generated due to noise alone, or failure in the command subsystem, and the state of the flip-flop would not be sampled. A second method for transferring this flip-flop state information to earth was to modulate an SCO with the reject/enable state information, and to modulate the transmitter with the SCO. During the missions, however, this SCO was not used due to the requirement to provide minimum threshold margin in the carrier by not modulating its energy out into sidebands.

For the above reasons only a general evaluation using the commanded functions as an evaluation source could be made. In all cases where a commanded function occurred, which should not have occurred, the anomalies were found to have been caused by ground or transmission problems.

Experience throughout all seven missions, although somewhat subjective, gave evidence only several times out of the hundreds of thousands of commands where the command subsystem might have been interrupted by noise causing a command reject.

## Bibliography


*Aerospace Telemetry.* Edited by H. Stiltz. Prentice-Hall, Inc., Englewood, N.J., 1961.

Kimball, K. R., *Characteristics and Operation of the Surveyor Low Level Differential Amplifier,* EPD-492. Jet Propulsion Laboratory, Pasadena, Calif., Apr. 26, 1967.

*Surveyor Failure Review Board, SC-4 AESP Switch Failures,* Report 78108. Hughes Aircraft Co., El Segundo, Calif., June 1967.

*Surveyor Spacecraft/DSIF System Interface Requirements, Surveyor* Project Control Document 6, Rev. 1, Jan. 1, 1964.

*Surveyor Spacecraft Equipment Specification, Section 6, Telecommunications Subsystems Requirements.* Hughes Aircraft Co., El Segundo, Calif., June 28, 1967.

*Surveyor Spacecraft Functional Description SC-1 Through SC-7,* Vols. I, II, and III, HAC Publication 70-93401. Hughes Aircraft Co., El Segundo, Calif., Nov. 1, 1964 (with revision sheets).

*Surveyor Spacecraft–Space Flight Operations, Interface Document Mission F,* PD-29, Rev. 9. Jet Propulsion Laboratory, Pasadena, Calif., Nov. 1, 1967.

*Surveyor Spacecraft System Bi-monthly Progress Summary,* No. SS111, SSD 3016R. Hughes Aircraft Co., El Segundo, Calif., Jan. 1963.

*Surveyor Spacecraft System Bi-monthly Progress Summary,* No. SS113, SSD 3377R. Hughes Aircraft Co., El Segundo, Calif., May 1963.

*Surveyor Spacecraft System Bi-monthly Progress Summary,* No. SS114, SSD 3486R. Hughes Aircraft Co., El Segundo, Calif., July 1963.

*Surveyor Spacecraft System Bi-monthly Progress Summary,* No. SS115, SSD 3110R. Hughes Aircraft Co., El Segundo, Calif., Sept. 1963.

# XXII. Spacecraft Scientific Instrument Payload

## A. Payload Evolution

The spacecraft payload discussed in this section is the group of special scientific instruments used to make the scientific observations at the landing site. However, this group of instruments excludes the basic spacecraft instrumentation, consisting of temperature transducers, strain gages, etc., which also provided useful scientific data.

Initial selection of the experiments, the responsibility of NASA, was made with extensive care to maximize the scientific information obtained from the limited number of landings planned for the project. Throughout the *Surveyor* Project, considerable attention was given to providing a scientifically meaningful payload for use in lunar observation. The payload selected, however, was based finally on the availability of instruments in conjunction with allowable payload weight. The exigencies of producing an operating spacecraft that would meet the basic engineering objectives of the project, including support of *Apollo* within the project time constraints, led to the adding of scientific instruments to the existing spacecraft design after successful mission performance had been demonstrated. Because of previous instrument work that had been carried out, this approach was successful.

The *Surveyor* spacecraft instruments had to be designed to withstand environmental conditions during the boost phase, during transit in space, during the soft landing, and also while operating on the lunar surface. Design, integration, and calibration of each instrument were undertaken to provide the principal investigator with data needed to conduct his experiment within the limits set by the power and communications bandwidth capabilities of the spacecraft. Although at the beginning of the project instrumentation specialists had little experience with problems of reliability, miniaturization, temperature control, material handling, etc. in the design of instruments for operation in space, their knowledge and awareness of these problems grew considerably during the time span covered by the *Surveyor* Project (1960–1968). Indeed, work on this project has had significant influence in bringing attention to space instrument development problems and in developing new techniques and materials for solution of these problems.

As shown in Table XXII-1, only three scientific instruments were finally used on the *Surveyor* missions, not including the bar magnets carried on *Surveyors IV–VII*. These instruments were (a) survey TV camera, (b) soil mechanics/surface sampler, and (c) alpha scattering instrument. All instruments performed their planned function on the successful missions, and much new and significant

**Table XXII-1. Scientific instrument payloads**

| Surveyor | Launch date | Survey TV camera | Soil mechanics/ surface sampler | Alpha scattering instrument | Remarks |
|---|---|---|---|---|---|
| I | May 30, 1966 | X[a] | | | Instrument operated successfully |
| II | September 20, 1966 | X[a] | | | Mission terminated before instrument operation |
| III | April 7, 1967 | X | X | | Instruments operated successfully |
| IV | July 14, 1967 | X | X | | Mission terminated before instrument operation |
| V | September 8, 1967 | X | | X | Instruments operated successfully |
| VI | November 7, 1967 | X | | X | Instruments operated successfully |
| VII | January 7, 1968 | X | X | X | Instruments operated successfully |

[a]Approach TV camera also carried but not used.

information was obtained on lunar-surface mechanical characteristics, composition, and topography.

At the beginning of the program, a nominal scientific payload weight of 345 lb was assumed. This weight was associated with a spacecraft weight of 2500 lb, which matched the capability of the *Centaur* launch vehicle known at that time. In preparation for the assembly of a 345-lb payload, work commenced at JPL and at HAC to develop and integrate a number of instruments with the spacecraft. To expedite selection, a decision was made to build an individual electronics auxiliary assembly for each scientific instrument. The purpose of the auxiliary assemblies was to match the power requirements of the instrument to the 22- and 29-VDC spacecraft power, to route commands to the instrument, and to accept and condition the output data from the instrument so that the format was compatible with the onboard signal handling equipment. This decision to build separate auxiliary assemblies proved valuable since it allowed payloads to be redefined without interfering unduly with spacecraft power, command, or signal handling conditions.

Principal changes in scientific payload during the *Surveyor* Project are shown in Table XXII-2, wherein major payload redirections are cited. Minor payload changes have been omitted for clarity.

In 1960–1961, work was performed mainly at JPL to determine the suitability for space operation of more than 20 instruments. The work performed varied from scientific feasibility studies to space instrument development. As time progressed, it became apparent that several instruments were not suitable for operation on the lunar surface; these were deleted from the payload. Work continued on other instruments until a major payload redefinition was made in the spring and summer of 1962, when two coincidental events narrowed the list of instruments for inclusion in the spacecraft scientific payload. In March 1962, *Centaur* was reassessed as having a capability of injecting a spacecraft of only 2100 lb into a lunar transfer trajectory. Accordingly, HAC was directed to redesign the spacecraft to reduce the weight from 2500 to 2100 lb. Such reduction in total spacecraft weight was immediately reflected in a reduced payload weight of 115 lb. At the same time, separate NASA and JPL reviews of instrument capabilities showed that further reduction in the list of candidate instruments for the scientific payload was necessary because of instrument development problems. On the basis of these two independent assessments, in October 1962 the payload was redefined and restricted to seven instruments:

(1) Survey television camera.

(2) Surface sampler.

(3) Sample processor.

(4) X-ray diffractometer.

(5) Soil mechanics instrument.

(6) Micrometeorite ejecta detector.

(7) Alpha scattering instrument.

The touchdown dynamics experiment was added to the list and the X-ray diffractometer and sample processor were deleted in 1963; work continued for about 2 yr on the newly defined payload. However, in an effort to concentrate on meeting the engineering objectives of the missions, the payload was reduced to only one instrument (TV) in late 1965.

After the successful soft landing of *Surveyor I* on the lunar surface on June 1, 1966, consideration was given to what items could be added for subsequent missions.

**Table XXII-2. Principal changes in the spacecraft scientific instrument payload definition**

| Date of change | Allowable payload weight, lb | Allowable spacecraft weight, lb | Reference document (JPL contract 950056) | Instruments included in spacecraft scientific payload[a] | |
|---|---|---|---|---|---|
| | | | | Total number | Items |
| September 1961 | 345 | 2500 | Modification 6 | 13 | Survey TV camera, subsurface sampler, X-ray, diffractometer, X-ray spectrograph, gas chromatograph, geophysical surface system, geophysical subsurface probe, magnetometer, plasma probe, seismometer, atmospheric pressure gage, radiation detector, surface sampler |
| April 1962 | 115 | 2100 | Modification 8 | 2 | TV and drill experiment |
| | 266 | 2500 | Modification 8 | 10 | Survey TV camera, subsurface geophysical instruments, X-ray diffractometer, gas chromatograph, surface geophysical instrument, surface sampler, sample processor, subsurface sampler, radiation detector, tape recorder |
| January 1963 | 114 | 2100 | Modification 15 | 7 | Survey TV camera, surface sampler, sample processor, X-ray diffractometer, soil mechanics, micrometeorite detector, alpha scattering instrument |
| April 1963 | 108 | 2100 | Change order 18 | 6 | Survey TV camera, surface sampler, micrometeorite detector, alpha-scattering instrument, single-axis seismometer, touchdown dynamics |
| June 1964 | 62.5 | 2150 | Modification 28 | 6 | Survey TV camera, surface sampler, alpha scattering instrument, seismometer, micrometeorite detector, touchdown dynamics |
| May 1965 | 114 | 2450 (A21A) | Modification 43 | 6 | Survey TV camera, surface sampler, alpha scattering instrument, seismometer, micrometeorite detector, touchdown dynamics |
| November 1965 | 62 | 2250 | Change order 101 | 1 | Survey TV camera,[b] (*Surveyors I* and *II* configuration) |
| August 1966 | 62 | 2250 | Modification 71 | 2 | Survey TV camera, soil mechanics/surface sampler (*Surveyors III* and *IV* configuration) |
| October 1966 | 62 | 2250 | Modification 73 | 2 | Survey TV camera, alpha scattering instrument (*Surveyors V, VI,* and *VII* configuration) |
| May 1967 | 71 (actual) | 2250 | Change order 156 | 3 | Survey TV camera, alpha scattering instrument, soil mechanics/surface sampler (*Surveyor VII* configuration) |

[a]Not included basic spacecraft telemetry instrumentation or bar magnets.

[b]Approach TV camera also carried but not used on *Surveyors I* and *II*.

The first in a series of decisions reinstating payload instruments occurred in August 1966, when it was decided to design and fabricate two flight and one spare soil mechanics/surface samplers (SM/SSs). These were simplified by deletion of the force-measuring instruments and the position-indicating potentiometers. The schedule constraints on the *Surveyor III* and *IV* spacecraft, for which these SM/SSs were intended, could not be modified. An electrical and mechanical interface was developed, enabling the simplified SM/SS to replace the approach TV camera without spacecraft modification.

Further consideration of the scientific payload led to the decision in October 1966 to add the alpha scattering instrument to the *Surveyor V, VI,* and *VII* spacecraft. The final addition to the *Surveyor* scientific payload was implemented in May 1967 when, as a result of continuing mission success, the simplified SM/SS was added to the *Surveyor VII* spacecraft. The existing spare flight SM/SS was used on this spacecraft. The mechanical interface between the SM/SS and the spacecraft was modified for *Surveyor VII*, enabling the SM/SS to pick up the deployed alpha scattering instrument sensor head

and move it to a different location on the lunar surface. The alpha scattering instrument could then analyze material from more than one site.

*Surveyor VII* was the only spacecraft which included all three instruments. The instrument weights are itemized in Table XXII-3. The total weight was approximately 71 lb.

The survey TV camera and the SM/SS were designed and constructed by HAC. The alpha scattering instrument was designed and built by the Laboratory of Astrophysics and Space Research of the University of Chicago. The JPL engineers under the direction of the *Surveyor* Project office had the overall responsibility for ensuring that these three instruments were designed and tested in accordance with the program requirements.

Of the three instruments, only the alpha scattering instrument was designed and built to the specifications of a principal investigator (A. Turkevich of the University of Chicago). The survey TV camera was designed at the beginning of the program as an engineering visual aid. By the time the principal investigator (E. Shoemaker of the United States Geological Service) was appointed, the design was in an advanced stage. Some modifications and additions were possible, however, and these improved the scientific capability so that the final version of the camera was well suited to its scientific task.

**Table XXII-3. Weight of scientific instruments**

| Instrument | Instrument component | Weight, lb |
|---|---|---|
| Survey TV camera | Camera | 17.40 |
| | Auxiliary assembly | 1.84 |
| | Miscellaneous hardware | 4.07 |
| | Total | 23.31 |
| Alpha scattering instrument | Sensor head | 5.23 |
| | Electronics | 4.70 |
| | Auxiliary assembly | 1.09 |
| | Thermal compartment | 5.79 |
| | Deployment mechanism | 3.55 |
| | Miscellaneous hardware | 6.99 |
| | Total | 27.35 |
| Soil mechanics/surface sampler | Mechanism | 8.38 |
| | Auxiliary assembly | 4.05 |
| | Thermal compartment | 2.25 |
| | Mounting substructure, etc. | 5.64 |
| | Total | 20.32 |

The SM/SS was originally conceived as a device to pick up rocks or pebbles on the lunar surface. It was part of a crushing and transport mechanism which collected and crushed the rocks and fed the powdered lunar material along a transport mechanism for analysis by the X-ray and alpha scattering instruments, both part of the original 345-lb payload. Because of engineering difficulties, work on the crushing and transport mechanism was discontinued in 1963. At about the same time, the original soil mechanics instrument was found to have major engineering problems, and work on it was also discontinued. The SM/SS was, therefore, retained to serve as a device that could be used to determine the surface characteristics of the lunar soil, and work proceeded to instrument the SM/SS with strain gages and accelerometers.

In 1964, a new principal investigator (R. Scott of the California Institute of Technology) was appointed by NASA. All activity was stopped on the SM/SS in 1965 by NASA direction in order to allow HAC to concentrate all their efforts on the first four spacecraft. Upon resumption of work in August 1966, only 110 days remained before the SM/SS was required for integration on *Surveyor III*. It was decided not to incorporate the strain gages, the accelerometers, and their associated electronics due to schedule limitations, so the SM/SS was built without these measuring devices. The two later models were also of the same simplified form.

Notwithstanding the development problems of the *Surveyor* scientific instrument development, the scientific results achieved from the program were excellent. This was due to two major factors. First, the spacecraft was designed to respond to a wide variety of commands from earth after soft-landing. This meant that the full flexibility of the instruments could be utilized. For example, of the instruments carried on the successful missions, the five TV cameras took a total of about 90,000 pictures, the two surface samplers dug many trenches and performed numerous dynamic-bearing-strength tests, and the three alpha scattering instruments performed their analysis on six lunar surface samples. Thus the flexibility of using earth commands allowed a considerable amount of unique observational science to be carried out. The second factor was the calibration: Each instrument was carefully calibrated before launch to the maximum extent possible. This factor was partly responsible for the amount of scientific interpretation made of the observations. The alpha scattering instrument was subjected to a thermal-vacuum calibration using known material samples after loading of the radioactive sources at Kennedy Space Center. This calibration

was undertaken by a combined JPL–University of Chicago team. The SM/SS was also calibrated on the spacecraft at Kennedy Space Center by a JPL–HAC team. Calibration of distances traveled by the scoop for given commands, and of forces which were exerted under various extensions of the unit, was made. Although these values could not be directly applied when the SM/SS was used on the lunar surface because of the change in ambient gravity, the observations proved to be useful for better interpretation of the lunar results. The survey TV camera was also given an extensive calibration by a JPL team at Kennedy Space Center. The camera was calibrated for light transfer characteristics, sine wave response, geometric linearity, polarimetric constants, erasure characteristics, photogrammetric characteristics and colorimetric or polarizing filter light transfer characteristics.

This report will concentrate on the three instruments which were carried on the spacecraft. In addition, several of the instruments which were in various stages of development when work was discontinued will be briefly discussed.

## B. Television Cameras

### 1. Introduction

The first design of the *Surveyor* spacecraft included three survey TV cameras and one approach TV camera. All of these imaging systems used a 600-line vidicon system with a picture-taking capability of one frame every 3.6 sec. The survey TV cameras were to be mounted around the spaceframe at 120-deg intervals to provide a full 360-deg stereoscopic coverage of the lunar scene. Each of the three survey TV cameras was mounted so that the vidicon faceplate was facing upwards, and wide or narrow angle views of the lunar scene were obtained by reflecting light from a mirror which could be positioned in elevation and azimuth. The approach TV camera employed a fixed-focus lens system set to infinity and it, too, operated in a 600-line mode to provide a view of the lunar surface just before the spacecraft commenced its final descent sequence.

As the project matured, the number of cameras on the vehicle decreased and the TV capability was improved. Initially a reduction in survey TV cameras from three to two was made. This considerably narrowed the angle over which stereo viewing was possible, because of the obstruction caused by spacecraft components, but aided the design of the spacecraft and the feasibility of operating the TV cameras by ground command. It was finally decided that only one survey TV camera would be flown on all missions and that an approach TV camera would be flown only on *Surveyors I* and *II*.

While these changes were being made a principal investigator for the TV cameras (E. Shoemaker of the United States Geological Service) was appointed. This appointment was made because the survey TV camera had the potentiality of being a scientific instrument and not just a qualitative viewing device to support engineering investigations. In conjunction with the principal investigator, JPL and HAC made considerable efforts to upgrade the cameras to enable them to be used as scientific instruments. These efforts resulted in camera and mirror unit design changes, additional testing, and extensive scientific calibration. The flight version of the TV cameras performed their functions well on all missions.

The scientific objectives of the survey TV camera are expressed as follows:

(1) Provide, as the primary objective, panoramic photographic information of the visible lunar surface in the immediate vicinity of the spacecraft, up to and including the local horizon.

(2) Provide measurements of feature size, shape, and range, through photogrammetry.

(3) Provide photometric, and colorimetric or polarimetric measurements of selected regions of the visible lunar surface, to aid in differentiating the observed features.

(4) Produce topographic or form-line maps of the observable vicinity of the spacecraft, for use in geologic interpretation of the observed features.

(5) Accurately locate the spacecraft landing position on the lunar surface by stellar position measurements.

(6) Observe lunar surface features at different angles of solar illumination to assist in differentiating and correlating the visual information, in identifying the lunar surface features, and in enhancing the accuracy of the topographic measurements.

(7) Observe phenomena taking place on the lunar surface, such as the formation of new craters by micrometeoroids and secondary solid particles, by successive observations of regions of the lunar surface and coordination with the results of other payload experiments.

The major characteristics of the survey TV camera which were determined to be necessary to fulfill the above objectives are stated below.

(1) The camera should have a resolution of at least 2 mrad in wide angle mode (i.e., 8 mm at 4 m), and a resolution of ½ mrad in narrow angle mode (i.e., 2 mm at 4 m).

(2) Azimuth and elevation axes of the camera should be determined within 2½ min of arc with respect to the camera coordinate system.

(3) Photometric characteristic of the camera should be known so that the error in relative light intensity measurement between incremental steps of 1:1.414 shades of gray, as well as over the entire dynamic range, should not exceed ±10%. Dynamic range to be such that at least eight such steps be distinguishable at highlight luminance of 800 ft-L. Accommodation of lunar scene intensity from 50 to 2600 ft-L should be obtainable.

(4) Colorimetric measurements (where applicable) should be known to within 15% of true coordinate positions (relative to the International Commission on Illumination system of color measurements).

(5) Polarimetric measurements (where applicable) should be made to determine the percentage of polarization as well as the polarization angle (phase of maximum transmission) and the spectral intensity of incident light from objects within the field of view.

(6) Calibration of the camera should include the following items:

  (a) Light transfer characteristics of the TV camera and the spacecraft.

  (b) Camera location on spacecraft.

  (c) Camera orientation angle.

  (d) Reseau pattern location.

  (e) Video signal-to-noise ratio.

  (f) Aperture response.

  (g) Distortions, including sensor tube shading.

  (h) Field corrections.

  (i) Spectral and/or polarimetric response.

  (j) Vignetting.

In meeting its objectives the survey TV camera performed the following (the approach TV camera was not used on those missions in which it was included):

(1) Observations of the lunar surface. Necessary data was obtained for general visual and topographic assessments of the landing sites.

(2) Surveillance of the other scientific instruments before, during, and after deployment to the lunar surface.

(3) Colorimetric surveys on *Surveyors I, III,* and *V* using a filter wheel containing filters plus a clear position.

(4) Polarimetric measurements on *Surveyors VI* and *VII* using a filter wheel containing polarizing filters which replaced color filters on previous *Surveyor* cameras. The polarizing measurements provided unique opportunities to compare polarimetric surveys from terrestrial telescopes with those made on the lunar surface.

(5) Observations of the solar corona (following sunset).

(6) Observations of the lunar surface illuminated after sunset by light reflected by the earth and light refracted through the earth's atmosphere during a solar eclipse.

(7) Observations of the earth including the viewing of earth-based laser beams.

(8) Surveys of rocks from which rock sizes and locations could be determined.

(9) Surveys of the lunar surface as disturbed by the spacecraft's footpads, crushable blocks, gas jets, SM/SS, and vernier engines.

(10) Surveys of portions of the spacecraft.

The pictures obtained by the TV camera provided valuable clues concerning the lunar surface properties and lunar processes. In performing the above operations the camera accommodated scene luminance levels from approximately $8 \times 10^{-5}$ ft-L to 2600 ft-L.

The survey TV camera was operated by ground command. Preplanned tapes were utilized to command the camera to take panoramic surveys. In addition, a considerable amount of manual commanding of the various camera functions was also performed when individual visual observations were required. Many thousands of commands were sent to the survey TV camera on all of the successful missions and the camera demonstrated great flexibility.

## 2. Design of the TV Cameras

*a. General description.* The TV camera carried on *Surveyors I* and *II* consisted of the slow-scan survey TV camera (capable of panoramic viewing) and an approach TV camera (downward looking), along with a TV auxiliary assembly for processing commands and telemetry data and two photometric charts. On *Surveyor III* and later missions, the approach TV camera was deleted.

Figure XXII-1 illustrates the functional elements of the survey TV camera. The mirror assembly shown is the new design used on *Surveyors VI* and *VII*. Of the six major assemblies, five of them (vidicon tube, shutter, variable focal length lens and iris, filter wheel, and mirror head) were mounted in the same housing, known as the survey TV camera, which was mounted on the spaceframe between legs 2 and 3 (Fig. XXII-2). It was about $5 \times 5 \times 22$ in. in size and weighed 16.1 lb (7.5 kg). The remaining

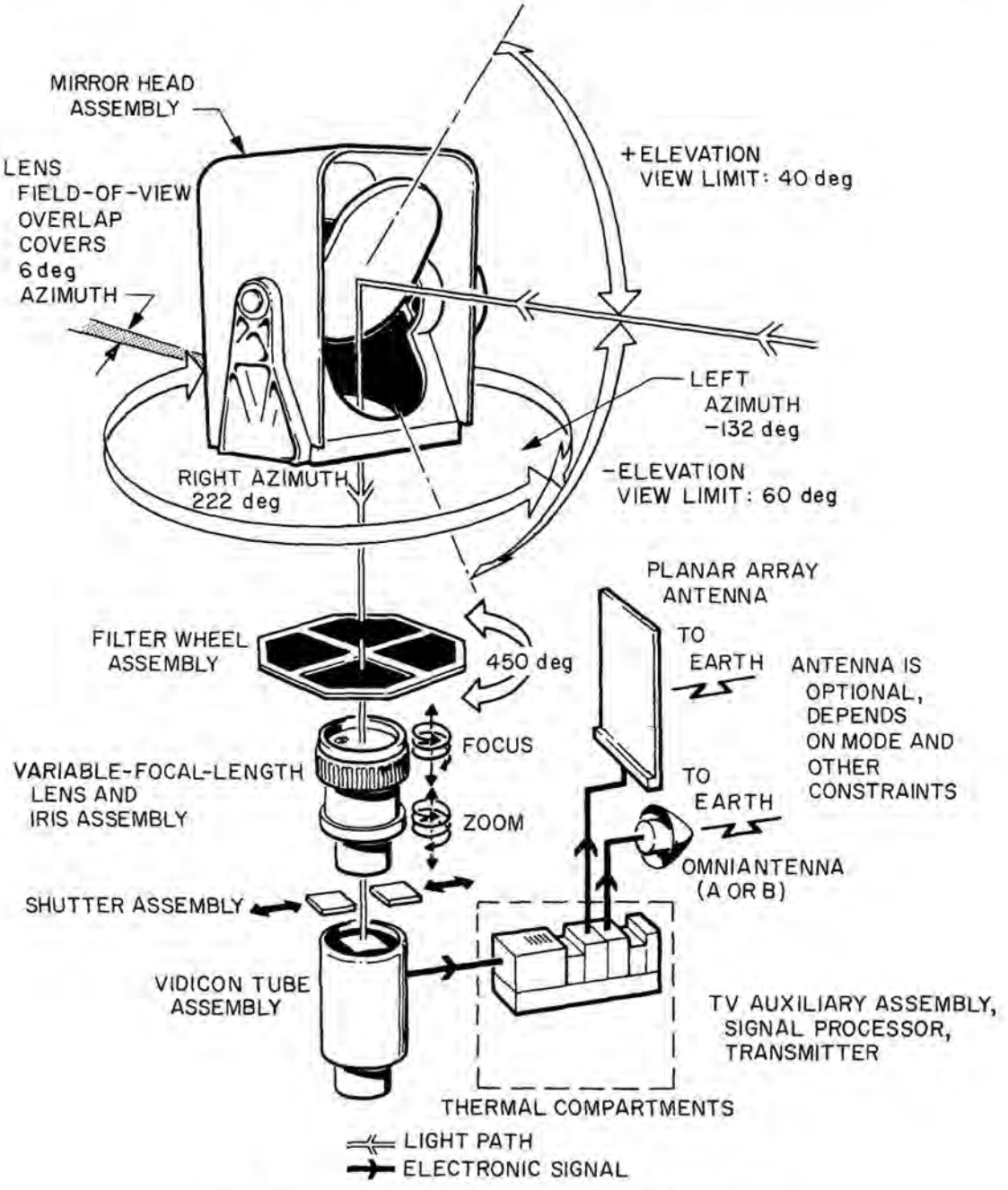



**Fig. XXII-1. Exploded view of *Surveyor* TV camera**

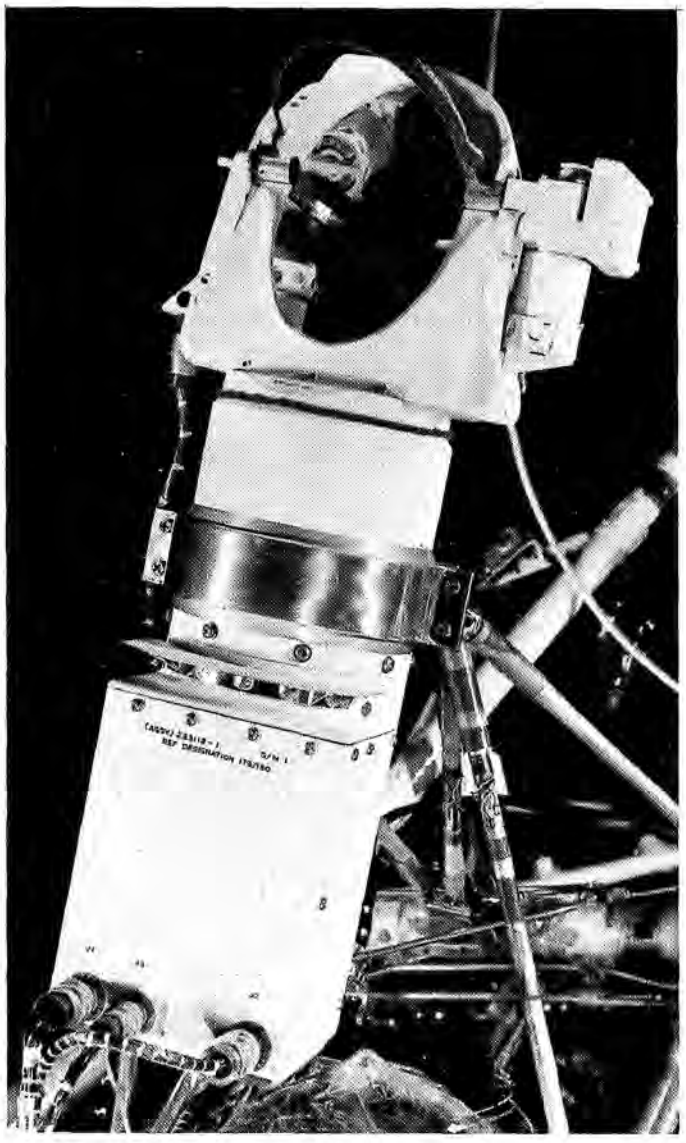


**Fig. XXII-2. Survey TV camera on the spacecraft (*Surveyor I*)**

assembly, known as the TV auxiliary assembly, was located within thermal compartment A. Figure XXII-3 shows a cutaway view of the survey TV camera.

The survey TV camera was designed to transmit either 600- or 200-line pictures. The 600-line pictures were transmitted in analog form together with added pulse-code-modulated (PCM) TV data as a frequency modulated signal through the planar array antenna of the spacecraft. A video bandwidth of 220 kHz was available, and the camera had the capability of photographing the scene once every 3.6 sec in the 600-line mode. Pictures taken in the 200-line mode could be repeated every 61.8 sec and could be transmitted via an omni-antenna using a bandwidth of only 1.2 kHz. The 200-line pictures were used in the missions only when one of the following conditions prevailed: (1) immediately after touchdown when the planar array was not yet oriented on earth, or (2) when the spacecraft or camera characteristics indicated that there might be problems in operating the spacecraft in the 600-line mode. Of the total of approximately 87,500 pictures recorded from all *Surveyor* missions, more than 99% were taken in the 600-line mode.

The pointing mirror concept was used to obtain a panoramic view around the spacecraft without rotating the main body of the camera. Although this concept considerably simplified the design of the camera, it was responsible for a rotation and a change in shape of the picture, as viewed through the ground equipment, as the camera mirror turned. This effect, although somewhat inconvenient, did not substantially reduce the operational effectiveness. The mirror head assembly was mounted to the top of the camera body. An elliptical mirror was used, pivoted in elevation about an axis in the plane of the mirror front surface which intersected the lens optical axis perpendicularly. Azimuth motion was produced by rotating the mirror head assembly about the lens optical axis (camera Z azis).

The focal plane shutter was designed to give an exposure of 150 msec on the survey camera. This was considered to be an optimum value for the lunar light conditions encountered. The variable focal length lens and iris assembly was adjustable from 25 to 100 mm focal length even though all operations were conducted at the two end stops which had undergone precision calibrations. These two focal positions allowed a wide and a narrow angle view to be taken of the lunar scene. The lens could be focused from infinity down to approximately 4 ft. The near focal position allowed detailed views of the visible part of the spacecraft and the lunar surface to be obtained. The iris was adjustable; the aperture was controlled by ground command to be compatible with the scene luminance and the vidicon characteristics. However, an automatic adjustment, based on a servo control actuated by the light incident on the camera, was also provided.

A four-position filter wheel assembly was mounted above the lens. On *Surveyors I–V*, this wheel was used to house one clear filter and three color filters. The colors chosen were red, green, and blue. On *Surveyors VI* and *VII*, three polarizing filters were used in place

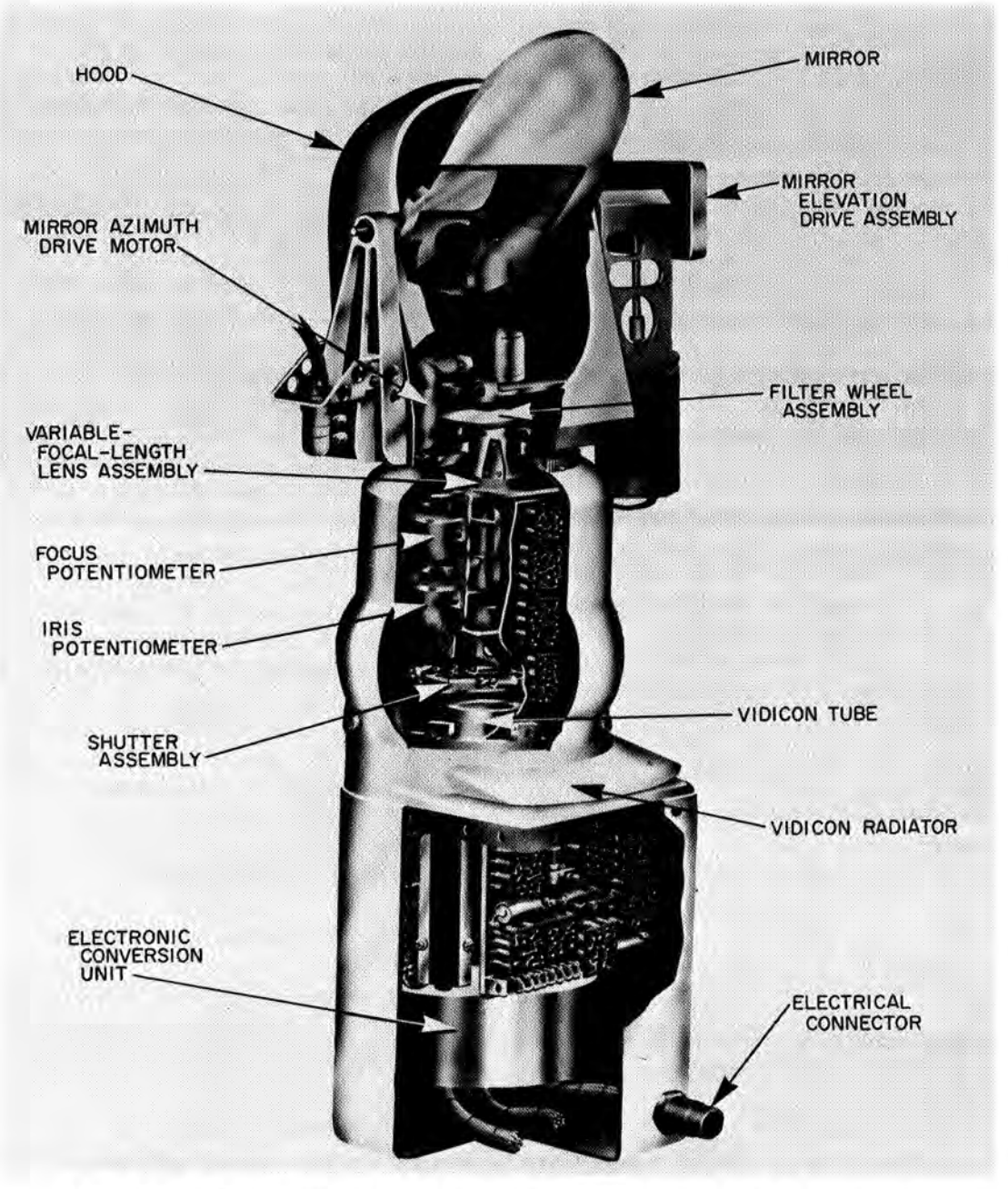



**Fig. XXII-3. Cutaway view of the survey TV camera (model used on *Surveyor I*)**

of the color filters to investigate the polarization of light reflected from the lunar surface and from the earth, and of light refracted from the lunar ballistic atmosphere.

The approach TV camera was similar in design to the survey TV camera but it had simplified optics and could operate only in the 600-line mode. A fixed infinity-focus, 100-mm focal length lens was used without a mirror. The same type of shutter assembly was used with a 20-msec exposure time. No color filters were employed. The approach TV camera was never operated on a mission but it was carried on *Surveyors I* and *II*. A thermally focused lens was designed to be used with the approach TV camera to compensate for focus shifts in the lens as the temperature changed.

***b. Major characteristics.*** The major characteristics of the survey TV cameras that were used on *Surveyor* missions were similar. The subsequent paragraphs provide a summary of the general characteristics of the cameras used on *Surveyors VI* and *VII*.

*1. Power requirements.* Power to operate the cameras required two sources. The 29-V regulated and 22-V unregulated lines were used for these sources. The camera on command required 9.2 W nominal in either no video, or video sequence modes from the 29-V regulated line. The vidicon heater, also powered from this line, required 2.7-W, nominal. Power requirements from the 22-V unregulated line for the camera on command were 0.55 W, nominal, in the no video and 46 W nominal in the video sequence mode. The electronic heater, powered from the 22-V unregulated line, required 38 W nominal.

*2. Commands.* The survey camera could accept and respond to 26 commands maximum. The TV auxiliary assembly could accept the two commands for camera thermal control.

*3. Video output signals.* There were two identical video outputs from the survey TV camera to provide required redundancy. The scan mode video signals (600- or 200-line) were routed to the TV auxiliary assembly located in thermal compartment A.

*4. Thermal capabilities.* The thermal capabilities specified were as follows:

| Area | Range, °F |
|---|---|
| Vidicon tube face | −20 to 150 |
| Electronic conversion unit | −20 to 165 |
| Lens assembly | −25 to 165 |
| Shutter mechanism | −65 to 165 |
| Electronics | −20 to 165 |
| Mirror head assembly | −50 to 180 |

The operating characteristics of the survey TV camera and the TV auxiliary assembly are given in Table XXII-4.

*c. Vidicon tube assembly.* The process of converting light into a corresponding electrical signal was accomplished by the vidicon tube assembly (Fig. XXII-4). The vidicon was the heart of the camera and much of the design was made to match the vidicon characteristics.

The principle by which a video signal was produced from the photo-conductive target layer is illustrated by Fig. XXII-5. A low-velocity scanning beam struck one surface of the target layer, the other side of which received illumination through a signal plate, from which the video signal was taken. When the photoconductive target surface was scanned, electrons deposited from the scanning beam charged the surface to the potential of the cathode of the electron gun. The conductivity was so low under dark conditions that very little current would flow across the target. If, on the other hand, the target was illuminated, the conductivity increased, the capacitively stored electron charge flowed across the target layer, and the scanned surface became more and more positive as it discharged in the interval between successive scans. During the next scan, the beam deposited only the number of electrons necessary to recharge the partially discharged surface back to cathode potential, thereby generating the video signal. The photoconducter incorporated in the *Surveyor* vidicon sensor consisted of a selenium derivative.

Integral to the photoconductor surface on the *Surveyor* vidicon was a 5 × 5-in. matrix of opaque dots comprising a reseau that could be used in correcting the image information for electronic scan nonlinearities and distortions. An opaque mark was also included in each

**Table XXII-4. Survey TV camera operating characteristics**

| Characteristic | 200-line mode | 600-line mode |
|---|---|---|
| **Video timing** | | |
| Vertical blanking, msec | 600 | 200 |
| Active video output, sec | 20 | 1 |
| Frame identification, msec | 600 | 200 |
| Total transmission time, sec | 21.1 | 1.4 |
| Erasure time (excluding picture readout), sec | 40.6 | 2.2 |
| Sync pulse time, μsec | 8 | 0.1336 |
| Back porch time, μsec | 8 | 0.1336 |
| Line scan time, msec | 84 | 1.403 |
| Vertical scan time (including retrace), sec | 20.6 | 1.2 |

## Table XXII-4 (contd)

| Characteristic | 200-line mode | 600-line mode |
|---|---|---|
| **Video output amplitude**[a] | | |
| Sync pulse amplitude: +2.5 V | | |
| Back porch amplitude: +1.5 V | | |
| White saturation, peak: −2.6 V | | |
| PCM zero: −2.5 V | | |
| PCM one: −1.5 V | | |
| **Radio frequency transmission** | | |
| Carrier frequency, MHz | 2295 | 2295 |
| Carrier deviation, MHz | ±0.005 | ±1.25 |
| Modulating signal bandwidth, MHz | 1.2 | 220 |
| Modulation index | 5.0 | 5.71 |
| Receiver signal-to-noise ratio | | |
| Upper margin, db | 8.2 | 16.9 |
| Lower margin, db | 4.51 | 12.6 |
| Threshold, db | 4.50 | 10.5 |
| Nominal transmitter output power, W | 0.10 (low power) | 10 (high power) |
| Nominal antenna gain, db | 0 (omnidirectional) | 27 (planar array) |
| **Performance specifications** | | |
| Minimum video signal-to-noise-ratio, db | 30 | 35 |
| Minimum horizontal relative response (for 600-line scan and SNR = 42 db in 600-line mode) | | |
| 1. 600 lines center | | 0.05 |
| 2. 450 lines (corner average) | | 0.14 |
| 3. 450 lines center | | 0.22 |
| 4. 300 lines center | | 0.54 |
| 5. 200 lines center | 0.40 | 0.80 |
| Minimum vertical relative response (for 600-line scan and SNR = 42 db in 600-line mode) | | |
| 1. 550 lines center | | 0.05 |
| 2. 450 lines center | | 0.15 |
| 3. 450 lines (corner average) | | 0.08 |
| 4. 300 lines center | | 0.35 |
| 5. 200 lines center | 0.40 | 0.60 |
| Gamma | 1.0 ±0.3 | 1.0 ±0.3 |
| Dynamic range | 4:1 | 11:1 |
| Grey level distinguishing capability | 5 $(2)^{1/2}$ | 8 $(2)^{1/2}$ |
| Luminance range, with iris at f/4 | 85–300 | 50–150 |
| Line-to-line jitter | <75 | <0.5 |

[a]Referenced to rest carrier = 0 V.

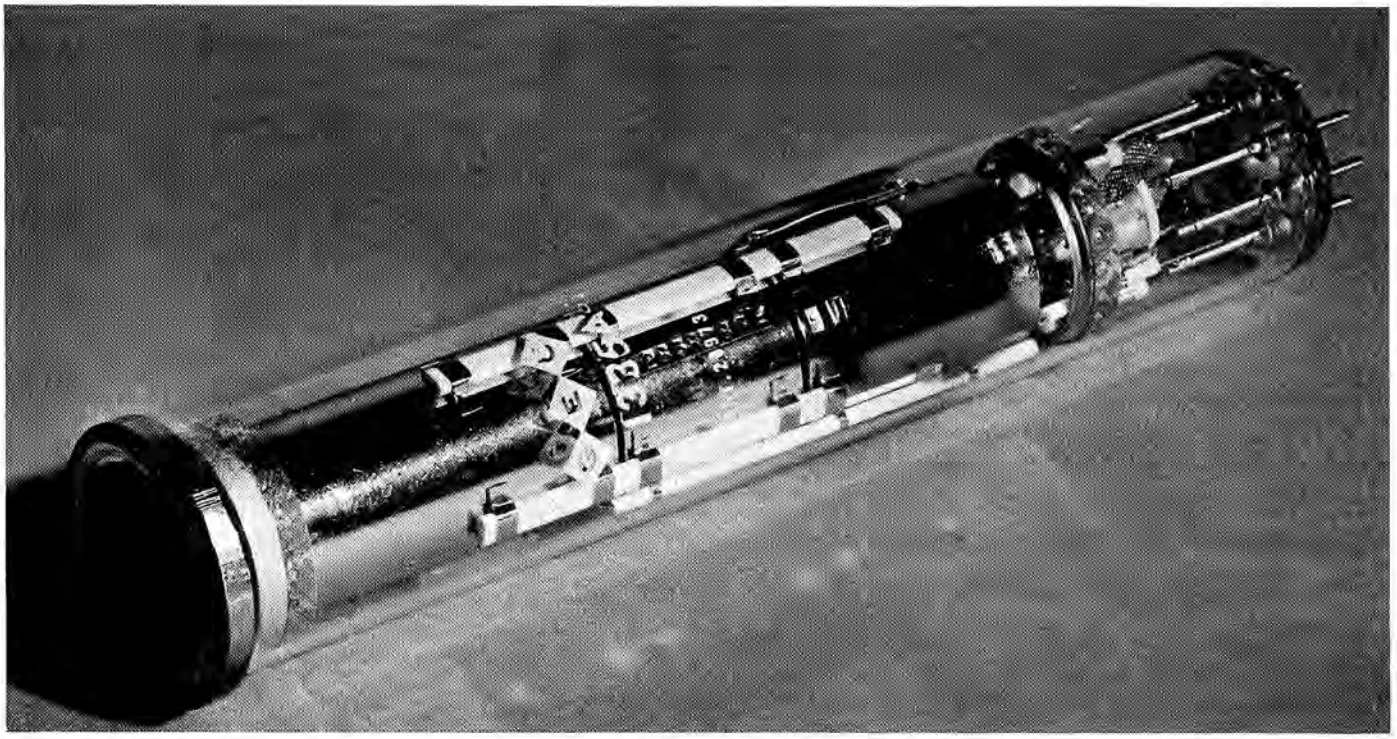


**Fig. XXII-4. One-inch vidicon tube assembly**

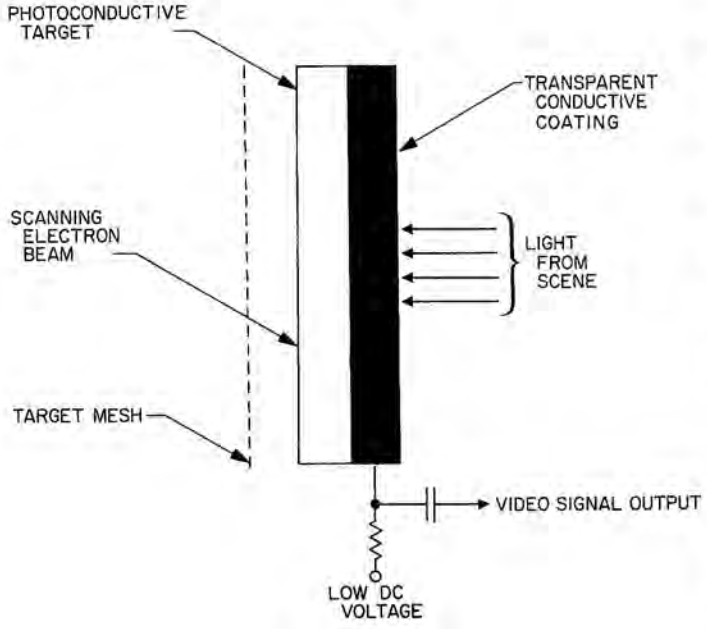



**Fig. XXII-5. Vidicon tube assembly functional diagram**

corner of the scanned format, which provided a black reference level in the video signal.

The vidicon tube assembly consisted of a 1-in.-diameter vidicon tube, lower housing subassembly, shroud, chassis, mirror logic chassis, and electronic circuitry. The tube assembly was positioned 0.2 in. behind the shutter. The vidicon cell subassembly consisted of the vidicon tube, a vidicon tube socket, deflection yoke and magnetic shield, and provision for longitudinal focus adjustment. Near the vidicon face was a boron nitride collar with the properties of high thermal conductance and high electrical resistance. Attached to this collar were four copper thermal conducting wires which connected to an exterior flat aluminum radiator as shown in Fig. XXII-3. The vidicon thermal radiator was a passive device to control the vidicon faceplate temperature during lunar operation.

*d. Shutter assembly.* Figure XXII-6 shows the shutter assembly which was used in the camera. This was situated approximately ¼ in. above the vidicon faceplate and mounted between it and the lens. The shutter blades were sequentially driven by solenoids across an aperture in the shutter base plate. The delay between the passage of the blades provided the exposure. The shutter assembly was commanded by ground command to give an exposure of 150 msec (normal mode), or it could be used in an open-shutter mode with 1–2 sec effective exposure time. A further provision enabled the camera to be operated indefinitely with the shutter open. This method of operation, the integrate mode, was used to increase the sensitivity of the camera by several orders

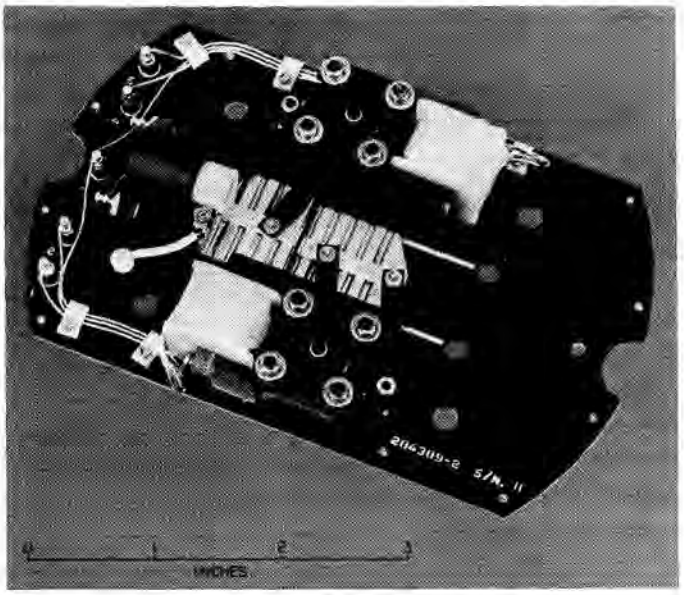


**Fig. XXII-6. Shutter assembly**

of magnitude so that an image of low-luminance-level scenes could be transmitted. The mode was implemented by opening the shutter assembly and turning off the vidicon electron beam. After the desired exposure had been obtained, the camera was restarted and the picture transmitted. Scene luminance as low as $8 \times 10^{-5}$ ft-L were reproduced in this mode.

A reflex beam splitter was provided between the lens and shutter assembly to sample the total incident light intensity. If this sampled intensity reached a predetermined value, the circuitry driving the shutter assembly was inhibited and the shutter assembly was prevented from opening until the excess light was removed. This prevented damage to the vidicon from direct or indirect sunlight. The design operating life of the shutter assembly was not less than 60,000 cycles.

*e. Variable focal length lens and iris assembly.* The variable focal length lens was responsible for the optical formation of the image on the vidicon faceplate. Figure XXII-3 shows it mounted approximately in the middle of the camera and just above the shutter assembly. The lens could vary its focus from 1.23 m to infinity by means of a rotating focus cell. The lens was of a zoom type, but it was calibrated and operated only at the two extreme positions: 25- or 100-mm focal length. These two positions correspond to a wide-angle field of view of $25.2 \times 25.2$ deg and a narrow-angle field of view of $6.4 \times 6.4$ deg, respectively. When operated in narrow-angle mode, the angular resolution of the camera was more than 0.5 mrad at 15% relative response. This resoluition permitted discrimination of objects on the lunar surface slightly less than 1 mm in diameter at the distance of the spacecraft footpads from the camera (1.6 m).

The lens and iris assembly included an adjustable iris that could be operated by ground command to give 11 positions for calibration. This resulted in the capability of changing the aperture area by a factor of 1.414 to the values of: $f/4$, $f/4.8$, $f/5.6$, $f/6.7$, $f/8$, $f/9.5$, $f/11$, $f/13$, $f/16$, $f/19$, and $f/22$. The iris could also operate in an automatic mode in which the iris position was controlled by the integrated scene luminance detected by a photocell in the lens. The reflex beam splitter described above provided the necessary light sample (10% of incident light) for operation of the iris in the automatic mode. Potentiometers geared to the iris, focal length, and focus elements allowed readout of these functions.

The lens and iris assembly, as shown in Fig. XXII-7, was mounted inside the lens support structure. Two chassis containing lens and mirror function (drive and logic) electronics were mounted to the sides of the lens support structure. Figure XXII-8 shows the nearly completed survey TV camera after the lens and iris assembly support structure and electronics chassis had been mounted to the deck structure. Another chassis (chassis 6) mounted parallel to the lens and mirror function chassis is shown. Not shown is the shutter assembly which was mounted between the main deck and the lens support structure.

*f. Filter wheel assembly.* The filter wheel assembly is shown in Fig. XXII-3 just above the lens and iris assembly. The filter wheel assembly was divided into four sectors as shown in Fig. XXII-9. On *Surveyors I–V*, the filter wheel contained three color filters and one clear piece of glass. The filter characteristics were tailored so that the camera responses, including the spectral response of the image sensor, the lens, and the mirror matched as nearly as possible with the standard CIE[1] tristimulus value curve (Fig. XXII-10). It was thus possible to reconstruct a color picture using the television imaging system after taking separate pictures with each of the three colored filters placed in the light path between the lunar scene and the vidicon. The color reconstituted pictures were used in determining lunar properties. On *Surveyors VI* and *VII*, the color filters were replaced by polarization filters. The plane of polarization of these three filters differed by 45 deg.

[1]Commission Internationale d'Eclairage.

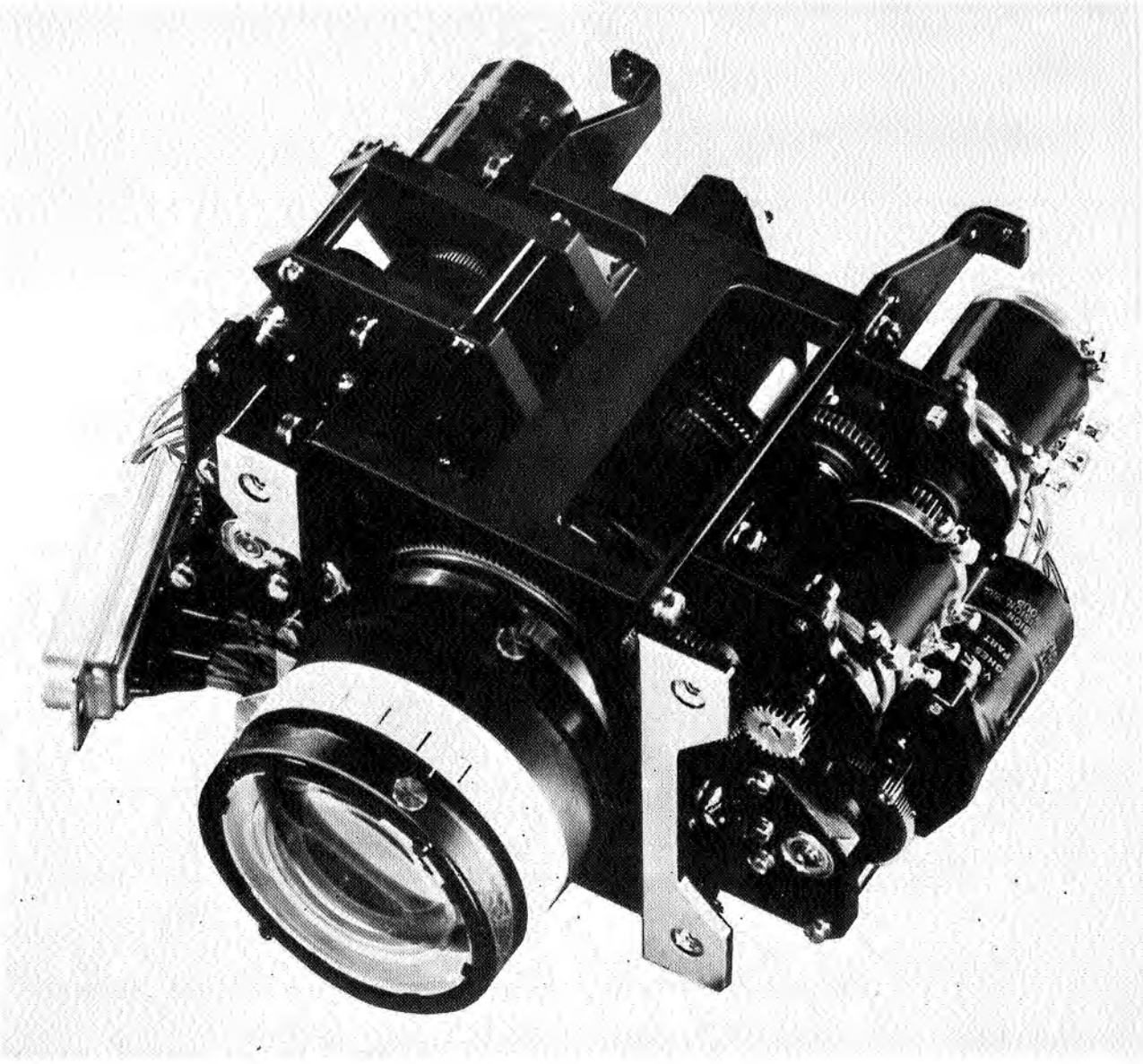


**Fig. XXII-7. Variable focal length lens and iris assembly**

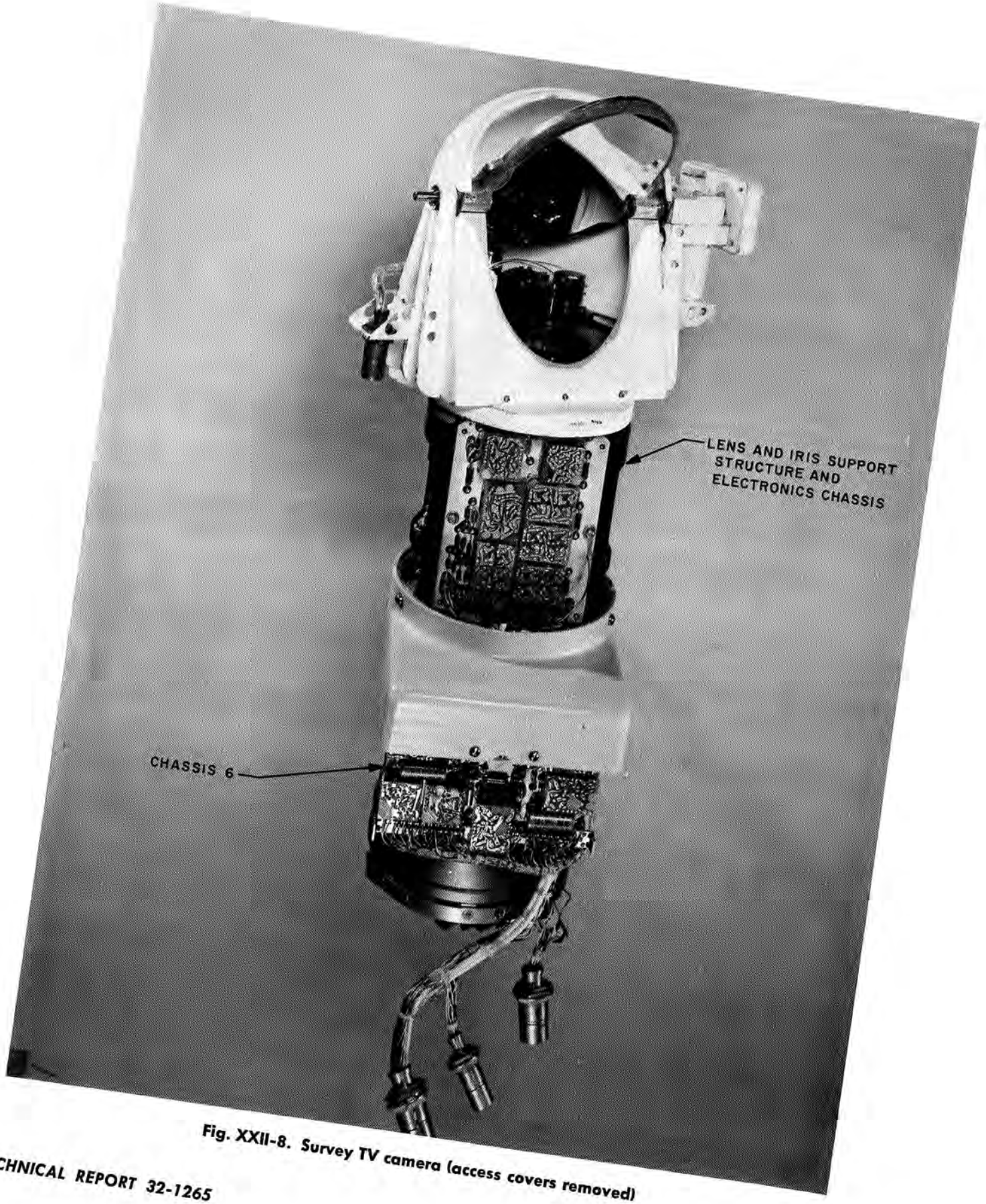



Fig. XXII-8. Survey TV camera (access covers removed)

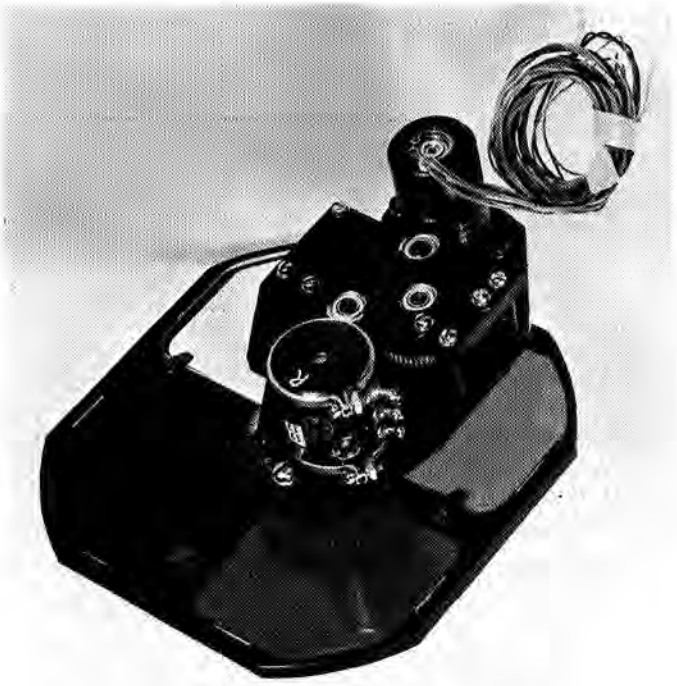


**Fig. XXII-9. Filter wheel assembly**

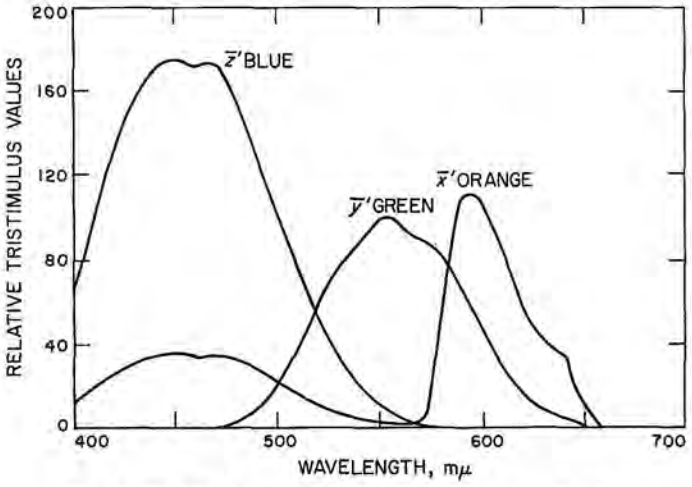



**Fig. XXII-10. Relative tristimulus values of color filter elements**

The filter wheel assembly consisted primarily of a gearbox supporting a stepper drive motor, a filter wheel rotating about a fixed hub, and a potentiometer position readout. The potentiometer provided an analog voltage output that indicated which filter was located over the lens. The total travel capability was 360 deg. The step time to the adjacent filter was less than 1 sec, the step size being 90 ±2 deg.

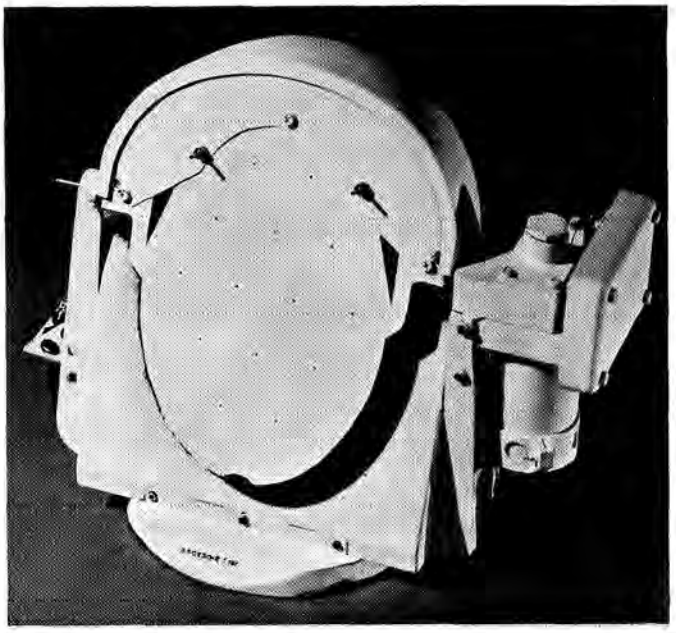


**Fig. XXII-11. Mirror head assembly (as used on *Surveyor I*)**

*g. Mirror head assembly.* Light which emanated from a lunar scene was reflected from a rotatable mirror in the mirror head assembly and was focused by the lens and iris assembly to produce an image on the faceplate of the vidicon. The mirror could be rotated in azimuth and elevation relative to a line through the center of the vidicon and the lens and iris assembly (camera Z axis). Figure XXII-1 shows the geometric outline of this light path; Fig. XXII-11 shows the mirror assembly in more detail.

The mirror rotation of the camera on *Surveyors I–V* (camera serial No. 284312) provided image scanning over a 360-deg horizontal panorama and from 40 deg above the plane normal to the camera Z-axis to −60 deg below this plane. The mirror head assembly was redesigned for *Surveyors VI* and *VII* (camera serial No. 290512) and the corresponding angles representing the range of vertical scanning remained approximately the same as for the earlier design. The new mirror head assembly was easily recognized because it had a hood that was more rectangular (compare Figs. XXII-11 and XXII-1). In the course of the redesign, the pointing accuracy, repeatability, and reliability were considerably improved.

The actual mirror employed was formed by vacuum-depositing an aluminum surface on a 10.5 × 15-cm beryllium elliptical mirror. The final surface was obtained

by depositing a layer of Kanogen finished with an overcoat of silicon monoxide. The overall thickness of the mirror was approximately 0.5 in.

Both axes of rotation of the mirror were geared to potentiometers so that the mirror position could be determined. The whole assembly (except for the elevation motor, gear drive, and potentiometer) was enclosed by a sheet metal hood painted white on the outside for temperature control and black on the inside to reduce reflections. Various external black paint patterns were used on cameras on different missions to attempt to minimize spurious reflections.

*1. Design characteristics.* The mirror head assembly characteristics included the following:

(1) Mirror reflectivity between 4000 and 7000 Å.
   a. Specular, 86%.
   b. Diffuse, less than 0.25%.

(2) Azimuth travel range of line of sight.
   a. Clockwise, 322 deg.
   b. Counterclockwise, 132 deg.

(3) Azimuth stepping
   a. Step size, 3 ±0.1 deg.
   b. Step rate, 2 per sec.

(4) Elevation travel range of line of sight from normal to camera Z axis.
   a. Above, +40 deg.
   b. Below, −60 deg.

(5) Elevation stepping.
   a. Step size, 5 ±0.2 deg.
   b. Step rate, 2 per sec.

(6) Life expectancy.
   a. Elevation, greater than 50,000 steps.
   b. Azimuth, greater than 100,000 steps.

***h. Photometric and colorimetric reference charts.*** Combined photometric and colorimetric charts were mounted on the spacecraft in view of the camera to assess TV photometric, colorimetric, and resolution performance. *Surveyors I–VI* were each equipped with two of these charts, one on leg 2 and one on omniantenna B. *Surveyor VII* had an additional chart on omniantenna A.

Each photometric chart was approximately 3½ in. in diameter and was constructed on substrate approximately 0.032 in. thick. The charts attached to leg 2 were made on aluminum substrate; those attached to the antenna booms were made on epoxy-fiber glass substrate so that they did not affect the omniantenna pattern.

Figure XXII-12 shows a photometric chart and its target format. Each chart was identical and contained a series of 13 gray wedges arranged circumferentially around the chart. These reference levels were used to check the photometric calibration of the camera and to determine that the right combination of aperature, filter, and shutter condition were being used. The actual dynamic range of the vidicons which were used in the missions varied from about 10:1 to 25:1. The total response range of the camera by use of filters, apertures and exposure times, however, was approximately $10^6$:1.

Three color wedges with known CIE chromaticity coordinates were located radially from the chart center. A series of radial lines was incorporated to provide gross estimates of camera resolution. Each chart also contained a centerpost which helped to determine solar angles after lunar landing by means of shadow information. Before launch, each chart was aligned and calibrated goniophotometrically to allow an estimate of postlanding camera dynamic range and to aid in photometric and colorimetric data reduction.

***i. Auxiliary mirrors.*** Auxiliary mirrors were used on *Surveyors III–VII* to allow the survey TV camera to view areas which would otherwise be blocked by spacecraft items. *Surveyors III* and *IV* each had one large and one small flat mirror mounted near leg 1 next to the retrorocket to allow viewing of vernier engine 3, crushable block 3, and the lunar surface beneath these. *Surveyor V* was equipped with two spherical mirrors that replaced the flat ones on *Surveyors III* and *IV*. One of these

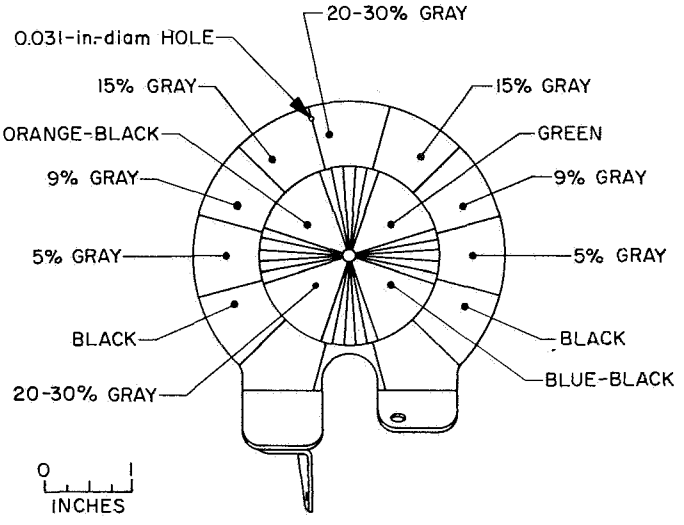



**Fig. XXII-12. Television photometric–colorimetric reference chart**

mirrors allowed the camera to view the possible deployment areas of the alpha scattering instrument. A third curved mirror was added on *Surveyors VI* and *VII*. The combination of the three mirrors allowed viewing of the areas under the vernier engines, the crushable blocks, and the possible alpha scattering instrument deployment sites. Also on *Surveyor VII*, a 9.5 × 3.5-in. mirror was attached to the *Surveyor* planar array mast to:

(1) Allow stereoscopic photographs of a portion of the lunar surface within the SM/SS operational area. The coverage obtainable was approximately 17% of the SM/SS operational area.

(2) Provide imagery of a portion of the lunar surface near the spacecraft for the TV photogrammetic experiment.

*j. Electronic circuitry and functional operation.* The complete command and data handling electronics for the survey TV camera was distributed among the camera, the auxiliary assembly, the central command decoder, the central signal processor, and the transmitters and receivers that were contained on the spacecraft.

The output of the vidicon tube assembly went to a video amplifier. This provided amplification and direct current clamping of the video signal. The video signal output from the camera was two identical single-frame composites applied to summing amplifiers in the TV auxiliary assembly through individual cables for redundancy.

Camera synchronizing and blanking pulses were generated continuously while the camera was operating; the horizontal and vertical generators were free running. A command signal was generated from the vertical blanking pulses and used to switch the transmitter automatically to the high power mode when the video was to be transmitted. This command signal also opened a gate to allow the video signal to pass to the summing circuits.

Frame identification data containing electronic, optical, and thermal data from the camera and mirror head assembly together with the angular setting of the mirror were also applied to the summing amplifier through an enable gate. This frame identification signal consisted of analog data that had been serially commutated in the TV auxiliary assembly and then converted to digital form. These data were summed with the composite video and transmitted as pulse coded frame identification data immediately after the composite video information. When operating in normal 600-line sequence, the video and frame identification signal was used to frequency modulate the high power spacecraft transmitted feeding the high-gain planar array antenna. Commands for the camera were processed by the telecommunications command decoder with further processing by the TV auxiliary assembly.

The first data transmitted during a picture-taking sequence were the horizontal sync pulses superimposed upon the vertical blanking pulses. This allowed Deep Space Instrumentation Facility monitors to be synchronized with the horizontal sync pulses prior to receipt of picture video. Single-frame picture readout occurred in the interval following vertical blanking. Transmission of the composite video information required 1.2 sec nominal, and terminated at the start of the next (second) vertical blanking pulse. The leading edge of the second blanking pulse reset the shutter, closed the video gate, and generated an enable pulse to open the frame identification input gate in the summing amplifier of the TV auxiliary assembly. Several complete sequences of frame identication data (about four or five) were transmitted during the enable pulse. The trailing edge of the second vertical blanking pulse terminated the enable pulse to close the frame identification input gate, and restored the transmitters to the low power mode, ending transmission for that particular sequence.

Three frame periods were required for proper vidicon erasure. Therefore, a subsequent start frame command was delayed until after the third vertical blanking pulse of a frame sequence. This constraint permitted three erasure frames (picture readout being the first) to occur during a nominal period of 3.6 sec for the 600-line scan mode.

*k. Approach TV camera.* The approach TV camera was similar to that of the survey TV camera. The primary differences were omission of the mirror head assembly, vidicon radiator and the complex lens and iris assembly with its associated electronic circuitry. The approach camera TV lens was supported by a simple shroud and had a manually adjustable iris. The TV auxiliary assembly was shared between the approach and survey TV cameras. Coded commands were processed by the decoder in the central command decoder; only six commands were required to operate the approach camera. Commutation was performed in the engineering signal processor in either the central command decoder or the TV auxiliary assembly. The approach TV camera transmitted in 600-line scan mode only, requiring transmitter high power, a 220-kHz bandwidth and the planar array antenna. No frame identification data was transmitted.

The approach TV camera was designed to take pictures of the landing site during lunar approach beginning approximately 1000 mi from the lunar surface and to continue at discrete intervals until the planar array no longer faced the earth. Because of the success of the *Ranger* Project in providing high-resolution approach pictures of the lunar surface, the *Surveyor* approach TV camera was not used.

### 3. Procurement and Fabrication History

***a. Vidicon tube assembly.*** Selection and procurement of the best suited vidicon tube assembly for the *Surveyor* missions was a major problem. Vidicon tube assemblies from four major suppliers were evaluated for a number of characteristics, ranging from resolution to survival temperatures. The General Electrodynamics Corporation 7226A assembly was selected on a preliminary basis during the design study phase because of its sensitivity and temperature survival characteristics.

The *Surveyor* mission required a vidicon photosensitive surface with incompatible characteristics of long persistence and rapid erasure. The Westinghouse WX 5100-series assembly and the existing General Electrodynamics Corporation 1335-A series assembly yielded best results; on the fourth scan (readout, two erase scans, and readout) the remaining image was 6% or less.

The 1335-A vidicon tube assembly was finally selected for the *Surveyor* camera mainly because of its ability to operate at high temperatures. This assembly with its modified selenium compound surface, also met requirements of dark current and erasure at 149°F with only minor spots that disappeared at lower temperatures.

The requirement to survive transit phase temperatures as low as −160°F was also shown to be met after some tests and analysis. Cryogenic tests were conducted on vidicon tubes and vidicon yokes. Vidicon tube assembly cryogenic survival varied from batch to batch as the manufacturer was unable to control the photosensitive surface properly. Enough of the 1335-A assemblies were qualified for transit survival during tests.

When subsequent tests indicated that these vidicon tube assemblies might be capable of lunar night survival, a requirement was set that the assemblies survive lunar night temperatures. Vidicon tube assemblies were subjected to liquid nitrogen temperatures (−310°F) for varying periods of time. However, in almost all cases, the vidicon photosensitive surface peeled away from the fused quartz faceplate and the tube was rejected. The GEC 1335-A assembly survived this test if the transition from room temperature to −310°F was made at a rate of 1.8°F/min or less. Since calculations of camera cooldown rates indicated that this would not be violated during cooldown, assemblies were eventually selected for flight use from groups that survived this liquid nitrogen cool soak test, showed no change in spectral characteristics, and still met the resolution requirements for the *Surveyor* camera.

When a further batch of vidicon tube assemblies was ordered for *Surveyors V–VII*, the new tubes could not survive the expected lunar night or even earth-moon transit temperatures. A 2-W vidicon survival heater was therefore added to the camera and the lunar night survival requirement relinquished. The heater was sufficient to hold the temperature above the survival value of −60°F under all transit conditions.

To improve the chance of lunar night survival, an effort was made to use cameras containing vidicon tube assemblies from the original batch, which possessed the best night-survival characteristics. Thus, *Surveyor V* used the original flight spare camera and the camera used on *Surveyors VI* and *VII* were recalled for replacement of the new vidicon tube assembly by the older series.

The camera on *Surveyor II* was observed to have black spots on the vidicon faceplate causing small marks to appear on the pictures. It is thought that these spots were small particles of epoxy and solid lubricant from inside of the camera body. On later cameras, a cleaning port was built into the camera housing and the particles were vacuum-cleaned from the vidicon faceplate by a special attachment without disassembly of the camera.

The vidicon yoke was found to be producing a nonlinear magnetic field superposition problem on some of the later cameras. This phenomenon manifested itself in a change of picture resolution when one yoke winding was reversed. This effect was investigated, and it was decided to make use of the increased resolution by reversing the direction of scan on the cameras on *Surveyors VI* and *VII*. Changes were made in the ground equipment so that the pictures were displayed correctly on the monitors.

***b. Shutter assembly.*** There were numerous problems with the reliability of the first shutter assembly designed for the *Surveyor* Project by a subcontractor. After many

attempts to improve the design and fabrication technique, it was decided to replace the shutter assembly. Jet Propulsion Laboratory supplied a design based on the shutter used in the *Ranger* TV camera to HAC, and this type of shutter assembly proved to be extremely reliable.

*c. Variable focal-length lens and iris assembly.* The type approval test camera indicated that the camera could not provide the required resolution when focused at infinity under high temperature conditions. This effect was caused by an aluminum lens mounting support structure that expanded with temperature and varied the lens–vidicon relationship. An Invar support structure was designed as a solution but was not adopted because of schedule problems. The vidicon tube assembly was eventually readjusted to a compromise position to compensate for the support structure shift. This decreased the high temperature problem, but resulted in a reduction in the near-field resolution capability. Correction curves were developed for mission operations to compute focus distance vs temperature.

Ultrahigh vacuum and temperature tests of the lens and iris assembly were carried out in 1965. During this test, cold-welding of the wiper arms to the wire was observed in the indicating potentiometers. From that time until the end of the project considerable effort was expended in improving the operation of the potentiometers in space. A complete solution to this problem was never found. However, the only problem involving a potentiometer occurred on *Surveyor I*, and this caused only a minor inconvenience.

Veiling glare and flare measurements on the lens and iris assembly were performed in 1964. Light from non-image forming rays arriving at the image plane, which does not originate from a corresponding point in the object space, can result in a reduction of contrast ratio by veiling of the low light image information. Contributing factors are multiple reflections and scattering from the lens surfaces and the edges of the lens and lens mount. The veiling glare contributed by the lens varied from approximately 4 to 11%. The lower value applied near the center of the field of view and increased in all directions as the test progressed outward from the center.

*d. Mirror head assembly.* The mirror head assemblies used on *Surveyors I–V* were of an original design made early in the project. Difficulties were experienced in meeting the pointing accuracy repeatability requirements for mirror positioning. In addition, the frictional forces acting at the mirror bearings were so great at the end stop positions that there were occasions during test when the mirror stuck in position and could not be repositioned. On the first missions, therefore, the camera was launched with the mirror in an open position to insure that pictures would be obtained. On *Surveyor III* there was a considerable amount of dust on the surface of the mirror that was presumably deposited there during the landing sequence, in which the vernier engines remained on until after the first two touchdowns.

Several changes were made to the mirror head assembly throughout the life of the project. The camera on *Surveyor III* had a small bonnetlike hood extension to reduce glare from direct or reflected sunlight. A similar shade was carried on the cameras of *Surveyors IV* and *V*. Cameras on *Surveyors IV–VII* utilized improved mirror stepping motors which gave improved reliability. The mirror head assembly on *Surveyors VI* and *VII* was completely redesigned and proved to be markedly superior in many respects.

*e. Electronic circuitry and functional operation.* As a result of continuing reviews, much upgrading of the electronic design of the TV camera was carried out during the project. Changes made included adding logic for the integrate mode on the camera, improving the performance of the video amplifier, improving linearity, overscanning the vidicon tube assembly to improve the wide temperature response of the camera, and many others. Because of substantial variations in characteristics between individual vidicon tube assemblies, and lack of clear interface definitions, changes in allowable video amplifier output had to be made in several cameras to prevent overdeviating the transmitters during peak white signal levels.

### 4. Test Program

The components, assemblies, and the complete survey TV camera were subjected to a rigorous testing program in conformance with *Surveyor* Project requirements. Because of extensive changes in the TV camera during the project two type approval cameras were fabricated and tested.

*a. Assembly tests.* The first major series of tests was conducted at the assembly level. After a functional test each assembly received a conformal coating and a three-cycle cryogenic test. This low-temperature test was necessary to check that the coating was sufficiently thin to prevent cracking of the components. The assembly was then tested for functional performance over its

designed temperature range, and upon completion of these tests it was mounted in the camera.

Individual acceptance and functional tests were carried out on components such as motors, vidicon tubes and potentiometers.

***b. Type approval tests.*** Two type approval test cycles were conducted on the TV camera: the first covered the *Surveyors I–V* configuration; the second, the *Surveyors VI* and *VII* configuration. The test sequence was as follows:

(1) Ambient full functional tests.

(2) Three axes of vibration.

(3) Partial functional tests.

(4) Thermal vacuum exposure and simultaneous partial functional test.

(5) Ambient full functional test.

The full functional tests consisted of measurement of the following parameters:

(1) Response to each command at low, nominal, and high input voltage.

(2) Nonresponse to spurious commands.

(3) Horizontal and vertical response at four line frequencies at the center and four corners of the video format for 600-line mode.

(4) Horizontal and vertical relative response at one line frequency at the center and four corners of the video format for 200-line mode.

(5) Signal-to-noise ratio at optimum light input in both 600- and 200-line mode operation.

(6) Light transfer function (i.e., light input vs voltage output).

(7) Linearity and line-to-line jitter.

Partial functional tests consisted of measurements selected from the above list to best evidence survival after exposure to vibration or the thermal vacuum chamber.

***c. Flight acceptance tests.*** Flight-acceptance tests were carried out on all flight TV cameras. They were similar in nature to the type approval tests excepting:

(1) The tests were conducted on each flight article.

(2) Vibration levels were 50% lower and 50% shorter in duration.

(3) Thermal vacuum exposure covered the same temperature extremes but was shorter in duration.

(4) Full functional tests were not quite as extensive, e.g., response to command at ambient was verified only at minimum voltages.

After a camera rework cycle, which may have been caused either by a failure at the system level or because of the incorporation of an engineering change, the extent of the flight acceptance test was reduced to verify only suitable rework. In all cases, however, the unit was again subjected to one axis of vibration and some thermal vacuum exposure. The flight TV cameras experienced considerable difficulty in meeting the system level tests and were consequently reworked and returned for flight acceptance tests on many occasions.

***d. Spacecraft system tests.*** As a part of the overall spacecraft testing program, many system tests involving the TV camera, the TV auxiliary assembly, the central signal processor, the central command decoder, the transmitters, and the receivers were carried out. These tests were to determine that the camera was compatible with the spacecraft as well as to confirm that the camera was still functioning before, during, and at the conclusion of the overall system testing program.

Tests were carried out on the TV camera during all phases of flight spacecraft system testing. These tests included checks of the following parameters for both 600- and 200-line modes while the camera was mounted in the spacecraft:

(1) Sensitivity and dynamic range.

(2) Video signal-to-noise ratio.

(3) Horizontal relative response.

(4) Vertical relative response.

(5) Imaging capability.

(6) System gain.

(7) System demodulated signal-to-noise ratio.

General testing of the following items was also carried out:

(1) Subsystem telemetry calibration.

(2) Mounting alignment.

(3) Subsystem warmup.

### 5. Television Camera Scientific Calibration

Although the TV camera was originally intended to function as an essentially qualitative viewing device which would support engineering investigation, its design was of adequate quality to permit transformation of the camera into a scientific instrument. This transformation was assistetd by a scientific calibration program which defined the TV camera performance accurately enough to allow scientific interpretation of the mission data.

The calibration program was conducted by JPL personnel. This included development of the optical and electronic calibration equipment, conducting the calibration, processing the data, and utilization of the results. Information on the TV camera and the spacecraft was supplied by HAC.

*a. Component calibration.* Prior to system calibration some aspects of the vidicon tube assembly, the color filters, the polarizing filters, and the photometric charts were calibrated by measurements on the individual components. For the vidicon tube assembly, the relative spectral response was measured. These data were used to develop certain response conversion factors and as a basis for calculation of the thickness of elements of the blue and green filters. Each blue or green filter consisted of a combination of two glass filters of different colors. The total thickness of the combination was constrained by the filter wheel design. Therefore, it was necessary to calculate the thickness of each glass element of the combination so that the combined response of the filter and the vidicon tube assembly would meet the scientific requirements. Absolute spectral response of each filter was measured. This, with the vidicon spectral response, enabled interpretation and reconstitution of color pictures taken during the mission.

The gray steps and color wedges of the photometric charts were calibrated, using a spectroradiometer on which incidence angle could be controlled. The spatial distribution of the spectral radiance factor of each step and wedge was calibrated in this fashion. For the *Surveyors VI* and *VII* TV cameras, on which the color filters were replaced by polarization filters, the absolute transmission of each filter was measured as a function of the angle between the polarization planes of the filter and a plane polarized light source.

*b. System calibration.* System calibration involved the precise measurement of the output for a precisely defined input. The input was the light, such as that coming from an object serving as a luminance source, being viewed by the camera on the spacecraft. The output was an image recorded on film or a signal recorded on magnetic tape produced by the television-ground data handling system (TV-GDHS). In this context, the system was not the spacecraft only but included the ground equipment.

Simultaneous calibration of the complete system was not feasible logistically. Instead, a method was used which, although not requiring simultaneous calibration of the spacecraft and of the TV-GDHS, resulted in a direct overall calibration.

Figures XXII-13 and XXII-14 show configurations used for TV calibration. Figure XXII-13 illustrates calibration of the spacecraft only, in the spacecraft checkout facility at Kennedy Space Center about 2 mo before launch of a spacecraft. The data were recorded in frequency modulated (FM) form on magnetic tape. Figure XXII-14 illustrates completion of the calibration, about 1 mo before launch, at the TV-GDHS locations at DSS 11 and at the Space Flight Operations Facility (SFOF). In the interim the tape recorder, which was part of the calibration test set used at Kennedy Space Center, was transported to DSS 11. There, the magnetic tape recorded at Kennedy Space Center was played into the TV-GDHS. Assuming that the tape recording and playback process had not influenced the data, the film or tape output of the TV-GDHS was compared to the calibration light source luminance to determine the exact response of the entire system.

The validity of the above assumption concerning the fidelity of the tape recorder can be explained as follows. The spacecraft transmitted an FM signal of 2295 MHz. The signal passed through amplifier and frequency conversion stages in the ground system receiver of the system test equipment assembly and in the calibration test set, resulting in an FM signal at a 4-MHz carrier frequency.* The base band data were intact because they were not affected by amplification or frequency conversion. The FM signal, at a high signal-to-noise ratio to prevent data loss, was then direct recorded on the video tape recorder. The tape recorder could corrupt the FM signal if the speed of the tape relative to the speed of the head was not maintained constant. Speed variation while recording was prevented by using crystal control of capstan and head speed. At the same time a crystal controlled reference signal was recorded on one channel. This permitted control of speed during playback by minimization

*The values given in this description apply to 600-line camera operation only.

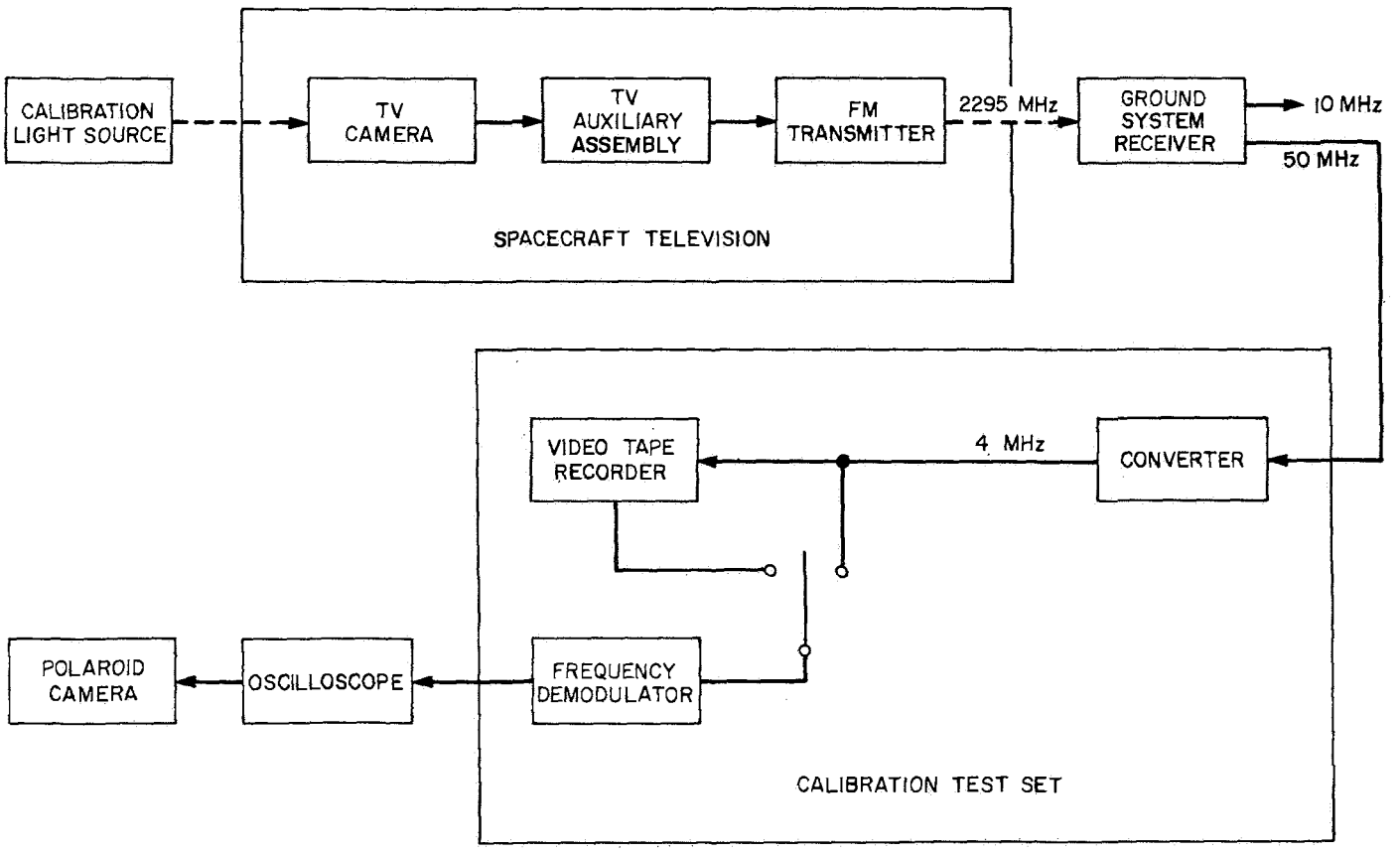



**Fig. XXII-13. Television calibration configuration at the Spacecraft Checkout Facility**

of a feedback error signal, which was derived by comparison of the reference signal frequency to the crystal frequency.

Playback was patched in at a compatible 4-MHz frequency level (Fig. XXII-14) bypassing only amplifier and frequency converter stages. At DSS 11 film and tape records were made including a predetection recording. Simultaneously, the signal was sent by microwave transmission to SFOF, where a similar set of records was made at the TV-GDHS in that location. In each case, the predetection recording was a duplicate, which could thereafter be played into the TV-GDHS to check for any day-to-day drift of demodulator and video processsor performance during a mission.

*c. Calibration equipment.* The *Surveyor* TV calibration test set (Fig. XXII-15) was designed and built by JPL. Its major functions were frequency conversion, tape recording, demodulation, and display. The input signal was the 50-MHz FM carrier at the first intermediate frequency stage of the system test equipment assembly) receiver. This was converted to a 4-MHz level, which was direct recorded, or to a 500-KHz level which was FM recorded, for 600-line or 200-line camera operation, respectively.

The tape recorder was an Ampex rotating head, helical scan machine, specially modified. The data recorded included the video channel, a time code signal, a voice annotation signal and a crystal controlled speed reference signal.

To monitor during calibration or to review tape playback, the video channel signal was supplied to an appropriate, carefully calibrated, frequency demodulator. The demodulator output was displayed on the Tektronix oscilloscope where a Polaroid photograph was made. Three crystal oscillators in the equipment, which represented carrier nominal center frequency and band edge frequencies, could be recorded on the tape as references or to test the tape recorder, or could be demodulated to calibrate the Polaroid prints.

The calibration test set served several vital functions besides those for which it was built. First, it demonstrated the extent of spacecraft frequency deviation on

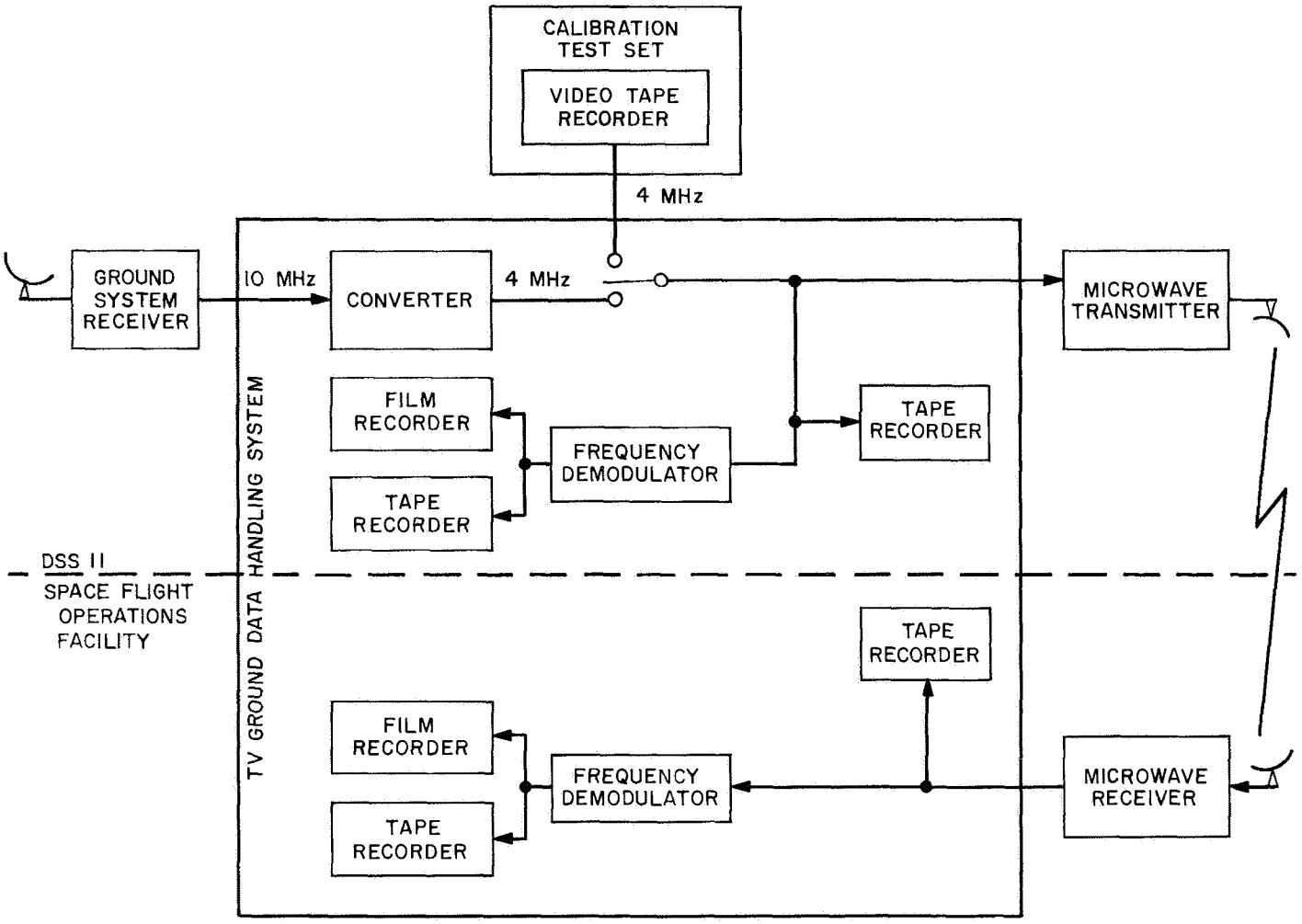



**Fig. XXII-14. Television calibration at DSS 11 and the Space Flight Operations Facility**

the *Surveyor IV* and *V* missions and showed video degradation which this could cause. Using the video tapes to simulate *Surveyors IV* and *V*, a nonstandard tracking station operating procedure was developed for the missions to avoid video degradation. Detection of this problem also permitted a design change in the *Surveyor VI* and *VII* cameras which prevented excessive frequency deviation on these spacecraft.

At DSS 14 the equipment served as a backup TV-GDHS during the *Surveyor I* Mission and for special tests during the second lunar day of *Surveyor VII*. During all missions, the conversion function of the equipment was used to enable predetection recording of telemetry as backup to DSS 11 so that loss of communication lock between the spacecraft and DSS 11 would not result in loss of telemetry data during critical phases of the mission. Of particular importance was the protection against any possible loss of strain gage data during *Surveyor I* touchdown.

The major item of optical equipment built for calibration was the *Surveyor* TV calibration light source, shown set up for calibration of a spacecraft in Fig. XXII-16. The source used two xenon lamps in an integrating hemisphere to generate an $8 \times 8$-line luminance field flat to $\pm 3\%$. The luminance level was continuously adjustable from 4 to 2600 ft-L. Adjustment was very simple, by iris control, involving no change in color temperature. Luminance level was continuously monitored by a fiber optics probe leading to a photometer.

Calibration slides, consisting of 8-in. square film transparencies mounted between glass plates, were fastened

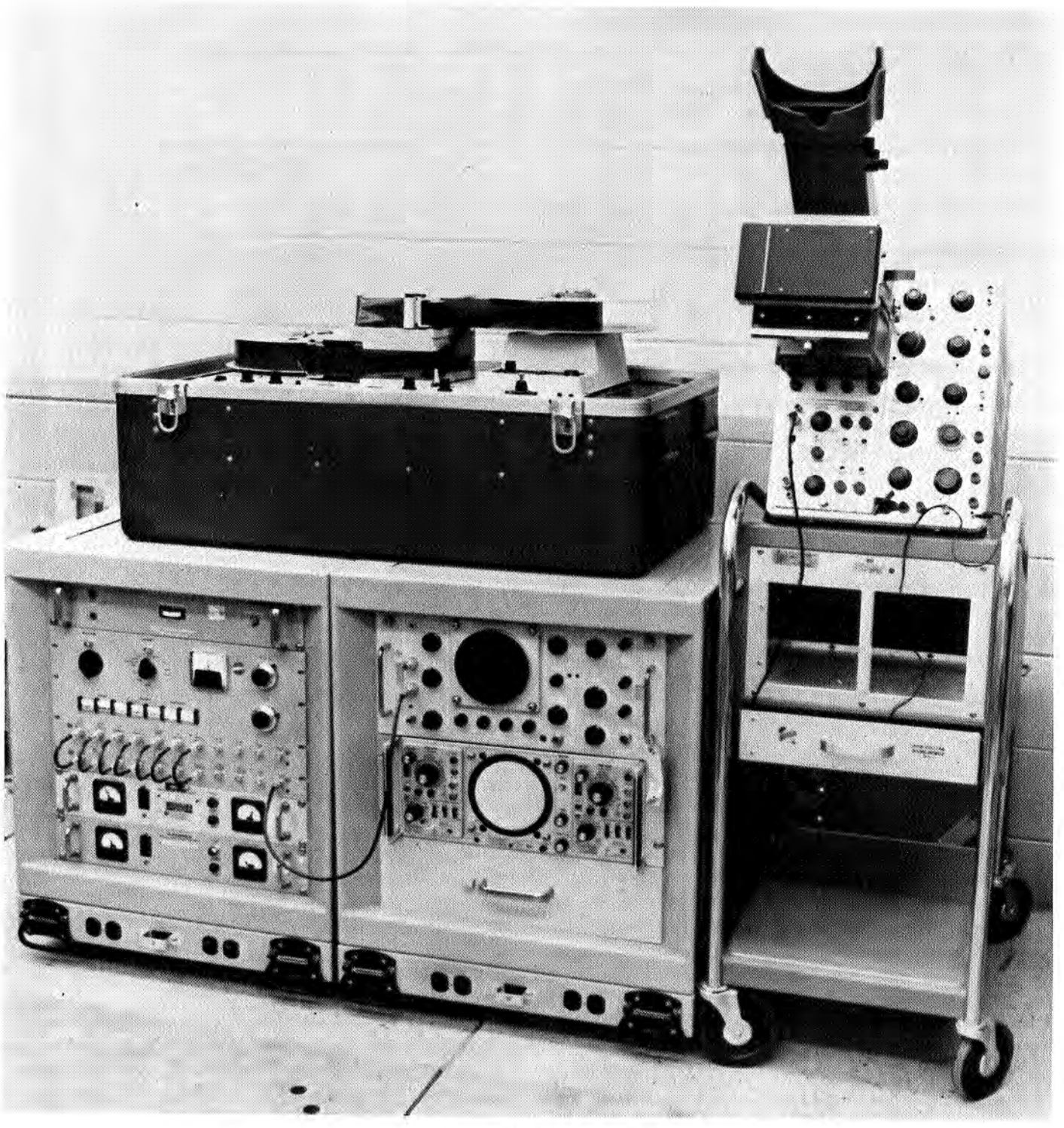


**Fig. XXII-15. Calibration test set**

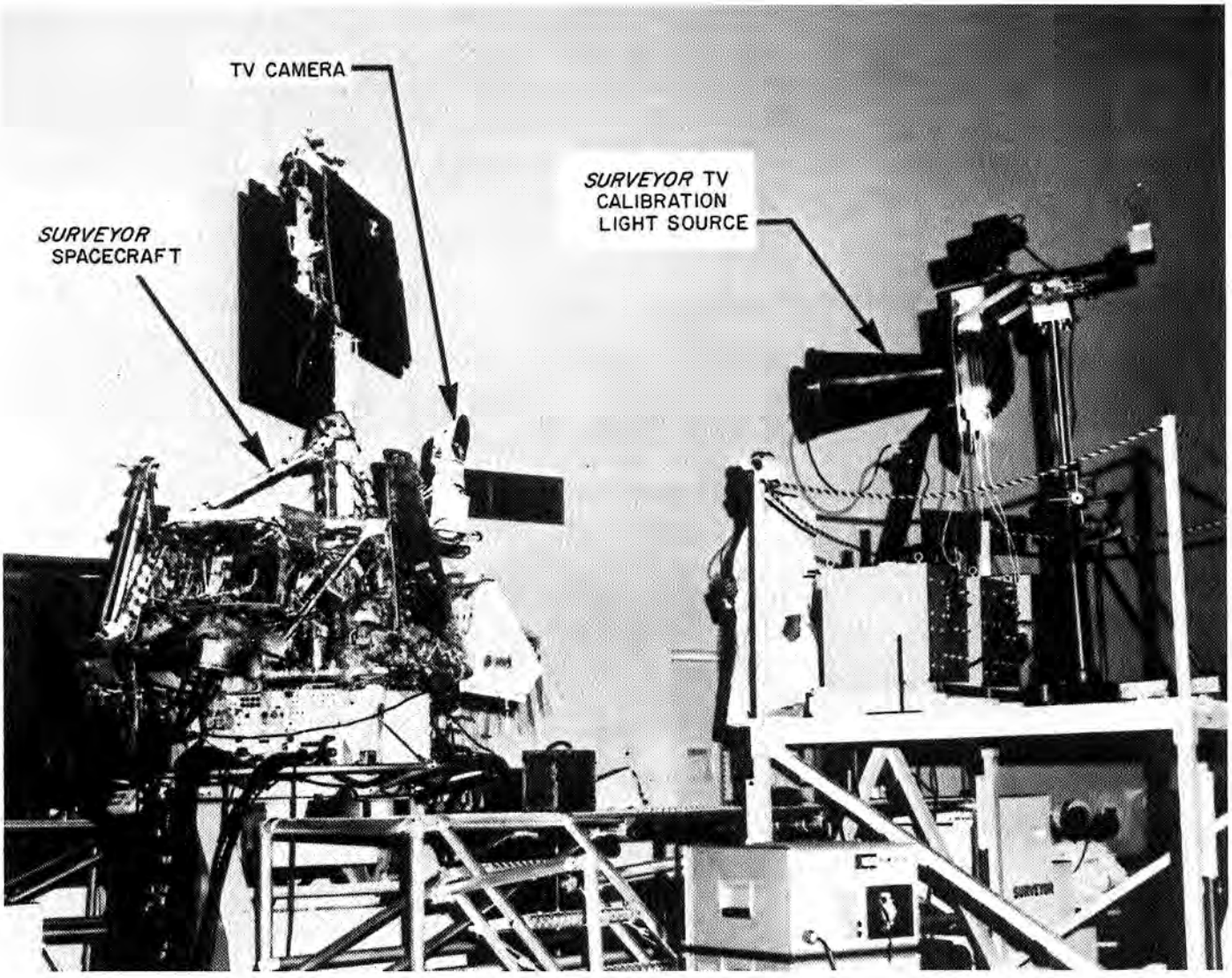



**Fig. XXII-16. Calibration light source**

to the front of the light source, where they could be rotated easily. They included a 10-level gray wedge for erasure determination, low contrast sine wave slides for modulation transfer measurements, and an accurately measured grid pattern to calibrate geometric distortion. In addition there were special assemblies for color and polarization measurements.

***d. Calibration data.*** Figure XXII-17 shows one example of calibration data in the form of the camera light transfer characteristics in the 600-line scan mode for the center of the frame, using transmitter A for *Surveyor III* with $f$ stop and exposure modes as parameters. Other items calibrated were light transfer functions for each color filter, polarimetric constants, shading over the frame, erasure response, modulation transfer function, geometric linearity, response of the automatic iris control, iris repeatability, and intersection of the optical axis with the vidicon target. In integrate exposure mode, vidicon dark current was measured as a function of exposure time.

Spatial radiance factors of the photometric charts were checked. This procedure utilized a small collimator which could be directed at each chart over a variety of incidence angles.

Accurate photogrammetric measurement from mission data requires a knowledge of the location of the optical axis of the TV camera for each combination of mirror

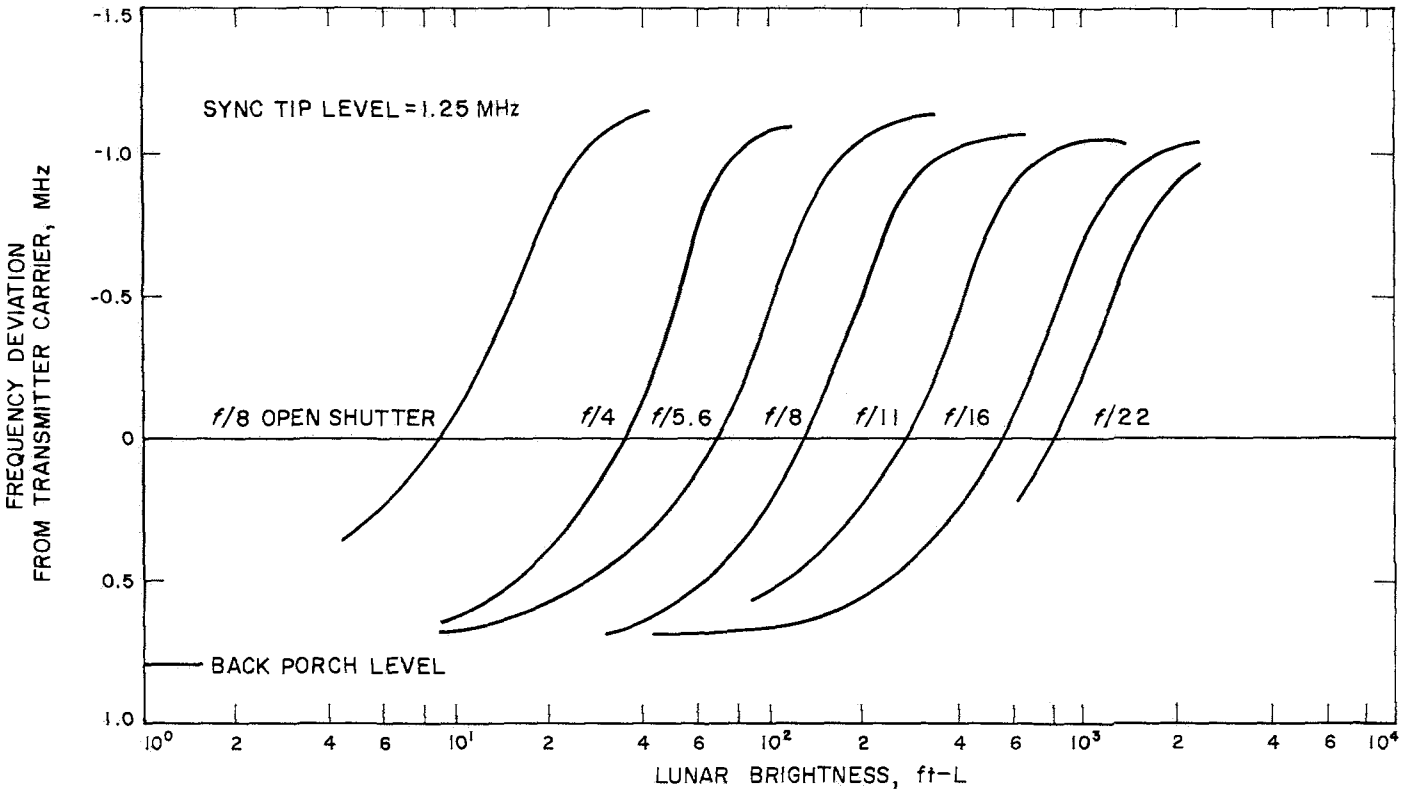



**Fig. XXII-17. Camera light transfer characteristics**

azimuth and elevation. The angular matrix for all steps permitted angular measurement over a pair or a group of scenes.

The pointing accuracy was measured by taking TV pictures of a set of crosshair-type targets at scattered points in the area surrounding the spacecraft. In each picture the position of the crosshair intersection was measured relative to the intersection of the optical axis with the vidicon target. The optical axis of the mirror head assembly was previously determined by theodolite survey, as were the angles to each crosshair intersection. The reduced data gave the relative angle matrix for the camera pointing system. By survey of points on the spaceframe the camera coordinate system was then referenced to the spacecraft coordinate system.

On *Surveyor VII* the stereo mirror plane was located, by survey, relative to the camera. This was necessary to calculate stereo photo base distance which was used in distance calculations. A degree of calibration for auxiliary viewing mirror distortion was obtained by tape recording TV pictures of patterns used as an aid to mirror alignment.

Certain amplitude and timing characteristics of the video signal were measured during calibration. A typical example of the data is shown in Table XXII-5.

*e. Application of data.* After calibrating a spacecraft, the data illustrated in Table XXII-5 were supplied to the TV-GDHS. There the constants were entered into the video simulator, frequency filters were chosen for sync and back porch predetection channels, and the system was set up for the type of signal expected from the spacecraft. The calibration tapes were then played into the TV-GDHS to complete calibration.

Considerable data reduction was required to convert the calibration light source luminance to equivalent lunar luminance. When this was completed a set of characteristic curves was prepared which would then be used by space science analysis and command group personnel during the mission as a guide for selection of exposure or other operating points.

A calibration report, issued for each mission, included a brief description of the calibration effort, the characteristic curves, signal characteristics, Polaroid photographs of interest, and a record of the tape sequences

**Table XXII-5. Composite video signal characteristics for *Surveyor III***

| Frequency deviation[a] | | |
|---|---|---|
| **Function** | **Deviation level transmitter A, MHz** | **Deviation level transmitter B, MHz** |
| Sync tip | 1.16 | 1.22 |
| Back porch | 0.70 | 0.72 |
| Black | 0.60 | 0.61 |
| PCM one | 0.56 | 0.83 |
| PCM zero | 1.06 | 1.33 |
| Average white saturation | 1.25 | 1.28 |

| Timing | |
|---|---|
| **Function** | **Duration** |
| Sync pulse | 138 msec |
| Back porch | 124 msec |
| Line (active) | 1.40 msec |
| Line (total) | 1.67 msec |
| PCM | 202 msec |
| Vertical blanking | 202 msec |
| Frame (active) | 1.00 sec |
| Frame (total) | 1.20 sec |

[a]Expressed as frequency deviation from transmitter carrier.

played during TV-GDHS calibration. A large number of appendixes were in the report, including the complete detailed calibration procedure, the calibration logs, the luminance correction factor calculations, the telemetry calibration, the results of the photogrammetric calibration, serial numbers of TV camera parts critical to the calibration, a map of the reseau pattern on the vidicon, precise values of focal length at the endpoints of focal length range, and tables of functional control position of temperature vs telemetry units. This telemetry calibration included mirror azimuth and elevation angles, focus distance, iris *f* stop, vidicon faceplate temperature, mirror baseplate temperature, electronic chassis temperature, and electronic conversion unit temperature.

The principal use of the calibration data was for correction of mission data (Ref. XXII-1). To prepare for this use, the image processing laboratory digitized the video data obtained during calibration and then developed computer programs to compensate for the errors introduced by TV camera response.

If it was desired to correct a given picture from a mission, the video data from that mission was likewise digitized. The appropriate computer programs were then used to correct the mission data. In some cases a printout of the corrected data was used by the investigator to measure the characteristics of a part of the viewed scene. In other cases corrected photographic negatives and prints were produced for visual interpretation.

Among the characteristics corrected in this way were linearity, intensity (shading), and modulation transfer function. Examples are shown in Figs. XXII-18 through XXII-20. Figure XXII-21 shows a combination of correction for modulation transfer function and removal of glare from scattered light.

### 6. Mission Performance

The TV camera configurations for the *Surveyor* missions are indicated in Table XXII-6. The survey TV camera, carried on each mission, was turned on only after a successful landing. The TV cameras on the unsuccessful missions, *Surveyors II* and *IV*, were never operated. Approach TV cameras were carried on *Surveyors I* and *II* only, and were not used.

Immediately after launch, heat drained rapidly away from the survey TV camera, and the mirror temperature stabilized at about −120°F and the camera body stabilized at −130°F within 15 h. About 5 h before touchdown, the heaters in the camera were switched on. One hour before touchdown the vidicon heaters were also commanded on. The heaters were turned off for the critical terminal descent period and then were commanded back on after touchdown. Thus, immediately after a soft landing had been achieved, the camera was at operating temperature.

Table XXII-7 summarizes the performance of the *Surveyor* TV camera on the lunar surface. All planned scientific observations were conducted and mission scientific objectives were met. In addition, the camera was used to perform other scientific and engineering measurements of interest on the lunar surface. Noteworthy among these are the pictures made under earthshine by using the integrate mode on the camera, views of the earth with the color or polarizing filters, views of an eclipse of the sun by the earth, and a view of two laser beams aimed at the moon from the western United States.

Although stereoscopic views of the surface were not anticipated since only one survey TV camera was carried on each spacecraft, some degree of stereo was obtained. As indicated in Table XXII-7, stereo was obtained by

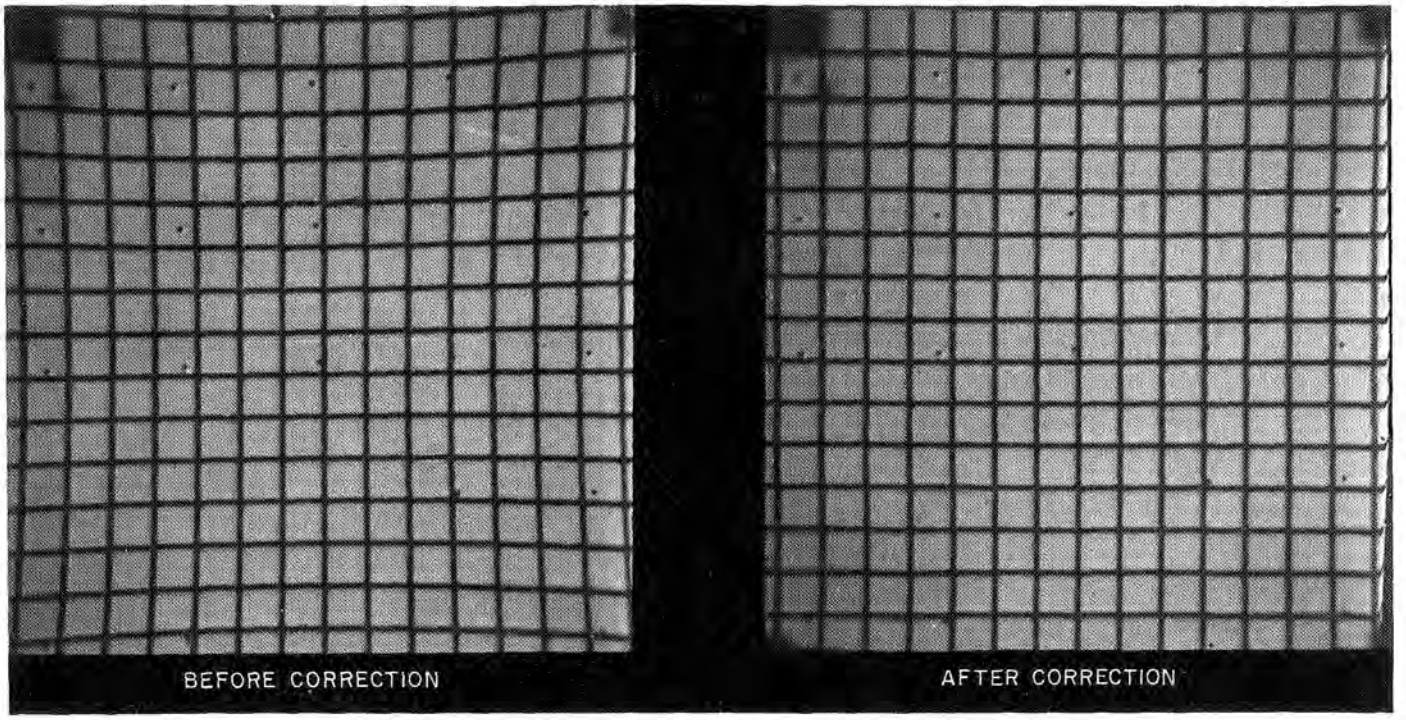



**Fig. XXII-18. Television picture linearity correction**

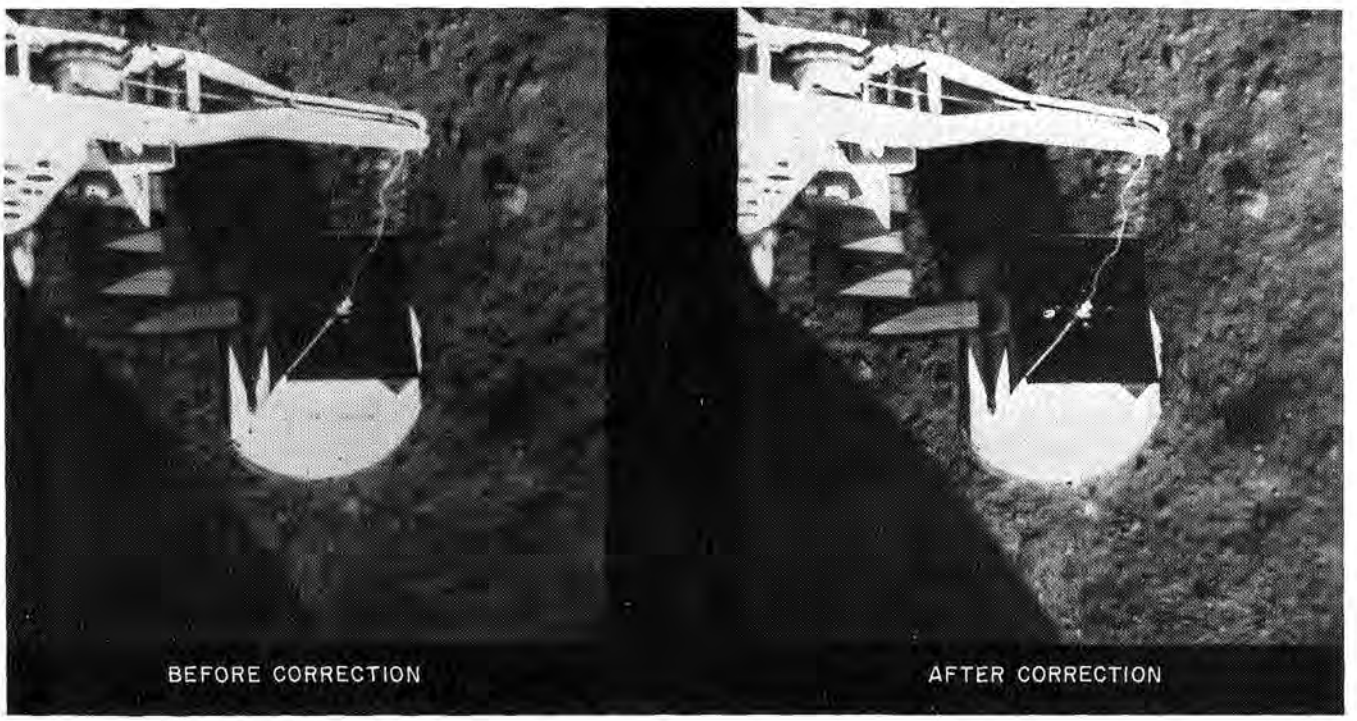



**Fig. XXII-19. Television picture intensity correction**

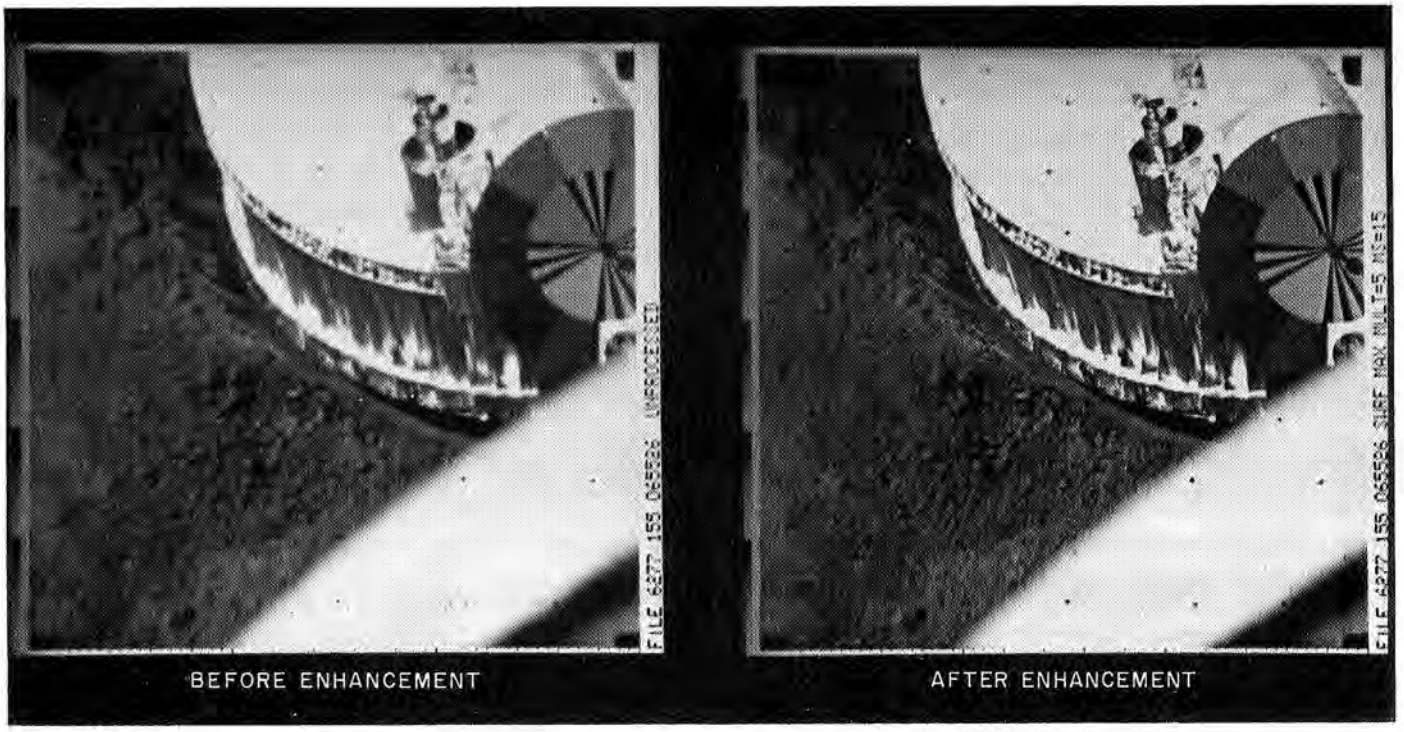



**Fig. XXII-20.** ***Surveyor I*** **footpad pictures illustrating correction of modulation transfer function**

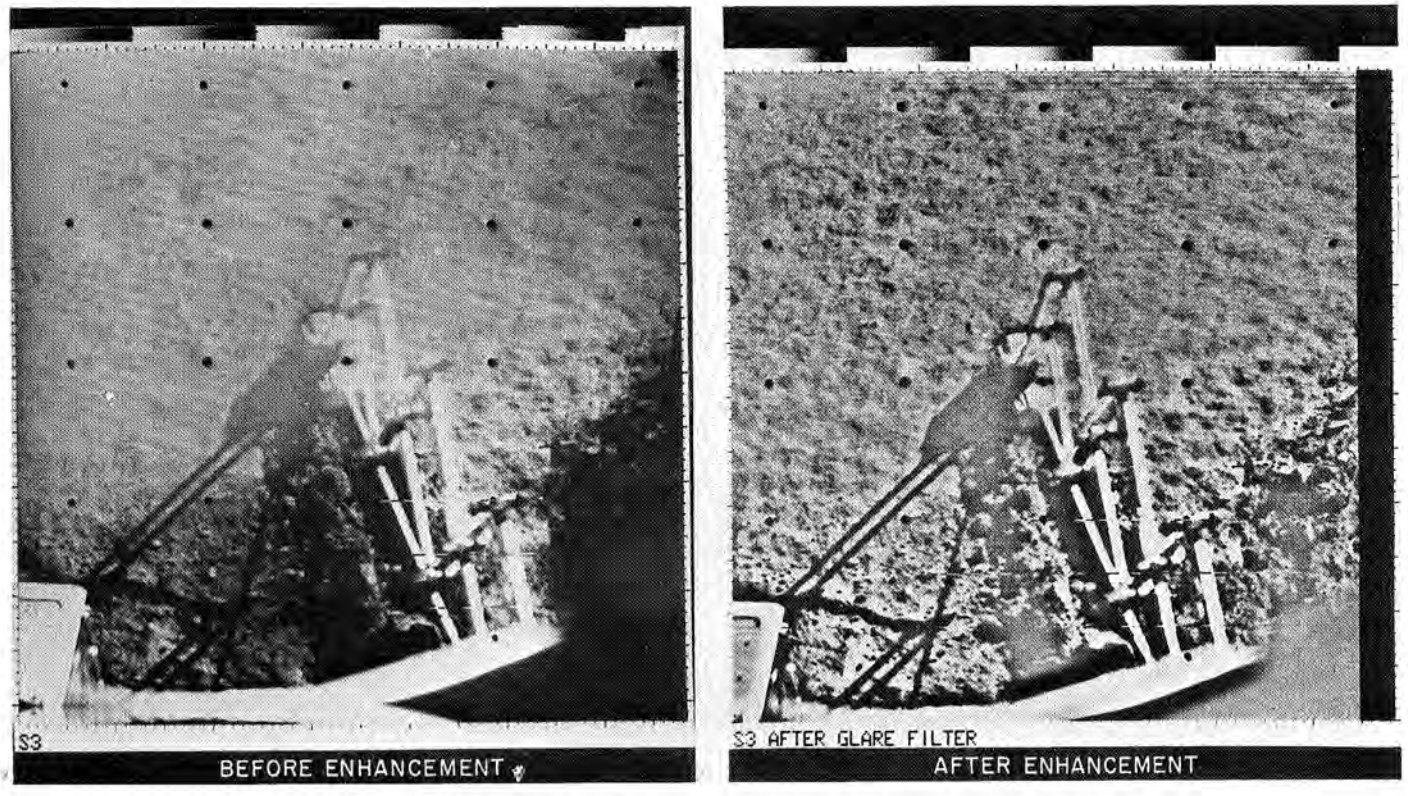



**Fig. XXII-21.** ***Surveyor III*** **view of soil mechanics/surface sampler**

## Table XXII-6. Television camera configurations

| Item | Surveyor mission | | | | | | |
|---|---|---|---|---|---|---|---|
| | I | II | III | IV | V | VI | VII |
| Survey TV camera | X | X | X | X | X | X | X |
| Photometric charts | 2 | 2 | 2 | 2 | 2 | 2 | 3 |
| Approach TV camera (not used) | X | X | | | | | |
| Auxiliary viewing mirrors | | | | | | | |
| 1 For surface under vernier engine 3 | | | 9 x 10 in. flat mounted inside spaceframe | Same as *Surveyor III* | 9 x 10-in. convex 70-in. spherical radius mounted inside spaceframe | Same as *Surveyor V* | Same as *Surveyor V* |
| 2 For surface under vernier engine 2 | | | 3.5 x 9.5-in. flat mounted inside spaceframe | Same as *Surveyor III* | | 3.5 x 6.7-in. convex 25-in. spherical radius, mounted inside spaceframe | Same as *Surveyor VI* |
| 3 For alpha scattering instrument deployment area | | | | | 3.5 x 6.7-in. convex 25-in. spherical radius, mounted inside spaceframe | 2.6 x 4.8-in. convex 25-in. spherical radius, mounted inside spaceframe | Same as *Surveyor VI* |
| 4 For stereo viewing | | | | | | | 3.5 x 9.5-in. flat, mounted on A/SPP mast |
| 5 For particle viewing | | | | | | | ½-in. hex flat, mounted in various locations on spacecraft |
| Mirror hood extension | | | X | X | X | | |
| Redesigned mirror head assembly | | | | | | X | X |
| Three color filters plus clear glass | X | X | X | X | X | | |
| Three polarizers plus neutral density filter | | | | | | X | X |
| Vertical scan direction reversed | | | | | | X | X |
| 10% horizontal overscanning | | | | | | X | |
| Mirror elevation at launch | Wide open | Wide open | Wide open | Wide open | 1 step open | Closed | Closed |

## Table XXII-6 (contd)

| Item | *Surveyor* mission | | | | | | |
|---|---|---|---|---|---|---|---|
| | *I* | *II* | *III* | *IV* | *V* | *VI* | *VII* |
| Amount of dust on mirror after landing | Some | — | Considerable | — | Little | Very little | Very little |
| Elevation coverage from −65 deg to — deg | +40 | +40 | +40 | +40 | +40 | +60 | +60 |
| Iris half-stop capability | | | | | | X | X |

## Table XXII-7. Major television operations performed on lunar surface

| Television operation | *Surveyor* mission | | | | |
|---|---|---|---|---|---|
| | *I* | *III* | *V* | *VI* | *VII* |
| Wide- and narrow-angle panoramas of visible lunar surface | X | X | X | X | X |
| Viewing spacecraft including other scientific instruments | X | X | X | X | X |
| Color (C) or polarimetric (P) surveys | X(C) | X(C) | X(C) | X(P) | X(P) |
| Focus ranging sequences | X | X | X | X | X |
| Shadow progression | X | X | X | X | X |
| Earthviewing (with color or polarizing filters) | | X(C) | | | X(P) |
| Sun eclipsed by earth (in color) | | X | | | |
| Postsunset viewing: using integrate mode | X | X | X (4 hr) | X (6 hr) | X (16 hr) |
| Postsunset diffraction pattern | | | | X | X |
| Lunar surface illuminated by earthshine after sunset or during eclipse (with color or polarizing filters) | X | X(C) | X | X(P) | X(P) |
| Laser experiment viewing | | | | | X |
| Viewing or solar corona | X | | X | X | X(P) |
| Viewing of planets and stars | X (Gemini) | X | X (Scorpius) | X | X (Orion) |
| Polarizing filter introspection | | | | X | |
| Stereo viewing effects resulting from: | | | | | |
| Shifts in reflected nodal point position | X | X | X | X | X |
| Spacecraft hop experiment | | | | X | |
| Spacecraft leg shift | | | | X | X |
| Soil mechanics/surface sampler stereo mirror | | | | | X |

viewing directly and via a mirror (*Surveyor VII*) and also by viewing before and after the spacecraft hop experiment was performed (*Surveyor VI*). A stereo effect, with a very small baseline, was also possible when a small change in leg position occurred on *Surveyors VI* and *VII*. A further, small stereo effect was seen because a discrete movement of the reflected entrant nodal point occurred when the mirror was stepped to a new position.

In summary, the survey TV camera performed its function as an observational tool and scientific instrument. Notwithstanding some anomalies in the camera functions as noted below, it was possible to conduct experiments and obtain measurements on all five successful missions, and this resulted in a significant amount of new scientific data on the properties of the moon.

Table XXII-8 gives a brief summary of the performance of the survey TV camera on each mission. None of the anomalies noted prevented the cameras from taking many good quality pictures on each mission. The most serious difficulty occurred on *Surveyor III* when the spacecraft rebounded two times before coming to rest on the lunar surface. When the camera was switched on, severe glare conditions were found. This was believed to be due to dust on the mirror surface or pitting of the surface that had been produced by the continued operation of the vernier engines during the landing sequence. After several days of operation on this mission, intermittent difficulty was first encountered in azimuth stepping and then in elevation stepping. These difficulties became worse and, at the end of the mission, the azimuth position was locked.

On *Surveyor V*, the spacecraft was operated on the first, the second, and the fourth lunar day. An electronic problem appeared to be responsible for the stoppage of response to the focus, filter, and focal length commands at the end of the first lunar day. The system recovered, however, and these functions operated correctly until close to the end of the second lunar day when the problem reoccurred.

There were no problems on the TV cameras on the first lunar days of *Surveyors VI* and *VII*. The redesigned mirror system performed well.

At the beginning of the program it was not anticipated that the TV camera would be expected to work after being subjected to the low temperature extreme of the lunar night. From Table XXII-8 it will be seen that for the three missions on which the Spacecraft System responded on the second lunar day, the TV camera survived and was operated, although significant degradation occurred on *Surveyors V* and *VII*.

## C. Soil Mechanics/Surface Sampler

### 1. Introduction

A surface sampler, first designed early in the *Surveyor* Project, was conceived to be a device that could be used to pick up rocks or samples of the lunar surface and deposit them in a small grinding mechanism. The final output was a finely ground powder that was to be supplied to two or more analysis instruments.

The payload of *Surveyor* at that time (1960) included a soil mechanics instrument designed to make several measurements of lunar surface mechanical properties. However, work on this instrument was stopped in 1963, and the surface sampler was examined to see whether it was suitable for use in a simplified soil mechanics experiment. It was concluded that with the addition of strain gages and accelerometers, the surface sampling device could produce meaningful data on the mechanical properties of the lunar surface; thus, work continued on an engineering model of the instrument.

After *Surveyor I* successfully soft-landed on the lunar surface in June 1966, various ideas were discussed for designing a device to test the surface for cohesiveness and bearing strength which could be added to a later spacecraft in the *Surveyor* series. It was decided that the surface sampler could be built in a shorter time than other untried instruments and HAC was redirected to build two surface samplers for use on *Surveyors III* and *IV*, plus a spare flight unit. Because only 110 days were available between redirection and the required delivery of the first unit, strain gages and accelerometers were deleted from the unit and the electrical interface with the Spacecraft System was simplified. The flight version of the instrument was renamed the soil mechanics/surface sampler.

The SM/SS was flown on *Surveyors III* and *IV*. It performed its required function on *Surveyor III* but *Surveyor IV* was lost during terminal descent. Because of the early successes of the *Surveyor* Project, it was decided to fly the spare flight unit on *Surveyor VII*. Much useful data on lunar surface properties was produced from the successful *Surveyor III* and *VII* Missions.

Originally, the surface sampler was used simply as a tool to pick up lunar rocks, pebbles, and soil. The

**Table XXII-8. Survey TV camera performance summary**

| Item | *Surveyor* mission | | | | |
|---|---|---|---|---|---|
| | *I* | *III* | *IV* | *VI* | *VII* |
| Lunar days operated | 1, 2 | 1 | 1, 2, 4 | 1 | 1, 2 |
| Pictures obtained on first lunar day | 10,341 | 6,326 | 18,006 | 29,952 | 20,993 |
| Pictures obtained on second lunar day | 899 | — | 1,048 | — | 45 (200-line) |
| Pictures obtained on fourth lunar day | — | — | 64 | — | — |
| Total number of pictures (87,647) | 11,240 | 6,326 | 19,118 | 29,952 | 21,038 |
| Mirror steps in azimuth (approximately) | 7,100 | 10,000 | 24,000 | 46,000 | 30,000 |
| Mirror steps in elevation | 15,900 | 3,600 | 8,300 | 13,000 | 9,000 |
| Television anomalies: | | | | | |
| First lunar day | Elevation potentiometer failure | Azimuth and elevation stepping erratic but usable. Mirror contaminated | Focus, filter, and focal length not commandable at end of day (electronic problem) | None | None |
| Second lunar day | As above | — | System recovered. Focus, filter, and focal length problem repeated at end of second day. Video signal very low | — | 600-line scan inoperative |
| Fourth lunar day | — | — | Extremely low video signal. Focal length would not change | — | — |
| Comments on mission | First lunar soft landing | Spacecraft re-bounded twice before final touchdown | Spacecraft landed with 20-deg tilt inside small crater | Spacecraft hop experiment conducted on lunar surface | Landing site of about 40-deg south latitutde caused camera to run hot |

redesignated SM/SS was used to determine bearing strength, cohesiveness, and general mechanical properties of the lunar soil. On *Surveyor VII*, which carried both an alpha scattering instrument and the SM/SS, the SM/SS had the dual purpose of manipulating the soil and lifting and moving the alpha scattering instrument. In addition, it assisted in deploying the alpha scattering instrument head when it became stuck in its background-count position. The SM/SS thus became an operable hand on the *Surveyor* spacecraft.

The flight design SM/SS was essentially a noninstrumented subsystem: there were no position potentiometers, strain gages, or accelerometers to indicate forces

or action of the SM/SS. On *Surveyor VII*, measurements of motor currents were obtained that aided in the understanding of the forces exerted by the motors in the various operations. All other information was obtained via TV pictures.

### 2. Description of the SM/SS

The SM/SS, attached to the *Surveyor* spacecraft (Fig. XXII-22), was designed to operate in all three coordinate planes, i.e., *X*, *Y*, and *Z*. The SM/SS could elevate and lower, extend and retract, move left and right azimuth, as well as open and close a door on its scoop. The scoop was forward mounted, assembled to lazy tongs, an extendable linkage that permitted digging, scratching, pushing, moving, and grasping lunar surface material. Each plane of operation was actuated by a small DC motor. The motor was operated by timed pulses so that the operator could position the scoop at a desired location.

TV pictures could not be taken while the SM/SS was operating, so the SM/SS was moved, photographed, and moved again until accurately positioned. An SM/SS

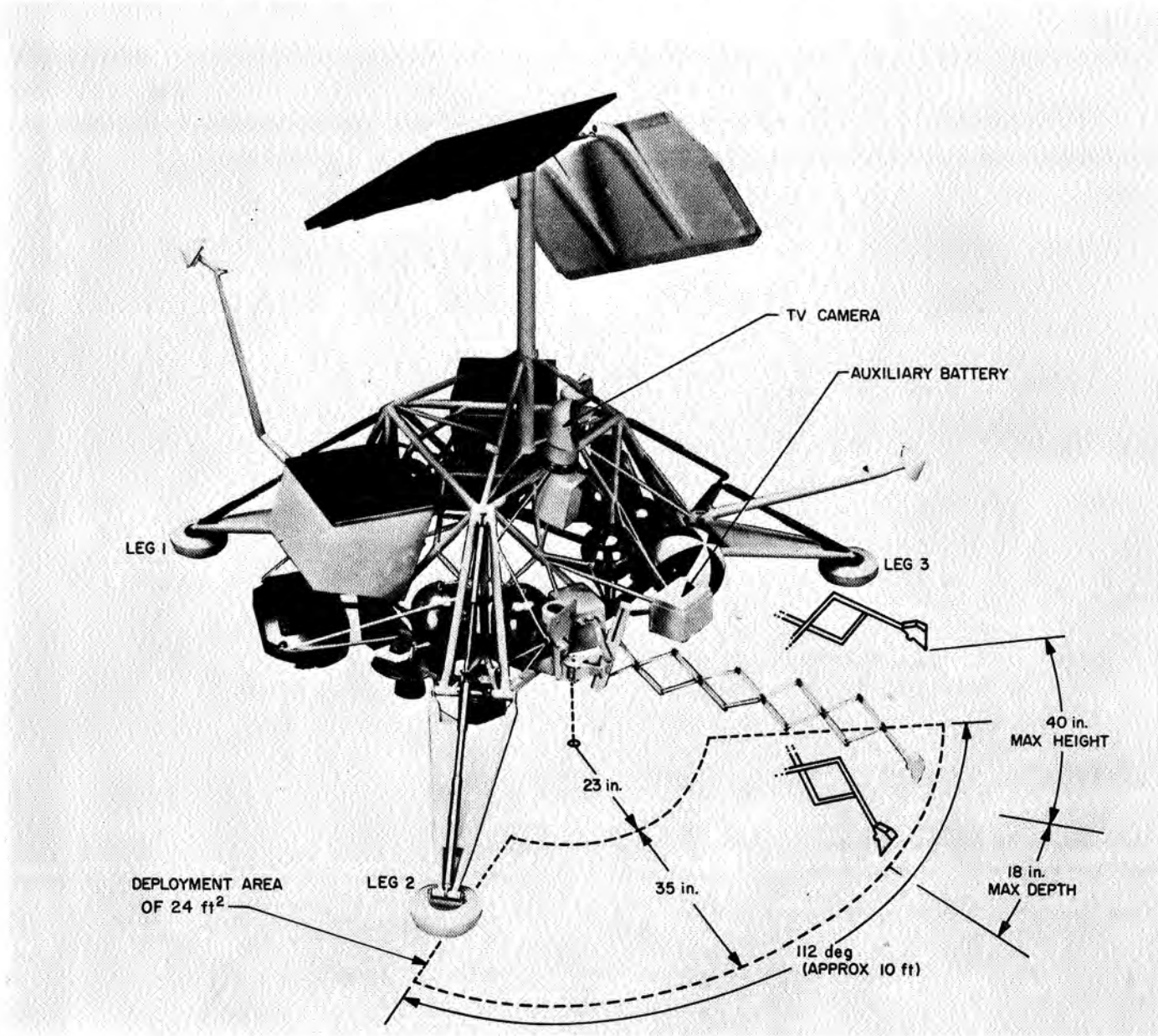



**Fig. XXII-22. Soil mechanics/surface sampler deployment envelope**

electronics auxiliary assembly was provided to function as the electrical interface between the SM/SS and the Spacecraft System.

*a. General description.* The SM/SS consisted of a mount, a squib-operated release mechanism, a support bracket which served as an azimuth hinge for the SM/SS, the lazy tongs to provide the operable mechanism, and a scoop, with a door that could be opened and closed on command for digging and grasping. Four DC motors provided the SM/SS motion (Fig. XXII-23). The basic design derived from the original need for a device to acquire a portion of lunar soil and to transport it to, and deposit in, an analyzing mechanism. The basic design was retained in the flight model, although several design improvements were made during development.

The lazy-tongs were retracted into an open channel and locked in this position for stowage by a spring-loaded yoke, which was restrained in locking position by a clevis and pin. To disengage the yoke for releasing the lazy tongs, a squib-operated pinpuller was fired, moving the pin from its locking position in the clevis. Upon release, the spring-loaded yoke rotated, releasing

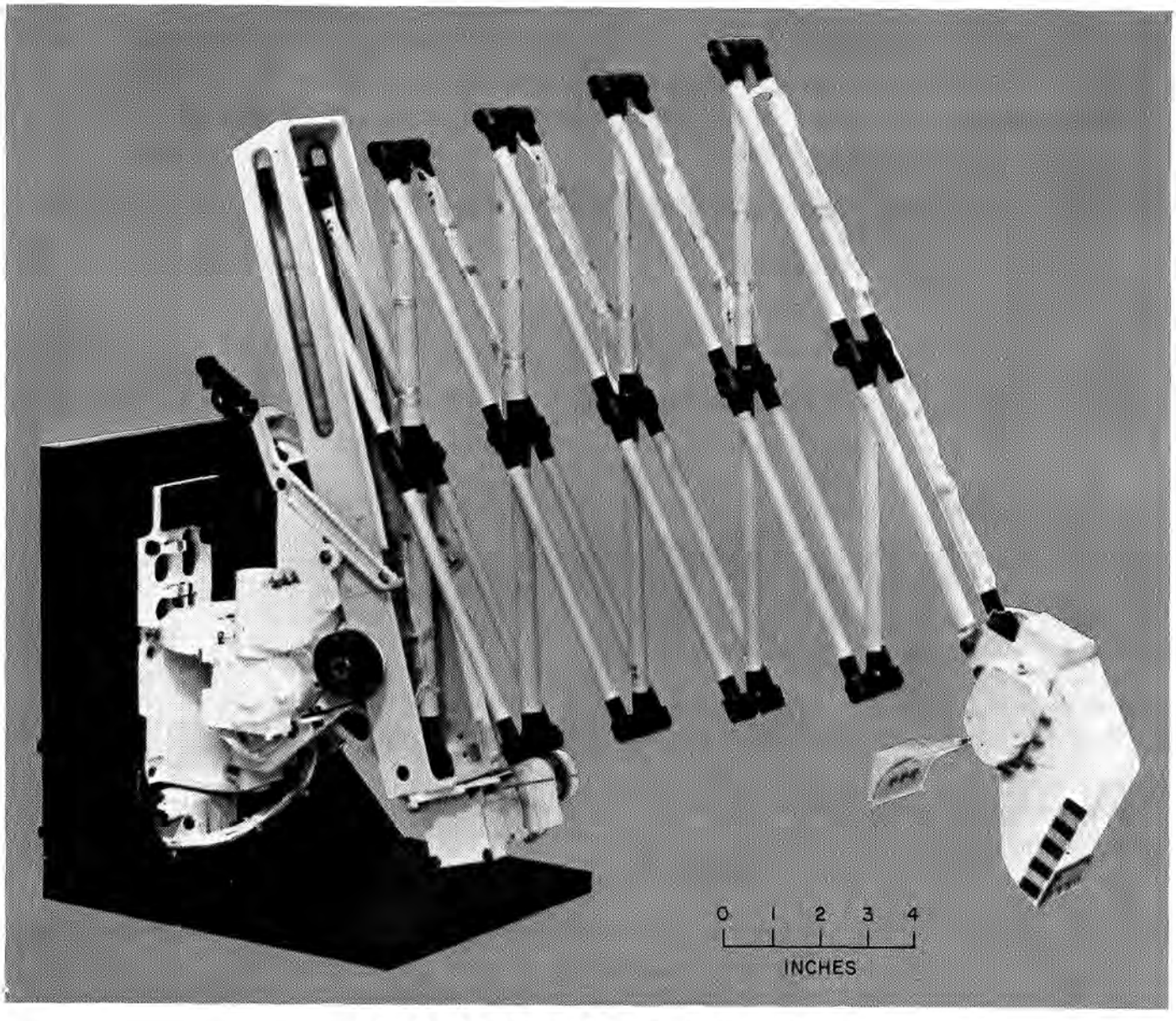



**Fig. XXII-23. Soil mechanics/surface sampler**

the lazy tongs. The lazy tongs, though released, were restrained by steel retraction tape.

A double-coiled spring, wrapped about each exposed joint, applied continual extension force (the original design had only used two extension springs). The total extension force, approximately 1.5 lb, was applied by the springs acting collectively. A motor-operated spool, mounted to the base of the channel, unwound the steel restraining tape thus permitting the lazy tongs to extend. Rotated in the opposite direction, the spool rewound the tape, causing retraction of the lazy tongs and applying a maximum pull of approximately 20 lb on the scoop.

The azimuth motor and gears provided azimuth motion. The lateral force which could be exerted was small. An elevation motor and gear provided angular motion in the vertical plane. The scoop encased its own motor for operation of the scoop door. The use of internal gears for elevation drive was a design modification. Early designs used a tape winding and unwinding simultaneously onto a double-ended spool. This caused difficulties because the tape either had to be loose (causing sloppy motion) or tended to break when wound from one to the other extreme. The SM/SS was capable of moving 112 deg in azimuth and 54 deg in elevation. This motion permitted the scoop to move to a possible penetration depth of about 18 in., assuming a level lunar surface. On *Surveyor III* the SM/SS was positioned to permit the scoop, at one end of its azimuth travel, to extend about 2 in. over spacecraft footpad 2. The SM/SS scoop is shown in Fig. XXII-24 as it approached footpad 2 on the *Surveyor III* Mission. On *Surveyor VII* the SM/SS was positioned to pick up the alpha scattering instrument with no overlap of footpad 2 provided.

The scoop consisted of a hydroformed case, the scoop door (operated by its motor through a coiled flat spring), and a hardened steel chopping plate mounted to the scoop edge. The scoop door was strengthened by the addition of a laminated plastic base which also provided a pressure plate for soil-bearing tests.

The scoop door operation was modified for the final design. Previously, the scoop door was rigidly attached to a motor shaft and limit switches were used to stop the door motor at the appropriate time. Several difficulties existed in this mode of operation:

(1) Either the motor coasted to a point beyond closing of the door, causing the shaft to break loose and continue to rotate while the door remained stationary, or the motor stopped before complete closing of the door.

(2) If the door were closed on a rigid object or on loose sand, there was no way to exert continuous pressure on the grasped object.

The redesigned scoop shaft solved these problems by not connecting the motor shaft directly to the door. Instead the scoop door was attached to a shaft which, in turn, was connected to the motor shaft through a flat clock-type spring. This spring permitted 108-deg rotation of the motor shaft relative to the scoop door shaft and placed a 2.3-in.-lb torque loading on the scoop door. Therefore, if sand, or a rigid object, were grasped between the scoop and the scoop door, the door, because of spring action, would continue to press on the object even when the motor was off.

The SM/SS included a chopping or picking spring which could apply a downward force of approximately 8 lb. The design also incorporated a solenoid-operated elevation clutch. By elevating the SM/SS scoop above the lunar surface and instantaneously disengaging the elevation drive from the lazy tongs, the knife edge of the scoop (with the scoop door opened) or the laminated plastic pressure plate attached to the door (with the scoop door closed) would sharply impact whatever existed below the scoop. Experiments at HAC indicated that the SM/SS used in this manner was capable of chopping or splitting a common building brick in two. When the SM/SS was extended in a plane horizontal to the *X-Y* plane of the spacecraft, 16.2-in.-lb preloading existed on the SM/SS.

White paint was considered for the SM/SS because of the thermal properties, but eliminated by the probability of TV flare. Black paint was discarded because of little anticipated contrast with the lunar surface. A light gray paint was acceptable to TV and thermal interests. However, because there was a color wheel using a clear filter plus three different color filters, and since a pastel paint offered equal thermal values to gray paint, it was decided to paint the SM/SS a light blue. This permitted the operators to vary the contrast of the SM/SS relative to the lunar surface by simply varying the color filters during lunar operation.

***b. The SM/SS electronic auxiliary assembly and control of the SM/SS.*** Prior to the development of the SM/SS electronics auxiliary assembly for *Surveyors III* and *IV*, an interface constraint established that the auxiliary assembly must employ only those electrical interfaces which had previously been used for the approach TV camera. This was done to minimize the changes

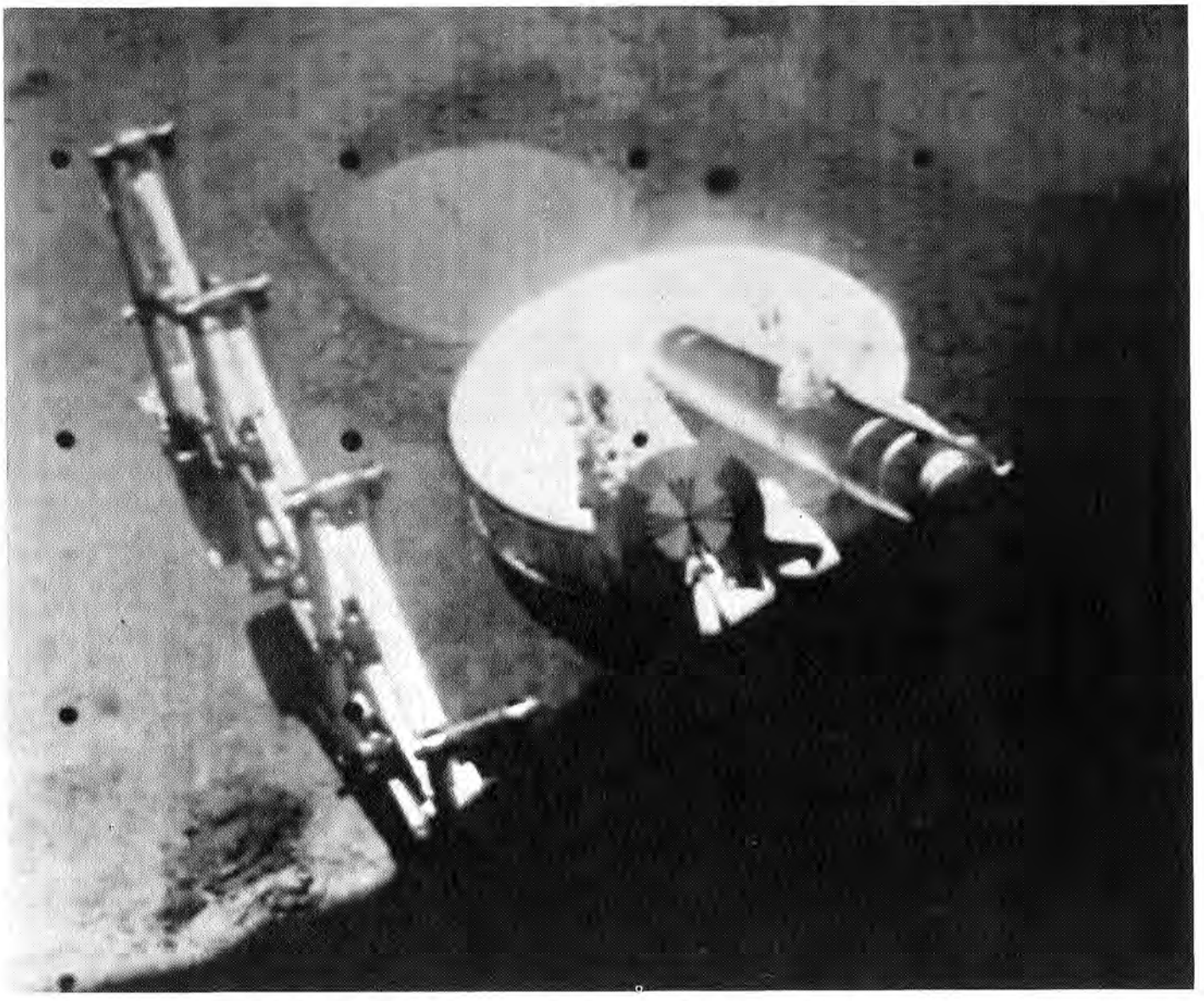


**Fig. XXII-24. Soil mechanics/surface sampler approaching footpad 2**

needed to integrate the unit and the spacecraft. The approach TV camera electrical interface had only six command leads, only two of which were directly related to temperature control. In addition, there was no squib firing interface with the auxiliary assembly.

Since a minimum of fifteen commands was required for deployment and control of the SM/SS and only four usable commands existed in the approach TV camera electrical interface, a unique approach was employed in the generation of SM/SS commands. In the standard *Surveyor* command structure a series of digital bits was transmitted to the spacecraft. The logic levels and sequence of the series of bits determined the routing of a command signal through the spacecraft electrical interfaces. As an end result, a single on-off pulse of nominally 20-msec duration appeared on a specific command lead. By utilizing two such command leads, it was possible to construct an N-element shift register capable of generating $2^N$ unique logical combinations. When this was accomplished, all that remained was to provide a decoding matrix, a signal which initiated execution of the coded command, and a means of clearing the shift register for use in generating subsequent coded commands.

The foregoing philosophy was implemented by designing the SM/SS electronics auxiliary assembly to

provide a clock pulse conditioner, four-element command register, count register, command enable latch, command pulse amplifier, sixteen command decoding matrix, and a reset buffer one-shot. A functional block diagram of the SM/SS electronics auxiliary assembly, along with its electrical interfaces, appears in Fig. XXII-25. The four usable command signals from the approach TV camera interface, together with their octal reference, were reassigned as follows:

(1) 0131 SM/SS power on/execute.

(2) 0132 SM/SS digital one.

(3) 0133 SM/SS digital zero/reset.

(4) 0134 SM/SS power off.

The SM/SS was released from the stowed position by electrically activating the squib-operated pin puller, allowing the spring-loaded yoke to disengage from the mechanism. The normal *Surveyor* method of activating explosive devices was to first execute an interlock command and, during the short dwell time of the interlock signal, transmit a second command which selected and activated the desired device. This sequence enabled a semiconductor switch, which was wired to the squib bridge, and simultaneously activated an electronic conversion unit in the engineering mechanisms auxiliary, which supplied current to the squib. The current source was activated only during the dwell time of the second command, nominally 20 msec.

Since the SM/SS was required to mate directly, without modification, to the existing approach TV camera electrical interface, no interface with the auxiliary assembly was available. This resulted in divergence from the normal *Surveyor* method of controlling detonation of explosive devices. Since inadvertent deployment of the SM/SS during mission-critical times, such as during the launch phase, could have catastrophic results on the mission, the SM/SS squib-firing circuitry was designed very carefully.

After landing and releasing the SM/SS from its stowed position by activation of the squib-operated pinpuller device, the SM/SS was controlled by the four reversible electric motors. Bidirectional motor operation was possible because each of the four motors had two opposing field windings. Excitation was applied to the armature (rotor) and rotational direction was selected by completing the circuit through the appropriate field winding.

Two timing cycles were provided for the control of the motors. A 2- or 0.1-sec mode could be selected by command. When the auxiliary decoder power switch was enabled, the 0.1-sec mode was automatically selected.

Operation of the timing cycle was as follows: When a motor switch was turned, solenoid control initiated operation of either the 2- or 0.1-sec delay circuit, depending on which mode had been selected. At the conclusion of the given delay period, a signal from the delay circuit was sent to motor control. This signal turned off the motor and solenoid control module and, hence, turned off the motor switch. The circuitry was designed so that false turnon of a motor also initiated the timer cycle, which turned off the motor after either 2- or 0.1-sec, depending upon the mode the timer was in. Aside from turnoff by means of the delay circuits, the motors could be turned off by the motors off command. The electromechanical solenoid, which was provided to disengage the elevation drive train and the mechanism to be impelled downward to impact the lunar surface, functioned only in the 2-sec timing mode.

In addition to power management, which also included fusing, current limiting, and command decoding, the SM/SS electronics auxiliary assembly provided four telemetry signals: two digital and two analog. The analog signals were digitized by the analog-to-digital converter on the spacecraft and transmitted to earth as PCM data at rates selected by ground command. Each analog data word was composed of 11 bits. The digital telemetry signals occupied 1 bit of an 11-bit data word. The SM/SS telemetry words appeared in the auxiliary engineering signal processor commutator, a 120-word commutator, and on the engineering signal processor mode two commutator, which was a 100-word commutator. During SM/SS operation, a bit rate of 4400 bits/sec was selected. At this rate, during a 2-sec motor activation period on *Surveyor III*, the SM/SS telemetry words were sampled six or seven times, depending upon what part of the sequence the commutation was in when a motor was commanded on. On *Surveyor VII*, five commutator positions were used and the readout was accomplished approximately 40 times during the 2-sec motor-activation period.

Two digital telemetry signals were provided: power on/off and command entered. The power on/off signal was derived from the output of the SM/SS on/off power switch and indicated a digital *one* when SM/SS power was on and a digital *zero* when SM/SS power was off.

The command entered signal was derived from the SM/SS auxiliary count register and indicated a digital *one* after four bits had been entered in the command register. Before four bits were entered in the command register and when the command register was reset, the command entered signal indicated a digital *zero*.

Two analog telemetry signals were provided: electronics temperature and motor current. The electronics temperature signal was implemented by supplying a current pulse from a constant-current source to a precision temperature-sensitive resistor and reading the voltage drop across the resistor. Motor current telemetry was derived by placing a precision 0.04-Ω resistor in the common return lead from all motors and the clutch solenoid. Since only one motor on the solenoid was active at any particular time, only one telemetry signal was required. The voltage developed across the 0.04-Ω resistor was amplified by a factor of 50 before being presented to the analog-to-digital converter and further processed for PCM transmission to earth.

### 3. Critical Design Considerations of the SM/SS

Three areas of the design required serious attention and evaluation: the motor design, the joint design used in the lazy tongs, and the structural integrity of the SM/SS under critical loading conditions.

The SM/SS used DC brush-commutated motors of a design dating back to 1960. The lubricant used in the original design of the motors became stiff at low temperatures. When the SM/SS was redesigned in 1966, a motor rework program was initiated to improve the lubrication over the anticipated temperature range and also to improve the brush material to reduce wear. Final motor design incorporated Lubeco 905 as a lubricant, and Boeing 046-45 compact brush material to extend brush life.

The original lazy-tongs joint design used a glass-reinforced Teflon bearing, and there were some indications that the joint might become unsatisfactory in operation in ultrahigh vacuum conditions. A new joint was designed using Lubeco 905 lubrication and a 5-wk test program in a thermal-ultrahigh vacuum chamber was initiated. The results clearly indicated the superiority of the newer joint, and this joint was adopted for the final design.

There were three periods of critical loading of the SM/SS. The first occurred during the boost phase at launch. The second was at touchdown on the lunar surface. The third (and most severe) was due to loads encumbered when the SM/SS was used to pick and dig on the lunar surface. Because of severe weight restrictions, the weight and size were kept to a minimum and careful analysis was made to ensure that the SM/SS would perform under all anticipated conditions. The minimum acceptable margins of safety for the design loads were 0.10 for yield strength and 0.25 for ultimate strength. Fatigue life was also assessed.

### 4. Mission Performance

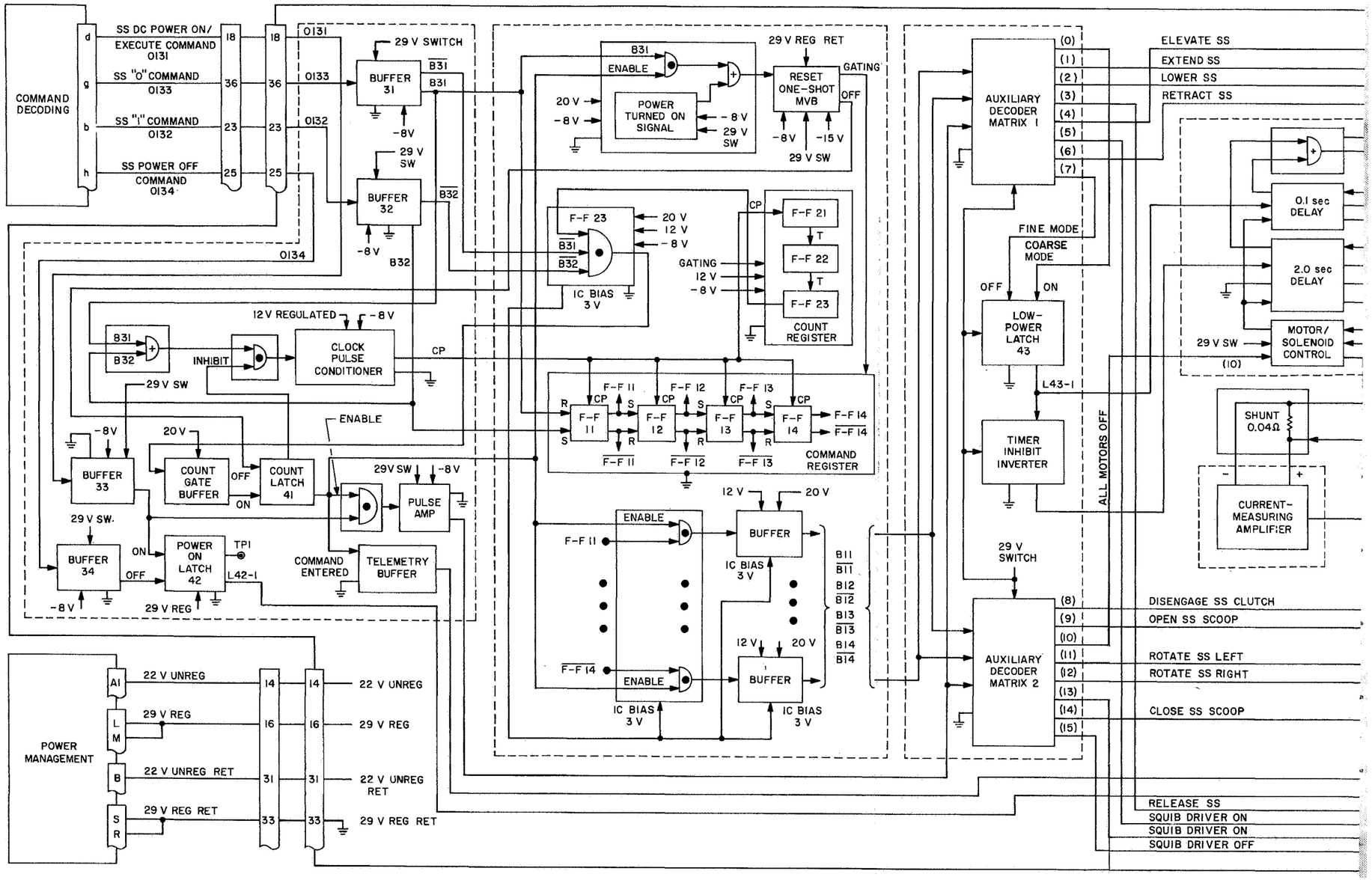
The SM/SS was carried on *Surveyors III, IV,* and *VII*. A summary of its operations on the lunar surface is given in Table XXII-9. *Surveyor IV* was terminated before landing.

***a. Summary of Surveyor III performance.*** As shown in Table XXII-9, the SM/SS was used very successfully on this mission. This was the first time that it was possible to command mechanical operations on the lunar surface and to obtain information on lunar surface properties. Because of an anomaly in spacecraft telemetry it was not possible to interpret the SM/SS motor currents. However, TV observation of the SM/SS enabled the operations to be conducted. The extension/retraction motion under no-load conditions was approximately 50% of the value obtained under preflight calibration conditions. The exact cause for this anomaly could not be determined, but it is thought to have been due either to a minor problem in the motor or to increased stiffness in a joint.

Figure XXII-26 shows the location of the tests conducted on the *Surveyor III* mission. The test locations can be related to the position of footpad 2 and part of the spaceframe. It can be seen that one trench (No. 3) was widened on two occasions and that the large number of tests were made.

***b. Summary of Surveyor VII performance.*** The SM/SS was operated extensively on this mission also. No anomalies in the performance of the unit were reported.

The SM/SS operations included six bearing tests, five with the scoop door open and one near the wall of a deep trench. A total of seven trenches were dug, two of these were subjected to multiple trenching operations. Four rocks were moved or manipulated. One rock was weighed several times by comparing the increase in motor current when it was picked up with the current observed for the same motion when the scoop was


COMMAND DECODING
SS DC POWER ON/ EXECUTE COMMAND 0131
SS "0" COMMAND 0133
SS "1" COMMAND 0132
SS POWER OFF COMMAND 0134
BUFFER 31
BUFFER 32
29 V SWITCH
29 V SW
-8V
B31
B32
ENABLE
20 V
-8 V
POWER TURNED ON SIGNAL
29 V REG RET
RESET ONE-SHOT MVB
GATING
OFF
-15 V
F-F 23
IC BIAS 3 V
12 V
F-F 21
F-F 22
COUNT REGISTER
12V REGULATED
CLOCK PULSE CONDITIONER
INHIBIT
CP
F-F 11
F-F 12
F-F 13
F-F 14
COMMAND REGISTER
BUFFER 33
COUNT GATE BUFFER
COUNT LATCH 41
ON
PULSE AMP
BUFFER 34
POWER ON LATCH 42
TP1
L42-1
COMMAND ENTERED
TELEMETRY BUFFER
29 V REG
BUFFER
B11
B12
B13
B14
AUXILIARY DECODER MATRIX 1
FINE MODE
COARSE MODE
LOW-POWER LATCH 43
L43-1
TIMER INHIBIT INVERTER
ALL MOTORS OFF
ELEVATE SS
EXTEND SS
LOWER SS
RETRACT SS
0.1 sec DELAY
2.0 sec DELAY
MOTOR/ SOLENOID CONTROL
SHUNT 0.04Ω
CURRENT-MEASURING AMPLIFIER
AUXILIARY DECODER MATRIX 2
DISENGAGE SS CLUTCH
OPEN SS SCOOP
ROTATE SS LEFT
ROTATE SS RIGHT
CLOSE SS SCOOP
RELEASE SS
SQUIB DRIVER ON
SQUIB DRIVER ON
SQUIB DRIVER OFF
POWER MANAGEMENT
22 V UNREG
29 V REG
22 V UNREG RET
29 V REG RET

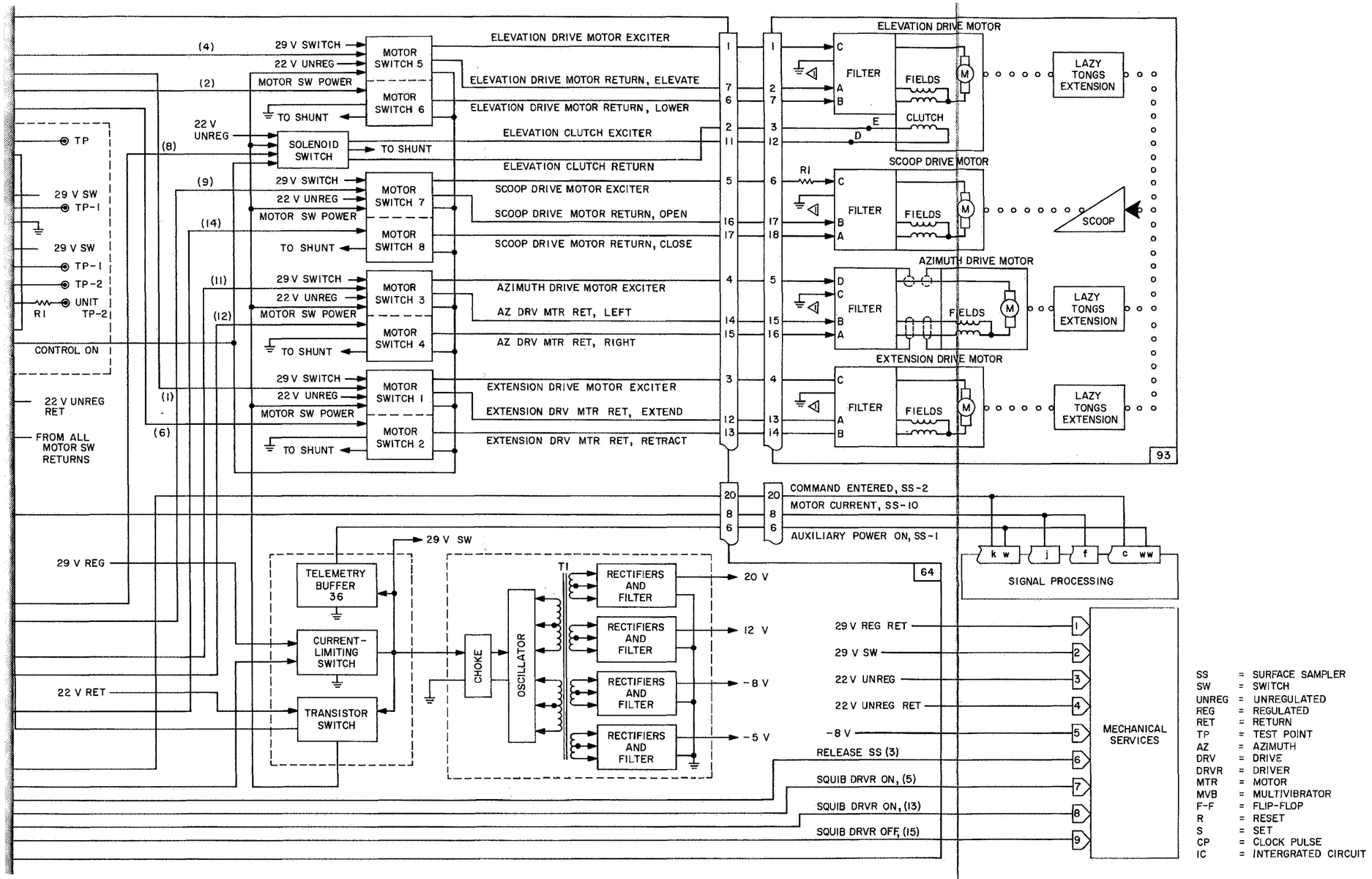



**Fig. XXII-25. Block diagram of soil mechanics/surface sampler auxiliary assembly**

**Table XXII-9. Summary of SM/SS operations on Surveyor missions**

| Operation | Surveyor missions | |
|---|---|---|
| | III | VII |
| Total time on | 18 hr, 22 min | 36 hr, 21 min |
| Number of earth commands | 5,879 | 12,639 |
| Number of mechanism movements | 1,898 | 4,397 |
| Number of bearing tests | 8 | 16 |
| Number of trenches dug | 4 | 7 |
| Number of impact tests | 14 | 2 |
| Tests with magnet | No | Yes |

empty. This rock was photographed from several positions on the lunar surface to provide a stereo view. Another rock was broken by the SM/SS.

Two magnets were mounted on the scoop door of the SM/SS on *Surveyor VII*. Several tests were made to determine the amount of material that stuck to the magnets.

The SM/SS was used to assist the alpha scattering instrument sensor head deploy to the surface on the *Surveyor VII* Mission. When commanded to release the sensor head, the deployment mechanism did not operate, and repeated commands were unsuccessful. Since the envelope of operation of the SM/SS included the position where the head was suspended, an attempt was made to release the head by nudging it with the scoop of the SM/SS. When first attempts failed, it was apparent that a downward force had to be exerted. From analysis and test on spacecraft models at JPL and HAC, the SM/SS was used to lever the alpha scattering instrument about the spacecraft helium tank. This exerted a downward force on the retaining cord, suspending the sensor head and causing the head to descend. Further downward taps by the SM/SS on the top of the head were made and in this manner the instrument was successfully deployed to the surface.

Later in the mission the SM/SS was used on two occasions to redeploy the alpha scattering sensor head to new locations. This redeployment, which was preplanned, allowed an elemental analysis to be made of three lunar samples. One of the samples was subsurface material which had been exposed by operation of the SM/SS. During a period close to lunar noon, the SM/SS scoop was positioned so that it produced a shadow on the sensor head. This maintained the alpha scattering instrument below its survival temperature.

On the second lunar day, the SM/SS was found to have survived the lunar night and was operated again. However, the SM/SS was not used for further testing.

## D. Alpha Scattering Instrument

### 1. Introduction

In September 1966, after the successful *Surveyor I* Mission, it was decided to include the alpha scattering instrument as part of the *Surveyor V, VI,* and *VII* scientific instrument payload. The alpha scattering instrument was used to perform elemental analysis of lunar surface material. A. Turkevich of the University of Chicago was appointed principal investigator. The objectives of the alpha scattering instrument analyses were to assist in determining the nature and origin of the material. The analyses provided the means to establish the following:

(1) Identification of the mass numbers of elements present in the lunar material by means of the energy spectrum of scattered alpha particles.

(2) Identification of certain lighter elements in the lunar material by means of the energy spectrum of protons emitted in alpha-proton nuclear reactions.

(3) Determination of the relative abundances of elements in the lunar material by means of both of these spectra.

The alpha scattering detector–analyzer system was capable of detecting scattered alpha particles from all elements except hydrogen and helium. The proton detector–analyzer system could detect protons from lithium, boron, nitrogen, fluorine, sodium, magnesium, aluminum, silicon, phosphorus, and sulfur. Sensitivity of the measurement varied from one element to another, but the detection threshold was about 1% by weight. Operation of the instrument was impaired by surface contaminants thicker than 0.1 $\mu$m because alpha particles could penetrate only a few microns into typical material.

### 2. Description of the Alpha Scattering Instrument

When the instrument was operated, a sample was bombarded with 6 MeV alpha particles from a source within the instrument as shown in Fig. XXII-27. Backward scattered alpha particles as well as protons, generated

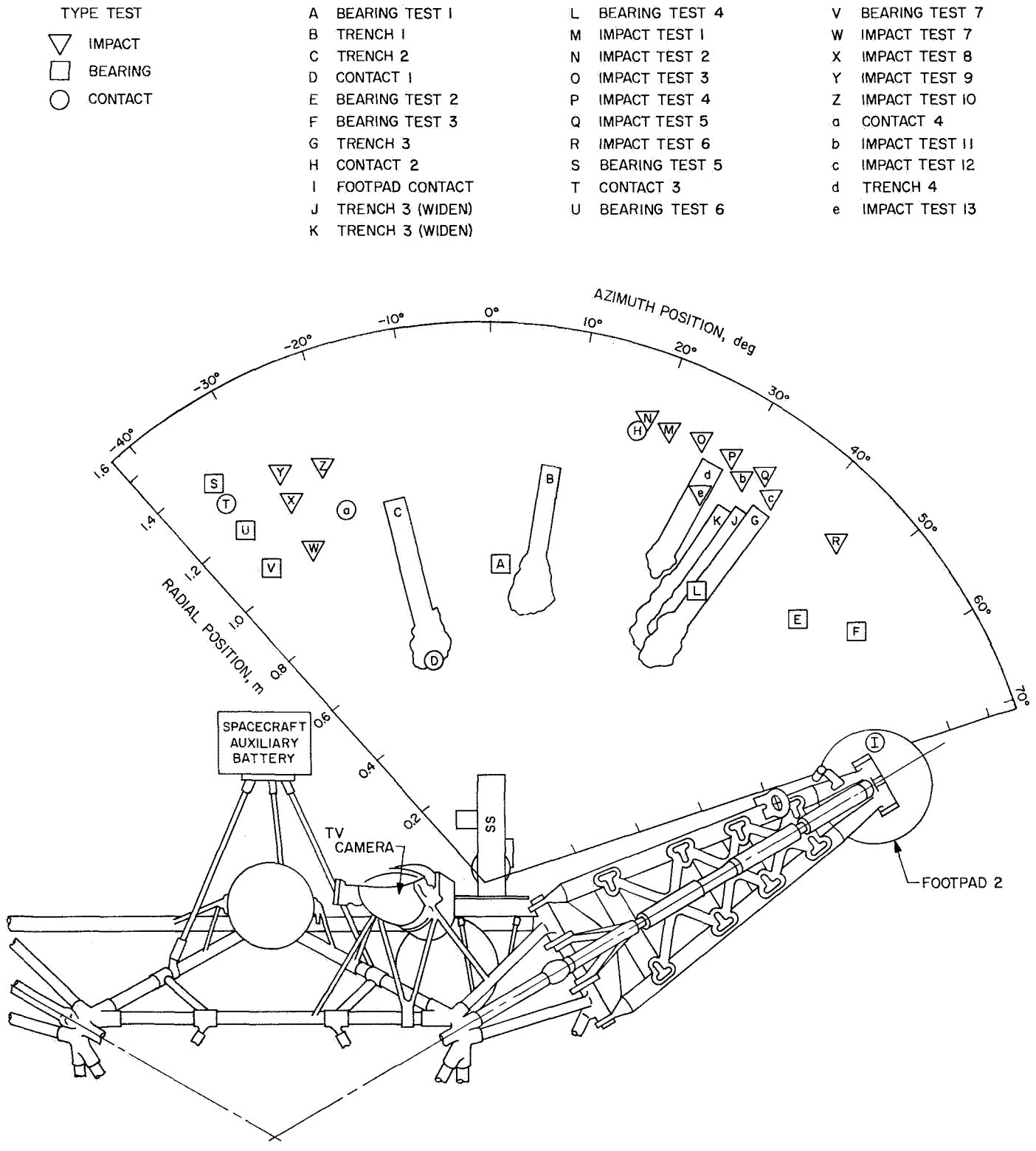



**Fig. XXII-26. Soil mechanics/surface sampler activity on *Surveyor III* mission**

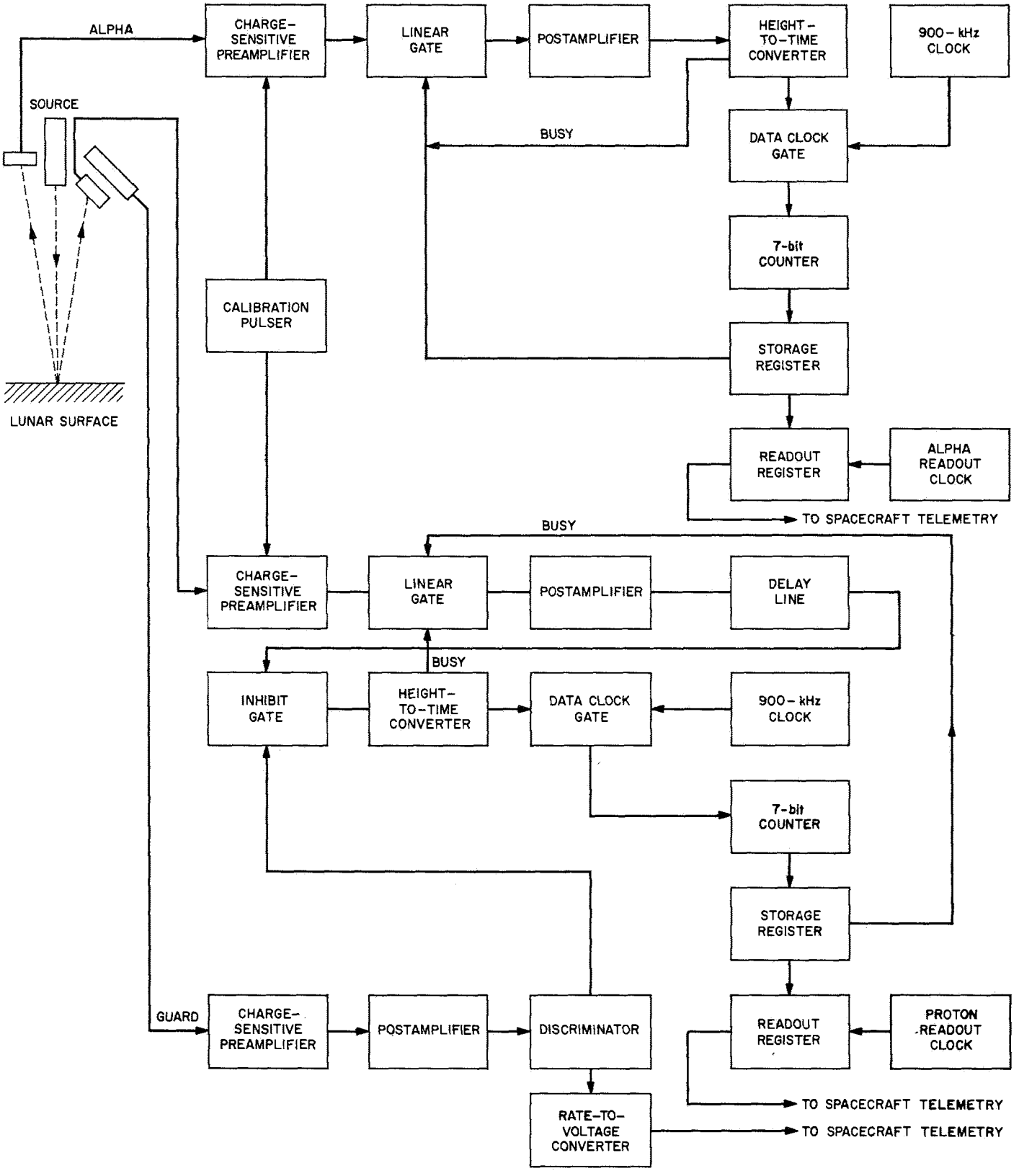



**Fig. XXII-27. Alpha scattering instrument simplified block diagram**

within the sample by the incident alpha particles, were detected with solid-state alpha and proton detectors. The proton detectors were covered with a thin metal foil to stop scattered alpha particles, and backed by an anti-coincidence guard detector to minimize background effects.

The varying charges on the detectors were converted to electrical pulses with amplitudes proportional to the energy of the detected particle by a charge-sensitive preamplifier-voltage amplifier system. The pulses were then routed to a height-to-time converter, and there translated into gating pulses. The durations of the gating pulses were directly related to the amplitude of the incoming pulses and therefore were time analogues of the energy possessed by the backscattered particles. The gating pulses steered the output of a 900-kHz clock into a 7-bit binary counter, thus completing the analog-to-digital conversion. The count contained in the 7-bit counter was then parallel transferred to a storage register to minimize dead-time effects, and then into an output register where it was sequentially scanned, most significant bit first, into the next telemetry data word. A sync bit and a parity bit were added to make a 9-bit word for telemetry. During the time that a height-to-time conversion was being performed, or that the storage registers were full, a busy signal was generated to inhibit the preamplifier outputs and prevent interference effects.

The guard amplifier system was similar to that described above; however, after mixing and amplification, the signal was fed to a pulse-height discriminator which inhibited the proton height-to-time converter. The four proton preamplifiers were identical to the alpha system, except for the addition of a delay-line to permit the guard system to reject an event if a detected particle were to trigger the guard discriminator. Discriminator events were converted to a voltage proportional to the event rate and telemetered, as were the 7- and 24-V supply voltages.

The calibration system injected known amounts of charge into the preamplifier inputs to give a two-point calibration of the system to determine linearity and offset. The charge inputs, with an additional point obtained from a radioactive calibration source within the sensor head, permitted the energy scale to be determined.

The alpha scattering instrument consisted of the digital electronics, the sensor head, and the electronics auxiliary assembly. A deployment mechanism, which contained the standard sample assembly, was also provided. The alpha scattering instrument was integrated in the existing spacecraft design for *Surveyors V, VI,* and *VII* by locating the sensor head in almost the same position occupied by the auxiliary battery on previous missions. The auxiliary battery was no longer required due to a redesign of the spacecraft power subsystem. The digital electronics and electronics auxiliary assembly were placed in a new compartment (compartment C), which also contained a heater. Compartment C was placed above and behind the sensor head, on the spacecraft.

***a. Sensor head.*** The sensor head, designed to be deployed to the lunar surface, contained the radioactive source of alpha particles, alpha detectors, proton-guard detector assemblies, and sensor head electronics. Figure XXII-28 is a view of the interior of the sensor head as seen from the viewing port. This view is a closeup from underneath the head, as seen from the lunar surface. The photo shows six radioactive sources, two alpha detectors, and four proton-guard detectors. The radioactive source of alpha particles consisted of six metal disks on which were deposited curium 242, collimators, protective films, and holders. Because curium 242 has a half-life of 163 days, and because of precautions necessary in handling radioactive materials, the sources were installed about 2 wk before launch.

The semiconductor-type detectors used produced charge signals in response to ionizing radiation. The two alpha detectors, mounted adjacent to the alpha sources to obtain the required geometry, were protected from light entry by very thin films. The four proton-guard detector assemblies, mounted close to the sample to obtain a higher event rate, consisted of a gold foil to stop alpha particles, a proton detector, and a coaxially mounted guard detector to intercept background radiation from above the proton detector.

When measuring composition in a vacuum, the instrument required an alpha source of 25–100 mCi of curium 242. However, it was not necessary to use a flight source in vacuum to test the instrument. Weak sources were mounted close to the detector so that reproducible spectra were obtained at atmospheric pressure. For vacuum tests, a different set of sources were employed. Tests were of sufficient length to allow accumulation of enough counts to avoid large statistical uncertainties. If system noise is defined as the uncertainty in the background count, then a ratio of the counts in a particular channel to the noise in the same channel needed to exceed 3:1 to be statistically significant. The tests were conducted

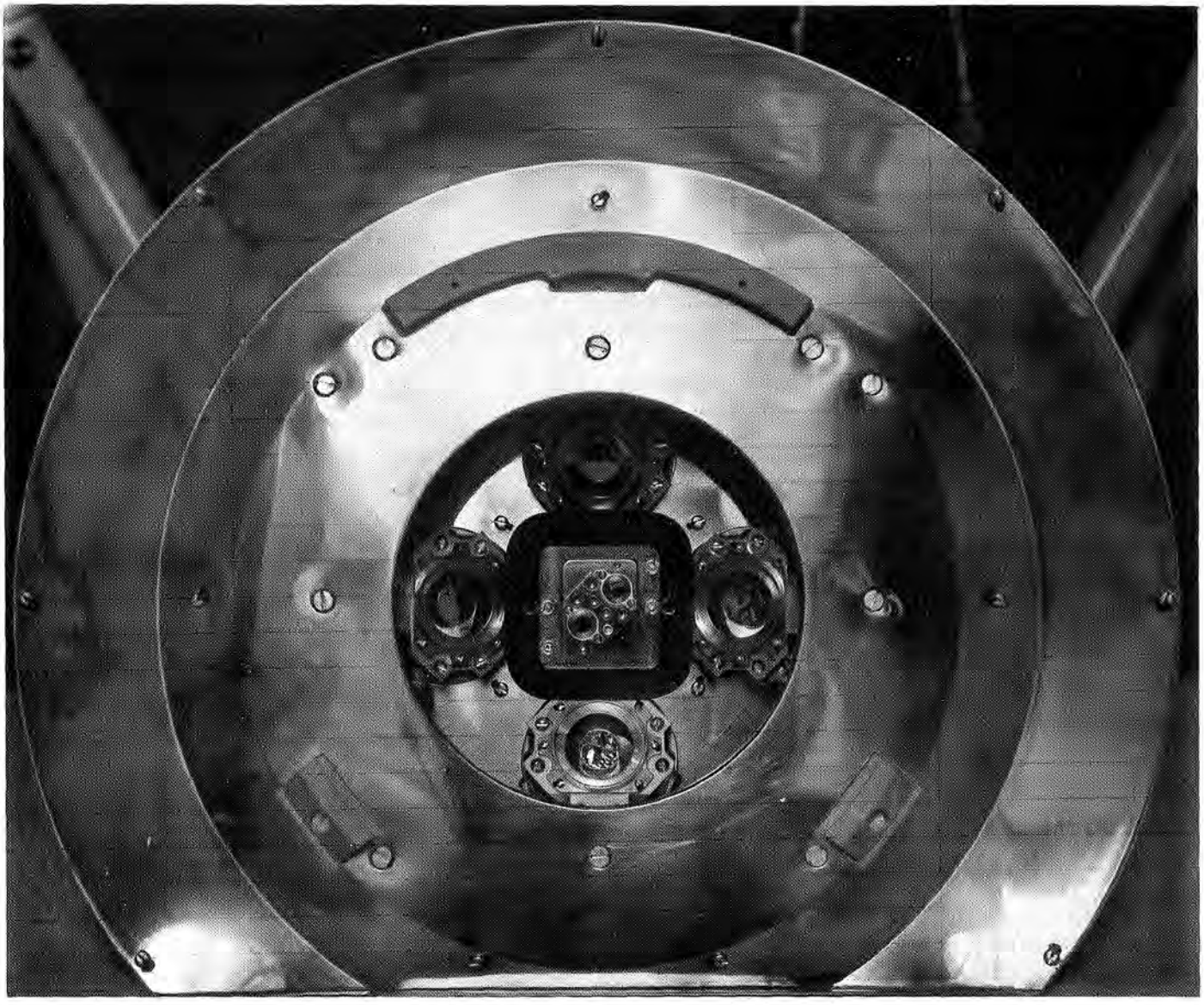


**Fig. XXII-28. Sensor head interior**

over a period sufficient to obtain count/noise ratios exceeding 10:1 on the lunar surface, average alpha signal-to-noise ratios were about 30:1, and in the proton spectra, 5:1 or 10:1.

*b. Digital electronics.* Digital electronics provided the circuitry to process the commands from the auxiliary assembly and to control the detector preamplifier switches located in the sensor head. Circuitry was also provided to convert the variable-width pulses from the sensor head into synchronous binary data for transmission, and to provide engineering telemetry functions of the detector switch states for both alpha and proton systems. The logic circuits for the alpha and proton data were identical except for the readout rates of 550 bits/sec for proton and 2200 bits/sec for alpha. A telemetered data word contained a sync bit, 7 data bits, and a parity check bit. If no data were to be transmitted, the sync bit followed by eight zeros was transmitted to maintain sync. The instrument power supply was also located in the digital electronics.

*c. Auxiliary assembly.* The auxiliary assembly, built by HAC, was used to provide the electrical interface between the alpha scattering instrument and the *Surveyor*

spacecraft. The auxiliary assembly supplied the electronics for command decoding, telemetry signal processing, power used by the alpha scattering instrument, and the electrical current to fire two squibs on the deployment mechanism.

*d. Deployment mechanism/standard sample.* The deployment mechanism provided stowage of the sensor head, and deployment to the background position and lunar surface. The sensor head was mounted to the deployment mechanism by means of three support lugs on the bottom plate. Deployment mechanism clamps that engaged these support lugs were released during the deployment operation. Figure XXII-29 illustrates the two-stage operation of the deployment mechanism. From the stowed position, the sensor head was first released on command to a position 22 in. above the nominal lunar surface by activation of an explosive pinpuller device. From the background position, the sensor head was then lowered directly to the lunar surface by activation of another explosive pinpuller device. Deployment velocity was controlled by an escapment.

A sample of specially treated glass containing magnesium, sodium, iron, silicon, and oxygen was attached to the platform on which the sensor head was mounted in the stowed position. This standard sample covered the circular opening in the bottom of the sensor head during spacecraft transit and landing to minimize entrance of dust and light and to provide a means of assessing instrument performance soon after the spacecraft landed on the moon. The standard sample and mounting platform moved down when the sensor head was deployed to the background position.

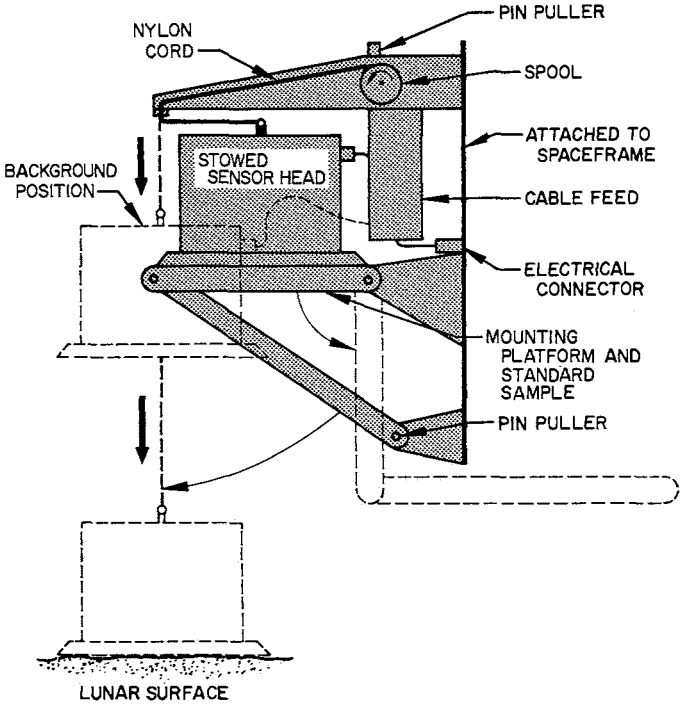



**Fig. XXII-29. Alpha scattering instrument deployment mechanism**

### 3. Development and Test History

Preliminary studies were made by A. Turkevich of the University of Chicago in 1961 to show that the energy spectrum of backscattered alpha particles was characteristic of the elements present in the material tested. A. Turkevich proposed that an experiment be conducted using an alpha scattering instrument to provide an elemental analysis of the lunar surface. A grant was awarded to him in January 1963 by NASA for a breadboard and a prototype for evaluation. A breadboard of the sensor head was built and tested and then delivered to JPL for evaluation.

Contract negotiations were held at the University of Chicago in June 1963 for the construction and test of four prototype alpha scattering instruments, identified as P-1, P-2, P-3, and P-4, for the *Surveyor* Project. Construction was to start immediately on P-1 and P-2, whereas P-3 and P-4 construction would be started at a later date.

*a. Development of P-1 and P-2.* Construction of P-1 was started in July 1963, and it was scheduled for delivery to JPL in October 1963. However, due to design changes and detector failures, the instrument was not delivered to JPL until April 1964. Delivery of P-2 was also delayed (until August 1964) because of the P-1 problems, the requirement for better components, and testing and detector difficulties. The principal investigator used P-1 during the summer months of 1964 for scientific investigation. In October 1964, P-1 was delivered to HAC where it successfully passed *Surveyor* electrical tests.

During acceptance testing, P-2 exhibited gain errors and zero offsets that did not satisfy the design specification that a design review in October 1963 indicated would be satisfied.

After P-2 had completed acceptance tests, it was delivered to JPL for scientific investigation by the coexperimenter at JPL. Then P-2, with flight sources installed, was used to test various kinds of materials and rocks to

build up a library of elemental and compound plots for use as references when data were received from the moon. This work was done over a period of approximately 3 yr.

*b. Design review.* The design review was held at the Laboratory for Astrophysics and Space Research (LASR) of the University of Chicago to assist LASR in improving the instrument. Some changes in P-1 and P-2 were made because of the design review, but problems were continually encountered during the testing of the two instruments. Development of the alpha scattering instrument continued through 1964 and 1965. Mechanical and electrical improvements were added as continued testing and environmental conditions disclosed that changes were required.

*c. Second-generation alpha scattering instrument.* Because the alpha scattering instrument was not meeting the requirements of the experiment in all respects, JPL undertook the construction of a backup sensor head. The sensor head contained the analog section of the instrument, and the new design was expected to increase the long-term stability of the unit to 1%, rather than the drift figure of approximately 5% exhibited by P-1 and P-2.

The work was started at the beginning of 1964 and a second-generation sensor head was delivered to LASR in the later part of the year for test and evaluation (Ref. XXII-2). Testing by LASR indicated that the new design was good and that the sensor head was stable; however, the sensor head built by LASR was selected as the instrument for the *Surveyor* spacecraft. The second-generation instrument effort was cancelled at the beginning of 1965. It should be noted that the laboratory-built instrument was gradually improved over the 2½ yr of testing and redesign, so that it would meet the design specification.

*d. Thermal and humidity requirements.*

*1. Thermal requirements.* Characteristics of the detectors in the sensor head were the constraining factors on the allowable instrument temperature. Detector upper temperature limits were 122°F (operating) and 167°F (nonoperating). Special considerations were made in the thermal and mechanical design of the instrument to insure that these temperatures were not exceeded under typical test conditions.

A subcontract was awarded the Illinois Institute of Technology Research Institute for thermal studies of the alpha scattering instrument. Data were provided by HAC on expected spacecraft temperature and the spacecraft view of the sensor head. The thermal tests were conducted by JPL on the thermal model; JPL worked with the Institute on the solar simulator tests at the Boeing space simulator and participated in design changes to keep the detectors in a cooler environment. At the beginning of 1967, a Vycor mirror was added to the top plate of the sensor head to further reduce sensor head temperature. Studies showed that the sensor head, when on the moon, would approach the 122°F temperature limit. With the Vycor mirror added, the temperature was calculated to be approximately 104°F on the moon.

*2. Humidity requirements.* In November 1966, two humidity requirements were implemented: the detectors should not be exposed to a relative humidity greater than 50%; a continuous dry nitrogen purge of the sensor head should be provided from the time of source loading to spacecraft launch. A nipple was added to the sensor head to pipe dry nitrogen into the head when the humidity went above 50% or when the sources were installed.

*e. Development and type-approval testing of P-3 and P-4.* Construction of P-3 and P-4 was delayed to allow for the inclusion of high-reliability and screened parts that were supplied by JPL for use in the multilayer circuit boards. In May 1964, delivery of P-3 was rescheduled to August 1964. Construction of P-4 was suspended at that time. Vendors were changed for the multilayer circuit boards, and such changes as adding a mechanical relay to give two additional calibration points and a redefinition of the *Surveyor* Program caused delivery of P-3 to be rescheduled to September 1965. Acceptance tests were finally conducted on P-3 in February and March 1966. Then P-3 was delivered to JPL for use as a type approval instrument.

The type-approval tests conducted on the instrument were: vibration, temperature-vacuum, thermal shock, mechanical shock, and static acceleration. An acoustical test was run on the head only, to test the films covering the detectors and sources. Both the sensor head and the digital electronics failed the first vibration test. One of the four bolts that held the digital electronics broke while mounting the unit to the vibration table. New bolts were designed and no further trouble was encountered.

The sensor head was held by clamping three of the feet on the bottom of the sensor head to a fixture. One clamp was adjustable to apply pressure for holding the

head. The three feet were an integral part of the bottom plate to which the detectors and analog electronics were fastened. During the first vibration test, the sensor head almost flew off the fixture before the test could be stopped. The bottom plate was redesigned. During the next vibration test, the bottom plate broke around one of the feet. The bottom plate was again redesigned, and the sensor head passed the next vibration test. The instrument passed the rest of the type approval tests without major difficulties.

*f. Flight instruments.* A new contract, written for the alpha scattering instruments in July 1965, called for the construction and testing of five flight instruments (P-4 and F-1 through F-4) and continued testing of the type approval instrument, P-3. The designation P-4 was used for the first flight unit. Because of *Surveyor* Project changes, F-4 was eliminated later in the year.

The flight instruments were completed and acceptance tested in Chicago, where some difficulty was encountered due to detectors becoming noisy. During the flight acceptance testing at JPL, there were also a number of detector failures during the temperature–vacuum tests.

*g. Problems.* There were two major instrument problems throughout the testing program. The most important problem was the frequent failure of detectors. The five instruments (P-3 through F-3) had a total of 49 detector failures. The detector problem was investigated throughout the lifetime of the project but no conclusive reason for failure was discovered. Some handling procedures and manufacturing processes were improved as a result of investigations, and detector reliability did show improvement near the end of the program. After the instruments had completed all testing at JPL and HAC, only three detectors failed in system tests.

Calibration relays used to feed pulses to the electronics to simulate detector operation accounted for the second major instrument problem. Requirements for the operation of relays were almost beyond the state of the art, and only through most selective screening were relays obtained. Additionally, once relays were selected, there was no assurance that they would stay in specification. After a number of relay failures, JPL gave the direction to select the best relay for each instrument, with the understanding that a failed relay would not be replaced. The principal investigator agreed to this requirement as there were other calibration methods of readout. The only way in which the instrument could be calibrated in less than an hour, however, was to use the relay. Thus a bad relay increased the instrument running time during the spacecraft test cycle.

*h. Spacecraft testing.* Once installed on a spacecraft, the alpha scattering instrument was given a complete checkout with the rest of the spacecraft subsystems. The instrument was given four Spacecraft System tests: mission sequence, electromagnetic interference, solar-thermal-vacuum, and vibration. Because of extensive type approval, flight acceptance, and payload system tests conducted at HAC, instrument problems encountered during system tests were minimal.

### 4. Air Force Eastern Test Range Operations

Before each alpha scattering instrument was installed on the *Surveyor* spacecraft, it was scientifically calibrated to include temperature and vacuum tests and the installation of flight sources.

University of Chicago personnel, an integral part of the calibration team, were responsible for radioactive source handling. A separate cleanroom facility, located near the JPL spacecraft checkout area, was used. Room temperature of the four-room facility, which used an air conditioner separated from the rest of the building, was maintained at 72°F and 20% relative humidity. The cleanroom facility was provided with a laminar flow bench, radioactive-source handling facilities, two vacuum chambers, and two sets of electronic support equipment.

One of the vacuum chambers was specially built so that samples could be inserted in the chamber (under the sensor) for calibration. A supply of both liquid and dry nitrogen was piped into the rooms for the vacuum chambers, and a high-purity source of dry nitrogen was used to purge the sensor head and the sources.

A complete alpha scattering procedure system was set up for this calibration operation. Nine handling and operating procedures were written and closely followed. After each flight instrument was subjected to a calibration sequence of approximately 10 days, it was finally delivered to the spacecraft about 6 days before launch. Before calibration of the flight instruments, a spare instrument was calibrated so that it was available for use as a flight-ready spare. Just before the instrument was returned to the spacecraft and immediately before encapsulation, a data review meeting was held. In this meeting, data relevant to the instrument was collected and given to HAC as part of the contractual requirements necessary for the delivery of government-furnished property. At this time, too, the principal investigator

reviewed the scientific data and certified that the instrument was suitable for its task on the mission.

### 5. Mission Performance

The alpha scattering experiment was completely successful on *Surveyor V, VI,* and *VII* missions. No failures occurred when the instrument was operating within its design temperature limits, and in several instances the instrument returned useful data even when operated beyond its design limits.

The *Surveyor VII* mission was of particular interest because of the target-area location in the region of the crater Tycho. Lunar surface analyses of a highland area could be compared with those of the mare areas, and could possibly reveal information relating to the origin of the moon.

Postlanding operations of the alpha scattering instrument were initiated shortly after the first TV survey, with the subsequent operations being conducted during intervals when the TV camera was not being utilized.

***a. Surveyor V.*** The *Surveyor V* used P-4. The possible effects of aluminum oxide particles contained within the main retro motor exhaust stream on the performance of the alpha scattering instrument were unknown. In addition, a planned static firing of the vernier engines was to commence less than 20 hr after touchdown. These two factors partially influenced the decision to reduce the duration of posttouchdown data accumulation in both the stowed and background positions. Data received from both the stowed and background positions indicated that instrument operation was normal and deployment to the lunar surface had been accomplished.

During the second power turnon after landing, the calibration pulser turned on. A command from earth was required to shut off the pulser and to allow standard date accumulation to proceed.

Overall performance of P-4 was excellent. The total lunar operating time was 93.5 hr. Figure XXII-30 shows a comparison of prelaunch data with data received during the transit phase. Figure XXII-31 presents the spectrum of the standard sample obtained on the moon compared with a computer-generated curve.

After the vernier engine static firing, the sensor head was observed to have moved approximately 10 cm, which allowed a new lunar surface area to be analyzed. The instrument was subjected to an operating temperature range of 126 to −69°F, the lower temperature occurring shortly before lunar sunset. This lower temperature was 29°F below the specified minimum operating limit, and no preflight data had ever been accumulated at such a low temperature. The value of this low-temperature operation is doubtful, however, since the effects of temperature on the sensor head are nonlinear, and in the case described, undefined.

Each of the 10 sensor-head detectors functioned properly. Only once, during a period of rapidly changing temperatures, was there suggestion of noise in the proton system. Sharp breakpoints in sample spectra showed that the high quality of the curium 242 sources had been preserved. The films covering the sources and alpha detectors had survived the launch, midcourse maneuver, and terminal descent phases. The electronics, calibration pulser, and einsteinium sources performed properly as evidenced by the sharpness of calibration peaks and agreement with prelaunch data. The guard detector and autocoincidence system worked as designed; guard monitor voltage and proton background spectrum agreed well with predicted values.

The digital electronics, instrument power supply, and electronic auxiliary assembly performed as designed. Circuits used to monitor engineering parameters provided good data. Nearly 600 commands were transmitted to the alpha scattering instrument, and, except for one, all commands gave the expected response. The deployment mechanism functioned properly in spite of the 19.5-deg tilt of the spacecraft.

The communications link from the spacecraft was excellent; a bit error rate of less than $10^{-6}$ was estimated from the parity-incorrect spectra. In general, deviations from this high-quality data reception occurred only when the spacecraft was being tracked near the earth's horizon. Both major alpha scattering computer programs and associated equipment provided excellent processing of the science data.

***b. Surveyor VI.*** The *Surveyor VI* used F-1. After approximately 53 hr of lunar surface operation, at a temperature of 109°F and rising, traces of noise were observed in the proton spectra. At this time, lunar noon was approaching, and the instrument was turned off. The sensor head was turned on again after lunar noon and, after only a short interval, the noise disappeared. Proton 3 detector was the detector involved with the noise. In general, detectors noisy in simulated lunar

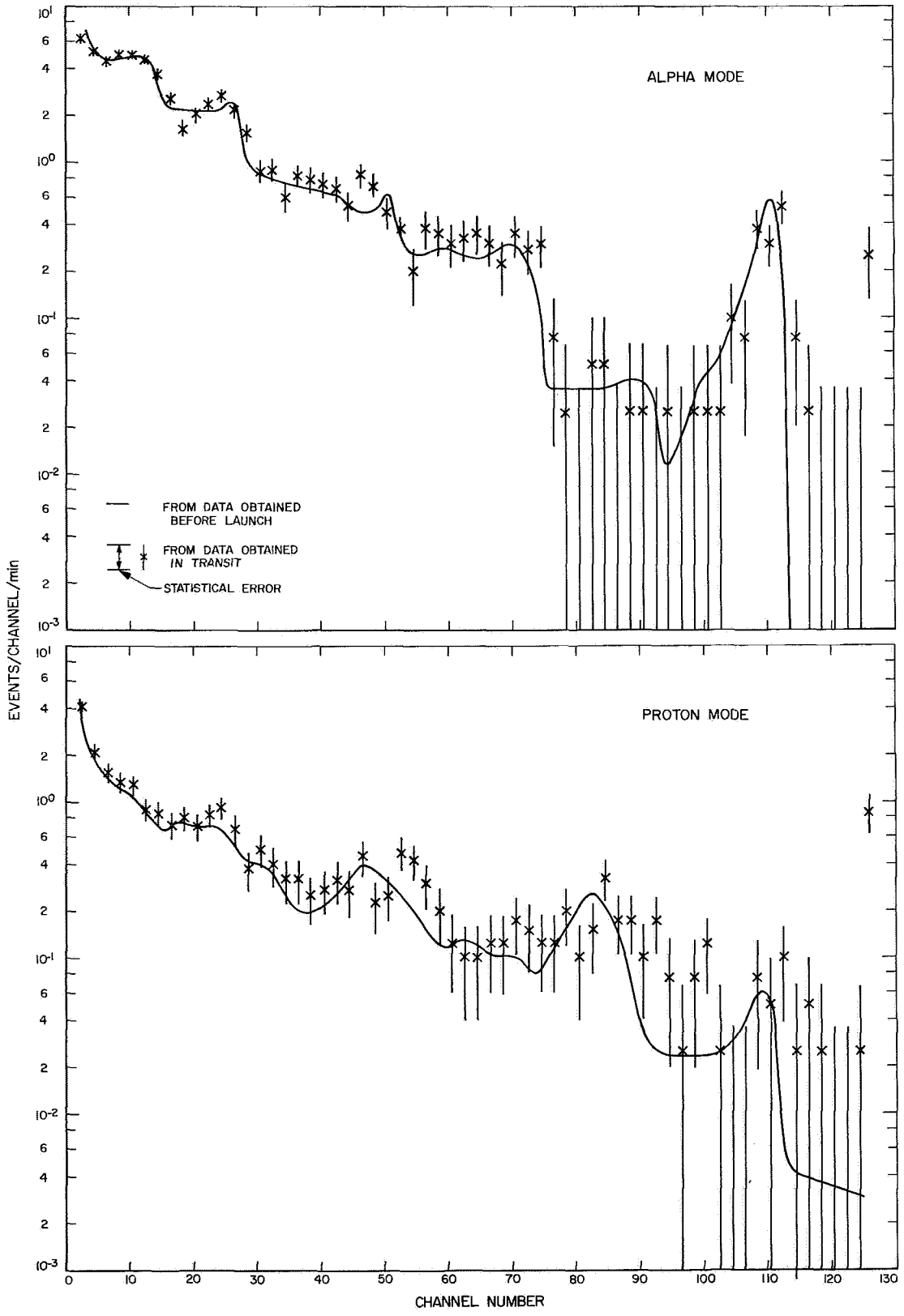



**Fig. XXII-30. Comparison of prelaunch and transit phase data**

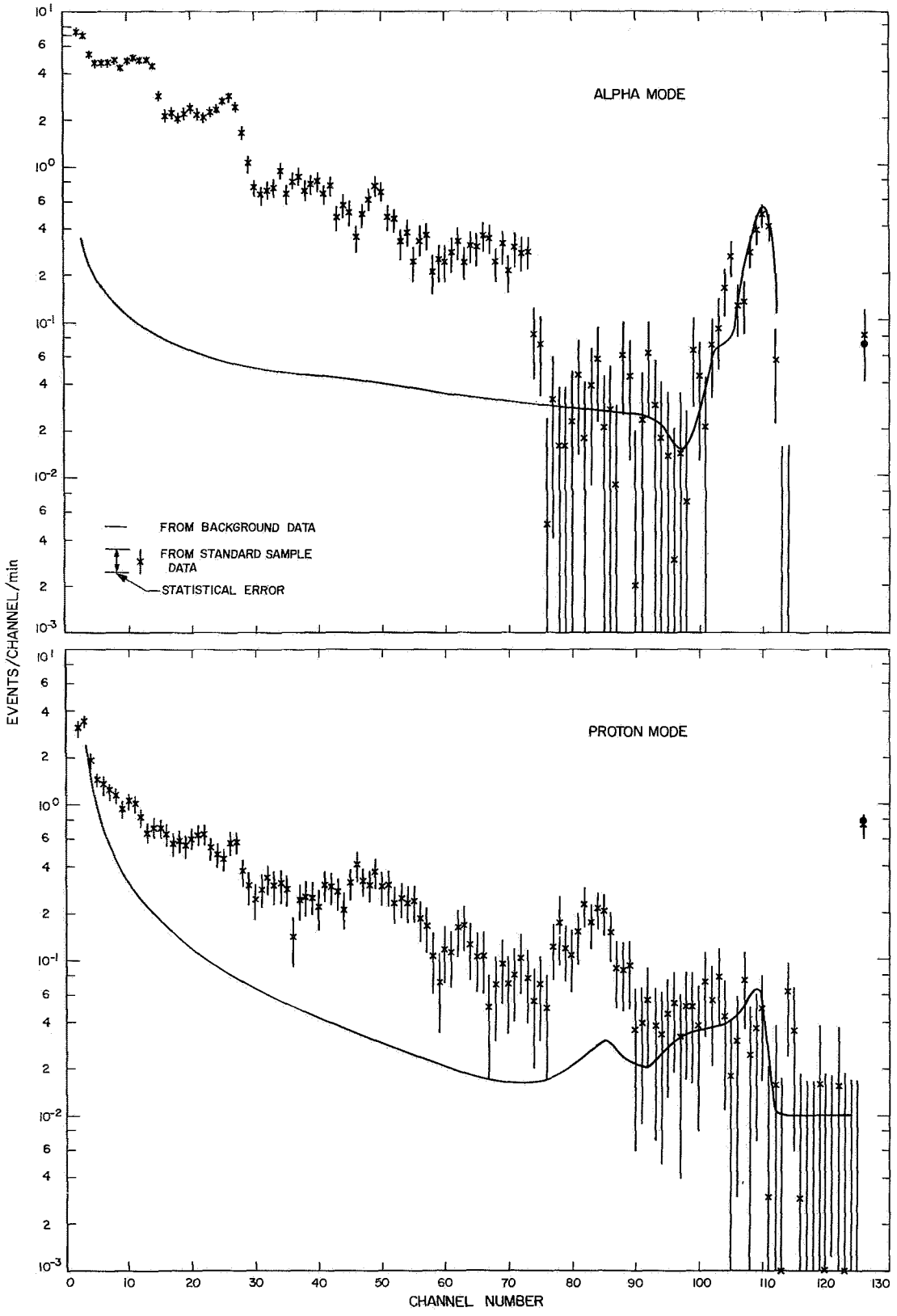



**Fig. XXII-31. Comparison of standard sample spectrum and computer-generated curve**

environment during testing did not recover spontaneously; however, in the actual lunar environment, proton 3 did recover as no further noise was encountered. Except for the proton 3 noise problem, F-1, together with the deployment mechanism and spacecraft auxiliary, performed as anticipated.

Following the spacecraft hop experiment, the instrument was observed to be upside down, with the sample port viewing space. Under these conditions, the sensor head temperature rose to 144°F. Operation of the instrument later in the lunar day showed that it was functioning electronically in a normal manner, but that urium 242 contamination was present in the sensor head, indicating that at least one of the source-protective films had broken. Data accumulated by the instrument in the inverted position provided additional information on cosmic ray activity.

Operation of the instrument on the second lunar day was attempted, but the alpha mode digital processing circuitry was not working properly.

*c. Surveyor VII.* *Surveyor VII* used F-2. The instrument was successfully deployed to the background count position, and the data received indicated proper operation of all instrument functions. However, the deployment mechanism did not lower the instrument to the lunar surface when commanded. A TV survey confirmed that the pinpuller had fired and that the escapement mechanism had not operated properly. Fortunately, the SM/SS was able to reach the sensor head and force it to the surface. Later investigations pointed to a stiffening of the nylon cord as the probable cause.

Once deployed, F-2 performed as expected over the period of lunar operations except during a brief interval when the sensor head was operated at 144°F. When more than one guard detector was operating, the guard monitor event rate was observed to increase. Individually, the count rate was normal, indicating that the energy threshold of the guard anticoincidence circuitry was dropping with each added active detector. This problem did not appear while F-2 was being operated within its designed temperature range. The SM/SS was employed to redeploy F-2 twice, providing analyses of three different lunar samples. *Surveyor VII* was the only spacecraft flying both the alpha scattering instrument and the SM/SS.

Second lunar day operation of F-2 revealed that the alpha 2 detector was noisy, whereas the alpha 1 detector seemed to be operating properly. The proton system did not function properly due to a malfunction in the digital electronics that entered all proton counts in channel 110. Later, all proton events were entered in channel 126. In both instances, no useful proton data were gathered on the second lunar day.

## E. Instruments Not Used on *Surveyor* Missions

Prior to the definition of the spacecraft scientific payload in 1964 and 1965, a number of instruments were in various stages of development. Many of these were in the scientific feasibility stage and never reached the status of flight instruments. Eight instruments that were in an advanced stage of development are described in this section. Each of these instruments was being developed for use on the spacecraft when development ceased because it was not selected for the payload, or because major engineering problems occurred in the development.

### 1. X-Ray Diffractometer

*a. Introduction.* The objective of the X-ray diffractometer experiment was to provide a mineralogical analysis of lunar material. This analysis was to include, as much as possible, the following information:

(1) Identification of mineral types.

(2) Relative quantities of mineral types.

(3) Identification of individual components of complex mineral types.

Operation of the X-ray diffractometer was based on the principle that X rays impinging on mineral samples at an angle $\theta$ will be selectively diffracted by different minerals within the sample. A detector, mounted so that it could rotate with respect to the sample tray, detected the coherently scattered X rays from the sample material. A plot of the detected flux vs the scattering angle ($2\theta$) produced a presentation in which peaks occurred that were ideally unique to individual minerals within the sample.

Detection of glass was expected to pose a problem in interpretation of diffractometer data, due to the single broad statistical maximum which glasses produce. In the event that crystals of other minerals were present in heterogenous mixtures that also contained glass, it was expected that diffraction peaks from the other mineral crystals would obscure the broad diffraction maximum

obtained from glass. It was also doubtful that the composition of glasses could be determined from the diffraction maximum. An elementary representation of the operation appears in Fig. XXII-32.

***b. Development.*** Since X-ray diffraction (based on Bragg's law) is a proven method for mineral analysis, the decision to employ X-ray diffraction for lunar rock analysis did not require development of new technologies or concepts. It did, however, pose a difficult engineering problem to develop a diffractometer suitable for a space program.

Perhaps the most difficult area initially was weight. No concerted effort had previously been made toward significant weight reduction. Standard commercial diffractometers weighed well over 1000 lb. The *Surveyor* X-ray diffractometer development was thus directed toward producing a lightweight unit with structural integrity for survival of spacecraft launch and lunar landing, which would produce diffraction data at least roughly comparable to commercial diffractometers while operating in the extreme lunar environment.

The feasibility of using X-ray diffraction for petrological analysis was demonstrated in early 1961 at Philips Electronics Instruments. The possible reduction of physical dimensions of the X-ray optical system was demonstrated by the first prototype, model A. This diffractometer was used with available laboratory X-ray tubes to show that useful diffraction data could be obtained with a miniaturized diffractometer and to prove proposed methods for goniometer drive and data presentation using solid-state electronics.

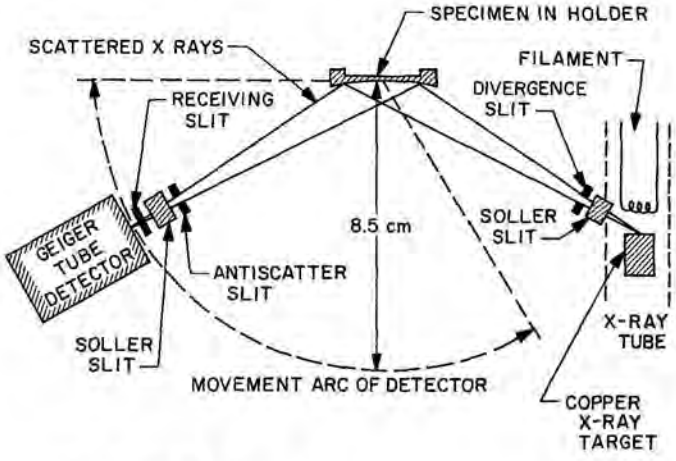



**Fig. XXII-32. X-ray diffractometer operation**

Next, models B and C were procured approximately concurrently, with efforts directed toward production that would meet both functional and environmental requirements.

The model D phase was directed toward improving overall performance, ruggedizing the diffractometer and providing a type approval test specimen. These tasks were accomplished by concurrent procurement of two diffractometers, designated P-3 and P-3D. These diffractometers were identical, except that the P-3D diffractometer had been subjected to extremely rigorous developmental tests in vibration, shock, high and low temperature, and vacuum operation. The P-3 diffractometer had been subjected to only limited testing so that a nonfatigued diffractometer could be delivered for type approval tests.

One of the significant developments in the model D phase was the X-ray tube. The 25-kV copper target X-ray tube was 5 in. long and weighed 13 oz. This tube is shown in Fig. XXII-33 along with an earlier, larger model.

The most readily apparent change in the P-3 diffractometer from earlier models was the use of an aluminum casting for the dust-cover housing. The new configuration (Fig. XXII-34), without cover plates, reduced the number of components and the volume by 50%.

The development stages produced the P-3 diffractometer shown in Fig. XXII-35. The process of miniaturization was relatively successful. The functional performance of the *Surveyor* diffractometer, in spite of

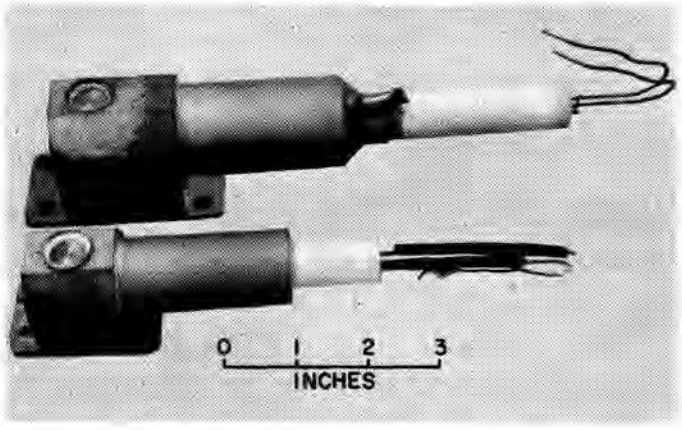



**Fig. XXII-33. X-ray diffractometer 25-kV X-ray tube (lower unit)**

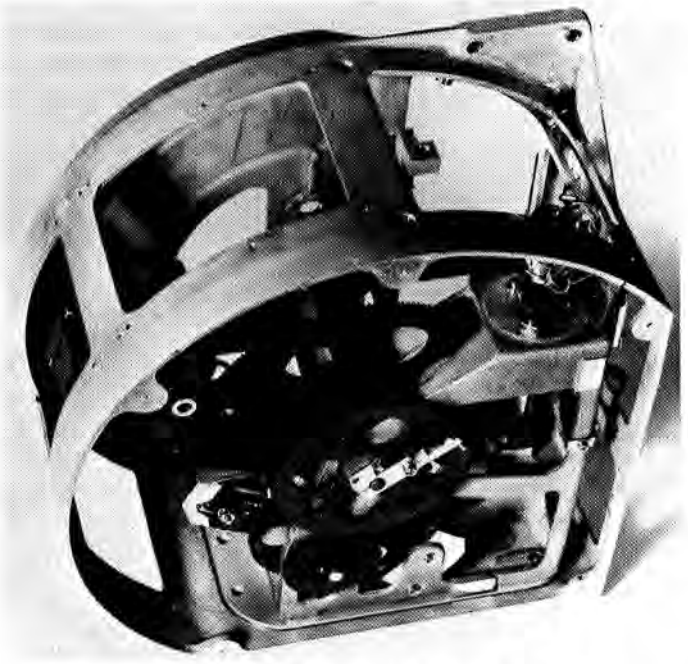


**Fig. XXII-34. P-3 X-ray diffractometer head without cover plates**

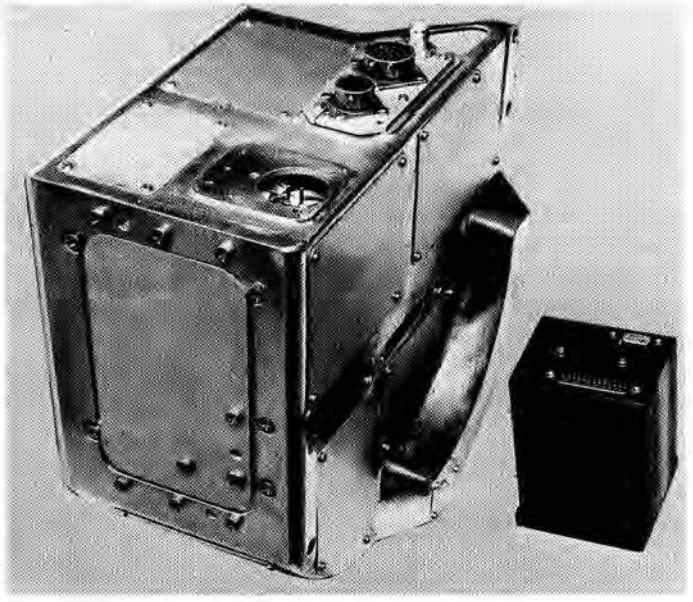


**Fig. XXII-35. P-3 X-ray diffractometer**

its ultraminiaturization, compared favorably with a standard laboratory diffractometer (Fig. XXII-36). In Fig. XXII-36, the entire *Surveyor* diffractometer, including power supply and electronics, is on the table in the foreground. The weight of the P-3 diffractometer was slightly increased during the developmental testing phase, due to requirements for stiffening indicated during the vibration tests. The P-3 sensor head weighed 10 lb, the electronics 1 lb, and the power supply approximately 8½ lb.

The functional acceptance test for the P-3 diffractometer was performed at the facilities of Philips Space Development in Mount Vernon, New York, and yielded the results shown in Table XXII-10, as compared with the design specification requirements. Two major problems were found when the diffractometer was operated at JPL. There was a major problem with arcing of the 25-kV power supply and tube assembly. In addition, the reliability of the unit was poor and the mean time between failures was only a few hours. Both problems were under invesigation at JPL when a redirection of the *Surveyor* Project occurred and work on the instrument ceased.

### 2. X-Ray Spectrometer

*a. Introduction.* The objective of the *Surveyor* X-ray spectrometer experiment was to determine the elemental composition of lunar surface materials. With the aid of the first design of the surface sampler, provisions were made to allow the analysis of subsurface lunar material.

The technique involved for the X-ray spectrometer was derived from the fact that any material, when bombarded by high-energy electrons, will emit X rays of wavelengths which are characteristic of the elements contained in the sample. In the *Surveyor* X-ray spectrometer, 25-kV electrons produced by a self-biased electron gun struck the target at the bottom of the spectrometer producing primary X rays and an X-ray continuum. These X rays were emitted upward into the spectrometer. X-rays of the proper energy, corresponding to elements of interest, were selectively diffracted by crystals of each particular channel. Eleven Geiger counters and four proportional counters were employed to detect the number of X rays diffracted into the different channels corresponding to each of the elements of interest.

Measurement of the quantity of X rays detected in each channel indicated the relative quantity of each of the elements contained in the sample under investigation. Figure XXII-37 is a pictorial representation of the X-ray spectrometer operation.

In addition to the above dispersive channels, a nondispersive channel detected X rays of all energies and performed an electronic pulse height analysis of the proportional counter output pulses to provide additional



**Fig. XXII-36. Comparison of *Surveyor* X-ray diffractometer and commercial X-ray diffractometer**

information concerning the relative quantities of the elements of interest.

*b. Development.* Figure XXII-38 shows the prototype model C X-ray spectrometer. Performance of this spectrometer was not satisfactory from several standpoints. Alignment of the crystal collimators was not readily accomplished without disrupting other portions of the package. Operation of several channels concurrently proved to be almost impossible due to electrical crosstalk and RF pickup. Additionally, the channel amplifiers were susceptible to damage at the occurrence of corona discharge or high-voltage arcing at the electron gun.

**Table XXII-10. 1011 quartz peak characteristics of the X-ray diffractometer**

| Characteristics | Specification | P-3 performance |
|---|---|---|
| Width at 1/2 peak height, deg (2$\theta$) | $\leq$0.22 | 0.19 |
| Width at 1/10 peak height, deg ($\theta$) | $\leq$0.43 | 0.36 |
| Asymmetry | $\leq$1.12 | 1.08 |
| Peak/background intensity ratio | $\geq$27 | 42 |
| Peak intensity, pulses/sec | $\geq$2300 | 4326 |
| Reproducibility of peak intensity, % | $\leq$3 | 0.6 |

During and after the model C spectrometer acceptance tests, a difficult problem concerning the method of sample excitation arose. When a sample possessing the electrical characteristics of an insulator was bombarded by the electron beam, it built up a negative charge which would effectively reduce the energy of the impinging electrons and deflect the beam from the proper focal spot to an extent that crystal alignment was incorrect.

This problem was investigated from several points of view, including:

(1) Providing a conductive pin in the sample cup.

(2) Providing a conductive screen embedded in the sample surface.

(3) Spraying the sample surface with a conductive material.

(4) Mixing the sample with graphite.

It was believed that the graphite mixture coupled with proper compaction would produce the best results.

The vendor was directed to continue development of the model D spectrometer, with emphasis on removing the functional difficulties found present in the model C

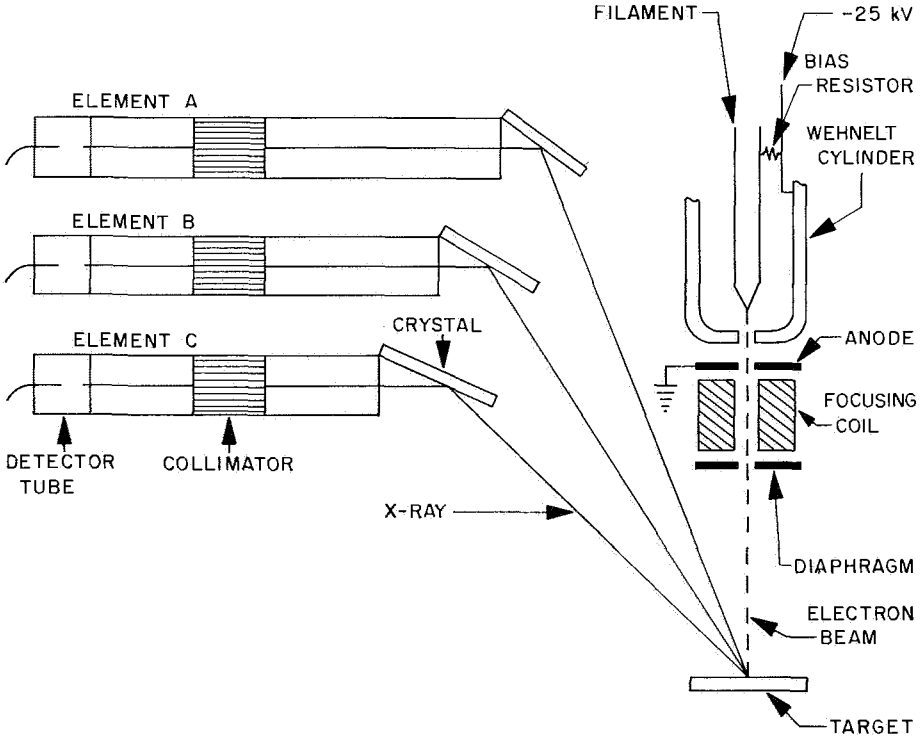



**Fig. XXII-37. X-ray spectrometer operation**

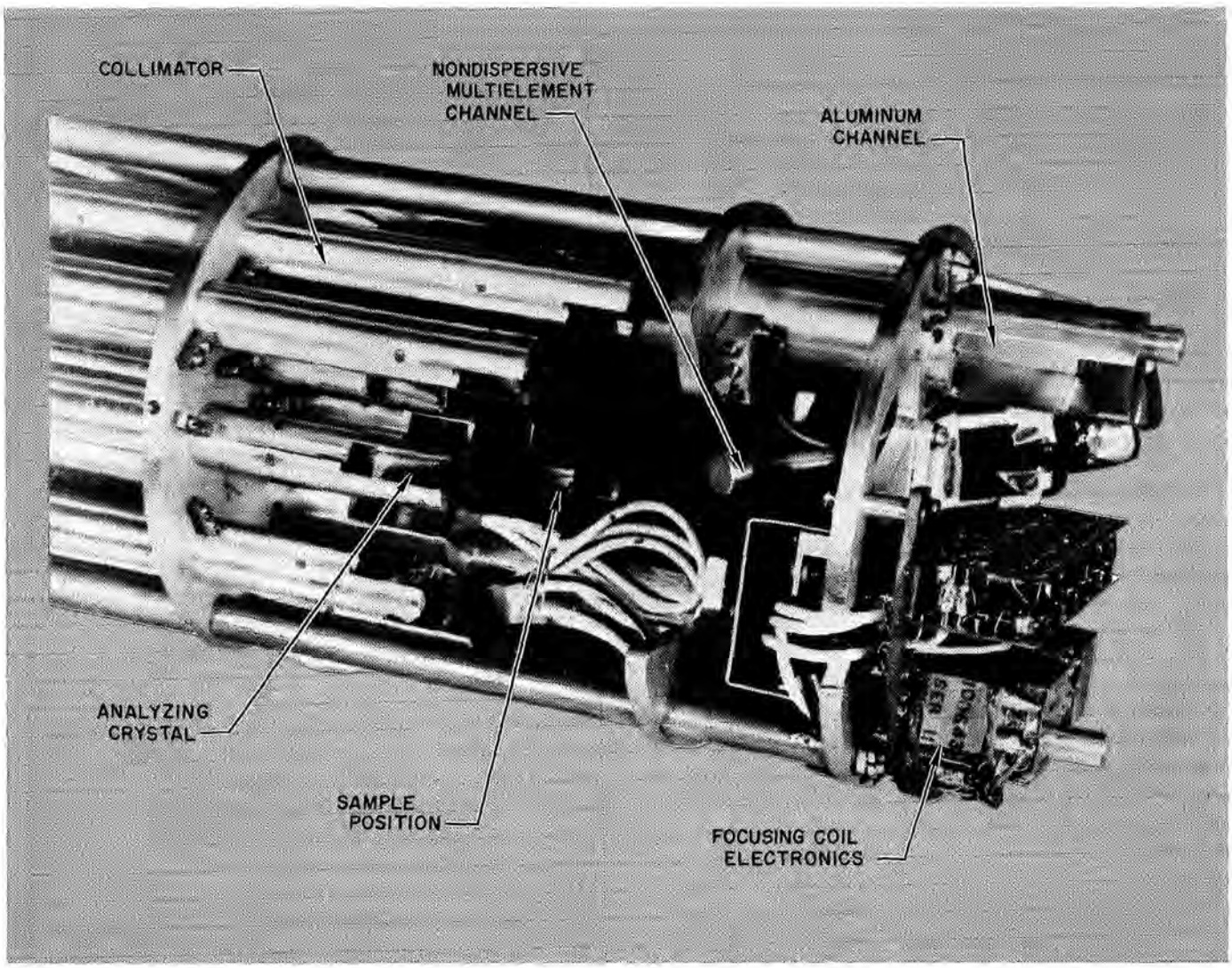



**Fig. XXII-38. Prototype model C X-ray spectrometer with dust cover removed**

spectrometer. At the same time, model C was to be shipped in functional order to JPL for evaluation and study. During shipment, however, the unit was involved in an airline crash, resulting in total loss.

The model D spectrometer, delivered to JPL on November 14, 1963, had nonlinearity problems with the pulse-height analyzers. At the time, most of the nonlinearity was traced to the linear gate circuitry employed. Recommendations regarding this particular problem and others, such as wiring techniques and potentiometer adjustments, were made by the vendor.

In general, the analytical performance of the model D spectrometer was adequate, although channel 14 (sodium) was inoperative. This, however, was caused by the inability to construct a tube with a mica window thin enough to pass a usable number of sodium $K_2$ photons. After considerable effort to make a suitable tube, the vendor finally recommended elimination of the sodium channel.

Detection of aluminum, silicon, sulphur, chlorine, potassium, calcium, titanium, chromium, and iron was very successful, with a mean detectable limit between 0.01 and 0.1%. Nickel and copper were identified with a mean detectable limit between 0.1 and 0.2%. Manganese was discernible within a mean detectable limit between 0.2 and 0.25%. The ability to resolve magnesium was rather poor, with a mean detectable limit of approximately 0.25%.

After the model D spectrometer, no further instruments were built, as modifications to the *Surveyor* payload required the deletion of this experiment.

### 3. Gas Chromatograph

*a. Introduction.* The gas chromatograph was to analyze volatile constituents in the lunar crust material. Samples of the lunar crust material were to be collected by the appropriate sampling devices on the *Surveyor* spacecraft and delivered to the gas chromatograph for analysis. The gas chromatograph was to have been capable of identifying the following 28 gaseous materials in concentration of equal to or greater than $1 \times 10^{-10}$ moles per sample.

(1) Hydrogen.
(2) Oxygen.
(3) Nitrogen.
(4) Carbon monoxide.
(5) Carbon dioxide.
(6) Water vapor.
(7) Methane.
(8) Ethane.
(9) Propane.
(10) Butane.
(11) Methanol.
(12) Ethanol.
(13) Propanol.
(14) Formic acid.
(15) Acetic acid.
(16) Butyric acid
(17) Formaldehyde.
(18) Acetaldehyde.
(19) Propionaldehyde.
(20) Acetone.
(21) Acetonitrile.
(22) Hydrocyanic acid.
(23) Benzene.
(24) Toluene.
(25) Ammonia.
(26) Hydrogen sulfide.
(27) Nitrous oxide.
(28) Hydrogen cyanide.

*b. Description.* A simplified schematic of the gas chromatograph appears in Fig. XXII-39. The delivered sample was passed through a funnel in the top of the chromatograph, into a small oven. The oven was then sealed by a pneumatically operated mechanism and heated to release gaseous material that might be in the sample. Gaseous materials thus liberated were injected into a helium carrier gas stream in the form of a tight slug. The sample gas stream was then divided and swept through analytical packed columns. Constituents of the sample gas had (more or less) affinity for the packing material in the columns. By means of adsorption and/or chemical equilibrium, passage of each constituent through the columns was impeded for a distinct, reproducible time interval unique for each unknown. This retention time was measured by a signal from a detector, located at the effluent end of each column, which was capable of sensing the presence of any unknown material other than the helium carrier gas. Outputs from the detectors were fed into the spacecraft for data processing and transmission back to earth. From these transmitted data, the identity and approximate quantity of each unknown volatile constituent in the sample was determined.

*1. Oven.* The oven was designed to accept a 3-$cm^3$ sample of lunar material. After the sample was sealed within the oven, it was heated to one of three temperatures (150, 325, or 500°C) selected on command. Oven seal leakage could not exceed $10^{-6}$ $cm^3$/sec of helium, which would represent a sample loss of 0.01% during the oven heating cycle. For obvious reasons, no organic materials could be exposed to the sample within the oven, which meant that the oven seal had to be metal-to-metal. Numerous sealing techniques were evaluated before a modified K-ring seal finally evolved. This seal was built into the oven cap. The upper surface of the oven, which sealed against this cap, was ground optically flat. This upper surface was made from Stellite, which has a Rockwell hardness of 60 to 62. The K-ring was heavily goldplated to eliminate any possibility of cold welding (due to the high lunar vacuum) to the upper surface of the oven during the seal. It was also necessary to provide a small brush of glass fibers imbedded in an epoxy resin so that any sample particles which landed on the sealing surface of the oven would be removed before allowing surface contact with the plated K-ring seal. This technique provided an oven seal which met the low-leak-rate requirement for over 100 consecutive sealings.

Mechanisms for moving the oven into different positions for accepting the delivered sample, sealing, and dumping the spent sample were actuated by double O-ring pneumatic pistons, which were pressured from the helium carrier gas cylinder. Many problems were encountered in designing the complex oven moving mechanism with sufficient structural strength to withstand the severe vibration environment.

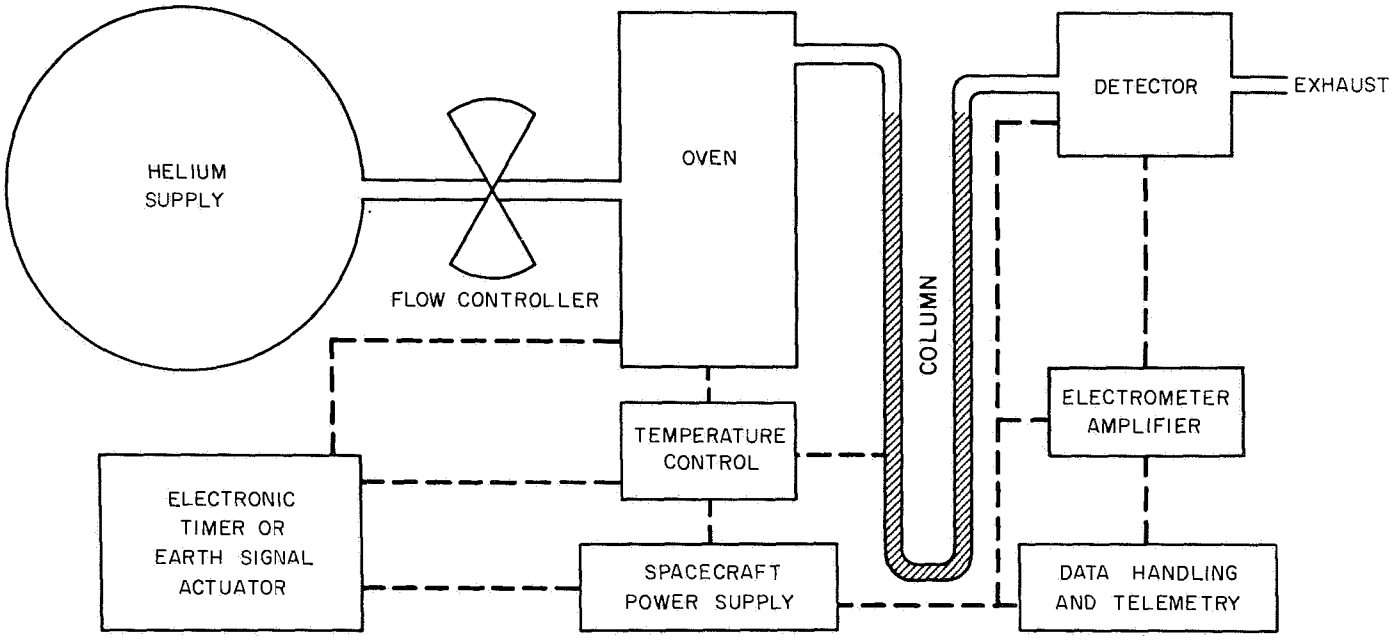



**Fig. XXII-39. Gas chromatograph schematic**

*2. Column and detector assembly.* The three parallel columns in the chromatograph were:

(1) A 7-ft molecular sieve column for separating the fixed gases.

(2) A 15-ft column was Carbowax 1540 on T-6 Teflon particle support for separating water and most of the hydrocarbons.

(3) A 12-ft column with Apiezon L, Carbowax 20M, and phosphoric acid on a support, called Chromosorb, for separating organic acids.

These columns were wound on the outside of a threaded magnesium mandrel together with a heater and temperature sensor element. A 7½-ft sample loop was wound on the inside of this mandrel.

The columns were temperature-controlled to 105°C. Electronics associated with the column temperature controller were mounted with the columns. Heat dissipated by the controller was used to partially heat the column and detector assembly. This column temperature controller provided full proportional temperature control and maintained the column temperature within 0.1°C. To prevent condensation on detector components, the detector block was maintained 5 to 10°C hotter than the columns. The assembly was enclosed in a super-insulation-covered box to reduce loss of heat by radiation and was structurally mounted by insulating mounting blocks.

The three detectors used in this chromatograph were glow discharge-type devices that acted electrically similar to a gas-filled voltage regulator tube. Figure XXII-40 shows a typical gas chromatograph detector signal. Under fixed conditions with a specific carrier gas (in this case, helium), the detectors had a specific breakdown voltage $V_d$. Introducing a contaminant gas (in this case, a sample component) to the carrier caused this breakdown voltage to change by an amount $U_p$. When the contaminant had passed, the breakdown voltage returned to its original value. These peaks of voltage as a function of time contained the information needed to identify the amount and type of sample component in the carrier.

One of the main problems which had to be overcome in the use of these detectors was that of zeroing the detectors in the absence of a sample. Many automatic

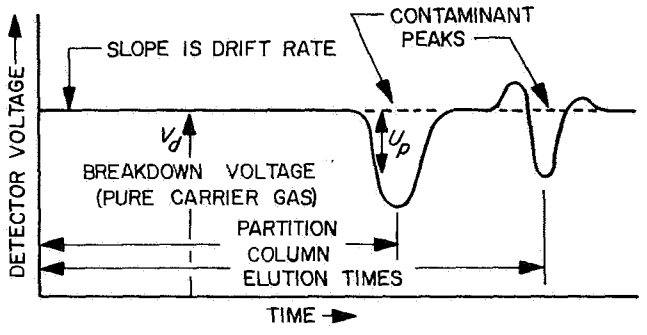



**Fig. XXII-40. Typical gas chromatograph detector signal**

servo-type systems were considered and discarded. It was finally decided to use a derivative readout of the chromatographic peaks, thereby eliminating the effect of DC drift associated with the breakdown voltage of the detectors.

3. *Pneumatic subsystem.* The pneumatic subsystem of the gas chromatograph consisted of a helium container, pressure regulator and solenoid valve, and a standard sample container.

The helium carrier gas container was a titanium sphere. The cylinder was designed to a burst pressure of 10,000 lb/in.$^2$, a proof pressure of 8000 lb/in.$^2$, and a working pressure of 6000 lb/in.$^2$ In use, the cylinder was loaded to 2200 lb/in.$^2$ at 25°C. This provided sufficient helium as carrier gas and as pneumatic operating gas for approximately 70 hr, or double that which would have been required to complete the lunar mission.

The pressure regulator, a two-stage regulator with the first stage regulating to 200 lb/in.$^2$, was completely temperature-compensated. The solenoid valve shut off the helium supply until needed.

The standard sample container, when properly actuated, injected a reproducible volume of the standard sample into the carrier gas. The sample volume delivered in each injection was approximately 0.15 cm$^3$.

4. *Sample valve.* The sample valve performed in coordination with the programmed pneumatic and electrical functions of the chromatograph. A motor-driven idler gear drove the geared pneumatic valve and a geared rotary switch. The pneumatic valve consisted of an optically flat drilled rotor with O-rings running against it for seals.

The O-rings, the most critical parts of the valve, had to meet leakage requirements over several hundred cycles and over the entire operating temperature range of −30 to 100°C. More specifically, those O-rings, made of Viton A, had to meet the following stringent demands:

(1) Withstand freezing in a static position during the lunar night and, on reaching operating temperature the second lunar day, regain the required resiliency to provide a satisfactory seal.

(2) Withstand lunar vacuum without deterioration.

***c. Development tests.*** The gas chromatograph was deleted from the payload, and consequently flight units were never built; however, a prototype model P-2 was constructed and tested. Before delivery, prototype model P-2 was acceptance-tested by the manufacturer to the requirements set forth in the JPL design and functional specifications, including determination of molecular weight of 28 gaseous materials from hydrogen to butyric acid. These 28 key materials were chosen so that the gas chromatograph would have a certain resolution capability consistent with its lunar mission. Of the 28 materials chosen, the instrument did not demonstrate the resolution requirement for the following six: formaldehyde, acetonitrile, hydrogen cyanide, carbon dioxide, hydrogen sulfide, and butyric acid. Formaldehyde and hydrogen sulfide appeared to be irreversibly adsorbed in the three columns and did not appear at the detectors. Acetonitrile was not satisfactorily resolved from hydrogen cyanide. Carbon dioxide could not be resolved on any of the three columns selected for this instrument, and the resolution required on butyric acid could not be demonstrated because this component would not elute from the column. Butyric acid appeared to be irreversibly adsorbed in the walls of the tubing and in the column itself.

The quantitative sensitivity specified for the gas chromatograph was $3 \times 10^{-10}$ moles for each of the 28 required materials. During the acceptance tests, the instrument failed to demonstrate the quantitative sensitivity for ethane. This requirement probably could have been met with some adjustment in the flow of the particular column.

Except for these deviations, all other specified requirements were demonstrated by the prototype model P-2 gas chromatograph. For example, the detector signal processor was demonstrated to have the required linearity, dynamic range, output level, and constancy of gain and zero over the operating temperature range of −30 to 100°C. Another demonstrated requirement was low helium leakages in the pneumatic components. The various pneumatic fittings, valves, etc., were required to have leakages of less than $10^{-3}$ or $10^{-4}$ cm$^3$/sec, depending on their location. During the acceptance tests, it was demonstrated that most leakages within the instrument were less than $10^{-6}$ cm$^3$/sec of helium.

In the development of the gas chromatograph, several mechanical and thermal environmental tests were run on components, subassemblies, and the complete gas chromatograph. In the thermal area, all subassemblies were reduced in temperature to that expected during the lunar night (approximately −185°C) and returned to normal operating temperatures with no loss in performance

capability. Items of major concern which passed these tests successfully were the Viton A O-rings, electronics, glass-insulated detectors, and Viton A diaphragms in the pressure regulator. All subassemblies passed the upper survival temperature limit, which corresponded with the upper operating-temperature limit.

The mechanical environment most severe to the gas chromatograph was the sinusoidal portion of the vibration encountered during launch. Components and subassemblies which passed individual vibration tests at least as severe as the type approval requirements were the rotary programming switch of the sample valve, the oven crucible, and the oven. An extensive vibration test was run at JPL on a portion of the gas chromatograph consisting of the complete case and structure of the chromatograph and some components. Components not included in this test specimen were simulated by dummy weights. Components present included the oven, the sample valve, and the column and detector assembly. The components represented by the simulated weights were the standard sample container, helium cylinder, solenoid valve and pressure regulator subassembly, and two electronics H-frame subassemblies. This test specimen was tested to the complex-tape portion of the type approval specification. The severity of the vibration test during the three-axes sweeps, caused seven accelerometers to vibrate loose. The results of the test showed that, except for the need for added stiffening in the cross panel, the overall structural integrity of the gas chromatograph was satisfactory. The stiffening was provided by a perpendicular partition with a curved cutout to provide room for the helium container. The design philosophy of the gas chromatograph was to provide a rigid structure with an overall resonance frequency of approximately 500 Hz. With this in mind, all subassemblies were mounted rigidly between the top and bottom panels of the chromatograph or to a perpendicular cross panel. Both the top and bottom panels and the cross panel were made from ⅜-in.-thick honeycomb aluminum, sandwiched between aluminum facing sheets. Inserts were provided in the honeycomb at places where various structures and subassemblies were fastened.

#### 4. Physical Parameters Instruments

*a. Introduction.* A series of experiments, at the beginning of the *Surveyor* Program, was designed to measure the physical parameters of the lunar surface. In 1962 it was decided that all of these experiments could be combined in one composite instrument known as the lunar parameters instrument. Designed in conjunction with a lunar drill, this composite instrument included the following instruments with the specified objectives:

(1) Density instrument to measure the density of the lunar material in its immediate neighborhood.

(2) Acoustic velocity instrument to measure the acoustic velocity between an acoustic source on the face and various depths in a drill hole.

(3) Magnetic susceptibility instrument to measure the AC magnetic susceptibility of lunar material surrounding the subsurface sonde at various depths.

(4) Temperature instrument to measure the temperature of lunar material at various depths.

(5) Thermal diffusivity instrument to measure the thermal diffusivity of lunar material at various depths.

(6) Caliper instrument to measure the average diameter of a drill hole at various depths.

The above instruments used a subsurface sonde (Fig. XXII-41). It was necessary that the total weight of the subsurface sonde be held to a minimum. A force of 15 lb was sufficient to drive the subsurface sonde into consolidated material making a hole with a diameter of 1.25–2 in., and the sonde was capable of withstanding a withdrawal force of 125 lb or less.

Another *Surveyor* instrument planned for measurement of physical properties, but not part of the subsurface sonde, was the penetrability instrument. Development work on all of these instruments ceased in 1963 when the *Surveyor* payload was redefined. At that time, work was still in progress defining the feasibility of these lunar experiments.

*b. Density instrument.* The density instrument (Fig. XXII-42) used the method of gamma-gamma logging in which a directed radiation source (approximately 40 millicuries of $Ir^{192}$) was located a known distance from a Geiger–Müller counter tube. Density was then derived from the knowledge that radiation received from the source due to scattering was related to the density of the material subjected to the experiment. Accurate measurements required that any background effects be accounted for. Background levels could be determined and any ambiguity in interpretation resolved by observing the level detected by the same Geiger–Müller tube prior to insertion in the hole (or unconsolidated material). The source was actuated through earth commands. Temperature corrections were to be made by measuring the temperature of the Geiger–Müller tube.

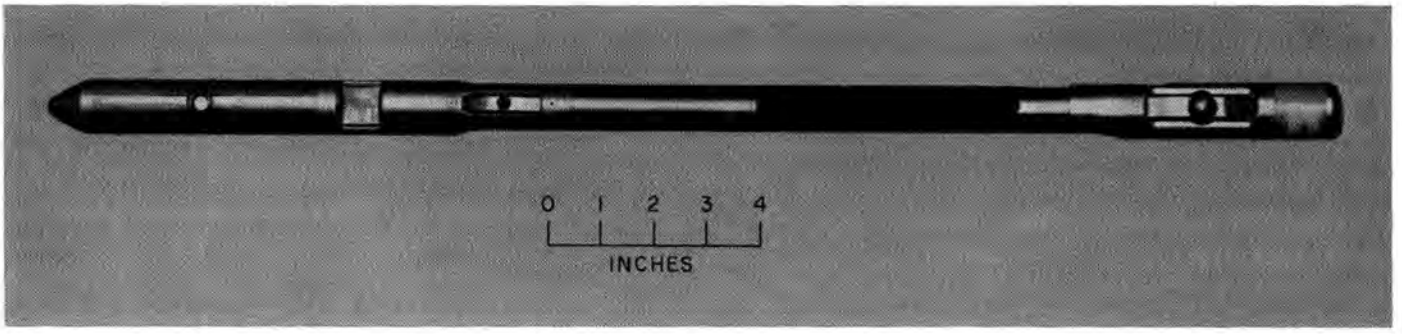



**Fig. XXII-41. Subsurface sonde**

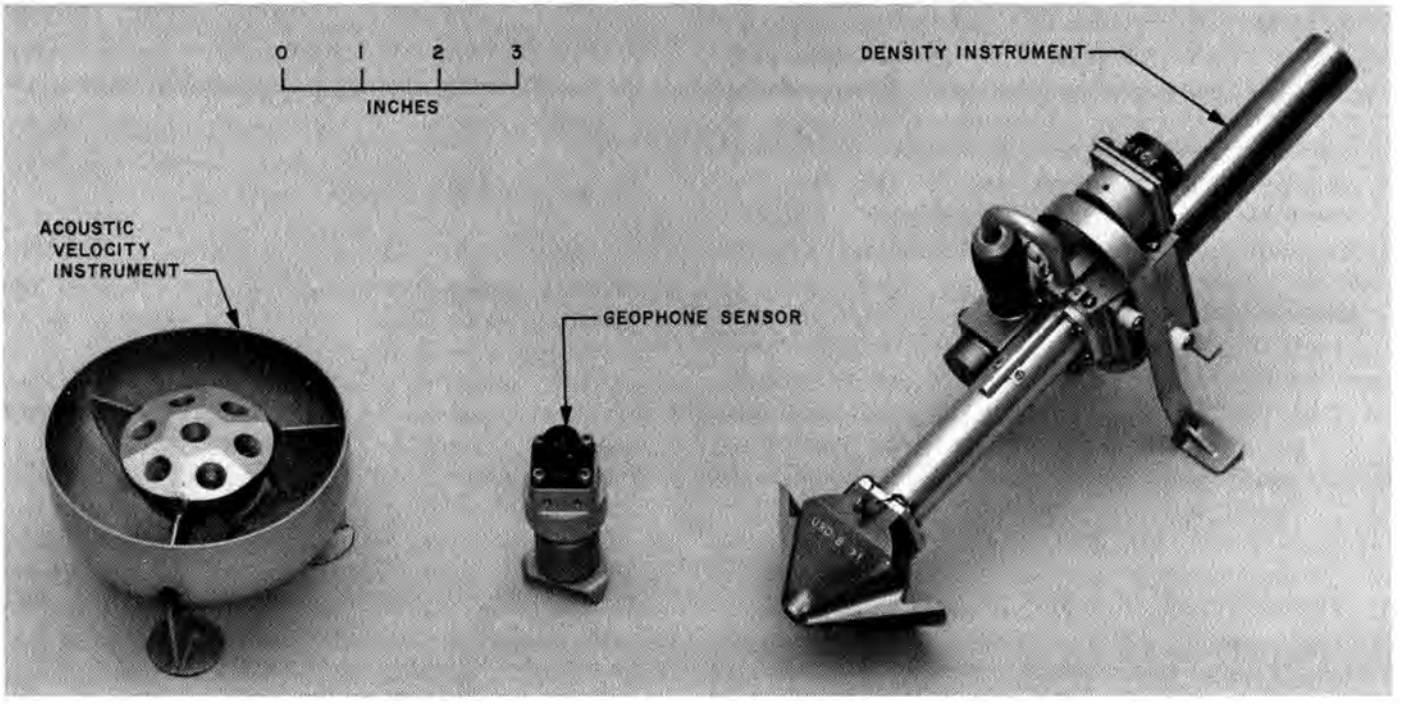



**Fig. XXII-42. Acoustic velocity instrument, geophone sensor, and density instrument**

*c. Acoustic velocity instrument.* The designed function of the acoustic velocity instrument (Fig. XXII-42) was to measure the speed of sound through lunar material. This was to be accomplished by (1) measuring the acoustic velocity between a known point on the lunar surface and a known point below the surface, (2) detonating a small explosive charge on the lunar surface, and (3) detecting the resultant signal transmitted through the lunar material. This signal was to be detected by using an acoustic sensor mounted on the subsurface probe and in pressure contact with the wall of the drill hole and two geophone sensors (Fig. XXII-43) deployed to the lunar surface. Acoustic velocity was to be determined from a knowledge of the separation of the acoustic source and detector and a measurement of the in-transit time of the acoustic signal. Proper decoupling between source and detector was required to ensure measurement through lunar material. Explosive charges were to be included in the surface acoustic source which was required both for surface and subsurface instruments. The instrument had the capability of measuring the acoustic velocities of the compression waves in the range of 300–25,000 ft/sec. Signal amplitude attenuation of a material varies as (1/distance) $\alpha$, where $\alpha$, may vary from 1–2.5 ft/sec.

*d. Magnetic susceptibility instrument.* The magnetic susceptibility instrument employed a transformer with

an output voltage vector variation proportional to the susceptibility and conductivity variation of the surrounding media. Measurements were made by measuring the input current and the susceptibility and conductivity vectors of the output voltage with the subsurface sonde in a known medium. These parameters were measured again with the sonde inserted in the lunar material. The difference between the output-voltage susceptibility vector amplitudes measured under these two conditions was proportional to the magnetic susceptibility. Data corrections were made possible by measuring the temperature of the transformer coils and the variations in input current. The output was reduced to zero to attain the required resolution and accuracy. Measurement capabilities of the instrument were:

| Parameter | Result |
|---|---|
| Range of susceptibility | $10^{-5}$ to $2 \times 10^{-1}$ cgs units |
| Resolution | $10 \times 10^{-6}$ cgs units |
| Conductivity | Undetermined |
| Sensitivity | Undetermined |
| Temperature sensitivity | Undetermined |

*e. Temperature instrument.* The temperature instrument provided the capability for measuring subsurface temperatures. Drill-hole-wall temperature or unconsolidated lunar-material temperature at various distances below the lunar surface was to be determined by two independent methods: a contact sensor and an interferometer spectrometer. Knowledge of the depth of each sensor below the lunar surface would then allow determination of the vertical temperature gradient in the lunar crust. The contact sensor was to be mounted on a bow-spring to ensure proper sensor-to-wall contact. The temperature instrument had the capability of measuring a range of hole-wall temperatures from 120 to 400°K.

*f. Thermal diffusivity instrument.* As the name indicates, the thermal diffusivity instrument (Fig. XXII-43) was designed for measuring thermal diffusivity. A protected radiant heat source was used to supply thermal energy to a small section of the borehole. The variation in hole-wall temperature was monitored by a detector located at the focus of a reflecting mirror. A semicylindrical window was used in front of the source and detector to protect the instrument from unconsolidated material. After empirical calibration, the rate of temperature rise of the detector was an indication of the diffusivity of the hole's wall. Body temperature was sensed with a separate sensor. The instrument had capabilities enabling it to accept:

| Parameter | Result |
|---|---|
| Range of hole-wall temperature | 120–400°K |
| Range of conductivity | $5 \times 10^{-1}$ to $1 \times 10^{-2}$ cal/cm²/sec/°C |
| Range of thermal diffusivity | $1 \times 10^{-6}$ to $2 \times 10^{-2}$ cm²/sec |

*g. Caliper instrument.* The caliper instrument was used to measure drill-hole size. Drill-hole size was measured by using the subsurface sonde decentralizer spring. This spring was mechanically coupled to a potentiometer in the hole to determine electrically the position of the spring relative to the side wall of the probe by recording the potentiometer slide wire position. The caliper could accept a range of hole sizes from 1.25 to 2.0 in. The caliper could exert a sidewise force of 3 lb at maximum (2-in.) extension.

*h. Penetrability instrument.* The penetrability instrument was used to investigate lunar surface hardness by recording the deceleration-time history of a dropped weight at three locations. Three weights (each containing an accelerometer) were allowed to drop a few inches in essentially free fall. The accelerometer output signal was used to empirically determine lunar surface hardness characteristics. Of the three weights used, two were to have compound points and one was to have a hemispherical impact point. The depth of penetration ranged between approximately ½ in. for soft materials, such as loose sand, and a few thousandths of an inch for very hard materials.

Required capabilities of the penetrability instrument were as follows:

| Parameter | Result |
|---|---|
| Range of hardness | Vacuum-sifted dust to quartzite |
| Range of drop heights | 7–25 in. (lunar) |
| Accelerometer linear range | 1–1500 $g$ (earth) |
| Accelerometer linearity | More than 5% |
| Repeatability between instruments | ±2.5% |

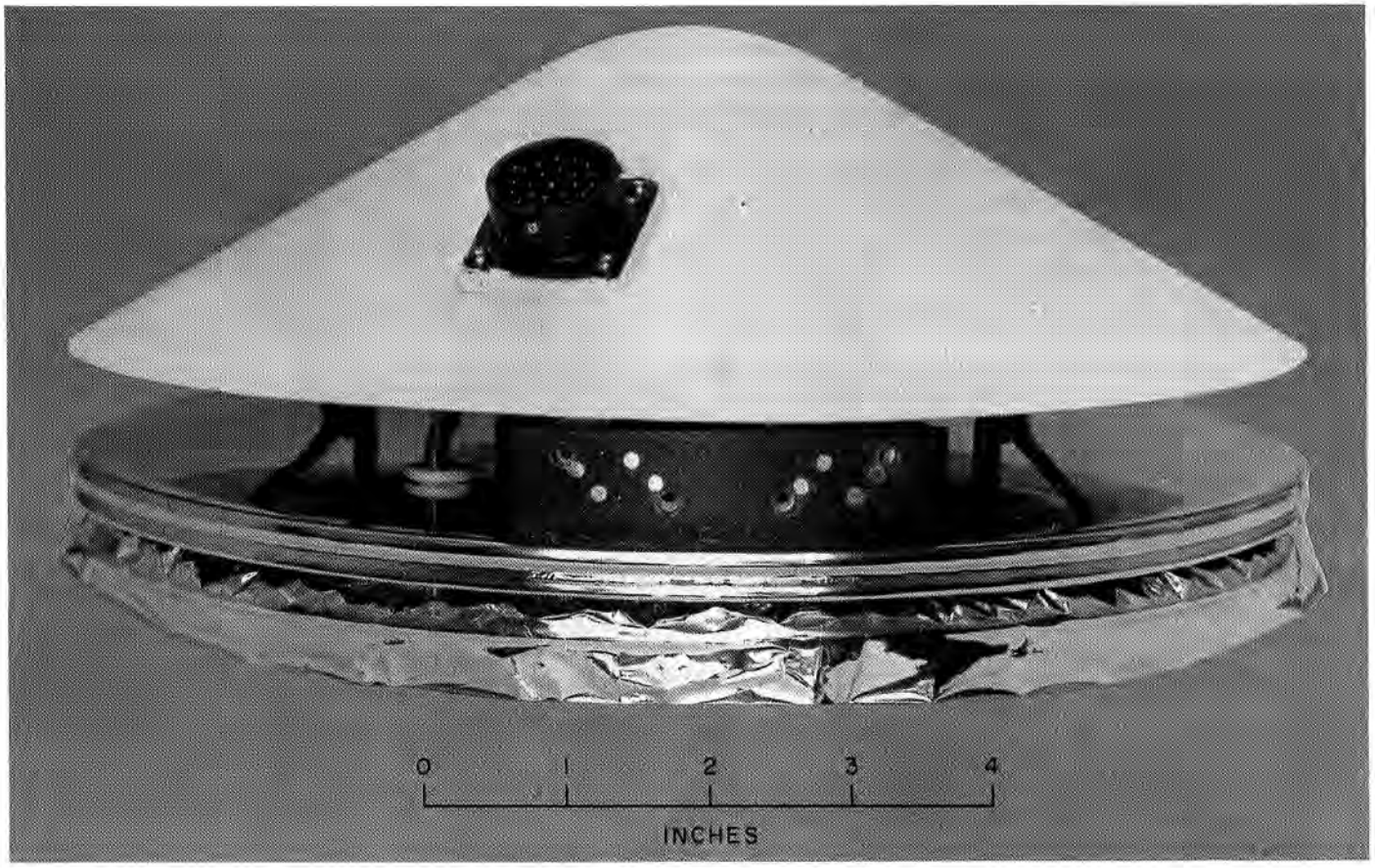



**Fig. XXII-43. Thermal diffusivity instrument**

### 5. Seismometer

*a. Introduction.* The objective of the seismometer was to provide data which could be used to determine physical properties and structural details of the moon as a geophysical body.

Although analysis of seismic activity recorded by devices similar to the seismometer was not a new area of exploration, certain mechanical constraints and unusual environmental conditions precluded the use of off-the-shelf devices and techniques for a lunar-based device. While earth-bound seismometers can be carefully placed, leveled, and adjusted as necessary, this seismometer had to be capable of performing all of these functions automatically and reliably. The development of a suitable seismometer which would compensate for lunar slope variations from the horizontal up to ±15 deg was needed for reliable seismometer performance. To accomplish the leveling function, two systems were employed. The first, a coarse-leveling mechanical system, reduced the angular error to less than 5 deg; the second, a servomechanism, accomplished the remaining leveling function necessary to maintain the seismometer longitudinal axis to within 10-min. of arc of lunar vertical.

The electrical and mechanical compliance of the seismometer had to encompass a 46 db (200:1) intensity range within a frequency range from 0.05 to 20 Hz. The upper frequency limit was imposed by the spacecraft telemetry equipment. An upper limit of approximately 300 Hz could have been realized from the seismometer.

The electrical output of the seismometer was an analog voltage signal. The spacecraft digitized this voltage for transmission to earth, where the electrical data was to be reduced to geophysical data.

*b. Development.* The original seismometer envisioned for *Surveyor* was a four-component instrument capable of being deployed to the lunar surface. The instrument was designed to have a surface compliance up to ±30

deg. The first prototype instrument, built by International Telephone and Telegraph Federal Laboratories, met all functional requirements except for weight. The instrument needed more development for use on the lunar surface, and before this could be carried out the *Surveyor* payload was redefined and work on the instrument ceased.

Later, in October 1962, NASA instructed JPL to develop a single-axis seismometer as a possible backup instrument for four missions which were, at that time, planned to follow the initial four *Surveyor* missions. The requirement was set forth that the single-axis seismometer be developed with minimum spacecraft redesign and testing. After extensive engineering evaluation, the feasibility of using the short-period vertical component of the original four-component seismometer in a modified form, as a single-axis seismometer, was demonstrated. In addition, a separate effort was launched to determine the feasibility of modifying a commercially available seismometer to operate reliably in the lunar environment. This seismometer was not considered a primary flight instrument but was envisioned for the purposes of investigation and possible backup use in the event that modification to existing flight-type hardware was not possible or practical. In particular, the development and procurement of springs which met the requirements of lunar operation posed a problem.

Figure XXII-44 shows the major assemblies of the single-axis seismometer. In September 1965, fabrication of two prototype and four flight seismometers was begun. By April 27, 1966, the last flight seismometer was delivered to JPL.

These seismometers were fitted with earth-type springs to allow testing under conditions of earth gravity. For the actual flight and subsequent lunar operation, it was intended to equip the sensors with springs made from an alloy, Elinvar Extra, that had a thermal elastic coefficient of expansion close to zero over the temperature range expected.

Acceptance testing of the six seismometers was performed at Geotech Corp., using a vibration table mounted on a seismic pier. Figure XXII-45 is a graph depicting the operation of the F-3 seismometer during these tests.

The F-3 seismometer successfully passed thermal-vacuum and vibration testing at type approval levels. The four flight seismometers did not undergo any flight acceptance testing, because of redefinition of the *Surveyor* payload, and were put in storage at JPL.

### 6. Touchdown Dynamics Instruments

***a. Introduction.*** The primary objectives of the touchdown dynamics instruments were to obtain data on the lunar surface character and to determine the spacecraft motions during landing. Data on the lunar surface would include information regarding contour in the landing area, and mechanical properties, such as coefficient of friction had it proved to be hard or the effect of surface penetration had it proved to be soft. Recording the spacecraft motions during landing would indicate the suitability of vehicles equipped with leg-type landing gears for operation in the actual lunar environment.

To meet experiment objectives, the approach was to equip the spacecraft with simple sensors of high reliability, and monitor their outputs during the landing. These sensors would measure:

(1) Three mutual orthogonal components of spacecraft translational acceleration.

(2) Three mutual components of spacecraft angular velocity about three mutually orthogonal spacecraft axes.

(3) Axial forces in the six landing leg struts and three shock absorbers.

(4) Angular position of each landing leg.

(5) Initial contact time of each footpad and crushable block.

Work was in progress on the engineering models of the instruments at HAC when, in 1966, the touchdown dynamics instruments were deleted from the scientific payload on *Surveyor* and work ceased.

***b. Description.*** The touchdown dynamics instruments design consisted of seven major items:

(1) Touchdown dynamics auxiliary assembly.

(2) Inertial measurement unit.

(3) Strain gages.

(4) Strain gage electronics.

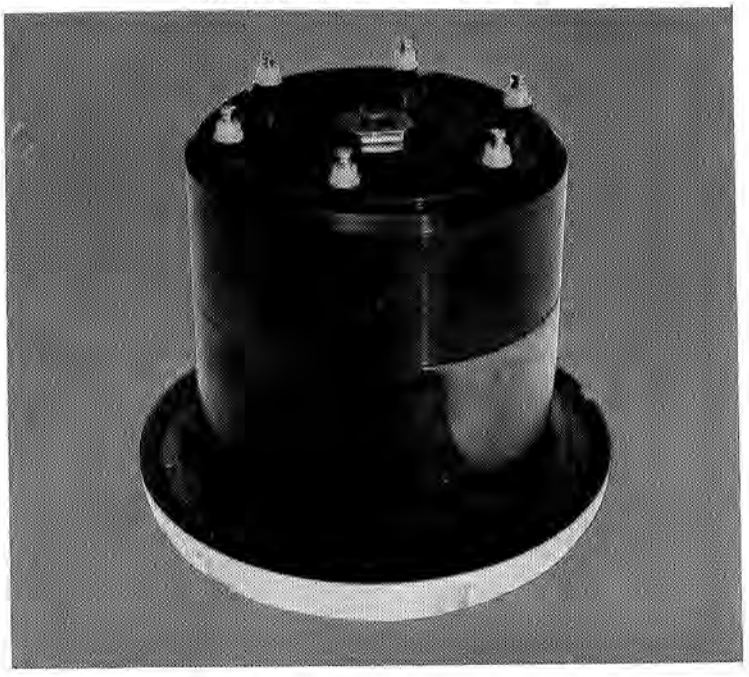
(5) Leg-position potentiometers.

(6) Contact switches.

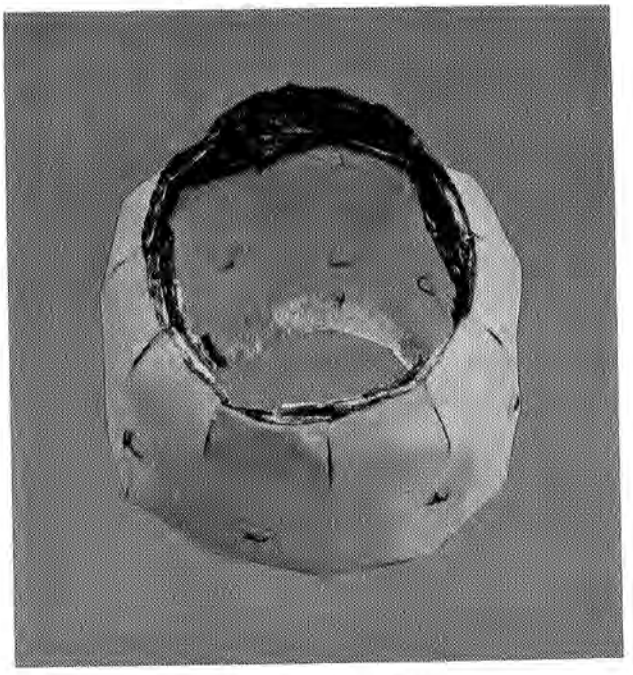
(7) Tape recorder.

The touchdown dynamics auxiliary assembly was designed to provide interface between the experiment and the *Surveyor* spacecraft. The functions were command

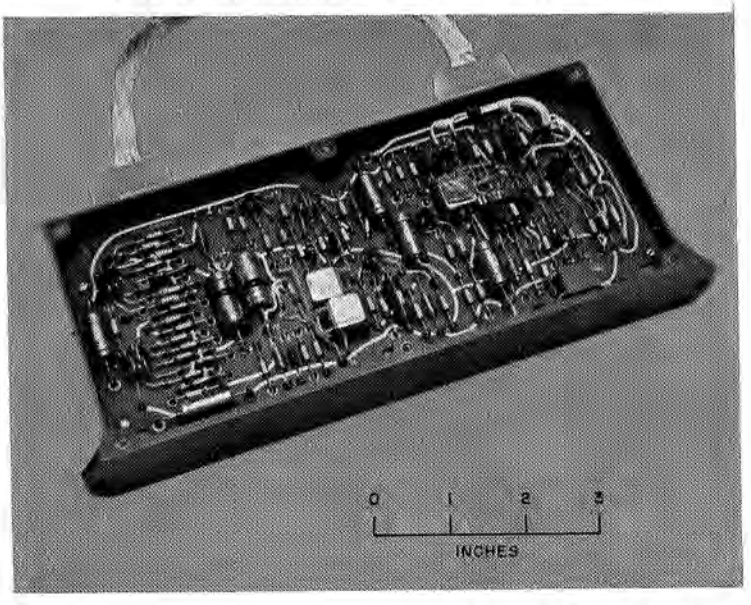
SENSOR MASS AND SPRING ASSEMBLY



RADIATION SHIELD ASSEMBLY



FLIGHT ELECTRONICS CIRCUIT BOARD AND HOUSING




THERMAL SHELL UPPER DOME



**Fig. XXII-44. Seismometer major assemblies**

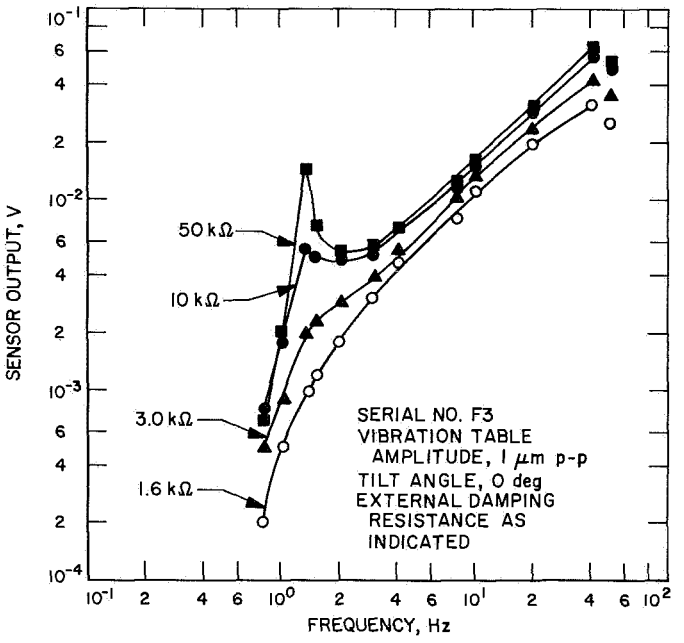



**Fig. XXII-45. Seismometer sensor frequency response curve**

decoding and signal processing, which included six subcarrier oscillators for real-time telemetry, power switching, logic, and calibration generation.

The inertial measurement unit consisted of three hermetically sealed and viscous damped rate gyros and three hermetically sealed and viscous damped linear accelerometers mounted in precise relationship to sense angular rates and linear accelerations about three mutually orthogonal axes. The unit included all electronics and power-conversion circuitry needed to enable the unit to operate from the 22-VDC unregulated bus and to provide signal outputs compatible with subcarrier oscillators in the tape recorder and the touchdown dynamics auxiliary assembly.

Strain gage bridges were applied to each spacecraft leg strut and shock-absorber strut. A total of nine bridges were required. Each bridge comprised four active strain elements. Active arms were located and oriented to cancel the effects of bending stresses and loop stresses, since the parameter to be measured was axial stress. Gages were of the foil type. The three strain gage bridges on each leg were excited by one power supply. A separate amplifier was provided for each bridge.

The strain gage electronics amplified and conditioned the outputs of the strain gages to a level suitable for recording. Three packages were provided, each including three amplifiers and the necessary power conversion and regulation for strain gage operation.

Three leg potentiometers were used to determine the extension angle of the landing gear legs during touchdown on the lunar surface. The leg-position potentiometers were located on the landing-gear hinge line of each landing gear. A linkage connected the rotating shaft of the leg-position potentiometers to a lower tube in the landing-gear A-frame, thus providing an electrical output proportional to the extension angle of the landing gear.

Contact switches were used to signal the time the footpads and crushable blocks contacted the lunar surface. One contact switch was located on the underside of each footpad and crushable block. The design objective was to determine relative time of contacts with the lunar surface.

The tape recorder with associated electronics was to be capable of recording simultaneously twenty-one channels of analog data, and one time-reference channel, using FM saturation recording. Sequential playback was provided, with the time reference and one selected data channel being played back each time. The recorder would use an endless tape loop and have an end of tape sensor. The recorder was capable of recording 65–75 sec of continuous data and playing back at the same tape speed used for recording. The recorder had one playback amplifier connected to the time reference channel head and a second playback amplifier switched to sequentially play back each of the recorded data channels. Sequencing was internal to the recorder. The FM signal obtained from the heads on playback was not demodulated but filtered and amplified only. The tape recorder was self-contained, requiring only 22-V power, pulse commands, and signal input and output connections.

Parameters which were to be recorded on the instrument tape recorder were:

(1) Angular positions of the three landing legs.

(2) Angular velocity about each of the spacecraft *X*, *Y*, and *Z* axes.

(3) Forces on left and right struts of each of the three landing legs.

(4) Forces on shock absorber of each of the three landing legs.

(5) Spacecraft velocity along each of the spacecraft *X*, *Y*, and *Z* axes.

(6) Spacecraft acceleration along each of the spacecraft $X$, $Y$, and $Z$ axes.

(7) Altitude mark of 13 ft.

(8) Initial contact time of each footpad and crushable block.

Data that was to be telemetered to earth in real-time were:

(1) Gyro outputs for $X$, $Y$, and $Z$ axes.

(2) Accelerometer outputs for $X$, $Y$, and $Z$ axes, including 13-ft mark. Table XXII-11 cites what the experiment sequence of events would be before and after touchdown $T$.

### 7. Micrometeorite Ejecta Detection Instrument

*a. Introduction.* The objectives of the micrometeorite ejecta detection instrument were to:

(1) Assist in the study of the evolutionary processes of the moon.

(2) Assist in the study of the nature of the lunar surface, as determined by interaction between the surface and the impacting particles.

(3) Evaluate the influx rate of interplanetary material on the lunar surface.

**Table XXII-11. Touchdown dynamics experiment sequence of events**

| Time, sec | Event | Event initiated by |
|---|---|---|
| $T-300$ | Turn on auxiliary assembly control logic | Earth command |
| $T-11$ | Turn on inertial measurement unit and auxiliary assembly | Delay-delayed burnout |
| $T-25$ | Tape recorder, strain gage electronics, and remaining power on | 1000-ft mark |
| $T-23$ | Start recording and calibration | Auxiliary assembly timer |
| $T-19$ | Stop calibration | Auxiliary assembly timer |
| $T+48$ | Subsystem off | Tape recorder end of tape signal |
| $T+$time compatible with other mission requirements | Play back recorded data | Earth command |

(4) Investigate the contribution of lunar ejecta material to dust particle distribution in interplanetary, cislunar, and near-earth space.

(5) Evaluate the hazards confronting manned and unmanned explorations of the lunar surface.

The approach to be used to meet the experiment objectives was to equip the spacecraft with sensors of high reliability and monitor their outputs after landing on the lunar surface. The sensor outputs, along with calibration data, would provide information regarding:

(1) Number of impacting particles.

(2) Mass of each particle.

(3) Mass of distribution of events.

(4) Speed distribution, from momentum and kinetic energy measurements of each particle.

The instrument was deleted from the *Surveyor* scientific payload and work ceased in 1966.

*b. Description.* The micrometeorite ejecta detection instrument design included three major items: an auxiliary assembly, a sensor head, and an electronics unit.

The instrument was developed by W. M. Alexander of the Goddard Space Flight Center, and the flight instrument was fabricated by Marshall Laboratories, Inc., of Torrance, Calif.

The auxiliary assembly was designed to provide interface between the instrument and the *Surveyor* spacecraft. The functions performed by the assembly included command decoding, signal processing, thin film protection, and experiment power management. Electronic components required to accomplish these function include a subsystem command decoder, two power switches, a $-12$-VDC electronic conversion unit, and one subcarrier oscillator. Current limiting protection was provided for both the 22-V power to the electronic conversion unit and the 29-V switched power. The subsystem decoder received signals from the central command decoder and decoded all commands addressed to the micrometeorite ejecta detection experiment. Six input command pulses were required by the instrument:

(1) Power on.

(2) Power off.

(3) Film protection emergency off.

(4) Readout command.

(5) Calibrate command.

(6) Clear command.

The signal processing channel used one subcarrier oscillator with necessary filtering and attenuation circuitry. The subcarrier oscillator received its input from a commutator in the electronics unit. The subcarrier oscillator output was routed to summing amplifiers in the central signal processor for transmission via the telecommunications subsystem.

The sensor head consisted of a pair of thin-film capacitor plates (approximately $8 \times 10$ in.) mounted on opposite sides of a sounding board to which an acoustical transducer (microphone) also was bonded. A second acoustical transducer was bonded to the sounding board to serve as a calibration stimulus.

In operation, ejecta particles, arriving from side A or side B, first pierced the film and then struck the sounding board. As the film was pierced, a momentary discharge of the thin-film capacitor delivered a signal to the film amplifiers which indicated direction of the hit and supplied an output signal for pulse-height analysis. This latter signal was related to the kinetic energy of the incoming particle. To guard against the possibility of a short circuit disabling the capacitor circuits, a current pulse was available to burn away the shorting particles. A short circuit was indicated by the film status circuit, which added a count to the film accumulator register. A $-12$-V film protection voltage was supplied to the thin-film capacitors by the auxiliary assembly any time internal power was not supplied. This kept the capacitors charged and prevented the accumulation of shorts while the sensor was not in operation. After piercing, the thin-film particles impacted upon the sounding board and were detected by the acoustical transducer. The signal from the acoustical transducer was related to the impulse delivered to the sounding board by the impacting particle. This signal, a function of the momentum, was pulse height analyzed and stored for readout.

The electronics unit contained pulse-height analysis circuitry, accumulation registers, power supply, capacitor-film clearing circuitry, detector-calibration circuitry, noise-coincidence circuitry, and commutation circuitry. Capacitor film and microphone signals from the sensor head were sent to the electronics unit for pulse-height analysis. Every impact on the sensor, above threshold, was counted and stored in the accumulation registers. During intervals when no ejecta impacts occurred, the commutator cycled once every 10 sec. When a particle hit occurred, the commutator cycled one time and read out the data from the pulse-height analysis circuits and from the other registers. As the commutator cycled, it generated a 19-bit data word readout at 100 bits/sec. Data content of the word bits appear in Table XXII-12.

**Table XXII-12. Word-bit data**

| Bit | Character | Function |
|---|---|---|
| 1 | 0 | Three-bit sequence, signaling the start of the 19-bit sequence |
| 2 | 0 | |
| 3 | 1 | |
| 4 | X | Three-bit number, giving pulse-height-analysis information |
| 5 | X | |
| 6 | X | |
| 7 | X | Identification of which side of film impacted |
| 8 | X | |
| 9 | X | Four-bit number giving pulse-height-analysis information |
| 10 | X | |
| 11 | X | |
| 12 | X | |
| 13 | X | Three-bit number giving contents of microphone accumulator |
| 14 | X | |
| 15 | X | |
| 16 | X | Spacecraft noise-coincidence detector |
| 17 | X | Three-bit number indicating contents of film accumulator |
| 18 | X | |
| 19 | X | |

### 8. Soil Mechanics

*a. Introduction.* The soil mechanics experiment was devised in 1961 with the following objectives:

(1) In cooperation with the TV cameras, to provide a qualitative evaluation of the lunar surface response to applied stresses by means of surface pictures before and after instrument operation.

(2) To determine whether the lunar surface has a yield strength within the maximum force limitations of the soil mechanics instrument, at the point tested by the instrument.

(3) To classify the penetrability of the lunar surface material in qualitative terms of lunar model, material type, discontinuities, and nonhomogeneities, at or below the surface.

(4) To calculate engineering properties describing the lunar surface material in the yield process, including bearing and shear strength.

(5) To determine empirical parameters describing the lunar surface material in flow-type behavior, permitting evaluation in terms of surface trafficability for land locomotion studies.

The approach used to meet the experiment objectives was to design an instrumented mechanism capable of imparting bearing and shear forces to the lunar surface in close proximity to the spacecraft. Sensors were included to measure:

(1) Bearing force applied to two circular flat penetration pads of different area.

(2) Penetration displacement of two penetration pads.

(3) Penetration displacement of a shear device.

(4) Bearing force applied to a shear device.

(5) Angular force applied to a shear device.

(6) Angular displacement of a shear device.

Evaluation of the sensor data would lead to quantitative determination of the following properties of the lunar surface:

(1) Density.

(2) State of compaction.

(3) Shearing or crushing strength.

(4) Angle of internal friction.

(5) Compressibility.

(6) Elastic modulus or moduli.

(7) Coefficient of sinkage.

After a series of design reviews and an attempt at a redesign by JPL, it was concluded that certain elements of the design of this instrument would not allow it to work on the lunar surface and work on the instrument was terminated in April 1963.

***b. Description.*** The soil mechanics included three major items: a soil-mechanics instrument, an instrument positioner, and an instrument auxiliary.

The soil mechanics instrument consisted of two bearing plates and a shear ring, held together by a triangular framework. Bearing-strength measurements were performed by applying thrust to the bearing plates and continuously monitoring displacement and thrust until a maximum of 9-in. displacement of approximately 30-earth-lbf thrust was reached. A prototype of the complete instrument is shown in Fig. XXII-46.

Shear strength was determined by applying torque to a spudded angular ring under a series of three axial loads. At each load, torque was measured as a function of angular displacement. The determination of maximum torque provided the relation between shear strength and applied normal stress which could be expressed in terms of effective cohesion coefficient and friction angle of the soil.

The instrument temperature was measured by monitoring the no-load output of the strain gage bridges. If the instrument temperature was within operating limits, the device would be extended approximately 15 in. by a spring-actuated tube into the field of view of the survey TV camera, and lowered as much as 16 in. by a deployment motor, until the bearing and shear plates were approximately 1 in. above the lunar surface. A sensor switch activated with less than 0.1-lb/in. force on contact with the lunar surface and stopped the deployment motor. An explosive pinpuller was provided to drop the instrument to the lunar surface in the event of failure of either the horizontal or vertical deployment mechanisms.

The soil mechanics positioner was a one-shot spring–actuated mechanism used to deploy the soil mechanics instrument after lunar landing. The purpose of the positioner was to locate the instrument in a position where lunar soil testing could be viewed by TV camera. The positioner consisted of one stationary tube rigidly attached to the spaceframe and two telescoping tubes contained within the stationary tube.

The stationary tube was mounted to the spaceframe at one end with a bracket that encircled the tube to which it was bonded. The bracket represented a split clamp configuration in attaching to the spaceframe. The stationary tube was attached, at its center, to the spaceframe by a bonded bracket. This bracket also mounted an explosive pinpuller.

The positioner was to be locked in the stowed position during launch, flight, and touchdown by an explosive pinpuller. The instrument was held by the positioner and by a bracket attached to the spaceframe.

In the deployment sequence, the instrument was lowered by its deployment motor until the sway bracket pins were cleared by the instrument. With the instrument in this position, the positioner pinpuller was actuated.

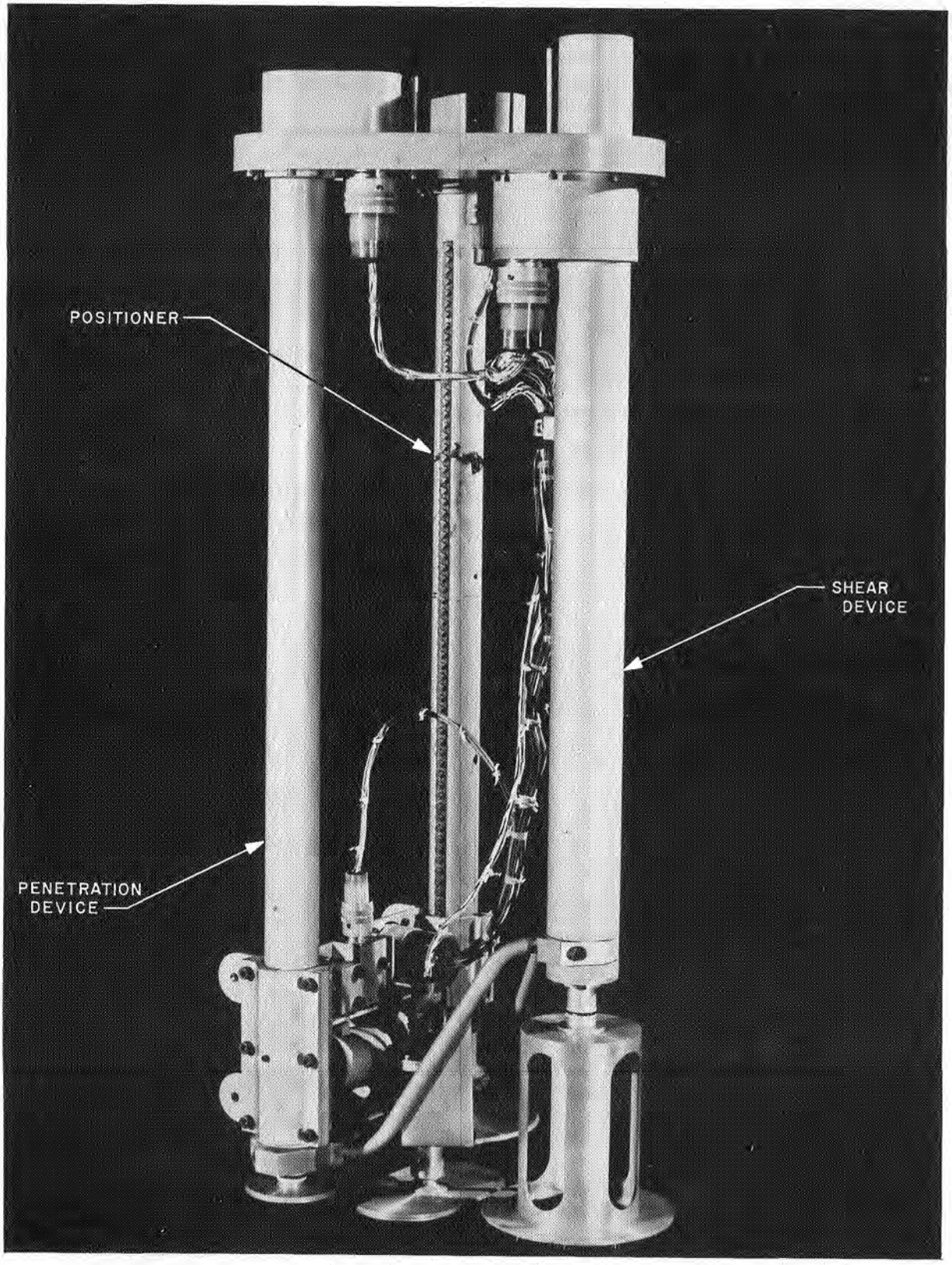



**Fig. XXII-46. Prototype soil mechanics instrument**

Free of this restraint, the spring contained within the positioner tube propelled the instrument to its extended position. The positioner was guided out and maintained in an upright position by an antirotation guide-rail bonded to the tubes and located in stationary and middle tubes. Outward stopping and positioning of tubes were attained by seating of two male and female self-locking tapered cones. These cones were located internal to the mechanism and bonded to the tubes. The three tubes used in the mechanism were made from standard aluminum tubing. There was no machining necessary on the tube diameters. The individual fitting of each of the cone rings (female) and end rings (male cone) to its respective tube eliminated the necessity for close tolerances on the tube diameters.

Designed to provide electrical interface between the soil mechanics and the *Surveyor* spacecraft, the soil mechanics instrument auxiliary assembly was used also to command decoding, signal processing, and power switching.

Command decoding was implemented by the use of a 20-channel subsystem decoder. Commands required for this instrument included:

(1) Temperature sensor power on.

(2) Temperature sensor power off.

(3) Potentiometer and strain gage power on.

(4) Potentiometer and strain gage power off.

(5) Deployment motor power on.

(6) Deployment motor power off.

(7) Energize explosive pinpuller.

(8) Small bearing plate motor power on.

(9) Small bearing plate motor power off.

(10) Large bearing plate motor power on.

(11) Large bearing plate motor power off.

(12) Shear trust motor power on.

(13) Shear thrust motor power off.

(14) Shear torque motor power on.

(15) Shear torque motor power off.

Signal processing was implemented by using a modified channel commutator employed to time-multiplex instrument outputs to the central signal processor. Signals required to be processed from the instrument included:

(1) Force exerted by small bearing-plate penetration unit.

(2) Force exerted by large bearing-plate penetration unit.

(3) Linear force exerted by shear unit.

(4) Torsional force exerted by shear unit.

(5) Displacement of small bearing-plate penetration unit pad.

(6) Displacement of large bearing-plate penetration unit pad.

(7) Displacement of shear unit pad.

(8) Angular displacement of shear pad.

(9) Voltage applied to strain gages.

(10) Voltage applied to displacement gages.

(11) Temperature sensor.

Power switching included three current limiting switches to regulate maximum torque of the vertical deployment and bearing-plate motors. Four regulated-voltage sources were provided for control of the shear device bearing and rotational motors.

## References


XXII-1. Smokler, M. I., "Calibration of the *Surveyor* Television System," *J. SMPTE*, Vol. 77, No. 4, pp. 317–323, Apr. 1968.

XXII-2. Harrington, T., and Marshall, J. H., "Pulse-Height Analyzer for Charged Particle Spectroscopy on the Lunar Surface," *Rev. Sci. Instr.*, Vol. 39, No. 2, pp. 184–194, 1968.

# XXIII. Summary of Recommendations

This section summarizes recommendations for consideration on future projects based on *Surveyor* Project experience. Emphasis has been placed on recommended procedures and design features which were not implemented on *Surveyor* or which deserve greater attention than was given early in the *Surveyor* Project. No attempt has been made to include all the features and techniques that were fully implemented and are described in other sections of this report.

## A. Technology

In the use of multiple-beam, single-frequency doppler radars, protection against cross-coupled lockups of one receiver tracker on a side-lobe of another beam should avoid the technique used on *Surveyor* of breaking the beam lock. This technique disabled the radar until relock, and without the roll constraints which were imposed, could have been as catastrophic to successful landing as a cross-lobe lock. A better technique would have been to introduce nonlinearity in the IF amplifier or in the RF system to cause small signal suppression, that would completely avoid locking onto a low-power side-lobe in the presence of the main power return.

Magnetically coupled isolators for telemetry of power and current measurements should be considered instead of the direct-coupled shunts used on *Surveyor*. The direct coupling proved to give noisy data, and considerably compounded the common ground loop problems with the spacecraft. Also, the capability for simultaneous transmission of scientific and engineering data should be designed into the spacecraft system. Inability to monitor spacecraft conditions during science instrument data periods made it necessary to reconfigure the spacecraft periodically for engineering data. This resulted in lost time and data for both science and engineering.

Where independent gas pressurization systems are used (such as the fuel and attitude control systems on *Surveyor*), incorporation of emergency cross-feed valves should be considered to permit alternate gas use for increased reliability.

The use of parabolic antennas makes sun pointing impossible; sun pointing could damage feed components at the focus. Planar arrays, light-opaque Fresnel lenses, or RF transparent covers should be used.

Conductive thermal switches were very effective temperature control devices when they operated properly at the required set point. However, further materials investigation should be carried out and rigorous qualification testing conducted to assure switches of high reliability.

For multimission projects, flexibility for change of telemetry measurements from mission to mission should be designed into the data processing system. Data channel changes of engineering measurements on successive *Surveyor* missions, as a result of the experience on previous flights, required harness rewiring which was difficult and jeopardized established reliabilities.

Proprietary designs should be approached with caution because system analyses and tradeoffs are difficult to make without in-depth knowledge of design. Lack of this knowledge for integrated components can lead to serious functional problems.

Monte Carlo techniques should be considered for obtaining quantitative statistical performance evaluations leading to optimum allocations of nominal parameters and tolerances. Monte Carlo techniques are effective in realistically integrating system element dispersions to obtain realistic design and operating margins and to assess performance of complex systems.

## B. Qualification Testing and Quality Assurance

Configuration control of low unit production spacecraft should not be encumbered with the mass production (military standard) unit serialization and modification system used on *Surveyor*. This system changed the serial number of each unit as major modifications or retrofits were made, making unit tracing and histories almost impossible.

In a lengthy program, such as *Surveyor*, reliance on initial parts qualification tests at the beginning of the program is not sufficient. Due to changes in manufacturing techniques, changes in materials suppliers, and personnel turnover in the component manufacturing area, it is necessary to continue requalifying parts by batch and sample testing and sometimes by 100% testing to assure a continued supply of uniformly acceptable parts.

On projects of this type, two quality assurance techniques which should be applied are high-power microscopic inspection and in-line/in-series (tollgate) inspection. Tollgate inspection compensates for shortcomings associated with limited production runs, which are not readily adaptable to standard inspection methods associated with large serialized runs.

The Project Office should insure an effective reliability program by continuous sponsorship throughout the life of the project. The trouble/failure report system proved a very powerful tool in assuring the launch readiness of the *Surveyor* spacecraft; however, it must have continuous high-level management attention to be effective.

Complete validation of components must be made before assembly into subsystems and validation of subsystems before integration into the systems test and operations. This necessitates care to assure a proper cone of tolerances wherein no subunit, once qualified to its tolerances, can fail to pass the tolerances on the next higher level of assembly qualification.

Spacecraft should be designed with adequate performance margins in all areas to permit complete and repeatable demonstrations of required deep-space performance in earth-based test environments. The *Surveyor* radar altimeter and doppler velocity sensor (RADVS) illustrates the importance of this concept. The RADVS was designed for only 4.5 min of actual mission operation. However, during testing, the RADVS was required to operate for longer periods; this necessitated an auxiliary blower. Extensive test setup time was required for installation of this blower, and unit damage was repeatedly experienced during solar-thermal-vacuum testing due to overheating problems.

Requirements should be established and the system designed for easy test accessibility, manufacturability, and maintainability, including:

(1) Appropriate built-in test connectors in harnesses to minimize make/break of flight connectors and associated flexing of the harnesses.

(2) Wiring harnesses designed for realistic handling requirements. This implies sufficient wire size, insulation, and service loops, even at the expense of additional weight.

Structural/flight control interaction of low-level buzz tests should be conducted at the system level. A reasonable range of force inputs should be used so that it can be observed that the effects of structural nonlinearities at high levels do not give lower control-loop amplifications than those at low levels where the system acts linearly without limiting.

System level flight acceptance tests should include solar-thermal-vacuum, vacuum profile (including decompression), and vibration–shock environments at expected upper bound flight levels to uncover latent defects not detected at unit or subsystem level or in ambient system level test.

For a highly complex spacecraft system like *Surveyor*, in addition to the proof test model a system level engineering model spacecraft should be provided and maintained in the latest configuration to permit system level problem solving and the proofing of changes. This spacecraft should be the pathfinder for hardware and procedural changes which would otherwise pose a risk to the integrity and test schedules of the proof test model or flight spacecraft by involving one or more of them in experimental cut-and-try-type actions.

System test techniques should include the automatic programming of tests with automatic alarm for repeated out-of-tolerance responses from the spacecraft. The incorporation of such techniques on *Surveyor* effected a vast improvement in test proficiency, including major reductions in the amount of time required to perform spacecraft tests and prelaunch checkout.

Test facilities should incorporate all necessary safety provisions to permit complete spacecraft design and flight system validation in areas and in tests which might otherwise be minimal or completely omitted because of their hazardous nature. Prime examples are propulsion, pyrotechnic, radioactive, and pressurized components and subsystems.

Spacecraft testing should include a rigorous, mission-like validation of the spacecraft–DSN interface as an element of spacecraft design certification. A test phase involving the extended operation of a test spacecraft at Goldstone in conjunction with necessary elements of the DSN proved extremely beneficial to *Surveyor*.

Careful consideration should be given to human factors in the design of test equipment and procedures to preclude faults and failures being induced into the test program through human errors or oversights during periods of stress.

In computerizing the processing and display of spacecraft hardline and telemetry data, the hardware and software that are generated should be applicable to both system test and flight operations. This would result in minimum transition between test and flight phases of spacecraft operations and permit the same performance criteria and assessment techniques to apply. Duplications in hardware, software, and analysis personnel would be minimized, and a better overall base for the conduct of flight operations would be established.

Computer programs developed for automatic monitoring, English unit conversions, and alarms during spacecraft testing must be written in modular blocks to permit the flexibility demanded by varying spacecraft parameters and test requirements.

Consideration should be given to the utilization of integrated ground command and control using automatic sequencing for time-critical functions. Examples of the flexibility provided by this concept on *Surveyor* were: the ability to turn off *Surveyor III* flight control power by command from the ground, the nonstandard terminal descent of *Surveyor V*, the postlanding hop experiment of *Surveyor VI*, and the use of the soil mechanics/surface sampler to assist alpha scattering instrument deployment on *Surveyor VII*. The flexibility provided by a ground command system, however, requires that careful consideration be given in the design to protective features for potentially destructive and nonreversible functions. Interlock commands were incorporated into the *Surveyor* system for critical command functions.

## C. Contractual Aspects

Extreme care should be given to the exact method and philosophy of providing technical direction to the contractor. To maintain consistency, integrity, and effectiveness during the life of the contract, it is recommended that all technical direction given to a contractor:

(1) Be delivered to the contractor in writing as clear and succinct as possible; the direction should always contain the reasons why the directive is being issued.

(2) Be cleared through a single focal point to ensure consistency and appropriateness from an overall systems view.

(3) Be screened by the cognizant procurement personnel for consistency with the provisions of the contract.

(4) Be acknowledged by the contractor as to receipt and implementation.

(5) Be followed by JPL as to the contractor's response and performance.

At the outset of the project or the contract, it should be carefully decided what documentation will be or will become controlling and the precise method by which that documentation will be changed if such changes are necessary during the course of the contract. Normally, the less documentation which exists to control and describe the contractor's performance requirements, the more likely confusion and disputes will arise regarding that performance.

Extreme care should be given to the selection of discrete work packages on which the contractor will be estimating and performing work during the life of the contract. Selection of work packages which are easy for JPL to understand may be difficult categories on which to report because of the contractor's internal organization or cost control system. The ease of reporting and analysis should be predominant criteria for establishing these work packages.

It is recommended that cost monitoring on large projects be designed to operate on an exception basis. The system should be structured to highlight deviations from previous estimates and other abnormal or unusual trends and occurrences so they can be evaluated rapidly and in appropriate depth.

# Glossary

| | |
|---|---|
| AAL | automatic acceleration limiter |
| ABC | auxiliary battery control |
| A/D | analog-to-digital |
| A/DC | analog/digital converter |
| AESP | auxiliary engineering signal processor |
| AFC | automatic frequency control |
| AFETR | Air Force Eastern Test Range |
| AGC | automatic gain control |
| AGE | aerospace ground equipment |
| AMR | altitude marking radar |
| APC | automatic phase control |
| ARPA | Advanced Research Projects Agency |
| AS | alpha scattering |
| ASACG | Alpha Scattering Analysis and Command Group |
| ASFOD | assistant spaceflight operations director |
| ASI | alpha scattering instrument |
| A/SPP | antenna/solar panel positioner |
| AVS | altitude velocity sensor |
| BCD | binary-coded decimal |
| BCR | battery charge regulator |
| BDA | Bermuda station |
| BECO | booster engine cutoff |
| B/R | booster-regulator |
| CCD | central command decoder |
| CC&S | central computer and sequencer |
| CCSLL | cross-coupled side-lobe logic |
| CDC | command data console |
| CDS | computer data system |
| CPC | command preparation and control |
| CPCG | command preparation and control group |
| CRO | Carnarvon (Australia) radar designation; cathode-ray oscilloscope |
| CRT | composite readiness test |
| CSP | central signal processor |
| CST | combined systems test |
| CSTS | combined systems test stand |
| CTL | consent-to-launch |
| CTS | consent-to-ship |
| CW | continuous wave |
| DC | direct command |
| DET | design evaluation test |
| DFR | dual frequency receiver |
| DIS | data input subsystem |
| DPS | data processing system |
| DSIF | Deep Space Instrumentation Facility |
| DSN | Deep Space Network |
| DSS | Deep Space Station |
| DVS | doppler velocity sensor |
| ECA | engineering change authorization |
| ECO | engineering change order |
| ECP | engineering change proposal (plan) |
| ECR | engineering change request |
| ECU | engineering conversion unit |
| EDR | engineering data reduction |
| EMA | engineering mechanism auxiliary |
| ESF | explosive-safe facility |
| ESP | engineering signal processor |
| FA | flight acceptance (test, testing) |
| FACT | flight acceptance composite test |
| FAR | flight altitude radar |
| FCSG | flight control sensor group |
| FPA | flight path analysis |
| FPAA | flight path analysis area |
| FPAC | flight path analysis and command |
| FSG | Flight Support Group |
| G&A | general and administrative |
| GCF | ground communications facility |
| GD/A | General Dynamics/Astronautics |
| GD/C | General Dynamics/Convair |
| GDHS | ground data handling system |
| GHE | ground handling equipment |
| GSE | ground support equipment |
| HAC | Hughes Aircraft Company |
| HSD | high-speed data |
| HSDL | high-speed data line |
| IF | intermediate frequency |
| I/O | input/output |
| IRIG | interrange instrument group |
| ISCO | integrated systems checkout |
| J-FACT | joint flight acceptance composite test |
| KPSM | klystron power supply modulator |
| KSC | Kennedy Space Center |
| LASR | Laboratory for Astrophysics and Space Research |
| LeRC | Lewis Research Center |
| LF | low frequency |

## Glossary (contd)

| | |
|---|---|
| LOC | launch operations console |
| LOS | loss of signal |
| LP | launch platform, launch pad |
| LV | launch vehicle |
| LVPS | low-voltage power supply |
| MAC | maneuver analysis and command |
| MACG | maneuver analysis and command group |
| MAPAR | material and process acceptance requirements |
| MC | midcourse |
| MCDR | media conversion data recovery |
| MCDRS | media conversion data recovery subsystem |
| MCFR | media conversion film recording |
| MCFRS | media conversion film-recording subsystems |
| MDL | master data library |
| MECO | main engine cutoff |
| MES | main engine start |
| MO | mission operations |
| MOPS | mission operations paging system |
| MOS | Mission Operations System |
| MPC | mandatory product control |
| MPS | main power switch |
| MRB | Materiel Review Board |
| MS | mission sequence |
| MSA | mission support area |
| MSFC | Marshall Space Flight Center (Huntsville, Ala.) |
| MSFN | Manned Space Flight Network |
| MTGOP | midcourse and terminal guidance operation program |
| MTGS | midcourse and terminal guidance system |
| MVA | mechanism vehicle assembly |
| NAA | narrow-angle acquisition |
| NACA | National Advisory Committee for Aeronautics |
| NAMG | narrow-angle Mars gate |
| NASC | National Aeronautics and Space Council |
| NASCOM | NASA Communications Network (worldwide) |
| NAS—NRC | National Academy of Sciences—National Research Council |
| NBVCXO | narrow-band voltage-controlled crystal oscillator |
| NCAR | National Center for Atmospheric Research (Boulder, Colo.) |
| NSF | National Science Foundation |
| NSSCC | National Space Surveillance Control Center (Cambridge Research Center) |
| OAMS | orbital attitude maneuvering system |
| OAO | Orbiting Astronomical Observatory |
| OART | Office of Advanced Research and Technology (NASA) |
| OAT | operating ambient temperature |
| OCC | operations control center |
| OCR | optimum-charge regulator |
| OGE | operational ground equipment |
| OLF | orbital launch facility |
| OLO | orbital launch operations |
| OLV | orbital launch vehicle |
| OMR | operations management report |
| OMSF | Office of Manned Space Flight (NASA) |
| ORT | operational readiness test |
| OSDP | on-site data processing |
| OSDR | on-site data recovery |
| OSE | operational support equipment |
| OSFD | Office of Space Flight Development (NASA) |
| OSFR | on-site film recorder |
| OTA | optical tracking aid |
| OTC | overload trip circuit |
| PA | performance analysis (group) |
| PCC | pneumatic control console |
| PCE | power conditioning equipment |
| PCM | pulse-code modulation |
| PCS | pressure control system |
| PCU | power control unit |
| PD | project document |
| PDP | project development plan |
| PE | project engineer |
| PERT | program evaluation and review technique |
| PFM | pulse-frequency modulation |
| P/FR | problem/failure report |
| PIPS | post-injection propulsion system |
| PLAS | postlanding attitude determination |
| PLM | pulse-length modulation |
| PM | phase modulation |
| PMR | project management report |

## Glossary (contd)

| | |
|---|---|
| PPL | preferred parts list |
| PPM | pulse-position modulation |
| PPS | primary propulsion system |
| PRB | problem review board |
| PRD | program requirements document |
| PRF | pulse-repetition frequency |
| PSD | power spectral density |
| PSNR | power signal-to-noise ratio |
| PSP | program support plan |
| PTM | proof test model |
| PU | propellant utilization |
| PVT | performance verification test |
| PWM | pulse-width modulation |
| RA | radar altimeter |
| RADVS | radar altimeter and doppler velocity sensor |
| RCS | reentry control system |
| RDS | receiver decoder selector |
| RIG | radio inertial guidance |
| RIS | Range Instrumentation Ship |
| RMD | Reaction Motors Division, Thiokol Chemical Corp. |
| RODVS | reliable-operate doppler velocity sensor |
| RORA | reliable-operate radar antenna |
| ROTI | recording optical tracking instrument |
| RPI | relay position indicator |
| RSC | range safety command test |
| RSPWG | range safety and planning work group |
| RSS | radio subsystem |
| R-T | receive-transmit |
| RTC | real-time command |
| RTCF | real-time computer facility |
| RTCS | Real-Time Computer System, Kennedy Space Center |
| RTG | radioisotope thermoelectric generator |
| RTV | reentry test vehicle |
| RV | reentry vehicle |
| SAA | S-band acquisition aid |
| SADL | Sterilization Assembly Development Laboratory |
| SAF | Spacecraft Assembly Facility (JPL or AFETR as defined) |
| SBR | Santa Barbara Research (Santa Barbara, Calif.) |
| SBRC | Santa Barbara Research Center (Goleta, Calif.) |
| SCCF | Spacecraft Checkout Computer Facility |
| SCF | Spacecraft Checkout Facility |
| SCO | subcarrier oscillator |
| SCR | silicon-controlled rectifier |
| SDA | systems data analysis |
| SDAT | systems data analysis team |
| SDC | signal data converter |
| SDCC | simulated data conversion center |
| SECO | sustainer engine cutoff |
| SET | solar energy thermionic (conversion system) |
| SFO | Space Flight Operations |
| SFOC | Space Flight Operations Center; Space Flight Operations Complex |
| SFOD | Space Flight Operations Director |
| SFOF | Space Flight Operations Facility |
| SFOG | Space Flight Operations Group |
| SFOP | Space Flight Operations Plan |
| SFOS | Space Flight Operations System |
| SFT | system functional test |
| SIRD | support instrumentation requirements document |
| SM/SS | soil mechanics/surface sampler |
| SMAC | soil mechanics analysis and command (group) |
| SOC | *Surveyor* Operations Center |
| SOCP | *Surveyor* on-site computer program |
| SP | signal processor |
| SPA | signal processing auxiliary |
| SPAA | spacecraft performance analysis area |
| SPAC | spacecraft performance and analysis command |
| SPODP | single-precision orbit-determination program |
| SPP | solar panel positioner |
| SRT | systems readiness test |
| SRV | system readiness verification |
| SS&A | separation, sensing, and arming |
| SSAC | space science analysis and control |
| SSACA | space science analysis and control area |
| SSB | single sideband |
| SSD | subsystem decoder |
| SSE | standard sequence of events |
| ST | systems test |
| STCDS | systems test complex data system |
| STEA | system test equipment assembly |
| STL | Space Technology Laboratory |
| STP | standard temperature and pressure |
| STS | space telecommunications system |
| STV | solar-thermal-vacuum |

## Glossary (contd)

| | |
|---|---|
| TA | type approval (test, testing) |
| TCA | thrust chamber assembly |
| TCP | telemetry and command processor |
| TCR | temperature control reference |
| TCVA | thrust control vector assembly |
| TDA | tracking data analysis |
| T&DA | Tracking and Data Acquisition (office) |
| TDH | tracking data handling |
| TDP | tracking data processor |
| T&DS | Tracking and Data System |
| T&FA | trend and failure analysis |
| T/FR | trouble/failure report |
| TOP | test and operations plan |
| TPAC | television performance analysis and command |
| TSAC | television science analysis and command |
| TSP | telemetry simulation program |
| TWT | traveling-wave tube |
| VCO | voltage-controlled oscillator |
| VECO | vernier engine cutoff |
| VEV | vernier engine vibration |
| VFSW | variable-frequency sine wave |
| VPS | vernier propulsion system |
| VSWR | voltage standing-wave ratio |
| VTVM | vacuum tube voltmeter |
| WBVCXO | wide-band voltage-controlled crystal oscillator |